UNIVERSIDADE DE LISBOA
FACULDADE DE CIÊNCIAS

Multi-elemental and isotope geochemistry of metapelites from the Volcano-Sedimentary Complex (Iberian Pyrite Belt, Portugal): unravelling fingerprints of different sources, sedimentary environments and exhalative-hydrothermal activity

" Documento Definitivo"

Doutoramento em Geologia
Especialidade em Metalogenia

Filipa Alexandra Diamantino da Luz

Tese orientada por:
António Manuel Nunes Mateus

Documento especialmente elaborado para a obtenção do grau de doutor

2020

UNIVERSIDADE DE LISBOA
FACULDADE DE CIÊNCIAS

Multi-elemental and isotope geochemistry of metapelites from the Volcano-Sedimentary Complex (Iberian Pyrite Belt, Portugal): unravelling fingerprints of different sources, sedimentary environments and exhalative-hydrothermal activity

Doutoramento em Geologia

Especialidade em Metalogenia

Filipa Alexandra Diamantino da Luz

Tese orientada por:

António Manuel Nunes Mateus

Júri:

Presidente:

- Maria da Conceição Pombo Freitas, Professora Catedrática, Faculdade de Ciências da Universidade de Lisboa

Vogais:

- Fernando Manuel Pereira de Noronha, Professor Catedrático Emérito, Faculdade de Ciências da Universidade do Porto
- Maria dos Anjos Marques Ribeiro, Professora Associada, Faculdade de Ciências da Universidade do Porto
- José António Paulo Mirão, Professor Associado com Agregação, Escola de Ciências e Tecnologia da Universidade de Évora
- António Manuel Nunes Mateus, Professor Catedrático, Faculdade de Ciências da Universidade de Lisboa, Orientador
- Jorge Manuel Todrigues de Sancho Telvas, Professor Associado com Agregação, Faculdade de Ciências da Universidade de Lisboa

Documento especialmente elaborado para a obtenção do grau de doutor

Com o apoio da Fundação para a Ciência e Tecnologia (PD/BD/114485/2016)

2020

Audaces fortuna juvat

(Virgílio, Eneida X, 284)

*This thesis is dedicated to my Mariazinha**

Acknowledgements

This study was performed with the financial support of the Fundação para a Ciência e Tecnologia through the grant PD/BD/114485/2016. Additional backing from the project FCT/UID/GEO/50019/2019 (IDL).

First, I would like to express my genuine thanks to my supervisor, António Mateus. It makes ten years that we've been working together…One decade! I've to admit that was not easy all the times but looking back now with other perspective (maybe due to my age), probably were the best years of my life. I had the opportunity to share his dream of being part of a scientific team working for the industry and trust me to be a team leader of a junior geologist's group (I'm still junior at the time). And I learned so much with this experience. He teached me how to be an exploration geologist and a scientist, he was patient when I didn't know how to see streaks, when I draw folds like mandalas or when he let me hit with my head on the walls to learn about numerical handling of isotopic data. But it was worth it, for sure! I don't know words in English to express my feelings about all the hours in the field, the guidance, the support, the huge effort (and hours) during all my manuscript reviews…MUITO OBRIGADO CHEFE!
Also, I want to acknowledge to my unofficial co-supervisor Jorge Figueiras. I'll never forget (and I think you not too) that day, when I cannot walk well because of my knee, but we're on the other side of the river looking to the outcrop and somehow, I became a truly geologist. *Audaces fortuna juvat* will be always on my mind! Thanks for oblige me to think about all the scenarios and hypotheses.

Cazé and Ezequiel, my younger unofficial supervisors, I'm deeply acknowledge to you. Both had a tremendous patient and availability to discuss with me and at the same time being highly demanding, compelling to "out of the box" thoughts. We learned a lot together, and I hope the future allow us to more collaborations.

I would also like to acknowledge to the Companies that provide me the opportunity to work and learn more about mining and exploration activities, i.e.:

- EPOS, S.A. for all the financial support before this PhD when the driven questions for this research arise. Luís Gonçalves, for the interest demonstrated along our collaboration and, later on, during the PhD plan, for all the logistic and technical support. A special mention regarding the two assistants from EPOS at Rio Maior warehouse; without their help with the drilling core boxes it was impossible to do the re-logging work in duly time;
- Teixeira Duarte, S.A., specifically to António Costa Vilar and Pedro Nunes. Thank you for introducing to me the "drilling world" and a bit of geotechnical stuff. I'll never forget the days at the Albernoa drilling site, and the sharing moments when you tried to convince me that geotechnics is better than mining, while I attempted to show you the reverse. Again, a special mention to Arlindo, Pedro, Vítor and Manuel for all the hours spent in the middle of nowhere, and all the pranks that you did to me (e.g. a

massive sulphide core from Neves Corvo in the middle of our drill-core or a death mouse);
- ALMINA and Lundin Mining for gave me the permission to access their drill-cores and underground mining samples. A special thanks to João Gonçalves, Inês Braz, Nélson Pacheco, Ricardo, Tiago Reis and Paulo Caetano;
- EDM and ESAN MET for providing me access to historical and exploration drills, for all the technical and logistic issues related to Gavião and Monte das Mesas prospects, respectively. Pedro Santos for the continuous support and for always believe in this research. At ESAN MET, I would like to thank Ilkay Cevik for believing the value of my work since the first day and for his help with everything he could; a special mention also to Nélson Martins and Jorge Hilário for the continuous support;
- Avrupa Minerals for providing me access to recent discoveries at Sesmarias. Paul Kuhn was always available to my work proposals and to discuss them.

I would like to thank Célia Lee and Pedro Rodrigues for their administrative and technical support during my PhD, respectively.

I would also thanks to the C6, 4th ground, researchers: Jorge Relvas, Álvaro Pinto, Miguel Gaspar, Mário Gonçalves, Isabel Costa and Raul Jorge, for everything they teach me along the years. You're partially responsible for my decision to be Economic Geologist. All the best, and I hope the future bring us freedom to discuss new ideas together. To João Mata for always have a nice word and support me when I needed.

I'm especially grateful to the Super Brigada team (Erica, Murphy, Marta e Barros). For all the hours spent in "our" Alentejo, with 40 degrees or running away from the cows… we're a fantastic team! Marta and Barros, despite the end of the project, were always present and helping me with their suggestions. I miss work with you!

The different versions of *Marmitex gang* colleagues and friends. Thank you for your friendship, for all the coffees, for shared lunched full of laughing geology. David, Ana Costa, João Carvalho, Sandra (my pizza partner) and a big hug for Cyntia, Sofia, Marta and Inês.

EarthSystem crew 2016, despite all our differences, this path will be different without you. I like palinha, dance at the office, the gentleman, miar e comer ratos, Fogooo (Porto accent), talk like a gun, ta tranquilo and second chances! And one ES 2015, Rodrigo, my solar friend, amazing our conversations and all I learn about renewables with you (I don't forget our collaboration!). All the best for you guys!

The C6, 4th ground, friends (as manas Pereira, Sofia e Inês, Jorge, Cristiana) for all the days of cheat conversation, but for believing that I'm "their metal girl". A special thanks to Violeta Lourenço for the days helping me to pack the drills and make me dance in the corridors.

A special thanks goes to Ana Jesus for all the friendship and all the things I learn with you! You probably don't know, but you secretly gave me strength to become a better scientist!

My “little GE€COS”, all the 4 generations, a lot of “sons and daughters”, some more distant, other closer like a real family. We learn so much together, I’am always learning with you! Thanks for all the hours that you help me in the lab, for complaining with me when we’re not satisfied with our supervisors, sing Hakuna Matata, bring me postcards and our famous coffee at Globo or our beer at the Muro. Ohhh life is good with “my GE€COS”. Sandra, Luís, Roseiro, Filipe, Rita Ferraz, Frederico, Marcelo, Rita Pereira, Linda, Gabi, Maria, Rita dos Santos, Diogo Ribeiro, Pedro, João and all the others! A bright future for you!

My “special GE€COS”, Ivo, Soares and André for bringing some happiness, rationality mixed with craziness. For always listening me! A bright future for you my darlings
André for being my IPB partner and the best PhD mate, sharing is caring, and you know it! I don’t forget (Santos & Luz, *in prep*; personal communication, Glasgow 2019).

Exploration team with my friends Mifi, Pedro and Joana. You’re always on the back supporting me personally and professionally! OBRIGADO! Somos a equipa Maravilha, só os investidores não vêem isso. Mifi, my older sister, for you I don’t need words =) always together*

As some might know, the PhD change the people…and one think that no one tells you is that “Being a PhD shouldn’t be bad for your health” and I only keep me safe because all the people that surround me, family and friends are here.

To all my friends (Fim do Mundo + além, Caramelos, Bazinga) that never let me goes down keeping me strong and into a normal life. Jantaradas cá em casa, viagens pelo mundo incluindo assar os pés na estrada mais antiga de Roma, o melhor afilhado, dançar até de manhã, fazer babysitting, os melhores cocktails in the town! E mesmo em tempos de quarentena os jantares e os treinos, obrigando-me a ter horários para a tese e para vocês! Obrigado!!!

An extra and special acknowledgment to my two coaches, André Barão and Catarina Palma during the quarantine exercise my legs, my arms, thousands of burpees, my first “man” push-ups…you put me in the line and without knowing keep my brain healthy!

A very special thanks to all my family without all your support it was impossible to be your Doutora! (Obrigado Pai, Mãe, Rita, Buga, Francisco, Catarina, Fernanda, Vítor e Avós Malveiro). Finalmente vou ter tempo para almoços, passeatas, petiscadas e férias sem levar os livros atrás =)

Finally, and the most important person (despite he doesn’t know yet what I was really doing these last four years), my João. All the words in the world are not enough to express my gratefulness!! But I let you with something special for us “Everything familiar has disappeared! The world looks brand-new. A new year…a fresh clean start. A day full of possibilities…It’s a magical world buddy”. João let’s go exploring…

Abstract

Over the last two decades, promising steps have been made in the development of new greenfield and brownfield exploration methods for massive sulphide ore-forming systems in the Iberian Pyrite Belt (IPB). However, the effects of lateral and vertical facies variations in metasedimentary piles forming the two main lithostratigraphic units that potentially host massive sulfide deposits [the Phyllite-Quartzite Group (PQG) and the Volcanic-Sedimentary Complex (VSC)] on mineral exploration remain unknown. Massive sulphide deposits of the IPB document the progression of ore-forming processes in the SW Iberian Variscides, throughout uppermost Devonian to Early Carboniferous. Sulphide ores are usually hosted in volcanic-dominated or shale-dominated successions belonging to the VSC (Late Fammenian to Late Visean). Yet, several important orebodies at Neves Corvo are sitting within upper sections (Fammenian) of the early deposited Phyllite-Quartzite Group (PQG). Four key sectors of the Portuguese segment of IPB were revisited and 262 samples collected to characterize the geochemical features of metapelites from PQG and VSC sequences in barren and fertile settings. The selected sectors include active (Neves Corvo and Aljustrel) and old (Lousal) mines, besides promising brownfield (Gavião) and greenfield (Sesmarias) prospects, and other lithostratigraphic sections without known mineralization. The composition of PQG and VSC metapelites is similar and mainly controlled by a mixture of clayey-derived and quartz sandy-derived components largely resulting from different sources of granitic to granodiorite/quartz-diorite composition. Mineral transformations during diagenesis and/or hydrothermal alteration/mineralization partially overprinted the primary composition. During sedimentation/diagenesis, prevalent redox conditions were mostly confined to oxic environments, at places transiting to suboxic. Subsequent multi-stage interaction with reducing hydrothermal fluids (to which the sulphide mineralization is related) generated heterogeneous anoxic signs. Significant hydrothermal/mineralization imprints exist when $Fe_2O_3/TiO_2 \geq 10$ and $Al_2O_3/(Al_2O_3+Fe_2O_3+MnO) \leq 0.6$. The $5x[(Fe_2O_3+MgO+MnO)/Al_2O_3]$, (Cu+Zn+Pb)/Sc and (As+Sb)/Sc geochemical ratios were recently proposed to separate barren from altered/mineralized metasedimentary successions in the IPB. When all these three ratios are above 10, a realistic vectoring towards massive sulphide accumulations occurs.

From this dataset, 98 samples were chosen to conduct a Pb-Nd-Sr isotope study from different sections of the PQG and VSC successions (from Givetian to Upper Visean), including footwall and hanging wall domains of mineralized horizons in Neves Corvo, Aljustrel and Lousal. An extensive review of the isotopic data for pelite rocks in the IPB allow the evaluation of their

sources and the potential of radiogenic isotopes as exploration tools, when combined with trace element geochemistry. The whole-rock Nd and Sr isotopic compositions along with Th/Sc ratios shows that PQG and VSC sediments are mostly composed of a silicilastic mix supplied by the dismantling of an old basement: $-11 \leq \varepsilon Nd_i \leq -8$; $^{87}Sr/^{86}Sr_i$ up to 0.727; and TDM ages ranging from 1.08 to 1.91 Ga ($\bar{x} = 1.67 \pm 0.16$ Ga). The rising of εNd_i values recorded by many samples of *upper* VSC (up to ± 0.2 in the Aljustrel sector) is interpreted as a result of local incorporation of volcanic-derived contributions completed during sedimentation processes during and after Upper Tournaisian**.** The PQG succession, at times complemented by VSC thick piles, represent the main crustal reservoirs of metals that supplied the hydrothermal inflows in IPB, which were dominated by modified seawater. Other sources, more radiogenic, should be involved in the IPB metal budget when the role of Sn- and Cu-rich fluids became central in the ore system, as documented for the Neves Corvo deposit. The increasing of $^{207}Pb/^{204}Pb_i$ ratios in sediments is sensitive to the circulation of mineralizing fluids. On the contrary, significant rise in $^{206}Pb/^{204}Pb_i$ (and $^{207}Pb/^{204}Pb$) values in sediments bearing disseminated sulphides other than pyrite only occur when conditions for a protracted interaction with radiogenic hydrothermal inflows of moderate to high temperature existed. The proximity to massive sulphide ore systems could be recognized in sedimentary levels of PQG and VSC whenever $^{207}Pb/^{204}Pb_i > 15.60$ together with other multi-elemental geochemical ratios such as Fe_2O_3/TiO_2 and $(Cu+Zn+Pb)/Sc > 10$.

Keywords

Iberian Pyrite Belt,

Massive sulphide deposits

Alteration/mineralization indexes

Metasedimentary successions

Sediment and metal sources

Resumo alargado

O presente resumo encontra-se redigido segundo as normas do Acordo Ortográfico de 1945.

Nas últimas duas décadas foram dados importantes passos no desenvolvimento de métodos de prospecção em contexto *greenfield* e *brownfield* para a sulfuretos maciços na Faixa Piritosa Ibérica (FPI). Estes estudos debruçaram-se sobre: i) os factores que condicionam a arquitectura, desenvolvimento e evolução da bacia que originou a FPI; ii) os constrangimentos temporais proporcionados por estudos palinológicos e de cronologia absoluta na delimitação do intervalo de tempo onde os sulfuretos maciços se desenvolveram; iii) a vulcanologia física do Complexo Vulcano-Sedimentar (CVS), com vista à reconstrução especial dos centros vulcânicos e a sua relação com a mineralização; iv) fontes de fluidos envolvidos no processo metalogenético através de estudos de geoquímica multi-elementar e isotópica; v) os modelos metalogenéticos híbridos que contemplam processos vulcanogénicos e exalativo-hidrotermais, entre outros.

No entanto, as variações laterais e verticais de fácies ao longo das sucessões metasedimentares que potencialmente hospedam sulfuretos maciços [Grupo Filito-Quartzitico (GFQ) e Complexo Vulcano-Sedimentar (CVS)] e a sua importância para a prospecção, mantêm-se desconhecidas. Os depósitos de sulfuretos maciços da FPI documentam processos de formação de minério durante a transição Devónico-Carbónico. Geralmente estes sulfuretos maciços estão hospedados em sucessões vulcânicas ou sedimentares que pertencem ao CVS (Fameniano superior a Viseano Superior). No entanto, diversas massas do depósito de Neves Corvo associam-se a níveis superiores do GFQ (Fammeniano). Neste trabalho foram revisitados quatro sectores do segmento português da FPI através de uma extensa amostragem (n=262) permitindo a caracterização geoquímica dos metapelitos do GFQ e do CVS em domínios mineralizados ou estéreis. Os sectores selecionados incluem minas activas (Neves Corvo e Aljustrel) e inactivas (Lousal). No sentido de tornar o estudo mais representativo, foram também estudadas sucessões metasedimentares em áreas concessionadas para a prospecção em contextos: *brownfield* (Gavião) e *greenfield* (Sesmarias e Monte das Mesas) e outros sectores da região sem mineralização reconhecida até ao momento.

A composição química dos metapelitos do GFQ e CVS é semelhante e essencialmente controlada pela mistura de uma componente argilosa e de outra quartzo-arenosa que resultam de fontes essencialmente de composição granítica a granodiorítica/quartzo-diorítica. Estas podem ser identificadas considerando um conjunto de razões geoquímicas: Al_2O_3/TiO_2, Th/Sc, Sc/TiO_2, Ga/TiO_2, Zr/TiO_2 and SiO_2/Al_2O_3. A componente argilosa caracteriza-se por $\approx 25 \leq Al_2O_3/TiO_2 \leq \approx 30$, $\approx 0.5 \leq Th/Sc \leq \approx 0.8$ e $\approx 0.0005 \leq Zr/TiO_2 \leq \approx 0.001$ e está representanda

essencialmente nas secções do CVS intermédio e superior. Por sua vez, a componente quartzo-arenosa apresenta valores de Al_2O_3/TiO_2 mais baixos (≈10 – 20), ≈ 0.5 ≤ Th/Sc ≤ ≈ 1 e ≈ 0.001 ≤ Zr/TiO_2 ≤ ≈ 0.025 que caracterizam os metapelitos do GFQ e o CVS inferior. Uma terceira componente de origem vulcânica foi identificada e tem especial expressão nas secções do CVS superior. Esta evidencia pequenos desvios aos valores mencionados: ≈ 45 ≤ Al_2O_3/TiO_2 ≤ ≈ 65, Th/Sc > 1 e valores baixos mas irregulares de Zr/TiO_2 (< 0.05).

As transformações minerais que ocorrem durante a diagénese e/ou o processo de alteração hidrotermal e mineralizante sobrepõem-se parcialmente às características primárias destes metapelitos. Durante o processo da sedimentação/diagénese, as condições redox das várias sub-bacias da FPI apontam para ambientes essencialmente óxicos, em alguns locais transitando para sub-óxicos (0 < U/Th < 1.25; V/Cr < 2). Posteriormente, a interação episódica com fluidos hidrotermais associados à mineralização geram sinais anóxicos heterogéneos (U/Th < 4.25; V/Cr > 2).

As razões $Fe_2O_3/TiO_2 \geq 10$ e $Al_2O_3/(Al_2O_3+Fe_2O_3+MnO) \leq 0.6$ permitem colocar em evidência metapelitos que foram sujeitos a processos de alteração/mineralização significativos. Existem algumas excepções, associadas a exemplars com altos conteúdos em aluminossilicatos. Os metapelitos do grupo "Py-bearing" apresentam intervalos mais estreitos para estas razões (Fe_2O_3/TiO_2 entre 5 - 10 e [$Al_2O_3/(Al_2O_3+Fe_2O_3+MnO)$ em torno de 0.6/0.7], sobrepondo-se parcialmente ao campo definido pelas amostras do grupo "Mineralized". A menor amplitude de valores registada pode estar relacionada com: i) o desenvolvimento da pirite durante a diagénese; ii) actividade hidrotermal de baixa temperatura e consequente deposição de pirite ± esfalerite; ou iii) interacção incipiente com fluidos hidrotermais de relativa alta temperatura que terão proporcionado a recristalização da pirite e a formação de calcopirite acessória.

Recentemente, outras três razões geoquímicas multi-elementares foram propostas para separar sucessões metasedimentares da FPI associadas ou não a domínios de alteração/mineralização hidrotermal: (5x[$(Fe_2O_3+MgO+MnO)/Al_2O_3$], (Cu+Zn+Pb)/Sc e (As+Sb)/Sc). Quando estas três razões apresentam valores acima de 10, tornam-se úteis na vectorização de acumulações de sulfuretos maciços. A conjugação das razões (Cu+Zn+Pb)/Sc e (As+Sb)/Sc e a sua co-variação positiva apresentam-se como uma valiosa ferramenta para a vectorização em relação ao horizonte mineralizante. Considerando apenas a abundância relativa de sulfuretos ("No-sulphide", "Py-bearing" e "Mineralized) nem sempre é possível distinguir tendências. No entanto, a discriminação quanto à posição das amostras do horizonte mineralizante (tecto ou muro) permite uma aproximação directa aos domínios mineralizados, principalmente para domínios a muro e/ou horizonte mineralizante. Os metapelitos a tecto apresentam grande

variabilidade da razão (As+Sb)/Sc (≈ 0.1 -50) e menor amplitude embora consistente, da razão (Cu+Zn+Pb)/Sc (≈ 10 – 50) que em conjunto poderão relacionar-se com a dispersão/re-distribuição de elementos químicos ocorrida antes, durante ou após deformação Varisca.

Para o estudo isotópico multi-sistema (Pb-Nd-Sr; rocha-total) foram escolhidas 98 amostras das diferentes secções do GFQ e do CVS, incluindo amostras a tecto e a muro dos horizontes mineralizados (Neves Corvo, Aljustrel e Lousal). Para enquadrar melhor os resultados deste trabalho, procedeu-se à construção de uma base de dados que contempla os dados isotópicos conhecidos para metapelitos e minérios da FPI (segmento português e espanhol). As composições isotópicas de Nd-Sr cruzadas com Th/Sc indicam que os sedimentos do GFQ e do CVS resultam essencialmente de uma mistura siliciclástica que deriva do desmantelamento do soco: $-11 \leq \varepsilon Nd_i \leq -8$; $^{87}Sr/^{86}Sr_i \leq 0.727$; e idades modelo entre 1.08 e 1.91 Ga ($\bar{x} = 1.67 \pm 0.16$ Ga). O incremento de valores de εNd_i, visível essencialmente em amostras do CVS superior (até 0.2) é interpretado como resultado da incorporação de componentes vulcano-derivadas durante o processo de sedimentação (sin- a pós- Tournaisiano superior). O GFQ, na sua maioria, mas também o CVS, representam os principais reservatórios crustais de metais que alimentam os influxos hidrotermais relacionados com a génese de sulfuretos maciços da FPI, estes dominados por água do mar modificada. Outras fontes, mais radiogénicas, devem ser consideradas nomeadamente quando os fluidos se tornam ricos em Sn + Cu, como é o caso de Neves Corvo. O aumento da razão $^{207}Pb/^{204}Pb_i$ em metapelitos é sensível à circulação de fluidos mineralizantes. Por sua vez, as razões $^{206}Pb/^{204}Pb_i$ e $^{207}Pb/^{204}Pb_i$ aumentam quando existe interação prolongada com influxos hidrotermais de temperatura moderada-alta. O cruzamento dos indicadores geoquímicos multi-elementares com razões isotópicas (sistema Pb-Pb) permite reconhecer sucessões sedimentares do GFQ e do CVS que se aproximam de domínios proximais aos depósitos de sulfuretos maciços. Isto verifica-se quando a razão $^{207}Pb/^{204}Pb_i > 15.60$, Fe_2O_3/TiO_2 e (Cu+Zn+Pb)/Sc > 10.

Palavras-Chave:

Faixa Piritosa Ibérica

Sulfuretos Maciços

Índices de alteração/mineralização

Sucessões metasedimentares

Fontes de metais e proveniências sedimentares

Table of Contents

List of Tables

List of Figures

Preface

The research activities for this thesis started at the beginning of 2016 with FCT co-funding through the EarthSystem Doctoral School (FCT/UID/GEO/20019/2019) and the Instituto Dom Luiz (IDL) grant (PD/BD/114485/2016). The work began at Faculdade de Ciências da Universidade de Lisboa (FCUL) facilities in close collaboration with EPOS S.A., EDM, ALMINA, Lundin Mining, ESAN MET and AVRUPA Minerals. Later on, collaboration with the Centro de Pesquisas Geocronológicas (CPGeo) at the University of São Paulo, Brazil, was established.

Between 2006 and the present, the exploration endeavours in the Iberian Pyrite Belt (IPB) have grown significantly (see data provided by the national mining authority, DGEG), bringing new life to old issues, which were not completely abandoned during the investment breaks between mid-90s and 2004, but regained a renewed significance.

During the last two decades, several multidisciplinary studies (e.g. Leistel *et al.*, 1998; Tornos *et al.*, 1998; Sáez *et al.*, 1999; Matos *et al.*, 2000; Rosa *et al.*, 2004; Rosa *et al.*, 2008; 2010; Oliveira *et al.*, 2011) contributed to noteworthy advances in the IPB knowledge, mainly regarding: (i) the factors that directly and indirectly conditioned the architecture, formation and evolution of the basin that gave rise to the IPB (e.g. Tornos *et al.*, 2002; Oliveira *et al.*, 2005); (ii) the role of physical volcanology in Volcano-Sedimentary Complex (VSC) interpretation, providing criteria useful to spatial reconstruction of volcanic centers and associated mineralization (e.g. Soriano & Mart, 1999; Rosa, 2007; Rosa *et al.*, 2008, 2010); (iii) the constraints imposed by palynology and absolute geochronology and consequent definition of the interval in which the ore-forming systems have been developed (e.g. Barrie *et al.*, 2002; Pereira *et al.*, 2007; Valenzuela et al, 2011; Oliveira *et al.*, 2013); (iv) the characterization of possible sources of metals and fluids involved in the metallogenic processes, making use of multi-elemental and isotopic data (e.g. Marcoux, 1998; Relvas *et al.*, 2001; Tornos *et al.*, 2008; Jorge, 2009; Carvalho, 2016); and (v) the proposal of hybrid genetic models, mostly involving both volcanogenic and exhalative-hydrothermal processes in sedimentary settings (e.g. Almodóvar *et al.*, 1998; Sáez *et al.*, 1999, 2011; Relvas, 2000; Oliveira *et al.*, 2005; Relvas *et al.*, 2006b; Tornos & Heinrich, 2008).

Notwithstanding these developments, several questions remain open, particularly those related to vertical and lateral variations in the VSC successions and their significance in mineral exploration. These are indeed important issues to better organize local stratigraphic columns and realize the main physical-chemical features constraining the basin evolution, providing

additional key elements for the location of concealed ore-forming systems of economic significance. In this regard it should be emphasized that the historical track record clearly shows that improvements in conceptual geological models, along with advances in geophysical data multi-method acquisition and modelling, were critical for the discovery of: (i) Neves Corvo in 1977 (e.g. Leca *et al.*, 1983; Carvalho *et al.*, 1999; Relvas *et al.*, 2002; Oliveira *et al.* 2004, 2013; Carvalho, 2016); (ii) Lagoa Salgada in 1992 (e.g. Oliveira *et al.*, 1998); (iii) Las cruces in 1994 (e.g. Yesares *et al.*, 2015; Tornos *et al.*, 2017); and (iv) in 2014, the technically successful exploration programs undertaken by AVRUPA in the Alvalade prospect (Avrupa Minerals, 2014) and by MATSA at La Magdalena (e.g. Granda *et al.*, 2016). These discoveries have prompted discussions on the performance of mineral exploration surveys and, particularly, on the role of geochemical exploration methods, which has triggered multiple thematic seminars and research projects considering current practicalities and modern approaches. This thesis has grown and taken shape alongside this evolution, greatly benefiting from discussions with different actors in the field.

List of original publications

This thesis is based on the following main publications:

i. **Luz, F.**, Mateus, A., Figueiras, J., Tassinari, C.C.G., Ferreira, E., Gonçalves, L., (2019) *Recognizing metasedimentary sequences potentially hosting concealed massive sulfide accumulations in the Iberian Pyrite Belt using geochemical fingerprints*. Ore Geology Reviews 107, 973-998, https://doi.org/10.1016/j.oregeorev.2019.03.020

ii. **Luz, F.,** Mateus, A., Rosa, C., Figueiras, J., (2020). *Geochemistry of Famennian to Visean metapelites from the Iberian Pyrite Belt: Implications for Provenance, Paleo-redox Conditions and Vectoring to Massive Sulfide Deposits, Natural Resources Research, - DOI: 10.1007/s11053-020-09686-4*

iii. **Luz, F.**, Mateus, A., Ferreira, E., Tassinari, C.G., Figueiras, J. *Pb-Nd-Sr isotope geochemistry of metapelites from the Iberian Pyrite Belt and its relevance in vectoring massive sulphide ore systems,* Economic Geology (under review, submitted in 3 June 2020)

In addition to these main publications, some preliminary data and interpretations were presented in international scientific meetings, such as:

(i) **Luz, F**., Mateus, A., Figueiras, J., Tassinari, C.G., Gonçalves, L. 2017. Whole-rock chemistry and Pb Isotope Compositions in metasediments of the Iberian Pyrite Belt; relevance to Mineral Exploration, Goldschmidt Conference, Paris – poster presentation;

(ii) **Luz, F**., Mateus, A., Figueiras, J., 2018. Elemental geochemistry of metasediments from the Aljustrel area, Iberian Pyrite Belt (IPB), Portugal: implications for mineral exploration. SEG Conference, Colorado (EUA) – poster presentation;

(iii) **Luz, F**., Mateus, A., 2019. Unravelling the geochemistry of dark-grey to black metapelites in the Iberian Pyrite Belt (Portugal): the relation to massive sulphide ores, 15th Biennal Meeting, Glasgow, Scotland – oral presentation.

(iv) **Luz, F**., Mateus, A., Rosa, C., Ferreira, E., Figueiras, J., Tassinari, C.G., 2020. Geochemistry of metapelites: the forgotten link to provenances and vector massive sulphide ores in the Iberian Pyrite Belt. Ore Deposit Hub, 29th May – oral presentation (https://www.youtube.com/watch?v=2ANBxcKWw8w).

Furthermore, outreach and training activities under the scope of the PhD research were also developed, the most relevant being the:

(i) Participation as a speaker at Raw Materials University Day – FCUL, Portugal International Mining Business and Investment (PIMBIS) for mining investors, Lisbon, Portugal (2016);

(ii) Accredited training to high-school teachers on mineral deposits and sustainable development (2019 onwards);

(iii) 14th and 16th Short courses in Economic Geology: Iron Oxide Copper Gold and Iron Oxide Deposits (2016) and Zinc Deposits (2018), TU Bergakademie, Freiberg Germany;

(iv) Radiogenic and Non-traditional Isotopes: Analytical Methods and Application – 7th to 10th of March 2017, Goethe University, Frankfurt, supervision Axel Gerdes (Goethe University);

(v) *EarthSystem Summer Course*: Introduction to numerical modelling using Underworld Software: 12th to 16th of September 2016, at Faculty of Sciences – University of Lisbon, under supervision of Nicolas Riel (University of Durnham)

SECTION 1

1. Introduction

The South Portuguese Zone (SPZ) represents the southernmost geotectonic unit of the Iberian Variscides and records a series of geological processes closely related to the evolution of the SW Iberian Variscan suture (*e.g.* Julivert *et al.*, 1994; Ribeiro *et al.*, 1990, 2007, 2010; Quesada, 1998; Oliveira *et al.*, 2019). The Iberian Pyrite Belt (IPB; **Figure 1.1**) is located immediately to the south of the Pulo do Lobo terrane that, together with the Beja Acebuches Ophiolite Complex, outline this Variscan suture (*e.g.* Ribeiro *et al.,* 1990, 2007, 2010; Silva *et al.,* 1990; Quesada *et al.,* 1984; Quesada, 1991, 1998). This geotectonic setting was critical for the establishment of conditions that ended up determining the generation of a wide range of massive sulphide ore systems, mostly from the upper Fammenian (Strunian ≈ 360 Ma) until to middle Tournaisian (*e.g.* Boulter, 1996; Nesbitt *et al.,* 1999; Mathur *et al.,* 1999; Barrie *et al.,* 2002; Pereira *et al.,* 2007, 2012; Rosa *et al.,* 2009; Matos *et al.,* 2011; Valenzuela *et al.,* 2011; Inverno *et al.,* 2015; Oliveira *et al.,* 2013 a, 2019; Tornos *et al.,* 2015; Li *et al.,* 2019).

The left-lateral transpressive convergence between SPZ and the Iberian Terrane during Carboniferous favoured the generation of tectonically controlled assymetric (2nd and 3rd order) basins within a shallow continental platform (*e.g.* Silva *et al.,* 1990; Oliveira *et al.,* 2013, 2019). A thick (> 2000 m), pre-orogenic and siliciclastic mega-sequence from the Givetian to Fammenian, known as the Phyllite-Quartzite Group (PQG), covered the continental platform (*e.g.* van den Boogard, 1963; Shermerhorn, 1971; Oliveira, 1990; Oliveira *et al.,* 2013 a, 2019; Moreno *et al.,* 1996; Jorge *et al.,* 2007; Pereira *et al.,* 2007; Faria *et al.,* 2015). The gradual development of those fault-bounded basins makes them the preferred focus for deposition of volcanic products whenever suitable physical conditions were locally met, quite often using the main fault zones as magma conduits. Bimodal magmatic activity generate different successions of volcanic rocks (with a wide of facies variety) that are frequently intercalated and/or inter-fingered with fine-grained siliciclastic successions, forming the Late Fammenian to Late Visean Volcano Sedimentary Complex (VSC) that may be up to 600 m thick (*e.g.* Schermerhorn, 1971; Carvalho *et al.,* 1999; Soriano and Martí, 1999; Valenzuela *et al.,* 2002; Donaire *et al.,* 2002; Rosa *et al.,* 2011; Oliveira *et al.,* 2019). The predominant host of the IPB massive sulphide ores is either the volcanic-dominated or the shale-dominated successions of the VSC. Most of these ores occur as stratiform bodies, quite often displaying large mineralized stockworks at their footwall. Overlying the VSC, a thick (> 1600 m) syn-orogenic flysch succession (Baixo Alentejo Flysch Group, BAFG) is developed, gradually younger in age

towards the SW (upper Visean to Sepkuvian-Moscobian) (*e.g.* Schermerhorn, 1971; Oliveira, 1990; Pereira *et al.,* 2007, 2010; Rodrigues *et al.,* 2015).

During the tectonic inversion triggered by the SPZ – Iberian Terrane oblique collision, an SE verging thin-skinned fold/thrust belt was developed (Schermerhorn and Stanton 1969; Silva *et al.* 1990, 2013; Quesada 1991) along with metamorphic recrystallization (315 ± 7 Ma) under increasingly lower PT conditions from NE (greenschist facies) to SW (prehnite-pumpellyite facies) (Priem *et al.* 1978; Munhá 1979, 1981, 1983, 1990; Munhá and Kerrich 1980; Abat *et al.* 2001). Despite the tectonic dismembering and stacking of slices belonging to PQG, VSC or BAFG, the main characteristics of the pre- and syn-orogenic sequences can be assessed in various lithostratigraphic sections.

The PQG siliciclastic pile comprises, at present, phyllites, quartzites and meta-quartzwackes, locally complemented with meta-limestone lenses in the upper levels of the sequence (e.g. Moreno *et al.* 1996; Jorge *et al.* 2007; Oliveira *et al.* 2019). The VSC includes a large variety of sedimentary rocks but with clear prevalence of shale/silty facies indicating deposition primacy in confined basins affecting the siliciclastic platform. *Lower* to *middle* VSC sections are represented by a monotonous succession of black metapelites or fine interfingerings of metapelites and metasiltstone levels disrupted by volcanic rocks or evolving gradually (either vertically or laterally) to volcaniclastic (matrix-supported) sediments (*e.g.* Schermerhorn, 1971; Leistel *et al.,* 1998 a; Oliveira *et al.,* 2013 a, 2019). Volcanic rocks in the VSC are predominantly submarine and document events between *ca.* 360 and 345 Ma, although peaking around 355–350 Ma (Nesbitt *et al.,* 1999; Mathur *et al.,* 1999; Carvalho *et al.,* 1999; Barrie *et al.,* 2002; Dunning *et al.,* 2002; Rosa *et al.,* 2009; Valenzuela *et al.,* 2011; Oliveira *et al.,* 2013 a, 2019; Solá *et al.,* 2015) The prevalence of felsic rocks (rhyodacitic/rhyolitic) is not regularly distributed, and products of mafic (basaltic) to intermediate (andesitic) composition can be significant in some VSC sections (*e.g.* Leca *et al.,* 1983; Munhá, 1981, 1983; Mitjavilla *et al.,* 1997; Thièblemont *et al.,* 1998; Carvalho *et al.,* 1999; Rosa *et al.,* 2004, 2006, 2008, 2011; Codeço *et al.,* 2018; Conde and Tornos, 2019; Donaire *et al.,* 2020).

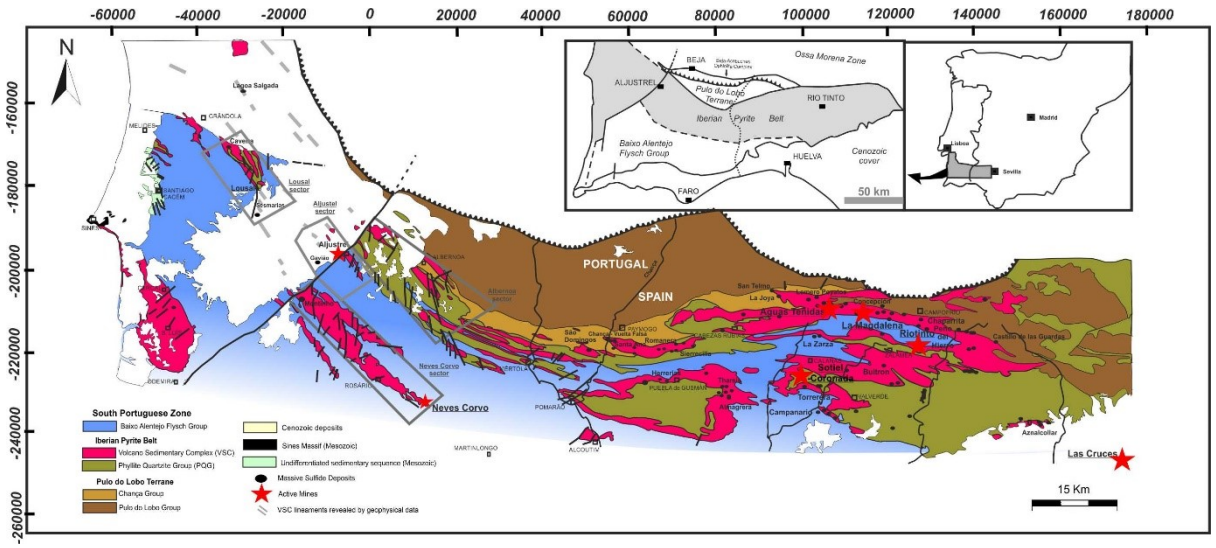

Figure 1.1 - Geological setting and simplified geological map of the South Portuguese Zone in SW Iberia, illustrating the IPB extension and the main massive sulphide ore deposits location. The four sectors considered in this study are traced by grey-polygons. Modified after Oliveira (1992), Barriga *et al.*, (1997, Marcoux (1998), Leistel *et al.*, (1998), Carvalho *et al.*, (1999), Matos *et al.*, (2000, 2006) and Tornos (2006).

The Massive Sulphide ore systems of IPB

The IPB hosts ≈2500 Mt of massive sulphide ores distributed over *ca*. 90 known deposits, eight of them classified as giant (> 100 Mt), namely: Riotinto, Tharsis, Aznallcóllar-Los Frailes, Masa Valverde, Sotiel-Migollas and La Zarza, in Spain; Aljustrel and Neves Corvo, in Portugal (*e.g.* Strauss, 1970; Strauss *et al.,* 1977; Sáez *et al.,* 1996, 1999; Barriga *et al.,* 1997; Leistel *et al.,* 1998b; Tornos *et al.,* 2000; Relvas *et al.,* 2002; Inverno *et al.,* 2015; Martín-Izard *et al.,* 2015, 2016).

The geological processes involved in the formation of these giant, metal-rich (including more than 20 Mt Cu, 35 Mt Zn, 15 Mt Pb and ≈0.8 Mt Au) sulphide accumulations are not consensual. However, as documented in many studies, the metallogenic models for the IPB massive sulphides can be classified as hybrid for most cases between volcanogenic systems and exhalative-hydrothermal processes in sedimentary settings (*e.g.* Barriga, 1983; Barriga and Fyfe 1988; Almodóvar *et al.,* 1998; Sáez *et al.,* 1999, 2011; Relvas *et al.,* 1994, 2001, 2002, 2006 a, b; Solomon *et al.,* 2002; Solomon and Quesada, 2003; Tornos, 2006; Tornos and Heinrich, 2008; Inverno *et al.,* 2008, Huston *et al.,* 2011). A recent assessment of mineral associations and textures displayed by the IPB sulphide ores (Almodóvar *et al.,* 2019) shows in addition that early deposited mineralization changed significantly its composition through protracted interaction with hydrothermal fluids with distinct chemical nature. These changes, acting over the (PQG and) VSC sections during successive ore-forming stages, could be further subjected to ore-zone refinements and/or geochemical dispersion. The latter processes should

document the progression of long-lived mass advection concurrent of Variscan deformation and metamorphism, afterwards followed by the propagation/reactivation of strike-slip fault zones in Late Variscan times (Quesada, 1998; Relvas, 2000; Marignac *et al.,* 2003; Castroviejo *et al.,* 2011; Codeço *et al.,* 2018; Almodóvar *et al.,* 2019). Apart from the variable intensity of late transformations experienced by massive sulphide ores, the development of early mineralization should reflect seafloor hydrothermal activity during upper Fammenian (Strunian) to mid Tournaisian. Venting of hydrothermal fluids onto the uppermost PQG and/or *lower* to *middle* VSC sections that comprise distinct successions of siliciclastic and volcaniclastic sediments led to different mineralization styles: sulphide mounts, stratiform exhalative and/or replacive bodies. These differences are related to variations in permeability of the geological setting, fluctuations in water/rock ratios, chemical reactivity and/or oscillations on local redox conditions presented by the siliciclastic and volcaniclastic successions (*e.g*. Barriga and Fyfe, 1998; Tornos *et al.,* 2015; Tornos, 2006; Relvas *et al.,* 2006 a). Nonetheless, according to the preserved geological record, the stratiform exhalative bodies are definitely the most common style of massive sulphide mineralization in the IPB, and the wanning stages of rhyolitic/rhyodacitic volcanic events within the variably thick VSC successions represent the most common mineralizing periods.

The emphasis ascribed in many studies to the mineralization setting has reinforced the "volcanic-hosted *vs*. shale-hosted" dichotomy, leading to a series of overviews about the separation of the two group deposits (Tornos, 2006; Tornos *et al.,* 1998, 2008, 2015; Tornos and Conde, 2002; Tornos and Heinrich, 2008; Velasco-Acebes *et al.,* 2018). Following this perspective, the orebodies distributed along the northern IPB (as Riotinto, Aguas Teñidas, La Zarza, Aljustrel or Lagoa Salgada) are sited in the apical domains of felsic domes and their development largely related to replacement processes of the hosting volcanic rocks in mid-Tournaisian. In contrast, the orebodies spreading all over the southern IPB (as Sotiel-Migollas, Tharsis, Neves Corvo, Lousal, Las Cruces, Aznalcóllar-Los Frailes or Masa Valverde) are mostly shale-hosted and typically larger (although often pyrite-enriched), representing a product of exhalative or replacement processes in euxinic basins during the Upper Fammenian (Strunian). This classification, altough appealing in many features, is not free of controversy, as documented for some important exceptions, such as Neves Corvo (*e.g.* Relvas *et al.,* 2001, 2006 a, b; Li *et al.*, 2019).

Despite of different views on the progression of ore-forming processes in the IPB, a generalized consensus exists on the alteration/mineralization patterns affecting the orebodies footwall.

These patterns are characterized by low sulphidation mineral assemblages developed in multi-stage processes under mildly acidic and low to moderate temperature conditions (≈100 ± 25 ºC to ≈300 ± 15 ºC; average values considering the ranges reported in *e.g.* Barriga, 1983; Leistel *et al.,* 1998b; Relvas, 2000; Sánchez-España *et al.,* 2000; Inverno *et al.,* 2008; Moura, 2008; Oliveira *et al.,* 2011). In addition, it should be noted that these ore-related secondary mineral assemblages overprint partly or obliterate completely the mineral/textural changes previously developed in PQG and VSC rocks due to the interaction with modified seawater. These early developed changes, triggered by seafloor metasomatism, are often labelled as "regional alteration" (*e.g.* Munhá and Kerrich, 1980; Munhá *et al.,* 1980; Barriga and Kerrich, 1984; Munhá *et al.,* 1986).

PhD aims and thesis outline

The main focus of the research carried out during this PhD was on the metasedimentary successions forming several sections of PQG and VSC in the Portuguese sector of the IPB, aiming at:

i. The distinction of fundamental constituents of these rocks and their prevalent sources;

ii. The assessment of critical factors in sedimentary environment analysis and/or subsequent geological evolution; and

iii. The identification of potential useful guides/criteria to the conceptual design of new exploration surveys in the IPB, seeking for concealed and high-grade massive sulphide accumulations.

To this end, an extensive sampling plan was performed in four key sectors (**Figure 1.1**) labelled as: Lousal (including the Sesmarias prospect), Aljustrel (including the Gavião and Monte das Mesas prospects), Albernoa (including Píncaros, Ervidel-Roxo and Entradas sub-sectors), and Neves Corvo (including the Montinho prospect). The geological context of each group of samples was characterized as much detailed as possible, allowing to document the lateral and vertical facies variations, as well as the change of attributes when close to massive sulphide orebodies. These macroscopic features were further complemented with petrography examination of all samples and detailed mineralogical inspection in representative sets of samples. The latter sets were also subjected to whole-rock multi-elemental geochemistry analysis and to a multi-system (Sr, Nd and Pb) isotope study.

Details on the sampled geological settings and on the analytical methods used will be reported in the following sections, preparing the grounds for results presentation and subsequent interpretation. Accordingly:

Section 2 will provide the information needed to characterize the geological context of each sample set;

Section 3 will portray the main geochemical tools used and the reasoning behind their combined application, besides disclosing relevant features on the analytical methods and sample preparation;

Section 4 will summarize the most relevant findings discussed in the three peer-reviewed papers, two of them already published, and whose integral versions are in Appendix 1;

Section 5 will deliver a concise report on the available mineral chemistry data and their interpretation, with particular emphasis on phyllosilicates which, along with other mineral phases, can be used as vectors to ore-forming systems;

Section 6 will sum up the pertinent results and their integrative interpretation; and

Section 7 will disclose future research lines to address unanswered topics, as well as the main challenges posed to geochemical exploration surveys in the IPB.

SECTION 2

2. Geological Appraisal and Sampling Program

2.1. Sampling overview

The first sampling survey was performed between 2013 and 2016 under the scope of a technical-scientific partnership between FFCUL and EPOS, S.A. One hundred and thirty-three samples of fine-grained metasediments were selected from various PQG and VSC sections in the Albernoa sector. Results from this sampling survey provided the main guidelines for the PhD research project and for the subsequent follow-ups. Indeed, the re-logging of selected drillings performed in the Albernoa sector (some of them historical) evidenced several features in the intersected metasedimentary successions that were poorly depicted or not described at all so far in published reports on the IPB. Moreover, preliminary geochemical results for these samples outlined enrichment patterns in some chemical elements and multi-elemental ratios that were interpreted as consequence of processes related to seafloor metasomatism and exhalative-hydrothermal activity (Luz *et al.*, 2015, 2017, 2018).

Samples from the first campaign were collected mainly in the northern part of the IPB Portuguese segment, namely across the Albernoa sector (Luz *et al.*, 2019), complemented with a few samples picked in three historical drillings, intended to inspect the SE extension of the Feitais structure (Aljustrel). The focus of the second sampling survey was on the active mining centres in the Portuguese IPB segment (Aljustrel and Neves Corvo), allowing to evaluate which geochemical fingerprints indicative of ore-forming processes could be effectively identified; this innovative geochemical data has the potential to support the definition of additional mineral exploration guides, as discussed in forthcoming sections. In these two mining centres, three main sampling criteria were considered: (i) mineralized or non-mineralized; (ii) lithostratigraphic position (PQG or *lower, middle* and *upper* VSC) and (iii) spatial representativeness, considering that each mining centre has more than one sulphide orebody and the corresponding footwall/hanging-wall. The third sampling survey included some mineral exploration prospects in other sectors of the IPB Portuguese segment (Gavião and Monte das Mesas), as well as an old mining centre (Lousal) and the recent discovery of a hidden massive sulphide mass (Sesmarias). In all these locations, different metasedimentary facies were considered, trying to cover all the macroscopically detectable variations, as well as the representativeness of different geological formations described in the literature. The gathered samples totalized 292 (100 from outcrops and underground mining works, and 192 from drill-cores), distributed across the four sectors above presented: Lousal (including the Sesmarias

prospect), Aljustrel (including the Gavião and Monte das Mesas prospects), Albernoa (including Píncaros, Ervidel-Roxo and Entradas subsectors) and Rosário-Neves Corvo (including the Montinho prospect). In the interest of time and logistic issues, other relevant sectors of the IPB Portuguese segment (such as Odemira, Cercal and Alcoutim) were not examined, but some additional data was compiled form literature, whenever available, to build a more complete regional database. **Figure 2.1** illustrates the spatial distribution of the sampling survey that supports the present work, and **Table 2-1** provides a general information on the number of samples collected in each sector. Supplementary information on sampling, including the coordinates of each sampling site, is disclosed in Appendix 2.

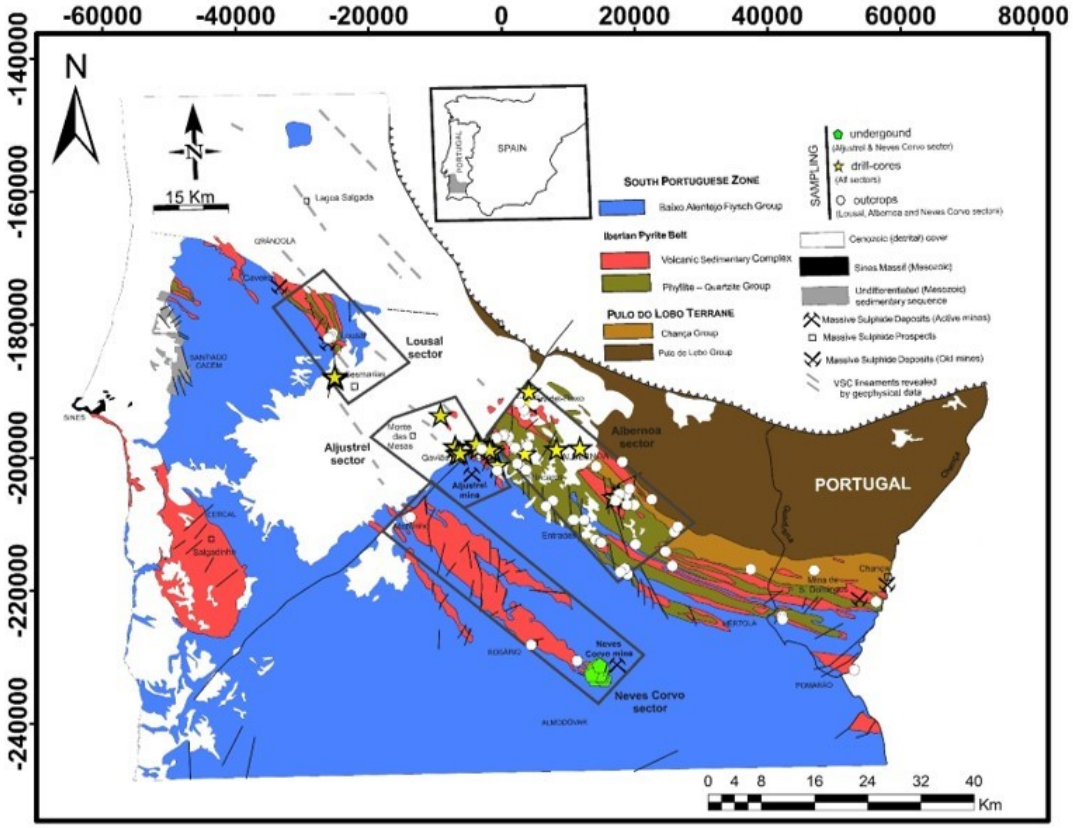

Figure 2.1 - Synthetic geological map of the Portuguese segment of IPB, illustrating the location of the main massive sulphide deposits (old and active mines), as well as the relevant prospects. The four sectors considered in this study are delimited by black polygons. Modified after Oliveira (1990), Barriga et al., (1997), Leistel et al., 1998, Carvalho et al., (1999) and Matos et al. (2000, 2006). A general distribution of the sampling survey is also presented. More details on each sample are shown in the Appendix 3.

Table 2-1 - Sectors/sub-sectors and number of samples picked in various PQG and VSC sections forming the the IPB Portuguese segment. Reference samples used for comparison purposes (Gafo, Ribeira de Limas, Santa Iria Formations, besides PQG and VSC successions) were collected in outcrops across the IPB Portuguese segment where previous studies provided critical information on age constraints.

Sector	*Sub-Sector*	*N (nr. of samples)*
Albernoa	*Albernoa*	*133*
Lousal	*Lousal old mine*	*4*
	Sesmarias	*18*
Aljustrel	*Aljustrel mine area*	*49*
	Gavião	*19*
	Monte das Mesas	*14*
Neves Corvo	*Neves Corvo mine area*	*42*
	Montinho/Algaré (Rosário Anticline)	*5*
Reference samples	*Mértola region*	*8*

2.2. Main facies and fundamental features

Previous detailed studies led to the identification of different types of metapelites in the Portuguese segment of the IPB (*e.g.* Schermerhorn, 1971; Oliveira *et al.,* 2013; Jorge, 2009). Macroscopic criteria were defined to characterize metasedimentary facies and/or successions in distinct sections of PQG and VSC. At first, these criteria considered only macroscopic observations but after detailed petrography they were readjusted (**Figure 2.2**). The re-logging of all the selected drillings was performed according to these criteria. The stratigraphic correlations are presented in section 2.4, compiling the information from all the lateral and vertical variations observed in the examined metasedimentary successions. Nine metasedimentary lithotypes were identified (MS1 to MS9) and separated from volcanic rocks (metavolcaniclastic – MV1, coherent felsic to intermediate composition – MV2 and mafic composition – MV3), but latter were not studied in detail during this PhD program. The main characteristics of the metasedimentary lithotypes are as follows:

i. **MS1 –** Reddish metapelite, displaying strong weathering effects;

ii. **MS2 –** Green metapelite;

MS2a – Green metapelite with significant siliceous component;

MS2b – Rhythmic succession of green metapelites (sericite-rich) including thin intercalations of levels with variable abundance of accessory mineral phases;

MS2c – Green metapelite with possible (minor and distal) volcanic contribution; in the Aljustrel sector dark-green to black matrix resulting from the deposition of volcanic ash is common;

iii. **MS3 –** Dark coloured metapelite intercalations or inter-fingerings in a brighter coloured metapelite bearing a fine-grained psammitic component;

iv. **MS4 –** Metapelite similar to MS3, although presenting a textural rhythmic succession;

v. **MS5 –** Grey metapelite, texturally homogeneous;

vi. **MS6 –** Dark coloured to black metapelite, sometimes comprising abundant graphite-like phases, but texturally homogeneous;

vii. **MS7 –** Rhythmic sequence (~cm) of black metapelites and fine-grained quartzites;

viii. **MS8 –** Metasediment with a dominant (very) fine-grained psammitic component, further classified as a meta-siltstone.

MS8a – Meta-quartzwacke;

MS8b – Fine-grained, impure quartzite;

ix. **MS9 –** Coloured metapelites, from violet-green to green (inter-fingered and/or intercalated), usually coexisting and showing transitional gradations;

MS9a – Interfingered, purple and greenish metapelites, often recording features ascribable to a possible distal volcanic contribution;

MS9b – Purple metapelite ("borra-de-vinho");

x. **MV1 –** Metavolcaniclastic rock *s.l.,* mainly felsic to intermediate composition

xi. **MV2** – Felsic to intermediate metavolcanic rocks *s.l.*

xii. **MV3** – Mafic metavolcanics rocks *s.l.*

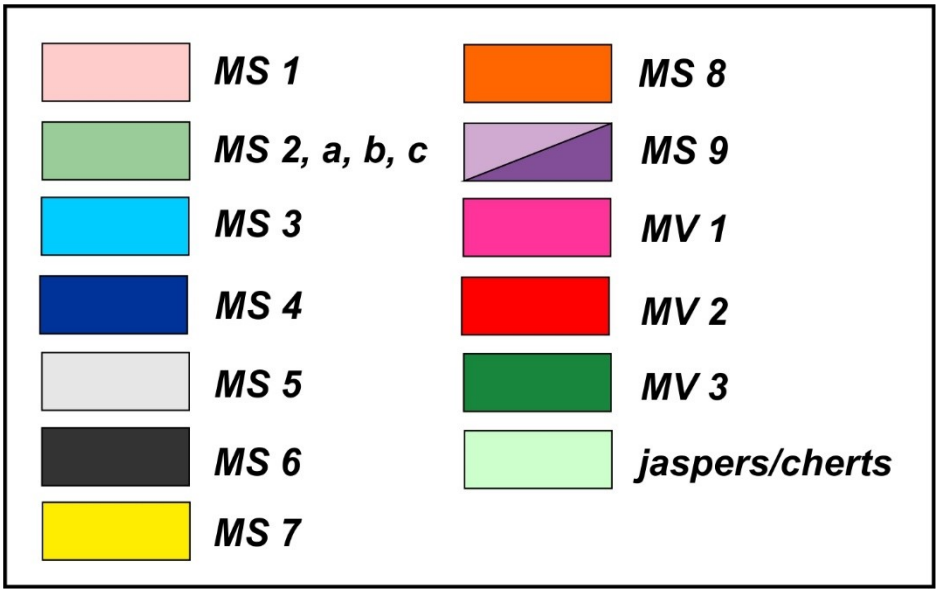

Figure 2.2 - Colour code for the main metasedimentary lithotypes (and metavolcanics) recognized in different PQG and VSC sections of the IPB Portuguese segment

The main features displayed by metasedimentary successions observed in each sector, as well as the sampled drillings/outcrops and the corresponding geological settings, will be presented in the next sub-section.

Figure 2.3 and **Figure 2.4** illustrate the main macroscopic features of each metasedimentary facies.

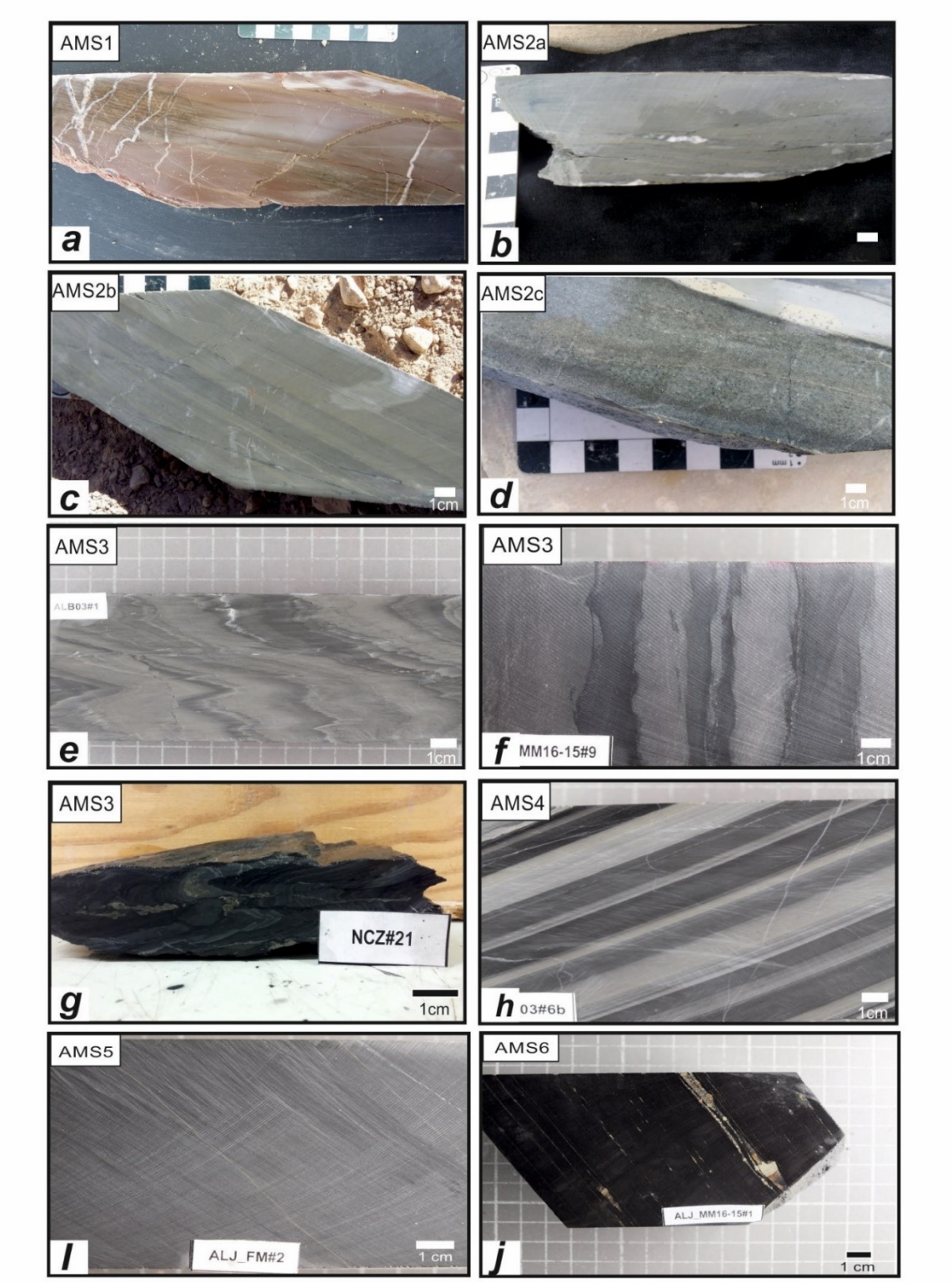

Figure 2.3 - Representative samples of different metapelite facies intersected in various sections of the Portuguese segment of IPB: **(a)** Reddish, weathered metapelite (ALB02– 21.00 m); **(b)** Green metapelite (abundant sericite), with significant siliceous component (ALB03 – 70.30 m; **(c)** Intercalated/inter-fingered bands in green metapelites (sericite enriched) possibly determined by differences in relative abundance of various accessory mineral phases (ALB03 – 245.45 m); **(d)** Green metapelite with possible volcanic contribution (ALB03 - 303.00m); **(e)**, **(f)** and **(g)** Intercalating/inter-fingering of dark coloured and lighter metapelites (ALB03 – 130 m; MM16-15 – 340 m; NCZ – Zambujal footwall);**(h)** Rhythmic succession of dark coloured and lighter metapelite enriched in a sandy-derived component (ALB03 – 213.80 m);**(i)** Grey metapelite (Alj_FM – 98.59 m) *note that the sample show cutting saw marks; **(j)** Dark coloured to black metapelite, sometimes comprising graphite-like phases, and often pyrite-rich. (Alj_MM16-15 - 237.00 m).

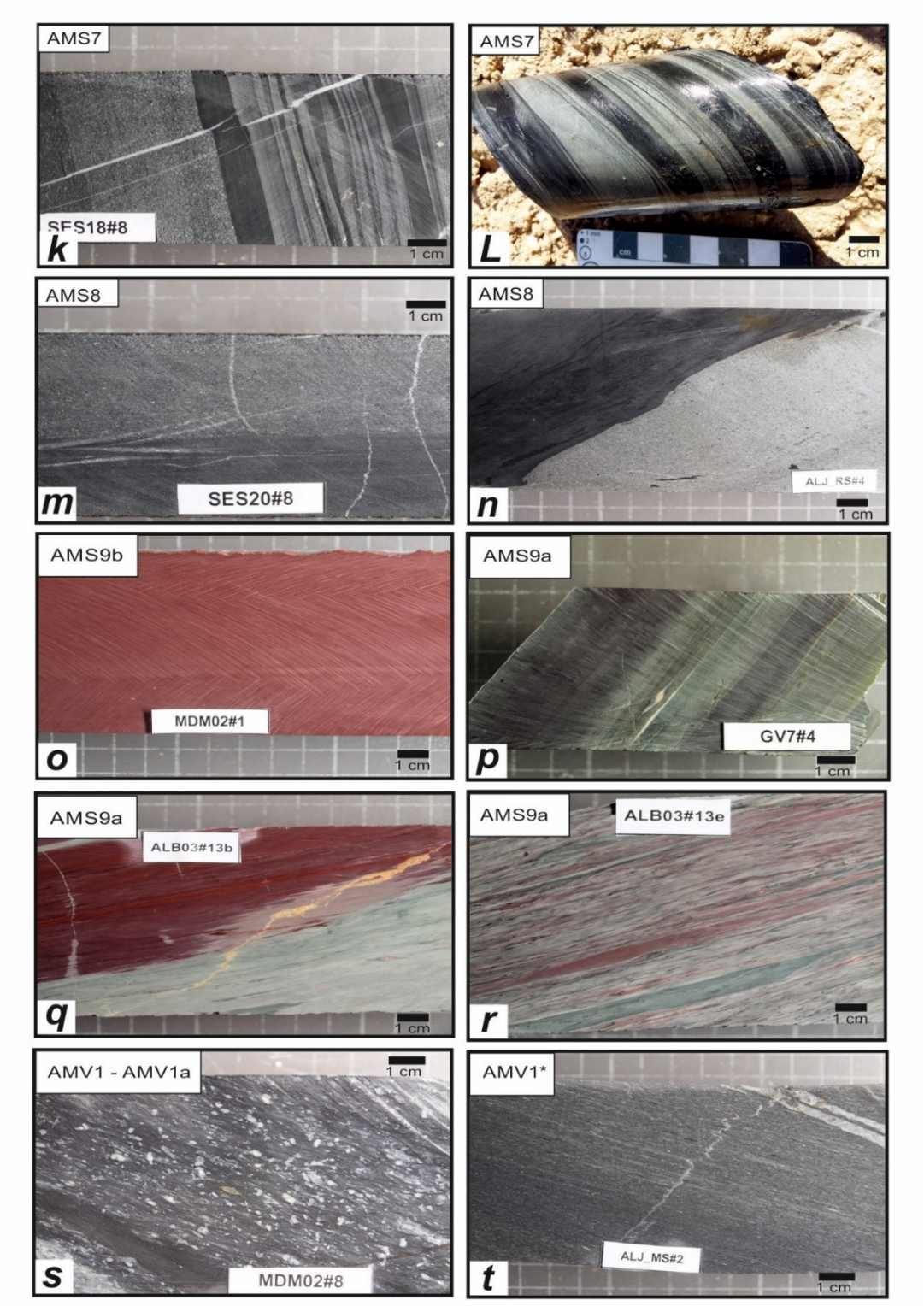

Figure 2.4 - Representative samples of different metapelite facies intersected in various PQG and VSC sections of the IPB Portuguese segment: **(k)** and **(L)** Rhythmic succession of black metapelites and fine-grained quartzites (SES18 – 483.26 m; ALB03 - 490.60m); **(m)** Metasediment with a dominant fine-grained psammitic component, meta-quarzwacke (SES20 – 406.20 m) and **(n)** impure quartzite (Alj_RS – 449.45m); **(o)** Purple metapelite ("xisto borra-de-vinho) (MDM02 – 85.50 m); **(p)**, **(q)** and **(r)** Coloured metapelites, from violet-green to green, often recording a possible distal volcanic contribution (GV7 – 797.00 m; ALB03 – 299.40 m; ALB03 – 315.90 m): **(s)** Metavolcaniclastic rockwith black matrix and mineraloclasts of quartz and feldspar (MDM02 – 361.70 m); **(t)** Metapelite with a volcanic-derived component – fine matrix (but resolvable to naked eye), commonly dark to black possibly resulting from the deposition of volcanic ash. (Alj_MS – 68 m).

2.3. Sectors

2.3.1. Albernoa

The Albernoa sector is located along the northern sector of the Portuguese segment of IPB and presents numerous outcrops of the two main lithostratigraphic units selected for the present study, PQG and VSC. The lowermost metasedimentary succession, ascribed to PQG, includes black metapelites, metasiltstones and quartzites. This succession displays several distinguishable features, namely an important sandy-derived component, prevalent whenever quartzite lenses are present (especially in the SE of the Albernoa sector), but relevant all over the succession, as recorded by the systematic presence of metasiltstones. The PQG section preserves miospore assemblages of the VH biozone (Upper Famennian; Pereira *et al.*, 2007, 2008). At the top of this section, minor metapelites with volcanic-derived components and metavolcaniclastic rocks records a gradual transition toward the stratigraphically overlying VSC (Luz *et al.*, 2019). This latter lithostratigraphic unit includes mostly rhyodacitic to rhyolitic rocks dated of ≈357 to 355 Ma (U-Pb, LA-ICP-MS in zircon; Rosa *et al.*, 2004), developing prevalent hyaloclastite piles that involve coherent facies (Rosa *et al.*, 2004; Codeço, 2015; Codeço *et al.*, 2018). The volcanic succession progresses laterally and vertically to metasedimentary sequences comprising dark-grey to black metapelites, purple-green metapelites, fine-grained metavolcanocclastic units (locally with fiamme), siliceous metapelites and minor metapelites with volcanic-derived component (Luz *et al.*, 2019; 2020). Dark-grey to black metapelites included in these successions yielded miospore assemblages from Pu (Upper Tournaisian-Lower Visean) to NL biozones (Visean; Pereira *et al.*, 2007, 2008). The Freixial Formation, assigned to the upper part of this lithostratigraphic column, is characterized by a flysch succession with carbonates (Faria *et al.*, 2015).

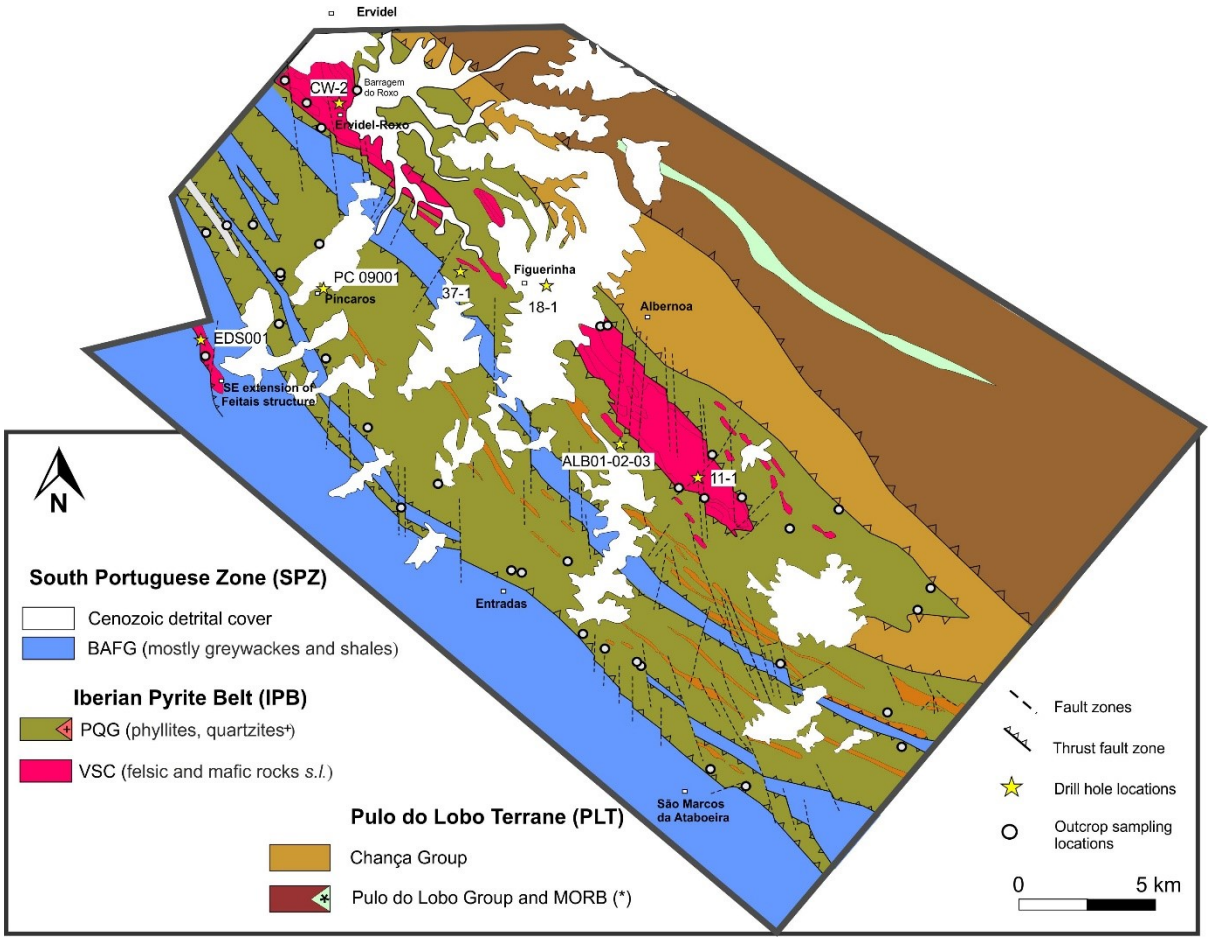

Figure 2.5 - Simplified geological map of the Albernoa area showing the location of sampled drill-holes and outcrops. Adapted from the Geological Map of Portugal at 1: 200.000 (Oliveira, 1990) and unpublished technical reports after detailed mapping at 1: 10.000 (Mateus et al., 2014, 2015 a,b).

Outcrop samples

Fifty-four samples of fine-grained siliciclastic rocks and metapelites with a volcanic-derived component were collected, representing the two main stratigraphic units (PQG and VSC). Their spatial position is shown in **Figure 2.5**.

Eight reference samples for comparison purposes were collected, considering the outcrop descriptions and age constraints reported in Pereira *et al.* (2008). These samples represent well-defined horizons of PQG and VSC, besides some other stratigraphic levels laterally equivalent to PQG or beneath it, as follows:

i. Santa Iria Formation, at the Santa Iria village;

ii. Ribeira de Limas Formation, at the Serpa-Mina de São Domingos road;

iii. Gafo Formation, near the Vuelta Falsa mine (Chança river);

iv. Gafo Formation, at the Corte de Sines Cemetery;

v. Gafo Formation, at the Mértola-Corte de Gafo road;

vi. PQG, at the São Domingos mine;

vii. PQG, Guadiana river (to the north of Mértola);

viii. VSC (lower level), at the Pomarão village.

Historical drill-holes

The reassessment of historical drillings was performed in 2014 in collaboration with Marta Codeço (EPOS-FCUL contract; Mateus *et al.*, 2014, 2015 a, b). The information collected was harmonized on a later stage (2016-2020), using criteria presented in section 2.2.

EDS0001

The Esteval da Serra drilling (EDS0001) was performed by *Portuglobal/Exmin* in 2000 at coordinates (ETRS89) $m = -256.557$ and $p = -201023.145$. It was designed with 225º azimuth and 75º dip.

The first 260 m are characterized by intercalations of meta-greywackes (with calcite occasionally sealing interstitial spaces in the rock matrix) and predominant black metapelites, ascribed to the Mértola Formation (BAFG). The lithological contacts are sharp (dipping 50-65º in relation to long core axis) and frequently transposed by fault zones. Locally, the development of quartz or calcite veinlets is noteworthy. At ca. 301 m, a reverse fault zone separates this unit from a VSC section.

The intersected VSC (*upper unit*, known as the Paraíso Formation) is dominated by metapelites often including a volcanic-derived component. Moreover, the drilling intersected dark-grey to black metapelites with frequent pyrite dissemination, besides purple metapelites and metajaspers. Metapelites with a volcanic-derived component preserve evidence of significant, although irregular, hydrothermal alteration (silicification ± chloritization ± sericitization ± hematitization). Volcanic rocks (mostly volcaniclastic) prevail after 500 m of drilling. The VSC section is affected by various fault zones, which are indicated by significant crushing and brecciation. (**Figure 2.6**) displays the interpretative geological cross-section for EDS0001 drill-hole using the collected information.

CW-2

The CW-2 drilling was designed by the "Consórcio Faixa Piritosa" Minaport-EDM and performed in 1993 at coordinates (ETRS89) $m = 4228.317$ and $p = -191707.105$ (Monte do

Chaparral W, Ervidel). The drilling, with 225º azimuth and 60º dip, was completed to check a gravimetric anomaly running along the NW-SE direction.

A monotonous VSC succession was intersected, comprising felsic metavolcaniclastic rocks and metapelites with a volcanic-derived component; locally, intermediate to mafic metavolcanics rocks occur, as well as green metapelites. This succession is crossed by three main fault zones outlined by intense crushing. The fault-related hydrothermal activity is expressed by late (polyphasic) quartz infillings coupled with accessory amounts of sulphides.

Metavolcaniclastic rocks show quartz and feldspar mineraloclasts scattered in a green coloured matrix (chlorite ± sericite ± epidote) which is interpreted as a result of "regional alteration". From ca. 107 to 126 m, an intersection of metajaspers display late milky-quartz veins with chlorite and pyrolusite. At ca. 486-490 m, a fault zone separates the above, volcanic-dominant, succession from a metasedimentary series. This series comprises mainly grey to black metapelites (often in intercalations with siliceous metapelites) and metajaspers. The entire VSC succession intersected by the CW-2 drilling displays abundant generations of milky quartz veins. Early quartz infillings are frequently folded, and their local reopening marked by the deposition of Fe ± Mn oxides or pyrite, chalcopyrite and pyrrothite. The late quartz veins comprise accessory amounts of chlorite ± sericite ± epidote ± carbonate. **Figure 2.7** displays the interpretative geological section for CW-2 drill-hole using the collected information.

37-1

The 37-1 drilling was designed by Riofinex and performed in 1983 at coordinates (ETRS89) $m = 8303.401$ and $p = -198699.04$. The drilling, with ca. 195º azimuth and ca. 30º dip, was performed to test a gravimetric anomaly in that area.

The drilling intersected a monotonous VSC metasedimentary succession mainly composed by dark-grey to black metapelites with frequent meta-siltstones (to fine-grained quartzite) intercalations that decrease in abundance towards the end of the drill-hole. Occasionally, green metapelites develop inter-fingers with fine-grained and impure quartzites. Pyrite is frequent, along with millimetric-quartz veinlets, in metapelites forming the lowermost levels of the metasedimentary succession. Also common are veinlet networks (quartz ± carbonate ± chlorite ± pyrite), locally affecting syn-sedimentar slumps. Some few sections show highly brecciated textures, generally fault-related, preserving effects of intense hydrothermal alteration. **Figure 2.8** displays interpretative geological section for 37-1 drill-hole using the collected information.

18-1

The geophysical (gravimetric and electromagnetic) anomaly nº18, located near the Figueirinha railway station, was checked by Riofinex in 1983 by means of a drilling at coordinates m= 11823.394 and p = -1984880.996, with 230º azimuth and 45º dip.

The first 26 m intersected the Cenozoic detrital cover. The subsequent succession can be grouped into three sections according to their main macroscopic features. The first section (up to 77.60 m) comprises intercalations of metapelites with a volcanic-derived component and purple metapelites (locally silicified) with abundant pyrite in S_0 and S_1 plans. Gradually and vertically, the purple metapelites are replaced by siliceous metasediments and, subsequently, by black metapelites. A reverse fault zone separates the first section from the second one, which is mostly composed of siliceous metapelites (sometimes including fine levels of chemogenic siliceous rocks), black metapelites, metavolcaniclastic rocks and felsic to intermediate metavolcanic rocks. Immediately before the second reverse fault zone, some levels of fine-grained quartzites and meta-siltstones, both presenting effects of hematization, were observed. The third section comprises mainly intermediate to mafic metavolcanic rocks with few intercalations of dark-grey to black metapelites usually pyrite-rich. Frequent pre-deformation veins/veinlets (quartz + carbonate ± chlorite ± sulphide ± oxides) were also identified in metavolcanic and metasedimentary rocks. Less abundant are the late-fractures filled with quartz ± carbonate ± sericite ± chlorite ± sulphide ± Fe-Mn oxides. Evidence of hydrothermal alteration is mostly confined to rock domains affected by intense, fault-controlled, brecciation Some metasedimentary levels intersected by the 18-1 drilling preserve a radiolaria association. A team from University of Lisbon (Sofia Pereira) and Russian colleagues (Ed. Amon and Marina Afanasieva) identified a junior population of *Bientactinosphaera? Cf. vetusta (Hinde*) and *Entactinia? Cf. herculean (Foreman)* that assign these rocks to the Upper Devonian – Lower Carboniferous transition. **Figure 2.9** displays the interpretative geological section for 18-1 drill-hole using the collected information.

11-1

The vertical drilling 11-1 was design by Riofinex at coordinates (ETRS89) m = 17603.483 and *p = -205798.913*. A thick metavolcaniclastic succession (up to 312.60 m) was intersected. Metavolcanic rocks present highly contrasting textures due to the heterogeneous progression of hydrothermal alteration (chloritization, sericitization, epidotization and silicification), mostly depending on the permeability distribution and local compositional constrasts. The textures could be characterized considering: (i) the dimension, nature and abundance of

fenocrystals (generally quartz and feldspar); (ii) the clast dimension and its composition when in presence of in-situ developed breccias; (iii) the mineralogical composition of the matrix composition and its granularity; and (iv) the relative abundance of amigdales and their mineral fillings. These metavolcanic rocks, usually showing late veinlets filled with quartz + chlorite (and scarce sulphides), are comparable (and spatially nearby) to those dated by Rosa *et al.*, 2009b (357.2 ± 2 Ma). The basal section of the drilling intersects a series of dark-grey to black metapelites that occasionally show quartz (± chlorite) veinlets with Fe-oxides. These black metapelites preserve miospore assemblages from the VCo biozone (Pereira *et al.*, 2008) which allowed ascribe this section to the PQG. **Figure 2.10** displays the interpretative geological section for 18-1 drill-hole using the collected information.

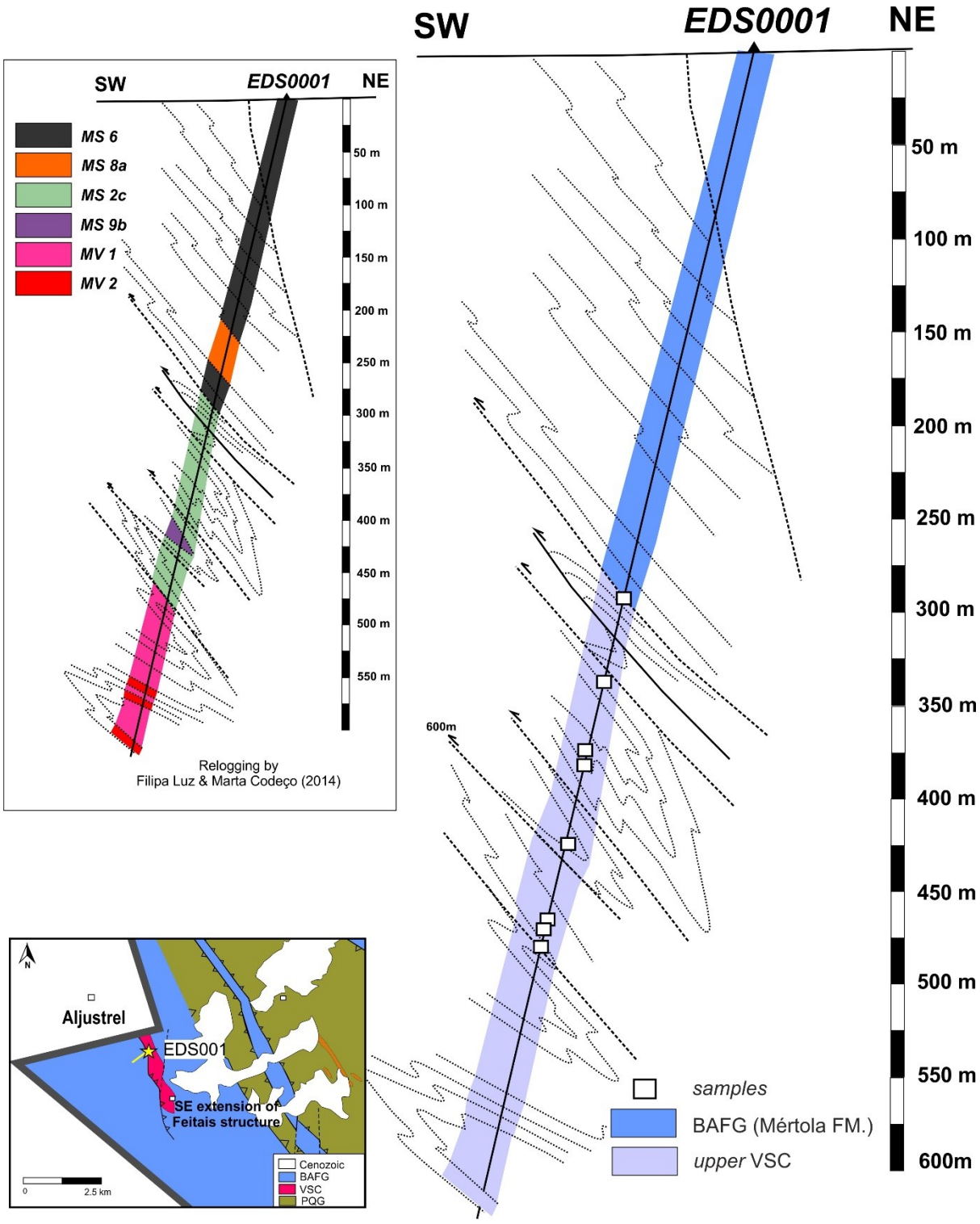

Figure 2.6 - Interpretative geological cross-section comprising the EDS0001 historical drill-hole, considering the observed polarity criteria and S_0-S_n angular relationships. Relative position and direction of the drilling in the geological map taken from *Figure 2.5*.

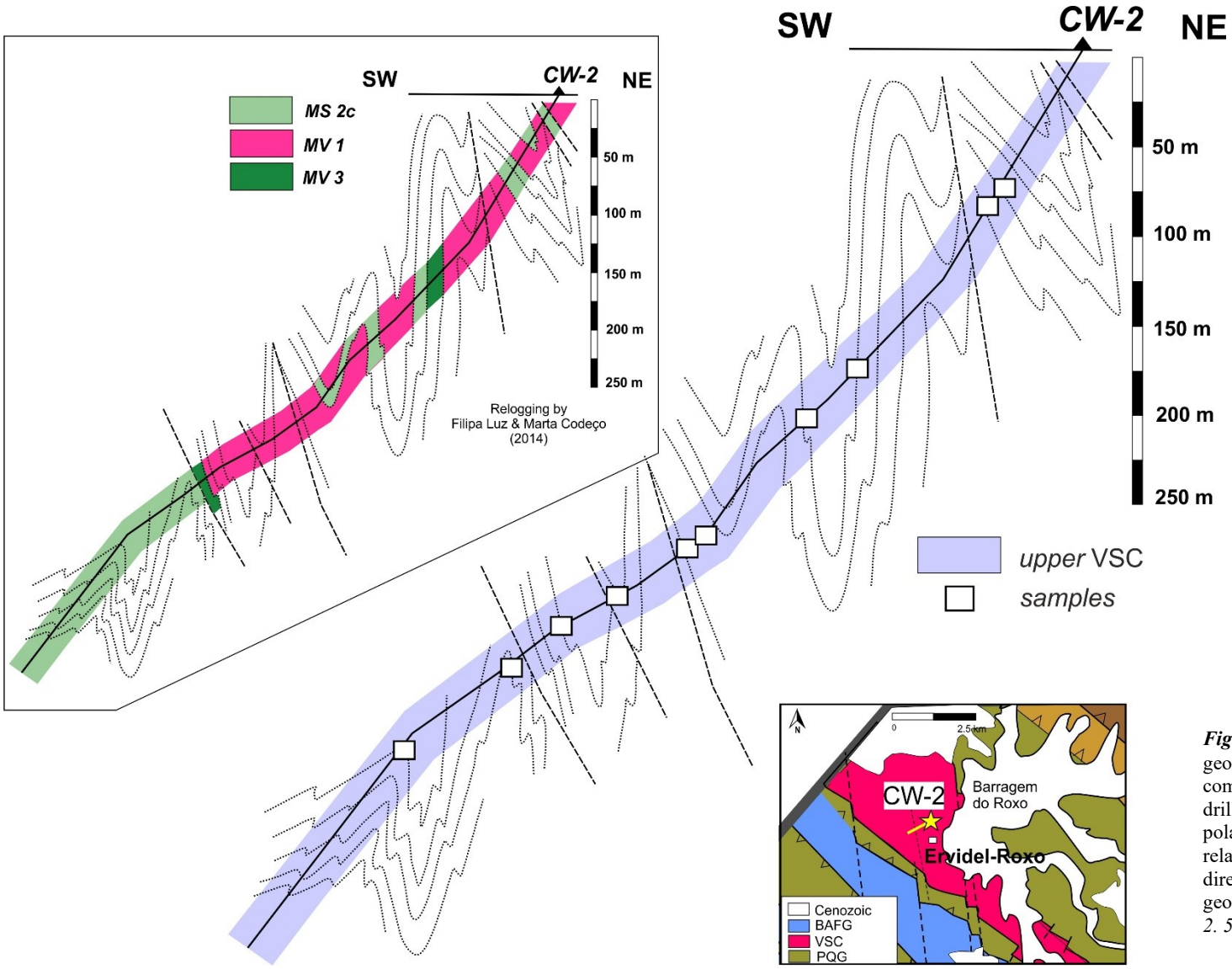

Figure 2.7 - Interpretative geological cross-section comprising the CW-2 historical drill-hole, considering the observed polarity criteria and S_0-S_n angular relationships. Relative position and direction of the drilling in the geological map taken from *Figure 2. 5.*

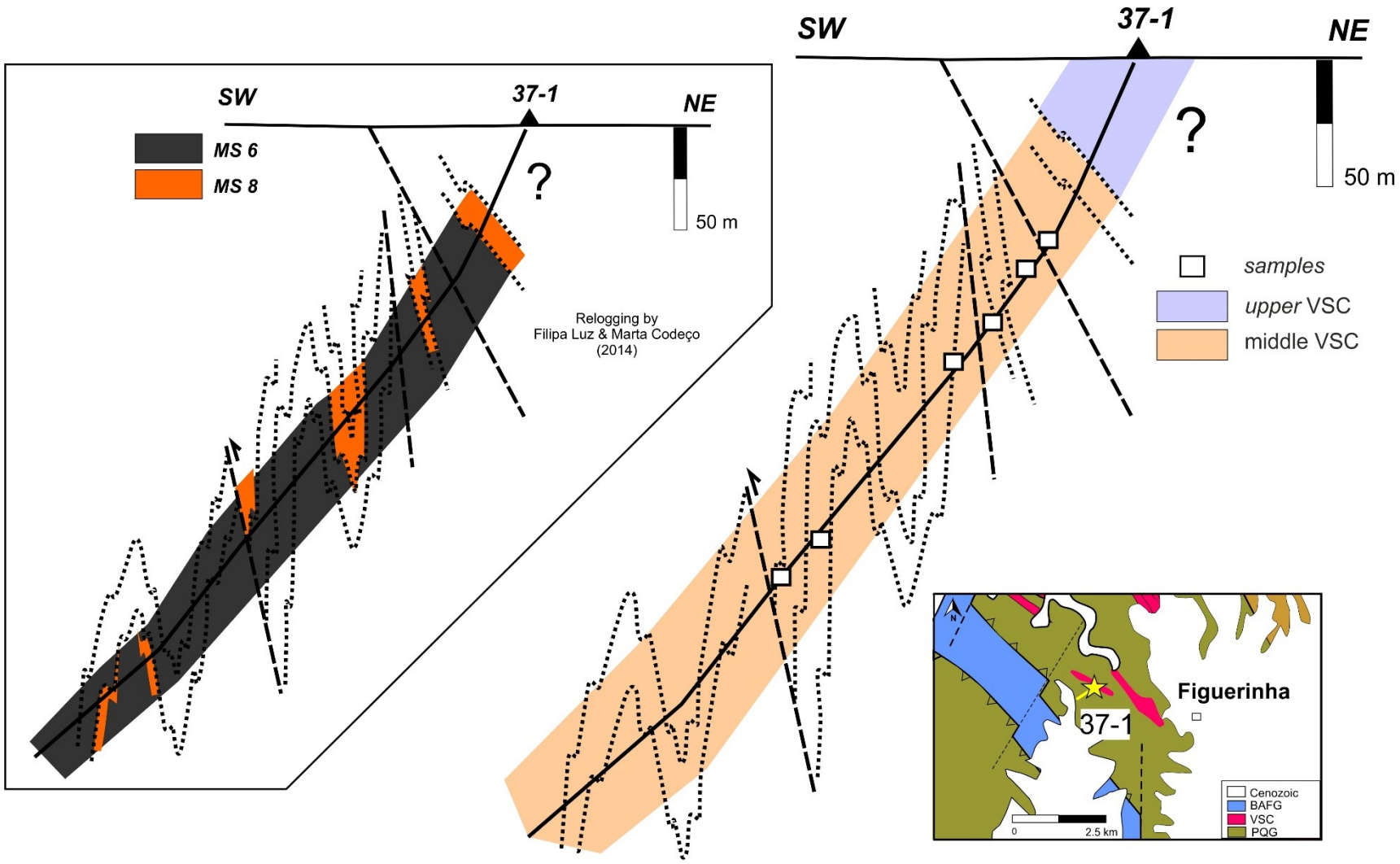

Figure 2.8 - Interpretative geological cross-section comprising the 37-1 historical drill-hole, considering the observed polarity criteria and S_0-S_n angular relationships. Relative position and direction of the drilling in the geological map taken from *Figure 2.5*.

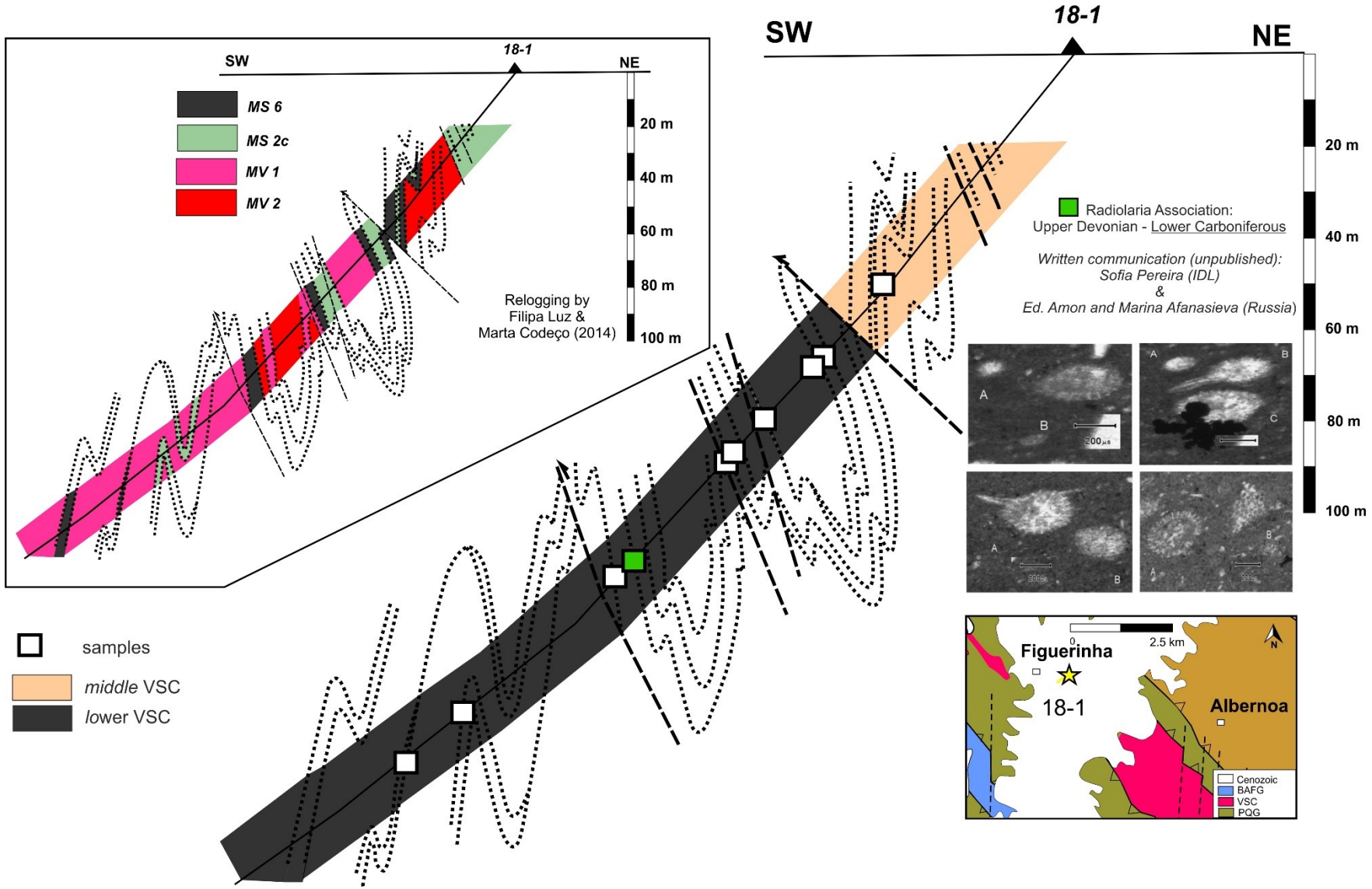

Figure 2.9 – Interpretative geological cross-section comprising the 18-1 historical drill-hole, considering the observed polarity criteria and S_0-S_n angular relationships. Relative position and direction of the drilling in the geological map taken from *Figure 2.5.*

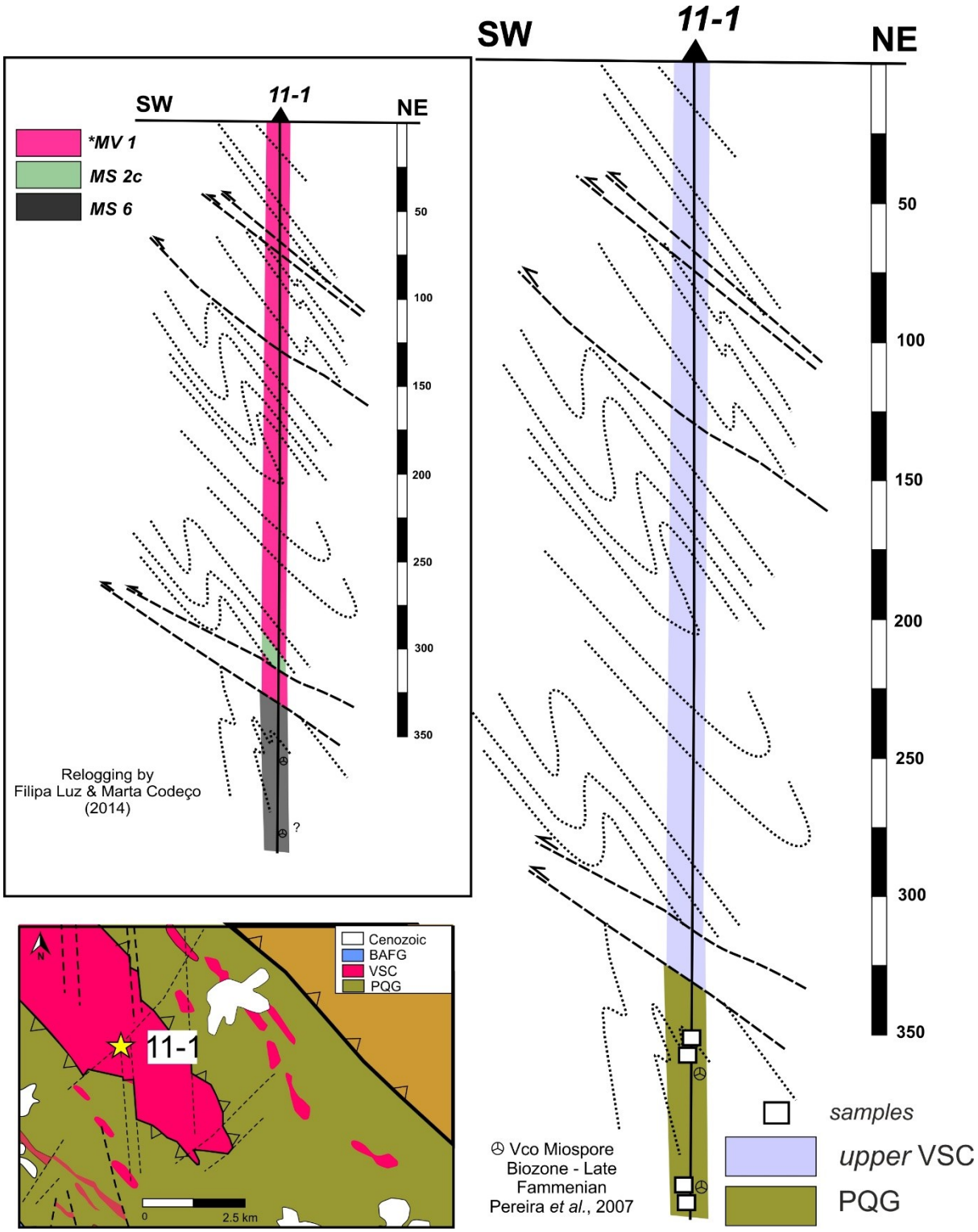

Figure 2.10 - Interpretative geological cross-section comprising the 11-1 historical drill-hole, considering the observed polarity criteria and S_0-S_n angular relationships. Relative position of the drilling in the geological map taken from *Figure 2.5*.

Recent exploration drills

Píncaros

The Píncaros drill-hole (PC09001) was performed by *AGC – Minas de Portugal, Unipessoal* in 2009 at coordinates (ETRS89) *m = 3556.55* and *p = -199306.418.* The conductive target identified in depth (≈1000 meters) along with a previously recognized gravimetric anomaly were the main reasons to design this drilling. According to the technical reports, the drilling achieved the real depth of 951.95 meters without cross the geophysical anomaly; and after an electromagnetic well-log, the target was abandoned.

Despite the unsuccessful result of the drilling from the mineral exploration point of view, it represents an important way to access and characterize the deeper PQG levels in this region. In general, the Píncaros re-logging revealed a monotonous sequence of dark coloured to black metapelites (locally enriched in graphitic-like material), with no evidence of volcanic-derived component. Frequently, these dark coloured metapelites show very fine-grained sandy-derived components (that may hinder the schistosity development) and/or are interbedded with metasiltstones levels. Recurrently, the deformation shows a syn-sedimentary character, possibly triggered by gravitational instabilities. The clay-rich/sandy-rich intercalations are observed from micro to macroscopic scales and could give rise, at deeper levels, to quartzite/meta-quarztwackes horizons (or lenses) of metric thicknesses, although continuously interbedded with thin metapelitic levels. The entire succession is affected by an intense, yet irregular, hydrothermal alteration traced by pervasive albitization, evident chemical corrosion of some primary minerals (e.g. quartz), chloritization and heterogeneous carbonation. Nonetheless, this hydrothermal alteration is not coeval of significant mineralizing process, as confirmed by the sporadic presence of pyrite + chalcopyrite ± cobaltite and other Ni-bearing sulphides/arsenates.

The detailed study of vertical facies variations demonstrated that the Píncaros drill-hole intersected several thrust fault zones, separating different stacked sections with distinct internal lithostratigraphic arrangements. These lithostratigraphic differences were later confirmed based on the basis of whole-rock geochemistry data, clearly splitting clearly section IV from the remaining others. **Figure 2.11** displays the interpretative geological section for PC09001 using the collected information.

ALB drill-holes (ALB01, ALB02 and ALB03)

The ALB01, ALB02 and ALB03 drill-holes were performed by Teixeira Duarte to check a geophysical anomaly recognized at ca. 600 m depth (Mateus *et al.*, 2015, 2015a). The ALB01 drilling was positioned at coordinates (ETRS89) *m* = 14779.878 and *p* = -204978.684, dipping ≈ 80º to the SW. After various technical problems, the ALB01 was abandoned and the ALB02 and ALB03 were executed a few meters away from the first location, dipping ca. 85º to the NE. The drillings intersected a VSC section up to ca. ≈500 meters. The first 50 meters includes a series of weathered reddish metapelites; the less weathered domains show relics of green coloured (sericite-rich) metapelites. Up to ≈200 m, the metasedimentary succession comprises intercalations and/or inter-fingerings of dark coloured metapelites with lighter coloured metapelites bearing a distinctive fine-grained sandy component. Frequently, the latter facies show gradual transitions to green metapelites (with or without minor distal volcanic contributions) that occasionally develop texturally rhythmic successions. Across this upper metasedimentary section, black metapelites were only intersected by ALB01.

From ca. 200 to 280 meters, the metasedimentary succession is similar to the upper section just referred, notwithstanding the higher abundance of fine intercalations of dark grey to black metapelites. A decimetric to metric intersection of fine-grained, impure quartzite was also recognized. A monotonous succession of black metapelites (often graphite-rich) was intersected between 280 and 310 meters.

From ca. 310 to 400 meters the drillings crossed a metasedimentary succession composed of black and coloured metapelite intercalations or inter-fingerings with lighter coloured metapelites bearing a fine-grained sandy component. The series of coloured metapelites starts at ca. 320 meters (from purple shale, purple-green to green), often including in their composition volcanic-derived components. From ≈340 to 350 meters, the intercalations of green metapelites and black metapelites are quite evident. Metavolcanic rocks were intersected between ≈ 400 and 450 meters, being mostly hosted in black and green metapelites with a volcanic-derived component, sometimes evolving to a (matrix-supported) metavolcaniclastic rock. The succession of metavolcanic rocks include lenses of different texture and composition. The basal monotonous metasedimentary succession, characterized by centimetric intercalations (often in a rhythmic succession) of black metapelites and fine-grained metasediments (from metasiltstones to quartzites), was interpreted as representing the PQG.

Several sections of the ALB01, ALB02 and ALB03 drillings show evidence of significant deformation. Recurrently, S_0 is transposed by S_1 and ranges between 0º (vertical) and ≈45º in

relation to long core axis. Fault zones are common, the most important of which intersected at: ≈80 m, ≈221 m, ≈283 m, ≈341 m and ≈492 m. These discontinuities were interpreted as thrust faults (with top to the S-SW).

Evidence of alteration and mineralization processes in the VSC succession is discrete until ca. 280 meters. In the uppermost metasedimentary succession, these processes are mostly recorded by epigenetic, fracture-controlled, hydrothermal mineral precipitates that include chlorite + carbonate ± albite + pyrite ± chalcopyrite. The development of these relatively late mineral infillings is independent of the host lithology, but their recurrence and intensity are typically higher in green (sericite-rich) metapelites displaying frequent quartz veinlets (locally deformed) with disseminated euhedral pyrite. The intensity of pre-deformation alteration (since the secondary mineral assemblages are affected by S_1) tends to increase in depth, being clearly higher between ≈399 to 417 meters and possibly reflecting a compositional contrast between the volcanogenic facies and hydrothermal fluids. The alteration intensity co-varies with the relative abundance of sulphides (pyrite ± chalcopyrite) disseminated in the matrix of different facies and/or filling dense fracture-networks. A significant part of these sulphides was formed before the Variscan deformation (and metamorphic recrystallization), as documented by the abundant deformed sulphide grains on foliation plans. **Figure 2.12** shows an interpretative geological section for the ALB01, ALB02 and ALB03 drillings.

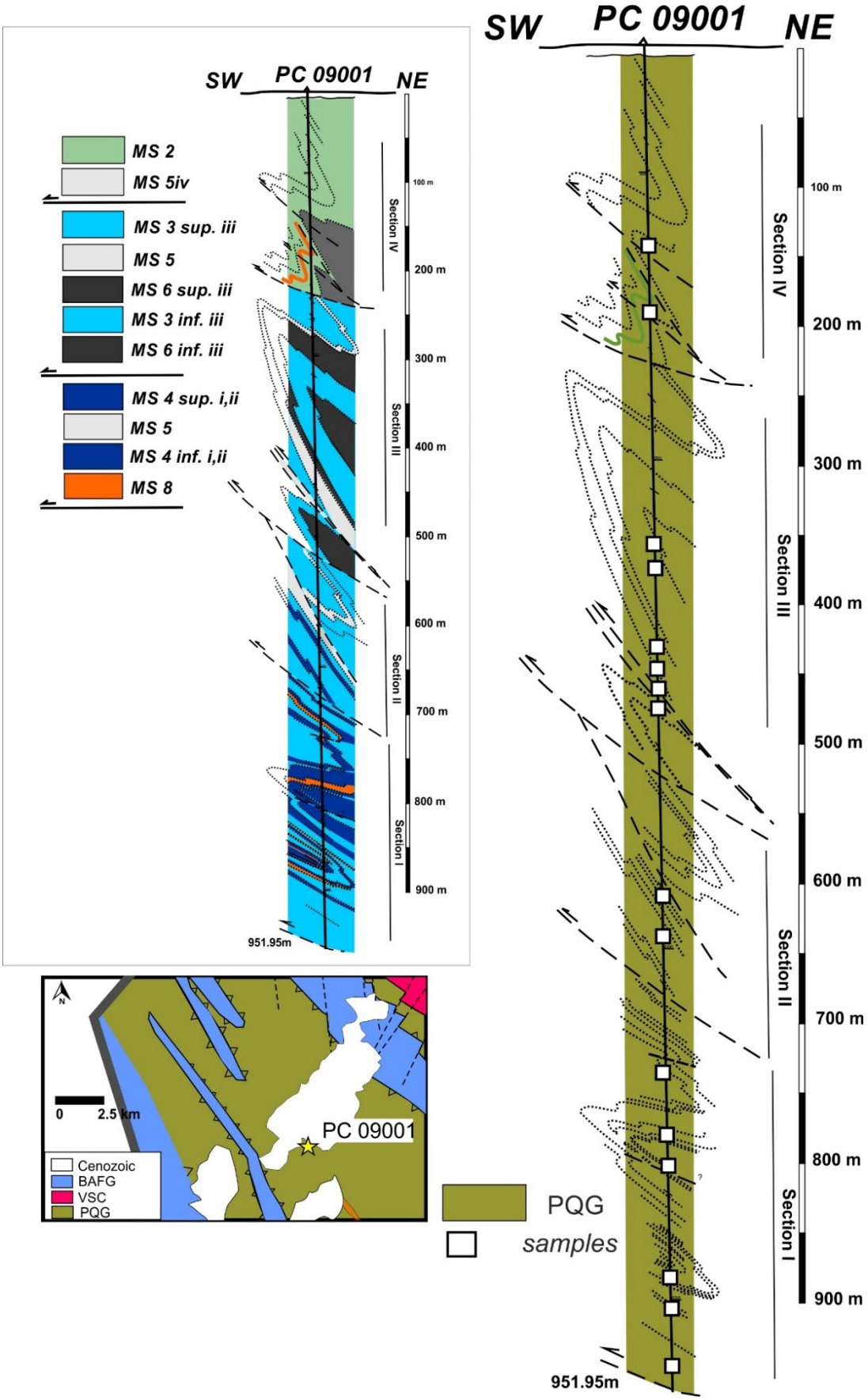

Figure 2.11 - Interpretative geological cross-section comprising the PC09001 exploration drill-hole, considering the observed polarity criteria and the S_0-S_n angular relationships. Relative position of the drilling in the geological map taken from *Figure 2.5*.

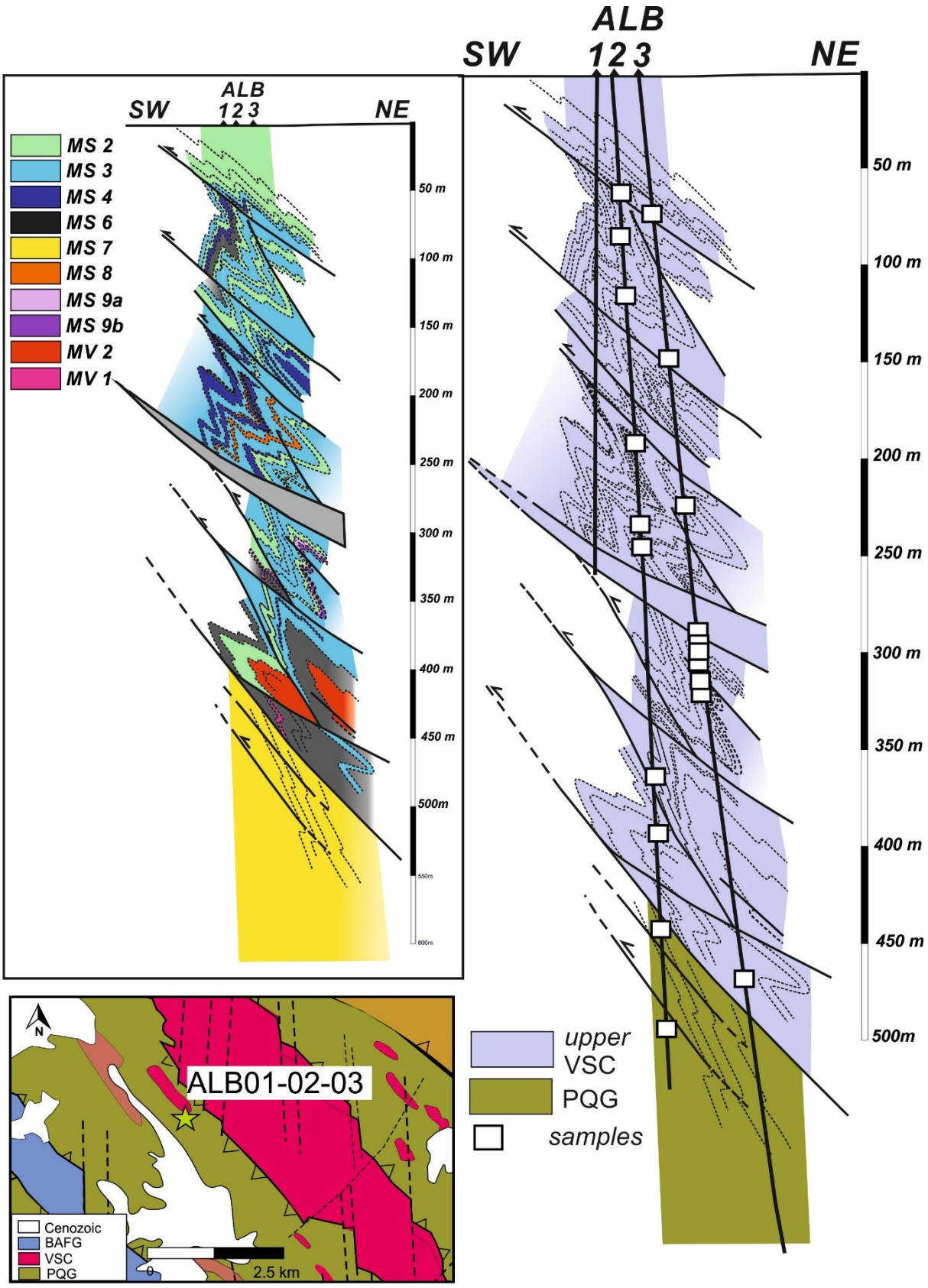

Figure 2.12 **-** Interpretative geological cross-section including information gathered for ALB01, ALB02 and ALB03 exploration drill-holes, considering the observed polarity and the S_0/S_n angular relationships. Relative position of drillings in the geological map taken from *Figure 2.5*.

2.3.2. Lousal and Sesmarias

At Lousal, the PQG comprises the Lower and Upper Corona metasedimentary units where Lem (Givetian) and LN (Strunian) miospore biozone assemblages were recognized, respectively (Oliveira *et al.*, 2006; Pereira *et al.*, 2007). These units include mainly metapelites with carbonaceous components, meta-siltstones and quartzites (*e.g.* Strauss, 1970: Strauss *et al.*, 1977; Fernandes, 2011; Relvas *et al.*, 2012). The *lower* VSC succession incorporates felsic metavolcanic rocks dated of 359 ± 3 Ma (U-Pb, LA-ICP-MS in zircon; Rosa *et al.*, 2009) intercalated with dark grey to black metapelites of Strunian age (Oliveira *et al.*, 2006) hosting the mineralization, besides minor intrusive metavolcanics. The *middle* VSC comprises an undifferentiated pile of metapelites (with some mafic metavolcanic rocks) that is overlain by siliceous and volcanic-derived metapelites forming the *upper* VSC section, which also includes some mafic to intermediate metavolcanic rocks. The BAFG flysch (Mértola Formation) on top of the VSC succession comprises grey to dark-grey metapelites preserving miospore assemblages of NL local biozone (corresponding to the NM biozone at the European scale), Visean in age (Pereira *et al.*, 2007). The lithostratigraphic column of the Sesmarias sub-sector is comparable to that of Lousal.

Lousal mine area

Sampling at the Lousal mine area was performed along the Ribeira de Corona (Ermidas do Sado), as illustrated in **Figure 2.13 a.** The outcrops near this stream allowed the observation of the lithostratigraphic units forming the Lousal/Azinheira de Barros succession. Recent works (e.g. Relvas *et al.*, 2012) specify some variations of the VSC metasedimentary succession in this area. From the lowermost to the uppermost levels, the VSC presents black metapelites that host the mineralization, felsic metavolcanics rocks, siliceous and black metapelites without evidence of mineralization and mafic metavolcanic rocks. One of the collected samples represents the PQG succession from the Upper Corona unit (Strunian), to the NW of the Lousal mine, whereas the other characterizes the *lower* VSC hosting the mineralization. Two additional samples of siliceous and non-mineralized black metapelites, typify the *upper* VSC succession.

Sesmarias

Sesmarias is located to the SSW of the Lousal mine (**Figure 2.13 b**). In 2014, AVRUPA Minerals reported an intersection of 57.85 meters of massive sulphides with a Cu grade ranging from 0.32 to 1.48 % and a Zn grade varying between 1.95 and 4.65 %, besides significant Au

and Ag abundances (0.45g/t and 25.1 g/t, respectively). Since then, fifty-four drillings were performed to delimitate and characterize this sulphide lense. According to the available press releases, ten drillings intersected the massive sulphides hosted in black metapelites and displaying various grades of Cu, Zn and Pb (AVRUPA Minerals, 2017). The company provided access to two selected drillings for sampling. Detailed re-logging focused on the metasedimentary succession, despite of a brief revision of the remaining rock types crossed. The SES20 and SES18 drillings were chosen because: (i) SES20 evidenced more than one massive sulphide intersection in black metapelites; and (ii) SES18 intersected a higher variety of metasediments without visible indicators of sulphide mineralization.

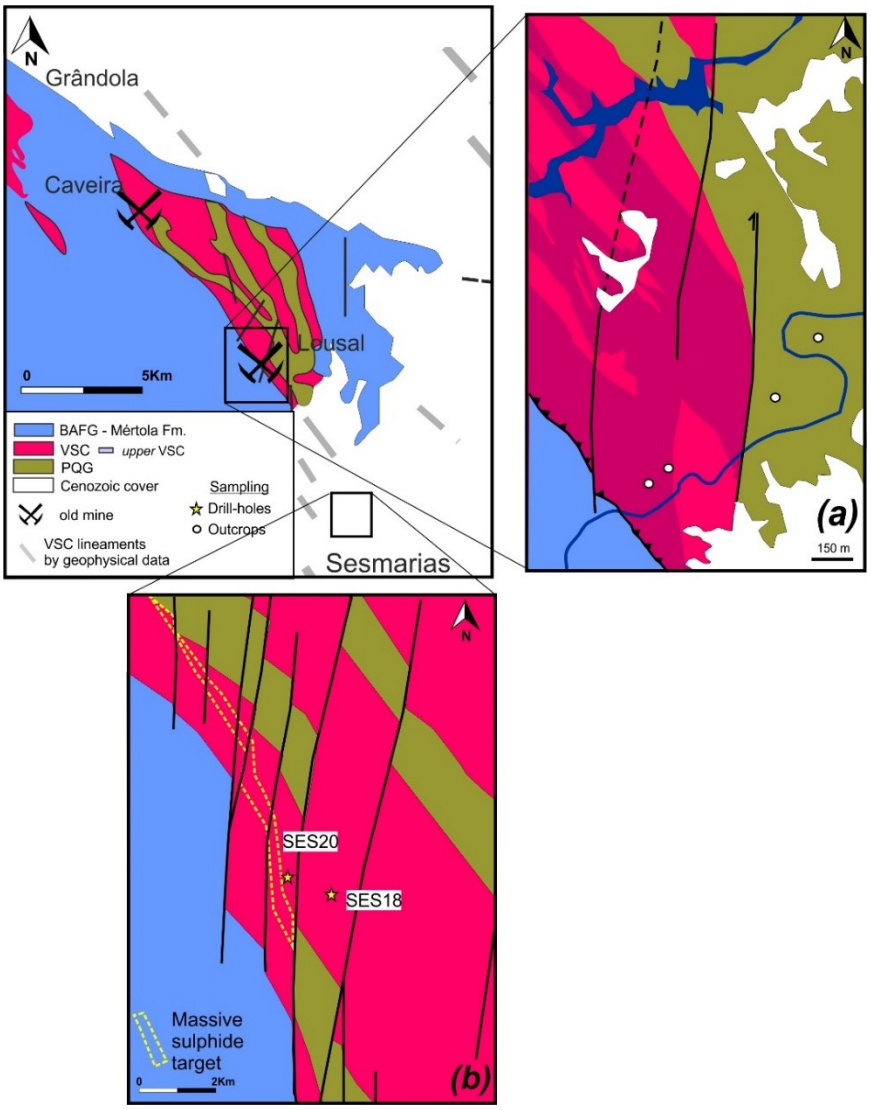

Figure 2.13 - Schematic geological map of Lousal are showing the location of sampled drill-holes and outcrops. Adapted from the Geological Map of Portugal at 1: 200.000 (Oliveira, 1992). **(a)** Main geological features of Lousal area (adapted from Relvas et al., 2012); **(b)** Geological interpretations of the sub-surface geology in the Sesmarias prospect (adapted from AVRUPA Minerals, 2017).

SES20

SES20 was designed by AVRUPA Minerals with 225' azimuth and 70' dip at coordinates (ETRS89) *m = -2566.249* and *p = -187755.89.* The first 121 meters are characterized by Cenozoic detrital cover on the top of Paleozoic basement, which is basically composed by a VSC succession down to 375 meters. The upper part of this VSC section (up to 219.05 m) includes green metapelites with (minor and distal) volcanic contribution overlying mafic metavolcanic rocks (dark green basalt flows, followed by a massive gabbro sill). From 219 to 267 m, the drilling crossed a monotonous metasedimentary succession composed of dark-coloured metapelite intercalations or interfingerings with lighter coloured meta-siltstones, locally (from ca. 263 to 267 m) interrupted by green metapelite levels with a volcanic derived component. At ca. 355 meters, the VSC succession comprises ca. 80 meters of massive sulphides hosted in black metapelites. This succession marks the end of the VSC section at 375 meters, although cut by a thin gabbro sill (1-2 meters).

The second part of the drilling crossed a metasedimentary succession characterized by intercalations (often expressed as rhythmic successions) of black metapelites and fine-grained metasediments (impure quartzites and/or metagreywackes). This succession was interpreted by the company as part of the Mértola Formation (BAFG). However, it displays many similarities with the succession crossed by the Píncaros drilling, ascribed to deeper PQG levels. Without age control and due to strong macroscopic similarities, both interpretations should be considered.

In general, several sections of this drill-hole show deformation/folding effects and fault zones. Frequently, S_0 is transposed by S_1 and ranges from 40º to 60º in relation to the long core axis. Three thrust faults zones (top to S) split the VSC succession. At ca. 355 meters a major interpreted thrust fault zone separates the VSC from the siliciclastic metasedimentary succession, from which the relative age is currently controversial (BAFG or PQG). The VSC succession display sericitic and/or chloritic alteration and mineralization, mainly expressed in green metapelites and some sections of metavolcanics rocks. Hydrothermal precipitates, typically epigenetic (quartz ± carbonate ± pyrite) are also common, crisscrossing the metasedimentary succession. In addition, there is evidence of an early (pre-deformation) hydrothermal pattern associated with pyrite ± chalcopyrite disseminations of variable intensity, mostly in black metapelites. The drilled massive sulphide intersection displays banded textures (mostly composed of fine-grained pyrite, partially recrystallized, disseminated sphalerite and occasional veinlets with sphalerite) to stockwork textures (quartz + pyrite ± chalcopyrite). The fined-grained metasediments from the siliciclastic succession (BAFG or PQG) often presents

pyrite dissemination. **Figure 2.14** shows the interpretative geological section for SES20 using the collected information.

SES18

SES18 was designed by AVRUPA Minerals with 225º and 70º dip at coordinates (ETRS89) *m* = -24931.078 and *p* = -187850.188. The first 115 meters represent the Cenozoic detrital cover on the top of Paleozoic basement which includes a VSC succession down to 428.28 meters. The upper part of this VSC succession (up to ≈ 250 m) includes an intercalation of three main metasedimentary lithotypes, whose relative abundance is as follows: (i) green metapelites with a minor volcanic-derived component; (ii) dark coloured metapelite intercalations with light coloured metapelites bearing an evident meta-siltstone component; and (iii) black metapelites. From ca. 187 to 213 m the drill-hole crossed massive lava flows and foliated greyish-green dacite volcaniclastic rocks, and at ca. 250 m a monotonous succession of dark-grey to black metapelites with minor meta-siltstones. The lower part of this section (down to 410 m) cuts through a volcaniclastic (dacitic) pile, sometimes evolving to metapelites with a fine-grained volcanic-derived component. This metavolcanic pile is hosted in a metasedimentary succession that includes green metapelites with a minor volcanic-derived component and dark-grey metapelite intercalations (and/or interfingerings) with light coloured metapelites bearing an evident siltitic component. From ca. 410 to 428, a monotonous succession of black metapelites with minor meta-siltstones is interrupted (at ≈427 m) by a light green gabbro sill.

The second section of the drilling crossed a metasedimentary succession characterized by intercalations (often expressed as rhythmic succession) of black metapelites and fine grained impure quartzites and/or metagreywackes. This succession was interpreted by the company as part of the Mértola Formation (BAFG). However, it shows many similarities with the Píncaros drill-hole ascribed to the deeper levels of PQG. Therefore, without additional stratigraphic/chronological constraints both interpretations should be considered.

Several sections of this drill-hole show intense deformation/folding effects and fault zones. Frequently, S_0 is transposed by S_1 and ranges from 30º to 60º in relation to the long core axis. Deformation effects are quite evident in rocks forming the metavolcanic pile, particularly those of volcaniclastic nature. Various fault zones disrupt the VSC succession, and a major (thrust?) fault zone separates this succession from the basal siliciclastic pile whose relative age is currently controversial (BAFG and PQG). Effects of alteration and mineralization are discrete in metasedimentary facies forming the VSC succession. The metasediments, mainly black

metapelites and green metapelites with minor volcanic-derived component, display pyrite (disseminated and as stringer infillings), occasionally crossed by millimetric veinlets of quartz and carbonate (post-deformation). The crossed metavolcanic rocks show strong sericitic alteration and effects of silicification, but with no evident dissemination of sulphides. The fine-grained metasediments (impure quartzites and/or metagreywackes) included in the basal siliciclastic plie (BAFG or PQG?) display most often pyrite disseminated in the matrix and preserve evidence of (pre-deformation) alteration effects, usually indicated by the developmente of (micro) quartz ± chlorite veinlets. **Figure 2.15** shows the interpretative geological section for SES18 using the collected information.

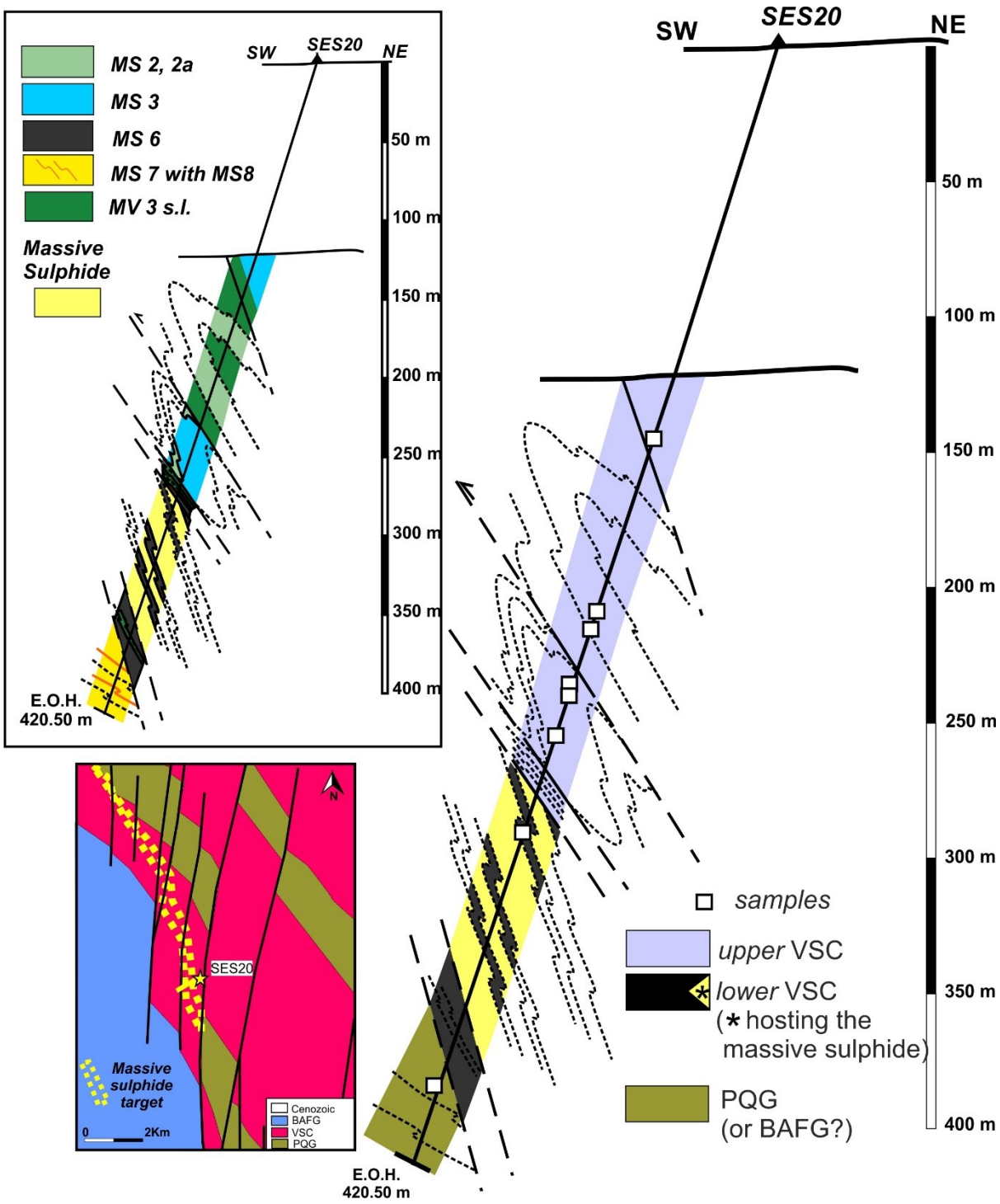

Figure 2.14 - Interpretative geological cross-section comprising the SES20 exploration drill-hole, considering the observed polarity and the S_0/S_n angular relationships. Relative position and direction of the drilling in the geological map taken from *Figure 2.13*.

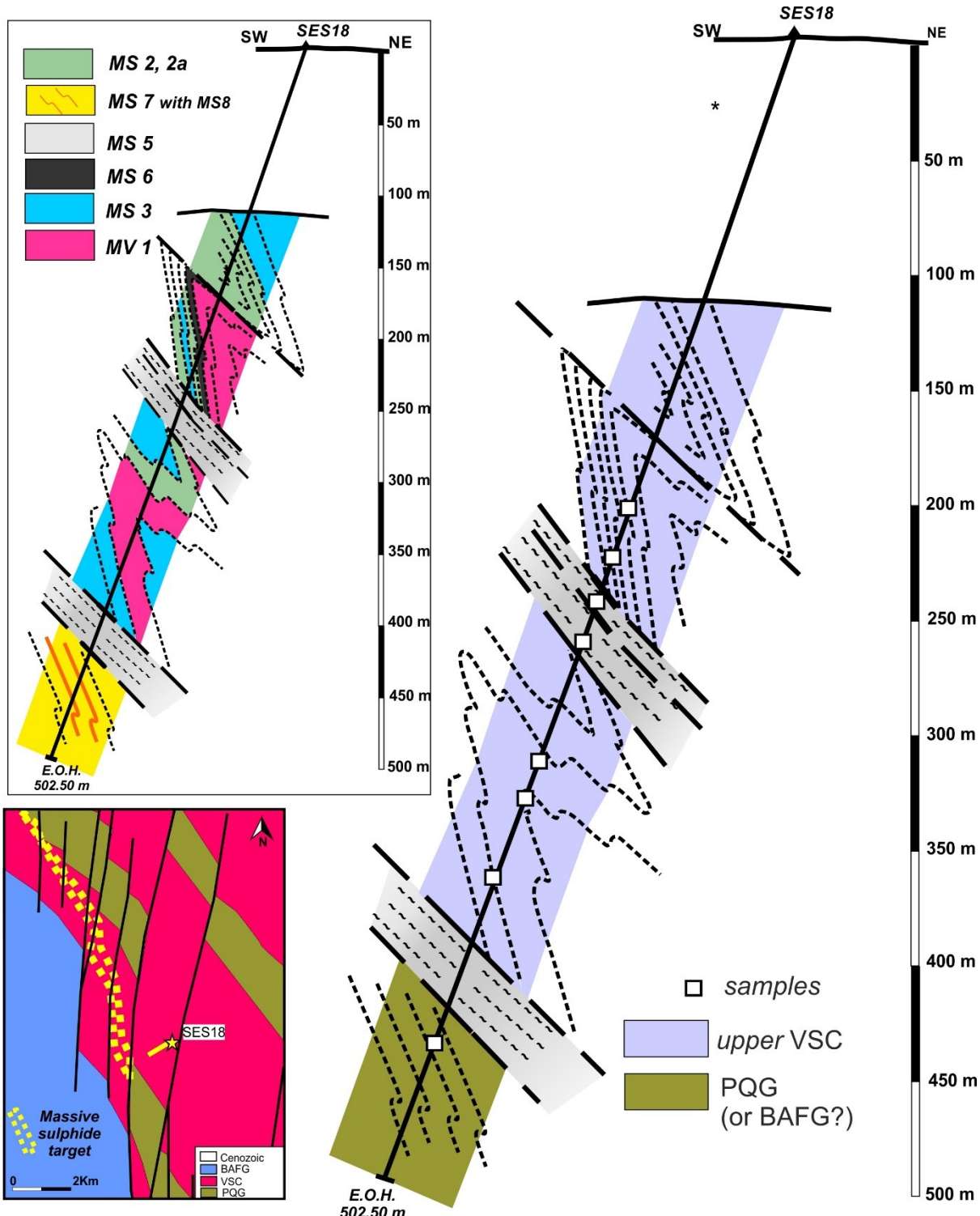

Figure 2.15 - Interpretative geological cross-section comprising the SES18 exploration drill-hole, considering the observed polarity and the S_0/S_n angular relationships. Relative position and direction of the drilling in the geological map taken from *Figure 2.13*.

2.3.3. Aljustrel

The Aljustrel sector comprises three sub-sectors (**Figure 2.16**): the Aljustrel mine area, Monte das Mesas and Gavião. Up until now, at Aljustrel, the metasedimentary succession that forms the PQG was not recognized and the local lithostratigraphy is dominated by a thick pile (up to 200 m) of metavolcanic rocks with intercalations of black metapelites whose precise age remains unknown, despite several attempts to resolve this issue. The volcanic succession was addressed in many studies aiming at the characterization of their geochemical (rhyolitic to dacitic) affinity, facies types and features developed during seafloor metasomatism, lately overprinted by (mineralizing) hydrothermal alteration (*e.g.* Schermerhorn and Stanton, 1969; Barriga and Kerrich, 1984; Barriga, 1983; Barriga and Fyfe, 1998; Relvas, 1991; Leitão, 1997, 2014; Carvalho *et al.*, 1999; Dawson and Caessa, 2003; Barret *et al.*, 2008; Inverno *et al.*, 2008; Oliveira *et al.*, 2013a, b). In this work, the thick volcanic pile was divided into two series: the *lower* one including rock types confined to the 364 ± 2 Ma time window (U-Pb, LA-ICP-MS in zircon; Rosa *et al.*, 2009) and the *upper*, hosting the main ore horizon, dated of 352.4 ± 1.9 Ma (U-Pb, TIMS in zircon; Barrie *et al.*, 2002). Overlying the latter volcanic pile, an extensive (and thick) metajasper/chert lens occurs, laterally equivalent to the metapelites succession forming the Paraíso Formation, part of the *upper* VSC. The Paraíso Formation is composed of purple and green metapelites (often interfingered), black metapelites/meta-siltstones, metapelites with volcanic-derived components and (less voluminous) mafic metavolcanics rocks *(e.g.* Barriga, 1983; Leitão, 2014). Palynological studies on metapelites from the Paraíso Formation yielded miospore assemblages of CM and Pu biozones (Lower Visean to Upper Tournaisian; Pereira *et al.*, 2007). Resting on top of the VSC succession, metapelites from the Mértola Formation (BAFG) include miospores from the NL biozone (Mid-Upper Visean; Pereira *et al.*, 2007; Oliveira *et al.*, 2009; Pereira and Matos, 2014). Despite of differences in detail, not properly characterized at present, the observed lithostratigraphic succession observed in the nearby sub-sectors of Gavião and Monte das Mesas follows the general (and simplified) column of Aljustrel.

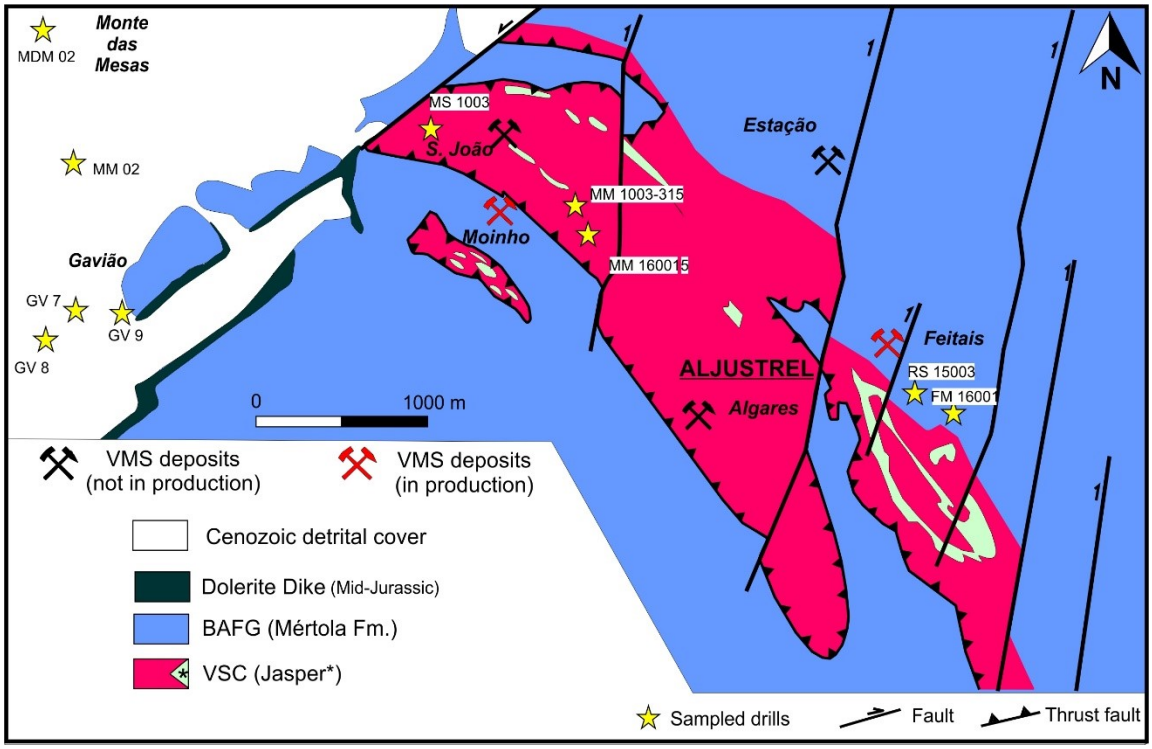

Figure 2.16 - Simplified geological map of the Aljustrel sector (adapted from Andrade and Schermerhorn, 1971; Inverno et al. 2008), showing the three sub-sectors: (i) the Aljustrel mine area and its orebodies with active (Feitais e Moinho) and suspended (S.João, Algares and Estação) underground mining works; (ii) the exploration prospect of Monte das Mesas; and (iii) the advanced exploration prospect of Gavião, hosting an estimated global amount of ca. 40 Mt of massive sulphides.

Aljustrel mine

The sampling survey at Aljustrel mine area was conducted at the ALMINA facilities and comprised two phases. The first one covered some domains of the mining underground works at Moinho and Feitais orebodies. Five samples were collected, representing different features, as follows: (i) at the Feitais orebody (≈390 m of depth), stockwork and metapelites from the hanging wall; and (ii) at the Moinho orebody (≈400 - 480 m of depth), metapelites forming the ore horizon and the hydrothermally altered metapelite at hanging wall position. The second sampling phase was planned based on the available drilling grid, representing historical and current exploration/exploitation activities. Five drill-holes were selected considering the variety of metasedimentary lithotypes crossed and their proximity to massive sulphide orebodies.

Using the logging information shared by the Company along with information from previous sampling surveys and the observations made in selected segments of each drilling, it was possible to advance some proposals for interpretative geological sections including each drill-

hole. In this exercise, the lithotype codes used by the company were harmonized with those applied in this work (**Figure 2.17**).

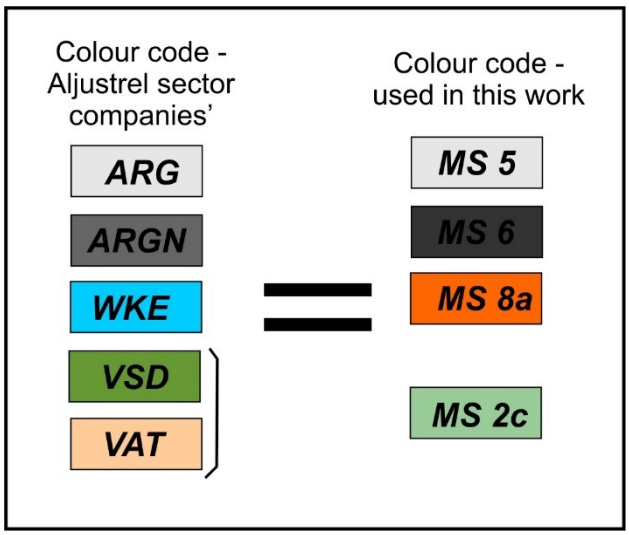

Figure 2.17 - Harmonization criteria for metasedimentary successions intersected in Aljustrel mine area. On the left the code used by ALMINA; on the right correspondence to our metasedimentary facies index.

Feitais orebody – FM16001

The production drill-hole FM16001 at Feitais was designed with ≈215º azimuth and 37º to 23º dip at coordinates (ETR89) *m = -1303.371* and *p = -199029.089*. The first one-hundred meters intersected a metasedimentary succession composed of grey to black metapelites interbedded with fine-grained metaquartzwacke, ascribed to the Mértola Formation (BAFG). The second section intersected up to ≈145 meters of a metasedimentary succession composed of green metapelites with volcanic-derived component that lay on chemogenic (exhalative?) siliceous facies (e.g. cherts), frequently interbedded with jaspers (Paraíso Formation – *upper* VSC). After some meters of volcaniclastic rocks, and from ca. 175 m to almost the end of the drill-hole (347.50 m), a pyritic stockwork (hosted in rhyolitic rocks) and a massive sulphide body (enriched in pyrite and sphalerite) were intersected. In general, several sections of this drill-hole preserve deformation/folding effects; commonly, S_0 is transposed by S_1 and ranges from 15º to 35º in relation to the long core axis. The most important tectonic discontinuities were interpreted as thrust fault zones with top to S-SW.

Fine disseminations of pyrite in black, often "graphite"-rich, metapelites belonging to the Mértola Formation and in metasediments of the *upper* VSC succession are common, despite any evidence of significant hydrothermal alteration. The metavolcanic rocks that host the

stockwork and the massive sulphide accumulations display intense chlorite-sericite alteration along with the growth of bands bearing fine-grained pyrite. **Figure 2.18** displays an interpretative geological section for FM16001 using the collected information.

Feitais orebody – RS15003

The exploration drill-hole RS15003 at Feitais was designed with ≈200º azimuth and ≈83º to 77º dip at coordinates (ETRS89) *m = -1728.974* and *p = -198713.595*. The first four-hundred meters intersected the Mértola Formation (BAFG), almost exclusively composed of grey and fine-grained metaquartzwacke with minor intervals of black metapelites. The VSC succession was drilled down to the end of the drill at 1049.05 m, after a major tectonic discontinuity at ca. 450 m. The upper section of the VSC succession (Paraíso Fm. – *upper* VSC) comprises metapelites with a volcanic-derived component, (minor) green metapelites and chemogenic (exhalative) siliceous facies. The Paraíso Formation overlies a series of metavolcanic rocks (of rhyolitic nature). At ca. 644 m, a tick body of massive sulphides is intersected and followed by stockwork hosted in a metavolcanic pile of rhyolitic nature. Tectonic discontinuities are commonly found, often tracing fault zones of variable importance; these are interpreted as thrust faults (with top to the S-SW).

The drilled section of Mértola Formation frequently shows disseminations of fine pyrite in the matrix of metagreywackes and black metapelites, and less common in quartz ± carbonate veinlets. Rocks forming the Paraíso Formation do not display macroscopic evidence of hydrothermal alteration and mineralization, except some halos adjoining fault zones variably silicified and enriched in chlorite ± sericite together with fine pyrite disseminations. Metavolcanic intersections show evidence of intense chloritization, occasionally superimposed with sericite alteration. Stockwork intersections are pyrite rich. **Figure 2.19** illustrates the interpretative geological section for RS15003 using the collected information

Moinho orebody – MM160015

The drill-hole MM160015, geometrically located at the footwall of the Moinho deposit, was designed with ≈230º azimuth and 28º to 21º dip at coordinates (ETRS89) *m* = -3468.778 and *p* = -198136.617. The VSC succession is intersected all along the drilling, up to 384.20 m. The first 106.30 m consists mostly of metavolcanic rocks, varying between rhyolites *s.l.* and porphyritic rhyolites. These metavolcanic rocks host a sequence of more than one-hundred

meters of stockwork and a massive sulphide lense (up to 221.25 m). After a major fault zone, and some few meters of volcaniclastic rocks, the Paraíso Formation is crossed, comprising metapelites with a volcanic-derived component interbedded with green metapelites that might preserve signs of distal volcanic contribution too. Rarely, there are also intercalations of "graphite"-rich black metapelites. The Paraíso Formation, overlying the metavolcanics rocks, includes also a thick layer of chemogenic (exhalative?) siliceous facies (cherts).

Some sections of this drill-hole preserve evidence of significant folding. Frequently, S_0 is transposed by S_1 and ranges from 60º to 80º in relation to the long core axis. Tectonic discontinuities are common, corresponding to fault zones with inverse kinematics (top to the S-SW). At ca. 221.25 m, the drill intersects the massive sulphide lense.

Signs of sericitic alteration can be observed all along the drilled rocks. In depth, chlorite alteration is stronger and overlaps the secondary mineral assemblages bearing sericite; nonetheless, evident chloritization is just preserved in metavolcanic rocks. Metasedimentary successions show pyritic dissemination in the matrix, mainly in green metapelites with volcanic-derived component and black metapelites. Frequently, chemogenic (exhalative?) siliceous facies display pyrite and magnetite dissemination. **Figure 2.20** shows the interpretative geological section for MM160015 using the compiled information.

Moinho orebody – MM10003-315

The drill-hole MM10003-315, was designed with ≈245º azimuth and 50º to 40º dip at coordinates (ETRS89) *m* = -3531.374 and *p* = -198454.217. The VSC succession was crossed along the 311.80 m of this drilling, excluding the section from ca. 77-20 to 99.50 m that comprises a series of fine and grey metagreywackes ascribed to the Mértola Formation (BAFG). The VSC succession is composed of rhyolitic volcaniclastic rocks that are overlaid by metasediments in the upper part of the section; similar rocks host a stockwork and a massive sulphide lense in the lower part of the section. The VSC metasedimentary succession comprises chemogenic (exhalative?) siliceous facies and metapelites with a volcanic-derived component that evolve to black metapelites, besides green metapelites with volcanic contribution. Despite the strong tectonic dismembering, the main folding pattern can be reconstructed and, as observed in cores from other drillings, S_0 is often transposed by S_1, ranging from 20º to 40º in relation the long core axis.

Fingerprints of hydrothermal alteration are present along all the drilled metavolcanics, mainly denoted by the development of chlorite ± quartz in the matrix, and some sericite as fracture

infillings. Metasediments present some carbonate alteration and black metapelites often show disseminations of fine-grained pyrite. Stockwork and massive sulphide intersections are pyrite rich. **Figure 2.21** shows the interpretative geological section for MM1003-315 using the collected information.

São João - MS10003

The exploration drill-hole MS1003 started on surface, near São João. It was designed with ≈200º azimuth and 60º to 55º dip at coordinates (ETRS89) *m* = -3794.782 and *p* = -197813.722. The first 95.00 m intersected the Mértola Formation (BAFG) comprising black metapelites and fine-grained grey meta-quartzwackes. From ≈95.00 m down to the end of the drilling (440.50 m), only a metavolcanic sequence composed of rhyolitic metavolcaniclastic rocks was intersected. At ca. 112.80 m a fine layer of green metapelites with volcanic-derived component overly the metavolcanic pile.

Frequently, S_0 is transposed by S_1 and ranges from 25º to 50º in relation to the long core axis. Tectonic discontinuities are common, the most important of which corresponding to fault zones. The upper metasedimentary succession often exhibits disseminated pyrite and some oxides. Alteration patterns are visible mainly in the metavolcanic pile, expressed as chlorite ± sericite. **Figure 2.22** shows the interpretative geological section for MS10003 using the collected information.

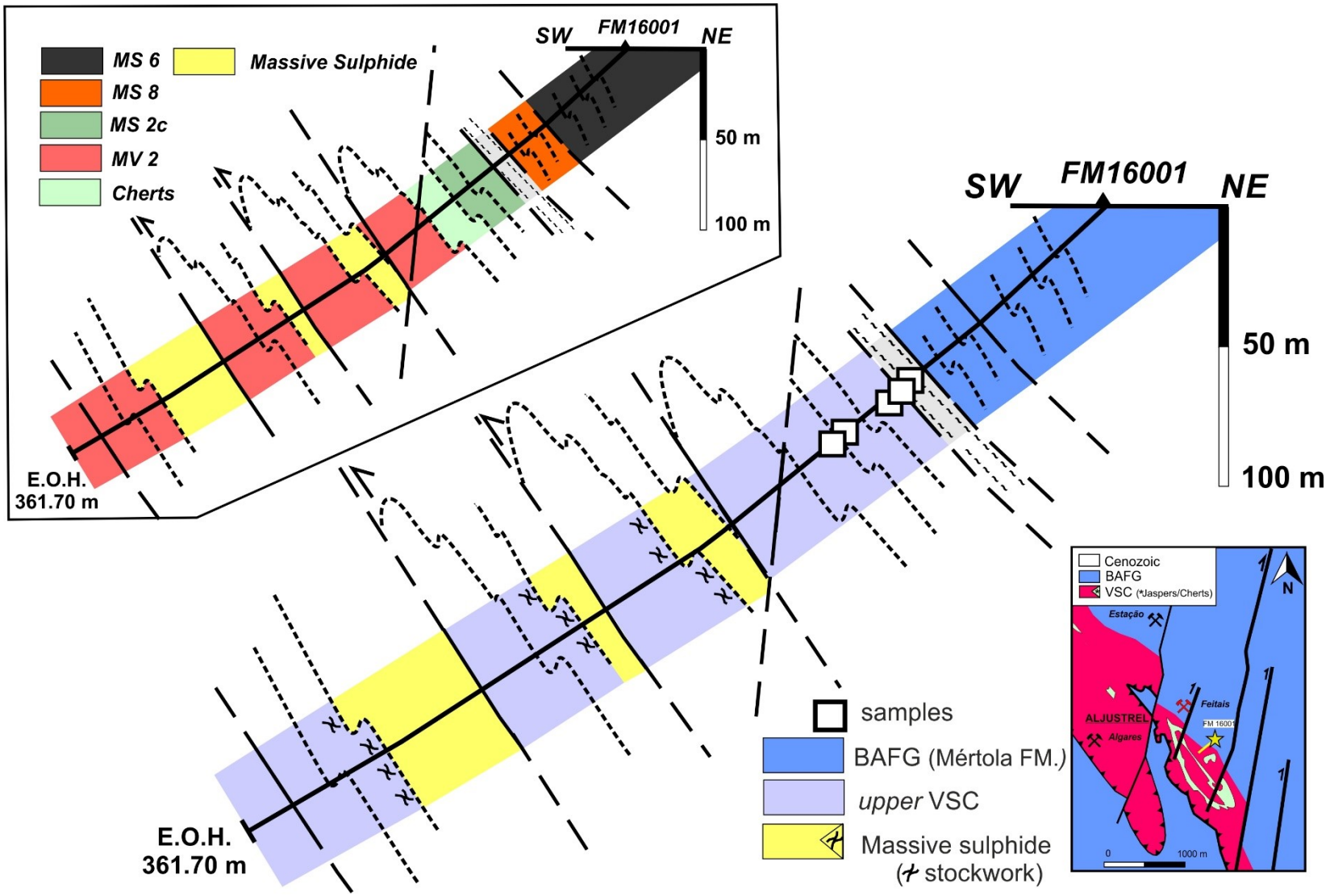

Figure 2.18 - Interpretative geological cross-section comprising the FM16001 exploration drill-hole from Feitais orebody (Aljustrel mine), considering the observed polarity and the S_0/S_n angular relationships. Relative position and direction of the drilling in the geological map taken from *Figure 2.16.*

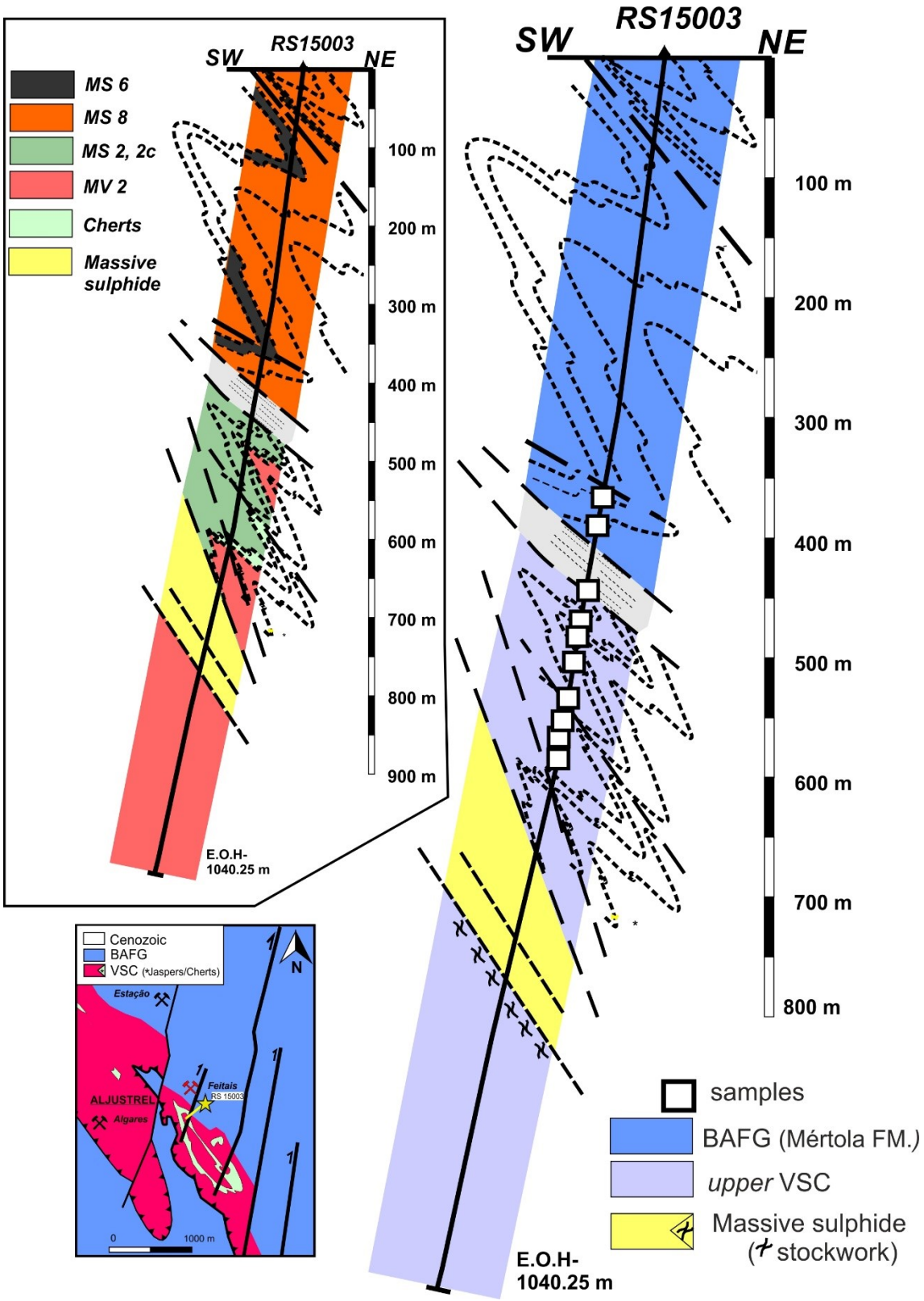

Figure 2.19 - Interpretative geological cross-section comprising the RS1003 exploration drill-hole from Feitais orebody (Aljustrel mine) , considering the observed polarity and the S_0/S_n angular relationships.. Relative position and direction of the drilling in the geological map taken from *Figure 2.16.*

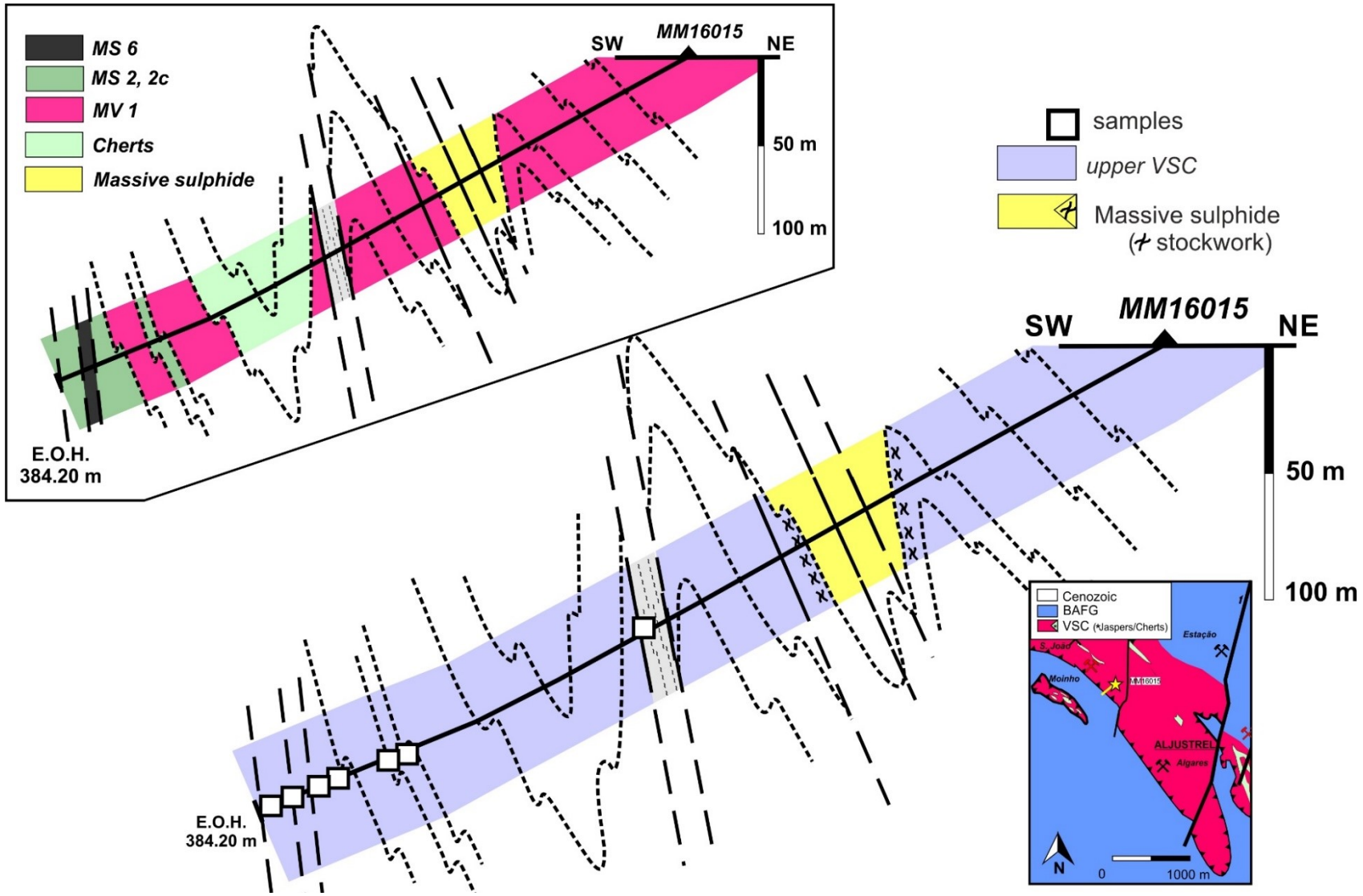

Figure 2.20 - Interpretative geological cross-section comprising the MM16015 production drill-hole from Moinho orebody (Aljustrel mine), considering the observed polarity and the S_0/S_n angular relationships. Relative position and direction of the drilling in the geological map, taken from *Figure 2.16*.

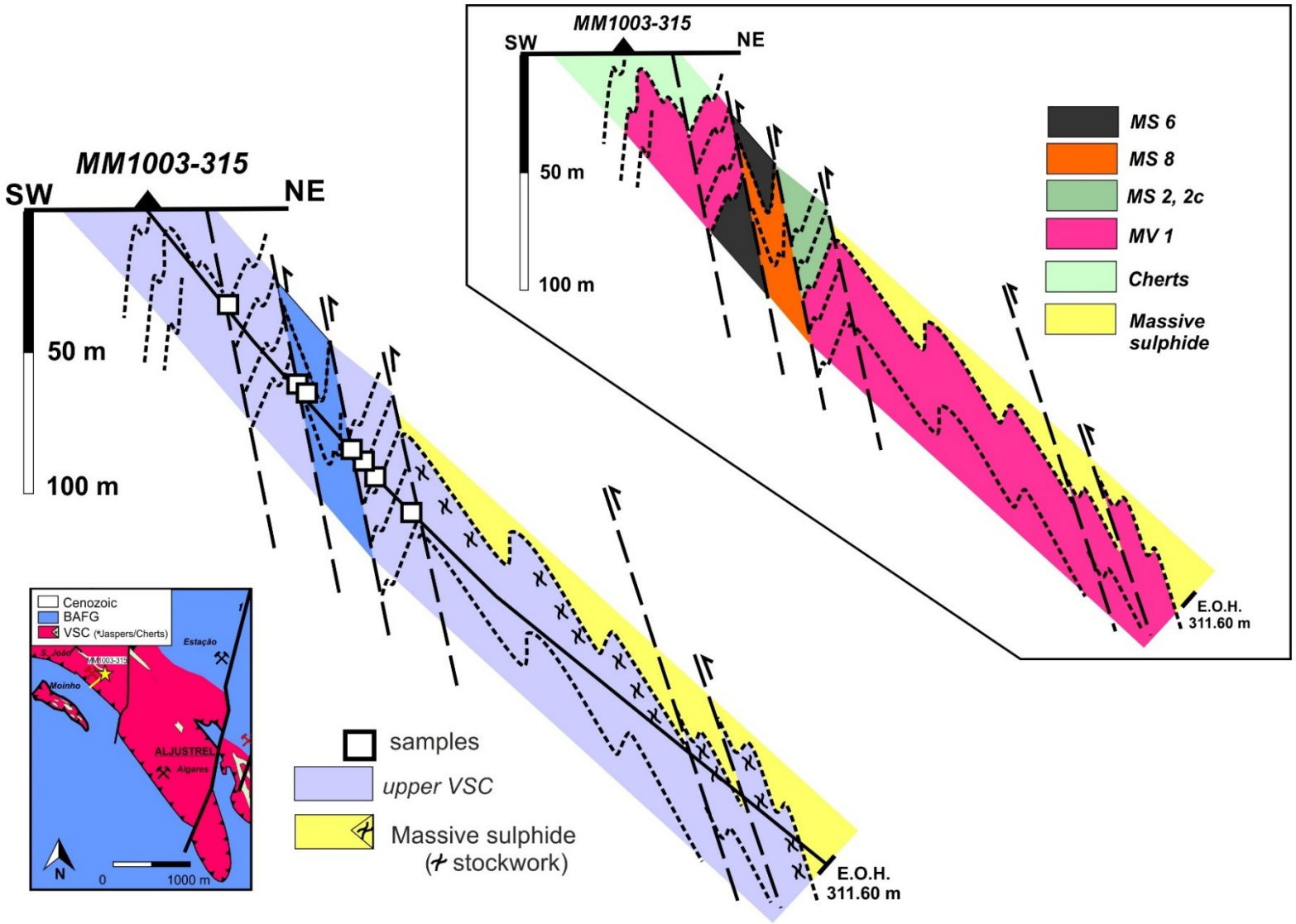

Figure 2.21 - Interpretative geological cross-section comprising the MM1003-315 production drill-hole from Moinho orebody (Aljustrel mine). , considering the observed polarity and the S_0/S_n angular relationships. Relative position and direction of the drilling in the geological map taken from *Figure 2.16.*

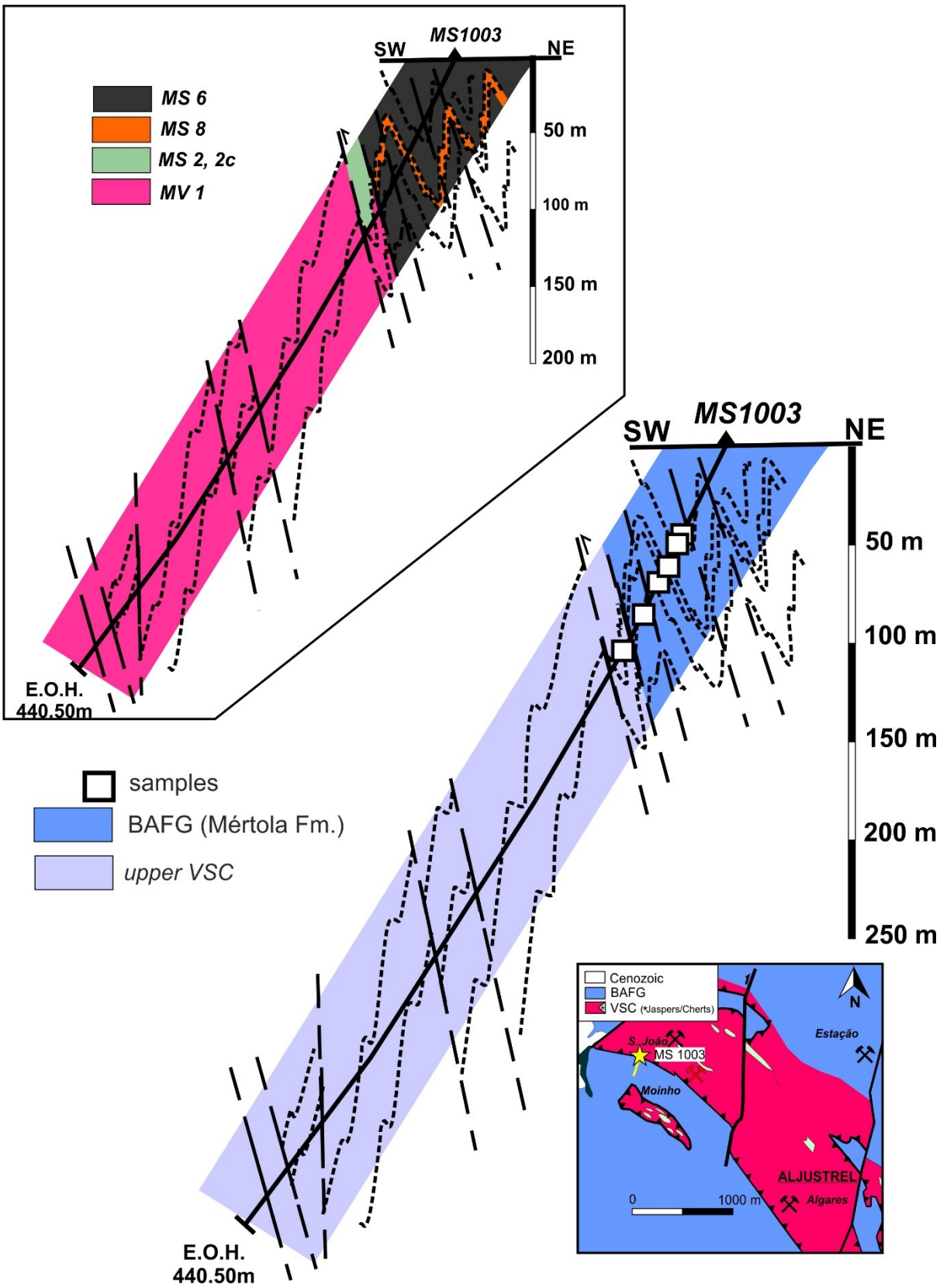

Figure 2.22 - Interpretative geological cross-section comprising the MS100 exploration drill-hole (Aljustrel mine), considering the observed polarity and the S_0/S_n angular relationships. Relative position and direction of the drilling in the geological map taken from *Figure 2.16*.

Gavião

The sampling survey of Gavião was performed at the EDM facilities in Aljustrel. Three drillings were selected, considering: (i) the variety of intersected metasedimentary lithotypes and (ii) their proximity to massive sulphide lenses. Only the metasedimentary successions were carefully re-assessed. Data from metavolcanic piles were extracted from EDM reports and their respective logs as well as the classification types.

GV7

The exploration drill-hole GV08007 was designed with ≈230º azimuth and 65º to 42º dip at coordinates (ETRS89) *m = -6402.80* and *p = -199157.5*. The first fifty meters correspond to the Cenozoic detrital cover on top of the Paleozoic basement. The VSC succession was intersected almost along the whole drilling, only interrupted between ca. 85 and 145 m by a series of fine-grained grey metaquartzwacke, possibly representing the Mértola Formation (BAFG). The *upper* VSC succession (Paraíso Formation) includes metapelites with volcanic derived components scattered in a black or dark-green matrix and black metapelites. The metavolcanic pile, from 205 to 750 m, is composed essentially by Quartz-Eye Tuff (lowermost section) and Mine Tuff (uppermost section). The latter hosts the massive sulphide lenses intersected at ≈ 745 m. As observed in many cores of other drillings, S_0 is often transposed by S_1 and ranges from ca. 15 to 70º in relation to the long core axis. Tectonic discontinuities are common, the most important representing fault zones interpreted as thrust faults (with top to the S-SW).

Effects of alteration are clear in green metapelites with volcanic derived contribution and usually marked by the growth of chlorite along with fine-grained quartz; the metavolcanic pile evidences also a superimposed sericitic alteration. Thin pyrite-rich layers, always concordant with the mainly foliation plans, occasionally including sphalerite, are common. Massive sulphide intersections are mostly composed of pyrite + sphalerite ± chalcopyrite. **Figure 2.23** displays the interpretative geological section for GV7 using the collected information.

GV8

The exploration drill GV08008 was designed with ≈225º azimuth and 63º (to 47º) dip at coordinates (ETRS89) *m = -6663.25* and *p = -199330.90*. Similarly, to the previous drill-hole, the first fifty meters represent the Cenozoic detrital cover on the top of the Paleozoic basement. Below this cover only the VSC succession were intersected, specifically the *upper* VSC (Paraíso Formation) comprising mostly metapelites with a volcanic derived component in a black and/or dark-green matrix. Fine chemogenic (exhalative?) siliceous facies (cherts) were drilled between the metapelites and the monotonous volcanic pile (Mine Tuff). At ca. 323 m, the latter pile hosts massive sulphide lenses (sphalerite + pyrite ± chalcopyrite). Often S_0 is transposed by S_1 and ranges from 20 to 40º in relation to the long core axis. Tectonic discontinuities are common, developing fault zones of variable expression, interpreted as thrust faults (with top to the S-SW).

The hydrothermal alteration pattern is discrete and often traced by the growth of chlorite in metasedimentary successions and sericite in metavolcanic piles. Again, thin pyrite-rich layers containing subordinate amounts of sphalerite, always concordant with the mainly foliation plans, are common. The chemogenic facies show frequently disseminated pyrite ± magnetite. The massive sulphide lenses include pyrite + sphalerite ± chalcopyrite ± galena. **Figure 2.24** shows the interpretative geological section for GV8 using the collected information.

GV9

The exploration drill GV08008 was designed with ≈234º azimuth and 63º (to 37º) dip at coordinates (ETRS89) *m = -6219.42* and *p = -199246.93*. The first seventy meters represent the Cenozoic detrital cover on the top of the Paleozoic basement. Only the VSC succession was intersected by this drilling, down to 797.50 m. An extensive metasedimentary series of the *upper* VSC (Paraíso the Formation) was intersected, from 70 to 300m, comprising two distinct sections: (i) green metapelites with a volcanic-derived component; and (ii) dark grey coloured to black metapelites with volcanic-derived components, evolving to dark-coloured and black metapelites with intercalations and/or interfingering of meta-siltstones, frequently presenting a rhythmic intercalation. The locally abundant volcanic-derived component (and the mineral/clast-size) in these black metapelites resembles a metavolcaniclastic rock. Frequently, thin intercalations and/or interfingerings of coloured metapelites from violet-green to green evolve gradually to deep purple metapelites. The metavolcanic pile, extending from ≈300 to 730 m is mostly composed of two lithotypes: (i) the lower one, Quartz-Eye tuff; and (ii) the

upper one, Mine tuff. At ca. 730 m, thirty meters of massive sulphides were intersected; the contacts with adjoining rocks are of tectonic nature.

Several sections of this drill-hole show deformation/folding effects and fault zones. Often S_0 is transposed by S_1 and ranges from 15 to 70º in relation to the long core axis. The prevalent fault zones were interpreted as thrust faults (with top to the S-SW).

The alteration/mineralization pattern in rocks forming the *upper* VSC section is quite discrete when affecting metasediments. However, grey to dark-grey to black metapelites and intercalated meta-siltstones often display anastomosed quartz structures with fine grained pyrite ± sphalerite. The crossed massive sulphide accumulation comprises pyrite + sphalerite ± chalcopyrite ± galena. **Figure 2.25** shows the interpretative geological section for GV9 using all collected information.

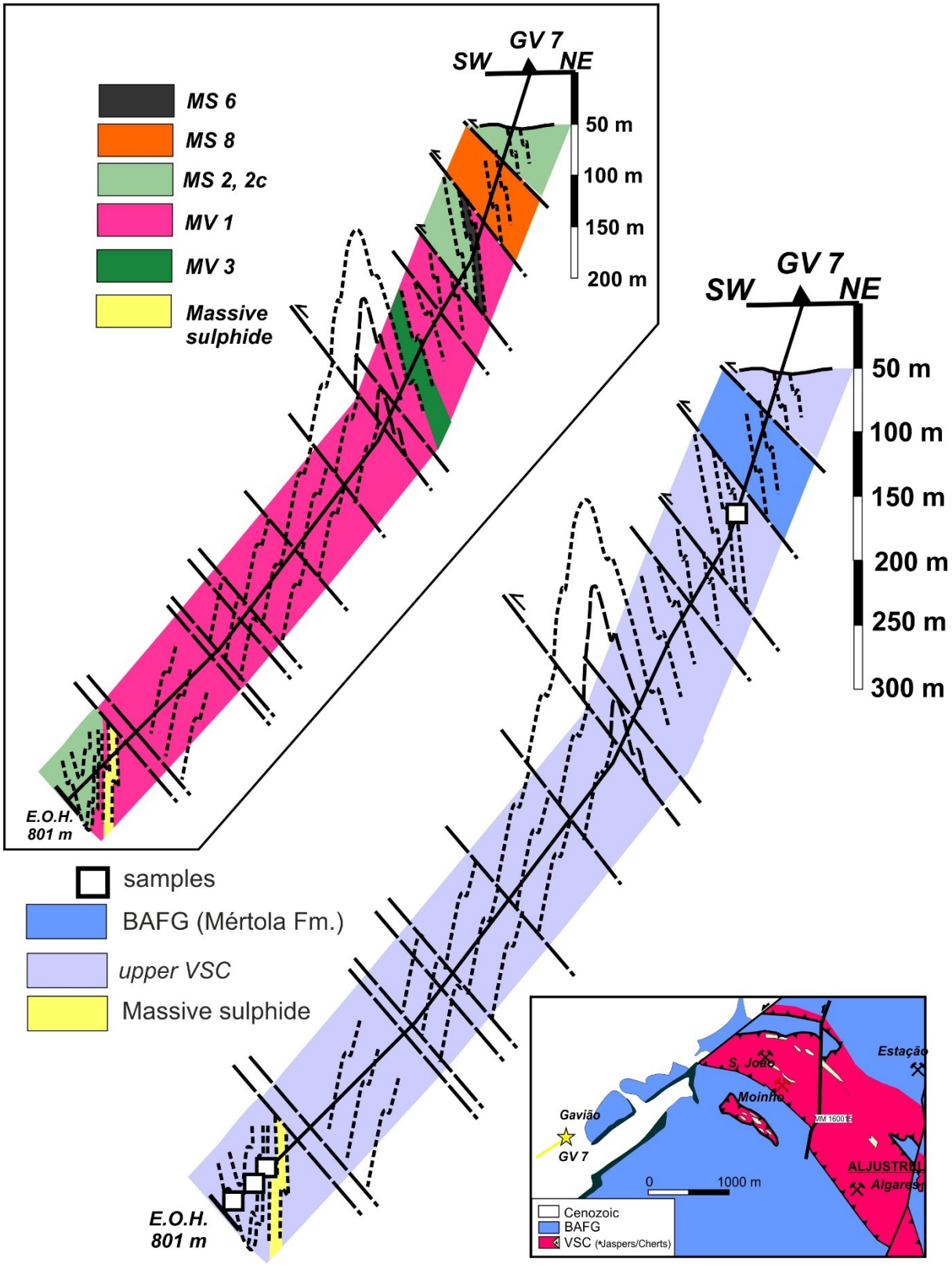

Figure 2.23 - Interpretative geological cross-section comprising the GV7 exploration drill-hole from Gavião sub-sector, considering the observed polarity and the S_0/S_n angular relationships. Relative position and direction of the drilling in the geological map taken from *Figure 2.16.*

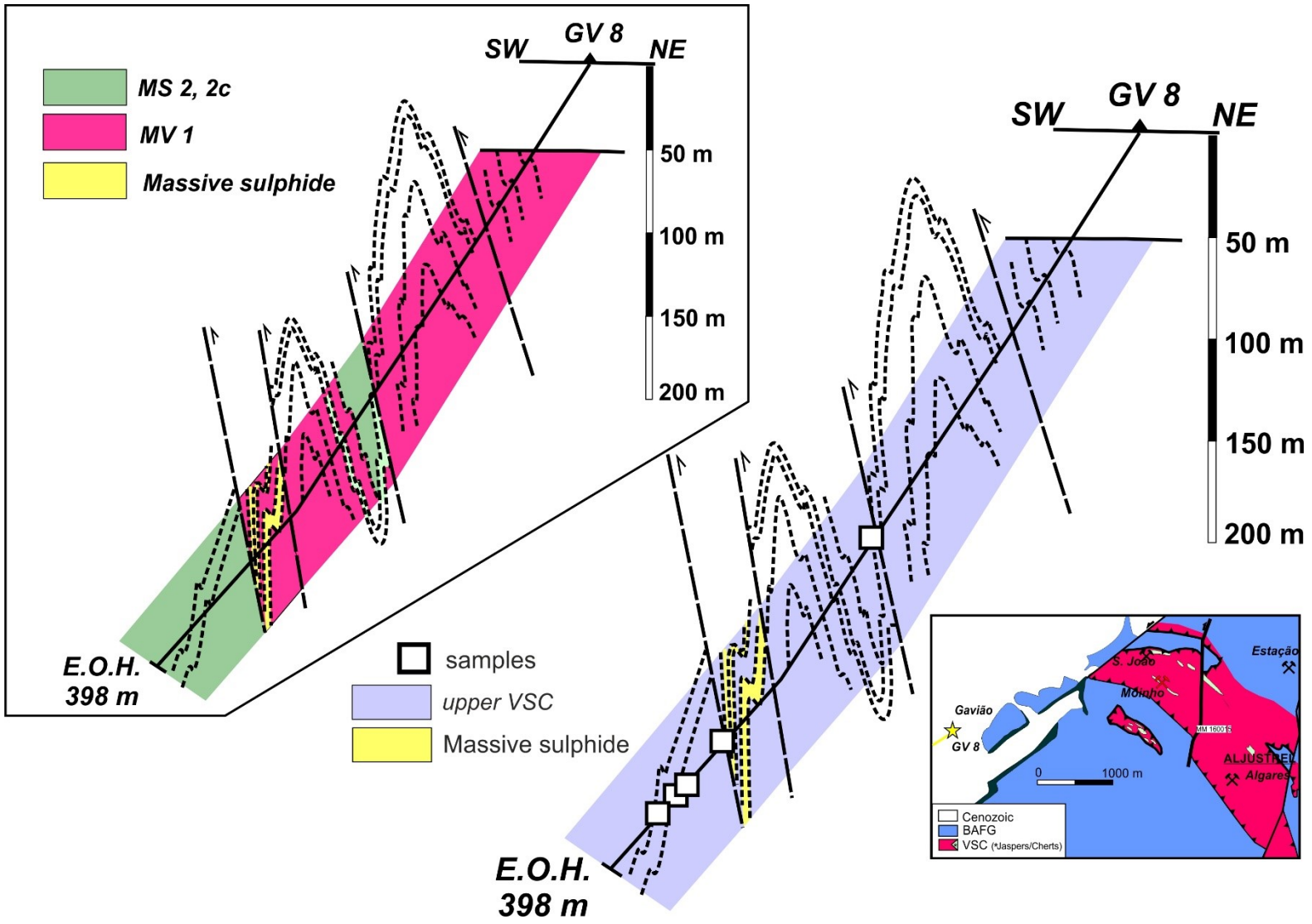

Figure 2.24 - Interpretative geological cross-section comprising the GV8 exploration drill-hole from Gavião sub-sector, considering the observed polarity and the S_0/S_n angular relationships. Relative position and direction of the drilling in the geological map taken from *Figure 2.16.*

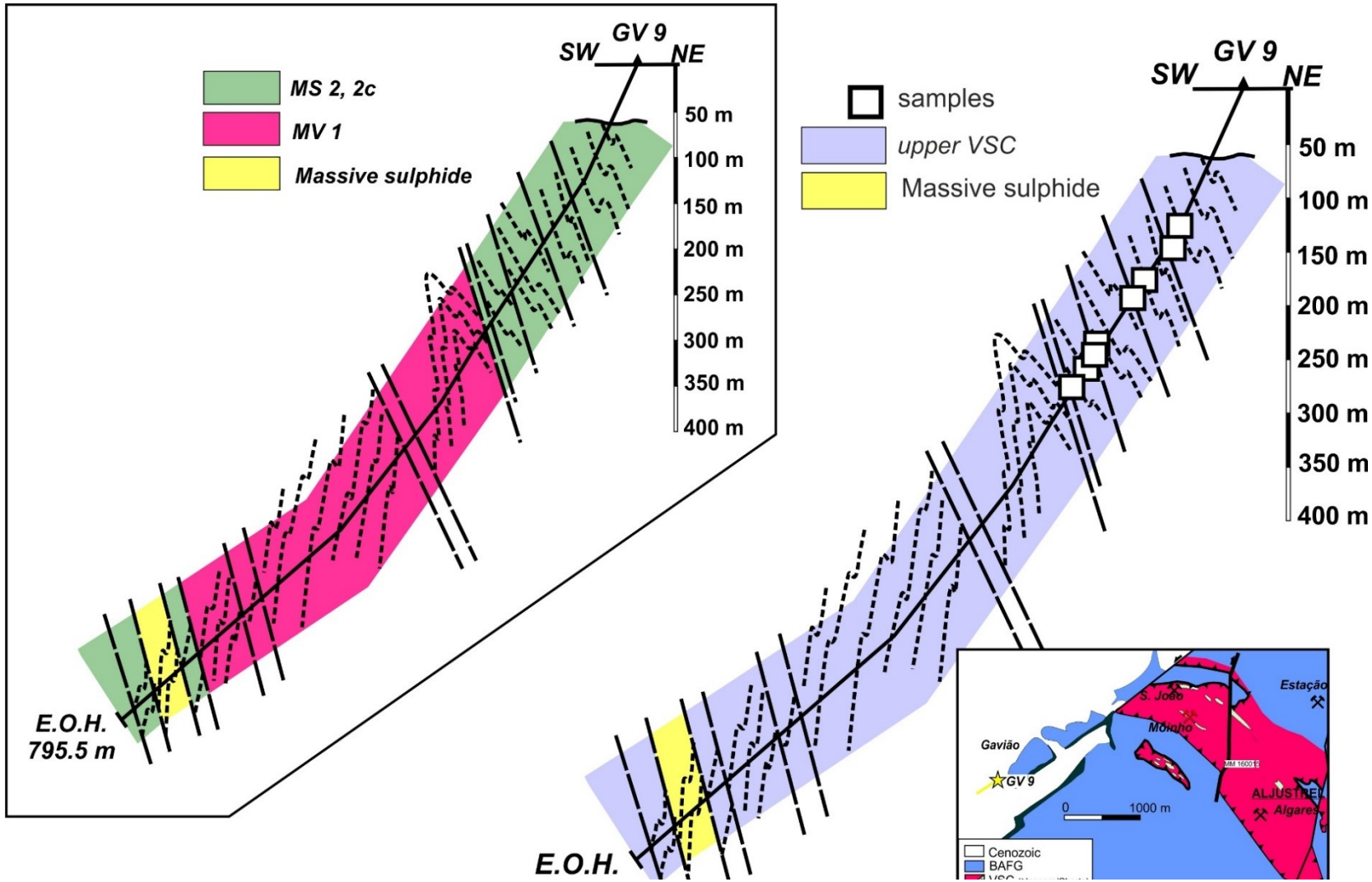

Figure 2.25 - Interpretative geological cross-section comprising the GV9 exploration drill-hole from Gavião sub-sector, considering the observed polarity and the S_0/S_n angular relationships. Relative position and direction of the drilling in the geological map taken from *Figure 2.16*.

Monte das Mesas

The sampling campaign in Monte das Mesas was performed at the ESAN MET facilities. The criteria used to choose the drill-holes was based on the variety of metasedimentary lithotypes and the proximity to other known massive sulphide ore systems (Gavião and Aljustrel). Due to the lack of time, a carefully detailed re-logging was not performed. Therefore, the following general description is based on the Company's reports and on the observations of Carpinteira (2020).

MM02

The MM02 is an historical exploration drill-hole performed at coordinates (ETRS89) *m = -6931.38* and *p = -198313*. The first ninety-seven meters correspond to Cenozoic detrital cover on the top of the Paleozoic basement. The Mértola Formation (BAFG) was intersected from 97 to 162 m and contains medium to coarse-grained meta-quarzwackes intercalated with dark-grey to black metapelites. A tectonic contact separates this unit from the *upper* VSC. The latter unit, crossed between 164 and 220 m, is essentially a metasedimentary succession that comprises black metapelites bearing a fine-grained meta-siltstone component. Frequently, rhythmic intercalations between minor meta-greywacke and black metapelites were observed. Palynological studies using samples picked at ca. 194 m identify miospore assemblages from the NL biozone, pointing to mid-Late Visean age. At ca. 207 m, a monotonous pile of greenish felsic metavolcaniclastic rocks (with quartz and feldspar clasts) is crossed by a shear zone. This structure separates the metavolcaniclastic pile from the overlaying succession with green-purple and grey metapelites. Small intersections of magnetite-rich metajaspers can be observed at ca. 262 m. The basal segment of the drilling intersects metavolcanic rocks of intermediate composition. According to the ESAN MET reports this VSC succession was interpreted as the NE limb of Gavião anticline. However, no major evidences of mineralization were observed. **Figure 2.26** show the interpretative geological section for MM02 using all collected information.

MdM02

The exploration MdM02 drill-hole was design by ESAN MET in 2017 at the coordinates *m = -9154.87* and *p = -193552.26* (ETRS89). The drilling has 225º azimuth with 75º dip and was performed to investigate a geophysical target (based on resistivity data).

The Cenozoic detrital cover was intersected in the first 16.45 meters. The next 400 m were interpreted as an *upper* VSC succession. The observed metasediments include purple-green metapelites with a frequent volcanic-derived component and black metapelites. The metavoclanic pile is predominantly felsic, comprising massive/coeherent rhyolitic lavas, sericite-rich metavolcaniclastic rocks and foliated metavolcaniclastic rocks (locally displaying sericite-chlorite rich levels). Frequently, the metavolcaniclastic rocks display intercalations of pyrite-rich black metapelites (Carpinteira, 2020).

At ca. 386 and 475 m, two fault zones put in contact the *upper* VSC succession with a siliciclastic unit ascribed to the Mértola Formation (BAFG) characterized by a monotonous intercalation of "graphitic" black metapelites (pyrite-rich) and metaquartzwackes, frequently developing a rthymic succession.

As observed in the ESAN MET reports, the geophysical anomaly might be related to the "graphitic" component presented by black metapelites and disseminated (although interconnected) pyrite grains. **Figure 2.27** shows the interpretative geological section for MdM02 using all collected information.

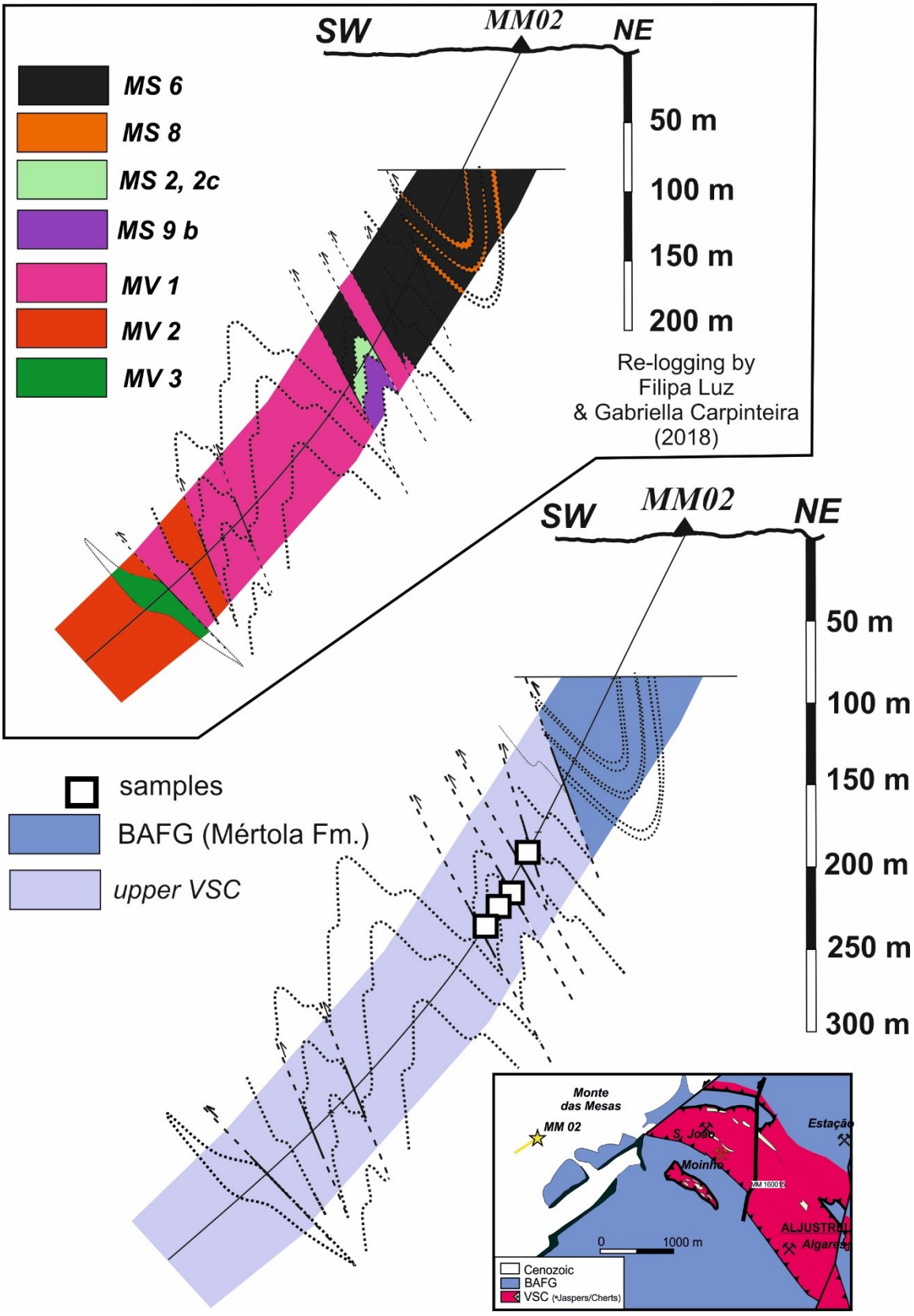

Figure 2.26 - Interpretative geological cross-section comprising the MM02 historical drill-hole from Monte das Mesas sub-sector, considering the observed polarity and the S_0/S_n angular relationships. Relative position and direction of the drilling in the geological map taken from *Figure 2.16.*

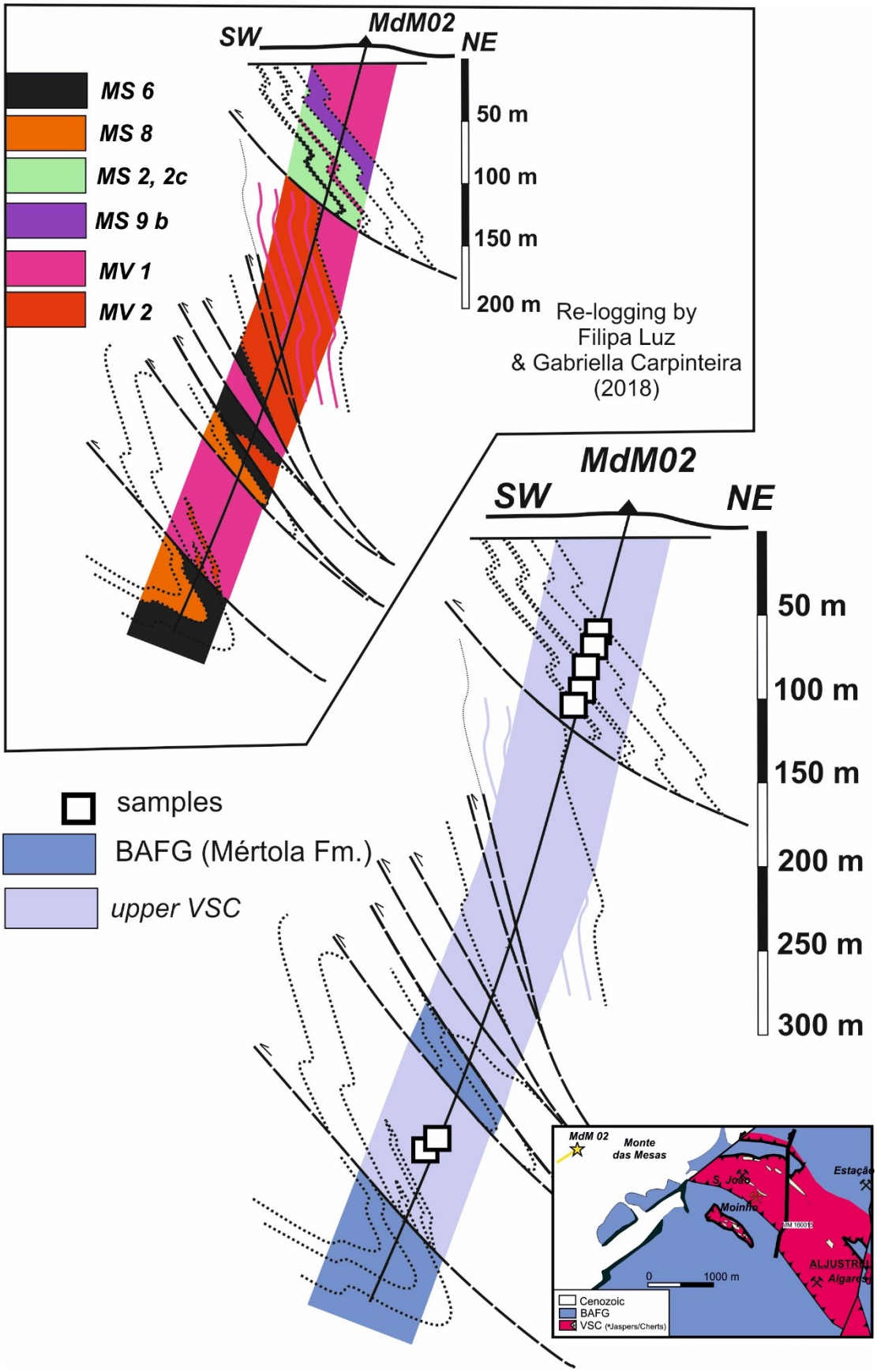

Figure 2.27 -- Interpretative geological cross-section comprising the MdM02 exploration drill-hole from Monte das Mesas sub sector, considering the observed polarity and the S_0/S_n angular relationships. Relative position and direction of the drilling in the geological map taken from *Figure 2.16*

2.3.4. Neves Corvo

Neves Corvo, located at the SE termination of the Rosário antiform, has been the focus of numerous comprehensive studies addressing stratigraphy, structural geology, physical volcanology, ore-forming processes and geochronology (e.g. Leca *et al.* 1983; Relvas et al, 2001, 2006a, b; Rosa *et al.* 2008; Oliveira *et al.* 2004, 2013; Solá *et al.* 2015; Albardeiro *et al.* 2017). The base of the stratigraphic succession comprises the PQG, forming a thick (more than 100 m) pile of dark-grey to black metapelites with intercalations of meta-siltstones and quartzites. These metapelites are likely of Upper Givetian to Upper Famenian (TA, BM and VCo Miospore biozones; Oliveira *et al.* 2004; Mendes *et al.* 2018). An erosive *hiatus* was suggested due to the absence of Frasnian miospore assemblages (e.g. Mendes *et al.* 2018). The overlying succession of the VSC comprises three informal divisions (*lower, middle* and *upper*). From bottom to top, the *lower* VSC succession consists of: (i) felsic metavolcanic rocks (Rhyolite 1; 363 ± 2.5 Ma – U/Pb, LA-ICP-MS in zircon; Solá *et al.* 2015; Albardeiro *et al.* 2017) and abundant layers with fiamme interpreted as pyroclastic (Rosa *et al.* 2008) interbedded with black, grey and green metapelites that typically include carbonate nodules (Corvo Formation, FC miospore biozone, Upper Fammenian); (ii) pyrite-rich black metapelites with intercalations of meta-siltstones (Neves Formation, LN miospores biozone, Strunian) interbedded with felsic metavoclanic rocks (mainly Rhyolite 2 – 360.5 ± 2.6 Ma, U/Pb, LA-ICP-MS in zircon; Solá *et al.* 2015; Albardeiro *et al.* 2017) characterized by coherent facies with thick and abundant hyaloclastite envelopes (Rosa *et al.* 2008); (iii) ore horizon, stratigraphically above Rhyolite 2, interbedded with the Neves Formation and dated of Strunian (360.7 ± 0.7 Ma; Oliveira *et al.*, 2004, Matos *et al.* 2011; Albardeiro *et al.*, 2017); and (iv) metajaspers (metacherts) and carbonates, locally including sericitic/chloritic metapelites, that may rest on the top of the orebodies or, more commonly, are found within the Neves Formation. The lithostratigraphy of the Rosário anticline is less well studied but, in general, similar to the one described for Neves Corvo. One difference is the voluminous mafic metavolcanic rocks at the base or in some sections of the lithostratigraphic succession. The *middle* VSC sequence, spreading from the LN to TS miospore biozones, includes mainly undifferentiated grey-siliceous to black metapelites, often bearing siliceous- phosphatic nodules (Graça Formation – TS miospore biozone). The *upper* VSC succession comprises several metasedimentary formations and a pile of felsic metavolcanic rocks (Rhyolite 3 – 353-349 Ma, U/Pb, LA-ICP-MS in zircon; Albardeiro *et al.* 2017) dominated by coherent and hyaloclastic facies (Rosa *et al.* 2008). The *upper* VSC metasedimentary series contains, from bottom to top: (i) intercalations of siliceous and black metapelites bearing carbonate/phosphate nodules

(Grandaços Formation, NM miospore biozone); (ii) purple and green (sericitic) to grey metapelites developing intercalations or inter-fingerings in one another; (iii) grey-green siliceous metapelites and meta-siltstones incorporating fine-grained volcanic-derived components (Godinho Formation, NM miospore biozone); and (iv) pyrite-rich black metapelites with layers of meta-siltstones (Brancanes Formation) at the transition to the overlying Mértola Formation (BAFG) which includes metapelites preserving miospore assemblages of the NM, VF and NC biozones (upper Visean to lower Serpukhovian; e.g. Oliveira *et al.* 2004; Mendes *et al.* 2018) interbedded with meta-greywackes.

Neves Corvo mine

The sampling survey at the Neves Corvo mine area was performed by the Lundin Mining team, according to their own logistic conditions. The sampling plan was previously discussed with geologists from Lundin Mining and further undertaken according to: (i) the representativeness of different Neves Corvo orebodies; (ii) the variety of metasedimentary facies / different ages / recognized formations of VSC and PQG units; and (iii) sulphide abundance, including the relative proximity to the orebodies. A total of forty-two samples were collected, mostly in underground mining works (29), complemented with five samples picked in drill-cores. The sampling survey appears to be downsized, particularly given the scale of this world class deposit; however, considering the available timeframe and logistic constraints, the 42 samples represent an acceptable solution that also supports the intended research and its goals.

In general, the collected VSC samples close to all the Neves Corvo orebodies vary between grey to black metapelites, also including intercalations or inter-fingerings of dark-grey metapelites in light-coloured metapelites bearing an evident silty component, besides less common green metapelites enriched in a siliceous component or volcanic-derived fraction. Due to logistic limitations, PQG samples were only collected near the Lombador orebody and varying between grey and black metapelites and fine-grained quartzite. For each lithostratigraphic unit there are samples with strong alteration/mineralization patterns, although some others are less overprinted by these changes. Nonetheless, almost all the samples clearly show mineralization fingerprints. **Figure 2.28**, **Figure 2.29** and **Figure 2.30** illustrate the relative position of most of the studied samples in different Neves Corvo geological cross-sections.

Montinho/Algaré

The sampling survey in Montinho and Algaré, two exploration prospects in the Rosário anticline) were collected in outcrops. Two samples were picked at Montinho, both representing the *upper* VSC succession (a mineralized black metapelite and a purple metapelite). Near the Rosário village, a sample from Grandaços Formation (according with unpublished Company reports) was picked; in Algaré, a sample of purple metapelite was collected. The purpose of this local sampling was to have some information on metapelite levels included in the very same Formations but located far from the Neves Corvo sulphide ore system.

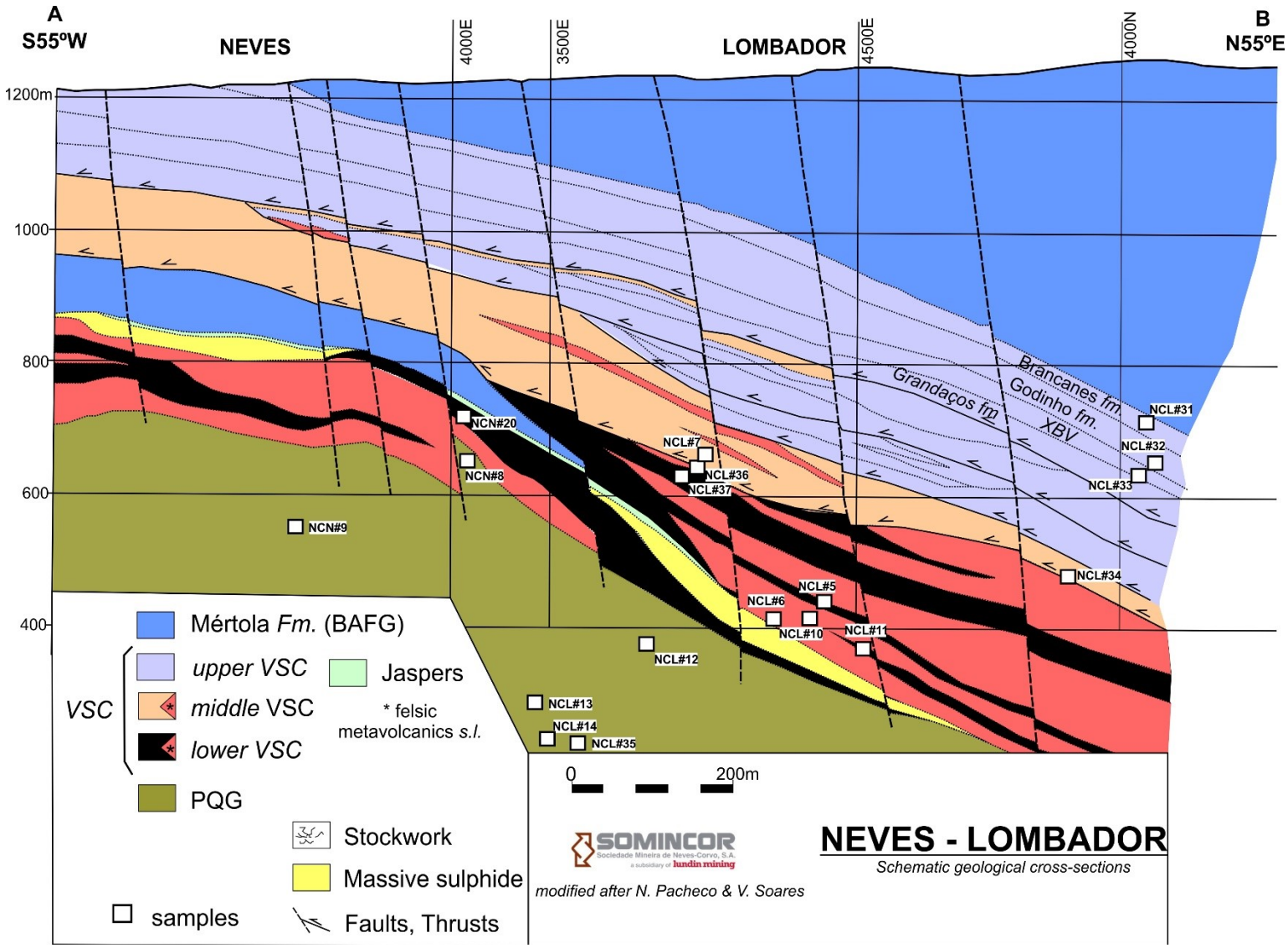

Figure 2.28 - Sampling distribution in a geological cross section of the Neves Corvo mine (Lombador and Neves orebodies, Neves Corvo sector.

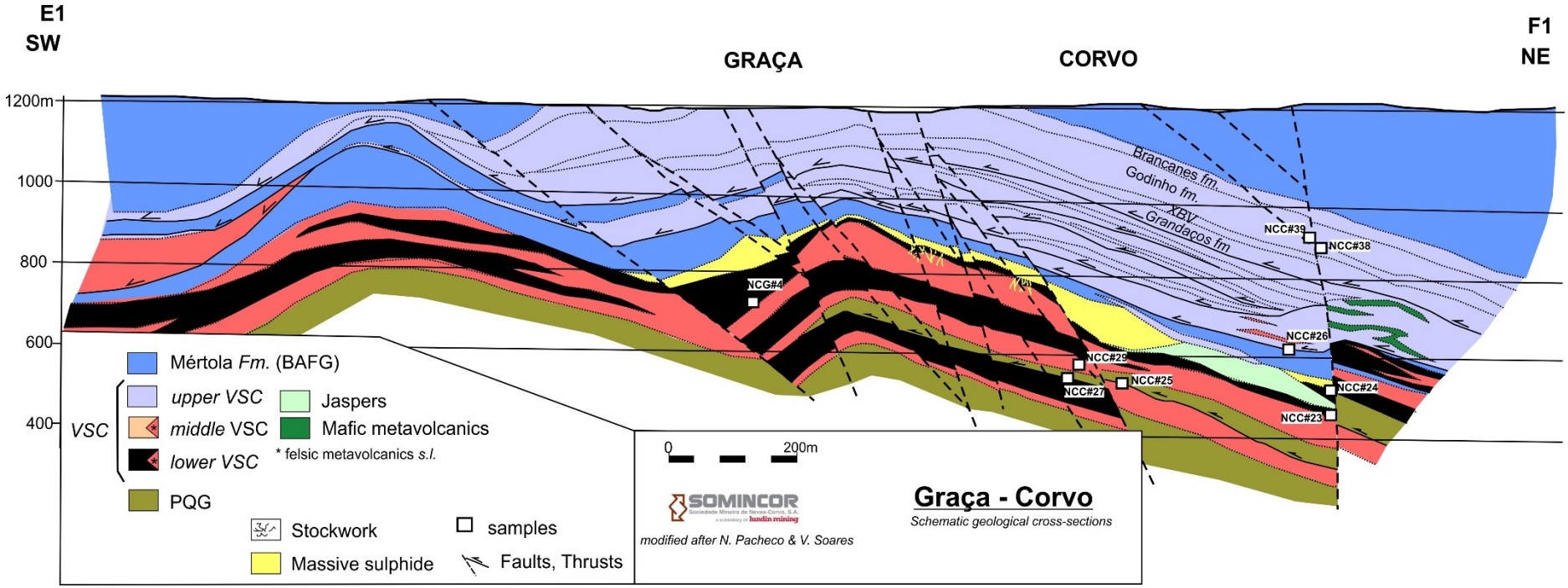

Figure 2.29 - Sampling distribution in a geological cross section of Neves Corvo mine (Graça-Corvo orebodies, Neves Corvo sector).

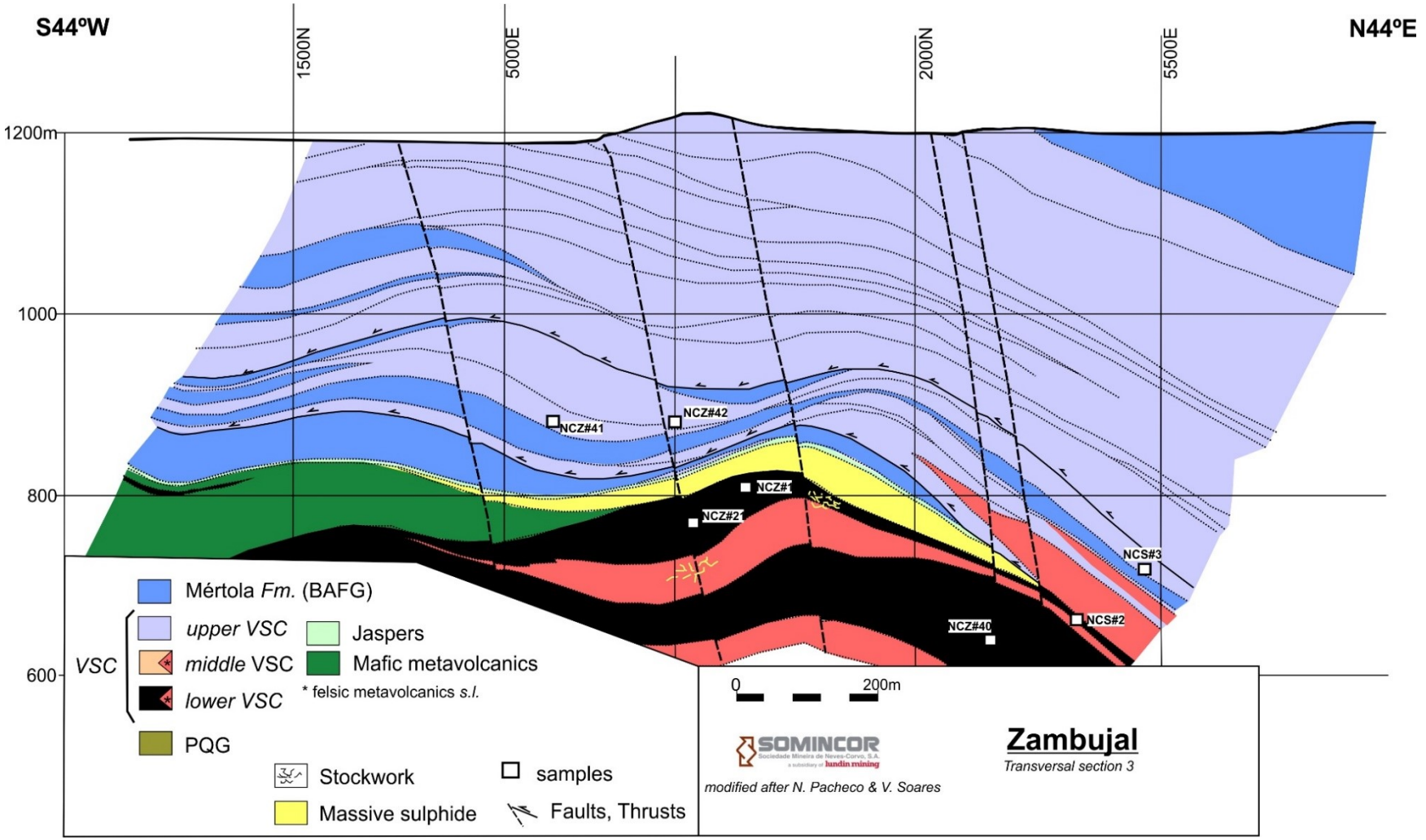

Figure 2.30 - Sampling distribution in a geological cross section of the Neves Corvo mine (Zambujal orebody. Neves Corvo sector).

2.4. Chrono-stratigraphic correlation

All the sampled sectors were presented in a concise way, although providing the relevant information to better constrain the main features of each sector and support the relative positioning (and understanding) of vertical/lateral facies variations recorded by the examined metapelites. Considering the information summarized in previous sections, the observations compiled for the final dataset (282 samples) and results from previous studies, a plausible chrono-stratigraphic correlation between the four studied sectors was established. Despite the specific attributes of each stratigraphic column (**Figure 2.31**), some general features could be recognized across all sectors. Since Neves Corvo is the best-constrained column, the age and relative positioning of different units were used as the main anchor to support the proposed correlation.

Main features of the stratigraphic units *(focusing on the studied sectors of the IPB Portuguese segment):*

I. PQG

Age constrains (Pereira *et al*., 2007, 2008; Oliveira *et al.,* 2004; Mendes *et al*., 2018, 2020)**:** The older age was found at the São Francisco da Serra anticline (AD miospore biozone, Eiafelian-Givetian) and recently in Neves Corvo mine (TA miospore biozone – middle Givetian). The PQG succession extends up to LN miospore biozone (Strunian), recognized in the Rosário and Albernoa anticlines.

Main features: This lithostratigraphic unit is characterized by a silicilastic succession mainly comprising black metapelites, quartzites, meta-siltstones and meta-quartzwackes, besides local meta-limestone lenses (e.g. Albernoa and Rosario Anticlinal). The Píncaros drill-hole (deeper PQG levels), located between Aljustrel and Albernoa, show a monotonous succession of dark-grey to black metasediments, continuously with an important fine-grained sandy quartz component (highly distal to facies), complemented with minor coarse-grained silicilastic rocks. To the SE, the relative abundance of coarse-grained siliciclastic rocks (mainly quartzites) tends to increase and becoming again quite significant once more in the IPB Spanish segment. Evidence of alteration and mineralization processes in the PQG sequences varies from discrete to intense. At Albernoa, the alteration intensity co-varies with the relative abundance of sulphides (pyrite ± chlacopyrite) often disseminated in the matrix and/or filling dense

fracture networks. At Neves Corvo, mainly at Lombador and Corvo orebodies, the PQG hosts the massive sulphide mineralization.

II. *lower* VSC

Age constrains (Pereira *et al*., 2007, 2008; Oliveira *et al.,* 2004, 2013 a, b; Rosa *et al.,* 2009; Solá *et al*., 2015; Albardeiro *et al*., 2017)**:** The older age recognized for this unit was found at the Neves Corvo mine (Vco miospore biozone), spreading up to LN miospore biozone, both belonging to Strunian (Upper Fammenian) and also recognized in other places of the Rosário Anticline, besides the Lousal and Azinheira de Barros sectors.

Main features: The *lower* VSC is characterized by a metasedimentary succession crossed by some metavolcanic rocks *s.l.* (see Rosa *et al*., 2004, 2008, 2009; Codeço *et al*., 2018, Carpinteira, 2020 for details on metavolcanics). The succession is mainly composed of black (dark-grey) metapelites that often host sulphide mineralization. Often, these metapelites present intercalations and/or inter-fingerings with levels including a significant fine-grained sandy quartz component. At Neves Corvo, there are two well-constrained Formations (Corvo and Neves, older to younger – respectively). The Neves Formation seems to correlate with the lithostratigraphic section hosting the mineralization in the Lousal mining area.

III. *middle* VSC

Age constrains (Pereira et al., 2007, 2008; Oliveira et al., 2013 a, b)**:** The *upper* VSC is poorly constrained, but it spreads between *lower* and *upper* VSC, so above the LN miospore biozone and below the CM miospores biozone. In general, it should represent the sedimentary deposition (irregularly?) occurred during the Lower Tournaisian.

Main features: The *middle* VSC metasedimentary pile comprises undifferentiated metapelites, occasionally including levels bearing fine-grained volcanic-derived components. Sulphide disseminations are rare, although late-Variscan veinlets with accessory amounts of pyrite ± chalcopyrite can be observed in some sections. At Albernoa and Lousal sectors, this metasedimentary sequence is crossed by metavolcanic rocks *s.l.* At the Rosario Anticlinal and Neves Corvo, this chronostratigraphic unit is represented by the Graça Formation.

IV. *upper* VSC

Age constrains (Pereira *et al*., 2007, 2008; Oliveira *et al.,* 2004, 2013 a, b; Rosa *et al.,* 2009; Solá *et al*., 2015; Albardeiro *et al*., 2017; EDM and ESAN MET technical reports): The Pu miospore biozone (Upper Tournasian to Lower Visean) is the most common timeframe indicated for metapelites forming the *upper* VSC. However, at the Gavião area, the Cm miospore biozone was identified. Thus, the lower limit of this unit should be placed close to the CM biozone, and its upper boundary near the NL miospore biozone (≈Upper Visean). At the Aljustrel mining area and surrounding exploration prospects, this unit is usually known as the Paraíso Formation. At Neves Corvo, the unit includes three formations (Godinho, purple metapelites and Grandaços).

Main features: The *upper* VSC is essentially a metasedimentary succession with occasional metavolcanoclastic rocks (see Barriga, 1983; Relvas, 1991; Leitão 1997, 2014; Barrie *et al.,* 2002; Barret *et al*., 2008; Inverno *et al*., 2008 for details on metavolcanics). The succession is composed of intercalations and/or inter-fingerings of purple-green, grey, black and siliceous metapelites; levels of metapelites with a distal volcanic-derived component and meta-jaspers/cherts are also common, although displaying quite variable thicknesses and macroscopic features. At Neves Corvo, some specific features were documented for this metasedimentary sequence, such as carbonate nodules (Grandaços *Fm*.). Commonly, the piles of green metapelites preserve effects related to alteration and mineralization processes, which are often denounced by folded veinlets or fracture infillings incorporating pyrite ± chalcopyrite ± pirrotite ± galena. Black metapelites are usually pyrite-rich, and metapelites with a volcanic-derived component display frequently disseminations of pyrite ± chalcopyrite. At Aljustrel, early-developed fractures (preceding the Variscan folding) are filled with carbonate ± chalcopyrite ± pyrite ± Co-Ni and Ni-Sb bearing sulphides ± As-Ni (Sb) bearing sulphosalts.

V. BAFG (Mértola *Fm.*)

Age constrains (Pereira *et al*., 2007, 2008): Palynological studies on metapelites forming the Mértola Formation indicates systematically NL^1 miospores biozone, excepting at Neves Corvo where miospore assemblages from the NL to NC biozones were described.

Main features: Typical flysch sequence, including intercalations of meta-greywackes and dark grey metapelites displaying quite variable thicknesses.

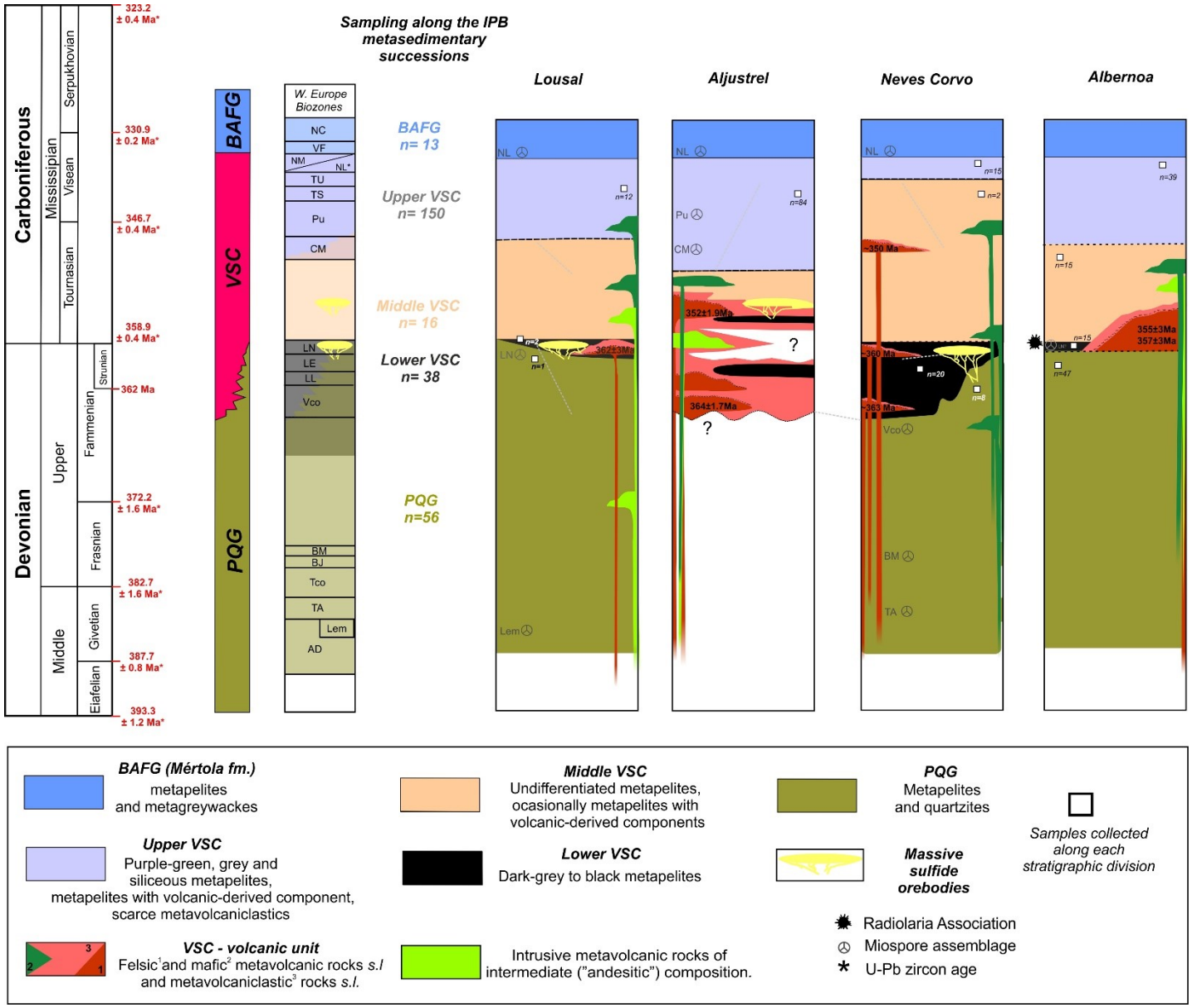

Figure 2.31 - Reconstructed lithostratigraphic columns of key sectors and chrono-stratigraphic regional correlation for the Portuguese segment of IPB (modified after Oliveira *et al.* 2013). Each column considers the available information on particular stratigraphic sections, comprehensively studied in recent years. All data from miospore assemblages/ages are from Pereira *et al.* (2007), Oliveira *et al.* (2013), Mateus et. al. (2014), Mendes *et al.* (2018), besides unpublished technical reports from ESAN MET and EDM. Metavolcanic rocks were dated by means of: (i) U-Pb, LA-ICP-MS in zircon for the Lousal sector (Oliveira *et al.* 2013); (ii) U-Pb, TIMS in zircon (Barrie *et al.*, 2002), and U-Pb and Lu-Hf, LA-ICP-MS in zircon (Rosa *et al.* 2009) for the Aljustrel sector; (iii) U-Pb, TIMS in zircon for the Rosario sector (Oliveira *et al.* 2013); (iv) U-Pb, LA-ICP-MS in zircon for the Neves Corvo sub-sector (Oliveira *et al.*, 2013; Solá *et al.* 2015; Albardeiro *et al.* 2017); and (v) U-Pb and Lu-Hf, LA-ICP-MS in zircon for Albernoa sector (Rosa *et al.* 2009). Twelve metapelite samples from the BAFG were collected and analyzed but not reported in this work..

2.5. Concise petrographic characterization of metapelites

2.5.1. Metapelites

The PQG comprises a metasedimentary succession dominated by black to dark-grey (locally greenish) metapelites with intercalations of variable thickness (from ~1 cm up to metric) of meta-siltstones, meta-quartzwackes and/or quartzites. In general, the relative abundance of coarse-grained metasediments in the examined four key sectors decreases from ENE to WSW, possibly reflecting constraints imposed by the sedimentary basin paleo-morphology (strongly segmented and asymmetric, increasingly deeper towards W-WSW) and proximity to the supplying continental sources.

Black to dark-grey (locally greenish) metapelites displays lenticular bedding composed by dark coloured (phyllosilicate-rich) metapelite in a lighter coloured metapelite bearing a fine-grained (quartz-dominated) sandy component. These rocks are mostly composed of very fine-grained white mica and quartz, and the common accessory minerals are tourmaline and rutile. Coarse-grained metasediments include poorly sorted quartz grains besides variable amounts of subordinate white mica/chlorite ± zircon ± rutile; sulphides are observed but their abundance is highly variable and most often related to quartz ± chlorite ± pyrite ± chalcopyrite hydrothermal infillings of structures developed (or reactivated) during Late-Variscan strike-slip faulting. Dark-grey (locally greenish) metapelites do not commonly incorporate sulphide phases, despite the presence of sub millimetric-sized pyrite ± chalcopyrite disseminations in a few places, irregularly coupled with discrete pyrite ± quartz infillings of micro-fracture networks. The PQG section at Neves Corvo is the sole known exception, specifically at the Lombador orebody where a voluminous stockwork (variably Cu-Zn enriched) exists. In this case, the rock mineral assemblage includes enhanced amounts of quartz (± chlorite ± carbonate ± REE-bearing phosphates), pyrite and chalcopyrite (± tetrahedrite ± sphalerite ± galena).

The *lower* VSC comprises mainly dark-grey to black metapelites associated with felsic metavolcanic rocks. This lithostratigraphic unit is considered the main host of massive sulphide ores in the Portuguese segment of IPB, possibly excluding the Aljustrel sector (that includes Gavião and Monte das Mesas prospects) where it was not firmly recognized so far. The dark-grey to black metapelites are made of sub(-rounded) quartz grains scattered in a groundmass of fine-grained white mica variably enriched in non- or poorly-structured organic matter; higher abundances of quartz grains, sometimes displaying coarser sizes, generate the observed intercalations of black meta-siltstones. These metapelites typically contain framboidal pyrite

and sub-millimeter sized disseminations of pyrite ± chalcopyrite ± sphalerite ± galena, at times along with folded veinlets/veins of quartz (± siderite) + pyrite ± pyrrhotite ± sphalerite. Limited to well-developed mineralized stockworks are observed in *lower* VSC at Lousal/Sesmarias and Neves Corvo, respectively. In some of these samples, namely at Sesmarias, early-developed cassiterite grains were found, as well as As-, Co- and Ni-bearing sulphide phases of imprecise identification due to their small size; several cassiterite grains are crossed by fracture-controlled infillings of quartz ± siderite ± chlorite + pyrite + chalcopyrite ± galena, which were also reported in other studies on samples from the Lousal mine (e.g. Fernandes, 2011).

The *middle* VSC, well-preserved in the Albernoa sector and recognized at Neves Corvo, includes grey-greenish to dark-grey and light purple metapelites, the latter being somewhat siliceous. Usually, these rocks comprise variable proportions of quartz and white mica, besides accessory amounts of zircon and rutile; sometimes, the relative proportion of quartz is high enough to classify the sample as a meta-siltstone. In some lithostratigraphic sections, these metapelites are interfingered with similar rocks incorporating distinct volcanic-derived components (see below). Sulphides are not commonly observed, despite of rare (pyrite?) box-works. However, late-developed veinlets of quartz ± chlorite ± pyrite ± chalcopyrite (criss-crossing S_1 and textural arrangements due to deformation and metamorphic recrystallization) can be frequent, particularly in rock domains adjoining Late-Variscan strike-slip fault zones.

The *upper* VSC is mostly composed of fine-grained metasediments, locally complemented by metavolcaniclastic rocks. The metasedimentary pile includes voluminous dark-grey to black metapelites with minor interbedded meta-siltstones that frequently came along with facies arrays characterized by intercalations and/or inter-fingerings of green-purple, dark-grey to black, and grey (siliceous) metapelites; stratigraphic levels incorporating volcanic-derived components and metajaspers/cherts are also present in many sections of this facies arrays. Black and dark-grey metapelites forming the *upper* VSC sequences have a mineralogical composition similar to comparable rock types in PQG and other VSC sections. The green purple metapelites comprise very fine-grained quartz grains embedded in a dominant phyllosilicate-rich matrix. This matrix includes abundant disseminated hematite (± magnetite) as a distinct mineral phase of purple metapelites, often also enclosing elongated aggregates (like *rod* structures *sensu lato*) of quartz ± Mg-rich carbonate ± chlorite ± apatite ± pyrite ± chalcopyrite ± digenite that replace primary components of possible volcaniclastic origin (Luz et al., 2019). Green metapelites consist mainly of white mica (that prevails over chlorite) and

contain tourmaline, rutile and authigenic apatite as main accessory minerals; in some samples, disseminations of very fine-grained pyrite are significant (Luz et al., 2019).

In the Portuguese segment of IPB, the *upper* VSC is not recognized as a horizon that potentially may host noteworthy massive sulphide ores, notwithstanding the common observation of sulphides in the sedimentary series with dominant black or green metapelites. In the former rocks, disseminations of framboidal pyrite and/or pyrite ± chalcopyrite are usual. Many green metapelites show abundant, early developed (because affected by S_1) micro-quartz structures with disseminated pyrite ± chalcopyrite ± pirrotite ± galena. At the Aljustrel sector, these rocks comprise frequent disseminations and/or early-fracture infillings of As-Co-Ni- and Ni-Sb-bearing sulphides along with As-Co-Ni- and As-Ni(-Sb)-bearing sulphosalts. Ulmannite, gersdorffite and cobaltite are the prevailing mineral phases so far identified (Luz *et al*., 2019), regularly coming together with chalcopyrite (Aljustrel mine and Monte das Mesas prospect) and/or REE-bearing phosphates (Gavião prospect). These mineral phases are less abundant in the studied metapelites from the *upper* VSC of Neves Corvo mine, even though the smaller grains of As-Ni(-Sb)-bearing sulphosalts in some samples were recognized. **Figure 2.32** highlight the main features of metapelites

2.5.2. Metapelites with volcanic-derived components

Metapelites incorporating volcanic-derived components were identified in all the previously described PQG (confined to the uppermost levels of this lithostratigraphic unit), *lower* VSC, *middle* VSC and *upper* VSC sections; their higher abundance is recorded in the *upper* VSC, occurring near sequences that comprises metavolcanic rocks. These metapelites comprise variable proportions of (sub-)millimetic sized quartz and/or feldspar ($Ab_{87.5-99.9}$) mineral fragments within a very fine-grained (violet to green-coloured in hand sample) matrix mostly composed of white mica (± chlorite) that is locally enriched in dolomite and/or calcite. Volcanic-derived components can reach up to 50 vol.% and consist of: (i) quartz fragments showing angular to sub-rounded shapes that commonly display late dissolution features due to pressure solution; (ii) feldspar fragments, typically displaying angular shapes and effects of hydrolysis of variable intensity; and (iii) elongated aggregates of quartz ± Mg-rich carbonate ± chlorite ± apatite ± pyrite ± chalcopyrite ± digenite (rimming chalcopyrite) that likely replace primary volcaniclastic components (Luz *et al*., 2019). **Figure 2.33** highlight the main features of metapelites with a volcanic derived component.

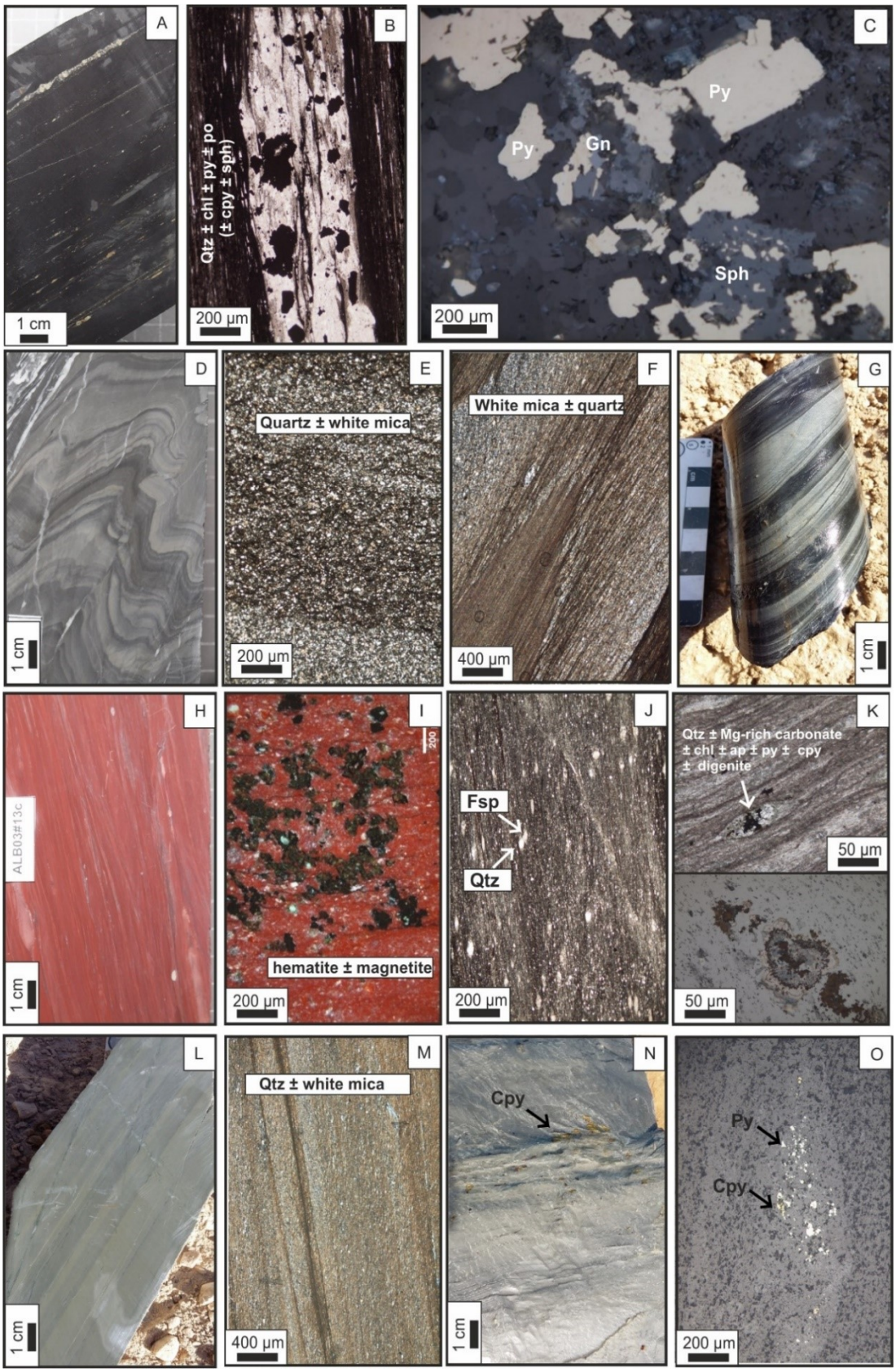

(caption next page)

Figure 2.32 - Selected hand samples and photomicrographs representing the main metapelite subgroups. Black metapelites **[A to C]: (A)** Pyritic black metapelite (EDS1-B, 304.56 m); **(B)** Early fractures (prior to S_1) filled with quartz + chl + py ± cpy ± sph (EDS1-C, 305.15 m); **(C)** Local enrichments in py ± sph ± gn in black metapelite (18-1-E, 80.70 m); Grey(-greenish) to dark-grey metapelites **[D to G]**: **(D)** Intercalations/inter-fingering of dark-grey to grey(-greenish) metapelites enriched in fine-grained sandy component (ALB02, 244.15 m); **(E)** fine-grained sandy layer (impure quartzite) (ALB03#35, 562.00 m); **(F)** Inter-fingering of metapelites and sandy-rich layers (ALB03#1, 64.05 m); **(G)** Rhythmic succession of dark colored and lighter (sandy-rich) metapelites (ALB03#9, 213.80 m); Purple metapelites **[H to K]: (H)** Typical purple metapelite (ALB03#13c, 311.50m); **(I)** Hematite (± magnetite) enrichments (X47, outcrop sample); **(J)** Purple metapelite recording volcanic-derived (feldspar and quartz) contribution (ALB03#13c, 311.50 m); **(K)** upper image (transmitted light) - elongated aggregates of quartz ± Mg-rich carbonate ± chlorite ± apatite ± pyrite ± chalcopyrite ± digenite replacing primary components of possible volcanogenic origin (EDS1-K, 427.40 m); lower image (reflected light) – detail of previous aggregate revealing distribution of neo-formed sulphide grains; Green metapelites **[L to O]: (L)** Intercalation/inter-fingering bands in green metapelites (abundant very fine-grained white mica) caused by differences in the relative abundance of various mineral phases (mostly quartz and phyllosilicates; ALB02, 245.45 m); **(M)** Typical green metapelite, mainly composed of quartz and white mica (ALB03#18, 301.70m); **(N)** Sulphide association in common early-developed quartz veinlets with pyrite and chalcopyrite (ALB02#15, 94.05 m); **(O)** Fine disseminations of pyrite ± chalcopyrite in the matrix of green metapelites (ALB02#15, 94.05 m).

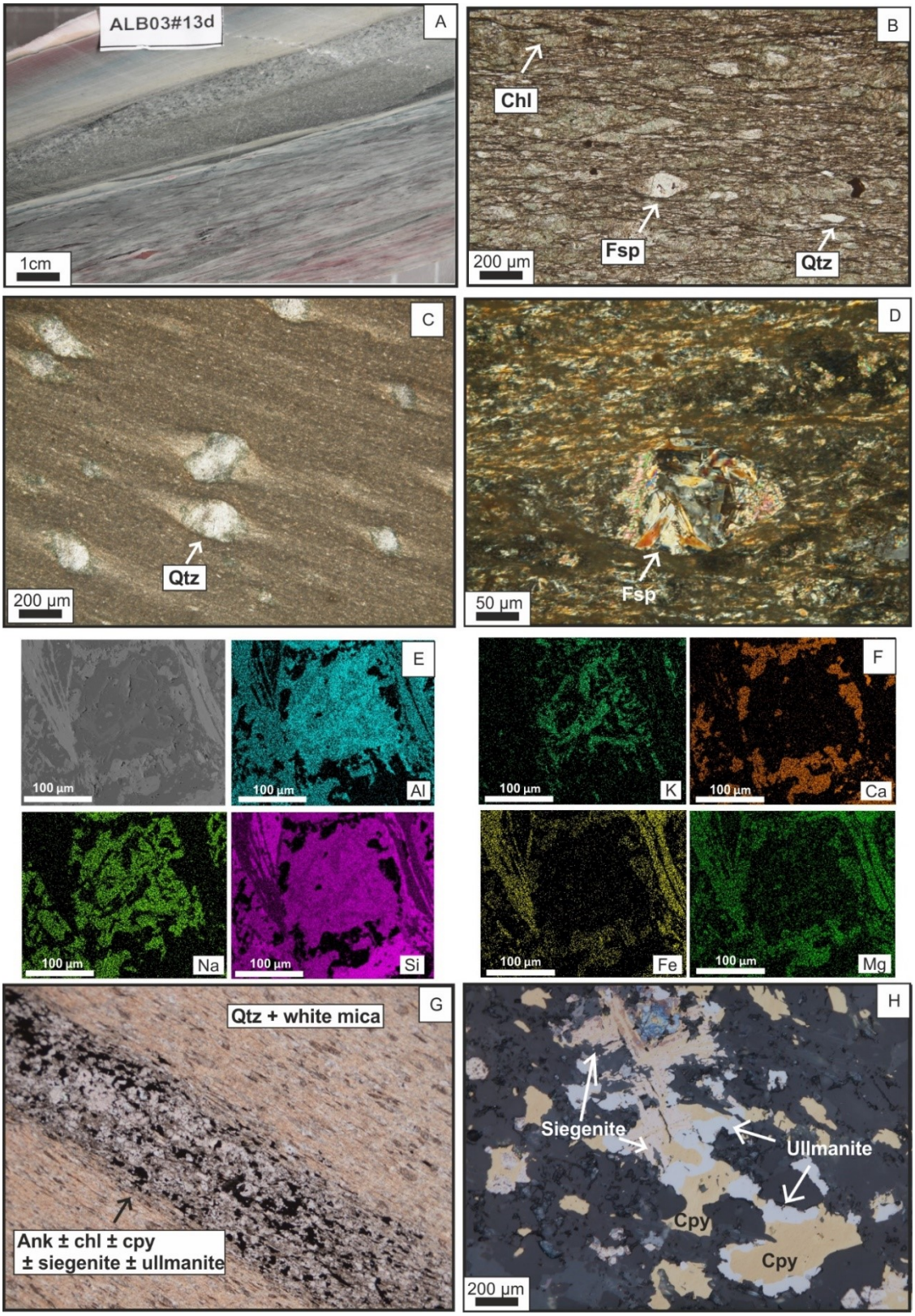

Figure 2.33 - Selected hand samples and photomicrographs representing tuffaceous metapelites **[A to H]: (A)** Green-violet metapelite incorporating volcanic-derived feldspar ± quartz (ALB03#13d, 311.50 m); **(B)** Quartz and feldspar deformed porphyroclasts in a fine-grained metasedimentary matrix mostly composed of muscovite ± chlorite (ALB03#13a, 305.40m); **(C) (D)** Details of altered (sericitized) feldspar deformed prophyroclasts (ALB03#13a, 305.40m); **(E)** and **(F)** Chemical map compositions highlighting the feldspar alteration by K-phyllosilicate (ALB03#13a, 305.40m). **(G)** and **(H)** Early fractures (prior to S_n) filled with carbonate + chalcopyrite ± pyrite ± Co-Ni- and Ni-Sb-bearing sulphides ± As-Co-Ni and As-Ni (-Sb)-bearing sulfosalts (EDS1-H, 385.20 m).

SECTION 3

3. Geochemical tools and analytical methods

3.1. The approach

Considering the aims of the PhD program, a combination of methods was chosen to address the intended issues regarding mineral chemistry, multi-elemental lithogeochemistry and multi-system isotopic (Sr, Nd and Pb) whole-rock geochemistry.

After careful examination, one-hundred and seventy-five samples were selected from petrographic studies which soon showed the need to recognize the type and relative abundance of sulphide phases in metapelites. This allowed to categorize the samples into three main sets, as follows: (i) samples lacking sulphide phases at a macro and micro-scale (shortly referred hereafter as "No-sulphide"); (ii) pyrite-bearing samples ("Py-bearing") where pyrite (diagenetic and/or recrystallized) is the sole sulphide present or largely prevails over sphalerite coupled with rare chalcopyrite; and (iii) samples including the typical sulphide assemblage in the IPB ("Mineralized"), i.e., pyrite + sphalerite ± chalcopyrite ± galena along with trace or minor amounts of As, Co, Ni ± Sb mineral phases (**Figure 3.1**). Such categorization was preserved during the subsequent analytical data handling (whole-rock lithogeochemistry and multi-system isotope geochemistry).

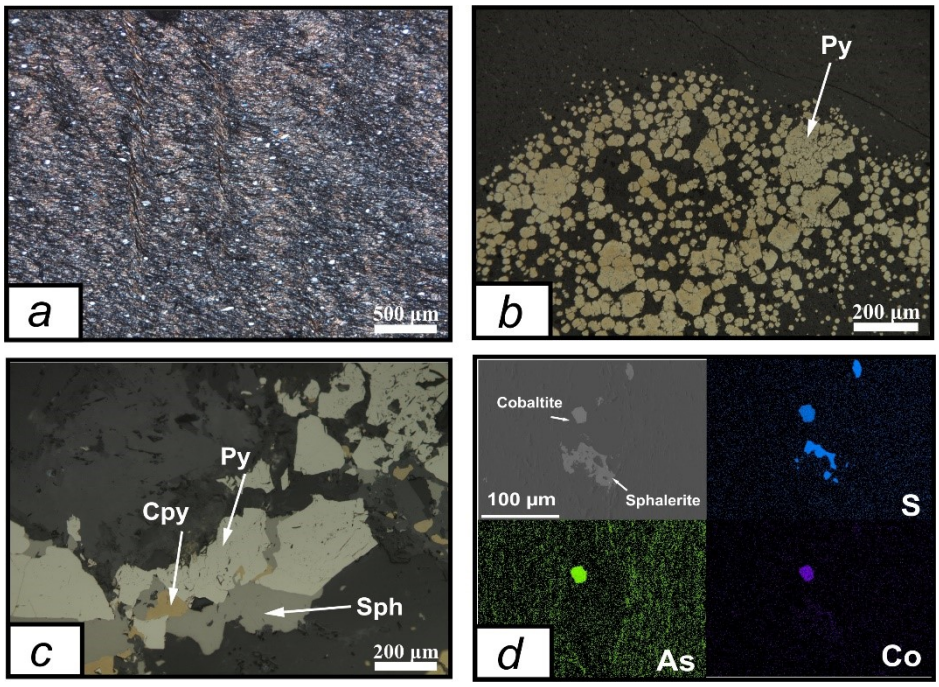

Figure 3.1 - Selected photomicrographs representing the three categories based on the sulphide assemblage and abundance; (a) metapelite belonging to the "No-sulphide" group (ALB03#16, 334 m); (b) Framboidal pyrite aggregates partially recrystallized in a metapelite sample of the "Py-bearing" group (NCN#7, underground, Neves Corvo mine); (c) Typical sulphide assemblage (pyrite ± chalcopyrite ± sphalerite) found in samples of the "Mineralized" group (NCC#20, underground, Neves Corvo mine); (d) Accessory mineral phases bearing As, Co, Ni ± Sb, such as cobaltite associated with chalcopyrite in early fractures (prior to S_1) displaying quartz infillings (FM#5, 113.50 m).

3.2. Mineral chemistry studies

The mineral chemistry studies were performed in 40 selected samples with an Electron-Microprobe Analyser (EPMA). More than 1000 quantitative analyses of different mineral phases were obtained. This approach allowed to:

i. Confirm some mineral identifications made under optical microscopy whenever in presence of doubtful observations, mostly due to the extreme fine granularity displayed by the metapelitic rocks;

ii. Identify mineral phases whose optical chracteristics and/or occurence modes hindered precise recognition;

iii. Put in evidence compositional differences between different generations of the same mineral phase and assess their influence in the characterization of geochemical tendencies or in the estimation of some key parameters (such as the temperature conditions);

iv. Distinguish compositional differences between settings in which the same generation of mineral phase occurs, and evaluate the effect of local chemical gradients irrespectively of their origin;

v. Ascertain the mineral phases hosting minor and trace elements detected by whole-rock geochemistry, thus contributing to the understanding of key features related to the relevance of these chemical elements in provenance studies and/or subsequent transformations (*e.g.* hydrothermal processes); and

vi. Ensure the statistical significance of the results obtained, whenever possible, and document new and/or uncommonly described mineral phases forming the examined rock types.

3.2.1. Analytical methods and conditions

All the polished thin sections (*ca.* 30 μm) were prepared and petrographically inspected at FCUL. Mineral chemistry studies used the EPMA at FCUL, a JEOL JXA8200 equipped with four wavelength-dispersive spectrometers and calibrated with metallic and mineral standards provided by Astimex Scientific, Ltd. The EPMA was operated with an accelerating voltage of 15kV, a beam current of 25 nA, a beam diameter of 5 μm and an acquisition time of 20 s for peaks and 5 s for background.

The EPMA data were numerically processed by considering the ideal stoichiometry of each mineral group and an unpublished algebraic procedure which extends the method reported by

Droop (1987) for valence partitioning of multivalent elements, which considers all relevant stoichiometric relationships. **Table 3-1**, **Table 3-2** and **Table 3-3** shows the elements, crystals and detection limits used for different mineral phases at the FCUL facilities.

Table 3-1 *– Detection limits and analytical condition of the microprobe for each mineral group; Chlorite and Apatite.*

Element	Crystals	Standards	Detection limit (ppm)
		Chlorite	
Ca	PETJ	Bustamite	134
Si	PETH	Pyrope	115
Cr	PETJ	Chromium Oxide	199
Na	TAP	Jadeiite	114
Cs	PETJ	Pollucite	336
K	PETH	Sanidine	66
Mn	PETJ	Bustamite	252
Mg	TAP	Chlorite	103
Zn	LIF	Sphalerite	568
Fe	LIFH	Almandine	187
Al	TAP	Chlorite	120
Ni	LIF	Nickel Sulfide	403
Ba	LIFH	Benitoite	423
		Apatite	
F	TAP	Apatite	871
Sr	PETJ	Celestite	605
P	PETH	Apatite	131
Nd	PETJ	REE 6	417
Na	TAP	Jadeite	1224
Ce	LIF	Monazite	964
Ca	PETH	Diopside	77
Mn	PETJ	Bustamite	249
Mg	TAP	Periclase	87
Cl	PETJ	Tugtupite	96
Fe	LIFH	Almandine	191

Table 3-2 *- Detection limits and analytical condition of the microprobe for each mineral group; Feldspar. Mica, Zircon and Carbonate.*

Element	Crystals	Standards	Detection limit (ppm)	Element	Crystals	Standards	Detection limit (ppm)
		Feldspar				*Zircon*	
Mn	PETJ	Bustamite	367	**La**	PETJ	Monazite	444
Al	TAP	Pyrope	201	**Ca**	PETJ	Apatite	165
Fe	LIFH	Almandine	279	**Ti**	PETJ		233
F	TAP	Fluorite	559	**Al**	TAP	Almandine	154
Cl	PETH	Tugtupite	91	**Mg**	TAP	Periclase	114
Si	PETH	Sanidine	95	**F**	TAP		909
Mn	PETJ	Bustamite	230	**Zr**	TAP		393
Na	TAP	Tugtupite	97	**Ce**	LIF	Monazite	1237
		Mica		**Th**	PETJ	Monazite	1016
				P	PETJ	Apatite	372
Si	PETJ	Olivine	273	**Fe**	LIFH	Almandine	239
Rb	PETH	CAL.STD	499	**Nd**	LIFH	REE 6	434
Ti	PETJ	Rutile	211	**Hf**	LIFH		610
Na	TAP	Jadeite	115	**Si**	PETH		195
K	PETH	Sanidine	61				
		Chromium				*Carbonate*	
Cr	PETJ	Oxide	182				
Mg	TAP	Chlorite	109	**Mg**	TAP	Almandine	122
Cs	PETJ	Pollucite	351	**Ca**	PETJ	Calcite	146
Ba	LIFH	Barite	328	**Fe**	LIFH	Magnetite	213
Mn	PETJ	Bustamite	244	**Mn**	PETJ	Bustamite	290
Al	TAP	Almandine	126	**Zn**	LIFH	Sphalerite	390
		Nickel					
Ni	LIF	Silicide	380	**Sr**	PETH	Celestite	234
Fe	LIFH	Kaersutite	186	**Ba**	PETJ	Barite	441
F	TAP	Fluorite	770	**Na**	TAP	Jadaite	107
Cl	PETJ	Tugtupide	106	**Ti**	PETJ	Rutile	236
				Ce	PETJ	Monazite	515
				La	PETJ	Monazite	459

Table 3-3 *- Detection limits and analytical condition of the microprobe for each mineral group; Rutile and Sulphides.*

Element	Crystals	Standards	Detection limit (ppm)
		Rutile	
P	PETJ	Apatite	301
Na	TAP	Jadeite	111
S	PETJ	Stibinite	234
Ba	LIFH	Benitoite	496
Bi	PETJ	Bismuth Selenide	690
Mg	TAP	Priclase	89
Pb	PETJ	Galena	457
V	LIFH	V	195
Ag	PETJ	Ag	282
As	TAP	Galium Arsenide	339
K	PETJ	Sanidine	137
Cr	LIFH	Chromium Oxide	202
Ca	PETJ	Diposide	158
Al	TAP	Plagioclase	100
Sn	PETJ	Cassiterite	361
Fe	LIFH	haematite	201
Zn	LIF	Willemite	637
Si	TAP	Rutile	135
Ni	LIFH	Nickel Silicide	249
Ti	PETJ	Rutile	260
Ta	LIF	LiTaO3	1117
Zr	TAP	Zirconia	268
Mn	PETJ	Rhodonite	284
Cu	LIFH	Cuprite	304
Co	LIF	Skutterudite	302
Nb	TAP	Metallic Nb	293
W	LIF	Metallic W	1195

Element	Crystals	Standards	Detection limit (ppm)
		Sulphides	
S	PETH	Pyrite	99
Fe	LIFH	Pyrite	283
Cu	LIFH	Cuprite	470
Zn	LIF	Spahlerite	1040
Pb	PETJ	Galena	861
As	TAP	Galium Arsenide	344
Sb	PETJ	Stibinite	416
Ni	LIF	Pentlandite	594
Sn	PETJ	Metallic Sn	359
Co	LIFH	Skutterudite	288
Mn	PETJ	Bustamite	386
Au	PETH	Au	411
Ag	PETJ	Ag	359
Bi	PETJ	Bismuth Selenide	3931
Ge	TAP	Metallic Ge	291
Se	TAP	Bismuth Selenide	244
In	PETJ	metallic In	414
Cd	PETJ	Cd	366
Mo	PETH	Molybdnite	594
Ga	TAP	Metallic Ga	241
Te	PETJ	CAL-STD	392

3.3. Whole-rock geochemistry studies

The whole-rock geochemistry analyses were performed in two-hundred and sixty-two samples considering the four sampled sectors, the main lithostratigraphic units (PQG, VSC – *lower*, *middle*, *upper*), proximity to massive sulphide orebodies and relative position to mineralized horizons (footwall and hanging-wall). The multi-elemental analyses were done in a certified commercial lab, Activation Laboratories (ActLABS, Canada) that offers a pre-defined package – 4E research (with ICP-MS option); for more details see below. This analytical package provides 60 elements and low detection limits, allowing to:

i. Characterize the chemical fingerprint of metasedimentary stratigraphic units, using the data to better constrain and/or infer about the sediment sourcing, sedimentary environments and regional overprints (such as seafloor metasomatism and further transformations triggered by Variscan metamorphism);

ii. Verify which element variations typify the sedimentary settings surrounding and/or hosting the IPB sulphide mineralization; and

iii. Define, if possible, which element variations can be used as proxies for sulphide ore-forming systems in the IPB (syn- and epigenetic).

3.3.1. Analytical methods

The 270 powder samples (including duplicates and replicates) for whole-rock geochemistry were prepared at FCUL. The analytical methods included in the 4E research analytical package offered by Activation Laboratories Ltd (ActLABS, Canada) comprised inductively coupled plasma mass spectrometry (ICP-MS) and instrumental neutron activation analysis (INAA) after a total digestion and lithium metaborate/tetraborate fusion. All the details and detection limits of this analytical package is shown on **Table 3-4**.

Table 3-4 – Elements analyzed and respective detection limits and methods (ActLABS, Canada).

Element	*Unit*	*Detection Limit*	*Method*	*Element*	*Unit*	*Detection Limit*	*Method*
SiO_2	%	0.01	FUS-ICP	**U**	ppm	0.01	FUS-MS
Al_2O_3	%	0.01	FUS-ICP	**V**	ppm	5	FUS-ICP
Fe_2O_3 (T)	%	0.01	FUS-ICP	**Y**	ppm	1	FUS-ICP
MnO	%	0.001	FUS-ICP	**Zr**	ppm	1	FUS-ICP
MgO	%	0.01	FUS-ICP	**La**	ppm	0.05	FUS-MS
CaO	%	0.01	FUS-ICP	**Ce**	ppm	0.05	FUS-MS
Na_2O	%	0.01	FUS-ICP	**Pr**	ppm	0.01	FUS-MS
K_2O	%	0.01	FUS-ICP	**Nd**	ppm	0.05	FUS-MS
TiO_2	%	0.001	FUS-ICP	**Sm**	ppm	0.01	FUS-MS
P_2O_5	%	0.01	FUS-ICP	**Eu**	ppm	0.005	FUS-MS
LOI	%		FUS-ICP	**Gd**	ppm	0.01	FUS-MS
Total	%	0.01	FUS-ICP	**Tb**	ppm	0.01	FUS-MS
Ba	Ppm	1	FUS-ICP	**Dy**	ppm	0.01	FUS-MS
Be	Ppm	1	FUS-ICP	**Ho**	ppm	0.01	FUS-MS
Bi	Ppm	0.1	FUS-MS	**Er**	ppm	0.01	FUS-MS
Cd	Ppm	0.5	TD-ICP	**Tl**	ppm	0.05	FUS-MS
Cs	Ppm	0.1	FUS-MS	**Tm**	ppm	0.005	FUS-MS
Cu	Ppm	1	TD-ICP	**Yb**	ppm	0.01	FUS-MS
Ga	Ppm	1	FUS-MS	**Lu**	ppm	0.002	FUS-MS
Ge	Ppm	0.5	FUS-MS	**Au**	ppb	1	INAA
Hf	Ppm	0.1	FUS-MS	**Ag**	ppm	0.5	MULT INAA/TD-ICP
I	Ppm	0.1	FUS-MS	**As**	ppm	1	INAA
Mo	Ppm	2	FUS-MS	**Br**	ppm	0.5	INAA
Nb	Ppm	0.2	FUS-MS	**Co**	ppm	0.1	INAA
Ni	Ppm	1	TD-ICP	**Cr**	ppm	0.5	INAA
Pb	Ppm	5	TD-ICP	**Hg**	ppm	1	INAA
Rb	Ppm	1	FUS-MS	**Ir**	ppb	1	INAA
S	%	0.001	TD-ICP	**Sb**	ppm	0.1	INAA
Sn	Ppm	1	FUS-MS	**Sc**	ppm	0.01	INAA
Sr	Ppm	2	FUS-ICP	**Se**	ppm	0.5	INAA
Ta	Ppm	0.001	FUS-MS	**W**	ppm	1	INAA
Th	Ppm	0.05	FUS-MS	**Zn**	ppm	1	MULT INAA/TD-ICP

3.4. Isotope geochemistry

One hundred and twelve samples were selected and suitably prepared for multi-system (Pb-Nd-Sr) isotopic geochemistry. The selection criteria were similar to that presented in the previous section (section 3.3). However, as Neves Corvo has been subjected to a wide series of studies using stable and radiogenic isotopes, all the samples collected in this sector were analysed to assist as reference. The integrative interpretation of whole-rock Pb, Nd and Sr isotopic compositions was used to:

i. Trace the primary sources involved in the rock-forming processes and characterize the sedimentary environments where the topmost PQG and VSC metapelites were deposited;

ii. Infer about fluid sources that could be related to the main hydrothermal events, including those related to mineralizing processes);

iii. Define geochemical/isotopic criteria useful to characterize hydrothermal alteration patterns and, if possible, infer about the targets with high metal content and/or large tonnage.

3.4.1. Analytical method and conditions

The whole-rock Pb, Nd and Sr isotopic analyses were performed at the Centro de Pesquisas Geocronológicas (CPGeo), Instituto de Geociências, University of São Paulo, Brazil. About 75 to 100 mg of the same powders used for whole-rock elemental analysis were taken into solution by acid digestion (3:1 mixture of HF + HNO_3) in Savillex beakers on hot plate at 110ºC for 10 days; no spikes were added. The Sr, Nd and Pb were separated from the same sample solution in ion-exchange columns following the procedures described in Sato *et al.* (1995), Tassinari *et al.* (1996) and Babinski *et al.* (1999). The $^{87}Rb/^{86}Sr$, $^{147}Sm/^{144}Nd$, $(^{206}Pb/^{204}Pb)_i$, $(^{207}Pb/^{204}Pb)_i$ and $(^{206}Pb/^{204}Pb)_i$ ratios were calculated using Rb, Sr, Sm, Nd, U, Th and Pb abundances determined in the same rock-powders by ICP-MS in ActLabs and previously used in whole-rock geochemistry multi-elemental analysis (Luz *et al.*, 2020). The Sr isotopic compositions were determined with a Thermo Triton mass spectrometer and the $^{87}Sr/^{86}Sr$ ratio was normalized to $^{86}Sr/^{88}Sr = 0.1194$. Replicate analysis of NBS 987 standard (n = 100) yielded a mean $^{87}Sr/^{86}Sr$ ratio of 0.710254 ± 0.000018 (2σ) during the period when the analytical work was performed. The Nd isotopic ratios were performed on a Thermo Neptune Plus ICP-MS. Measurements of $^{143}Nd/^{144}Nd$ were normalized to $^{146}Nd/^{144}Nd = 0.7129$ and the average (n = 107) of $^{143}Nd/^{144}Nd$ ratio for the JNdi-1 standard was 0.512003 ± 0.00003 (2σ). Pb isotopic

compositions were measured with a Finnigan MAT 262 Mass Spectrometer. Replicate analysis (n = 60) of NBS-981 common Pb standard yielded $^{206}Pb/^{204}Pb = 16.892 \pm 0.006$, $^{207}Pb/^{204}Pb = 15.430 \pm 0.008$, $^{208}Pb/^{204}Pb = 36.509 \pm 006$. The Pb ratios were corrected for mass fractionation of 0.12% amu ($^{207}Pb/^{204}Pb$) and 0.13% amu ($^{206}Pb/^{204}Pb$, $^{208}Pb/^{204}Pb$) based on the NBS-981 analysis. Procedure blanks are 169 ± 76 pg for Sr, 83 ± 21 pg for Nd and 100 ± 30 pg for Pb and, considered to be negligible for the size of the analysed samples.

The age-corrections of Sr, Nd and Pb isotopic compositions were performed considering 360 Ma for PQG/*lower* VSC and 350 Ma for *middle/upper* VSC (Luz *et al.,* 2020 and references therein). The Nd T_{DM} model ages were calculated assuming a linear depletion model with present-day depleted values of $^{143}N/^{144}Nd = 0.513151$ and $^{147}Sm/^{144}Nd = 0.2137$ (Peucat *et al.*, 1998). Two-stage T_{DM} model ages were computed for samples with $^{147}Sm/^{144}Nd$ ratio outside the typical range of upper continental crust-derived sediments (0.09 - 0.13; e.g. Goldstein *et al.*, 1984); a $^{147}Sm/^{144}Nd$ value of 0.114 was used to estimate the sample evolution path prior to depositional age (Goldstein and Jacobsen, 1988; Li and Schoornmaker, 2014).

SECTION 4

4. Overview of the published and submitted papers

4.1. Statement of own contribution

As already mentioned in Section 1, two papers were already published and a third one recently submitted, all of them gathering the contribution of different authors. Hereby I confirm that the information provided below on the involvement of each author is accurate and complete.

Section 4.1. - **Luz, F.**, Mateus, A., Figueiras, J., Tassinari, C.C.G., Ferreira, E., Gonçalves, L., (2019) *Recognizing metasedimentary sequences potentially hosting concealed massive sulfide accumulations in the Iberian Pyrite Belt using geochemical fingerprints*. Ore Geology Reviews 107, 973-998, https://doi.org/10.1016/j.oregeorev.2019.03.020

(i) **F.L**. was involved in sample preparation and subsequent data collection, management and analysis, as well as the numerical handling of isotopic data in cooperation with E. Ferreira. All the authors participate in the interpretation of results. The first version of the manuscript was written by **F.L**. and A. Mateus, incorporating comments and contributions from E. Ferreira and J. Figueiras. The final version was edited after receiving constructive comments and English improvements from Prof. Reinaldo Saéz (Univ. Huelva, Spain), Jan Peter (Geological Survey of Canada) and an anonymous reviewer. **F.L**. was also responsible for the editing of all the figures and tables;

Section 4.2. - **Luz, F.,** Mateus, A., Rosa, C., Figueiras, J., (2020). *Geochemistry of Famennian to Visean metapelites from the Iberian Pyrite Belt: deepening criteria to resolve sedimentary issues and exploration targeting for massive sulphide deposits, Natural Resources Research, DOI: 10.1007/s11053-020-09686-4*

(ii) **F.L**. carried out the re-logging of various drillings and sampling, besides all data collection and management. Data interpretation was iteratively done with A. Mateus. Significant insights on regional comparative lithostratigraphy were gathered through fruitful discussions with C. Rosa. A first draft of the manuscript was prepared by **F.L.**, along with all the figures and tables. A deep revision of this early version was afterwards done by A. Mateus, considering the comments as well of C. Rosa and J. Figueiras. The final version of the manuscript was prepared after receiving the suggestions of minor and major revisions raised by an anonymous reviewer and Marcus Kuzamn (CSIRO, Australia), respectively;

<u>Section 4.3.</u> - **Luz, F.**, Mateus, A., Ferreira, E., Tassinari, C.C.G., Figueiras, J. (submitted to Economic Geology). *Pb-Nd-Sr isotope geochemistry of metapelites from the Iberian Pyrite Belt and its relevance in vectoring massive sulphide ore systems*.

(iii) **F.L.** accomplished all the tasks regarding sample preparation and isotopic data handling. The analytical dataset was obtained at Universidade de São Paulo (Brazil) and involved the support of its resident technical staff. **F.L** wrote the early version of the manuscript and edited all the figures and tables, considering the comments and suggestions from the remaining authors. A thoroughly revision of this version was afterwards done by A. Mateus, considering as well further comments raised by E. Ferreira. The compilation and integrative interpretation of the available isotopic data on IPB were done by **F.L.** and A. Mateus. Detailed interpretation of results was carried out in deep collaboration with E. Ferreira, A. Mateus and C.C.G. Tassinari.

4.2. Recognizing metasedimentary sequences potentially hosting concealed massive sulfide accumulations in the Iberian Pyrite Belt using geochemical fingerprints

DOI: https://doi.org/10.1016/j.oregeorev.2019.03.020

Results of a multi-element geochemical study of 133 samples representing PQG and VSC metasedimentary rocks selected from drill-holes and outcrops throughout the Albernoa area (≈713 km^2) are reported in this paper along with Sr, Nd and Pb isotopic data for a subset of 12 samples from VSC (see the full version in Appendix 1.1). The main findings can be summarized as follows:

(i) The Zr/Sc, Th/Sc, Eu/Eu* relationships indicate that an evolved "felsic source" (resulting from sediment recycling) was the source of the prevalent siliciclastic component in of all the samples analysed, irrespectively of the lithostratigraphic unit.

(ii) The source-areas implicated in the basin supply were most likely the same and, according to the Chemical Index of Alteration (CIA) values, were significantly weathered while supplying sediment to the basin from Middle Devonian to Visean time.

(iii) The main sedimentary fractions comprise a clayey-derived component ($20 \leq Al_2O_3/TiO_2 \leq 30$, $Sc/TiO_2 > 0.002$, $Ga/TiO_2 > 0.001$) and a (fine-grained) sandy-derived component ($\approx 5 \leq Al_2O_3/TiO_2 \leq 20$, $Sc/TiO_2 < 0.002$, $Ga/TiO_2 < 0.001$, $0.01 \leq Zr/TiO_2 \leq 0.1$).

(iv) The clayey- and sandy-derived components are, in places, variable mixed with volcanic-derived fractions in metapelites that are typical of VSC, but also present in the uppermost sections of PQG. The incorporation of volcanic-derived material is recorded by a clear increase of Al_2O_3/TiO_2 ratios (from ≈15-20 up to 45-65) along with a variable increase in Sc/TiO_2 and Ga/TiO_2 values and variably decreased Zr/Al_2O_3 ratios.

(v) Samples including the prevalent clayey-derived component are mostly confined to VSC sections, irrespectively of the sampled sector. In contrast, the sandy-derived component is predominant in a vast number of samples representing different VSC settings and various PQG lithostratigraphic levels. The volcanogenic component is distinctly more abundant in some metapelites from the Ervidel-Roxo and Figueirinha-Albernoa sectors. In general, VSC samples have the following chemical characteristics $2.5 \leq SiO_2/Al_2O_3 \leq 6.5$, $0.02 \leq TiO_2/Al_2O_3 \leq 0.06$

and 0.2 ≤ (Cao+Na_2O+K_2O)/Al_2O_3 ≤ 0.25, whereas PQG samples display 2.5 ≤ SiO_2/Al_2O_3 ≤ 12, 0.08 ≤ TiO_2/Al_2O_3 ≤ 0.58 and (CaO+Na_2O+K_2O)/Al_2O_3 ≤ 0.3. The cross-plot Al_2O_3/TiO_2 *vs*. Zr/Al_2O_3 (**Figure 4.1**) illustrates quite well the relative contribution of each main component.

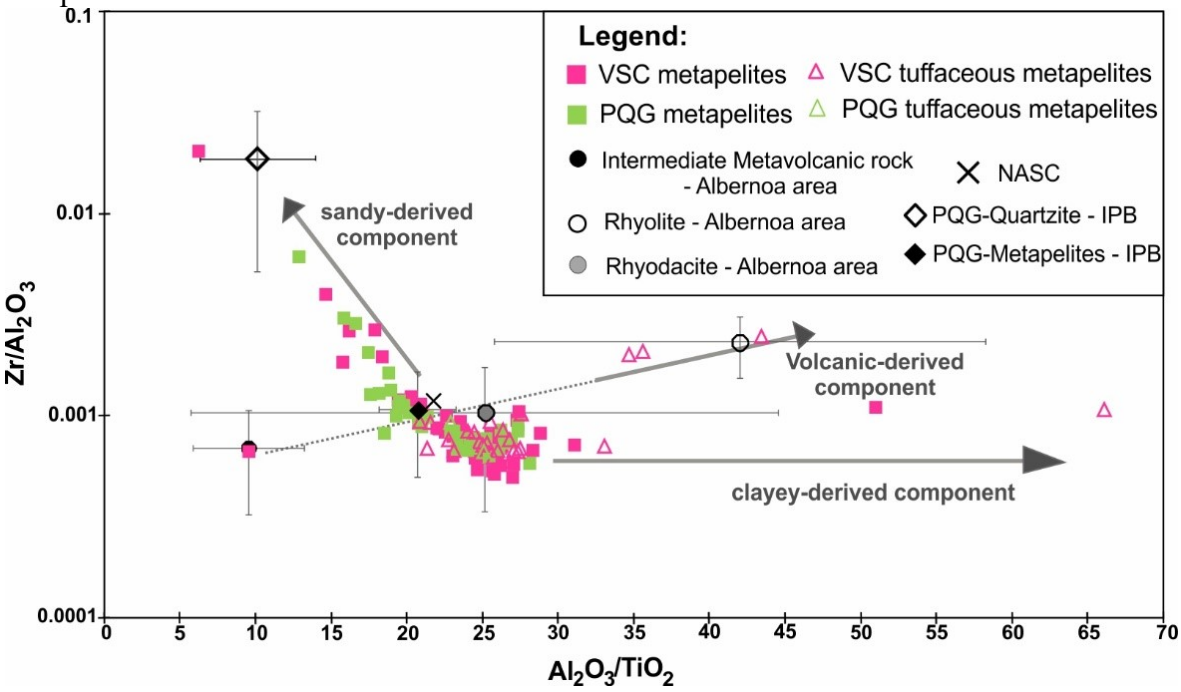

Figure 4.1 - Zr/Al_2O_3 vs. Al_2O_3/TiO_2 plot illustrating the main composition deviations displayed by the examined samples (n = 133); mixtures of clayey-derived or (fine-grained) sandy-derive continental components with volcanic-derived (and/or hydrothermal) fractions. For reference, and besides the ratios typifying NASC (Condie, 1993), the average ratios and corresponding standard deviation measures calculated for PQG-quartzite and metapelite (n = 75; different sites of IPB, Jorge, 2009) and VSC-metavolcanic rocks of Albernoa (intermediate composition n = 9, rhyodacite n = 27, rhyolite n = 22; Codeço et al., 2018) are displayed.

(vi) Samples with Fe_2O_3/TiO_2 ratios ≥ 10 and Al_2O_3/(Al_2O_3+Fe_2O_3+MnO) ratios ≤ ≈0.6 (**Figure 4.2**) record the influence of early-developed (pre-Variscan metamorphism and deformation) hydrothermal imprint on the prevalent siliciclastic component that, in the case of some metapelites, is variably mixed with volcanic-derived fractions; and

(vii) The ratios 5×[(Fe_2O_3+MgO+MnO)/Al_2O_3], (As+Sb)/Sc and (Cu+Zn+Pb)/Sc can be used as discriminants of barren and altered/mineralized metasedimentary sequences in the IPB (**Figure 4.3**). Values for all the three ratios between 1.0 and 10.0 indicate the influence of seafloor metasomatism processes, and when ≥ 10.0 indicates close proximity to hydrothermal vent site that may potentially be associated with massive sulfide mineralization.

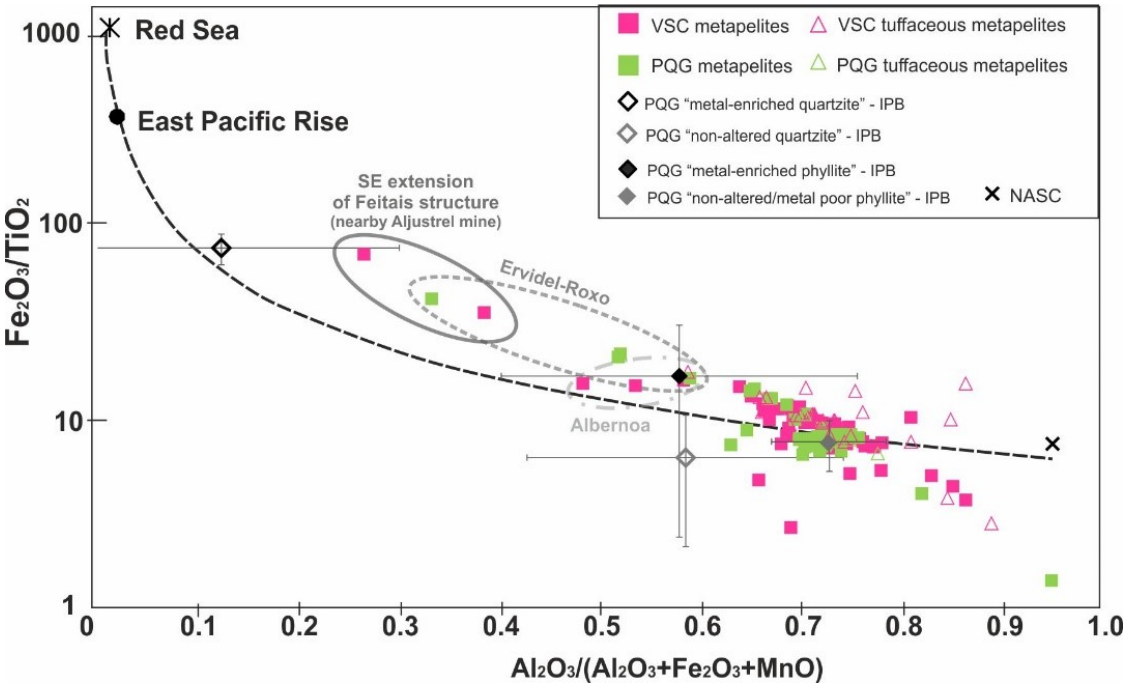

Figure 4.2 **-** Fe_2O_3/TiO_2 vs. $Al_2O_3/(Al_2O_3+Fe_2O_3+MnO)$ diagram for the complete Albernoa dataset illustrating a possible mixing strip between a "terrigenous" end-member (given by the samples clustering) and a conceptual "exhalative-hydrothermal" term represented by the composition of the East Pacific Rise and/or the Red Sea brine pool (*e.g.* Marchig et al., 1982; Goodfellow et al., 2003). NASC and PQG phyllites and quartzites (metal enriched and non-altered/metal poor) were plotted for reference (Condie, 1993; Jorge, 2009, respectively). The mixing strip is represented by the black dashed line and the samples where the "hydrothermal component" is more evident separated by ellipses with sector labels.

(viii) Sr and Nd isotopic characteristics for a small subset of 12 samples from VSC sections show highly radiogenic $^{87}Sr/^{86}Sr_{(360\ Ma)}$ and negative $\varepsilon Nd_{(360\ Ma)}$ values that indicate derivation mostly from an old, reworked, upper continental crustal source.

(ix) Pb isotope signatures for these 12 samples also support an upper crustal derivation without significant juvenile contamination. Isotope ratios characterizing the main siliciclastic components are somewhat disturbed by the addition of volcanic-derived components, recording also modifications by hydrothermal alteration/mineralization processes from less radiogenic fluids. Close proximity to a concealed sulfide mineralization hosted in VSC might be indicated by a decreased $^{87}Sr/^{86}Sr_{(360\ Ma)}$, and increased $\varepsilon Nd_{(360\ Ma)}$, $^{207}Pb/^{204}Pb$ and $^{206}Pb/^{204}Pb$ (age-corrected) isotopic ratios (**Figure 4.4**).

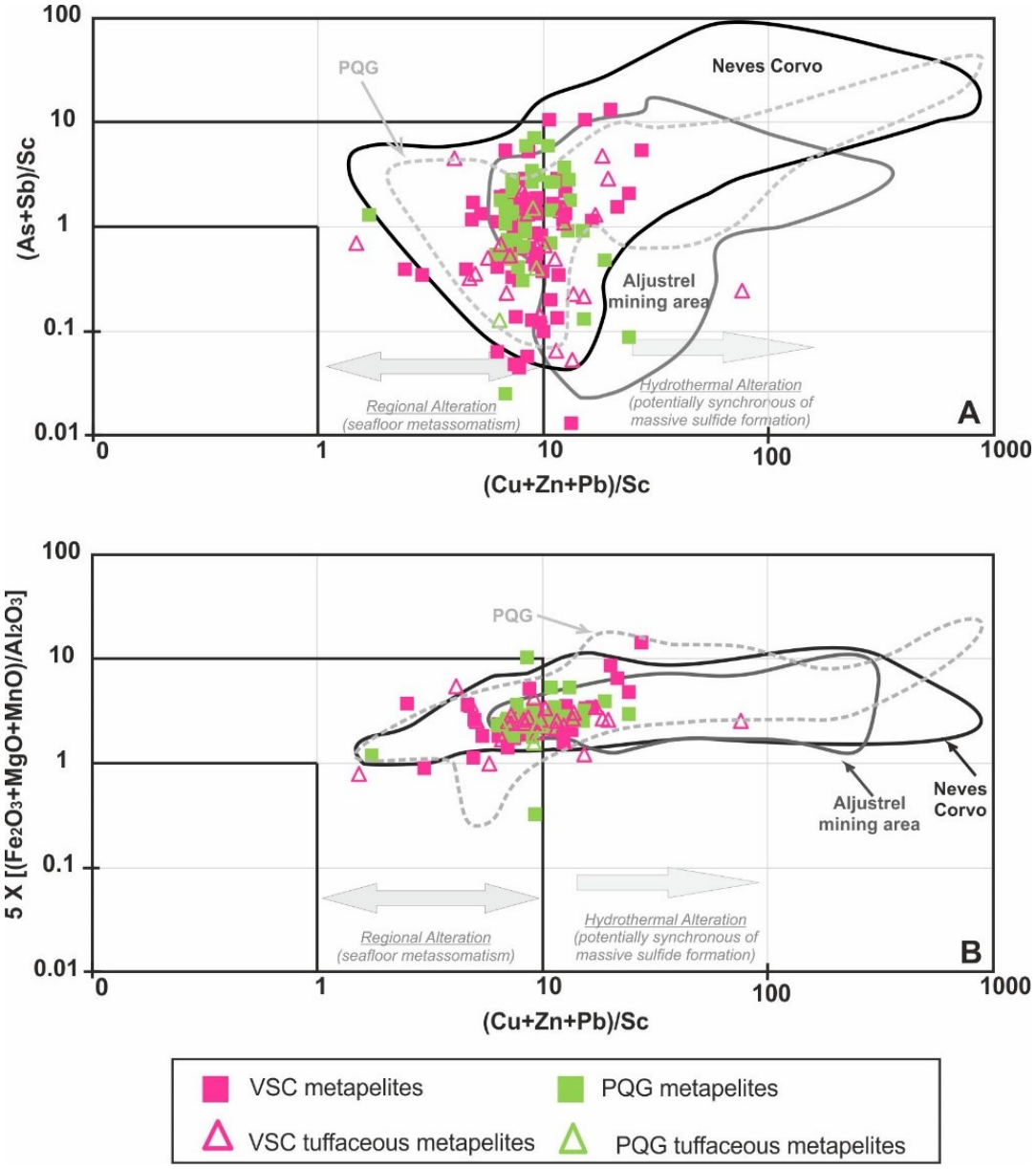

Figure 4.3 – (As+Sb)/Sc vrs.(Cu+Zn+Pb)/Sc and (Fe_2O_3+MgO+MnO)/Al_2O_3 vrs. (As+Sb)/Sc diagrams illustrating the chemical effects related to post-sedimentary transformations. Values between 1.0 and 10.0 of these geochemical ratios trace, conceivably, the influence of oceanic metasomatism processes (regional alteration pattern); ratios above 10.0 indicate the proximity of hydrothermal discharges potentially related to ore-forming systems. For comparison purposes, compositional fields for the Aljustrel and Neves Corvo mining areas are indicated using the available whole-rock geochemical data for metasedimens. Delimitation of the Aljustrel field considered 79 samples of VSC metapelites and tuffaceous metapelites picked in (i) exploitation drillings [Feitais and Moinho orebodies], (ii) underground-mining works [Feitais and Moinho orebodies] and (iii) recent exploration brownfield drillings [S. João, Gavião and Monte das Mesas]; for details see Luz et al. (2018). The Neves Corvo field was delineated on the basis of 42 samples of PQG and VSC metapelites and tuffaceous metapelites collected in various levels of the underground-mining works in Zambujal, Semblana, Graça, Lombador, Neves and Corvo orebodies (ongoing research). The PGQ compositional field includes 75 samples representing (non-altered and altered/mineralized) phyllites and quartzites reported in Jorge (2009).

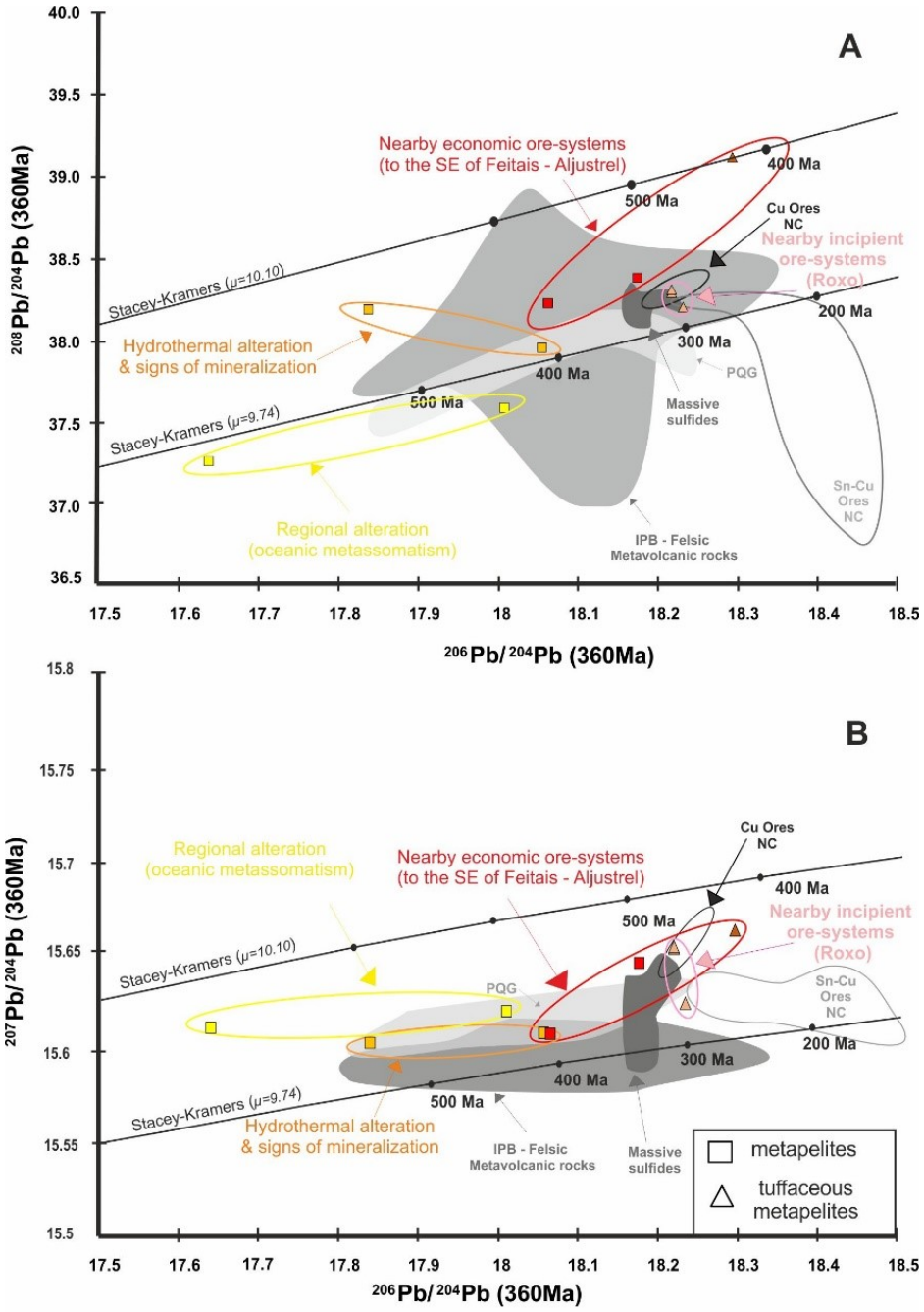

Figure 4.4 - $^{206}Pb/^{204}Pb$ versus $^{207}Pb/^{204}Pb$ and $^{208}Pb/^{204}Pb$ (age-corrected, 360Ma) diagrams for selected samples of VSC metapelites and tuffaceous metapelites from the Albernoa area. Reference fields of IPB sulfide ores (Marcoux, 1998, Pomiès et al., 1998; Relvas et al., 2001) were classified into three groups: (i) Sn-Cu- ores from Neves Corvo (n = 8); (ii) Cu-ores from Neves Corvo (n = 8); and (iii) common massive sulfide ores (São Domingos n = 3, Lousal n = 4, Aljustrel n = 11, Lagoa Salgada n = 3, Riotinto n = 14, and some other deposits in Spain n = 18). The (age corrected) Pb-Pb ratios for metavolcanic (n = 14) and metasedimentary (n = 5) rocks were calculated considering data reported in Marcoux (1998) and in Jorge (2009), respectively. In the $^{206}Pb/^{204}Pb$ vrs $^{208}Pb/^{204}Pb$ diagram, the large extension of the "metavolcanic field" reflects the correction made: given the lack of whole-rock concentration values for Th, the $^{232}Th/^{204}Pb$ ratio was estimated for each sample on the basis of their $^{238}U/^{204}Pb$ values, assuming $^{232}Th/^{238}U = 3.62$ (as in Marcoux, 1998).

4.3. Geochemistry of Famennian to Visean Metapelites from the Iberian Pyrite belt: implications for Provenance, Paleo-Redox Conditions and Vectoring to Massive Sulfide Deposits

DOI: https://doi.org/10.1007/s11053-020-09686-4

As documented in sections 2 and 3, four key sectors of the IPB Portuguese segment were revisited and 262 samples collected to characterize the geochemical features of metapelites from PQG and VSC representing barren and fertile settings. The full version of this paper can be found in Appendix 1.2), supporting the following main conclusions.

(i) The surveyed PQG and VSC successions include a large variety of fine-grained clastic sediments deposited from Fammenian to Visean, lately (≈315 Ma) subjected to metamorphic recrystallization under low grade conditions.

(ii) The shale/silty facies prevail in VSC, indicating deposition in confined, tectonic-controlled, basins that affect the previously developed siliciclastic platform and may comprise also different volcanic products.

(iii) No major compositional differences exist between metapelites forming the examined PAG and VSC sections, and the observed geochemical trends mostly represent different proportions of clay/mud-rich and quartz-rich components. Thus, SiO_2 concentrations range from ≈55 to ≈70 wt% for most of the samples. The Al_2O_3 and K_2O concentrations are also relatively high and mostly distributed in the ≈15-20 wt% and ≈2-4 wt% intervals, respectively. Total iron, as Fe_2O_3, hardly exceeds 10 wt%, except when metapelites are mineralized. Abundances of CaO, MgO, Na_2O and MnO are typically low (< ≈2 wt%, ≈2 wt%, ≈1.5 wt% and ≈0.5 wt%, respectively). TiO_2 and P_2O_5 contents rarely exceeds 0.25 wt% and 0.75 wt%, respectively.

(iv) Incorporation of volcanic-derived components (such as feldspar clasts) contribute to some compositional deviations. In addition, mineral transformations developed during diagenesis and/or hydrothermal alteration/mineralization processes (particularly chloritization and silicification, often coupled with carbonate deposition, quite evident in samples forming the pre horizon or placed at the orebodies footwall) superimpose an imprint on the primacy composition. This imprint is better resolved with minor and trace elements (see concluding remark vii). Nonetheless, higher median abundances of SiO_2. Fe_2O_3 and MnO characterize mineralized samples in Neves Corvo, Aljustrel, Lousal and Sesmarias; and MgO

concentrations, albeit irregular, tend to increase in samples forming the "Py-Bearing" group. Consistent comparison readings require normalization of abundances of elemental oxides in relation to Al_2O_3 or TiO_2, which display a good positive correlation ($r = 0.72$; *p-value* < 0.05) despite some scatter related to metapelites bearing an important quartz sandy-derived fraction (common in PQG). As a result, Fe_2O_3/TiO_2 ratios above 10 are the most reliable indicator of hydrothermal/mineralizing processes, separating all metapelite samples from ore horizons or orebodies footwall. The MgO/TiO_2 (or MgO/Al_2O_3) and ratios of alkali or alkaline-earth elements relative to Al_2O_3 or TiO_2 show considerable dispersion and do not coherently separate subsets of samples sharing similar mineralogical features, even though sensitive to the presence of secondary mineral phases, such as chlorite or carbonates.

(v) The detected clay/mud-rich and quartz-rich components forming the examined metasediments largely derived from different sources of felsic (granitic) to intermediate (granodiorite to quartz-diorite) composition (**Figure 4.5**).

(vi) A significant number of PQG metapelites display features indicative of high compositional maturity of the primary sediments to which they are related, pointing also to accessory contributions from old-sedimentary sources. Incorporation of volcanic-derived fractions contribute to some compositional deviations, evident in several *upper* VSC sections (**Figure 4.5**).

(vii) Mineral transformations developed during diagenesis and/or hydrothermal alteration/mineralization processes superimpose an imprint on the primary composition. In general, the normalized patterns for minor and trace elements are internally consistent (**Figure 4.6**) revealing a gradual increase in the abundances of As, Sb, Cu, Zn, Pb, Co, Ni (± V) as the amount and diversity of sulphide phases enlarge. In mineralized samples, As and Sb positive anomalies are quite often above 100×NASC, going up to 50-300×NASC for Cu, Zn and Pb; for Ni, Co and V the maximum values recorded are 5-20×NASC. This elemental increase is coupled by a distinct, although irregular, decline of Rb, Sr and Ba contents, reflecting the progression of compositional changes likely related to hydrothermal alteration processes (namely chloritization).

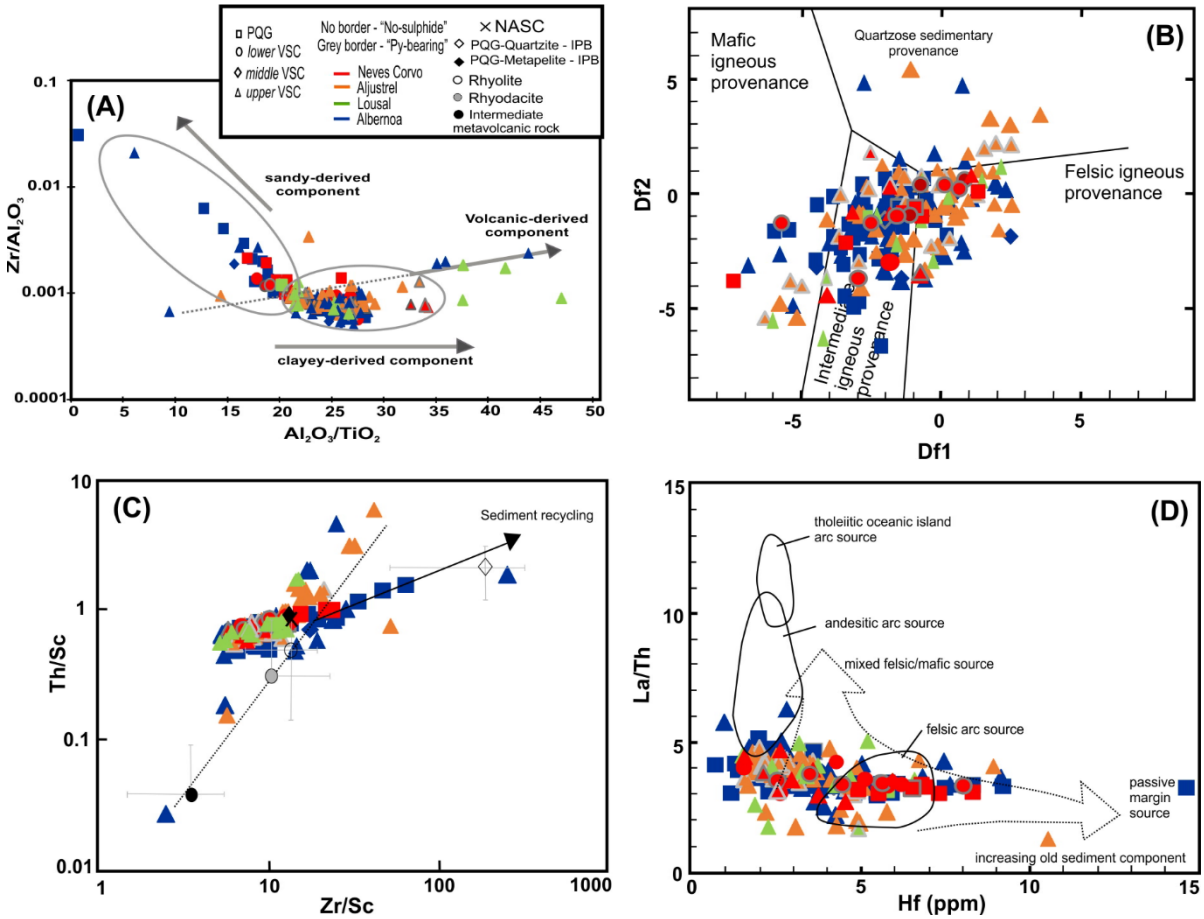

Figure 4.5 - Al_2O_3/TiO_2 vs. Zr/Al_2O_3 plot (**A**). Discrimination function diagram for the provenance signatures of clastic sedimentary rocks using major element ratios (after Roser and Korsch, 1988) applied to IPB metapelites (**B**). Provenance diagrams Zr/Sc vs. Th/Sc (**C**) and La/Th vs. Hf (**D**), after Slack et al. (2004) and Floyd and Leveridge (1987), respectively. Because abundances of some elements were considerably disturbed during hydrothermal alteration and mineralization processes, only samples forming the "No-sulphide" and "Py-bearing" groups (n = 224) were plotted. The discriminant functions used in (**B**) are: $Df1 = 30.638TiO_2/Al_2O_3 - 12.541Fe_2O_3(total)/Al_2O_3 + 7.329MgO/Al_2O_3 + 12.031Na_2O/Al_2O_3 + 35.402K_2O/Al_2O_3 - 6.382$; $Df2 = 56.500TiO_2/Al_2O_3 - 10.879Fe_2O_3(total)/Al_2O_3 + 30.875MgO/Al_2O_3 - 5.404Na_2O/Al_2O_3 + 11.112K_2O/Al_2O_3 - 3.89$. In (**C**) and (**D**), for comparison purposes, the ratios typifying NASC (Condie, 1993), as well as the average ratios and corresponding standard deviation measures calculated for PQG-quartzite and metapelite (n = 75; different sites of IPB; Jorge, 2009) and VSC-metavolcanic rocks of Albernoa (intermediate composition, n = 9, rhyodacite, n = 27, rhyolite, n = 22; Codeco et al. 2018) are also displayed.

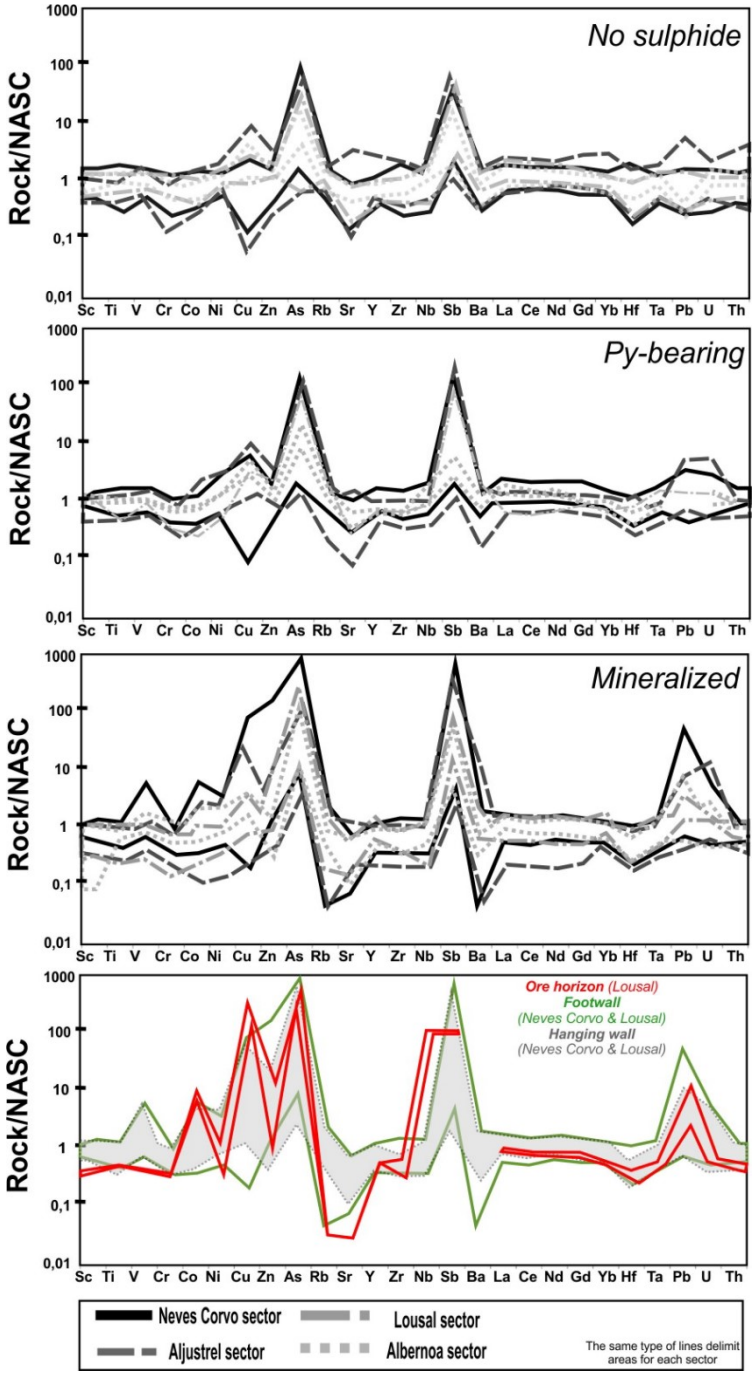

Figure 4.6 - NASC-normalized, multi-element patterns for IPB metapelites. For each sampling sector, the patterns were assembled in accordance to the previously defined groups: "No-sulphide", "Py-bearing" and "Mineralized".

(viii) Prevalent redox conditions in the confined basins were mostly oxic (at places transitional to suboxic), later on getting heterogeneous anoxic signs due to multi-stage interaction with reducing hydrothermal fluids. This interaction is quite variable and could be limited to early hydrothermal venting/exhalation into unconsolidated sediments, or evolve afterwards to

intense high-temperature, fracture-controlled, fluid flow prior to Variscan deformation and metamorphism. Considering just the dark-grey and black metapelites (n = 60), the V/Cr ratios vary largely between 1 and 2, indicative of a redox boundary near the sediment-water interface, exceeding 2 when belonging to the "Py-bearing" group (**Figure 4.7**). Many mineralized samples from PQG and *lower* VSC at the orebodies footwall of Neves Corvo are not limited to the anoxic setting implied by V/Cr > 2. For the same set of dark-grey and black metapelites, similar readings on redox conditions are supported by the U/Th ratios, spreading mostly from 0.14 to 1.25 and so covering the oxic and suboxic fields up until the suboxic/anoxic boundary, using the thresholds reported in Wignall & Myers (1988), Jones and Manning (1994) and Wignall & Twichett (1996). In particular, dark-grey to black metapelites included in the "No-sulphide" or "Py-bearing" groups record U/Th ratios that point to: oxic conditions, in the cases of Lousal (*lower* VSC) and Albernoa (*middle* and *upper* VSC sections); oxic and suboxic conditions, in the case of Neves Corvo (*lower* VSC); and oxic to suboxic/anoxic conditions, in the case of Aljustrel (*upper* VSC). The redox conditions deduced on the basis of U/Th ratios do not vary significantly for the mineralized dark-grey to black metapelites picked in Neves Corvo (PQG, *lower* and *middle* VSC), Lousal (*middle* VSC) or Aljustrel (*upper* VSC), despite the anomalous value of 2.94 obtained for one sample from Aljustrel, close to the lower limit of euxinic conditions (Figure 4.7).

(ix) As documented for other cases in the IPB (e.g. Saéz et al. 2011), whole rock abundances of S and Fe do not co-vary in the sampled metapelites. In general, S concentrations in dark-grey to black metapelites lacking sulphides or just bearing pyrite vary from ≈2 to 8 wt%, clustering in the 3-6 wt% interval; these values rise up to ≈19 wt% when the rock is evidently mineralized. Total Fe abundances are usually below 1 wt% in metapelites of the "No-sulphide" group, increasing irregularly up to ≈6 wt% and ≈8.5 wt% in samples forming the "Py-bearing" and "Mineralized" groups, respectively. Accordingly, most of the samples forming the three groups display S/Fe ratios below 0.52, pointing again to oxic conditions (e.g. Rainswell et al. 1988 and Georgiev et al. 2012); the exceptions are confined to 6 "Py-bearing" and 4 "Mineralized" samples from the *lower* and *upper* VSC sections in Neves Corvo and Aljustrel, whose S/Fe ratios suggest (local?) prevalence of anoxic or anoxic/euxinic transitional conditions.

(x) Consistent increasing in Fe_2O_3/TiO_2, (Cu+Zn+Pb)/Sc and (As+Sb)/Sc ratios to values above 10 represents a valuable footprint towards ore horizons (**Figure 4.8** and **Figure 4.9**), confirming the preliminary results reported in the previous published paper.

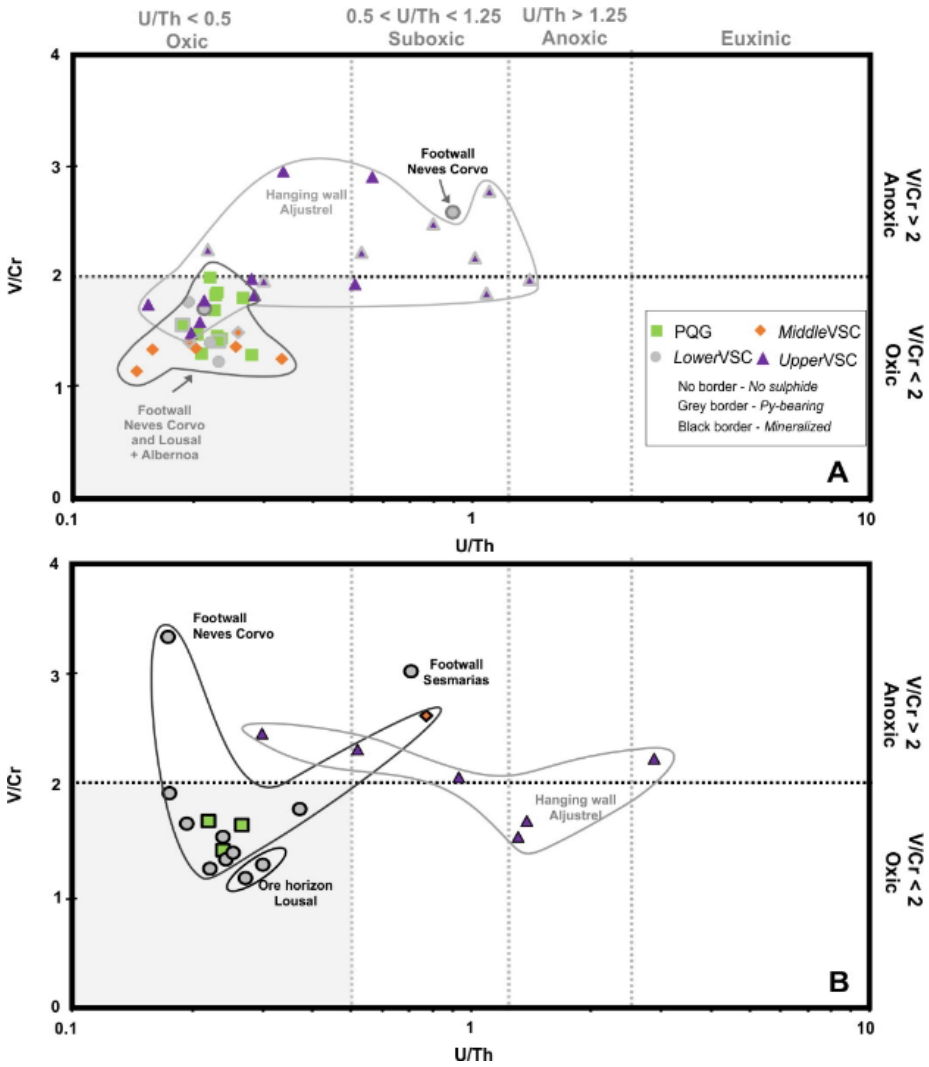

Figure 4.7 **-** Variations of U/Th vs. V/Cr ratios recorded by dark-grey to black metapelites (n = 60) sampled in Neves Corvo, Aljustrel, Lousal and Albernoa sectors, separating the "No-sulphide" and "Py-bearing" groups (**A**) from the "Mineralized" group (**B**). Thresholds of redox conditions from Wignall and Myers (1988), Jones and Manning (1994), and Wignall and Twichett (1996).

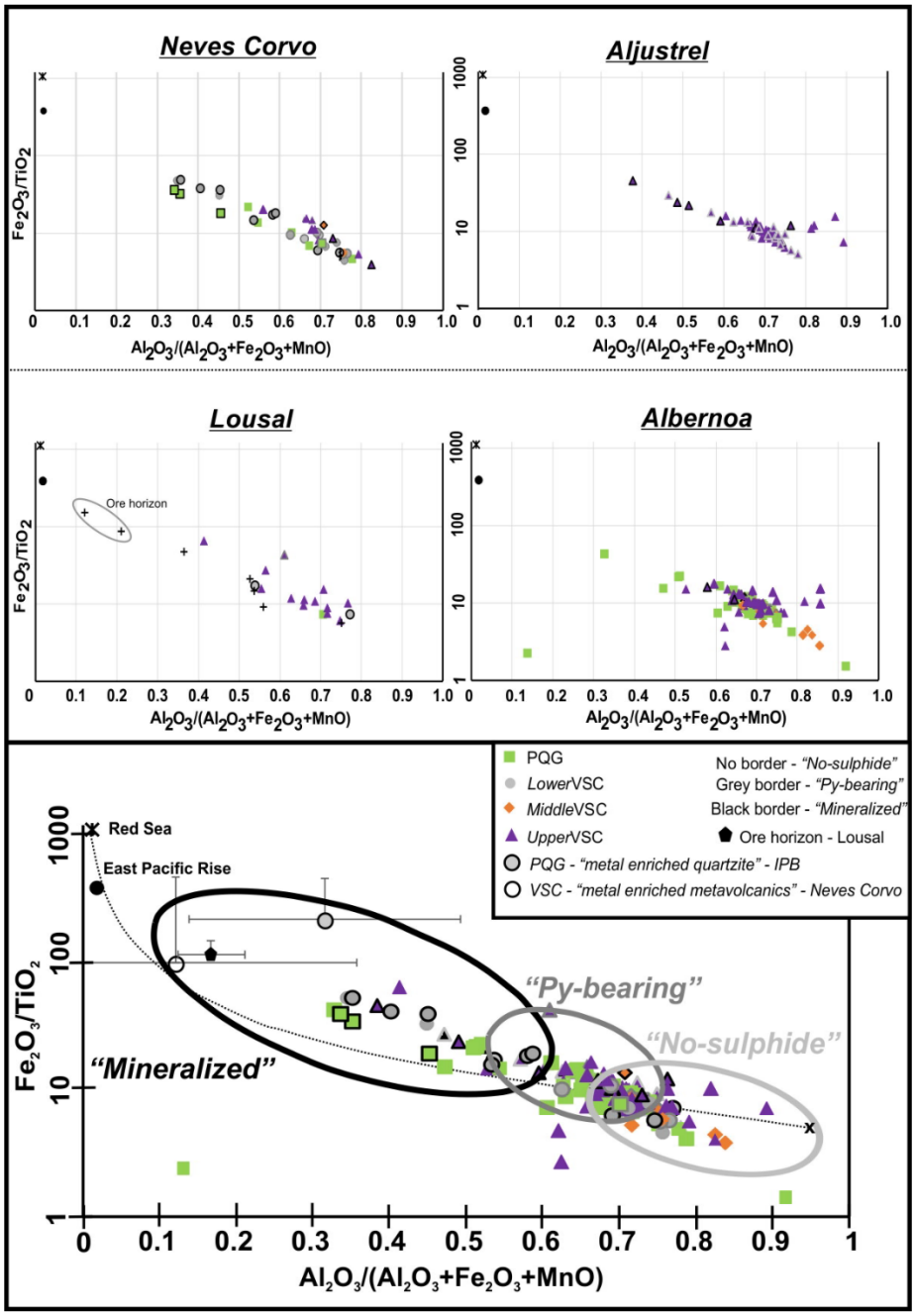

Figure 4.8 **-** Fe_2O_3/TiO_2 vs. $Al_2O_3/(Al_2O_3+Fe_2O_3+MnO)$ diagram for the four sectors (Neves Corvo = 46, Aljustrel = 84, Lousal = 16 and Albernoa = 116) illustrating the mixing strip between a "terrigenous" end-member (given by the NASC projection, Condie, 1993) and a conceptual "exhalative-hydrothermal" term represented by the composition of the East Pacific Rise and/or Red Sea brine pool (e.g. Marchig et al., 1982; Goodfellow et al., 2003). Metal-enriched PQG quartzites and VSC metavolcanics were plotted for reference (data from Jorge 2009, and Relvas et al. 2006a, respectively). The average and standard deviation values for "No-sulphide", "Py-bearing" and "Mineralized" groups are plotted as diamonds and error bars. The ore horizon of Lousal is represented by 7 non-weathered samples (+) reported in Fernandes (2011).

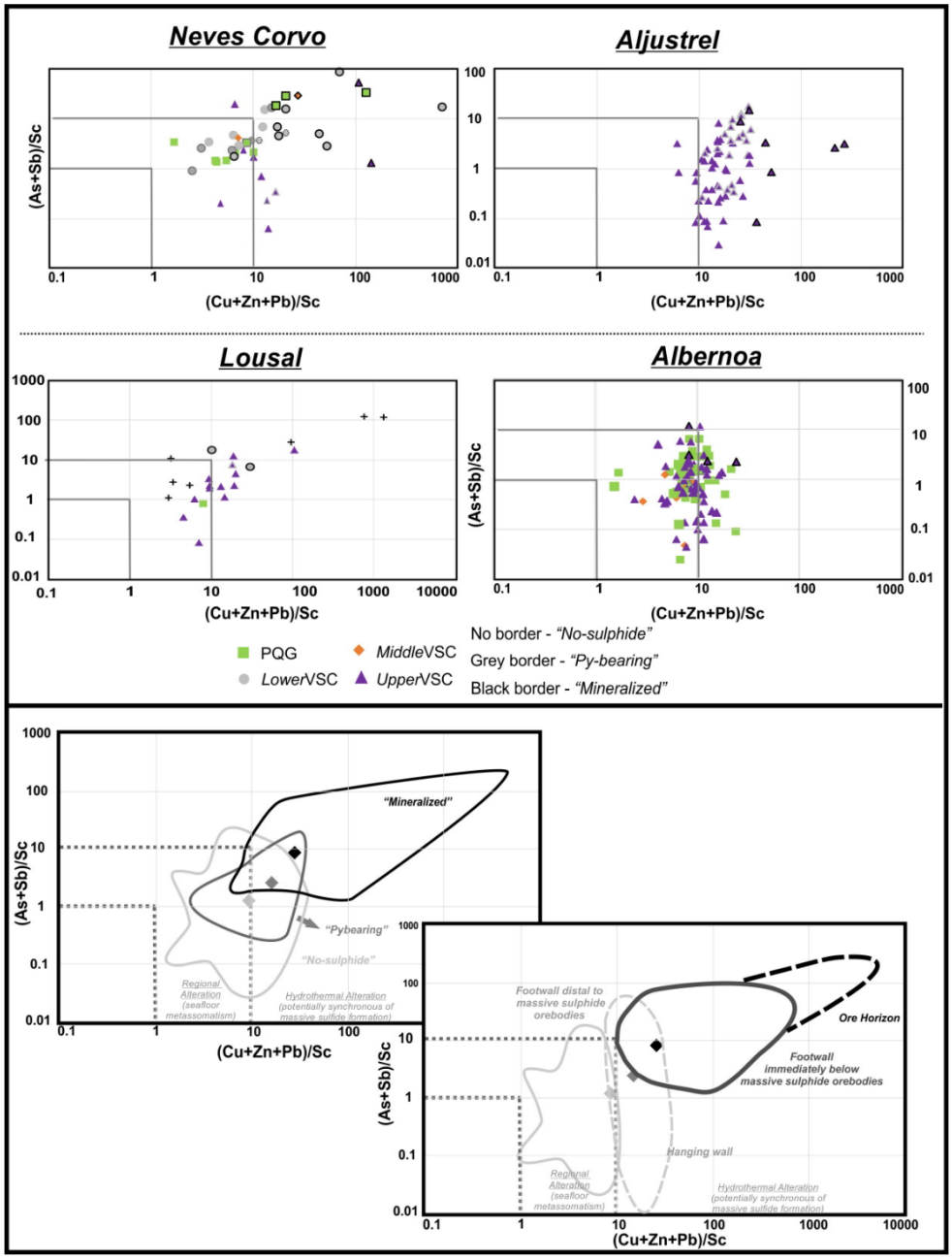

Figure 4.9 **-** (As+Sb)/Sc vrs.(Cu+Zn+Pb) diagram illustrating the chemical effects related to post-sedimentary transformations. Values between 1.0 and 10.0 of these geochemical ratios trace effects ascribed to oceanic metasomatism processes (regional alteration pattern); ratios above 10.0 indicate the proximity of hydrothermal discharges potentially related to ore-forming systems. The ore horizon of Lousal is represented by 7 non-weathered samples (+) reported in Fernandes (2011).

4.3. Pb-nd-Sr isotope geochemistry of metapelites from the Iberian Pyrite Belt and its relevance in vectoring massive sulfide ore systems

Paper *under review*

A Pb-Nd-Sr isotope study was conducted for a large number (n = 98) of samples representing fine-grained sediments in different sections of PQG and VSC successions of the IPB (from Givetian to Upper Visean), including the footwall and hanging wall domains of mineralized horizons in Neves-Corvo, Aljustrel and Lousal deposits. The full version of the submitted manuscript is in Appendix 1.3 and the main results can be summarized as follows.

(i) The examined samples are chemically similar and the joint inspection of whole-rock Nd and Sr isotopic compositions along with Th/Sc ratios shows that they are mostly composed of a siliciclastic mix supplied by an old basement ($-11 \leq \varepsilon Nd_i \leq -8$ and $(^{87}Sr/^{86}Sr)_i$ up to 0.727), slightly changed via mixing with volcanic-derived fractions and interaction with modified seawater at the Devonian-Carboniferous boundary (**Figure 4.10**).

(ii) For the studied samples, the Nd T_{DM} ages vary from 1.08 to 2.02 Ga and their distribution has a mean value of 1.73 ± 0.17 Ga. Three samples representing the Gafo, Ribeira de Limas and Sta. Iria Formations (ca. 370 Ma, included in the Chança and Pulo do Lobo Groups), stratigraphically below to lateral equivalent of PQG, were also analysed for comparison purposes. These samples display the lowest εNd_i values, between -10.7 and -9.5, and a mean T_{DM} age of 1.90 ± 0.04 Ga, resembling metasedimentary rocks involved in the Meguma Terrane ≈ 1.94 ± 0.06 (**Figure 4.11**). This suggests that a source of similar isotopic characteristics could have supplied the shallow SPZ continental platform in Devonian times (see also Pereira et al., 2019 and references therein). If so, mixtures of clasts derived from the dismantling of old metasediments and subvolcanic/granitoid rocks (in a proportion that roughly range from 0.75 : 0.25 to 0.55 : 0.45, assuming εNd_i values of -12 and -3 for each rock type, respectively) could explain the isotopic signature displayed by the siliciclastic mix involved in PQG and *lower* VSC sections.

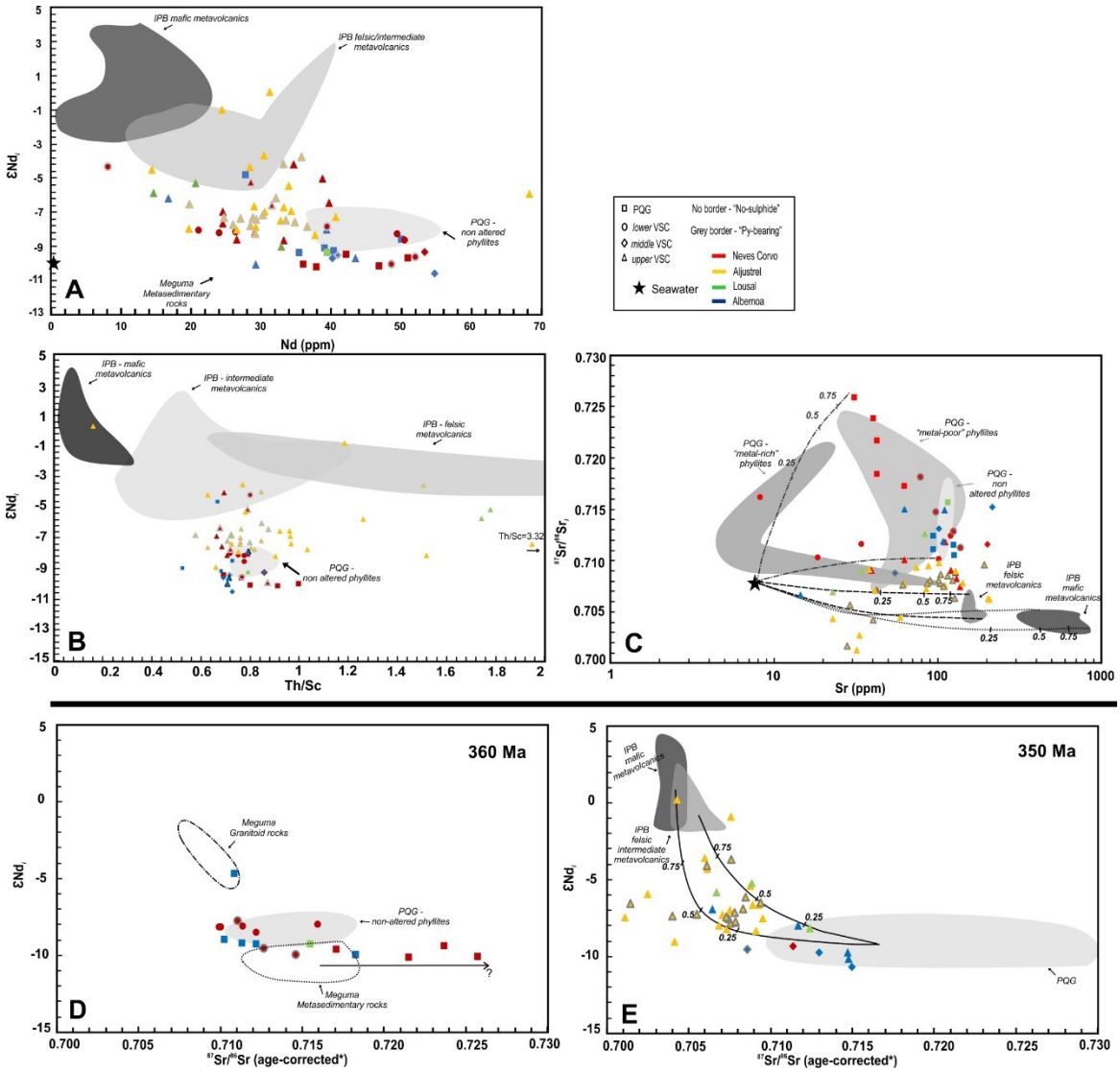

Figure 4.10 - Sr and Nd isotopic compositions and trace element ratios for PQG and VSC samples included in "No-sulfide" and "Py-bearing" groups (n = 75)**: (A)** Nd (ppm) vs. εNd_i; **(B)** Th/Sc **vs.** εNd_i; **(C)** $^{87}Sr/^{86}Sr_i$ vs. Sr (ppm) and **(D)** $^{87}Sr/^{86}Sr_i$ vs**.** εNd_i for PQG and lower VSC at 360 Ma. **(E)** $^{87}Sr/^{86}Sr_i$ vs**.** εNd_i for middle and upper VSC at 350 Ma. Crustal reservoirs data from the literature (Clarke & Halliday, 1985; Clarke et al., 1988, 1997; Mitjavilla et al., 1997; Jorge, 2009; Donaire et al., 2020). The star indicates an exploratory reference for ambient seawater at Devonian-Carboniferous boundary that could have acted as an end-member of simple binary mixtures established with siliciclastic and/or volcanic rocks

(iii) A close inspection of the data shows in addition that, despite some overlap, the T_{DM} ages tend to become gradually younger from the bottom to the top of the stratigraphic sequence, notwithstanding the associated uncertainties and the limited number of samples representing the *middle* VSC sections: 1.83 ± 0.09 Ga for PQG; 1.85 ± 0.08 for *lower* VSC; 1.80 ± 0.03 for *middle* VSC; and 1.68 ± 0.17 Ga for *upper* VSC. Similarly to the T_{DM} ages, the range of εNd_i values obtained for samples representing the *middle* and *upper* VSC sections (from -10.6 to -8.5 and from -10 to +0.2, respectively) also overlaps to a great extent the range displayed by PQG and *lower* VSC samples, indicating the presence of a common siliciclastic mix across the whole PQG and VSC succession, which is irregularly modified in some *upper* VSC levels.

The rising of εNd_i and T_{DM} ages values recorded by many samples of *upper* VSC (up to +0.2 in the Aljustrel sector) implies the involvement of a distinct and more juvenile source of clastic sediments supplying the basin in Upper Tournaisian to Visean times. This isotopic fingerprint is interpreted as a result of the local incorporation of volcanic-derived contributions completed during the sedimentation.

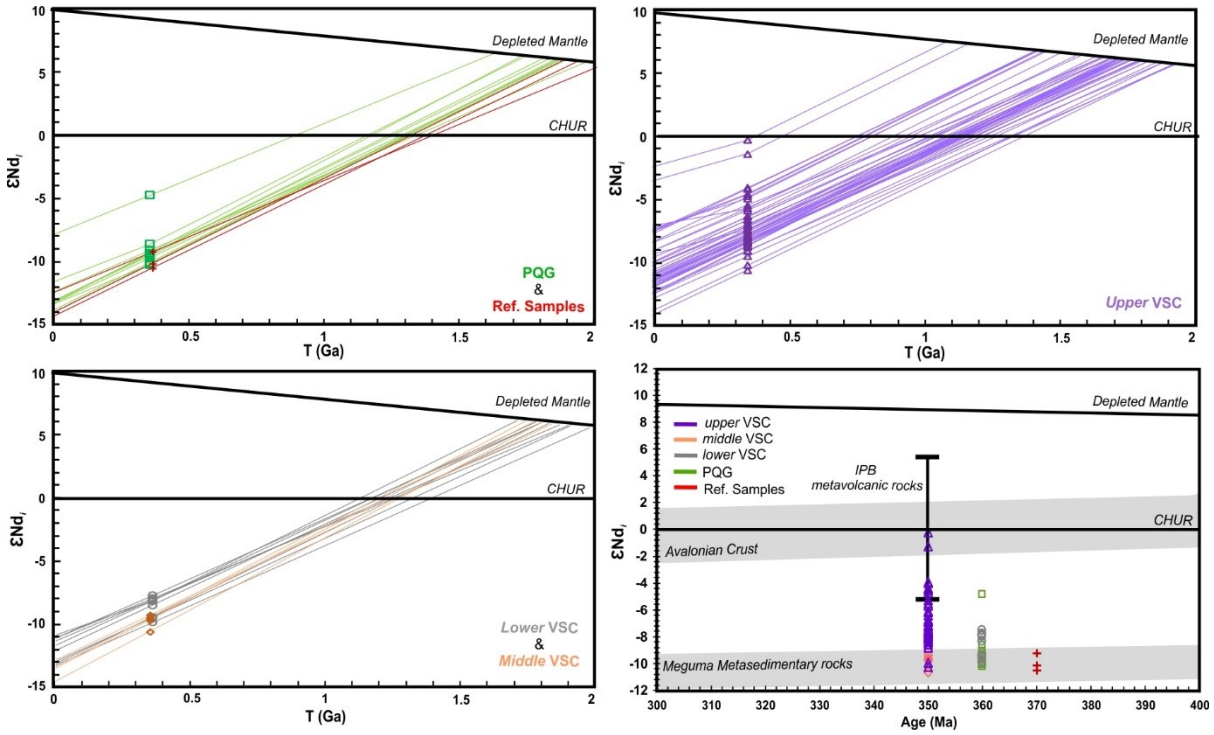

Figure 4.11 - εNd_i vs. time diagrams: **(A)** Time in Ga, The Nd T_{DM} model ages were calculated assuming a linear depletion model with present-day depleted values of $^{143}N/^{144}Nd = 0.513151$ and $^{147}Sm/^{144}Nd = 0.2137$ (Peucat et al., 1998). Two-stage T_{DM} model ages were computed for samples with $^{147}Sm/^{144}Nd$ ratio outside the typical range of upper continental crust-derived sediments (0.09 - 0.13; e.g. Goldstein et al., 1984); a $^{147}Sm/^{144}Nd$ value of 0.114 was used to estimate the sample evolution path prior to depositional age (Goldstein and Jacobsen, 1988; Li and Schoornmaker, 2014) **.(B)** Time in Ma, comparing Sm-Nd isotope data for PQG, lower VSC, middle VSC, upper VSC and reference samples of Gafo, Ribeira de Limas and Sta. Iria formations with data for the Meguma Metasedimentary rocks (Clark et al., 1980, 1988, 1997), the Avalonia crust (Murphy et al., 1996, 2000) and the IPB volcanic rocks (Mitjavilla et al., 1997; Donaire et al., 2020). Depleted mantle evolution curve from the model of De Paolo (1981).

(iv) The Pb isotopic fingerprints displayed by the studied sediments are consistent with published data for IPB ores and country rocks (**Figure 4.12**). When included in footwall levels contiguous of the Neves Corvo orebodies, the metapelites tend to display a Pb isotopic signature close to the trends disclosed in previous studies for the corresponding ore types (e.g. Relvas, 2000; Carvalho, 2016). The metapelites forming the levels immediately below the ore horizons at the Lousal mine or at the neighbouring Sesmarias prospect show $^{206}Pb/^{204}Pb_i$ values

below the empirical threshold defined for the Portuguese IPB massive sulphide ores (≈18.16), even though displaying comparable $^{207}Pb/^{204}Pb_i$ ratios (≈15.62). At the hanging wall (*upper* VSC) of massive sulphide orebodies in Aljustrel, metapelites display ≈18.12 ≤ $^{206}Pb/^{204}Pb_i$ ≤ ≈18.34, but $^{207}Pb/^{204}Pb_i$ ≥ 15.62. In the *upper* VSC sections of the Albernoa sector, the most common metapelites are characterized by $^{206}Pb/^{204}Pb_i$ ≤ ≈18.10 and $^{207}Pb/^{204}Pb_i$ ≈ 15.60.

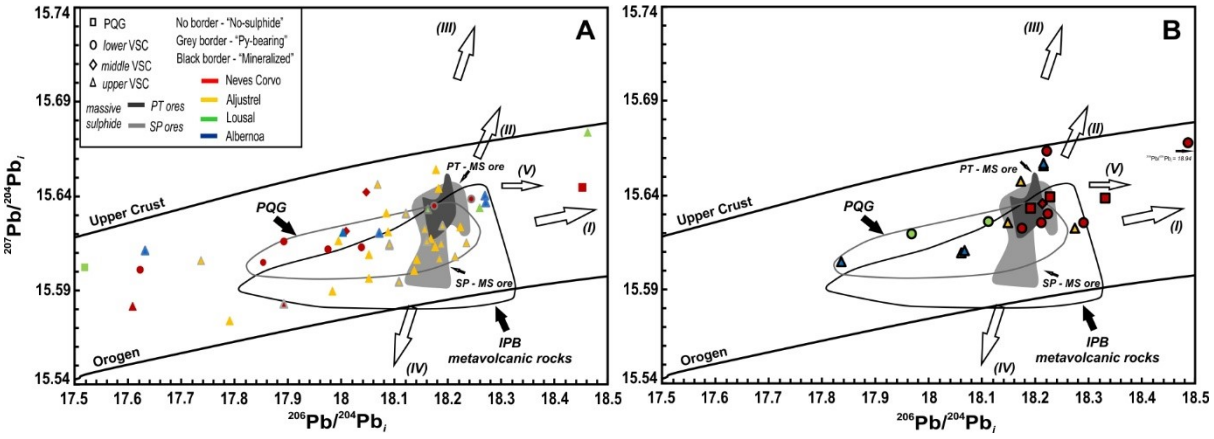

Figure 4.12 - $^{206}Pb/^{204}Pb_i$ vs. $^{207}Pb/^{204}Pb_i$ diagrams for studied samples (n = 75). The common massive sulfide ores in the Portuguese and Spanish segments of IPB were separated into two fields, considering the data (n =106) reported in Marcoux (1998), Pomiés et al. (1999), Relvas et al. (2001), Jorge et al. (2007) and Carvalho (2016). The numbered arrows illustrated the trends for Neves Corvo on the basis of published data (n=42; Marcoux, 1998; Relvas et al., 2001; Jorge et al., 2007; Carvalho, 2016).

(v) As indicated in previous studies, the obtained results suggest that the PQG succession, at times complemented by VSC thick piles, should represent the main crustal reservoirs of metals involved in the supply of common hydrothermal inflows in IPB during the Fammenian-Tournaisian transition, which were dominated by modified seawater. Other sources, more radiogenic, should be involved in the IPB metal budget when the role of Sn- and Cu-rich fluids became central in the ore system, as thoroughly documented for the Neves-Corvo deposit.

(vi) The increasing of $^{207}Pb/^{204}Pb_i$ ratios in sediments is sensitive to the circulation of mineralizing fluids, namely those implicated in the deposition of common IPB massive sulphides. On the contrary, significant rises in $^{206}Pb/^{204}Pb_i$ (and $^{207}Pb/^{204}Pb_i$) values in sediments bearing disseminated sulphides other than pyrite only occur when a protracted interaction with radiogenic hydrothermal inflows of moderate to high temperature is recorded.

(vii) The proximity to massive sulphide ore systems could be recognized in sedimentary levels of PQG and VSC whenever $^{207}Pb/^{204}Pb_i$ > 15.60, correlating well with several other multi-element geochemical ratios such as Fe_2O_3/TiO_2 >10 and (Cu+Zn+Pb)/Sc > 10 (**Figure 4.13**).

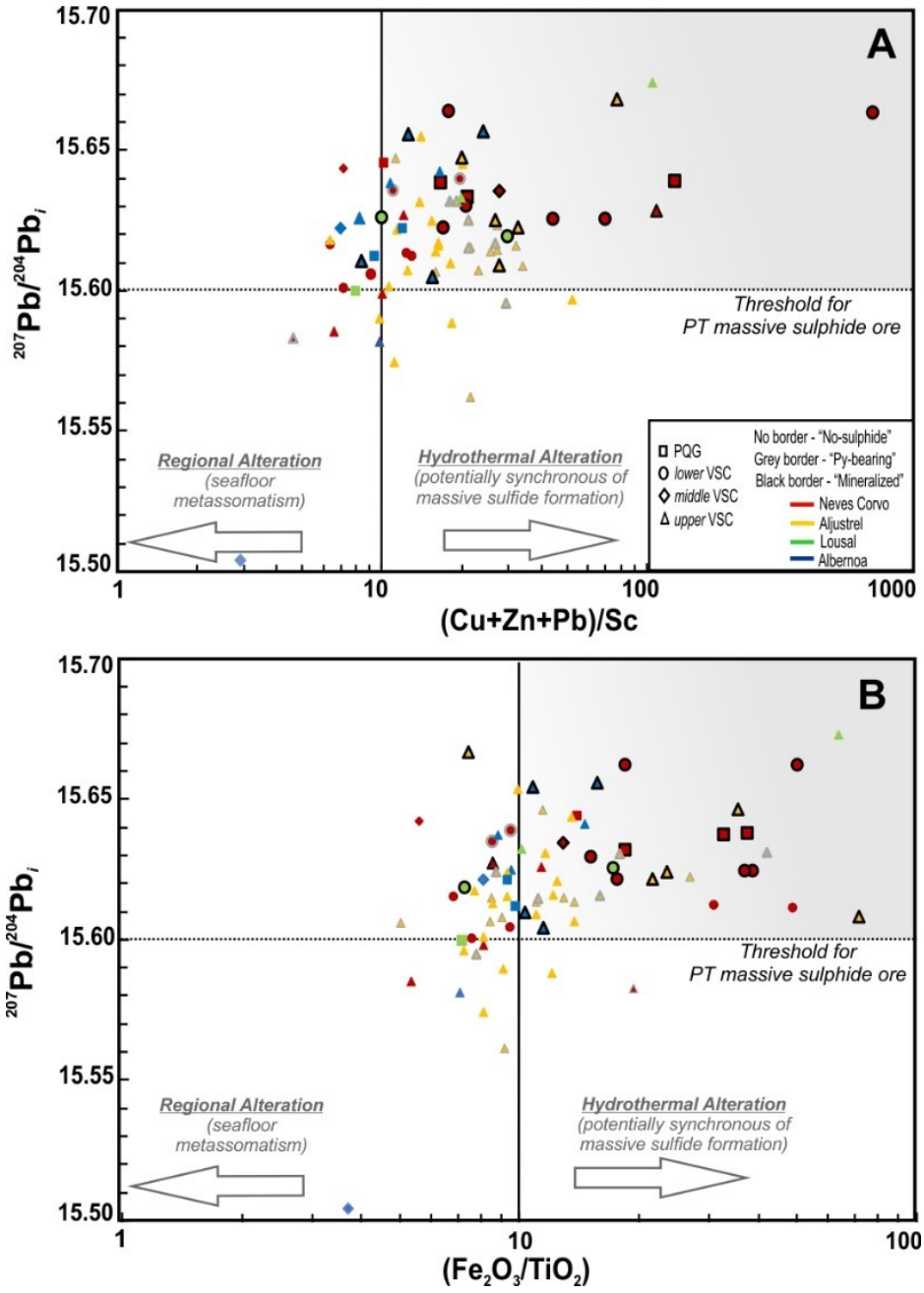

Figure 4.13 -(Cu+Zn+Pb)/Sc and Fe_2O_3/TiO_2 vs. $^{207}Pb/^{204}Pb_i$ diagrams showing the potential use of these cross-plots in vectoring massive sulfide accumulations. (Cu+Zn+Pb)/Sc and Fe_2O_3/TiO_2 thresholds (>10) described in Luz et al. (2019, 2020). $^{207}Pb/^{204}Pb_i$ for Portuguese massive sulfide ores according with literature data (n = 106; Marcoux, 1998; Pomiés et al., 1999; Relvas et al., 2001; Jorge et al., 2007; Carvalho, 2016).

SECTION 5

5. Micro-chemical fingerprints provided by mineral associations and compositions

The mineral phases analysed with EPMA were silicates (feldspars, mica, chlorite and zircon), carbonates (calcite, siderite, ankerite/dolomite), phosphates (fluorapatite, xenotime, monazite), sulphides and sulphosalts (pyrite, sphalerite, chalcopyrite, galena, besides various As-Co-Ni-Sb bearing species) and oxides (rutile *s.l.*). Phyllosilicates were the main focus of the study since they represent the prevalent phases of the examined metasedimentary rocks, forming a key constituent of the hydrothermal alteration haloes related to the mineralizing processes.

5.1. Chlorite

The comprehensive assessment of chlorite composition in many samples is often constrained by the reduced size of the crystals, which are smaller than the electron beam diameter and prevent the acquisition of high-quality (< 2% error) quantitative analyses. Even so, 267 analyses displayed enough quality to be numerically processed, further grouped according to petrographic criteria into: (i) early-formed chlorites, preceding the Variscan deformation events and thus preserving effects of strain accommodation; and (ii) late-formed chlorites, included in fracture infillings that crisscross (micro)structural arrangements developed during the Variscan deformation events. Data inspection considered first a general comparison with published results on chlorite composition for Aljustrel, Gavião, Neves Corvo and Lousal (e.g. Barriga, 1983; Relvas, 1991, 2000; Fernandes, 2011; Carvalho, 2016). Subsequently, the obtained data was examined considering each sector and, whenever possible, separating the two chlorite groups. The data reported in other studies were always used to realize the representativeness of the obtained compositions for each chlorite group. In some cases, the dataset is enough robust, but the information gaps detected in other contexts provide several suggestions that may support additional lines of research in the future (see Section 7).

The chlorite composition can be written as $[R^{2+}_{(6-x-y)}(R^{3+},R^{4+})_{(x+2y)}\square_y](Si_{4-x}\,R^{3+}_x)O_{10}\,(OH)_8$ where □ stands for the vacancies, and the divalent (Mg, Fe^{2+}, Mn and Zn), trivalent (Al, Fe^{3+}, Cr^{3+}) and tetravalent (Ti) cations are represented by $R^{2+,}$ R^{3+} and R^{4+}, respectively (*e.g.* Foster, 1962; Bayliss, 1975; Bailey, 1988; Laird, 1988). The simplified formula (Mg, Fe^{2+}, Fe^{3+}, Mn, Al)$_6$[(Si, Al)$_4$O$_{10}$](OH)$_{16}$ documents a crystal structure comprising regular alternations of octahedral "brucite-like" sheets and tetrahedral-octahedral-tetrahedral sheets in a 2:1 proportion (Deer *et al*., 2008).

Table 5-1 - Summary of descriptive statistics for chlorite analyses, in wt% (n = 267), Appendix 3, *chlorite sheet* show all the spot analyses.

		Mean	St deviation	Median	Min	Max
Neves Corvo (n = 84)	*TiO2*	0.06	0.18	0.03	0.00	1.20
	SiO2	24.96	1.34	24.40	23.70	30.27
	Fe2O3	0.24	2.19	0.06	0.00	20.19
	Cr2O3	0.07	0.02	0.07	0.02	0.14
	Al2O3	21.84	0.75	21.81	20.03	23.63
	ZnO	0.06	0.06	0.06	0.00	0.19
	NiO	0.02	0.02	0.01	0.00	0.08
	FeO	33.94	4.74	35.72	12.37	38.37
	MnO	0.20	0.09	0.18	0.04	0.42
	MgO	7.41	2.72	6.48	5.18	18.35

		Mean	St deviation	Median	Min	Max
Lousal (n = 14)	*TiO2*	0.03	0.02	0.03	0.00	0.08
	SiO2	25.05	0.68	25.13	24.08	26.76
	Fe2O3	0.00	0.00	0.00	0.00	0.00
	Cr2O3	0.16	0.10	0.21	0.02	0.31
	Al2O3	20.89	1.02	20.16	19.77	22.42
	ZnO	0.07	0.04	0.06	0.01	0.13
	NiO	0.02	6.29	0.60	0.00	0.06
	FeO	32.35	3.84	0.09	28.13	39.76
	MnO	1.15	0.57	1.47	0.05	1.81
	MgO	8.78	3.08	10.28	1.70	11.79

		Mean	St deviation	Median	Min	Max
Aljustrel (n = 73)	*TiO2*	0.06	0.19	0.03	0.00	1.67
	SiO2	25.51	1.17	25.31	23.66	31.75
	Fe2O3	0.05	0.42	0.00	0.00	3.70
	Cr2O3	0.08	0.03	0.07	0.02	0.19
	Al2O3	21.56	0.92	21.41	19.23	24.62
	ZnO	0.08	0.06	0.08	0.00	0.22
	NiO	0.02	0.03	0.00	0.00	0.11
	FeO	28.56	3.91	29.05	14.92	32.91
	MnO	1.71	1.19	1.04	0.18	4.05
	MgO	10.83	2.37	10.59	7.86	20.04

		Mean	St deviation	Median	Min	Max
Albernoa (n = 93)	*TiO2*	0.07	0.14	0.12	0.00	0.74
	SiO2	25.28	1.83	25.04	21.09	36.35
	Fe2O3	0.00	0.00	0.07	0.00	0.00
	Cr2O3	0.08	0.03	0.08	0.02	0.14
	Al2O3	23.68	4.64	22.51	20.14	39.98
	ZnO	0.07	0.06	0.07	0.00	0.25
	NiO	0.01	0.04	0.00	0.00	0.18
	FeO	27.46	4.63	28.82	13.68	33.21
	MnO	0.47	0.31	0.42	0.04	1.35
	MgO	11.19	4.88	10.84	0.76	24.92

The general chlorite dataset presents deviations from the chamosite end member towards the Fe-amesite and sudoite compositions. These chemical variations are justified mainly by three cationic substitutions (e.g. Bailey *et al.,* 1988; Vidal *et al.,* 2005): (i) $(Fe^{2+})^{vi} = (Mg^{2+})^{vi}$ – **Figure 5.1**; (ii) $(Si^{4+})^{vi} + (R^{2+})^{vi} = (Al^{3+})^{iv} + (Al^{3+})^{vi}$ – **Figure 5.2** and (iii) $3(R^{2+})^{vi} = 2(Al^{3+})^{vi} + \square^{vi}$ – **Figure 5.3**, where R^{2+} represent any divalent cation (Fe^{2+}, Mg, Mn, Zn, Ni) in octahedral (vi) positions, $\square^{vi}$ the octahedral vacancies and (iv) the tetrahedral (iv) positions. The extent of FM (= Fe-Mg interchange, where Mg could be partly replaced by Mn) substitution in octahedral positions is substantial, as illustrated in **Figure 5.1**. Nonetheless, higher median #Fe [= $Fe^{2+}/(Fe^{2+}+Mg+Mn)$] values characterize chlorite aggregates from Neves Corvo (#Fe = 0.75) and Lousal (#Fe = 0.66), whereas similar ratios typify chlorite aggregates from Aljustrel (#Fe = 0.58) and Albernoa (#Fe = 0.53). Considering just the data reported in literature, chlorites from Neves Corvo, Aljustrel and Lousal display #Fe > 0.50, and those from Gavião (a sub-sector of Aljustrel) show #Fe ≈ 0.60. All the presented#Fe are median values and consider literature data. **Figure 5.2** highlight the deviations towards the sudoite endmember for Neves Corvo where samples are marked by lower R^{2+} contents and proportional increment of Al^{3+}.

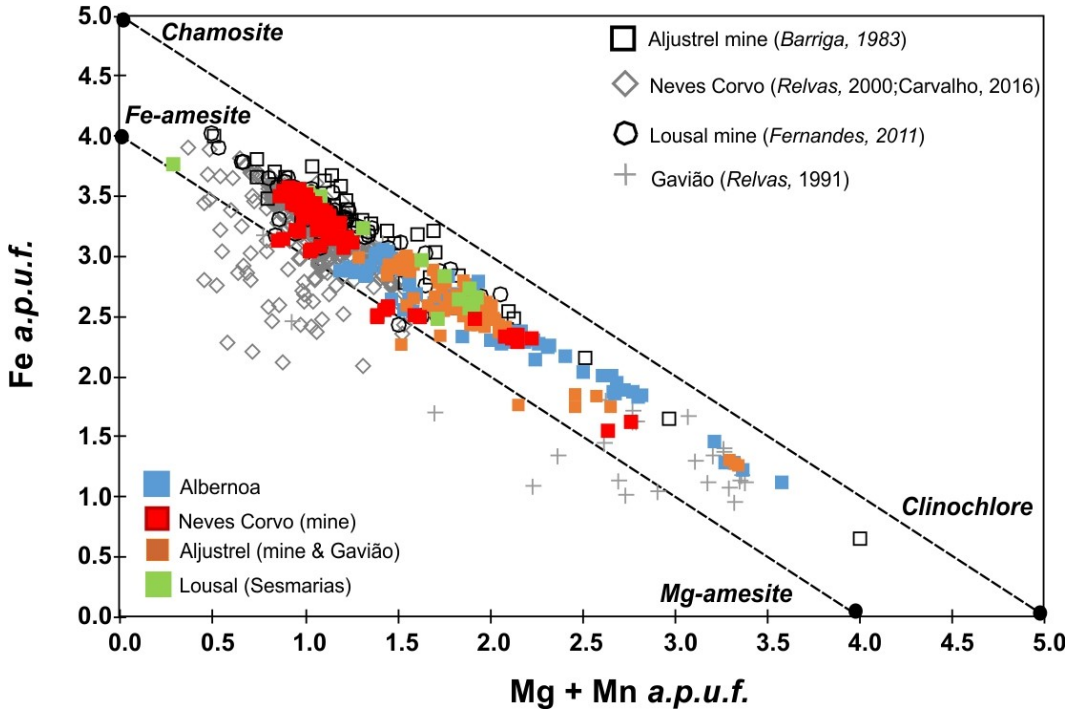

Figure 5.1 - Cross-plot showing the FM substitution vector, the predominant exchange mechanism in this chlorite dataset. For reference and comparison purposes, the literature data were plotted for Aljustrel mine (stockwork/ore and HW position; n = 44; Barriga, 1983), Neves Corvo (stockwork/ore and FW position from Corvo n = 57 and Lombador n = 410 orebodies, Relvas, 2000 and Carvalho, 2016, respectively), Lousal mine (FW position and Late tectono-metamorphic, n = 64; Fernandes, 2011) and for Gavião prospect (regional and hydrothermal - FW and lateral to ore horizon, n = 31; Relvas, 1991). HW = orebody hanging wall; FW = orebody footwall. The literature dataset include outliers that might represent analytical shifts.

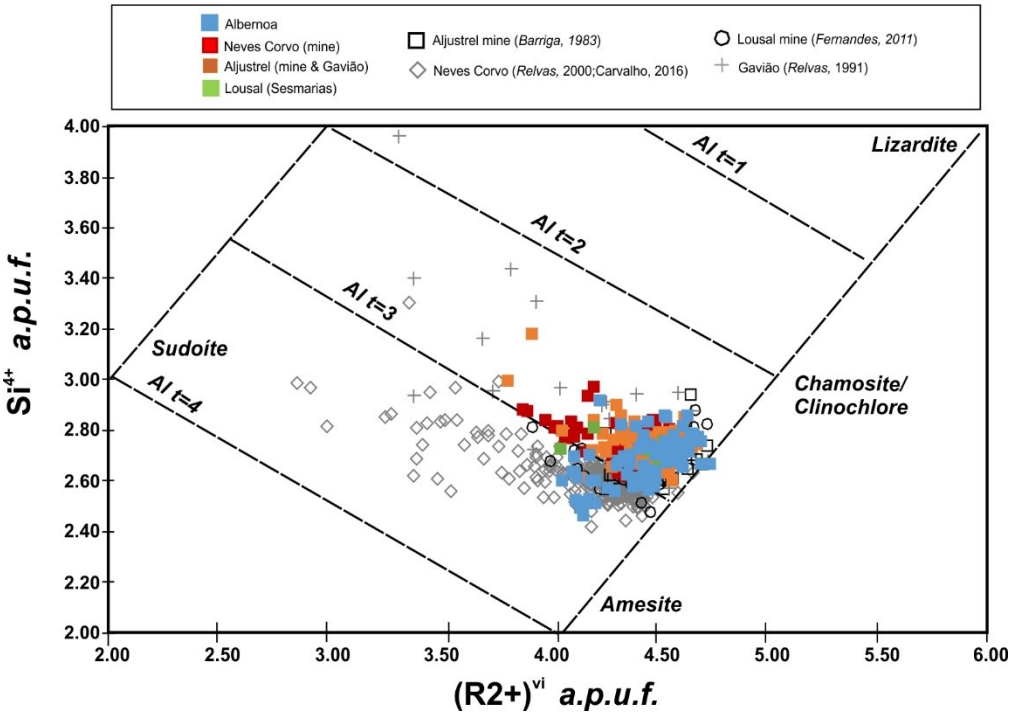

Figure 5.2 - Position of the analyzed chlorite in the R^{2+} vs. Si^{4+} diagram (Wiewiora, et al., 1990). For reference and comparison purposes, the literature data were plotted for Aljustrel mine (stockwork/ore and HW position; n = 44; Barriga, 1983), Neves Corvo (stockwork/ore and FW position from Corvo n = 57 and Lombador n = 410 orebodies, Relvas, 2000 and Carvalho, 2016, respectively), Lousal mine (FW position and late tectono-metamorphic, n = 64; Fernandes, 2011) and for Gavião prospect (regional and hydrothermal - FW and lateral to ore horizon, n = 31; Relvas, 1991). The literature dataset includes outliers that might represent analytical shifts.

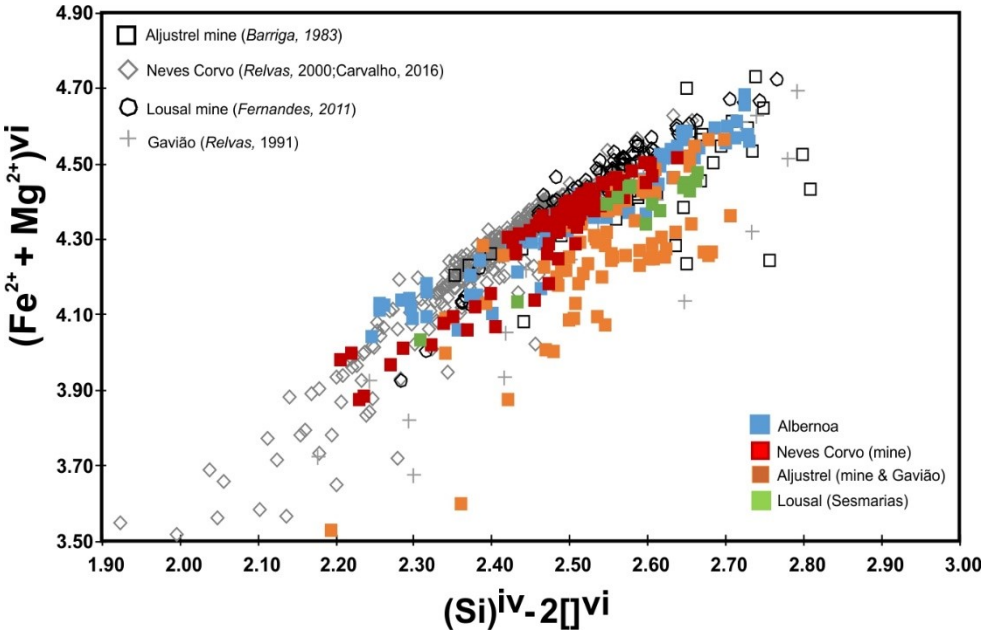

Figure 5.3 - Cross-plot showing the $(R^{2+})^{vi}$ vs. $(Si^{iv} – 2[]^{vi})$ relationship. For reference and comparison purposes, the literature data were plotted for Aljustrel mine (stockwork/ore and HW position; n = 44; Barriga, 1983), Neves Corvo (stockwork/ore and FW position from Corvo n = 57 and Lombador n = 410 orebodies, Relvas, 2000 and Carvalho, 2016, respectively), Lousal mine (FW position and late tectono-metamorphic, n = 64; Fernandes, 2011) and for Gavião prospect (regional and hydrothermal - FW and lateral to ore horizon, n = 31; Relvas, 1991). The literature dataset includes outliers that might represent analytical shifts

5.1.1. Chlorite by sectors and generations

The most noteworthy compositional variation recorded by chlorite is related to the FM substitution, which is complemented by the Tschermak vector [$(Si^{4+})^{vi} + (R^{2+})^{vi} = (Al^{3+})^{iv} + (Al^{3+})^{vi}$], leading often to significant incorporation of Al^{3+} in tetrahedral positions. The $3(R^{2+})^{vi} = 2(Al^{3+})^{vi} + \square^{vi}$ exchange mechanism is also relevant in many chlorite analyses from Neves-Corvo, if data compiled from literature were considered. Nevertheless, all these compositional variations seem to record the influence of local chemical gradients rather than differences between early or late-formed chlorite, regardless of the tendency for an increase in Fe contents in early chlorite generations. **Figure 5.4** show the chlorite variations through sectors.

At Neves Corvo only early formed chlorites were identified and analysed. However, if the dataset obtained in samples nearby different orebodies is separately considered, some few differences in Fe and (Mg + Mn) contents emerge, suggesting delicate variations imposed either by the chemistry of hydrothermal fluids or the sedimentary media, both with implications on the temperature formation of chlorites. In this context, chlorites from Lombador, Corvo and Zambujal present higher median #Fe (0.75) whereas those from Neves display a relatively constant Fe content and smaller (Mg + Mn) values (#Fe = 0.64). Two analyses from Corvo present lower #Fe values (0.37) but, according to the available information, they should record the influence of local chemical gradients related to the sediment composition, deviating from the most common chlorites found in the Corvo's stockwork or other hydrothermally altered samples at the orebody footwall.

For the Aljustrel sector the dataset was divided, firstly by sub-sectors (mine, Gavião and Monte das Mesas prospect and Feitais extension structure) and later by chlorite generations. Here, the compositional differences between early and late-formed chlorites are clear, the former being Fe-richer and the later displaying a strong tendency to be (Mg ± Mn)-richer. With few exceptions (three analyses from the Aljustrel mine), the composition of chlorites forming the infillings of late-Variscan veinlets is similar to that presented by chlorites ascribed to regional alteration (seafloor metasomatism) in samples from the Gavião prospect (Relvas, 2000). In addition, it should be noted that the dataset gathered for early-formed chlorites are fully consistent with data reported in other studies, especially for early-chlorite from Gavião ("hydrothermal"). Chlorite samples from the Feitais orebody (Barriga, 1983) display higher median #Fe ratios (0.71) irrespectively of their proximity to the hydrothermal feeder zone(s).

In the Lousal sector, data reported in Fernandes (2011) and gathered from samples picked in the Sesmarias subsector were considered. In both cases, better than in the other studied sectors,

it is possible to control the proximity to hydrothermal feeder zones, where it is clear the increment of Fe contents in chlorite towards the places where the effects of alteration/mineralization are more evident. Late-formed chlorites were identified by Fernandes (2011), and these display compositions somewhat distinct from the early chlorites, being slighter to evidently enrich in (Mg + Mn). To a large extent, chlorites from Sesmarias spread over the compositional field described for Lousal.

For samples collected in the Albernoa sector, two main chlorite generations were recognised. Early-formed chlorite, possibly related to seafloor metasomatism and developing oriented aggregates, is chemically characterized by median #Fe ratios around 0.60. Late-formed chlorite that represent infillings of fractures crosscutting S_1 has distinctly more Mg-enriched (median #Fe = 0.55) compositions.

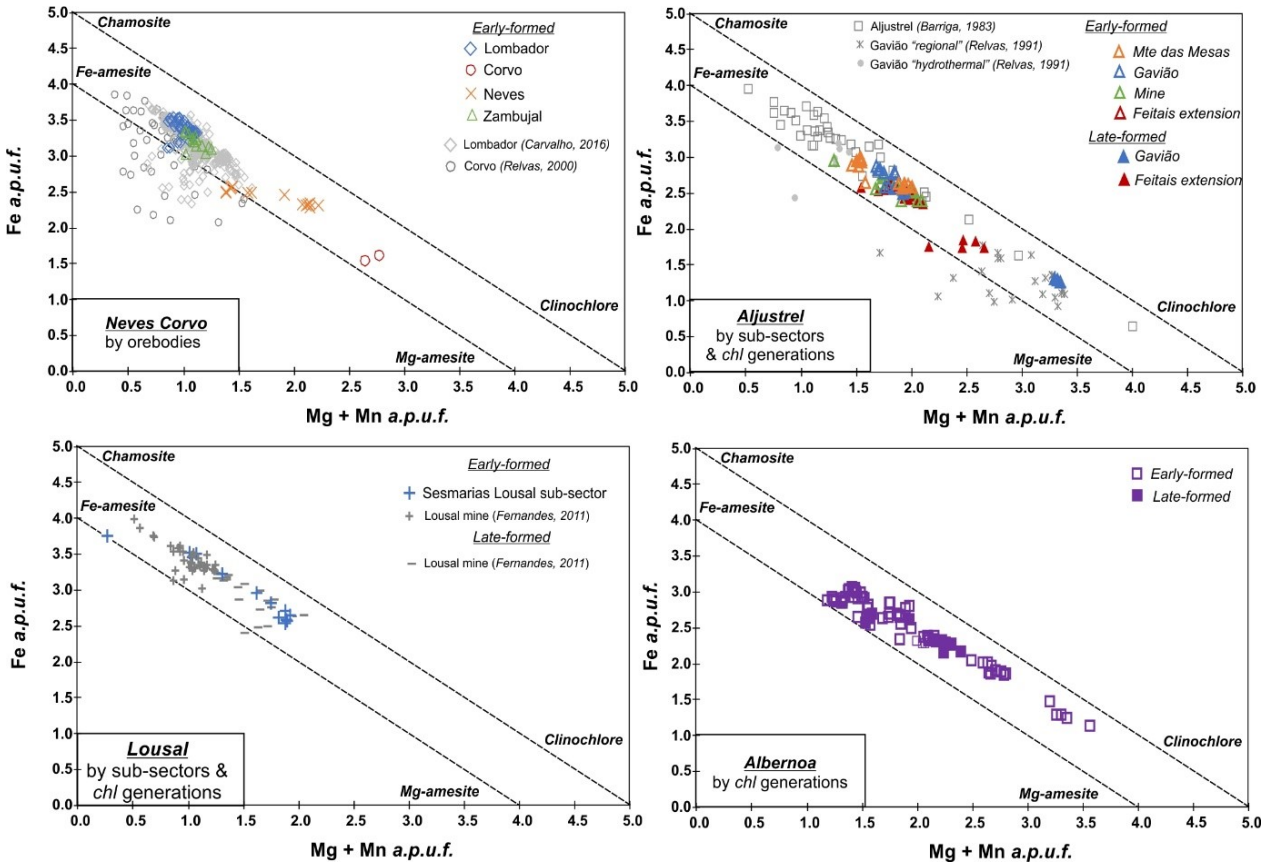

Figure 5.4 - Cross-plots showing the FM substitution vector by sectors. Dataset from Neves Corvo sector was divided by orebodies (all chlorites analysed are early-formed); the Aljustrel sector considered the three sub-sectors (Aljustrel mine, Gavião and Mte das Mesas prospect) and, whenever possible, early and late-formed chlorites were separated; the Lousal sector includes data from the Lousal mine and the Sesmarias prospect; and the Albernoa sector comprises analyses of early and late-formed chlorite. For reference and comparison purposes, the literature data were plotted for Aljustrel mine (stockwork/ore and HW position; n = 44; Barriga, 1983), Neves Corvo (stockwork/ore and FW position from Corvo n = 57 and Lombador n = 410 orebodies, Relvas, 2000 and Carvalho, 2016, respectively), Lousal mine (FW position and Late tectono-metamorphic, n = 64; Fernandes, 2011) and for Gavião prospect (regional and hydrothermal – FW and lateral to ore horizon, n = 31; Relvas, 1991).

5.1.2. Chlorite geothermometers

The chemical variation of chlorite is sensitive to (P-)T conditions. This involves the main chemical elements in chlorite composition like Fe, Mg, Al and Si. Cationic changes in octahedral positions or interchanges with tetrahedral positions are the basis of various geothermometric approaches (e.g. Cathelineau, 1988; Kranidiots & macLean, 1987; Jowett, 1991; zang & Fyfe, 1995; Walshe, 1986; Vidal *et al.,* 2001, 2005, 2006; Inoue *et al*., 2009; Bourdelle *et al*., 2013; Lanari *et al*., 2014). The main three mechanisms implicated in these changes are:

i. $(Fe^{2+})^{vi} = (Mg^{2+})^{vi}$;
ii. $(Si^{4+})^{vi} + (R^{2+})^{vi} = (Al^{3+})^{iv} + (Al^{3+})^{vi}$;
iii. $3(R^{2+})^{vi} = 2(R^{3+})^{vi} + []^{vi}$.

The most reliable empirical method to estimate the temperature formation of chlorite depends on its Al^{iv} content, calibrated in active geothermal systems and making use of neoformed chlorite aggregates (Cathelineau, 1988). Later, other authors attempted to improve this method, considering the influence of R^{2+} cations in the Al partitioning between octahedral and tetrahedral positions (Kranidiots & MacLean, 1987; Jowett, 1991; Zang & Fyfe, 1995). However, this method presents many limitations (e.g. de Caritat et al. 1993; Bourdelle and Cathelineau, 2015) and only yields reasonable results when the system is Al_2O_3-saturated.

Conceptually, the thermodynamic-based approaches can solve these limitations but other problems emerge when they are applied, namely: uncertainties in PT conditions used in model calibration; the exact thermodynamic conditions of the solid solution end-member and the better model for the dataset in study, considering substitution mechanisms (Grosh *et al.*, 2012). The accurate Fe^{3+} measurement is still a constraint, but it could be suitably circumvented in several thermodynamic-based approaches by using adequate solid solution models (e.g. Vidal *et al.*, 2001, 2005, 2006; Inoue *et al.*, 2009; Bourdelle *et al.*, 2013; Lanari *et al.*, 2014).

The chlorite formation temperature for the compiled dataset considered the thermodynamic-based approaches reported in Bourdelle *et al.* (2013) and Lanari *et al.* (2014). The latter approach fits better the observed compositional variation. Often, the Al content in octahedral and tetrahedral positions are quite similar and, occasionally, $Al^{iv} > Al^{vi}$ which hinders the use of the Bourdelle *et al*. (2013) model.

The thermodynamic model of Lanari *et al.* (2014) considers four independent end-members and two dependent end-members, as follows: C_1= *Mg amesite* ($[Mg_4Al_2][Si_2Al_2]O_{10}(OH)_8$)*;* C_3 = *clinochlore* ($[Mg_5Al][Si_3Al]O_{10}(OH)_8$)*;* C_4 = *daphnite* ($[Fe^{2+}{}_5Al][Si_3Al]O_{10}(OH)_8$) and *$C_5$* =

Mg sudoite ($[Mg_2Al_3\square][Si_3Al]O_{10}(OH)_8$)*;* the two dependent end-members are C_2 = *Fe amesite* ($[Fe^{2+}{}_4Al_2][Si_2Al_2]O_{10}(OH)_8$) and *C6 = Fe sudoite* ($[Fe^{2+}{}_2Al_3\square][Si_3Al]O_{10}(OH)_8$). From this six-member solid solution, the three following reactions can be established:

$$5\ Fe\text{-}am^* + 4\ clin = 5\ Mg\text{-}am + 4\ daph$$

$$Mg\text{-}am + 2\ Fe\text{-}sud^* = Fe\text{-}am^* + 2\ Mg\text{-}sud$$

$$2\ clin + 5\ Fe\text{-}sud^* = 2\ daph + 5\ Mg\text{-}sud$$

two of which linearly independent with two members (*) compositionally dependent. This approach considers the ordered cationic distribution model as proposed by Vidal et al. (2001, 2005, 2006):

$Al^{M4} = 1 - (Fe^{3+})^{vi}$

$\square^{M1} = 6 - \text{total vi}$

$Al^{M2\text{-}M3} = 2 \times \square^{vi}$

$Al^{M1} = 1 - (Fe+Mg+\square)^{M1}$

$(Fe + Mg)^{M1} = (Fe + Mg)_{total} - (Fe + Mg)^{M2\text{-}M3}$

$(Fe + Mg)^{M2\text{-}M3} = 4 - Al^{M2\text{-}3}$

$Mg^{M1} = [Mg / (Mg + Fe] \times (Fe + Mg)^{M1}$

$Fe^{M1} = \{1 - [Mg/(Mg+Fe)]\} \times (Fe+Mg)^{M1}$

$Mg^{M2\text{-}M3} = Mg_{total} - Mg^{M1}$

$Fe^{M2\text{-}3} = Fe_{total} - Fe^{M1}$

Therefore:

$(XSi)^{T2} = (Si - 2) / 2$

$(XAl)^{T2} = (4 - Si) / 2 = Al^{iv}/2$

$$(XSi)^{T2} + (XAl)^{T2} = 1.000$$

$(XMg)^{M1} = Mg^{M1}$

$(XFe)^{M1} = Fe^{M1}$

$(XAl)^{M1} = Al^{M1}$

$(X\square)^{M1} = \square^{M1}$

$(XMg)^{M1} + (XFe)^{M1} + (XAl)^{M1} + (X\square)^{M1} = 1.000$

$(XMg)^{M2\text{-}M3} = Mg^{M2\text{-}M3}/4$

$(XFe)^{M2\text{-}M3} = Fe^{M2\text{-}M3}/4$

$(XAl)^{M2\text{-}M2} = Al^{M2\text{-}M3}/4$

$(XMg)^{M2\text{-}M3} + (XFe)^{M2\text{-}M3} + (XAl)^{M2\text{-}M3} = 1.000$

$(XFe^{3+})^{M4} = (Fe^{3+})^{vi}$

$(XAl)^{M4} = Al^{M4}$

$(XFe^{3+})^{M4} + (XAl)^{M4} = 1.000$

In the Lanari et al. (2014) model the three parameters linearly independent are defined as:

$$x = \frac{4X_{Fe-am} + 5X_{daph} + 2X_{Fe-sud}}{4X_{Fe-am} + 5X_{daph} + 4X_{am} + 5X_{clin} + 2X_{Mg-sud} + 2X_{Fe-sud}} = \frac{Fe}{Fe + Mg} = X(Fe)$$

$$y = X_{Mg-am} + X_{Fe-am} + {}^{1}/_{2}\left(X_{clin} + X_{daph} + X_{Mg-sud}\right) = (XAl)^{M1}$$

$$z = X_{Mg-sud} = (X\square)^{M1}$$

where:

$X(Fe) = Fe^{2+}/(Fe^{2+}+Mg)$, so that $x = X(Fe)$

$Al^{iv} = 4 - (Si+Ti)$

$Al^{vi} = Al_{total} - Al^{iv}$

$R1 = Na+ K$

$\square = ½ (Al^{vi} - Al^{iv} + Fe^{3+} - R1)$, resulting $z = \square$

$Al^{M4} = 1- Fe^{3+}$

$Al^{M2\text{-}M3} = 2\square^{M1}$

$Al^{M1} = Al^{vi} - (Al^{M3} + Al^{M4})$, yielding $y = Al^{M1}$

The resultant structural formula is $(Al)_1(Mg,Fe,Al)_4(Mg,Fe,Al,\square)_1(Si,Al)_2O_{10}(OH)_8$ and the activity of the four independent members are:

$a_{C1} = a_{Mg\text{-}am} = k_1 (X_{Mg,M2\text{-}M3})^4 (X_{Al,M1}) (X_{Al,T2})^2$

$a_{C3} = a_{clin} = k_2 (X_{Mg,M2\text{-}M3})^4 (X_{Mg,M1}) (X_{Al,T2}) (X_{Si,T2})$

$a_{C4} = a_{daph} = k_4 (X_{Fe,\ M2\text{-}M3})^4 (X_{Fe,M1}) (X_{Al,T2}) (X_{Si,T2})$

$a_{C5} = a_{Mg\text{-}sud} = k_5 (X_{Al,\ M2\text{-}M3})^2 (X_{Mg,M2\text{-}M3})^2 (X_{\square,M1}) (X_{Al,T2}) (X_{Si,T2})$

with $k_1 = 1$; $k_3 = 4 = k_4$; $k_5 = 64$.

The reaction used in temperature estimation is $2C_3 + 3C_4 = 4C_1 + 7SiO_2 + 4H_2O$ (with $k = a^4_{C1}/(a^2_{C2} \times a^3_{C5})$, and if $\Sigma Fe = (Fe^{2+} + Fe^{3+})$:

$$T\ (ºC) = \frac{1723410}{-R\ logk + 315.149} - 273.15$$

where R = 8.3144 $J.K^{-1}.mol^{-1}$.

Table 5- shows the summary of descriptive statistics for chlorite temperatures considering only the studied sectors and the literature data. It is important to note that data collected from literature can be tentatively used for comparison purposes, notwithstanding the difficulties imposed by the analytical quality of some sets of analyses (e.g. errors likely above 2%) and the imprecise descriptions of textural arrangements that include all the analysed chlorite aggregates.

Table 5-2 - Summary of descriptive statistics for chlorite temperatures calculated with the model of Lanari *et al.* (2014).

Dataset		*n*	average	st. deviation	median
Neves Corvo		*80*	319	5	333
Aljustrel		*66*	347	8	345
Lousal (Sesmarias)		*14*	340	9	349
Albernoa		*82*	347	5	344
Literature					
Aljustrel mine	*Barriga, 1983*	*38*	398	12	379
NevesCorvo	*Relvas, 2000 & Carvalho, 2016*	*443*	348	2	352
Lousal	*Fernandes, 2011*	*43*	360	20	356
Gavião	*Relvas, 1991*	*21*	352	23	346

In general, the temperature formation of chlorite in the studied IPB metasedimentary successions range between 319 ± 5 and 347 ± 8 ºC (n = 267), not differing significantly from the values estimated on the basis of the data compiled from literature (**Figure 5.5**; Barriga, 1983; Relvas, 1991, 2000; Fernandes, 2011; Carvalho, 2016). In the latter dataset, several chlorite analyses yield geologically implausible temperature values (above ≈450ºC), which figure as outliers of each distribution per sector. These "anomalous" temperature values should be discarded as they likely represent inadequacy of the used solid solution model to describe the compositional features displayed by those chlorite aggregates. Nevertheless, the number of

chlorite analyses in this situation is minor and do not jeopardise the statistically representativeness of the central tendency measures that characterize the distribution of T values for each sector.

The obtained results can be summarised as follows (**Figure 5.6**):

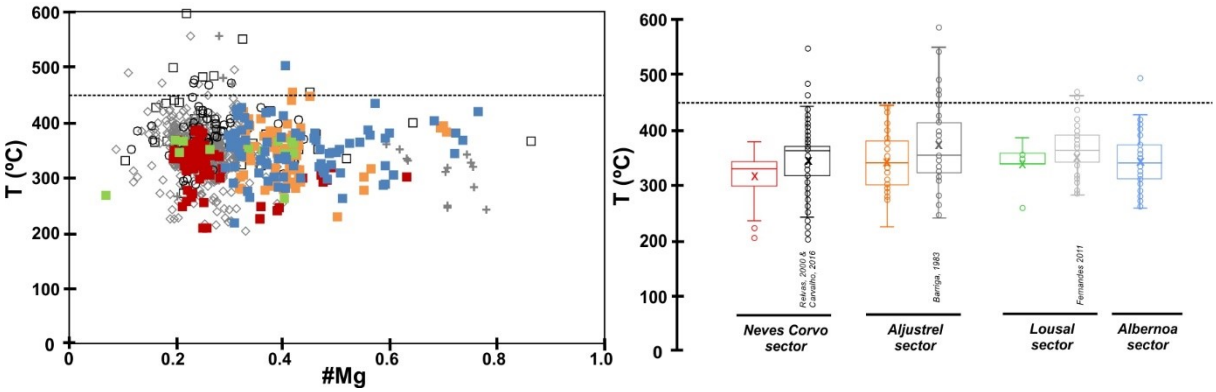

Figure 5.5 - On the left: Plot of #Mg vs. temperature for all dataset of chlorite calculated with the model of Lanari et al. (2014). On the right, box whiskers for all the chlorite dataset and the reference data for comparison. Both diagrams considered data collected from literature: Aljustrel mine (n = 44; Barriga, 1983), Neves Corvo (n = 467, Relvas, 2000, Carvalho, 2016), Lousal mine n = 64; Fernandes, 2011) and for Gavião prospect (n = 31; Relvas, 1991).

(i) Chlorite analyses from Neves Corvo display slightly differences in formation temperatures: *Lombador* = 334 ± 5º C, *n* = 453; *Corvo* = 332 ± 10º C, *n* = 39; *Neves* = 288 ± 10º C, *n* = 16 and *Zambujal* = 328 ± 7º C, *n* = 15. The #Mg [= Mg/(Fe+Mg)] ratios are similar (≈ 0.2) and only chlorites from Neves present #Mg > 0.25.

(ii) The late-formed chlorites from Gavião prospect and Feitais extension show always #Mg > 0.4, but a wide range of temperatures, from ≈ 200ºC up to 350 ºC (excluding 1 outlier). These chlorites are compositionally similar to those reported in Relvas (1991), interpreted as part of the "regional alteration" mineral assemblages due to seafloor metasomatism. The composition of early-formed chlorites, irrespectively of the sub-sector included in the Aljustrel sector, point to temperature conditions ranging from 250º C to 350ºC, like those observed in samples from Neves Corvo sector, regardless of differences in #Mg ratios.

(iii) For the Lousal mine, temperature values are somewhat higher (368 ± 5ºC) than those gathered for the previous sectors, even so consistent with the global range indicated by the chlorite analyses compiled from literature; as aforementioned, late-formed chlorite in samples from Lousal presents #Mg > 0.3, whereas early-formed chlorite shows #Mg < 0.3. In samples

from Sesmarias, the temperature formation of early-formed chlorite is 353 ± 3ºC and their #Mg ratios vary from less than 0.1 to ≈ 0.5.

(iv) The early-formed chlorites from samples of Albernoa are more enriched in Mg (0.2 < #Mg < 0.8) and their temperature formation is 349 ± 5ºC, somewhat above the values depicted by the late-formed chlorites (323 ± 8ºC). The total of analyses available for each chlorite generation is, however, quite distinct, and the differences found in temperature conditions may not be so relevant if the late chlorite generation includes a larger number of data.

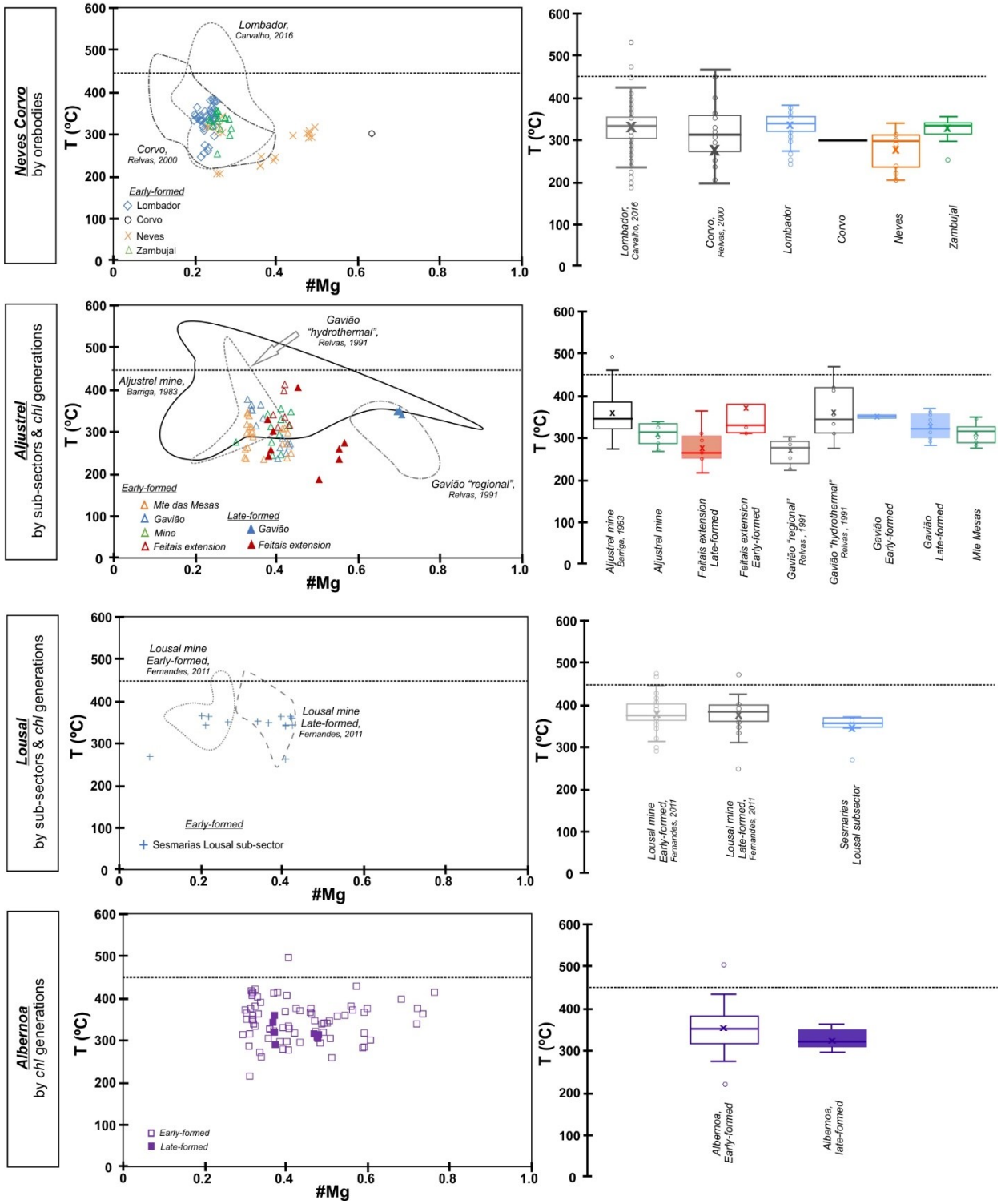

Figure 5.6 - On the left: Plot of #Mg vs. temperature of chlorite formation, separating sectors and chlorite generations. On the right, box whiskers with temperature ranges. Both plots use temperature values estimated on the basis of the model of Lanari et al., (2014). Dataset from Neves Corvo sector was divided by orebodies (all chlorites analysed are early-formed); the Aljustrel sector considers the three sub-sectors (Aljustrel mine, Gavião and Mte das Mesas prospect) and, whenever possible, the early- and late-formed chlorites were separated); the Lousal sector considers data from Sesmarias prospect (early-formed chlorites); and Albernoa includes data representing early- and late-formed chlorite. For reference and comparison purposes, literature data were plotted for Aljustrel mine (stockwork/ore and HW position; n = 44; Barriga, 1983), Neves Corvo (stockwork/ore and FW position from Corvo n = 57 and Lombador n = 410 orebodies, Relvas, 2000 and Carvalho, 2016, respectively), Lousal mine (FW position and Late tectono-metamorphic, n = 64; Fernandes, 2011) and for Gavião prospect (regional and hydrothermal - FW and lateral to ore horizon, n = 31; Relvas, 1991).

5.2. White mica

The dioctahedral K-mica, commonly termed muscovite or sericite according to the grain size, is one of the main mineral phases forming the studied metasedimentary rocks. This mica can result from metamorphic recrystallization of siliciclastic materials (clays), hydrolysis of volcanogenic-derived feldspar clasts incorporated in the sedimentary matrix or from different chemical reactions triggered by exhalative-hydrothermal activity potentially related to massive sulphide deposition. In the IPB, some authors (e.g. Barriga, 1983; Relvas, 1991, 2000) used the relative abundance of this phyllosilicate and its composition to distinguish the alteration haloes associated with the massive sulphide ore systems. Accordingly, the profusion and compositional variations recorded by white micas could be used as a footprint (vector) to the ore-forming system. As in the chlorite group, the common small dimension of white mica plates (in most case below the electron beam diameter) results in analyses with errors above 2% and for that excluded from the subsequent numerical processing. Nonetheless, 217 analyses of the total performed showed enough quality and were handled to conveniently characterize this mineral group in the studied IPB metasedimentary rocks. The petrographic inspection did not allow the separation of different mica generations. Most of the analyses were spotted in matrix domains (mainly early formed mica?), few of them also representing also hydrolysis products of feldspar grains. The analyses forming the latter group display errors above 2% and were discarded. **Figure 5.7 A** and **B** illustrate the two groups identified.

The general formula of dioctahedral mica is $(R^{+})^{xii}(R^{3+}_{(x-2)}R^{2+}_{x}\square)^{vi}(R^{4+}_{(3+x)}R^{2+}_{(1-x)}\square)^{iv}O_{10}(OH)_2$, as described in many studies (e.g. Velde, 1960; Bailey, 1986; Mateus, 1996). **Table 5-2** summarises the chemical variations obtained for white mica in samples picked in each sector. In addition, data from literature were compiled and separated into the categories defined by the authors of these studies; (i) regional (seafloor metasomatism, Relvas, 1991; Gavião prospect); (ii) hydrothermal - sericite *IIa* and *IIb*, outlining the distance to the feeder zones (Aljustrel and Neves Corvo, Barriga, 1983; Relvas, 2000; Carvalho, 2016).

The ternary diagram of Velde (1960) allow to separate and identify the different types of phyllosilicates (**Figure 5.8**). General trends could be identified using the data compiled from literature, shifting regularly from the ideal composition of muscovite towards the pyrophyllite end-member, with some minor deviations to montmorillonite-illite. White mica in samples from the Neves Corvo and Aljustrel mines (literature data) develop a regular array from muscovite-like compositions (sericite *IIa*) to those characterized by higher Si contents and lower occupancy of *xii* positions (sericite *IIb*). Regional and sericite *IIa* in samples from Gavião

prospect displays minor deviations from the ideal muscovite composition, although recording a significant amounts of R^{2+} cations (mostly Fe^{2+} and Mg) which become much higher in white micas found in samples from the Lousal mine (evidently deviating towards the phengite end-member, irrespectively of the sericite type). The obtained dataset shows similar compositional trends: (i) white micas in samples from Neves Corvo (mostly representing footwall positions, nearby the ore horizon) plot near the field of sericite *IIa;* (ii) white micas in samples from Albernoa, Aljustrel and Lousal are quite similar to sericite *IIa* and *IIb* from the Lousal mine; and (iii) in many cases, there is no evident compositional contrast between white micas forming the "regional alteration" assemblages and those ascribed to the superimposed halos of hydrothermal alteration.

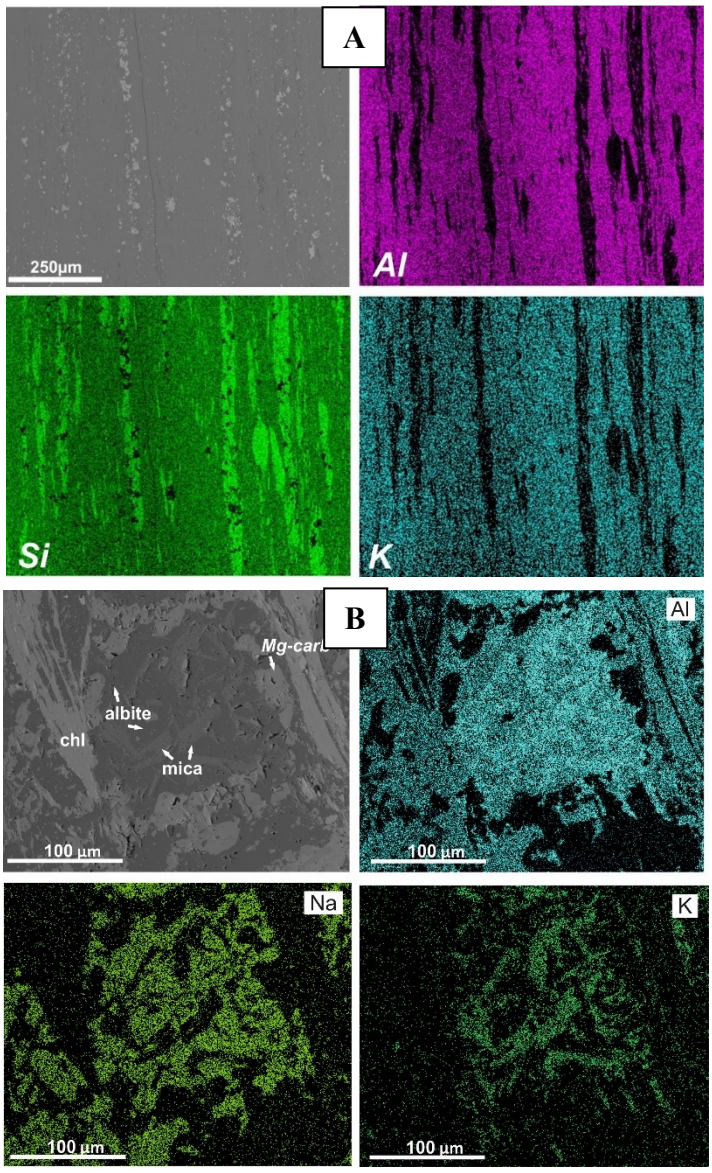

Figure 5.7 - **(A)** Back-scattered image of a common metapelite, where white mica is the predominant mineral phase. Chemical maps of the main mica components (Al, Si, K). (MFM#3 underground mine sample from Moinho orebody – Aljustrel). **(B)** Back scattered image of a hydrolyzed feldspar (ALB03#13a, 305.40 m, Albernoa sector).

Table 5-2 - Summary of descriptive statistics for white mica analyses, in wt% (n = 217). Appendix 3, *white mica sheet* show all the spot analyses

		Mean	St deviation	Median	Min	Max
Neves Corvo (n = 64)	*SiO2*	48.60	3.44	48.13	38.05	60.14
	Al2O3	33.42	3.12	34.34	24.99	38.05
	FeO	1.03	1.15	0.45	0.00	5.66
	Fe2O3	1.29	2.98	0.30	0.00	15.32
	MnO	0.01	0.01	0.00	0.00	101.81
	MgO	0.86	0.63	0.63	0.00	2.93
	CaO	0.04	0.04	0.03	0.00	0.12
	Na2O	0.58	0.25	0.51	0.07	1.34
	K2O	8.54	1.23	8.86	5.69	11.34
	F	0.15	0.10	0.16	0.00	0.39
	TiO2	0.46	0.54	0.22	0.01	2.62
	Cr2O3	0.07	0.02	0.07	0.02	0.11
	BaO	0.15	0.04	0.15	0.05	0.23

		Mean	St deviation	Median	Min	Max
Lousal (n = 20)	*SiO2*	50.05	3.52	49.07	42.54	59.45
	Al2O3	31.97	2.53	32.50	24.69	34.62
	FeO	1.29	1.45	1.19	0.00	7.09
	Fe2O3	0.63	0.70	0.24	0.00	2.22
	MnO	0.02	0.03	0.01	0.00	0.15
	MgO	1.30	0.31	1.24	1.04	2.54
	CaO	0.04	0.02	0.05	0.00	0.08
	Na2O	0.23	0.11	0.21	0.13	0.69
	K2O	9.69	0.96	9.94	6.50	10.57
	F	0.19	0.08	0.19	0.00	0.32
	TiO2	0.28	0.38	0.15	0.09	1.69
	Cr2O3	0.06	0.03	0.05	0.02	0.12
	BaO	0.22	0.07	0.22	0.11	0.34

		Mean	St deviation	Median	Min	Max
Aljustrel (n = 107)	*SiO2*	48.56	2.36	48.23	39.79	59.21
	Al2O3	32.74	2.28	32.98	21.20	36.02
	FeO	1.24	1.11	0.24	0.00	5.08
	Fe2O3	0.44	1.15	0.00	0.00	6.91
	MnO	0.05	0.15	0.02	0.00	1.39
	MgO	1.51	1.20	1.11	0.38	9.84
	CaO	0.05	0.06	0.04	0.00	0.55
	Na2O	0.45	0.53	0.36	0.12	6.20
	K2O	9.89	1.15	10.06	3.51	11.34
	F	0.16	0.11	0.14	0.00	0.53
	TiO2	0.25	0.41	0.13	0.00	3.05
	Cr2O3	0.06	0.03	0.06	0.00	0.13
	BaO	0.36	0.30	0.23	0.01	1.14

		Mean	St deviation	Median	Min	Max
Albernoa (n = 43)	*SiO2*	49.22	2.75	48.74	44.55	57.70
	Al2O3	32.47	3.10	32.52	25.15	37.79
	FeO	1.54	1.19	1.22	0.00	4.66
	Fe2O3	0.16	0.68	0.00	0.00	3.91
	MnO	0.03	0.09	0.02	0.00	0.52
	MgO	1.24	0.68	0.87	0.23	2.64
	CaO	0.09	0.08	0.07	0.01	0.31
	Na2O	0.88	0.86	0.44	0.19	3.20
	K2O	8.62	1.63	9.00	5.59	10.76
	F	0.12	0.09	0.09	0.00	0.44
	TiO2	0.35	0.60	0.12	0.00	3.07
	Cr2O3	0.07	0.02	0.07	0.02	0.12
	BaO	0.12	0.05	0.11	0.04	0.29

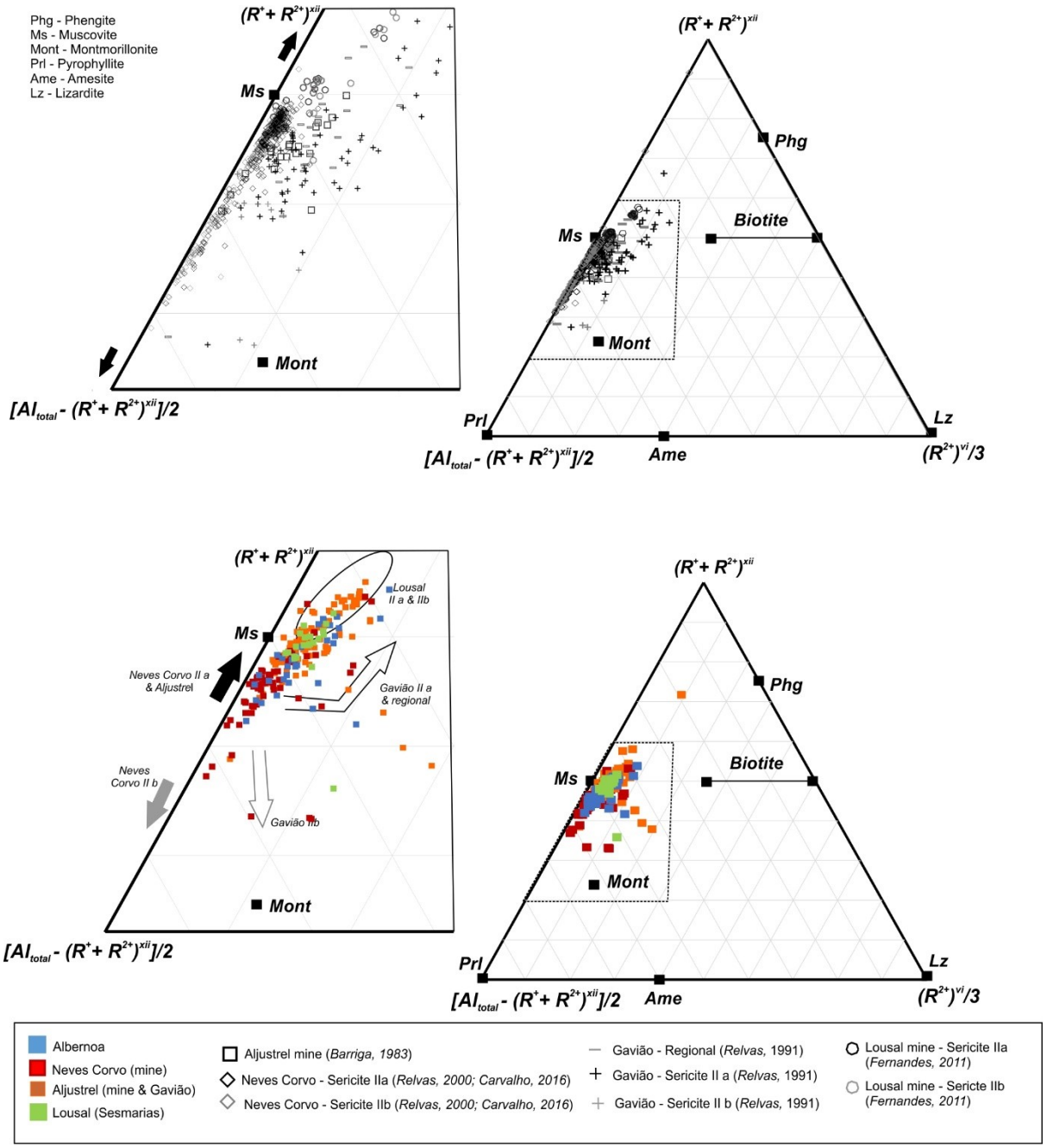

Figure 5.8 - Triangular plot (Velde, 1965) discriminating different phyllosilicates. Mineral compositions used as reference were taken from the Handbook of Mineralogy. On top, data from literature: Aljustrel (n = 21, stockwork/ore and HW position; Barriga, 1983), Neves Corvo (stockwork/ore and FW position from Corvo n = 108 and Lombador n = 368 orebodies, Relvas, 2000 and Carvalho, 2016, respectively), Lousal mine (FW position and late tectono-metamorphic, n = 30; Fernandes, 2011) and for Gavião prospect (regional and hydrothermal - FW and lateral to ore horizon, n = 97; Relvas, 1991). On the bottom, the studied dataset by sectors and the main trends defined on the basis of published data.

Four main substitution mechanisms explain the compositional variation recorded by the analysed white micas (**Figure 5.9**). The deviation from dioctahedral to trioctahedral K-micas is minor, although evident for many analyses, denoting a partial occupancy of the third octahedral position by divalent cations, as illustrated in the R^{3+} *vs.* Fe+Mg+Mn+Ti+(Si-3) plot. The Tschermark interchange mechanism [$(Si^{4+})^{iv} + (R^{2+})^{vi} = (Al^{3+})^{iv} + (Al^{3+})^{vi}$] is significant, mostly for white micas in samples from Aljustrel, Albernoa and Lousal. The incorporation of $R^{4+} = Ti^{4+}$ in octahedral positions according to the $(Al^{3+})^{vi} + (Si^{4+})^{vi} = (R^{4+})^{vi} + (Al^{3+})^{vi}$ cationic balance appears to be somewhat relevant in the analysed white micas, thus excluding most of the data compiled in literature. In dodecahedral positions, the main exchanges are $(K^{+})^{xii} = (Na^{+})^{xii}$ which are complemented in many cases with minor additions of $(R^{2+})^{xii}$ (mostly Ca and Ba) in accordance to the $(R^{+})^{xii} + (Al^{3+})^{vi} = (R^{2+})^{xii} + (R^{2+})^{vi}$ substitution mechanism.

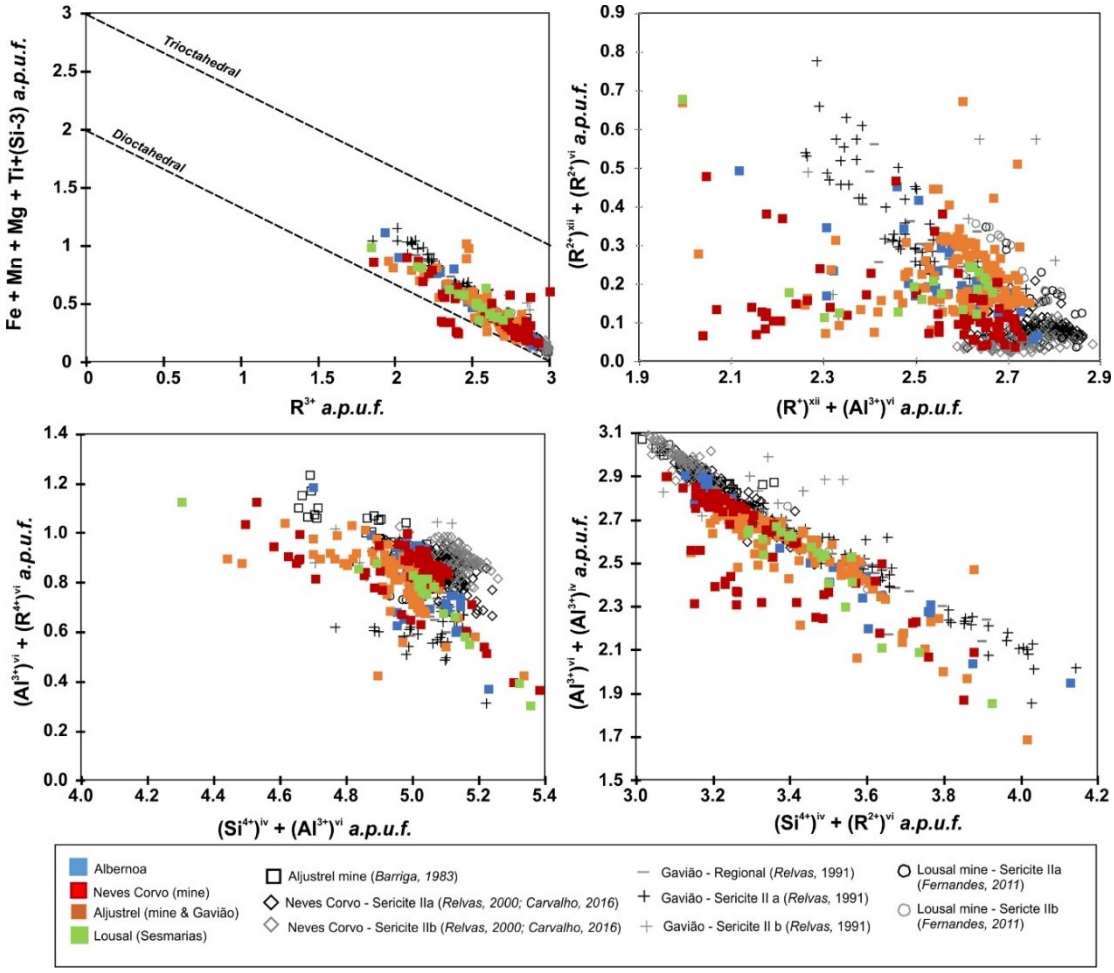

Figure 5.9 - Prevailing substitution mechanisms in the analysed white mica. Reference data from literature: Aljustrel (n = 21, stockwork/ore and HW position; Barriga, 1983), Neves Corvo (stockwork/ore and FW position from Corvo n = 108 and Lombador n = 368 orebodies, Relvas, 2000 and Carvalho, 2016, respectively), Lousal mine (FW position and late tectono-metamorphic, n = 30; Fernandes, 2011) and for Gavião prospect (regional and hydrothermal - FW and lateral to ore horizon, n = 97; Relvas, 1991).

5.3. Carbonates

Carbonates are common in the studied IPB fine-grained metasedimentary rocks. Their occurrence can denote a primary feature (e.g. upper PQG successions bearing carbonate-rich levels) or a secondary attribute related to seafloor metasomatism or exhalative-hydrothermal alteration processes. Distinction between these different environments is not simple, in particularly the latter two, due to the strong chemical reactivity of carbonates, which promotes the dissolution and re-precipitation of these phases, and favours their compositional re-homogenization according to local chemical gradients. Nonetheless, as in other studies (*e.g.* Relvas, 2000; Fernandes, 2011; Carvalho, 2016), considering the sulphide-rich mineral assemblages bearing carbonates and the textural arrangements, two main generations can be recognised: (i) carbonates related to the hydrothermal/mineralizing episodes; and (ii) carbonates included in late tectono-metamorphic veins/veinlets. Primary carbonate-rich levels from PQG were not sampled because this study was focused on the fine-grained siliciclastic sediments. A total of 105 EPMA analyses were used to characterize the compositional variation displayed by carbonates. For comparison purposes, data from Aljustrel (Barriga, 1983), Neves Corvo (e.g. Relvas, 2000; Carvalho, 2016) and Lousal (Fernandes, 2011) were compiled. The median composition for carbonates associated with the hydrothermal-mineralizing episodes is highlighted in **Table 5-3** and belong to the siderite group.

Table 5-3 - Median compositions of carbonates associated with the mineralizing episodes. Appendix 3 show all the spot analyses

Sector			*n*	Median composition
Neves Corvo (mine subsector)			17	$(Ca_{0.008}Mn_{0.014}Fe_{0.749}Mg_{0.231})CO_3$
Aljustrel (mine, Gavião subsectors)			4	$(Ca_{0.194}Mn_{0.006}Fe_{0.736}Mg_{0.194})CO_3$
Lousal (Sesmarias subsector)			27	$(Ca_{0.007}Mn_{0.005}Fe_{0.936}Mg_{0.049})CO_3$
Albernoa			0	-
Literature data				
Neves Corvo	*Relvas, 2000*	Corvo	34	$(Ca_{0.005}Mn_{0.020}Fe_{0.843}Mg_{0.227})CO_3$
	Carvalho, 2016	Lombador	233	$(Ca_{0.010}Mn_{0.015}Fe_{0.730}Mg_{0.245})CO_3$
Aljustrel	*Barriga, 1983*	stockwork & ore	14	$(Ca_{0.950}Mn_{0.023}Fe_{0.012}Mg_{0.012})CO_3$
		Paraíso *Fm.* HG	36	$(Ca_{0.512}Mn_{0.172}Fe_{0.048}Mg_{0.015})CO_3$
Lousal	*Fernandes, 2011*	host rocks	35	$(Ca_{0.008}Mn_{0.012}Fe_{0.962}Mg_{0.018})CO_3$

When plotted in the ternary diagram $MgCO_3$ – $CaCO_3$ – $FeCO_3$ the analytical data evidence clear differences for the two main carbonate generations and minor variances throughout the sampled sectors. Three types of carbonates were identified: calcite ($CaCO_3$, n = 35); dolomite/ferroan-dolomite ([$CaMg(CO_3)_2$ – $Ca(Fe,Mg)(CO_3)_2$], n = 23) and, the most abundant, siderite ($FeCO_3$, n = 47) often including significant amounts of Mg (**Figure 5.10**).

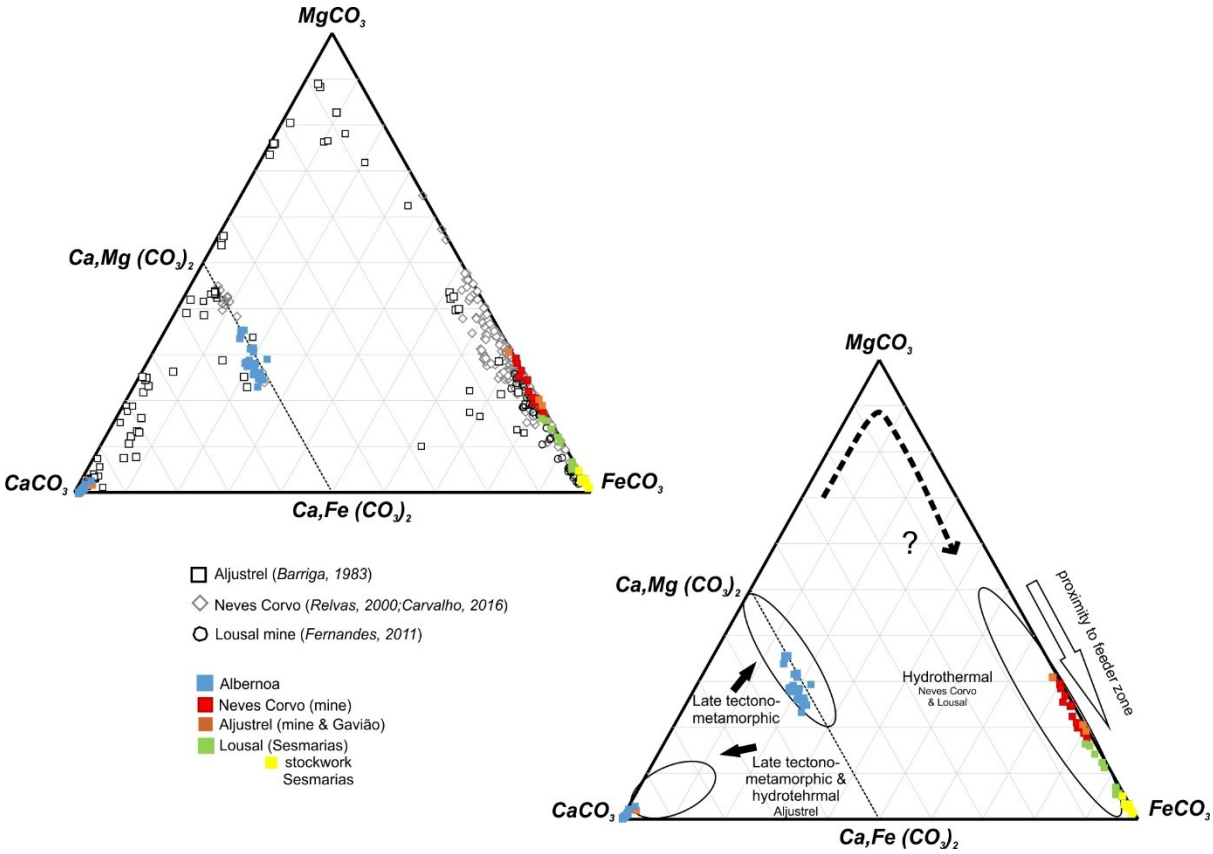

Figure 5.10 - Ternary diagram for carbonate phases $CaCO_3$ – $MgCO_3$ – $FeCO_3$. For reference and comparison purposes, literature data were collected: for Neves Corvo (n = 293), Relvas (2000) and Carvalho (2016); for Aljustrel (n = 90), Barriga (1983); and for Lousal (n = 35), Fernandes (2011).

The composition of preserved (or slightly modified) hydrothermal carbonates can be used to infer the chemical evolution of mineralizing fluids, mainly through their Fe and (Mg + Mn) contents. This variation has been described by different authors for several ore-forming systems in the IPB (e.g. Relvas, 2000; Carvalho, 2016) and in the Abitibi province, Kidd Creek deposit (e.g. Hannington et al., 1999).

Metapelite samples from Neves Corvo and Sesmarias (Lousal sub-sector) placed at the footwall of massive sulphide orebodies include carbonates with higher median Fe contents: #Fe = 0.75 and #Fe = 0.95, respectively. The increment towards the ideal composition of siderite ($FeCO_3$) is clear when carbonates forming samples from stockwork domains are considered. Carbonates

found in metapelite samples from the hanging-wall of the same locals display small compositional deviations with less Fe and Mn abundances. The obtained results are fully consistent with data already published for Neves Corvo (#Fe = 0.76; Relvas, 2000; Carvalho, 2016) and Lousal (#Fe = 0.89; Fernandes, 2011).

At Aljustrel, only few (n = 4) carbonate analyses show #Fe values (0.74) similar to those gathered in metapelites from Neves Corvo and Lousal. In fact, carbonates included in sulphide ore and stockwork samples are mostly Ca-rich and carbonates from samples placed at the hanging-wall of massive sulphides show always limited Fe abundances and a wide range (Mg + Mn) contents. These differences in composition suggest that carbonates in Aljustrel were subjected to significant late chemical transformations, thus becoming deprived of their initial Fe (±Mg, Mn) contents, or that carbonate deposition occurred significantly after the development of massive sulphides, when the circulating (residual) fluids were no longer enriched in those chemical elements. The latter hypothesis is possibly correct considering the observed textural relationships between carbonates, chlorite (± white mica) and sulphides in metapelites, usually indicating a relatively late growth of carbonates. Nonetheless, additional data are needed to confirm or infirm this interpretation, namely extending significantly the sampling program in order to include all the orebodies forming the Aljustrel ore system.

Late tectono-metamorphic carbonates were only identified in samples picked in different places of the Albernoa sector. These carbonates form two compositionally distinct groups: calcite and dolomite/ferroan-dolomite. Calcite was observed as interstitial grains and discrete (irregular) veinlets in few metapelites from Ervidel-Roxo, a specific sub-sector of the Albernoa sector; they display a median composition close to $Ca_{0.973}Mn_{0.010}Fe_{0.006}Mg_{0.005}CO_3$. The dolomite/ferroan-dolomite with median composition of $Ca_{0.525}Mn_{0.014}Fe_{0.195}Mg_{0.242}CO_3$ is very common but denoting a chemical environment distinct from that of Neves Corvo where the late tectono-metamorphic carbonates without evident relationship with sulphide-remobilization show compositions close to ($Ca_{0.048}Mn_{0.015}Fe_{0.504}Mg_{0.381}CO_3$). Once again, a wider sampling program is needed to investigate in detail these differences and suitably interpret their real geological meaning. **Figure 5.11** evidence the geochemical discrimination of carbonates by sectors.

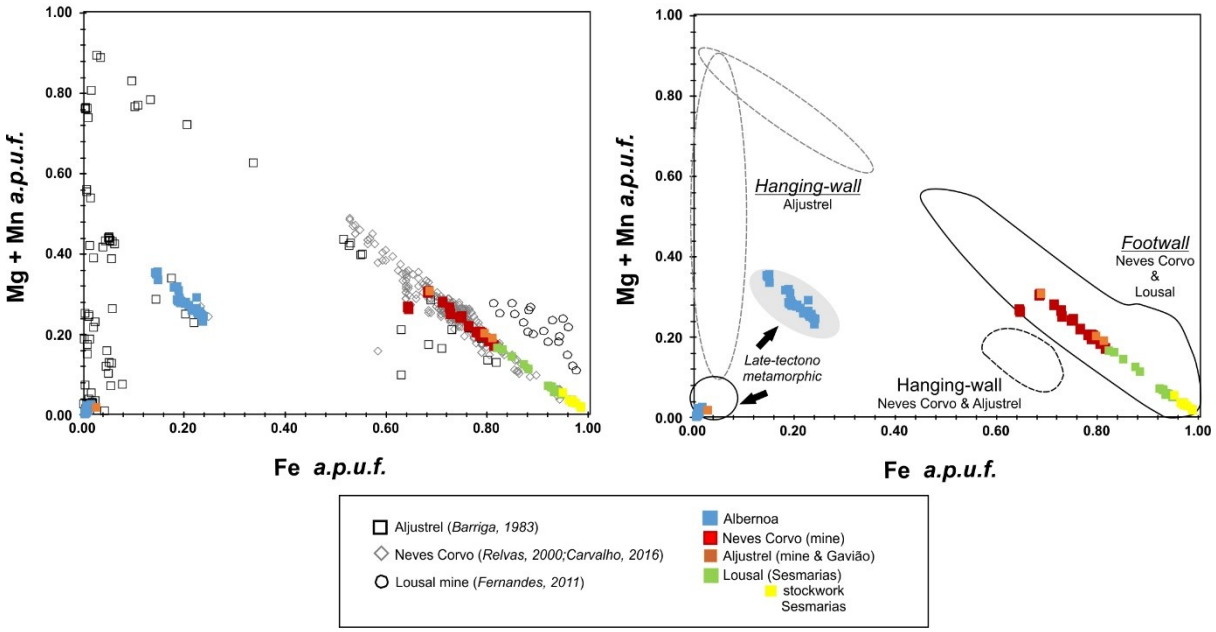

Figure 5.11 - Geochemical discrimination of carbonates by sectors based on Fe vs. Mg+Mn contents. Literature data were used to constraint proximity to feeder zones (Relvas, 2000, Fernandes, 2011, Carvalho, 2016).

5.4. Other mineral phases

5.4.1. Feldspars

The feldspars occur as an accessory mineral in coarse grained siliciclastic metasediments (e.g. meta-quartzwacke) and in metapelites comprising a volcanic-derived component; the latter rocks are quite frequent in the *upper* VSC sections. Feldspar EPMA data were essentially collected in samples from Aljustrel and Albernoa sectors (n = 42).

Table 5-4 - Summary of descriptive statistics, in wt%, for feldspars s.l. composition. Appendix 3, *feldspars table* show all the spot analyses.

		Average	St Deviation	Median	Min	Max
Albernoa (n=19)	**An %**	2.62	3.36	1.77	0.00	12.38
	Ab%	96.95	3.60	98.13	87.52	99.70
	Or %	0.43	0.64	0.20	0.00	2.70
Aljustrel (n=22)	**An %**	1.47	1.26	0.87	0.06	3.97
	Ab%	98.20	1.46	98.89	95.13	99.90
	Or %	0.33	0.42	0.16	0.00	1.67

The general formula for this group is MT_4O_8 where the tetrahedral positions are occupied by Si^{4+} and Al^{3+}, and the M positions by alkaline cations (mostly K^+, Ca^+ and Na^+). Based on the obtained analyses the molar fraction of each main component was estimated: $CaAl_2Si_2O_8$ (Anortite %) – $NaAlSi_3O_8$ (Albite %) – $KalSi_3O_8$ (Ortoclase %); **Table 5-4** highlights the ranges calculated for each component. In both sectors, the prevalent composition is albite: 96.65% and 98.20% for Albernoa and Aljustrel, respectively. Most of these analyses represent fractured or relic grains, but 4 spots document albite in an early-formed veinlet including carbonates (ferroan-dolomite + calcite) ± quartz ± chlorite ± sulphides (chalcopyrite, pyrite, siegenite, ulmannite e gersdorffite); no significant chemical differences exist between this albite and the fractured grains scattered in the siliciclastic matrix. The feldspar median composition in samples from Aljustrel is $(Na_{0.974}Ca_{0.009}K_{0.002})(Si_{3.003}Al_{0.987})O_8$ and in samples from Albernoa is $(Na_{0.984}Ca_{0.018}K_{0.002})(Si_{2.986}Al_{1.003})O_8$.

5.4.2. Zircon

Zircon is a common accessory mineral phase in the studied metasedimentary rocks, often displaying a grain size below the electron beam diameter. Compositional variations displayed by zircon can be useful to infer about their provenance or even to characterise possible late (hydrothermal) imprints. The Hf >> Th proportion and the main trivalent cation (Fe^{3+}), suggest that the analysed zircon grains are mainly detrital.

Table 5-5 - Summary of descriptive statistics, in wt%, for zircon composition Appendix 3, zircon table show all the spot analyses.

	Average	St deviation	Median	Min	Max
SiO2	32.86	0.72	32.74	30.84	34.75
ZrO2	64.41	1.57	64.87	58.98	66.32
P2O5	0.16	0.39	0.04	0.00	2.39
HfO2	1.17	0.20	1.16	0.73	1.52
La2O3	0.02	0.02	0.00	0.00	0.09
Ce2O3	0.06	0.09	0.03	0.00	0.40
ThO2	0.06	0.09	0.02	0.00	0.47
Nd2O3	0.01	0.02	0.00	0.00	0.09

Three main zircon types were distinguished on the basis of textural arrangements provided by high resolution images (**Figure 5.12**): (i) fractured grains; (ii) fractured grains with corroded borders; and (iii) fractured grains with coatings and/or fracture infillings of xenotime (YPO_4) ± REE-phosphate.

These three zircon types do not display significant compositional variations, remaining close to the ideal formula ($Zr_{3.86\pm0.11}Si_{4.03\pm0.06}O_4$), even though displaying a slightly deviating Si:Zr proportion, possibly due to minor cation substitution and analytical errors. According to the available data (**Table 5-5**) and to the results reported in several studies on zircon composition: (1) the total R^{4+} cations in *A* coordination sites should be (Zr + Hf + U + Th) instead of Zr, as proposed by Fowler *et al*. 2002); (2) the proportion of R^{3+} cations in *A* sites must be similar to the proportion of P^{5+} at the *B* sites, according to the coupled-substitution mechanism Zr^{4+} + Si^{4+} = $(Y, REE)^{3+}$ + P^{5+} (e.g. Speer 1980, Hanchar *et al.* 2001); (3) Al^{3+} is preferentially incorporated in *B* sites, according to the coupled substitution (P^{5+} + Al^{3+}) = $2Si^{4+}$, as indicated by Uher & Černý (1998) and Akhtar & Wassem (2001); and (4) the trace (and irregular) amounts of R^{2+} cations, likely occupying interstitial sites (*int*), could be related to the following mechanism of charge balance for the (Y, REE) in excess of P: $R^{2+}_{(int)}$ + $3(Y, REE)^{3+}$ + P^{5+} = $3Zr^{4+}$ + Si^{4+} (Romans *et al*. 1975, Hoskin *et al*. 2000).

5.4.2. Rutile

Rutile is the second more common accessory mineral phase in the studied metasedimentary rocks. The chemical variation in rutile could be useful as pathfinder to the ore-forming systems. However, in the 27 spot analyses performed on Neves Corvo, Aljustrel and Albernoa sectors no differences were observed. **Table 5-6** summarize the rutile compositions and further information on cation distribution are in Appendix 3 - rutile.

Table 5-6 - Summary of descriptive statistics, in wt %, for rutile compositions. Appendix 3, rutile table show all the spot analysis.

	Average	**St deviation**	**Median**	**Min**	**Max**
Ta2O5	0.05	0.07	0.00	0.00	0.28
Nb2O5	0.37	0.14	0.36	0.06	0.73
TiO2	97.94	0.79	98.07	96.07	99.36
Fe2O3	0.63	0.30	0.58	0.21	1.59
Cr2O3	0.04	0.10	0.01	0.00	0.53
CuO	0.07	0.12	0.02	0.00	0.47
ZrO2	0.06	0.08	0.04	0.00	0.39

Detailed petrography and subsequent EPMA observations allow the identification of two rutile types. The first one includes detrital rutile grains with almost no visible alteration. The second type comprises rutile grains in close association with uncommon mineral assemblage: chalcopyrite + REE-phosphates + rutile (**Figure 5.12**). These rutile grains display irregular ZrO_2 abundances, up to 0.012 wt%, pointing to maximum temperature conditions of about 500 ºC

or ranging from ca. 490 to 500ºC ($0.7 \leq aSiO_2 \leq 1.0$), if the geothermometric approaches of Watson et al. (2006) and Ferry and Watson (2007) are considered, respectively. Since rutile deposition precedes the chalcopyrite growth in the aforementioned mineral aggregates, it is plausible to assume that the estimated temperatures represent the upper limit for the early hydrothermal fluid inflows into metapelites. However, to confirm or not this inference in future other analytical methods than EPMA should be used to better characterise the composition of rutile (such as LA-ICP-MS).

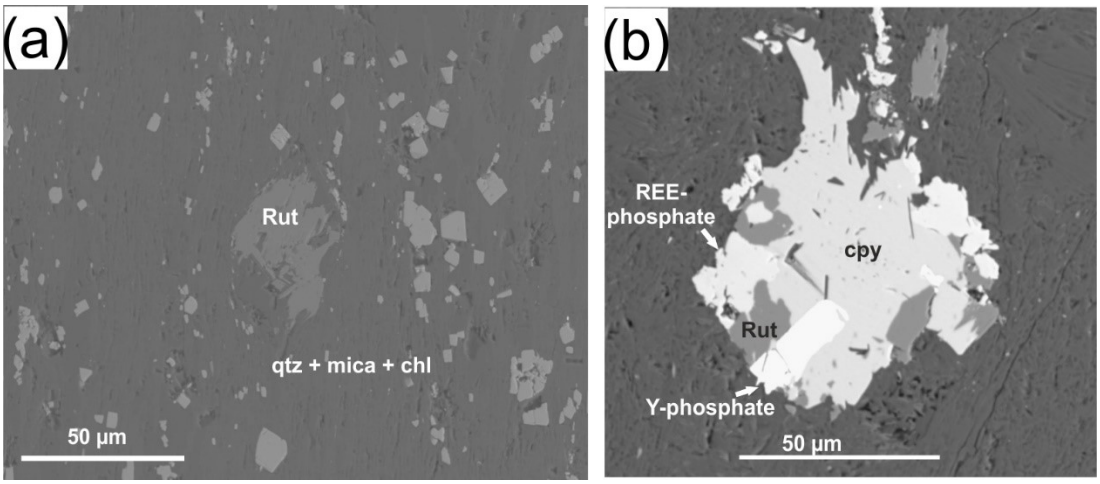

Figure 5.12 - Back scattered electron images from the two main rutile types. On the left, a detrital (fractured and corroded) rutile (MFM#3, underground mine - Aljustrel sector). On the right, rutile associated with REE- and Y-bearing phosphates and sulphides (ALB03#22a, 401.50 m – Albernoa sector).

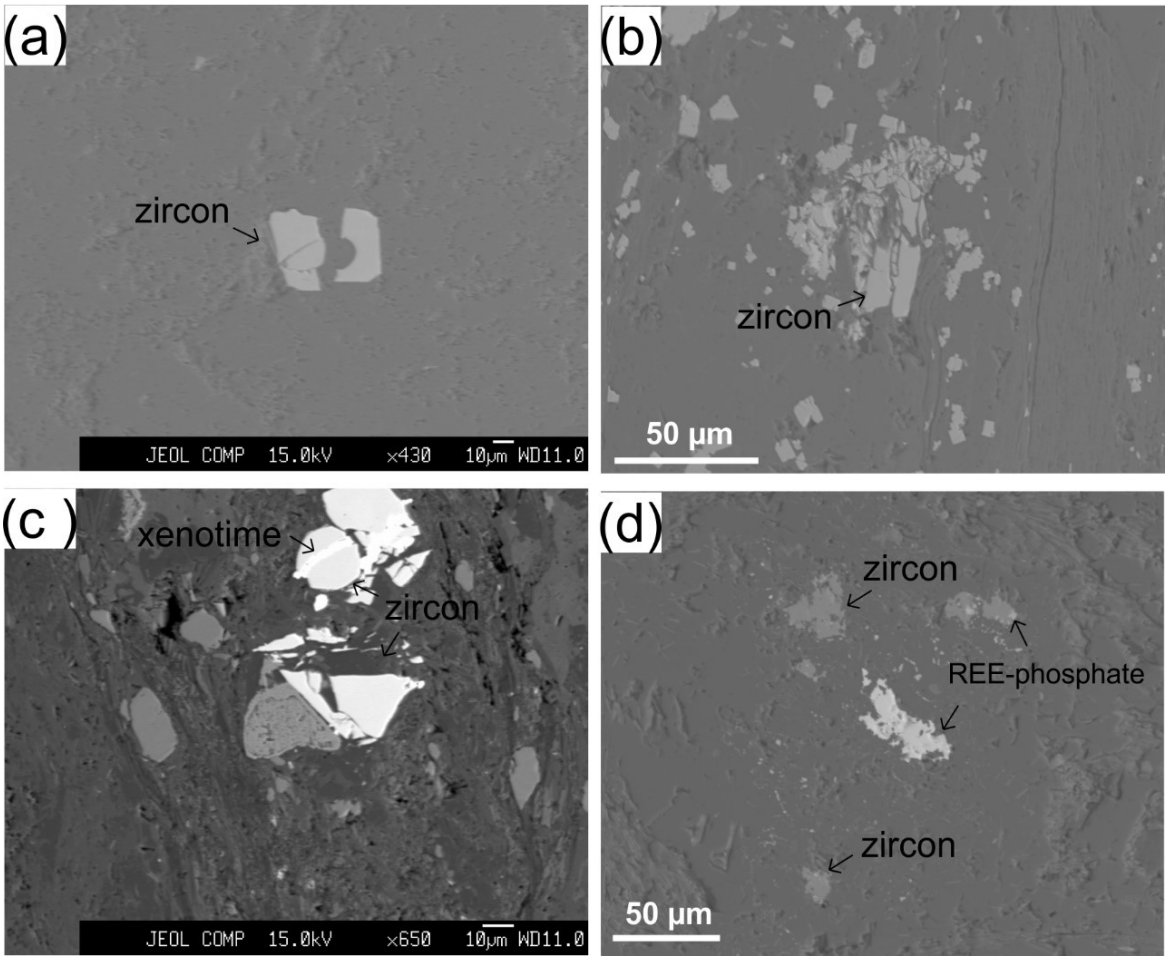

Figure 5.13 -Back-scattered images of zircons representing the three main groups: (a) outcrop sample – T73, Albernoa sector; (b) underground sample, Aljustrel mine – MFM#3; and (c) drill-core sample 18-1-G2, 89.75 m, Albernoa sector; (d) underground sample, Neves Corvo, Zambujal orebody.

5.5. Sulphide phases

Sulphide phases were not the focus of this study. However, some spot analysis was done to control possible chemical variations. **Figure 5.14** illustrates the principal textural features observed involving sulphide phases. All the EPMA analytical data are in Appendix 3.

Pyrite

The available analytical dataset shows that pyrite composition is close to the ideal one ($Fe_{0.999\pm0.07}S_{1.992\pm0.008}$), revealing traces as well (< 0.001 a.p.u.f.) of As, Co and Ni. Despite of 170 spot analyses done in framboidal to partially crystallized pyrite grains and pyrite aggregates clearly associated with hydrothermal mineral assemblages (quartz ± sericite ± chlorite ± sulphides), no evident chemical variations were detected with the EPMA. Some pyrite grains included in mineralized domains show higher abundances of trace elements, like Co and Ni, but these are quite irregular to sustain any convincing statement. Nonetheless, these compositional signs should be explored in the future with LA-ICP-MS, clarifying possible chemical differences between diagenetic and hydrothermal pyrite in the IPB.

Chalcopyrite

According to the obtained EPMA data, the general composition of chalcopyrite in the examined samples is $Cu_{0.98\pm0.01}Fe_{0.008\pm0.008}S_{2.02\pm0.001}$, incorporating always trace amounts of Co, Zn and Pb, sporadically coupled with As. Despite the strong chemical similarity of the analysed chalcopyrite grains/aggregates (n = 61), they represent two distinct types, found in quite different textural arrangements. In the first one, related to the massive sulphide mineralizing episodes, chalcopyrite comes along with pyrite ± sphalerite and sometimes with other mineral phases, such as REE- and Y-bearing phosphates and As-Co-Ni-S-bearing mineral phases. This "chalcopyrite type" occurs mostly in samples from mining centres: Neves Corvo, Lousal and Aljustrel, following the order of occurrence frequency. In the second type, recognised in many samples from Albernoa sector, chalcopyrite is generally associated with mineral infillings of late-formed veinlets, namely: (i) quartz ± carbonate (calcite and/or ferroan-dolomite) ± pyrite ± chalcopyrite; and (ii) calcite ± ferroan-dolomite ± chalcopyrite. Matrix disseminated chalcopyrite is rare although observed in few samples together with pyrite.

Sphalerite

The existing dataset for sphalerite demonstrates that all the spot analyses (n = 41) are close to the ideal formula ($Zn_{0.927\pm0.05}S_{1.014\pm0.009}$), despite of the usual presence of some minor and trace elements. Iron is common (up to 0.05 a.p.u.f.), occasionally coupled with Cu and Pb (up to

0.014 a.p.u.f.); Co and Cd abundances are quite irregular and typically negligible (< 0.01 a.p.u.f.). In samples from the Albernoa sector, sphalerite disseminations were identified mostly in metapelites with a volcanic-derived component and affected by fault-controlled hydrothermal alteration. In the other sectors, mainly Neves Corvo and Aljustrel, two sphalerite types were distinguished: (i) fine-grained sphalerite disseminations in non-altered rock matrix, suggesting that their occurrence might be related with redox conditions established during sedimentation and/or diagenesis; and (ii) well-developed sphalerite grains/aggregates along with other sulphides (pyrite ± chalcopyrite ± galena) and the typical hydrothermal alteration assemblage (quartz + chlorite ± sericite), related to exhalative-hydrothermal activity. The first occurrence type is common in samples from Aljustrel and few samples from Neves Corvo. The second occurrence type was only recognised in samples from Neves Corvo, especially from the Lombador and Zambujal orebodies.

Galena

The available analytical (n=14) dataset shows that galena composition is close to the ideal one ($Pb_{0.992\pm0.014}S_{0.982\pm0.010}$), revealing traces of Cu up to 0.03 a.p.u.f. Galena is present mainly where effects of hydrothermal activity were recognized irrespectively of the sampled sector. At mine centers (Neves Corvo and Lousal) and Sesmarias prospect it occurs as small grains due to replacement and/or exsolutions in pyrite and chalcopyrite.

Arsenopyrite & Cassiterite

Arsenopyrite and cassiterite are two mineral phases only identified at Neves Corvo and Lousal mine, respectively. Both present analyses which are above the admitted error (> 2%) and for that reason were not processed. Arsenopyrite grains occurred associated with the typical hydrothermal (secondary) mineral assemblage or in some hanging wall samples that at some point were affected by high-temperature fluids channelized into fault zones. At Sesmarias prospect cassiterite grains were identified in one sample from stockwork. These cassiterite grains seems to be altered and involved (and crossed when fractures) by the stockwork assemblage (quartz ± carbonate ± chlorite ± pyrite ± chalcopyrite ± galena) related to the main mineralizing event. The host rock, a black metapelite whose matrix is enriched in quartz and apatite, should be the focus of future detailed studies, using the P content to infer the depositional event and its relationship with cassiterite grains on matrix. More sampling in this prospect is needed to better understand the process involved in the development of massive sulphide lense.

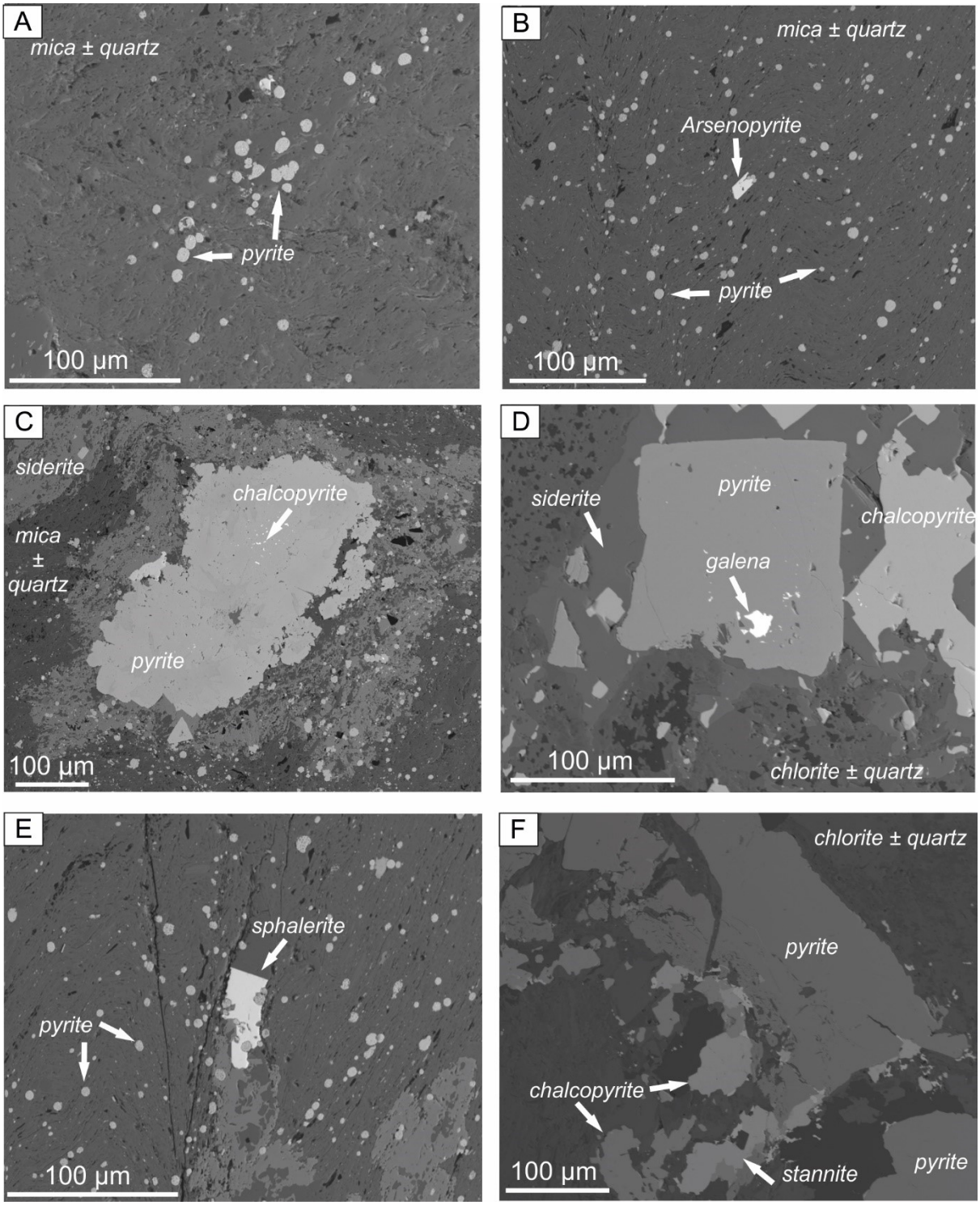

Figure 5.14 - Back-scattered images of the common sulphide phases identified in the studied metasedimentary rocks from the IPB: **(A)** Framboidal pyrite (SES20#10, 288.60 m, FW position); **(B)** Framboidal pyrite with arsenopyrite (underground mine, NCL#6, HG position). **(C)** Recrystallized pyrite with chalcopyrite exsolutions (SES20#10, 288.60 m, FW position); **(D)** Sesmarias stockwork: quartz ± chlorite ± siderite ± sulphides (SES20#9, 279 m); **(E)** Framboidal pyrite with sphalerite (underground mine, NCL#6, HG position); **(F)** Stockwork hosted in black metapelites, Lombador orebody (underground mine, NCL#10, FW position).

Other sulphide and sulphosalt phases

The common sulphide phases recognised in the studied metasedimentary rocks is quite simple, comprising mostly pyrite, sphalerite, chalcopyrite and galena. However, a suite of other sulphides and sulphosalts (As-Co-Ni-Sb-Ni-bearing phases) have been described mainly for the Spanish IPB segment (e.g. Marcoux et al., 1999; Almodóvar et al., 2019). In the examined metapelites, these mineral phases are often fine grained, and the preserved textural relationships are not clear enough to support any correlation with the four-stage evolution reported in Almodóvar et al. (2019). Nonetheless, they seem to be relatively common despite of the difficulties posed by the tiny dimension of grains in their optical identification and composition assessment.

A wide group of different mineral phases were identified but only for cobaltite it was possible to gather significant number of quantitative analyses (n = 15), which documents a composition close to the ideal: $Co_{0.81\pm0.08}As_{0.92\pm0.02}S_{0.99\pm0.02}$ also displaying significant trace amounts of Ni and Fe. For this reason, **Figure 5.15** illustrates the main identified sulphide phases identified and, whenever possible, the respective compositional map. These mineral phases were recognised in samples from all the studied sectors, but preferentially in those representing metasedimentary rock domains adjoining feeder zones of massive sulphide ore-forming systems or hydrothermal alteration haloes enclosing (late?) fault-zones.

At the Aljustrel sector, early-developed (prior to Variscan deformation/metamorphism) fractures filled with carbonate + pyrite ± siegenite [$(Ni,Co)_3S_4$] ± ullmannite [(Ni,Sb)S] ± gersdorffite [(Ni,As)S] are common in metapelites with a volcanic-derived component. Often, other sulphide phases, like cobaltite [(Co,As)], ikunolite [$Bi_4(S,Se)_3$] and kharaelakhite [$(Cu,Pt,Pb,Fe,Ni)_9S_8$] (± chalcopyrite ± pyrite), occur as fine-grained disseminations in the rock matrix. Nevertheless, a straightforward paragenetic sequence is not easy to establish because all these mineral phases occur nearby fault-zones that record multiple hydrothermal circulation imprints. This is also the case of some samples from the Albernoa sector. In samples from Neves Corvo and Sesmarias (Lousal sub-sector), representing footwall levels nearby feeder zones, the aforementioned As-Co-Ni-Sb-bearing sulphide assemblages were also identified, coming along with quartz + chlorite ± carbonate ± common sulphides. For the Lousal mine, other Bi- and Au-bearing occurrences associated with fault-controlled Late-Variscan hydrothermal activity were reported in other studies (e.g. Oliveira et al., 2011; Fernandes, 2011).

The relationships of these sulphides and sulphosalts with the common sulphide assemblage forming the massive ores are not well known, at least in the shale-hosted systems of the IPB. Therefore, complementary studies are needed to better understand this mineralogical finger/footprint in the framework of massive sulphide ores deposition and evolution.

Figure 5.15 -(next page) – Back-scattered images of the less common sulphide phases identified in the studied metasedimentary rocks- **(A)** Early fractures filled with carbonate + chalcopyrite ± pyrite ± ullmannite ± siegenite ± gersdorfitte (EDS1-H, 385.20 m, HG position); **(B)** and **(C)** Bi- and Pb-bearing phases in quartz + chlorite ± carbonate rock matrix, nearby fault zones recording evidence of multi-stage hydrothermal circulation. **(D)** Compositional map for the back-scattered image in (C) (MDM02#4, 117 m, HG position); **(E)** and **(F)** One of the common relationship of cobaltite and pyrite and the corresponding compositional map (underground mine, NCN#17, FW position); **(G)** and **(H)** Cobaltite grain with chalcopyrite disseminated in the rock matrix and their respective compositional map (MM16#9, 340 m, HG position,). All compositional maps include only the main elements to characterize the uncommon sulphide phases.

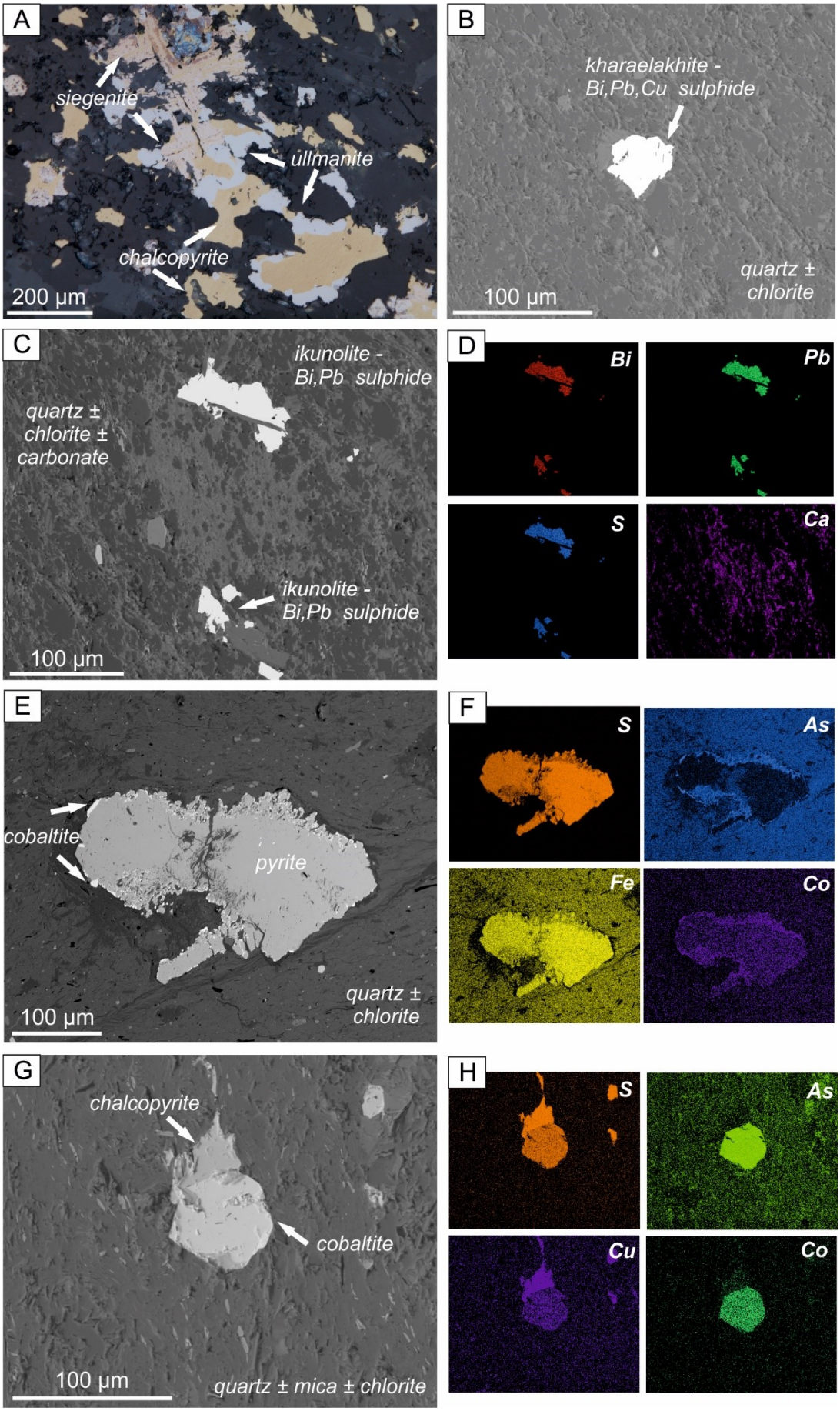
A
siegenite
üllmanite
chalcopyrite
200 µm
B
kharaelakhite -
Bi,Pb,Cu sulphide
quartz ±
chlorite
100 µm
C
ikunolite -
Bi,Pb sulphide
quartz ±
chlorite ±
carbonate
ikunolite -
Bi,Pb sulphide
100 µm
D
Bi
Pb
S
Ca
E
cobaltite
pyrite
quartz ±
chlorite
100 µm
F
S
As
Fe
Co
G
chalcopyrite
cobaltite
100 µm
quartz ± mica ± chlorite
H
S
As
Cu
Co

SECTION 6

6. Summary results of the main research topics

The detailed characterization of metasedimentary successions included in the PQG and VSC lithostratigraphic units is fundamental to better understand the geological evolution of the IPB basins, namely through the characterization of depositional environments and identification of the main siliciclastic sources involved. Furthermore, as massive sulphides are often hosted in metasedimentary rocks, it is possible to conceive new exploration vectors in the IPB for massive sulphide accumulations based on geochemical/mineralogical fingerprints and footprints.

To better support and contextualise the new gathered data and interpretations, whole-rock chemistry results and isotopic information obtained in key-studies performed in the past were extensively compiled. For mineral chemistry, reference data picked in previous works were mostly limited to samples from active or old mines in the Portuguese sector of the IPB; this database in clearly incomplete and should be expanded in the near future.

This section presents a summing up of the main results obtained in the last four years of research under the scope of the PhD project introduced in section 1.

6.1. Sediment sourcing

The combination of geochemical ratios and Nd-Sr isotopic compositions is a useful tool to determine the sediment provenance. The prevalent siliciclastic constituent forming metapelites included in the PQG and VSC metasedimentary successions are derived from the same continental source (Luz *et al*., 2019, 2020). This source is dominated by weathered products of felsic (granitic) to intermediate composition (granodiorite to quartz-diorite), typified by similar Th/Sc and Zr/Sc ratios (Slack *et al.,* 2004) and well-bounded La/Th : Hf proportions (Floyd and Leveridge, 1987); additional contributions from an old metasedimentary source (Hf ≥ ≈7) are also recognisable in many samples, mostly from PQG . Two main components resulting from the continental source erosion can be distinguished based on Al_2O_3/TiO_2, Zr/Al_2O_3, Sc/TiO_2, Ga/TiO_2 and Th/Sc ratios (Luz et al., 2020). The first component is clayey-derived, dominant in metapelites from the *middle* to *upper* VSC sections and denoted by Al_2O_3/TiO_2 between 25 and 30, and Zr/Al_2O_3 ranging from 0.0005 to 0.001 (Th/Sc ≈ 0.5 to 0.8). The second component is (fine-grained) sandy-derived, quite relevant in metapelites forming the *upper* PQG and some of the sampled *lower* VSC sections, and are characterised by lower Al_2O_3/TiO_2 ratios (between 10 and 20) and higher Zr/Al_2O_3 ratios (from 0.001 to 0.025), without significant changes in Th/Sc ratios (≈ 0.5 to 1). These two components have indistinguishable isotopic

compositions as indicated by the similar whole-rock εNd_i values (-11 to -8) obtained for siliciclastic sediments deposited in the IPB from the Givetian to the Upper Fammenian (e.g. Jorge, 2009; Luz *et al*., 2020). Therefore, the composition of metasediments included in PQG and *lower* VSC successions mainly reflect the fingerprint of a regional siliciclastic mixing derived from the dismantling of an older crust which, locally, and according to the Sr-isotope systematics, might be somewhat modified by seawater during Devonian-Carboniferous boundary (Luz *et al*., submitted).

A third, volcanic-derived component is significant in many metapelites forming several of the sampled *upper* VSC sections. The incorporation of this component yields distinctly higher Al_2O_3/TiO_2 ratios (from 45 to 65) along with relatively low Zr/Al_2O_3 values (between 0.001 and 0.025) and Th/Sc often above 1. In these samples, the whole-rock εNd_i increases up to +0.2, towards the isotopic compositional field of the IPB metavolcanic rocks, clearly reflecting local volcanic-derived additions of variable proportion to the siliciclastic mixture deposited during the time period from the Upper Tournaisian to Visean times. Significantly, higher Th/Sc values coupled with meaningful εNd_i rises reflect the incorporation of felsic (rhyolitic-rhyodacitic) volcanic-derived components (as documented for the Aljustrel and Lousal sectors), whereas lower Th/Sc ratios and minor increments in εNd_i denote lesser contributions of the third component and/or the inclusion of volcanic-derived components of intermediate ("andesite"-like) composition (e.g. Mitjavilla *et al*., 1997; Donaire *et al*., 2020; Luz *et al*., submitted)

The higher whole-rock $(^{87}Sr/^{86}Sr)_i$ values (up to 0.727) together with εNd_i values around -10 recorded by basal units (PQG and *lower* VSC) are consistent with siliciclastic sources related to an old (more radiogenic) basement. The obtained T_{DM} ages, ranging from 1.08 to 2.02 Ga, also support this interpretation. Samples stratigraphically below and laterally equivalent to the PQG (Gafo, Rib. Limas and Sta. Iria formations) present the lowest εNd_i values (-10.7 to -9.5) and the oldest T_{DM} ages (1.90 ± 0.04 Ga), similar to those ascribed to the Meguma Terrane (1.94 ± 0.06 Ga; Clarke & Halliday, 1985; Clarke *et al*., 1997; Braid et al., 2012). So, mixtures resulting from the dismantling of old metasediments and granitoid rocks alike of those described for the Meguma Terrane result in similar signatures to those showed by the IPB basal units.

The T_{DM} ages vary with stratigraphy and are younger in the upper units: PQG: 1.83 ± 0.09 Ga; *lower* VSC: 1.85 ± 0.08 Ga; *middle* VSC: 1.80 ± 0.03 Ga and *upper* VSC: 1.68 ± 0.17 Ga.

Metapelites from PQG and *lower* VSC record a common derivation whereas those from the *upper* VSC should include evident contributions of more juvenile sources. The latter overprint the Meguma-type source (Clarke & Halliday, 1985; Clarke *et al*., 1997; Braid *et al*., 2012) and could be explained by irregular contributions of the Avalonia Terrane crustal sources (Murphy et al., 1996, 2000). Nevertheless, the favoured interpretation ascribes the increasing of in εNd_i values and younger T_{DM} ages to the local input of volcanic-derived components related to the IPB magmatic activity, as supported by field and petrographic observations.

6.2. Chemical constrains on sediment deposition

Trace element variations are sensitive to many environmental physical-chemical parameters, thus providing critical information about the sedimentary settings and their paleo-redox conditions. Isotopic compositions (mainly Pb-Pb) allow to refine some of the inferences related to chemical constraints posed to sediment deposition and subsequent modifications triggered by exhalative-hydrothermal activity (e.g. Luz *et al*., 2019; Piercey & Krammer, 2019; Luz *et al*., submitted).

According to the assembled information for metapelites in the IPB, the whole-rock V/Cr ratios should mostly record redox conditions established during sedimentation/diagenesis, whereas elemental ratios involving Co and Ni do not represent an inherited feature and could trace late hydrothermal imprints. The U/Th ratio, a frequently used redox proxy, should be evaluated carefully because it may change significantly during sediment interaction with radiogenic (U-enriched) hydrothermal fluids. Combining all the geochemistry data gathered, deposition of the IPB's Late Fammenian to Visean fine-grained sediments should have occurred in 2nd or 3rd order basins that:

i. Evolved from oxic to suboxic (occasionally anoxic) conditions during the sedimentation and/or diagenesis. This is essentially due to microbial reactions that might locally constrain the initial stages of mineralizing processes; or
ii. Progressed under oxic (often transitional to suboxic) conditions, subsequently affected by multistage interaction with reduced hydrothermal fluids, which generates heterogeneous anoxic signatures. These chemical changes could involve sediments subjected to different stages of consolidation, but the most efficient fluid inflows should be related to fault-controlled, high-temperature, hydrothermal activity established prior to Variscan deformation/metamorphism.

Several basins along the IPB host different types and styles of massive sulphide mineralization and syn-sedimentation/diagenesis redox conditions. The latter could have ruled the formation of some ore occurrences, at least influencing the onset of the mineralizing process to which they are related. However, according to the obtained data for the Portuguese segment of the IPB, the sedimentary settings where the most significant (in terms of relative tonnage and metal content) shale-hosted massive ores occur were not subjected to suboxic/anoxic conditions. On the contrary, the prevalent redox conditions of those settings were oxic/suboxic, thus considerably limiting the influence of microbial mechanisms in sulphide deposition (Luz et al., 2019, 2020, submitted).

For Neves Corvo, dark-grey to black metapelite samples do not show signs of U-enrichment and present low U/Th (< 0.5) and V/Cr (< 2) ratios, even when portraying abundant sulphide dissemination. These geochemical features are typical of pelites developed in oxic settings (Wignall and Myers, 1988; Jones and Mensing, 1994; Wignall and Twichett, 1996). Therefore, the documented rise of Pb abundancies coupled with other base metals (such as Cu and Zn), should trace the advancement of ore-forming processes through intense hydrothermal activity. This is consistent with the Pb isotopic compositions displayed by these samples (Luz et al., submitted), which are near those typifying the IPB massive sulphide ores [($^{207}Pb/^{204}Pb)i \approx$ 15.62 and ($^{206}Pb/^{204}Pb)i \approx 18.16$; Marcoux, 1998; Pomiés *et al*., 1999; Relvas *et al*., 2001; Jorge *et al*., 2007; Carvalho, 2016).

Dark-grey to black metapelites from the Aljustrel sector show a wide range of U/Th (0.5 to 4.5) and V/Cr (≈ 1.5 up to 3) values, spreading the redox conditions of the sedimentary setting from oxic to anoxic. This range of redox conditions explain the commonly observed framboidal pyrite in "Py-bearing" samples, possibly formed nearby the water-sediment interface during the initial evolving stages. Nonetheless, other similar samples, displaying a wider sulphide assemblage (and so labelled as "Mineralized"), should have chemically reacted with fault-controlled, reduced mineralizing fluids (Luz *et al.,* 2019, 2020); once again, these samples show increments in ($^{207}Pb/^{204}Pb)i$ values (> 15.61), narrowing around the ($^{206}Pb/^{204}Pb)i$ range delimited for the IPB massive sulphide ores.

Black metapelite samples from the Lousal mine display geochemical features similar to that indicated for Neves Corvo, with U/Th < 0.5 and V/Cr < 2, and pointing out to initial oxic conditions further on disturbed due to interaction with a reduced hydrothermal fluid, as also supported by the available Pb-Pb isotopic systematics. On the contrary, black metapelite samples collected in the orebody footwall of the Sesmarias prospect, present higher U/Th (0.79)

and V/Cr (> 2) ratios, suggesting that (at least) part of the sulphide deposition might have been ruled by local suboxic/anoxic redox conditions during diagenesis, which is consistent with the distinct ($^{206}Pb/^{204}Pb$)*i* values (≈17.98) obtained.

The U/Th and V/Cr ratios displayed by dark-grey to black metapelites from the Albernoa sector indicate also prevalent oxic conditions during sedimentation/diagenesis. No significant changes were detected based on redox sensitive elements and Pb-Pb isotopic compositions, thus suggesting incipient interactions (under low water/rock ratios) between the sampled metasedimentary piles and late (reduced and mineralised) hydrothermal fluids. In fact, all through the all examined VSC sections there is no clear evidence of a vigorous/productive massive sulphide system (Codeço *et al*., 2018; Luz *et al*., 2019, 2020).

The textural and mineralogical evolution along the IPB ores reported in Almodóvar *et al*. (2019) for the Spanish segment of the IPB is, to a large extent, consistent with the interpretative trends described above. The same is true for the inferences supported by whole-rock Pb-Pb isotopic compositions reported for "shale-like" rocks in various studies (Jorge *et al*., 2007; Jorge, 2009); Pircey and Krammers, 2019; Luz *et al.*, submitted).

6.3. Fingerprints and footprints of exhalative-hydrothermal activity in the IPB

One of the main goals of this PhD research project was the identification of useful guides/criteria to design new exploration surveys in the IPB, vectoring massive sulphide accumulations. Considering the whole-rock geochemical dataset obtained for metapelites from various lithostratigraphic sections, significant hydrothermal/mineralization imprints exist when $Fe_2O_3/TiO_2 \geq 10$ and $Al_2O_3/(Al_2O_3+Fe_2O_3+MnO) \leq 0.6$ (Luz *et al.,* 2019, 2020). Samples representing the basal units (PQG and *lower* VSC) from footwall positions at Neves Corvo, Lousal and Sesmarias validate these thresholds, which indicate proximity to sulphide mineralized sites. Some exceptions to this vectoring trend were found, although always related to samples displaying anomalous high abundances of aluminosilicate minerals. The "Py-bearing" metapelites display narrower ranges of Fe_2O_3/TiO_2 and $Al_2O_3/(Al_2O_3+Fe_2O_3+MnO)$ ratios (from ≈5 to 10 and from ≈0.6 to 0.7, respectively) but, according to the observed features, this is caused by: (i) pyrite growth during diagenesis; (ii) low-temperature hydrothermal activity, leading to pyrite ± sphalerite deposition; and (iii) incipient interaction with (relatively) high-temperature fluids, promoting the recrystallization of early pyrite and the formation of minor amounts of chalcopyrite. In conclusion, the two geochemical ratios initially proposed to

identify metalliferous sediments in present-day or recent analogues (e.g. Marchig *et al.,* 1982) could be used as a first approach in the recognition of proximal settings to massive sulphide ore-forming systems in the IPB. Yet, they do not separate properly "barren" settings (when pyrite is the sole sulphide or largely prevails over other sulphide phases) from those variably enriched in base metal sulphides.

The 5x[(Fe_2O_3+MgO+MnO)/Al_2O_3], (Cu+Zn+Pb)/Sc and (As+Sb)/Sc geochemical ratios were recently proposed to separate barren from altered/mineralized metasedimentary successions in the IPB (Luz *et al.,* 2019, 2020). When all these three ratios are above 10, a realistic vectoring towards massive sulphide accumulations exists. Metapelites from the Neves Corvo footwall (stockwork domains of Lombador and Neves orebodies) and from the Lousal ore horizon were used as "end-members" to trace these trends (for more details see Luz *et al*., 2019, 2020). A valuable footprint towards ore horizons is provided by consistent increasing of (Cu+Zn+Pb)/Sc and (As+Sb)/Sc ratios. Some overlap is observed when the "No-sulphide", "Py-bearing" and "Mineralized" groups of samples are considered together; however, when the samples are separated according to their position in relation to the ore horizon, the discrimination is clear. The (Cu+Zn+Pb)/Sc and (As+Sb)/Sc ratios co-variate positively, particularly close to the ore horizons and the footwall domains of high-grade orebodies. In metapelites representing the hanging wall of orebodies, the (As+Sb)/Sc ratio varies widely (≈0.1 to 50) due to chemical dispersion/redistribution completed previously and/or subsequently to the Variscan deformation/metamorphism, co-varying roughly with the (Cu+Zn+Pb)/Sc ratio (≈ 10 – 50). To become directly applied by Companies during exploration surveys, the same ratios were tested but normalizing to Th instead of Sc, to which the trends and thresholds remained the same. This is relevant because Th is readily measured with portable XRF, an equipment frequently used in mineral exploration activities (see Luz *et al*., 2020 for more details).

The circulation of mineralizing fluids, namely those implicated in the deposition of common massive sulphides affect the $^{207}Pb/^{204}Pb_i$ ratios in sediments, frequently evidenced by their increase. The other two Pb isotopic ratios ($^{206}Pb/^{204}Pb_i$ and $^{207}Pb/^{204}Pb_i$) record changes when host sediments bearing disseminated sulphides other than pyrite are exposed to a protracted interaction with radiogenic hydrothermal inflow (moderate to high temperature). The proximity to massive sulphide ore systems could be recognized in sedimentary levels of PQG and VSC whenever $^{207}Pb/^{204}Pb_i > 15.60$, correlating well with several other multi-element geochemical ratios such as $Fe_2O_3/TiO_2 >10$ and (Cu+Zn+Pb)/Sc > 10.

From all the mineral phases analysed with EPMA (silicates, carbonates, phosphates, sulphides and sulphosalts) and despite overall higher number of data (n ≈ 1000), more sampling is needed to better understand the chemical variations and/or mode of occurrence. This might support future lines of investigation (see Section 7). Despite its Fe-rich composition close to the feeder zones, there are few suggestions that chlorite composition could record local chemical gradients. For Neves Corvo, slightly variations in Fe and (Mg+Mn) contents can be observed when considering each orebody; on the other hand, the Gavião prospect presents Mg-rich chlorites similar to the composition of those developed in settings related to Late-Variscan hydrothermal activity. However, more sampling should be performed to support these suggestions. Using the chlorite dataset, their formation in this IPB metasedimentary successions range between 319 ± 5 and 347 ± 8 ºC (n = 267), not differing significantly from the values estimated on the basis of the data compiled from literature (Barriga, 1983; Relvas, 1991, 2000; Fernandes, 2011; Carvalho, 2016). In general, the white micas from these IPB metasedimentary successions show similar trends, but often there is not evident compositional contrast between white micas forming the "regional alteration" mineral assemblages and those ascribed to the superimposed halos of hydrothermal alteration. Carbonates placed at the footwall of massive sulphide orebodies include Fe-rich carbonates (#Fe > 0.75), towards the ideal composition of siderite ($FeCO_3$), consistent with previous data for Neves Corvo (Relvas, 2000; Carvalho, 2016). Carbonates found in hanging wall and stockwork/ore samples from Aljustrel, frequently present higher Ca contents and a wide range of values for Mg+Mn (and low Fe). The latter suggests that these carbonates were affected by late chemical transformations depriving their initial Fe (±Mg, Mn) contents and/or their deposition occur after de massive sulphide development being related to circulation of residual fluids.

In common sulphide assemblages, pyrite incorporates irregular amounts of Co, As and Ni, often significant but not defining consistent trends (at least considering just the EPMA data). Uncommon sulphide and sulphosalts phases highlight the incorporation of trace elements like As, Sb, Co, Ni and Bi, even though the relationships with common sulphides forming the massive ores are not enough clear, at least in the shale-hosted systems of the IPB. For better understanding of the mineral finger/footprints in the massive sulphide ores deposition and evolution, additional studies are required.

SECTION 7

7. Future directions of geochemical exploration in the IPB

The combination of methods [mineral chemistry, whole-rock multi-element chemistry and multi-system (Sr, Nd and Pb) isotopic characterization] used in this PhD research program allowed a comprehensive inspection of several metasedimentary successions forming different PQG and VSC sections in the Portuguese segment of IPB. To further complement the gathered data and provide robust interpretations, a large whole-rock and isotopic geochemistry dataset was compiled from previous key studies, to which relevant mineral chemistry data from Aljustrel, Gavião, Lousal and Neves Corvo were added. The main questions posed at the beginning were answered, but many other were raised during the study, as expected in any scientific investigation.

Future research lines in the IPB should consider more micro-analytical studies. The latter can lead to significant knowledge improvements, expanding the current understanding on geochemical processes that may provide noteworthy model refinements regarding the geodynamic evolution of the IPB and the genesis of economic, massive sulphide ore centres. Accordingly, new advances and/or adjustments of the exploration guidelines proposed in this PhD research can be accomplished. Some major highlights can be stated for the foreseen research lines, as follows:

- Petrography and whole-rock chemistry results fully justify the separation of metapelites into three main categories, in conformity with the type and relative abundance of existing sulphide phases; these were labelled as “No-sulphide”, “Py-bearing” (diagenetic) and “Mineralized”. Besides an improved characterization of trace element abundances in critical mineral phases (mainly sulphides and phyllosilicates) with LA-ICP-MS, X-ray maps and MLA, it might be useful to understand if the composition of these minerals is enough sensitive to subtle environmental changes with geological meaning (i.e. representing delicate variations in local textural arrangements or specific genetic features).
- For the “Mineralized” group it is important to identify and characterize the chemical composition of As-Sb-Co (Ni±Bi±Pb)-bearing phases and their genetic link with the main massive sulphide accumulations
- Microanalytical studies (through EPMA and LA-ICP-MS) that allow to better characterize the composition of some mineral phases affected by the hydrothermal fluids, such as chlorite, rutile or zircon, could be helpful to use as a geothermometer to estimate temperatures of hydrothermal fluid inflows.

- Black metapelites are present along all the PQG and *lower* to *upper* VSC sections and do no record significant compositional differences besides the evident increase in base metals (and other trace elements) when mineralized. Considering field observations and the literature data, black metapelites included in the basal units (*upper* PQG and *lower* VSC) frequently host massive sulphide ores and their chemical evolution could influence the early mineralizing stages. Therefore, an extended sampling program of these particular metasediments in the Portuguese sector of IPB should be considered, complemented by a thorough investigation of their composition, to better constrain the redox conditions of the sedimentary settings and their role in metallogenic processes (making use of parameters additional to those already employed, such as Mo, Fe^{2+}, Fe^{3+}, organic C, sulphur and carbon isotopes).

- Another question related to black metapelites concerns the distinction of PQG and *lower* VSC sections when other facies criteria (such as the presence of coarse-grained siliciclastic rocks or volcaniclastic levels) cannot be tentatively applied. In Aljustrel, the PQG was not recognized so far, and field observations and some drill-core re-logging suggest that the local basin should have been deeper, thus favouring calmer, hemipelagic sedimentation. Consequently, the identified black metapelite levels within the lower intra-volcanic successions might correspond to *lower* VSC or to *upper* PQG. Additional palynological studies are needed to unravel the issue, possibly complemented by a detailed examination of the relative abundance and composition of accessory (small) siliciclastic mineral phases.

- A systematic study on depositional environments all through the IPB should be performed to better understand if microbial processes are indeed unavoidable in the development of "shale-hosted" massive sulphide accumulations. The available data, although significant, is quite fragmented and does not suitably represent either many types/styles of mineralization or the "regional context" (far from the main ore centres). Furthermore, a harmonized database is needed, assembling multi-parameter information in both the Portuguese and Spanish segments of the IPB, establishing the conditions to suitably investigate the "shale-hosted" and "volcanic-hosted" massive ores dichotomy.

- Purple metapelites are commonly defined as a guide level in the *upper* VSC sections and in some cases, they are found overlying the ore horizons or massive sulphide mineralization. However, these rock types are frequently associated with

intercalations/inter-fingerings of purple-green and grey metapelites with a significant volcanic-derived component. Thus, a detailed study focusing on these "purple" metapelites is important to: (i) understand if they are really metapelites in *strict sense* or should they be classified in accordance to the frequently incorporated volcanic-derived contribution; and (ii) realize if the aforementioned intercalations represent specific sediment environments subjected to particular redox gradients developed during diagenesis and/or triggered by late hydrothermal imprints.

- The geodynamic evolution of SPZ, where the IPB basins are found, did not affect the Spanish segment in the same way that in the Portuguese segment; differences in details may lead to major contrasting results. Effects of the diachronic opening of the 2nd and 3rd order basins in sedimentation and volcanic processes, and their connection with mineralizing events, are not conveniently explored. The same is true for the major fault zones that played a critical role as magma conduits, as well as preferred channels for the focusing of high-temperature fluid inflows, potentially enriched in Cu and Sn (besides other metals). Furthermore, according to some authors (e.g. Almodóvar et al., 2019 and references therein), the ore-refinement process recorded by some massive sulphide ores in the Spanish segment of IPB should be related to fluids released during the emplacement of later volcanic piles of mafic nature. Although controversial, the evidence reported by these authors are scientific valid and should not be discarded, thus raising alternative interpretations for the genesis of several mineralization styles that should be tested in other sites.

- A systematic detailed work about how Variscan metamorphism and deformation affect all the IPB sequences (PQG, VSC and even flysch – Mértola Fm.) and their ores should be done, examining in particular the role of these processes in metals redistribution and the consequential effects in geochemical guides used in mineral exploration.

SECTION 8

8. References

Abat, I., Mata, J.P., Nieto, F., Velilla, N., 2001, The phyllosilicates in diagenetic-metamorphic rocks of the South Portuguese Zone, Southwestern Portugal: Canadian Mineralogist, v. 39, p. 1571-1589.

Albardeiro, L., Solá, R., Salgueiro, R., Morais, I., Matos, J.X., Mendes, M., Pereira, M.L., Inverno, C., Oliveira, D., Rosa, D., Pacheco, N., (2017). Insights into the timing mineralization in the Neves Corvo VMS deposit (Iberian Pyrite Belt). *14th SGA Biennal Meeting*, Vol. 3, 989-992.

Almodóvar, G.R., Saéz, R., Pons, J.M., Maestre, A., Toscano, M., Pascual, E., 1998, Geology and genesis of the Aznalcóllar massive sulfide deposits, Iberian Pyrite Belt, Spain: Mineralium Deposita, v. 33, p. 111-136.

Almodóvar, G.R., Yesares, L., Sáez, R., Toscano, M., González, F., Pons, J.M., 2019, Massive sulfide ores in the Iberian Pyrite Belt: mineralogical and textural evolution: Minerals, v. 9, p. 653.

Akhtar, M.J., & Wassem, S., 2001. Atomistic simulation studies of zircon. *Chem. Phys*. **274**, 109-120.

Andrade, R.F., Schermerhorn, L.J.G., 1971. Aljustrel e Gavião. In: D. Carvalho, J.A.C. Goinhas, L.J.G. Schermerhorn, (Eds). Principais jazigos minerais do sul de Portugal. I Congresso Hispano-Luso-Americano de Geologia Económica, Lisboa, Direcção-geral de Minas e Serviços Geológicos, Livro-Guia da Excursão, nº4, 32-59.

AVRUPA Minerals, 2014. Avrupa and Antofagasta intersect copper-rich VMS in Pyrite Belt, Portugal [Press release]. Retrieved from: http://www.avrupaminerals.com/_resources/news/nr_2014_02_07.pdf.

AVRUPA Minerals, 2017. Avrupa Minerals reports on progress in Kosovo and Portugal [Press release]. Retrieved from: https://avrupaminerals.com/category/2017/.

Ayuso, R. A., Kelley, K. D., Leach, D. L., Young, L. E., Slack, J. F., Wandless, G., Lyon, A. M., Dillingham, J. D., 2004, Origin of the Red Dog Zn-Pb-Ag deposits, Brooks Range, Alaska: Evidence from regional Pb and Sr isotope sources: Economic Geology, v. 99, p. 1533-1553.

Babinski, M., Van Schmus, W.R., Chemale Jr, F., 1999. Pb-Pb dating and Pb isotopic geochemistry of Neoproterozoic carbonate rocks from the São Francisco basin, Brazil: implications for the mobility of Pb isotopes during tectonism and metamorphism. Chemical geology 160, 175-199.

Bathia, M.R., 1983. Plate tectonics and the geochemical of sandstones. *The Journal of Geology*, *91(6),* 611-627.

Bathia, M.R. & Crook, K.A.W., 1986. Trace element characteristics of greywackes and tectonic setting discrimination of sedimentary basins. *Contributions to Mineralogy and Petrology, 92*, 181-193.

Barret, J.T., Jarvis, I., Javis, K.E., (1990). Rare earth element geochemistry of massive sulfides-sulfates and gossans on the southern Explorer Ridge. *Geology, 18*, 583-586

Barrett, J.T., Dawson, G.L., MacLean, W.H., 2008, Volcanic stratigraphy, alteration, and seafloor setting of the Paleozoic Feitais massive sulfide deposit, Aljustrel, Portugal: Economic Geology, v. 103, p. 215-239.

Barrie, T., Cousens, B. L., Hannington, M. D., Bleeker, W., Gibson, H., 1999, Lead and neodymium isotope systematics of the giant Kidd Creek mine stratigraphic sequence and ore: Economic Geology Monograph 10, p. 497-510.

Barrie, C., Amelin, Y., Pascual, E., 2002, U-Pb geochronology of VMS mineralization in the Iberian Pyrite Belt: Mineralium Deposita, v. 37/8, p. 684-703.

Barriga, F.A.J.S., 1983, Hydrothermal Metamorphism and Ore Genesis at Aljustrel, Portugal. PhD thesis, University of Western Ontario, 368 p.

Barriga, F. A. J. S. & Kerrich, R., 1984. Extreme ^{18}O-enriched volcanics and ^{18}O-evolved marine water, Aljustrel, Iberian Pyrite Belt: transition from high to low Rayleigh number convective regimes. Geochemica Cosmochmica Acta 48, 1021-1031.

Bailey, S.W., 1988: Chlorites: structure and crystal chemistry. In: hydrous Phyllosilicates (Exclusive of Micas) (S.W. Bailey, eds), Mineral Society of America, Reviews in Mineralogy 19, 348-403.

Bayliss, 1975. Nomenclature of the trioctahedral chlorites. Canadian Mineralogist 13, 178-180.

Barriga, F.A.J.S., Carvalho D., Ribeiro A., 1997, Introduction to the Iberian Pyrite Belt. In: Barriga, F.A.J.S., Carvalho, D. (Eds), Geology and VMS Deposits of the Iberian Pyrite Belt. Society of Economic Geologists, Guidebook series 27, p. 1-20.

Barriga, F.J.A.S, Fyfe, W.S., 1998, Multi-phase water-rhyolite interaction and ore fluid generation at Aljustrel, Portugal: Mineralium Deposita, v.33, p. 188-207.

Boulter, C.A., 1996, Extensional tectonics and magmatism as drivers of convection leading to Iberian massive sulfide deposits?: Journal of Geological Society of London, v. 153, p. 181-184.

Bourdelle, F., Parra, T., Beissac, O., Chopin, C., Vidal, O., 2013. Clay minerals as geo-thermometer: A comparative study based on high spatial resolution analyses of illite and chlorite in Gulf Coast sandstones (Texas, U.S.A.). American Mineralogist 8, 914-926.

Braid, J.A., Murphy, J.B., Quesada, C., Bickerton, L., Mortensen, J.K., 2012. Probing the composition of unexposed basement, South Portuguese Zone, southern Iberia: implications for the connections between the Appalachian and Variscan Orogen. Canadian Journal of Earth Science 49, 591-613.

Carpinteira,G., 2020. Comprehensive characterization of the Volcano-Sedimentary complex section at Monte das Mesas prospect and assessment of its potential to host massive sulphide mienralization. MSc thesis, University of Lisbon, 125 pp.

Carvalho, D., Barriga, F.J.A.S., Munhá, J., 1999, Bimodal-siliciclastic systems – the case of the Iberian Pyrite Belt: Reviews in Economic Geology, v. 8, p. 375-408.

Carvalho, J. R. S., 2016, Zinc metallogenesis, and indium and selenium distribution at the Neves Corvo Deposit, Iberian Pyrite Belt, Portugal. PhD thesis, University of Lisbon, Portugal, 817 p.

Castroviejo R., Quesada C., Soler M., 2011, Post-depositional tectonic modification of VMS deposits in Iberia and its economic significance: Mineralium Deposita, v.46, p. 615-637.

Cathelineau, M., 1988. Cation site occupancy in chlorites and illites as a function of temperature: Clay Mineralogist 23, 471-485.

Clarke, D.B., Halliday, A.N., 1985, Sm/Nd isotopic investigation of the age and origin of the Meguma Zone Metasedimentary rocks: Canadian Journal of Earth Science, v. 22, p. 102-107.

Clarke, D.B., Halliday, A.N., Hamilton, P.J., 1988, Neodymium and Strontium isotopic constraints on the origin of the peraluminous granitoids of the South Mountain batholith, Nova Scotia, Canada: Chemical Geology, v. 73, p. 15-24.

Clarke, D.B., MacDonald, M.A., Tate, M.C., 1997, Late Devonian mafic-felsic magmatism in the Meguma Zone, Nova Scotia. *In* The nature of magmatism in the Appalachian orogen. *Edited by* A.K. Sinha, J.B. Whalen and J.P. Hogan: Geological Society of America, Memoir 191, p. 107-127.

Codeço, M., 2015. Estudo comparative das sequências vulcânicas constituintes dos eixos Ervidel-Roxo e Figueirinha-Albernoa (Faixa Piritosa Ibérica) e respective relevância na prospecção de sulfuretos maciços polimetálicos. MSc thesis, University of Lisbon, 253 pp.

Codeço, M., Mateus, A., Figueiras, J., Gonçalves, L., Rodrigues, P., 2018. Development of the Ervidel-Roxo and Figueirinha-Albernoa volcanic sequences in Iberian Pyrite Belt, Portugal: metallogenic and geodynamic implications. Ore Geology Reviews 98: 80-108.

Conde, C., Tornos, F., 2019, Geochemistry and architecture of the host sequence of the massive sulfides in the northern Iberian Pyrite Belt: Ore Geology Reviews, https://doi.org/10.1016/j.oregeorev.2019.103042

Condie, K.C., 1993. Chemical composition and evolution of the Upper Continental Crust: contrasting results from surface samples and shales. Chemical Geology 104, 1-37.

Dawson, G.L. & Caessa, P., 2003. Geology of the Aljustrel Mine area, southern Portugal. *GEODE – Global Comparison Massive Sulphide Project Field Workshop: "The Geology of the Volcanic-Hosted Massive Sulphides of the Iberian Pyrite Belt*", pp. 26.

Deer, W.A., Howie, R.A., Zussaman, J., 2008. Minerais constituintes das rochas – uma introdução. Tradução de C.A.R. Macedo. Fundação Calouste Gulbenkian, 727 pp.

De Paolo, D.J., 1981. Neodymium isotopes in the Colorado Front Range and crust-mantle evolution in the Proterozoic: Nature, v. 291, p. 193-196.

Donaire, T., Sáez, R., Pascual., E., 2002, Rhyolitic globular peperites from the Aznalcóllar mining district (Iberian Pyrite Belt, Spain): physical and chemical controls: Journal of Volcanology and Geothermal Research, v. 114, p. 119-128.

Donaire, T., Pascual, E., Sáez, R., Pin, C., Hamilton, M.A., Toscano, M., 2020, Geochemical and Nd isotopic signature of felsic volcanic rocks as a proxy of Volcanic-Hosted Massive Sulphide deposits in the Iberian Pyrite Belt (SW, Spain): the Paymogo Volcano-Sedimentary Alignment: Ore Geology Reviews, v. 120, 10.1016/j.oregeorev.2020.103408

Dunning, G.R., Díez-Montes, A., Matas, J., Martín Parra, L.M., Almarza, J., Donaire, M., 2002, Geocronologia U/Pb del volcanismo ácido y granitódies de la Faja Pirítica Ibérica (Zona Sud Portuguesa): Geogaceta, v. 32, p. 127-130.

Faria, R., Pereira, Z., Matos, J.X., Rosa, C., Caetano Alves, M.I., Oliveira, J.T., 2015, Palynostratigraphic study of the Malhadinha sector, NE of Alvares, Mértola, Iberian Pyrite Belt: Comunicações Geológicas, v. 102(1), p. 5-11.

Faure, G., Mensing. T.M., 2005. Isotopes: Principles and Applications, Wiley. 928 pp.

Fedo, C.M., Nesbitt H.W., Young G.M., (1995). Unraveling the effects of potassium metasomatism in sedimentary rocks and paleosols with implications for paleoweathering conditions and provenance. *Geology, 23*, 921-934.

Fernandes, A. 2011. Caracterização petrográfica, mineralógica e geoquímica do padrão de alteração hidrotermal a muro das massas de sulfuretos maciços do Lousal, Faixa Piritosa Ibérica. MSc thesis, University of Lisbon, pp. 194.

Ferry, J.M., Watson, E.B., 2007. New thermodynamic models and revised calibrations for the Ti-in-zircon and Zr-in-rutile thermometers. Contributions to Mineralogy and Petrology, 154(4), 429–437

Floyd, P.A. & Leveridge, B.E., (1987). Tectonic environment of the Devonian Gramscatho basin, south Cornwall: framework mode and geochemical evidence from turbiditic sandstone. *Journal of Geological Society*, *144*, 531–542.

Foster, 1962. Interpretation of the composition and a classification of the chlorites. U.S.G.S. Professional Paper, 414-A, 1-33.

Fowler, A., Prokoph, A., Stern, R. & Dupuis, C., 2002. Organization of oscillatory zoning in zircon: analysis, scaling, geochemistry and model of a zircon from Kipawa, Quebec, Canada. Geochim. Cosmochim. Acta 66, 311-328.

Granda, A., Granda, T., Pons, J.M., Videira, J.C., 2016. The leading role of geophysical methods in the discovery of La Magdalena VMS deposit in Pyrite Belt, Huelva. First Break 34.

Goldstein, S.L., O´Nions, R.K., Hamilton, P.J., 1984. A Sm-Nd isotopic study of atmospheric dust and particulates from major river systems. Earth Planet. Sci. Lett. 70, 221-236.

Goldstein, S.L., Jacobsen, S.B., 1988. Nd and Sr isotopic systematics of river water suspended material: Implications for crustal evolution. Earth Planetary Science Letters 87; 249-265.

Goodfellow, W.D., Peter, J.M., Winchester, J.A., van Staal, C.R., 2003. Ambient Marine Environment and Sediment Provenance during Formation of Massive Sulfide Deposits in the Bathrust Mining Camp: Importance of Reduced Bottom Waters to Sulfide Precipitation and Preservation. Economic Geology, Monograph 11, 129-156.

Georgiev, S., Stein, H.J., Hannan, J.L., Weiss, H.M., Bingen, B., Xu, G., Rein, E., Hatlo, V., Loseth, H., Nali, M., Piasecki, S., (2012). Chemical signals for oxidative weathering predict Re-Os isochroneity in black shales, East Greenland. *Chemical Geology*, *324-325*, 108-121.

Girty, G.H., Ridge, D.L., Knaack, C., Johnson, D., Al-Riyami, R.K., (1996). Provenance and depositional setting of Paleozoic chert and argillite, Sierra Nevada, California. *Journal of Sedimentary Research*, 66, 107–118.

Haley, B.A., Klinkhammer, G.P., McManus, J., (2004). Rare earth elements in pore waters of marine sediments. *Geochimica et Cosmochimica Acta*, *68*, 1265–1279.

Hanchar, J.M., Finch, R.J., Hoskin, P.W.O., Watson, E.B., Cherniak, D.J. & Mariano, A.N., 2001. Rare earth elements in synthetic zircon. 1. Synthesis, and rare earth element and phosphorus doping. American Mineralogist 86, 667-680.

Hoffman, D.L., Algeo, T.J., Maynard, J.B., Joachimski, M.M., Hower, J.C., Kaminski, J., (1998). Regional stratigraphic variation in bottom waters anoxia in offshore core shales of Upper Pennsylvanian cyclotherms from Eastern Midcontinent Shelf (Kansas), USA. In: Schieber, J., Zimmerle, W., Sethi, P. (eds) *Shales and mudstones* (pp. 234-269). Schweizerbart´sche Verlagsbucchandlung, Stuttgart.

Hollis, S.P., Podmore, D., James, M., Mole, D.R., Turner, O., Kneeshaw, A., Beaton, R., (2019). Targeting VHMS mineralization at Erayinia in the Eastern Goldfields Superterrane using lithogeochemistry, soil chemistry and HyLogger data. *Journal of Geochemical Exploration, 207*, 106379.

Hoskin, P.W.O., Kinny, P.D., Wyborn, D. & Chappell,B.W., 2000. Identifying accessory mineral saturation during differentiation in granitoid magmas: an integrated approach. Journal of Petrorology. 41, 1365-1396.

Huston, D.L., Relvas, J.M.R.S., Gemmel, J.B., Drieberg, S., 2011, The role of granites in volcanic-hosted ore forming systems: an assessment of magmatic-hydrothermal contributions: Mineralium Deposita, v. 46, p. 473-507.

Inoue, A., Meunier, A., Patrier-Mas, P., Rigault, C., beuaufort, D., Vieilalrd, P., 2009. Application of chemical geothermometry to low-temperature trioctahedral chlorites. Clays and Caly Mineralogy 57, 371-382.

Inverno, C.M.C., Solomon, M., Barton, M.D., Foden, J., 2008. The Cu stockwork and massive sulfide ore of the Feitais volcanic-hosted massive sulfide deposit, Aljustrel, Iberian Pyrite Belt, Portugal: a mineralogical, fluid Inclusion, and isotopic investigation: Economic Geology, v. 103, p. 241-267.

Inverno, C., Díez-Montes, A., Rosa, C., García-Crespo, J., Matos, J., García-Lobón, J.L., Carvalho, J., Bellido, F., Castello-Branco, J.M., Ayala, C., Batista, M.J., Rubio, F., Granado, J., Tornos, F., Oliveira, J.T., Rey, C., Araújo, V., Sánchez-Garcá, T., Pereira, Z., Represas, P., Solá, A.R., Sousa, P., 2015. Introduction and geological setting of the Iberian Pyrite Belt. In: Weihed, P. (Eds.),3D, 4D and Predictive Modelling of Major Mineral Belts in Europe: Mineral Resources Reviews, Switzerland, Springer, p. 191-208.

Julivert, M., Fontboté, J.M., Ribeiro, A., Conde, L., 1974. Memoria explicative del Mapa Tectónico de la Península Ibérica y Baleares. 1: 1.000.000, IGME, Madrid, 1-101.

Jones, B., & Manning, D.A.C., (1994), Comparison of geochemical indices used for interpretation of paleoredox conditions in ancient mudstones. *Chemical Geology*, *111*,111-129.

Jorge, R. C. G. S., 2009, Caracterização petrográfica, geoquímica e isotópica dos reservatórios metalíferos crustais, dos processos de extracção de metais e dos fluidos hidrotermais envolvidos em sistemas mineralizantes híbridos na Faixa Piritosa Ibérica: PhD thesis, University of Lisbon, Portugal, 272 p.

Jorge, R.C.G.S., Relvas, J.M.R.S., Matos, J.X., (2006). Geochemistry of metasediments from the Phyllite-Quartzite Group, Iberian Pyrite Belt: implications for provenance and source-area weathering (progress report), *VII Congresso Nacional de Geologia, Livro de Resumos I*, Estremoz, Universidade de Évora, Portugal, pp. 175-178.

Jorge, R. C. G. S., Pinto, A. M. M., Tassinari, C. C. G., Relvas, J. M. R. S., Munhá, J., 2007, VHMS metal sources in the Iberian Pyrite Belt: new insights from Pb isotope data. In: Andrew CJ *et al.* (eds) Digging deeper: Special Publication of the Irish Association for Economic Geology, p. 1097-1100.

Jorge, R.C.G.S., Pinto, A.M.M., Tassinari, C.C.G, Relvas, J.M.R.S., Munhá, J., 2007, VHMS metal sources in the Iberian Pyrite Belt: new insights from Pb isotope data [ext. abs.]: 9th Biennal SGA Meeting Dublin, Ireland, 2007, Extended Abstract, p. 1097-1100

Jowett, E.C., 1991. Fitting iron and magnesium into the hydrothermal chlorite geothermometer: GAC/MAC/SEG Joint Annual Meeting (Toronto, May 27-29, 1991), Program with Abstracts 16, A62.

Julivert, M., Fontboté, J., Ribeiro, A., Igme, L.C., & Madrid, U., 1974. Memoria explicative del mapa tectónico de la Peninsula Ibérica y baleares. Madrid.

Kranidiots, P., & MacLean, W.H., 1987. Systematics of chlorite alteration at the Phelps Doge massive sulfide deposit, Matagami, Quebec. Economic Geology 82, 1898-1911.

Laird, J., 1988. Chlorites: metamorphic petrology. In: Hydrous Phyllosilicates (Exclusive Micas) (S.W. Bailey, eds.), Reviews in Mineralogy 19, Mineral Society of America, 405-453.

Lanari, P., Wagner, T., Vidal, O., 2014. A thermodynamic model for di-trioctahedral chlorite from experimental and natural data in the system MgO-FeO-Al2O3-SiO2-H2O: applications to P-T sections and geothermometry. Contributions to Mineralogy and Petrology 167, 968.

Leca, X., Ribeiro, A., Oliveira, J.T., Silva, J.B., Albouy, L., Carvalho, P., Merino, H., 1983, Cadre géologique des minéralisations de Neves Corvo (Baixo-Alentejo, Portugal)- Lithostratigraphie, paléogéographie et tectonique: *Mémories BRGM,* 121-1983. Éditions du BRGM, Orléans, France, p. 79.

Leistel, J. M., Marcoux, E., Deschamps, Y., 1998a, Chert in the IPB. Mineralium Deposita, v. 33, p. 59-81.

Leistel, J.M., Marcoux, E., Thiéblemont, D., Quesada, C., Sánchez, A., Ruiz de Amodóvar, G., Pascual, E., Sáez, R., 1998b, The volcanic-hosted massive sulphide deposits of the Iberian Pyrite Belt: Mineralium Deposita, v. 33, p. 2-30.

Leitão, J. 1997. Geology of the Aljustrel massive sulfide deposits. Society of Economic Geologists Field Trip Guidebook Series, *27*: 82-97.

Leitão, J.C.R., 2014. Architecture of the Aljustrel volcanic-sedimentary basins. Comunicações Geológicas, *101*, Especial I, 469-474.

Li, Y.-H., Schoonmaker, J.E., 2014, Chemical composition and mineralogy of marine sediments. In: Holland, H.D., Turekian, K.K. (Eds.), Sediments, Diagenesis and Sedimentary Rocks: Treatise on Geochemistry 2nd edition, Vol. 9. Elsevier Ltd., p. 1-32.

Li, X., Zhao, K.D., Jiang, S.Y., Palmer, M.R., 2019, *In situ* U-Pb geochronology and sulfur isotopes constrains the metallogenesis of the giant Neves Corvo deposit, Iberian Pyrite Belt: Ore Geology Reviews, v. 105, 223-235.

Luz, F., Mateus, A., Figueiras, J., Rodrigues, P., Gonçalves, L., 2015. Fingerprints of Pre-Metamorphic Hydrothermal Alteration Affecting Metapelites from the Iberian Pyrite Belt; Implications for Massive

Ore Exploration. X Congresso Ibérico de Geoquímica/XVIII Semana de Geoquímica Abs., Alfragide, Portugal, pp. 43-46

Luz, F., Mateus, A., Figueiras, J., Tassinari, C.G., Gonçalves, L., 2017. Whole-rock chemistry and Pb Isotope Compositions in metasediments of the Iberian Pyrite Belt; relevance to Mineral Exploration. Goldschmidt Conference, Paris.

Luz F., Mateus A., Figueiras J., 2018. Elemental geochemistry of metasediments from Aljustrel area, Iberian Pyrite Belt (IPB): implications for mineral exploration. SEG Conference: Metals, Minerals, and Society Keystone, Colorado, USA, September 22-25th.

Luz, F., Mateus, A., Figueiras, J., Tassinari, C.C.G., Ferreira, E., Gonçalves, L., 2019, Recognizing metasedimentary sequences potentially hosting concealed massive sulphide accumulations in the Iberian Pyrite Belt using geochemical fingerprints: Ore Geology Reviews v. 107, p. 973-998.

Luz, F., Mateus, A., Rosa, C., Figueiras, J., 2020, Geochemistry of Famennian to Visean metapelites from the Iberian Pyrite Belt: Implications for Provenance, Paleo-Redox Conditions and Vectoring to Massive Sulfide Deposits: Natural Resources Research. DOI: 10.1007/s11053-020-09686-4

Mathur, R., Ruiz, J., Tornos, F., 1999, Ages and sources of the ore at Tharsis and Rio Tinto, Iberian Pyrite Belt, from Re-Os isotopes: Mineralium Deposita, v. 34, p. 790-793.

Marcoux, 1998. Lead isotope systematics in the giant massive sulphide deposits in the Iberian Pyrite Belt. Mineralium Deposit 33, 45-48.

Marchig, V., Gundalach, H., Möller, P., Schley, M., 1982. Some geochemical indicators for discrimination between diagenetic and hydrothermal metalliferous sediments. Marine Geology 50, 241-256.

Marignac, C., Diagana, B., Cathelineau, M., Boiron, M.C., Banks, D., Fourcade, S., Vallance, J., 2003, Remobilisation of base metals and gold by Variscan metamorphic fluids in the south Iberian Pyrite Belt: evidence from Tharsis VMS deposit: Chemical Geology, v. 194, p. 143-165.

Martin-Izard, A., Arias, D., Arias, M., Gumiel, P., Sanderson, D.J., Castañon, C., Lavandeira, A., Sanchez, J., 2015, A new 3D geological model and interpretation of structural evolution of the world-class Rio Tinto VMS deposit, Iberian Pyrite Belt (Spain): Ore Geology Reviews, v. 71, p. 457-476.

Martín-Izard, A., Arias, D., Arias, M., Gumiel, P., Sanderson, D.J., Castañon, C., Sanchez, J., 2016. Ore deposit types and tectonic evolution of the Iberian Pyrite Belt: From transtensional basins and magmatism to transpression and inversion tectonics: Ore Geology Reviews, v. 79, p. 254-267.

Mateus, A., Figueiras, J., Monteiro Santos, F., Luz, F., Khalill, M., Codeço, M., Gonçalves, S., Godinho, E., Santos, E., Rodrigues, P., 2014. Prospeção Mineral no "Polígono de Albernoa" (Faixa Piritosa Ibérica, Portugal); Avaliação integrada de dados geológicos e geofísicos existentes; novas informações mineralógicas e geoquímicas e follow-up. Unpublished Report, Lisbon, Portugal, pp. 260.

Matos, J.X., Barriga, F.J.A.S., Oliveira, V.M-J., Relvas, J.M.R.S., Conceição, P., 2000. The structure and hydrothermal alteration of the Lagoa Salgada orebody (Iberian Pyrite Belt – Sado Tertiary Basin). In: Volcanic Environments and Masisve Sulfide Deposits. SEG/CODES International Conference Abstract Volume, Tasmania, Australia, pp. 119-121.

Matos, J.X., Pereira, Z., Rosa, C.J.P., Rosa, D.R.N., Oliveira, J.T., Relvas, J.M.R.S., 2011. Late Strunian age: a key time frame for VMS deposit exploration in the Iberian Pyrite Belt. [ext. abs] 11th SGA Biennal Meeting: Let's talk about Ore Deposits, Antofagasta, Chile, 2011. Extended Abstracts, p. 790-792.

MATSA, A Mubadala & Transfigura Company, 2018. Mina de Aguas Teñidas. [Corporate Presentation]. Retrieved from: https://www.matsamining.com/media/3925/2018matsacorporatepresentation.pdf

Mendes, M., Pereira, Z., Matos, J.X., Albardeiro, L., Morais, I., Solá, R., Pacheco, N, Araújo, V., (2018). Middle-upper Devonian Palynostratigrapgy of the Phyllite-Quartzite Group in the Neves-Corvo mine region, Iberian Pyrite Belt correlation with the South Portuguese Zone. *Cuadernos del Museu Geominero*, *27*, 357-365.

Mendes, M., Pereira, Z., Matos, J.X., Albardeiro, L., Morais, I., Solá, R., Salgueiro, R., Pacheco, N., Araújo, V., Inverno, C., Oliveira, J.T., 2020. New insignts on the midlle Givetian/middle Frasnian palynofloras from the Phyllite-Quartzite Formation in the Neves Corvo mine region (Iberian Pyrite Belt, Portugal). Revue de micropaléontologie 68, 100447.

Mitjavilla, J., Martí, J., Soriano, C., 1997, Magmatic evolution and tectonic setting of the Iberian Pyrite Belt: Journal of Petrology, v. 38, p. 727-755.

Moura, A., 2008, Metallogenesis at the Neves Corvo VHMS deposit (Portugal): A contribution from the study of fluid inclusions: Ore Geology Reviews, v. 34(3), p. 354-368.

Moreno, C., Sierra, S., Saéz, R., 1996, Evidence for catastrophism at the Famennian-Dinantian boundary in the Iberian Pyrite Belt. in Strogen, P., Sommerville, I.D., Jones, J.L. (Ed.), Recent Advances in Lower Carboniferous Geology, London, The Geological Society of London, Special Publication, v. 106, p. 153-162.

Munhá, J., 1979, Blue amphiboles, metamorphic regime and plate tectonic modelling in the Iberian Pyrite Belt: Contributions to Mineralogy and Petrology, v. 69, p. 279-289

Munhá, J., 1981, Igneous and metamorphic petrology of the Iberian Pyrite Belt volcanic rocks: Doctoral Thesis, University of Western Ontario, Canada.

Munhá, J., 1983, Low-grade regional metamorphism in the Iberian Pyrite Belt: Comunicações dos Serviços Geológicos de Portugal, v. 69, p. 3-36.

Munhá, J., 1990, Metamorphic evolution of the South Portuguese/ Pulo do Lobo Zone, in: Dallmeyer, R.D., Martínez García, E. (Eds), Pre-Mesozoic Geology of Iberia, Berlin, Springer Berlin Heidelberg, p. 363-369. Munhá, J., Barriga, F.J.A.S., Kerrich, R., 1986, High ^{18}O ore-forming fluids in volcanic-hosted base metal massive sulfide deposits; geologic, $^{18}O/^{16}O$, and D/H evidence from the Iberian Pyrite Belt; Crandon, Wisconsin; and Blue Hill, Maine: Economic Geology, v. 81(3), p. 530-552.

Munhá, J., Fyfe, W.S., Kerrich, R., 1980, Adularia, the characteristic mineral of felsic spilites: Contributions to Mineralogy and Petrology, v. 75, p. 15-19.

Munhá, J., Kerrich, R., 1980. Seawater basalt interaction in spilites from the Iberian Pyrite Belt: Contributions to Mineralogy and Petrology, v. 73, p. 191-200.

Murphy, J.B., Keppie, J.D., Dostal, J., Waldron, J.W.F., Cude, M., 1996, Geochemical and isotopic characteristics of Early Silurian clastic sequences in Antigonish Highlands, Nova Scotia, Canada: constraints on the accretion of Avalonia in the Appalachian – Caledonide Orogen: Canadian Journal of Earth Sciences, v. 33(3), p. 379-388.

Murphy, J.B., Strachan, R.A., Nance, R.D., Parker, K.D., Fowler, M.B., 2000, Proto-Avalonia: a 1.2-1.0 Ga tectonothermal event and constraints for the evolution of Rodinia: Geology, v. 28(12), p. 1071-1074.

Nesbitt, R.W., Pascual, E., Fenning, C.M., Toscano, M., Sáez, R., Almodóvar, R.G., 1999, U-Pb dating of stockwork zircons from the eastern Iberian Pyrite Belt: Journal of Geological Society of London, v. 156, p. 7-10.

Oliveira, D.P.S., Matos, J.X., Rosa, C.J.P., Rosa, D.R.N., Figueiredo, M.O., Silva, T.P., Guimarães, F., Carvalho, J.R.S., Pinto, Á.M.M., Relvas, J.M.R.S., Reiser, F.K.M., 2011, The Lagoa Salgada orebody, Iberian Pyrite Belt, Portugal: Economic Geology, v. 106, p. 1111-1128.

Oliveira, J.T., 1990, Stratigraphy and syn-sedimentary tectonism in the South Portuguese Zone. in: Dallmeyer, R.F. & Martinez-Garcia (Eds). Pre-Mesozoic Geology of Iberia, Springer-Verlag, p. 334-347.

Oliveira, J.T., Pereira, E., Ramalho, M., Antunes, M.T., Monteiro, J.H., 1992. Carta Geológica de Portugal, Escala 1: 200000. Instituto Geológico e Mineiro, Lisbon.

Oliveira, V., Matos, J.X., Bengala, M., Silva, N., Sousa, P., Torres, L., 1998. Geology and geophysics as successful tools in the discovery of the Lagoa Salgada orebody (Sado tertiary Basin – Iberian Pyrite Belt), Grândola, Portugal, Mineral Deposita 33, 170-187.

Oliveira, J.T., Pereira, Z., Carvalho, P., Pacheco, N., Korn, Dieter., 2004. Stratigraphy of the tectonically imbricated lithological succession of the Neves Corvo mine area, Iberian Pyrite Belt, Portugal. Miner. Depos. 39(49), 422-436.

Oliveira, J.T., Pereira, Z., Rosa, C., Rosa, D., Matos, J., 2005 Recent advances in the study of the stratigraphy and the magmatism of the Iberian Pyrite Belt, Portugal. In: Carosi, R., Dias, R., Iacopini, D., Rosenbaum, G. (eds) The southern Variscan belt. Journal of the Virtual Explorer, Electronic Edition 19,1441-8142.

Oliveira, J.T., Relvas, J.M.R.S., Pereira, Z., Matos, J.X., Rosa, C.J., Rosa, D., Munhá, J.M., Jorge, R.C.G.S., Pinto, A.M.M., 2006. O Complexo Vulcano-Sedimentar da Fiaxa Piritosa Ibérica: estrtigrafia, vulcanismo e mineralizações associadas e evolução tectonoestratigráfica no context da Zona Sul Portuguesa. In: Dias, R., Araújo, A., Terrinha, P., Kullberg, J.C., (Eds.), Geologia de Portugal na Ibérica. VII Congresso Nacional de Geologia, Univ. Évora, Portugal, pp. 207-214.

Oliveira, J.T., Relvas, J.M.R.S., Pereira, Z., Matos, J.X., Rosa, C.J., Rosa, D., Munhá, J.M., Fernandes, P., Jorge, R.C.G.S., Pinto, A.M.M., 2013a, Geologia da Zona Sul Portuguesa, com ênfase na estratigrafia, vulcanologia física, geoquímica e mineralizações da Faixa Piritosa, in: Dias, R., Araújo, A., Terrinha, P.E., Kullberg, J.C. (Eds). Geologia de Portugal. Vol. I – Geologia Pré-Mesozóica de Portugal, Escolar Editora, p. 673-766.

Oliveira, J.T., Quesada, C., Pereira, Z., Matos, J.X., Solá, A.R., Rosa, D., Albardeiro L., Díez-Montes, A., Morais, I., Inverno, C., Rosa, C., Relvas, J., 2019, South Portuguese Terrane: A continental affinity

exotic unit, in: C. Quesada and J. T. Oliveira (eds.), The Geology of Iberia: A Geodynamic Approach, Regional Geology Reviews, vol. 2, Springer-Verlag, p. 173-206.

Pereira, Z., Matos, J., Fernandes, P., Oliveira, J.T., 2007, Devonian and Carboniferous palynostratigraphy of the South Portuguese Zone, Portugal – an overview: Comunicações Geológicas, v. 94, p. 53-79.

Pereira, Z., Matos, J.X., Fernandes, P., Jorge, R.G.S., Oliveira, J.T., 2010, Qual a idade mais antiga da Faixa Piritosa. Nova idade Givetiano inferior para o Grupo Filito-Quartzítico (Anticlinal São Francisco da Serra), Faixa Piritosa: Revista Electrónica de Ciências da Terra, v. 17(13), p. 4.

Pereira, Z., Matos, J.X., Rosa, C., Oliveira, J.T., 2012, Palynostratigraphic importance of the Strunian in the Iberian Pyrite Belt. [ext. abs]: 45th Annual Meeting AASP Abs, Lexington, KY, USA, Extended Abstract, p. 42-43.

Peucat, J.J., Vidal, O., Bernard-Griffiths, J., Condie, K.C., 1989, Sr, Nd, and Pb isotopic systematics in the Archean low- to high-grade transition zone of southern India: syn-accretion vs post-accretion granulites: Journal of Geology, v. 97, p. 537-549.

Piercey S. J., Kamber, B. S., 2019, Lead isotope geochemistry of shales from the Wolverine volcanogenic massive sulfide deposit, Yukon: implications for Pb isotope vectoring in exhalative ore systems: Economic Geology, v. 114, p. 47-66.

Pomiès, C., Cocherie, A., Guerrot, C., Marcoux, E., Lancelot, J., 1998, Assessment of the precision and accuracy of lead-isotope ratios measured by TIMS for geochemical applications: example of massive sulphide deposits (Rio Tinto, Spain): Chemical Geology, v. 144, p. 137-149.

Priem, H.N.A., Boelrijk, N.A.I.M., Hebeda, E.H., Schermerhorn, L.J.G., Verdurmen, E.A.Th., Verschure, R.H., 1978, Sr isotopic homogenization through whole-rock systems under low greenschist facies metamorphism in Carboniferous pyroclastics at Aljustrel (Southern Portugal): Chemical Geology, v. 21, p. 307-314.

Quesada, C., 1991, Geological constraints on the Paleozoic tectonic evolution of the tectonostratigraphic terranes in the Iberian Massif: Tectonophysics, v. 185, p. 225-245.

Quesada, C., 1998, A reappraisal of the structure of the Spanish segment of the Iberian Pyrite Belt: Mineralium Deposita, v. 33, p. 31-44.

Quesada, C., Fonseca, P., Munhá, J., Oliveira, J., Ribeiro, A., 1984, The Beja-Acebuches Ophiolite (Southern Iberia Variscan fold belt): geological characterization and geodynamic significance: Boletin Geológico y Minero, v. 105(1), p. 3-49.

Rainswell, R., Buckley, F., Berner, R.A., Anderson, T.F., 1988. Degree of pyritization of iron as a paleoenvironment indicator of bottom-water oxygenation. Journal of Sedimentary petrology 58, 812-819.

Relvas, 1991. Estudo Geológico e Metalogenético da área do Gavião, Baixo Alentejo, Unpublished MSc thesis, University of Lisbon, 319 pp.

Relvas, J.M.R.S., 2000, Geology and metallogenesis at the Neves Corvo, Portugal: PhD Thesis. University of Lisbon, Portugal, 250 p.

Relvas, J.M.R.S., Barriga, F.J.A.S., Bernardino, F.B.C.P., Oliveira, V.M.S., Matos, J.X., 1994, Ore zone hydrothermal alteration in drill hole IGM-LS1 Lagoa Salgada, Grândola, Portugal: A first report on pyrophyllite in a central stockwork: Boletín Sociedad Española Mineralogia, v. 17, p. 157-158.

Relvas, J.M.R.S., Barriga, F.J.A.S., Pinto, A., Ferreira, A., Pacheco, N., Noiva, P., Barriga, G., Baptista, R., Carvalho, D., Oliveira, V., Munhá, J., Hutchinson, R.W., 2002, The Neves-Corvo deposit, Iberian Pyrite Belt, Portugal: Impacts and future, 25 years after the discovery, in: Goldfarb R, Nielsen J (Ed) Integrated Methods for discovery. SEG Special Publication 9, p. 155-176.

Relvas, J. M. R. S., Tassinari, C. C. G., Munhá, J., Barriga, F. J. A. S., 2001, Multiple sources for ore-forming fluids in the Neves-Corvo VHMS deposit of the Iberian Pyrite Belt (Portugal): strontium, neodymium and lead isotope evidence: Mineralium Deposita, v. 36, p. 416-427.

Relvas, J.M.R.S., Barriga, F.J.A.S., Ferreira, A., Noiva, P.C., Pacheco, N., Barriga, G., 2006a, Hydrothermal alteration and mineralization in the Neves-Corvo volcanic hosted massive sulfide deposit, Portugal: I. Geology, mineralogy and geochemistry: Economic Geology, v. 101, p. 791-804.

Relvas, J.M.R.S., Barriga, F.J.A.S., Longstaffe, F.J., 2006b, Hydrothermal alteration and mineralization in the Neves-Corvo volcanic-hosted massive sulfide deposit, Portugal: II. Oxygen, hydrogen, and carbon isotopes: Economic Geology, v. 101, p. 753-790.

Ribeiro, A., Quesada, C., Dallmeyer, R.D., 1990, Geodynamic evolution of the Iberian Massif, in: Dallmeyer, R.D., Martínez Garcia, E. (Ed), Pre-Mesozoic Geology of Iberia, Berlin, Springer Berlin Heidelberg, p. 334-347.

Ribeiro, A., Munhá, J., Dias, D., Mateus, A., Pereira, E., Ribeiro, L., Fonseca, P., Araújo, A., Oliveira, J.T., Romão, J., Chaminé, H., Coke, C., Pedro, J., 2007, Geodynamic evolution of the SW Europe Variscides: Tectonics, v. 26, TC6009.

Ribeiro, A., Munhá, J., Fonseca, P.E., Araújo, A., Pedro, J.C., Mateus, A., Tassinari, C., Machado, G., Jesus, A.P., 2010, Variscan ophiolite belts in the Ossa-Morena Zone (Southwest Iberia): geological characterization and geodynamic significance: Gondwana Research, v. 17, p. 408-421.

Rodrigues, B., Chew, D.M., Jorge, R.C.G.S., Fernandes, P., Veiga-Pires, C., Oliveira, J.T., 2015, Detrital zircon geochronology of the Carboniferous Baixo Alentejo Flysch Group (South Portugal); constraints on the provenance and geodynamic evolution of the South Portuguese Zone: Journal of the Geological Society, v. 172, p. 294-308.

Romans, P.A., Brown, L.L. & White, J.C., 1975. An electron microprobe study of yttrium, rare earth, and phosphorus distribution in zoned and ordinary zircon. American Mineralogist 60, 475-480.

Rosa, C.J.P., McPhie, J., Relvas, J., 2011, Sediment-matrix igneous breccias at the top contacts of felsic units in the IPB: implications for VHMS exploration, [ext. abs.]11th SGA Biennal Meeting Abstracts, Antofagasta, Chile, Extended abstract, p. 754-756.

Rosa, C.J.P., McPhie, J., Relvas, J., 2011, Sediment-matrix igneous breccias at the top contacts of felsic units in the IPB: implications for VHMS exploration, [ext. abs.]11th SGA Biennal Meeting Abstracts, Antofagasta, Chile, Extended abstract, p. 754-756.

Rosa, C.J.P., McPhie, J., Relvas, J., Pereira, Z., Oliveira, T., Pacheco, N., 2008. Volcanic setting of the giant Neves Corvo massive sulfide deposit, Iberian Pyrite Belt, Portugal. Mineralium Deposita 43: 449-466.

Rosa, D., Inverno, C., Oliveira, V., Rosa, C., 2004, Geochemistry of volcanic rocks, Albernoa area, Iberian Pyrite Belt, Portugal: International Geology Reviews, v. 46, p. 366-383.

Rosa, D., Inverno, C., Oliveira, V., Rosa, C., 2006. Geochemistry and geothermometry of volcanic rocks from Serra Branca, Iberian Pyrite Belt, Portugal. Gondwana Research 10: 328-339.

Rosa, D.R.N., Finch, A.A., Andersen, T., Inverno, C.M.C., 2009, U-Pb geochronology and Hf isotope ratios of magmatic zircons from the Iberian Pyrite Belt: Mineralogy and Petrology, v. 95, p. 47-69.

Roser, B.P., Korsch, R.J., 1988. Provenance signature of sandstone-mudstone suit determined using discriminant function analysis of major element data. Chemical Geology 67, 518-527

Saéz, R., Almodóvar, G.R., Pascual, E., 1996, Geological constraints on massive sulphide genesis in the Iberian Pyrite Belt: Ore Geology Reviews, v. 11, p. 429-451.

Saéz, R., Pascual, E., Toscano, M., Almodóvar, G.R., 1999, The Iberian type of volcano-sedimentary massive sulphide deposits: Mineralium Deposita, v. 34, p. 549-570.

Saéz, R., Moreno, C., González, F., Almodóvar, G.R., 2011, Black shales and massive sulfide deposits: causal or casual relationships? Insights from Rammelsberg, Tharsis, and Draa Sfar: Mineralium Deposita, v. 46, p. 585-614.

Sánchez-España, J., Velasco, F., Yusta, I., 2000, Hydrothermal alteration of felsic volcanic rocks associated with massive sulfide deposition in the northern Iberian Pyrite Belt (SW Spain): Applied Geochemistry, v. 15, p. 1265-1290.

Sato, K., Tassinari, C.G.C., Kawashita, K., Petronillo, L., 1995. O método geocronológico Sm-Nd no IG-USP e suas aplicações. Anais da Academia Brasileira de Ciências 67, 313-336.

Schermerhorn, L.J.G., 1971, An outline stratigraphy of the Iberian Pyrite Belt: Boletin Geológico y Minero, v. 82 (3/4), p. 239-268.

Schermerhorn, L.J.G., Stanton, W.I., 1969, Folded overthrusts at Aljustrel (South Portugal). Geological Magazine, v. 160(2), p. 130-141.

Silva, J.B., Oliveira, J.T., Ribeiro, A., 1990, Structural outline of the South Portuguese Zone. in: Dallmeyer, R.D., Martínez García, E. (Eds.), Pre-Mesozoic Geology of Iberia, Berlin, Springer Berlin Heidelberg, p. 348-362.

Silva, J.B., Pereira, M.F., Chichorro, M., 2013, Estruturas das áreas internas da Zona Sul Portuguesa, no contexto do órogeno Varisco, in: Dias, R., Araújo, A., Terrinha, P.E., Kullberg, J.C. (Eds). Geologia de Portugal. Vol. I – Geologia Pré-Mesozóica de Portugal, Escolar Editora, p. 767-780.

Simancas, J.F., Tahiri, A., Azor, A., Lodeiro, F.G., Poyatos, D.J.M., 2005. The tectonic frame of the Variscan-Alleghanian orogen in Southern Europe and Northern Africa. Tectonophysics 398, 181-198.

Slack, J.F., Dumoulin, J.A., Schmidt, J.M., Young, L.E., Rombach, C.S., 2004. Paleozoic sedimentary rocks in the Red Dog Zn-Pb-Ah district and vicinity, western metallogenic significance. Econ. Geol. 99, 1385-1414.

Solá, A.R., Salgueiro, R., Pereira, Z., Matos, J.X., Rosa, C., Araújo, V., Neto, R., Lains, J.A., 2015. Time span of the volcanic setting of the Neves-Corvo VHMS deposit. [ext. abs]: X Congresso Ibérico de Geoquímica/XVII Semana da Geoquímica, Extended Abstract, p. 120-123.

Solomon, M., Quesada, C., 2003, Zn-Pb-Cu massive sulphide deposits: brine-pool types occur in collisional orogens, black smoker types occur in back arc and/or arc basins: Geology, v. 31, p. 1029-1032.

Solomon, M., Tornos, F., Gaspar, O.C., 2002, A possible explanation for many of the unusual features of the massive sulfide deposits of the Iberian Pyrite Belt: Geology, v. 30, p. 87-90.

Soriano, C., Martí, J., 1999, Facies analysis of volcano-sedimentary successions hosting massive sulfide deposits in the Iberian Pyrite Belt, Spain: Economic Geology, v. 94, p. 867-882.

Speer, J.A., 1980. Zircon. *In* Orthosilicates (P.H. Ribbe, ed.). Rev. Mineral. 5, 67-112.

Stacey, J.S., Kramers, J.D., 1975. Approximation of terrestrial lead isotope evolution by a two stage model. Earth Planet. Sci. Lett. 26, 207-221

Strauss, G., 1970, Sobre la geologia de la provincia piritífera del SW de la Península Ibérica y de sus yacimientos, en especial sobre la mina de pirita de Lousal (Portugal): Memoria Instituto Tecnológico Geominero de España, v. 77, 266 p.

Strauss, G.K., Madel, J., Fernández Alonso, F. 1977, Exploration practice for stratabound volcanogenic sulphide deposits in the Spanish-Portuguese Pyrite Belt: Geology, geophysics, and geochemistry, in: Klemm, D.D., Schneider, H.J. (eds.). Time and stratabound ore deposits. Berlin, Springer-Verlag, p. 55-93.

Tassinari, C.G., Cordani, U.G., Nutman, A.P., Schmus, W.R.V., Bettencourt, J.S., Taylor, P.N., 1996. Geochronological systematics on basement rocks from the Rio Negro-Juruena Province (Amazonian Craton) and tectonic implications. International Geology Review 38, 161-175.

Tessalina S. G., Herrington, R. J., Taylor, R. N., Sundblad, K., Maslennikov, V.V., Orgeval, J.-J., 2016, Lead isotopic systematics of massive sulphide deposits in the Urals: applications for geodynamic setting and metal sources: Ore Geology Reviews, v. 72, p. 22-36.

Thiéblemont, D., Pascual, E., Stein, G., 1998, Magmatism in the Iberian Pyrite Belt: petrological constraints on a metallogenetic model: Mineralium Deposita, v. 33, p. 98-110.

Thorpe, R. I., 1999, The Pb isotope linear array for volcanogenic massive sulfide deposits of the Abitibi and Waawa subprovinces, Canadian Shield: Economic Geology Monograph 10, p. 555-575.

Tornos, F., 2006, Environment of formation and styles of volcanogenic massive sulfides: the Iberian Pyrite Belt: Ore Geology Reviews, v. 28, p. 259-307.

Tornos, F., Barriga, F., Marcoux, E., Pascual, E., Pons, J.M., Relvas, J., Velasco, F., 2000, The Iberian Pyrite Belt, in: Large, R., Blundell, D. (Eds), Database on global VMS districts: CODES-GEODE, p. 19-52.

Tornos, F., Conde, C., 2002, La influencia biogénica en la formación de los yacimientos de sulfuros masivos de la Faja Pirítica Ibérica: Geogaceta, v. 32, p. 235-238.

Tornos, F., Heinrich, C.A., 2008. Shale basins, sulfur-deficient ore brines and the formation of exhalative base metals deposits: Chemical Geology, v. 247, p. 195-207.

Tornos, F., Solomon, M., Conde, C., Spiro, B., 2008, Formation of the Tharsis massive sulfide deposit, Iberian Pyrite Belt: geological, lithogeochemical, and stable Isotope evidence for a deposition in a brine Pool: Economic Geology, v. 103, p. 185-214.

Tornos, F., Peter, J.M., Allen, R.L., Conde, C., Peter, F., Conde, R., 2015, Controls on the siting and style of volcanogenic massive sulphide deposits: Ore Geology Reviews, v. 68, p. 142-163.

Tornos, F., Velasco, F., Slack, J.F., Delgado, A., Gomez-Miguelez, N., Escobar, J.M., Gomez, C., 2017. The high-grade Las Cruces copper deposit, Spain: a product of secondary enrichment in an evolving basin. Miner. Depos. 52, 1-34.

Turner S., Foden J., Sandiford M., Bruce D., 1993. Sm-Nd isotopic evidence for the provenance of sediments from the Adelaide Fold Belt and southeastern Australia with implications for episodic crustal addition. Geochim. et Cosmochim Acta 57(1): 1837-1856.

Uher, P. & Čern´y, P., 1998,. Zircon in Hercynian granitic pegmatites of the western Carpathians, Slovakia. Geol. Carpathica 49, 261-270

Valenzuela, A., Donaire, T., Pascual, E., 2002, Secuencia de fácies volcânicas en el area del rio Odiel (Faja Piritica Iberica, España): Geogaceta, v. 32, p. 131-134.

Valenzuela, A., Donaire, T., Pin, C., Toscano, M., Hamilton, M., Pascual, E., 2011, Geochemistry and U-Pb Dating of felsic volcanic rocks in the Rio Tinto-Nerva unit, Iberian Pyrite Belt, Spain: crustal thinning, progressive crustal melting and massive sulphide genesis: Journal of the Geological Society, v. 168, p. 717-731.

Van den Boogard, M., 1963, Conodonts of Upper Devonian and Lower Carboniferous age from southern Portugal: Geologie en Mijnbouw, v. 42, p. 248-259.

Varnavas P., Cronan D.S., 1988. Arsenic, antimony and bismuth in sediments and waters from the Santorini hydrothermal field, Greece. Chem. Geol. 67(3-4), 295-305.

Velde, B., 1965. Phengite micas: synthesis, stability and natural occurrence. American Journal of Science 263, 886-913.

Velasco-Acebes, J., Tornos, F., Kidane, A., Wiedenbeck, Mi, Velasco, F., 2018, Isotope geochemistry tracks the maturation of submarine massive sulfide mounds (Iberian Pyrite Belt): Mineralium Deposita, v. 54(6), p. 913-934.

Vidal, O., Parra, T., Trotet, F., 2001. A thermodynamic model of Fe-Mg aluminous chlorite using data from phase equilibrium experiments and natural pelitic assemblages in the 100º to 600ºC, 1 to 25 kb range. American Journal of Science 301, 557-592.

Vidal, O., Parra, T., Vieillard., P., 2005. Thermodynamic properties of the Tschermak solid solution in Fe-chlorite: Application to natural examples and possible role of oxidation. American Mineralogist 90, 347-358.

Vidal, O., De Andrade, V., Lewin, E., Munoz, M., Parra, T., Pascarelli, S., 2006. P-T-deformation Fe^{3+}/Fe^{2+} mapping at the thin section scale and comparison with XANES mapping: Application to a garnet-bearing metapelite from the Sambagawa metamorphic belt (Japan). Journal of Metamorphic Geology 24, 669-683.

Yesares, L., Sáez, R., Nieto, J.M., Almodóvar, G.R., Gómez, C., Escobar, J.M., 2015. The Las Cruces deposit, Iberian Pyrite Belt, Spain. Ore Geology Reviews 66, 25–46.

Young, G.M., Nesbitt, H.W., 1998. Processes controlling the distribution of Ti and AI in weathering profiles, siliciclastic sediments and sedimentary rocks. J. Sed. Research 68(3), 448- 455.

Watson, E.B., Wark, D.A., Thomas, J.B., 2006. Crystallization thermometers for zircon and rutile. Contrib Mineral Petrol 151:413–433

Wiewiora, A., 1990. Crystallochemical classifications of phyllosilicates based on the unified system of projection of chemical composition: I. The mica group. Clay Minerals V.25, Issure 1, 73-81.

Wiewiora, A., Weiss, Z., 1990. Crystallochemical classifications of phyllosilicates based on the unified system of projection of chemical composition: II. The chlorite group. Clay Minerals V.25, Issure 1, 73-81.

Wignall, P., Myers, K., 1988. Interrpeting benthic oxygen levels in mudrocks: A new approach. Geology 16 (5).

Wignall, P., Twichett, R.J., 1996. Oceanic Anoxia and the End Permian Mass Extinction. Sience 272(5265): 1155-8.

Zhao, J.X., McCulloch, M.T., Bennet, V.C., 1992. Sm-ND and U-Pb zircon isotopic constraints on the provenance of sediments from the Amadeus Basin, central Australia: Evidence for REE fractionation. Geochim. Cosmochim. Acta. 56, 921-940.

Zang, W., Fyfe, W.S., 1995. Chloritization of the hydrothermally altered bedrock at the Igarapá bahia gold deposit, Carajás, Brazil, Mineralium Deposita 30, 30-38.

Zartman, R.E., Doe B.R., 1981. Plumbotectonics - the model. Tectonophysics 75, 135-162

Appendix 1.1

Recognizing metasedimentary sequences potentially hosting concealed massive sulfide accumulations in the Iberian Pyrite Belt using geochemical fingerprints

Ore Geology Reviews - 2019

Filipa Luz
António Mateus
Jorge Figueiras
Colombo C.G. Tassinari
Ezequiel Ferreira
Luís Gonçalves

Ore Geology Reviews 107 (2019) 973–998

Contents lists available at ScienceDirect

Ore Geology Reviews

journal homepage: www.elsevier.com/locate/oregeorev

Recognizing metasedimentary sequences potentially hosting concealed massive sulfide accumulations in the Iberian Pyrite Belt using geochemical fingerprints

Filipa Luz[a,*], António Mateus[a], Jorge Figueiras[a], Colombo C.G. Tassinari[b], Ezequiel Ferreira[a], Luís Gonçalves[c]

[a] Dep. Geologia and IDL Instituto Dom Luiz, Faculdade de Ciências, Universidade de 14 Lisboa, Ed. C6, Piso 4, 1749-016 Lisboa, Portugal
[b] Instituto de Geociências, Universidade de São Paulo, Rua do Lago, 562, 05508-900 São Paulo, SP, Brazil
[c] EPOS – Empresa Portuguesa de Obras Subterrâneas, S.A., Lagoas Park, Ed. 1, 16 2740-264 Porto Salvo, Portugal

ARTICLE INFO

Keywords:
Metasediments geochemistry
Alteration/mineralization index
Massive sulfide deposits
Iberian Pyrite Belt
Mineral exploration

ABSTRACT

Promising advances in the development of new greenfield and brownfield exploration methods and methodologies for massive sulfide ore-systems in the Iberian Pyrite Belt (IPB) have been made over the last two decades. However, the effects of lateral and vertical facies variations in metasedimentary piles forming the two main lithostratigraphic units that potentially host massive sulfide deposits [the Phyllite-Quartzite Group (PQG) and the Volcanic-Sedimentary Complex (VSC)] on mineral exploration remain unknown. Herein we report on results of a multi-element geochemical study of 133 samples representing PQG and VSC metasedimentary rocks from the Albernoa area (≈713 km^2); this dataset is complemented by whole-rock Sr, Nd and Pb isotopic data for a subset of 12 VSC metasedimentary rock samples.

The prevalent siliciclastic component in the analyzed rocks derives from an evolved "felsic source" (as suggested by the Zr/Sc, Th/Sc, Eu/Eu* relationships) that, according to CIA values, should have been affected by significant weathering before they were deposited in the basin from Middle Devonian to Visean time. The siliciclastic component comprises clay and (fine-grained) sand whose relative abundance can be distinguished on the basis of Al_2O_3/TiO_2, Sc/TiO_2, Ga/TiO_2, Zr/TiO_2 and SiO_2/Al_2O_3 ratios. These terrigenous components are, in places, variably mixed with volcanic-derived fractions, leading to the formation of tuffaceous metapelites typical of the VSC sequences but also present in the upper stratigraphic sections of the PQG. In general, VSC samples display the following parameters $2.5 \leq SiO_2/Al_2O_3 \leq 6.5$, $0.02 \leq TiO_2/Al_2O_3 \leq 0.06$ and $0.2 \leq (CaO + Na_2O + K_2O)/Al_2O_3 \leq 0.25$, whereas PQG samples display $2.5 \leq SiO_2/Al_2O_3 \leq 12$, $0.08 \leq TiO_2/Al_2O_3 \leq 0.58$ and $(CaO + Na_2O + K_2O)/Al_2O_3 \leq 0.3$. Fe_2O_3/TiO_2 ratios ≥ 10 and $Al_2O_3/(Al_2O_3 + Fe_2O_3 + MnO)$ ratios ≤ ≈0.6 indicate the strong influence of an early-developed (prior to Variscan metamorphism and deformation) hydrothermal component on the prevalent siliciclastic component sometimes mixed with a variable volcanic-derived fraction. Moreover, values of (As + Sb)/Sc, (Cu + Zn + Pb)/Sc and $5 \times [(Fe_2O_3 + MgO + MnO)/Al_2O_3]$ ratios between 1 and 10 indicate the influence of seafloor metasomatism processes, and ratios ≥ 10 indicate close proximity to hydrothermal discharge potentially associated with massive sulfide mineralization.

The Sr, Nd, Pb isotopic data show that VSC metasedimentary rocks are mostly derived from old, reworked, upper continental crust. Isotope ratios characterizing the main siliciclastic component are somewhat disturbed by the significant presence of volcanic-derived components and/or mineral changes due to early hydrothermal alteration/mineralization processes, which should have involved isotopically distinct fluids.

1. Introduction

The Iberian Pyrite Belt (IPB) hosts ≈2500 Mt of massive sulfide accumulations distributed within ca. 90 deposits in Portugal and Spain (Fig. 1) and is one of the most important worldwide metallogenic provinces (*e.g.* Barriga et al., 1997; Tornos et al., 2000; Relvas et al.,

* Corresponding author at: Dep. Geologia and IDL Instituto Dom Luiz, Faculdade de Ciências, Universidade de Lisboa, Ed. C6, Piso 4, 1749-016 Lisboa, Portugal.
E-mail address: faluz@fc.ul.pt (F. Luz).

https://doi.org/10.1016/j.oregeorev.2019.03.020
Received 31 July 2018; Received in revised form 3 March 2019; Accepted 18 March 2019
Available online 22 March 2019
0169-1368/

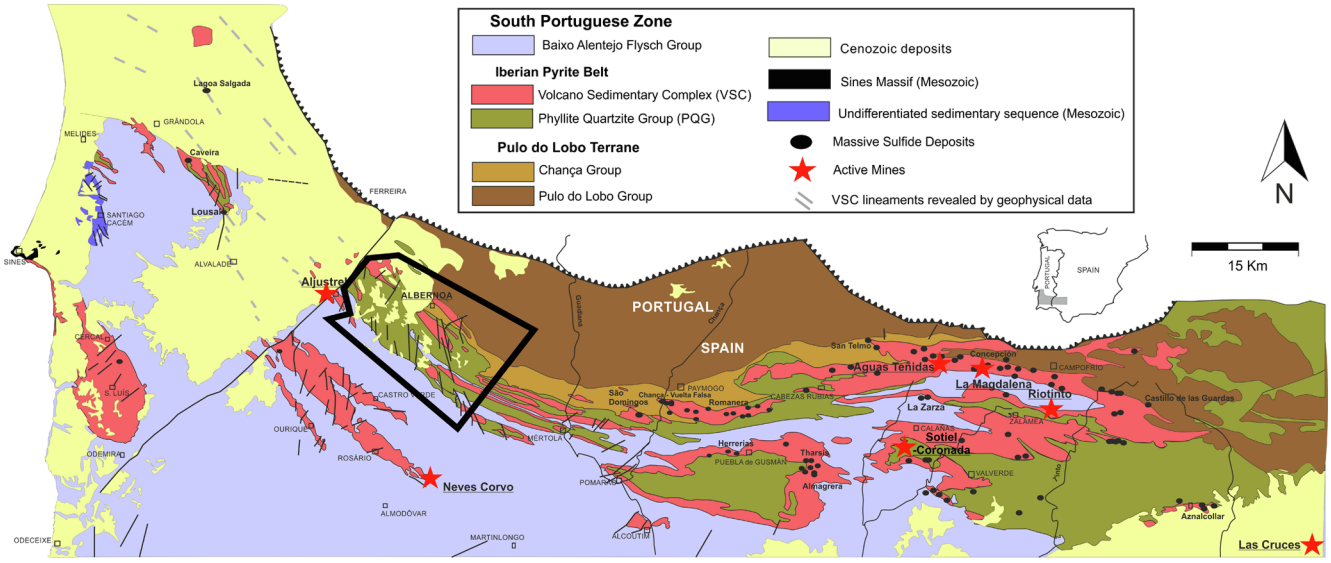

Fig. 1. Synthetic geological map of SW Iberia, illustrating the location of the main sulfide ore deposits and related Fe-Mn occurrences. The outer limit of the Albernoa area is traced by the black polygon. Modified after Oliveira (1992), Barriga et al. (1997), Leistel et al. (1998), Carvalho et al. (1999), Matos et al. (2000, 2006), Tornos (2006).

2002; Inverno et al., 2015). These deposits are of varying size and metal content and are mostly hosted in the Volcano-Sedimentary Complex (VSC) of Upper Fammenian to Upper Visean age. Their economic importance is historically indisputable and, at present, the seven active mining centers (Neves Corvo, Aljustrel, Las Cruces, Aguas Teñidas, RioTinto, Sotiel-Coronada and La Magdalena) have a strong regional/national impact, and are responsible for a significant part of the copper produced in the European Union (*e.g.* Mateus et al., 2017). Two of these centers (Neves Corvo and Aljustrel) will soon produce zinc concentrates, joining Aguas Teñidas, La Magdalena and Sotiel-Coronada (MATSA, 2018) as some of the few active base metal mines in Europe.

During the last two decades, several multidisciplinary studies (e.g. Leistel et al., 1998; Tornos et al., 1998; Saéz et al., 1999; Matos et al., 2000; Rosa et al., 2004, 2008, 2010; Oliveira et al., 2011) significantly contributed to advances in the geoscientific understanding of the IPB, namely: (i) the factors that directly and indirectly influenced the architecture, formation and evolution of the basin in which the IPB formed (e.g. Tornos et al., 2002; Oliveira et al., 2005); (ii) the physical volcanological control on VSC deposition, including spatial reconstruction of volcanic centers and associated mineralization (e.g. Soriano and Martí, 1999; Rosa, 2007; Rosa et al., 2008, 2010); (iii) the constraints imposed by palynology and absolute age appraisals, and consequent definition of the interval in which the ore-forming systems have been developed (*e.g.* Barrie et al., 2002; Pereira et al., 2007; Valenzuela et al., 2011; Oliveira et al., 2013; Li et al., 2019); (iv) the identification of metal sources of and fluids involved in the metallogenic process, making use of multi-elemental and isotopic data (*e.g.* Marcoux, 1998; Relvas et al., 2001; Tornos et al., 2008; Jorge, 2009; Li et al., 2019); and (v) the development of hybrid genetic models, mostly transitional from volcanic-hosted to sedimentary-hosted massive sulfides (*e.g.* Almodóvar et al., 1998; Saéz et al., 1999, 2011; Relvas, 2000; Oliveira et al., 2005; Relvas et al., 2006; Tornos and Heinrich, 2008; Li et al., 2019*)*. Notwithstanding these developments, several questions remain, particularly those related to the lateral and vertical facies variations in VSC and their significance in mineral exploration. Better organization of local stratigraphic columns and documentation of the main physical-chemical features constraining the basin evolution are needed to understand the controls on siting of concealed ore-forming systems of economic significance. In this regard it should be emphasized that the historical track record clearly shows that improvements in conceptual geological models, along with advances in geophysical data multi-method acquisition and modelling, were critical for the discovery of: (i) Neves Corvo in 1977 (*e.g.* Leca et al., 1983; Carvalho et al., 1999; Relvas et al., 2002; Oliveira et al., 2004, 2013; Carvalho, 2016); (ii) Lagoa Salgada in 1992 (e.g. Oliveira et al., 1998); (iii) Las Cruces in 1994 (*e.g.* Yesares et al., 2015; Tornos et al., 2017); and (iv) more recently, 2013–2014, the technically successful exploration programs undertaken by AVRUPA in the Alvalade license (Avrupa Minerals, 2014*)* and by MATSA at La Magdalena (e.g. Granda et al., 2016).

New greenfield and brownfield exploration methods and methodologies developed in the IPB employ high-resolution geological, mineralogical, geochemical and geophysical data obtained for the Albernoa area (≈713 km^2) (Mateus et al., 2014, 2015a,b; Codeço et al., 2015; Godinho et al., 2015; Luz et al., 2015, 2017; Moreira et al., 2015; Codeço et al., 2018). In the present study, the multi-element geochemical data for 133 metasedimentary rock samples from the IPB main units [Phyllite-Quartzite Group (PQG) and VSC] outcropping in the Albernoa area are reported and discussed, along with whole-rock Pb, Sr and Nd isotope data gathered for a selected group of samples representing non-altered and hydrothermally altered and mineralized sections of the sampled metasedimentary VSC stratigraphic sections. The specific purpose is twofold: (i) recognize the basic compositional features defining the "geochemical background" for metapelite rocks in the VSC and PQG sequences; and (ii) develop whole-rock geochemical fingerprints that can be used to detect pre-Variscan metamorphic and deformational seafloor hydrothermal activity that may be associated with massive sulfide ores. The data and interpretations here presented, resulting from a baseline "proof-of-concept" study, are part of an ongoing study of all the key metasedimentary sequences in the Portuguese sector of IPB which has the following broad objectives: (i) the identification and quantification of all sources of fundamental constituents of these rocks; (ii) evaluation of the main variables in sedimentary environment analysis and/or subsequent geological evolution; and (iii) identification of potential useful guides/criteria to the conceptual design of new exploration programs for concealed and high-grade massive sulfide accumulations in the IPB. In general, our approach to achieve these objectives follows similar research lines in some other relevant massive sulfide provinces (e.g. Lett and Bobrowsky, 1998; Lett, 2001; Canet et al., 2004; Jansson et al., 2018; Denhavi et al. 2018).

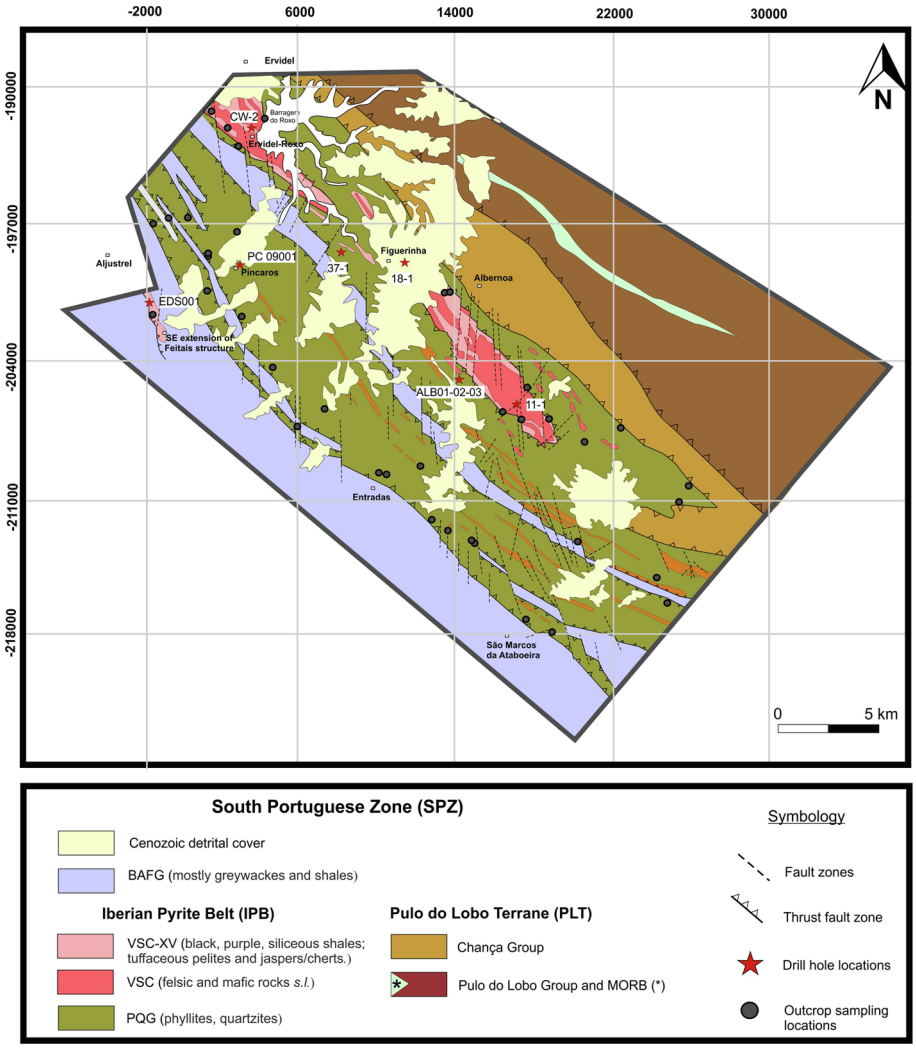

Fig. 2. Simplified geological map of the Albernoa area showing the location of sampled drill-holes and outcrops. Adapted from the Geological Map of Portugal at 1:200,000 (Oliveira,1992) and unpublished technical reports (Mateus et al. 2014, 2015a,b). Supplementary information on sampling is provided in Appendix 1.

2. Geological background

The South Portuguese Zone (SPZ) is one of the SW Iberian Variscides geotectonic domains (*e.g,* Silva et al. 1990, Quesada, 1998; Simancas et al. 2005; Ribeiro et al. 2007*)*. It includes from N to S (*e.g.* Carvalho et al. 1971, 1976; Oliveira, 1990): (i) the Pulo do Lobo Terrane; (ii) the Iberian Pyrite Belt (IPB); (iii) the Baixo Alentejo Flysh Group (BAFG), also known as the Culm Group; and (iv) the SW Portuguese Domain (SWP). The IPB stratigraphy comprises three main sequences (*e.g.* van den Boogard, 1963; Schermerhorn, 1971; Oliveira, 1990; Moreno et al., 1996; Pereira et al., 2018; Oliveira et al., 2013) that, from bottom to top, are known as: (i) the Phyllite-Quartzite Group (PQG); (ii) the Volcano-Sedimentary Complex (VSC); and (iii) the Mértola Formation, the lowermost part of the BAFG. The Middle to Late Devonian PQG corresponds to a siliciclastic succession mainly comprising phyllites, quartzites and *meta*-quartzwackes that, locally, may include metalimestone lenses (e.g. Moreno et al., 1996; Jorge et al., 2006). The Late Fammenian to Late Visean VSC is characterized by voluminous volcanic rocks emplaced during several volcanic episodes and typically developing inter-fingered successions with metasedimentary clastic rocks (*e.g.* Schermerhorn, 1971; Carvalho et al., 1999*;* Soriano et al., 1999*;* Valenzuela et al. 2002; Donaire et al., 2002; Rosa et al., 2011). The metavolcanic rocks are largely submarine and commonly bimodal in nature despite the prevailing rhyolitic/rhyodacitic nature observed in outcrops (*e.g.* Rosa et al., 2008, 2010; Codeço et al., 2018, and references therein). The metasedimentary component is composed of a large variety of rock types but with a clear prevalence of black metapelites and *meta*-siltstones (locally accompanied by minor *meta*-quartzwackes), excluding the upper part of the sequence which is dominated by siliceous metapelites, *meta*-jaspers (commonly *meta*-cherts) and purple metapelites (*e.g.* Tornos et al., 1998, 2008; Tornos and Spiro, 1999; Mateus et al., 2014, 2015a,b). The Mértola Formation (Upper Visean) is a typical flysch sequence that contains intercalations of variable thickness of prevalent meta-greywackes and metapelites (*e.g.* Oliveira, 1990; Oliveira et al., 2006; Rosa et al., 2008, 2010; Pereira et al., 2007).

Although heterogeneous, the Variscan deformation is intense throughout the SPZ, particularly along its northern border, close to the SW Iberian suture (*e.g.* Ribeiro and Silva, 1983; Silva et al., 1990; Quesada, 1998; da Silva et al., 2007; Ribeiro et al., 2010; Carvalho et al., 2016). The S-verging, thin-skinned thrust-fold belt represents the culmination of a significant crustal shortening within a left-lateral transpressive tectonic regime triggered by oblique continental collision during the Carboniferous. This deformation, typically involving strong strain partitioning, caused disturbances of different amplitude in the original stratigraphic relationships and internal facies arrangements (*e.g.* Schermerhorn, 1971; Moreno et al., 1996; Pereira et al., 2007), thus creating additional difficulties in lithostratigraphic reconstruction (*e.g.* Oliveira, 1990, 2008; Quesada, 1998; Tornos et al., 2002; Relvas et al. 2006; Martín-Izard et al., 2015). In addition, synorogenic

metamorphic recrystallization may have obliterated primary features, despite the prevalence of low grade conditions, i.e. from the prehnite-pumpellyite facies and progressing to greenschist facies conditions towards the northern border of IPB and PLT (*e.g.* Munhá, 1979, 1981, 1983a,b, 1990; Abat et al., 2001).

In the IPB, the sulfide ore-forming systems related to the large massive bodies are commonly rooted in stockworks of variable dimension hosted in hydrothermally altered volcanic and/or metasedimentary sequences (e.g. Barriga et al., 1997; Leistel et al. 1998; Tornos et al., 2000; Saéz et al., 2011). Conditions for the development of different sulfide ore-forming systems were mostly attained during VSC evolution. Nevertheless, evidence for syn- to late-orogenic ore remobilization (which improves metal grades in some deposits) is common (e.g. McKee, 2001; Castroviejo et al. 2011; Luz et al. 2012; 2014a,b). This is due to chemical and physical transformations that took place during Variscan metamorphism and tectonic stacking, further complemented by hydrothermal activity related to the propagation/reactivation of several (strike-slip) fault zones in late Variscan times (e.g. Quesada, 1998; Relvas, 2000; Marignac et al., 2003; Tornos, 2006*)*.

2.1. The Albernoa area

The Albernoa area extends along the Portuguese segment of the IPB northern sector (Fig. 2). The local lithostratigraphic column presents the PQG at the base, forming a metasedimentary succession with prevalent black metapelites, meta-siltstones and quartzites (*e.g.* Rosa et al., 2004; Rosa, 2007; Pereira et al., 2007; Mateus et al., 2014, 2015a,b). In general, throughout the area, the PQG displays: (i) an important sandy-derived component of relatively pure quartzite lenses with minor amounts of interstitial phyllosilicates that increase in abundance from NW to SE; (ii) widespread *meta*-siltstones; and (iii) minor tuffaceous metapelites and metavolcaniclastic rocks, tracing the gradual transition towards the stratigraphically overlying VSC (Mateus et al., 2014, 2015a). In this regard it should be noted that the term “tuffaceous” is here used as an adjective of metapelites, thus indicating the incorporation of a minor fraction of volcanic-derived particles in a fine-grained clay-rich sediment, the assemblage further subjected to metamorphism; our use of this terminology does not imply that this volcanic detritus was pyroclastically emplaced. Samples of black metapelites collected in drill-hole 11-1 (see Fig. 2) yielded miospores from the Upper Fammenian VH biozone (Pereira et al., 2007).

The Volcano-Sedimentary Complex sequence includes relatively thick piles of metavolcanic rocks that define two main alignments labeled as Ervidel-Roxo (ER) and Figueirinha-Albernoa (FA). The ER metavolcanics rock pile comprises mostly rhyolites and minor rhyodacite rocks, locally complemented with minor intermediate to mafic metavolcanic rocks. In contrast, the FA metavolcanic pile is mainly composed of coherent rocks of rhyodacitic composition interbedded with products of their fragmentation (autoclastic derivatives), forming an extensive metavolcaniclastic rock envelope (e.g. Codeço et al., 2018). Metasedimentary rocks in the VSC are characterized by a prevalent clayey component, although supplemented by a minor, but ubiquitous, fine-grained sandy fraction in some of the examined sections. Various metapelite sub-types can be distinguished based on their visual appearance and mineral composition; siliceous metapelites, dark-grey to black metapelites and sericitic metapelites are the most common, with the former two locally interbedded with thin layers of meta-siltstones or (very) fine-grained impure quartzites; tuffaceous metapelites occur typically near the metavolcanic sequence. The VSC sequences in Albernoa culminate with a succession of meta-jaspers (/meta-cherts), purple and black metapelites (Mateus et al., 2014, 2015a,b*;* Codeço et al., 2018). Two metapelite levels from this upper metasedimentary sequence (overlying metavolcanic rocks) preserve miospores from the lower Visean Pu Biozone to middle Visean NL Biozone (Pereira et al., 2007).

The Variscan metamorphic recrystallization conditions deduced for the Albernoa are of greenschist facies, locally reaching the chlorite-biotite zones transition as indicated by the development of biotite after chlorite in some metavolcaniclastic rocks (Codeço et al., 2018) and the sporadic occurrence of fine-grained (green) biotite in some metapelite samples.

There is also heterogeneous strain accommodation (moderate to intense) in places evidenced by various micro- to mesoscopic structures denoting the superposition of two main deformation events; the latter are clear at the SE extension of the Feitais structure (near the Aljustrel mine), Ervidel-Roxo and Entradas (Mateus et al., 2014, 2015a).

3. Sampling and analytical methods

One hundred and thirty-three samples of fine-grained siliciclastic and tuffaceous metapelites from PQG and VSC units were selected for petrography and whole-rock multi-element chemical analysis; sample locations are given in Appendix 1 and plotted on Fig. 2. The sampling was performed after detailed geological mapping and re-logging of the accessible historical mineral exploration drill cores (Mateus et al., 2014, 2015a,b); 54 samples are from outcrops and 79 from drill-cores (see also Appendix 1), the latter subgroup including 11 samples of the EDS0001 drilling at the SE extension of Feitais structure (≈ 2 km distant from the Aljustrel mine). All the samples were prepared at the University of Lisbon laboratories for petrographic, chemical and mineralogical analysis, and whole-rock geochemistry.

Mineral chemistry studies were performed on polished thin sections (selected after comprehensive petrographic examination) at the University of Lisbon using an Electron Probe Micro-Analyser (EPMA) – JEOL JXA8200 equipped with four wavelength-dispersive spectrometers and calibrated with metallic and mineral standards provided by Astimex Scientifc Ltd. The EPMA was operated with an accelerating voltage of 15 kV, a beam current of 25nA with a diameter of 5 μm and an acquisition time of 20 s for peaks and 5 s for a background radiation. EPMA analyses were numerically processed by considering the ideal stoichiometry of each mineral group and an unpublished algebraic procedure which extends the method reported in Droop (1987) for valence partitioning of multivalent elements, which takes into account all relevant stoichiometric relationships.

The whole-rock chemical analysis of 142 powder samples (including duplicates and replicates) was performed at Activation Laboratories Ltd (ActLABS), Ancaster, Ontario, Canada using their 4E-research analytical package. This package incorporate inductively coupled-plasma mass spectrometry (ICP-MS) and instrumental neutron activation analysis (INAA) after total digestion and lithium metaborate/tetraborate fusion (further details in http://www.actlabs.com – Code 4E Research).

Whole-rock Sr, Nd and Pb isotopic analyses were performed on a selected subset of samples ($n = 12$) at the Centro de Pesquisas Geocronológicas (CPGeo), Instituto de Geociências, Universidade de São Paulo, Brazil. About 75 to 100 mg of the same powders used for whole-rock elemental analysis were taken into solution by acid digestion (3:1 HF + HNO_3 mixture) in Savillex beakers on hot plate at 110 °C for 10 days; no spikes were added. The Sr, Nd and Pb were separated from the same sample solution in ion-exchange columns following the procedures described by Tassinari et al. (1996), Sato et al. (1995) and Babinski et al. (1999). $^{87}Rb/^{86}Sr$, $^{147}Sm/^{144}Nd$, ($^{206}Pb/^{204}Pb$)i, ($^{207}Pb/^{204}Pb$)i and ($^{206}Pb/^{204}Pb$)i ratios were calculated using Rb, Sr, Sm, Nd, U, Th and Pb abundances from the ICP-MS whole-rock analyses. The Sr isotopic compositions were determined on a Thermo Triton mass spectrometer. The $^{87}Sr/^{86}Sr$ ratio was normalized to $^{86}Sr/^{88}Sr = 0.1194$. Replicate analysis of NBS 987 standard (n = 100) yielded a mean $^{87}Sr/^{86}Sr$ ratio of 0.710239 ± 0.000016 (2σ) during the analytical period; the blanks for Sr were 5 ng. The Nd isotopic ratios were performed on a Thermo Neptune Plus ICP-MS. Measurements of $^{143}Nd/^{144}Nd$ were normalized to $^{146}Nd/^{144}Nd = 0.7129$. The average of $^{143}Nd/^{144}Nd$ for La Jolla and BCR-1 standards were

0.511847 ± 0.00005 (2σ) and 0.512662 ± 0.00005 (2σ), respectively; the blanks for Nd were < 0.03 ng. Pb isotopic compositions were measured on a Finnigan MAT 262 Mass Spectrometer. Replicate analysis (n = 60) of NBS-981 common Pb standard yielded $^{206}Pb/^{204}Pb$ = 16.899 ± 0.007, $^{207}Pb/^{204}Pb$ = 15.438 ± 0.007, $^{208}Pb/^{204}Pb$ = 36.539 ± 0.28. The Pb ratios were corrected for mass fractionation of 0.12% amu ($^{207}Pb/^{204}Pb$) and 0.13% amu ($^{206}Pb/^{204}Pb$, $^{208}Pb/^{204}Pb$) based on the NBS-981 analysis. Procedure blanks are ca. 140 pg for Sr, 59 pg for Nd and 470 pg for Pb, and considered to be negligible for the size of the samples analyzed.

4. Characteristic features of the metasedimentary rocks

Metapelites and tuffaceous metapelites sampled in the Albernoa area display similar (grano-)lepidoblastic textures. These rocks preserve a wide range of microstructures that record strong heterogeneous strain accommodation such as micro-folding, oriented fabrics, effects of strain hardening and incipient dynamic recrystallization, pressure solution and chemical softening. All these features are particularly evident at the SE extension of the Feitais structure (near the Aljustrel mine), Ervidel-Roxo and Entradas. In these locations, the prominent schistosity (S_n at a low angle with bedding, S_0, or transposing it) is folded and crenulated, and there is a recognizable late cleavage (S_{n+1}). Subsequent Late Variscan fracturing (affecting all the examined metasedimentary rocks and postdating S_n, and S_{n+1}, where present), shows discontinuous (non-oriented and non-strained) infillings of quartz ± chlorite ± pyrite ± chalcopyrite ± calcite.

Some samples of metapelites and tuffaceous metapelites preserve evidence of early-developed (pre-Variscan metamorphism and deformation) veinlets typically folded and filled with strained and variably recrystallized quartz + sulfides (± chlorite ± carbonates). The rock matrix surrounding these structures is enriched in phyllosilicates (± carbonate) and submillimeter sized quartz along with other accessory phases (apatite + rutile ± REE-bearing phosphates ± sulfides; the latter two groups are only recognized at high magnification during EPMA inspection) that document a moderate to intense alteration of a preexistent mineral assemblage. Since these rock constituents also develop oriented fabrics, it is likely that they represent products of hydrothermal processes prior to Variscan deformation, and this alteration event can be related to the formation of massive sulfide systems. Therefore, these mineral assemblages partly overprint or obliterate completely the mineral/textural changes that took place during diagenesis, most possibly involving modified seawater (the so called "regional alteration" triggered by the progression of seafloor metasomatism processes, that are prominent in metavolcanic rocks in the area – *e.g.* Munhá and Kerrich, 1980; Barriga and Kerrich, 1984; Munhá et al., 1986).

4.1. Metapelites

The prevailing mineral assemblage forming metapelites *sensu lato* in both PQG and VSC sequences comprises fine-grained white mica (± chlorite), quartz and accessory zircon, apatite, titanite, rutile and tourmaline. White mica is the most common mineral in metapelites, commonly in similar abundances to quartz. This phyllosilicate deviates from the ideal muscovite (Ms) composition mostly due to Tschermak substitution [i.e. $(R^{2+})^{vi}Si^{iv}_{-1}Al^{vi}_{-1}Al^{iv}$ where R^{2+} accounts mostly for Mg^{2+} and Fe^{2+}], recording also significant Na contents (up to 0.4 a.p.f.u.) in place of K (Fig. 3A and B). Early-formed chlorite (prior to Variscan deformation), which develops oriented aggregates together with white mica in some samples, is chemically characterized by average $Fe^{2+}/(Fe^{2+}+Mg)$ (= #Fe) ratios around 0.74 (Fig. 3D). Late-formed chlorite (postdating the main stages of Variscan strain accommodation) occurs in infillings of fractures that crosscut S_n (and S_{n+1}, where present), and has distinctly more Mg-enriched ($\#Fe_{average}$ = 0.53) compositions (Fig. 3D).

Differences in the abundances of the major and accessory mineral phases (that may show similar or different chemical compositions) define several metapelite subtypes, some of which are recognizable at the macroscopic scale: (i) black metapelites; (ii) grey(-greenish) to dark-grey metapelites; (iii) purple metapelites; and (iv) green metapelites.

Black metapelites (Fig. 4A) are variably enriched in non– or poorly-ordered organic matter and show (sub-)rounded quartz clasts within a groundmass of fine-grained white mica. Depending on the proportion, size and distribution of quartz clasts this subtype can resemble black meta-siltstone. Botryoidal pyrite and submillimeter sized disseminations of pyrite ± chalcopyrite ± sphalerite ± galena are common, and they may be accompanied with early- (prior to S_n) fracture infillings of pyrite ± pyrrhotite (± chalcopyrite ± sphalerite) (Fig. 4B and C).

Grey(-greenish) to dark-grey metapelites are commonly associated. This assembly typically comprises lenticular bedding of dark colored (phyllosilicate-rich) metapelite in (Fig. 4D) a lighter colored metapelite bearing a fine-grained (quartz-dominant) sandy component (Fig. 4E). These rocks are mostly composed of very fine-grained white mica and quartz (Fig. 4F), and the most common accessory minerals are tourmaline and rutile; in some samples, authigenic apatite is present as irregular grains, and its growth is related to (primary) P-enrichments due to accumulations of bio-derived products. Chlorite is mainly present in late-developed veins/veinlets along with quartz ± carbonates. Sulfides are not common, despite the presence of disseminations of submillimeter sized pyrite ± chalcopyrite in a few places. This metapelite sub-group typically occurs in PQG where well-foliated metapelites (phyllites) commonly display centimeter-thick rhythmic-sequences with fine-grained (impure) quartzites (Fig. 4G); in places, thicker quartzite layers display tight anastomosed networks of veinlets sealed with quartz ± chlorite ± pyrite.

Purple metapelites (Fig. 4H) contain abundant, although variable, disseminated fine-grained hematite (± magnetite) (Fig. 4I) within a groundmass of phyllosilicates and submillimeter sized quartz (Fig. 4J). These rocks may also enclose elongated aggregates (like *rod* structures *sensu lato*) of quartz ± Mg-rich carbonate ± chlorite ± apatite ± pyrite ± chalcopyrite ± digenite that replace primary components of possible volcaniclastic origin (Fig. 4K); a few similar structures filled only with quartz provide evidence of dynamic recrystallization.

Green metapelites (Fig. 4L) contain variable proportions of phyllosilicates and fine-grained (commonly very fine-grained) quartz. White mica prevails (Fig. 4M), but chlorite is also common present as: (i) early-formed and oriented aggregates (together with mica), and on this basis preceded the Variscan deformation; and (ii) late-formed aggregates in quartz-rich infillings (post-dating S_n and, where present, S_{n+1}) of irregular veins/veinlets. The typical accessory assemblage is tourmaline, rutile and (authigenic) apatite. These metapelites commonly display early-developed quartz microstructures (folded and affected by S_n and S_{n+1}) that contain variable amounts of pyrite and chalcopyrite (Fig. 4N, O).

4.2. Tuffaceous metapelites

Tuffaceous metapelites were identified in both lithostratigraphic sequences (PQG and VSC), even though they are far more predominant in VSC than in the PQG; they typically occur near sequences that include metavolcanic rocks. The tuffaceous metapelites include variable amounts of volcanic-derived and (sub-) millimeter sized quartz and/or feldspar ($Ab_{87.5-99.9}$) mineral fragments within a very fine-grained, violet to green-colored (in hand sample) matrix mostly composed of white mica (± chlorite) that is locally enriched in dolomite and/or calcite. Evident and possible volcaniclastic component (Fig. 5A and B) can reach up to 50 vol% and is characterized by: (i) quartz clasts showing angular to sub-rounded shapes, and which commonly display late dissolution features that are the result of pressure solution

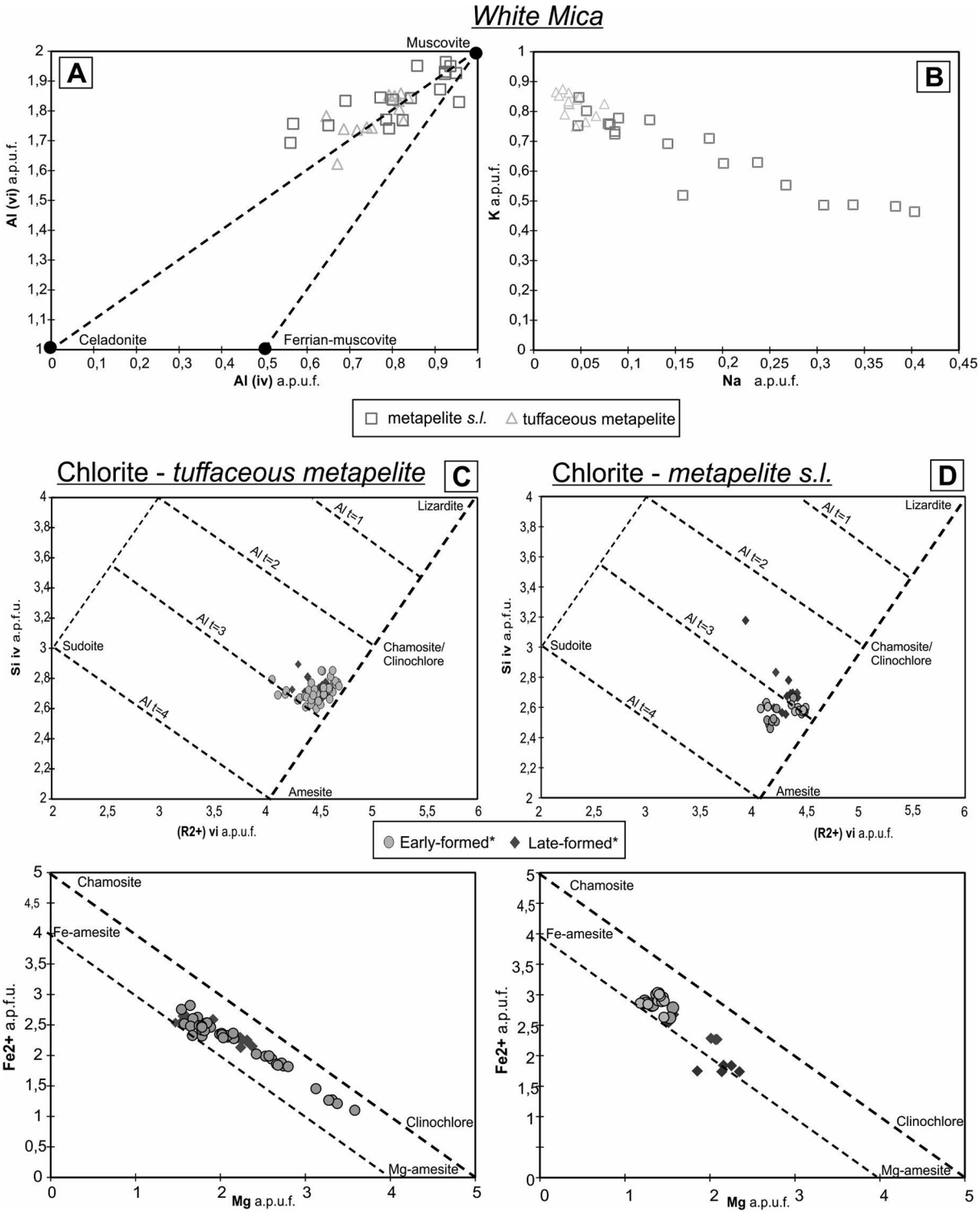

Fig. 3. Di-octahedral micas forming metapelites and tuffaceous metapelites plotted in the Al^{iv} vs. Al^{vi} (a.p.f.u. = atoms per formula unit) diagram (A), putting in evidence the main Tschermak cationic exchange, and in the Na vs. K (a.p.f.u.) diagram (B), documenting the clear enrichment in paragonitic content of micas from metapelite samples. Compositional variation displayed by early- and late-formed chlorites in tuffaceous metapelites (C) and metapelites (D) using the Si vs $(R^{2+})^{vi}$ and the Fe^{2+} vs Mg (a.p.f.u) plots, where $(R^{2+})^{vi}$ = (Mg,Fe^{2+}, Mn^{2+}, Ba, Zn). Representative EPMA data and correspondent ion distribution per formula unit for white micas and chlorites are given in Appendixes 2 and 3, respectively.

(Fig. 5C); (ii) feldspar fragments, typically displaying angular shapes and effects of hydrolysis of variable intensity (Fig. 5D); and (iii) elongated aggregates of quartz ± Mg-rich carbonate ± chlorite ± apatite ± pyrite ± chalcopyrite ± digenite (rimming chalcopyrite) that likely replaces primary volcaniclastic components. Other characteristic features in tuffaceous metapelites from Ervidel-Roxo are: (i) feldspar ($Ab_{96.8}$) clasts that commonly record effects of early albitization; (ii) intensely hydrothermally altered samples that commonly contain epidote, titanite and REE-bearing phosphates (Fig. 5E); and (iii) abundant pyrite in samples with a chlorite-calcite rich matrix, and in

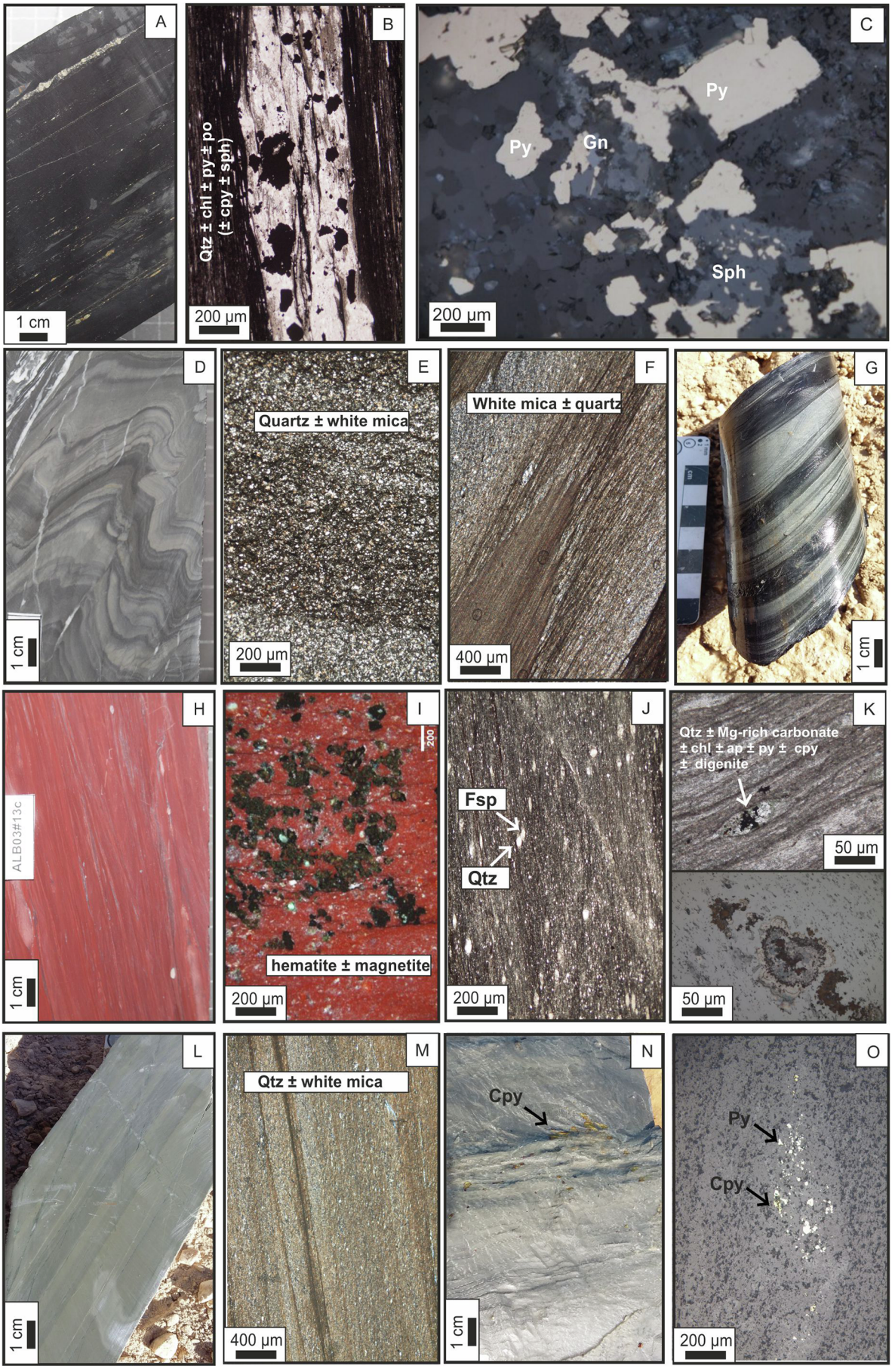

(caption on next page)

Fig. 4. Selected hand samples and photomicrographs representing the main metapelite subgroups. Black metapelites [A to C]: (A) Pyritic black metapelite (EDS1-B, 304.56 m); (B) Early fractures (prior to S_1) filled with *quartz + chl + py ± cpy ± sph* (EDS1-C, 305.15 m); (C) Local enrichments in *py ± sph ± gn* in black metapelite (18–1-E, 80.70 m); Grey(-greenish) to dark-grey metapelites [D to G]: (D) Intercalations/inter-fingering of dark-grey to grey(-greenish) metapelites enriched in fine-grained sandy component (ALB02, 244.15 m); (E) fine-grained sandy layer (impure quartzite) (ALB03#35, 562.00 m); (F) Inter-fingering of metapelites and sandy-rich layers (ALB03#1, 64.05 m); (G) Rhythmic succession of dark colored and lighter (sandy-rich) metapelites (ALB03#9, 213.80 m); Purple metapelites [H to K]: (H) Typical purple metapelite (ALB03#13c, 311.50 m); (I) Hematite (± magnetite) enrichments (X47, outcrop sample); (J) Purple metapelite recording volcanic-derived (feldspar and quartz) contribution (ALB03#13c, 311.50 m); (K) upper image (transmitted light) - elongated aggregates of *quartz ± Mg-rich carbonate ± chlorite ± apatite ± pyrite ± chalcopyrite ± digenite* replacing primary components of possible volcanogenic origin (EDS1-K, 427.40 m); lower image (reflected light) – detail of previous aggregate revealing distribution of neo-formed sulfide grains; Green metapelites [L to O]: (L) Intercalation/inter-fingering bands in green metapelites (abundant very fine-grained white mica) caused by differences in the relative abundance of various mineral phases (mostly quartz and phyllosilicates; ALB02, 245.45 m); (M) Typical green metapelite, mainly composed of quartz and white mica (ALB03#18, 301.70 m); (N) Sulfide association in common early-developed quartz veinlets with pyrite and chalcopyrite (ALB02#15, 94.05 m); (O) Fine disseminations of *pyrite ± chalcopyrite* in the matrix of green metapelites (ALB02#15, 94.05 m). (For interpretation of the references to colour in this figure legend, the reader is referred to the web version of this article.)

places occurring together with sphalerite ± galena (Fig. 5F). Some tuffaceous metapelite samples collected from the SE extension of the Feitais structure (near the Aljustrel mine) also show the development of early fractures (prior to S_n) filled with carbonate + chalcopyrite ± pyrite ± Co-Ni and Ni-Sb bearing sulfides ± As-Co-Ni and As-Ni (-Sb)-bearing sulfosalts (Fig. 5G and H).

The chemical composition of white mica in tuffaceous metapelites is similar to that in metapelites, displaying a similar extent of the main Tschermak cationic substitution but a significant narrower (< 0.1 a.p.f.u.) replacement of K by Na in interlayer positions (Fig. 3A, B). Chlorite compositions tend to cluster at an average #Fe $\approx$ 0.49 for chlorite that forms aggregates developed prior to rock cleavages, despite of the lower range of Mg-contents (< 2 a.p.f.u.) of chlorites in early-formed (folded) veinlets in comparison to chlorites in the rock matrix (Fig. 3C). The late-formed chlorite in quartz-rich fracture fillings that cut S_n (and S_{n+1}, where present) also display variable Mg contents ($\approx 1.3-2.4$ a.p.f.u.), its average #Fe is 0.55 (Fig. 3C). The average chemical composition of feldspars in tuffaceous metapelites is $Ab_{97.5}$; anorthite contents range from 0.1 to 12% but those of orthoclase are typically rather lower.

5. Geochemistry

5.1. Whole-rock chemistry

The inter-elemental correlation matrix shows various linear co-variations involving a relatively large number of elements (see Appendix 5). When grouped according to rock type (metapelites or tuffaceous metapelites) several differences are evident between them, as expected. However, no significant disparities are observed from VSC/PQG metapelites and VSC/PQG tuffaceous metapelites (See Tables 1A, 1B). In general, the prevailing whole-rock geochemical fingerprints are controlled largely by: (i) the relative abundance of quartz and phyllosilicates (white micas ± chlorite); and (ii) certain accessory minerals, such as zircon, titanite (± rutile), apatite and carbonates. The similarities between both rock types are evident when the median abundances of many chemical elements are considered, despite of minor irregularities in abundance displayed by some elements, which correlate well with differences in mineral assemblage as summarized previously (see boxplots in Appendix 5). High standard deviations indicate that element abundances are quite irregular, and values close to or above the average reflect the presence of outliers or extreme outliers (*e.g.* Soares, 2006); in the present study, these outliers (anomalous values) may denote effects of pre-Variscan hydrothermal alteration (and/or mineralization) of variable intensity.

Positive linear co-variations displaying correlation coefficients (r) from 0.75 to 0.95 (see Appendix 5), that also intersect the origin (on bivariate plots), are obtained for Al_2O_3 vrs: TiO_2, Sc, Th and Ga; the Al_2O_3 vrs Zr positive linear co-variation shows a lower correlation coefficient but its p-value (< 0.05) still is statistically significant. These co-variations suggest that all these elements display coherent geochemical behavior and are immobile, even though their relative abundance is controlled by the ratio between sandy- (or silt) and clayey-derived components forming each sample (Fig. 6A–D). Several sand-rich samples that contain variable abundances of Al-free accessory minerals (such as zircon) are responsible for a significant degree of dispersion in the Zr and Th vs. Al_2O_3 plots (Fig. 6A and C). There are also two particularly anomalous samples: (i) with the highest Al_2O_3 content (due to the presence of a dominant clayey component) and this sample might represent our most endmember metapelite composition; and (ii) with the high TiO_2, Sc and low Th abundances, indicative of the presence of titanite (± rutile ± magnetite), although the explanation for the high Sc ($\approx$ 45 ppm) is unknown.

5.1.1. Major elements

The examination of major elements behavior can be done by using Al_2O_3 as common reference (Fig. 7). The clearest negative co-variation between SiO_2 and Al_2O_3 records satisfactorily the dilution effect of the prevalent aluminum–silicate component by free silica (as quartz), regardless of its primary or secondary origin. Additionally, the strong positive co-variation between K_2O and Al_2O_3 for both rock types from each lithostratigraphic unit, documents well the influence of K- and Al-bearing phases (mostly white mica) on the bulk composition. Elemental oxides such as Fe_2O_3 and MgO present significant positive co-variations with Al_2O_3 ($r > 0.5$; see Appendix 5) for PQG samples, and may reflect the relative abundance of chlorite over other phyllosilicates, although always disturbed whenever Fe-bearing sulfides are present (see Appendix 5 for Fe_2O_3 and S correlation coefficients). Weaker linear correlations, but statistically significant (see Appendix 5), were observed for Na_2O and MnO vrs Al_2O_3 plots; the CaO vrs Al_2O_3 correlation is not statistically significant ($r < 0.5$, p-value > 0.05). Considering the primary mineral assemblages forming the analyzed rocks, abundances of CaO up to 0.5 wt% should trace the regional background for the IPB metapelites *sensu lato* despite the lithostratigraphic unit (VSC or PQG); CaO > 0.5 wt% indicates the presence of significant amounts of apatite (detrital or non-detrital, also impacting on P_2O_5 abundances) and carbonates (sulfide-related or not) that may or may not be associated with titanite and/or epidote. In the Al_2O_3 vrs Na_2O plot, the high Na outliers are due to the presence of abundant albite that is quite common in the tuffaceous metapelites, and also in samples with a significant sandy detrital component that have been moderately altered during regional seafloor metasomatism; in addition, the K ⇔ Na substitution in white micas forming many metapelite samples may also contribute to the measured Na_2O abundances. The MnO contents are commonly below 0.1 wt%, reflecting the incorporation of trace/minor amounts of manganese in some silicate phases (*e.g.* epidote and chlorite) and carbonate phases; higher abundances reflect the presence of Mn-bearing (hydr)oxides that have been documented either in drill-core or surface samples from the PQG and VSC.

Considering the aforementioned relationships established between whole-rock chemical analyses and mineral assemblages, the ratio-ratio plots incorporating SiO_2, (CaO + Na_2O + K_2O) and TiO_2 abundances normalized to Al_2O_3 are useful to investigate the main compositional trends that characterize the examined metasedimentary rocks. In fact,

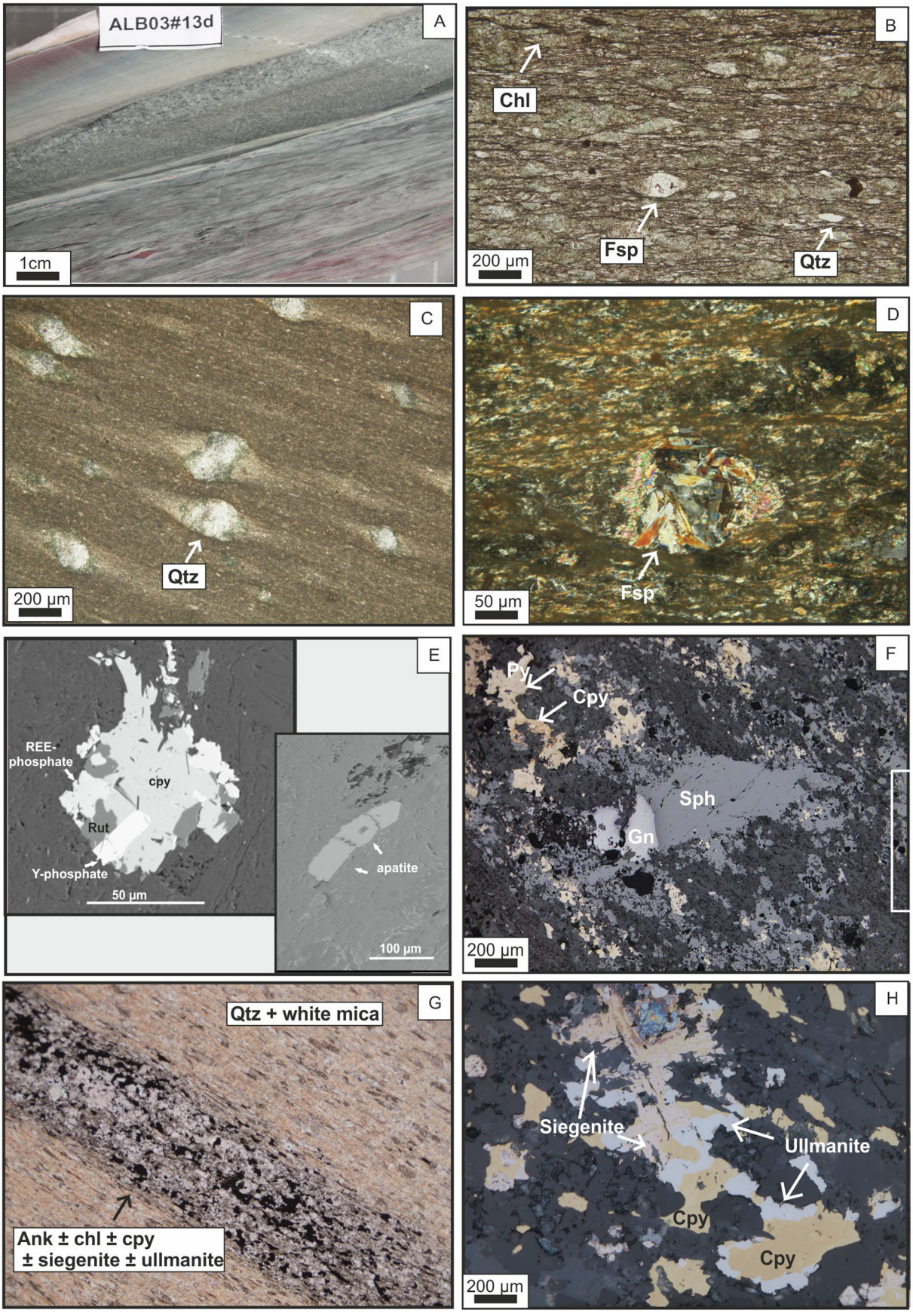

(caption on next page)

Fig. 5. Selected hand samples and photomicrographs representing tuffaceous metapelites [A to H]: (A) Green-violet metapelite incorporating volcanic-derived feldspar ± quartz (ALB03#13d, 311.50 m); (B) Quartz and feldspar deformed porphyroclasts in a fine-grained metasedimentary matrix mostly composed of muscovite ± chlorite (ALB03#13a, 305.40 m); (C) (D) Details of altered (sericitized) feldspar deformed prophyroclasts (ALB03#13a, 305.40 m); (E) upper - back scattered electron images of REE- and Y-bearing phosphates associated with sulfides (ALB03#22a, 401.50 m); lower – back scattered electron images of non-detrital apatite (EDS1-H, 385.20 m); (F) Chlorite-calcite enriched matrixes; pyrite is abundant, occasionally coming together with sphalerite ± galena (CW2-AA, 211.25 m). (G) and (H) Early fractures (prior to S_n) filled with carbonate + chalcopyrite ± pyrite ± Co-Ni- and Ni-Sb-bearing sulfides ± As-Co-Ni and As-Ni (-Sb)-bearing sulfosalts (EDS1-H, 385.20 m). (For interpretation of the references to colour in this figure legend, the reader is referred to the web version of this article.)

and despite some overlap, the ratio-ratio plots in Fig. 8A and B show that: (i) data for VSC lie within the following parameters $2.5 \leq SiO_2/Al_2O_3 \leq 6.5$, $0.02 \leq TiO_2/Al_2O_3 \leq 0.06$ and $0.2 \leq (CaO + Na_2O + K_2O)/Al_2O_3 \leq 0.25$; and (ii) data for PQG samples show $(CaO + Na_2O + K_2O)/Al_2O_3 \leq 0.3$, that range to higher SiO_2/Al_2O_3 and TiO_2/Al_2O_3 ratios (from 2.5 to 12 and 0.08 to 0.58, respectively) than VSC samples. Metasedimentary rocks from PQG with $(CaO + Na_2O + K_2O)/Al_2O_3$ ratios ≥ 0.3 represent samples with high albite contents that correspond to fine-grained *meta*-quartzwackes or centimeter-thick layers of meta-quartzwackes interbedded in the metapelites. Four samples of VSC (three metapelites and one tuffaceous metapelite) are outliers because of their high SiO_2/Al_2O_3 ratios and low $(CaO + Na_2O + K_2O)/Al_2O_3$. VSC metapelites with higher (> 10) SiO_2/Al_2O_3 ratios have a significant fine-grained sandy component in

Table 1A
Representative whole-rock multi-element analyses and statistic measures for VSC metapelites and tuffaceous metapelites (average ± standard deviation; median; two representative analyses) for Albernoa area. Major oxide-elements and S in wt% and minor elements in ppm; for each subgroup of rocks the number of available chemical analyses is indicated. Numbers 1 to 4 are representative analysis to each sub-group (*#1* – 11-1-MM (ordinary metapelite); *#2* – EDS1-B (mineralized metapelite); *#3* – CW2-O; *#4* – EDS1-H).

	metapelites (n = 62)				tuffaceous metapelites *(n = 27)*			
	mean ± σ	median	1	2	mean ± σ	median	3	4
SiO2	63,55 ± 8,83	62.05	62.59	47.04	69.44 ± 6.68	69.92	56.13	69.92
Al2O3	17,26 ± 5,42	17.06	16.98	12.27	14.37 ± 3.55	14	20.88	15.83
Fe2O3(T)	6,91 ± 2,58	6.91	8.32	19.42	5.06 ± 1.85	4.9	8.85	3.64
MnO	0,21 ± 0,32	0.129	0.085	0.16	0.18 ± 0.19	0.11	0.104	0.082
MgO	1,63 ± 0,98	1.5	1.94	1.31	1.82 ± 1.36	1.49	2.27	1.32
CaO	0,49 ± 0,51	0.23	0.65	0.45	0.69 ± 0.83	0.36	0.55	0.23
Na2O	0,83 ± 0,84	0.72	0.37	0.21	1.20 ± 1.09	0.79	0.18	0.89
K2O	3,30 ± 1,09	3.53	3.05	2.68	2.86 ± 1.09	2.62	5.57	3.54
TiO2	0,75 ± 0,27	0.78	0.843	0.536	0.53 ± 0.20	0.5	0.858	0.481
P2O5	0,11 ± 0,06	0.1	0.12	0.08	0.08 ± 0.03	0.07	0.09	0.07
Ba	514 ± 197	529	338	549	445.70 ± 168.99	476	497	606
Cs	7,58 ± 4,1	6.9	6.4	7.5	5.48 ± 2.81	4.8	6.1	9.9
Cu	39,8 ± 22,32	35.5	33	60	74.92 ± 154.52	36	86	106
Ga	23,97 ± 6,69	24.5	23	17	20.44 ± 4.72	21	27	22
Ge	2,33 ± 0,71	2.3	1.7	0.7	2.16 ± 0.66	2.3	1.9	2.3
Hf	3,78 ± 1,42	3.85	4.9	2.1	3.31 ± 1.71	2.9	4.1	3.1
Nb	12,95 ± 5,06	12.25	16.6	9.5	9.30 ± 3.38	8.8	14.2	13.8
Ni	64,56 ± 24,79	62.5	65	130	69.56 ± 43.40	67	65	167
Pb	24,05 ± 27,24	13	6	84	15 ± 13.23	11.5	5	7
Rb	152,26 ± 56,65	165	138	119	121.93 ± 48.37	111	158	178
S*	0,35 ± 1,5	0.0275	0.46	11.8	0.15 ± 0.44	0.02	2.11	0.015
Sr	87,87 ± 40,35	89.5	90	107	66.85 ± 31.71	65	39	67
Ta	1,07 ± 0,39	1.065	1.34	0.72	0.79 ± 0.24	0.83	1.24	0.98
Th	11,71 ± 3,84	12	13.7	8.43	10.17 ± 3.87	9.86	13.5	18
U	2,93 ± 1,65	2.66	3.16	11.9	2.09 ± 1.04	1.93	2.75	4.98
V	129,15 ± 42,68	135.5	158	138	100.85 ± 42.43	110	153	115
Y	25,82 ± 5,92	27	27	20	26.11 ± 11.28	23	26	21
Zr	155,79 ± 64,55	150	211	97	134.63 ± 70.26	120	173	111
La	41,92 ± 11,27	43.5	42	32.1	36.62 ± 9.81	37.3	42.3	44.2
Ce	82,04 ± 21,55	82.65	83	66.8	77.26 ± 18.95	74.8	79.4	105
Pr	9,41 v 2,38	9.71	9.51	7.52	8.35 ± 2.16	8.38	9.42	10.5
Nd	34,88 ± 8,57	36.1	35.5	28.2	31.24 ± 7.60	31.3	34.9	38.2
Sm	6,75 ± 1,61	6.99	6.8	5.63	6.26 ± 1.62	6.2	6.27	7.23
Eu	1,36 ± 0,34	1.34	1.42	1.12	1.14 ± 0.36	1.17	1.3	1.28
Gd	5,65 ± 1,35	5.8	5.66	4.52	5.29 ± 1.64	4.84	5.22	5.16
Tb	0,89 ± 0,22	0.92	0.9	0.69	0.85 ± 0.30	0.77	0.81	0.84
Dy	5,16 ± 1,25	5.27	5.26	3.91	4.98 ± 1.85	4.52	4.85	4.72
Ho	1,01 ± 0,24	1.05	1.01	0.73	0.99 ± 0.39	0.88	0.96	0.89
Er	2,92 ± 0,67	2.96	2.91	2.13	2.87 ± 1.13	2.55	2.91	2.58
Tl	0,68 ± 0,24	0.71	0.71	0.85	0.58 ± 0.23	0.55	0.71	0.95
Tm	0,43 ± 0,1	0.45	0.453	0.318	0.43 ± 0.16	0.39	0.443	0.393
Yb	2,86 ± 0,62	2.96	3	2.23	2.86 ± 1.14	2.65	2.95	2.65
Lu	0,43 ± 0,09	0.44	0.452	0.33	0.43 ± 0.17	0.37	0.438	0.366
As	28 ± 38,51	17	21	180	16.91 ± 19.68	8	27	14
Co	21,43 ± 10,94	19.4	18.2	70.7	22.15 ± 14.80	22.35	30.4	28.1
Cr	89,93 ± 31,03	87.5	86.7	81	62.64 ± 26.65	61.8	120	61.5
Sb	2,49 ± 3,27	13	1.2	19.9	1.52 ± 0.94	1.3	1.2	1.9
Sc	16,50 ± 5,91	16.25	15.9	13.7	13.92 ± 4.22	13.9	20	14
Zn	87,18 ± 28,11	96	110	128	79 ± 30.10	82	80	62

Table 1B
Representative whole-rock multi-element analyses and statistic measures for PQG metapelites and tuffaceous metapelites (average ± standard deviation; median; two representative analyses) for Albernoa area. Major oxide-elements and S in wt% and minor elements in ppm; for each subgroup of rocks the number of available chemical analyses is indicated. Numbers 1 to 3 are representative analysis to each sub-group (*#1* – X42 (ordinary metapelite); *#2* – X14 (higher sandy-component metapelite); *#3* – T18).

	metapelites (n = 40)				tuffaceous metapelites (n = 3)	
	mean ± σ	median	1	2	mean ± σ	3
SiO2	68.16 ± 9.26	66.01	65.72	72.81	72.02 ± 11.43	57.5
Al2O3	15.23 ± 5.01	16.24	12.96	12.7	14.31 ± 5.23	20.78
Fe2O3(T)	6.54 ± 2.3	6.74	11.81	5.19	5.21 ± 2.67	8.74
MnO	0.13 ± 0.15	0.11	0.117	0.095	0.06 ± 0.06	0.014
MgO	1.31 ± 0.73	1.36	1.42	1.02	0.99 ± 0.59	1.18
CaO	0.16 ± 0.21	0.1	0.1	0.01	0.07 ± 0.02	0.09
Na2O	0.74 ± 0.61	0.65	0.34	0.23	0.30 ± 0.13	0.45
K2O	2.58 ± 0.97	2.63	1.51	2.26	2.55 ± 1.10	3.9
TiO2	0.72 ± 0.27	0.74	0.539	0.489	0.59 ± 0.20	0.833
P2O5	0.09 ± 0.04	0.09	0.09	0.06	0.09 ± 0.03	0.1
Ba	397.41 ± 132.80	416	297	376	412.67 ± 183.14	648
Cs	4.94 ± 2.29	4.7	2.7	3.8	3.93 ± 1.31	4.6
Cu	53.39 ± 47.57	41	38	109	41 ± 15.30	20
Ga	21.57 ± 6.36	23	20	20	21 ± 6.98	30
Ge	2.68 ± 0.68	2.6	4.4	3.8	2.47 ± 1.06	3.8
Hf	4.32 ± 2.57	4.5	2.9	2.4	2.63 ± 0.78	3.6
Nb	12.05 ± 4.68	12.3	10.4	8.3	9.67 ± 3.10	12.6
Ni	55.71 ± 21.65	61.5	75	89	44 ± 27.09	48
Pb	20.33 ± 15.67	15	7		24 ± 2	22
Rb	126.33 ± 44.82	142	85	116	128.33 ± 53.61	188
S*	0.06 ± 0.14	0.006	0.07	0.006	0.02 ± 0.01	0.008
Sr	83.31 ± 35.14	88	62	46	103.67 ± 33.51	78
Ta	1 ± 0.36	1.01	0.86	0.76	0.69 ± 0.13	0.87
Th	10.85 ± 3.45	11.8	8.84	9.01	8.56 ± 3.12	12.4
U	2.53 ± 0.70	2.67	3.53	1.74	2.36 ± 0.13	2.36
V	122.87 ± 39.75	136	81	142	112.67 ± 23.16	127
Y	25.21 ± 7.33	26	22	21	19.33 ± 5.31	26
Zr	167.13 ± 96.26	160	99	85	103.33 ± 25.96	137
La	38.21 ± 11.35	40.9	30.1	35.3	49.37 ± 17.33	42.4
Ce	74.78 ± 23.96	77.33	55.6	77.3	65.37 ± 10.33	78.1
Pr	8.67 ± 2.51	9.16	7.33	7.75	9.61 ± 1.62	9.8
Nd	32.6 ± 9.62	33.8	28.6	28.4	31.83 ± 3.81	36.3
Sm	6.41 ± 1.88	6.84	5.78	5.46	5.80 ± 1.61	7.9
Eu	1.26 ± 0.37	1.33	1.08	1.34	1.09 ± 0.20	1.36
Gd	5.18 ± 1.52	5.37	4.88	3.98	4.21 ± 1.08	5.59
Tb	0.83 ± 0.24	0.88	0.84	0.65	0.65 ± 0.19	0.89
Dy	4.88 ± 1.43	5.04	4.85	4.1	3.78 ± 1.13	5.09
Ho	0.96 ± 0.27	0.97	0.89	0.79	0.74 ± 0.22	1.01
Er	2.77 ± 0.77	2.83	2.51	2.3	2.11 ± 0.54	2.77
Tl	0.49 ± 0.19	0.51	0.28	0.51	0.50 ± 0.17	0.7
Tm	0.41 ± 0.12	0.43	0.364	0.341	0.31 ± 0.09	0.418
Yb	2.77 ± 0.77	2.87	2.4	2.34	2.17 ± 0.58	2.9
Lu	0.43 ± 0.12	0.45	0.389	0.368	0.34 ± 0.08	0.441
As	21.68 ± 12.72	21	40	12	6.33 ± 4.19	2
Co	16.31 ± 7.76	17.75	22.3	22.2	17 ± 3.70	13.3
Cr	83.83 ± 29.28	89.5	60.6	58.6	76.60 ± 24.17	106
Sb	1.45 ± 1.87	0.8	2.5	0.7	1.20 ± 0.73	0.5
Sc	15.20 ± 4.94	16.5	14.1	13.2	14.16 ± 4.25	19.4
Zn	78.79 ± 34.12	90	139	90	56 ± 34.03	83

the form of thin (commonly rhythmic) meta-siltstone or (impure) quartzite layers; the tuffaceous metapelite sample displaying $SiO_2/Al_2O_3 > 10$ and $(CaO + Na_2O + K_2O)/Al_2O_3 < 0.25$ incorporates abundant volcanic-derived quartz fragments without signs of feldspar. The two samples with highest TiO_2/Al_2O_3 ratios contain high amounts of Ti-rich phases, such as rutile or titanite.

5.1.2. Minor and trace elements

The strong positive correlation coefficients ($r \geq 0.75$; see Appendix 5) between Al_2O_3 and some minor/trace elements (*e.g.* Ga, Nb, Rb, Cr and Sc) indicate that these elements are preferentially incorporated in phyllosilicates, irrespectively of the rock type and the lithostratigraphic unit; see also the supplementary plots in Appendix 5, using K_2O instead of Al_2O_3. For both PQG and VSC units, TiO_2 abundances show strong positive correlations ($r > 0.75$; see Appendix 5) with: Sc, Cr, HREE, Ta, Nb and Eu in the metapelite subgroup, and V, Ga and Ge in the tuffaceous metapelite subgroup.

As mentioned above, Zr, Th, Sc, Ti tend to behave as geochemically immobile elements (during weathering, transport and diagenetic-metamorphic processes). Thus, elemental ratios, such as Zr/Sc, Th/Sc, and Eu/Eu*, can be used to discriminate between dominant "felsic" or "mafic" sources in provenance studies (*e.g.* Middelburg et al., 1988; McLennan et al., 1993; Jorge et al., 2006). Most of the metapelites and tuffaceous metapelites from both lithostratigraphic units plot in the "felsic source" field (Fig. 9B), exception for few VSC samples from the Roxo area, near a predominantly rhyodacitic metavolcanic sequence that also includes intermediate-mafic volcaniclastic rocks (*e.g.* Codeço et al., 2018) which may have been sourced, resulting in the mafic source discrimination. Fig. 9A and B also indicates that an evolved "felsic source" (implying sediment recycling) should be the ultimate

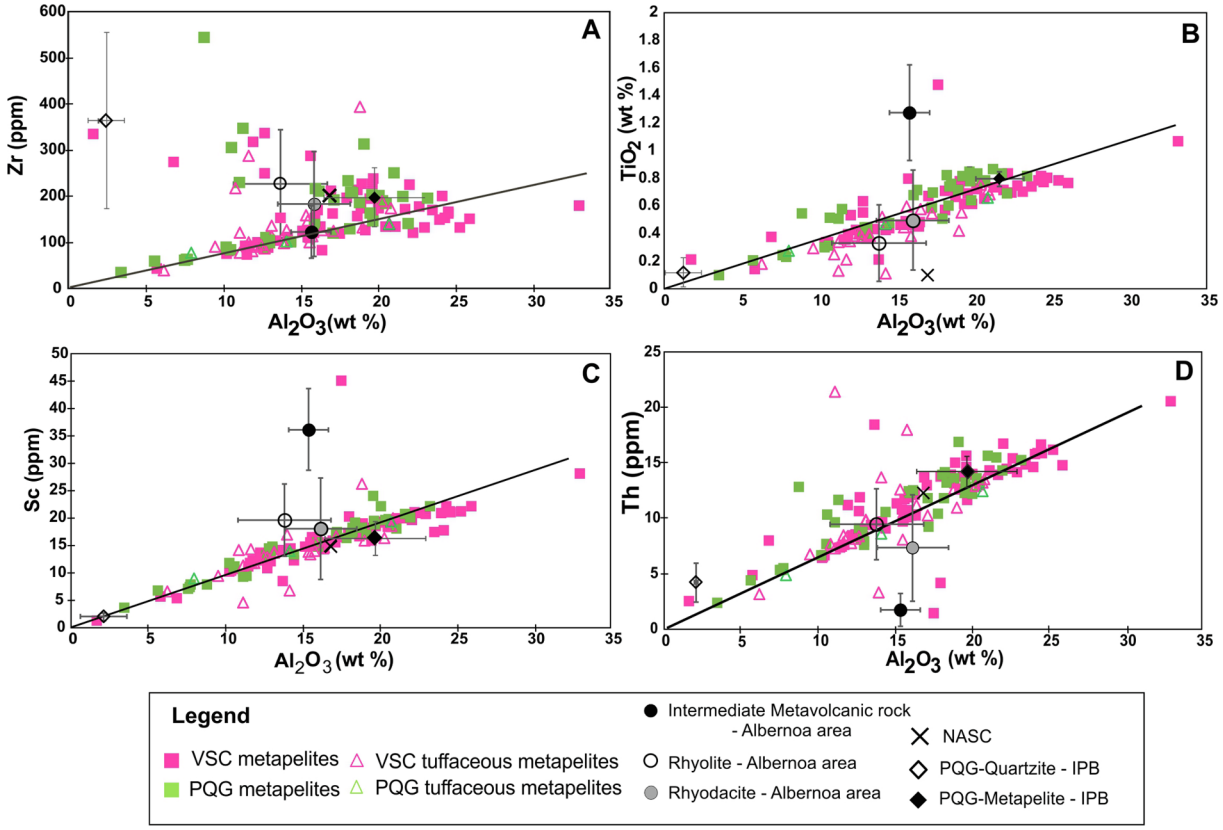

Fig. 6. [A to D]: Co-variations between: (A) Zr (ppm) vs. Al_2O_3 (wt %); (B) TiO_2 (wt %) vs. Al_2O_3 (wt %); (C) Th (ppm) vs. Al_2O_3 (wt %); and (D) Sc (ppm) vs. Al_2O_3 (wt %). For reference, and besides NASC contents (Condie, 1993), the average and standard deviation concentration measures calculated for PQG-quartzite and metapelite (n = 75; different sites of IPB; Jorge, 2009) and VSC-metavolcanic rocks of Albernoa (intermediate composition, n = 9, rhyodacite, n = 27, rhyolite, n = 22; Codeço et al. 2018) are displayed.

source of the prevalent siliciclastic component in the sedimentary rocks, irrespectively of their lithostratigraphic unit. Such an interpretation is fully consistent with the conclusions of other workers in the IPB (*e.g.* Jorge, 2009; Jorge et al., 2006; Tornos et al., 2008; Rodrigues et al., 2014). However, the involvement of unevolved "felsic sources" cannot be discarded for some metapelites or tuffaceous metapelites samples, as discussed below.

North American Shale Composition (NASC, Condie, 1993; Taylor & McLennan, 1995) normalized spider diagrams for minor and trace elements in metapelites and tuffaceous metapelites from both VSC and PQG units are shown in Fig. 10 – (a) for metapelites sensu lato and ***(b)*** for tuffaceus metapelites. The normalized patterns are quite similar, typified by systematic positive anomalies in As and Sb, which can reach 100 × NASC. Other elements show values below (mostly −10 × NASC) or ≈ 1, except in samples that contain appreciable volcanic-derived clastic detritus and/or record mineral/ geochemical changes due to hydrothermal alteration processes. Indeed, samples displaying visible enrichments in chlorite (± carbonate and disseminated sulfides) display always positive anomalies in Cu (up to 10–15 × NASC) that in some samples also show concomitant enrichments in Pb, Zn and Co (typically, 5–10 × NASC).

Drill-core samples from the SE extension of Feitais structure (near the Aljustrel mine) show consistently high (≈100 × NASC) positive Sb and As anomalies, together with concomitantly high Cu + Pb (± Zn ± Co). Samples from Ervidel-Roxo present anomalies similar to (albeit weaker) those typifying the SE extension of Feitais structure. Samples from the Figueirinha-Albernoa sector display a wide range of elemental abundances, and variable positive Cu, As, Sb, Co and Pb anomalies are the result of early local changes (achieved during diagenesis or seafloor regional metasomatism) and/or of late-Variscan hydrothermal alteration along reactivated strike-slip fault zones. PQG metapelites exhibit a consistent Cu positive anomaly in samples from Píncaros and Entradas, in agreement with the presence of quartz ± chlorite ± pyrite ± chalcopyrite filling late fractures. Tuffaceous metapelites from VSC in the SE extension of Feitais structure show minor negative Sc, V, Cr, Co, Sr, Nb and Hf anomalies and prevalent As, Sb, Cu ± Pb positive anomalies.

5.1.3. *Rare earth elements*

The (C1; Taylor and McLennan, 1995) chondrite-normalized REE patterns show the similarities in REE compositions for PQG and VSC, as this has been noted by previous workers (*e.g.* Jorge, 2009; Jorge et al., 2006). The patterns are characterized by strong light rare earth elements (LREE) enrichments (negative slope), negative Eu anomalies and relatively flat heavy rare earth element (HREE) abundances (Fig. 11). Subtle differences from these trends reflect minor differences in the abundance(s) of primary or secondary mineral phases that incorporate these elements.

5.2. *Isotope compositions*

5.2.1. *Sr and Nd*

The whole-rock Sr and Nd isotopic data obtained for selected samples of VSC metapelites and tuffaceous metapelites are shown in Tables 2 and 3. In metapelites, Rb and Sr abundances range from 4 to 278 ppm and from 18 to 207 ppm, respectively. In tuffaceous metapelites the Rb and Sr compositions range between 38 and 197 ppm and 14–95 ppm, respectively. The initial Sr-isotopic composition of metapelites, calculated for 360 Ma, is highly heterogeneous, ranging from 0.70702 to 0.71967 (Fig. 12A). The tuffaceous metapelites display lower

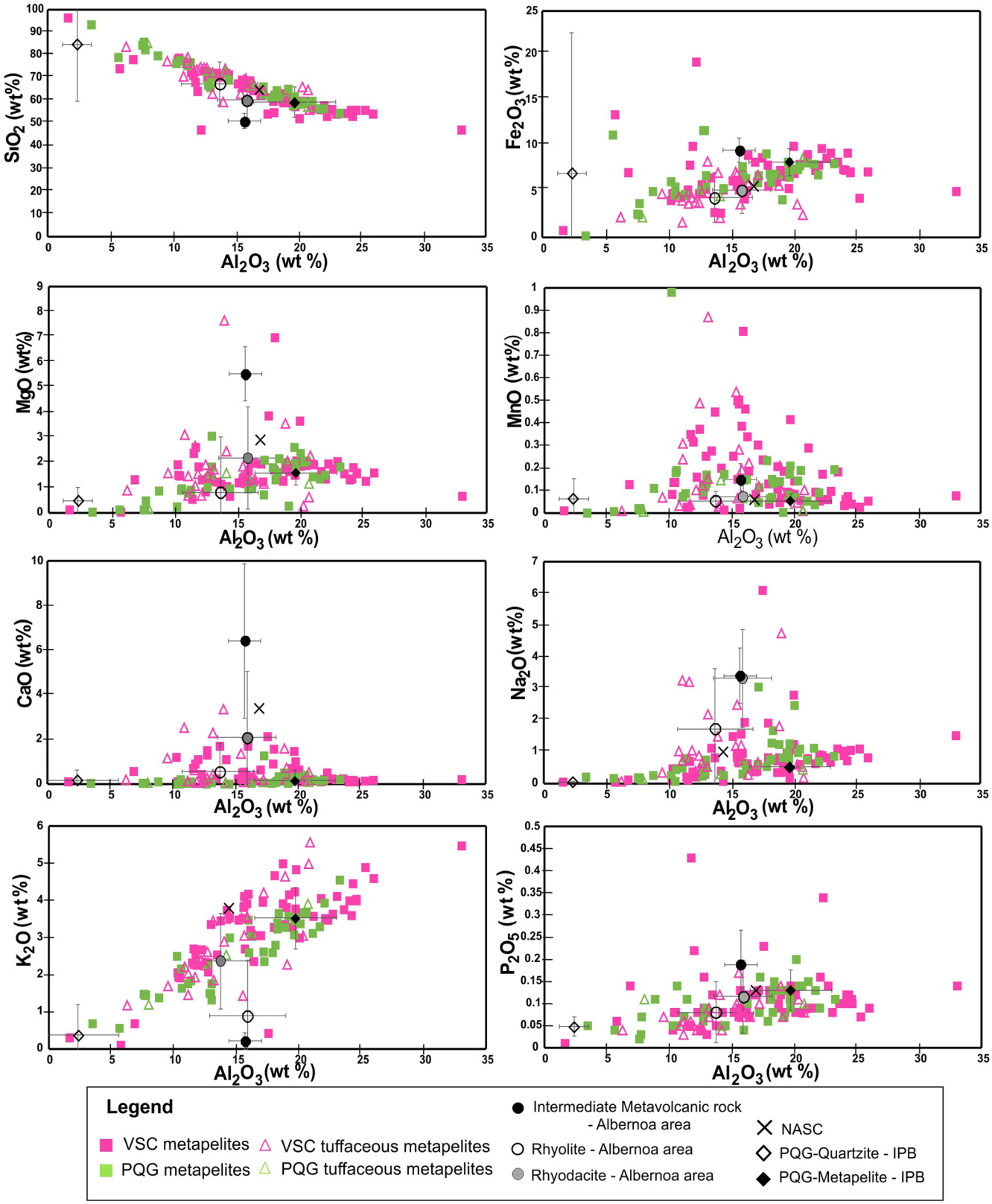

Fig. 7. Co-variations between Al_2O_3 and other major elements (SiO_2, Fe_2O_3, MgO, MnO, CaO, Na_2O, K_2O and P_2O_5) for all the Albernoa dataset. For reference, and besides NASC contents (Condie, 1993), the average and standard deviation concentration measures calculated for PQG-quartzite and metapelite (n = 75; different sites of IPB; Jorge, 2009) and VSC-metavolcanic rocks of Albernoa (intermediate composition, n = 9, rhyodacite, n = 27, rhyolite, n = 22; Codeço et al. 2018) are displayed.

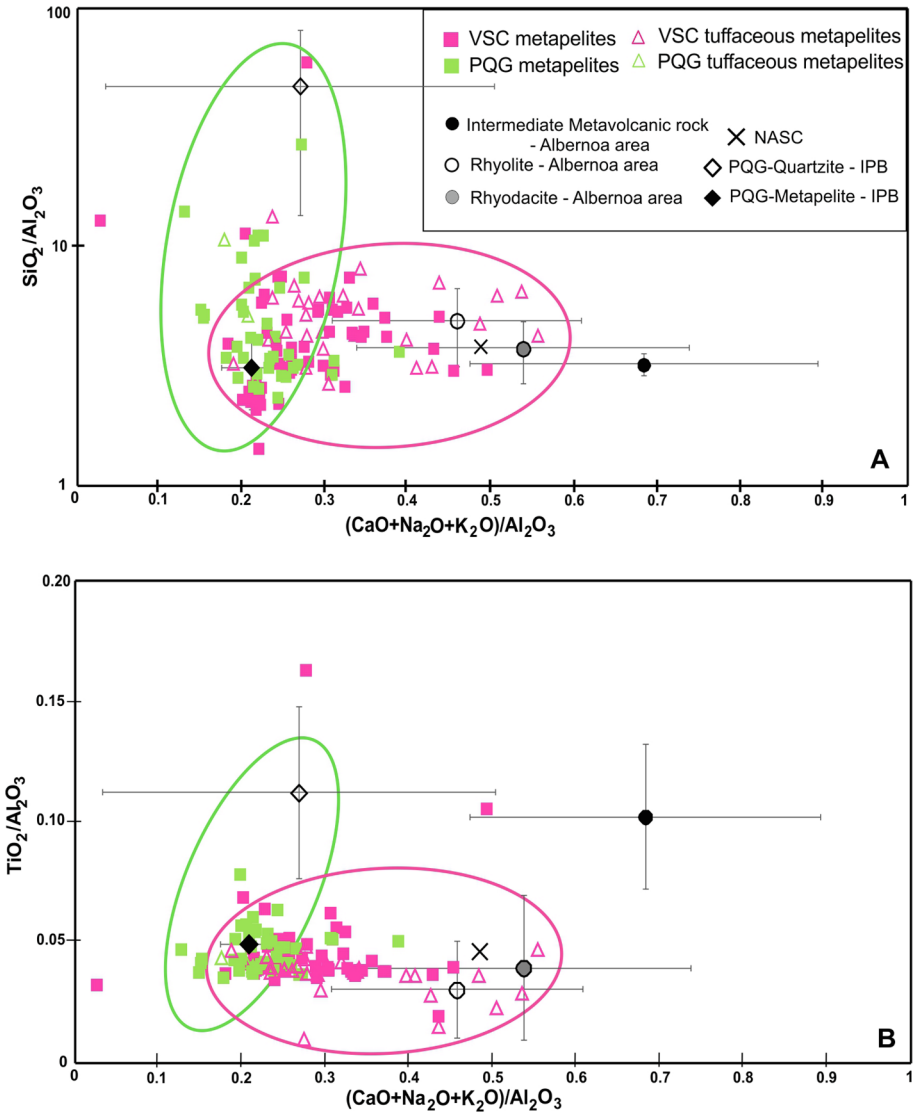

Fig. 8. Geochemical separation of the Albernoa dataset representing the two main lithostratigraphic units on the basis of the $(CaO + Na_2O + K_2O)/Al_2O_3$, SiO_2/Al_2O_3 and TiO_2/Al_2O_3 ratios (A and B). For reference, and besides the ratios typifying NASC (Condie, 1993), the average ratios and corresponding standard deviation measures calculated for PQG-quartzite and metapelite (n = 75; different sites of IPB; Jorge, 2009) and VSC-metavolcanic rocks of Albernoa (intermediate composition, n = 9, rhyodacite, n = 27, rhyolite, n = 22; Codeço et al. 2018) are displayed.

variability of the initial Sr-isotopic composition (0.70532 − 0.70938; Fig. 12A), except for sample EDS1-T that has a geologically unreasonably value of 0.67112 (which has been omitted on the plot of Fig. 12A). Such a low calculated value suggests an over-correction of in-situ generated ^{87}Sr (via radioactive decay of ^{87}Rb), indicating that the Rb/Sr ratio of this sample was increased either by Rb-addition or Sr-loss; for this reason, we did not consider further the isotopic data for EDS1-T.

The Sm-Nd isotopic data are relatively similar for metapelites and tuffaceous metapelites. Samarium contents display an average value of 6.3 ± 1.9 ppm (range from 3.6 to 9.7 ppm) for the metapelites and of 6.0 ± 1.8 ppm (range from 3.3 to 7.0 ppm) for tuffaceous metapelites, Neodymium contents are 34.0 ± 11.2 ppm (range from 20.3 to 54.7 ppm) for the metapelites and 30.7 ± 9.6 ppm (range from 16.8 to 38.6 ppm) for tuffaceous metapelites. The $^{147}Sm/^{144}Nd$ ratios range from 0.1066 to 0.1296 (0.1142 ± 0.0066), which are typical values for clastic sediments and similar to upper continental crust (~0.12; Goldstein et al. 1984; Zhao et al., 1992). Initial εNd values range between −6.3 and −10.6 ($\varepsilon Nd_{(360Ma)}$ = −8.2 ± 1.4; Fig. 12A) and depleted mantle model ages vary from 1.38 to 1.68 Ga (T_{DM} = 1.56 ± 0.11 Ga).

The obtained Sr-Nd isotopic data are similar to those reported in other works for non-altered PQG phyllites (Jorge, 2009) and sulfide ore samples (Relvas et al., 2001), and deviate from the isotopic signature displayed by various types of metavolcanic rocks lacking evident effects of hydrothermal alteration/mineralization (Mitjavilla et al., 1997). However, metasedimentary rocks slightly increase their $\varepsilon Nd_{(360Ma)}$ values (for equivalent Sm/Nd ratios) when volcanic-derived products are incorporated and/or when secondary mineral assemblages (due to hydrothermal alteration/mineralization) are observed (Fig. 12B). The $^{87}Sr/^{86}Sr$ data reported in Tornos (2006) for 10 black metapelites from PQG and VSC, along with additional $^{87}Sr/^{86}Sr$ data in Jorge (2009), are not showed in plots of Fig. 12 because no information on Sm-Nd isotope abundances is provided for these samples. Nonetheless, the documented ranges do not deviate significantly from those here indicated, as illustrated by the Sr- $^{87}Sr/^{86}Sr_{(360Ma)}$ and $^{87}Sr/^{86}Sr_{(360Ma)}$ – $^{87}Rb/^{86}Sr$ plots in Appendix 6.

5.2.2. Pb isotope compositions

The whole-rock Pb isotopic data for selected samples of VSC

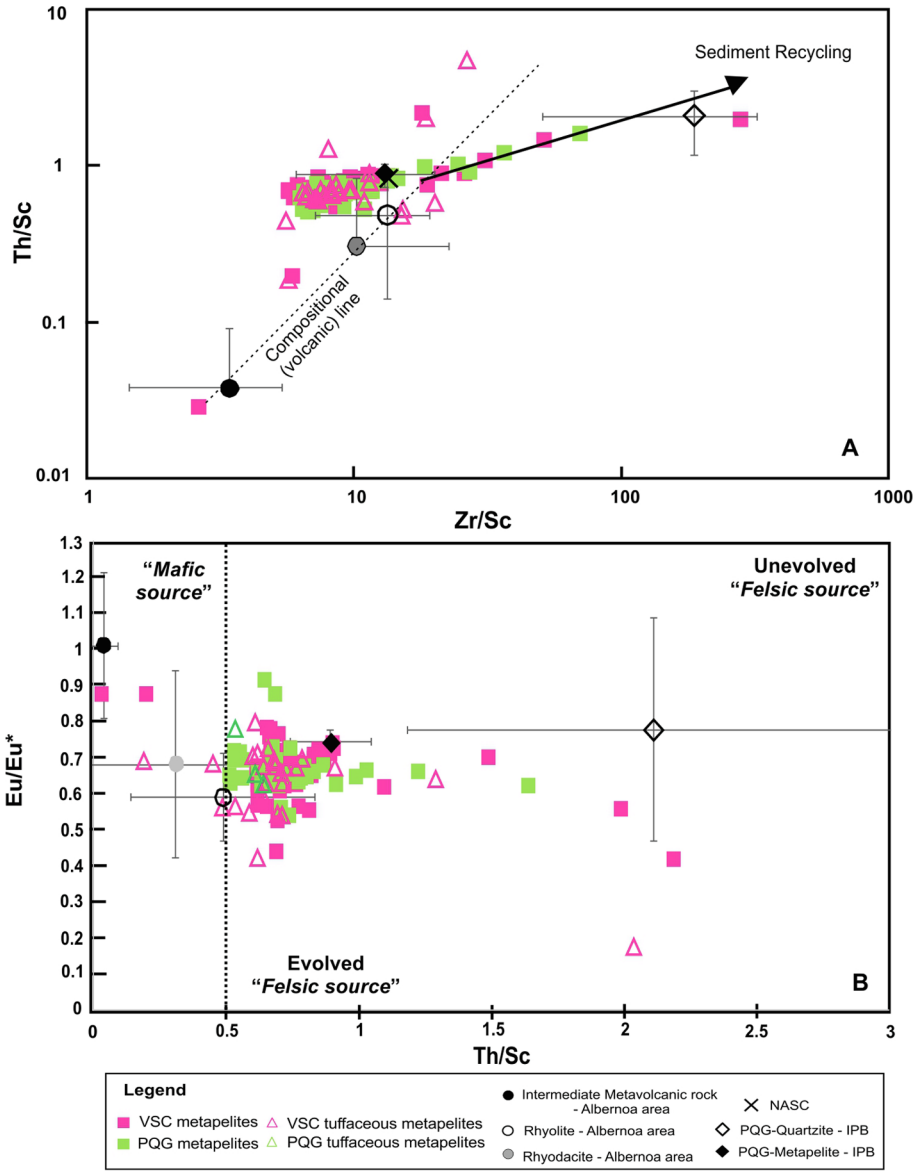

Fig. 9. Plotting of the Albernoa dataset on provenance/recycling diagrams Zr/Sc vs. Th/Sc (A) and Eu/Eu* vs. Th/Sc (B); modified after Slack et al. 2004. For reference, and besides the ratios typifying NASC (Condie, 1993), the average ratios and corresponding standard deviation measures calculated for PQG-quartzite and metapelite (n = 75; different sites of IPB; Jorge, 2009) and VSC-metavolcanic rocks of Albernoa (intermediate composition, n = 9, rhyodacite, n = 27, rhyolite, n = 22; Codeço et al. 2018) are displayed.

metapelites and tuffaceous metapelites are shown in Table 4. Abundances of Pb in metapelites range between 6 and 84 ppm; the tuffaceous metapelites have Pb contents that range between 12 and 133 ppm. Uranium abundances are also variable, ranging from 2.11 to 11.90 ppm in metapelites and from 0.57 to 2.91 ppm in tuffaceous metapelites. The correspondent U/Th ratios vary between 0.17 and 1.41 in metapelites, and tuffaceous metapelites display a more restricted, less variable range (0.17–0.23). However, four samples that have been hydrothermally altered and which contain sulfides (including those collected nearby the Aljustrel sulfide-ore system) are characterized by the higher U/Th ratios (up to 1.41).

Excluding two samples (37-1-B and X64), that have possibly been affected by ^{204}Pb-loss, the whole-rock Pb isotope values are fairly homogeneous, with a range of $^{206}Pb/^{204}Pb_{(360\ Ma)}$ values from 17.638 to 18.294, $^{207}Pb/^{204}Pb_{(360\ Ma)}$ values from 15.603 to 15.665 and $^{208}Pb/^{204}Pb_{(360\ Ma)}$ values from 37.274 to 39.120 (Fig. 13A and B). The age corrected Pb isotopic ratios for the tuffaceous metapelites are more homogeneous and less radiogenic than those of metapelites: $^{206}Pb/^{204}Pb_{(360\ Ma)}$ = 17.638 − 18.175 (17.963 ± 0.176), $^{207}Pb/^{204}Pb_{(360\ Ma)}$ = 15.605 − 15.647 (15.617 ± 0.014) and $^{208}Pb/^{204}Pb_{(360\ Ma)}$ = 37.274 − 38.387 (37.941 ± 0.389). The Pb reservoir(s) that contributed Pb to the samples analyzed are crustal (see $^{207}Pb/^{204}Pb$ versus $^{206}Pb/^{204}Pb$ and the $^{208}Pb/^{204}Pb$ - $^{206}Pb/^{204}Pb$ diagrams of Zartman and Doe (1981) in Appendix 6).

Our Pb isotope data, although limited, are consistent with the available information for the IPB (Pomiès et al., 1998; Marcoux, 1998; Leistel et al., 1998; Relvas et al. 2001, Jorge et al. 2007; Jorge, 2009). VSC metapelites that display effects of regional alteration overlap partly the (age-corrected) Pb-Pb fields documented for PQG, shifting towards higher $^{207}Pb/^{204}Pb$ and $^{206}Pb/^{204}Pb$ ratios when evidently affected by early hydrothermal alteration and mineralization processes (Fig. 13B). The Pb-Pb ranges for altered/mineralized samples plot within or nearby the fields characterizing the common massive sulfide ores of IPB, which are far more homogenous than those reported for the Neves Corvo deposit (Fig. 13A and B; see labels and data sources in caption).

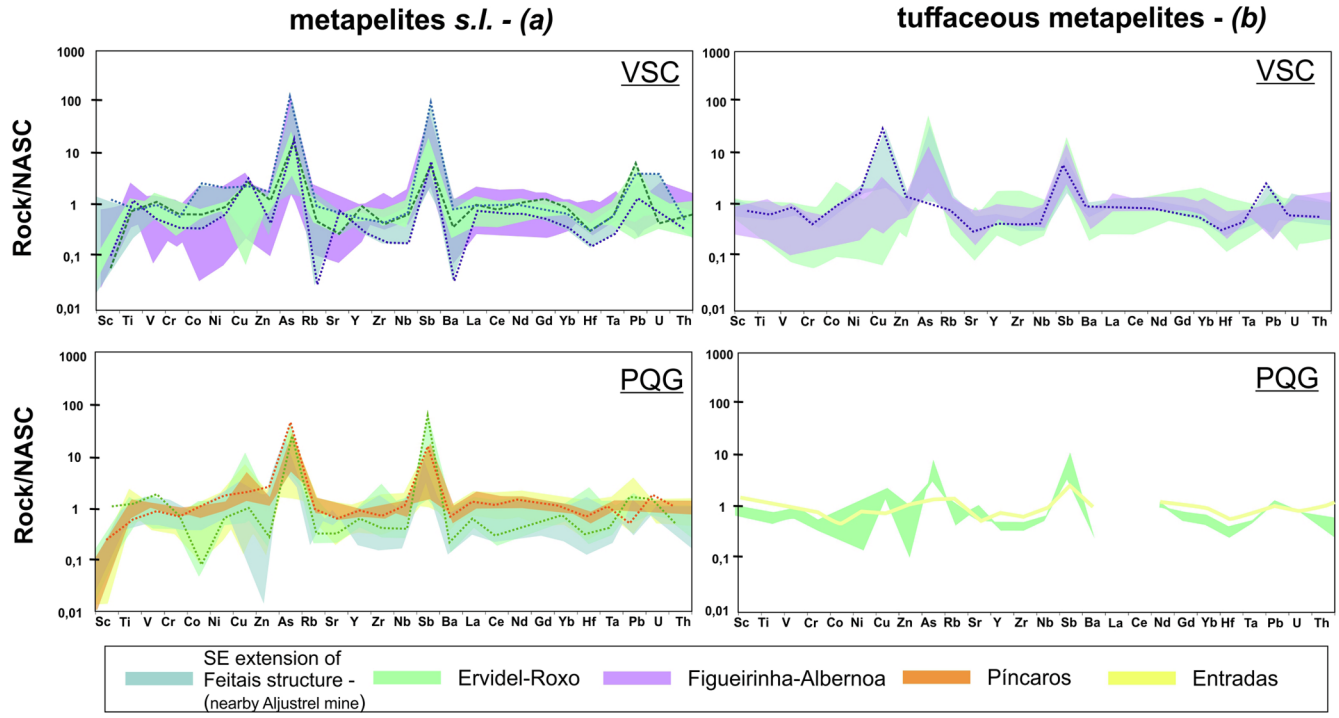

Fig. 10. NASC-normalized multi-element concentration patterns for metapelites s.L. and tuffaceous metapelites from VSC and PQG. Patterns are grouped by sampling sectors (all indicated in the map of Fig. 2) and the dotted lines represent samples with relevance for the Discussion section.

6. Discussion

6.1. Sediment provenance

Bulk geochemical data can be used to constrain the source-area composition and weathering conditions (*e.g.* Young & Nesbitt, 1998; Goodfellow et al. 2003; Jorge et al. 2006). Provenance studies should employ ratio-ratio plots utilizing immobile elements such as Zr, Th, Ti and Sc (as shown in Section 5.1), which are also predominantly incorporated in the suspended detrital fraction of seawater (Holland, 1972). Clustering and/or trending of samples on such discriminant plots can indicate source(s) that contributed to the metasedimentary rocks. VSC and PQG metasedimentary rocks are chemically alike; indeed, they all derive from the same continental source, although they

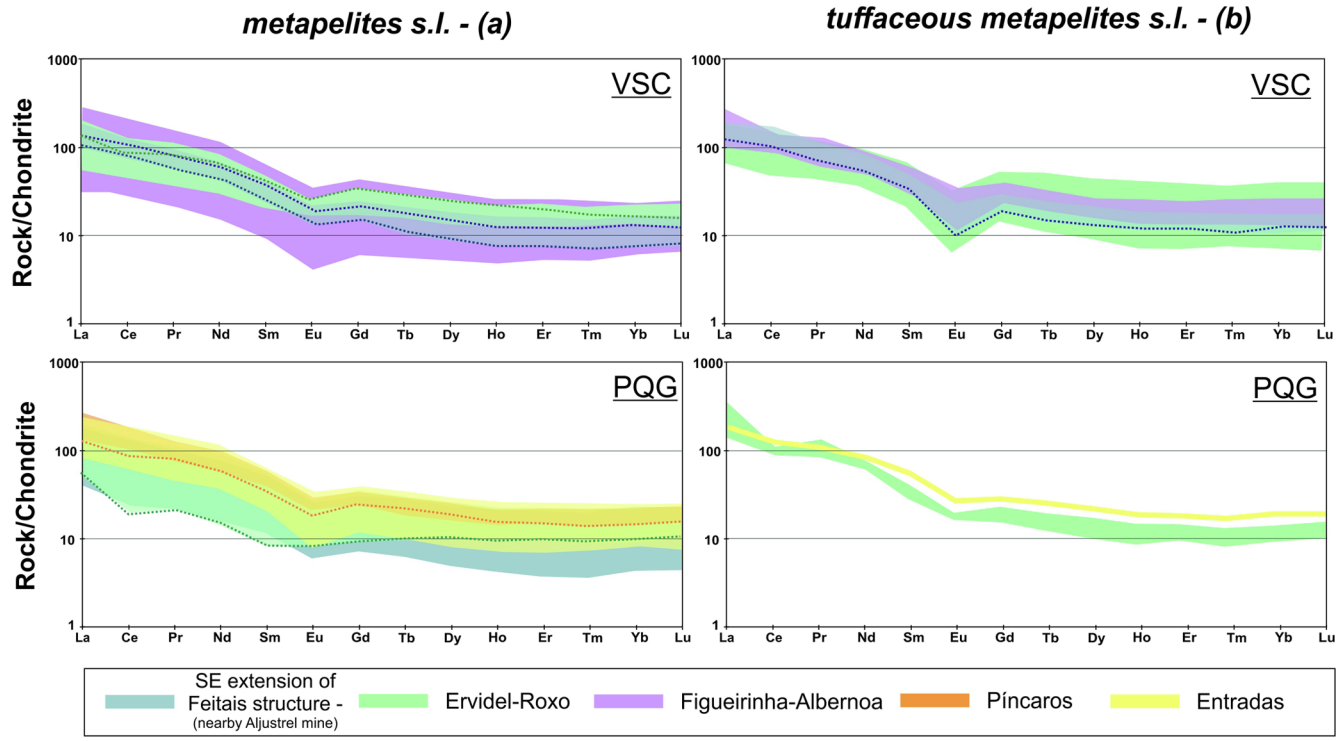

Fig. 11. Chondrite-normalized REE concentration patterns for metapelites and tuffaceous metapelites from VSC and PQG. Patterns are grouped by sampling sectors (all indicated in the map of Fig. 2) and the dotted lines represent samples with relevance for the Discussion section.

Table 2
Sm-Nd whole-rock and isotopic compositions for a selected VSC group samples (metapelites, n = 8; tuffaceous metapelites, n = 4). $\varepsilon Nd_{(0)}$ calculated relative to chondritic uniform reservoir (CHUR) with present-day composition of $^{143}Nd/^{144}Nd = 0.512638$ and $^{147}Sm/^{144}Nd = 0.1967$ (Jacobsen and Wasserburg, 1980). $\varepsilon Nd_{(i)}$ calculated for 360 Ma. Neodymium model ages (T_{DM}) calculated according to the depleted mantle model of DePaolo (1981). $f_{Sm/Nd} = (^{147}Sm/^{144}Nd)_{sample}/(^{147}Sm/^{144}Nd)_{CHUR} - 1$.

	Ref.	Sm (ppm)	Nd (ppm)	$^{147}Sm/^{144}Nd$	$^{143}Nd/^{144}Nd$	Error (± 2σ)	εNd(0)	εNd(i)	T_{DM} (Ga)	$f_{Sm/Nd}$
Metapelites	11-1-MM	6.80	35.5	0.1158	0.511966800	0.000003	−13.1	−9.4	1.67	−0.40
	37-1-B	9.73	54.7	0.1076	0.511884290	0.000003	−14.7	−10.6	1.66	−0.45
	X93	7.33	40.2	0.1103	0.511937800	0.000005	−13.7	−9.7	1.63	−0.44
	X64	7.40	41	0.1091	0.511944000	0.000004	−13.5	−9.5	1.60	−0.45
	18-1-FF	5.14	28.1	0.1106	0.512084940	0.000004	−10.8	−6.8	1.41	−0.44
	18-1-E	4.60	23.6	0.1179	0.512085470	0.000003	−10.8	−7.2	1.52	−0.40
	EDS1-B	5.63	28.2	0.1207	0.512022584	0.000005	−12.0	−8.5	1.67	−0.39
	X23	3.58	20.3	0.1066	0.512075376	0.000004	−11.0	−6.8	1.38	−0.46
Tuffaceous metapelites	RT49	3.34	16.8	0.1202	0.512134252	0.000004	−9.8	−6.3	1.48	−0.39
	CW2-CC	6.95	38.6	0.1089	0.512014317	0.000004	−12.2	−8.1	1.49	−0.45
	CW2-LL	7.01	32.7	0.1296	0.512117160	0.000003	−10.2	−7.1	1.68	−0.34
	EDS1-T	6.50	34.7	0.1133	0.512016065	0.000006	−12.1	−8.3	1.56	−0.42

are comprised of differing mixtures of two main components (Fig. 14). According to the available data, these components are characterized by: (i) a clayey-derived contribution with high (20–30) Al_2O_3/TiO_2 ratios, $Sc/TiO_2 > 0.002$, $Ga/TiO_2 > 0.001$ and $Zr/Al_2O_3 \approx 0.001$; and (ii) a (fine-grained) sandy-derived component indicated by lower (≈ 5–20) Al_2O_3/TiO_2 ratios that co-vary inversely with Zr/Al_2O_3 (≈ 0.001–0.002) and Zr/TiO_2 (0.01–0.1), also displaying $Sc/TiO_2 < 0.002$ and $Ga/TiO_2 < 0.001$. Markedly higher Al_2O_3/TiO_2 ratios (up to 45–65), together with higher Sc/TiO_2 and Ga/TiO_2 values, but variably lower Zr/Al_2O_3 ratios, indicate the contribution of a third, mostly volcanic-derived source. Overprints of hydrothermal processes are indicated by modifications of $Al_2O_3/(Al_2O_3 + Fe_2O_3 + MnO)$ and Fe_2O_3/TiO_2 (see below).

Samples with a prevalent clayey-derived component are predominantly from VSC sections, irrespectively of the surveyed sector. In contrast, the sandy-derived component is common in a vast number of samples representing different VSC settings and various PQG lithostratigraphic levels. The third component is distinctly higher for some tuffaceous metapelites from Ervidel-Roxo and Figueirinha-Albernoa sectors where the volcanic contribution is significant and tends to deviate towards the average compositions of metavolcanic rocks recognized in the Albernoa area. Two samples from the Figueirinha-Albernoa sector, collected from different drill-holes, are the main deviations to the general compositional trend obtained for VSC sections. One of these samples overlaps the average Al_2O_3/TiO_2 and Zr/Al_2O_3 ratios representing the intermediate metavolcanic rocks of Albernoa, and its mineral assemblage is clearly influenced by accessory amounts of Ti-bearing phases of (local?) volcanogenic origin. The second sample, typifying a rather pure meta-siltstone (devoid of significant amounts of interstitial phyllosilicates), presents the highest Zr/Al_2O_3 ratio and the lowest Al_2O_3/TiO_2 ratio, and is chemically analogous to a quartzite.

Sm-Nd isotope compositions plotted against trace elemental ratios can be used in provenance analysis (*e.g.* Linn et al., 1991; Turner et al., 1993; Cingolani et al., 2003, Jorge, 2009). In this regard, the $\varepsilon Nd_{(360Ma)}$ values and Th/Sc ratios obtained for a selected group of VSC samples fall in a relatively narrow cluster (Fig. 15), indicating a common siliciclastic, "felsic-dominated", upper-crust continental source, which is consistent with the Al_2O_3/TiO_2 and, Zr/Al_2O_3 ratios presented above, and other multi-element geochemical fingerprints.

Several studies used chemical ratios to determine the degree of weathering to which the source-areas of sediments were subjected. The chemical index of alteration (CIA; Nesbit & Young, 1982) is defined by the proportion of original minerals and secondary/alteration products, using major oxide-elemental ratios (alumina and alkaline oxides). The values range from 50 in fresh rocks to 100 in completely weathered rocks. Numerous estimates of the CIA for IPB metasedimentary rocks are reported in Jorge et al. (2006), who suggested that values below 70 indicate minimal weathering in source-areas, whereas values above 80 represent moderate to intense weathering or hydrothermal alteration. To a large extent, the Albernoa dataset yields CIA values above 65 (Fig. 16A), roughly distinguishing PQG from VSC metasedimentary rocks, as well as those that have a significant volcanic contribution (metapelites versus tuffaceous metapelites). The following broad conclusions may be drawn: (i) the terrigenous (clayey- or sandy-derived) source-areas of the analyzed PQG and VSC metasedimentary rocks are chemically similar; (ii) the source-areas were most likely the same or, if not, other suppliers to these metasedimentary rocks cannot be distinguished at light of the analytical data currently available; (iii) these

Table 3
Rb-Sr whole-rock and isotopic compositions for a selected VSC group samples (metapelites, n = 8; tuffaceous metapelites, n = 4). $^{87}Sr/^{86}Sr(i)$ calculated for 360 Ma. εSr(0) calculated relative to chondritic uniform reservoir (CHUR) with present-day composition of $^{87}Sr/^{86}Sr = 0.7042$ and $^{87}Rb/^{86}Sr = 0.0827$ (Faure and Mensing, 2005).

	Ref.	Rb (ppm)	Sr (ppm)	$^{87}Rb/^{86}Sr$	$^{87}Sr/^{86}Sr$	Error (± 2σ)	$^{87}Sr/^{86}Sr(i)$	εSr(0)	εSr(i)
Metapelites	11–1-MM	138	90	4.450	0.73500	0.00003	0.71219	433	115
	37–1-B	278	207	3.897	0.73442	0.00002	0.71445	425	147
	X93	216	98	6.402	0.74485	0.00002	0.71204	573	113
	X64	195	53	10.705	0.76188	0.00006	0.70702	815	42
	18–1-FF	101	18	16.393	0.80368	0.00014	0.71967	1408	221
	18–1-E	114	94	3.517	0.72805	0.00004	0.71002	334	84
	EDS1-B	119	107	3.224	0.72422	0.00002	0.70770	280	51
	X23	4	121	0.096	0.70960	0.00004	0.70911	72	71
Tuffaceous metapelites	RT49	38	14	7.885	0.74573	0.00004	0.70532	585	18
	CW2-CC	107	95	3.266	0.72612	0.00004	0.70938	307	75
	CW2-LL	64	42	4.420	0.73066	0.00004	0.70801	371	56
	EDS1-T	197	41	13.954	0.74264	0.00007	0.67112	541	−468

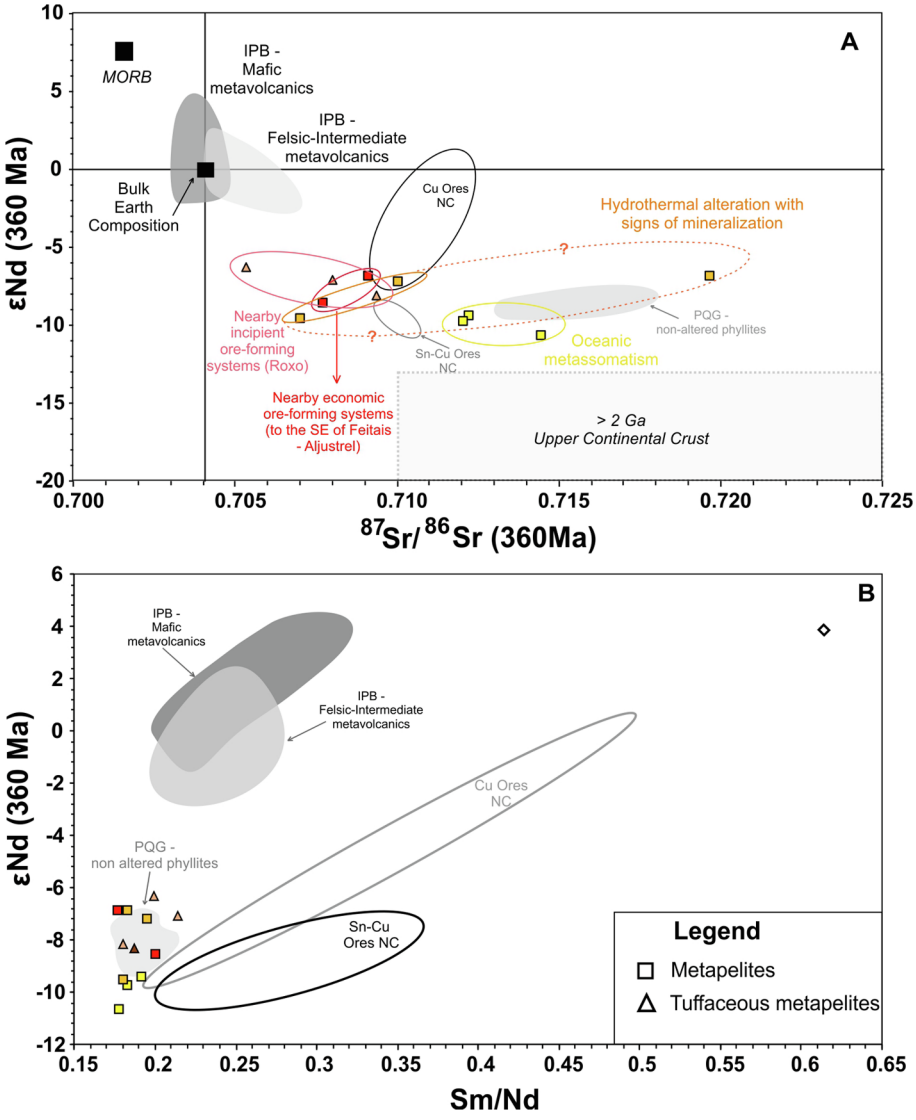

Fig. 12. $^{87}Sr/^{86}Sr_{(360\ Ma)}$ vs. $\varepsilon Nd_{(360\ Ma)}$ [A] and Sm/Nd vs. vs. $\varepsilon Nd_{(360\ Ma)}$ [B] for a selected group of VSC samples including metapelites (n = 8) and tuffaceous metapelites (n = 3). In both diagrams, the fields of "metavolcanic rocks" (mafic n = 7 and felsic n = 5), "non-altered phyllites" (n = 7) and "Neves Corvo ores" (Sn-Cu ores n = 5 and Cu ores n = 4) were delimited according to data reported in *Mitjavilla et al. (1991)*, Jorge (2009) and Relvas et al. (2001), respectively. The contour of Sn-Cu ores from Neves Corvo did not consider the sample indicated by the diamond marker.

source-areas were significantly weathered while they supplied sediment to the basin at least from Middle Devonian to Visean time (i.e. from AD miospore Biozone to NM miospore Biozone; Pereira et al., 2007,2010); and (v) during deposition of these terrigenous clastic sediments, they were variably mixed with volcanic-derived material to produce tuffaceous metapelites that are typical of VSC sequences but also recognized in the upper sections of PQG.

Fig. 16B, a $(CaO + Na_2O)$-Al_2O_3-K_2O (mole proportion) ternary diagram, show that the Albernoa data (particularly a subgroup of 8 samples – 6 VSC tuffaceous metapelites and 2 metapelites, 1 from PQG and another from VSC) define a trend towards the $(CaO + Na_2O)$ apex. One interpretation is that this indicates the presence of variable amounts of Na-rich plagioclase (volcanic-derived or resulting from the progression of regional seafloor metasomatism) in the tuffaceous metapelites; however, as mentioned above, it may also reflect relative enrichments in Ca due to the presence of variable amounts of other mineral phases (*e.g.* carbonates and titanite), some of them introduced during hydrothermal alteration and/or sulfide mineralization processes.

6.2. Hydrothermal alteration and mineralization fingerprints

The relative proportions of terrigenous (siliciclastic) and/or hydrothermal components involved in the sediment composition can be estimated on the basis of the Fe, Ti, Al and Mn contents (e.g. Boström, 1973; Marchig et al., 1982; Peter & Goodfellow, 1996; Goodfellow et al. 2003). In the Fe_2O_3/TiO_2 vrs $Al_2O_3/(Al_2O_3 + Fe_2O_3 + MnO)$ diagram (Fig. 17) our data define a general mixing trend between a hydrothermal end-member and a plausible "terrigenous end-member" (*e.g.* Marchig et al., 1982; Goodfellow et al., 2003). Although most samples cluster near the terrigenous end-member, some PQG and VSC metapelites plot nearer (though still far from it) the hydrothermal end-member: (i) the SE extension of Feitais structure (near the Aljustrel mine); (ii) Ervidel-Roxo and Entradas sectors; and (iii) ALB drill-hole (Albernoa). These samples show the effects of early-developed hydrothermal alteration and the presence of sulfide mineralization, particularly in the former two sectors. Therefore, Fe_2O_3/TiO_2 ratios above 10 and $Al_2O_3/(Al_2O_3 + Fe_2O_3 + MnO)$ ratios below ≈0.6 can be used to indicate the possible presence of a hydrothermal component over a detrital siliciclastic component that, for tuffaceous metapelites, also

Table 4
Lead whole-rock and isotopic compositions for a selected VSC group samples (metapelites, n = 8; tuffaceous metapelites, n = 4). All the Pb-Pb age corrected (360 Ma) isotopic ratios were estimated by considering the $^{238}U/^{204}Pb$, $^{235}U/^{204}Pb$ and $^{232}Th/^{204}Pb$ ratios determined on the basis of the measured Pb isotopic compositions (i.e. $^{206}Pb/^{204}Pb$, $^{207}Pb/^{204}Pb$ and $^{208}Pb/^{204}Pb$), and U, Th and Pb concentration values. Calculation of μ = $^{238}U/^{204}Pb$, ω = $^{232}Th/^{204}Pb$ and k = $^{232}Th/^{238}U$ values was performed using the age corrected $^{208}Pb/^{204}Pb$, $^{207}Pb/^{204}Pb$, $^{206}Pb/^{204}Pb$ ratios and the 3.7 Ga reference point of the Stacey and Kramers (1975) model.

	Ref	U ppm	Th ppm	Pb ppm	$^{206}Pb/^{204}Pb$	Error (± 2σ)	$^{207}Pb/^{204}Pb$	Error (± 2σ)	$^{208}Pb/^{204}Pb$	Error (± 2σ)	μ	ω	κ	$^{208}Pb/^{204}Pb(i)$	$^{207}Pb/^{204}Pb(i)$	$^{208}Pb/^{204}Pb(i)$
Metapelites	11–1-MM	3.16	13.7	6	19.636	0.006	15.720	0.005	40.074	0.011	9.98	37.19	3.73	17.64	15.61	37.27
	37–1-B	6.94	20.6	8	19.087	0.005	15.680	0.004	39.939	0.010	*10.94*	*55.30*	*5.05*	*15.83*	*15.51*	*36.81*
	X93	2.40	13.9	7	19.302	0.005	15.691	0.005	40.018	0.012	9.88	36.26	3.67	18.01	15.62	37.60
	X64	4.27	12.7	(*)	19.88	0.006	15.715	0.005	40.884	0.013	*10.22*	*50.31*	*4.92*	*16.60*	*15.54*	*37.73*
	18–1-FF	7.42	7.4	26	18.887	0.004	15.661	0.004	38.531	0.011	9.86	40.77	4.13	17.84	15.61	38.19
	18–1-E	1.73	7.3	12	18.584	0.004	15.638	0.004	38.680	0.010	9.81	37.72	3.84	18.06	15.61	37.96
	EDS1-B	11.90	8.4	84	18.694	0.006	15.675	0.005	38.506	0.013	9.95	39.93	4.01	18.18	15.65	37.39
	X23	2.11	4.8	30	18.319	0.005	15.623	0.004	38.419	0.010	9.81	39.16	3.99	18.06	15.61	38.23
Tuffaceous metapelites	RT49	0.57	3.0	12	18.405	0.005	15.635	0.004	38.503	0.009	9.84	38.03	3.87	18.23	15.63	37.39
	CW2-CC	2.91	13.9	99	18.325	0.005	15.661	0.004	38.461	0.011	9.97	39.25	3.93	18.22	15.66	38.30
	CW2-LL	1.25	7.5	133	18.252	0.007	15.658	0.008	38.384	0.027	9.98	39.39	3.95	18.23	15.66	38.19
	EDS1-T	2.67	11.6	58	18.464	0.008	15.674	0.008	39.359	0.024	10.00	43.38	4.34	18.29	15.67	39.12

(*) below the detection limit (i.e. < 5 ppm) of the analytical method used. Assuming a whole-rock concentration of Pb for sample X64 equal to 5 ppm, the calculated values are questionable, suggesting Pb loss. An overcorrection of radiogenic Pb, possibly due to Pb loss, occurred also in sample 37-1-B. These two samples were not used in plots of Fig. 13.

contains variably amounts of volcanic-derived products.

These guides may correlate with other geochemical indicators? The NASC-normalized spidergrams for the 133 metasedimentary rocks picked in the Albernoa area show that As and Sb are systematically enriched, followed by lesser enrichments of Cu, Zn and Pb in samples with disseminated sulfides (Luz et al., 2015, 2017). In addition, several studies have shown that variations in the relative abundances of some major element oxide (Fe_2O_3, MgO and MnO) can be used to separate hydrothermal alteration patterns related to the development of massive sulfide accumulations (e.g. Large et al. 2001; Relvas, 2001) or hydrothermal metalliferous sediments in modern analogues (*e.g.* Marchig et al., 1982). The whole-rock Cu, Zn and Pb whole-rock contents, together with Co, can also be used as proxies to define geochemical enrichment trends in areas hosting massive sulfide accumulations such as the IPB (*e.g.* Marcoux et al., 1996; Sánchez-España et al., 2000). Moreover, the relative increase in As (and Sb, Ni, etc.) is well known as a typical feature of sediments affected by exhalative-hydrothermal processes (e.g. Marchig et al., 1982; Varnavas and Cronan, 1988; Lottermoser, 1991; Gurvich, 2006; Hung et al., 2018).

These potential geochemical indicators, ratioed to geochemical immobile elements, can be used to generate three interdependent indexes that allow to discriminate between barren and altered/mineralized metasedimentary rocks in the IPB: (i) (As + Sb)/Sc, (ii) (Cu + Zn + Pb)/Sc, and (iii) $5 \times [(Fe_2O_3 + MgO + MnO)/Al_2O_3]$; the multiplier (5×) in the third index works just for scaling purposes. In plots using these indexes (Fig. 18A, B) for our data (Albernoa area), and grouping samples according to their petrographic features, values of (As + Sb)/Sc, (Cu + Zn + Pb)/Sc and $5 \times [(Fe_2O_3 + MgO + MnO)/Al_2O_3]$.: (i) between 1.0 and 10.0 may track the influence of seafloor metasomatism; and (ii) above 10.0, indicate close proximity of paleo-hydrothermal discharge that is potentially related to sulfide mineralization. This geochemical discrimination has recently been applied to VSC metapelites and tuffaceous metapelites from the Aljustrel area (Luz et al., 2018), and to PQG and VSC metapelites and tuffaceous metapelites from the Neves Corvo mine center (unpublished).

6.3. Isotopic signatures of VSC metasediments

As described above, our VSC Sr, Nd and Pb isotopic data agree with previous studies of the IPB (*e.g.* Pomiès et al., 1998; Marcoux, 1998; Leistel et al., 1998; Relvas et al. 2001, Jorge et al. 2007; Jorge, 2009; Tornos, 2006). However, the small number of analyses restrict us from over-generalizing. All the samples display radiogenic $^{87}Sr/^{86}Sr_{(360\ Ma)}$ and negative $\varepsilon Nd_{(360\ Ma)}$, indicating that these sedimentary rocks were derived from reservoirs characterized by high Rb/Sr and low Sm/Nd ratios; additionally, depleted mantle model ages, interpreted to reflect the mean crustal residence age of the sediment sources, are much older than the depositional age. Altogether, the Sr and Nd isotopic data suggest that the VSC metasedimentary rocks are mostly derived from an old, reworked, upper continental crust. The (co)variation of initial $^{87}Sr/^{86}Sr$ and $\varepsilon Nd_{(T)}$ may reflect either (i) a natural heterogeneity of the source terranes or (ii) mixing of predominant old continental crustal material and subordinate input of younger (volcanogenic?) material with lower $^{87}Sr/^{86}Sr$ and less negative εNd values. Notwithstanding this plausible interpretation, the specific petrographic characteristics of the samples allow additional inferences to be made (that should be the subject of future studies): (i) the four hydrothermally altered, and sulfide bearing samples (including those collected nearby the Aljustrel deposit) are confined to a narrow range of $^{87}Sr/^{86}Sr_{(360\ Ma)}$ and $\varepsilon Nd_{(360\ Ma)}$ values (≈0.705 − 0.709 and −9 to −6, respectively); (ii) hydrothermal altered metasedimentary rocks without significant sulfide mineralization show $-10 \leq \varepsilon Nd_{(360\ Ma)} \leq -7$ and $0.707 \leq {}^{87}Sr/^{86}Sr_{(360\ Ma)} \leq 0.720$; and (iii) metasedimentary rocks that do not display any evidence of hydrothermal alteration and mineralization have restricted ranges of $-12 < \varepsilon Nd_{(360\ Ma)} < -9$ and $0.712 < {}^{87}Sr/^{86}Sr_{(360\ Ma)} < 0.715$. Thus, a general decreasing trend of $^{87}Sr/^{86}Sr_{(360\ Ma)}$ values together with a slight increase in $\varepsilon Nd_{(360\ Ma)}$ in VSC metasediments result from a disturbance of the original (siliciclastic) isotopic signatures caused by: (i) the incorporation of volcanic-derived components in tuffaceous metapelites; and (ii) hydrothermal alteration and sulfide deposition progressed under systematically increased fluid/rock ratios.

These isotopic variations can be used to vector toward to massive sulfide mineralization. Our (age-corrected) lead isotope signatures ($\mu \approx 10$, $\approx 36 \leq \omega \leq 43$) for VSC sedimentary rocks also indicate derivation from upper crustal that has not been significantly contaminated by juvenile material. In addition, the spread of the (age-corrected) Pb isotopic ratios suggests that the lead isotopic signature of the VSC samples that have been affected by early hydrothermal alteration and mineralization processes show mixing of lead from distinct reservoirs, which results in shifts towards higher $^{207}Pb/^{204}Pb$ and $^{206}Pb/^{204}Pb$ ratios. As showed in Fig. 13A and B, the Pb-Pb fields for the IPB massive sulfide are broadly similar to the VSC metavolcanic rocks and PQG metasedimentary rocks. Furthermore, the $^{206}Pb/^{204}Pb$ range for the common IPB massive sulfide ores is narrower than that of

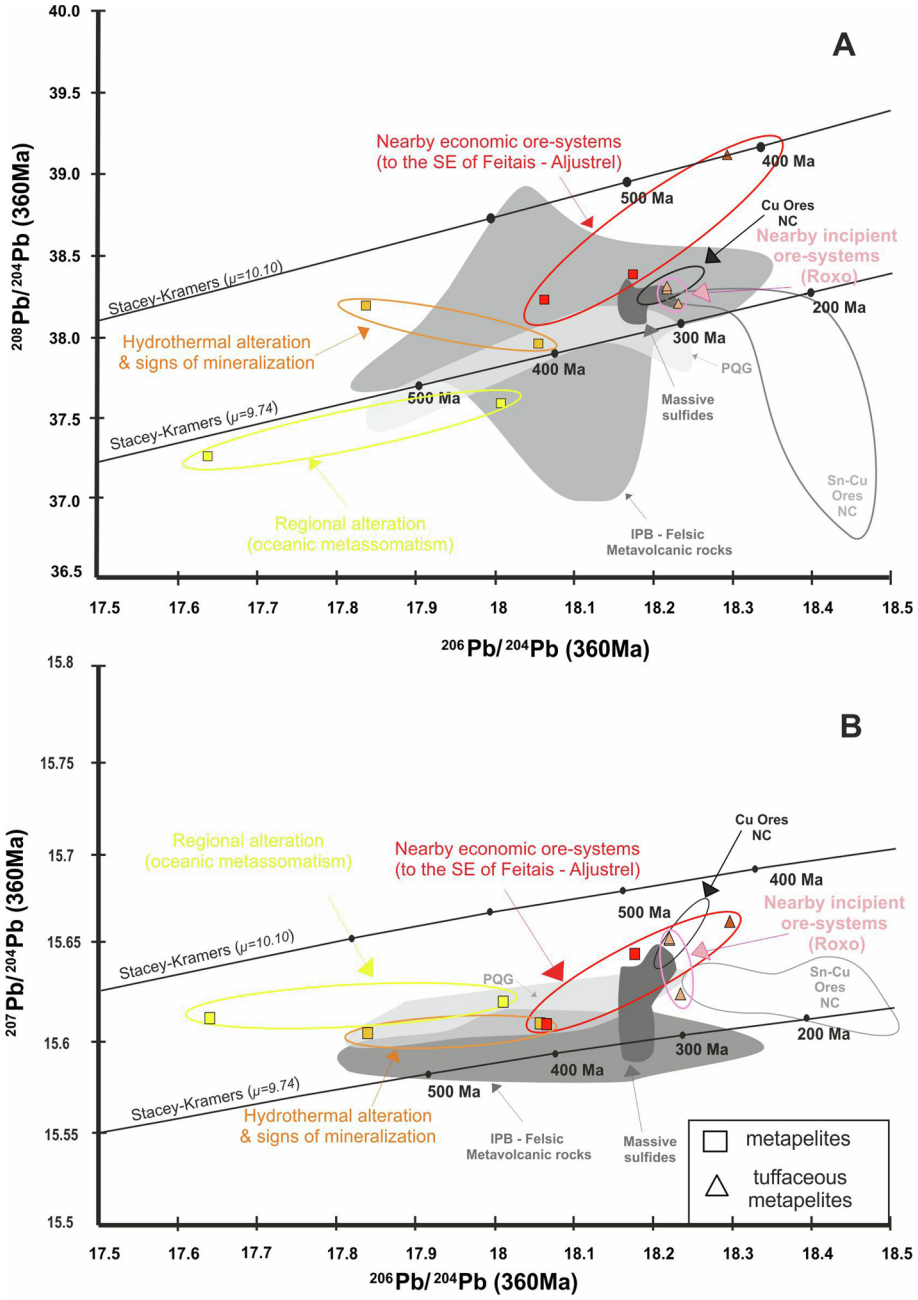

Fig. 13. $^{206}Pb/^{204}Pb$ versus $^{207}Pb/^{204}Pb$ and $^{208}Pb/^{204}Pb$ (age-corrected, 360 Ma) diagrams for selected samples of VSC metapelites and tuffaceous metapelites from the Albernoa area. Reference fields of IPB sulfide ores (Marcoux, 1998, Pomiès et al., 1998; Relvas et al., 2001) were classified into three groups: (i) Sn-Cu- ores from Neves Corvo (n = 8); (ii) Cu-ores from Neves Corvo (n = 8); and (iii) common massive sulfide ores (São Domingos n = 3, Lousal n = 4, Aljustrel n = 11, Lagoa Salgada n = 3, Riotinto n = 14, and some other deposits in Spain n = 18). The (age corrected) Pb-Pb ratios for metavolcanic (n = 14) and metasedimentary (n = 5) rocks were calculated considering data reported in Marcoux (1998) and in Jorge (2009), respectively. In the $^{206}Pb/^{204}Pb$ *vrs* $^{208}Pb/^{204}Pb$ diagram, the large extension of the "metavolcanic field" reflects the correction made: given the lack of whole-rock concentration values for Th, the $^{232}Th/^{204}Pb$ ratio was estimated for each sample on the basis of their $^{238}U/^{204}Pb$ values, assuming $^{232}Th/^{238}U = 3.62$ (as in Marcoux, 1998).

$^{207}Pb/^{204}Pb$, reflecting mixing of Pb from a reservoir with μ values similar or slightly above the Stacey-Kramers curve (i.e. 9.74) and from a distinct reservoir with higher μ values. The involvement of an unidentified higher-μ reservoir, noted in previous studies (*e.g.* Marcoux, 1998), is reinforced when Cu-ore samples from Neves Corvo are considered (see also Relvas et al., 2001). However, influence of a third reservoir characterized by higher $^{206}Pb/^{204}Pb$ ratios cannot be ruled out; such a reservoir is implicated in the development of the Neves Corvo Sn-rich ore samples from Graça and Corvo orebodies (Marcoux, 1998; Relvas et al., 2001; Li et al., 2019).

In summary, the isotopic signature of typical metapelites in the VSC ($\mu \approx 10$, $\approx 36 \leq \omega \leq 37$) results from a radiogenic reservoir that has a prevalent upper crustal component. This signature is somewhat disturbed by the addition of volcanic-derived components, but is mostly modified towards higher (age-corrected) $^{207}Pb/^{204}Pb$ and $^{206}Pb/^{204}Pb$ ratios in the course of the pre-Variscan hydrothermal alteration/mineralization processes.

7. Conclusions

Typical massive sulfide deposits in the IPB are hosted in volcano-sedimentary sequences. Their genesis is confined to a relatively short period of time that is not simply related in space and time to (felsic) volcanic rocks, and this provides the impetus for better characterizing the lateral and vertical facies variations in coeval metasedimentary rocks. The lower lithostratigraphic unit (PQG) comprises metamorphosed shales/sandstones that systematically grade to shale-dominant series commonly interbedded with tuffaceous metapelites, and these are (collectively) the prevailing sedimentary rocks in the overlying lithostratigraphic unit (VSC).

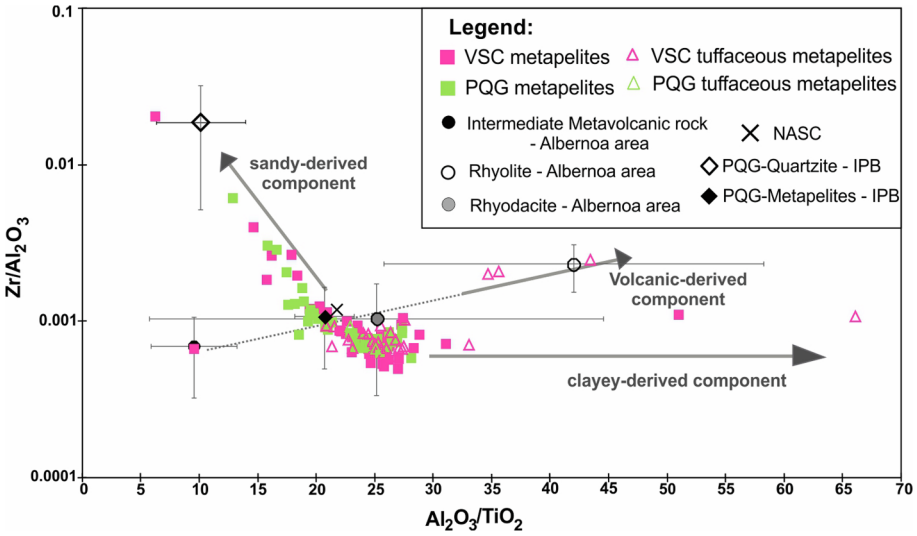

Fig. 14. Zr/Al_2O_3 vs. Al_2O_3/TiO_2 plot illustrating the main composition deviations displayed by the examined samples (n = 133): mixtures of clayey-derived or (fine-grained) sandy-derive continental components with volcanic-derived (and/or hydrothermal) fractions. For reference, and besides the ratios typifying NASC (Condie, 1993), the average ratios and corresponding standard deviation measures calculated for PQG-quartzite and metapelite (n = 75; different sites of IPB; Jorge, 2009) and VSC-metavolcanic rocks of Albernoa (intermediate composition, n = 9, rhyodacite, n = 27, rhyolite, n = 22; Codeço et al. 2018) are displayed.

A multi-element geochemical study of 133 representative samples of PQG and VSC metasedimentary rocks selected from drill-holes and outcrops throughout the Albernoa area show:

(I) The Zr/Sc, Th/Sc, Eu/Eu* relationships indicate that an evolved "felsic source" (resulting from sediment recycling) was the source of the prevalent siliciclastic component in of all the samples analyzed, irrespectively of the lithostratigraphic unit;

(II) The source-areas implicated in the basin supply were most likely the same and, according to the Chemical Index of Alteration (CIA) values, were significantly weathered while supplying sediment to the basin from Middle Devonian to Visean time;

(III) The main sedimentary fractions comprise a clayey-derived component ($20 \leq Al_2O_3/TiO_2 \leq 30$, $Sc/TiO_2 > 0.002$, $Ga/TiO_2 > 0.001$) and a (fine-grained) sandy-derived component ($\approx 5 \leq Al_2O_3/TiO_2 \leq 20$, $Sc/TiO_2 < 0.002$, $Ga/TiO_2 < 0.001$, $0.01 \leq Zr/TiO_2 \leq 0.1$);

(IV) The clayey- and sandy-derived components are, in places, variable mixed with volcanic-derived fractions in tuffaceous metapelites that are typical of VSC, but also present in the upper sections of PQG. Incorporation of volcanic-derived material is recorded by a clear increase of Al_2O_3/TiO_2 ratios (from ≈15-20 up to 45–65) along with a variable increase in Sc/TiO_2 and Ga/TiO_2 values and variably decreased Zr/Al_2O_3 ratios;

(V) Samples including the prevalent clayey-derived component are mostly confined to VSC sections, irrespectively of the sampled sector. In contrast, the sandy-derived component is predominant in a vast number of samples representing different VSC settings and various PQG lithostratigraphic levels. The volcanogenic component is distinctly more abundant in some tuffaceous metapelites from the Ervidel-Roxo and Figueirinha-Albernoa sectors. In general, VSC samples have the following chemical

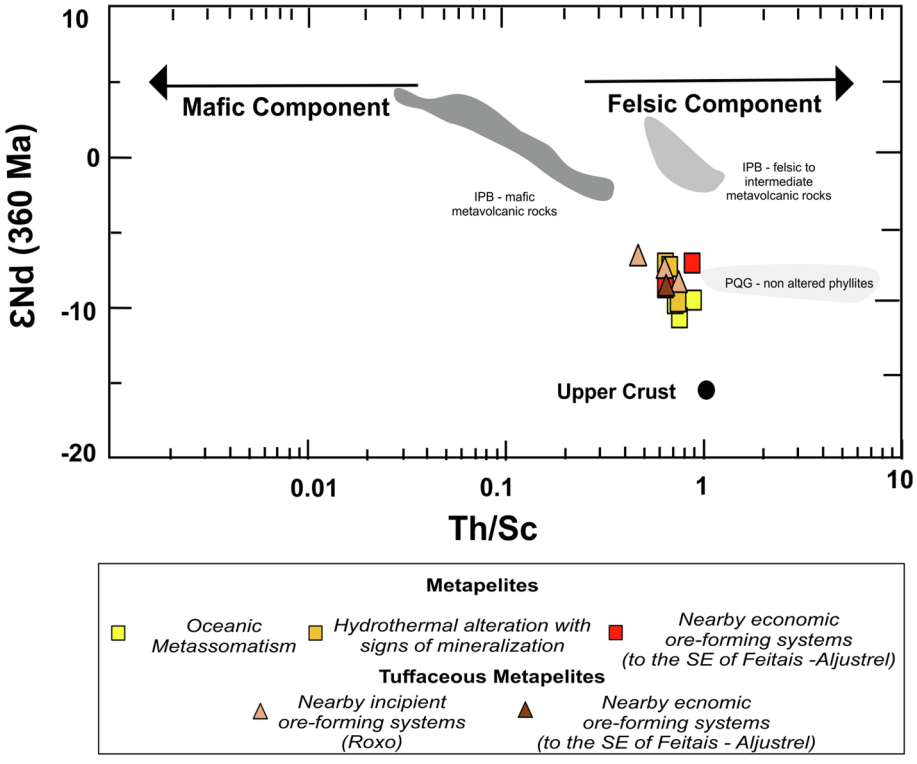

Fig. 15. Binary plot of $\varepsilon Nd_{(360\ Ma)}$ vs. Th/Sc for a selected group of VSC samples including metapelites (n = 8) and tuffaceous metapelites (n = 4), revealing a similar composition consistent with a prevalent common source-area (modified after McLennan et al. 1993). Reference fields of IPB metavolcanics (mafic n = 7 and felsic/intermediate n = 5) were delimited using data from *Mitjavilla et al. (1991)*. For the PQG field, 7 samples of non-altered phyllites (Jorge, 2009) were used.

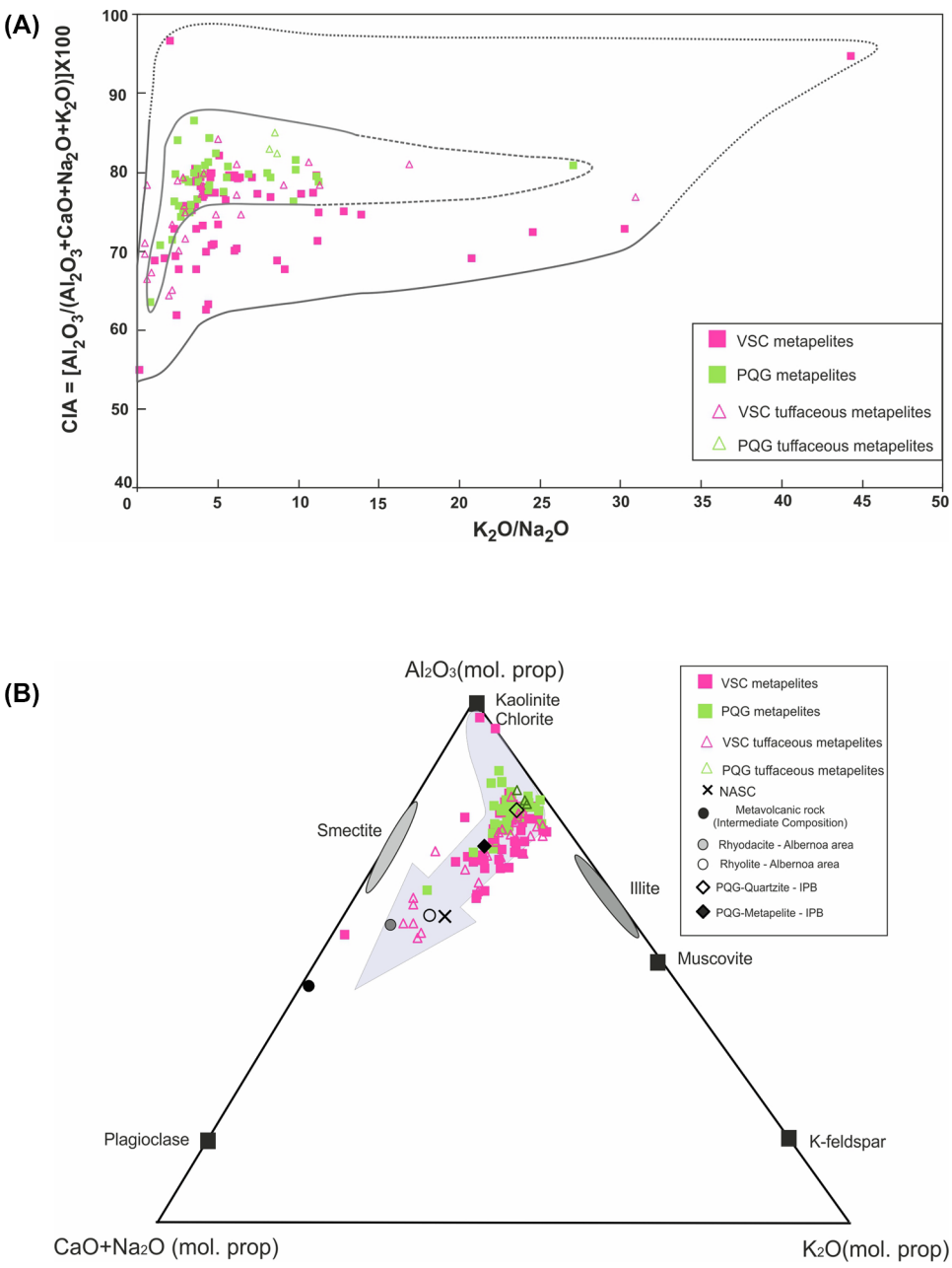

Fig. 16. Chemical Alteration Index (CIA) vs. K_2O/Na_2O (A) illustrating the intensity of source-rock weathering in the composition of the analyzed metasediments, possibly disturbed by exhalative-hydrothermal processes subsequent to sedimentation. (B) Ternary $(CaO + Na_2O)$-Al_2O_3-K_2O (mole proportion) diagram for the same samples. For reference, and besides NASC contents (Condie, 1993), the median values calculated for PQG-quartzite and metapelite (n = 75; different sites of IPB; Jorge, 2009) and VSC-metavolcanic rocks of Albernoa (intermediate composition, n = 9, rhyodacite, n = 27, rhyolite, n = 22; Codeço et al. 2018) are displayed. Ideal chemical compositions of mineral phases useful for reference purposes are also plotted. Modified after *McLennan et al. (1990)* and Goodfellow et al. (2003).

characteristics $2.5 \leq SiO_2/Al_2O_3 \leq 6.5$, $0.02 \leq TiO_2/Al_2O_3 \leq 0.06$ and $0.2 \leq (Cao + Na_2O + K_2O)/Al_2O_3 \leq 0.25$, whereas PQG samples display $2.5 \leq SiO_2/Al_2O_3 \leq 12$, $0.08 \leq TiO_2/Al_2O_3 \leq 0.58$ and $(CaO + Na_2O + K_2O)/Al_2O_3 \leq 0.3$;

(VI) Samples with Fe_2O_3/TiO_2 ratios ≥ 10 and $Al_2O_3/(Al_2O_3 + Fe_2O_3 + MnO)$ ratios ≤ ≈0.6 record the influence of early-developed (pre-Variscan metamorphism and deformation) hydrothermal imprint on the prevalent siliciclastic component that, in the case of tuffaceous metapelites, is variably mixed with volcanic-derived fractions; and

(VII) The ratios $5\times [(Fe_2O_3 + MgO + MnO)/Al_2O_3]$, (As + Sb)/Sc and (Cu + Zn + Pb)/Sc can be used as discriminants of barren and altered/mineralized metasedimentary sequences in the IPB. Values for all the three ratios between 1.0 and 10.0 indicate the influence of seafloor metasomatism processes, and ≥ 10.0 indicates close proximity to hydrothermal vent site that may potentially be associated with massive sulfide mineralization.

Strontium and Nd isotopic characteristics for a small subset of samples from VSC sections show highly radiogenic $^{87}Sr/^{86}Sr_{(360\ Ma)}$ and negative $\varepsilon Nd_{(360\ Ma)}$ values that indicate derivation mostly from an old, reworked, upper continental crustal source. Lead isotope signatures also support an upper crustal derivation without significant juvenile contamination. Isotope ratios characterizing the main siliciclastic components are somewhat disturbed by the addition of volcanic-derived components, recording also modifications by hydrothermal alteration/mineralization processes from less radiogenic fluids. Close proximity to of concealed sulfide mineralization hosted in VSC might be indicated by a decreased $^{87}Sr/^{86}Sr_{(360\ Ma)}$, and increased $\varepsilon Nd_{(360\ Ma)}$, $^{207}Pb/^{204}Pb$ and $^{206}Pb/^{204}Pb$ (age-corrected) isotopic ratios.

Acknowledgments

This work was funded by EPOS – Empresa Portuguesa de Obras Subterrâneas, S.A. Additional backing was provided through the FCT grant UID/GEO/50019/2019 – Instituto Dom Luiz. Filipa Luz

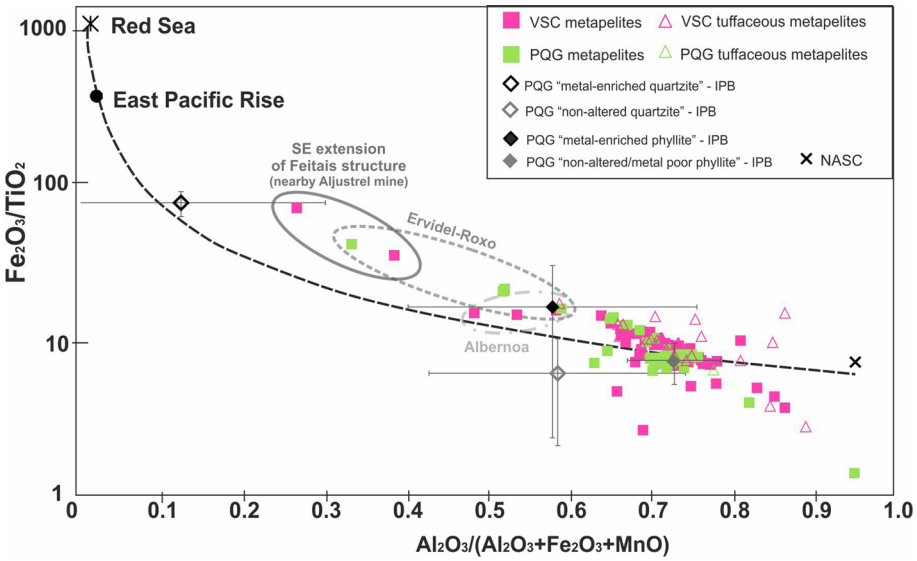

Fig. 17. Fe_2O_3/TiO_2 vs. $Al_2O_3/(Al_2O_3 + Fe_2O_3 + MnO)$ diagram for the complete Albernoa dataset illustrating a possible mixing strip between a "terrigenous" end-member (given by the samples clustering) and a conceptual "exhalative-hydrothermal" term represented by the composition of the East Pacific Rise and/or the Red Sea brine pool (*e.g.* Marchig et al. 1982; Goodfellow et al. 2003). NASC and PQG phyllites and quartzites (metal enriched and non-altered/metal poor) were plotted for reference (Condie, 1993; Jorge, 2009, respectively). The mixing strip is represented by the black dashed-line and the samples where the "hydrothermal component" is more evident separated by ellipses with sector labels. (For interpretation of the references to colour in this figure legend, the reader is referred to the web version of this article.)

acknowledges the support of Fundação para a Ciência e Tecnologia (FCT; PD/BD/114485/2016 grant). The authors warmly thanks the "SuperBrigada" for its continuous involvement in field and lab work, and Marta Codeço for discussion and comments on early versions of this text. Prof. R. Saéz (Univ. Huelva, Spain), Jan Peter (Geological Survey of Canada), and an anonymous reviewer are acknowledged for their constructive comments and suggestions which helped improved the final version of the manuscript.

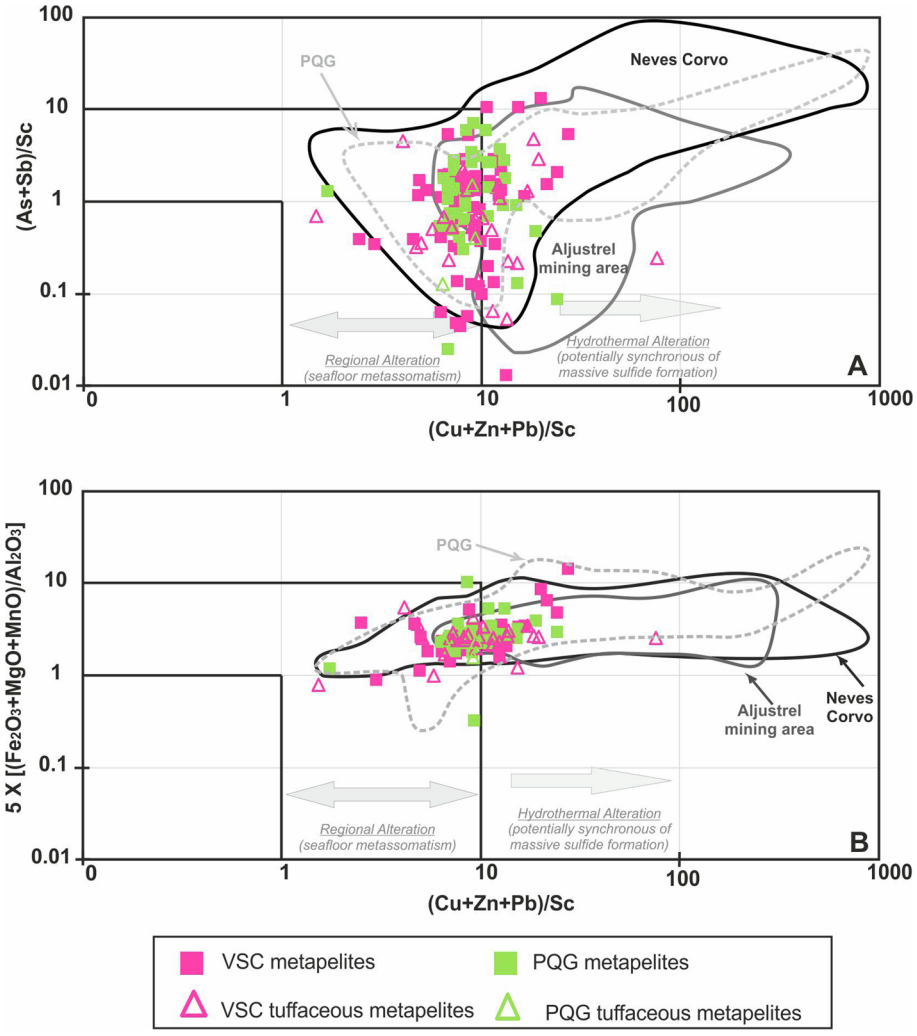

Fig. 18. (As + Sb)/Sc *vrs.*(Cu + Zn + Pb)/Sc and $(Fe_2O_3 + MgO + MnO)/Al_2O_3$ *vrs.* (As + Sb)/Sc diagrams illustrating the chemical effects related to post-sedimentary transformations. Values between 1.0 and 10.0 of these geochemical ratios trace, conceivably, the influence of oceanic metasomatism processes (*regional alteration pattern*); ratios above 10.0 indicate the proximity of hydrothermal discharges potentially related to ore-forming systems. For comparison purposes, compositional fields for the Aljustrel and Neves Corvo mining areas are indicated using the available whole-rock geochemical data for metasedimens. Delimitation of the Aljustrel field considered 79 samples of VSC metapelites and tuffaceous metapelites picked in (i) exploitation drillings [Feitais and Moinho orebodies], (ii) underground-mining works [Feitais and Moinho orebodies] and (iii) recent exploration brownfield drillings [S. João, Gavião and Monte das Mesas]; for details see Luz et al. (2018). The Neves Corvo field was delineated on the basis of 42 samples of PQG and VSC metapelites and tuffaceous metapelites collected in various levels of the underground-mining works in Zambujal, Semblana, Graça, Lombador, Neves and Corvo orebodies (ongoing research). The PGQ compositional field includes 75 samples representing (non-altered and altered/mineralized) phyllites and quartzites reported in Jorge (2009).

Appendix A. Supplementary data

Supplementary data to this article can be found online at https://doi.org/10.1016/j.oregeorev.2019.03.020.

References

Abat, I., Mata, J.P., Nieto, F., Velilla, N., 2001. The phyllosilicates in diagenetic-metamorphic rocks of the South Portuguese Zone, Southwestern Portugal. Can. Mineral. 39, 1571–1589.

Almodóvar, G.R., Saéz, R., Pons, J.M., Maestre, A., Toscano, M., Pascual, E., 1998. Geology and genesis of the Aznalcóllar massive sulfide deposits, Iberian Pyrite Belt, Spain. Mineral. Depos. 33, 111–136.

AVRUPA Minerals, 2014. Avrupa and Antofagasta intersect copper-rich VMS in Pyrite Belt, Portugal [Press release]. Retrieved from: http://www.avrupaminerals.com/_resources/news/nr_2014_02_07.pdf.

Babinski, M., Vans Schumus, W.R., Chemale Jr., F., 1999. Pb-Pb dating and Pb isotope geochemistry of Neoproterozoic carbonate rocks from the São Francisco basin, Brazil: implications for the mobility of Pb isotopes during tectonism and metamorphism. Chem. Geol. 160, 175–199.

Barrie, C., Amelin, Y., Pascual, E., 2002. U-Pb geochronology of VMS mineralization in the Iberian Pyrite Belt. Mineral. Depos. 37 (8), 684–703.

Barriga, F.J.A.S., Carvalho, D., Ribeiro, A., 1997. Introduction to the Iberian Pyrite Belt. In: Barriga, F.J.A., Carvalho, D. (Eds.), Geology and VMS Deposits of the Iberian Pyrite Belt. Society of Economic Geologists Guidebook series, pp. 1–20. https://doi.org/10.5382/GB.27.

Barriga, F., Kerrich, R., 1984. Extreme 18O-enriched volcanics and 18O-evolved marine water, ALjustrel, Iberian Pyrite Belt: transition from high to low Rayleigh number convective regimes. Geochim. Cosmochim. Acta 48 (5), 1021–1031.

Boström, K., 1973. The origin and fate of ferromanganoan active ridge sediments. Stockholm Contribut. Geol. 27, 147–243.

Canet, C., Alfonso, P., Melgarejo, J.C., Belyatsky, B.V., 2004. Geochemical evidences of sedimentary-exhalative origin of the shale-hosted PGE-Ag-Au-Zn occurrences of the Prades Mountains (Catalonia, Spain): trace-element abundances and Sm-Nd isotopes. J. Geochem. Explor. 82, 17–33.

Carvalho, D., Barriga, F.J.A.S., Munhá, J., 1999. Bimodal-siliciclastic systems – the case of the Iberian Pyrite Belt. Rev. Econ. Geol. 8, 375–408.

Carvalho, D., Correia, H.A.C., Inverno, C.M.C., 1976. Contribuição para o conhecimento geológico do Grupo de Ferreira Ficalho. Suas relações com o Grupo do Pulo do Lobo e com a Faixa Piritosa. Mem Not. (Univ. Coimbra) 82, 145–169.

Carvalho, D., Goinhas, J., Oliveira, V., Ribeiro, A., 1971. Observações sobre a Geologia do Sul de Portugal e consequências metalogenéticas: Estudos Notas Trabalhos, Serviço Fomento Mineiro, v. 20, Fas. 1-2, pp. 153–199.

Carvalho, J., 2016. Zinc metallogenesis, and indium and selenium distribution at Neves Corvo deposit, Iberian Pyrite Belt. University of Lisbon, Portugal, pp. 543 PhD thesis.

Carvalho, J., Inverno, C., Matos, J.X., Rosa, C., Granado, I., Branhc, T., Represas, P., Caracaneanu, L., Matis, L., Sousa, P., 2016. Subsurface mapping in the Iberia Pyrite Belt using seismic reflections profiling and potential-field data. Int. J. Eartth Sci. (Geol. Rundsch.). https://doi.org/10.1007/s00531-016-1340-1.

Castroviejo, R., Quesada, C., Soler, M., 2011. Post-depositional tectonic modifications of VMS deposits in Iberia and its economic significance. Mineral. Depos. 46, 615–637.

Cingolani, C.A., Manassero, M., Abre, P., 2003. Composition, provenance, and tectonic setting of Ordovician siliciclastic rocks in the San Rafale block: southern extension of the Precordillera crustal fragment, Argentina. J. South Amer. Earth Sci. 16 (1), 91–106.

Codeço, M., Mateus, A., Figueiras, J., Gonçalves, L., Rodrigues, P., 2018. Development of the Ervidel-Roxo and Figueirinha-Albernoa volcanic sequences in Iberian Pyrite Belt, Portugal: metallogenic and geodynamic implications. Ore Geol. Rev. 98, 80–108.

Codeço, M., Mateus, A., Figueiras, J., Rodrigues, P., Gonçalves, L., 2015. Zircon Saturation and Ti-in-Zircon Thermometry Applied to Felsic Volcanics of the Iberian Pyrite Belt; Useful Exploration Guides to Massive Sulphide Ores. X Congresso Ibérico de Geoquímica/XVIII Semana de Geoquímica Abs., Alfragide, Portugal, pp. 63–66.

Condie, K.C., 1993. Chemical composition and evolution of the Upper Continental Crust: contrasting results from surface samples and shales. Chem. Geol. 104, 1–37.

da Silva, N.V., Mateus, A., Monteiro Santos, F.A., Almeida, E.P., Pous, J., 2007. 3-D electromagnetic imaging of a Paleozoic plate-tectonic boundary segment in SW Iberian Variscides (S Alentejo, Portugal). Tectonophysics 445, 98–115.

Denhavi, A.S., lentz, D.R., McFarlane, C. R.M., Walker, J.A.,, 2018. Quantification of fluid-mobile elements in white mica by LA-ICP-MS: from chemical composition to a potential micro-chemical vectoring tool in VMS exploration. J. Geochem. Explorat. 188, 290–307.

DePaolo, D.J., 1981. Neodymium isotopes in the Colorado Front Range and crust–mantle evolution in the Proterozoic. Nature 291 (5812), 193–196.

Donaire, T., Saez, R., Pascual, E., 2002. Rhyolitic globular peperites from the Aznacollar mining district (Iberian Pyrite Belt, Spain): physical and chemical controls. J. Volcanol. Geotherm. Res. 114, 119–128.

Droop, G.T.R., 1987. A general equation for estimating Fe^{3+} concentrations in ferromagnesian silicates and oxides from microprobe analysis using stoichiometric criteria. Min. Mag. 51, 431–435.

Faure, G., Mensing, T.M., 2005. Isotopes: Principles and Applications. Wiley, pp. 928.

Granda, A., Granda, T., Pons, J.M., Videira, J.C., 2016. The leading role of geophysical methods in the discovery of La Magdalena VMS deposit in Pyrite Belt, Huelva. First Break 34.

Godinho, E., Figueiras, J., Mateus, A., Rodrigues, P., Gonçalves, L., 2015. Mineralogical and geochemical alteration patterns in metajaspers and metacherts: New Exploration Guides for Pollymetalic Massive Sulfides in the Iberian Pyrite Belt. In: X Congresso Ibérico de Geoquímica/XVIII Semana de Geoquímica Abs., Alfragide, Portugal, pp. 48–51.

Goldstein, S.L., ÓNions, R.K., Hamilton, P.J., 1984. A Sm-Nd isotopic study of atmospheric dust and particulates from major river systems. Earth Planet. Sci. Lett. 70, 221–236.

Goodfellow, W.D., Peter, J.M., Winchester, J.A., van Staal, C.R., 2003. Ambient marine environment and sediment provenance during formation of massive sulfide deposits in the bathrust mining camp: importance of reduced bottom waters to sulfide precipitation and preservation. Econ. Geol. Monograph 11, 129–156.

Gurvich, E.G., 2006. Metalliferous sediments of the World Ocean. Fundamental theory of deep-sea hydrothermal sedimentation. Springer-Verlag, Berlin.

Holland, H.D., 1972. The geologic history of seawater: an attempt to solve the problem. Geochim. Cosmochim. Acta 36, 637–651.

Hung, J.-J-., Yeh, H.-Y., Peng, S.-H., Chen, C.T.A., 2018. Influence of submarine hydrothermalism on sulfur and metal accumulation is surface sediments in the Kueishantao venting field off northeastern Taiwan. Mar. Chem. 198, 88–96.

Inverno, C., Díez-Montes, A., Rosa, C., García-Crespo, J., Matos, J., García-Lobón, J.L., Carvalho, J., Bellido, F., Castello-Branco, J.M., Ayala, C., Batista, M.J., Rubio, F., Granado, J., Tornos, F., Oliveira, J.T., Rey, C., Araújo, V., Sánchez-Garcá, T., Pereira, Z., Represas, P., Solá, A.R., Sousa, P., 2015. Introduction and geological setting of the Iberian Pyrite Belt. In: Weihed, P. (Ed.), 3D, 4D and Predictive Modelling of Major Mineral Belts in Europe. Mineral Resources Reviews, Springer, Switzerland, pp. 191–208.

Jacobsen, S., Wasserburg, G.J., 1980. Sm-Nd evolution of chondrites. Earth Planet. Sci. Lett. 50 (1), 139–155.

Jansson, N.F., Zetterqvist, A., Allen, L., Malmström, L., 2018. Geochemical vectors for stratiform Zn-Pb-Ag sulfide and associated dolomite-hosted Cu mineralization at Zinkgruvan Bergslagen, Sweden. J. Geochem. Explor. 190, 207–228.

Jorge, R.C.G.S., 2009. Caracterização petrográfica, geoquímica e isotópica dos reservatórios metalíferos crustais, dos processos de extracção de metais e dos fluidos hidrotermais envolvidos em sistemas mineralizantes híbridos na Faixa Piritosa Ibérica. PhD Thesis. University of Lisbon, Portugal, pp. 290.

Jorge, R.C.G.S., Pinto, A.M.M., Tassinari, C.C.G., Relvas, J.M.R.S., Munhá, J., 2007. VHMS metal sources in the Iberian Pyrite Belt: new insights from Pb isotope data. In: Proceed 9th Biennal SGA. Mtg Dublin, Ireland, pp. 1097–1100.

Jorge, R.C.G.S., Relvas, J.M.R.S., Matos, J.X., 2006. Geochemistry of metasediments from the Phyllite-Quartzite Group, Iberian Pyrite Belt: implications for provenance and source-area weathering (progress report) VII Congresso Nacional de Geologia, Livro de Resumos I. Estremoz. Universidade de Évora (Portugal), pp. 175–178.

Leca, X., Ribeiro, A., Oliveira, J.T., Silva, J.B., Albouy, L., Carvalho, P., Merino, H., 1983. Cadre Geólogique des Minéralisations de Neves-Corvo, Baixo Alentejo, Portugal: Lithostratigraphie, paléogeographie et téctonique. Mémoire Bureau de Recherches Geólogique et Minières 121, pp. 79.

Leistel, J.M., Marcoux, E., Thiéblemont, D., Quesada, C., Sánchez, A., Ruiz de Amodóvar, G., Pascual, E., Sáez, R., 1998. The volcanic-hosted massive sulphide deposits of the Iberian Pyrite Belt. Mineral. Depos. 33, 2–30.

Lett, R.E., 2001. Geochemical signatures around massive sulphide deposits in southern British Columbia. Geological Society, London, Special Publications, Canada, pp. 301–321.

Lett, R.E., Bobrowsky, P., Cathro, M., 1998. Geochemical pathfinders for massive sulphide deposits in the Southern Kootenay Terrane. Geological Fieldwork 1997 Paper 1998-1.

Li, X., Zhao, K.D., Jiang, S.Y., Palmer, M.R., 2019. *In situ* U-Pb geochronology and sulfur isotopes constrains the metallogenesis of the giant Neves Corvo deposit, Iberian Pyrite Belt. Ore Geol. Rev. 105, 223–235.

Linn, A.M., DePaolo, D.J., Ingersoll, R.V., 1991. Nd-Sr isotopic provenance analysis of Upper Cretaceous Great Valley fore-arc sandstones. Geology 19 (8), 803–806.

Lottermoser, B.G., 1991. Trace element composition of exhalites associated with the Boken Hill sulfide deposit, Australia. Econ. Geol. 86, 870–877.

Luz F., Mateus A., Figueiras J., 2018. Elemental geochemistry of metasediments from Aljustrel area, Iberian Pyrite Belt (IPB): implications for mineral exploration. SEG Conference: Metals, Minerals, and Society Keystone, Colorado, USA, September 22–25th.

Luz, F., Mateus, A., Figueiras, J., Rodrigues, P., Gonçalves, L., 2015. Fingerprints of Pre-Metamorphic Hydrothermal Alteration Affecting Metapelites from the Iberian Pyrite Belt; Implications for Massive Ore Exploration. In: X Congresso Ibérico de Geoquímica/XVIII Semana de Geoquímica Abs., Alfragide, Portugal, pp. 43-46.

Luz, F., Mateus, A., Figueiras, J., Tassinari, C.G., Gonçalves, L., 2017. Whole-rock chemistry and Pb Isotope Compositions in metasediments of the Iberian Pyrite Belt; relevance to Mineral Exploration. In: Goldschmidt Conference, Paris.

Luz, F., Mateus, A., Matos, J.X., Gonçalves, M.A., 2012. Geochemistry of stream sediments southwards of the SW Variscan suture in Portugal (Guadiana and Chança river basins): insights into element anomalies of variable origin and intensity. Applied Earth Science – Trans. Inst. Min. Metall. B 121 (3), 137–150.

Luz, F., Mateus, A., Matos, J.X., Gonçalves, M.A., 2014a. Cu- and Zn- Anomalies in the NE Border of the South Portuguese Zone (Iberian Variscides, Portugal) Identified by Multifractal and Geostatistical Analyses. Nat. Resour. Res. 23 (2), 195–215.

Luz, F., Mateus, A., Matos, J.X., Gonçalves, M.A., 2014b. Copper, Zn and Pb soil geochemistry data from the NW domain of the Iberian Pyrite Belt in Portugal: implications for mineral exploration. Geochem. Explorat. Environ. Anal. 14, 341–358.

Marchig, V., Gundalach, H., Möller, P., Schley, M., 1982. Some geochemical indicators for discrimination between diagenetic and hydrothermal metalliferous sediments. Marine Geol. 50, 241–256.

Marcoux, E., Moelo, Y., Leistel, J.M., 1996. Bismuth and cobalt minerals as indicators of stringer zones to massive sulphide deposits,. Iberian Pyrite Belt. Mineral. Depos. 31,

1–26.
Marcoux, E., 1998. Lead isotope systematics of the giant massive sulphide deposits in the Iberian Pyrite Belt. Mineral. Depos. 33, 45–58.
Mateus, A., Figueiras, J., Monteiro Santos, F., Luz, F., Khalill, M., Codeço, M., Gonçalves, S., Godinho, E., Santos, E., Rodrigues, P., 2014. Prospeção Mineral no "Polígono de Albernoa" (Faixa Piritosa Ibérica, Portugal); Avaliação integrada de dados geológicos e geofísicos existentes; novas informações mineralógicas e geoquímicas e follow-up. Unpublished Report, Lisbon, Portugal, pp. 260.
Mateus, A., Figueiras, J., Monteiro Santos, F., Luz, F., Khalill, M., Codeço, M., Gonçalves, S., Godinho, E., Farzamian, M., Moreira, B., Rodrigues, P., Jorge, R.C.G.S., Henriques, C., 2015a. Prospeção Mineral no "Polígono de Albernoa" (Faixa Piritosa Ibérica, Portugal); avaliação integrada e três áreas prioritárias recorrendo a dados multi-disciplinares e follow up. Unpublished Report, Lisbon, Portugal, pp. 291.
Mateus, A., Figueiras, J., Monteiro Santos, F., Luz, F., Khalill, M., Gonçalves, S., Farzamian, M., Rodrigues, P., Bernardo, I. 2015b. Prospeção Mineral no "Polígono de Albernoa" (Faixa Piritosa Ibérica, Portugal); Re-avaliação geofísica detalhada das três áreas prioritárias, refinamento lito-estratigráfico e geoquímico de sequências silto-pelíticas inferiors e follow-up. Unpublished Report, Lisbon, Portugal, pp. 291.
Mateus, A., Lopes, C., Martins, L., Carvalho, J., 2017. Towards a multi-dimensional methodology supporting a safeguarding decision on the future access to mineral resources. Miner. Econom. 30 (3), 229–255.
Matos, J.X., Barriga, F.J.A.S., Oliveira, V.M-J., Relvas, J.M.R.S., Conceição, P., 2000. The structure and hydrothermal alteration of the Lagoa Salgada orebody (Iberian Pyrite Belt – Sado Tertiary Basin). In: Volcanic Environments and Masisve Sulfide Deposits. SEG/CODES International Conference Abstract Volume, Tasmania, Australia, pp. 119–121.
Matos, J., Pereira, Z., Oliveira, V., Oliveira, J., 2006. The geological setting of the São Domingos pyrite orebody, Iberian Pyrite Belt. In: VII Congresso Nacional de Geologia, Estremoz, Universidade de Évora, Portugal.
Marignac, C., Diagana, B., Cathelineau, M., Boiron, M.C., Banks, D., Fourcade, S., Vallance, J., 2003. Remobilisation of base metals and gold by Variscan metamorphic fluids in the south Iberian Pyrite Belt: evidence from Tharsis VMS deposit. Chem. Geol. 194, 143–165.
Martín-Izard, A., Arias, D., Arias, A., Gumiel, P., Sanderson, D.J., Castañon, C., Lavandeira, A., Sanchez, J., 2015. A new 3D geological model and interpretation of structural evolution of the world-class Rio Tinto VMS deposit, Iberian Pyrite Belt (Spain). Ore Geol. Rev. 71, 457–476.
MATSA, Mubadala, A., Transfigura Company, 2018. Mina de Aguas Teñidas. [Corporate Presentation]. Retrieved from: https://www.matsamining.com/media/3925/2018matsacorporatepresentation.pdf.
McKee, G.S., 2001. Deformation and ore remobilisation within the Aguas Teñidas Este VMS deposit, Iberian Pyrite Belt. Trans. Inst. Min. Metall. 110, B50–B58.
McLennan, S.M., Hemming, S., McDanniel, D.K., Hanson, G.N., 1993. Geochemical approaches to sedimentation, provenance, and tectonics. Special Paper In: Johnsson, M.J., Basu, A. (Eds.), Processes Controlling the Composition of Clastic Sediments. Geological Society of America, pp. 21–40.
Middelburg, J.J., Van Der Weidjen, C.H., Woittiez, J.R.W., 1988. Chemical processes affecting the mobility of major, minor and trace elements during weathering of granitic rocks. Chem. Geol. 68, 253–273.
Mitjavilla, J., Martí, J., Soriano, C., 1997. Magmatic evolution and tectonic setting of the iberian pyrite belt volcanism. J. Petrol. 38 (6), 727–755.
Moreira, B., Figueiras, J., Mateus, A., Rodrigues, P., Jorge, R.C.G.S., Gonçalves, L., 2015. A new manganese mineralisation type in the Iberian Pyrite Belt? X Congresso Ibérico de Geoquímica/XVIII Semana de Geoquímica Abs., Alfragide, Portugal, pp. 135–138.
Moreno, C., Sierra, S., Saez, R., 1996. Evidence for catastrophism at the Famennian-Dinantian boundary in the Iberian Pyrite Belt. In: Strogen, P., Sommerville, I.D., Jones, G.L. (Eds.), Recent advances In Lower Carboniferous Geology. Geological Society Special publication, pp. 153–162.
Munhá, J., 1979. Blue amphiboles, metamorphic regime and plate tectonic modelling in the Iberian Pyrite Belt. Contrib. Mineral. Petrol. 69, 279–289.
Munhá, J., 1981. Igneous and metamorphic petrology of the Iberian Pyrite Belt volcanic rocks. Doctoral Thesis. University of Western Ontario, Canada.
Munhá, J., 1983a. Hercynian magmatism in the Iberian Pyrite Belt. In: Lemos de Sousa, M.J., Oliveira, J.T. (Eds.), The Carboniferous of Portugal. Mem. Serv. Geol. Port, pp. 39–81.
Munhá, J., 1983. Low-grade regional metamorphism in the Iberian Pyrite Belt. Comun. Serv. Geol. Port. 69, 3–36.
Munhá, J., 1990. Metamorphic evolution of the South Portuguese/ Pulo do Lobo Zone. In: Dallmeyer, R.D., Martínez García, E. (Eds.), Pre-Mesozoic Geology of Iberia. Springer, Berlin Heidelberg, Berlin, pp. 363–369.
Munhá, J., Barriga, F., Kerrich, R., 1986. High 10° ore-forming fluids in volcanic-hosted base metal massive sulfide deposits; geologic, 18°/16°, and D/H evidence from the Iberian Pyrite Belt; Crandon, Wisconsin; and Blue Hill,. Maine. Econ. Geol. 81 (3), 530–552.
Munhá, J., Kerrich, R., 1980. Seawater basalt interaction in spilites from the Iberian Pyrite Belt. Contrib. Miner. Petrol. 73, 191–200.
Oliveira, J.T., 1990. Stratigraphy and syn-sedimentary tectonism in the South Portuguese Zone. In: Dallmeyer, R.D., Martinez García, E. (Eds.), Pre-Mesozoic Geology of Iberia. Springer, Berlin Heidelberg, Berlim, pp. 334–347.
Oliveira, J.T., 1992. Notícia explicativa da Folha 8 da carta geológica de Portugal 1:200 000, Serviços Geológicos de Portugal, Lisboa.
Oliveira, V., Matos, J.X., Bengala, M., Silva, N., Sousa, P., Torres, L., 1998. Geology and geophysics as successful tools in the discovery of the Lagoa Salgada orebody (Sado tertiary Basin – Iberian Pyrite Belt),. Grândola, Portugal Miner. Depos. 33, 170–187.
Oliveira, J.T., Pereira, Z., Carvalho, P., Pacheco, N., Korn, Dieter, 2004. Stratigraphy of the tectonically imbricated lithological succession of the Neves Corvo mine area, Iberian Pyrite Belt,. Portugal. Miner. Depos. 39 (49), 422–436.
Oliveira, J.T., Pereira, Z., Rosa, C., Rosa, D., Matos, J., 2005. Recent advances in the study of the stratigraphy and the magmatism of the Iberian Pyrite Belt, Portugal. In: Carosi, R., Dias, R., Iacopini, D., Rosenbaum, G. (eds) The southern Variscan belt. J. Virtual Explor. 19, 1441–8142.
Oliveira, J.T., Relvas, J.M.R.S., Pereira, Z., Matos, J.X., Rosa, C.J., Rosa, D., Munhá, J.M., Jorge, R.C.G.S., Pinto, A.M.M., 2006. O Complexo Vulcano-Sedimentar da Fiaxa Piritosa Ibérica: estrtigrafia, vulcanismo e mineralizações associadas e evolução tectonoestratigráfica no context da Zona Sul Portuguesa. In: Dias, R., Araújo, A., Terrinha, P., Kullberg, J.C., (Eds.), Geologia de Portugal na Ibérica. VII Congresso Nacional de Geologia, Univ. Évora, Portugal, pp. 207–214.
Oliveira, J.T., Pereira, Z., Matos, J., Fernandes, P., 2008. A palinoestratigrafia no contexto da interpretação estrutural da Faixa Piritosa. VIII Reunião do Grupo de Geologia Estrutural e Tectónica (GCET). Faculdade de Ciências da Universidade do Porto, pp. 107–110.
Oliveira, D., Matos, J.X., Rosa, C., Rosa, D., Figueiredo, M., Silva, T., Guimarães, F., Carvalho, J., Pinto, A., Relvas, J., Reiser, F., 2011. The Lagoa Salgada Orebody, Iberian Pyrite Belt, Portugal. Econ. Geol., Soc. Econ. Geol. 106, 1111–1128.
Oliveira, J.T., Rosa, C.J.P., Rosa, D.R.N., Pereira, Z., Matos, J.X., Inverno, C.M.C., Andersen, T., 2013. Geology of the Neves-Corvo antiform, Iberian Pyrite Belt, Portugal: new insights from physical volcanology, palynostratigraphy and isotope geochronology studies. Mineral. Depos. 48, 748–766.
Pereira, Z., Matos, J.X., Fernandes, P., Jorge, R.G.S., Oliveira, J.T., 2010. Qual a idade mais antiga da Faixa Piritosa. Nova idade Givetiano inferior para o Grupo Filito-Quartzitico (Anticlinal São Francisco da Serra, Faixa Piritosa, Revista Electrónica de Ciências da Terra Vol. 17, n°13, pp. 4.
Pereira, Z., Matos, J., Fernandes, P., Oliveira, J.T., 2007. Devonian and Carboniferous palynostratigraphy of the South Portuguese Zone, Portugal – an overview. Comunicações Geológicas 94, 53–79.
Pereira, Z., Matos, J.X., Fernandes, P., Jorge, R.G.S., Oliveira, J.T., 2018. Stratigraphy of the Northern Pulo do Lobo Domain, SW Iberia Variscides: a palynological contribution, Geobio.
Peter, J.M., Goodfellow, W.D., 1996. Mineralogy, bulk and rare earth element geochemistry of massive sulphide-associated hydrothermal sediments of the Brunswick horizon, Bathurst Mining Camp, New Brunswick. Canadian J. Earth Sci. 33, 252–283.
Quesada, C., 1998. A reappraisal of the structure of the Spanish segment of the Iberian Pyrite Belt. Mineral. Depos. 33, 31–44.
Relvas, J.M.R.S., 2000. Geology and metallogenesis at the Neves Corvo, Portugal. PhD Thesis. University of Lisbon, Portugal, pp. 250.
Relvas, J.M.R.S., Barriga, F.J.A.S., Ferreira, A., Noiva, P.C., Pacheco, N., Barriga, G., 2006. Hydrothermal alteration and mineralization in the Neves-Corvo volcanic hosted massive sulfide deposit, Portugal: I. Geology, mineralogy and geochemistry. Econ. Geol. 101, 791–804.
Relvas, J.M.R.S., Barriga, F.J.A.S., Pinto, A., Pacheco, N., Noiva, P., Barriga, G., Baptista, R., Carvalho, D., Oliveira, V., Munhá, J., Hutchison, R.W., 2002. The Neves-Corvo deposit, Iberian Pyrite Belt, Portugal: Impacts and future, 25 years after the discovery. In: Goldfarb, R., Nielsen, J. (Eds.), Integrated Methods for discovery. SEG Special Publication pp. 155–176.
Relvas, J.M.R.S., Tassinari, C.C.G., Munhá, J., Barriga, F.J.A.S., 2001. Multiple sources for ore-forming fluids in the Neves Corvo VHMS Deposit of the Iberian Pyrite Bet (Portugal): strontium, neodymium and lead isotope evidence. Miner. Depos. 36, 416–427.
Ribeiro, A., Silva, J.B., 1983. Structure of the South Portuguese Zone. In: Lemos de Sousa, M., Oliveira, J.T. (Eds.), The Carboniferous of Portugal. Mem. Serv. Geol. Portugal, Lisboa pp. 83-89.
Ribeiro, A., Munhá, J., Dias, D., Mateus, A., Pereira, E., Ribeiro, L., Fonseca, P., Araújo, A., Oliveira, J.T., Romão, J., Chaminé, H., Coke, C., Pedro, J., 2007. Geodynamic evolution of the SW Europe Variscides. Tectonics 26, TC6009.
Ribeiro, A., Munhá, J., Fonseca, P.E., Araújo, A., Pedro, J.C., Mateus, A., Tassinari, C., Machado, G., Jesus, A.P., 2010. Variscan ophiolite belts in the Ossa-Morena Zone (Southwest Iberia): geological characterization and geodynamic significance. Gondwana Res. 17, 408–421.
Rodrigues, B., Chew, D.M., Jorge, R.C.G.S., Fernandes, P., Veiga-Pires, C., Oliveira, J.T., 2014. Detrital zircon geochronology of the Carboniferous Baixo Alentejo Flysh Group (South Portugal); constraints on the provenance and geodynamic evolution of the South Portuguese Zone. J. Geol. Soc. London. https://doi.org/10.1144/jgs2013-084.
Rosa, D., Inverno, C., Oliveira, V., Tosa, C., 2004. Geochemistry of volcanic rocks, Albernoa area, Iberian Pyrite Belt,. Portugal. Int. Geol. Rev. 46, 366–383.
Rosa, C.J.P., 2007. Facies Architecture of the Volcano Sedimentary Complex of the Iberian Pyrite Belt, Portugal and Spain. PhD thesis. University of Tasmania.
Rosa, C.J.P., McPhie, J., Relvas, J., Pereira, Z., Oliveira, T., Pacheco, N., 2008. Volcanic setting of the giant Neves Corvo massive sulfide deposit, Iberian Pyrite Belt, Portugal. Mineral. Deposita 43, 449–466.
Rosa, C.J.P., McPhie, J., Relvas, J., 2010. Type of volcanoes hosting the massive sulfide deposits of the Iberian Pyrite Belt. J. Volcanol. Geotherm. Res. 194, 107–126.
Rosa, C., McPhie, J., Relvas, J., 2011. Sediment-matrix igneous breccias at the top contacts of felsic units in the IPB: implications for VHMS exploration. In: 11th SGA Biennal Mtg Abs. Antofagasta, Chile, pp. 754–756.
Saéz, R., Pascual, E., Toscano, M., Almodóvar, G.R., 1999. The Iberian type of volcano-sedimentary massive sulfide deposits. Mineral. Depos. 34, 549–570.
Saéz, R., Moreno, C., González, F., Almodóvar, G.R., 2011. Black shales and massive sulfide deposits: causal or casual relationships? Insights from Rammelsberg, Tharsis, and Draa Sfar. Mineral. Depos. 46, 585–614.
Sánchez-España, J., Velasco, F., Yusta, I., 2000. Hydrothermal alteration of felsic volcanic rocks associated with massive sulphide deposition in the northern Iberian Pyrite Belt (SW Spain). Appl. Geochem. 15, 1265–1290.

Sato, K., Tassinari, C.G.C., Kawashita, K., Petronillo, L., 1995. O método geocronológico Sm-Nd no IG-USP e suas aplicações. Anais da Academia Brasileira de Ciências 67, 313–336.
Schermerhorn, L.J.G., 1971. An outline stratigraphy of the Iberian Pyrite Belt. Boletin Geológico y Minero 82 (3/4), 239–268.
Slack, J.F., Dumoulin, J.A., Schmidt, J.M., Young, L.E., Rombach, C.S., 2004. Paleozoic sedimentary rocks in the Red Dog Zn-Pb-Ah district and vicinity, western metallogenic significance. Econ. Geol. 99, 1385–1414.
Stacey, J.S., Kramers, J.D., 1975. Approximation of terrestrial lead isotope evolution by a two stage model. Earth Planet. Sci. Lett. 26, 207–221.
Silva, J.B., Oliveira, J.T., Ribeiro, A., 1990. Structural outline of the South Portuguese Zone. In: Dallmeyer, R.D., Martínez García, E. (Eds.), Pre-Mesozoic Geology of Iberia. Springer Berlin Heidelberg, Berlin pp. 348.362.
Simancas, J.F., Tahiri, A., Azor, A., Lodeiro, F.G., Poyatos, D.J.M., 2005. The tectonic frame of the Variscan-Alleghanian orogen in Southern Europe and Northern Africa. Tectonophysics 398, 181–198.
Soares, A., 2006. Geoestatística para as Ciências da Terra e do Ambiente. Eds: IST. Ensino da Ciência e da Tecnologia pp. 232.
Soriano, C., Martí, J., 1999. Facies Analysis of Volcano-Sedimentary Successions Hosting Massive Sulfide Deposits in the Iberian Pyrite Belt. Spain. Econ. Geol. 94, 867–882.
Taylor, S.R., McLennan, S.M., 1995. The geochemical evolution of the continental crust. Rev. Geophys. 33, 241–265.
Tornos, F., 2006. Environment of formation and styles of volcanogenic massive sulfides: The Iberian Pyrite Belt. Ore Geol. Rev. 28, 259–307.
Tornos, F., González-Clavijo, E., Spiro, B.F., 1998. The Filón Norte orebody (Tharsis, Iberian Pyrite Belt): a proximal low-temperature shale-hosted massive sulfide in a thin-skinned tectonic belt. Mineral. Depos. 33, 150–169.
Tornos, F., Spiro, B., 1999. The genesis of the shale hosted massive sulphides in the Iberian Pyrite Belt. In: Stanley, C.J. (Ed.), Mineral deposits: processes to processing. Balkema, Rotterdam, pp. 605–608.
Tornos, F., Barriga, F., Marcoux, E., Pascual, E., Pons, J.M., Relvas, J., Velasco, F., 2000. The Iberian Pyrite Belt. In: Large, R., Blundell, D. (Eds.), Database on global VMS districts. CODES-GEODE pp. 19–52.
F. Tornos C. Casquet J.M.R.S. Relvas F.J.A.S. Saéz 2002. The relationship between ore deposits in and oblique tectonics: the SW Iberian Variscan Belt D.R. Blundell F. Neubauer A. von Quadt The timing and location of major ore deposits in and evolving orogen. Geological Society London Special Publication London pp. 179–198.
Tornos, F., Heinrich, C.A., 2008. Shale basins, sulfure-deficient ore brines and the formation of exhalative base metals deposits. Chem. Geol. 247, 195–207.
Tornos, F., Solomon, M., Conde, C., Spiro, B., 2008. Formation of the tharsis massive sulfide deposit, Iberian pyrite belt: geological, lithogeochemical, and stable isotope evidence for a deposition in a brine pool. Econ. Geol. 103 (1), 185–214.
Tornos, F., Velasco, F., Slack, J.F., Delgado, A., Gomez-Miguelez, N., Escobar, J.M., Gomez, C., 2017. The high-grade Las Cruces copper deposit, Spain: a product of secondary enrichment in an evolving basin. Miner. Depos. 52, 1–34.
Turner, S., Foden, J., Sandiford, M., Bruce, D., 1993. Sm-Nd isotopic evidence for the provenance of sediments from the Adelaide Fold Belt and southeastern Australia with implications for episodic crustal addition. Geochim. Cosmochim. Acta 57 (1), 1837–1856.
Valenzuela, A., Donaire, T., Pascual, E., 2002. Secuencia de fácies volcânicas en el area del rio Odiel (Faja Piritica Iberica, España). Geogaceta 32, 131–134.
Valenzuela, A., Donaire, T., Pin, C., Toscano, M., Hamilton, M., Pascual, E., 2011. Geochemistry and U-Pb Dating of felsic volcanic rocks in the Rio Tinto-Nerva unit, Iberian Pyrite Belt, Spain: crustal thinning, progressive crustal melting and massive sulfide genesis. J. Geol. Soc. 168, 717–731.
van den Boogard, M., 1963. Conodonts of Upper Devonian and Lower Carboniferous age from Southern Portugal. Geologie en Mijnbow 42, 248–259.
Varnavas, P., Cronan, D.S., 1988. Arsenic, antimony and bismuth in sediments and waters from the Santorini hydrothermal field,. Greece. Chem. Geol. 67 (3–4), 295–305.
Yesares, L., Sáez, R., Nieto, J.M., Almodóvar, G.R., Gómez, C., Escobar, J.M., 2015. The Las Cruces deposit, Iberian Pyrite Belt, Spain. Ore Geol. Rev. 66, 25–46.
Young, G.M., Nesbitt, H.W., 1998. Processes controlling the distribution of Ti and AI in weathering profiles, siliciclastic sediments and sedimentary rocks. J. Sed. Res. 68 (3), 448–455.
Zartman, R.E., Doe, B.R., 1981. Plumbotectonics - the model. Tectonophysics 75, 135–162.
Zhao, J.X., McCulloch, M.T., Bennet, V.C., 1992. Sm-ND and U-Pb zircon isotopic constraints on the provenance of sediments from the Amadeus Basin, central Australia: evidence for REE fractionation. Geochim. Cosmochim. Acta. 56, 921–940.

Appendix 1.1

Supplementary material

Recognizing metasedimentary sequences potentially hosting concealed massive sulfide accumulations in the Iberian Pyrite Belt using geochemical fingerprints

Ore Geology Reviews - 2019

Filipa Luz
António Mateus
Jorge Figueiras
Colombo C.G. Tassinari
Ezequiel Ferreira
Luís Gonçalves

ALB03#22a (401.50 m): high resolution images of phosphate phases and associated minerals, and selected X-Ray elemental maps.

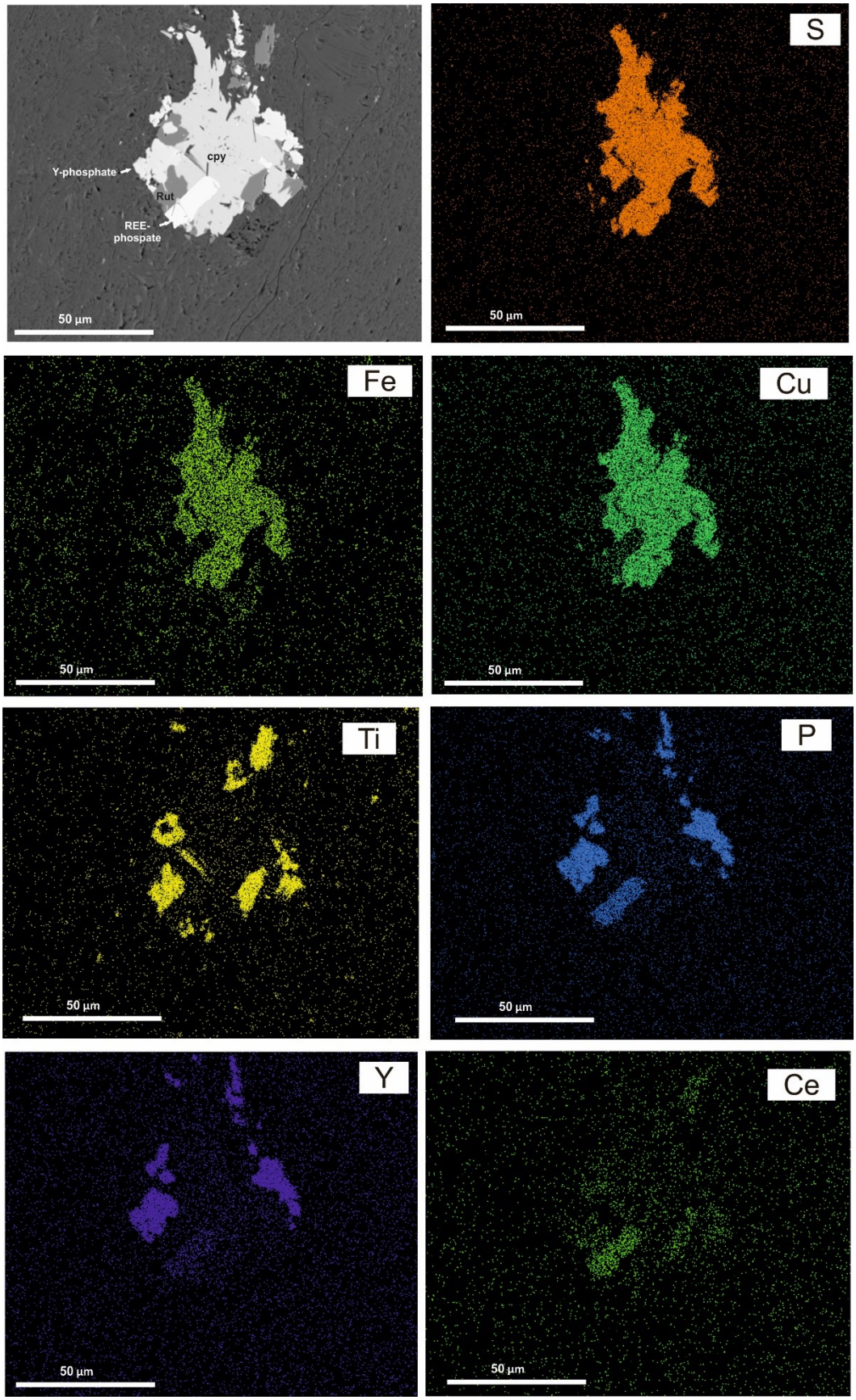

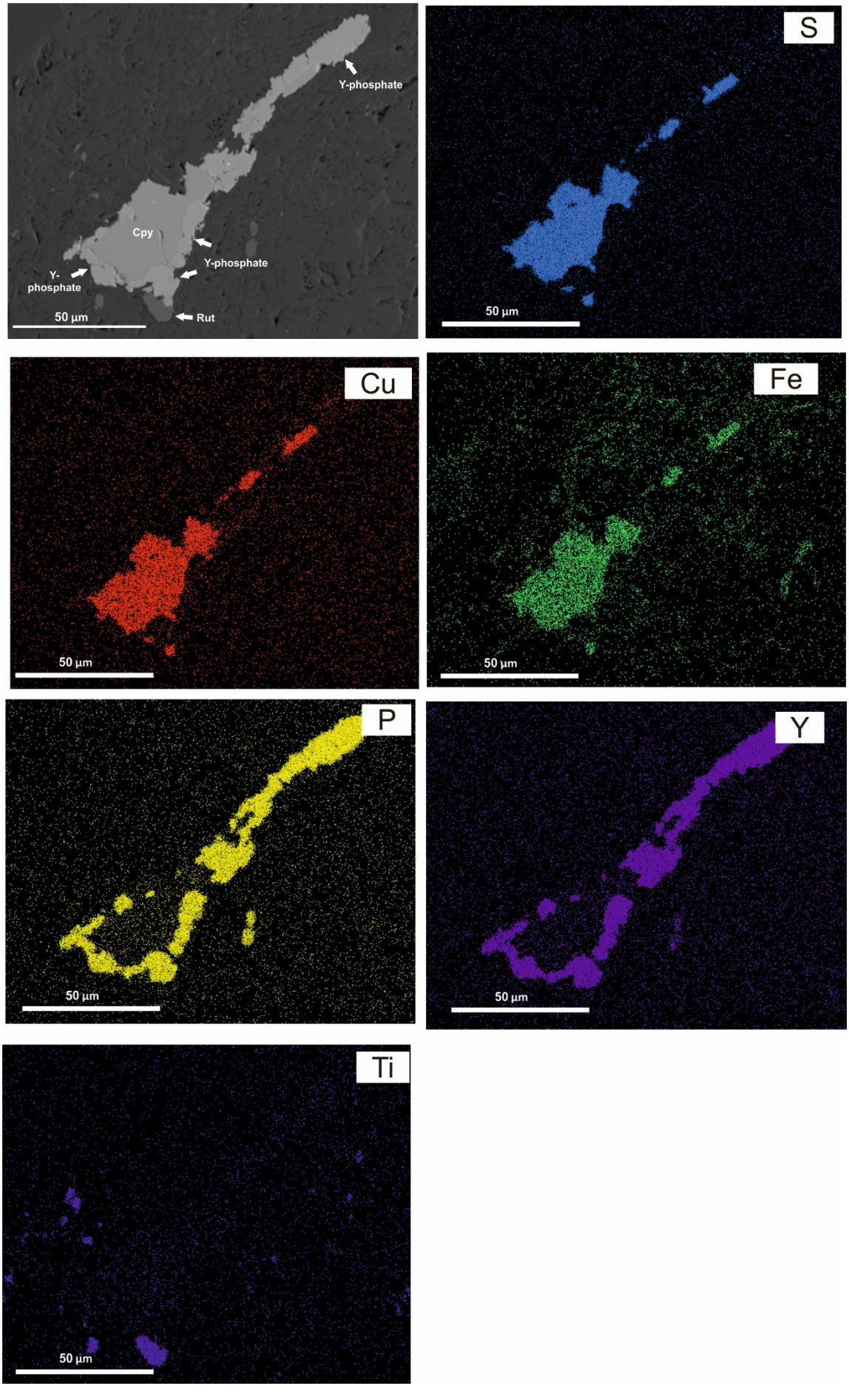
Y-phosphate
Cpy
Y-phosphate
Y-phosphate
Rut
50 µm
S
50 µm
Cu
50 µm
Fe
50 µm
P
50 µm
Y
50 µm
Ti
50 µm

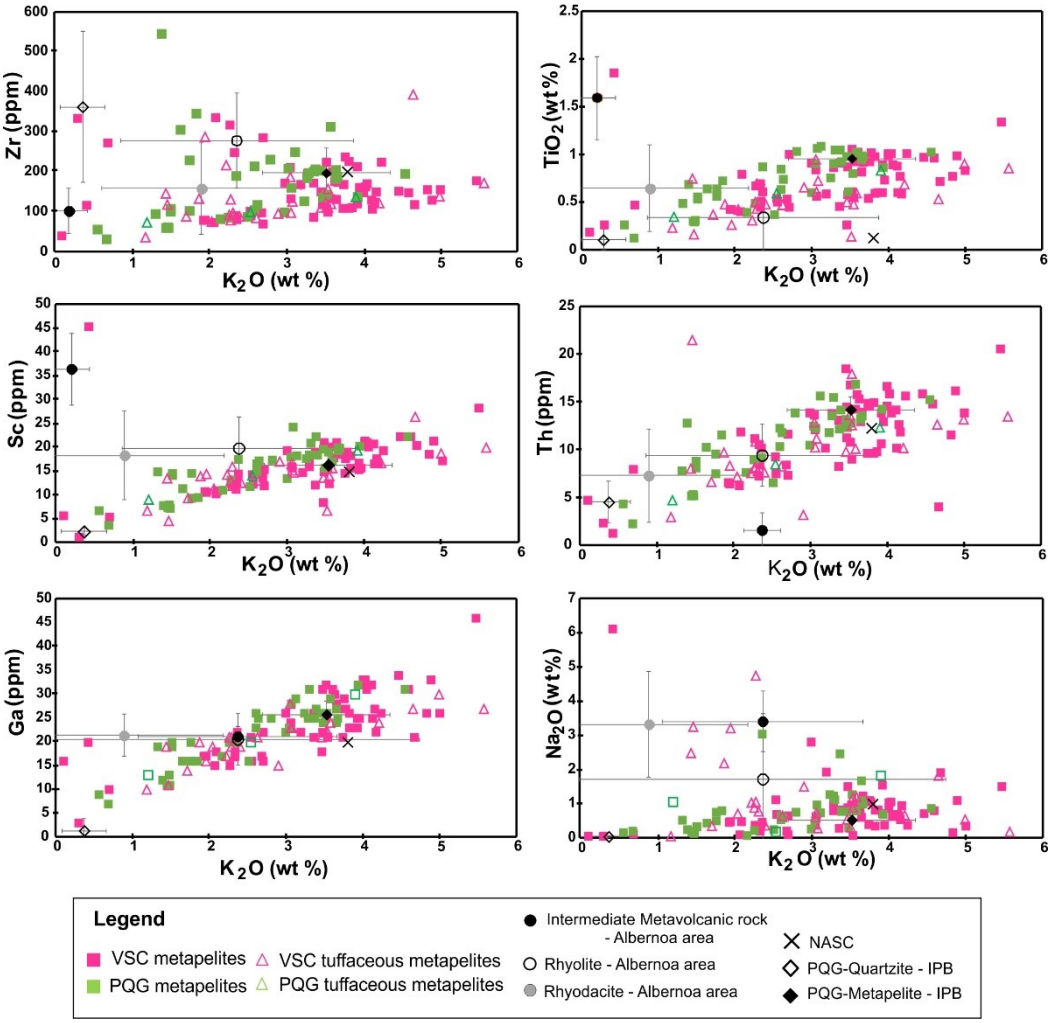

Representative co-variations between K_2O and other major, minor and trace elements for the Albernoa dataset. For reference, and besides the NASC (Condie, 1993), the average and standard deviation concentration measures calculated for PQQ-quartzite and metapelite (n=75; different sites of IPB; Jorge, 2009) and VSC-metavolcanic rocks of Albernoa (intermediate composition, n=9, rhyodacite, n=27, rhyolite, n=22; Codeço et al. 2018) are displayed.

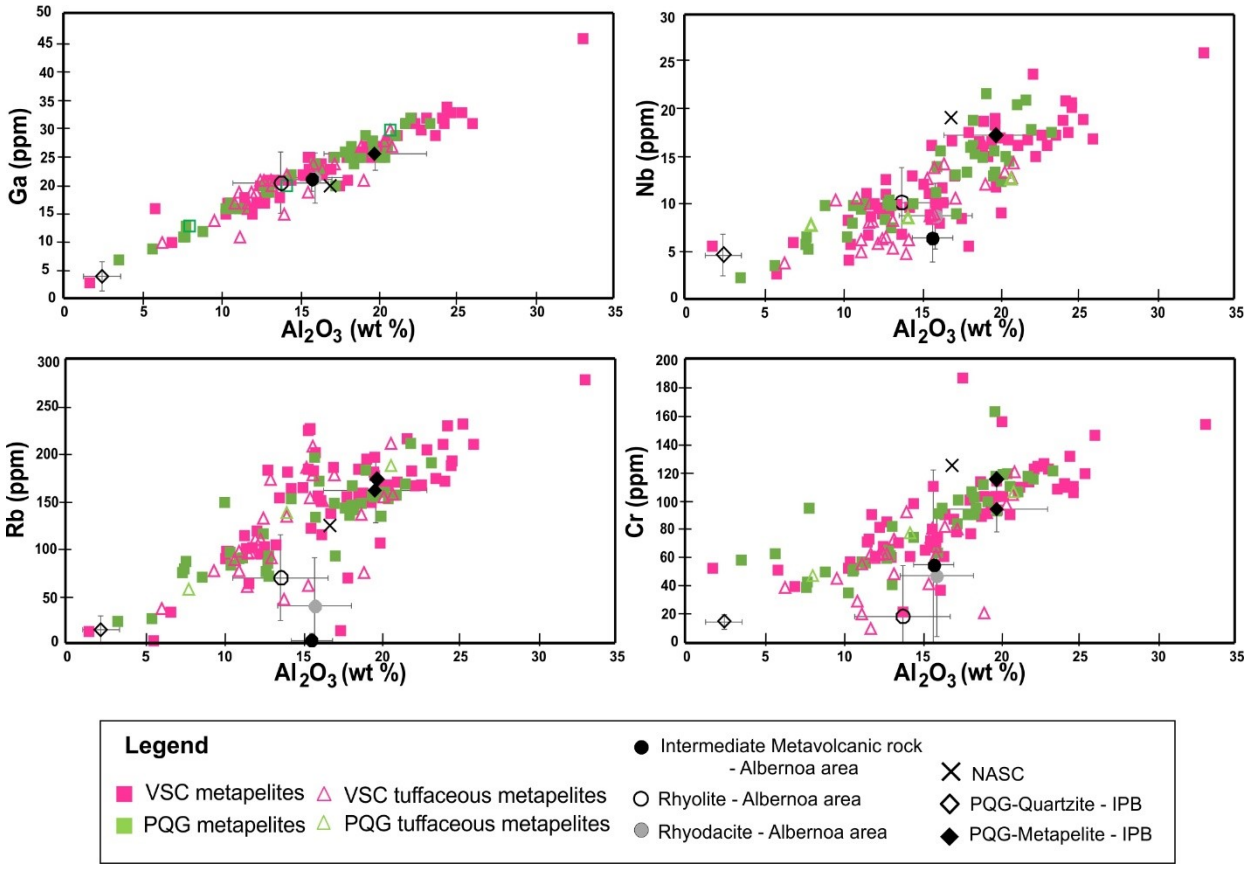

Representative co-variations (r≥0.75-1) between Al_2O_3 and minor/trace elements (Ga,Nb,Rb,Cr) for the Albernoa dataset. For reference, and besides the NASC (Condie, 1993), the average and standard deviation concentration measures calculated for PQQ-quartzite and metapelite (n=75; different sites of IPB; Jorge, 2009) and VSC-metavolcanic rocks of Albernoa (intermediate composition, n=9, rhyodacite, n=27, rhyolite, n=22; Codeço et al. 2018) are displayed.

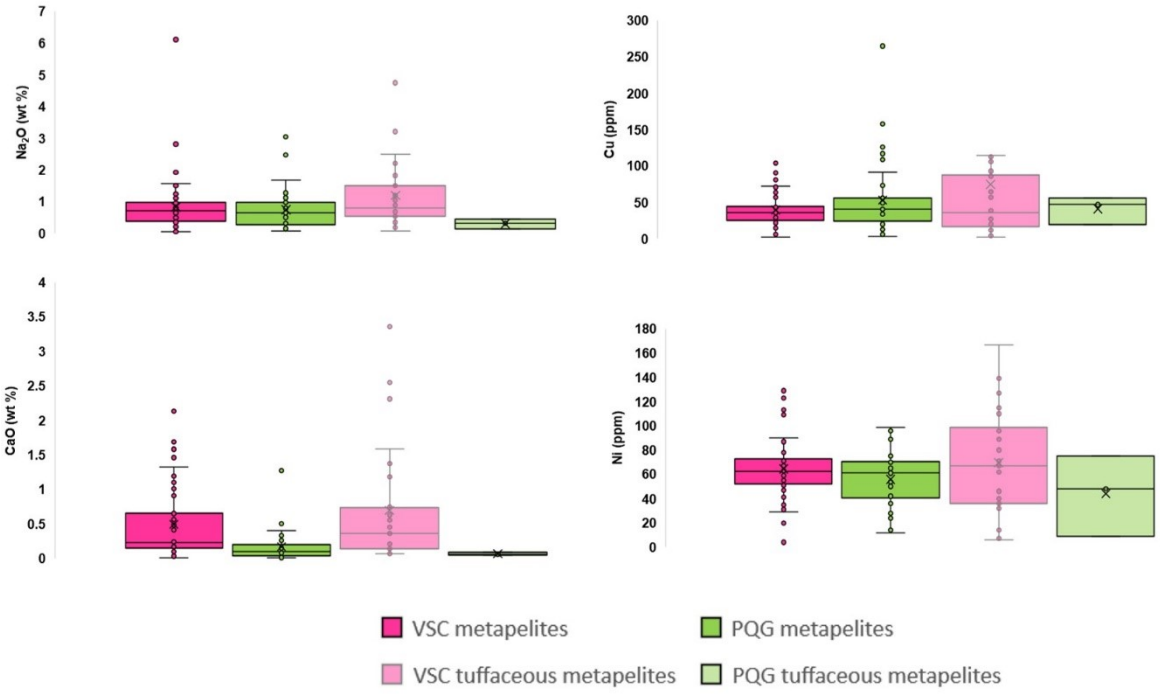

Selected boxplots illustrating similarities and minor deviations of element concentration from different rock types.

Correlation matrix for VSC metapelites (n=62)

VSC metapelites	SiO2	Al2O3	Fe2O3(T)	MnO	MgO	CaO	Na2O	K2O	TiO2	P2O5	Ba	Cs	Cu	Ga	Ge	Hf	Nb	Ni	Pb	Rb	S	Sr	Ta	Th	U	V	Y	Zr	La	Ce	Pr	Nd	Sm	Eu	Gd	Tb	Dy	Ho	Er	Tl	Tm	Yb	Lu	As	Co	Cr	Sb	Sc	Zn
SiO2	1.00																																																
Al2O3	-0.86	1.00																																																
Fe2O3(T)	-0.56	0.15	1.00																																														
MnO	0.19	-0.34	0.28	1.00																																													
MgO	-0.38	0.19	0.14	-0.22	1.00																																											
CaO	-0.01	-0.22	-0.01	0.30	0.45	1.00																																										
Na2O	-0.37	0.29	0.09	-0.06	0.52	0.33	1.00																																									
K2O	-0.63	0.77	-0.07	-0.29	0.13	-0.19	-0.05	1.00																																								
TiO2	-0.73	0.77	0.20	-0.38	0.31	0.06	0.61	0.36	1.00																																								
P2O5	-0.29	0.17	0.28	-0.05	0.28	0.28	0.26	-0.03	0.35	1.00																																							
Ba	-0.41	0.57	-0.07	-0.18	-0.23	-0.38	-0.08	0.75	0.18	-0.18	1.00																																						
Cs	-0.39	0.55	-0.03	-0.12	-0.15	-0.21	-0.01	0.67	0.25	-0.05	0.73	1.00																																					
Cu	0.09	-0.19	0.13	0.19	-0.06	-0.16	-0.24	-0.13	-0.27	-0.06	-0.10	-0.27	1.00																																				
Ga	-0.80	0.97	0.16	-0.22	0.04	-0.33	0.20	0.77	0.68	0.11	0.64	0.62	-0.14	1.00																																			
Ge	-0.15	0.34	0.04	0.39	-0.36	-0.39	-0.02	0.17	0.15	-0.10	0.34	0.33	0.05	0.47	1.00																																		
Hf	-0.07	0.15	-0.10	-0.33	-0.05	0.11	-0.03	0.01	0.37	0.20	-0.15	-0.09	-0.45	0.07	-0.10	1.00																																	
Nb	-0.68	0.84	0.13	-0.44	-0.07	-0.31	0.07	0.60	0.72	0.15	0.44	0.39	-0.17	0.82	0.23	0.40	1.00																																	
Ni	-0.05	-0.09	0.20	0.01	0.07	-0.08	-0.16	0.15	-0.24	-0.09	0.20	0.20	0.20	-0.03	-0.18	-0.50	-0.20	1.00																																	
Pb	-0.07	-0.24	0.42	0.13	0.18	0.01	0.29	-0.28	-0.21	0.35	-0.17	-0.16	0.24	-0.28	-0.25	-0.24	-0.21	0.15	1.00																																	
Rb	-0.53	0.74	-0.08	-0.23	-0.20	-0.34	-0.10	0.89	0.33	-0.11	0.87	0.81	-0.21	0.79	0.36	0.02	0.61	0.13	-0.33	1.00																																
S	-0.24	-0.14	0.63	-0.05	-0.03	0.03	-0.10	-0.10	-0.10	-0.03	-0.03	-0.03	0.13	-0.16	-0.38	-0.11	-0.08	0.35	0.37	-0.11	1.00																																
Sr	-0.66	0.68	0.27	-0.01	0.05	-0.04	0.46	0.31	0.69	0.18	0.32	0.43	-0.19	0.67	0.32	0.10	0.56	-0.20	-0.15	0.38	0.07	1.00																															
Ta	-0.66	0.83	0.09	-0.41	-0.08	-0.24	0.07	0.61	0.70	0.14	0.42	0.39	-0.19	0.80	0.21	0.45	0.95	-0.22	-0.25	0.59	-0.10	0.58	1.00																														
Th	-0.62	0.79	0.08	-0.27	-0.17	-0.24	-0.09	0.70	0.47	0.10	0.58	0.48	-0.18	0.80	0.32	0.39	0.82	-0.13	-0.24	0.73	-0.10	0.45	0.87	1.00																													
U	-0.38	0.17	0.41	-0.08	-0.10	0.02	-0.10	0.22	0.06	-0.01	0.22	0.18	0.17	0.17	-0.08	0.01	0.18	0.25	0.18	0.22	0.72	0.16	0.19	0.31	1.00																												
V	-0.68	0.59	0.29	-0.26	0.46	0.14	0.63	0.29	0.79	0.33	0.12	0.16	0.05	0.52	-0.01	-0.08	0.50	0.01	0.20	0.19	0.04	0.50	0.45	0.22	0.15	1.00																											
Y	-0.47	0.50	0.03	-0.20	0.12	0.20	0.26	0.42	0.45	0.53	0.26	0.20	-0.09	0.44	0.07	0.36	0.49	-0.09	0.12	0.38	-0.10	0.27	0.51	0.62	0.27	0.36	1.00																									
Zr	0.02	0.04	-0.11	-0.31	-0.08	0.14	-0.06	-0.07	0.29	0.18	-0.21	-0.15	-0.43	-0.05	-0.17	0.98	0.33	-0.47	-0.21	-0.07	-0.06	0.04	0.38	0.29	-0.01	-0.13	0.30	1.00																								
La	-0.62	0.79	0.11	-0.20	-0.24	-0.31	-0.13	0.73	0.41	0.10	0.67	0.58	-0.08	0.83	0.41	0.21	0.80	-0.02	-0.20	0.81	-0.11	0.44	0.81	0.94	0.28	0.23	0.58	0.13	1.00																							
Ce	-0.61	0.78	0.14	-0.21	-0.25	-0.32	-0.15	0.68	0.42	0.12	0.64	0.56	-0.13	0.82	0.40	0.26	0.79	0.01	-0.27	0.78	-0.09	0.42	0.80	0.95	0.28	0.19	0.56	0.17	0.98	1.00																						
Pr	-0.61	0.77	0.13	-0.22	-0.22	-0.29	-0.12	0.70	0.42	0.16	0.64	0.52	-0.07	0.80	0.38	0.23	0.78	-0.03	-0.15	0.78	-0.10	0.37	0.78	0.92	0.29	0.25	0.65	0.15	0.98	0.96	1.00																					
Nd	-0.61	0.75	0.12	-0.23	-0.20	-0.25	-0.10	0.69	0.43	0.20	0.62	0.49	-0.04	0.78	0.37	0.22	0.78	-0.04	-0.13	0.75	-0.10	0.37	0.76	0.89	0.31	0.29	0.69	0.14	0.96	0.94	0.99	1.00																				
Sm	-0.57	0.68	0.14	-0.22	-0.13	-0.17	-0.03	0.62	0.42	0.32	0.52	0.43	-0.07	0.69	0.30	0.24	0.67	-0.02	-0.04	0.68	-0.08	0.29	0.65	0.80	0.29	0.29	0.80	0.16	0.86	0.85	0.94	0.96	1.00																			
Eu	-0.66	0.70	0.28	-0.23	0.06	-0.07	0.13	0.52	0.58	0.48	0.37	0.40	-0.14	0.68	0.25	0.25	0.68	0.03	-0.02	0.53	-0.07	0.40	0.65	0.68	0.17	0.46	0.74	0.19	0.74	0.75	0.82	0.84	0.90	1.00																		
Gd	-0.54	0.59	0.15	-0.19	-0.01	0.00	0.09	0.49	0.42	0.50	0.35	0.30	-0.06	0.57	0.19	0.26	0.58	-0.05	0.06	0.50	-0.09	0.26	0.56	0.70	0.26	0.32	0.90	0.19	0.74	0.72	0.82	0.86	0.95	0.90	1.00																	
Tb	-0.56	0.61	0.11	-0.23	0.03	0.04	0.14	0.51	0.48	0.52	0.34	0.30	-0.11	0.58	0.18	0.32	0.60	-0.08	0.04	0.50	-0.10	0.30	0.59	0.71	0.25	0.35	0.93	0.24	0.73	0.71	0.81	0.84	0.93	0.89	0.99	1.00																
Dy	-0.54	0.58	0.11	-0.22	0.05	0.08	0.16	0.48	0.47	0.53	0.32	0.28	-0.13	0.54	0.15	0.36	0.57	-0.10	0.04	0.47	-0.11	0.29	0.57	0.70	0.24	0.33	0.95	0.29	0.70	0.69	0.78	0.81	0.91	0.87	0.98	0.99	1.00														
Ho	-0.52	0.57	0.05	-0.22	0.08	0.12	0.22	0.48	0.48	0.51	0.31	0.25	-0.13	0.52	0.13	0.36	0.54	-0.10	0.08	0.46	-0.13	0.27	0.55	0.68	0.22	0.36	0.97	0.29	0.66	0.65	0.75	0.78	0.88	0.83	0.96	0.98	0.99	1.00												
Er	-0.52	0.58	0.04	-0.22	0.09	0.12	0.24	0.49	0.48	0.45	0.32	0.24	-0.14	0.52	0.13	0.37	0.55	-0.12	0.06	0.46	-0.14	0.27	0.57	0.69	0.24	0.36	0.97	0.30	0.66	0.64	0.75	0.78	0.88	0.81	0.94	0.96	0.98	0.99	1.00										
Tl	-0.13	0.26	-0.15	0.27	-0.37	-0.24	-0.13	0.62	-0.08	-0.36	0.73	0.65	-0.15	0.40	0.30	-0.15	0.16	0.22	-0.16	0.78	0.07	0.23	0.17	0.35	0.28	-0.09	0.07	-0.19	0.42	0.36	0.37	0.35	0.28	0.04	0.09	0.07	0.04	0.06	0.09	1.00								
Tm	-0.54	0.61	0.01	-0.24	0.11	0.11	0.26	0.53	0.50	0.39	0.36	0.26	-0.14	0.56	0.11	0.39	0.59	-0.14	0.03	0.49	-0.13	0.32	0.61	0.72	0.26	0.38	0.96	0.30	0.69	0.66	0.76	0.78	0.86	0.78	0.92	0.94	0.95	0.97	0.99	0.16	1.00							
Yb	-0.55	0.60	0.02	-0.23	0.10	0.11	0.28	0.54	0.53	0.37	0.37	0.27	-0.17	0.56	0.11	0.40	0.59	-0.13	0.02	0.51	-0.12	0.31	0.59	0.70	0.23	0.39	0.95	0.32	0.66	0.64	0.74	0.76	0.85	0.77	0.89	0.92	0.94	0.96	0.98	0.19	0.99	1.00					
Lu	-0.49	0.55	0.00	-0.22	0.08	0.09	0.26	0.50	0.48	0.32	0.36	0.27	-0.19	0.52	0.11	0.42	0.54	-0.11	0.02	0.50	-0.13	0.26	0.56	0.69	0.23	0.34	0.93	0.34	0.65	0.63	0.73	0.75	0.84	0.74	0.88	0.90	0.92	0.95	0.96	0.21	0.97	0.98	1.00				
As	-0.20	-0.09	0.44	-0.03	0.01	0.06	-0.13	-0.01	-0.06	-0.03	-0.07	-0.02	0.30	-0.11	-0.35	-0.08	0.00	0.43	0.41	-0.05	0.67	-0.03	-0.03	-0.02	0.60	0.10	-0.02	-0.05	-0.02	0.00	0.00	0.00	0.01	-0.02	0.00	-0.02	-0.02	-0.04	-0.06	0.08	-0.06	-0.05	-0.03	1.00			
Co	-0.31	0.07	0.43	-0.11	0.11	0.02	-0.06	0.15	-0.01	0.00	0.14	0.22	0.19	0.07	-0.29	-0.28	-0.02	0.71	0.33	0.13	0.65	0.07	-0.02	0.03	0.58	0.15	-0.05	-0.26	0.09	0.12	0.07	0.05	0.05	0.09	0.01	-0.01	-0.03	-0.04	-0.07	0.16	-0.07	-0.06	-0.06	0.79	1.00		
Cr	-0.75	0.75	0.32	-0.32	0.27	-0.09	0.52	0.35	0.88	0.33	0.21	0.24	-0.11	0.69	0.18	0.17	0.69	-0.17	0.08	0.32	-0.04	0.61	0.64	0.42	0.07	0.80	0.33	0.11	0.44	0.43	0.45	0.46	0.42	0.60	0.41	0.44	0.41	0.40	0.39	-0.09	0.40	0.41	0.35	-0.01	0.06	1.00	
Sb	-0.23	-0.09	0.44	-0.01	0.05	0.21	0.08	-0.05	0.02	-0.01	-0.06	0.01	0.11	-0.12	-0.42	-0.17	-0.09	0.30	0.37	-0.07	0.77	0.13	-0.12	-0.17	0.53	0.19	-0.08	-0.14	-0.15	-0.17	-0.15	-0.15	-0.12	-0.08	-0.10	-0.11	-0.11	-0.11	-0.12	0.10	-0.12	-0.07	-0.09	0.73	0.72	0.05	1.00	
Sc	-0.77	0.75	0.22	-0.25	0.43	0.13	0.74	0.41	0.90	0.32	0.28	0.32	-0.18	0.68	0.17	0.02	0.53	-0.07	-0.18	0.37	-0.08	0.68	0.49	0.33	0.06	0.83	0.38	-0.07	0.32	0.31	0.32	0.34	0.34	0.50	0.36	0.40	0.39	0.41	0.41	0.05	0.43	0.46	0.40	-0.07	0.08	0.83	0.10	1.00	
Zn	-0.52	0.44	0.49	-0.15	0.17	-0.18	0.16	0.24	0.32	0.25	0.32	0.27	-0.29	0.42	0.13	0.00	0.31	0.30	0.20	0.33	0.13	0.20	0.29	0.37	0.08	0.25	0.24	-0.07	0.40	0.46	0.41	0.38	0.40	0.48	0.35	0.36	0.35	0.32	0.30	-0.01	0.28	0.29	0.30	0.00	0.26	0.34	-0.08	0.35	1.00

Correlation matrix for PQG metapelites (n=42)

PQG metapelites	SiO2	Al2O3	Fe2O3(T)	MnO	MgO	CaO	Na2O	K2O	TiO2	P2O5	Ba	Ce	Cu	Ga	Ge	Hf	Nb	Ni	Pb	Rb	S	Sr	Ta	Th	U	V	Y	Zr	La	Ce	Pr	Nd	Sm	Eu	Gd	Tb	Dy	Ho	Er	Tl	Tm	Yb	Lu	As	Co	Cr	Sb	Sc	Zn
SiO2	1.00																																																
Al2O3	-0.97	1.00																																																
Fe2O3(T)	-0.63	0.44	1.00																																														
MnO	-0.03	0.00	0.10	1.00																																													
MgO	-0.72	0.67	0.48	0.02	1.00																																											
CaO	-0.39	0.37	0.23	-0.03	0.48	1.00																																										
Na2O	-0.57	0.58	0.19	-0.06	0.61	0.84	1.00																																									
K2O	-0.83	0.91	0.23	0.12	0.47	0.27	0.46	1.00																																								
TiO2	-0.87	0.91	0.35	-0.10	0.60	0.40	0.61	0.81	1.00																																								
P2O5	-0.62	0.61	0.31	-0.07	0.66	0.61	0.75	0.46	0.78	1.00																																							
Ba	-0.79	0.86	0.24	0.17	0.36	0.16	0.35	0.93	0.74	0.36	1.00																																						
Ce	-0.79	0.87	0.27	0.11	0.44	0.28	0.43	0.92	0.79	0.48	0.84	1.00																																					
Cu	-0.12	0.09	0.03	-0.02	0.42	-0.08	0.04	-0.03	-0.07	-0.08	-0.02	-0.06	1.00																																				
Ga	-0.94	0.97	0.43	0.00	0.59	0.21	0.44	0.90	0.85	0.50	0.86	0.85	0.12	1.00																																			
Ge	0.05	-0.13	0.17	-0.19	-0.10	-0.39	-0.44	-0.20	-0.09	-0.17	-0.05	-0.25	0.05	0.00	1.00																																		
Hf	-0.17	0.21	-0.02	-0.09	0.09	0.13	0.18	0.18	0.52	0.51	0.20	0.22	-0.26	0.16	0.19	1.00																																	
Nb	-0.82	0.89	0.31	-0.10	0.41	0.12	0.36	0.82	0.89	0.53	0.79	0.80	-0.04	0.91	-0.02	0.40	1.00																																	
Ni	-0.59	0.49	0.52	0.21	0.67	0.10	0.19	0.37	0.25	0.18	0.35	0.33	0.45	0.52	0.13	-0.29	0.21	1.00																																	
Pb	0.27	-0.18	-0.24	0.20	-0.20	-0.29	-0.19	0.04	-0.24	-0.29	0.11	0.10	-0.06	-0.17	-0.16	-0.14	-0.20	-0.10	1.00																																	
Rb	-0.78	0.85	0.22	0.18	0.33	0.08	0.26	0.94	0.72	0.29	0.94	0.86	-0.02	0.89	-0.01	0.15	0.81	0.36	0.06	1.00																																
S	0.21	-0.15	-0.24	-0.16	-0.10	0.13	0.08	-0.16	-0.13	0.11	-0.27	-0.06	-0.20	-0.20	-0.31	-0.17	-0.16	0.13	0.08	-0.26	1.00																															
Sr	-0.50	0.55	0.10	0.22	0.35	0.27	0.42	0.49	0.52	0.42	0.48	0.48	-0.08	0.52	-0.30	0.13	0.50	0.15	0.10	0.43	0.27	1.00																													
Ta	-0.78	0.84	0.29	-0.13	0.39	0.18	0.36	0.77	0.90	0.62	0.74	0.78	-0.10	0.84	0.05	0.52	0.95	0.15	-0.23	0.74	-0.16	0.47	1.00																													
Th	-0.81	0.88	0.30	-0.08	0.45	0.20	0.40	0.83	0.93	0.60	0.81	0.83	-0.10	0.87	0.03	0.59	0.94	0.20	-0.13	0.81	-0.22	0.47	0.94	1.00																												
U	-0.61	0.55	0.56	-0.26	0.36	0.30	0.40	0.40	0.68	0.65	0.33	0.45	-0.23	0.50	0.05	0.41	0.60	0.00	-0.43	0.33	-0.04	0.34	0.65	0.62	1.00																											
V	-0.54	0.51	0.30	-0.28	0.43	0.25	0.36	0.47	0.43	0.32	0.33	0.44	0.19	0.50	-0.14	-0.19	0.37	0.30	-0.10	0.40	-0.12	0.11	0.32	0.32	0.42	1.00																										
Y	-0.71	0.74	0.36	-0.01	0.45	0.24	0.43	0.67	0.88	0.69	0.64	0.73	-0.14	0.70	0.01	0.68	0.80	0.10	-0.11	0.63	-0.19	0.52	0.84	0.90	0.71	0.25	1.00																									
Zr	-0.20	0.25	-0.01	-0.09	0.11	0.15	0.22	0.21	0.55	0.53	0.21	0.28	-0.26	0.19	0.11	0.99	0.43	-0.29	-0.12	0.17	-0.14	0.17	0.54	0.62	0.43	-0.18	0.72	1.00																								
La	-0.77	0.86	0.26	0.02	0.48	0.18	0.38	0.83	0.82	0.50	0.82	0.81	0.02	0.85	-0.04	0.47	0.86	0.26	0.00	0.80	-0.25	0.51	0.84	0.93	0.47	0.26	0.84	0.50	1.00																							
Ce	-0.77	0.86	0.20	0.03	0.49	0.21	0.42	0.84	0.84	0.53	0.81	0.83	0.03	0.84	-0.10	0.50	0.87	0.29	-0.11	0.79	-0.22	0.46	0.86	0.94	0.44	0.25	0.81	0.53	0.97	1.00																						
Pr	-0.76	0.84	0.24	0.04	0.45	0.15	0.36	0.81	0.86	0.54	0.81	0.81	-0.07	0.84	0.00	0.57	0.89	0.21	-0.08	0.80	-0.25	0.51	0.88	0.96	0.52	0.19	0.90	0.60	0.96	0.96	1.00																					
Nd	-0.75	0.83	0.24	0.08	0.45	0.18	0.39	0.80	0.85	0.55	0.80	0.81	-0.08	0.82	-0.03	0.58	0.88	0.19	-0.09	0.79	-0.26	0.52	0.86	0.95	0.53	0.18	0.90	0.61	0.95	0.96	1.00	1.00																			
Sm	-0.75	0.81	0.26	0.13	0.48	0.23	0.41	0.78	0.88	0.63	0.77	0.79	-0.11	0.80	-0.03	0.61	0.86	0.21	-0.15	0.76	-0.22	0.55	0.86	0.94	0.57	0.17	0.93	0.64	0.92	0.92	0.98	0.99	1.00																		
Eu	-0.78	0.82	0.35	0.10	0.53	0.28	0.46	0.75	0.87	0.66	0.73	0.79	-0.09	0.80	-0.04	0.56	0.83	0.28	-0.14	0.72	-0.18	0.56	0.83	0.92	0.59	0.22	0.93	0.60	0.90	0.90	0.95	0.96	0.97	1.00																	
Gd	-0.74	0.78	0.35	0.09	0.47	0.21	0.39	0.70	0.86	0.65	0.71	0.74	-0.12	0.76	0.00	0.63	0.84	0.18	-0.18	0.70	-0.18	0.58	0.84	0.91	0.62	0.15	0.95	0.66	0.87	0.85	0.95	0.95	0.97	0.97	1.00															
Tb	-0.72	0.75	0.38	0.05	0.45	0.15	0.34	0.65	0.85	0.62	0.67	0.69	-0.10	0.74	0.09	0.66	0.83	0.15	-0.21	0.67	-0.22	0.55	0.83	0.91	0.64	0.16	0.96	0.69	0.86	0.82	0.93	0.93	0.96	0.95	0.99	1.00														
Dy	-0.73	0.75	0.40	0.03	0.45	0.17	0.35	0.66	0.87	0.65	0.66	0.70	-0.11	0.74	0.09	0.66	0.82	0.15	-0.19	0.66	-0.21	0.53	0.84	0.91	0.68	0.20	0.98	0.69	0.85	0.82	0.92	0.92	0.95	0.95	0.98	0.99	1.00												
Ho	-0.73	0.75	0.37	0.02	0.45	0.17	0.37	0.67	0.88	0.65	0.66	0.71	-0.10	0.74	0.08	0.66	0.83	0.14	-0.16	0.67	-0.23	0.52	0.85	0.91	0.68	0.24	0.98	0.69	0.85	0.82	0.92	0.91	0.94	0.94	0.96	0.98	0.99	1.00										
Er	-0.73	0.75	0.36	0.00	0.46	0.18	0.39	0.68	0.88	0.66	0.68	0.71	-0.08	0.74	0.06	0.66	0.83	0.13	-0.14	0.67	-0.24	0.51	0.85	0.92	0.68	0.24	0.99	0.69	0.86	0.83	0.92	0.92	0.94	0.94	0.97	0.98	0.99	1.00	1.00									
Tl	-0.60	0.67	0.14	0.33	0.23	0.01	0.16	0.79	0.50	0.11	0.84	0.73	0.08	0.72	-0.13	0.00	0.62	0.31	0.11	0.88	-0.31	0.46	0.53	0.61	0.15	0.26	0.48	0.02	0.65	0.62	0.66	0.66	0.63	0.59	0.59	0.54	0.52	0.54	0.54	1.00							
Tm	-0.71	0.74	0.34	-0.01	0.43	0.19	0.37	0.68	0.88	0.64	0.67	0.72	-0.11	0.72	0.06	0.68	0.82	0.11	-0.12	0.67	-0.24	0.49	0.86	0.92	0.69	0.23	0.98	0.70	0.85	0.83	0.92	0.92	0.94	0.93	0.96	0.97	0.99	0.99	1.00	0.53	1.00						
Yb	-0.73	0.76	0.34	-0.01	0.46	0.19	0.38	0.71	0.89	0.64	0.70	0.73	-0.07	0.75	0.09	0.66	0.83	0.17	-0.11	0.70	-0.27	0.48	0.86	0.93	0.65	0.27	0.97	0.68	0.86	0.84	0.92	0.91	0.94	0.92	0.95	0.96	0.98	0.99	0.99	0.56	0.99	1.00					
Lu	-0.75	0.77	0.35	0.00	0.49	0.23	0.44	0.71	0.91	0.69	0.68	0.72	-0.07	0.74	0.06	0.67	0.82	0.17	-0.13	0.68	-0.25	0.47	0.85	0.92	0.68	0.30	0.97	0.69	0.84	0.83	0.90	0.90	0.93	0.92	0.93	0.94	0.97	0.98	0.98	0.50	0.98	0.99	1.00				
As	0.18	-0.19	0.04	-0.24	-0.23	0.06	0.08	-0.25	-0.09	0.11	-0.24	-0.17	-0.44	-0.25	-0.01	0.14	-0.11	-0.36	-0.36	-0.35	0.20	-0.14	-0.04	-0.11	0.17	-0.26	-0.06	0.15	-0.11	-0.11	-0.12	-0.11	-0.11	-0.08	-0.07	-0.09	-0.09	-0.11	-0.10	-0.45	-0.12	-0.16	-0.10	1.00			
Co	-0.62	0.55	0.43	0.24	0.65	0.23	0.32	0.44	0.37	0.32	0.44	0.40	0.39	0.54	0.03	-0.10	0.32	0.83	-0.03	0.38	0.26	0.24	0.28	0.31	0.03	0.17	0.21	-0.09	0.36	0.43	0.33	0.32	0.32	0.36	0.28	0.25	0.26	0.22	0.23	0.18	0.21	0.25	0.27	-0.24	1.00		
Cr	-0.80	0.81	0.33	-0.21	0.57	0.37	0.55	0.72	0.81	0.64	0.61	0.68	0.03	0.77	-0.11	0.15	0.69	0.36	-0.20	0.63	0.03	0.43	0.67	0.66	0.59	0.76	0.58	0.16	0.54	0.54	0.54	0.53	0.55	0.56	0.54	0.53	0.56	0.57	0.57	0.39	0.56	0.60	0.62	-0.19	0.38	1.00		
Sb	0.13	-0.24	0.38	-0.16	-0.26	0.18	-0.07	-0.26	-0.21	-0.10	-0.30	-0.13	-0.23	-0.26	-0.10	-0.19	-0.23	-0.24	0.11	-0.28	0.14	-0.17	-0.22	-0.24	0.29	0.29	-0.10	-0.17	-0.30	-0.38	-0.34	-0.34	-0.33	-0.23	-0.22	-0.20	-0.15	-0.14	-0.13	-0.27	-0.13	-0.16	-0.13	0.26	-0.34	-0.03	1.00	
Sc	-0.96	0.96	0.51	0.05	0.75	0.38	0.60	0.86	0.87	0.64	0.79	0.79	0.17	0.94	-0.10	0.13	0.79	0.59	-0.28	0.80	-0.17	0.52	0.74	0.78	0.55	0.57	0.68	0.15	0.76	0.76	0.75	0.74	0.75	0.77	0.72	0.70	0.71	0.71	0.71	0.64	0.69	0.73	0.74	-0.24	0.59	0.83	-0.21	1.00
Zn	-0.77	0.66	0.71	0.12	0.77	0.24	0.33	0.44	0.58	0.53	0.47	0.40	0.25	0.66	0.29	0.14	0.50	0.80	-0.30	0.44	-0.20	0.28	0.50	0.52	0.42	0.20	0.50	0.15	0.51	0.50	0.51	0.50	0.53	0.58	0.56	0.55	0.55	0.52	0.52	0.31	0.50	0.52	0.52	-0.13	0.75	0.46	-0.30	0.71

Correlation matrix for VSC tuffaceous metapelites (n=27)

VSC tuffaceous metapelites	SiO2	Al2O3	Fe2O3(T)	MnO	MgO	CaO	Na2O	K2O	TiO2	P2O5	Ba	Cs	Cu	Ga	Ge	Hf	Nb	Ni	Pb	Rb	S	Sr	Ta	Th	U	V	Y	Zr	La	Ce	Pr	Nd	Sm	Eu	Gd	Tb	Dy	Ho	Er	Tl	Tm	Yb	Lu	As	Co	Cr	Sb	Sc	Zn
SiO2	1.00																																																
Al2O3	-0.82	1.00																																																
Fe2O3(T)	-0.75	0.39	1.00																																														
MnO	-0.11	-0.07	0.33	1.00																																													
MgO	-0.41	0.00	0.36	-0.11	1.00																																												
CaO	-0.43	-0.08	0.45	0.18	0.76	1.00																																											
Na2O	-0.25	0.10	0.15	0.16	0.10	0.21	1.00																																										
K2O	-0.63	0.77	0.27	-0.13	0.09	-0.05	-0.33	1.00																																									
TiO2	-0.72	0.81	0.51	-0.08	0.02	-0.03	-0.08	0.54	1.00																																									
P2O5	-0.70	0.56	0.55	0.04	0.30	0.33	0.25	0.30	0.58	1.00																																								
Ba	-0.10	0.41	-0.08	0.08	-0.29	-0.39	-0.44	0.58	0.31	-0.06	1.00																																							
Cs	-0.14	0.28	0.17	0.04	-0.12	-0.25	-0.31	0.51	0.18	0.06	0.65	1.00																																						
Cu	0.17	-0.12	-0.11	0.33	-0.02	-0.17	-0.12	-0.11	0.00	-0.21	0.36	0.16	1.00																																					
Ga	-0.63	0.88	0.28	0.04	-0.16	-0.20	-0.22	0.82	0.72	0.35	0.66	0.47	0.02	1.00																																				
Ge	-0.02	0.38	-0.05	0.19	-0.61	-0.47	-0.36	0.21	0.55	0.10	0.58	0.28	0.26	0.55	1.00																																				
Hf	-0.40	0.40	0.00	-0.10	0.12	0.24	0.34	0.33	0.03	0.38	-0.01	-0.06	-0.20	0.33	-0.19	1.00																																				
Nb	-0.63	0.72	0.32	-0.04	-0.08	0.06	0.04	0.59	0.55	0.44	0.31	0.20	-0.14	0.64	0.25	0.54	1.00																																				
Ni	-0.03	-0.02	0.25	0.36	-0.02	-0.07	-0.20	0.06	0.13	-0.18	0.34	0.42	0.31	0.15	0.25	-0.50	-0.12	1.00																																				
Pb	0.24	-0.28	-0.23	0.22	-0.02	-0.11	0.17	-0.25	-0.29	-0.24	0.05	-0.09	0.74	-0.18	0.05	0.12	-0.30	-0.01	1.00																																				
Rb	-0.33	0.62	0.11	0.07	-0.33	-0.32	-0.41	0.79	0.46	0.13	0.77	0.73	-0.01	0.80	0.60	0.07	0.48	0.28	-0.24	1.00																																				
S	-0.51	0.43	0.47	-0.11	0.15	0.05	0.15	0.38	0.35	0.08	-0.05	-0.08	-0.01	0.22	-0.20	0.09	0.31	-0.03	-0.17	0.00	1.00																																				
Sr	-0.42	0.57	0.12	-0.04	-0.13	-0.12	0.61	0.07	0.48	0.50	0.04	0.03	-0.17	0.29	0.25	0.26	0.32	-0.14	-0.09	0.11	0.03	1.00																																				
Ta	-0.56	0.66	0.28	0.04	-0.09	0.06	0.07	0.59	0.42	0.40	0.21	0.15	-0.16	0.56	0.18	0.50	0.87	-0.12	-0.35	0.49	0.33	0.29	1.00																																				
Th	-0.18	0.47	-0.18	0.14	-0.35	-0.32	0.20	0.39	0.05	0.10	0.29	0.21	-0.11	0.36	0.21	0.34	0.46	-0.05	-0.24	0.49	0.13	0.40	0.62	1.00																																				
U	-0.03	0.26	-0.19	0.18	-0.35	-0.33	0.19	0.14	-0.03	-0.03	0.16	0.13	0.00	0.16	0.20	0.03	0.14	0.14	-0.10	0.33	0.09	0.23	0.22	0.80	1.00																																				
V	-0.34	0.35	0.45	-0.08	0.07	-0.12	-0.33	0.29	0.72	0.16	0.25	0.27	0.21	0.33	0.40	-0.55	0.15	0.48	-0.15	0.32	0.26	0.08	0.07	-0.24	-0.14	1.00																																				
Y	-0.30	0.28	-0.03	-0.03	0.20	0.30	0.07	0.40	-0.12	0.33	0.08	0.06	-0.25	0.33	-0.20	0.89	0.41	-0.47	0.01	0.17	-0.11	0.01	0.44	0.28	-0.04	-0.61	1.00																																				
Zr	-0.46	0.41	0.14	-0.05	0.15	0.31	0.33	0.35	0.09	0.46	-0.03	-0.02	-0.20	0.35	-0.19	0.97	0.57	-0.43	0.08	0.09	0.10	0.23	0.57	0.26	-0.09	-0.46	0.87	1.00																																				
La	-0.23	0.52	0.03	0.33	-0.57	-0.34	0.08	0.45	0.27	0.13	0.46	0.41	-0.11	0.55	0.53	0.29	0.51	0.08	-0.24	0.69	0.02	0.41	0.63	0.78	0.51	-0.04	0.25	0.29	1.00																																				
Ce	-0.19	0.49	-0.01	0.28	-0.54	-0.38	-0.01	0.49	0.25	0.08	0.52	0.50	-0.02	0.60	0.53	0.28	0.53	0.28	-0.19	0.74	-0.03	0.29	0.64	0.75	0.50	0.01	0.25	0.30	0.94	1.00																																				
Pr	-0.25	0.52	-0.03	0.30	-0.53	-0.28	0.09	0.47	0.22	0.16	0.42	0.38	-0.13	0.57	0.47	0.44	0.55	0.00	-0.20	0.66	-0.01	0.38	0.65	0.80	0.52	-0.17	0.40	0.43	0.98	0.93	1.00																																				
Nd	-0.28	0.52	-0.01	0.29	-0.46	-0.19	0.09	0.47	0.21	0.21	0.38	0.35	-0.15	0.56	0.42	0.55	0.60	-0.07	-0.19	0.62	-0.03	0.34	0.68	0.77	0.45	-0.24	0.52	0.54	0.94	0.90	0.99	1.00																																				
Sm	-0.24	0.44	-0.11	0.21	-0.30	-0.06	0.13	0.41	0.06	0.26	0.27	0.23	-0.21	0.49	0.25	0.74	0.50	-0.24	-0.08	0.48	-0.14	0.28	0.57	0.68	0.41	-0.48	0.75	0.71	0.77	0.74	0.88	0.92	1.00																																				
Eu	-0.50	0.48	0.38	0.15	-0.16	0.19	-0.02	0.40	0.46	0.49	0.17	0.28	-0.29	0.52	0.35	0.53	0.63	0.00	-0.29	0.43	-0.01	0.20	0.53	0.19	-0.04	0.04	0.49	0.62	0.54	0.55	0.61	0.68	0.67	1.00																																				
Gd	-0.29	0.32	-0.03	0.14	-0.01	0.24	0.12	0.34	-0.04	0.32	0.13	0.08	-0.23	0.37	0.00	0.87	0.49	-0.38	-0.05	0.26	-0.12	0.08	0.51	0.42	0.14	-0.59	0.92	0.85	0.46	0.44	0.61	0.71	0.89	0.67	1.00																																				
Tb	-0.30	0.31	-0.05	0.05	0.07	0.27	0.12	0.36	-0.08	0.33	0.10	0.05	-0.26	0.35	-0.09	0.90	0.47	-0.43	-0.03	0.23	-0.12	0.06	0.49	0.39	0.11	-0.63	0.97	0.87	0.36	0.36	0.52	0.63	0.85	0.59	0.98	1.00																																				
Dy	-0.29	0.29	-0.04	0.05	0.10	0.28	0.10	0.37	-0.12	0.30	0.09	0.05	-0.27	0.34	-0.13	0.88	0.43	-0.43	-0.01	0.22	-0.12	0.02	0.45	0.36	0.11	-0.64	0.98	0.86	0.33	0.33	0.49	0.59	0.82	0.54	0.97	0.99	1.00																																				
Ho	-0.30	0.28	-0.03	0.03	0.16	0.31	0.09	0.36	-0.12	0.30	0.08	0.06	-0.24	0.34	-0.16	0.89	0.42	-0.43	0.02	0.19	-0.11	0.00	0.43	0.30	0.03	-0.63	0.99	0.87	0.27	0.28	0.44	0.55	0.78	0.52	0.95	0.99	0.99	1.00																																				
Er	-0.30	0.28	-0.03	0.02	0.19	0.32	0.10	0.38	-0.14	0.28	0.08	0.06	-0.23	0.33	-0.20	0.89	0.40	-0.43	0.04	0.19	-0.09	-0.01	0.43	0.31	0.05	-0.63	0.99	0.86	0.26	0.27	0.42	0.53	0.77	0.48	0.94	0.98	0.99	1.00	1.00																																				
Tl	-0.24	0.47	0.17	0.17	-0.25	-0.35	-0.36	0.67	0.31	0.03	0.79	0.88	0.21	0.66	0.49	-0.07	0.35	0.46	-0.06	0.91	0.00	0.09	0.34	0.42	0.32	0.35	0.03	-0.06	0.58	0.66	0.53	0.47	0.31	0.25	0.08	0.05	0.06	0.04	0.04	1.00																																				
Tm	-0.32	0.25	-0.02	-0.01	0.27	0.40	0.10	0.37	-0.15	0.27	0.03	0.03	-0.25	0.29	-0.26	0.88	0.38	-0.43	0.03	0.14	-0.07	-0.03	0.41	0.27	0.01	-0.63	0.98	0.86	0.20	0.21	0.37	0.48	0.72	0.45	0.91	0.96	0.98	0.99	0.99	0.00	1.00																																				
Yb	-0.31	0.28	-0.04	-0.02	0.25	0.35	0.09	0.38	-0.14	0.28	0.06	0.03	-0.23	0.31	-0.24	0.89	0.40	-0.44	0.03	0.15	-0.07	-0.02	0.42	0.29	0.02	-0.63	0.99	0.86	0.20	0.21	0.37	0.48	0.72	0.44	0.91	0.96	0.98	0.99	0.99	0.01	1.00	1.00																																				
Lu	-0.31	0.28	-0.06	-0.03	0.26	0.33	0.10	0.39	-0.14	0.26	0.09	0.04	-0.21	0.32	-0.25	0.88	0.35	-0.44	0.06	0.15	-0.07	-0.01	0.36	0.27	0.02	-0.63	0.98	0.84	0.18	0.19	0.35	0.45	0.71	0.40	0.90	0.95	0.97	0.98	0.99	0.02	0.99	0.99	1.00																																				
As	-0.23	-0.01	0.24	-0.03	0.60	0.34	0.10	-0.01	0.14	0.05	-0.25	-0.24	-0.09	-0.20	-0.36	-0.28	-0.21	0.36	-0.35	-0.31	0.23	0.02	-0.18	-0.32	-0.19	0.31	-0.30	-0.27	-0.45	-0.38	-0.49	-0.50	-0.48	-0.32	-0.38	-0.36	-0.35	-0.32	-0.30	-0.21	-0.25	-0.26	-0.24	1.00																																				
Co	-0.17	-0.08	0.34	-0.03	0.59	0.28	-0.14	-0.04	0.17	0.22	-0.23	0.02	0.12	-0.17	-0.19	-0.46	-0.39	0.38	0.03	-0.21	0.13	-0.12	-0.44	-0.44	-0.17	0.45	-0.42	-0.44	-0.59	-0.53	-0.62	-0.64	-0.61	-0.39	-0.54	-0.50	-0.48	-0.45	-0.44	-0.05	-0.38	-0.39	-0.38	0.70	1.00																																				
Cr	-0.51	0.64	0.37	-0.22	0.09	-0.19	-0.27	0.50	0.86	0.23	0.30	0.16	0.03	0.57	0.41	-0.34	0.22	0.25	-0.34	0.39	0.48	0.24	0.16	0.01	0.09	0.86	-0.40	-0.33	0.03	0.02	-0.06	-0.12	-0.27	-0.02	-0.39	-0.41	-0.41	-0.41	-0.41	0.32	-0.41	-0.39	-0.38	0.32	0.39	1.00																																				
Sb	-0.08	0.14	0.05	-0.08	-0.34	-0.16	-0.07	0.21	0.12	-0.01	0.07	0.25	-0.09	0.14	0.26	0.14	0.24	-0.09	0.30	0.33	-0.09	0.14	0.14	0.08	0.03	0.13	0.06	0.12	0.32	0.28	0.32	0.30	0.21	0.35	0.10	0.08	0.08	0.06	0.05	0.32	0.05	0.02	0.00	-0.36	-0.21	-0.05	1.00																																				
Sc	-0.81	0.74	0.54	-0.03	0.29	0.30	0.05	0.69	0.68	0.59	0.29	0.30	-0.06	0.72	0.12	0.54	0.65	0.06	-0.10	0.41	0.31	0.30	0.55	0.03	-0.26	0.29	0.45	0.64	0.26	0.32	0.31	0.37	0.35	0.67	0.41	0.41	0.39	0.42	0.42	0.30	0.42	0.42	0.41	0.07	-0.01	0.35	0.11	1.00																																				
Zn	-0.19	0.09	0.48	0.51	-0.08	-0.04	0.10	0.10	0.06	0.10	0.23	0.40	0.29	0.26	0.15	0.09	0.08	0.47	0.42	0.22	0.00	-0.02	0.13	-0.08	-0.18	0.09	0.11	0.21	0.26	0.37	0.22	0.23	0.15	0.32	0.12	0.09	0.10	0.13	0.12	0.39	0.07	0.07	0.06	-0.08	-0.04	-0.13	0.15	0.35	1.00																																				

Correlation matrix for PQG tuffaceous metapelites (n=3)

PQG tuffaceous metapelites	SiO2	Al2O3	Fe2O3(T)	MnO	MgO	CaO	Na2O	K2O	TiO2	P2O5	Ba	Cs	Cu	Ga	Ge	Hf	Nb	Ni	Pb	Rb	S	Sr	Ta	Th	U	V	Y	Zr	La	Ce	Pr	Nd	Sm	Eu	Gd	Tb	Dy	Ho	Er	Tl	Tm	Yb	Lu	As	Co	Cr	Sb	Sc	Zn
SiO2	1.00																																																
Al2O3	-1.00	1.00																																																
Fe2O3(T)	-1.00	0.99	1.00																																														
MnO	0.02	0.03	-0.11	1.00																																													
MgO	-0.64	0.67	0.56	0.76	1.00																																											
CaO	-0.77	0.73	0.82	-0.66	-0.01	1.00																																										
Na2O	-0.99	1.00	0.98	0.11	0.73	0.68	1.00																																									
K2O	-1.00	1.00	0.99	0.05	0.68	0.72	1.00	1.00																																								
TiO2	-1.00	1.00	0.99	0.06	0.69	0.72	1.00	1.00	1.00																																							
P2O5	0.09	-0.14	0.00	-0.99	-0.82	0.57	-0.21	-0.15	-0.16	1.00																																							
Ba	-1.00	1.00	1.00	-0.03	0.62	0.78	0.99	1.00	1.00	-0.07	1.00																																					
Cs	-0.73	0.77	0.67	0.67	0.99	0.12	0.81	0.78	0.78	-0.74	0.72	1.00																																				
Cu	0.77	-0.73	-0.82	0.66	0.01	-1.00	-0.68	-0.72	-0.72	-0.57	-0.78	-0.12	1.00																																			
Ga	-1.00	1.00	1.00	-0.05	0.61	0.79	0.99	1.00	0.99	-0.05	1.00	0.71	-0.79	1.00																																		
Ge	-1.00	1.00	0.99	0.01	0.65	0.75	0.99	1.00	1.00	-0.11	1.00	0.75	-0.75	1.00	1.00																																		
Hf	-1.00	1.00	0.99	0.02	0.67	0.74	1.00	1.00	1.00	-0.13	1.00	0.76	-0.74	1.00	1.00	1.00																																		
Nb	-0.96	0.94	0.98	-0.31	0.38	0.92	0.91	0.93	0.93	0.21	0.96	0.50	-0.92	0.96	0.95	0.94	1.00																																	
Ni	-0.53	0.57	0.45	0.84	0.99	-0.14	0.63	0.58	0.59	-0.89	0.52	0.97	0.14	0.50	0.55	0.56	0.26	1.00																																	
Pb	1.00	-1.00	-1.00	-1.00	-1.00	-1.00	-1.00	-1.00	-1.00	1.00	-1.00	-1.00	1.00	-1.00	-1.00	-1.00	-1.00	-1.00	1.00																																	
Rb	-0.98	0.99	0.96	0.19	0.78	0.62	1.00	0.99	0.99	-0.29	0.97	0.86	-0.62	0.97	0.98	0.99	0.87	0.70	-1.00	1.00																																
S	0.95	-0.96	-0.91	-0.30	-0.85	-0.52	-0.98	-0.97	-0.97	0.40	-0.94	-0.91	0.52	-0.94	-0.96	-0.96	-0.81	-0.77	1.00	-0.99	1.00																																
Sr	0.86	-0.88	-0.81	-0.50	-0.94	-0.32	-0.91	-0.89	-0.89	0.59	-0.85	-0.98	0.32	-0.84	-0.87	-0.88	-0.67	-0.89	1.00	-0.94	0.98	1.00																																
Ta	-0.97	0.96	0.99	-0.25	0.44	0.89	0.94	0.96	0.95	0.14	0.98	0.56	-0.89	0.98	0.97	0.96	1.00	0.32	-1.00	0.90	-0.85	-0.72	1.00																																
Th	-1.00	1.00	0.99	0.04	0.68	0.73	1.00	1.00	1.00	-0.15	1.00	0.77	-0.73	1.00	1.00	1.00	0.94	0.58	-1.00	0.99	-0.97	-0.89	0.96	1.00																																
U	0.44	-0.48	-0.36	-0.89	-0.97	0.24	-0.55	-0.50	-0.51	0.93	-0.43	-0.93	-0.24	-0.41	-0.46	-0.47	-0.16	-0.99	1.00	-0.62	0.70	0.84	-0.22	-0.49	1.00																																
V	-0.79	0.82	0.73	0.60	0.98	0.21	0.86	0.83	0.83	-0.68	0.78	1.00	-0.21	0.77	0.80	0.81	0.57	0.94	-1.00	0.90	-0.94	-0.99	0.63	0.82	-0.90	1.00																																
Y	-1.00	1.00	0.99	0.01	0.65	0.75	0.99	1.00	1.00	-0.11	1.00	0.75	-0.75	1.00	1.00	1.00	0.95	0.55	-1.00	0.98	-0.96	-0.87	0.97	1.00	-0.46	0.80	1.00																																
Zr	-1.00	0.99	1.00	-0.07	0.60	0.80	0.98	0.99	0.99	-0.04	1.00	0.70	-0.80	1.00	1.00	1.00	0.97	0.49	-1.00	0.97	-0.93	-0.83	0.98	0.99	-0.39	0.76	1.00	1.00																																
La	0.68	-0.71	-0.61	-0.72	-1.00	-0.05	-0.76	-0.72	-0.73	0.79	-0.67	-1.00	0.05	-0.65	-0.69	-0.70	-0.43	-0.98	1.00	-0.82	0.88	0.96	-0.49	-0.72	0.96	-0.99	-0.69	-0.64	1.00																																
Ce	-1.00	1.00	0.99	0.04	0.68	0.73	1.00	1.00	1.00	-0.14	1.00	0.77	-0.73	1.00	1.00	1.00	0.94	0.58	-1.00	0.99	-0.96	-0.88	0.96	1.00	-0.49	0.82	1.00	0.99	-0.72	1.00																																
Pr	0.36	-0.41	-0.28	-0.92	-0.95	0.32	-0.48	-0.42	-0.43	0.96	-0.35	-0.90	-0.32	-0.33	-0.39	-0.40	-0.07	-0.98	1.00	-0.55	0.64	0.79	-0.14	-0.42	1.00	-0.86	-0.39	-0.32	0.93	-0.42	1.00																																
Nd	-0.50	0.46	0.58	-0.87	-0.35	0.94	0.39	0.44	0.43	0.82	0.51	-0.22	-0.94	0.53	0.48	0.47	0.73	-0.47	-1.00	0.31	-0.20	0.02	0.68	0.45	0.56	-0.14	0.48	0.54	0.30	0.45	0.62	1.00																																
Sm	-1.00	0.99	1.00	-0.07	0.59	0.80	0.98	0.99	0.99	-0.03	1.00	0.69	-0.80	1.00	1.00	1.00	0.97	0.48	-1.00	0.96	-0.93	-0.83	0.98	0.99	-0.39	0.75	1.00	1.00	-0.63	0.99	-0.31	0.55	1.00																																
Eu	-0.99	0.98	1.00	-0.18	0.51	0.86	0.96	0.98	0.97	0.07	0.99	0.62	-0.86	0.99	0.98	0.98	0.99	0.39	-1.00	0.93	-0.88	-0.76	1.00	0.98	-0.29	0.68	0.98	0.99	-0.55	0.98	-0.21	0.63	0.99	1.00																																
Gd	-1.00	1.00	1.00	-0.03	0.63	0.77	0.99	1.00	1.00	-0.08	1.00	0.73	-0.77	1.00	1.00	1.00	0.96	0.52	-1.00	0.98	-0.94	-0.85	0.98	1.00	-0.43	0.78	1.00	1.00	-0.67	1.00	-0.36	0.51	1.00	0.99	1.00																																
Tb	-1.00	1.00	0.99	0.01	0.66	0.75	1.00	1.00	1.00	-0.12	1.00	0.75	-0.75	1.00	1.00	1.00	0.95	0.56	-1.00	0.98	-0.96	-0.87	0.97	1.00	-0.47	0.81	1.00	1.00	-0.70	1.00	-0.39	0.47	1.00	0.98	1.00	1.00																																
Dy	-0.99	0.99	0.97	0.14	0.75	0.66	1.00	1.00	1.00	-0.24	0.99	0.83	-0.66	0.98	0.99	0.99	0.90	0.65	-1.00	1.00	-0.99	-0.93	0.93	1.00	-0.57	0.87	0.99	0.98	-0.78	1.00	-0.50	0.36	0.98	0.95	0.99	0.99	1.00																																
Ho	-1.00	1.00	0.99	0.05	0.69	0.72	1.00	1.00	1.00	-0.16	1.00	0.78	-0.72	0.99	1.00	1.00	0.93	0.59	-1.00	0.99	-0.97	-0.89	0.96	1.00	-0.50	0.83	1.00	0.99	-0.73	1.00	-0.43	0.44	0.99	0.97	1.00	1.00	1.00	1.00																																
Er	-1.00	1.00	0.98	0.07	0.70	0.71	1.00	1.00	1.00	-0.18	0.99	0.79	-0.71	0.99	1.00	1.00	0.93	0.61	-1.00	0.99	-0.97	-0.90	0.95	1.00	-0.52	0.84	1.00	0.99	-0.74	1.00	-0.45	0.42	0.99	0.97	0.99	1.00	1.00	1.00	1.00																																
Tl	-0.98	0.99	0.96	0.16	0.76	0.64	1.00	0.99	0.99	-0.26	0.98	0.84	-0.64	0.98	0.99	0.99	0.89	0.67	-1.00	1.00	-0.99	-0.93	0.92	0.99	-0.59	0.88	0.99	0.97	-0.80	0.99	-0.52	0.34	0.97	0.94	0.98	0.99	1.00	0.99	1.00	1.00																																
Tm	-1.00	1.00	0.99	0.05	0.69	0.72	1.00	1.00	1.00	-0.16	1.00	0.78	-0.72	0.99	1.00	1.00	0.93	0.59	-1.00	0.99	-0.97	-0.89	0.95	1.00	-0.50	0.83	1.00	0.99	-0.73	1.00	-0.43	0.44	0.99	0.97	1.00	1.00	1.00	1.00	1.00	0.99	1.00																																
Yb	-1.00	1.00	0.99	0.01	0.66	0.75	1.00	1.00	1.00	-0.12	1.00	0.75	-0.75	1.00	1.00	1.00	0.95	0.56	-1.00	0.98	-0.96	-0.87	0.97	1.00	-0.47	0.81	1.00	1.00	-0.70	1.00	-0.39	0.47	1.00	0.98	1.00	1.00	1.00	1.00	1.00	0.99	1.00	1.00																																
Lu	-1.00	1.00	0.99	0.06	0.69	0.71	1.00	1.00	1.00	-0.16	1.00	0.78	-0.71	0.99	1.00	1.00	0.93	0.59	-1.00	0.99	-0.97	-0.89	0.95	1.00	-0.51	0.83	1.00	0.99	-0.73	1.00	-0.44	0.43	0.99	0.97	1.00	1.00	1.00	1.00	1.00	0.99	1.00	1.00	1.00																																
As	0.96	-0.97	-0.93	-0.27	-0.83	-0.55	-0.99	-0.97	-0.98	0.37	-0.95	-0.90	0.55	-0.95	-0.96	-0.97	-0.83	-0.75	1.00	-1.00	1.00	0.97	-0.86	-0.97	0.68	-0.93	-0.96	-0.94	0.86	-0.97	0.62	-0.23	-0.94	-0.90	-0.95	-0.97	-0.99	-0.97	-0.98	-0.99	-0.97	-0.97	-0.98	1.00																																
Co	1.00	-1.00	-1.00	1.00	1.00	-1.00	-1.00	-1.00	-1.00	-1.00	-1.00	1.00	1.00	-1.00	-1.00	-1.00	-1.00	1.00	#DIV/0!	-1.00	1.00	1.00	-1.00	-1.00	-1.00	1.00	-1.00	-1.00	-1.00	-1.00	-1.00	-1.00	-1.00	-1.00	-1.00	-1.00	-1.00	-1.00	-1.00	-1.00	-1.00	-1.00	-1.00	-1.00	-1.00	1.00	1.00																																
Cr	-1.00	1.00	0.99	0.06	0.70	0.71	1.00	1.00	1.00	-0.17	1.00	0.79	-0.71	0.99	1.00	1.00	0.93	0.60	-1.00	0.99	-0.97	-0.89	0.95	1.00	-0.51	0.84	1.00	0.99	-0.73	1.00	-0.44	0.43	0.99	0.97	1.00	1.00	1.00	1.00	1.00	1.00	1.00	1.00	1.00	1.00	1.00	-0.98	-1.00	1.00																																
Sb	0.93	-0.95	-0.90	-0.34	-0.87	-0.49	-0.97	-0.96	-0.96	0.44	-0.93	-0.93	0.49	-0.92	-0.94	-0.95	-0.79	-0.80	1.00	-0.99	1.00	0.98	-0.83	-0.95	0.73	-0.96	-0.94	-0.92	0.90	-0.95	0.67	-0.16	-0.91	-0.87	-0.93	-0.94	-0.98	-0.96	-0.96	-0.98	-0.96	-0.95	-0.96	1.00	1.00	-0.96	1.00																																
Sc	-1.00	1.00	0.99	0.04	0.68	0.73	1.00	1.00	1.00	-0.15	1.00	0.77	-0.73	1.00	1.00	1.00	0.94	0.58	-1.00	0.99	-0.96	-0.88	0.96	1.00	-0.49	0.82	1.00	0.99	-0.72	1.00	-0.42	0.45	0.99	0.98	1.00	1.00	1.00	1.00	1.00	0.99	1.00	1.00	1.00	-0.97	-1.00	1.00	-0.95	1.00																																
Zn	-0.87	0.89	0.82	0.48	0.94	0.35	0.92	0.90	0.90	-0.57	0.86	0.97	-0.35	0.85	0.88	0.89	0.68	0.88	-1.00	0.95	-0.98	-1.00	0.73	0.90	-0.83	0.99	0.88	0.84	-0.95	0.89	-0.78	0.00	0.84	0.78	0.86	0.88	0.93	0.90	0.91	0.94	0.90	0.88	0.90	-0.97	-1.00	0.90	-0.99	0.90	1.00																																

Representative correlation values, *t Stat*, *p-values* and number of observations for some inter-elemental correlations

VSC and PQG metapelites and tuffaceous metapelites				
Al_2O_3 vs.	***r***	***t Stat***	***p-value***	***N***
Zr	0.18	2.1365	0.0345	131
TiO_2	0.82	15.9944	0.0000	131
Sc	0.82	16.0996	0.0000	131
Th	0.77	13.5724	0.0000	131
Ga	0.96	39.9708	0.0000	131
Nb	0.84	17.5661	0.0000	131
Rb	0.77	13.4933	0.0000	131
Cr	0.74	12.7743	0.0000	131
Fe_2O_3	0.33	3.9151	0.0001	131
MnO	0.2	-2.2703	0.0248	131
MgO	0.25	2.8788	0.0047	131
CaO	0.05	-0.5239	0.6012	131
Na_2O	0.27	3.1308	0.0022	131
K_2O	0.81	15.6124	0.0000	131

S *vs.*	***r***	***t Stat***	***p-value***	***N***
Fe2O3	0.48	6.1986	0.000	131

PQG				
Al_2O_3 vs.	***r***	***t Stat***	***p-value***	***N***
Fe_2O_3	0.5	3.4946	0.0012	42
MgO	0.66	5.6542	0.0000	42

Representative correlation values, *t Stat*, *p-values* and number of observations for some inter-elemental correlations

VSC and PQG metapelites				
TiO_2 vs.	***r***	***t Stat***	***p-value***	***N***
Sc	0.89	19.3779	0.0000	101
Cr	0.85	16.2924	0.0000	101
Ta	0.77	12.0183	0.0000	101
Nb	0.78	12.3412	0.0000	101
Eu	0.69	9.5363	0.0000	101
Gd	0.60	7.4696	0.0000	101
Tb	0.63	8.0459	0.0000	101
Dy	0.64	8.2069	0.0000	101
Ho	0.65	8.4194	0.0000	101
Er	0.65	8.4896	0.0000	101
Tm	0.66	8.7072	0.0000	101
Yb	0.68	9.2125	0.0000	101
Lu	0.66	8.7666	0.0000	101

VSC and PQG tuffaceous metapelites				
TiO_2 vs.	***r***	***t Stat***	***p-value***	***N***
V	0.73	5.5854	0.0000	30
Ga	0.75	5.9238	0.0000	30
Ge	0.61	4.1069	0.0003	30

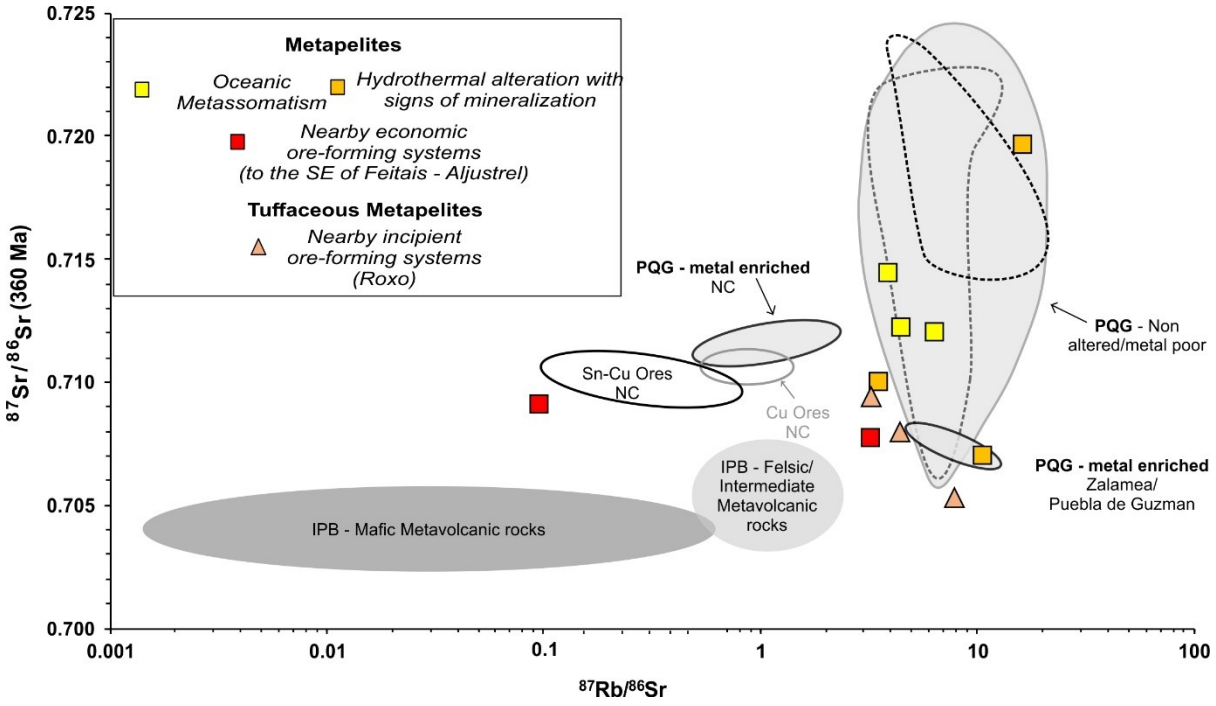

$^{87}Sr/^{86}Sr_{(360\ Ma)}$ vs. $^{87}Rb/^{86}Sr_{(360\ Ma)}$ for a selected group of VSC samples including metapelites (n = 8) and tuffaceous metapelites (n = 3). For reference purposes, various fields were delineated on the basis of published data: (i) "IPB metavolcanics" (mafic n = 7 and felsic n = 5; *Mitjavilla et al.*, *1997*); (ii) "non-altered PQG metasediments" (phyllites n = 20 and quartzites n = 1; *Jorge, 2009*); (iii) "metal enriched PQG metasediments" (phyllites n = 5; quartzites n = 1; *Jorge, 2009);* (iv) Neves Corvo ores (Sn-Cu ores n = 4; Cu ores n = 3; *Relvas et al. 2001*); (v) 4 VSC (black dash-line) and 6 PQG (grey dash-line) black metapelites (*Tornos et al. 2006*).

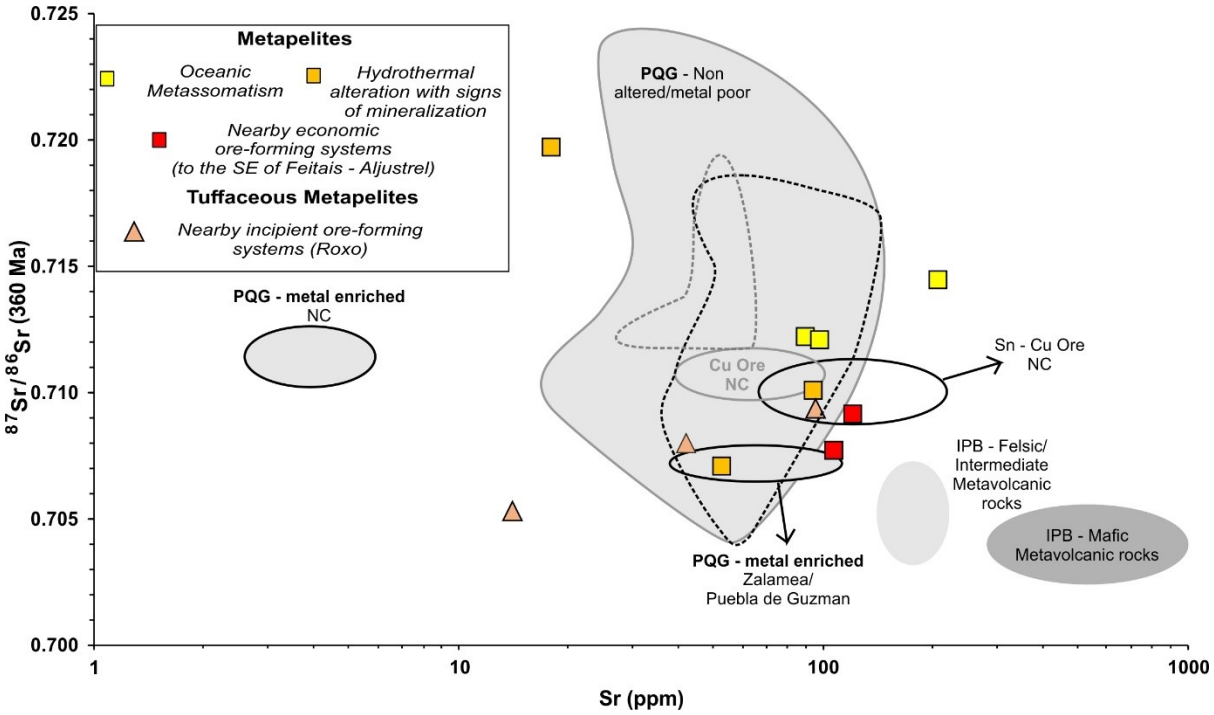

$^{87}Sr/^{86}Sr_{(360\ Ma)}$ vs. Sr (ppm) for a selected group of VSC samples including metapelites (n = 8) and tuffaceous metapelites (n = 3). For reference purposes, the following fields were delimited considering published data: (i) "IPB metavolcanics" (mafic n = 7 and felsic n = 5; *Mitjavilla et al.*, *1997*); (ii) "non-altered PQG metasediments" (phyllites n = 20 and quartzites n = 1; *Jorge, 2009*); (iii) "metal enriched PQG metasediments" (phyllites n = 5; quartzites n = 1; *Jorge, 2009*); (iv) Neves Corvo ores (Sn-Cu ores n = 4; Cu ores n = 3; *Relvas et al. 2001*); (v) 4 VSC (black dash-line) and 6 PQG (grey dash-line) black metapelites (*Tornos et al. 2006*).

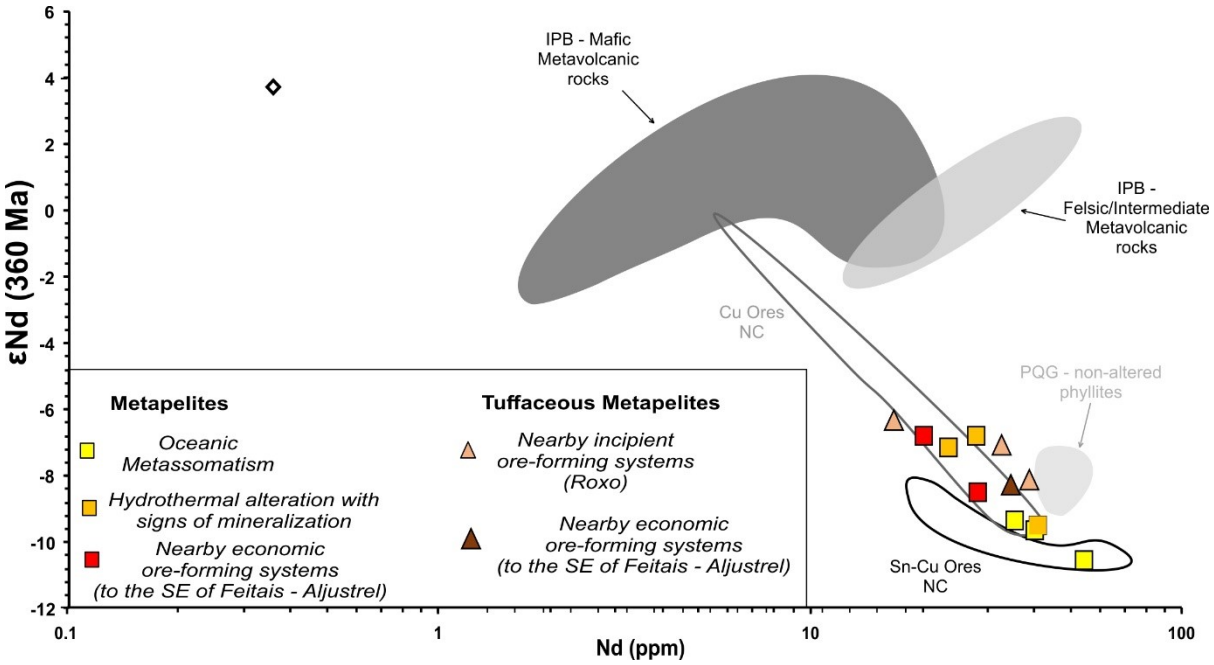

Nd (ppm) vs. εNd$_{(360\ Ma)}$ for a selected group of VSC samples including metapelites (n = 8) and tuffaceous metapelites (n = 4). For reference purposes, the fields of "IPB metavolcanics" (mafic n = 7 and felsic n = 5), **"**non-altered PQG phyllites" (n = 7) and Neves Corvo ores (Sn-Cu ores n = 5 and Cu ores n = 4) are plotted considering the data reported in *Mitjavilla et al.* (*1997*), *Jorge* (*2009*), and *Relvas et al.* (*2001*), respectively**.** The contour of Sn-Cu ores from Neves Corvo did not consider the sample indicated by the diamond marker.

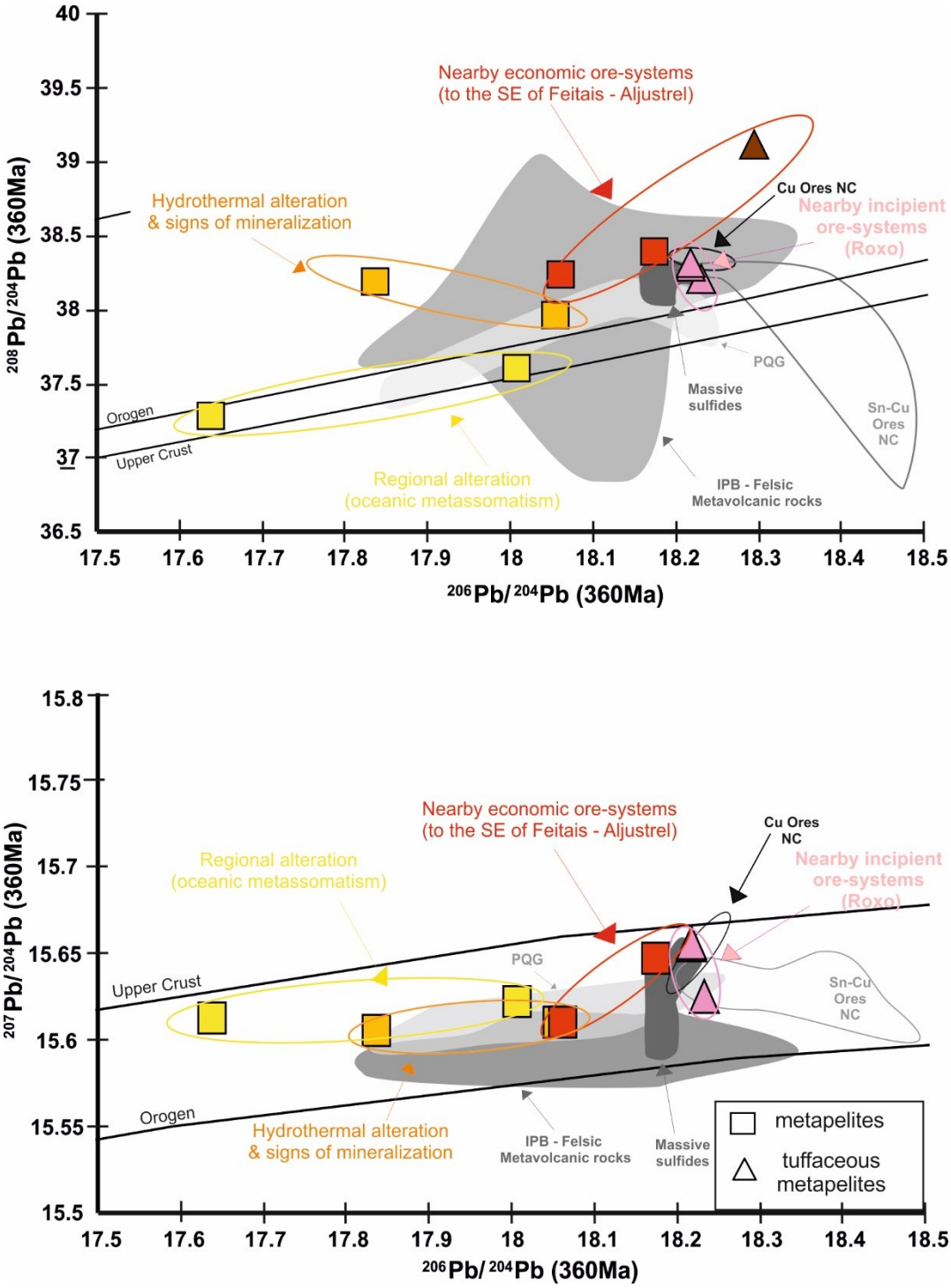

$^{206}Pb/^{204}Pb$ versus $^{207}Pb/^{204}Pb$ and $^{208}Pb/^{204}Pb$ (age-corrected, 360Ma) diagrams for selected samples of VSC metapelites and tuffaceous metapelites from the Albernoa area.Reference fields of IPB sulfide ores (*Marcoux, 1998, Pomiès et al., 1998; Relvas et al., 2001*) were classified into three groups: (i) Sn-Cu- ores from Neves Corvo (n = 8); (ii) Cu-ores from Neves Corvo (n = 8); and (iii) common massive sulfide ores (São Domingos n = 3, Lousal n = 4, Aljustrel n = 11, Lagoa Salgada n = 3, Riotinto n = 14, and some other deposits in Spain n = 18). The (age corrected) Pb-Pb ratios for metavolcanic (n = 14) and metasedimentary (n = 5) rocks were calculated on the basis of data reported in *Marcoux (1998)* and in *Jorge (2009*), respectively. In the

$^{206}Pb/^{204}Pb$ *vrs* $^{208}Pb/^{204}Pb$ diagram, the large extension of the “metavolcanic field” reflects the correction made: given the lack of whole-rock concentration values for Th, the $^{232}Th/^{204}Pb$ ratio was estimated for each sample on the basis of their $^{238}U/^{204}Pb$ values, assuming $^{232}Th/^{238}U = 3.62$ (as in *Marcoux, 1998*). The Zartman & Doe (1981) “upper crust” and “orogen” curves are also shown.

Appendix 1.2

Geochemistry of Fammenian to Visean metapelites from the Iberian Pyrite Belt: implications for provenance, paleo-redox conditions and vectoring massive sulfide deposits

Natural Resources Research - *2020*

Filipa Luz
António Mateus
Carlos Rosa
Jorge Figueiras

Natural Resources Research (© 2020)
https://doi.org/10.1007/s11053-020-09686-4

Original Paper

Geochemistry of Famennian to Visean Metapelites from the Iberian Pyrite Belt: Implications for Provenance, Paleo-Redox Conditions and Vectoring to Massive Sulfide Deposits

Filipa Luz[1,4] **António Mateus,**[1,2] **Carlos Rosa,**[1,3] **and Jorge Figueiras**[1,2]

Received 25 November 2019; accepted 28 April 2020

Massive sulfide deposits of the Iberian Pyrite Belt (IPB) document the progression of ore-forming processes in the SW Iberian Variscides, throughout uppermost Devonian to Early Carboniferous. Sulfide ores are usually hosted in volcanic-dominated or shale-dominated successions belonging to the Volcano-Sedimentary Complex (VSC; Late Famennian to Late Visean). Yet, several important orebodies at Neves-Corvo are sitting within upper sections (Famennian) of the early deposited Phyllite–Quartzite Group (PQG). Four key sectors of the Portuguese segment of IPB were revisited and 262 samples collected to characterize the geochemical features of metapelites from PQG and VSC sequences in barren and fertile settings. The selected sectors include active (Neves-Corvo and Aljustrel) and old (Lousal) mines, besides promising brownfield (Gavião) and greenfield (Sesmarias) prospects, and other lithostratigraphic sections without known mineralization. The composition of PQG and VSC metapelites is similar and mainly controlled by a mixture of clayey-derived and quartz sandy-derived components largely resulting from different sources of granitic to granodiorite/quartz diorite composition. A third component of local volcaniclastic origin could be significant in many samples of *upper* VSC sections. Mineral transformations during diagenesis and/or hydrothermal alteration/mineralization partially overprinted the primary composition. During sedimentation/diagenesis, prevalent redox conditions were mostly confined to oxic environments, at places transiting to sub-oxic. Subsequent multistage interaction with reducing hydrothermal fluids (to which the sulfide mineralization is related) generated heterogeneous anoxic signs. Consistent increases in Fe_2O_3/TiO_2, (Cu + Zn + Pb)/Sc and (As + Sb)/Sc ratios to values above 10 represent a valuable footprint toward ore horizons.

KEY WORDS: Alteration/mineralization indexes, Iberian Pyrite Belt, Massive sulfide deposit, Metasedimentary sequences.

INTRODUCTION

Massive sulfide ores of the Iberian Pyrite Belt (IPB) are hosted in volcanic-dominated or shale-dominated sequences, reflecting the progression of ore-forming processes mostly during the uppermost Devonian to Early Carboniferous (e.g., Barrie et al.

[1]Instituto Dom Luiz (IDL), Faculdade de Ciências, Universidade de Lisboa, Campo-Grande, 1749-016 Lisbon, Portugal.
[2]Dep. Geologia, Faculdade de Ciências, Universidade de Lisboa, Ed. C6, Piso 4, 1749-016 Lisbon, Portugal.
[3]CPR Lda Geology Consulting, Qta da Pedra Branca, Av. Casal Segulim, 1685-891 Famões, Portugal.
[4]To whom correspondence should be addressed; e-mail: geo.filipa.luz@gmail.com

Published online: 25 May 2020

2002; Pereira et al. 2007; Oliveira et al. 2013a, b, 2019; Inverno et al. 2015). Several lines of evidence suggest that these ores could be considered a subtype of the volcanic-hosted massive sulfide clan, transitional to the sedimentary-hosted massive sulfide group (Saéz et al. 1996, 1999). However, features supporting the genetic model proposed in Saéz et al. (1999), recently reassessed in Almodóvar et al. (2019), do not satisfactorily meet the data so far compiled for all the studied ore systems in IPB, as indicated for the remarkable exception of Neves-Corvo giant deposit (Relvas 2000; Relvas et al. 2001, 2006a, b; Li et al. 2019). More recently, the dichotomy ''volcanic-hosted vs. shale-hosted'' has been revisited and deepened (Tornos 2006; Tornos et al. 1998, 2008, 2015; Tornos and Conde 2002; Tornos and Heinrich 2008; Velasco-Acebes et al. 2019), leading to a series of overviews about the separation of the two groups of deposits. In this perspective, massive sulfide deposits distributed along the northern IPB (such as Riotinto Aguas Teñidas, La Zarza and Aljustrel) are necessarily sited in apical domains of felsic domes and were mostly generated by replacement processes of the hosting volcanic rocks in the middle Tournaisian. In contrast, massive sulfide deposits across the southern IPB (as Sotiel-Migollas, Tharsis, Neves-Corvo, Lousal, Las Cruces, Aznalcóllar-Los Frailes or Masa Valverde) are essentially shale-hosted and typically larger (although more enriched in pyrite), being developed in euxinic basins by means of exhalative or replacement processes during Famennian or Strunian. These general views, although appealing in some aspects, include straightforward extrapolations that are arguable and/or not supported by evidence gathered in known deposits or promising prospects sited in the Portuguese segment of IPB. Therefore, the search of new insights into the most suitable environments for the formation of massive sulfide ores in IPB must continue, in particular when these ores are spatially associated with metasedimentary sequences.

In the Portuguese segment of IPB, recent advances were made regarding the use of multi-elemental geochemical data to characterize the prevalent metapelites forming the two main lithostratigraphic units (Phyllite–Quartzite Group and Volcano-Sedimentary Complex) and unravel the compositional changes recorded by them due to exhalative hydrothermal activity concurrent of massive sulfides formation (Luz et al. 2019). This study builds on previous results by broadening the sampling surveys and further expanding the current knowledge on geochemical fingerprints/footprints for exploration targeting to massive sulfides in IPB. Whole-rock geochemical data obtained for 262 metapelite samples picked in PQG and VSC sections of four key sectors in Portugal will be reported and discussed. The dataset includes samples from distal (regional background) to proximal sites of massive sulfide ores, such as those under exploitation in the Aljustrel and Neves-Corvo mines. The vertical and lateral compositional/textural variations recorded by the sampled sedimentary sequences were considered to address the following objectives: (i) evaluation of geochemical features useful to the analysis of depositional environments, including redox conditions and/or geological evolution of the basin; and (ii) validation of geochemical vectors to massive sulfide ores.

GEOLOGICAL BACKGROUND

The South Portuguese Zone (SPZ), representing the southernmost geotectonic unit of the Iberian Variscides, records a series of geological processes largely determined by the SW Iberian Variscan suture evolution (e.g., Lötze 1945; Julivert et al. 1974; Ribeiro et al. 1990, 2007, 2010; Quesada 1998; Oliveira et al. 2019). In brief, the development of two main pre-orogenic mega-sequences was followed by a syn-orogenic flysch sequence; the succession experienced heterogeneous strain accommodation and low-grade metamorphism during the tectonic inversion triggered by oblique convergence and collision with the Ossa-Morena Zone (OMZ), to the north of SPZ, completed in the Carboniferous. Because of this evolution, an SW-verging, thin-skinned fold/thrust belt developed (e.g., Silva et al. 1990, 2013; Quesada 1991) along with metamorphic recrystallization under lower PT conditions from NE (greenschist facies) to SW (prehnite–pumpellyite; Priem et al. 1978; Munhá 1979, 1981, 1983, 1990; Munhá and Kerrich 1980; Abat et al. 2001).

Lithostratigraphy

Distinct preservation of lithostratigraphic sections forming the pre- and syn-orogenic sequences, as well as particular structural features, has been used as criteria to separate the main tectonic–stratigraphic domains forming the SPZ: (i) the Ibe-

rian Pyrite Belt (IPB); (ii) the Baixo Alentejo Flysh Group (BAFG), also known as the Culm Group and (iii) the SW Portuguese Domain. The IPB comprises mostly sections of variable extension of the two pre-orogenic mega-sequences (see below), whereas the latter two domains include different formations of the syn-orogenic flysch sequence, gradually younger in age toward SW and deposited from Upper Visean to Sepkhuvian-Moscovian (e.g., Schermerhorn 1971; Oliveira 1990; Pereira et al. 2008, 2010; Rodrigues et al. 2005).

The northern border of IPB is in thrust contact with the Pulo do Lobo Terrane (Fig. 1), interpreted as an accretionary prism located immediately to the south of the Variscan suture zone, presently outlined by the Beja-Acebuches Ophiolite Complex (*e.g.*, Munhá et al. 1986; Silva et al. 1990; Quesada 1991 1992; Quesada et al. 1994; Ribeiro et al. 2007, 2010; Oliveira et al. 2019). Several other NW–SE to WNW–ESE thrust faults disrupt the internal IPB litostratigraphic arrangement, often leading to tectonic dismembering and stacking of slices belonging to the main successions that, from bottom to top, are known as (e.g., Van den Boogard 1963; Schermerhorn 1971; Oliveira et al. 1990, 2013a, b, 2019; Moreno et al. 1996; Pereira et al. 2008; Faria et al. 2015): (i) the Phyllite–Quartzite Group (PQG); (ii) the Volcano-Sedimentary Complex (VSC); and (iii)

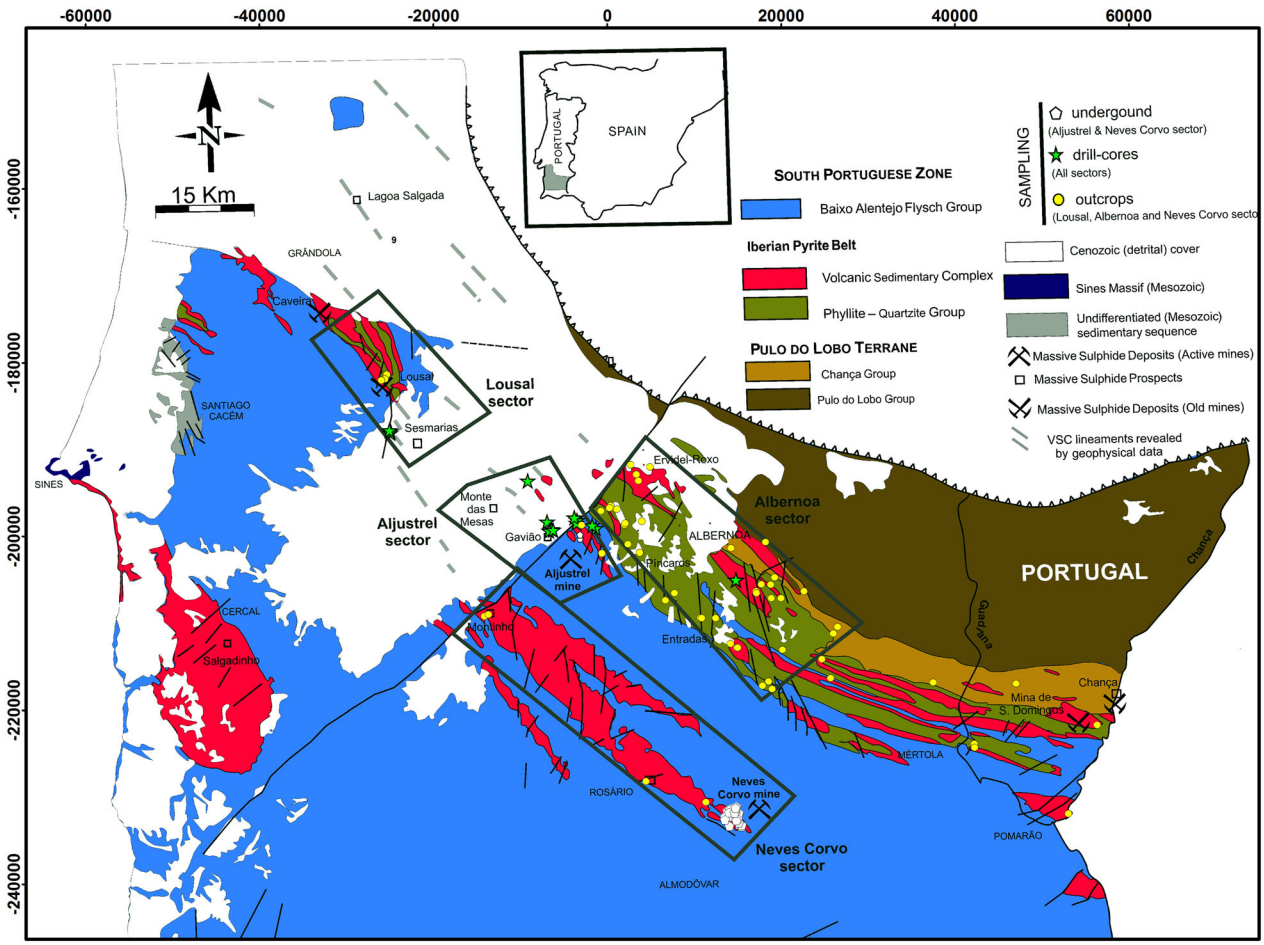

Figure 1. Synthetic geological map of the Portuguese segment of IPB, illustrating the location of the main massive sulfide deposits (old and active mines), as well as the most relevant prospects. The four sectors considered in this study are traced by black polygons. Modified after Oliveira (1990), Barriga et al. (1997), Leistel et al. (1998), Carvalho et al. (1999) and Matos et al. (2000, 2006). A general distribution of the sampling survey is also presented; in the "Neves-Corvo and Rosário anticline" sector, the small number of pelite samples picked in outcrops reflects mostly their poor preservation (due to strong weathering) and the large abundance of volcanic rocks. The stratigraphic setting of the 262 samples is summarized in Figure 2, and the exact location of each sample is provided in Electronic Supplementary Material 1 (ESM1.xlsx).

the Mértola Formation, the lowermost formation of the BAFG.

The Givetian to Famennian PQG corresponds to a thick siliciclastic pile that forms the early pre-orogenic mega-sequence developed in epicontinental marine environment, at present comprising phyllites, quartzites and metaquartzwackes, locally complemented with metalimestone lenses in upper levels of the sequence (e.g., Moreno et al. 1996; Jorge et al. 2006; Oliveira et al. 2019). The Late Famennian to Late Visean VSC represents the subsequent pre-orogenic mega-sequence composed of volcanic rocks intermittently emplaced throughout time and developing intercalated and/or interfingered successions with fine-grained sedimentary clastic rocks (e.g., Schermerhorn 1971; Carvalho et al. 1999; Soriano and Martí 1999; Valenzuela et al. 2002; Donaire et al. 2002; Rosa et al. 2010, 2016; Oliveira et al. 2019).

Constraints to Volcano-Sedimentary Complex Development

The VSC growth records a critical stage of the SPZ/OMZ boundary evolution, indicating the advancement of significant lithospheric stretching at the SPZ northern border and concomitant magmatic activity, because of subduction blocking (e.g., Jesus et al. 2007, Ribeiro et al. 2007, 2010). Considering the kinematic coupled system active during the Carboniferous left lateral transpressive collision (Jesus et al. 2007), the mechanical response of the pro-wedge domain (upcoming IPB) should have favored the generation of arrays of tectonic-controlled asymmetric (2^{nd} or 3^{rd} order) basins within the siliciclastic platform. Some of the fault zones bounding these basins attained conditions to serve as magma conduits, and when adequate physical conditions were met, several basins became the preferred locus of recurrent deposition of volcanic products. The main volcanic events are confined to the narrow time window $\sim$ 360 to 345 Ma, peaking at $\sim$ 355 to 350 Ma (Nesbitt et al. 1999; Mathur et al. 1999; Barrie et al. 2002; Dunning et al. 2002; Rosa et al. 2009; Valenzuela et al. 2011; Oliveira et al. 2013a, b, 2019; Solá et al. 2015).

The volcanic rocks in VCS are largely submarine and commonly bimodal in nature, despite the prevailing rhyolitic/rhyodacitic nature observed in present-day outcrops; the prevalence of felsic rocks is not regularly distributed and products of mafic (basaltic) or intermediate (andesitic) composition can be significant in some sections or increase in depth (e.g., Leca et al. 1983; Munhá 1983b; Mitjavilla et al. 1997; Thiéblemont et al. 1998; Carvalho et al. 1999; Rosa et al. 2004, 2006, 2008, 2010, 2016; Codeço et al. 2018; Conde and Tornos 2019). The sedimentary component of VSC includes a large variety of rock types but with clear prevalence of shale/silty facies that indicates deposition primacy in quieter confined basins affecting the siliciclastic platform. Therefore, such sedimentary record will be preserved in basins that underwent variable extension and with varying morphology where volcanic products of any kind are lacking or where the latter can be easily detectable or even dominate the entire sequence, depending on the vigor, lifetime and chemical nature of the magmatic activity in each basin. Accordingly, when lava flows and/or assortments of clast-supported volcaniclastic sediments (usually proximal to domes and partly extrusive cryptodomes) are present, the intercalated levels of shale/silt facies document pauses of volcanism. But, considering the sedimentary reworking potentially affecting volcaniclastic (matrix-supported) sediments, lateral and vertical interfingering with shale/silt facies can develop without difficulty (Rosa et al. 2010, 2016). This explains the main features observed in common lower sections of VSC, presently represented by monotonous series of (black) metapelites or by fine intercalations of metapelite/metasiltstone levels disrupted by volcanic rocks or evolving gradually (either vertically or laterally) to volcaniclastic (matrix-supported) sediments. In contrast, the upper VSC sections are dominated by siliceous metapelites (some of them incorporating distal volcanic-derived components), metajaspers (commonly metacherts) and purple metapelites (e.g., Oliveira et al. 2013a, b, 2019).

Massive Sulfide Deposits

Massive sulfide deposits of the IPB are mostly hosted in VSC volcanic-dominated or shale-dominated sequences, despite examples sitting within the upper sections of PQG in Neves-Corvo. These deposits were formed during the Upper Devonian (Famennian or Late Strunian, miospore biozone LN, 360.7 ± 0.7 to 362 Ma) to Early Carboniferous (mid-Tournasian) time (e.g., Nesbitt et al. 1999; Mathur et al. 1999; Barrie et al. 2002; Dunning et al. 2002; Pereira et al. 2007, 2012; Rosa et al. 2009;

Matos et al. 2011; Valenzuela et al. 2011; Oliveira et al. 2013a, b, 2019; Li et al. 2019). The influence of host sequences on the mineralization styles of the corresponding deposits is noteworthy, supporting different genetic models, namely hybrid for most cases between systems of volcanogenic affiliation and exhalative hydrothermal processes in sedimentary settings (e.g., Barriga and Fyfe 1998; Boulter 1993; Almodóvar et al. 1998, 2019; Saéz et al. 1999, 2011; Solomon et al. 2002; Relvas et al. 1994, 2001, 2002, 2006a, b; Tornos 2006; Tornos and Heinrich 2008; Inverno et al. 2008; Huston et al. 2011).

Irrespective of the metallogenic model, a generalized consensus exists about the hydrothermal alteration/mineralization haloes affecting host rocks forming the orebodies footwall, which are characterized by low-sulfidation mineral assemblages developed in a multistage process under mildy acidic conditions and low to moderate temperature conditions ($\sim 100 \pm 25$ °C to $\sim 300 \pm 15$ °C; e.g., Barriga 1983; Leistel et al. 1998, Relvas 2000; Sánchez-España et al. 2000; Inverno et al. 2008; Barrett et al. 2008; Moura 2008; Oliveira et al. 2011). These secondary haloes partly overprinted or completely obliterated the mineralogical and textural transformations previously experienced by the PQG or VSC rocks due to interaction with modified seawater, the so-called regional alteration triggered by seafloor metasomatic processes (e.g., Munhá 1980; Munhá and Kerrich 1980; Barriga and Kerrich 1984; Munhá et al. 1986).

Effects due to Variscan deformation/metamorphism, locally complemented by hydrothermal activity related to the propagation/reactivation of strike–slip fault zones in Late Variscan times, should also be considered when mineral/geochemical data of massive sulfide ores and their host rocks are examined. In fact, all these processes may cause redistribution of chemical elements, leading to mechanical ore-zone refinements and/or chemical dispersion by means of long-lived mass advection (Quesada 1998; Relvas 2000; Marignac et al. 2003; Castroviejo et al. 2011; Codeço et al. 2018; Almodóvar et al. 2019). Mass advection processes could inclusively generate significant metal remobilization from preexistent massive ores or their mineralized footwalls to fracture-controlled settings nearby or far from these sources, where the metal content in fluids could (at least in part) reprecipitate. Thus, signs of these secondary metal enrichments, often expressed as late deposited sulfides/sulfosalts in hanging wall domains, should not be confused with indicators of primary mineralization (*e.g.,* Codeço et al. 2018; Almodóvar et al. 2019).

Key Sectors

The sampled PQG and VSC sections are part of four key sectors whose main features will be concisely reported below. The information compiled for these four sectors provides several lines of evidence to further confine the relative lithostratigraphic positioning and understand the prevailing vertical/lateral facies variations recorded by sedimentary sequences along the Portuguese segment of IPB. The reconstructed lithostratigraphic columns of the four key sectors and their chronostratigraphic correlation, schematically illustrated in Figure 2, are based on the information available for various stratigraphic sections, including: biostratigraphy data (e.g., Pereira et al. 2007; Mateus et al. 2014; Mendes et al. 2018), U–Pb zircon geochronology data of volcanic rocks (e.g., Barrie et al. 2002; Rosa et al. 2009; Solá et al. 2015; Albardeiro et al. 2017) and structural reconstructions.

Neves-Corvo and Rosário Anticline

Neves-Corvo, located at the SE termination of the Rosário antiform, has been the focus of numerous comprehensive studies addressing stratigraphy, structural geology, physical volcanology, ore-forming systems and geochronology aspects (e.g., Leca et al. 1983; Relvas et al. 2001; 2006a, b; Rosa et al. 2008; Oliveira et al. 2004, 2013a, b; Solá et al. 2015; Albardeiro et al. 2017). The base of the stratigraphic succession comprises the PQG, forming a thick (more than 100 m) pile of dark gray to black metapelites with intercalations of metasiltstones and quartzites. These metapelites are likely of Upper Givetian to Upper Famenian (TA, BM and VCo Miospore biozones; Oliveira et al. 2004; Mendes et al. 2018). An erosive hiatus was suggested due to the absence of Frasnian miospore assemblages (e.g., Mendes et al. 2018). The overlying succession of the VSC comprises three informal divisions (*lower, middle* and *upper*). From bottom to top, the *lower* VSC succession consists of: (i) felsic metavolcanic rocks (Rhyolite 1; 363 ± 2.5 Ma–U/Pb, LA-ICP-MS in zircon; Solá et al. 2015; Albardeiro et al. 2017) and abundant units with fiamme interpreted as pyroclastic levels (Rosa et al. 2008) interbedded with

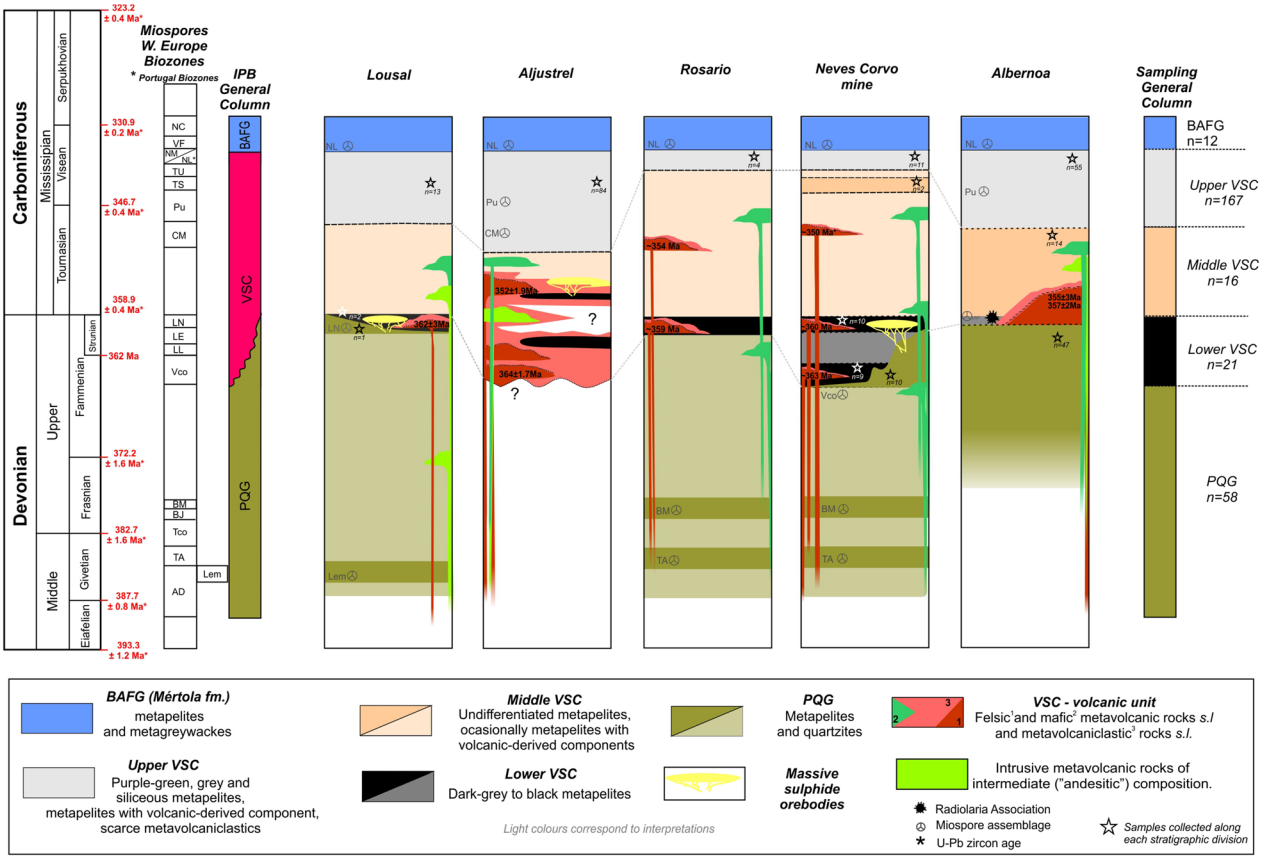

Figure 2. Reconstructed lithostratigraphic columns of key sectors and chronostratigraphic regional correlation for the Portuguese segment of IPB (modified after Oliveira et al. 2013a, b). Each column considers the available information on particular stratigraphic sections, comprehensively studied in recent years. All data from miospore assemblages/ages are from Pereira et al. (2007), Oliveira et al. (2013a, b), Mateus et al. (2014), Mendes et al. (2018), besides unpublished technical reports from ESAN and EDM. Metavolcanic rocks were dated by means of: (i) U–Pb, LA-ICP-MS in zircon for the Lousal sector (Oliveira et al. 2013a, b); (ii) U–Pb, TIMS in zircon (Barrie et al. 2002), and U–Pb and Lu–Hf, LA-ICP-MS in zircon (Rosa et al. 2009) for the Aljustrel sector; (iii) U–Pb, TIMS in zircon for the Rosario sector (Oliveira et al. 2013a, b); (iv) U–Pb, LA-ICP-MS in zircon for the Neves-Corvo sub-sector (Oliveira et al. 2013a, b; Solá et al. 2015; Albardeiro et al. 2017); and (v) U–Pb and Lu–Hf, LA-ICP-MS in zircon for Albernoa sector (Rosa et al. 2009). Twelve metapelite samples from the BAFG were collected and analyzed but not reported in this work. Supplementary information on sampling in Electronic Supplementary Material 1 (ESM1.xlsx).

black, gray and green metapelites that typically include carbonate nodules (Corvo Formation, FC miospore biozone, Upper Famennian); (ii) pyrite-rich black metapelites with intercalations of metasiltstones (Neves Formation, LN miospores biozone, Strunian) interbedded with felsic metavoclanic rocks, mainly Rhyolite 2 (360.5 ± 2.6 Ma, U/Pb, LA-ICP-MS in zircon; Solá et al. 2015; Albardeiro et al. 2017) characterized by coherent facies with thick and abundant hyaloclastite envelopes (Rosa et al. 2008); (iii) ore horizon, stratigraphically above Rhyolite 2, interbedded with the Neves Formation and dated of Strunian (360.7 ± 0.7 Ma; Oliveira et al. 2004, Matos et al. 2011; Albardeiro et al. 2017); and (iv) metajaspers(-metacherts) and carbonates, locally including sericitic/chloritic metapelites, that may rest on the orebodies or, more commonly, are found within the Neves Formation.

The lithostratigraphy of the Rosário anticline is less well studied but generally similar to the one observed for Neves-Corvo. One difference is the voluminous mafic metavolcanic rocks at the base or in some sections of the lithostratigraphic succession. The *middle* VSC sequence, spreading from the LN to TS miospore biozones, includes mainly undifferentiated gray siliceous to black metapelites, often bearing siliceous–phosphatic nodules (Graça Formation—TS miospore biozone). The *upper* VSC

succession comprises several metasedimentary formations and a pile of felsic metavolcanic rocks (Rhyolite 3) dated of 353–349 Ma, U/Pb, LA-ICP-MS in zircon (Albardeiro et al. 2017) and is dominated by coherent and hyaloclastic facies (Rosa et al. 2008). The metasedimentary series contains, from bottom to top: (i) intercalations of siliceous and black metapelites bearing carbonate/phosphate nodules (Grandaços Formation, NM miospore biozone); (ii) purple and green (sericitic) to gray metapelites developing intercalations or interfingerings in one another; (iii) gray–green siliceous metapelites and metasiltstones incorporating fine-grained volcanic-derived components (Godinho Formation, NM miospore biozone); and (iv) pyrite-rich black metapelites with layers of metasiltstones (Brancanes Formation) at the transition to the overlying this succession, the BAFG flysch (Mértola Formation) includes metapelites preserving miospore assemblages of the NM, VF and NC biozones (upper Visean to lower Serpukhovian; e.g., Oliveira et al. 2004; Mendes et al. 2018) interbedded with metagraywackes.

Aljustrel Sector (Including Gavião and Monte das Mesas Sub-Sectors)

At Aljustrel, the metasedimentary succession forming the PQG is not recognized and the local lithostratigraphy is dominated by a thick pile (up to 200 m) of metavolcanic rocks with intercalations of black metapelites whose age was not determined so far, despite several attempts to solve the issue. The volcanic succession was addressed in many studies aiming the characterization of their geochemical (rhyolitic to dacitic) affinity, facies types and features developed during early seafloor metasomatism lately overprinted by (mineralizing) hydrothermal alteration (e.g., Schermerhorn and Stanton 1969; Barriga and Kerrich 1984; Barriga 1983; Barriga and Fyfe 1998; Relvas 1991; Leitão 1997, 2014; Carvalho et al. 1999; Dawson and Caessa 2003; Barrett et al. 2008; Inverno et al. 2008; Oliveira et al. 2013a, b). In this work, the thick volcanic pile was divided into two series: the *lower* one including rock types confined to the 364 ± 2 Ma time window (U–Pb, LA-ICP-MS in zircon; Rosa et al. 2009) and the *upper*, hosting the main ore horizon, dated of 352.4 ± 1.9 Ma (U–Pb, TIMS in zircon; Barrie et al. 2002). Overlying the latter volcanic pile, an extensive (and thick) metajasper/chert lens occurs, laterally equivalent to metapelites forming the Paraíso Formation, part of the *upper* VSC. This formation is composed of purple and green metapelites (often interfingered), black metapelites/metasiltstones, metapelites with volcanic-derived components and (less voluminous) mafic metavolcanic rocks (e.g., Barriga 1983; Leitão 2014). Palynological studies on metapelites from the Paraíso Formation yielded miospore assemblages of CM and Pu biozones (Lower Visean–Upper Tournasian; Pereira et al. 2007). Resting on top of the VSC sequence, metapelites from the Mértola Formation include miospores from the NL biozone (Mid-Upper Visean; Pereira et al. 2007; Oliveira et al. 2009; Pereira and Matos 2014). Despite differences in detail, not all suitably characterized at present, the lithostratigraphic succession observed in the nearby sub-sectors of Gavião and Monte das Mesas follows the general (and simplified) column of Aljustrel.

Lousal (Including Sesmarias)

At Lousal, the PQG comprises the Lower and Upper Corona metasedimentary units where Lem (Givetian) and LN (Strunian) miospore biozone assemblages were recognized, respectively (Oliveira et al. 2006; Pereira et al. 2007). These units include mainly metapelites with carbonaceous components, metasiltstones and quartzites (e.g., Strauss 1970; Strauss et al. 1977; Fernandes 2011; Relvas et al. 2012). The *lower* VSC succession incorporates a felsic metavolcanic unit dated of 359 ± 3 Ma (U–Pb, LA-ICP-MS in zircon; Rosa et al. 2009) intercalated with dark gray to black metapelites of Strunian age (Oliveira et al. 2006) hosting the mineralization, besides minor intrusive metavolcanics. The *middle* VSC comprises an undifferentiated pile of metapelites (with some mafic metavolcanic rocks) that is overlain by siliceous and volcanic-derived metapelites forming the *upper* VSC section, which also includes some units of mafic to intermediate metavolcanics. The BAFG flysch (Mértola Formation) on top of the VSC succession comprises gray to dark gray metapelites preserving miospore assemblages of NL local biozone (corresponding to the NM biozone of the European scale), Visean in age (Pereira et al. 2007). The lithostratigraphic column of the Sesmarias sub-sector is comparable to that of Lousal.

Albernoa (Including Píncaros, Ervidel-Roxo and Entradas Sub-Sectors)

The lithostratigraphic column of Albernoa includes a PQG section characterized by a succession of black metapelites preserving miospore assemblages of VH biozone (Upper Famennian; Pereira et al. 2007), metasiltstones and quartzites. At the top of this section, the presence of minor metapelites with volcanic-derived components and metavolcaniclastic rocks records a gradual transition toward the stratigraphically overlying VSC (Luz et al. 2019). The latter unit includes mostly rhyodacitic to rhyolitic rocks dated of ≈ 357 to 355 Ma (U–Pb, LA-ICP-MS in zircon; Rosa et al. 2004), developing prevalent hyaloclastite piles that involve coherent facies (Rosa et al. 2004; Codeço et al. 2018). The volcanic succession progresses laterally and vertically to metasedimentary sequences comprising dark gray to black metapelites, purple green metapelites, fine-grained metavolcaniclastic units (locally with fiamme), siliceous metapelites and minor metapelites with volcanic-derived components (Luz et al. 2019). Samples representing some dark gray to black metapelite levels included in these successions yielded miospore assemblages from Pu (Upper Tournasian–Lower Visean) to NL biozones (Visean) (Pereira et al. 2007). The upper part of this lithostratigraphic column comprises a flysch succession with carbonates assigned to the Freixial Formation (Faria et al. 2015).

SAMPLING AND ANALYTICAL METHODS

Two hundred and sixty-two samples of fine-grained siliciclastic rocks (some of them with volcanic-derived components) from PQG, VSC and BAFG were collected according to the following criteria: (i) balanced geographic distribution all over the Portuguese segment of IPB; (ii) representativeness of lateral/vertical variations recorded by metasedimentary sequences forming the main lithostratigraphic units in the four key sectors (i.e., PQG, *lower* VSC, *middle* VSC, *upper* VSC and BAFG); (iii) proximity to different massive sulfide orebodies; and (iv) coverage of footwall and hanging wall domains of mineralized horizons when in mining centers. Far from the mining centers, the studied samples were collected in outcrops (n = 62) and cores from historical (n = 79) and recent (n = 43) exploration drillings. Within mining centers, the samples were picked from cores of production drillings (n = 37) and active exploitation fronts in underground works (n = 41). A general picture of sampling distribution is provided in Figure 1 and its stratigraphic setting summarized in Figure 2. The exact location of each sample is shown in Electronic Supplementary Material 1 (ESM1.xlsx); Figures 3 and 4 illustrate the distribution of some of the studied samples picked in cores of an exploration drilling PC09001 (at Píncaros, Albernoa sector) and in a cross section of the Neves-Corvo mine (Lombador orebody, Neves-Corvo mine).

All the samples were prepared at the University of Lisbon laboratories for petrography and whole-rock geochemistry. Whole-rock chemical analyses of 270 samples from PQG and VSC (including duplicates and replicates) were performed at Activation Laboratories Ltd (ActLABS), Ancaster, Ontario, Canada using the 4E-research analytical package. The methods included in this package were inductively coupled plasma mass spectrometry (ICP-MS) and instrumental neutron activation analysis (INAA) after total digestion and lithium metaborate/tetraborate fusion (for details see http://www.actlabs.com—Code 4E Research).

Previous petrography and comprehensive mineral chemistry studies showed that recognition of the type and relative abundance of sulfide phases in metapelites from IPB is of utmost importance to interpret correctly the whole-rock chemical data. Accordingly, three different categories were considered: (i) samples lacking sulfide phases at macro- and microscale (shortly referred hereafter as ''No-sulfide,'' Fig. 5E); (ii) pyrite-bearing samples (''Py-bearing'') where pyrite (diagenetic and/or recrystallized, Fig. 5F) is the sole sulfide present or largely prevails over sphalerite coupled with rare chalcopyrite; and (iii) samples including the typical sulfide assemblage in IPB (''Mineralized''), i.e., pyrite + sphalerite ± chalcopyrite ± galena along with trace or minor amounts of various As, Co, Ni ± Sb mineral phases (Fig. 5G, H, respectively).

PETROGRAPHY OF METAPELITES AND MAIN CHARACTERISTICS OF THEIR SETTINGS

Metapelites

The PQG comprises a metasedimentary succession dominated by black to dark gray (locally

greenish) metapelites with intercalations of variable thickness (from ~ 1 cm up to metric) of metasiltstones, metaquartzwackes and/or quartzites. In general, the relative abundance of coarse-grained metasediments in the four key sectors decreases from ENE to WSW, possibly reflecting constraints imposed by the sedimentation basin paleo-morphology (strongly segmented and asymmetric, increasingly deeper toward W–WSW) and proximity to the supplying continental sources.

The assemblage black to dark gray (locally greenish) metapelites displays lenticular bedding of dark-colored (phyllosilicate-rich) metapelite in a lighter-colored metapelite bearing a fine-grained (quartz-dominated) sandy component (Fig. 5A). These rocks are mostly composed of very fine-grained white mica and quartz, and the common accessory minerals are tourmaline and rutile. Coarse-grained metasediments include poorly sorted quartz grains besides variable amounts of subordinate white mica/chlorite ± zircon ± rutile; sulfides are observed, but their abundance is highly variable and most often related to quartz ± chlorite ± pyrite ± chalcopyrite hydrothermal infillings of structures developed (or reactivated) during Late Variscan strike–slip faulting. Dark gray (locally greenish) metapelites do not commonly incorporate sulfide phases, despite the presence of submillimeter-sized pyrite ± chalcopyrite disseminations in a few places, irregularly coupled by discrete pyrite ± quartz infillings of micro-fracture networks. The PQG section at Neves-Corvo is the sole known exception, specifically at the Lombador orebody where a voluminous stockwork (variably Cu–Zn enriched) exists. In this case, the rock mineral assemblage includes enhanced amounts of quartz (± chlorite ± carbonate ± REE-bearing phosphates), pyrite and chalcopyrite (± tetrahedrite ± sphalerite ± galena).

The *lower* VSC comprises mainly dark gray to black metapelites associated with felsic metavolcanic rocks. This lithostratigraphic unit is considered the main host of massive sulfide ores in the Portuguese segment of IPB, possibly excluding the Aljustrel sector (including Gavião and Monte das Mesas) where it was not firmly recognized so far. The dark gray to black metapelites are made of sub(-rounded) quartz grains scattered in a groundmass of fine-grained white mica variably enriched in non- or poorly structured organic matter; higher abundances of quartz grains, sometimes displaying coarser sizes, generate the observed intercalations of black metasiltstones. These metapelites typically contain framboidal pyrite and submillimeter-sized disseminations of pyrite ± chalcopyrite ± sphalerite ± galena, at times along with folded veinlets/veins of quartz (± siderite) + pyrite ± pyrrhotite ± sphalerite. Limited to well-developed mineralized stockworks are observed in *lower* VSC at Lousal/Sesmarias and Neves-Corvo, respectively. In some of these samples, namely at Sesmarias, early developed cassiterite grains were found, as well as Co- and Ni-bearing sulfide phases of imprecise identification due to their tiny size; several cassiterite grains are crossed by fracture-controlled infillings of quartz ± siderite ± chlorite + pyrite + chalcopyrite ± galena, which were also reported in other studies on samples from the Lousal mine (e.g., Fernandes 2011).

The *middle* VSC, well-preserved in the Albernoa sector and recognized at Neves-Corvo, includes gray greenish to dark gray and light purple metapelites, the latter being somewhat siliceous. Usually, these rocks comprise variable proportions of quartz and white mica, besides accessory amounts of zircon and rutile; sometimes, the relative proportion of quartz is high enough to classify the sample as a metasiltstone. In some lithostratigraphic sections, these metapelites are interfingered with similar rocks incorporating distinct volcanic-derived components (see below). Sulfides are not commonly observed, despite rare (pyrite?) box works. However, late developed veinlets of quartz ± chlorite ± pyrite ± chalcopyrite (crisscrossing S_1 and textural arrangements due to deformation and metamorphic recrystallization) can be frequent, particularly in rock domains adjoining Late Variscan strike–slip fault zones.

The *upper* VSC is mostly composed of fine-grained metasediments, locally complemented by metavolcaniclastic rocks. The metasedimentary pile includes voluminous dark gray to black metapelites with minor interbedded metasiltstones that frequently came along with facies arrays characterized by intercalations and/or interfingerings of green–purple (Fig. 5D), dark gray to black and gray (siliceous) metapelites; stratigraphic levels incorporating volcanic-derived components and metajaspers/cherts are also present in many sections of this facies arrays. Black and dark gray metapelites forming the *upper* VSC sequences have a mineralogical composition similar to that of comparable rock types in

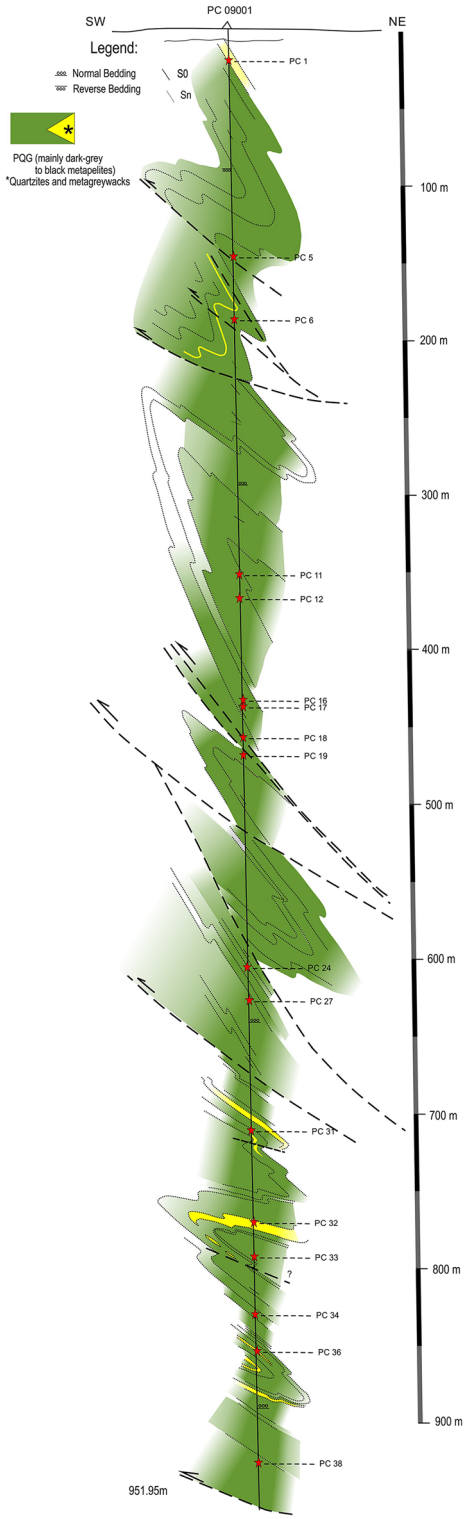

Figure 3. Sampling distribution in an interpretative geological cross section including the exploration drilling PC09001 performed at coordinates (ETRS89) $m = 3557$ and $p = -199306$ (Albernoa sector).

PQG and other VSC sections. The green–purple metapelites comprise very fine-grained quartz grains embedded in a dominant phyllosilicate-rich matrix. This matrix includes abundant disseminated hematite (± magnetite) as a distinct mineral phase of purple metapelites, often also enclosing elongated aggregates (like *rod* structures sensu lato) of quartz ± Mg-rich carbonate ± chlorite ± apatite ± pyrite ± chalcopyrite ± digenite that replace primary components of possible volcaniclastic origin (Luz et al. 2019). Green metapelites consist mainly of white mica (that prevails over chlorite) and contain tourmaline, rutile and authigenic apatite as main accessory minerals; in some samples, disseminations of very fine-grained pyrite are significant (Luz et al. 2019).

In the Portuguese segment of IPB, the *upper* VSC is not recognized as a horizon that potentially may host noteworthy massive sulfide ores, notwithstanding the common observation of sulfides in the sedimentary series with dominant black or green metapelites. In the former rocks, disseminations of framboidal pyrite and/or pyrite ± chalcopyrite are usual. Many green metapelites show abundant, early developed (because affected by S_1) micro-quartz structures with disseminated pyrite ± chalcopyrite ± pyrrhotite (?) ± galena. At the Aljustrel sector (including the Aljustrel mine, Gavião and Monte das Mesas prospects), these rocks comprise frequent disseminations and/or early fracture infillings of As–Co–Ni- and Ni–Sb-bearing sulfides along with As–Co–Ni- and As–Ni(–Sb)-bearing sulfosalts. Ulmannite, gersdorffite and cobaltite are the prevailing mineral phases so far identified (Luz et al. 2019), regularly coming together with chalcopyrite (Aljustrel mine and Monte das Mesas prospect) and/or REE-bearing phosphates (Gavião prospect). These mineral phases are less abundant in the studied metapelites from the *upper* VSC of Neves-Corvo mine, even though the minute grains of As–Ni(–Sb)-bearing sulfosalts in some samples were recognized.

Metapelites with Volcanic-Derived Components

Metapelites incorporating volcanic-derived components were identified in all the previously described PQG, *lower* VSC, *middle* VSC and *upper*

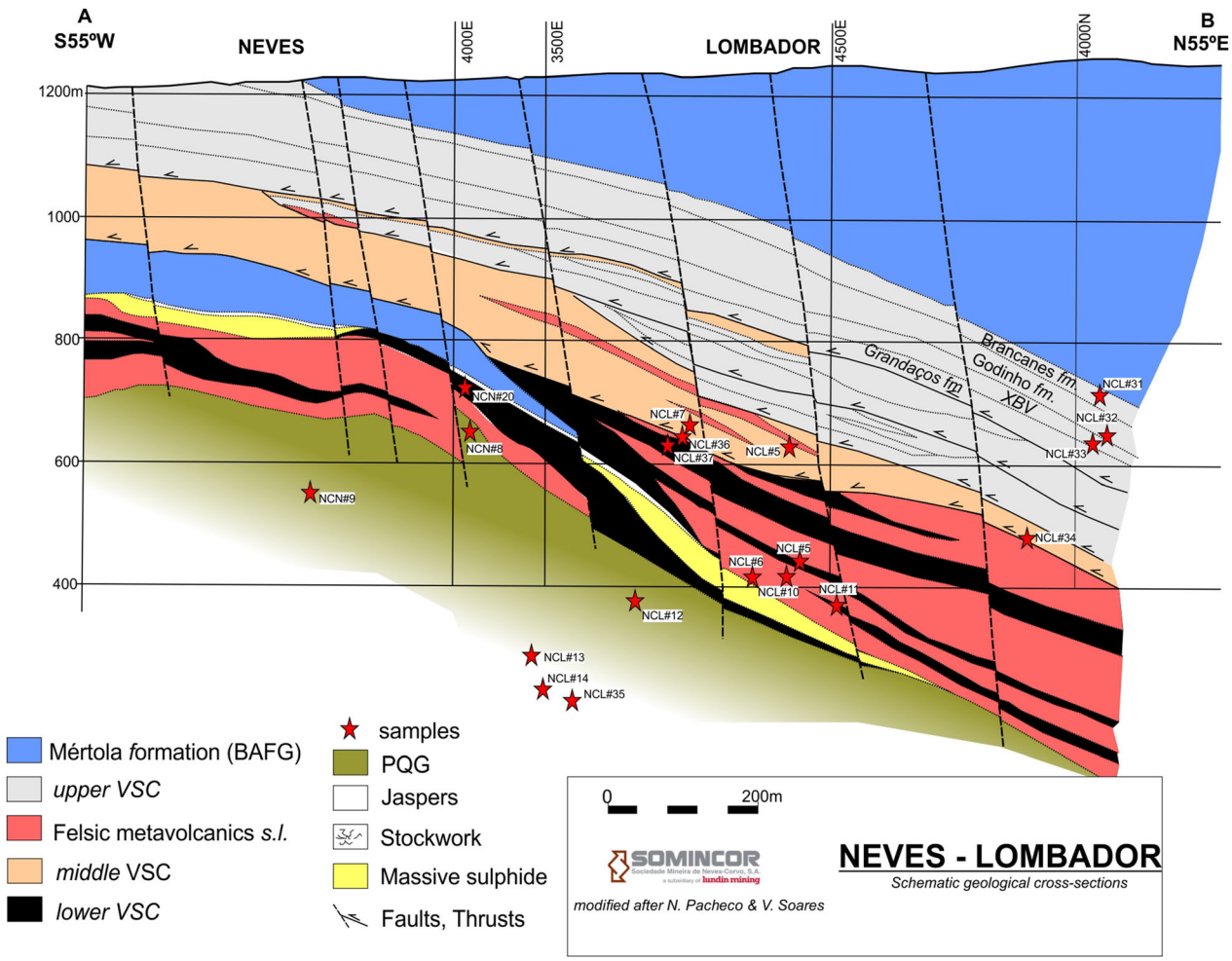

Figure 4. Sampling distribution in a geological cross section of the Neves-Corvo mine (Lombador and Neves orebodies, Neves-Corvo and Rosário sector).

VSC sections; their higher abundance occurs in the *upper* VSC, occurring near sequences comprising metavolcanic rocks. These metapelites comprise variable proportions of (sub-)millimeter-sized quartz and/or feldspar ($Ab_{87.5-99.9}$) mineral fragments within a very fine-grained (violet- to green-colored in hand sample) matrix mostly composed of white mica (± chlorite) that is locally enriched in dolomite and/or calcite. Volcanic-derived components can reach up to 50 vol.% and consist of: (i) quartz fragments showing angular to sub-rounded shapes that commonly display late dissolution features due to pressure solution; (ii) feldspar fragments, typically displaying angular shapes and effects of hydrolysis of variable intensity; and (iii) elongated aggregates of quartz ± Mg-rich carbonate ± chlorite ± apatite ± pyrite ± chalcopyrite ± digenite (rimming chalcopyrite) that likely replace primary volcaniclastic components (Luz et al. 2019).

WHOLE-ROCK CHEMISTRY

The analytical results obtained are summarized in Tables 1, 2, 3 and 4. A general inspection of these results shows that: (i) average or median concentrations of major elements do not deviate significantly from the values that typify very fine-grained mature clastic sediments derived from continental

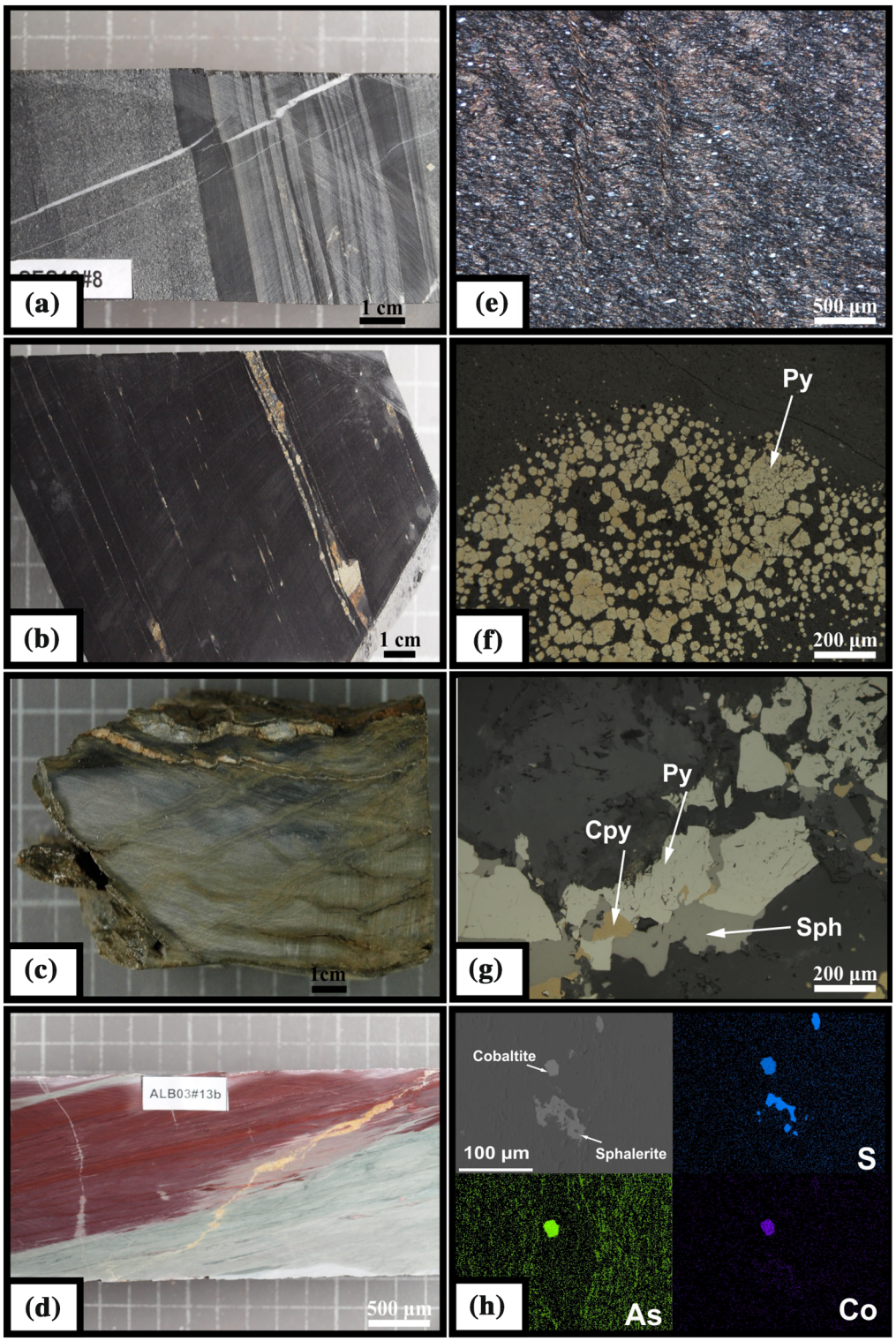
(a)
1 cm
(e)
500 µm
(b)
1 cm
(f)
Py
200 µm
(c)
1cm
(g)
Py
Cpy
Sph
200 µm
ALB03#13b
(d)
500 µm
(h)
Cobaltite
100 µm
Sphalerite
S
As
Co

◀ **Figure 5.** Selected hand samples and photomicrographs representing the main stratigraphic divisions and sulfide associations: (**a**) PQG sample displaying a siliciclastic succession of metapelite, quartzite and metaquartzwacke (SES18, 400 m); (**b**) Black metapelite from the *lower VSC* (NCN#20, underground Neves-Corvo mine); (**c**) gray greenish siliceous metapelites from *middle VSC* (X64, outcrop sample); (**d**) Green–purple metapelite from the *upper VSC* (ALB03#13b, 308.10 m); (**e**) metapelite belonging to the ''No-sulfide'' group (ALB03#16, 334 m); (**f**) Framboidal pyrite aggregates partially recrystallized in a metapelite sample of the ''Py-bearing'' group (NCN#17, underground Neves-Corvo mine); (**g**) Typical sulfide assemblage (pyrite ± chalcopyrite ± sphalerite) found in samples of the ''Mineralized'' group, (NCC#20, underground Neves-Corvo mine); (**h**) Accessory mineral phases bearing As, Co, Ni ± Sb, such as cobaltite associated with chalcopyrite in early fracture (prior to S_1) quartz infillings (FM#5, 113.50 m).

crust (Carmichael 1989; Ague 1991) and (ii) no major compositional differences exist between metapelites forming the surveyed PQG and VSC sequences. However, distinct chemical characteristics related to primary features or secondary processes affecting these rocks can be evidenced when concentrations of major element oxides and of minor/-trace elements are cross-examined.

Major Element Oxides

As illustrated in Figure 6, SiO_2 concentrations range from ~ 55 to ~ 70 wt% for most of the samples. The Al_2O_3 and K_2O concentrations are also relatively high and mostly distributed in the ~ 15 to 20 wt% and ~ 2 to 4 wt% intervals, respectively. Total iron, as Fe_2O_3, hardly exceeds 10 wt%, except when metapelites are mineralized. Abundances of CaO, MgO, Na_2O and MnO are typically low (< ~ 2 wt%, ~ 2 wt%, ~ 1.5 wt% and ~ 0.5 wt%, respectively); the same happens with TiO_2 and P_2O_5, rarely exceeding 0.25 wt% and 0.75 wt%, respectively. All these features together with the negative correlations displayed by Al_2O_3, Fe_2O_3, TiO_2, MgO and K_2O with SiO_2 (despite some data scattering, but always showing *p-values* < 0.05) are typical of pelite rocks. So, the observed compositional trends mostly represent different proportions of clay/mud-rich and quartz-rich components forming the original sediments, further leading to prevalent white mica and quartz throughout metamorphic recrystallization.

Incorporation of volcanic-derived components (such as feldspar clasts) contributes to some of the recorded compositional deviations. In addition, mineral transformations developed during diagenesis and/or hydrothermal alteration/mineralization processes (particularly chloritization and silicification, often coupled with carbonate deposition, quite evident in samples forming the ore horizon or placed at the orebodies footwall) superimpose an imprint on the primary composition. This imprint is better resolved with minor and trace elements, and will be addressed below. Nonetheless, it should be noted that: (i) higher median abundances of SiO_2, Fe_2O_3 and MnO characterize mineralized samples in Neves-Corvo, Aljustrel, Lousal and Sesmarias; and (ii) MgO concentrations, albeit irregular, tend to increase in samples forming the ''Py-bearing'' group. Consistent comparison readings require normalization of abundances of elemental oxides in relation to Al_2O_3 or TiO_2, which display a good positive correlation ($r = 0.72$; $p\ value < 0.05$) despite some scatter related to metapelites bearing an important quartz sandy-derived fraction (common in PQG). As a result, Fe_2O_3/TiO_2 ratios above 10 are the most reliable indicator of hydrothermal/mineralizing processes, separating all metapelite samples from ore horizons or orebodies footwall. The MgO/TiO_2 (or MgO/Al_2O_3) and ratios of alkali or alkaline earth elements relative to Al_2O_3 or TiO_2 show considerable dispersion and do not coherently separate subsets of samples sharing similar mineralogical features, even though they are sensitive to the presence of secondary mineral phases, such as chlorite or carbonates.

Minor and Trace Elements

Considering the median values of elemental concentration distributions for each key sector (Tables 1, 2, 3, 4), the most relevant minor elements entering the composition of IPB metapelites are: Ba (~ 460 to 560 ppm), Rb (~ 130 to 160 ppm), Zr (~ 110 to 160 ppm), S (~ 170 to 300 ppm, although reaching 2075 ppm in the Neves-Corvo sector) and V (~ 115 to 140 ppm). Following the same reasoning, the most significant trace elements are: Ga (~ 20 to 24 ppm), Sr (~ 65 to 85 ppm), La (~ 37 to 43 ppm), Ce (~ 80 to 90 ppm), Y (~ 23 to 29 ppm), Nd (~ 30 to 38 ppm), Sc (~ 12 to 16 ppm), Ni (~ 58 to 60 ppm), Cr (~ 65 to 90 ppm), Cu (~ 36 to 56 ppm), As (~ 17 to 20, but rising up to 59 ppm in the Neves-Corvo sector), Co (~ 18 to 22 ppm), Pb (~ 24 to 26 ppm) and Zn (~ 90 to 100 ppm). Variations in abundance of these 19 elements correlate well with many observed petrographic features, but

Table 1. Representative whole-rock multi-element analyses and statistic measures for PQG and VSC (*lower, middle and upper*) metapelites and metapelites with volcanic-derived components (average ± standard deviation; median; two representative analyses) for the Neves-Corvo sector (n = 46)

	Neves-Corvo dataset			PQG			Lower VSC			Middle VSC		Upper VSC		
	Average	St deviation n = 46	Median	No-sulfide NCL#13	Py-bearing NCL#14	Mineralized NCL#10	No-sulfide NCC#27	Py-bearing NCC#24	Mineralized NCZ#21	No-sulfide NCG#4	Mineralized NCL#34	No-sulfide NCZ#41	Py-bearing NCL#31	Mineralized NCL#6
SiO_2	60.59	8.04	58.92	58.24	58.53	44.47	62.84	61.76	56.41	55.46	67.07	62.44	69.62	47.85
Al_2O_3	16.81	4.07	15.87	23.5	20.19	13.7	15.46	15.48	15.8	21.91	14.17	18.85	12.5	23.55
Fe_2O_3 (T)	9.59	5.64	7.25	5.54	7.55	26.15	12.03	6.34	12.9	5.95	5.43	4.15	6.05	7.77
MnO	0.18	0.25	0.10	0.04	0.07	0.17	0.06	0.04	0.09	0.031	0.03	0.12	0.36	0.04
MgO	1.85	0.86	1.67	1.22	1.7	2.97	1.92	1.57	1.54	1.21	1.38	1.67	3.07	0.82
CaO	0.26	0.25	0.17	0.26	0.18	0.75	0.14	0.6	0.13	0.31	0.3	0.22	0.93	0.12
Na_2O	0.35	0.32	0.23	0.19	0.23	0.04	0.11	0.6	0.21	0.71	0.12	0.58	0.06	0.39
K_2O	3.26	1.36	3.53	5.74	4.47	1.09	2.66	2.88	3.14	4	4.19	4.23	2.52	6.33
TiO_2	0.75	0.27	0.72	1.164	1.00	0.687	0.85	0.61	0.84	1.052	0.42	0.77	0.39	0.89
P_2O_5	0.10	0.05	0.10	0.14	0.15	0.14	0.12	0.09	0.1	0.11	0.07	0.07	0.05	0.09
Ba	569.48	351.20	549.50	873	861	162	534	570	471	538	685	942	609	1196
Cs	7.17	3.82	7.15	7.3	6.2	1.6	3.9	10	6.8	10.3	7.7	10.9	5.1	14.3
Cu	121.17	309.06	36.00	4	122	1280	17	71	45	31	66	54	153	495
Ga	24.13	5.52	24.00	29	27	27	21	21	22	43	19	27	18	37
Ge	1.67	0.65	1.55	1.4	1.3	1.3	1.4	0.5	1.1	1.1	–	1.7	1.8	–
Hf	4.20	1.84	3.90	6.9	6.5	4	7.3	2.5	5.4	5.9	2.1	3.7	2.5	3.8
Nb	13.07	5.34	12.65	19.2	17.2	11.9	14.1	12.5	15.9	19.8	8.7	13.6	7.8	17.1
Ni	74.37	45.01	59.50	75	71	49	53	189	57	51	91	274	66	193
Pb	73.77	165.12	25.50	–	–	62	9	71	62	10	82	15	–	244
Rb	148.89	62.32	158.00	239	184	45	108	150	154	187	204	205	102	282
S	10580.65	17378.05	2075.00	260	4730	42200	2340	40100	36500	1140	27100	3380	450	43400
Sr	74.55	44.92	65.50	60	67	23	–	146	41	193	43	116	41	99
Ta	1.16	0.36	1.13	1.61	1.47	0.98	1.2	0.88	1.36	1.63	0.75	1.38	0.7	1.36
Th	12.42	3.50	12.00	17.9	16.6	10.7	13.6	9.53	13.9	17.1	9.13	12.5	9.97	14.7
U	3.51	2.23	3.30	4.26	3.87	2.43	3.26	8.63	3.2	4.4	7.24	5.14	1.44	14.1
V	156.48	90.79	138.50	186	171	117	123	223	109	147	190	207	83	246
Y	28.67	8.74	29.00	37	33	23	29	29	29	41	25	22	25	41
Zr	173.63	79.70	161	289	273	164	302	113	213	239	91	129	99	150
La	43.46	12.14	42.95	60.5	55.7	32.9	42.4	34.6	46.4	61.9	30.8	38.6	32.5	51.3
Ce	86.95	24.07	88.85	123	115	68.2	86.7	65.3	94.2	122	57.1	71.2	71.3	95.7
Pr	9.78	2.72	9.90	13.7	12.4	7.5	9.49	7.87	10.7	13.9	6.95	8.07	7.44	11
Nd	36.78	10.24	38.40	51	46	28.5	36.1	29.1	40.6	53.4	26.3	29.1	28.5	42.6
Sm	7.37	2.01	7.71	9.96	9.5	6.26	6.83	5.87	7.9	10.3	5.21	5.43	5.67	8.46
Eu	1.64	0.54	1.56	2.28	1.83	2.16	1.41	1.04	1.44	2.3	1.06	1.04	1.22	2.56
Gd	5.90	1.66	5.81	7.79	7.37	5.3	5.58	5.26	6.15	7.38	4.48	4.01	4.85	7.12
Tb	0.94	0.26	0.95	1.23	1.11	0.86	0.9	0.8	0.97	1.24	0.7	0.67	0.81	1.19
Dy	5.62	1.55	5.61	7.15	6.8	5.02	5.56	4.64	5.84	7.66	4.07	4.37	4.95	7.04
Ho	1.11	0.30	1.12	1.42	1.32	0.96	1.12	0.93	1.15	1.49	0.81	0.88	0.97	1.38

Table 1. continued

	Neves-Corvo dataset			PQG			Lower VSC			Middle VSC		Upper VSC		
	Average	St deviation	Median	No-sulfide	Py-bearing	Mineralized	No-sulfide	Py-bearing	Mineralized	No-sulfide	Mineralized	No-sulfide	Py-bearing	Mineralized
	n = 46			NCL#13	NCL#14	NCL#10	NCC#27	NCC#24	NCZ#21	NCG#4	NCL#34	NCZ#41	NCL#31	NCL#6
Er	3.21	0.85	3.32	4.03	3.68	2.73	3.33	2.85	3.36	4.46	2.3	2.66	2.71	3.91
Tl	8.59	16.21	2.43	1.99	1.39	1.57	2.58	1.7	4.27	5.71	1.94	3.16	3.1	96
Tm	0.47	0.12	0.49	0.59	0.54	0.38	0.50	0.41	0.50	0.625	0.357	0.40	0.39	0.57
Yb	3.11	0.78	3.19	3.94	3.71	2.49	3.03	2.61	3.34	4.06	2.31	2.66	2.54	3.86
Lu	0.47	0.12	0.47	0.61	0.52	0.39	0.45	0.41	0.50	0.65	0.33	0.42	0.37	0.58
As	132.73	216.75	58.50	78	67	416	26	206	272	77	323	306	4	1000
Co	27.37	26.54	21.35	26.2	31.5	147	21	21.9	34	19.6	17.1	86.6	11.7	127
Cr	84.33	25.66	85.50	130	121	69	84	87	87	107	71.5	96	53	117
Sb	7.88	16.23	3.35	2.2	4.1	8.6	3.3	31.8	8.4	3.6	31.5	14.9	0.4	103
Sc	16.21	4.22	16.40	23.4	21.1	12.6	13.6	13.9	17.9	19.3	12.2	16.4	12.6	20.7
Zn	413.00	1684.75	98.00	35	58	244	111	67	263	96	187	39	55	1500

Concentrations of major element oxides are in wt% and of minor elements in ppm. Representative analyses for metapelites in each stratigraphic unit and group (''No-sulfide,'' ''Py-bearing'' and ''Mineralized'') are showed

their real meaning must be examined by cross-checking the compositional signs provided by concentrations of both major element oxides and remaining trace elements.

Elements Indicative of Sediment Source

The abundances of several large-ion lithophile elements, like Rb and Cs, are variable and display a linear positive correlation with Al_2O_3 and a negative one with SiO_2, suggesting that they mainly reside in the mica fraction of the analyzed rocks. To a large extent, and as documented by the K/Rb and K/Cs ratios, this is an inherited feature resulting from ion exchanging during weathering only disturbed when volcanic-derived feldspar clasts (affected by heterogeneous hydrolysis) are present. Together with significant concentrations in Zr, Th and Hf, the inferred inherited feature points to felsic source compositions. In this regard, it should be noted that Zr abundances (reflecting mostly the presence of zircon) show considerable scatter relative to Al_2O_3, evident in many PQG samples and in VSC metapelites comprising a distinctive silt fraction or a significant volcanic-derived component. The correlation coefficient between Al_2O_3 and Zr for all samples is, therefore, low (r = 0.27), but the corresponding *p-value* <0.05 indicates a statistically valid linear positive covariation. The Al_2O_3 *vs*. Th and Al_2O_3 *vs*. Hf distributions are more regular and display acceptable linear positive correlations for all samples (r = 0.68 and 0.43, respectively).

Whole-rock abundances of total rare earth elements (REE) range from $\sim$ 41 to $\sim$ 758 ppm (with a median value of $\sim$ 190 ppm) and are linearly correlated with Al_2O_3 (r = 0.71), K_2O (r = 0.64), Rb (r = 0.63), SiO_2 (r = -0.61), TiO_2 (r = 0.57), Sc (r = 0.49) and Cr (r = 0.41), all the distributions having *p-values* < 0.05 (Fig. 7). This indicates that phyllosilicates play an important control on REE distribution, irregularly complemented by additional mineral phases, as suggested by the positive intercept in REE axis. Petrography and mineral composition data show that heavy minerals are important REE carriers in many metapelites, locally completed with phosphates and/or carbonates, which is consistent with the covariation between ΣREE, Zr, Y and Th (r = 0.51–0.75 and p values < 0.05; Fig. 7).

Smectite- and chlorite-type minerals might fix several transitional trace elements (e.g., Sc, V, Cr, Co and Ni) during weathering, and so, a source

Table 2. Representative whole-rock multi-element analyses and statistic measures for *upper* VSC metapelites and metapelites with volcanic-derived components (average ± standard deviation; median; two representative analyses) for the Aljustrel sector (n = 84)

	Aljustrel dataset			Upper VSC					
	Average	St deviation	Median	No sulfide		Py-bearing		Mineralized	
		n = 84		GV8#3	FFM#1	MM02#3	RS#1	GV9#7	MFM#1
SiO_2	67.54	8.60	68.97	76.76	61.25	73.04	52.73	56.73	79.99
Al_2O_3	13.98	2.97	13.88	11.17	17.66	13.98	13.89	14.4	10.05
Fe_2O_3 (T)	6.23	3.38	5.55	3.21	7.9	4.22	15.26	12.91	2.87
MnO	0.29	0.41	0.18	0.05	0.09	0.29	0.24	0.20	0.12
MgO	1.85	0.90	1.58	1.42	2.35	1.91	1.69	1.89	0.58
CaO	0.92	2.70	0.27	0.17	0.89	0.14	0.51	0.18	0.03
Na_2O	0.93	0.68	0.80	0.68	2.37	1.06	0.49	0.96	0.14
K_2O	2.90	0.96	2.83	2.5	2.58	2.6	2.72	2.86	1.97
TiO_2	0.52	0.18	0.53	0.52	0.86	0.45	0.56	0.59	0.24
P_2O_5	0.26	1.57	0.07	0.04	0.14	0.08	0.07	0.07	0.01
Ba	662.95	770.09	564.50	686	554	594	589	728	6886
Cs	10.06	3.65	7.35	7.6	6.1	6.5	8.8	7.1	18.3
Cu	84.18	114.13	55.50	50	35	124	71	125	44
Ga	20.60	6.71	20.00	15	22	19	18	21	71
Ge	2.20	0.92	2.20	2.5	1.4	2.5	0.7	1	6.7
Hf	3.12	1.49	2.70	2.4	4	4.5	2.3	3	2.1
Nb	9.70	3.44	9.30	9	9.4	10.9	8.9	10.6	4.7
Ni	80.71	39.97	77.50	81	45	69	137	178	9
Pb	61.99	203.43	25.50	6	16	11	94	84	22
Rb	143.23	51.05	135.50	128	104	117	124	136	91
S	8306.25	21776.54	270.00	100	1000	830	93100	71600	1720
Sr	91.68	66.81	82.50	65	194	83	118	88	35
Ta	0.82	0.28	0.79	0.71	0.82	0.82	0.73	0.8	0.59
Th	10.58	5.14	9.81	7.79	10.4	13.5	8.49	10.3	12.7
U	3.99	4.71	2.43	1.67	2.99	5.61	11.9	5.53	37.3
V	121.38	52.43	116.00	125	135	100	167	183	59
Y	28.68	28.05	23.00	21	23	29	24	20	12
Zr	126.21	52.44	111.00	102	159	190	100	122	77
La	39.81	20.02	37.10	34.2	36.9	42.7	32	38.9	7.34
Ce	80.07	25.07	78.80	67.5	72.2	94.7	67.9	81.9	15.4
Pr	8.88	3.84	8.35	7.65	7.83	9.9	7.19	8.42	1.7
Nd	32.83	15.57	30.35	28.8	28.4	35.8	26	30.2	5.85
Sm	6.60	3.32	6.06	5.08	5.45	7.3	5.12	5.74	1.43
Eu	1.27	0.90	1.23	1.1	1.33	1.27	1.23	1.21	0.34
Gd	6.00	4.65	5.24	4.33	4.82	6.56	4.66	4.94	1.3
Tb	0.95	0.74	0.80	0.67	0.77	1	0.75	0.79	0.33
Dy	5.52	4.32	4.74	3.85	4.52	5.72	4.6	4.55	2.34
Ho	1.09	0.87	0.93	0.72	0.9	1.13	0.9	0.88	0.51
Er	3.11	2.33	2.64	2.17	2.59	3.43	2.52	2.61	1.67
Tl	2.08	3.38	1.07	5	14.5	5.08	1.46	1.52	–
Tm	0.45	0.29	0.39	0.32	0.38	0.53	0.37	0.37	0.28
Yb	2.94	1.70	2.60	2.11	2.43	3.7	2.35	2.39	2.09
Lu	0.45	0.24	0.38	0.33	0.36	0.59	0.35	0.37	0.35
As	29.13	37.29	17.00	4	8	23	123	156	7
Co	21.46	13.13	20.60	12.9	17.5	14.9	61.8	53.6	3.3
Cr	63.04	24.65	65.00	70	73.5	34.5	82	78	26
Sb	4.39	7.15	1.70	4.6	0.9	7.5	23.3	11.8	7.9
Sc	11.84	3.54	11.60	10.8	16.6	8.95	13.5	12.3	6.17
Zn	119.79	139.94	101.00	51	111	57	203	192	1320

Concentrations of major element oxides are in wt% and of minor elements in ppm. Representative analyses for metapelites in each stratigraphic unit and group (''No-sulfide,'' ''Py-bearing'' and ''Mineralized'') are showed

Table 3. Representative whole-rock multi-element analyses and statistic measures for PQG and VSC (*lower and upper*) metapelites and metapelites with volcanic-derived components (average ± standard deviation; median; two representative analyses) for the Lousal sector (n = 16)

	Lousal dataset			PQG	Lower VSC	Upper VSC	
	Average n = 16	St deviation	Median	No sulfide L MS#1	Mineralized SES20#10	No sulfide SES18#3	Py-bearing SES20#6
SiO_2	62.27	8.41	64.39	63.03	58.54	72.01	47.18
Al_2O_3	15.72	3.65	15.90	18.4	19.46	10.57	21.95
Fe_2O_3 (T)	7.91	3.14	7.59	6.79	5.08	7.98	13.7
MnO	0.18	0.26	0.10	0.03	0.047	0.054	0.14
MgO	1.64	0.87	1.50	1.42	1.08	1.4	2.62
CaO	0.59	1.54	0.20	0.17	0.08	0.31	0.11
Na_2O	0.73	0.61	0.61	0.71	0.16	0.45	0.16
K_2O	2.85	0.99	2.97	2.98	5.78	2.1	5.35
TiO_2	0.64	0.26	0.61	0.93	0.69	0.497	0.32
P_2O_5	0.09	0.05	0.08	0.12	0.04	0.16	0.04
Ba	581.47	663.63	489.50	417	751	494	1300
Cs	8.39	5.50	7.10	6.8	29.9	7.3	21
Cu	65.68	72.91	42.50	22	48	52	81
Ga	21.03	7.24	21.00	25	27	15	29
Ge	2.31	0.90	2.20	2.6	1.5	1.7	3.3
Hf	3.76	1.94	3.40	5.9	3.3	1.6	5
Nb	11.12	4.56	10.40	14	11.9	5.3	10.6
Ni	62.77	32.24	63.00	58	99	62	30
Pb	34.70	63.67	23.50	6	60	10	28
Rb	140.77	52.25	142.00	161	363	99	308
S	5351.21	14657.90	295.00	40	16000	4830	27600
Sr	87.72	56.72	84.50	111	49	29	38
Ta	0.97	0.36	0.89	1.56	1.27	0.61	1.7
Th	10.68	2.99	10.55	14.8	12.6	7.41	10.8
U	3.39	3.84	2.62	3.07	9.19	1.29	3.65
V	121.63	50.38	130.50	162	342	96	120
Y	26.31	10.41	24.50	27	24	20	23
Zr	150.60	73.21	136.50	221	112	86	128
La	38.80	11.01	38.65	47.7	40.2	32.2	19.3
Ce	77.50	21.43	78.60	95.6	76.4	61.1	38.3
Pr	8.76	2.32	8.78	10.9	9.22	6.76	4.83
Nd	32.45	8.68	32.15	39.5	34.6	26	18.7
Sm	6.44	1.76	6.62	7.49	6.41	5.16	4.73
Eu	1.27	0.39	1.31	1.54	1.1	1.26	0.644
Gd	3.47	2.41	2.96	5.77	4.6	4.83	4.24
Tb	0.87	0.29	0.86	0.98	0.74	0.72	0.76
Dy	5.17	1.81	4.99	5.99	4.86	4.25	4.69
Ho	1.02	0.37	0.97	1.15	0.94	0.83	0.89
Er	2.95	1.08	2.82	3.26	2.9	2.45	2.53
Tl	1.82	5.08	0.70	5.79	45.5	0.6	27.7
Tm	0.43	0.16	0.41	0.518	0.425	0.364	0.358
Yb	2.87	1.06	2.77	3.22	2.88	2.42	2.2
Lu	0.44	0.16	0.42	0.464	0.427	0.364	0.33
As	34.32	53.53	20.50	14	74	12	98
Co	18.04	10.68	17.50	15	20.5	13.3	6.3
Cr	75.30	33.40	74.00	110	112	82	41
Sb	4.57	8.98	1.45	0.7	50.2	1.1	16.2
Sc	13.47	4.71	13.50	18.6	18.5	10.3	14.9
Zn	111.94	129.14	94.50	119	439	87	160

Concentrations of major element oxides are in wt% and of minor elements in ppm. Representative analyses for metapelites in each stratigraphic unit and group (''No-sulfide,'' ''Py-bearing'' and ''Mineralized'') are showed

Table 4. Representative whole-rock multi-element analyses and statistic measures for PQG and VSC (*middle and upper*) metapelites and metapelites with volcanic-derived components (average ± standard deviation; median; two representative analyses) for the Albernoa sector (n = 116)

	Albernoa dataset			PQG		Middle VSC		Upper VSCUpper VSC	
	Average n = 116	St deviation	Median	No sulfide X68	Py-bearing PC17	No sulfide 37-1-B	Py-bearing 37-1-E	No sulfide ALB02#2	Mineralized EDS1-B
SiO_2	65.84	9.26	64.30	68.8	61.69	47.07	59.67	64.61	47.04
Al_2O_3	16.29	5.44	17.14	15.68	19.73	33.05	20.1	16.41	12.27
Fe_2O_3 (T)	6.37	2.18	6.82	5.22	6.66	5.06	7.1	9.06	19.42
MnO	0.14	0.16	0.10	0.02	0.21	0.08	0.08	0.19	0.16
MgO	1.59	1.06	1.50	1.17	1.74	0.67	1.86	1.97	1.31
CaO	0.44	0.60	0.18	0.2	0.31	0.2	0.22	0.13	0.45
Na_2O	0.88	0.90	0.71	0.66	1.27	1.52	1.24	0.47	0.21
K_2O	2.97	1.14	3.12	2.7	3.53	5.47	3.67	2.36	2.68
TiO_2	0.73	0.28	0.75	1.00	0.80	1.35	0.92	0.61	0.54
P_2O_5	0.10	0.06	0.09	0.13	0.09	0.14	0.12	0.07	0.08
Ba	446.70	168.74	462.00	448	503	780	489	372	549
Cs	5.77	2.91	5.70	3.7	6.8	17.6	7.6	6.2	7.5
Cu	45.61	46.10	37.00	81	117	21	42	72	60
Ga	22.55	6.97	23.00	22	26	46	27	22	17
Ge	2.38	0.73	2.40	2.8	2.2	4.7	1.7	2.9	0.7
Hf	4.09	2.08	3.90	6.8	3.7	4.6	4.3	2.5	2.1
Nb	12.63	4.86	12.65	16.1	13.3	25.8	9	10.1	9.5
Ni	55.80	24.59	57.50	31	73	31	74	47	130
Pb	29.89	90.83	9.00			8	18	48	84
Rb	133.60	52.89	146.00	122	158	278	165	115	119
S	1507.65	3707.74	170.00	0.003	360	450	7750	400	118000
Sr	85.28	39.91	85.00	85	95	207	115	60	107
Ta	1.04	0.37	1.00	1.34	1.11	2.06	1.24	0.78	0.72
Th	11.39	3.85	12.30	11.7	12.8	20.6	14	10.2	8.43
U	2.62	1.08	2.64	2.66	2.42	6.94	3.65	1.6	11.9
V	122.39	45.71	133.00	121	144	194	155	103	138
Y	26.37	8.01	27.00	33	27	34	27	17	20
Zr	163.45	78.79	151.00	287	143	178	174	81	97
La	40.60	12.07	42.40	38.9	60.5	68.8	46.7	35.6	32.1
Ce	78.20	23.28	81.90	74.9	108	129	93	71.2	66.8
Pr	9.15	2.50	9.72	9.12	9.88	14.5	10.8	8.08	7.52
Nd	34.08	9.08	35.50	33.9	37.5	54.7	38.2	29.3	28.2
Sm	6.66	1.77	7.01	6.71	7.05	9.73	7.7	5.63	5.63
Eu	1.32	0.37	1.36	1.31	1.33	1.93	1.58	1.18	1.12
Gd	5.55	1.47	5.75	6.06	5.13	7.84	6.22	4.45	4.52
Tb	0.88	0.25	0.90	1.02	0.82	1.25	1.02	0.68	0.69
Dy	5.16	5.25	5.25	6.22	4.76	6.94	5.82	3.91	3.91
Ho	1.02	0.30	1.03	1.27	0.95	1.34	1.16	0.74	0.73
Er	2.93	0.85	2.96	3.65	2.82	3.82	3.24	2.1	2.13
Tl	0.57	0.23	0.57	0.45	0.6	1.1	0.77	0.29	0.85
Tm	0.44	0.13	0.44	0.54	0.42	0.57	0.47	0.31	0.32
Yb	2.87	0.86	2.94	3.6	2.87	3.72	3.15	2.05	2.23
Lu	0.44	0.12	0.45	0.54	0.46	0.54	0.52	0.318	0.33
As	25.81	43.99	16.50	9	28	8	33	16	180
Co	18.28	8.86	18.45	6.7	22.9	16.5	34.1	20.7	70.7
Cr	85.00	32.75	89.75	110	92.6	154	103	90	81
Sb	2.29	5.36	1.20	1	0.7	2.1	4.6	1.3	19.9
Sc	15.53	5.77	15.90	15.4	19	28.3	19.3	14.4	13.7
Zn	85.28	43.77	90.00	35	90	54	97	117	128

Concentrations of major element oxides are in wt% and of minor elements in ppm. Representative analyses for metapelites in each stratigraphic unit and group (''No-sulfide,'' ''Py-bearing'' and ''Mineralized'') are showed

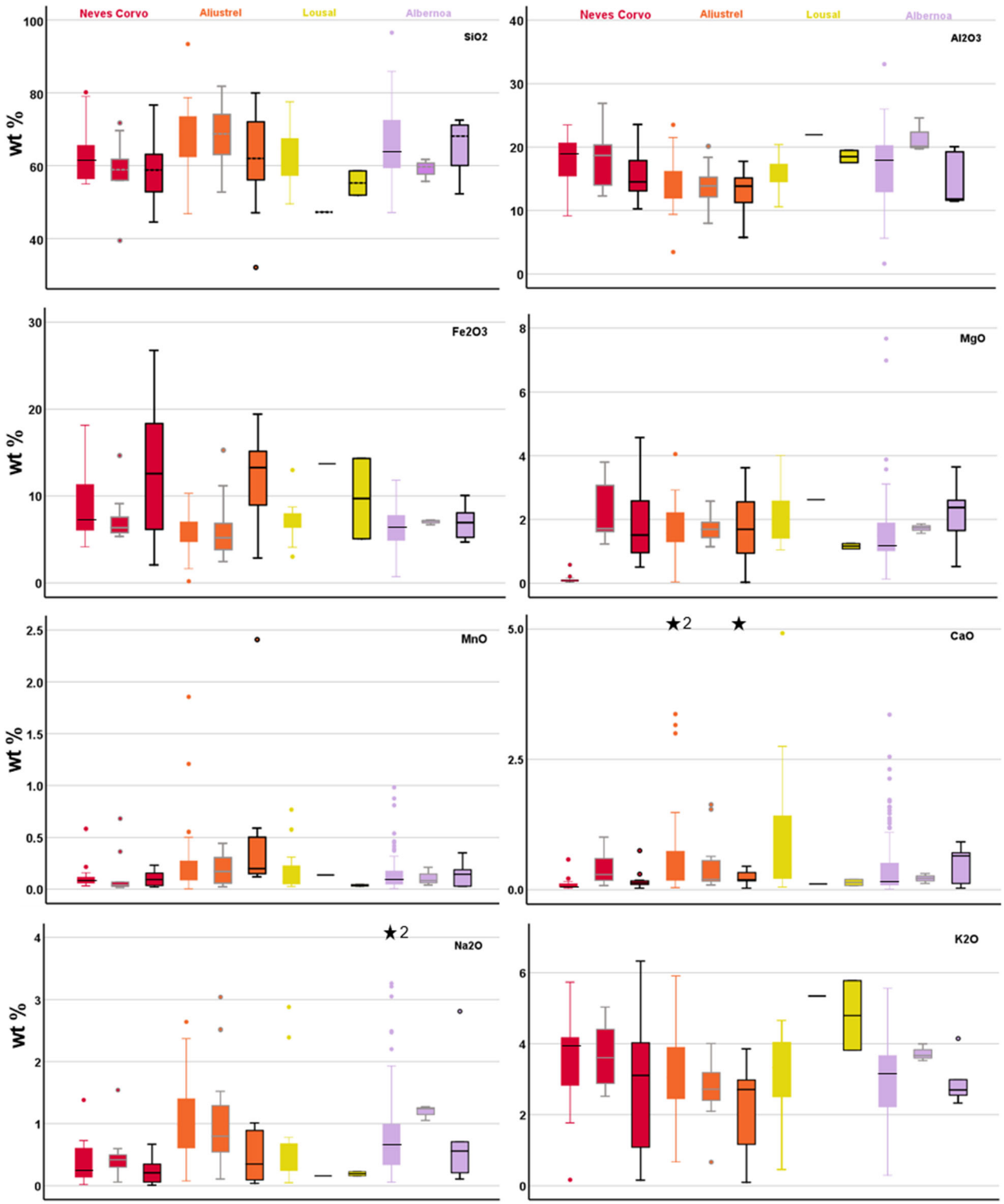

Figure 6. Box–whisker plots for major element oxides (SiO_2, Al_2O_3, Fe_2O_3, MgO, MnO, CaO, Na_2O and K_2O) differentiating the four sampled sectors (Neves-Corvo, Aljustrel, Lousal and Albernoa) by color. TiO_2 and P_2O_5 abundances do not show significant differences and their plots are not presented. Boxes without borders indicate samples included in the ''No-sulfide'' group; boxes with gray borders represent samples assigned to the ''Py-bearing'' group; boxes with black borders comprise ''Mineralized'' samples.

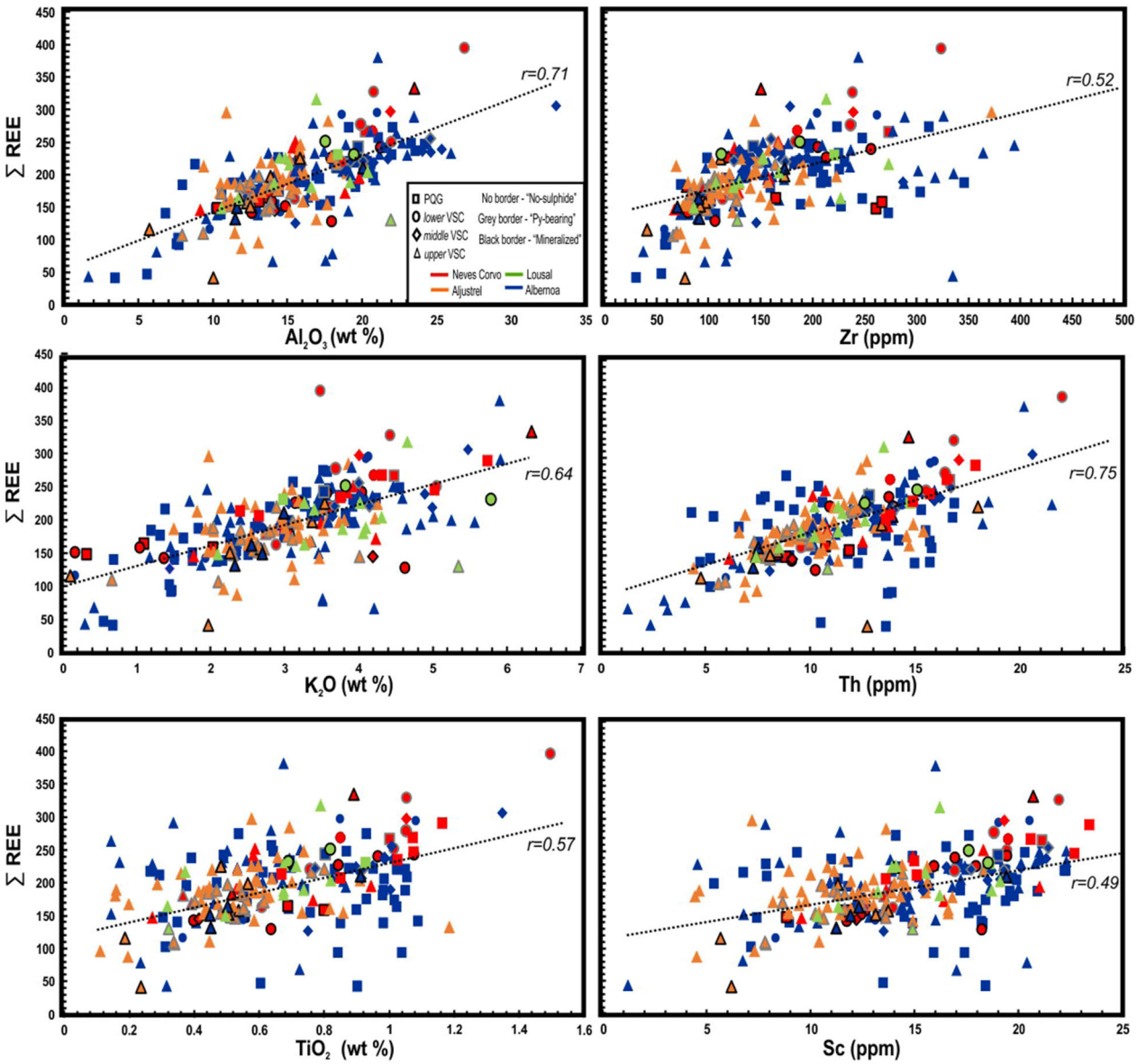

Figure 7. Whole-rock abundances of total REE (ΣREE) vs. Al_2O_3, K_2O, TiO_2, Zr, Th and Y. These selected plots document the most relevant covariations involving ΣREE for all the analyzed samples.

composition signal could be also transferred to pelites, as suggested by the good linear positive correlations of Sc and Cr with Al_2O_3 (r = 0.82 and r = 0.70 respectively), also roughly verified for V, but not followed by Co and Ni.

Redox-Sensitive and Sulfide-Forming Elements

The deviation observed for V in comparison with Cr, mostly confined to samples from PQG and *lower* VSC at Neves-Corvo, may denote the establishment of redox conditions during sedimentation

or diagenesis that favored its partial solubility or late dissolution/reprecipitation (e.g., Sadiq 1988; Breit and Wanty 1991; Wang and Wilhelm 2009). By contrast, the distinct behaviors of Co and Ni seem to record a non-inherited feature, reflecting late inputs into the clastic sediment possibly related to the mineralizing events (see below). This explains the positive covariation between Co and Ni abundances ($r = 0.61$; *p-value* <0.05) and the poor correlation displayed by V vs. Co ($r = 0.23$; *p-value* <0.05) and V vs. Ni ($r = 0.31$; *p-value* <0.05) distributions. To be noted also the range of V/Cr ratios vary from around 1 to 3 in samples that represent the footwall of orebodies at Neves-Corvo (PQG and *lower* VSC). For Lousal (*lower* VSC) the values clustering around 1.3 to 1.7. These values differ from the V/Cr ratios that characterize the *upper* VSC sequences of Neves-Corvo (including the orebodies hanging wall) and Aljustrel, which tend to show a wider variation (from 0.7 up to 5) but higher average or median values (~ 2). For the Albernoa sector, the V/Cr variation obtained for pelites forming the *middle* and *upper* VSC sections ranges from 0.2 to 3. In addition, it should be stressed that V and P_2O_5 abundances do not covary in the examined metasediments.

Pelite rocks from the orebodies footwall at Neves-Corvo (PQG and *lower* VSC) and Lousal (*lower* VSC) show also comparable median V/Ni ratios (2.41 and 2.32) despite differences in range (1.20–3.70 and 0.60–8.50, respectively). These median V/Ni ratios are significantly higher compared to those that characterize the *upper* VSC sequences of Neves-Corvo (including the orebodies hanging wall; 1.28) and the *upper* VSC at Aljustrel (1.45), for which the following ranges were obtained: 0.60–10.41 and 0.43–13.00, following the same order. The latter two ranges also compare well with the one obtained for the Albernoa pelites (0.70–11.33; *middle* and *upper* VSC sections), but in this case the median V/Ni values are much higher (2.24).

REE distribution patterns normalized to the PAAS composition (e.g., Lentz 2003; Fig. 8) show strong similarities for all the dataset, outlining mild enrichments in MREE over LREE ($La/Sm = 0.89 \pm 0.17$) and HREE ($Gd/Yb = 1.15 \pm 0.16$.), which significant increase in some of the mineralized metapelites of Aljustrel (*upper* VSC). In general, La/Yb ratios (1.05 ± 0.29) show small variations, consistent with minor fractioning between LREE and HREE, despite a shift toward slight HREE enrichments over LREE in several samples of the ''Py-bearing'' and ''Mineralized'' groups from *lower*, *middle* and *upper* VSC. The negative anomaly observed in several normalized patterns of the ''Mineralized'' group from Aljustrel is an artifact amplified by the positive La anomaly. But the $(Eu/Eu^*)_{PAAS}$ ratios represent the most notable feature with redox implications, which are commonly negative except in samples placed at the orebodies footwall, as observed for Neves-Corvo, in particular for the Lombador orebody. A similar compositional signal is observed in metapelites forming the ore horizon of Lousal, considering the analytical data of non-weathered samples reported in Fernandes (2011).

Arsenic and antimony are also two important redox-sensitive elements. For all the examined metapelites, As abundances (up to 1020 ppm) are significantly greater than those of Sb (up to 103 ppm) and correlate satisfactorily ($r = 0.62$; *p-value* < 0.05) with each other. Both elements do not covary linearly neither with P_2O_5 nor V. The S vs. As correlation is poor but statistically meaningful ($r = 0.40$; *p-value* < 0.05), improving for S vs. Sb ($r = 0.59$; *p-value* < 0.05). Individually or jointly, the As and Sb abundances show rough positive correlations ($0.30 \leq r \leq 0.55$; *p-values* < 0.05) with other sulfide-forming elements (such as Co, Ni, Cu, Pb and Zn), the most expressive with Co (or Co + Ni) and the less significant with (Cu + Pb + Zn). In this regard, it should also be noted that linear covariations of S with (Co + Ni), (Cu + Pb + Zn) and (Fe + Cu + Pb + Zn) are characterized by relatively low coefficients ($r = 0.46$, 0.37 and 0.45, respectively), despite the statistic relevance indicated by the correspondent *p-values* (always below 0.05). Many of these covariations improve considerably when the ''Mineralized'' group of samples is considered alone or is plotted together with the ''Py-bearing'' group, and this is quite evident for the Aljustrel sector (*upper* VSC), contrasting with the higher scattering of data representing Neves-Corvo (PQG and *lower* VSC).

Considering just the dark gray and black metapelites ($n = 60$), the V/Cr ratios vary largely between 1 and 2, indicative of a redox boundary near the sediment–water interface (Jones and Manning 1994), exceeding 2 when belonging to the ''Py-bearing'' group (Fig. 9A). Interestingly, many mineralized samples from PQG and *lower* VSC at the orebodies footwall of Neves-Corvo are not limited to the anoxic setting implied by $V/Cr > 2$ (Fig. 9B). For the same set of dark gray and black metapelites,

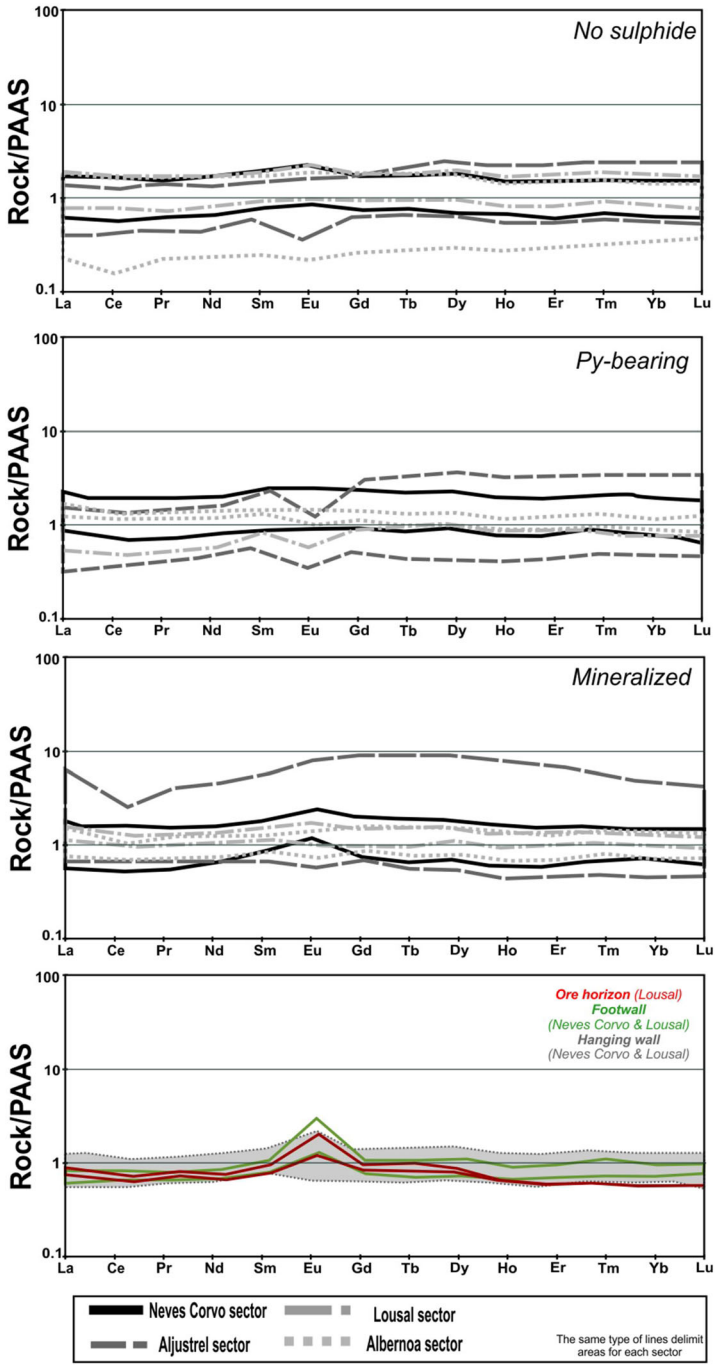

Figure 8. PAAS-normalized REE concentration patterns for IPB metapelites. For each sampling sector, the patterns were assembled in accordance to the previously defined groups: ''No-sulfide,'' ''Py-bearing'' and ''Mineralized''.

similar readings on redox conditions are supported by the U/Th ratios (Fig. 9A), spreading mostly from 0.14 to 1.25 and so covering the oxic and sub-oxic fields up until the sub-oxic/anoxic boundary, using the thresholds reported in Wignall and Myers (1988), Jones and Manning (1994) and Wignall and

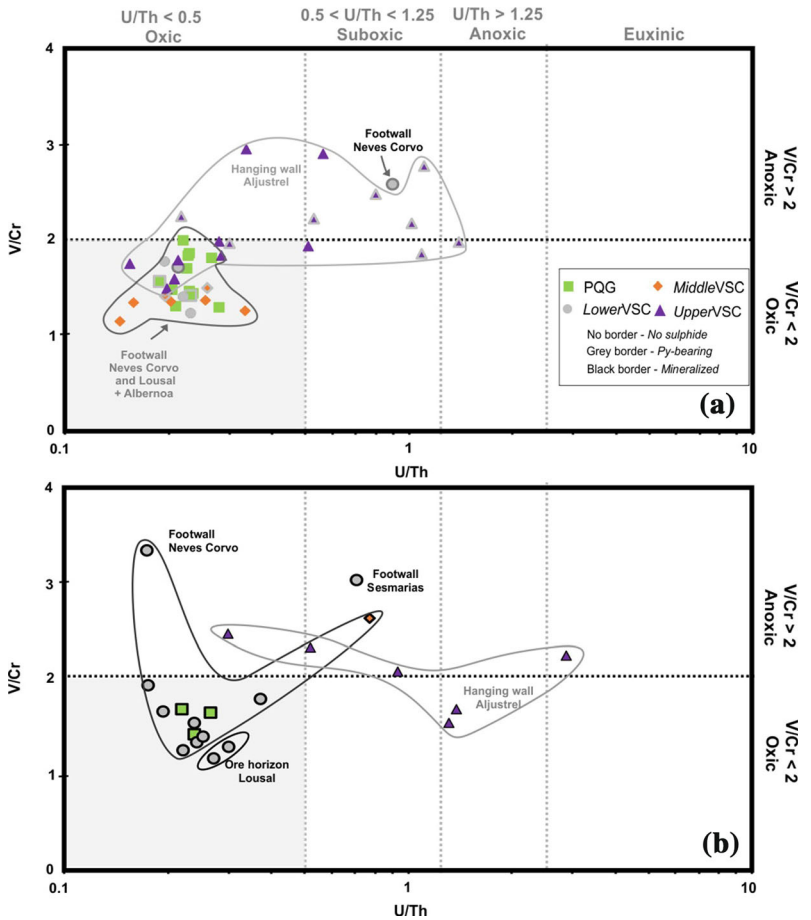

Figure 9. Variations of U/Th vs. V/Cr ratios recorded by dark gray to black metapelites (n = 60) sampled in Neves-Corvo, Aljustrel, Lousal and Albernoa sectors, separating the ''No-sulfide'' and ''Py-bearing'' groups (**A**) from the ''Mineralized'' group (**B**). Thresholds of redox conditions from Wignall and Myers (1988), Jones and Manning (1994), and Wignall and Twichett (1996).

Twichett (1996). In particular, dark gray to black metapelites included in the ''No-sulfide'' or ''Py-bearing'' groups record U/Th ratios that point to: (i) oxic conditions, in the cases of Lousal (*lower* VSC) and Albernoa (*middle* and *upper* VSC sections); (ii) oxic and sub-oxic conditions, in the case of Neves-Corvo (*lower* VSC); and (iii) oxic to sub-oxic/anoxic conditions, in the case of Aljustrel (*upper* VSC). The redox conditions deduced on the basis of U/Th ratios do not vary significantly for the mineralized dark gray to black metapelites picked in Neves-Corvo (PQG, *lower* and *middle* VSC), Lousal (*middle* VSC) or Aljustrel (*upper* VSC), despite the anomalous value of 2.94 obtained for one sample from Aljustrel, close to the lower limit of euxinic conditions (Fig. 9B).

Redox inferences based on V/Cr and U/Th ratios are in apparent divergence with indications provided by V/(V + Ni) ratios displayed by the three groups of metapelites (''No-sulfide,'' ''Py-bearing'' and ''Mineralized''), which are mostly scattered within the 0.6 to 0.9 interval, pointing to anoxic environments (Hoffman et al. 1998). However, this inconsistency may simply be due to the lowering of V/(V + Ni) ratios caused by the late input of Ni, as indicated above, thus variably obliterating the chemical proportionality achieved during sedimentation/diagenesis.

As documented for other cases in the IPB (e.g., Saéz et al. 2011), whole-rock abundances of S and Fe do not covary in the sampled metapelites. In general, S concentrations in dark gray to black meta-

pelites lacking sulfides or just bearing pyrite vary from ~ 2 to 8 wt%, clustering in the 3–6 wt% interval; these values rise up to ~ 19 wt% when the rock is evidently mineralized. Total Fe abundances are usually below 1 wt% in metapelites of the ''No-sulfide'' group, increasing irregularly up to ~ 6 wt% and ~ 8.5 wt% in samples forming the ''Py-bearing'' and ''Mineralized'' groups, respectively. Accordingly, most of the samples forming the three groups display S/Fe ratios below 0.52, pointing again to oxic conditions (e.g., Raiswell et al. 1988 and Georgiev et al. 2012); the exceptions are confined to 6 ''Py-bearing'' and 4 ''Mineralized'' samples from the *lower* and *upper* VSC sections in Neves-Corvo and Aljustrel, whose S/Fe ratios suggest (local?) prevalence of anoxic or anoxic/euxinic transitional conditions.

Multi-element Patterns of Hydrothermal Alteration and Mineralization Imprinting

Abundances of minor and trace elements were normalized to both the North American Shale Composition (NASC; Condie 1993, Taylor and McLennan 1995) and Average Shale (AS; Wedepohl 1971, 1995) composition; PAAS was not used in this approach because some elements of interest could not be normalized with this compositional reference. The NASC- and AS-normalized patterns are evidently similar, as expected, differing only in the relative intensity of anomalies (Electronic Supplementary Material 2). In general, the normalized patterns displayed by each group of samples (''No-sulfide,'' ''Py-bearing'' and ''Mineralized'') are internally consistent (Fig. 10), revealing a gradual increase in the abundances of As, Sb, Cu, Zn, Pb, Co, Ni (± V) as the amount and diversity of sulfide phases enlarge. In mineralized samples, As and Sb positive anomalies are quite often above 100 × NASC, going up to 50–300 × NASC for Cu, Zn and Pb; for Ni, Co and V, the maximum values recorded are 5–20 × NASC. This elemental increase is coupled by a distinct, although irregular, decline of Rb, Sr and Ba contents, reflecting the progression of compositional changes likely related to hydrothermal alteration processes (namely chloritization).

For the Neves-Corvo deposit, some of the detected compositional variations might be interpreted because of local geochemical gradients distinctly developed in the hanging wall (*upper* VSC) or footwall of different orebodies (PQG and *lower* VSC). In fact, two samples from hanging walls of Corvo and Lombador orebodies present intense As and Sb anomalies (~ 1000 × NASC) along with Cu and Zn (~ 20 × NASC), besides minor anomalies in Co, Ni and Pb (~ 10 × NASC). Metapelites from stockwork domains of the Corvo orebody display the stronger Cu anomalies (up to 100 × NASC) together with As and Sb (up to 100 × NASC), besides Co, Ni and Pb (up to 10 × NASC). Metapelites forming the footwall of the Lombador orebody show systematic enrichments in As and Sb, jointly reaching up to 100 × NASC, along with Cu, Zn, Pb and Co (all up to 50 × NASC). Metapelites from the footwall of Zambujal and Neves orebodies record the highest Zn (± Pb) anomalies in comparison with the other orebodies; for some mineralized samples from Neves, the Zn and Pb anomalies spread up to 100 × NASC and 50 × NASC, respectively. Compositional features of footwall samples compare well with those characterizing metapelites from the ore horizon of Lousal, for which the anomalies of As, Cu, Sb, Co and Pb attain 1000 × , 300 × , 100 × , 20 × and 20 × NASC, respectively (whole-rock geochemistry data of non-weathered samples reported in Fernandes 2011).

The studied metapelites from Aljustrel mine are confined to the *upper* VSC. The available dataset does not include a large number of mineralized samples (displaying compositional fingerprints similar to those gathered for the hanging walls of Corvo and Lombador orebodies), but the ''Py-bearing'' group is well represented. For the latter group of metapelites, the most significant signs can be summarized as follows: As and Sb, ~ 100 × NASC; Cu, Pb and Zn, 5–10 × NASC; and Co and Ni, usually up to 5 × NASC but increasing till ~ 10 × NASC in several metapelites containing volcanic-derived components. Metapelites from the Aljustrel mine and the nearby Gavião prospect show strong compositional similarities, but signs of hydrothermal and/or mineralization overprints are quite subtle in the Monte das Mesas prospect, some few kilometers to the W of Gavião.

DISCUSSION

Sediment Provenance

The results here reported compare well with other datasets available for the IPB (e.g., Jorge et al.

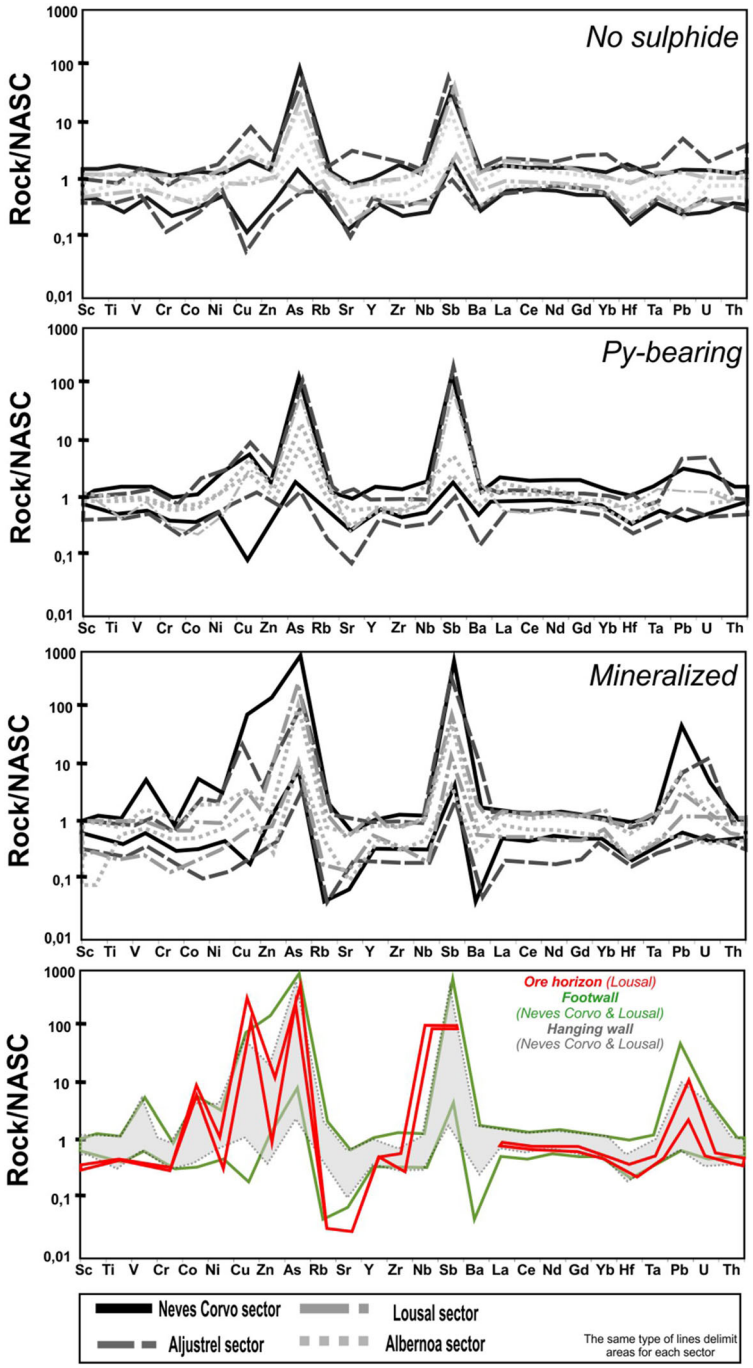

Figure 10. NASC-normalized, multi-element patterns for IPB metapelites. For each sampling sector, the patterns were assembled in accordance to the previously defined groups: ''No-sulfide,'' ''Py-bearing'' and ''Mineralized''.

2006; Saéz et al. 2011), showing that PQG and VSC metapelites derived from similar continental sources. These rocks are mostly composed of a mixture (in variable proportions) of clayey-derived and (fine-grained) quartz sandy-derived components. A third component, of local volcaniclastic origin, is also present in many VSC samples, most often when these rocks are part of *upper* VSC sections. The

Al_2O_3/TiO_2 and Zr/Al_2O3 ratios allow distinguishing the three components (Fig. 11A), which also display distinct ranges of Sc/TiO_2 and Ga/TiO_2 and Th/Sc values: (i) the clayey-derived component predominates in *middle* and *upper* VSC samples and is characterized by $\sim 25 \leq Al_2O_3/TiO_2 \leq \sim 30$, $\sim 0.5 \leq$ Th/Sc $\leq \sim 0.8$ and $0.0005 \leq Zr/Al_2O_3 \leq 0.001$; (ii) the sandy-derived component, clearly more significant in PQG and *lower* VSC metapelites, is indicated by $\sim 10 \leq Al_2O_3/TiO_2 \leq \sim 20$, $\sim 0.5 \leq$ Th/Sc $\leq \sim 1.0$ and $0.001 \leq Zr/Al_2O_3 \leq 0.025$; and (iii) the volcanic-derived component, quite evident in upper VSC sequences found in the Aljustrel sector, is typified by $\sim 45 \leq Al_2O_3/TiO_2 \leq \sim 65$, Th/Sc > 1.0 and irregular, although low (< 0.05), Zr/Al_2O_3 ratios.

The composition of PQG and VSC metapelites is mainly controlled by their sedimentary sources, which could record quite variable weathering effects. The chemical index of alteration (CIA; e.g., Nesbitt and Young 1982, 1984; Fedo et al. 1995; Young and Nesbitt 1998) is commonly used to

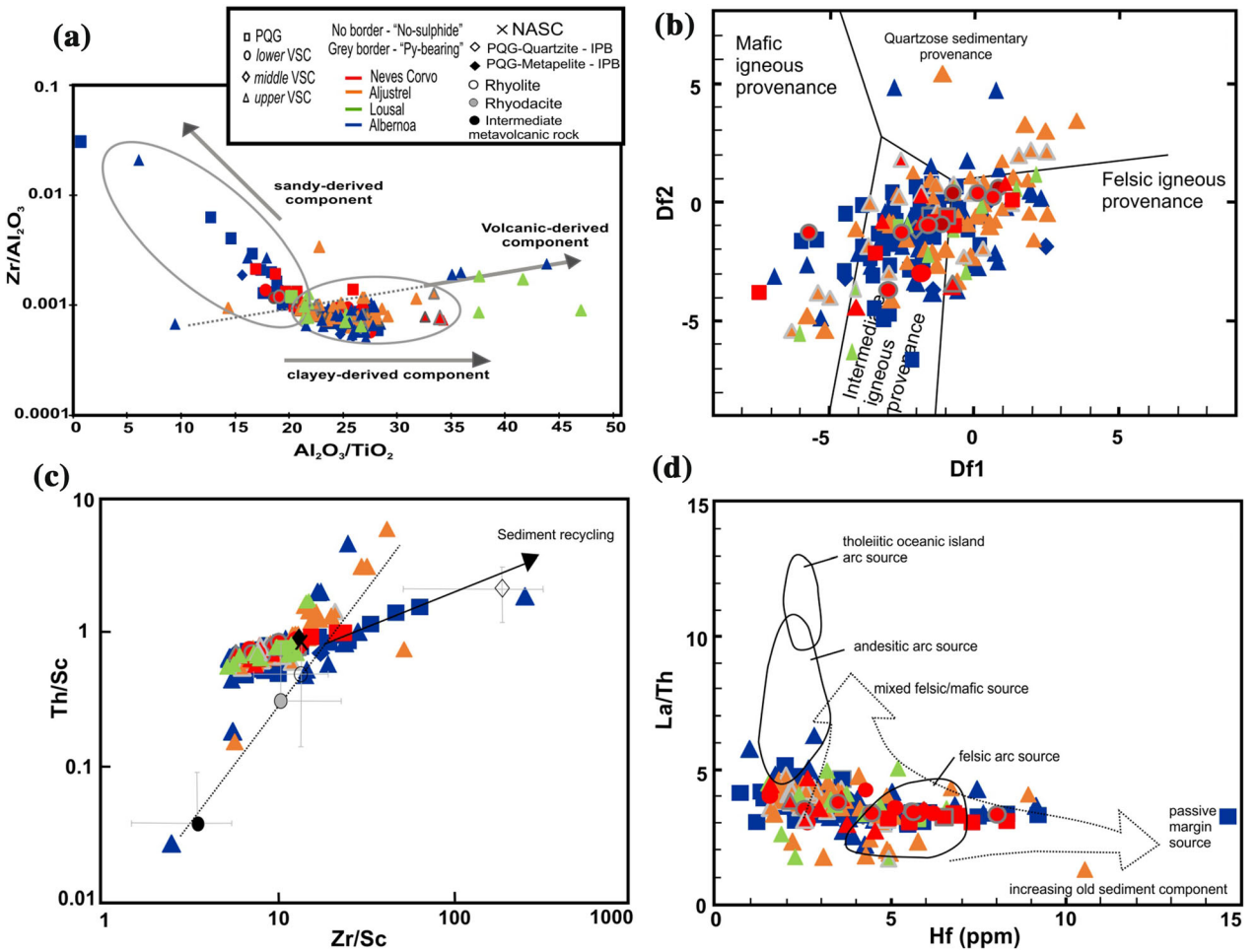

Figure 11. Al_2O_3/TiO_2 vs. Zr/Al_2O_3 plot (**A**). Discrimination function diagram for the provenance signatures of clastic sedimentary rocks using major element ratios (after Roser and Korsch 1986) applied to IPB metapelites (**B**). Provenance diagrams Zr/Sc vs. Th/Sc(**C**) and La/Th vs. Hf(**D**), after Slack et al. (2004) and Floyd and Leveridge (1987), respectively. Because abundances of some elements were considerably disturbed during hydrothermal alteration and mineralization processes, only samples forming the ''No-sulfide'' and ''Py-bearing'' groups ($n = 224$) were plotted. The discriminant functions used in (**B**) are: $Df1 = 30.638TiO_2/Al_2O_3 - 12.541Fe_2O_3(total)/Al_2O_3 + 7.329MgO/Al_2O_3 + 12.031Na_2O/Al_2O_3 + 35.402K_2O/Al_2O_3 - 6.382$; $Df2 = 56.500TiO_2/Al_2O_3 - 10.879Fe_2O_3(total)/Al_2O_3 + 30.875MgO/Al_2O_3 - 5.404Na_2O/Al_2O_3 + 11.112K_2O/Al_2O_3 - 3.89$. In (**C**) and (**D**), for comparison purposes, the ratios typifying NASC (Condie 1993), as well as the average ratios and corresponding standard deviation measures calculated for PQG quartzite and metapelite ($n = 75$; different sites of IPB; Jorge 2009) and VSC–metavolcanic rocks of Albernoa (intermediate composition, $n = 9$, rhyodacite, $n = 27$, rhyolite, $n = 22$; Codeço et al. 2018) are also displayed.

ascertain the intensity of source area weathering, and for the present study, it ranges from about 55 to 94 when samples evidently mineralized are excluded, although clustering between 70 and 79 (Fig. 12A). Thus, most of the sediments involved in the generation of IPB metapelites resulted from a chemical weathering of moderate to strong intensity. The discrimination function diagram for the provenance signatures of clastic sedimentary rocks using major element ratios (Roser and Korsch 1986) suggests in addition that the main provenances of these fine-grained clastic sediments were felsic (granite) and intermediate (granodiorite to quartz diorite) rocks (Fig. 11B). A similar inference emerges when Al_2O_3/TiO_2 ratios are used along with the ranges indicative of granitoid sources, as defined by Girty et al. (1996): For non-mineralized samples, the Al_2O_3/TiO_2 ratios vary between $\sim$ 12 and 32, with a large majority between 20 and 27 if metapelites bearing an important quartz sandy-derived component are separated, as well as some outliers with higher Al_2O_3/TiO_2 values (up to $\sim$ 50) representing metapelites from Aljustrel and Lousal sectors enriched in volcanic-derived components.

Using the Zr/Sc and Th/Sc ratios (Fig. 11C), a prevalent evolved felsic source, complemented with sediment recycling, can also be inferred for the IPB metapelites (Slack et al. 2004). This is consistent

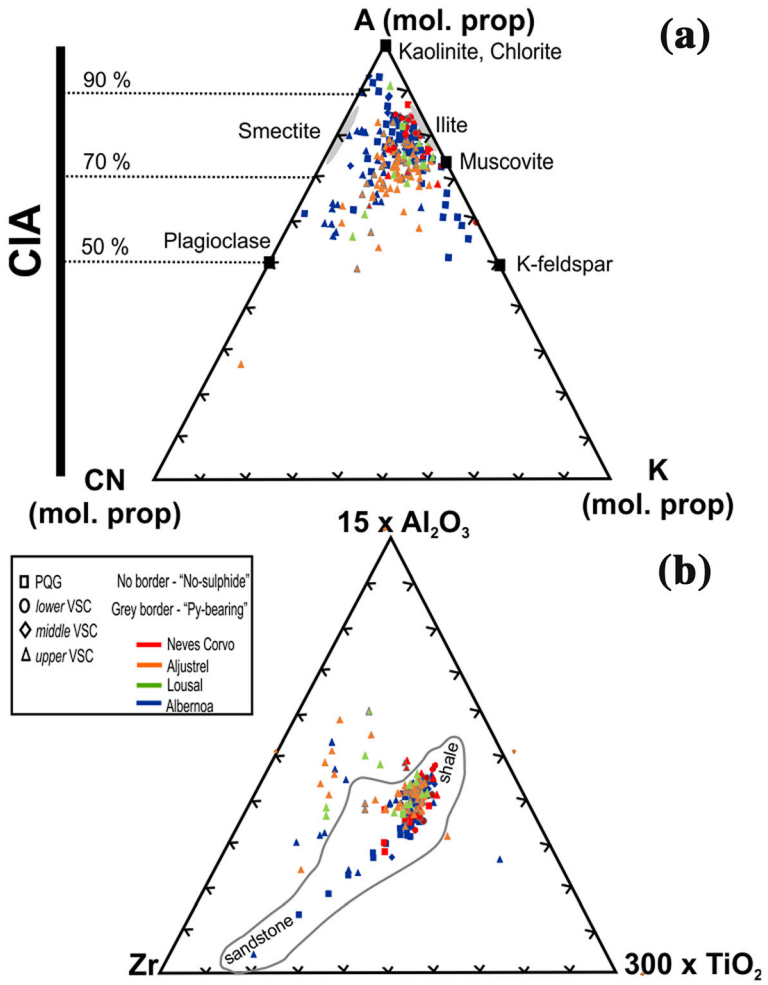

Figure 12. Ternary CN-A-K (= $CaO + N_2O - Al_2O_3 - K_2O$, mole proportions) diagram showing the scattering of CIA values (**A**) and $Zr - Al_2O_3$ ($\times$ 15) $- TiO_2$ ($\times$ 300) diagram (**B**) illustrating the compositional spreading displayed by metapelites of ''No-sulfide'' and ''Py-bearing'' groups picked in the four sectors (n = 224). In the ternary diagram (**B**), the solid line delineates the field of clastic sedimentary rocks, according to Garcia et al. (1994).

with the obtained $(Eu/Eu^*)_{CN}$ ratios (normalized to chondrite C1; Taylor and McLennan 1995), largely scattered within the 0.4 to 0.9 interval, and the Cr/Th ratios, varying within the range indicated by Cullers (1994) as typical of felsic rocks (from 2.5 to 17.5): median values characterizing the Cr/Th ratio distributions (not differing significantly from average values) fall within the narrow interval 6 to 9, despite the lower (< 2.5) Cr/Th ratios showed by some few samples from the Aljustrel, Lousal and Albernoa sectors. Such prevailing felsic source is likewise supported by the La/Th vs. Hf diagram of Floyd and Leveridge (1987), which suggests in addition a heterogeneous mixing of igneous-derived and old sediment components, the latter quite evident in many PQG and *lower* VSC samples picked in Neves-Corvo and Albernoa sectors, as well as in few pelites of *middle* and *upper* VSC from the Albernoa sector (Fig. 11D). Derivation from heterogeneous felsic to intermediate igneous sources are also indicated by the relatively uniform median (or average) values describing the distributions of La/Yb ratios for all the key sectors, ranging between ~ 13 and ~ 15, despite the wider data scattering generated by the aforementioned small subset of samples from Aljustrel, Lousal and Albernoa sectors.

Among major elements, Al and Ti are usually considered to be stable during weathering and accumulate in the residue, as happens with Zr, Th, Hf and Sc (e.g., Bathia 1983; Bathia and Crook 1986; Goodfellow et al. 2003; this study). The CIA values displayed by most of the IPB metapelites confirm this assertion, further corroborated by the cross-relationships between all these elements (see electronic supplementary material 3). Thus, the ternary Al_2O_3-Zr-TiO_2 plot is quite helpful to distinguish either the influence of sorting processes (Garcia et al. 1994) or the late incorporation of local volcanic-derived components (Fig. 12B). From this plotting, one may conclude that PQG metapelites, particularly those picked in the Albernoa sector, tend to display higher compositional maturity than most of the VSC samples, which are usually characterized by a narrower range of TiO_2-Zr variations. On the contrary, the influence of volcanic-derived components is solely evident for a limited set of VSC samples from all sectors except Neves-Corvo. Therefore, crisscrossing this indication with the aforementioned inferences based on the discrimination function diagram using major element ratios (Fig. 11B) and from the Zr/Sc vs. Th/Sc and La/Th vs. Hf plots (Fig. 11C, D), one may conclude that: IPB metapelites represent a wide variety of fine-grained clastic sediments with variable degree of sorting/maturity and intensity of chemical weathering, which were largely derived from different sources of felsic (granitic) to intermediate (granodiorite to quartz diorite) composition. A significant number of PQG metapelites display features indicative of high compositional maturity of the primary sediments to which they are related, pointing also to accessory contributions from old sedimentary sources. In contrast, significant incorporation of volcanic-derived components into pelite sediments is local and confined to some VSC sections, according to observations independently achieved. Additionally, the tendency of (fine-grained) quartz sandy-derived components is more significant in some PQG to *lower* VSC sections (as the case of metapelites at the footwall of Lombador and Corvo orebodies of Neves-Corvo mine), suggesting that differences in sedimentation processes existed for the same period. These differences could be quite limited, just controlled the local basin configuration, or a result of intermittent energy changes in sedimentation during the Upper Devonian, with significant implications in biogeochemical processes (see section ''Sediment Provenance'').

Geochemical characteristics of clastic sedimentary rocks could also be used to infer their tectonic settings (e.g., Bhatia 1983; Bhatia and Crook 1986), as shown in Fig. 13 by selecting two commonly used discrimination diagrams. The discriminant functions using major elements suggest that non-mineralized metapelite suites of PQG and VSC overlap extensively, and with few exceptions, plot nearby transitional fields from ''passive'' to ''active continental margins'' (Fig. 13A). These indications must be regarded carefully because they should be biased due to the general tendency for geochemical mobility of many elements included in Df1 and Df2 functions during the long-lived geological evolution experienced by these sediments after their deposition. The fingerprints provided by the immobile (see Electronic Supplementary Material 3) trace elements Th, Sc and Zr are slightly different and likely more reliable, pointing to a major cluster between fields of ''active continental margins and arcs'' (Fig. 13B), not far from the averages of PAAS and upper continental crust. In the Sc–Th-Zr/10 ternary plot, it is

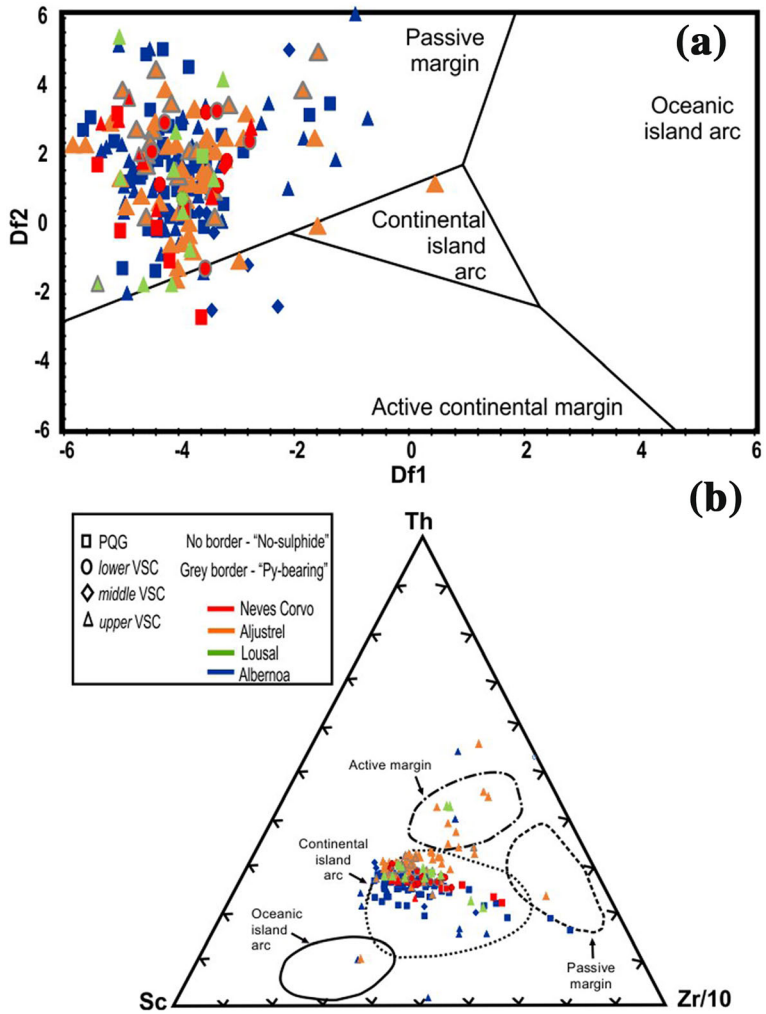

Figure 13. Unravelling tectonic settings for non-mineralized metapelites (n = 224) of IPB using (**A**) the discriminant function diagram of Bhatia (1983) and (**B**) the Sc–Th–Zr/10 diagram of Bhatia and Crook (1986). Discriminant functions in the first plot are: Df1 = $-0.0447SiO_2 - 0.972TiO_2 + 0.008Al_2O_3 - 0.267Fe_2O_3 + 0.208FeO - 3.082MnO + 0.140MgO + 0.195CaO + 0.719Na_2O - 0.032K_2O + 7.510P_2O_5 + 0.303$; Df2 = $-0.421SiO_2 + 1.988TiO_2 - 0.526Al_2O_3 - 0.551Fe_2O_3 - 1.610FeO + 2.720MnO + 0.881MgO - 0.907CaO - 0.177Na2O - 1.840K_2O + 7.244P_2O_5 + 43.57$. Fields as follows: **1**—oceanic island arc; **2**—continental island arc, **3**—active continental margin; and **4**—passive continental margin.

also clear that deviations toward the field of ''active continental margins'' are exclusively denoted by samples from *upper* VSC, whereas some PQG samples indicate the most evident shifts in direction of the ''passive continental margins'' field. These general inferences, matching those reported in Saéz et al. (2011), do not conflict with the geodynamic evolution proposed for the SPZ (see ''Geological Background'' section).

Paleo-Redox Conditions

Appraisals of redox conditions are critical to estimate the oxygen and hydrogen sulfide availability in bottom waters in equilibrium with clastic sediments, which is determinant for the progress of reactions assisting the development of some types of shale-hosted massive sulfide ores (e.g., Tornos 2006; Tornos and Heinrich 2008; Tornos et al. 2008; Sáez

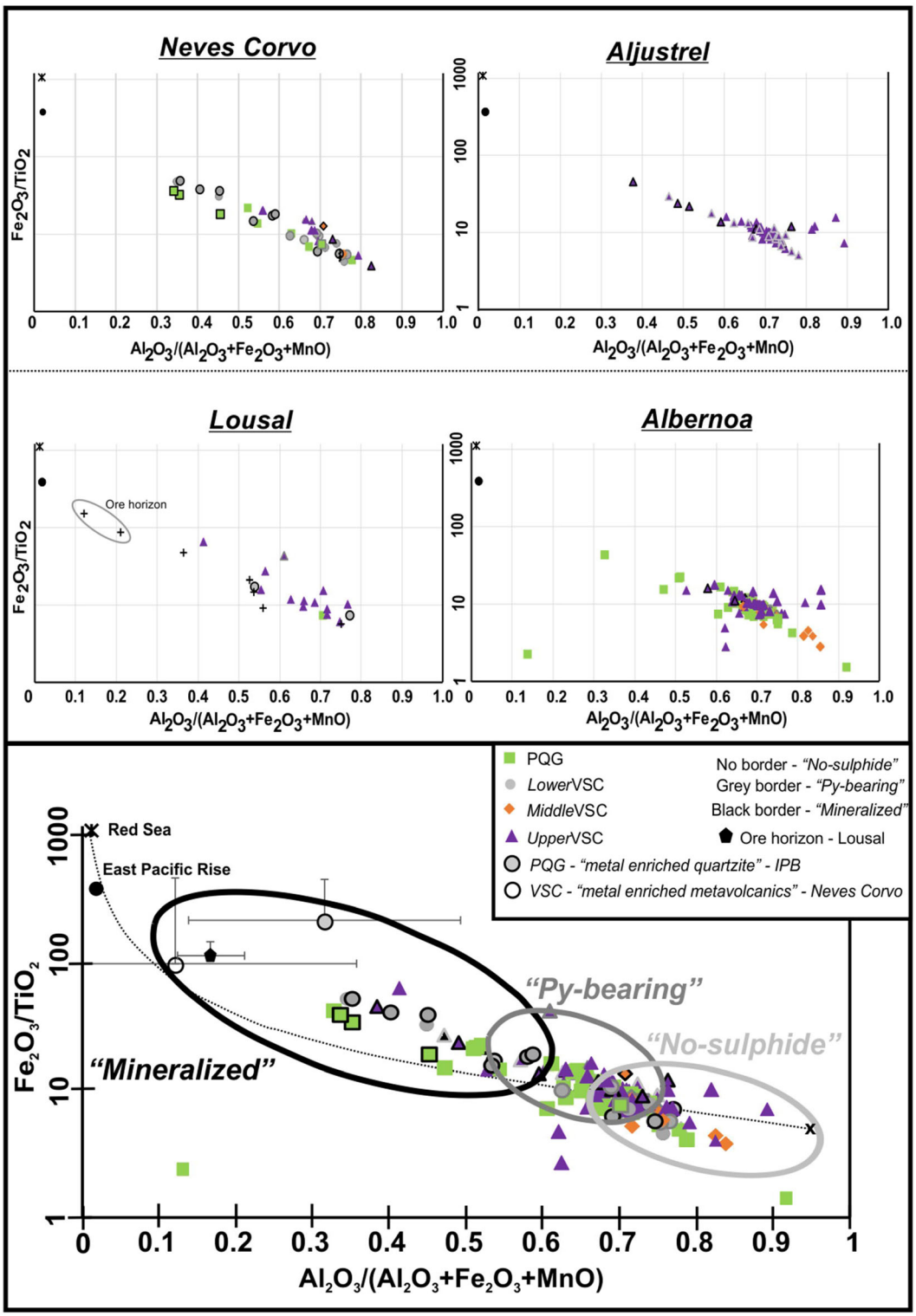
Neves Corvo
Aljustrel
Lousal
Albernoa
Ore horizon
Fe2O3/TiO2
Al2O3/(Al2O3+Fe2O3+MnO)
PQG
LowerVSC
MiddleVSC
UpperVSC
No border - "No-sulphide"
Grey border - "Py-bearing"
Black border - "Mineralized"
Ore horizon - Lousal
PQG - "metal enriched quartzite" - IPB
VSC - "metal enriched metavolcanics" - Neves Corvo
Red Sea
East Pacific Rise
"Py-bearing"
"No-sulphide"
"Mineralized"

◄ **Figure 14.** Fe_2O_3/TiO_2 vs. $Al_2O_3/(Al_2O_3 + Fe_2O_3 + MnO)$ diagram for the four sectors (Neves-Corvo = 46, Aljustrel = 84, Lousal = 16 and Albernoa = 116) illustrating the mixing strip between a ''terrigenous'' end member (given by the NASC projection, Condie 1993) and a conceptual ''exhalative hydrothermal'' term represented by the composition of the East Pacific Rise and/or Red Sea brine pool (e.g., Marchig et al. 1982; Goodfellow et al. 2003). Metal-enriched PQG quartzites and VSC metavolcanics were plotted for reference (data from Jorge 2009 and Relvas et al. 2006a, respectively). The average and standard deviation values for ''No-sulfide,'' ''Py-bearing'' and ''Mineralized'' groups are plotted as diamonds and error bars. The ore horizon of Lousal is represented by seven non-weathered samples (+) reported in Fernandes (2011).

et al. 2011; Velasco-Acebes et al. 2019). In these geological settings, early redox conditions are regulated by microbially mediated and abiotic reactions that ultimately destroy the organic matter throughout a long cascade of reactions, involving oxygen loss, manganese reduction, iron reduction, nitrate reduction, sulfate reduction and methanogenesis. So, the joint inspection of redox-sensitive elements that participate in these reactions (becoming enriched or depleted in sediments) could be used to infer the redox conditions in paleo-environments (e.g., Wignall and Myers 1988; Calvert and Pedersen 1993, 2007; Wignall and Twichett 1996; Morford and Emerson 1999; Algeo and Maynard 2004; Brumsack 2006; Tribovillard et al. 2006). In this regard, it should be emphasized that Mo systematics (a powerful redox proxy—e.g., Scott and Lyons 2012) could not be used in the present study because its concentration is almost always below the detection limits of the analytical methods used to characterize the whole-rock geochemistry of IPB metapelites.

As shown before, variations in redox-sensitive elements displayed by non-mineralized dark gray to black metapelites of PQG and VSC strongly suggest that deposition of their parental sediments occurred mainly in oxygenated environments, occasionally transitional to sub-oxic conditions. Moreover, dominant sub-oxic settings, sometimes attaining the sub-oxic/anoxic boundary, could be inferred for the hosting environments of protoliths of many ''Py-bearing'' metapelites from *upper* (sporadically, also *lower*) VSC sequences. This overall range of redox conditions is similar to that deduced for the locales where protoliths of the ''Mineralized'' group formed, notwithstanding the anoxic or anoxic to euxinic indications provided by some few mineralized metapelites from Neves-Corvo and Aljustrel. Significantly, with one exception (the *lower* VSC ore horizon at Sesmarias), the shift toward anoxic or anoxic/euxinic environments is denoted by mineralized metapelites included in *middle* and *upper* VSC sections of Neves-Corvo and Aljustrel, respectively.

In modern marine systems, the common association of V and P reflects temporal and spatial shifts in bottom water chemistry from sub-oxic (phosphate concentrated) to more reducing conditions that favor V accumulation (e.g., Breit and Wanty 1991). In addition, localized removal of P and V from pore waters has been demonstrated at micro-niches where sulfide phases are produced, possibly involving bacterial uptake and reduction of vanadate to insoluble V(III) by sulfides (Stockdale et al. 2008). Such processes might have affected the local abundances of V and P in the protoliths of IPB metapelites, particularly when subjected to transitional sub-oxic/anoxic conditions. Even so, according to the available information, evidence for differential removal/fixation of V and P is feeble and limited to few mineralized samples from the footwall of Corvo orebody at Neves-Corvo, which record a clear increase in V concentration. Note also that V and P_2O_5 abundances do not covary in the examined metapelites and this should reflect mostly a primary feature instead of a disturbance caused by differential removal/fixation at the sub-oxic/anoxic boundary.

Like V and P, As and Sb are controlled by both biological and redox reactions, their behaviors diverging at the sediment–water interface and near the sulfide boundary due to the relative stability of the III and IV species, as well as the methyl forms of dissolved As and Sb (e.g., Cutter 1991, 1992; Cutter and Cutter 2006). So, the common As and Sb fingerprints in IPB metapelites lacking any signs of mineralization are consistent with prevalent oxic/sub-oxic transitional conditions under which chemical speciation dissimilarities and differential adsorption/desorption by Mn/Fe oxyhydroxides are more favorable to As fixation in relation to Sb, emphasizing possible elemental concentration differences in water. Hence, the evident increasingly upgrading of As and Sb in metapelites of ''Py-bearing'' and ''Mineralized'' groups (along with Co, Ni, Cu, Zn and Pb) reflects later, multistage, exhalative/hydrothermal inputs rather than particular redox conditions achieved during sedimentation and diagenesis. This is not an uncommon process, as documented in many other studies (e.g., Marchig

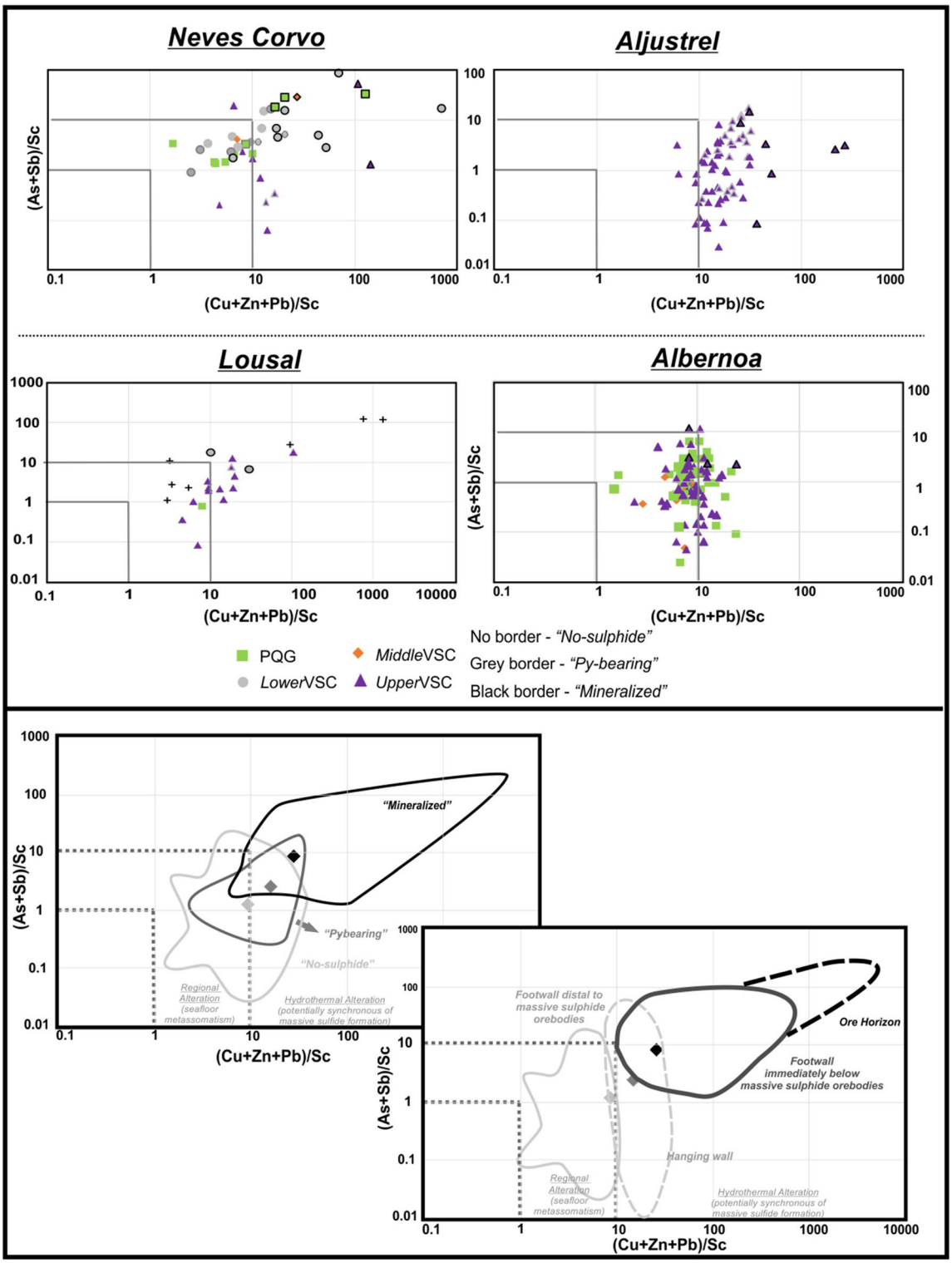
Neves Corvo
Aljustrel
Lousal
Albernoa
(As+Sb)/Sc
(Cu+Zn+Pb)/Sc
0.1
1
10
100
1000
10000
0.01
PQG
MiddleVSC
LowerVSC
UpperVSC
No border - "No-sulphide"
Grey border - "Py-bearing"
Black border - "Mineralized"
"Mineralized"
"Pybearing"
"No-sulphide"
Regional Alteration (seafloor metassomatism)
Hydrothermal Alteration (potentially synchronous of massive sulfide formation)
Footwall distal to massive sulphide orebodies
Ore Horizon
Footwall immediately below massive sulphide orebodies
Hanging wall

◀ **Figure 15.** (As + Sb)/Sc *vrs.*(Cu + Zn + Pb) diagram illustrating the chemical effects related to post-sedimentary transformations. Values between 1.0 and 10.0 of these geochemical ratios trace effects ascribed to oceanic metasomatism processes (*regional alteration pattern*); ratios above 10.0 indicate the proximity of hydrothermal discharges potentially related to ore-forming systems. The ore horizon of Lousal is represented by seven non-weathered samples (+) reported in Fernandes (2011).

et al. 1982; Lottermoser 1991; Gurvich 2006; Hung et al. 2018; Hollis et al. 2019). Note also that late hydrothermal inputs, also indicated by the positive $(Eu/Eu^*)_{PAAS}$ anomalies displayed by samples from the orebodies footwall at Neves-Corvo and the ore horizon at Lousal, correlate well with chemical transformations developed nearby the main discharge zones, as described for other massive sulfide accumulations (e.g., Michard et al. 1983; Barret et al. 1990; Goodfellow et al. 2003).

The MREE bulge displayed by several PAAS-normalized REE patterns points also to early oxic/sub-oxic sedimentary environments where Mn/Fe oxyhydroxides could efficiently and preferentially scavenge MREEs during their formation at the chemocline (e.g., Haley et al. 2004; Poulton and Canfeld 2011; Kim et al. 2012). Subsequent chemical transformations experienced by sediments under reducing and alkaline conditions will favor the reductive dissolution of Mn/Fe oxyhydroxides and the release of adsorbed MREE (and As). In these circumstances, the MREE bulge will be destroyed (as observed in the large majority of black metapelites) because no favorable conditions existed to incorporate or adsorb the released MREE into authigenic phases; arsenic will be preferentially incorporated in early formed pyrite (e.g., Tabelin et al. 2012; Large et al. 2014).

Total Fe abundances are low (< 1 wt%) in many dark gray to black metapelites of the studied PQG and VSC sequences, indicating that parental unconsolidated clastic sediments were largely impoverished in reactive iron. For some stratigraphic levels of *lower* and *middle* VSC, the Fe concentrations are fairly higher (up to ~ 2–4 wt%), but the lack of pyrite or other iron sulfide phase suggests low availability of reduced sulfur during sedimentation and diagenesis, thus favoring the fixation of reactive iron in carbonate phases. Therefore, the growth of early pyrite (usually evolving from fine framboids to colloform and coarser, recrystallized, (sub)euhedral aggregates) in some layers of the *lower* and *upper* VSC reflects just the local availability of reactive iron and reduced sulfur, strongly restraining the basin settings where real (sub-oxic to) anoxic conditions were attained. A relative shortage of reactive organic matter in the original sediments might explain the inferred deficiency in reduced sulfur; but a rapid sediment burial, hampering the interaction with sulfate-rich seawaters, could instead justify both that deficiency and the low Fe abundances for most of the studied PQG and VSC sequences.

Summarizing, prevalent redox conditions in the confined (2^{nd} or 3^{rd} order) basins where the fine-grained sedimentary pile developed, from late Famennian to Visean: (i) evolved from oxic to sub-oxic, or even anoxic, during sedimentation and diagenesis mostly by means of microbially mediated reactions that largely shaped the initial stages of mineralizing processes; or (ii) were mostly confined to oxic settings (at places transitional to sub-oxic), later on getting heterogeneous anoxic signs due to multistage interaction with reducing hydrothermal fluids (from early hydrothermal venting/exhalation into unconsolidated sediments to late, fracture-controlled, high-temperature fluid flow prior to Variscan deformation and metamorphism). Both alternatives are possible and could explain the variable geological/geochemical record so far documented for different basin settings hosting distinct styles of massive sulfide mineralization (impacting also the tonnage, grades and metal association in known orebodies). However, considering the information provided by redox-sensitive and sulfide-forming elements, the second alternative should be favored, suitably portraying the environmental redox evolution connected to the development of larger ore-forming systems with significant metal enrichment and diversity, at least in the Portuguese segment of IPB. Similar inferences can be done on the basis of both the textural and mineralogical evolution experienced by the IPB ores (e.g., Almodóvar et al. 2019) and changes in Pb isotopic signatures displayed by hydrothermally altered and mineralized metapelites (e.g., Jorge et al. 2007; Jorge 2009; Luz et al. 2019; Piercey and Krammer 2019).

Vectoring to Massive Sulfide Ore Systems in IPB

Hydrothermal/mineralization imprints over siliciclastic matrices can be assessed by means of

several geochemical criteria. For the IPB metasedimentary rocks, including metapelites with volcanic-derived components, these imprints are significant and represent a useful exploration footprint, when $Fe_2O_3/TiO_2 > 10$ and $Al_2O_3/(Al_2O_3 + Fe_2O_3 + MnO) \leq 0.6$ (Luz et al. 2019). A detailed inspection of the whole dataset (Fig. 14) corroborates these thresholds as indicative of mineralizing settings, aggregating almost all the PQG and *lower* VSC samples at the footwall of Lombador and Neves orebodies, as well as the black metapelites forming the ore horizon at Lousal and Sesmarias. There are some few exceptions to this trend, due to an atypical raising of $Al_2O_3/(Al_2O_3 + Fe_2O_3 + MnO)$ ratios and consequent shifting to compositional fields dominated by samples of the ''Py-bearing'' and ''No-sulfide'' groups. However, these exceptions (imposed by anomalously high aluminosilicate contents) do not influence the focal interpretation, as revealed by the plotting of statistical information regarding the very same geochemical ratios for ''metal-enriched quartzites'' and ''metal-enriched metavolcanics'' assessed on the basis of published datasets (Jorge 2009; Relvas et al. 2006a).

The $Al_2O_3/(Al_2O_3 + Fe_2O_3 + MnO)$ vs. Fe_2O_3/TiO_2 plot shows in addition that samples included in the ''Py-bearing'' group display narrow ranges of both geochemical ratios, namely $5 \leq Fe_2O_3/TiO_2 \leq 10$ and $0.6 < Al_2O_3/(Al_2O_3 + Fe_2O_3 + MnO) \leq 0.7$. Therefore, considering all the compositional features that characterize this particular group of metapelites, one may conclude that such small variation in both geochemical ratios represents: (i) sulfide growth during diagenesis (denoting availability of reactive iron and reduced sulfur) and/or (ii) effects resulting from low-temperature exhalative/hydrothermal activity that may expand the formation of iron sulfides (and recrystallization of those previously formed) along with accessory amounts of sphalerite and/or (iii) outcomes of delicate interactions with fluids of higher temperature, increasing the recrystallization path of early developed pyrite and favoring the deposition of minor amounts of other sulfides (chalcopyrite in particular). Thus, this transitional range of values displayed by the Fe_2O_3/TiO_2 and $Al_2O_3/(Al_2O_3 + Fe_2O_3 + MnO)$ ratios does not discriminate properly ''barren'' settings (where diagenetic pyrite is the sole sulfide) from places that could record the involvement of hydrothermal fluids, even if they correspond to lateral and/or distal variations in relation to massive sulfide ores.

The $5x[(Fe_2O_3 + MgO + MnO)/Al_2O_3]$, (Cu + Zn + Pb)/Sc and (As + Sb)/Sc ratios were recently proposed to separate barren from altered/mineralized metasedimentary sequences in IPB, the latter group displaying values above 10 for the three geochemical ratios (Luz et al. 2019). The usefulness of these thresholds was confirmed for the whole dataset, but the particular nature of the sampling now reported allows deepening some considerations (Fig. 15 and Electronic Supplementary Material 4). Separation of barren from the altered and mineralized metapelites in Neves-Corvo is clear: samples showing the strongest effects of alteration/mineralization come from the hosting settings of Lombador and Neves orebodies, whereas the less altered/mineralized samples represent mostly the envelop of Zambujal orebody, regardless of the stratigraphic position. Mineralized samples from Lombador represent mainly stockwork domains with quartz ± (Fe–Mg)-chlorite ± siderite + pyrite ± sphalerite ± chalcopyrite, whereas at Neves and Zambujal footwalls the dominant sulfides in mineralized metapelites are disseminated, conceivably representing hydrothermal replacements of primary sediments (e.g., Carvalho 2016). Samples from Aljustrel (*upper* VSC) plot largely above the (Cu + Zn + Pb)/Sc threshold, but close to it; usually, these samples present framboidal to recrystallized pyrite as the main sulfide phase, which does not necessarily imply strong interaction with late mineralizing fluids, as suggested by the (As + Sb)/Sc ratios < 10. Samples from Lousal and Sesmarias define compositional trends similar to those reported for Neves-Corvo, being noteworthy the extremely high (As + Sb)/Sc and (Cu + Pb + Zn)/Sc ratios (> 100 and 1000, respectively) recorded by the black metapelites of the ore horizon (*lower* VSC). On the contrary, the compositional variability documented for metapelites of the Albernoa sector (from PQG to *upper* VSC) reflects mostly geochemical imprints related to seafloor metasomatism, locally complemented by accessory signs of early sulfide growth (Luz et al. 2019).

According to the available data, consistent increase in (Cu + Zn + Pb)/Sc and (As + Sb)/Sc ratios represents a valuable footprint toward ore horizons, despite the partial overlapping of the areas encircling the ''No-sulfide,'' ''Py-bearing'' and ''Mineralized'' groups. The growing of (Cu + Zn + Pb)/Sc seems to proceed under higher rates in comparison

with rising of (As + Sb)/Sc, but the latter is not negligible, particularly near ore horizons or of stockworks at the footwall of high-grade orebodies. Metapelites from the hanging wall of known orebodies record often the effects of metal redistribution (prior or after the Variscan deformation); their (As + Sb)/Sc ratios vary widely, but values of (Cu + Zn + Pb)/Sc are apparently confined to the narrow range of $\sim$ 10 to 50. Finally, it should be noted that the trend under discussion are only slightly modified and remain clearly visible if Co and/or Ni are added to either the (As + Sb) or to the (Cu + Zn + Pb) totals. It is also noteworthy that these same trends can be also evidenced if normalization is made relative to Th instead of relative to Sc, as above. This is relevant because Th (unlike Sc) is readily measured with portable XRF apparatus (see Electronic Supplementary Material 5) commonly used in mineral exploration activities.

CONCLUSIONS

The surveyed PQG and VSC successions include a large variety of fine-grained clastic sediments deposited from Famennian to Visean, lately subjected to metamorphic recrystallization under low-grade conditions. The shale/silty facies prevail in VSC, indicating deposition in confined, tectonic-controlled, basins that affect the previously developed siliciclastic platform and may comprise different volcanic products. No major compositional differences exist between metapelites forming the examined PQG and VSC sections, and the observed geochemical trends mostly represent different proportions of clay/mud-rich and quartz-rich components largely derived from different sources of felsic (granitic) to intermediate (granodiorite to quartz diorite) composition. A significant number of PQG metapelites display features indicative of high compositional maturity of the primary sediments to which they are related, pointing also to accessory contributions from old sedimentary sources. Incorporation of volcanic-derived fractions contributes to some compositional deviations, evident in several *upper* VSC sections. Mineral transformations developed during diagenesis and/or hydrothermal alteration/mineralization processes superimpose an imprint on the primary composition.

Prevalent redox conditions in the confined basins were mostly oxic (at places transitional to suboxic), later on getting heterogeneous anoxic signs due to multistage interaction with reducing hydrothermal fluids. This interaction is quite variable and could be limited to early hydrothermal venting/exhalation into unconsolidated sediments, or evolve afterward to intense high-temperature, fracture-controlled, fluid flow prior to Variscan deformation and metamorphism. Consistent increase in Fe_2O_3/TiO_2, (Cu + Zn + Pb)/Sc and (As + Sb)/Sc ratios to values above 10 represents a valuable footprint toward ore horizons.

ACKNOWLEDGMENTS

The support of sampling surveys provided by Empresa Portuguesa de Obras Subterrâneas (EPOS, S.A), Lundin Mining, ALMINA, Empresa de Desenvolvimento Mineiro (EDM), ESAN and AVRUPA Minerals is truly appreciated. Filipa Luz acknowledges the FCT (Fundação para a Ciência e Tecnologia) Grant PD/BD/114485/2016. Additional backing from the Project FCT/UID/GEO/50019/2019 (IDL) is acknowledged. The first author warmly thanks André Cravinho Santos for discussion and comments on early versions of the manuscript. The authors acknowledge also Marcus Kunzmann (CSIRO), an anonymous reviewer and Dr. John Carranza (Editor-in-Chief, NRR) for valuable suggestions and useful comments that helped to improve the manuscript and the electronic supplementary material.

ELECTRONIC SUPPLEMENTARY MATERIAL

The online version of this article (https://doi.org/10.1007/s11053-020-09686-4) contains supplementary material, which is available to authorized users.

REFERENCES

Abat, I., Mata, J. P., Nieto, F., & Velilla, N. (2001). The phyllosilicates in diagenetic-metamorphic rocks of the South Portuguese Zone, Southwestern Portugal. *Canadian Mineralogist, 39,* 1571–1589.

Ague, J. J. (1991). Evidence for major mass transfer and volume strain during regional 960 metamorphism of pelites. *Geology, 19*(8), 855–858.

Albardeiro, L., Solá, R., Salgueiro, R., Morais, I., Matos, J.X., Mendes, M., et al. (2017). Insights into the timing mineral-

ization in the Neves-Corvo VMS deposit (Iberian Pyrite Belt). In *14th SGA Biennal Meeting* (Vol. 3, pp. 989–992).
Algeo, T. J., & Maynard, J. B. (2004). Trace-element behavior and redox facies in core shales of Upper Pennsylvanian Kansas-type cyclothems. *Chemical Geology, 206,* 289–318.
Almodóvar, G. R., Saéz, R., Pons, J. M., Maestre, A., Toscano, M., & Pascual, E. (1998). Geology and genesis of the Aznalcóllar massive sulfide deposits, Iberian Pyrite Belt, Spain. *Mineralium Deposita, 33,* 111–136.
Almodóvar, G. R., Yesares, L., Sáez, R., Toscano, M., González, F., & Pons, J. M. (2019). Massive sulfide ores in the Iberian Pyrite Belt: mineralogical and textural evolution. *Minerals, 9,* 653.
Barret, J. T., Jarvis, I., & Javis, K. E. (1990). Rare earth element geochemistry of massive sulfides-sulfates and gossans on the southern Explorer Ridge. *Geology, 18,* 583–586.
Barrett, T. J., Dawson, G. L., & MacLean, W. H. (2008). Volcanic stratigraphy, alteration, and seafloor setting of the Paleozoic Feitais massive sulfide deposit, Aljustrel, Portugal. *Economic Geology, 103,* 215–239.
Barrie, C., Amelin, Y., & Pascual, E. (2002). U-Pb geochronology of VMS mineralization in the Iberian Pyrite Belt. *Mineralium Deposita, 37*(8), 684–703.
Barriga, F. A. J. S. (1983). *Hydrothermal metamorphism and ore genesis at Aljustrel, Portugal* (p. 368). Ph.D. thesis, University of Western Ontario.
Barriga, J. A. S. F., Carvalho, D., & Ribeiro, A. (1997). Introduction to the Iberian Pyrite Belt. *SEG Neves-Corvo Field Conference*, *27*.
Barriga, F. J. A. S., & Fyfe, W. S. (1998). Multi-phase water-rhyolite interaction and ore fluid generation at Aljustrel, Portugal. *Mineralium Deposita, 33,* 188–207.
Barriga, F. J. A. S., & Kerrich, R. (1984). Extreme ^{18}O-enriched volcanics and ^{18}O-evolved marine water, Aljustrel, Iberian Pyrite Belt: Transition from high to low Rayleigh number convective regimes. *Geochimica et Cosmochimica Acta, 48,* 1021–1031.
Bathia, M. R. (1983). Plate tectonics and the geochemical of sandstones. *The Journal of Geology, 91*(6), 611–627.
Bathia, M. R., & Crook, K. A. W. (1986). Trace element characteristics of greywackes and tectonic setting discrimination of sedimentary basins. *Contributions to Mineralogy and Petrology, 92,* 181–193.
Boulter, C. A. (1993). High level peperitic sills at Rio Tinto, Spain: Implications for stratigraphy and mineralization. *Transactions of the Institutions of Mining and Metallurgy, 112,* B30–B38.
Breit, G. N., & Wanty, R. B. (1991). Vanadium accumulation in carbonaceous rocks: A review of geochemical controls during deposition and diagenesis. *Chemical Geology, 91,* 83–97.
Brumsack, H. J. (2006). The trace metal content of recent organic carbon-rich sediments: Implications for Cretaceous black shale formation. *Palaeogeography, Palaeoclimatology, Palaeoecology, 232,* 344–361.
Calvert, S. E., & Pedersen, T. F. (1993). Geochemistry of recent oxic and anoxic marine sediments: implications for the geological record. *Marine Geology, 113,* 67–88.
Calvert, S. E., & Pedersen, T. F. (2007). Elemental proxies for palaeoclimatic and palaeoceanographic variability in marine sediments: interpretation and application. In C. Hillaire-Marcel & A. De-Vernal (Eds.), *Developments in marine geology* (pp. 567–644). New York: Elsevier.
Carmichael, R. S. (1989). *Practical handbook of physical properties of rocks and minerals* (p. 741). Boca Raton: CRC Press.
Carvalho, J. (2016). *Zinc metallogenesis, and indium and selenium distribution at Neves-Corvo deposit, Iberian Pyrite Belt, Portugal* (p. 543). Ph.D. thesis, University of Lisbon, Portugal.
Carvalho, D., Barriga, F. J. A. S., & Munhá, J. (1999). Bimodal-siliciclastic systems—The case of the Iberian Pyrite Belt. *Rev. Economic Geology, 8,* 375–408.
Castroviejo, R., Quesada, C., & Soler, M. (2011). Post-depositional tectonic modification of VMS deposits in Iberia and its economic significance. *Mineralium Deposita, 46,* 615–637.
Codeço, M., Mateus, A., Figueiras, J., Gonçalves, L., & Rodrigues, P. (2018). Development of the Ervidel-Roxo and Figueirinha-Albernoa volcanic sequences in Iberian Pyrite Belt, Portugal: metallogenic and geodynamic implications. *Ore Geology Reviews, 98,* 80–108.
Conde, C., & Tornos, F. (2019). Geochemistry and architecture of the host sequence of the massive sulfides in the northern Iberian Pyrite Belt. *Ore Geology Reviews*. https://doi.org/10.1016/j.oregeorev.2019.103042.
Condie, K. C. (1993). Chemical composition and evolution of the Upper Continental Crust: contrasting results from surface samples and shales. *Chemical Geology, 104,* 1–37.
Cullers, R. L. (1994). The controls on the major and trace element variation of shale, siltstone and sandstone of Pennsylvanian-Permian age from uplifted continental blocks in Colorado to platform sediment in Kansas, USA. *Geochimica et Cosmichimica Acta, 58,* 4955–4972.
Cutter, G. A. (1991). Dissolved arsenic and antimony in the Black Sea. *Deep Sea Research. Part A. Oceanographic Research Papers, 38, suppl.,* S825–S843.
Cutter, G. A. (1992). Kinetic controls on the speciation of metalloids in seawater. *Marine Chemistry, 40,* 65–80.
Cutter, G. A., & Cutter, L. S. (2006). Biogeochemistry of arsenic and antimony in the North Pacific Ocean. *Geochemistry Geophysics Geosystems, 70*(5), Q05M08.
Dawson, G. L., & Caessa, P. (2003). Geology of the Aljustrel Mine area, southern Portugal. *GEODE—Global Comparison Massive Sulphide Project Field Workshop: ''The Geology of the Volcanic-Hosted Massive Sulphides of the Iberian Pyrite Belt*'' (p. 26).
Donaire, T., Saez, R., & Pascual, E. (2002). Rhyolitic globular peperites from the Aznacollar mining district (Iberian Pyrite Belt, Spain): physical and chemical controls. *Journal of Volcanology and Geothermal Research, 114,* 119–128.
Dunning, G. R., Díez Montes, A., Matas, J., Martín Parra, L. M., Almarza, J., & Donaire, M. (2002). Geocronología U/Pb del volcanismo ácido y granitoides de la Faja Pirítica Ibérica (Zona Surportuguesa). *Geogaceta, 32,* 127–130.
Faria, R., Pereira, Z., Matos, J. X., Rosa, C., Caetano Alves, M. I., & Oliveira, J. T. (2015). Estudo palinostratigráfico do setor Malhadinha, região NE Alvares, concelho de Mértola, Faixa Piritosa Ibérica. *Comunicações Geológicas, 102*(1), 5–11.
Fedo, C. M., Nesbitt, H. W., & Young, G. M. (1995). Unraveling the effects of potassium metasomatism in sedimentary rocks and paleosols with implications for paleoweathering conditions and provenance. *Geology, 23,* 921–934.
Fernandes, A. (2011). *Caracterização petrográfica, mineralógica e geoquímica do padrão de alteração hidrotermal a muro das massas de sulfuretos maciços do Lousal, Faixa Piritosa Ibérica* (p. 194). M.Sc. thesis, University of Lisbon.
Floyd, P. A., & Leveridge, B. E. (1987). Tectonic environment of the Devonian Gramscatho basin, south Cornwall: framework mode and geochemical evidence from turbiditic sandstone. *Journal of Geological Society, 144,* 531–542.
Garcia, D., Fonteilles, M., & Moutte, J. (1994). Sedimentary fractionations between Al, Ti, and Zr and the genesis of strongly Peraluminous granite. *The Journal of Geology, 102*(4), 411–422.
Georgiev, S., Stein, H. J., Hannan, J. L., Weiss, H. M., Bingen, B., Xu, G., et al. (2012). Chemical signals for oxidative weathering predict Re-Os isochroneity in black shales, East Greenland. *Chemical Geology, 324–325,* 108–121.

Girty, G. H., Ridge, D. L., Knaack, C., Johnson, D., & Al-Riyami, R. K. (1996). Provenance and depositional setting of Paleozoic chert and argillite, Sierra Nevada, California. *Journal of Sedimentary Research, 66,* 107–118.

Goodfellow, W. D., Peter, J. M., Winchester, J. A., & van Staal, C. R. (2003). Ambient marine environment and sediment provenance during formation of massive sulfide deposits in the Bathrust Mining Camp: importance of reduced bottom waters to sulfide precipitation and preservation. *Economic Geology, Monograph, 11,* 129–156.

Gurvich, E. G. (2006). *Metalliferous sediments of the World. Fundamental theory of deep-sea hydrothermal sedimentation* (p. 416). Berlin: Springer.

Haley, B. A., Klinkhammer, G. P., & McManus, J. (2004). Rare earth elements in pore waters of marine sediments. *Geochimica et Cosmochimica Acta, 68,* 1265–1279.

Hoffman, D. L., Algeo, T. J., Maynard, J. B., Joachimski, M. M., Hower, J. C., & Kaminski, J. (1998). Regional stratigraphic variation in bottom waters anoxia in offshore core shales of Upper Pennsylvanian cyclotherms from Eastern Midcontinent Shelf (Kansas), USA. In J. Schieber, W. Zimmerle, & P. Sethi (Eds.), *Shales and mudstones* (pp. 234–269). Stuttgart: Schweizerbart'sche Verlagsbucchandlung.

Hollis, S. P., Podmore, D., James, M., Mole, D. R., Turner, O., Kneeshaw, A., et al. (2019). Targeting VHMS mineralization at Erayinia in the Eastern Goldfields Superterrane using lithogeochemistry, soil chemistry and HyLogger data. *Journal of Geochemical Exploration, 207,* 106379.

Hung, J. J., Yeh, H. Y., Peng, S.-H., & Chen, C. T. A. (2018). Influence of submarine hydrothermalism on sulfur and metal accumulation is surface sediments in the Kueishantao venting field off northeastern Taiwan. *Marine Chemistry, 198,* 88–96.

Huston, D. L., Relvas, J. M. R. S., Gemmel, J. B., & Drieberg, S. (2011). The role of granites in volcanic-hosted ore forming systems: an assessment of magmatic-hydrothermal contributions. *Mineralium Deposita, 46,* 473–507.

Inverno, C., Díez-Montes, A., Rosa, C., García-Crespo, J., Matos, J., García-Lobón, J. L., et al. (2015). Introduction and geological setting of the Iberian Pyrite Belt. In P. Weihed (Ed.), *3D, 4D and predictive modelling of major mineral belts in Europe. Mineral resources reviews* (pp. 191–208). Cham: Springer.

Inverno, C. M. C., Solomon, M., Barton, M. D., & Foden, J. (2008). The Cu stockwork and massive sulfide ore of the Feitais volcanic-hosted massive sulfide deposit, Aljustrel, Iberian Pyrite Belt, Portugal: a mineralogical, fluid Inclusion, and isotopic investigation. *Economic Geology, 103,* 241–267.

Jesus, A. P., Munhá, J., Mateus, A., Tassinari, C., & Nutman, A. (2007). The Beja layered gabbroic sequence (Ossa Morena Zone, Southern Portugal): geochronology and geodynamic implications. *Geodinamica Acta, 20,* 139–157.

Jones, B., & Manning, D. A. C. (1994). Comparison of geochemical indices used for interpretation of paleoredox conditions in ancient mudstones. *Chemical Geology, 111,* 111–129.

Jorge, R. C. G. S. (2009). *Caracterização petrográfica, geoquímica e isotópica dos reservatórios metalíferos crustais, dos processos de extracção de metais e dos fluídos hidrotermais envolvidos em sistemas mineralizantes híbridos na Faixa Piritosa Ibérica* (p. 290). Ph.D. Thesis, University of Lisbon, Portugal.

Jorge, R.C.G.S., Pinto, A.M.M., Tassinari, C.C.G, Relvas, J.M.R.S., & Munhá, J. (2007). VHMS metal sources in the Iberian Pyrite Belt: new insights from Pb isotope data. In *9th Biennal SGA, Meeting Dublin*, Ireland (pp. 1097–1100).

Jorge, R. C. G. S., Relvas, J. M. R. S., & Matos, J. X. (2006). Geochemistry of metasediments from the Phyllite-Quartzite Group, Iberian Pyrite Belt: implications for provenance and source-area weathering (progress report). In *VII Congresso Nacional de Geologia, Livro de Resumos I*, Estremoz (pp. 175–178). Universidade de Évora, Portugal.

Julivert, M., Fontboté, J., Ribeiro, A., Igme, L.C., & Madrid, U. (1974). *Memoria explicative del mapa tectónico de la Península Ibérica y Baleares*. Madrid.

Kim, J. H., Torres, M. E., Haley, B. A., Kastner, M., Pohlman, J. W., Riedel, M., et al. (2012). The effect of diagenesis and fluid migration on rare earth element distribution in pore fluids of the northern Cascadia accretionary margin. *Chemical Geology, 291,* 152–165.

Large, R. R., Halpin, J. A., Danyushevsky, L. V., Maslennikov, V. V., Bull, S. W., Long, J. A., et al. (2014). Trace element content of sedimentary pyrite as a new proxy for deep-time ocean-atmosphere evolution. *Earth and Planetary Science Letters, 389,* 209–220.

Leca, X., Ribeiro, A., Oliveira, J.T., Silva, J.B., Albouy, L., Carvalho, P., et al. (1983). Cadre géologique des minéralisations de Neves-Corvo (Baixo-Alentejo, Portugal)- Lithostratigraphie, paléogéographie et tectonique. In *Mémories BRGM,* 121–1983 (p. 79). Éditions du BRGM, Orléans, France.

Leistel, J. M., Marcoux, E., Thiéblemont, D., Quesada, C., Sánchez, A., Ruiz de Amodóvar, G., et al. (1998). The volcanic-hosted massive sulphide deposits of the Iberian Pyrite Belt. *Mineralium Deposita, 33,* 2–30.

Leitão, J. (1997). Geology of the Aljustrel massive sulfide deposits. *Society of Economic Geologists Field Trip Guidebook Series, 27,* 82–97.

Leitão, J. C. R. (2014). Architecture of the Aljustrel volcanic-sedimentary basins. *Comunicações Geológicas, 101, Especial I,* 469–474.

Lentz, D. (2003). Geochemistry of sediments and sedimentary rocks: historical research perspectives. In D. Lentz (Ed.), *Geochemistry of sediments and sedimentary rocks: Evolutionary considerations to mineral deposit-forming environments* (pp. 1–6). St. John's: Geological Association of Canada, GEOtext 4.

Li, X., Zhao, K. D., Jiang, S. Y., & Palmer, M. R. (2019). *In situ* U-Pb geochronology and sulfur isotopes constrains the metallogenesis of the giant Neves-Corvo deposit, Iberian Pyrite Belt. *Ore Geology Reviews, 105,* 223–235.

Lottermoser, G. G. (1991). Trace element composition of exhalites associated with the Boken Hill sulfide deposit, Australia. *Economic Geology, 86,* 870–877.

Luz, F., Mateus, A., Figueiras, J., Tassinari, C. C. G., Ferreira, E., & Gonçalves, L. (2019). Recognizing metasedimentary sequences potentially hosting concealed massive sulfide accumulations in the Iberian Pyrite Belt using geochemical fingerprints. *Ore Geology Reviews, 107,* 973–998.

Marchig, V., Gundalach, H., Möller, P., & Schley, M. (1982). Some geochemical indicators for discrimination between diagenetic and hydrothermal metalliferous sediments. *Marine Geology, 50,* 241–256.

Marignac, C., Diagana, B., Cathelineau, M., Boiron, M. C., Banks, D., Fourcade, S., et al. (2003). Remobilisation of base metals and gold by Variscan metamorphic fluids in the south Iberian Pyrite Belt: evidence from Tharsis VMS deposit. *Chemical Geology, 194,* 143–165.

Mateus, A., Figueiras, J., Monteiro Santos, F., Luz, F., Khalill, M., Codeço, M., et al. (2014). *Prospeção Mineral no ''Polígono de Albernoa'' (Faixa Piritosa Ibérica, Portugal); Avaliação integrada de dados geológicos e geofísicos existentes; novas informações mineralógicas e geoquímicas e follow-up* (p. 260). Unpublished Report, Lisbon, Portugal.

Mathur, R., Ruiz, J., & Tornos, F. (1999). Ages and sources of the ore at Tharsis and Rio Tinto, Iberian Pyrite Belt, from Re-Os isotopes. *Mineralium Deposita, 34,* 790–793.

Matos, J. X., Pereira, Z., Rosa, C. J. P., Rosa, D. R. N., Oliveira, J. T., & Relvas, J. M. R. S. (2011). Late Strunian age: a key time frame for VMS deposit exploration in the Iberian Pyrite Belt.

In *11th SGA Biennal Meeting: Let's talk about Ore Deposits*, Antofagasta, Chile (pp. 790–792).

Mendes, M., Pereira, Z., Matos, J. X., Albardeiro, L., Morais, I., Solá, R., et al. (2018). Middle-upper Devonian Palynostratigrapgy of the Phyllite-Quartzite Group in the Neves-Corvo mine region, Iberian Pyrite Belt correlation with the South Portuguese Zone. *Cuadernos del Museu Geominero, 27,* 357–365.

Michard, A., Albarede, F., Michard, G., Minster, J. F., & Charlou, J. I. (1983). Rare-earth elements and uranium in high-temperature solutions from East Pacific Rise hydrothermal vent field (13ºN). *Nature, 303,* 795–797.

Mitjavilla, J., Martí, J., & Soriano, C. (1997). Magmatic evolution and tectonic setting of the Iberian pyrite belt volcanism. *Journal of Petrology, 38*(6), 727–755.

Moreno, C., Sierra, S., & Saéz, R. (1996). Evidence for catastrophism at the Famennian-Dinantian boundary in the Iberian Pyrite Belt. In P. Strogen, I. D. Sommerville, & J. L. Jones (Eds.), *Recent advances in lower carboniferous geology* (pp. 153–162). London: The Geological Society of London, Special Publication 106.

Morford, J. L., & Emerson, S. (1999). The geochemistry of redox sensitive trace metals in sediments. *Geochimica et Cosmochimica Acta, 63,* 1735–1750.

Moura, A. (2008). Metallogenesis at the Neves-Corvo VHMS deposit (Portugal): A contribution from the study of fluid inclusions. *Ore Geology Reviews, 34*(3), 354–368.

Munhá, J. (1979). Blue amphiboles, metamorphic regime and plate tectonic modelling in the Iberian Pyrite Belt. *Contributions to Mineralogy and Petrology, 69,* 279–289.

Munhá, J. (1981). *Igneous and metamorphic petrology of the Iberian Pyrite Belt volcanic rocks*. Doctoral Thesis, University of Western Ontario, Canada.

Munhá, J. (1983). Low-grade regional metamorphism in the Iberian Pyrite Belt. *Comunicações dos Serviços Geológicos de Portugal, 69,* 3–36.

Munhá, J. (1990). Metamorphic evolution of the South Portuguese/Pulo do Lobo Zone. In R. D. Dallmeyer & E. Martínez García (Eds.), *Pre-Mesozoic Geology of Iberia* (pp. 363–369). Berlin: Springer.

Munhá, J., Barriga, F., & Kerrich, R. (1986). High ^{18}O ore-forming fluids in volcanic-hosted base metal massive sulfide deposits; geologic, $^{18}O/^{16}O$, and D/H evidence from the Iberian Pyrite Belt; Crandon, Wisconsin; and Blue Hill, Maine. *Economic Geology, 81*(3), 530–552.

Munhá, J., & Kerrich, R. (1980). Seawater basalt interaction in spilites from the Iberian Pyrite Belt. *Contributions to Mineralogy and Petrology, 73,* 191–200.

Nesbitt, R. W., Pascual, E., Fanning, C. M., Toscano, M., Saéz, R., & Almodovar, G. R. (1999). U-Pb dating of stockwork zircons from the eastern Iberian Pyrite Belt. *Journal of the Geological Society (London)*, *156*, 7–10.

Nesbitt, H. W., & Young, G. M. (1982). Early Proterozoic climates and plate motions inferred from major element chemistry of lutites. *Nature, 299,* 715–717.

Oliveira, J. T. (1990). Stratigraphy and syn-sedimentary tectonism in the South Portuguese Zone. In R. F. Dallmeyer & E. Martinez-Garcia (Eds.), *Pre-Mesozoic Geology of Iberia* (pp. 334–347). Berlin: Springer.

Oliveira, D. P. S., Matos, J. X., Rosa, C. J. P., Rosa, D. R. N., Figueiredo, M. O., Silva, T. P., et al. (2011). The Lagoa Salgada orebody, Iberian Pyrite Belt, Portugal. *Economic Geology, 106,* 1111–1128.

Oliveira, J. T., Pereira, Z., Carvalho, P., Pacheco, N., & Korn, D. (2004). Stratigraphy of the tectonically imbricated lithological succession of the Neves-Corvo mine area, Iberian Pyrite Belt, Portugal. *Mineralium Deposita, 39*(4), 422–436.

Oliveira, J.T., Pereira, Z., Matos, J.X., & Fernandes, P. (2009). Investigação Palinostratográfica da região da Mina de Aljustrel—Relatório Final. *Unpublished technical report* (pp. 1–19), Alfragide, LNEG.

Oliveira, J. T., Quesada, C., Pereira, Z., Matos, J. X., Solá, A. R., Rosa, D., et al. (2019). South Portuguese Terrane: A continental affinity exotic unit. In C. Quesada & J. T. Oliveira (Eds.), *The geology of Iberia: A geodynamic approach, regional geology reviews* (pp. 173–206). Berlin: Springer.

Oliveira, J. T., Relvas, J. M. R. S., Pereira, Z., Matos, J. X., Rosa, C. J., Rosa, D., et al. (2013a). Geologia da Zona Sul Portuguesa, com ênfase na estratigrafia, vulcanologia física, geoquímica e mineralizações da Faixa Piritosa. In R. Dias, A. Araújo, P. E. Terrinha, & J. C. Kullberg (Eds.), *Geologia de Portugal. Vol. I—Geologia Pré-Mesozóica de Portugal* (pp. 673–766). Forte da Casa: Escolar Editora.

Oliveira, J. T., Relvas, J. M. R. S., Pereira, Z., Matos, J. X., Rosa, C. J., Rosa, D., et al. (2006). O Complexo Vulcano-Sedimentar da Faixa Piritosa Ibérica: estratigrafia, vulcanismo e mineralizações associadas e evolução tectonoestratigráfica no contexto da Zona Sul Portuguesa. In R. Dias, A. Araújo, P. Terrinha, & J. C. Kullberg (Eds.), *Geologia de Portugal na Ibérica. VII Congresso Nacional de Geologia* (pp. 207–214). Évora: VII Congresso Nacional de Geologia.

Oliveira, J. T., Rosa, C. J. P., Rosa, D. R. N., Pereira, Z., Matos, J. X., Inverno, C. M. C., et al. (2013b). Geology of the Neves-Corvo antiform, Iberian Pyrite Belt, Portugal: new insights from physical volcanology, palynostratigraphy and isotope geochronology studies. *Mineralium Deposita, 48,* 748–766.

Pereira, Z., & Matos, J. X. (2014). Datações das sequências volcano-sedimentares da área do Monte das Mesas (Aljustrel), Faixa Piritosa—Relatório Final. Unpublished technical report (pp. 1-31), EDM, S.A./LNEG.

Pereira, Z., Matos, J. X., Fernandes, P., Jorge, R. G. S., & Oliveira, J. T. (2010). Qual a idade mais antiga da Faixa Piritosa. Nova idade Givetiano inferior para o Grupo Filito-Quartzitico (Anticlinal São Francisco da Serra, Faixa Piritosa. *Revista Electrónica de Ciências da Terra, 17*(13), 4.

Pereira, Z., Matos, J. X., Fernandes, P., & Oliveira, J. T. (2007). Devonian and Carboniferous palynostratigraphy of the South Portuguese Zone, Portugal—An overview. *Comunicações Geológicas, 94,* 53–79.

Pereira, Z., Matos, J. X., Fernandes, P., Oliveira, J. T. (2008). Palynostratigraphy and systematic palynology of the Devonian and Carboniferous successions of the South Portuguese Zone, Portugal. *Memórias do INETI*, *34*, 1–176.

Piercey, S. J., & Kamber, B. S. (2019). Lead isotope geochemistry of shales from the Wolverine volcanogenic massive sulphide deposit, Yukon: Implications for Pb isotope vectoring exhalative ore systems. *Economic Geology*, *114*, 537–549.

Poulton, S. W., & Canfeld, D. E. (2011). Ferruginous conditions: A dominant feature of the ocean through Earth's history. *Elements, 7,* 107–112.

Priem, H. N. A., Boelrijk, N. A. I. M., Hebeda, E. H., Schermerhorn, L. J. G., Verdurmen, E A Th, & Verschure, R. H. (1978). Sr isotopic homogenization through whole-rock systems under low greenschist facies metamorphism in Carboniferous pyroclastics at Aljustrel (Southern Portugal). *Chemical Geology, 21,* 307–314.

Quesada, C. (1991). Geological constraints on the Paleozoic tectonic evolution of the tectonostratigraphic terranes in the Iberian Massif. *Tectonophysics, 185,* 25–245.

Quesada, C. (1998). A reappraisal of the structure of the Spanish segment of the Iberian Pyrite Belt. *Mineralium Deposita, 33,* 31–44.

Quesada, C., Fonseca, P., Munhá, J., Oliveira, J., & Ribeiro, A. (1994). The Beja-Acebuches Ophiolite (Southern Iberia Variscan fold belt): geological characterization and geodynamic significance. *Boletin Geológico y Minero, 105*(1), 3–49.

Raiswell, R., Buckley, F., Berner, R. A., & Anderson, T. F. (1988). Degree of pyritization of iron as a paleoenviron-

mental indicator of bottom water oxygenation. *Journal of Sedimentary Petrology*, *58*, 812–819.

Relvas, J. M. R. S. (1991). *Estudo Geológico e metalogenético da área de Gavião, Baixo Alentejo* (p. 250). M.Sc. Thesis, University of Lisbon.

Relvas, J. M. R. S. (2000). *Geology and metallogenesis at the Neves-Corvo*, Portugal (p. 250). Ph.D. Thesis. University of Lisbon, Portugal.

Relvas, J. M. R. S., Barriga, F. J. A. S., Bernardino, F. B. C. P., Oliveira, V. M. S., & Matos, J. X. (1994). Ore zone hydrothermal alteration in drill hole IGM-LS1 Lagoa Salgada, Grândola, Portugal: A first report on pyrophyllite in a central stockwork. *Boletín Sociedad Española Mineralogia, 17,* 157–158.

Relvas, J. M. R. S., Barriga, F. J. A. S., Ferreira, A., Noiva, P. C., Pacheco, N., & Barriga, G. (2006a). Hydrothermal alteration and mineralization in the Neves-Corvo volcanic hosted massive sulfide deposit, Portugal: I. Geology, mineralogy and geochemistry. *Economic Geology, 101,* 791–804.

Relvas, J. M. R. S., Barriga, F. J. A. S., & Longstaffe, F. J. (2006b). Hydrothermal alteration and mineralization in the Neves-Corvo volcanic-hosted massive sulfide deposit, Portugal: II. Oxygen, hydrogen, and carbon isotopes. *Economic Geology, 101,* 753–790.

Relvas, J. M. R. S., Pinto, A. M. M., & Matos, J. X. (2012). Lousal, Portugal: a successful example of rehabilitation of a closed mine in the Iberian Pyrite Belt. *SGA News, 31,* 6–16.

Relvas, J. M. R. S., Tassinari, C. C. G., Munhá, J., & Barriga, F. J. A. S. (2001). Multiple sources for ore-forming fluids in the Neves-Corvo VHMS Deposit of the Iberian Pyrite Bet (Portugal): strontium, neodymium and lead isotope evidence. *Mineralium Deposita, 36,* 416–427.

Ribeiro, A., Munhá, J., Dias, D., Mateus, A., Pereira, E., Ribeiro, L., et al. (2007). Geodynamic evolution of the SW Europe Variscides. *Tectonics, 26,* TC6009.

Ribeiro, A., Munhá, J., Fonseca, P. E., Araújo, A., Pedro, J. C., Mateus, A., et al. (2010). Variscan ophiolite belts in the Ossa-Morena Zone (Southwest Iberia): geological characterization and geodynamic significance. *Gondwana Research, 17,* 408–421.

Ribeiro, A., Quesada, C., & Dallmeyer, R. D. (1990). Geodynamic evolution of the Iberian Massif. In R. D. Dallmeyer & E. Martínez Garcia (Eds.), *Pre-Mesozoic Geology of Iberia* (pp. 334–347). Berlin: Springer.

Rodrigues, B., Chew, D. M., Jorge, R. C. G. S., Fernandes, P., Veiga-Pires, C., & Oliveira, J. T. (2005). Detrital zircon geochronology of the Carboniferous Baixo Alentejo Flysch Group (South Portugal); constraints on the provenance and geodynamic evolution of the South Portuguese Zone. *Journal of the Geological Society, 172,* 294–308.

Rosa, D. R. N., Finch, A. A., Andersen, T., & Inverno, C. M. C. (2009). U-Pb geochronology and Hf isotope ratios of magmatic zircons from the Iberian Pyrite Belt. *Mineralogy and Petrology, 95,* 47–69.

Rosa, D., Inverno, C., Oliveira, V., & Rosa, C. (2004). Geochemistry of volcanic rocks, Albernoa area, Iberian Pyrite Belt, Portugal. *International Geology Review, 46,* 366–383.

Rosa, D., Inverno, C., Oliveira, V., & Rosa, C. (2006). Goechemistry and geothermometry of volcanic rocks from Serra Branca, Iberian Pyrite Belt, Portugal. *Gondwana Research, 10,* 328–339.

Rosa, C., McPhie, J., & Relvas, J. (2010). Type of volcanoes hosting the massive sulfide deposits of the Iberian Pyrite Belt. *Journal of Volcanology and Geothermal Research, 194,* 107–126.

Rosa, C., McPhie, J., & Relvas, J. (2016). Distinguishing peperite from other sediment-matrix igneous breccias: Lessons from the Iberian Pyrite Belt. *Journal of Volcanology and Geothermal Research, 315,* 28–39.

Rosa, C. J. P., McPhie, J., Relvas, J., Pereira, Z., Oliveira, T., & Pacheco, N. (2008). Volcanic setting of the giant Neves-Corvo massive sulfide deposit, Iberian Pyrite Belt, Portugal. *Mineralium Deposita, 43,* 449–466.

Roser, B. P., & Korsch, R. J. (1986). Determination of tectonic setting of sandstone–mudstone suites using SiO_2 content and K_2O/Na_2O ratio. *Journal of Geology, 94,* 635–650.

Sadiq, M. (1988). Thermodynamic solubility relationships of inorganic vanadium in the marine environment. *Marine Chemistry, 23,* 87–96.

Saéz, R., Almodóvar, G. R., & Pascual, E. (1996). Geological constraints on massive sulphide genesis in the Iberian Pyrite Belt. *Ore Geology Reviews, 11,* 429–451.

Saéz, R., Moreno, C., González, F., & Almodóvar, G. R. (2011). Black shales and massive sulfide deposits: causal or casual relationships? Insights from Rammelsberg, Tharsis, and Draa Sfar. *Mineralium Deposita, 46,* 585–614.

Saéz, R., Pascual, E., Toscano, M., & Almodóvar, G. R. (1999). The Iberian type of volcano-sedimentary massive sulfide deposits. *Mineralium Deposita, 34,* 549–570.

Sánchez-España, J., Velasco, F., & Yusta, I. (2000). Hydrothermal alteration of felsic volcanic rocks associated with massive sulphide deposition in the northern Iberian Pyrite Belt (SW Spain). *Applied Geochemistry, 15,* 1265–1290.

Schermerhorn, L. J. G. (1971). An outline stratigraphy of the Iberian Pyrite Belt. *Boletin Geológico y Minero, 82*(3/4), 239–268.

Schermerhorn, L. J. G., & Stanton, W. I. (1969). Folded overthrusts at Aljustrel (South Portugal). *Geological Magazine, 160*(2), 130–141.

Scott, C., & Lyons, T. W. (2012). Contrasting molybdenum accumulation in sediments underneath a nitrogeneous water column and implications for the reconstruction of paleo-redox conditions based on molybdenum isotopes. *Geochimica and Cosmochimica Acta*, *213*, 400–417.

Silva, J. B., Oliveira, J. T., & Ribeiro, A. (1990). Structural outline of the South Portuguese Zone. In R. D. Dallmeyer & E. Martínez García (Eds.), *Pre-mesozoic geology of Iberia* (pp. 348–362). Berlin: Springer.

Slack, J. F., Dumoulin, J. A., Schmidt, J. M., Young, L. E., & Rombach, C. S. (2004). Paleozoic sedimentary rocks in the Red Dog Zn-Pb-Ah district and vicinity, western metallogenic significance. *Economic Geology, 99,* 1385–1414.

Solá, A. R., Salgueiro, R., Pereira, Z., Matos, J. X., Rosa, C., Araújo, V. et al. (2015). Time span of the volcanic setting of the Neves-Corvo VHMS deposit. In *X Congresso Ibérico de Geoquímica/XVII Semana da Geoquímica* (pp. 120-123).

Solomon, M., Tornos, F., & Gaspar, O. C. (2002). A possible explanation for many of the unusual features of the massive sulfide deposits of the Iberian Pyrite Belt. *Geology, 30,* 87–90.

Soriano, C., & Martí, J. (1999). Facies analysis of volcano-sedimentary successions hosting massive sulfide deposits in the Iberian Pyrite Belt, Spain. *Economic Geology, 94,* 867–882.

Stockdale, A., Davison, W., & Zhang, H. (2008). High-resolution two-dimensional quantitative analysis of phosphorus, vanadium and arsenic, and qualitative analysis of sulfide, in a freshwater sediment. *Environmental Chemistry, 5,* 143–149.

Strauss, G. (1970). Sobre la geologia de la provincia piritífera del SW de la Península Ibérica y de sus yacimientos, en especial sobre la mina de pirita de Lousal (Portugal). *Memoria Instituto Tecnológico Geominero de España - ITGE, 77,* 266.

Strauss, G. K., Madel, J., & Fernández Alonso, F. (1977). Exploration practice for stratabound volcanogenic sulphide deposits in the Spanish-Portuguese Pyrite Belt: Geology, geophysics, and geochemistry. In D. D. Klemm & H. J. Schneider (Eds.), *Time and stratabound ore deposits* (pp. 55–93). Berlin: Springer.

Tabelin, C. B., Igarashi, T., Tamoto, S., & Takahashi, R. (2012). The roles of pyrite and calcite in the mobilization of arsenic

and lead from hydrothermally altered rocks excavated in Hokkaido, Japan. *Journal of Geochemical Exploration, 119–120,* 17–31.

Taylor, S. R., & McLennan, S. M. (1995). The geochemical evolution of the continental crust. *Reviews in Geophysics, 33,* 241–265.

Thiéblemont, D., Pascual, E., & Stein, G. (1998). Magmatism in the Iberian Pyrite Belt: petrological constraints on a metallogenetic model. *Mineralium Deposita, 33,* 98–110.

Tornos, F. (2006). Environment of formation and styles of volcanogenic massive sulfides: the Iberian Pyrite Belt. *Ore Geology Reviews, 28,* 259–307.

Tornos, F., & Conde, C. (2002). La influencia biogénica en la formación de los yacimientos de sulfuros masivos de la Faja Pirítica Ibérica. *Geogaceta, 32,* 235–238.

Tornos, F., González, Clavijo E., & Spiro, B. (1998). The Filon Norte orebody (Tharsis, Iberian Pyrite Belt): a proximal low-temperature shale hosted massive sulfide in a thin-skinned tectonic belt. *Mineralium Deposita, 33,* 150–169.

Tornos, F., & Heinrich, C. A. (2008). Shale basins, sulfur-deficient ore brines and the formation of exhalative base metals deposits. *Chemical Geology, 247,* 195–207.

Tornos, F., Peter, J. M., Allen, R. L., Conde, C., Peter, F., & Conde, R. (2015). Controls on the siting and style of volcanogenic massive sulphide deposits. *Ore Geology Reviews, 68,* 142–163.

Tornos, F., Solomon, M., Conde, C., & Spiro, B. (2008). Formation of the Tharsis massive sulfide deposit, Iberian Pyrite Belt: geological, lithogeochemical, and stable Isotope evidence for a deposition in a brine Pool. *Economic Geology, 103*(1), 185–214.

Tribovillard, N., Algeo, T. J., Lyons, T., & Riboulleau, A. (2006). Trace metals as paleoredox and paleoproductivity proxies: An update. *Chemical Geology, 232,* 12–32.

Valenzuela, A., Donaire, T., & Pascual, E. (2002). Secuencia de fácies volcânicas en el area del rio Odiel (Faja Piritica Iberica, España). *Geogaceta, 32,* 131–134.

Valenzuela, A., Donaire, T., Pin, C., Toscano, M., Hamilton, M., & Pascual, E. (2011). Geochemistry and U-Pb Dating of felsic volcanic rocks in the Rio Tinto-Nerva unit, Iberian Pyrite Belt, Spain: crustal thinning, progressive crustal melting and massive sulfide genesis. *Journal of the Geological Society, 168,* 717–731.

Van den Boogard, M. (1963). Conodonts of Upper Devonian and Lower Carboniferous age from southern Portugal. *Geologie en Mijnbouw, 42,* 248–259.

Velasco-Acebes, J., Tornos, F., Kidane, A., Wiedenbeck, M., & Velasco, F. (2019). Isotope geochemistry tracks the maturation of submarine massive sulfide mounds (Iberian Pyrite Belt). *Mineralium Deposita, 54,* 913–934.

Wang, D., & Wilhelm, S. A. S. (2009). Vanadium speciation and cycling in coastal waters. *Marine Chemistry, 111,* 52–58.

Wedepohl, K. H. (1971). *Environmental influences on the chemical composition of shales and clays* (pp. 310–320). Gottingen: Geochemisches Institut, Universitit Gottingen.

Wedepohl, K. H. (1995). The composition of the continental crust. *Geochimica et Cosmochimica Acta, 59*(7), 1217–1232.

Wignall, P. B., & Myers, K. J. (1988). Interpreting benthic oxygen levels in mudrocks: A new approach. *Geology, 16*(5), 452–455.

Wignall, P. B., & Twichett, R. J. (1996). Oceanic anoxia and the end permian mass extinction. *Science, 272,* 1155–1159.

Young, G. M., & Nesbitt, H. W. (1998). Processes controlling the distribution of Ti and Al in weathering profiles. Siliciclastic sediments and sedimentary rocks. *Journal of Sedimentary Research, 68*(3), 448–455.

Appendix 1.2

Supplementary material 1 -
Table providing all the relevant information of the studied samples

Geochemistry of Fammenian to Visean metapelites from the Iberian Pyrite Belt: implications for provenance, paleo-redox conditions and vectoring massive sulfide deposits

Natural Resources Research - 2020

Filipa Luz
António Mateus
Carlos Rosa
Jorge Figueiras

Supplementary Material 1 – Table providing all the relevant information of the studied samples (coordinates, stratigraphy, mineralization type, whole-rock chemistry, etc.)

Sample Ref		NCL#9	NCL#10	NCL#11	NCL#12	NCL#13	NCL#14	NCL#15	NCL#35	NCC#25	NCC#27	NCZ#1	NCZ#21	NCZ#40	NCS#2	NCS#3	NCL#7
Sector		Neves Corvo	Neves Corvo	Neves Corvo	Neves Corvo	Neves Corvo	Neves Corvo	Neves Corvo	Neves Corvo	Neves Corvo	Neves Corvo	Neves Corvo	Neves Corvo	Neves Corvo	Neves Corvo	Neves Corvo	Neves Corvo
Stratigraphic division		*PQG*	*PQG*	*PQG*	*PQG*	*PQG*	*PQG*	*PQG*	*PQG*	*PQG*	*PQG*	*lower* VSC	*lower* VSC	*lower* VSC	*lower* VSC	*lower* VSC	*lower* VSC
Mineralization type/occurrence		*Mineralized*	*Mineralized*	*Mineralized*	*No sulphide*	*No sulphide*	*Py-bearing*	*No sulphide*	*No sulphide*	*No sulphide*	*No sulphide*	*Mineralized*	*Mineralized*	*Mineralized*	*No sulphide*	*Py-bearing*	*Mineralized*
Footwall/Hangingwall		*Footwall*	*Footwall*	*Footwall*	*Footwall*	*Footwall*	*Footwall*	*Footwall*	*Footwall*	*Footwall*	*Footwall*	*Footwall*	*Footwall*	*Footwall*	*Footwall*	*Footwall*	*Footwall*
Location - ETRS89	**x**	13812	14419	14509	14254	14110	14120	14078	*n.a.*	14745	14648	15175	15143	*n.a.*	15436	15480	14305
	y	-231566	-231437	-231432	-231370	-231465	-231418	-231379	*n.a.*	-231837	-231786	-233119	-232927	*n.a.*	-233332	-233202	-231809
Depth (m)		*n.a.*	*n.a.*	*n.a.*	*n.a.*	*n.a.*	*n.a.*	*n.a.*	*n.a.*	*n.a.*	*n.a.*	*n.a.*	*n.a.*	*n.a.*	*n.a.*	*n.a.*	*n.a.*
SiO_2	%	58.58	44.47	59.45	56.8	58.24	58.53	55.94	57.47	66.29	62.84	56.72	56.41	59	55.95	58.84	50.15
Al_2O_3	%	10.26	13.7	13.07	21.41	23.5	20.19	20.59	16.94	16.86	15.46	13.92	15.8	17.87	20.72	18.66	14.85
Fe_2O_3(T)	%	18.34	26.15	14.99	8.13	5.54	7.55	11.11	14.87	7.21	12.03	20.15	12.9	12.21	8.19	7.29	26.75
MnO	%	0.154	0.165	0.093	0.046	0.042	0.069	0.067	0.112	0.033	0.061	0.155	0.092	0.231	0.056	0.018	0.161
MgO	%	4.57	2.97	2.44	1.41	1.22	1.7	1.84	2.82	1.24	1.92	1.93	1.54	1.49	2.22	3.35	3.24
CaO	%	0.08	0.75	0.17	0.22	0.26	0.18	0.16	0.26	0.15	0.14	0.08	0.13	0.18	0.16	0.08	0.1
Na_2O	%	0.01	0.04	0.11	0.17	0.19	0.23	0.14	0.11	0.14	0.11	0.06	0.21	0.22	0.33	0.37	-
K_2O	%	0.32	1.09	2.02	5.03	5.74	4.47	4.32	2.4	3.76	2.66	1.04	3.14	3.2	4.21	3.61	0.16
TiO_2	%	0.55	0.687	0.798	1.077	1.164	0.999	1.074	0.669	1.028	0.851	0.513	0.842	0.683	0.852	0.757	0.525
P_2O_5	%	0.07	0.14	0.07	0.14	0.14	0.15	0.13	0.21	0.13	0.12	0.06	0.1	0.13	0.1	0.04	0.06
Ba	*ppm*	49	162	316	654	873	861	616	528	897	534	153	471	427	677	559	34
Cs	*ppm*	0.7	1.6	2.8	9.6	7.3	6.2	7.9	3.5	5.9	3.9	1.5	6.8	4.1	7.7	6.6	0.3
Cu	*ppm*	14	1280	25	4	4	122	26	6	8	17	130	45	4	71	157	6
Ga	*ppm*	14	27	19	28	29	27	28	23	23	21	24	22	26	28	26	23
Ge	*ppm*	1.2	1.3	1.1	1.4	1.4	1.3	1.5	1.8	1.5	1.4	2.2	1.1	2.5	1.7	1.3	2.7
Hf	*ppm*	5.1	4	5.8	4.9	6.9	6.5	6.8	5.5	8.3	7.3	2.2	5.4	3	4.5	3.7	2.3
Nb	*ppm*	6.4	11.9	10.8	18.1	19.2	17.2	18	14	16	14.1	10.5	15.9	12.4	18.5	14.5	10.3
Ni	*ppm*	30	49	36	57	75	71	54	77	41	53	74	57	110	96	114	56
Pb	*ppm*	22	62	37	-	-	-	-	-	-	9	6	62	25	10	53	7
Rb	*ppm*	13	45	84	211	239	184	179	91	152	108	50	154	172	170	131	6
S	%	4.1	4.22	3.28	0.039	0.026	0.473	0.154	0.114	0.007	0.234	0.628	3.65	0.58	0.14	1.48	0.058
Sr	*ppm*	22	23	26	39	60	67	30	41	-	-	30	41	57	98	132	11
Ta	*ppm*	0.72	0.98	1.14	1.5	1.61	1.47	1.48	1.1	1.4	1.2	0.83	1.36	1.18	1.4	1.13	0.83
Th	*ppm*	8.79	10.7	11.8	15.7	17.9	16.6	16.5	13.8	14.9	13.6	8.1	13.9	10.9	13.8	12.2	8.41
U	*ppm*	2.42	2.43	2.93	3.85	4.26	3.87	3.84	2.96	3.93	3.26	1.47	3.2	1.97	3.01	3.54	1.66
V	*ppm*	101	117	102	176	186	171	168	145	130	123	147	109	270	231	169	114
Y	*ppm*	18	23	23	29	37	33	32	29	36	29	24	29	24	37	31	15
Zr	*ppm*	261	164	266	209	289	273	277	236	364	302	94	213	117	186	149	89
La	*ppm*	31.9	32.9	31.3	51.2	60.5	55.7	56.9	43.1	47	42.4	35.1	46.4	51.3	59.1	47	32
Ce	*ppm*	63.5	68.2	63.6	106	123	115	116	89	96.6	86.7	60.6	94.2	87.8	104	89.2	60.3
Pr	*ppm*	6.85	7.5	6.87	11.5	13.7	12.4	12.6	9.89	10.6	9.49	7.65	10.7	11.9	13	10.5	6.97
Nd	*ppm*	25.5	28.5	26	42.2	51	46	46.9	38	40.5	36.1	29.3	40.6	43.9	49.5	39.4	26.6
Sm	*ppm*	4.98	6.26	5.3	8.22	9.96	9.5	8.77	8.09	8	6.83	5.85	7.9	8.88	9.69	7.95	5.36
Eu	*ppm*	1.55	2.16	3.14	1.8	2.28	1.83	1.95	1.54	1.43	1.41	1.04	1.44	1.78	2	1.48	2.18
Gd	*ppm*	3.82	5.3	4.83	6.54	7.79	7.37	6.34	7.13	6.38	5.58	4.99	6.15	6.28	7.86	6.36	3.98
Tb	*ppm*	0.59	0.86	0.78	0.99	1.23	1.11	1	1.03	1.05	0.9	0.81	0.97	0.9	1.26	0.99	0.62
Dy	*ppm*	3.45	5.02	4.79	5.65	7.15	6.8	6.09	5.83	6.62	5.56	4.89	5.84	5.38	7.44	5.99	3.49
Ho	*ppm*	0.72	0.96	0.92	1.14	1.42	1.32	1.17	1.09	1.36	1.12	0.99	1.15	1	1.45	1.16	0.67
Er	*ppm*	2.18	2.73	2.86	3.31	4.03	3.68	3.51	3	3.79	3.33	2.83	3.36	3.03	4.07	3.35	1.92
Tl	*ppm*	1.29	1.57	4.97	2.3	1.99	1.39	1.27	0.83	5.35	2.58	1.72	4.27	1.55	2.56	2.02	6.06
Tm	*ppm*	0.318	0.377	0.428	0.497	0.594	0.542	0.53	0.43	0.6	0.5	0.415	0.497	0.438	0.589	0.495	0.277
Yb	*ppm*	2.19	2.49	2.75	3.28	3.94	3.71	3.53	2.93	3.72	3.03	2.81	3.34	2.82	3.88	3.25	1.84
Lu	*ppm*	0.366	0.393	0.415	0.494	0.606	0.522	0.536	0.422	0.562	0.445	0.422	0.502	0.418	0.611	0.513	0.295
As	*ppm*	157	416	326	45	78	67	26	21	20	26	62	272	108	65	77	55
Co	*ppm*	10.1	147	13.5	23.8	26.2	31.5	18.4	24	10.4	21	27.1	34	28.8	20.8	40.6	36.9
Cr	*ppm*	61	69	71.5	120	130	121	115	89	100	84	75.5	87	80	107	90	65
Sb	*ppm*	5.4	8.6	6.3	3.5	2.2	4.1	1.8	1	2.2	3.3	1.7	8.4	3.4	3.5	6.8	1.6
Sc	*ppm*	8.8	12.6	11.6	22.7	23.4	21.1	20.6	15.1	15	13.6	12.6	17.9	15.9	19.5	16.9	12.4
Zn	*ppm*	110	244	179	148	35	58	64	77	56	111	418	263	242	97	120	206

Supplementary Material 1 – Table providing all the relevant information of the studied samples (coordinates, stratigraphy, mineralization type, whole-rock chemistry, etc.)

Sample Ref		**NCL#36**	**NCL#37**	**NCN#16**	**NCN#17**	**NCN#18**	**NCN#19**	**NCN#22**	**NCN#30**	**NCC#23**	**NCC#24**	**NCC#26**	**NCC#28**	**NCG#4**	**NCL#34**	**NCZ#41**	**NCZ#42**	**NCL#6**	**NCL#31**
Sector		**Neves Corvo**	**Neves Corvo**	**Neves Corvo**	**Neves Corvo**	**Neves Corvo**	**Neves Corvo**	**Neves Corvo**	**Neves Corvo**	**Neves Corvo**	**Neves Corvo**	**Neves Corvo**	**Neves Corvo**	**Neves Corvo**	**Neves Corvo**	**Neves Corvo**	**Neves Corvo**	**Neves Corvo**	**Neves Corvo**
Stratigraphic division		***lower* VSC**	***lower* VSC**	***lower* VSC**	***lower* VSC**	***lower* VSC**	***lower* VSC**	***lower* VSC**	***lower* VSC**	***lower* VSC**	***lower* VSC**	***lower* VSC**	***lower* VSC**	***middle* VSC**	***middle* VSC**	***upper* VSC**	***upper* VSC**	***upper* VSC**	***upper* VSC**
Mineralization type/occurrence		***No sulphide***	***No sulphide***	***Mineralized***	***Py-bearing***	***Py-bearing***	***Mineralized***	***No sulphide***	***No sulphide***	***Mineralized***	***Py-bearing***	***Py-bearing***	***No sulphide***	***No sulphide***	***Mineralized***	***No sulphide***	***No sulphide***	***Mineralized***	***Py-bearing***
Footwall/Hangingwall		***Footwall***	***Footwall***	***Footwall***	***Footwall***	***Footwall***	***Footwall***	***Footwall***	***Footwall***	***Footwall***	***Footwall***	***Footwall***	***Footwall***	***Footwall***	***Footwall***	***Hangingwall***	***Hangingwall***	***Hangingwall***	***Hangingwall***
Location - ETRS89	**x**	*n.a.*	*n.a.*	13545	13984	13990	14041	13544	13544	15127	15134	15048	14869	14054	14755	*n.a.*	*n.a.*	14385	14861
	y	*n.a.*	*n.a.*	-232243	-232270	-232270	-232220	-232592	-232592	-231817	-231811	-232493	-232654	-233292	-231210	*n.a.*	*n.a.*	-231332	-231090
Depth (m)		*n.a.*	*n.a.*	*n.a.*	*n.a.*	*n.a.*	*n.a.*	*n.a.*	*n.a.*	*n.a.*	*n.a.*	*n.a.*	*n.a.*	*n.a.*	*n.a.*	*n.a.*	*n.a.*	*n.a.*	*n.a.*
SiO_2	%	64.8	58.74	52.78	39.43	55.93	65.24	61.63	55.25	60.88	61.76	55.92	55.21	55.46	67.07	62.44	58.1	47.85	69.62
Al_2O_3	%	9.79	14.52	17.92	26.89	20.79	15.61	18.62	21.01	21.19	15.48	19.89	19.94	21.91	14.17	18.85	19.86	23.55	12.5
Fe_2O_3(T)	%	18.14	17.23	11.95	14.64	5.77	5.98	4.84	6.51	6.13	6.34	9.1	7.02	5.95	5.43	4.15	7.77	7.77	6.05
MnO	%	0.095	0.119	0.032	0.06	0.026	0.035	0.088	0.061	0.02	0.04	0.017	0.097	0.031	0.028	0.12	0.076	0.043	0.363
MgO	%	2.15	1.98	0.51	3.8	1.71	0.96	1.23	1.52	1.47	1.57	1.76	2.22	1.21	1.38	1.67	2.55	0.82	3.07
CaO	%	0.07	0.14	0.16	0.29	0.26	0.17	0.82	0.17	0.13	0.6	0.15	0.25	0.31	0.3	0.22	0.41	0.12	0.93
Na_2O	%	0.02	0.1	0.31	0.45	0.5	0.35	0.63	0.73	0.66	0.6	0.42	0.47	0.71	0.12	0.58	1.38	0.39	0.06
K_2O	%	0.17	1.93	4.62	3.47	4.41	3.56	4.09	4.13	4.03	2.88	3.68	4.15	4	4.19	4.23	3.49	6.33	2.52
TiO_2	%	0.365	0.55	0.636	1.495	1.053	0.964	1.081	0.849	1.074	0.606	1.051	1.014	1.052	0.415	0.766	0.944	0.891	0.392
P_2O_5	%	0.03	0.03	0.12	0.25	0.18	0.13	0.12	0.12	0.11	0.09	0.12	0.14	0.11	0.07	0.07	0.16	0.09	0.05
Ba	*ppm*	58	260	616	454	627	434	540	570	577	570	491	682	538	685	942	636	1196	609
Cs	*ppm*	0.3	2.6	7.9	17.1	12.5	8	10.7	11.1	9.1	10	10.3	11.1	10.3	7.7	10.9	8	14.3	5.1
Cu	*ppm*	3	20	282	4	5	7	47	37	22	71	41	34	31	66	54	55	495	153
Ga	*ppm*	17	26	26	35	28	21	24	28	28	21	26	27	43	19	27	26	37	18
Ge	*ppm*	2.3	2.3	0.8	1.7	0.9	1	1	1.5	1.1	0.5	0.6	1.1	1.1	-	1.7	2	-	1.8
Hf	*ppm*	1.5	2.6	2.7	8	5.6	6.1	6.2	5.1	5	2.5	5.8	5.8	5.9	2.1	3.7	4.5	3.8	2.5
Nb	*ppm*	4.2	9.4	12	28.1	19.5	14.9	19.1	18.3	18.3	12.5	20.1	19.5	19.8	8.7	13.6	10.7	17.1	7.8
Ni	*ppm*	38	64	122	61	39	37	42	52	61	189	63	58	51	91	274	54	193	66
Pb	*ppm*	8	14	903	-	-	255	-	6	6	71	36	13	10	82	15	26	244	-
Rb	*ppm*	9	99	248	163	198	162	178	196	191	150	170	180	187	204	205	145	282	102
S	%	0.139	1.21	8.28	0.401	0.513	1.98	0.284	0.191	0.427	4.01	3.34	0.302	0.114	2.71	0.338	0.033	4.34	0.045
Sr	*ppm*	8	33	64	148	120	79	104	115	131	146	93	106	193	43	116	131	99	41
Ta	*ppm*	0.62	0.95	0.91	2.27	1.59	1.38	1.62	1.51	1.47	0.88	1.66	1.55	1.63	0.75	1.38	1.12	1.36	0.7
Th	*ppm*	5.96	9.85	10.2	22	16.8	13.7	15.7	15.9	15.8	9.53	16.4	16.3	17.1	9.13	12.5	13.7	14.7	9.97
U	*ppm*	1.2	1.92	3.93	6.04	4.25	3.46	3.69	3.56	3.17	8.63	4.3	3.79	4.4	7.24	5.14	3.6	14.1	1.44
V	*ppm*	83	144	170	182	143	109	127	141	187	223	136	135	147	190	207	162	246	83
Y	*ppm*	19	15	21	52	43	35	41	39	30	29	40	40	41	25	22	27	41	25
Zr	*ppm*	57	91	106	323	238	256	262	204	205	113	236	238	239	91	129	158	150	99
La	*ppm*	24.4	30.6	21.8	76.1	59.9	46.9	54.1	58.2	51.1	34.6	57.4	55.7	61.9	30.8	38.6	38.9	51.3	32.5
Ce	*ppm*	45.4	59	42.5	153	120	94	109	116	104	65.3	115	111	122	57.1	71.2	80.8	95.7	71.3
Pr	*ppm*	5.57	7.09	5.55	17.5	13.7	10.6	12.3	13.1	11.2	7.87	12.9	12.7	13.9	6.95	8.07	9.36	11	7.44
Nd	*ppm*	21.2	26.4	21.9	65	52	40.5	46.6	50.5	41	29.1	48.6	46.9	53.4	26.3	29.1	34.7	42.6	28.5
Sm	*ppm*	4.45	5.45	5.03	13.4	10.3	8.64	9.12	9.83	7.62	5.87	9.8	9.43	10.3	5.21	5.43	7.52	8.46	5.67
Eu	*ppm*	1.01	1.08	1.63	2.93	2.12	2.34	1.99	1.96	1.53	1.04	2.05	2	2.3	1.06	1.04	1.56	2.56	1.22
Gd	*ppm*	3.63	3.62	4.43	11.2	8.94	7.09	7.5	7.95	5.39	5.26	7.94	7.64	7.38	4.48	4.01	5.5	7.12	4.85
Tb	*ppm*	0.65	0.58	0.7	1.73	1.4	1.16	1.2	1.26	0.9	0.8	1.29	1.25	1.24	0.7	0.67	0.93	1.19	0.81
Dy	*ppm*	4.1	3.21	4.19	10.2	8.25	6.76	7.39	7.53	5.52	4.64	7.75	7.4	7.66	4.07	4.37	5.57	7.04	4.95
Ho	*ppm*	0.76	0.67	0.87	1.99	1.54	1.34	1.49	1.45	1.11	0.93	1.52	1.46	1.49	0.81	0.88	1.12	1.38	0.97
Er	*ppm*	2.13	1.85	2.58	5.76	4.48	3.95	4.27	4.19	3.39	2.85	4.26	4.18	4.46	2.3	2.66	3.06	3.91	2.71
Tl	*ppm*	0.35	1.54	15.1	30.3	40.6	12.5	32.8	18.7	5.82	1.7	3.9	13.1	5.71	1.94	3.16	2.01	96	3.1
Tm	*ppm*	0.329	0.278	0.402	0.833	0.651	0.582	0.608	0.608	0.5	0.406	0.624	0.601	0.625	0.357	0.4	0.469	0.574	0.393
Yb	*ppm*	1.97	1.84	2.61	5.36	4.15	3.8	4.05	4.03	3.31	2.61	4.08	4.05	4.06	2.31	2.66	3.13	3.86	2.54
Lu	*ppm*	0.271	0.285	0.393	0.797	0.634	0.559	0.619	0.575	0.512	0.408	0.578	0.586	0.65	0.33	0.421	0.458	0.58	0.371
As	*ppm*	126	86	285	59	55	42	66	56	32	206	58	79	77	323	306	34	1000	4
Co	*ppm*	30.3	34.9	18.5	21.4	12.8	12.4	16	19	22.1	21.9	23.5	25.1	19.6	17.1	86.6	25.4	127	11.7
Cr	*ppm*	42	61	94.5	147	108	81.5	104	101	112	87	97	102	107	71.5	96	79	117	53
Sb	*ppm*	1.6	4.4	37.4	5.8	3	5.9	6.4	5.8	2.7	31.8	8.8	8.1	3.6	31.5	14.9	2.4	103	0.4
Sc	*ppm*	8.3	13.1	18.2	27.5	21.9	16.9	19	20.5	19.4	13.9	18.8	18.4	19.3	12.2	16.4	21	20.7	12.6
Zn	*ppm*	96	127	11600	165	62	623	23	104	98	67	127	70	96	187	39	130	1500	55

Supplementary Material 1 – Table providing all the relevant information of the studied samples (coordinates, stratigraphy, mineralization type, whole-rock chemistry, etc.)

Sample Ref		NCL#33	NCN#20	NCC#38	NCC#39	NCL#5	NCC#29	X23	EDS1-B	EDS1-E	EDS1-L	EDS1-R	GV7#1	GV7#2	GV7#3	GV7#4	GV8#1	GV8#2	GV8#3	GV8#4
Sector		Neves Corvo	Neves Corvo	Neves Corvo	Neves Corvo	Neves Corvo	Neves Corvo	Aljustrel	Aljustrel	Aljustrel	Aljustrel	Aljustrel	Aljustrel	Aljustrel	Aljustrel	Aljustrel	Aljustrel	Aljustrel	Aljustrel	Aljustrel
Stratigraphic division		*upper* VSC	*upper* VSC	*upper* VSC	*upper* VSC	*upper* VSC	*upper* VSC	*upper* VSC	*upper* VSC	*upper* VSC	*upper* VSC	*upper* VSC	*upper* VSC	*upper* VSC	*upper* VSC	*upper* VSC	*upper* VSC	*upper* VSC	*upper* VSC	*upper* VSC
Mineralization type/occurrence		*No sulphide*	*Mineralized*	*Mineralized*	*No sulphide*	*No sulphide*	*No sulphide*	*Mineralized*	*Mineralized*	*No sulphide*	*No sulphide*	*No sulphide*	*Py-bearing*	*No sulphide*	*Mineralized*	*Py-bearing*	*Py-bearing*	*No sulphide*	*No sulphide*	*No sulphide*
Footwall/Hangingwall		*Hangingwall*	*Hangingwall*	*Hangingwall*	*Hangingwall*	*Hangingwall*	*Hangingwall*	*n.a.*	*n.a.*	*n.a.*	*n.a.*	*n.a.*	*Hangingwall*	*Hangingwall*	*Hangingwall*	*Hangingwall*	*Hangingwall*	*Hangingwall*	*Hangingwall*	*Hangingwall*
Location - ETRS89	**x**	14848	14018	*n.a.*	*n.a.*	14444	14662	-624	-257	-257	-257	-257	-6403	-6403	-6403	-6403	-6663	-6663	-6663	-6663
	y	-231110	-231726	*n.a.*	*n.a.*	-231728	-231774	-201919	-201023	-201023	-201023	-201023	-199158	-199158	-199158	-199158	-199331	-199331	-199331	-199331
Depth (m)		*n.a.*	*n.a.*	*n.a.*	*n.a.*	*n.a.*	*n.a.*	*n.a.*	-304.56	-350.57	-434.28	-478.23	-162.70	-778.60	-782.30	-797.00	-243.70	-337.55	-345.60	-365.85
SiO_2	%	80.18	63.1	76.65	65.33	64.68	54.94	74.19	47.04	78.7	67.87	66.09	52.86	66.94	55.4	67.79	70.36	70.6	76.76	65.55
Al_2O_3	%	9.14	12.55	12.32	14.52	15.37	15.52	5.76	12.27	10.49	15.55	15.64	15.6	15.13	13.82	14.71	15.25	14.27	11.17	16.18
Fe_2O_3(T)	%	4.34	14.9	2.07	6.12	6.59	11.51	13.58	19.42	4.85	5.88	5.78	11.18	6.28	13.92	5.2	3.57	4.72	3.21	5.62
MnO	%	0.215	0.104	0.093	0.581	0.106	0.159	2.407	0.16	0.137	0.501	0.487	0.172	0.35	0.194	0.444	0.08	0.045	0.045	0.272
MgO	%	1.41	2.58	0.64	1.66	1.33	2.61	0.03	1.31	1.48	1.25	1.25	1.66	2.41	1.62	1.89	1.74	1.81	1.42	1.35
CaO	%	0.15	0.03	0.12	1.07	0.27	0.19	-	0.45	0.12	0.49	0.54	1.63	0.31	0.16	0.61	0.09	0.13	0.17	0.52
Na_2O	%	0.23	0.06	0.67	0.67	0.32	0.21	0.05	0.21	0.47	0.83	0.67	0.96	1.09	0.49	1.52	1.02	0.96	0.68	1.08
K_2O	%	1.77	1.36	3.08	3	3.85	3.93	0.1	2.68	1.93	3.82	4.12	3.19	2.45	2.74	3.19	3.8	2.96	2.5	4.22
TiO_2	%	0.272	0.396	0.517	0.531	0.583	0.586	0.186	0.536	0.43	0.594	0.606	0.631	0.598	0.58	0.448	0.702	0.638	0.521	0.588
P_2O_5	%	0.04	0.03	0.03	0.07	0.08	0.08	0.06	0.08	0.08	0.07	0.08	0.1	0.07	0.08	0.07	0.04	0.04	0.04	0.08
Ba	*ppm*	252	207	504	714	831	2260	24	549	325	845	811	572	619	732	733	609	910	686	541
Cs	*ppm*	4.2	1.8	6	7	10.7	12.7	0.4	7.5	5.1	17.8	15.8	8.5	7.2	7.9	11.3	15.2	8.6	7.6	15.2
Cu	*ppm*	79	35	1720	29	83	5	91	60	45	7	-	96	80	82	34	90	58	50	11
Ga	*ppm*	14	21	19	21	21	24	16	17	17	23	25	20	22	20	20	20	19	15	22
Ge	*ppm*	1.6	1.9	1.9	2.4	2.3	3.7	4.7	0.7	2.2	3	2.5	1.4	2.3	0.6	2.1	3.6	2.4	2.5	2.6
Hf	*ppm*	1.5	2.2	1.8	2.9	2.8	3.8	1.1	2.1	2.1	2.8	2.9	3.1	3.6	2.6	4.7	3.3	3.4	2.4	3.5
Nb	*ppm*	5.4	7.9	4.9	6.7	9.7	11.3	2.6	9.5	5.7	8.8	8.4	9.5	9.6	8.6	8.8	12.6	15.4	9	11.6
Ni	*ppm*	101	52	66	90	41	56	41	130	113	74	90	117	100	137	64	65	52	81	99
Pb	*ppm*	-	94	-	37	-	-	30	84	-	29	21	22	36	152	33	74	12	6	25
Rb	*ppm*	78	73	146	144	184	197	4	119	98	225	226	140	114	126	157	215	150	128	212
S	%	0.014	0.145	0.181	0.015	0.092	0.138	0.017	11.8	0.025	0.006	0.007	6.02	0.046	8.33	0.008	0.037	0.058	0.01	0.009
Sr	*ppm*	38	18	105	125	107	60	121	107	42	109	79	116	153	149	122	59	82	65	84
Ta	*ppm*	0.52	0.74	0.83	0.93	0.89	0.92	0.34	0.72	0.46	0.69	0.7	0.78	0.83	0.72	0.78	0.98	1.08	0.71	0.93
Th	*ppm*	6.12	9.09	8.79	10.8	10.1	10.7	4.75	8.43	6.59	9.64	10.2	10.5	12.2	9.28	13.1	10.6	9.89	7.79	12.2
U	*ppm*	1.06	2.07	6.62	2.07	1.61	1.46	2.11	11.9	1.38	2.06	2.23	10.8	1.89	12.5	2.76	15	1.96	1.67	2.12
V	*ppm*	92	111	687	115	112	116	76	138	85	118	117	182	117	149	93	166	115	125	112
Y	*ppm*	18	31	15	23	34	32	12	20	20	22	22	23	28	23	32	25	28	21	25
Zr	*ppm*	67	80	79	107	125	167	41	97	80	110	108	119	151	111	188	142	144	102	147
La	*ppm*	28	28.9	36.3	39.8	48.3	42.8	25.9	32.1	28.7	40.6	39.7	35.7	46.6	38.6	38.4	42.6	41.5	34.2	43.2
Ce	*ppm*	67.2	53	88.7	80.9	94.5	90.9	50.4	66.8	62.2	77.8	80.7	74.6	100	81.4	78.9	81.6	85	67.5	87.2
Pr	*ppm*	6.48	6.39	8.18	9.04	10.4	9.91	5.43	7.52	6.58	8.96	8.69	8.08	10.1	8.44	8.95	9.54	9.57	7.65	9.26
Nd	*ppm*	24.6	24.1	29.1	33.3	39.7	38.8	20.3	28.2	24.1	32	31.9	30	37	30.6	33.2	34.8	35.1	28.8	33.8
Sm	*ppm*	4.78	5.42	5.33	6.95	8.26	8.32	3.58	5.63	5.14	6.38	6.47	6.25	7.25	5.95	7.28	6.79	6.85	5.08	6.58
Eu	*ppm*	0.972	0.844	1.01	1.36	1.56	1.72	0.776	1.12	0.942	1.22	1.23	1.31	1.38	1.15	1.27	1.33	1.49	1.1	1.37
Gd	*ppm*	3.97	5.08	3.54	5.15	6.78	7.13	3.1	4.52	4.3	4.77	4.89	5.24	6.37	5.13	6.55	5.65	5.73	4.33	5.49
Tb	*ppm*	0.57	0.97	0.56	0.82	1.01	1.14	0.41	0.69	0.67	0.8	0.77	0.8	0.96	0.79	1.07	0.84	0.93	0.67	0.87
Dy	*ppm*	3.36	6.16	3.32	4.74	5.82	6.63	2.26	3.91	3.83	4.68	4.34	4.74	5.6	4.79	6.32	5.03	5.5	3.85	4.94
Ho	*ppm*	0.68	1.23	0.66	0.94	1.13	1.36	0.43	0.73	0.73	0.94	0.89	0.91	1.12	0.92	1.25	0.98	1.08	0.72	0.99
Er	*ppm*	2.02	3.59	1.86	2.74	3.41	3.91	1.27	2.13	1.98	2.63	2.44	2.62	3.14	2.62	3.71	2.82	3.06	2.17	2.9
Tl	*ppm*	0.84	2.95	0.93	0.85	16.4	34.1	-	0.85	0.61	1.02	1.21	4.95	1.38	2.22	2.09	4.23	6.26	5	2.58
Tm	*ppm*	0.301	0.523	0.299	0.409	0.507	0.554	0.183	0.318	0.289	0.386	0.373	0.392	0.484	0.378	0.56	0.44	0.444	0.318	0.432
Yb	*ppm*	1.88	3.25	2.03	2.85	3.49	3.64	1.22	2.23	1.99	2.61	2.76	2.69	3.06	2.41	3.61	2.85	2.92	2.11	2.78
Lu	*ppm*	0.278	0.473	0.3	0.436	0.557	0.536	0.204	0.33	0.304	0.425	0.406	0.41	0.449	0.354	0.539	0.435	0.439	0.33	0.419
As	*ppm*	-	1020	15	8	31	1	31	180	17	-	3	64	4	69	2	22	1	4	1
Co	*ppm*	22.7	18.9	15.9	28.6	8.9	6.8	9.9	70.7	30.3	22.4	24.7	31	22.6	51.8	18.1	15.6	10.5	12.9	25.3
Cr	*ppm*	47	65.5	50	44	53	56	50.6	81	51.8	70.7	79.5	84	67	96	30	84	77	70	55
Sb	*ppm*	0.6	5.2	1.2	1.5	2.5	2.5	1.7	19.9	0.6	2	2.7	13.2	11.2	45.6	1.9	10.9	1.8	4.6	3.3
Sc	*ppm*	9.55	11.7	12.3	13.6	14.9	18.3	5.63	13.7	10.7	15.6	16.6	16.8	15.6	13.9	15.5	14	13	10.8	11.9
Zn	*ppm*	56	681	34	98	31	79	34	128	86	104	101	195	101	136	106	58	64	51	111

Supplementary Material 1 – Table providing all the relevant information of the studied samples (coordinates, stratigraphy, mineralization type, whole-rock chemistry, etc.)

Sample Ref		GV9#2	GV9#4	GV9#5	GV9#7	GV9#8	GV9#9	GV9#10	GV8#5	GV9#3	GV9#6	ALJ_FM#4	ALJ_FM#5	ALJ_RS#7	ALJ_RS#8	ALJ_RS#9	ALJ_RS#10	FFM#1	FFM#2	ALJ_MM10-03#3
Sector		Aljustrel	Aljustrel	Aljustrel	Aljustrel	Aljustrel	Aljustrel	Aljustrel	Aljustrel	Aljustrel	Aljustrel	Aljustrel	Aljustrel	Aljustrel	Aljustrel	Aljustrel	Aljustrel	Aljustrel	Aljustrel	Aljustrel
Stratigraphic division		*upper* VSC	*upper* VSC	*upper* VSC	*upper* VSC	*upper* VSC	*upper* VSC	*upper* VSC	*upper* VSC	*upper* VSC	*upper* VSC	*upper* VSC	*upper* VSC	*upper* VSC	*upper* VSC	*upper* VSC	*upper* VSC	*upper* VSC	*upper* VSC	*upper* VSC
Mineralization type/occurrence		*Mineralized*	*No sulphide*	*No sulphide*	*Mineralized*	*No sulphide*	*No sulphide*	*Py-bearing*	*No sulphide*	*No sulphide*	*No sulphide*	*No sulphide*	*Py-bearing*	*No sulphide*	*No sulphide*	*Py-bearing*	*Py-bearing*	*No sulphide*	*No sulphide*	*Py-bearing*
Footwall/Hangingwall		*Hangingwall*	*Hangingwall*	*Hangingwall*	*Hangingwall*	*Hangingwall*	*Hangingwall*	*Hangingwall*	*Hangingwall*	*Hangingwall*	*Hangingwall*	*Hangingwall*	*Hangingwall*	*Hangingwall*	*Hangingwall*	*Hangingwall*	*Hangingwall*	*Hangingwall*	*Hangingwall*	*Hangingwall*
Location - ETRS89	x	-6219	-6219	-6219	-6219	-6219	-6219	-6219	-6663	-6219	-6219	-1303	-1303	-1729	-1729	-1729	-1729	*n.a.*	*n.a.*	-3531
	y	-199247	-199247	-199247	-199247	-199247	-199247	-199247	-199331	-199247	-199247	-1999029	-1999029	-198714	-198714	-198714	-198714	*n.a.*	*n.a.*	-198454
Depth (m)		-148.65	-175.90	-201.90	-244.20	-246.75	-271.45	-294.05	-391.20	-160.45	-223.60	-107.23	-113.50	-486.15	-501.45	-519.85	-529.90	*n.a.*	*n.a.*	-63.50
SiO_2	%	61.97	75.46	46.79	56.73	63.44	59.93	62.78	69.7	72.29	75.1	74.26	77.46	76.09	69.76	76.95	81.84	61.25	59.53	74.34
Al_2O_3	%	17.75	10.74	10.93	14.4	17.95	15.2	16.05	12.54	13.87	11.94	10.99	10.61	11.09	14.37	10.79	7.97	17.66	19.01	9.35
Fe_2O_3(T)	%	7.71	4.95	4.11	12.91	6.62	6.34	7.07	5.28	4.3	2.42	5.13	3.47	3.97	5.47	2.83	2.46	7.9	7.48	4.42
MnO	%	0.587	0.38	1.856	0.204	0.224	1.208	0.113	0.394	0.329	0.221	0.143	0.1	0.047	0.043	0.035	0.035	0.088	0.081	0.022
MgO	%	1.75	1.4	1.67	1.89	2.21	2.92	2.17	1.62	1.34	1.83	1.41	1.31	1.4	1.82	1.42	1.15	2.35	2.28	1.49
CaO	%	0.19	0.29	15.14	0.18	0.15	3.37	1.54	0.64	0.12	1.28	0.74	0.12	0.15	0.27	0.17	0.19	0.89	0.92	0.64
Na_2O	%	0.82	0.4	1.11	0.96	1.83	0.56	2.51	0.83	0.89	0.77	0.79	0.47	0.41	0.85	0.61	0.11	2.37	2.02	3.04
K_2O	%	3.86	1.96	1.97	2.86	3.18	2.8	2.22	2.04	2.8	2.36	1.99	2.41	2.67	3.04	2.64	2.1	2.58	3.35	0.67
TiO_2	%	0.692	0.423	0.393	0.589	0.733	0.577	0.817	0.468	0.546	0.197	0.414	0.402	0.483	0.621	0.481	0.341	0.858	0.91	0.337
P_2O_5	%	0.09	0.03	0.2	0.07	0.07	0.09	0.14	0.09	0.05	0.06	0.1	0.03	0.05	0.06	0.04	0.02	0.14	0.16	0.03
Ba	*ppm*	684	367	331	728	781	496	453	529	517	428	891	597	340	364	311	257	554	661	126
Cs	*ppm*	10.2	4	4.9	7.1	7.4	6.8	4.9	5	5.6	5.9	11	16.3	13.2	13.9	13.8	13.3	6.1	7.4	2.4
Cu	*ppm*	358	55	8	125	114	96	49	131	163	15	40	81	24	23	102	66	35	41	37
Ga	*ppm*	25	18	21	21	24	22	21	20	23	16	16	15	15	18	15	12	22	25	12
Ge	*ppm*	3.1	2.1	1.6	1	1.6	1.8	1.7	1.9	2.3	1.7	1.9	2.1	2.1	2	1.8	1.8	1.4	1.6	1.1
Hf	*ppm*	3.5	2	8.8	3	3.5	3	4.8	2.3	2.3	2.3	2.6	1.9	2	2.2	2	1.5	4	5	1.8
Nb	*ppm*	13.8	7.4	12.1	10.6	12.5	10	11	6.7	8.6	5.4	11.8	6.8	6.7	7.6	9.1	5.5	9.4	11.3	6.3
Ni	*ppm*	85	109	14	178	100	111	47	72	120	12	67	68	56	59	69	68	45	51	92
Pb	*ppm*	20	9	22	84	-	-	26	11	58	16	14	17	12	16	49	25	16	11	42
Rb	*ppm*	191	92	92	136	144	129	95	100	127	117	120	170	137	149	142	120	104	133	32
S	%	0.009	0.01	0.015	7.16	1.33	0.101	0.473	0.069	0.014	0.03	0.171	0.022	0.004	0.006	0.051	0.252	0.1	0.029	2.58
Sr	*ppm*	105	64	489	88	127	118	158	104	100	107	60	28	40	67	51	27	194	198	184
Ta	*ppm*	1.04	0.58	0.81	0.8	0.9	0.73	0.82	0.57	0.75	0.81	0.98	0.63	0.62	0.85	0.65	0.48	0.82	0.84	0.53
Th	*ppm*	12.4	7.6	12.7	10.3	11.6	10.4	10.6	8.88	9.6	6.85	8.36	7.32	7.82	9.48	7.58	5.59	10.4	11.1	5.95
U	*ppm*	2.82	1.72	3.15	5.53	5.96	2	3.33	1.45	2.78	6.23	1.33	1.42	1.34	1.72	4.05	1.69	2.99	3.14	6.66
V	*ppm*	176	92	38	183	156	118	134	81	142	22	94	82	100	114	133	98	135	143	149
Y	*ppm*	26	18	95	20	25	25	22	23	18	16	24	19	19	20	16	10	23	26	21
Zr	*ppm*	144	81	372	122	142	118	197	106	102	78	129	82	84	105	86	66	159	191	69
La	*ppm*	61.4	31.3	51.6	38.9	47.5	37	33	38.4	37.9	17.2	36.4	35	32.8	37.7	32.7	23.9	36.9	35.7	23
Ce	*ppm*	124	71.2	108	81.9	104	83.2	66.8	81.8	86.4	36.5	83.7	76.6	66.8	78.3	65.4	46.4	72.2	72.8	43.1
Pr	*ppm*	12.8	6.72	12.9	8.42	10.6	8.23	7.4	8.74	8.19	4.05	8.36	7.87	7.28	8.35	7.46	5.14	7.83	8.07	5.27
Nd	*ppm*	48.9	24.6	51.9	30.2	38	29.7	27.4	32.1	29.2	14.4	30.6	28.8	26.6	29.7	27.2	18.4	28.4	30.4	19.8
Sm	*ppm*	9.75	4.68	12.7	5.74	6.91	5.97	5.33	6.38	5.36	3.4	6.13	5.59	5.21	5.69	5.17	3.24	5.45	5.95	4.04
Eu	*ppm*	2.38	0.967	1.32	1.21	1.44	1.14	1.19	1.28	0.893	0.406	1.39	1.06	1.01	1.23	0.964	0.595	1.33	1.46	0.642
Gd	*ppm*	8.2	4.09	14.4	4.94	5.48	5.24	4.95	5.54	4.23	2.97	5.44	4.62	4.44	4.39	4.19	2.48	4.82	5.47	3.46
Tb	*ppm*	1.15	0.61	2.53	0.79	0.84	0.86	0.8	0.89	0.66	0.52	0.9	0.71	0.64	0.69	0.59	0.34	0.77	0.84	0.55
Dy	*ppm*	6.21	3.5	15.9	4.55	4.91	5.06	4.53	5.11	3.69	2.91	5.23	3.93	3.76	4.1	3.29	1.96	4.52	5.22	3.33
Ho	*ppm*	1.1	0.67	3.21	0.88	0.99	0.99	0.9	0.98	0.72	0.56	1.03	0.79	0.75	0.77	0.65	0.42	0.9	0.99	0.68
Er	*ppm*	2.98	1.99	9.49	2.61	2.81	2.84	2.64	2.85	2.12	1.62	2.92	2.23	2.19	2.34	1.83	1.3	2.59	2.82	1.89
Tl	*ppm*	0.97	0.46	0.41	1.52	1.12	0.88	0.68	0.95	0.6	0.73	0.83	1.2	0.55	0.53	0.74	0.63	14.5	5.02	1.59
Tm	*ppm*	0.427	0.287	1.36	0.373	0.408	0.412	0.394	0.419	0.312	0.244	0.404	0.311	0.318	0.326	0.271	0.201	0.379	0.407	0.288
Yb	*ppm*	2.87	1.88	9.15	2.39	2.74	2.86	2.64	2.79	2.07	1.56	2.56	2.08	2.03	2.23	1.74	1.36	2.43	2.66	1.87
Lu	*ppm*	0.434	0.288	1.44	0.373	0.406	0.432	0.403	0.406	0.328	0.23	0.379	0.312	0.339	0.351	0.312	0.225	0.363	0.409	0.335
As	*ppm*	-	7	-	156	46	15	30	4	39	4	61	49	-	-	16	11	8	20	120
Co	*ppm*	22.6	22.4	7.3	53.6	28.1	28.5	16.9	18	26.3	4.9	13.4	14.3	12.1	13.4	21.5	20.8	17.5	20.6	10.4
Cr	*ppm*	73.5	48.5	15	78	81	67.5	90	41	56	14	45.5	48	63	70	60	50	73.5	72.5	54
Sb	*ppm*	1.1	0.6	0.2	11.8	1.4	0.3	1.8	1.2	3	0.4	5.5	6.5	1.1	1	2	2.6	0.9	1	6.5
Sc	*ppm*	13.6	8.95	7.15	12.3	14.4	13	16.6	11.1	11.3	4.5	8.65	8.65	10.4	12.6	10.2	7.81	16.6	14.4	7.77
Zn	*ppm*	144	110	87	192	116	100	124	92	108	51	87	87	74	83	172	71	111	108	170

Supplementary Material 1 – Table providing all the relevant information of the studied samples (coordinates, stratigraphy, mineralization type, whole-rock chemistry, etc.)

Sample Ref		MFM#1	ALJ_FM#6	ALJ_RS#11	ALJ_RS#12	ALJ_RS#13	ALJ_RS#14	ALJ_RS#15	ALJ_MM10-03#1	ALJ_MM10-03#2	ALJ_MM10-03#4	ALJ_MM10-03#5	ALJ_MM16-15#9	ALJ_MM16-15#10	ALJ_MM16-15#11	ALJ_MS#5	ALJ_FM#1	ALJ_FM#2	ALJ_RS#1	ALJ_RS#2
Sector		Aljustrel	Aljustrel	Aljustrel	Aljustrel	Aljustrel	Aljustrel	Aljustrel	Aljustrel	Aljustrel	Aljustrel	Aljustrel	Aljustrel	Aljustrel	Aljustrel	Aljustrel	Aljustrel	Aljustrel	Aljustrel	Aljustrel
Stratigraphic division		*upper* VSC	*upper* VSC	*upper* VSC	*upper* VSC	*upper* VSC	*upper* VSC	*upper* VSC	*upper* VSC	*upper* VSC	*upper* VSC	*upper* VSC	*upper* VSC	*upper* VSC	*upper* VSC	*upper* VSC	*upper* VSC	*upper* VSC	*upper* VSC	*upper* VSC
Mineralization type/occurrence		*Mineralized*	*No sulphide*	*No sulphide*	*No sulphide*	*No sulphide*	*No sulphide*	*No sulphide*	*No sulphide*	*No sulphide*	*No sulphide*	*No sulphide*	*No sulphide*	*No sulphide*	*No sulphide*	*No sulphide*	*Py-bearing*	*Py-bearing*	*Py-bearing*	*Py-bearing*
Footwall/Hangingwall		*Hangingwall*	*Hangingwall*	*Hangingwall*	*Hangingwall*	*Hangingwall*	*Hangingwall*	*Hangingwall*	*Hangingwall*	*Hangingwall*	*Hangingwall*	*Hangingwall*	*Hangingwall*	*Hangingwall*	*Hangingwall*	*Hanginwall*	*Hanginwall*	*Hanginwall*	*Hanginwall*	*Hanginwall*
Location - ETRS89	x	*n.a.*	-1303	-1729	-1729	-1729	-1729	-1729	-3531	-3531	-3531	-3531	-3469	-3469	-3469	-3795	-1303	-1303	-1729	-1729
	y	*n.a.*	-1999029	-198714	-198714	-198714	-198714	-198714	-198454	-198454	-198454	-198454	-198137	-198137	-198137	-197814	-1999029	-1999029	-198714	-198714
Depth (m)		*n.a.*	-115.45	-542.42	-550.93	-560.85	-576.93	-585.55	-41.50	-50.95	-77.35	-109.20	-340.47	-356.55	-383.80	-113.00	-94.45	-98.59	-408.55	-416.70
SiO_2	%	79.99	73.89	72.01	76.49	71.42	73.64	61.81	73.1	73.15	53.81	72.46	68.97	66.84	63.26	67.51	61.92	63.53	52.73	60.74
Al_2O_3	%	10.05	13.07	11.5	10.44	13.3	11.47	15.83	13.8	14.1	16.96	12.67	13.85	15.21	13.81	12.39	15.25	18.36	13.89	20.12
Fe_2O_3(T)	%	2.87	4.46	6.93	4	5.3	4.16	10.95	1.78	1.8	9.25	3.9	4.17	7.16	8.29	10.05	8.59	6.52	15.26	6.59
MnO	%	0.119	0.161	0.167	0.071	0.046	0.064	0.17	0.02	0.025	0.065	0.066	1.05	0.629	0.447	0.051	0.196	0.32	0.238	0.433
MgO	%	0.58	1.46	1.15	1.16	1.46	1.57	2.47	3.66	4	6.77	3.08	1.42	1.53	2.19	2	1.91	2.57	1.69	2.51
CaO	%	0.03	0.12	0.94	0.89	0.23	0.56	0.19	0.23	0.19	1.58	0.59	2.16	0.54	1.93	0.4	0.2	0.16	0.51	0.35
Na_2O	%	0.14	0.5	2.07	0.63	0.75	0.55	0.07	0.46	0.39	0.71	0.11	0.32	0.73	0.71	0.05	0.6	0.76	0.49	2.52
K_2O	%	1.97	3.11	1.5	2.43	3.18	2.73	2.99	3.01	2.77	3.1	3.29	3.37	2.96	2.3	2.64	3.1	3.52	2.72	2.89
TiO_2	%	0.236	0.504	0.437	0.422	0.56	0.518	0.657	0.159	0.158	1.184	0.199	0.566	0.565	0.512	0.552	0.613	0.762	0.556	0.8
P_2O_5	%	0.01	0.03	0.09	0.04	0.05	0.04	0.1	0.01	0.02	0.2	0.06	0.13	0.08	0.08	0.19	0.06	0.06	0.07	0.09
Ba	*ppm*	6886	1128	257	352	653	902	2832	537	522	517	452	699	686	567	441	562	743	589	639
Cs	*ppm*	18.3	18.3	10.3	21.9	27.3	27	27.6	11.2	8.6	9.3	8.6	8.8	12.3	6.1	8	8.6	9.7	8.8	8.4
Cu	*ppm*	44	95	15	54	33	29	41	6	7	29	10	470	23	191	93	164	188	71	186
Ga	*ppm*	71	17	15	15	17	16	22	21	21	22	18	19	20	18	17	21	24	18	25
Ge	*ppm*	6.7	2.5	2.3	2.3	2.2	3.1	5.7	1.5	1.7	1.6	1.4	2.1	2.3	1.2	2.6	0.8	2.1	0.7	1.9
Hf	*ppm*	2.1	2.2	2.1	2.7	2.3	2.1	3.5	5.1	5	4.2	4.4	4.2	2.1	1.7	2.7	2.7	3.5	2.3	3.2
Nb	*ppm*	4.7	9	8	10.8	9.3	8	13.4	9.7	9	6.9	7.7	10.5	6.6	5.6	10.7	10.2	12.5	8.9	12.9
Ni	*ppm*	9	88	79	75	60	42	53	5	1	55	5	64	86	103	58	148	56	137	78
Pb	*ppm*	22	41	29	10	26	14	-	13	11	30	9	31	30	58	15	53	28	94	15
Rb	*ppm*	91	221	87	164	208	201	217	166	133	135	121	164	148	101	141	140	157	124	135
S	%	0.172	0.017	0.006	0.01	0.007	0.03	0.019	0.006	0.011	1.71	1.83	0.049	0.004	3.04	0.008	3.27	0.09	9.31	0.346
Sr	*ppm*	35	27	139	31	37	34	24	82	94	57	20	136	124	111	13	86	99	118	217
Ta	*ppm*	0.59	0.78	0.73	0.91	0.84	0.71	1.08	1.09	0.94	0.49	0.79	0.93	0.78	0.59	0.9	0.87	1.02	0.73	1.08
Th	*ppm*	12.7	9.19	8.19	7.88	8.99	8.06	12	15.4	14.6	4.42	14.7	13.4	9.86	7.87	8.22	9.96	11.8	8.49	12
U	*ppm*	37.3	1.4	1.32	1.32	1.63	1.4	2.17	2.05	3.92	1.78	4.26	3.55	2.15	5.6	3.25	8.05	2.57	11.9	2.64
V	*ppm*	59	143	94	76	135	110	216	6	13	227	15	93	122	133	167	195	180	167	156
Y	*ppm*	12	18	23	21	20	20	32	57	57	38	46	29	28	18	21	19	25	24	22
Zr	*ppm*	77	106	93	111	103	95	158	157	140	163	150	173	113	88	127	122	164	100	147
La	*ppm*	7.34	39.3	37.1	34.2	36.3	32.3	50.8	32.2	31.8	21.6	28.9	40.5	42.5	29.3	35.9	35.3	44.3	32	45.5
Ce	*ppm*	15.4	89.7	84.3	77.3	75.3	65.7	92.9	70.4	67.1	46.3	63.6	84.1	80.9	65.3	63.2	75.1	96.8	67.9	99.9
Pr	*ppm*	1.7	9.12	8.57	7.7	8.16	7.33	11.4	8.13	7.67	5.87	7.38	9.27	9.25	6.72	8.02	7.88	10.1	7.19	10.3
Nd	*ppm*	5.85	33.6	31.3	29	29.3	27	40.6	31.2	29.8	24.4	27.7	34	34.3	24.7	29.3	28.5	36.6	26	36.5
Sm	*ppm*	1.43	6.52	6.15	5.66	5.89	5.1	8.28	7.66	7.08	6	6.95	6.99	6.79	4.93	5.66	5.53	7.01	5.12	6.79
Eu	*ppm*	0.338	1.21	1.39	1.11	1.17	1.14	1.72	0.615	0.564	1.52	0.504	1.39	1.47	1.08	1.25	1.09	1.3	1.23	1.31
Gd	*ppm*	1.3	5.28	5.26	4.68	4.5	4.21	7.09	8.27	7.73	6.87	6.92	5.96	5.9	4.33	4.81	4.4	5.46	4.66	5.51
Tb	*ppm*	0.33	0.78	0.85	0.71	0.71	0.65	1.16	1.63	1.4	1.14	1.35	0.95	0.92	0.64	0.76	0.71	0.86	0.75	0.86
Dy	*ppm*	2.34	4.36	4.96	4.06	4.11	3.7	6.95	10.5	9.66	7.09	8.62	5.68	5.43	3.78	4.74	4.23	5.09	4.6	5.02
Ho	*ppm*	0.51	0.8	0.95	0.79	0.82	0.71	1.41	2.17	1.99	1.41	1.78	1.12	1.08	0.72	0.92	0.81	1.02	0.9	0.93
Er	*ppm*	1.67	2.21	2.75	2.27	2.34	2.14	3.96	6.31	6.02	3.98	5.18	3.07	3.15	2.01	2.69	2.35	2.93	2.52	2.65
Tl	*ppm*	> 1000	1.83	0.49	1.15	1.46	2.67	7.38	0.85	1.22	0.88	0.92	1.11	0.76	1.34	0.31	2.12	1.25	1.46	1.05
Tm	*ppm*	0.275	0.319	0.402	0.345	0.332	0.306	0.571	0.952	0.932	0.545	0.792	0.452	0.431	0.291	0.4	0.342	0.413	0.369	0.386
Yb	*ppm*	2.09	1.99	2.45	2.23	2.3	2.09	3.77	6.41	6.3	3.53	5.09	2.89	3.16	1.9	2.49	2.26	2.78	2.35	2.6
Lu	*ppm*	0.347	0.308	0.359	0.354	0.338	0.345	0.584	0.97	0.967	0.511	0.749	0.435	0.458	0.284	0.366	0.355	0.417	0.348	0.384
As	*ppm*	7	97	1	27	17	17	37	1	-	21	29	9	-	48	4	116	3	123	7
Co	*ppm*	3.3	23.8	21.3	21.4	14.1	7.4	8.8	2.6	0.6	26.4	3	19	19.5	31.2	14.9	47.8	8.1	61.8	14.4
Cr	*ppm*	26	57.5	52.5	43	65	53.5	77	6.5	5.5	166	11	44.5	68.5	69	74	79	80.5	82	92
Sb	*ppm*	7.9	2.8	1.5	4.7	2.9	4.3	6.8	0.3	0.4	2.3	1.6	0.8	1.1	21.1	0.4	29.3	1.7	23.3	0.5
Sc	*ppm*	6.17	10.5	9.55	8.15	9.75	8.9	11.6	4.63	4.4	27.7	9.43	11.3	12.6	13.6	11.6	12.4	14.4	13.5	18.3
Zn	*ppm*	1320	87	112	69	90	65	135	65	59	116	39	84	90	115	112	121	115	203	99

Supplementary Material 1 – Table providing all the relevant information of the studied samples (coordinates, stratigraphy, mineralization type, whole-rock chemistry, etc.)

Sample Ref		ALJ_RS#5	ALJ_RS#6	LJ_MM16-15	ABNSTR1	11-1-KK	11-1-LL	11-1-MM	11-1-NN	ALB03#30	ALB03#31	ALB03#32	ALB03#34	PC34	PC32	PC38	PC6	PC19	PC27	X32
Sector		Aljustrel	Aljustrel	Aljustrel	Albernoa	Albernoa	Albernoa	Albernoa	Albernoa	Albernoa	Albernoa	Albernoa	Albernoa	Albernoa	Albernoa	Albernoa	Albernoa	Albernoa	Albernoa	Albernoa
Stratigraphic division		*upper* VSC	*upper* VSC	*upper* VSC	PQG	PQG	PQG	PQG	PQG	PQG	PQG	PQG	PQG	PQG	PQG	PQG	PQG	PQG	PQG	PQG
Mineralization type/occurrence		*No sulphide*	*No sulphide*	*Py-bearing*	*No sulphide*	*No sulphide*	*No sulphide*	*No sulphide*	*No sulphide*	*No sulphide*	*No sulphide*	*No sulphide*	*No sulphide*	*No sulphide*	*No sulphide*	*No sulphide*	*No sulphide*	*No sulphide*	*No sulphide*	*No sulphide*
Footwall/Hangingwall		*Hanginwall*	*Hanginwall*	*Hanginwall*	*n.a.*	*n.a.*	*n.a.*	*n.a.*	*n.a.*	*n.a.*	*n.a.*	*n.a.*	*n.a.*	*n.a.*	*n.a.*	*n.a.*	*n.a.*	*n.a.*	*n.a.*	*n.a.*
Location - ETRS89	x	-1729	-1729	-3469	53032	17603	17603	17603	17603	14790	14790	14790	14790	3557	3557	3557	3557	3557	3557	5307
	y	-198714	-198714	-198137	-231885	-205799	-205799	-205799	-205799	-204961	-204961	-204961	-204961	-199306	-199306	-199306	-199306	-199306	-199306	-204250
Depth (m)		-454.50	-461.75	-237.00	*n.a.*	-363.60	-365.65	-399.80	-400.80	-513.60	-542.80	-577.95	-593.20	*n.a.*	*n.a.*	*n.a.*	*n.a.*	*n.a.*	*n.a.*	*n.a.*
SiO_2	%	78.37	72.15	65.27	71.42	59.58	61.5	62.59	71.15	57.86	78.15	55.71	54.37	58.6	62.69	61.8	58.92	64.59	54.46	67.13
Al_2O_3	%	9.37	12.2	13.56	14.44	19.69	19	16.98	12.74	22.11	6.84	24.21	23.6	20.13	17.25	18.42	20.6	18.28	23.31	16.01
Fe_2O_3(T)	%	3.83	6.35	5.88	5.22	5.46	7.41	8.32	5.74	7.96	7.2	7.4	8.32	7.58	6.87	6.98	7.93	6.08	8.2	6.74
MnO	%	0.201	0.09	0.027	0.014	0.067	0.068	0.085	0.082	0.053	0.127	0.059	0.182	0.071	0.112	0.135	0.189	0.149	0.194	0.146
MgO	%	1.3	1.24	1.45	0.65	1.5	1.88	1.94	1.29	1.34	1.31	1.36	1.55	2.37	2.1	2.16	2.08	1.59	1.82	1.26
CaO	%	0.65	0.67	0.25	0.01	1.46	0.45	0.65	1.52	0.22	0.56	0.16	0.23	0.32	1.27	0.33	0.4	0.12	0.21	0.08
Na_2O	%	0.61	1.06	0.8	0.08	0.38	0.35	0.37	0.27	0.91	0.13	1.02	1.1	2.47	3.05	1.69	1.11	1.28	0.86	0.65
K_2O	%	1.82	2.04	4.01	3.54	4.24	3.82	3.05	2.33	3.52	0.69	3.6	3.75	3.37	2.36	3.65	3.65	3.24	4.55	2.6
TiO_2	%	0.359	0.456	0.526	0.553	1.016	0.983	0.843	0.697	1.055	0.471	1.025	0.931	1.05	0.877	0.953	0.986	0.757	1.025	0.852
P_2O_5	%	0.04	0.31	0.07	0.05	0.14	0.13	0.12	0.09	0.16	0.14	0.12	0.1	0.2	0.16	0.15	0.14	0.08	0.11	0.11
Ba	*ppm*	288	311	460	529	509	452	338	251	477	110	516	520	461	323	450	533	505	652	447
Cs	*ppm*	6.1	6.7	11.4	6.5	9.4	7.9	6.4	5	10.8	1.5	10.5	10.8	6.6	4.3	7.1	8.6	6.4	9.4	4.5
Cu	*ppm*	171	25	57	64	28	37	33	29	15	16	30	33	54	35	54	39	49	56	34
Ga	*ppm*	14	16	18	21	26	26	23	17	32	10	31	29	25	20	24	27	26	31	23
Ge	*ppm*	2.1	2.4	1.1	2.7	1.8	2.2	1.7	1.4	2.1	3	2.6	2.4	1.5	1.7	1.7	2.4	2.1	2.2	3.6
Hf	*ppm*	1.8	1.7	2.6	2.4	5.6	5.6	4.9	5.6	5.9	6.2	4.6	3.8	4.7	4.7	4.9	4.5	3.2	4.9	5.7
Nb	*ppm*	6	6.2	10.4	12.9	18.9	18.6	16.6	12.5	23.5	5.9	20.7	17.1	12.3	8.9	15.2	14.4	16.1	17.4	13.9
Ni	*ppm*	93	84	93	63	56	65	65	44	59	35	64	52	64	52	57	62	77	63	54
Pb	*ppm*	18	25	42	23	5	6	6	5	5	-	-	8	-	-	-	-	-	-	65
Rb	*ppm*	88	92	197	164	181	159	138	102	182	34	172	175	135	93	142	153	146	191	134
S	%	0.027	0.008	3.46	0.018	0.156	0.059	0.46	0.46	0.282	0.049	0.088	0.09	0.132	0.159	0.082	0.026	0.01	0.102	0.003
Sr	*ppm*	85	98	39	16	96	83	90	80	107	28	117	119	103	121	85	101	90	161	90
Ta	*ppm*	0.55	0.69	0.78	0.85	1.49	1.51	1.34	1.4	1.69	0.55	1.73	1.48	1.01	0.81	1.21	1.26	1.08	1.47	1.2
Th	*ppm*	6.88	8.7	8.07	9.06	15.7	15	13.7	10.6	16.8	7.95	15.8	14.9	12.2	9.21	13.2	13.3	11.8	15.3	12.3
U	*ppm*	1.15	1.47	8.85	2.4	4.24	3.35	3.16	2.46	2.94	1.67	2.72	2.53	3.35	2.83	3.02	2.82	2.17	3.01	2.64
V	*ppm*	119	108	138	145	185	179	158	115	145	44	145	142	162	133	159	148	136	151	104
Y	*ppm*	19	27	24	33	32	31	27	23	32	21	29	26	32	24	32	31	24	31	28
Zr	*ppm*	69	86	98	99	225	226	211	248	224	273	200	169	200	189	204	182	126	194	214
La	*ppm*	30	39.9	31.1	43.2	48.4	44.7	42	34.7	58.8	27.3	52.7	51.6	40.9	30.9	44.6	45.2	46.9	52.9	42.2
Ce	*ppm*	70.2	92.6	57.2	77.7	96.3	86.5	83	67.9	118	59.5	107	103	85.5	63.7	92.9	91.8	104	107	75.7
Pr	*ppm*	6.92	8.92	7	12.4	11.2	9.91	9.51	7.82	12.9	6.68	11.7	11.3	9.56	7.16	10.4	10.1	10.4	11.4	9.24
Nd	*ppm*	26.3	32.8	27.1	50	42.9	36.8	35.5	29	46.5	25.4	41.9	40.6	37.8	27.9	39.3	38.2	40.4	43.2	33.5
Sm	*ppm*	4.99	6.65	5.27	10.9	7.97	6.9	6.8	5.29	8.85	5.04	8.15	7.69	7.41	5.93	8	7.67	7.3	8.35	6.52
Eu	*ppm*	0.993	1.64	1.08	2.21	1.59	1.36	1.42	1.18	1.87	1.09	1.72	1.6	1.59	1.26	1.48	1.59	1.49	1.58	1.26
Gd	*ppm*	4.71	5.86	4.42	9.03	6.64	5.88	5.66	4.49	7.65	4.45	6.7	5.97	6.21	4.85	6.31	6.04	5.33	6.32	5.17
Tb	*ppm*	0.66	0.9	0.69	1.36	1.06	0.96	0.9	0.74	1.24	0.71	1.07	0.93	0.94	0.71	0.99	0.94	0.8	1.02	0.86
Dy	*ppm*	3.56	5.34	3.88	7.4	6.06	5.59	5.26	4.2	7.23	4.16	6.3	5.53	5.72	4.25	5.81	5.73	4.58	6.03	5.24
Ho	*ppm*	0.7	1.06	0.78	1.43	1.17	1.12	1.01	0.87	1.32	0.79	1.21	1.06	1.13	0.85	1.15	1.11	0.93	1.16	1.05
Er	*ppm*	1.97	3.03	2.32	4.13	3.43	3.27	2.91	2.51	3.66	2.21	3.51	3.09	3.3	2.47	3.44	3.26	2.74	3.34	3.06
Tl	*ppm*	0.5	0.36	1.53	0.71	0.75	0.74	0.71	0.53	0.57	0.12	0.41	0.45	0.52	0.37	0.52	0.56	0.46	0.7	0.42
Tm	*ppm*	0.306	0.417	0.339	0.578	0.524	0.502	0.453	0.36	0.543	0.31	0.505	0.42	0.471	0.368	0.513	0.486	0.406	0.506	0.453
Yb	*ppm*	1.93	2.79	2.25	3.83	3.44	3.34	3	2.42	3.68	2.07	3.19	2.81	3.14	2.48	3.41	3.08	2.77	3.38	3.13
Lu	*ppm*	0.301	0.42	0.354	0.586	0.506	0.52	0.452	0.388	0.565	0.343	0.47	0.424	0.53	0.407	0.552	0.523	0.454	0.548	0.494
As	*ppm*	2	-	32	17	26	22	21	18	38	8	30	16	32	27	25	15	41	24	13
Co	*ppm*	21.2	20.8	17.3	10	16.6	17.5	18.2	13.3	23.3	13.4	24.5	19.8	20	18.5	20.9	19.8	23.2	25.2	17.3
Cr	*ppm*	49	59	74.5	97.6	103	90.6	86.7	62.5	122	38.5	109	108	118	100	94.1	110	89.5	121	90.5
Sb	*ppm*	0.6	1	9.6	1.3	1.2	1.1	1.2	1.1	2.9	0.7	1.1	1.1	2	2	2.2	0.6	0.6	1.2	1.2
Sc	*ppm*	9.98	12	10.6	12.4	19.4	18.3	15.9	11.8	19.7	5.35	17.8	17.6	22.2	17.5	19.3	19.9	17.6	22.3	14.9
Zn	*ppm*	94	99	173	61	71	100	110	76	109	99	108	95	97	86	84	101	80	97	93

Supplementary Material 1 – Table providing all the relevant information of the studied samples (coordinates, stratigraphy, mineralization type, whole-rock chemistry, etc.)

Sample Ref		X42	X43	X44	X46	X47	X48	X50	X51	X60	X61	X29	X30	X31	X7	X10	X11	X12	X13	X14
Sector		**Albernoa**	**Albernoa**	**Albernoa**	**Albernoa**	**Albernoa**	**Albernoa**	**Albernoa**	**Albernoa**	**Albernoa**	**Albernoa**	**Aljustrel**	**Aljustrel**	**Aljustrel**	**Albernoa**	**Albernoa**	**Albernoa**	**Albernoa**	**Albernoa**	**Albernoa**
Stratigraphic division		**PQG**	**PQG**	**PQG**	**PQG**	**PQG**	**PQG**	**PQG**	**PQG**	**PQG**	**PQG**	**PQG**	**PQG**	**PQG**	**PQG**	**PQG**	**PQG**	**PQG**	**PQG**	**PQG**
Mineralization type/occurrence		***No sulphide***	***No sulphide***	***No sulphide***	***No sulphide***	***No sulphide***	***No sulphide***	***No sulphide***	***No sulphide***	***No sulphide***	***No sulphide***	***No sulphide***	***No sulphide***	***No sulphide***	***No sulphide***	***No sulphide***	***No sulphide***	***No sulphide***	***No sulphide***	***No sulphide***
Footwall/Hangingwall		***n.a.***	***n.a.***	***n.a.***	***n.a.***	***n.a.***	***n.a.***	***n.a.***	***n.a.***	***n.a.***	***n.a.***	***n.a.***	***n.a.***	***n.a.***	***n.a.***	***n.a.***	***n.a.***	***n.a.***	***n.a.***	***n.a.***
Location - ETRS89	**x**	10725	10868	14163	14903	14989	14989	18960	25690	18540	18540	2366	3728	3728	3957	1986	2050	1070	370	370
	y	-209321	-209353	-212329	-212789	-212768	-212768	-217525	-216294	-216670	-216670	-200888	-201856	-201856	-198222	-198632	-198465	-196842	-196470	-196470
Depth (m)		*n.a.*	*n.a.*	*n.a.*	*n.a.*	*n.a.*	*n.a.*	*n.a.*	*n.a.*	*n.a.*	*n.a.*	*n.a.*	*n.a.*	*n.a.*	*n.a.*	*n.a.*	*n.a.*	*n.a.*	*n.a.*	*n.a.*
SiO_2	%	65.72	66.01	56.3	85.85	76.43	71.67	56.32	77.81	61.31	65.14	76.77	93.38	57.69	79.2	79.67	75.5	69.13	67.21	72.81
Al_2O_3	%	12.96	17.2	21.69	7.68	10.26	13.05	22.05	10.57	17.89	19.18	11.38	3.46	19.6	5.63	8.82	11.15	14.45	15.96	12.7
Fe_2O_3(T)	%	11.81	6.11	8.09	2.53	6.16	6.86	6.95	4.65	9.21	4.18	4.74	0.18	8.34	11.32	5.05	4.6	5.39	7.87	5.19
MnO	%	0.117	0.046	0.037	0.02	0.981	0.169	0.089	0.18	0.235	0.005	0.087	0.002	0.082	0.007	0.109	0.075	0.175	0.063	0.095
MgO	%	1.42	0.73	1.36	0.13	0.25	3.06	1.5	0.9	1.79	0.28	0.91	0.04	2.61	0.13	0.87	0.77	0.97	0.97	1.02
CaO	%	0.1	0.06	0.15	0.03	0.02	0.08	0.16	0.01	0.05	0.04	0.12	0.04	0.18	-	0.1	0.03	0.02	-	0.01
Na_2O	%	0.34	0.6	1.12	0.18	0.26	0.53	0.71	0.08	0.54	0.81	0.8	0.21	0.98	0.16	0.25	0.5	0.27	0.31	0.23
K_2O	%	1.51	2.63	3.3	1.45	2.51	1.32	3.93	2.16	2.6	3.58	1.84	0.68	3.07	0.56	1.39	1.76	2.99	3.48	2.26
TiO_2	%	0.539	0.741	1.051	0.306	0.377	0.49	0.87	0.394	0.639	1.026	0.724	0.127	1.067	0.265	0.692	0.644	0.605	0.612	0.489
P_2O_5	%	0.09	0.08	0.13	0.03	0.05	0.08	0.09	0.05	0.06	0.07	0.11	0.05	0.13	0.04	0.11	0.07	0.05	0.04	0.06
Ba	*ppm*	297	414	644	290	447	223	591	260	392	526	361	82	443	91	254	295	485	584	376
Cs	*ppm*	2.7	3.8	5.4	1.8	4.7	2.4	6.7	3.4	6	9.1	3.3	0.7	5.7	1	2.3	3.3	5	7.9	3.8
Cu	*ppm*	38	38	62	56	3	158	40	92	126	21	24	6	73	20	24	15	13	44	109
Ga	*ppm*	20	25	31	11	16	19	32	17	26	29	16	7	28	9	12	16	22	24	20
Ge	*ppm*	4.4	3.2	2.7	1.9	1.8	2.6	3.2	1.9	2.8	2.4	3.2	2.2	3.6	2.5	3.1	3.4	3.1	3.4	3.8
Hf	*ppm*	2.9	3.3	5.2	1.4	2	2.1	3.6	2	2.4	7.6	9.3	0.8	4.8	1.3	14.7	6	2.6	3.7	2.4
Nb	*ppm*	10.4	13	20.8	6.5	6.5	7.5	17.7	7.9	13.3	21.5	10	2.2	12.9	3.5	9.8	9.4	10	11.1	8.3
Ni	*ppm*	75	42	61	16	53	68	55	64	99	12	28	-	96	26	27	29	71	77	89
Pb	*ppm*	7	8	-	-	33	24	-	-	-	-	-	27	6	24	-	15	-	36	-
Rb	*ppm*	85	148	169	80	149	72	211	97	144	183	91	24	157	27	71	90	153	197	116
S	%	0.07	0.01	0.004	0.009	0.004	0.002	0.005	0.006	0.002	0.006	0.004	0.78	0.005	0.034	0.003	0.003	0.005	0.005	0.006
Sr	*ppm*	62	92	164	35	132	139	108	26	77	120	67	127	66	31	58	65	59	70	46
Ta	*ppm*	0.86	1.11	1.59	0.51	0.44	0.53	1.27	0.63	1	1.63	0.92	0.21	1.03	0.34	0.87	0.87	0.88	0.92	0.76
Th	*ppm*	8.84	11.8	15.5	5.22	6.6	7.84	14.3	7.65	10.4	16.9	11.6	2.27	12.3	4.33	12.8	9.56	10.5	12.4	9.01
U	*ppm*	3.53	2.84	2.88	1.33	1.34	1.92	2.17	1.32	2.07	3.64	2.37	1.34	2.68	2.82	2.74	2	1.91	2.15	1.74
V	*ppm*	81	103	150	84	45	113	140	101	142	136	65	64	203	177	53	61	148	94	142
Y	*ppm*	22	24	33	11	22	23	26	13	19	37	28	7	28	15	34	23	19	30	21
Zr	*ppm*	99	117	197	59	86	95	137	81	103	312	346	31	160	55	545	228	97	136	85
La	*ppm*	30.1	42.9	52.4	22	29.5	40.9	50.6	28	32.3	55.3	38.8	9.44	36.9	13.3	42	31.2	35.7	46.7	35.3
Ce	*ppm*	55.6	79.6	97.5	43.9	53.7	69.3	94.8	62.9	70.4	113	76.9	15	70.9	12.9	87.6	61.5	78	79	77.3
Pr	*ppm*	7.33	9.79	11.6	5.09	7.47	8.57	11.2	6.31	7.59	13.4	9.08	2.07	8.82	2.05	10.5	7.59	8.29	10.6	7.75
Nd	*ppm*	28.6	35	43.2	18.5	30.9	32	42	23.7	27.2	52	34.7	7.26	33.1	6.93	40.8	27.8	30.7	38.4	28.4
Sm	*ppm*	5.78	6.84	8.34	3.09	6.62	6.23	7.93	4.74	5.14	9.71	6.73	1.76	7.18	1.37	8.23	5.32	5.49	7.25	5.46
Eu	*ppm*	1.08	1.35	1.68	0.486	1.26	1.31	1.56	0.843	1.01	1.83	1.32	0.36	1.37	0.488	1.54	1.06	0.981	1.48	1.34
Gd	*ppm*	4.88	5.16	7.37	2.27	5.37	5.34	6.84	3.37	4.2	7.69	5.5	1.53	5.76	1.93	6.9	4.44	3.96	6.14	3.98
Tb	*ppm*	0.84	0.86	1.2	0.36	0.81	0.88	1.04	0.47	0.67	1.26	0.91	0.23	1	0.38	1.15	0.7	0.61	0.97	0.65
Dy	*ppm*	4.85	5.04	6.8	2.16	4.62	4.89	5.57	2.66	3.63	7.24	5.23	1.25	5.83	2.67	6.59	4.29	3.67	5.8	4.1
Ho	*ppm*	0.89	0.96	1.31	0.44	0.89	0.96	1.03	0.54	0.71	1.44	1.01	0.24	1.16	0.55	1.25	0.89	0.76	1.13	0.79
Er	*ppm*	2.51	2.8	3.84	1.33	2.47	2.74	2.99	1.59	2.06	4.09	2.95	0.64	3.22	1.6	3.66	2.51	2.23	3.32	2.3
Tl	*ppm*	0.28	0.47	0.8	0.48	0.83	0.46	0.75	0.54	0.62	0.8	0.29	0.06	0.58	0.08	0.21	0.3	0.52	0.91	0.51
Tm	*ppm*	0.364	0.416	0.55	0.196	0.362	0.392	0.435	0.239	0.288	0.611	0.44	0.095	0.47	0.244	0.557	0.364	0.34	0.517	0.341
Yb	*ppm*	2.4	2.69	3.8	1.34	2.35	2.62	2.86	1.74	2.1	4.05	2.91	0.71	3.52	1.59	3.55	2.47	2.37	3.53	2.34
Lu	*ppm*	0.389	0.432	0.562	0.196	0.365	0.386	0.43	0.272	0.311	0.602	0.451	0.117	0.545	0.272	0.563	0.399	0.356	0.496	0.368
As	*ppm*	40	28	19	21	8	7	-	20	2	21	31	27	7	32	22	60	7	9	12
Co	*ppm*	22.3	10.5	18.5	3.2	16	14.9	19	9.7	25.1	2.1	8.5	-	20.2	1.3	11.3	10.5	26	17.2	22.2
Cr	*ppm*	60.6	83.2	117	41.8	34.4	40.1	115	49.6	89.5	99.1	55.7	57.7	163	62	49.4	56.1	73.5	62.4	58.6
Sb	*ppm*	2.5	0.8	0.8	0.4	1.3	0.5	0.5	0.8	0.2	2.6	0.8	1.5	0.6	11.6	0.4	0.7	0.6	2.4	0.7
Sc	*ppm*	14.1	17.2	20.9	7.41	11.8	14.9	20.3	11	16.5	17.1	9.5	3.7	24.2	6.77	7.83	9.33	13.5	15.7	13.2
Zn	*ppm*	139	73	113	10	54	100	98	54	126	8	66	1	119	13	64	68	71	90	90

Supplementary Material 1 – Table providing all the relevant information of the studied samples (coordinates, stratigraphy, mineralization type, whole-rock chemistry, etc.)

Sample Ref		X16	X17	X19	ALB02#51	PC1	PC5	PC24	PC17	ABNSTR7	ABNSTR2	T8	T18	T59	L MS#2	SES20#10	37-1-A	37-1-B	37-1-C	37-1-D
Sector		Albernoa	Albernoa	Albernoa	Albernoa	Albernoa	Albernoa	Albernoa	Albernoa	Albernoa	Albernoa	Albernoa	Albernoa	Albernoa	Lousal	Lousal	Albernoa	Albernoa	Albernoa	Albernoa
Stratigraphic division		PQG	PQG	PQG	PQG	PQG	PQG	PQG	PQG	PQG	PQG	PQG	PQG	PQG	lower VSC	lower VSC	middle VSC	middle VSC	middle VSC	middle VSC
Mineralization type/occurrence		*No sulphide*	*No sulphide*	*No sulphide*	*No sulphide*	*No sulphide*	*No sulphide*	*No sulphide*	*Py-bearing*	*No sulphide*	*No sulphide*	*No sulphide*	*No sulphide*	*No sulphide*	*Mineralized*	*Mineralized*	*Py-bearing*	*No sulphide*	*No sulphide*	*No sulphide*
Footwall/Hangingwall		*n.a.*	*n.a.*	*n.a.*	*n.a.*	*n.a.*	*n.a.*	*n.a.*	*n.a.*	*n.a.*	*n.a.*	*n.a.*	*n.a.*	*n.a.*	*Footwall*	*Footwall*	*n.a.*	*n.a.*	*n.a.*	*n.a.*
Location - ETRS89	x	252	-730	-730	144787	3557	3557	3557	3557	42206	56327	3957	-730	18540	-25573	-25066	8303	8303	8303	8303
	y	-196686	-197030	-197030	-204973	-199306	-199306	-199306	-199306	-223825	-221658	-198221	-197030	-216670	-181885	-187756	-198699	-198699	-198699	-198699
Depth (m)		*n.a.*	*n.a.*	*n.a.*	*n.a.*	*n.a.*	*n.a.*	*n.a.*	*n.a.*	*n.a.*	*n.a.*	*n.a.*	*n.a.*	*n.a.*	*n.a.*	-288.50	-82.85	-91.57	-124.40	-134.50
SiO_2	%	77.56	70.01	82.46	59.72	61.48	60.83	59.29	61.69	62.44	81.99	85.43	73.14	57.5	51.86	58.54	55.64	47.07	59.64	55.72
Al_2O_3	%	10.63	13.05	7.77	21.11	19.67	18.9	20.39	19.73	18.14	0.71	7.97	14.18	20.78	17.54	19.46	24.61	33.05	20.57	25.34
$Fe_2O_3(T)$	%	5.62	5.61	3.78	8.23	7.27	6.86	7.5	6.66	6.99	3.06	2.28	4.61	8.74	14.31	5.08	7.24	5.06	8.11	4.36
MnO	%	0.189	0.133	0.014	0.055	0.172	0.141	0.142	0.211	0.065	0.004	0.006	0.146	0.014	0.027	0.047	0.04	0.077	0.056	0.027
MgO	%	0.95	1.84	0.49	1.43	1.99	2.02	2.01	1.74	1.31	0.04	0.19	1.59	1.18	1.25	1.08	1.57	0.67	1.89	1.26
CaO	%	0.19	0.08	0.03	0.19	0.26	0.5	0.33	0.31	0.06	0.06	0.06	0.05	0.09	0.2	0.08	0.12	0.2	0.15	0.14
Na_2O	%	0.44	0.76	0.15	0.75	0.79	1.23	0.99	1.27	0.76	0.03	0.14	0.31	0.45	0.23	0.16	1.05	1.52	0.61	1.1
K_2O	%	1.64	1.76	1.47	3.12	3.46	3.28	3.67	3.53	2.8	0.21	1.2	2.54	3.9	3.82	5.78	4	5.47	3.65	4.89
TiO_2	%	0.645	0.563	0.295	1.089	0.983	0.903	0.98	0.803	1.039	1.397	0.35	0.594	0.833	0.819	0.689	1.009	1.347	0.824	0.986
P_2O_5	%	0.14	0.08	0.07	0.15	0.11	0.13	0.14	0.09	0.11	0.05	0.11	0.05	0.1	0.18	0.04	0.11	0.14	0.08	0.07
Ba	*ppm*	298	319	232	416	462	435	552	503	384	811	199	391	648	421	751	617	780	673	894
Cs	*ppm*	4	3.2	3.2	8.9	6.3	6.6	7.8	6.8	6	2.5	2.1	5.1	4.6	7.6	29.9	9.2	17.6	7.8	11.9
Cu	*ppm*	16	265	47	15	41	37	51	117	35	377	47	56	20	82	48	32	21	59	25
Ga	*ppm*	16	20	13	29	26	25	25	26	25	3	13	20	30	25	27	33	46	28	33
Ge	*ppm*	3.5	3	2.9	2	2.4	2.1	1.8	2.2	2.5	1.4	1.2	2.4	3.8	1.8	1.5	2.7	4.7	2.6	2.3
Hf	*ppm*	8.4	2.7	1.6	5.6	5	4.8	4.8	3.7	5.6	5	1.7	2.6	3.6	5.6	3.3	4.1	4.6	3.5	3.2
Nb	*ppm*	9.8	9.8	5.2	20.3	15.5	14.8	14.9	13.3	15.9	21.6	7.8	8.6	12.6	16.2	11.9	20.1	25.8	16.7	18.8
Ni	*ppm*	36	76	24	64	65	63	63	73	50	3	9	75	48	29	99	54	31	61	51
Pb	*ppm*	11	-	27	-	-	-	-	-	9	570	26	-	22	37	60	-	8	7	10
Rb	*ppm*	83	93	87	157	155	148	160	158	136	8	58	139	188	185	363	188	278	168	232
S	%	0.006	0.031	0.011	0.381	0.003	0.021	0.226	0.036	0.005	1.84	0.041	0.017	0.008	1.89	1.6	0.047	0.045	0.108	0.283
Sr	*ppm*	69	61	51	97	94	91	120	95	159	57	151	82	78	80	49	142	207	135	216
Ta	*ppm*	1.37	0.81	0.53	1.6	1.25	1.33	1.34	1.11	1.42	1.83	0.57	0.64	0.87	1.6	1.27	1.71	2.06	1.45	1.61
Th	*ppm*	10.3	7.53	5.37	15.7	13.2	13.6	13.6	12.8	13.9	15.1	4.76	8.53	12.4	15.1	12.6	16.7	20.6	13	16.2
U	*ppm*	2.34	1.81	2.67	2.9	2.6	2.89	3.86	2.42	3.52	4.23	2.52	2.2	2.36	3.73	9.19	3.29	6.94	2.07	2.34
V	*ppm*	63	113	210	130	145	144	153	144	131	36	80	131	127	153	342	148	194	121	138
Y	*ppm*	26	20	18	36	30	28	31	27	39	31	13	19	26	33	24	29	34	22	24
Zr	*ppm*	304	101	60	248	202	184	188	143	231	209	74	99	137	188	112	160	178	132	130
La	*ppm*	35	27.9	21.9	53.3	45.7	45.7	45.3	60.5	45.4	58.2	73.2	32.5	42.4	52.5	40.2	57.3	68.8	44.9	55
Ce	*ppm*	70.5	58	31.1	108	93.5	93.5	93.3	108	86.5	107	52.8	65.2	78.1	103	76.4	107	129	88.7	102
Pr	*ppm*	8.43	6.47	4.94	12.3	10.3	10.4	10.4	9.88	10.7	12.4	11.5	7.54	9.8	12.1	9.22	12.1	14.5	9.72	11.3
Nd	*ppm*	31	24.1	18.4	44.8	38.8	40	39.1	37.5	40.3	44.7	32.2	27	36.3	44.3	34.6	45.4	54.7	36.7	42.4
Sm	*ppm*	6.73	4.73	3.57	8.88	7.63	7.66	8.09	7.05	8.42	7.4	3.99	5.52	7.9	8.81	6.41	8.18	9.73	6.48	6.98
Eu	*ppm*	1.25	0.905	0.684	1.84	1.49	1.58	1.58	1.33	1.64	1.41	0.875	1.02	1.36	1.93	1.1	1.62	1.93	1.28	1.37
Gd	*ppm*	5.51	4.08	3.02	7.69	5.74	5.79	6.51	5.13	7.09	4.87	2.95	4.09	5.59	7.08	4.6	6.77	7.84	4.93	5.33
Tb	*ppm*	0.88	0.67	0.49	1.19	0.96	0.91	0.97	0.82	1.16	0.89	0.42	0.64	0.89	1.16	0.74	1.03	1.25	0.75	0.88
Dy	*ppm*	5.01	4.07	2.88	7.24	5.8	5.57	5.79	4.76	6.98	5.51	2.34	3.92	5.09	7.05	4.86	5.91	6.94	4.33	4.97
Ho	*ppm*	0.97	0.81	0.61	1.38	1.09	1.09	1.12	0.95	1.38	1.15	0.47	0.74	1.01	1.36	0.94	1.16	1.34	0.84	0.95
Er	*ppm*	2.83	2.44	1.82	3.93	3.11	3.15	3.36	2.82	4.03	3.43	1.44	2.13	2.77	3.88	2.9	3.51	3.82	2.52	2.71
Tl	*ppm*	0.33	0.34	0.31	0.5	0.42	0.55	0.69	0.6	0.61	1.41	0.28	0.53	0.7	3.16	45.5	0.99	1.1	0.79	0.96
Tm	*ppm*	0.434	0.361	0.263	0.585	0.487	0.476	0.518	0.415	0.603	0.535	0.197	0.308	0.418	0.568	0.425	0.532	0.574	0.379	0.458
Yb	*ppm*	2.94	2.47	1.76	3.72	3.32	3.26	3.32	2.87	3.92	3.57	1.47	2.14	2.9	3.71	2.88	3.27	3.72	2.51	2.88
Lu	*ppm*	0.435	0.387	0.272	0.576	0.494	0.496	0.497	0.457	0.589	0.552	0.242	0.343	0.441	0.54	0.427	0.486	0.537	0.371	0.4
As	*ppm*	41	1	28	32	11	9	26	28	11	391	12	5	2	308	74	11	8	6	24
Co	*ppm*	11.5	32.8	2.9	23.3	29.8	18.2	17	22.9	9.7	7.8	-	20.7	13.3	20.3	20.5	19	16.5	21.9	22.6
Cr	*ppm*	50.8	81.5	94.4	106	117	111	119	92.6	106	30.9	46.8	77	106	99	112	105	154	90.1	119
Sb	*ppm*	0.6	0.3	3.5	2.7	0.3	0.4	3.4	0.7	0.7	55.3	2.2	0.9	0.5	11.9	50.2	1.2	2.1	1.1	2.2
Sc	*ppm*	11.3	14.6	7.9	18.2	19.6	18.4	19.8	19	17.4	4.81	8.98	14.1	19.4	17.6	18.5	21.4	28.3	18.5	21.3
Zn	*ppm*	74	87	25	103	95	96	95	90	99	408	8	77	83	56	439	111	54	119	68

Supplementary Material 1 – Table providing all the relevant information of the studied samples (coordinates, stratigraphy, mineralization type, whole-rock chemistry, etc.)

Sample Ref		37-1-F	X68	X71	X93	X64	X54	T67	T83	RT56	S3-B	S3-F	S3-I	S3-J	CW2-CC	CW2-LL	CW2-QQ	CW2-ZZ
Sector		Albernoa	Albernoa	Albernoa	Albernoa	Albernoa	Albernoa	Albernoa	Albernoa	Albernoa	Albernoa	Albernoa	Albernoa	Albernoa	Albernoa	Albernoa	Albernoa	Albernoa
Stratigraphic division		*middle* VSC	*middle* VSC	*middle* VSC	*middle* VSC	*middle* VSC	*middle* VSC	*middle* VSC	*middle* VSC	*middle* VSC	*upper* VSC	*upper* VSC	*upper* VSC	*upper* VSC	*upper* VSC	*upper* VSC	*upper* VSC	*upper* VSC
Mineralization type/occurrence		*No sulphide*	*No sulphide*	*No sulphide*	*No sulphide*	*Py-bearing*	*No sulphide*	*No sulphide*	*No sulphide*	*No sulphide*	*No sulphide*	*No sulphide*	*No sulphide*	*No sulphide*	*Mineralized*	*Mineralized*	*No sulphide*	*No sulphide*
Footwall/Hangingwall		*n.a.*	*n.a.*	*n.a.*	*n.a.*	*n.a.*	*n.a.*	*n.a.*	*n.a.*	*n.a.*	*n.a.*	*n.a.*	*n.a.*	*n.a.*	*n.a.*	*n.a.*	*n.a.*	*n.a.*
Location - ETRS89	x	8303	22622	19970	19263	26497	24677	22622	18808	3587	-597	-597	-597	-597	4228	4228	4228	4228
	y	-198699	-206283	-207079	-204661	-210362	-214114	-206283	-205487	-193577	-201299	-201299	-201299	-201299	-191707	-191707	-191707	-191707
Depth (m)		-250.00	*n.a.*	*n.a.*	*n.a.*	*n.a.*	*n.a.*	*n.a.*	*n.a.*	*n.a.*	-262.20	-313.60	-350.63	-359.38	-214.75	-333.70	-412.00	-517.84
SiO_2	%	55.86	68.8	54.41	56.28	60.01	61.24	64.91	66.16	66.04	72.16	72.1	67.32	68.94	52.2	68.1	54.92	68.75
Al_2O_3	%	24.63	15.68	24.06	21.78	19.25	18.93	20.77	20.33	15.54	14.23	13.47	15.17	15.51	20.08	11.77	18.05	16.15
$Fe_2O_3(T)$	%	7.2	5.22	7.46	7.42	6.91	6.91	2.54	3.64	6.96	2.71	6.56	6.26	5.71	10.04	8.04	5.7	4.25
MnO	%	0.041	0.022	0.033	0.094	0.188	0.048	0.012	0.048	0.067	0.199	0.277	0.254	0.149	0.144	0.351	0.041	0.462
MgO	%	1.59	1.17	1.31	1.65	1.65	1.75	0.63	0.29	1.87	1.04	1.22	1.21	1.38	3.65	2.6	6.98	1.98
CaO	%	0.12	0.2	0.12	0.12	0.12	0.17	0.17	0.14	0.36	1.11	0.23	0.25	0.2	0.65	0.92	1.58	0.3
Na_2O	%	1.06	0.66	0.88	0.64	0.56	0.83	0.55	0.61	2.49	0.41	1.12	1.5	0.97	2.81	0.71	1.92	1.93
K_2O	%	4.03	2.7	4	4.05	4.15	3.36	4.99	3.05	1.44	3.74	2.54	3.47	3.52	2.99	2.55	4.67	3.19
TiO_2	%	1.011	1.004	0.986	0.898	0.772	0.916	0.904	0.95	0.751	0.541	0.543	0.585	0.615	0.913	0.502	0.723	0.591
P_2O_5	%	0.1	0.13	0.1	0.09	0.08	0.12	0.08	0.11	0.17	0.08	0.12	0.08	0.08	0.08	0.43	0.11	0.08
Ba	*ppm*	625	448	593	640	861	560	736	476	248	535	461	951	654	429	250	166	492
Cs	*ppm*	9.3	3.7	8	6	4.2	6.4	4.4	4.3	2.9	15.8	5.3	11.7	12.9	3.8	3.8	4.2	6.7
Cu	*ppm*	27	81	43	28	72	45	8	45	20	69	37	-	10	41	71	33	2
Ga	*ppm*	33	22	32	31	27	26	30	28	19	21	21	22	25	26	16	21	22
Ge	*ppm*	2.8	2.8	3.2	3.3	2.8	2.9	3.3	3.8	2.3	2.2	2.5	2.3	2.7	1.7	1.3	0.9	2.2
Hf	*ppm*	4.1	6.8	3.9	4.4	3	4.3	3.8	4.9	3.4	2.4	2.3	3	2.6	4.2	2.1	3	4.6
Nb	*ppm*	20.5	16.1	18.7	16.7	14.9	15.7	12.7	13.3	8.7	9.6	9.9	12	11	16.9	8.6	5.5	7.9
Ni	*ppm*	52	31	56	56	67	64	32	39	40	78	109	72	113	58	56	71	50
Pb	*ppm*	-	-	7	7	-	17	-	5	-	11	-	37	13	99	133	5	53
Rb	*ppm*	193	122	210	216	195	159	211	155	62	181	105	165	184	107	64	70	156
S	%	0.041	0.003	0.002	0.002	0.003	0.005	0.007	0.007	0.004	0.397	0.006	0.004	0.004	0.688	0.136	0.02	0.005
Sr	*ppm*	141	85	120	98	53	123	100	106	119	100	61	100	58	95	42	78	85
Ta	*ppm*	1.53	1.34	1.37	1.3	1.09	1.21	0.99	0.97	0.71	0.82	0.79	1.04	0.99	1.34	0.73	0.52	0.66
Th	*ppm*	15.9	11.7	14.6	13.9	12.7	13.1	13.2	12.9	8.04	9.68	9.32	11.3	10.8	13.9	7.52	4.03	10.2
U	*ppm*	3.23	2.66	2.27	2.4	4.27	3.62	2.65	2.66	2.24	3.14	1.75	2.87	2.34	2.91	1.25	1.06	3.99
V	*ppm*	150	121	145	127	148	157	137	110	123	107	103	105	118	234	156	144	89
Y	*ppm*	29	33	25	24	23	31	27	34	20	25	22	27	22	32	33	20	35
Zr	*ppm*	164	287	148	170	124	172	139	187	146	109	102	123	110	173	90	118	168
La	*ppm*	53.2	38.9	52.8	48.1	48	43.8	49.1	46.1	26.9	43.1	34.1	42.9	37.5	48.1	33.2	13.7	32.2
Ce	*ppm*	97.8	74.9	99	95.3	94.3	83.1	91.2	89.2	50.1	74.1	76.8	81	80.4	81.7	57	28.5	60.1
Pr	*ppm*	11.2	9.12	11.6	10.9	10.9	9.79	11.1	11	6.03	8.77	7.63	9.43	8.16	10.6	8.05	3.57	7.64
Nd	*ppm*	40.9	33.9	41.9	40.2	41	37.3	39.1	41.8	23.1	32.4	28.2	34.8	30.3	38.6	32.7	14.4	28.7
Sm	*ppm*	7.71	6.71	7.73	7.33	7.4	7.23	7.51	9.05	4.9	5.9	5.36	6.48	5.46	6.95	7.01	3.33	6.98
Eu	*ppm*	1.51	1.31	1.48	1.52	1.28	1.5	1.13	1.94	1.01	1.28	1.27	1.3	1.23	1.45	1.52	0.986	1.15
Gd	*ppm*	6.39	6.06	6.06	5.83	5.34	6.21	5.4	7.93	3.92	5	4.57	5.73	4.42	6	7.17	3.54	6.36
Tb	*ppm*	1.01	1.02	0.97	0.91	0.82	1.04	0.89	1.23	0.66	0.77	0.66	0.85	0.71	0.96	1.12	0.61	1
Dy	*ppm*	5.78	6.22	5.35	5.22	4.64	6.22	5.18	6.81	3.77	4.64	3.95	4.96	4.12	5.62	6.51	3.56	5.88
Ho	*ppm*	1.12	1.27	1.05	1.05	0.91	1.22	0.99	1.35	0.73	0.94	0.81	0.98	0.81	1.19	1.28	0.73	1.26
Er	*ppm*	3.24	3.65	2.94	3.01	2.66	3.4	2.96	3.62	2.04	2.63	2.31	2.94	2.44	3.56	3.4	2.2	3.77
Tl	*ppm*	0.78	0.45	0.75	0.86	0.85	0.63	0.71	0.52	0.27	0.92	0.63	0.87	1.04	0.59	0.25	0.35	0.9
Tm	*ppm*	0.469	0.54	0.437	0.45	0.389	0.487	0.441	0.508	0.301	0.386	0.341	0.443	0.349	0.556	0.456	0.344	0.555
Yb	*ppm*	3.17	3.6	2.99	3.04	2.53	3.17	2.99	3.52	2.07	2.6	2.33	2.98	2.39	3.62	2.9	2.28	3.76
Lu	*ppm*	0.461	0.536	0.442	0.448	0.392	0.488	0.462	0.529	0.312	0.381	0.368	0.441	0.398	0.558	0.41	0.34	0.573
As	*ppm*	8	9	-	11	15	28	12	7	7	22	6	3	-	41	26	7	-
Co	*ppm*	17.3	6.7	19.6	18.7	20.6	13.8	6.5	14.3	36.6	36.7	22.3	19.6	23.9	22.7	18	19.3	16.1
Cr	*ppm*	110	110	112	113	102	103	104	96.6	73.4	60	69.7	64.4	71.4	156	89.5	76.2	36.4
Sb	*ppm*	1.1	1	1	0.8	1	1.9	1.7	1.7	0.5	9	0.5	1.7	0.9	4.1	1.2	1.3	3
Sc	*ppm*	21.1	15.4	21	20.1	17.7	19.1	18.7	16.5	13.5	14.6	14.3	14.9	15.5	19.4	12.3	20.4	14.8
Zn	*ppm*	106	35	108	105	90	105	20	45	77	21	96	80	109	104	92	55	105

Supplementary Material 1 – Table providing all the relevant information of the studied samples (coordinates, stratigraphy, mineralization type, whole-rock chemistry, etc.)

Sample Ref		X72	X84	X92	18-1-E	18-1-H	18-1-FF	18-1-T	18-1-U	18-1-OO	ALB02# 2	ALB02# 15	ALB02# 4	ALB02# 6	ALB02# 9	ALB02# 24	ALB02# 28	ALB02# 45	ALB02# 48	ALB03#3
Sector		Albernoa	Albernoa	Albernoa	Albernoa	Albernoa	Albernoa	Albernoa	Albernoa	Albernoa	Albernoa	Albernoa	Albernoa	Albernoa	Albernoa	Albernoa	Albernoa	Albernoa	Albernoa	Albernoa
Stratigraphic division		*upper* VSC	*upper* VSC	*upper* VSC	*upper* VSC	*upper* VSC	*upper* VSC	*upper* VSC	*upper* VSC	*upper* VSC	*upper* VSC	*upper* VSC	*upper* VSC	*upper* VSC	*upper* VSC	*upper* VSC	*upper* VSC	*upper* VSC	*upper* VSC	*upper* VSC
Mineralization type/occurrence		*No sulphide*	*No sulphide*	*No sulphide*	*Mineralized*	*No sulphide*	*Mineralized*	*No sulphide*	*No sulphide*	*No sulphide*	*No sulphide*	*No sulphide*	*No sulphide*	*No sulphide*	*No sulphide*	*No sulphide*	*No sulphide*	*No sulphide*	*No sulphide*	*No sulphide*
Footwall/Hangingwall		*n.a.*	*n.a.*	*n.a.*	*n.a.*	*n.a.*	*n.a.*	*n.a.*	*n.a.*	*n.a.*	*n.a.*	*n.a.*	*n.a.*	*n.a.*	*n.a.*	*n.a.*	*n.a.*	*n.a.*	*n.a.*	*n.a.*
Location - ETRS89	x	14234	17717	17164	11823	11823	11823	11823	11823	11823	14787	14787	14787	14787	14787	14787	14787	14787	14787	14790
	y	-201324	-205484	-206482	-198489	-198489	-198489	-198489	-198489	-198489	-204973	-204973	-204973	-204973	-204973	-204973	-204973	-204973	-204973	-204961
Depth (m)		*n.a.*	*n.a.*	*n.a.*	-80.70	-90.38	-159.60	-130.22	-133.20	-204.50	-93.80	-75.25	-124.50	-197.75	-244.16	-260.00	-378.25	-411.30	-473.00	-88.70
SiO_2	%	70.98	73.23	64.82	72.5	76.36	71.16	57.51	54.1	59.73	64.61	53.21	56.42	54.23	53.08	64.11	60.35	96.52	59.64	56.25
Al_2O_3	%	12.98	12.5	17.14	11.48	10.29	11.61	19.77	17.57	18.73	16.41	22.33	21.2	23.04	24.37	11.98	19.73	1.63	18.01	22.72
$Fe_2O_3(T)$	%	5.34	4.86	6.06	4.71	4.11	5.24	7.58	8.87	6.18	9.06	9.85	9.13	9.37	9.35	10.05	7.22	0.72	8	8.71
MnO	%	0.252	0.372	0.302	0.026	0.085	0.028	0.417	0.236	0.206	0.187	0.173	0.29	0.098	0.073	0.318	0.088	0.011	0.131	0.06
MgO	%	1.26	0.85	1.24	0.53	1.91	2.37	2.08	3.88	1.26	1.97	1.96	1.91	2.03	1.79	1.82	1.73	0.14	1.7	1.75
CaO	%	0.1	0.09	0.06	0.03	1.19	0.71	1.01	2.13	0.17	0.13	0.52	0.17	0.2	0.18	1.1	0.23	0.09	0.91	0.24
Na_2O	%	0.3	0.33	0.39	0.21	0.1	0.11	0.16	6.11	0.36	0.47	0.89	0.8	0.69	0.72	0.38	1.07	0.06	0.81	0.81
K_2O	%	3.36	2.34	3.95	2.33	2.07	2.7	4.83	0.42	5	2.36	3.47	3.58	4.11	4.46	2.27	3.77	0.3	3.28	3.63
TiO_2	%	0.46	0.509	0.732	0.451	0.407	0.449	0.774	1.857	0.835	0.611	0.874	0.925	0.884	0.973	0.674	1.023	0.266	0.89	0.943
P_2O_5	%	0.03	0.04	0.13	0.05	0.04	0.05	0.11	0.23	0.09	0.07	0.34	0.09	0.08	0.12	0.22	0.13	0.01	0.13	0.14
Ba	*ppm*	521	575	522	382	494	355	623	86	565	372	566	579	624	734	333	610	48	428	579
Cs	*ppm*	7.7	2.8	5.3	3.4	2.7	5.7	6.8	1.1	7.5	6.2	9.8	9.5	12.4	13.1	3.8	7.8	0.4	6.7	9.6
Cu	*ppm*	36	35	39	57	42	104	21	24	71	72	30	38	41	35	22	24	6	35	25
Ga	*ppm*	21	20	25	18	15	16	26	20	26	22	31	29	32	34	15	27	3	25	30
Ge	*ppm*	2.3	2.5	2.2	0.9	1.9	1.7	2.1	2	2.1	2.9	2.4	2.4	2.7	2.8	1.7	2.1	0.9	1.5	2.7
Hf	*ppm*	2	2.2	3.9	2.1	1.8	1.7	4	2.9	3.9	2.5	3.6	4.1	4	3.5	6.9	5.4	6.9	4.5	4
Nb	*ppm*	9.2	8.9	12.9	11	8.2	6.7	11.7	8.4	16.5	10.1	14.9	16.1	16.1	17.4	10	18.2	5.5	17.4	17.1
Ni	*ppm*	38	87	73	56	53	129	63	29	70	47	66	59	68	62	47	55	4	90	63
Pb	*ppm*	9	8	13	12	6	26	-	-	-	48	7	-	-	-	15	-	-	55	-
Rb	*ppm*	183	95	186	114	90	101	197	15	184	115	167	171	205	230	102	177	14	155	168
S	%	0.002	0.006	0.005	0.876	0.013	0.835	0.038	0.016	0.017	0.04	0.023	0.013	0.051	0.03	1.65	0.075	0.041	1.58	0.008
Sr	*ppm*	28	50	71	94	36	18	41	175	59	60	113	100	93	106	79	89	11	104	101
Ta	*ppm*	0.67	0.74	1.12	0.9	0.65	0.65	0.94	0.63	1.37	0.78	1.11	1.21	1.17	1.36	0.88	1.35	0.44	1.33	1.46
Th	*ppm*	8.32	8.46	13	7.27	6.32	7.4	11.6	1.29	13.9	10.2	14.5	14.3	14.2	15.9	11.2	14.6	2.38	13.8	15.4
U	*ppm*	2.9	1.39	2.2	1.73	1.5	7.42	2.67	1.26	2.91	1.6	4.64	3.12	2.25	2.66	3.44	3.34	0.99	3.37	2.48
V	*ppm*	90	96	145	111	132	153	131	309	136	103	143	139	135	152	76	141	10	139	145
Y	*ppm*	17	17	28	19	17	22	23	27	27	17	36	23	23	28	33	28	7	28	30
Zr	*ppm*	87	90	161	91	73	70	156	117	155	81	119	133	130	152	318	237	335	196	177
La	*ppm*	38.1	31.3	41.8	29	30.8	32.3	41.9	8.15	44.7	35.6	54.2	50.2	50.6	54.2	38	49.4	8.91	47.1	53.5
Ce	*ppm*	68.1	65.8	81.9	53.8	56.3	60.8	80.1	19.9	86.2	71.2	110	100	99.9	108	79.8	102	18.1	96.9	107
Pr	*ppm*	8.84	7.1	9.36	6.28	6.64	7.1	9.39	2.94	9.77	8.08	12.4	11.2	11.2	12.1	9.18	11.5	2.07	10.9	11.7
Nd	*ppm*	32.5	25.7	34.2	23.6	25.8	28.1	34.7	14.1	36.7	29.3	46.9	40.1	39.6	43.5	35.2	42.1	7.31	39.4	42.2
Sm	*ppm*	5.53	4.36	7.32	4.6	4.83	5.14	6.5	3.92	6.77	5.63	9.48	7.42	7.59	8.3	7.76	8.39	1.42	7.72	8.21
Eu	*ppm*	0.674	0.991	1.51	0.791	0.917	1.02	1.27	1.22	1.12	1.18	2.05	1.54	1.59	1.78	1.78	1.64	0.245	1.57	1.82
Gd	*ppm*	3.95	3.65	5.78	3.99	4.13	4.54	5.39	4.61	5.63	4.45	8.83	5.99	6.16	6.86	7.24	6.55	1.26	6.38	7.11
Tb	*ppm*	0.63	0.58	0.92	0.58	0.6	0.68	0.84	0.78	0.88	0.68	1.4	0.92	0.93	1	1.1	0.96	0.21	1	1.13
Dy	*ppm*	3.57	3.36	5.27	3.38	3.4	3.83	4.93	4.71	5.1	3.91	7.89	5.36	5.25	5.73	6.87	5.82	1.33	5.86	6.58
Ho	*ppm*	0.69	0.69	1.07	0.67	0.66	0.78	0.97	1	1.04	0.74	1.46	1.01	1.01	1.08	1.26	1.2	0.28	1.14	1.25
Er	*ppm*	2.04	2	3.05	1.95	1.96	2.29	2.91	2.89	2.96	2.1	3.99	2.96	2.84	3.11	3.57	3.49	0.9	3.14	3.57
Tl	*ppm*	0.89	0.4	0.92	0.57	0.4	0.54	0.75	0.19	0.77	0.29	0.52	0.58	0.64	0.88	0.42	0.7	-	0.78	0.51
Tm	*ppm*	0.295	0.296	0.466	0.312	0.297	0.34	0.4	0.414	0.437	0.31	0.566	0.455	0.42	0.46	0.506	0.518	0.137	0.462	0.513
Yb	*ppm*	2.13	2.03	3.14	1.96	1.99	2.01	2.95	2.93	2.99	2.05	3.5	2.96	2.68	2.95	3.36	3.42	1.03	3.2	3.38
Lu	*ppm*	0.332	0.313	0.433	0.315	0.293	0.316	0.421	0.416	0.436	0.318	0.509	0.452	0.414	0.469	0.495	0.539	0.171	0.494	0.482
As	*ppm*	-	4	8	26	16	133	24	11	99	16	12	-	36	-	67	21	3	189	2
Co	*ppm*	11.2	21.3	18.4	14.8	9.9	54.9	28.2	15.1	18.2	20.7	23.6	22.2	23.4	23.1	17.7	22.5	0.9	59.5	19.4
Cr	*ppm*	59.2	66.9	77.4	70.5	51.5	72.5	92.8	187	88.5	90	124	109	122	131	60	114	51.5	100	126
Sb	*ppm*	1.2	0.6	2.2	8.6	2.1	4.6	9.6	7.2	2.7	1.3	1.6	0.9	1.3	1.4	3.7	1.2	0.7	12.7	0.9
Sc	*ppm*	12.1	12.8	15.7	11.2	10.3	11.9	18.6	45.4	17.2	14.4	21.1	20.1	20.8	22.3	12.4	19	1.2	17.4	21
Zn	*ppm*	77	107	85	25	66	53	70	87	47	117	132	121	118	106	70	95	8	96	135

Supplementary Material 1 – Table providing all the relevant information of the studied samples (coordinates, stratigraphy, mineralization type, whole-rock chemistry, etc.)

Sample Ref		ALB03#7	ALB03#12b	ALB03#13c	ALB03#14	ALB03#29	S3-H	CW2-O	CW2-P	CW2-BB	CW2-II	CW2-VV	RT49	RT59-1	RT59-2	T24	T73	T88
Sector		Albernoa	Albernoa	Albernoa	Albernoa	Albernoa	Aljustrel	Albernoa	Albernoa	Albernoa	Albernoa	Albernoa	Albernoa	Albernoa	Albernoa	Albernoa	Albernoa	Albernoa
Stratigraphic division		*upper* VSC	*upper* VSC	*upper* VSC	*upper* VSC	*upper* VSC	*upper* VSC	*upper* VSC	*upper* VSC	*upper* VSC	*upper* VSC	*upper* VSC	*upper* VSC	*upper* VSC	*upper* VSC	*upper* VSC	*upper* VSC	*upper* VSC
Mineralization type/occurrence		*No sulphide*	*No sulphide*	*No sulphide*	*No sulphide*	*No sulphide*	*No sulphide*	*No sulphide*	*No sulphide*	*No sulphide*	*No sulphide*	*No sulphide*	*No sulphide*	*No sulphide*	*No sulphide*	*No sulphide*	*No sulphide*	*No sulphide*
Footwall/Hangingwall		*n.a.*	*n.a.*	*n.a.*	*n.a.*	*n.a.*	*n.a.*	*n.a.*	*n.a.*	*n.a.*	*n.a.*	*n.a.*	*n.a.*	*n.a.*	*n.a.*	*n.a.*	*n.a.*	*n.a.*
Location - ETRS89	x	14790	14790	14790	14790	14790	-597	4228	4228	4228	4228	4228	4905	3354	3354	2684	14234	17133
	y	-204961	-204961	-204961	-204961	-204961	-201299	-191707	-191707	-191707	-191707	-191707	-191952	-192818	-192818	-191737	-201324	-206276
Depth (m)		-233.25	-299.40	-311.50	-322	-478	-321	-82	-93	-212	-303	-478	*n.a.*	*n.a.*	*n.a.*	*n.a.*	*n.a.*	*n.a.*
SiO_2	%	70.07	62.99	59.87	70.44	60.9	73.9	56.13	59.46	59.64	59.38	73.08	83.75	64.3	69.08	74.04	79.06	74.91
Al_2O_3	%	12.75	18.72	15.98	13.73	19.51	11.91	20.88	18.91	19.08	14	11.69	6.24	17.2	15.65	14.18	11.15	12.2
$Fe_2O_3(T)$	%	5.85	6.46	7.74	2.76	6.94	4.4	8.85	5.72	6.82	7.14	3.78	2.27	6.91	6.21	2.19	1.67	3.96
MnO	%	0.124	0.106	0.808	0.449	0.095	0.342	0.104	0.21	0.098	0.032	0.036	0.009	0.119	0.282	0.041	0.309	0.105
MgO	%	1.38	1.3	1.69	1.15	1.86	1.57	2.27	3.57	2.08	7.67	1.08	0.9	1.16	1.5	2.45	0.7	0.68
CaO	%	1.32	0.17	1.72	1.69	0.69	0.12	0.55	1.59	0.74	3.36	0.74	0.21	0.19	0.12	0.07	0.13	0.07
Na_2O	%	0.49	0.72	0.96	0.82	0.97	1.06	0.18	1.82	4.75	1.5	3.21	0.07	0.68	0.74	0.31	3.26	0.39
K_2O	%	2.09	3.92	4.17	3.46	3.28	2.28	5.57	4.65	2.28	2.9	1.95	1.18	4.21	3.06	3.51	1.46	2.4
TiO_2	%	0.795	0.9	0.589	0.27	0.867	0.438	0.858	0.533	0.698	0.66	0.27	0.234	0.691	0.611	0.144	0.169	0.485
P_2O_5	%	0.16	0.1	0.12	0.05	0.13	0.05	0.09	0.14	0.07	0.12	0.06	0.04	0.1	0.08	0.04	0.06	0.04
Ba	*ppm*	367	556	558	566	423	444	497	580	319	192	161	151	486	385	518	254	654
Cs	*ppm*	4.4	7	7.9	4.2	6.2	5	6.1	7.3	2.6	3.1	2.3	2.6	9.8	7.6	4.7	3	5.4
Cu	*ppm*	16	28	16	38	45	113	86	5	39	27	22	24	4	12	2	18	33
Ga	*ppm*	18	25	22	18	25	19	27	27	21	15	16	10	24	23	22	11	19
Ge	*ppm*	2.1	2.5	2.2	2.3	2	1.8	1.9	1.4	1.5	0.9	1.4	1.6	2.4	2.9	1.4	1.7	2.5
Hf	*ppm*	7.7	4.8	3.2	4	4.2	1.9	4.1	9.1	3.2	2.5	7.4	0.9	2.6	2.2	4.2	3.6	2.6
Nb	*ppm*	10.9	15.8	9.5	6.8	16.5	8.1	14.2	16.4	12	4.7	8	3.8	10.6	8.8	6.2	6.2	5.8
Ni	*ppm*	43	63	123	20	59	139	65	14	67	82	7	9	71	91	6	14	96
Pb	*ppm*	-	-	15	13	-	-	5	11	12	-	40	12	19	-	-	13	-
Rb	*ppm*	103	158	202	154	149	97	158	137	76	48	61	38	178	154	135	78	111
S	%	0.04	0.006	0.005	0.011	0.061	0.02	2.11	0.015	1.09	0.208	0.115	0.003	0.004	0.003	0.006	0.003	0.012
Sr	*ppm*	89	71	68	41	91	55	39	83	136	71	68	14	103	65	29	119	66
Ta	*ppm*	1	1.41	0.9	0.85	1.41	0.73	1.24	1.27	0.89	0.43	0.66	0.28	0.89	0.84	0.6	0.93	0.44
Th	*ppm*	11.9	13.9	11.9	18.5	13.8	8.24	13.5	12.7	10.9	3.17	8.4	3	10.2	10.3	13.7	21.5	7.69
U	*ppm*	2.64	2.86	2.46	5.38	2.87	1.71	2.75	0.4	2.07	0.92	2.38	0.57	1.48	1.77	3.6	4.27	1.33
V	*ppm*	75	129	86	44	151	106	153	26	122	143	15	81	159	119	12	16	103
Y	*ppm*	29	28	33	37	29	19	26	67	12	23	42	11	26	25	45	25	21
Zr	*ppm*	336	213	151	151	194	79	173	394	131	96	288	37	122	97	124	119	89
La	*ppm*	41.2	47.4	48.8	47.5	48.2	33	42.3	44.2	33.4	10.2	34.4	16.8	44.4	45.9	27.4	54.5	37.3
Ce	*ppm*	86.4	96.2	87.5	98.2	98.2	73.1	79.4	92.3	62.1	20.8	70.3	30.7	83.3	92.4	53.6	92.2	68.6
Pr	*ppm*	9.32	10.5	10.9	10.9	10.9	7.32	9.42	11.2	7.04	2.75	8.82	4.31	9.54	10	7.08	12	8.38
Nd	*ppm*	35.4	37.8	40.6	40.2	38.9	27	34.9	45	25.1	12.7	34.4	16.8	33.9	36.8	26.7	42.5	31.3
Sm	*ppm*	7.04	7.28	8.2	7.97	7.6	5.15	6.27	10.1	4.16	3.32	8.34	3.34	6.2	6.51	6.9	8.37	5.83
Eu	*ppm*	1.3	1.49	1.7	1.04	1.58	0.84	1.3	1.89	0.808	0.807	1.44	0.692	1.35	1.25	0.395	0.695	1.24
Gd	*ppm*	5.85	5.82	7.3	7.15	6.42	4.33	5.22	10.5	3.2	3.83	7.73	2.85	4.31	4.73	6.71	5.87	4.86
Tb	*ppm*	0.94	0.97	1.15	1.15	1.03	0.63	0.81	1.84	0.51	0.65	1.32	0.42	0.7	0.74	1.26	0.89	0.69
Dy	*ppm*	5.48	5.69	6.87	7.04	6.07	3.52	4.85	10.9	2.73	3.92	8.09	2.27	4.13	4.57	8.14	5.01	4.02
Ho	*ppm*	1.09	1.14	1.35	1.41	1.19	0.72	0.96	2.31	0.53	0.83	1.64	0.41	0.81	0.95	1.65	0.92	0.79
Er	*ppm*	3.13	3.28	3.87	4.16	3.46	2.11	2.91	6.61	1.54	2.55	4.8	1.13	2.29	2.7	4.91	2.73	2.29
Tl	*ppm*	0.59	0.54	0.86	0.81	0.31	0.55	0.71	0.61	0.41	0.29	0.26	0.19	0.94	0.75	0.64	0.4	0.5
Tm	*ppm*	0.47	0.461	0.549	0.624	0.5	0.311	0.443	0.956	0.241	0.441	0.698	0.19	0.341	0.397	0.714	0.405	0.35
Yb	*ppm*	2.94	3.17	3.59	3.91	3.39	2.05	2.95	6.68	1.61	2.83	4.56	1.23	2.25	2.65	5.04	2.69	2.34
Lu	*ppm*	0.465	0.458	0.533	0.607	0.485	0.31	0.438	0.977	0.263	0.443	0.699	0.18	0.334	0.366	0.781	0.394	0.351
As	*ppm*	21	19	8	10	12	60	27	9	32	82	4	14	5	-	4	-	6
Co	*ppm*	17	18.1	24.5	9.4	18.8	31.6	30.4	4.1	19.7	75.4	3	38.4	25	33.1	-	4.8	10.8
Cr	*ppm*	84.4	113	73.8	20.6	95	59.4	120	20	91.2	92	9	38.3	79.6	79.9	-	19.2	61.6
Sb	*ppm*	0.7	0.6	1.7	0.5	1.9	0.6	1.2	0.6	1.3	0.7	3.4	1.7	4.2	2.2	0.8	1	2.4
Sc	*ppm*	10.9	16.8	16.6	8.48	15.9	11.9	20	26.4	16	17	14.4	6.72	16.8	15.2	6.74	4.53	12.5
Zn	*ppm*	86	107	125	54	112	106	80	117	81	42	101	19	97	136	42	38	85

Supplementary Material 1 – Table providing all the relevant information of the studied samples (coordinates, stratigraphy, mineralization type, whole-rock chemistry, etc.)

Sample Ref		18-1-F	18-1-EE	18-1-II	EDS1-G	EDS1-H	EDS1-I	EDS1-P	EDS1-T	ALB02# 18	ALB03#13b	ALB03#13e	L MS#3	L MS#4	SES20#2	SES20#4	SES20#5
Sector		**Albernoa**	**Albernoa**	**Albernoa**	**Aljustrel**	**Aljustrel**	**Aljustrel**	**Aljustrel**	**Aljustrel**	**Albernoa**	**Albernoa**	**Albernoa**	**Lousal**	**Lousal**	**Lousal**	**Lousal**	**Lousal**
Stratigraphic division		***upper* VSC**	***upper* VSC**	***upper* VSC**	***upper* VSC**	***upper* VSC**	***upper* VSC**	***upper* VSC**	***upper* VSC**	***upper* VSC**	***upper* VSC**	***upper* VSC**	***upper* VSC**	***upper* VSC**	***upper* VSC**	***upper* VSC**	***upper* VSC**
Mineralization type/occurrence		***No sulphide***	***No sulphide***	***No sulphide***	***No sulphide***	***No sulphide***	***No sulphide***	***No sulphide***	***No sulphide***	***No sulphide***	***No sulphide***	***No sulphide***	***No sulphide***	***No sulphide***	***No sulphide***	***No sulphide***	***No sulphide***
Footwall/Hangingwall		***n.a.***	***n.a.***	***n.a.***	***n.a.***	***n.a.***	***n.a.***	***n.a.***	***n.a.***	***n.a.***	***n.a.***	***n.a.***	***Hangingwall***	***Hangingwall***	***Hangingwall***	***Hangingwall***	***Hangingwall***
Location - ETRS89	**x**	11823	11823	11823	-527	-527	-527	-527	-527	14787	14790	14790	-26006	-26006	-25066	-25066	-25066
	y	-198489	-198489	-198489	-201023	-201023	-201023	-201023	-201023	-204973	-204961	-204961	-181998	-181998	-187756	-187756	-187756
Depth (m)		-88	-157	-173	-372	-385	-387	-474	-497	-302	-309	-316	*n.a.*	*n.a.*	-236.46	-252.20	-255.60
SiO_2	%	77.56	73.03	70.82	68.05	69.92	74.37	76.92	74.31	63.12	72.49	63.09	66.01	77.56	65.74	72.07	67.37
Al_2O_3	%	9.53	11.7	10.86	15.84	15.83	12.71	11.14	12.5	13.18	13.16	15.4	9.25	10.82	16.93	14.13	14.48
Fe_2O_3(T)	%	4.85	5.09	4.52	6.24	3.64	4.99	4.06	3.82	8.4	4.9	7.22	12.97	3.02	5.92	4.1	7.92
MnO	%	0.072	0.04	0.034	0.195	0.082	0.123	0.241	0.491	0.874	0.152	0.538	0.574	0.048	0.048	0.034	0.051
MgO	%	1.59	2.66	3.11	1.3	1.32	1.49	1.46	1.91	1.74	1.43	1.44	2.79	1.05	1.58	1.28	1.82
CaO	%	1.18	0.63	2.55	0.5	0.23	0.26	0.14	0.17	2.31	0.45	1.37	0.22	0.05	0.42	0.21	0.38
Na_2O	%	0.35	0.79	1.04	1.21	0.89	0.65	0.72	0.89	2.2	0.54	1.19	0.05	0.13	0.36	0.51	0.63
K_2O	%	1.71	2.31	2.22	3.58	3.54	2.62	2.04	2.26	1.87	3.46	3.54	0.46	2.55	4.66	3.78	3.26
TiO_2	%	0.375	0.49	0.314	0.594	0.481	0.472	0.43	0.506	0.48	0.501	0.561	0.2	0.293	0.79	0.675	0.675
P_2O_5	%	0.07	0.05	0.05	0.09	0.07	0.04	0.03	0.05	0.09	0.07	0.1	0.09	0.03	0.06	0.05	0.19
Ba	*ppm*	490	350	252	785	606	473	536	671	279	469	535	442	1449	744	883	841
Cs	*ppm*	2.2	6.3	4.1	14.8	9.9	7.6	4.8	6.5	2.7	6.7	6.7	2.5	5.6	14.3	13	13.4
Cu	*ppm*	93	57	8	-	106	65	115	827	22	45	60	17	20	86	37	46
Ga	*ppm*	14	17	17	24	22	21	19	21	20	21	22	12	14	24	19	21
Ge	*ppm*	2.3	1.5	1.4	2.6	2.3	2.3	2.3	2.9	2.2	2.2	2.6	4.4	2.3	2.3	1.8	2.1
Hf	*ppm*	2.1	2.2	5	2.9	3.1	2.2	1.9	2.3	2.8	1.6	4	1.9	2.3	5.3	2.4	3.8
Nb	*ppm*	10.4	10	10.6	8.9	13.8	6.5	4.9	6.3	8.2	5.3	12.6	3.3	4.6	25.6	8.3	17.5
Ni	*ppm*	46	36	46	80	167	129	115	110	99	127	89	62	21	83	55	66
Pb	*ppm*	-	7	-	9	7	13	15	58	7	7	23	73	30	94	10	< 5
Rb	*ppm*	78	96	89	208	178	133	98	111	91	174	186	25	137	210	188	176
S	%	0.074	0.029	0.035	0.039	0.015	0.011	0.015	0.029	0.061	0.009	0.019	0.007	0.004	0.048	0.013	0.511
Sr	*ppm*	32	27	37	94	67	55	50	48	58	29	47	33	22	33	41	44
Ta	*ppm*	0.83	0.76	1	0.69	0.98	0.53	0.45	0.58	0.74	0.9	0.94	0.6	0.76	2.33	0.91	1.35
Th	*ppm*	6.65	7.79	7.59	10.1	18	8.29	7.22	8.05	9.78	9.86	12.6	8.92	10.4	13.5	9.53	11.3
U	*ppm*	1.1	1.75	0.7	2.29	4.98	1.59	1.7	1.93	2.87	2.08	2.82	4.9	4.02	2.51	1.68	1.74
V	*ppm*	86	145	56	100	115	115	99	131	69	130	104	39	41	173	137	122
Y	*ppm*	23	21	39	26	21	17	17	17	28	22	30	55	24	38	22	26
Zr	*ppm*	89	98	217	120	111	85	75	92	134	111	157	83	94	213	107	152
La	*ppm*	26.8	31.3	30.1	44.9	44.2	34.4	32.8	31.2	42.4	38	47.1	24	19.3	69.8	40	47.6
Ce	*ppm*	54.7	61.2	59.7	81.8	105	75.6	68.7	66.9	74.8	86.1	89.7	42	40.5	136	79.4	96.2
Pr	*ppm*	5.93	6.97	7.26	9.79	10.5	7.73	6.89	7.08	9.89	8.25	10.5	5.43	4.34	15.1	8.79	10.7
Nd	*ppm*	23.6	27.6	29.4	35.6	38.2	28.2	25.1	26.2	37.3	29.5	38.9	20.7	14.7	54.1	32.4	40.4
Sm	*ppm*	4.52	5.16	6.27	7.14	7.23	5.58	5.04	5.01	7.61	5.93	7.52	5.69	2.8	10.4	6.16	7.33
Eu	*ppm*	0.953	1.17	1.17	1.32	1.28	1.05	0.835	0.615	1.54	1.17	1.57	0.649	0.332	2.44	1.05	1.72
Gd	*ppm*	4.72	4.68	6.39	5.76	5.16	4.02	3.62	3.91	6.68	4.77	6.77	7.17	2.89	8.34	4.82	6.09
Tb	*ppm*	0.78	0.71	1.1	0.88	0.84	0.64	0.56	0.57	1.01	0.77	1.08	1.39	0.59	1.24	0.75	0.91
Dy	*ppm*	4.41	3.98	6.68	5.26	4.72	3.54	3.31	3.26	6.12	4.52	6.24	9.03	4.19	7.54	4.51	5.47
Ho	*ppm*	0.88	0.83	1.41	1.06	0.89	0.7	0.68	0.69	1.18	0.84	1.2	1.89	0.94	1.44	0.88	1.1
Er	*ppm*	2.39	2.4	4.11	3.05	2.58	2.02	1.97	2.03	3.34	2.4	3.45	5.69	2.83	4.33	2.63	3.16
Tl	*ppm*	0.39	0.44	0.34	1.11	0.95	0.7	0.55	0.72	0.41	0.69	0.83	0.68	1.46	1.26	1.95	1.87
Tm	*ppm*	0.358	0.35	0.673	0.445	0.393	0.3	0.285	0.293	0.491	0.352	0.5	0.869	0.411	0.624	0.392	0.487
Yb	*ppm*	2.34	2.31	4.42	2.84	2.65	2.04	1.86	2.06	3.17	2.24	3.29	5.79	2.78	3.88	2.64	3.11
Lu	*ppm*	0.331	0.355	0.617	0.458	0.366	0.325	0.334	0.323	0.462	0.348	0.497	0.855	0.394	0.623	0.396	0.469
As	*ppm*	12	7	3	2	14	-	35	2	7	-	-	79	22	48	19	19
Co	*ppm*	13	5.6	12.2	22.6	28.1	27.8	25.9	29.4	18.4	22.1	22.6	29.4	7.3	18.3	10.5	13.7
Cr	*ppm*	44.8	61.8	28.4	67	61.5	62	55	61.8	47.5	72.6	40.5	22	31	136	106	74
Sb	*ppm*	1	1.2	1.7	1.7	1.9	0.7	0.4	1.3	0.6	0.9	3.2	9.9	4.3	4.9	2.8	7.3
Sc	*ppm*	9.41	11.9	14.3	15.6	14	13	11.4	13.1	13.9	13.7	13.9	5	5.95	16.2	13.2	14.1
Zn	*ppm*	69	57	60	99	62	98	92	118	97	105	108	431	68	127	77	85

Supplementary Material 1 – Table providing all the relevant information of the studied samples (coordinates, stratigraphy, mineralization type, whole-rock chemistry, etc.)

Sample Ref		SES18#3	SES20#1	SES20#3	SES18#1	SES18#2	SES18#4	SES18#5	MM02#2	MM02#3	MDM02#1	MDM02#2	MDM02#3	MDM02#4	MDM02#5	MDM02#6
Sector		Lousal	Lousal	Lousal	Lousal	Lousal	Lousal	Lousal	Aljustrel	Aljustrel	Aljustrel	Aljustrel	Aljustrel	Aljustrel	Aljustrel	Aljustrel
Stratigraphic division		*upper* VSC	*upper* VSC	*upper* VSC	*upper* VSC	*upper* VSC	upper VSC	upper VSC	upper VSC	upper VSC	upper VSC	upper VSC	upper VSC	upper VSC	upper VSC	upper VSC
Mineralization type/occurrence		*No sulphide*	*No sulphide*	*No sulphide*	*No sulphide*	*No sulphide*	*No sulphide*	*No sulphide*	*No sulphide*	*Py-bearing*	*No sulphide*	*No sulphide*	*No sulphide*	*Mineralized*	*No sulphide*	*Mineralized*
Footwall/Hangingwall		*Hangingwall*	*Hangingwall*	*Hangingwall*	*Hangingwall*	*Hangingwall*	*Hangingwall*	*Hangingwall*	*Hangingwall*	*Hangingwall*	*Hangingwall*	*Hangingwall*	*Hangingwall*	*Hangingwall*	*Hangingwall*	*Hangingwall*
Location - ETRS89	x	-24931	-25066	-25066	-24931	-24931	-24931	-24931	-6931	-6931	-9155	-9155	-9155	-9155	-9155	-9155
	y	-187850	-187756	-187756	-187850	-187850	-187850	-187850	-198313	-198313	-193552	-193552	-193552	-193552	-193552	-193552
Depth (m)		-277.10	-166.30	-240.20	-262.35	-214.55	-340.30	-361.40	-238.45	-255.30	-86.50	-110.25	-114.00	-117.00	-136.20	-145.80
SiO_2	%	57.54	67.56	72.01	56.15	49.49	56.93	67.22	69.63	73.04	64.98	58.01	60.44	32.04	59.14	59.76
Al_2O_3	%	20.39	14.88	10.57	19.19	16.63	15.17	11.71	14.1	13.98	17.45	23.51	16.72	10.21	19.28	15.9
$Fe_2O_3(T)$	%	7.3	6.98	7.98	8.03	7.88	5.89	8.72	5.94	4.22	6.99	2.45	10.29	16.35	8	10.16
MnO	%	0.051	0.062	0.054	0.212	0.766	0.31	0.188	0.552	0.291	0.273	0.266	0.157	0.418	0.101	0.138
MgO	%	1.87	1.42	1.4	2.67	4.01	2.8	1.36	1.44	1.91	1.53	4.05	2.21	3.21	2.3	3.62
CaO	%	0.3	1.02	0.31	1.5	4.92	2.75	0.18	0.47	0.14	0.18	0.2	0.34	19.28	0.27	0.21
Na_2O	%	0.39	0.43	0.45	0.65	0.12	0.78	0.08	1.26	1.06	1.67	1.34	1.94	0.04	0.58	1.01
K_2O	%	4.31	4.02	2.1	4.09	4.06	3.4	3.26	3.59	2.6	4.18	5.91	3.9	0.37	5.25	3.1
TiO_2	%	0.82	0.713	0.497	0.736	0.676	0.372	0.318	0.502	0.454	0.694	0.336	0.636	0.349	0.673	0.737
P_2O_5	%	0.08	0.05	0.16	0.1	0.09	0.08	0.11	0.09	0.08	0.09	0.11	0.07	14.21	0.08	0.08
Ba	*ppm*	528	521	494	573	431	233	186	746	594	621	672	432	102	670	357
Cs	*ppm*	8.1	7.6	7.3	6	6.1	6.6	3.4	16.6	6.5	9.4	12.8	9.5	0.9	9.5	6.4
Cu	*ppm*	38	69	52	28	11	7	86	-	124	14	2	26	92	15	130
Ga	*ppm*	27	19	15	26	23	23	15	19	19	27	28	25	16	27	22
Ge	*ppm*	1.6	1.8	1.7	2.3	2.3	1.5	1.3	2.4	2.5	2.4	2.3	2.9	2.8	2.7	2.3
Hf	*ppm*	4.3	3.3	1.6	3.5	3.4	6.7	4.8	3.1	4.5	3.4	10.4	4.8	1.7	4.3	3.9
Nb	*ppm*	11.1	13.5	5.3	8.7	9.5	6.1	6	9.5	10.9	13.8	23.6	18.1	5.8	14.5	13.6
Ni	*ppm*	66	73	62	58	68	2	3	68	69	99	194	77	53	59	62
Pb	*ppm*	29	19	10	-	7	-	45	58	11	54	35	107	1760	187	291
Rb	*ppm*	191	140	99	177	161	158	121	168	117	198	266	196	15	244	149
S	*%*	1.44	0.04	0.483	0.017	0.073	0.113	2.59	0.004	0.083	0.003	0.007	0.003	0.048	0.009	0.038
Sr	*ppm*	100	34	29	80	80	71	12	84	83	71	72	60	299	29	26
Ta	*ppm*	1.27	1.17	0.61	1.06	1.04	0.98	0.61	0.79	0.82	1.03	2.4	1.21	0.28	1.27	0.97
Th	*ppm*	12.6	10.2	7.41	11.3	10.2	11.5	8.48	10.1	13.5	12.5	48	15	5.65	18.2	11.3
U	*ppm*	2.88	2.07	1.29	1.95	1.6	2.74	2.38	2.63	5.61	2.72	6.45	2.24	7.23	2.18	3.48
V	*ppm*	160	122	96	128	96	17	17	90	100	125	84	172	223	139	255
Y	*ppm*	23	25	20	22	25	42	36	25	29	27	36	40	256	30	38
Zr	*ppm*	168	152	86	130	124	273	227	130	190	140	326	198	76	153	167
La	*ppm*	43.7	49.2	32.2	40.4	38.5	39.5	29.9	40.3	42.7	49.7	59	59.9	190	43.1	55.8
Ce	*ppm*	87.6	96.3	61.1	80.7	76.1	85.2	62.6	79.3	94.7	108	131	110	206	81.5	92.4
Pr	*ppm*	9.83	10.6	6.76	9.24	8.76	9.98	7.39	8.97	9.9	10.6	13.8	13.8	36.1	9.53	12.3
Nd	*ppm*	35.7	40.2	26	32.9	31.8	38.4	29.9	33.2	35.8	37.7	48.4	50.7	149	34.9	45.5
Sm	*ppm*	6.83	7.4	5.16	6.62	6.68	9.41	6.74	6.93	7.3	7.26	9.02	10.3	31.5	6.97	9.17
Eu	*ppm*	1.35	1.63	1.26	1.45	1.39	1.66	1.67	1.38	1.27	1.43	0.937	1.88	8.61	1.23	1.79
Gd	*ppm*	5.1	5.98	4.83	4.74	5.1	8.44	6.7	5.63	6.56	5.99	7.86	9.21	42.7	5.89	8.42
Tb	*ppm*	0.79	0.89	0.72	0.75	0.82	1.37	1.09	0.86	1	0.92	1.24	1.51	6.7	1	1.28
Dy	*ppm*	4.86	5.36	4.25	4.72	4.76	8.6	6.81	5.02	5.72	5.42	7.34	8.66	39.4	5.94	7.72
Ho	*ppm*	0.93	1	0.83	0.91	0.94	1.67	1.36	0.96	1.13	1.03	1.39	1.69	7.91	1.17	1.51
Er	*ppm*	2.73	2.97	2.45	2.57	2.7	4.95	4.07	2.88	3.43	2.94	4.11	4.77	20.9	3.35	4.49
Tl	*ppm*	0.69	0.5	0.6	0.39	0.47	0.66	0.59	8.47	5.08	1.61	1.75	1.21	0.37	1.06	0.74
Tm	*ppm*	0.431	0.42	0.364	0.386	0.388	0.743	0.592	0.424	0.528	0.44	0.606	0.706	2.48	0.498	0.631
Yb	*ppm*	2.61	2.85	2.42	2.56	2.51	4.65	3.8	2.71	3.7	2.85	3.84	4.41	13.9	3.28	4.32
Lu	*ppm*	0.417	0.425	0.364	0.386	0.351	0.69	0.562	0.455	0.592	0.411	0.569	0.657	1.9	0.47	0.609
As	*ppm*	35	32	12	1	17	3	146	2	23	16	21	5	20	18	37
Co	*ppm*	27.3	17.4	13.3	20.8	20.1	0.8	7.9	14.5	14.9	22.1	38.7	16.8	14.2	11	16.9
Cr	*ppm*	157	112	82	152	136	-	6	44	34.5	71	18.5	82	80.5	79	102
Sb	*ppm*	19	1.7	1.1	0.7	1.9	3.2	16	1.7	7.5	2.8	3	1.3	0.8	1	1.2
Sc	*ppm*	19.1	13.9	10.3	18.7	16.2	15.5	11.3	10.5	8.95	13.8	7.8	11.4	7.05	10.9	12.3
Zn	*ppm*	115	96	87	104	82	63	80	88	57	124	137	166	122	155	154

Supplementary Material 1 – Table providing all the relevant information of the studied samples (coordinates, stratigraphy, mineralization type, whole-rock chemistry, etc.)

Sample Ref		**MM02#1**	**MDM02#8**	**MDM02#9**	**MDM02#10**	**R MS#1**	**R MS#2**	**R MS#4**	**R MS#5**	**L MS#1**	**X99**	**X100**	**ABNSTR7**	**ABNSTR2**	**SES20#7**	**SES18#6**
Sector		**Aljustrel**	**Aljustrel**	**Aljustrel**	**Aljustrel**	**Neves Corvo**	**Neves Corvo**	**Neves Corvo**	**Neves Corvo**	**Lousal**	**Albernoa**	**Albernoa**	**Albernoa**	**Albernoa**	**Lousal**	**Lousal**
Stratigraphic division		**upper VSC**	**upper VSC**	**upper VSC**	**upper VSC**	**upper VSC**	**upper VSC**	**upper VSC**	***upper* VSC**	**PQG**	**PQG**	**PQG**	**PQG**	**PQG**	**BAFG (Flysch)**	**BAFG (Flvsch)**
Mineralization type/occurrence		***No sulphide***	***No sulphide***	***No sulphide***	***No sulphide***	***No sulphide***	***No sulphide***	***No sulphide***	***No sulphide***	***No sulphide***	***No sulphide***	***No sulphide***	***No sulphide***	***No sulphide***	***No sulphide***	***No sulphide***
Footwall/Hangingwall		***Hangingwall***	***Hangingwall***	***Hangingwall***	***Hangingwall***	***Hangingwall***	***Hangingwall***	***Hangingwall***	***Hangingwall***	***Footwall***	***n.a.***	***n.a.***	***n.a.***	***n.a.***	***n.a.***	***n.a.***
Location - ETRS89	**x**	-6931	-9155	-9155	-9155	-14111	-13674	4457	11359	*n.a.*	*n.a.*	*n.a.*	*n.a.*	*n.a.*	-25066	-24931
	y	-198313	-193552	-193552	-193552	-209159	-208943	-228160	-230546	*n.a.*	*n.a.*	*n.a.*	*n.a.*	*n.a.*	-187756	-187850
Depth (m)		-230.80	-361.70	-371.55	-377.30	*n.a.*	*n.a.*	*n.a.*	*n.a.*	*n.a.*	*n.a.*	*n.a.*	*n.a.*	*n.a.*	*n.a.*	*n.a.*
SiO_2	%	73.33	67.69	71.45	76.43	65.77	67.54	75.01	79.05	63.03	84.41	66.75	62.44	81.99	60.31	55.93
Al_2O_3	%	13.23	15.32	11.5	13.07	15.93	15.4	11.77	10.35	18.4	7.58	12.84	18.14	0.71	17.32	16.81
Fe_2O_3(T)	%	4.94	3.24	3.88	1.8	6.6	6.06	3.61	4.16	6.79	2.57	11.81	6.99	3.06	7.14	7.55
MnO	%	0.192	0.019	0.028	0.016	0.406	0.141	0.033	0.107	0.026	0.021	0.116	0.065	0.004	0.086	0.239
MgO	%	1.63	3.04	1.69	1.21	2.02	0.89	1.14	0.31	1.42	0.13	1.46	1.31	0.04	2.4	1.99
CaO	%	0.24	0.51	0.15	0.42	0.03	0.09	0.19	0.03	0.17	0.03	0.1	0.06	0.06	1.29	2.17
Na_2O	%	0.86	1.85	0.53	3.57	0.16	0.46	0.08	0.11	0.71	0.18	0.34	0.76	0.03	2.39	0.57
K_2O	%	2.14	3.18	3.13	2.18	3.23	3.71	3	2.26	2.98	1.48	1.51	2.8	0.21	2.47	3.89
TiO_2	%	0.533	0.288	0.447	0.111	0.663	0.563	0.501	0.432	0.929	0.312	0.558	1.039	1.397	0.818	0.764
P_2O_5	%	0.06	0.07	0.06	0.17	0.05	0.04	0.05	0.04	0.12	0.02	0.08	0.11	0.05	0.15	0.09
Ba	*ppm*	304	736	344	468	865	608	297	338	417	274	289	384	811	491	633
Cs	*ppm*	5.9	6.7	7.1	4.9	6.8	11.6	7	3.6	6.8	1.7	2.5	6	2.5	5.9	10
Cu	*ppm*	39	18	56	10	50	11	48	110	22	43	24	35	377	39	69
Ga	*ppm*	21	22	16	19	23	21	17	17	25	11	19	25	3	22	24
Ge	*ppm*	2.4	1.4	1.4	1.8	2.2	2.7	2.6	2.4	2.6	2.2	2.8	2.5	1.4	1.7	1.4
Hf	*ppm*	2.5	5.9	1.8	3.2	3.4	2.4	1.8	2.4	5.9	1.5	2.4	5.6	5	3.7	3.1
Nb	*ppm*	9.1	9.3	6.5	8.7	12.8	5.8	4.9	5.8	14	5.7	10	15.9	21.6	6.2	9.2
Ni	*ppm*	126	19	61	3	56	85	37	74	58	14	70	50	3	44	76
Pb	*ppm*	20	24	43	21	44	32	11	-	6	-	6	9	570	20	68
Rb	*ppm*	88	110	127	77	147	207	152	103	161	76	77	136	8	104	178
S	*%*	0.009	0.992	1.81	0.256	0.006	0.003	0.004	0.004	0.004	0.003	0.058	0.005	1.84	0.256	2.68
Sr	*ppm*	82	70	22	81	56	82	22	22	111	36	62	159	57	188	127
Ta	*ppm*	0.73	0.89	0.62	0.85	0.96	0.98	0.92	0.69	1.56	0.45	0.8	1.42	1.83	0.89	1.16
Th	*ppm*	9.76	14.9	6.89	7.44	11.1	10.6	8.46	7.42	14.8	5.21	8.11	13.9	15.1	10.3	12.7
U	*ppm*	2.1	5.82	3.92	3.93	2.31	1.5	3.34	1.38	3.07	1.28	3.36	3.52	4.23	3.2	8.36
V	*ppm*	98	40	291	10	125	116	103	99	162	84	83	131	36	130	183
Y	*ppm*	19	42	21	33	16	26	20	14	27	11	22	39	31	23	23
Zr	*ppm*	104	223	73	96	138	98	75	90	221	58	107	231	209	137	116
La	*ppm*	38.2	37.1	24.1	14.2	30.9	45.7	31.4	26.9	47.7	20.6	29.3	45.4	58.2	32	44.8
Ce	*ppm*	92.1	78.7	41.4	34.4	66.1	93.9	60.8	65.6	95.6	38.7	53.5	86.5	107	67.3	90.9
Pr	*ppm*	8.72	8.96	5.3	4.14	6.77	10.5	7.01	6.37	10.9	4.55	7.15	10.7	12.4	7.81	10.3
Nd	*ppm*	31.9	33	19.8	15.8	24	39.6	26.6	23.4	39.5	17.1	26.8	40.3	44.7	30.9	37.8
Sm	*ppm*	6.03	7.42	3.97	5.16	4.41	7.79	5.28	4.8	7.49	3.17	5.35	8.42	7.4	6.44	7
Eu	*ppm*	1.15	0.804	0.712	0.398	0.924	1.63	1.03	0.854	1.54	0.469	1.16	1.64	1.41	1.47	1.45
Gd	*ppm*	4.79	7.36	3.71	5.89	3.51	6.29	4.39	3.3	5.77	2.22	4.89	7.09	4.87	5.1	4.97
Tb	*ppm*	0.74	1.25	0.56	1.06	0.57	1.02	0.72	0.55	0.98	0.37	0.78	1.16	0.89	0.85	0.8
Dy	*ppm*	4.23	7.79	3.3	6.18	3.41	5.85	4.27	3.22	5.99	2.03	4.44	6.98	5.51	5.03	4.99
Ho	*ppm*	0.81	1.53	0.67	1.1	0.72	1.13	0.84	0.64	1.15	0.4	0.81	1.38	1.15	0.97	0.95
Er	*ppm*	2.21	4.52	1.93	2.66	2.24	3.33	2.24	1.84	3.26	1.19	2.35	4.03	3.43	2.75	2.79
Tl	*ppm*	25	3.45	2.52	1.87	0.73	1.56	1.05	0.84	5.79	0.34	0.29	0.61	1.41	4.29	0.96
Tm	*ppm*	0.329	0.709	0.289	0.348	0.351	0.5	0.359	0.291	0.518	0.193	0.343	0.603	0.535	0.435	0.411
Yb	*ppm*	2.38	4.68	1.79	2.22	2.44	3.27	2.25	1.88	3.22	1.37	2.23	3.92	3.57	2.85	2.76
Lu	*ppm*	0.37	0.747	0.269	0.323	0.362	0.472	0.316	0.295	0.464	0.196	0.321	0.589	0.552	0.438	0.39
As	*ppm*	2	13	18	3	4	-	21	7	14	21	40	11	391	15	77
Co	*ppm*	21.7	4.8	9.6	-	6.5	21.3	10	12.4	15	2.8	21.4	9.7	7.8	21	28.3
Cr	*ppm*	58.5	37	101	-	95	69	76	42	110	38.3	64.7	106	30.9	82	140
Sb	*ppm*	0.4	2	5.2	0.3	0.6	1.6	2.5	0.6	0.7	0.3	1.9	0.7	55.3	1	22.5
Sc	*ppm*	11.1	10.6	10.4	7.28	16.4	16.5	11.3	10.4	18.6	7.11	14.5	17.4	4.81	18.4	17.1
Zn	*ppm*	112	78	67	79	101	95	51	21	119	9	126	99	408	101	76

Supplementary Material 1 – Table providing all the relevant information of the studied samples (coordinates, stratigraphy, mineralization type, whole-rock chemistry, etc.)

Sample Ref		ALJ_MM16-15#.	ALJ_MS#1	ALJ_MS#3	ALJ_MS#4	X38	X57	X62	T58
Sector		Aljustrel	Aljustrel	Aljustrel	Aljustrel	Albernoa	Albernoa	Albernoa	Albernoa
Stratigraphic division		BAFG (Flysch)	BAFG (Flysch)	BAFG (Flysch)	BAFG (Flysch)	BAFG (Flysch)	BAFG (Flysch)	BAFG (Flysch)	BAFG (Flysch)
Mineralization type/occurrence		*No sulphide*	*No sulphide*	*No sulphide*	*No sulphide*	*No sulphide*	*No sulphide*	*No sulphide*	*No sulphide*
Footwall/Hangingwall		*n.a.*	*n.a.*	*n.a.*	*n.a.*	*n.a.*	*n.a.*	*n.a.*	*n.a.*
Location - ETRS89	x	-3469	-3795	-3795	-3795	6684	20152	17865	20152
	y	-198137	-197814	-197814	-197814	-207298	-213030	-217172	-213030
Depth (m)		-238.60	-61.50	-72.35	-77.00	*n.a.*	*n.a.*	*n.a.*	*n.a.*
SiO_2	%	69.5	59.11	56.12	59.61	59.43	62.24	58.35	84.02
Al_2O_3	%	15.64	16.72	21.51	18.82	19.42	18.59	20.67	9.58
$Fe_2O_3(T)$	%	1.63	7.37	7.36	7.62	8.31	6.49	7.37	1.92
MnO	%	0.033	0.123	0.092	0.1	0.115	0.034	0.071	0.004
MgO	%	2.89	1.89	2.12	2.17	1.83	1.01	1.19	0.15
CaO	%	1.48	3	0.57	1.14	0.1	-	0.09	0.02
Na_2O	%	0.09	1.4	0.99	2.28	0.66	0.53	0.8	0.3
K_2O	%	4.82	2.74	4.11	2.64	3.16	3.18	3.33	2.08
TiO_2	%	0.179	0.786	1.044	0.931	0.862	0.925	0.814	0.38
P_2O_5	%	0.03	0.11	0.15	0.14	0.1	0.06	0.08	0.03
Ba	*ppm*	684	395	600	410	496	439	510	357
Cs	*ppm*	12.9	5.9	9.2	5.7	5.6	4.8	4.5	2.3
Cu	*ppm*	7	47	60	52	35	46	87	17
Ga	*ppm*	23	21	27	22	30	26	29	14
Ge	*ppm*	1.9	1	1.5	1.3	4.2	2.7	3	1.9
Hf	*ppm*	5.8	3.7	4.1	4.4	3.7	4.5	3.3	2.2
Nb	*ppm*	10.1	11	13	11.9	15.3	16.1	16.3	8.5
Ni	*ppm*	2	55	61	52	53	58	73	7
Pb	*ppm*	12	36	20	15	13	-	9	-
Rb	*ppm*	230	120	179	112	168	152	175	109
S	*%*	0.247	1.38	0.71	0.521	0.003	0.016	0.004	0.016
Sr	*ppm*	43	124	115	133	97	83	133	35
Ta	*ppm*	1.14	0.93	1.16	1.01	1.22	1.38	1.22	0.51
Th	*ppm*	16.8	10.8	13.9	11.6	13.6	13.4	13.1	5.56
U	*ppm*	4.82	6.52	5.85	9.69	2.78	3.94	3.62	1.24
V	*ppm*	13	136	175	151	127	156	130	63
Y	*ppm*	70	23	29	29	29	27	23	13
Zr	*ppm*	167	160	189	200	129	190	125	95
La	*ppm*	40.2	33.8	42.7	35.4	43.2	44.3	45.6	20.3
Ce	*ppm*	87.5	70	88.3	73.7	82	84.8	89.8	43.3
Pr	*ppm*	9.98	7.72	9.78	8.3	9.88	9.83	10.4	4.27
Nd	*ppm*	38.8	28.6	36.4	30.8	36.7	36.4	38.8	14.8
Sm	*ppm*	9.71	5.69	7.12	6.45	6.89	7.18	6.96	2.74
Eu	*ppm*	0.66	1.35	1.61	1.47	1.38	1.43	1.31	0.638
Gd	*ppm*	10.5	4.79	5.64	5.88	5.96	5.58	5.48	2.02
Tb	*ppm*	1.83	0.79	0.94	0.89	0.95	0.9	0.85	0.38
Dy	*ppm*	12.1	4.63	5.69	5.56	5.71	5.18	4.91	2.32
Ho	*ppm*	2.47	0.95	1.14	1.11	1.14	1.04	0.94	0.49
Er	*ppm*	7.24	2.63	3.3	3.16	3.19	3.05	2.7	1.44
Tl	*ppm*	2.14	0.64	0.75	0.49	0.58	0.6	0.75	0.4
Tm	*ppm*	1.13	0.375	0.488	0.453	0.475	0.478	0.416	0.206
Yb	*ppm*	7.5	2.48	3.21	2.96	3.2	3.24	2.77	1.45
Lu	*ppm*	1.18	0.387	0.487	0.443	0.511	0.476	0.391	0.263
As	*ppm*	10	35	26	13	12	8	17	-
Co	*ppm*	1.4	20	25	19.8	19.8	9.3	15.2	-
Cr	*ppm*	2.5	72.5	88.5	83.5	95.8	106	99.2	53
Sb	*ppm*	1.4	4.3	2	1.4	0.4	0.9	0.4	0.8
Sc	*ppm*	4.25	14.4	22.6	19.6	18.3	18.9	18.9	9.35
Zn	*ppm*	57	102	122	120	113	87	102	9

Appendix 1.2

Supplementary material 2

Geochemistry of Fammenian to Visean metapelites from the Iberian Pyrite Belt: implications for provenance, paleo-redox conditions and vectoring massive sulfide deposits

Natural Resources Research - 2020

Filipa Luz
António Mateus
Carlos Rosa
Jorge Figueiras

Electronic Supplementary Material 2

Geochemistry of Famennian to Visean metapelites from the Iberian Pyrite Belt: implications for provenance, paleo-redox conditions and vectoring of massive sulphide deposits

Filipa Luz[1], António Mateus[2,1], Carlos Rosa[3,1], Jorge Figueiras[2,1]

[1] Instituto Dom Luiz (IDL), Faculdade de Ciências, Universidade de Lisboa, Campo-Grande 1749-016 Lisboa, Portugal – ORCID ID: 0000-0002-2913-2803

[2] Dep. Geologia, Faculdade de Ciências, Universidade de Lisboa, Ed. C6, Piso 4, 1749-016 Lisboa, Portugal

[3] CPR Lda Geology Consulting, Qta da Pedra Branca, Av. Casal Segulim, 1685-891 Famões, Portugal

*geo.filipa.luz@gmail.com

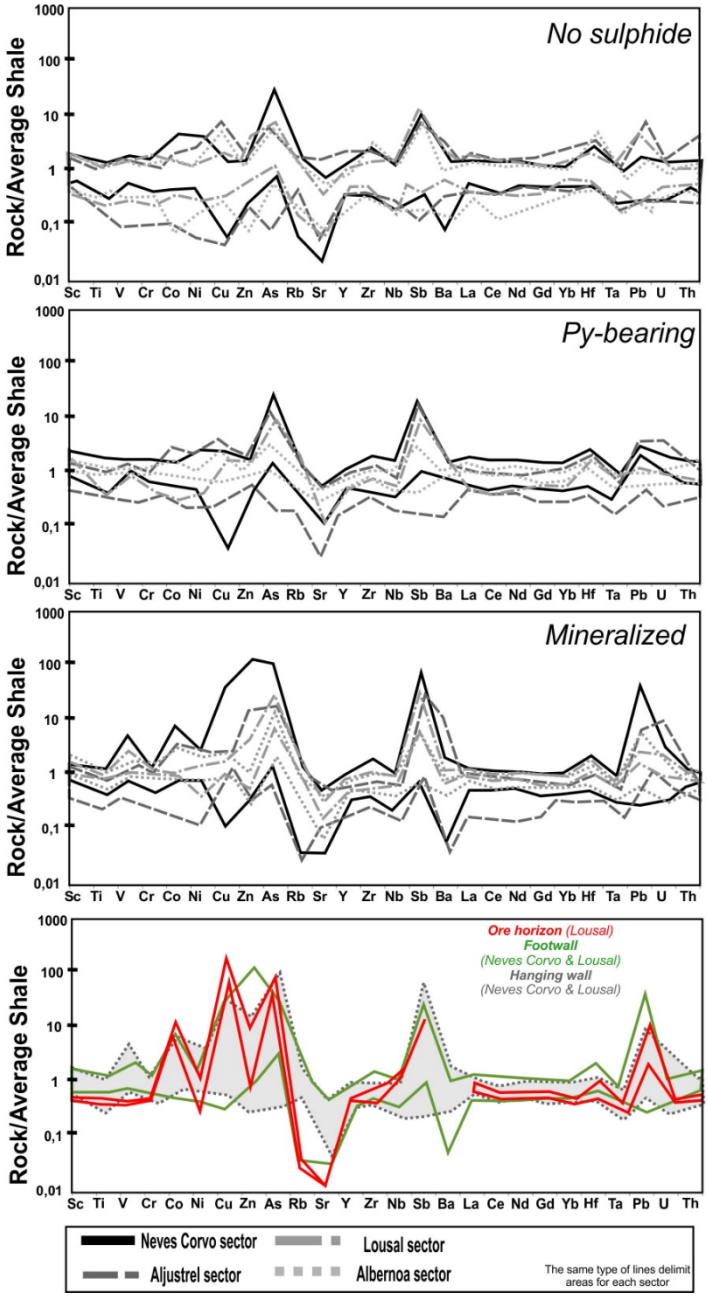

Electronic Supplementary Material 2 – PAAS-normalized, multi-element patterns for IPB metapelites. For each sampling sector, the patterns were assembled in accordance to the previously defined groups: “No-sulphide”, “Py-bearing” and “Mineralized”.

Electronic Supplementary Material 3

Geochemistry of Famennian to Visean metapelites from the Iberian Pyrite Belt: implications for provenance, paleo-redox conditions and vectoring of massive sulphide deposits

Filipa Luz[1*], António Mateus[1,2], Carlos Rosa[3], Jorge Figueiras[1,2]

[1] Instituto Dom Luiz (IDL), Faculdade de Ciências, Universidade de Lisboa, Campo-Grande 1749-016 Lisboa, Portugal – ORCID ID: 0000-0002-2913-2803

[2] Dep. Geologia, Faculdade de Ciências, Universidade de Lisboa, Ed. C6, Piso 4, 1749-016 Lisboa, Portugal

[3] CPR Lda Geology Consulting, Qta da Pedra Branca, Av. Casal Segulim, 1685-891 Famões, Portugal

*geo.filipa.luz@gmail.com

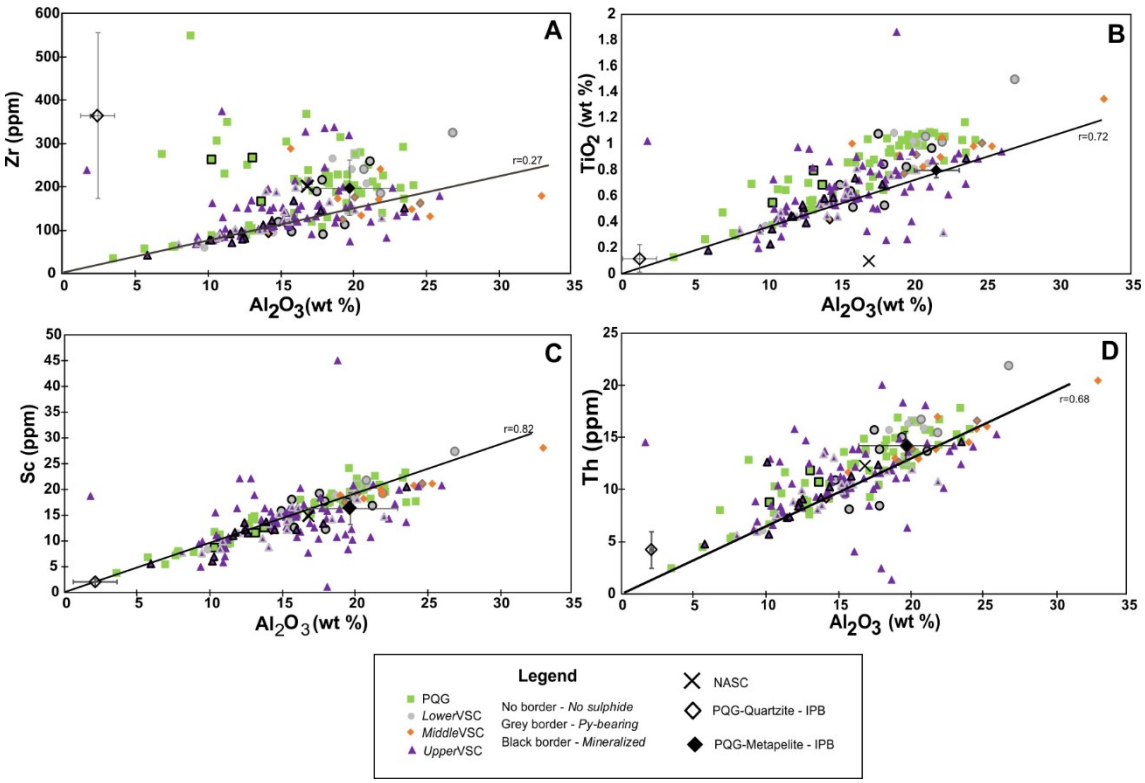

Electronic Supplementary Material 3 – Co-variation between Zr (ppm) vs. Al_2O_3 (wt %); TiO2 (wt %) vs. Al_2O_3 (wt %), Th (ppm) vs. Al_2O_3 (wt %) and Sc (ppm) vs. Al_2O_3 (wt %), to test the immobile behaviour. For reference, and besides NASC contents (Condie, 1993), the average and standard deviation concentration measures calculated for the PQG-quartzite and metapelites (n=75, different IPB sites, Jorge, 2009).

Reference: Jorge, R.C.G.S., (2009). *Caracterização petrográfica, geoquímica e isotópica dos reservatórios metalíferos crustais, dos processos de extracção de metais e dos fluídos hidrotermais envolvidos em sistemas mineralizantes híbridos na Faixa Piritosa Ibérica*. PhD Thesis, University of Lisbon, Portugal, pp.290.

Electronic Supplementary Material 4

Geochemistry of Famennian to Visean metapelites from the Iberian Pyrite Belt: implications for provenance, paleo-redox conditions and vectoring of massive sulphide deposits

Filipa Luz[1*], António Mateus[1,2], Carlos Rosa[3], Jorge Figueiras[1,2]

[1] Instituto Dom Luiz (IDL), Faculdade de Ciências, Universidade de Lisboa, Campo-Grande 1749-016 Lisboa, Portugal – ORCID ID: 0000-0002-2913-2803

[2] Dep. Geologia, Faculdade de Ciências, Universidade de Lisboa, Ed. C6, Piso 4, 1749-016 Lisboa, Portugal

[3] CPR Lda Geology Consulting, Qta da Pedra Branca, Av. Casal Segulim, 1685-891 Famões, Portugal

*geo.filipa.luz@gmail.com

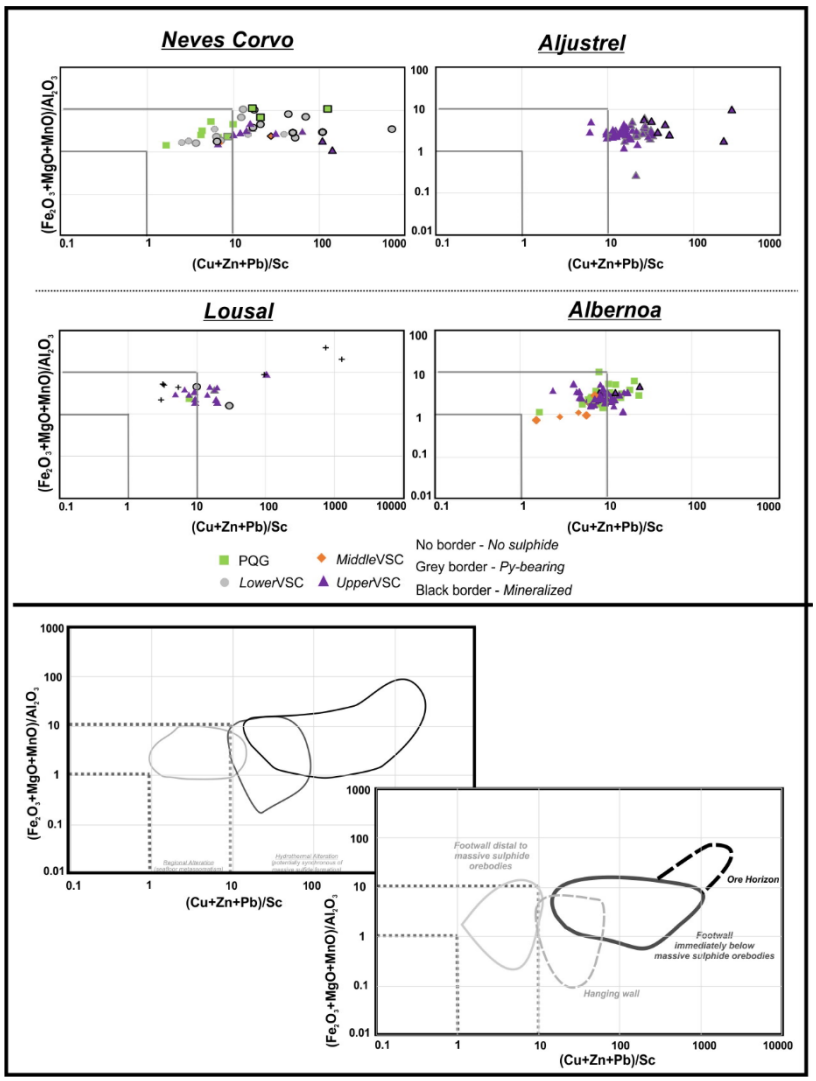

Electronic Supplementary Material 4 – (Fe_2O_3+MgO+MnO)/Al_2O_3 *vrs* (Cu+Zn+Pb)/Sc diagram illustrating the chemical effects related to post-sedimentary transformations. Values between 1.0 and 10.0 of these geochemical ratios trace effects ascribed to oceanic metasomatism processes (*regional alteration pattern*); ratios above 10.0 indicate the proximity of hydrothermal discharges potentially related to ore-forming systems. The ore horizon of Lousal is represented by 7 non-weathered samples (**+**) reported in Fernandes (2011).

Reference: Fernandes, A. (2011). *Caracterização petrográfica, mineralógica e geoquímica do padrão de alteração hidrotermal a muro das massas de sulfuretos maciços do Lousal, Faixa Piritosa Ibérica*. MSc thesis, University of Lisbon, pp. 194.

Electronic Supplementary Material 5

Geochemistry of Famennian to Visean metapelites from the Iberian Pyrite Belt: implications for provenance, paleo-redox conditions and vectoring of massive sulphide deposits

Filipa Luz[1*], António Mateus[1,2], Carlos Rosa[3], Jorge Figueiras[1,2]

[1] Instituto Dom Luiz (IDL), Faculdade de Ciências, Universidade de Lisboa, Campo-Grande 1749-016 Lisboa, Portugal – ORCID ID: 0000-0002-2913-2803

[2] Dep. Geologia, Faculdade de Ciências, Universidade de Lisboa, Ed. C6, Piso 4, 1749-016 Lisboa, Portugal

[3] CPR Lda Geology Consulting, Qta da Pedra Branca, Av. Casal Segulim, 1685-891 Famões, Portugal

*geo.filipa.luz@gmail.com

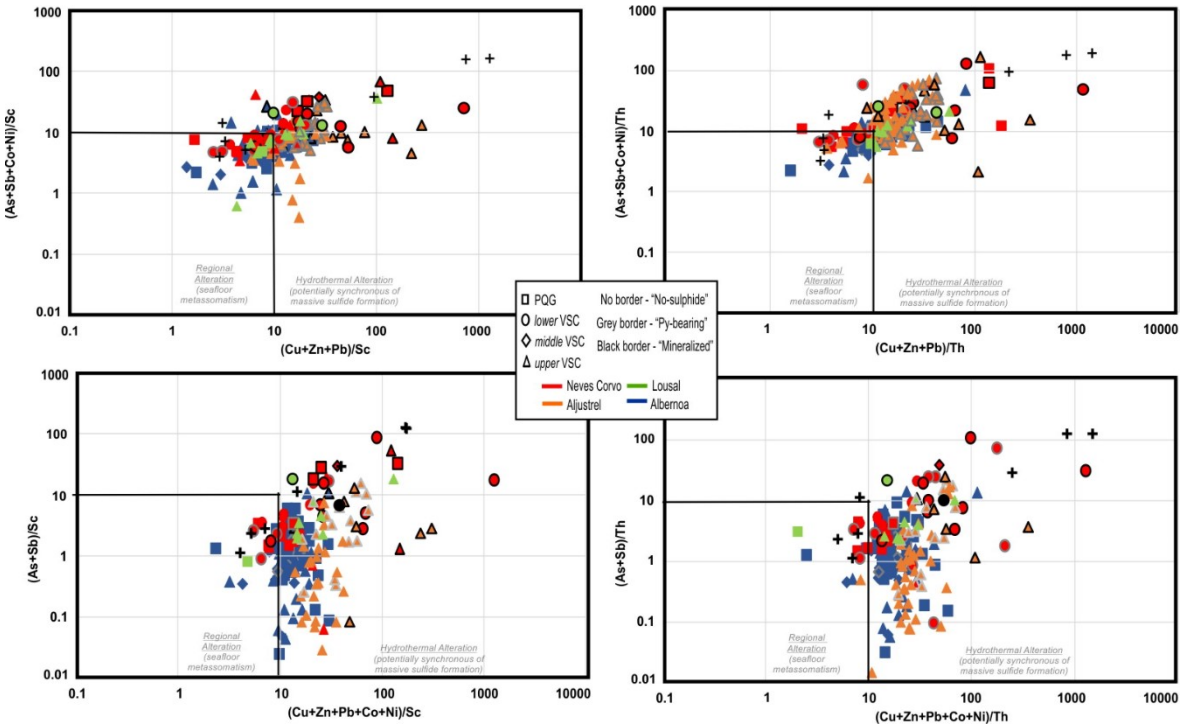

Electronic Supplementary Material 5 – (Cu+Zn+Pb)/Sc v. (As+Sb+Co+Ni)/Sc, (Cu+Zn+Pb+Co+Ni)/Sc vs. (As+Sb)/Sc, (Cu+Zn+Pb)/Th v. (As+Sb+Co+Ni)/Th, (Cu+Zn+Pb+Co+Ni)/Th vs. (As+Sb)/Th, diagram illustrating the chemical effects related to post-sedimentary transformations. Values between 1.0 and 10.0 of these geochemical ratios trace effects ascribed to oceanic metasomatism processes (*regional alteration pattern*); ratios above 10.0 indicate the proximity of hydrothermal discharges potentially related to ore-forming systems. The ore horizon of Lousal is represented by 7 non-weathered samples (**+**) reported in Fernandes (2011).

Reference: Fernandes, A. (2011). *Caracterização petrográfica, mineralógica e geoquímica do padrão de alteração hidrotermal a muro das massas de sulfuretos maciços do Lousal, Faixa Piritosa Ibérica*. MSc thesis, University of Lisbon, pp. 194.

Appendix 1.3

Pb-Nd-Sr isotope geochemistry of metapelites from the Iberian Pyrite Belt and its relevance in provenance analysis and mineral exploration surveys

under review in Economic Geology

Filipa Luz
António Mateus
Ezequiel Ferreira
Colombo C. G. Tassinari
Jorge Figueiras

Economic Geology

Pb-Nd-Sr isotope geochemistry of metapelites from the Iberian Pyrite Belt and its relevance in provenance analysis and mineral exploration surveys

--Manuscript Draft--

Manuscript Number:	SEG-D-20-00118R1
Full Title:	Pb-Nd-Sr isotope geochemistry of metapelites from the Iberian Pyrite Belt and its relevance in provenance analysis and mineral exploration surveys
Article Type:	Regular Paper
Corresponding Author:	Filipa Luz Universidade de Lisboa Faculdade de Ciencias Lisbon, PORTUGAL
Corresponding Author Secondary Information:	
Corresponding Author's Institution:	Universidade de Lisboa Faculdade de Ciencias
Corresponding Author's Secondary Institution:	
First Author:	Filipa Luz
First Author Secondary Information:	
Order of Authors:	Filipa Luz
	António Mateus
	Ezequiel Ferreira
	Colombo G. Tassinari
	Jorge Figueiras
Order of Authors Secondary Information:	
Abstract:	The Iberian Pyrite Belt (IPB) is a world-class metallogenic district from the Devonian-Carboniferous boundary in Iberian Variscides. The IPB massive sulfide ores are hosted in the lower unit of Volcano-Sedimentary Complex (VSC; Late-Famennian to Late-Visean), however at the Neves Corvo deposit occur in the uppermost levels of the Phyllite-Quartzite Group (PQG) too. A multi-system isotopic dataset (Pb-Nd-Sr; n=98) was applied to fine-grained sediments from the IPB (from Givetian to Upper-Visean), including footwall-hanging wall domains of mineralized horizons in Neves Corvo, Aljustrel and Lousal. A revision and new isotopic data for pelite rocks in the IPB was done to evaluate the sources and the potential as exploration tools together with geochemistry data. The Nd-Sr isotopic whole-rock with Th/Sc ratios shows that the IPB sediments are composed of a silicilastic mix supplied by the dismantling of an old basement. ƐNd i increments is interpreted as an incorporation of volcanic-derived contributions during sedimentation processes along/after Upper Tournaisian . The PQG succession and VSC thick piles, represent the crustal reservoirs of metals that supplied the hydrothermal inflows in IPB, which were dominated by modified seawater. More radiogenic sources should be involved when Sn- and Cu-rich fluids arise, as in Neves Corvo. The increasing of 207 Pb/ 204 Pb i ratios is sensitive to the circulation of mineralizing fluids. Rises in 206 Pb/ 204 Pb i (and 207 Pb/ 204 Pb i) in sediments bearing disseminated sulfides occur reflect a protracted interaction with radiogenic hydrothermal inflows of moderate-high temperature. The proximity to massive sulfide ore systems in the IPB sedimentary levels is observed when 207 Pb/ 204 Pb i >15.60 and Fe 2 O 3 /TiO 2 or (Cu+Zn+Pb)/Sc>10.

Subject: Manuscript Revision

Pb-Nd-Sr isotope geochemistry of metapelites from the Iberian Pyrite Belt and its relevance in provenance analysis and mineral exploration surveys

Authors: Filipa Luz; António Mateus; Ezequiel Ferreira; Colombo G. Tassinari Jorge Figueiras

(geo.filipa.luz@gmail.com; amateus@fc.ul.pt; ezequiel.geo@gmail.com; ccgtassi@usp.br; jmvf@fc.ul.pt)

Dear Larry Meinert,

Following your invitation to improve the manuscript entitled "*Pb-Nd-Sr isotope geochemistry from the Iberian Pyrite Belt and its relevance in provenance analysis and mineral exploration surveys*" we examined your specific comments.

We acknowledge the careful suggestions. All the changes were added using blue colour.

In the submitted version of the manuscript, critical information on the geological context of analysed samples were provided in Tables 1 to 4, along with the isotopic data. We recognize, however, that sampling location and the respective lithostratigraphic setting were incipiently addressed. Therefore, following your recommendation: (1) two new sentences were added to section 4; (2) a new table was created, listing all the studied samples and their attributes (site coordinates, lithostratigraphic position, relationship to the massive sulphide orebodies, etc.); and (3) figure 6 was extensively revised. In the revised version of the manuscript, and despite the information compiled in the new table (Table 1), the format of pre-existent tables (now renumbered) were kept facilitating the read each time the tables are consulted. During this revision, some typo errors were corrected, and the figure captions were improved whenever necessary, thus providing information on the data sources used in each case.

The last section (Discussion) was also checked carefully, thus ensuring that: (1) all the data needed to build up the presented plots are available in the submitted files; and (2) all the geological information required for the context of geochemical/isotopic data is provided. In consequence, some minor rephrasing or specific adding's were done.

The improvements made in this new version of the manuscript leave us confident that the work now can be revised for publication in Economic Geology.

Yours sincerely,

Filipa Luz
(Corresponding author)

Pb-Nd-Sr isotope geochemistry of metapelites from the Iberian Pyrite Belt and its relevance in provenance analysis and mineral exploration surveys

Filipa Luz[1], António Mateus[2,1], Ezequiel Ferreira[1], Colombo G. Tassinari[3], Jorge Figueiras[2,1]

[1] Instituto Dom Luiz (IDL), Faculdade de Ciências, Universidade de Lisboa, Campo-Grande 1749-016 Lisboa, Portugal – ORCID ID: 0000-0002-2913-2803

[2] Dep. Geologia, Faculdade de Ciências, Universidade de Lisboa, Ed. C6, Piso 4, 1749-016 Lisboa, Portugal

[3] Instituto de Geociências, Universidade de São Paulo, Rua do Lago, 562, 05508-900 São Paulo, SP, Brazil

Abstract

The Iberian Pyrite Belt (IPB) is a world-class metallogenic district from the Devonian-Carboniferous boundary in Iberian Variscides. The IPB massive sulfide ores are hosted in the lower unit of Volcano-Sedimentary Complex (VSC; Late-Famennian to Late-Visean), however at the Neves Corvo deposit occur in the uppermost levels of the Phyllite-Quartzite Group (PQG) too. A multi-system isotopic dataset (Pb-Nd-Sr; *n=98*) was applied to fine-grained sediments from the IPB (from Givetian to Upper-Visean), including footwall-hanging wall domains of mineralized horizons in Neves Corvo, Aljustrel and Lousal. A revision and new isotopic data for pelite rocks in the IPB was done to evaluate the sources and the potential as exploration tools together with geochemistry data. The Nd-Sr isotopic whole-rock with Th/Sc ratios shows that the IPB sediments are composed of a siliciclastic mix supplied by the dismantling of an old basement. εNd_i increments is interpreted as an incorporation of volcanic-derived contributions during sedimentation processes along/after Upper Tournaisian**.**

The PQG succession and VSC thick piles, represent the crustal reservoirs of metals that supplied the hydrothermal inflows in IPB, which were dominated by modified seawater. More radiogenic sources should be involved when Sn- and Cu-rich fluids arise, as in Neves Corvo. The increasing of $^{207}Pb/^{204}Pb_i$ ratios is sensitive to the circulation of mineralizing fluids. Rises in $^{206}Pb/^{204}Pb_i$ (and $^{207}Pb/^{204}Pb_i$) in sediments bearing disseminated sulfides occur reflect a protracted interaction with radiogenic hydrothermal inflows of moderate-high temperature. The proximity to massive sulfide ore systems in the IPB sedimentary levels is observed when $^{207}Pb/^{204}Pb_i>15.60$ and Fe_2O_3/TiO_2 or $(Cu+Zn+Pb)/Sc>10$.

Introduction

The usefulness of information provided by radiogenic isotope systems to constrain both the metal sources involved in the formation of massive sulfide deposits and their age is conclusively documented in a myriad of studies addressing volcanic- and sediment-hosted ores developed in different geological settings and timeframes (e.g. Franklin and Thorpe, 1982; Godwin and Sinclair, 1982; Swinden and Thorpe, 1984; Maas et al., 1986; Kerrich, 1991; Thorpe, 1999; Barrie et al., 1999; Prior et al., 1999; Tosdal et al., 1999; Jiang et al., 2000; Chiaradia and Fontboté, 2001; Solomon et al., 2004; Ayuso et al., 2004; Mortensen et al., 2006, 2008; Layton-Matthews et al., 2013; Turner and Kamber, 2012; Tessalina et al., 2016; Piercey and Kamber, 2019). In what concerns massive sulfide deposits of Iberian Pyrite Belt (IPB, SW Europe), radiogenic isotopes have been also crucial to significant improvements of genetic models, tracing the contribution of multiple sources for ore-forming fluids and providing additional support to explain the co-existence of different styles of mineralization (e.g. Marcoux, 1998; Pomiés et al., 1998; Mathur et al., 1999; Relvas et al., 2001; Munhá et al., 2005; Jorge et al., 2007; Carvalho, 2016). Yet, the focus of these studies has been largely the mineral phases forming the exploited ores in some paradigmatic deposits of IPB, only complemented by few surveys on the volcanic or sedimentary host rocks (e.g. Mitjavila et al., 1997; Jorge et al., 2007; Jorge, 2009). This fact strongly restrains the use of the available radiogenic isotopic data in the design of mineral exploration endeavours oriented to concealed deposits, particularly when they are hosted in shale-dominated sequences, as is the case of many sectors of the IPB.

The present study builds on preliminary results reported in Luz et al. (2019) and provides new whole-rock Pb-Nd-Sr isotopic data for 98 metapelite samples picked in four key sectors of the Portuguese segment of IPB. These samples were selected from a larger (274) collection of specimens that were comprehensively characterized by petrography and whole-rock multi-

element geochemistry (Luz et al., 2020), aiming at the: (i) assessment of geochemical features useful to the analysis of depositional environments, including redox conditions and/or geological evolution of the basin; and (ii) validation of geochemical vectors to massive sulfide ores. The selected samples represent various sections of the two main IPB lithostratigraphic units (the Phyllite-Quartzite Group and Volcano-Sedimentary Complex), typifying distal (regional background) and proximal sites of massive sulfide ores, such as those under exploitation in the Aljustrel and Neves Corvo mines. Accordingly, the main purpose of this study is to review and complement the existent isotopic information for metapelite rocks in the IPB, evaluating the sources of their main constituents and the potential of radiogenic isotopes as exploration tools, when combined with trace element geochemistry. In addition, and to better frame the interpretation of the obtained results, a thorough appraisal of published isotopic data for the IPB massive sulfide ore systems will be presented.

Regional geology

The IPB is a fundamental unit of the South Portuguese Zone (SPZ) placed immediately to the south of the Pulo do Lobo Terrane (Fig.1) that, together with the Beja-Acebuches Ophiolite Complex, outlines the SW Variscan suture (e.g. Ribeiro et al., 1990, 2007, 2010; Silva et al., 1990; Quesada et al., 1984; Quesada, 1991, 1998; Oliveira et al., 2019). This geotectonic setting was critical to the establishment of suitable conditions for the generation of numerous massive sulfide ore systems in a relatively short period of time, mostly from the Famennian/Late Strunian to mid Tournaisian (e.g. Boulter, 1996; Nesbitt et al. 1999; Mathur et al. 1999; Barrie et al. 2002; Dunning et al., 2002; Pereira et al., 2007, 2012; Rosa et al., 2009; Matos et al., 2011; Valenzuela et al., 2011; Inverno et al. 2015; Oliveira et al., 2013a, 2019; Tornos et al., 2015; Li et al. 2019). Indeed, the stress regime related to the progression of the left-lateral transpressive convergence between SPZ and the Iberian Terrane (to the north) during Carboniferous should have favoured the generation of arrays of tectonic-controlled

asymmetric (2^{nd} or 3^{rd} order) basins within a shallow continental platform covered by a thick (> 2000 m), pre-orogenic, siliciclastic mega-sequence dated of Givetian to Famennian (the so-called Phyllite-Quartzite Group, PQG; e.g. van den Boogaard, 1963; Schermerhorn, 1971; Oliveira, 1990; Oliveira et al. 2013a, 2019; Moreno et al., 1996; Jorge et al., 2006; Pereira et al., 2007; Faria et al. 2015). Some of the fault zones bounding these basins attained conditions to serve as magma conduits and, when adequate physical conditions were met, several basins became the preferred locus of recurrent deposition of volcanic products. As a result of intermittent bimodal magmatic activity, different successions of volcanic rocks (that may include a wide variety of facies) intercalated and/or inter-fingered with fine-grained sedimentary clastic rocks developed, generating the Late Famennian to Late Visean Volcano-Sedimentary Complex (VSC) whose thickness could locally exceeds 600 m (e.g. Schermerhorn, 1971; Carvalho et al., 1999; Soriano and Martí, 1999; Valenzuela et al. 2002; Donaire et al. 2002; Rosa et al. 2011; Oliveira et al. 2019). The volcanic-dominated or shale-dominated successions of VSC are the predominant hosts of the IPB massive sulfide deposits, which occur mostly as stratiform bodies often displaying large mineralized stockworks at their footwall.

The PQG and VSC pre-orogenic mega-sequences were followed by a thick (> 1600 m) syn-orogenic flysch succession (the Baixo Alentejo Flysh Group, BAFG, also known as the Culm Group), gradually younger in age towards SW and deposited from Upper Visean to Sepkhuvian-Moscovian (e.g. Schermerhorn, 1971; Oliveira, 1990; Pereira et al., 2007; 2010; Rodrigues et al., 2005). During the subsequent tectonic inversion triggered by the SPZ – Iberian Terrane oblique collision, an SW-verging, thin-skinned fold/thrust belt developed (e.g. Schermerhorn and Stanton, 1969; Silva et al. 1990, 2013; Quesada, 1991) along with metamorphic recrystallization under increasingly lower PT conditions from NE (greenschist facies) to SW (prehnite-pumpellyite; Priem et al., 1978; Munhá, 1979, 1981, 1983, 1990;

Munhá and Kerrich, 1980; Abat et al., 2001). The metamorphism is dated of 315 ± 7 Ma (Priem et al., 1978).

Despite the tectonic dismembering and stacking of slices belonging to PQG, VSC or BAFG (Fig.1), the main characteristics of pre- and syn-orogenic sequences can be assessed in various lithostratigraphic sections. The PQG siliciclastic pile comprises at present phyllites, quartzites and meta-quartzwackes, locally complemented with meta-limestone lenses in upper levels of the sequence (e.g. Moreno et al., 1996; Jorge et al., 2006; Oliveira et al., 2019). The VSC includes a large variety of sedimentary rocks but with a clear prevalence of shale/silty facies indicating deposition primacy in confined basins affecting the siliciclastic platform. In general, the lower (to intermediate) sections of VSC are represented by monotonous series of (black) metapelites or fine interchanges of metapelite/meta-siltstone levels disrupted by volcanic rocks or evolving gradually (either vertically or laterally) to volcaniclastic (matrix-supported) sediments (e.g. Schermerhorn, 1971; Soriano and Martí, 1999; Valenzuela et al., 2002; Donaire et al., 2002; Rosa et al., 2011; Oliveira et al., 2019). The upper VSC sections are, on the contrary, dominated by siliceous metapelites (some of them incorporating distal volcanic-derived components), meta-jaspers (commonly meta-cherts) and purple-green metapelites (e.g. Schermerhorn, 1971; Leistel et al., 1998a; Oliveira et al., 2013a, 2019). Volcanic rocks in VSC are largely submarine and document various events usually bracketed in the ≈360-345 Ma interval, although peaking at ≈355-350 Ma (Nesbitt et al., 1999; Mathur et al., 1999; Carvalho et al., 1999; Barrie et al., 2002; Dunning et al., 2002; Rosa et al., 2009; Valenzuela et al., 2011; Oliveira et al., 2013, 2019; Solá et al., 2015). The prevalence of felsic rocks (rhyolitic/rhyodacitic) is not regularly distributed and products of mafic (basaltic) or intermediate (andesitic) composition can be significant in some VSC sections or increase in depth (e.g. Leca et al., 1983; Munhá, 1981, 1983; Mitjavila et al., 1997; Thiéblemont et al.,

1998; Carvalho et al., 1999; Rosa et al. 2004, 2006, 2008, 2010; Codeço et al., 2018; Conde and Tornos, 2019; Donaire et al., 2020).

The massive sulfide ore systems of IPB

The IPB hosts ≈2500 Mt of massive sulfide ores distributed over ca. 90 known deposits (e.g. Strauss, 1970; Strauss et al., 1977; Sáez et al., 1996, 1999; Barriga et al., 1997; Leistel et al., 1998b; Tornos et al., 2000; Relvas et al., 2002; Inverno et al., 2015; Martín-Izard et al., 2015, 2016), eight of them classified as giant (>100 Mt), namely: Riotinto, Tharsis, Aznalcóllar-Los Frailes, Masa Valverde, Sotiel-Migollas and La Zarza, in Spain; Aljustrel and Neves Corvo, in Portugal. The origin of this huge accumulation of sulfide ores, containing more than ≈20 Mt Cu, ≈35 Mt Zn, ≈15 Mt Pb and ≈0.8 Mt Au, is not free of controversy, as documented in many studies discussing different genetic models, namely hybrid for most cases between systems of volcanogenic affiliation and exhalative-hydrothermal processes in sedimentary settings (e.g. Barriga, 1983; Barriga and Fyfe, 1988; Almodóvar et al., 1998; Sáez et al., 1999, 2011; Relvas et al., 1994, 2001, 2002, 2006a, b; Solomon et al. 2002; Solomon and Quesada, 2003; Tornos, 2006; Tornos and Heinrich, 2008; Inverno et al., 2008; Huston et al., 2011). A recent assessment of mineral associations and textures displayed by the IPB sulfide ores (Almodóvar et al., 2019) shows that early-deposited mineralization changed significantly its composition through protracted interaction with hydrothermal fluids. These changes record the progression of hydrothermal activity all along the VSC formation besides ore-zone refinements and/or chemical dispersion related to long-lived mass advection processes concurrent of Variscan deformation/metamorphism and subsequent propagation/reactivation of strike-slip fault zones in Late Variscan times (Quesada, 1998; Relvas, 2000; Marignac et al., 2003; Castroviejo et al., 2011; Codeço et al., 2018; Almodóvar et al., 2019).

Notwithstanding the variable intensity of late transformations experienced by massive sulfide ores, the early-formed mineralization should reflect seafloor hydrothermal activity during Famennian/Late Strunian to mid Tournaisian. Venting of hydrothermal fluids into (topmost PQG and/or) lower to intermediate VSC sections that comprise distinct sequences of siliciclastic and volcaniclastic sediments (with contrasting permeability, chemical reactivity and/or subjected to variable redox conditions) led to different mineralization styles: sulfide mounts, stratiform exhalative and/or replacive bodies (e.g. Barriga and Fyfe, 1998; Tornos et al., 2005; Tornos, 2006; Relvas et al., 2006a). The stratiform exhalative bodies are by far the most common style of mineralization and the preferred period for massive sulfide deposition is by large the waning stages of rhyolitic/rhyodacitic volcanic events within the variably thick VSC. Nonetheless, the emphasis ascribed in many studies to the mineralization setting has reinforced the "volcanic-hosted *vs*. shale-hosted" dichotomy, leading to a series of overviews about the separation of the two groups of deposits (Tornos 2006; Tornos et al. 1998, 2008, 2015; Tornos and Conde, 2002; Tornos and Heinrich 2008; Velasco-Acebes et al., 2019). Following this perspective, the orebodies distributed along the northern IPB (as Riotinto, Aguas Teñidas, La Zarza, Aljustrel or Lagoa Salgada) are sited in apical domains of felsic domes and were mostly generated by replacement processes of the hosting volcanic rocks in mid-Tournaisian. The orebodies spreading all over the southern IPB (as Sotiel-Migollas, Tharsis, Neves Corvo, Lousal, Las Cruces, Aznalcóllar-Los Frailes or Masa Valverde) are, on the contrary, mainly shale-hosted and typically larger (although more enriched in pyrite), their formation involving exhalative or replacement processes in euxinic basins during the Famennian/Late Strunian. This classification, although appealing in many aspects, is not free of controversy, as documented for some important exceptions, namely Neves Corvo (e.g. Relvas et al., 2001, 2006a, b; Li et al., 2019).

Regardless of the perspective on ore-forming processes, a generalized consensus exists about the alteration/mineralization patterns affecting host rocks at the orebodies footwall. These patterns are characterized by low-sulphidation mineral assemblages developed in a multi-stage process under mildly acid conditions and low to moderate temperature conditions (≈100 ± 25ºC to ≈300 ± 15ºC, considering the range of average values reported in several studies; e.g. Barriga, 1983; Leistel et al., 1998b, Relvas 2000; Sánchez-España et al. 2000; Inverno et al. 2008; Barrett et al. 2008; Moura 2008; Oliveira et al. 2011). In addition, it should be noted that these ore-related secondary mineral assemblages overprint partly or obliterate completely the mineral/textural changes previously developed in PQG or VSC rocks due to interaction with modified seawater; the so-called "regional alteration" triggered by seafloor metasomatism (e.g. Munhá and Kerrich, 1980; Munhá et al., 1980; Barriga and Kerrich, 1984; Munhá et al., 1986).

Metallogenic constraints provided by isotopic data

The relevance of hydrothermal activity in the formation of massive sulfide ores in IPB was first recognized during fieldwork performed in the seventies (Carvalho, 1976). Thus far, a wide number of petrological and geochemical studies has provided critical inputs to the understanding of the origin and evolution of these ore systems. Invaluable insights on the sources of fluids and metals involved in the mineralizing processes, as well as on their age, were provided by isotope geochemistry.

Stable isotopes

O and H isotopes

The predominance of modified seawater in the hydrothermal fluid budget of typical IPB sulfide deposits was first suggested by $\delta^{18}O$ and δD whole rock (WR) and mineral data (e.g. Munhá and Kerrich, 1984; Barriga and Kerrich, 1984; Barriga and Fyfe, 1998; Tornos and Spiro, 1999; Lerouge et al., 2001). The variable shifting of the estimated $\delta^{18}O_{Fluid}$ (up to 6‰) and δD_{Fluid}

(from ≈ -4‰ to +3‰) values in relation to $\delta^{18}O_{SMOW}$ and δD_{SMOW} were mainly interpreted as a result of isotope fractionation due to the progression of water-rock interaction under different temperature conditions and fluid/rock ratios. Accordingly, the development of common IPB massive sulfide systems should have not involved significant inputs from fluids other than deeply circulated seawater, connate waters equilibrated with the PQG siliciclastic sediments and/or combinations of these with low-grade dewatering fluids in variable mixing proportions. This reasoning is not valid for all the IPB sulfide deposits and other hypotheses should be considered to better interpret the $\delta^{18}O_{Fluid}$ and δD_{Fluid} values inferred for Neves Corvo (-0.4‰ ≤ $\delta^{18}O_{Fluid}$ ≤ +10.2‰, -37‰ ≤ δD_{Fluid} ≤ -10‰; Relvas, 2000; Relvas et al., 2006b) and several other deposits along the northern IPB (+2.7‰ ≤ $\delta^{18}O_{Fluid}$ ≤ +13.1‰, -45‰ ≤ δD_{Fluid} ≤ -10‰; Sánchez-España et al., 2003). Boiling processes and/or significant incorporation of magmatic fluids (+5‰ ≤ $\delta^{18}O_{Fluid}$ ≤ +10‰, -80‰ ≤ δD_{Fluid} ≤ -40‰) allow explain the observed isotopic shifting, as well as the high salinity (up to 24 wt% eq. NaCl; Sánchez-España et al., 2003) of hydrothermal fluids implicated in these particular ore systems. Nonetheless, within the range of the inferred isotopic fluid compositions ($\delta^{18}O_{Fluid}$ and δD_{Fluid} up to +13‰ and -45‰, respectively), the $\delta^{18}O$ and δD values do not represent by themselves irrefutable indications of the fluid origin (e.g. Huston, 1999), because they may equally document effects related to partial or total isotopic reactivation during the Variscan metamorphism and/or other late thermal events (Moura et al., 1999; Marignac and Cathelineau, 2005; Moura, 2008).

Notwithstanding the problematic origin of mineralizing fluids, a general tendency for temperature decreasing from the central zone to the periphery of the massive sulfide orebodies (≈400 to 200ºC in stockwork, ≈200 to 150ºC in massive pyritic ore and ≈150 to 100ºC in hydrothermal cherts) were evidenced with isotopic geothermometry and fluid inclusion microthermometry (Munhá et al., 1986; Almodóvar et al., 1998; Inverno et al., 2000; Sánchez-España et al., 2003; Relvas et al., 2006b). Haloes of relative $\delta^{18}O_{WR}$ depletion in felsic volcanic

rocks were also identified at Aljustrel, La Zarza and Riotinto (Barriga and Kerrich, 1984; Lerouge et al., 2001), correlating well with the type and spatial distribution of ore-related hydrothermal alteration: chloritic, stockwork ($\delta^{18}O_{WR}$ = +4 to +11‰); sericitic, peripheral ($\delta^{18}O_{WR}$ = +9 to +15‰). For Aljustrel (Estação and Feitais orebodies), Barriga and Kerrich (1984) demonstrated too that isotopic changes related to sulfide mineralization occurred in volcaniclastic rocks previously enriched in ^{18}O (as a result of "regional alteration"), further evolving with fluid/water ratio lowering and temperature increase.

C and S isotopes

Additional evidence for the involvement of modified seawater in early evolving stages of some (low temperature) IPB mineralization styles came from $\delta^{13}C$ and $\delta^{18}O$ isotopic compositions of carbonate concentrates. Results from the deposits of Aguas Teñidas ($\delta^{18}O$ = +15.3 to +18.3‰, $\delta^{13}C$ = -7.55 to +4.12‰; Sanchez-España et al., 2003), Neves Corvo ($\delta^{18}O$ = +15.6 to +22.4‰, $\delta^{13}C$ = -7.06 to -2.12‰; Relvas, 2000, Relvas et al., 2006b), Tharsis ($\delta^{18}O$ = +15.0 to +23.4‰, $\delta^{13}C$ = -10.10 to -6.4‰; Tornos et al., 1998) and Sotiel-Migollas ($\delta^{18}O$ = +14.1 to +27.8‰, $\delta^{13}C$ = -12.2 to -5.2‰; Velasco-Acebes et al., 2018) indicate that carbonates formed largely within the ≈100-175ºC temperature range. In these conditions, the $^{13}C/^{12}C$ isotopic fractioning is strongly mitigated by kinetic factors and the $\delta^{13}C_{\Sigma CO2\text{-}aqueous}$ could be used directly to characterize the C-sources of carbonates (Ohmoto, 1986). Therefore, the available isotopic compositions for carbonates forming some IPB ores suggest mixed contributions of carbon, derived from marine CO_2 ($\delta^{13}C \approx 0$‰) and oxidation of organic matter (-30‰ < $\delta^{13}C$ < -10‰) included in black shales of PQG and VSC. In general, the relevance of organic C-derived components is higher when co-existing sulfides are strongly depleted in $\delta^{34}S$.

Common IPB massive sulfide ores show a wide range of $\delta^{34}S$ values, mostly from -42‰ to +12‰; the isotopic composition of the rare barite occurrences associated with sphalerite-rich ores (peripheral domains of some deposits) varies from +15‰ to +24‰, and pyrite

disseminated in cherty rocks displays $\delta^{34}S$ values exclusively negative and around -30‰ (e.g. Yamamoto et al., 1993; Sáez et al., 1996, 1998, 2011; Velasco et al., 1998; Tornos et al., 1998, 2008; Tornos and Heinrich, 2008; Velasco-Acebes et al., 2018). Negative $\delta^{34}S$ values prevail in distal orebodies and are typical of massive sulfide ores preserving primary (sedimentary/diagenetic) arrangements, whereas sulfides recording recrystallization and/or hydrothermal replacement textures (characteristic of stockworks and of Cu-rich, matured massive sulfide ores) show more uniform and positive $\delta^{34}S$ values (usually from ≈ +3‰ to +6‰). This evident heterogeneity of $\delta^{34}S$ values reflects different mechanisms of sulphur derivation and/or sources, namely (e.g. Ohomoto, 1986; Habicht and Canfield 1997, 2001; Rudnicki et al., 2001; Seal, 2006; Shanks, 2014; Hannington, 2014; Lode et al., 2017): (i) direct contribution of seawater sulphate ($\delta^{34}S_{Sulphate}$ ≈ +15 to +20‰) in the case of the rare barite-rich occurrences; (ii) biogenic origin via microbial/biogenic sulphate reduction of seawater sulphate, microbial sulfide oxidation and microbial disproportionation of intermediate sulphur components ($\Delta^{34}S_{Sulfide\text{-}SO4}$ ≈ -40 ± 20‰), in the case of incipiently modified (early-deposited) sulfides typified by strongly negative $\delta^{34}S$ values; and (iii) hydrothermal supplying related to thermochemical reduction of seawater sulphate ($\Delta^{34}S_{Sulfide\text{-}SO4}$ ≈ -20 to 0‰ in T-pH-fO_2 conditions typical of sulfide deposition) during efficient interaction with volcanic rocks, in the case of mature sulfide ores. Subordinate incorporation of volcanogenic sulphur ($\delta^{34}S$ ≈ 2.5‰) could not be discarded in stockworks displaying $\delta^{34}S$ ≈ 0‰, even though redox fluctuations affecting $\Delta^{34}S_{Sulfide\text{-}Fluid}$ in mineralizing fluids might explain largely the range of $\delta^{34}S$ values recorded by matured massive sulfides. Nonetheless, magmatic contributions to the mineralizing process were proposed for the cassiterite ores of Neves Corvo (Li et al., 2019), considering the clustering of their $\delta^{34}S$ values near 0‰. Cassiterite samples from these ore types yield U-Pb ages of 363-366 Ma (Li et al., 2019), consistent with the age of host volcanic

rocks (Oliveira et al., 2013b) and the 347 ± 25 Ma timing estimated for the sulfide/cassiterite mineralization event using Rb-Sr isotopic analyses (Relvas et al., 2001)

Radiogenic Isotopes

Sr isotopes

The available Sr isotope data for whole-rock and ore samples from IPB are plotted in Fig. 2A, considering the initial $^{87}Sr/^{86}Sr$ values and the measured Sr abundances. Six Cu and Zn-rich sulfide ore samples were discarded of this plot due to their meaningless $(^{87}Sr/^{86}Sr)_i$ ratios, conceivably reflecting Sr losses and/or Rb gains during ore-related hydrothermal processes or late tectonic-metamorphic changes (Carvalho, 2016). Ore types from the Neves Corvo deposit display quite variable Sr abundances, although clearly higher in cassiterite-rich ores (128 ± 45 ppm) in comparison with Cu-rich (≈11 to 76 ppm) or Zn-rich (≈4 to 27 ppm) sulfide ores. The $(^{87}Sr/^{86}Sr)_i$ values obtained for these ore types are distinct (0.70993 ± 0.00043 for Sn-rich ores, 0.70979 ± 0.00152 for Cu-rich ores, and 0.71390 ± 0.00139 for Zn-rich ores), differing as well from the Sr isotope composition of both ore-related siderite (0.710881 to 0.71183; Relvas et al., 2001, Carvalho, 2016) and carbonate fractions separated from slightly altered pelitic rocks (0.70911; Velasco-Acebes et al., 2018) – Fig. 2A. Carbonate-rich ores from Tharsis and Sotiel-Migollas deposits display $^{87}Sr/^{86}Sr$ ratios similar to those of ore-related siderite at Neves Corvo, mostly ranging from 0.70934 to 0.71276 (Tornos, 2006) and from 0.70846 to 0.71284 (Velasco-Acebes et al., 2018), respectively (Fig. 2A). However, the $^{87}Sr/^{86}Sr$ ratios of carbonate fractions separated from altered metapelites of Sotiel-Migollas (0.70846 to 0.71354) expand to more radiogenic values than the values reported for comparable rocks at Neves-Corvo (Velasco-Acebes et al., 2018). All these $^{87}Sr/^{86}Sr$ ratios deviate from the range of values indicated for seawater during the Devonian-Carboniferous boundary (≈0.7080; Veizer et al., 1999), thus suggesting that other sources should have controlled the Sr isotope composition of

the fluids involved in the deposition of different ore types and carbonate-alteration of their host rocks (Fig. 2A).

Numerical approaches assuming binary mixtures (e.g. Velasco-Acebes et al., 2018) show that ambient seawater could have supplied ca. 39 to 95% of the total Sr measured in carbonate-rich ores and in carbonate fractions separated from altered metapelites. The remaining Sr incorporated in this set of samples should be related to more radiogenic sources (not completely homogenised) and modelling results suggest that footwall siliciclastic sediments represent the most plausible origin of it. Following similar reasoning, the $(^{87}Sr/^{86}Sr)_i$ values obtained for other IPB ore types are interpreted as a result of Sr mixing and homogenization between seawater-dominated hydrothermal fluids and a crustal reservoir mostly formed by the PQG and VSC siliciclastic and volcanic piles. For this reason, the $(^{87}Sr/^{86}Sr)_i$ values of non-altered PQG shales (0.71491 ± 0.0023) vary with hydrothermal alteration/mineralization intensity (0.71746 ± 0.00476 in metal-poor samples and 0.71197 ± 0.00479 in metal-rich samples), as reported in Jorge (2009; Fig. 2B). Equivalent trends are expected for volcanic rocks, but no published isotopic data exist to suitably document the anticipated shifting of $(^{87}Sr/^{86}Sr)_i$ values in comparison with those that characterize non-altered rhyolites (0.70604 ± 0.00073) and mafic/intermediate rock types (0.70406 ± 0.00052. Fig. 2B; Mitjavilla et al., 1998).

Thus, extensive infiltration of seawater into PQG and VSC sequences should be considered a key mechanism to promote compositional changes in the circulating hydrothermal fluids and rocks with which they interacted. The intensity of these changes could be quite variable, considering its dependency on many factors such as temperature conditions, permeability anisotropy, fluid/rock ratio, mixing with connate waters and depth of the circulation path, besides the chemical reactivity, Sr abundances and isotopic composition of the rock sequences crossed. Note also that, under suitable permeability conditions, the modified-seawater circuits

may eventually reach the basement beneath the thick PQG sequences, as suggested in various works (e.g. Marcoux, 1998; Relvas, 2000; Tornos, 2006).

Nd isotopes

Variations in initial ƐNd values for different ore types from Neves Corvo are evident (Fig. 3) and suggest that their formation should have involved distinct hydrothermal fluid sources and variable mixing processes. Zn-rich sulfide ores display a wide range of ƐNd (from -8.6 to +2.1) and Nd contents (0.2 to 34 ppm). This Zn-rich ore trend exclude six samples with ƐNd values < -11, Nd < 10 ppm and Sm/Nd ratios > 0.35 clearly affected by changes in REE abundances triggered by late tectono-metamorphic processes (Carvalho, 2016). High Sm/Nd ratios are related to REE fractionation along time, but after sulfide deposition, which explain the extreme negative ƐNd values. Copper-rich sulfide ores are characterized by Nd abundances extending from 0.5 to 39.24 ppm, Sm/Nd ratios of 0.33±0.11 and ƐNd ranging from -0.47 to -9.55, whereas the cassiterite-rich ores present somewhat higher Nd contents (0.363 to 69.27 ppm), similar Sm/Nd ratios (0.33±0.15) but a narrower range (-8.88 ± 1.08) of ƐNd values (Relvas et al., 2001; Carvalho, 2016). These observations suggest different Nd – ƐNd trends (Fig.3), indicating that the three ore types should have incorporated REE derived from distinct sources, which is compatible with geological information independently gathered (for details see Relvas et al., 2001; Jorge et al., 2007; Jorge, 2009; Carvalho, 2016). The compositional variations in Zn-rich sulfide ores not significantly affected by late transformations involving high-temperature hydrothermal fluids are consistent with mixing processes between three reservoirs of REE: (i) the non-altered PQG siliciclastic sediments displaying Nd = 46.59 ± 4.93 and ƐNd = -8.13 ± 0.61 (Jorge, 2009); (ii) metavolcanic rocks from VSC (mafic and felsic) with Nd = 18.03 ± 8.41 with ƐNd = -1.51 ± 2.73; and (iii) a fluid characterized by extreme lower Nd = 4.2 ppt and ƐNd ≈ -10, within the range of values inferred for seawater in epicontinental sea during Carboniferous (e.g. Li et al., 2000; Woodard et al., 2013). These REE sources should

have also be involved in the hydrothermal system related to the deposition of Cu-rich massive sulfide ores, besides chalcopyrite and pyrite in stockworks, but more extensively mixed with regional mafic/felsic VSC metavolcanic rocks (Mitjavilla et a., 1997; Donaire et al., 2020). In contrast, ℇNd values of cassiterite-rich ores denote prevalent REE derivation from a distinct reservoir without significant admixture from the VSC volcanic piles. This external reservoir could be either related to metamorphic fluids deeply circulated through older basement rocks or to high-evolved deep-seated magmatic sources different from that related to common IPB felsic melts (Relvas et al., 2001; Munhá et al., 2005).

Os isotopes

Osmium abundances discriminate well different ore types from the Neves Corvo deposit, being comparatively lower in stockwork domains (9-105 ppt and 23-109 ppt in sulfide-rich and cassiterite-rich, respectively) than in massive sulfide ores (19-669 ppt); still, no regular patterns were observed for Re distribution (Munhá et al., 2005). Considering also the Re-Os data for Tharsis and Riotinto deposits (Mathur et al., 1999), initial $^{187}Os/^{188}Os$ ratios calculated for IPB ores are too radiogenic (0.376-7.85) to represent mantle sources ($0.105 < {}^{187}Os/^{188}Os < 0.152$; Shirey and Walker, 1998), indicating the prevalence of crustal components in the ore-forming fluids. High initial $^{187}Os/^{188}Os$ ratios of pyrite in cassiterite-rich stockworks of Neves Corvo (4.89-7.85) suggest that metals in these particular ore types could not have derived exclusively from the same crustal sources involved in the development of sulfide-rich stockworks or massive sulfide ores in that deposit (Munhá et al., 2005). Indeed, the initial $^{187}Os/^{188}Os$ ratios for the latter two sulfide ore types are significantly lower, ranging from 0.451 to 1.08 and from 0.376 to 0.982, respectively (Munhá et al., 2005), which compare well with results gathered for massive sulfide ores from Aljustrel and Tharsis, excepting two $(^{187}Os/^{188}Os)_i$ values close to 4 of the Tharsis deposit.

Sulfide samples in the $^{187}Re/^{188}Os$ - $^{187}Os/^{188}Os$ isochron for the IPB (356 ± 26 Ma; Munhá et al., 2005) point to an initial $^{187}Os/^{188}Os$ ratio of 0.57 ± 0.29, which decreases to 0.49 ± 0.07 if samples other than sulfide-rich stockworks of Neves Corvo are excluded. This initial $^{187}Os/^{188}Os$ ratio is similar to that inferred for Late Devonian seawater (0.59 ± 0.05; Creaser et al., 2002) strongly suggesting that Os in these sulfides should have included significant contributions from a seawater-derived component. Extensive, although variable, interaction of seawater with radiogenic Os-rich shales included in PQG and VSC, or its mixing with connate waters trapped in these sequences, provides a plausible explanation for the initial $^{187}Os/^{188}Os$ compositions obtained for the remaining sulfides (mostly from ≈0.8 to ≈1.5, but reaching up to 4 at Tharsis). Therefore, the contrastingly high (4.89 - 7.85) radiogenic Os-signature of pyrite in the Neves Corvo cassiterite-rich stockworks indicates an additional source, conceivably related to basement rocks forming some portions of the lower continental crust (Chesley and Ruiz, 1998). This is consistent with the low εNd values for the cassiterite-rich ores.

Pb isotopes

Lead isotope systematics in the IPB was comprehensively addressed by Marcoux (1998) and so far supplemented by the works of Pomiés et al. (1999), Relvas et al. (2001), Jorge et al. (2007), Jorge (2009) and Carvalho (2016). Excluding data from Neves Corvo, the massive sulfide ores display a fairly homogeneous initial lead isotopic composition: $^{206}Pb/^{204}Pb$ = 18.18 ± 0.02, $^{207}Pb/^{204}Pb$ = 15.62 ± 0.06 and $^{208}Pb/^{204}Pb$ = 38.20 ± 0.05 (Fig. 4A). These isotopic ratios are broadly similar to the range presented by VSC felsic metavolcanic rocks ($^{206}Pb/^{204}Pb$ = 18.11 ± 0.12, $^{207}Pb/^{204}Pb$ = 15.61 ± 0.02 and $^{208}Pb/^{204}Pb$ = 38.09 ± 0.37) and PQG metasedimentary rocks ($^{206}Pb/^{204}Pb$ = 18.07 ± 0.15 $^{207}Pb/^{204}Pb$ = 15.61 ± 0.01 and $^{208}Pb/^{204}Pb$ = 37.84 ± 0.26).

All these isotopic results plot close to the Stacey and Kramers (1975) model values for contemporaneous lithospheric lead and above the orogenic curve of Doe and Zartman (1979;

Fig. 4B), suggesting the involvement of similar crustal reservoirs. This Pb isotope matching is consistent with the proposed origin for felsic magmatism in IPB (e.g. Munhá, 1981, 1983; Mitjavila et al. 1997; Thiéblemont et al. 1998; Rosa et al. 2008, 2010; Codeço et al. 2018) and, as noted in other studies (e.g. Marcoux, 1998; Relvas et al., 2001; Jorge et al., 2007), strongly suggests that hydrothermal fluids involved in deposition of common IPB massive sulfides should have equilibrated previously with the entire crustal segment underneath the shallow ore-forming systems.

A closer inspection of the available Pb-Pb data (Fig. 5A and 5B; see also Appendic Fig. 1 and Table 2 for information on $^{208}Pb/^{204}Pb$ ratios) shows, in addition, that the $^{206}Pb/^{204}Pb$ variation for common IPB massive sulfide ores is narrower than the variation displayed by $^{207}Pb/^{204}Pb$, reflecting mixing of Pb from two crustal reservoirs: one having μ values similar or slightly above the Stacey-Kramers curve (μ = 9.74) and another with higher μ values. This is particularly evident for some massive ores in the IPB Spanish segment (notably for Aznalcóllar-Los Frailles, La Zarza, Riotinto), besides Lagoa Salgada in Portugal, irrespectively of their location along the northern ("volcanic-hosted") or southern ("shale-hosted") branches of the belt. Significantly also is the deviation towards higher $^{206}Pb/^{204}Pb$ ratios showed by the sulfide ores of La Zarza, Riotinto, Aljustrel, Sierricita, Lomero-Potayos and Herrerias, possibly documenting the influence of a third crustal reservoir. These $^{207}Pb/^{204}Pb$ and/or $^{206}Pb/^{204}Pb$ shifts, already noted in previous studies (Marcoux, 1998), become clear when data from Neves Corvo are added to the dataset (Fig. 5B and C).

The exceptional nature of the Neves Corvo deposit resides in the much larger variability of initial Pb isotope compositions displayed by various ore types, coming from different orebodies or representing domains of the very same orebody variably enriched in different metals (Relvas et al., 2001; Jorge et al., 2007; Jorge, 2009; Carvalho, 2016). Polymetallic-complex, copper-rich and pyritic massive sulfide ores from the Neves orebody show heterogeneous $^{206}Pb/^{204}Pb$

and $^{207}Pb/^{204}Pb$ values, ranging from 18.20 to 18.29 and from 15.62 to 15.66, respectively (Marcoux, 1998; Carvalho, 2016). Bornite ores from the Neves orebody present isotopic ($^{206}Pb/^{204}Pb$, $^{207}Pb/^{204}Pb$) ratios varying from (18.13, 15.59), typical of IPB common massive sulfides, to (18.43, 15.87), defining a steep linear trend (Jorge et al., 2007); the lowest $^{207}Pb/^{204}Pb$ - $^{206}Pb/^{204}Pb$ bornite ore data plot close to the Stacey & Kramers (1975) model Pb-growth curve, providing a model age of ca. 348 Ma, in agreement with other geochronological estimations. The Pb isotopic ratios obtained for cassiterite concentrates representing early "stringer and massive cassiterite ores" from the Corvo orebody (Relvas et al., 2001) vary from values slightly above the massive sulfides ($^{206}Pb/^{204}Pb$ = 18.47, $^{207}Pb/^{204}Pb$ = 15.65) to highly radiogenic values ($^{206}Pb/^{204}Pb$ = 35.03, $^{207}Pb/^{204}Pb$ = 16.78). The Cu/Sn-rich ores from Corvo and Graça orebodies deviate towards high $^{206}Pb/^{204}Pb$ and/or $^{207}Pb/^{204}Pb$ ratios, scattering in between the trends defined for Cu-rich and Sn-rich massive ores (Marcoux, 1998). The Zn-rich sulfide ores of the Lombador, Corvo (SE area), Neves, Graça (SW area) and Zambujal orebodies present $^{206}Pb/^{204}Pb$ and $^{207}Pb/^{204}Pb$ ratios ranging from 18.14 to 18.25 and from 15.57 to 15.65, respectively (Carvalho, 2016), differing considerably from the radiogenic enrichment trends evidenced for the other ore types. In this regard, as noted in Carvalho (2016), the lowest $^{207}Pb/^{204}Pb$ ratio represents distal, carbonate-rich semi-massive to massive zinc ores.

Summing up the available data, five different trends of $^{207}Pb/^{204}Pb$ and/or $^{206}Pb/^{204}Pb$ variation can be distinguished, as follows (Fig. 5A to C and electronic supplementary material Appendix Fig. 1 and Table 2 for $^{208}Pb/^{204}Pb$):

(i) An exceptional increase of both Pb isotopic ratios, particularly well-documented for cassiterite-rich ores of Neves Corvo deposit and requiring the involvement of high radiogenic crustal Pb-sources external to PQG and VSC sequences, as also indicated by εNd values and $(^{187}Os/^{188}Os)_i$ ratios;

(ii) A clear increase of $^{207}Pb/^{204}Pb$ ratios coupled with slighter $^{206}Pb/^{204}Pb$ changes, displayed by common (massive and stockwork) sulfide ores of IPB, that should record the influence of different metal extractions from crustal reservoirs largely made of PQG and VSC sequences, but with noteworthy contributions of volcanic rocks and/or other crustal sources when the ores are Cu-rich;

(iii) A steep increase of $^{207}Pb/^{204}Pb$ ratios along with less important $^{206}Pb/^{204}Pb$ variations, typifying the bornite ores of Neves Corvo, which should indicate the involvement of a distinct metal source, such as old (high $^{207}Pb/^{204}Pb$) crustal rocks;

(iv) A combined decrease of $^{207}Pb/^{204}Pb$ and $^{206}Pb/^{204}Pb$ isotopic ratios, evident for common Zn-rich sulfide ores and low Cu-grade pyritic massive ores in IPB, that should denote metal supplying from PQG and/or VSC crustal reservoirs, although dominated by siliciclastic (namely shale) components; and

(v) An increase of $^{206}Pb/^{204}Pb$ without substantial changing in $^{207}Pb/^{204}Pb$ values, observed in massive ores affected by late tectono-metamorphic imprints and/or in late-stage, high-temperature Cu(± Bi, Se, Ag)-rich ores of Neves Corvo deposit (Carvalho, 2016).

Thus, metal extraction processes from PQG and VSC sequences progressing under different temperature conditions and involving seawater-dominated hydrothermal fluids were vital to the formation of common sulfide ores in the IPB. However, the development of ores displaying significant enrichments in tin and/or copper, required the participation of other fluid types and the supply of Pb from additional crustal sources to the IPB metal budgets. This supply was particularly relevant in some orebodies forming the Neves Corvo deposit, but could not be discarded in many other Cu-rich sulfide ores of IPB. Late metal inputs and/or redistributions related to mass advection mechanisms concurrent of Variscan deformation and metamorphism were locally relevant and strong enough to cause disturbances in some isotopic ratios.

Samples and analytical procedures

Ninety-eight samples of fine-grained siliciclastic rocks (some of them with volcanic-derived components) from the PQG and VSC units were chosen from a collection of 274 samples examined for multi-element geochemistry (Luz et al., 2020). The map in Fig. 6A illustrates the distribution of sampling sites and drillings across the four sectors considered in this study, from NW to SE: Lousal (including Sesmarias prospect), Aljustrel (active mine and including Gavião and Monte das Mesas prospects), Albernoa, and Neves Corvo mine.

The sampling survey was designed in accordance with the following criteria: (i) geographic distribution in the Portuguese segment of the IPB; (ii) lateral and/or vertical variations recorded by metasedimentary sequences forming the main lithostratigraphic units of the studied sectors (i.e. PQG, *lower* VSC, *middle* VSC and *upper* VSC); (iii) proximity to different massive sulfide ore bodies; and (iv) footwall and hanging-wall domains of mineralized horizons whenever in mining centres. The diagram in Fig. 6B summarizes the sampling distribution across the stratigraphic unit and sectors, making use of reconstructed lithostratigraphic columns and chronostratigraphic regional correlation for the Portuguese segment of the IPB, as comprehensively reported in Luz et al. (2020). The coordinates of each sample, as well as other supplementary information, are provided in Table 1. Far from the mining centres, the samples were collected in outcrops (n = 12) and cores from historical (n = 11) and recent (n = 14) exploration drillings. In the mining centres, the samples were picked from cores of production drillings (n = 27) and active exploitation fronts in underground mining works (n = 41).

Petrography results reported in Luz et al. (2019, 2020) show that the type and relative abundance of sulfide phases in metapelites are instrumental in correct interpretations of geochemical (multi-elemental and/or isotopic) data. Accordingly, three main categories were considered: (i) samples lacking sulfide phases at macro and micro-scale (shortly referred hereafter as “No-sulfide”); (ii) pyrite-bearing samples (“Py-bearing”) where pyrite (diagenetic

and/or recrystallized) is the sole sulfide present or largely prevails over sphalerite coupled with rare chalcopyrite; and (iii) samples including the typical sulfide assemblage in IPB ("Mineralized"), i.e. pyrite + sphalerite ± chalcopyrite ± galena along with minor or trace amounts of various As, Co, Ni ± Sb mineral phases.

Whole-rock Sr, Nd and Pb isotopic analyses were performed at the Centro de Pesquisas Geocronológicas (CPGeo), Instituto de Geociências, University of São Paulo, Brazil. About 75 to 100 mg of the same powders used for whole-rock elemental analysis were taken into solution by acid digestion (3:1 mixture of HF + HNO_3) in Savillex beakers on hot plate at 110ºC for 10 days; no spikes were added. The Sr, Nd and Pb were separated from the same sample solution in ion-exchange columns following the procedures described in Sato et al. (1995), Tassinari et al. (1996) and Babinski et al. (1999). The $^{87}Rb/^{86}Sr$, $^{147}Sm/^{144}Nd$, $(^{206}Pb/^{204}Pb)_i$, $(^{207}Pb/^{204}Pb)_i$ and $(^{206}Pb/^{204}Pb)_i$ ratios were calculated using Rb, Sr, Sm, Nd, U, Th and Pb abundances determined in the same rock-powders by ICP-MS in ActLabs and previously used in whole-rock geochemistry multi-elemental analysis (Luz et al., 2020). The Sr isotopic compositions were determined with a Thermo Triton mass spectrometer and the $^{87}Sr/^{86}Sr$ ratio was normalized to $^{86}Sr/^{88}Sr = 0.1194$. Replicate analysis of NBS 987 standard (n = 100) yielded a mean $^{87}Sr/^{86}Sr$ ratio of 0.710254 ± 0.000018 (2σ) during the period when the analytical work was performed. The Nd isotopic ratios were performed on a Thermo Neptune Plus ICP-MS. Measurements of $^{143}Nd/^{144}Nd$ were normalized to $^{146}Nd/^{144}Nd = 0.7129$ and the average (n = 107) of $^{143}Nd/^{144}Nd$ ratio for the JNdi-1 standard was 0.512003 ± 0.00003 (2σ). Pb isotopic compositions were measured with a Finnigan MAT 262 Mass Spectrometer. Replicate analysis (n = 60) of NBS-981 common Pb standard yielded $^{206}Pb/^{204}Pb = 16.892 \pm 0.006$, $^{207}Pb/^{204}Pb = 15.430 \pm 0.008$, $^{208}Pb/^{204}Pb = 36.509 \pm 006$. The Pb ratios were corrected for mass fractionation of 0.12% amu ($^{207}Pb/^{204}Pb$) and 0.13% amu ($^{206}Pb/^{204}Pb$, $^{208}Pb/^{204}Pb$) based on the NBS-981

analysis. Procedure blanks are 169 ± 76 pg for Sr, 83 ± 21 pg for Nd and 100 ± 30 pg for Pb and, considered to be negligible for the size of the analysed samples.

The age-corrections of Sr, Nd and Pb isotopic compositions were done considering 360 Ma for PQG/*lower* VSC and 350 Ma for *middle/upper* VSC (Luz et al. 2020 and references therein). All the unreasonable initial values shown in Tables 1, 2 and 3 were not considered in data interpretations. The Nd T_{DM} model ages were calculated assuming a linear depletion model with present-day depleted values of $^{143}N/^{144}Nd = 0.513151$ and $^{147}Sm/^{144}Nd = 0.2137$ (Peucat et al., 1998). Two-stage T_{DM} model ages were computed for samples with $^{147}Sm/^{144}Nd$ ratio outside the typical range of upper continental crust-derived sediments (0.09 - 0.13; e.g. Goldstein et al., 1984); a $^{147}Sm/^{144}Nd$ value of 0.114 was used to estimate the sample evolution path prior to depositional age (Goldstein and Jacobsen, 1988; Li and Schoornmaker, 2014).

Results

Rb-Sr isotope systematics

The whole-rock Sr results are presented in Table 1. Rb and Sr abundances for the PQG metapelites vary from 13 to 239 ppm and from 22 to 121 ppm, respectively. For the VSC metapelites, the Rb and Sr concentrations show wider variations, ranging from 4 to 363 ppm and from 8 to 363 ppm, respectively. General trends of relative variation in Rb and Sr contents correlate well with the mineral assemblage forming the "No-sulfide", "Py-Bearing" and "Mineralized" groups of samples. Relative enrichments in Rb (co-varying with K) and depletions in Sr reflect the prevalence of K-bearing minerals, namely fine-grained white micas, regardless of the group type. Secondary growth of carbonate phases usually account for relative minor enrichments in Sr (co-varying with Ca and Ba) observed in many samples forming these groups of rocks. When other phyllosilicates instead of mica (such as chlorite) prevail, both Rb and Sr abundances decrease significantly. In some "Mineralized" samples from Neves Corvo and Lousal sectors, documenting rock domains close to massive sulfide ores or other

mineralization styles, carbonates are occasionally coupled with REE-bearing phosphates (e.g. Relvas et al., 2006; Carvalho, 2016; Luz et al., 2019).

The initial Sr-isotopic composition for all dataset is highly variable, ranging from 0.7018 to 0.7270 (Fig. 7). Three samples displaying $(^{87}Sr/^{86}Sr)_i$ ratios below 0.700 (ALJ_RS#15, EDS1-T and SES20#6) and one above 0.800 (ABNSTR1) were discarded. These anomalous $(^{87}Sr/^{86}Sr)_i$ values likely reflect Sr losses and/or Rb gains related to disturbances caused by early hydrothermal processes or late tectono-metamorphic modifications. Considering separately the "No-sulfide", "Py-bearing" and "Mineralized" group of samples, no significant differences are observed. The higher and consequently more radiogenic $(^{87}Sr/^{86}Sr)_i$ values in the bottom units (PQG and *lower* VSC) tend to decrease to the upper units (*upper* VSC). PQG samples are characterized by 0.7174 ± 0.0052 of $(^{87}Sr/^{86}Sr)_i$ similar to values presented by Jorge (2009) for non-altered phyllites (0.7150 ± 0.0028). However, the obtained dataset show a wider variation of $(^{87}Sr/^{86}Sr)_i$ values, between 0.7103 and 0.7257, expanding the field of PQG metassediments. Equivalent $(^{87}Sr/^{86}Sr)_i$ values are presented by samples of *lower* VSC (0.7123 ± 0.0028) and *middle* VSC (0.7116 ± 0.0022). Less radiogenic values of $(^{87}Sr/^{86}Sr)_i$ characterize the *upper* VSC samples (0.7079 ± 0.0067). Therefore, the strong similarity of $(^{87}Sr/^{86}Sr)_i$ values should reflect mostly the influence of primary (siliciclastic) constituents of metapelites, despite possible variations in composition of the involved sources. For samples in the *upper* VSC sections, their lower $(^{87}Sr/^{86}Sr)_i$ values can be explained by the incorporation of local volcanic-derived fractions.

Sm-Nd isotope systematics

The Sm-Nd isotopic results are shown in Table 2. Abundances of Sm and Nd in PQG samples range from 5 to 7.7 ppm and from 25.5 to 51 ppm, respectively. For VSC metapelites, the Sm and Nd concentrations are also variable (1.4 – 14 ppm and 5.9 – 68 ppm, respectively) and no differences exist to clearly separate samples from *lower*, *middle* or *upper* sections. On the

contrary, the εNd_i values reveal some significant disparities between samples grouped according to stratigraphic criteria (Fig. 8). Samples from PQG and lower VSC sections show εNd_i scattered in the interval -11 and -7.8, consistent with the average values reported for non-altered phyllites (-8.2 ± 0.7; Jorge, 2009). This interval comprises as well the εNd_i values calculated for samples forming the sampled *middle* VSC sections, but an evident increase of εNd_i characterizes metapelites collected across the *upper* VSC sections (εNd_i up to 0). For samples included in the "Mineralized" group the calculated εNd_i values vary from -6.83 to -10 and their Nd contents do not differ significantly from those displayed by the other two groups, which agrees with the REE normalized patterns previously reported for all the samples (Luz et al., 2020). Furthermore, there are no evident isotopic differences for metapelites picked across the footwalls or hanging walls of massive sulfide orebodies.

The T_{DM} model age for the whole dataset is 1.73 ± 0.17 Ga if just the $^{147}Sm/^{144}Nd$ values between 0.09 and 0.13 are considered, i.e. the range that characterize the upper continental crust. The TDM ages are virtually indistinct for metapelites from PQG (1.83 ± 0.09 Ga) and *lower*/*middle* VSC (1.85 ± 0.08 Ga and 1.80 ± 0.03 Ga). The *upper* VSC samples display a somewhat lower T_{DM} age (1.68 ± 0.17 Ga). Thus, taking together the variations in Nd abundances, εNd_i values and T_{DM} ages it is plausible to infer a mixture of two main components: one characterized by high Nd concentrations, low εNd_i values and older T_{DM} ages, reflecting the prevalent siliciclastic source; another, typified by lower Nd abundances, relatively higher εNd_i values and younger T_{DM} ages, documenting mixing effects due to the incorporation of volcanic derived components, which are quite evident in samples forming the *upper* VSC sections (Luz et al., 2020).

Pb isotope systematics

Pb isotopic compositions for the whole dataset are shown in Table 3. The Pb abundances in PQG samples vary between 5 and 62 ppm, whereas in those from the VSC range from 5 to 903

ppm. The U and Th abundances in PQG samples are scattered within narrow ranges, spanning from 2.17 to 4.26, and from 8.79 to 17.9 ppm, respectively. Concentrations in U and Th are, in general, higher (0.57 – 37.3 and 13 – 22 ppm, respectively) for VSC samples, but subgroups representing the *lower*, *middle* and *upper* sections of this lithostratigraphic unit do not show significant differences.

Considering separately the "No-sulfide", "Py-bearing" and "Mineralized" groups of samples, no significant differences are observed in Th abundances, but U and Pb concentrations vary in presence of sulfides. In "Mineralized" samples, the Pb concentrations spread from values below the detection limit of the analytical method used (5 ppm) to 903 ppm, whereas in "No-sulfide" samples they do not exceed 99 ppm, and cluster at ca. 94 ppm in "Py-bearing" samples. The U concentrations tend also to increase from "No-sulfide" samples (0.57 to 6.94 ppm) to "Py-bearing" samples (1.40 to 15 ppm) and further to "Mineralized" samples (1.25 to 37.30 ppm).

In present-day $^{207}Pb/^{204}Pb$ and $^{208}Pb/^{204}Pb$ vs. $^{206}Pb/^{204}Pb$ diagrams, the analysed samples spread over three different groups (Fig. 9). The first and most representative group includes less radiogenic samples which are characterized by $^{206}Pb/^{204}Pb \leq 19.5$ and no significant variation of $^{207}Pb/^{204}Pb$ ratios. Samples forming the second group show a limited variation of $^{206}Pb/^{204}Pb$ ratios (from ≈19.5 to 20.5) coupled by a restricted but continuous increase of $^{207}Pb/^{204}Pb$ and $^{208}Pb/^{204}Pb$ ratios. Samples within the third group show $^{206}Pb/^{204}Pb > 20.5$ and plot along a linear array (positive co-variation between $^{207}Pb/^{204}Pb$, $^{208}Pb/^{204}Pb$ vs. $^{206}Pb/^{204}Pb$) up to 25.45. Additional insights on the real meaning of these groups are provided by the U/Pb and Th/Pb vs. U/Th ratios (Fig. 10A), and the measured Pb concentrations (Fig. 10B). In fact, when Pb abundances rest below 5 ppm, the U/Pb and Th/Pb ratios are inevitably high, but no significant U/Th variations are recorded; these samples are about the same that display high $^{207}Pb/^{204}Pb$ and $^{208}Pb/^{204}Pb$ ratios coupled with $^{206}Pb/^{204}Pb > 20.5$. When Pb abundances are

low (5 to 10 ppm), rough positive co-variations between U/Pb and Th/Pb vs. U/Th are observed. However, this separation could be over evaluated because Pb abundances below 5 ppm are not accurately measured, and so there is a strong possibility of these two subgroups become a single set. When Pb > 10 ppm, no significant variations in U/Pb and Th/Pb ratios occur, excluding a limited group of samples showing higher U/Th ratios (possibly related to U enrichment during deposition under oxygen-depleted conditions), and minor differences in $^{207}Pb/^{204}Pb$, $^{208}Pb/^{204}Pb$ vs. $^{206}Pb/^{204}Pb$ ratios are observed. Thus, considering the geochemical immobile behaviour of Th in the analysed samples (Luz et al., 2019, 2020), high U/Pb values in samples displaying low U/Th ratios could be used as a sign of significant Pb-loss. Similar inferences are supported by the Th/Pb vs. U/Th relationships, reinforcing the interpretation plausibility. In this regard, it should be noted that the enrichment in U could not be used to explain the recorded disparity because U/Th ratio is generally low for samples with high Th/Pb and U/Pb values and highly radiogenic Pb compositions (see discussion for further details).

To better constrain the Pb sources, initial Pb compositions were calculated assuming a closed system behaviour in correction of the U-decay, as reported in other studies (e.g. Marcoux, 1998; Piercey et al., 2019). Considering the reasons above presented, all the samples with Pb < 5 ppm (n =19) were excluded from the initial compositions diagrams, as well as few (n =4) samples recording overcorrected values due to radiogenic Pb. The results obtained (Fig. 11) show that "No-sulfide" samples are characterized by a wide range of initial isotopic compositions: $17.52 \leq {}^{206}Pb/^{204}Pb_i \leq 18.46$, $15.50 \leq {}^{207}Pb/^{204}Pb_i \leq 15.67$ and $36.85 \leq {}^{208}Pb/^{204}Pb_i \leq 38.45$. The initial isotopic compositions become gradually confined to smaller ranges as sulfide abundances increase. For the "Py-bearing" samples, $17.74 \leq {}^{206}Pb/^{204}Pb_i \leq 18.24$, $15.56 \leq {}^{207}Pb/^{204}Pb_i \leq 15.65$ and $37.60 \leq {}^{208}Pb/^{204}Pb_i \leq 38.31$). And for "Mineralized" samples, $17.84 \leq {}^{206}Pb/^{204}Pb_i \leq 18.94$), $15.60 \leq {}^{207}Pb/^{204}Pb_i \leq 15.67$ and $37.96 \leq {}^{208}Pb/^{204}Pb_i \leq 39.56$, approaching the values typical of IPB massive sulfide ores ($^{206}Pb/^{204}Pb \approx 18.25$,

$^{207}Pb/^{204}Pb \approx 15.63$ and $^{208}Pb/^{204}Pb \approx 38.15$; Marcoux, 1998; Relvas et al., 2001; Carvalho, 2016), despite of some few exceptions.

Discussion

Provenance of siliciclastic sediments

The combination of Nd and Sr isotopic compositions along the whole-rock immobile trace element ratios are useful to trace the provenance of siliciclastic sediments included in the PQG and VSC successions (e.g. Luz et al., 2019, 2020). In this analysis, "Mineralized" samples were excluded, fully ensuring that possible inputs related to mineralizing processes do not disturb early fingerprints preserved in samples lacking sulfide phases ("No-sulfide") or where pyrite is mainly diagenetic even if partially recrystallized ("Py-bearing"). The examined "Mineralized" metapelites only include accessory amounts of sulfides, and their Nd and Sr isotopic variations do not deviate significantly from the other two groups of samples, as showed in section 5. However, multiple REE sources are potentially involved in the formation of IPB massive ores and their alteration haloes (Relvas et al., 2001; Jorge et al., 2007; Jorge, 2009; Carvalho, 2016, Donaire et al., 2020). Furthermore, Cu- and Zn-rich ores from Neves Corvo record also considerable Sr losses and/or Rb gains due to hydrothermal activity related to ore-forming processes and/or late tectono-metamorphic reworking (e.g. Carvalho, 2016).

Metasedimentary rocks in PQG and VSC are chemically alike (Luz et al., 2019, 2020). According to discriminant geochemical factors, these rocks derive from an equivalent continental source of prevalent felsic (granitic) to intermediate (granodiorite to quartz-diorite) composition, with accessory contribution of old sedimentary rocks, although comprising different proportions of clay/mud-rich and quartz-rich components (Luz et al. 2020). The incorporation of volcanic-derived fractions during sedimentation contribute to some compositional deviations quite evident in several *upper* VSC sections (Luz et al., 2019, 2020), but other supplies should be investigated to explain the compositional variations recorded for

PQG rocks. All these component mixtures cause a spread of Nd and Sr isotopic compositions and consequent data point scattering in joint cross-plots with elemental Nd and Sr concentrations or with Th/Sc ratios (Fig. 12 A, B, C and D; Sc concentrations are listed in the electronic supplementary material 2).

Most samples display similar Nd abundances (≈30 to 54 ppm), also comparable with those presented by non-altered phyllites from PQG (45.59 ± 4.9 ppm, Fig. 12A; Jorge, 2009). The Th/Sc ratio for this particular siliciclastic mix varies between 0.5 and 1 (Fig. 12B), which is also equivalent to the range displayed by PQG and *lower* VSC samples. Therefore, sediments deposited from Giveatian to Upper Famennian times are characterized by $-11 \leq \varepsilon Nd_i \leq -8$, expanding the reference value so far used for PQG ($\varepsilon Nd_i \approx -9$; Jorge, 2009). Increments of εNd_i values and deviations towards the compositional fields of IPB metavolcanics rocks observed in the VSC metapelites reflect the variable incorporation of volcanic-derived components in the regional siliciclastic mix. This incorporation is quite variable although attaining significant weight in pelites forming several sections of the *upper* VSC (Upper Tournasian – Visean) for which the εNd_i values vary between -8 and +0.2. To summarize, the $-11 \leq \varepsilon Nd_i \leq -8$ range displayed by the Neves Corvo, Lousal and Albernoa basal units (PQG and *lower* VSC) should reflect mostly the fingerprint of regional siliciclastic mix supplied by a dismantled old crust, slightly changed via interaction with modified seawater at the Devonian-Carboniferous boundary. The binary mixing line between the two crustal reservoirs (PQG and VSC) suggests that the rising εNd_i values, up to +0.2 in the *upper* VSC section of Aljustrel sector, should be taken as an evidence for volcanic-derived contributions completed during sedimentation processes in the Upper Tournaisian to Visean times, disturbing the regional siliciclastic-derived geochemical fingerprint.

The relevance of volcanic-derived components for the whole-rock geochemical range displayed by the *upper* VSC samples is better resolved using εNd_i vs. Th/Sc plot (Fig. 12B; Appendix Table 2). Samples from Neves Corvo and part of those from the Aljustrel sector show a slight decrease in Th/Sc ratios along with an increase in εNd_i values, towards metavolcanic rocks of intermediate composition. The rise in Th/Sc ratios coupled with evident growths of εNd_i values reflect the incorporation of felsic volcanic-derived components. Recent studies (Donaire et al., 2020) extend the Nd isotopic field for IPB felsic metavolcanic rocks, and the possible presence of similar facies with Th/Sc ratios up to 4 and $\varepsilon Nd_i \approx -3$, could explain the anomalous trend displayed by some samples from Aljustrel and Lousal sectors. The incorporation of this volcanic-derived fraction in samples representing the *upper* VSC of Albernoa is minor and so they cluster nearby the PQG compositional field.

The Sr isotopic compositions also reveal differences between basal units (PQG and *lower* VSC) and the *upper* VSC. Data reported in Jorge (2009) for non-altered PQG phyllites indicate Sr abundances of ≈100 ppm and $(^{87}Sr/^{86}Sr)_i$ values around 0.715, but the dataset now compiled shows that $(^{87}Sr/^{86}Sr)_i$ values for PQG rocks spread up to 0.727. In general, samples from PQG and *lower* VSC are more radiogenic (0.710 to 0.727) than those forming the *middle* and *upper* sections of VSC (0.701 to 0.710). Most of the *upper* VSC samples from Neves Corvo and Albernoa plot within the "non-altered" and "metal-poor" PQG phyllites (Fig. 12C), but those from the remaining sectors (in particular from Aljustrel) plot along mixing lines between the seawater composition at the Devonian-Carboniferous transition (Veizer et al., 2008) and the crustal reservoirs. This suggests Sr mixing and further homogenization between seawater-dominated hydrothermal fluids and the "non-altered" PQG siliciclastic and VSC volcanic piles (Fig. 12C). In such circumstances, the high radiogenic values displayed by PQG and *lower* VSC samples could be interpreted as an imprint of compositional changes occurred during that fluid-rock interaction, under high fluid/rock ratios and involving fluids previously equilibrated

with highly radiogenic basement rocks beneath the PQG (e.g. Marcoux, 1998; Relvas et al., 2001; Tornos, 2006). Nonetheless, the observed high deviations (up to 0.727) in $(^{87}Sr/^{86}Sr)_i$ values together with almost constant and low εNd_i values of the PQG and *lower* VSC sediments can also be interpreted as an early fingerprint favouring the possibility of have a siliciclastic mix directly derived from an old basement (Fig.12D and Fig. 12E). Additional evidence supporting this interpretation come from the T_{DM} model ages.

The T_{DM} ages vary from 1.08 to 2.02 Ga and their distribution has a mean value of 1.73 ± 0.17 Ga. Three samples representing the Gafo, Ribeira de Limas and Sta. Iria formations (ca. 370 Ma, included in the Chança and Pulo do Lobo Groups – Fig. 1; Pereira et al., 2007; Oliveira et al., 2013), stratigraphically below to lateral equivalent of PQG, were also analysed for comparison purposes. These samples display the lowest εNd_i values, between -10.7 and -9.5, and a mean T_{DM} age of 1.90 ± 0.04 Ga, resembling metasedimentary rocks involved in the Meguma Terrane ≈ 1.94 ± 0.06 (Fig.13; Clarke & Halliday, 1985; Clarke et al., 1997; Braid et al., 2012). This suggests that a source of similar isotopic characteristics could have supplied the shallow SPZ continental platform in Devonian times (see also Pereira et al., 2019 and references therein). If so, mixtures of clasts derived from the dismantling of old metasediments and subvolcanic/granitoid rocks (in a proportion that roughly range from 0.75 : 0.25 to 0.55 : 0.45, assuming εNd_i values of -12 and -3 for each rock type, respectively) could explain the isotopic signature displayed by the siliciclastic mix involved in PQG and *lower* VSC sections.

A close inspection of the data shows in addition that, despite some overlap, the T_{DM} ages tend to become gradually younger from the bottom to the top of the stratigraphic sequence, notwithstanding the associated uncertainties and the limited number of samples representing the *middle* VSC sections (Fig. 13): 1.83 ± 0.09 Ga for PQG; 1.85 ± 0.08 for *lower* VSC; 1.80 ± 0.03 for *middle* VSC; and 1.68 ± 0.17 Ga for *upper* VSC. Similarly to the T_{DM} ages, the range of εNd_i values obtained for samples representing the *middle* and *upper* VSC sections (from -

10.6 to -8.5 and from -10 to +0.2, respectively) also overlaps to a great extent the range displayed by PQG and *lower* VSC samples, indicating the presence of a common siliciclastic mix across the whole PQG and VSC succession, which is irregularly modified in some *upper* VSC levels. The rising of εNd_i values and T_{DM} ages recorded by many samples of *upper* VSC could be explained by a contribution of a distinct and more juvenile source of clastic sediments supplying the basin, regionally or locally, modifying the isotopic fingerprint related to the aforementioned Meguma-type source. One hypothesis is to envisage a sporadic contribution of crustal sources alike of the Avalonia Terrane (Sm-Nd data reported in, e.g., Murphy et al., 1996; 2000) to the sedimentation process occurred in the IPB during and after the Upper Tournaisian. Another possibility, much simpler and consistent with field observations, petrographic information and multi-elemental geochemical data (Luz et al., 2020), is to consider the local input of volcanic-derived components related to the IPB magmatic activity, as briefly addressed in section 2.

Metal sources

To better constrain the metal sources involved in the IPB mineralizing processes it is central to first gather some information on U, Th, Pb and their respective ratios. As illustrated in Fig. 9 and Fig. 10, and discussed in section 5.3, samples having Pb abundances below 10 ppm display an evident increase in the present-day $^{206}Pb/^{204}Pb$, $^{207}Pb/^{204}Pb$ and $^{208}Pb/^{204}Pb$ isotopic ratios. Consequently, the very same samples show high U/Pb and Th/Pb ratios but almost invariable and low U/Th values, suggesting the possibility of depletion of the original Pb abundances. This possibility is favoured because samples with low Pb concentrations also display evident depletions in other base metals (such as Cu and Zn), as documented by the multi-element patterns normalized to NASC or AS (Luz et al., 2020). Thus, if Pb was leached during diagenesis or hydrothermal alteration, the U/Pb and Th/Pb ratios would tend to increase, enhancing the growth of uranogenic and thorogenic Pb in these samples and, as a consequence,

of the respective Pb isotopic ratios. Nonetheless, considering just the samples with Pb abundances above 10 ppm, the corresponding isotopic compositions do not seem to have experienced significant changes through time, as indicated by the minor variations of their regressed isotopic ratios. Nevertheless, in this group of samples some display high (0.5 to 4.5) U/Th values, whereas the large part is characterized by low (up to 0.5) U/Th values (Fig. 14). For the former subgroup, mostly confined to the *upper* VSC in Aljustrel, the incorporation of Pb into sulfides should have occurred below the water-sediment interface, with the enrichment in U (± Pb) conceivably related to depositional processes under reducing conditions. For the latter subgroup of samples, the low U/Th ratios should reflect largely the siliciclastic composition.

The initial Pb isotopic variations for the whole dataset (*n=75*), excluding samples with Pb abundances below the detection limit of the analytical procedure used (5 ppm), are illustrated in Fig. 15. The spreading above the Zartman & Zoe (1981) orogen curve suggests that Pb derived mostly from a radiogenic reservoir with a prevalent upper crustal component. Samples included in the "No-sulfide" and "Py-bearing" groups (that also represent distal footwall to hanging wall levels in relation to known orebodies) show a considerable scattering (Fig. 15A). However, with some exceptions, most of the data points overlap the Pb isotopic compositional fields encircling data points provided in previous studies for PQG phyllites (Jorge, 2009) and IPB felsic metavolcanics (Marcoux, 1998). The few (*n = 6*) samples displaying $^{206}Pb/^{204}Pb_i$ ratios below 17.9 are characterised by Pb abundances up to 15 ppm and the possibility of some loss of the original metal content cannot be discarded; if so, the plotted isotopic ratios are overcorrected. In the same cross-plots, samples forming the "Mineralized" group also display some dispersion (Fig. 15B), although revealing:

(i) A tendency to cluster nearby the Pb isotopic compositional field of massive sulfide ores in the Portuguese segment of IPB or to follow the isotopic trends discussed in section 3.2.4, when included in footwall levels contiguous of the Neves Corvo orebodies;

(ii) $^{206}Pb/^{204}Pb_i$ values below the empirical threshold defined for the Portuguese IPB massive sulfide ores (≈18.16), even though displaying comparable $^{207}Pb/^{204}Pb_i$ ratios (≈15.62), when part of the levels immediately below the ore horizons at the Lousal mine or at the neighbouring Sesmarias prospect;

(iii) $\approx 18.12 \leq {}^{206}Pb/^{204}Pb_i \leq \approx 18.34$, but $^{207}Pb/^{204}Pb_i \geq 15.62$, when representing the hanging wall (*upper* VSC) of massive sulfide orebodies at Aljustrel; and

(iv) $^{206}Pb/^{204}Pb_i \leq \approx 18.10$ and $^{207}Pb/^{204}Pb_i \approx 15.60$, when documenting *upper* VSC sections in the Albernoa sector, excluding two samples that plot together with those of Aljustrel.

Samples from Neves Corvo included in the "Mineralized" group (PQG, *lower* and *middle* VSC) do not show evidence of U enrichment. Their U/Th ratios (< 0.5, excepting 1 case) are typical of oxic environments and the increase in Pb contents (as well as in other elements; see Luz et al., 2020) should be related to the ore-forming hydrothermal activity, yielding limited $^{206}Pb/^{204}Pb_i$ (15.62-15.66) and $^{207}Pb/^{204}Pb_i$ (18.19-18.33) isotopic variations. In Neves Corvo, the combined decrease of $^{207}Pb/^{204}Pb$ and $^{206}Pb/^{204}Pb$ ratios recorded by few samples represent situations where sphalerite is the main disseminated sulfide phase (along with minor chalcopyrite), as described for the Lombador orebody (Carvalho, 2016). One sample display a steep increase in the $^{207}Pb/^{204}Pb$ ratio, accompanying the trend defined by Cu-rich sulfide ores (see section 3.2.4). The remaining samples plot nearby the isotopic field of IPB ores in Portugal, and the $^{206}Pb/^{204}Pb_i$ increase shown by two of them represent metapelites affected by late tectono-metamorphic imprints, being thus comparable with similar trends found in some ore samples as reported in Carvalho (2016).

Like the *lower* VSC at the footwall of some orebodies in Neves Corvo, the sample representing the level immediately below the ore horizon at the Lousal mine shows U/Th < 0.5, despite the slight deviation of its $^{206}Pb/^{204}Pb_i$ value (≈ 18.10) in relation to the empirical threshold defined for the Portuguese IPB massive sulfide ores (≈ 18.16). This contrasts with the situation represented by the sample collected at the Sesmarias prospect (Lousal sector), also illustrating a *lower* VSC level beneath the drilled ore horizon, but with U/Th ratio of 0.79. In this case, sulfide deposition could be, at least in part, associated with local redox conditions explaining also the shift to lower (≈17.98) $^{206}Pb/^{204}Pb_i$ values. The Lousal and Sesmarias ore systems share many features with the Tharsis deposit in Spain, where deposition of massive sulfide ores was mostly related to fault-controlled hydrothermal discharges in local basins with low oxygen content (e. g. Sáez et al., 2011; Fernandes, 2011). Thus, an exploratory interpretation of the Pb isotopic results for Lousal and Sesmarias samples suggests that $^{207}Pb/^{204}Pb_i$ ratio are more sensitive to mineralizing hydrothermal influxes than $^{206}Pb/^{204}Pb_i$. The latter ratio may preserve the memory of conditions attained during sedimentation/diagenesis unless the local has been affected by a vigorous and long-lived hydrothermal system of moderate to high temperature, involving radiogenic fluids.

The *upper* VSC samples from Aljustrel display the highest $^{207}Pb/^{204}Pb_i$ (15.57 to 15.65) and U/Pb (up to 4.5) ranges, along with low (up to 0.5, excepting 1 case) Th/Pb and U/Pb ratios. Considering the available data (see also Luz et al., 2020), many of these sediments should have been deposited in suboxic to anoxic conditions, favouring the early growth of pyrite, as clearly documented by the samples included in the "Py-bearing" group. Nevertheless, samples classified as "Mineralized" in this sector preserve evidence of interaction with fault-controlled mineralizing fluids, leading to epigenetic mineral assemblages enriched in sulfides and sulphosalts (Luz et al., 2019, 2020). The same is true for two "Mineralized" samples from Albernoa. These sulfides and sulphosalts are not voluminous but the hydrothermal process to

which they are related was enough contrasting to trigger a significant rise in $^{207}Pb/^{204}Pb_i$ values (≥ 15.61) together with a relative narrowing of the $^{206}Pb/^{204}Pb_i$ range (≈18.12-18.34) in comparison with the "No-sulfide" or "Py-bearing" samples.

In what concerns the remaining "Mineralized" samples from *upper* VSC sections of Albernoa sector, for which U/Th < 0.5, the interaction provided by the available Pb-Pb results clearly point to incipient hydrothermal discharges unable to change significantly the $^{206}Pb/^{204}Pb_i$ and $^{207}Pb/^{204}Pb_i$ ratios in comparison with samples of the same stratigraphic levels included in the "No-sulfide" or "Py-bearing" groups. This agrees with petrographic and geochemical evidence so far gathered for the Albernoa sector, where no signs of a robust and long-lived mineralizing system were recognized yet (Codeço et al., 2018; Luz et al. 2019, 2020).

In short, all the Pb isotopic fingerprints displayed by the studied sediments are consistent with published data for IPB ores and country rocks, as summarized in section 3. For common massive sulfide ores in IPB, the siliciclastic PQG succession should represent the main crustal reservoir of metals supplying the hydrothermal inflows dominated by modified seawater. Additional contributions for the metal budget come from VSC thick piles, but other sources should be involved when the ores are particularly enriched in Cu and Sn. These are evident in Neves Corvo deposit, leaving also signs in sediments at the footwall of orebodies as indicated by the consistent rise in $^{206}Pb/^{204}Pb_i$ and $^{207}Pb/^{204}Pb_i$ values. The $^{207}Pb/^{204}Pb_i$ ratio is quite sensitive to the circulation of mineralizing fluids. On the contrary, a protracted interaction with radiogenic hydrothermal inflows of moderate to high temperature appears to be necessary to shift significantly the $^{206}Pb/^{204}Pb_i$ (along with $^{207}Pb/^{204}Pb_i$) values of PQG and VSC sediments when bearing disseminated sulfides. Samples with Pb abundances below 5 ppm but enriched in radiogenic Pb, mostly from Neves Corvo, should represent extremely leached domains of the siliciclastic successions due to vigorous (high-temperature?) hydrothermal activity. Therefore, the joint use of Pb isotopic ratios with U/Th ratios allows to resolve several

ambiguities posed by C and S isotopes in what concerns the role of local redox conditions in the development of IPB massive sulfides ores.

Vectoring massive sulfide ore systems

The geochemical ratios can be used to assess hydrothermal mineralization in the IPB siliciclastic sequences reported in previous studies (Appendix Table 2; Luz et al., 2019, 2020). The imprints are significant and represent a useful exploration tool when Fe_2O_3/TiO_2 >10 and $Al_2O_3/[(Al_2O_3+Fe_2O_3+MnO)] \leq 0.6$. Other ratios, such as $5 \times [(Fe_2O_3+MgO+MnO/Al_2O_3)]$, (Cu+Zn+Pb)/Sc and (As+Sb)/Sc separate quite well barren and altered/mineralized sediments when above 10 (Luz et al., 2019, 2020). Crisscrossing these geochemical ratios with $^{207}Pb/^{204}Pb$ values (Fig. 16) some vectors for massive sulfide ores emerge. All the samples included in the "Mineralized" group plot above $^{207}Pb/^{204}Pb_i = 15.60$, which represents the lower limit of the uncertainty associated with the mean value estimated for the common IPB massive sulfide ores in Portugal (15.62 ± 0.02; Marcoux, 1998). Samples from PQG and *lower* VSC sections display a good positive relationship between multi-element geochemical ratios and $^{207}Pb/^{204}Pb_i$ values, reflecting the expected fingerprints related to the ore-forming processes when included in the "Mineralized" group. The same is true for samples from middle VSC despite the limited number of data points available and reduced spatial distribution, being confined to Neves Corvo and Albernoa sectors. The settings represented by samples from *upper* VSC sections are diverse and generate some scattering. Nonetheless, with very few exceptions, the *upper* VSC samples included in the "No sulfide" group tend to plot below or near the threshold values. Those forming the "Py-bearing" group tend to plot slightly above or near the thresholds but with a restrained $^{207}Pb/^{204}Pb_i$ range, in some cases possibly reflecting minor imprints of hydrothermal mineralization over early (sedimentary/diagenetic) features. And the *upper* VSC samples classified as "Mineralized" plot above thresholds without define any consistent

relationship with the remaining samples from the same stratigraphic level, documenting the irregular character of this mineralization style.

Conclusions

A Pb-Nd-Sr isotope study was conducted for a large number (n = 98) of samples representing fine-grained sediments in different sections of PQG and VSC successions of the IPB (from Givetian to Upper Visean), including the footwall and hanging wall domains of mineralized horizons in Neves-Corvo, Aljustrel and Lousal deposits. These sediments are chemically similar and the joint inspection of whole-rock Nd and Sr isotopic compositions along with Th/Sc ratios shows that they are mostly composed of a siliciclastic mix supplied by an old basement ($-11 \leq \varepsilon Nd_i \leq -8$ and $(^{87}Sr/^{86}Sr)_i$ up to 0.727), slightly changed via mixing with volcanic-derived fractions and interaction with modified seawater at the Devonian-Carboniferous boundary. The rising of εNd_i and T_{DM} ages values recorded by many samples of *upper* VSC (up to +0.2 in the Aljustrel sector) implies the involvement of a distinct and more juvenile source of clastic sediments supplying the basin in Upper Tournaisian to Visean times. This isotopic fingerprint is interpreted as a result of the local incorporation of volcanic-derived contributions completed during the sedimentation.

The Pb isotopic fingerprints displayed by the studied sediments are consistent with published data for IPB ores and country rocks. The PQG succession, at times complemented by VSC thick piles, represent the main crustal reservoirs of metals that supplied the common hydrothermal inflows in IPB, which were dominated by modified seawater. Other sources, more radiogenic, should be involved in the IPB metal budget when the role of Sn- and Cu-rich fluids became central in the ore system, as thoroughly documented for the Neves-Corvo deposit.

The increasing of $^{207}Pb/^{204}Pb_i$ ratios in sediments is sensitive to the circulation of mineralizing fluids, namely those implicated in the deposition of common IPB massive sulfides. On the contrary, significant rises in $^{206}Pb/^{204}Pb_i$ (and $^{207}Pb/^{204}Pb_i$) values in sediments bearing disseminated sulfides other than pyrite only occur when a protracted interaction with radiogenic hydrothermal inflows of moderate to high temperature is recorded. The proximity to massive sulfide ore systems could be recognized in sedimentary levels of PQG and VSC whenever $^{207}Pb/^{204}Pb_i > 15.60$, correlating well with several other multi-element geochemical ratios such as $Fe_2O_3/TiO_2 >10$ and $(Cu+Zn+Pb)/Sc > 10$.

Acknowledgements

The support of sampling surveys provided by Empresa Portuguesa de Obras Subterrâneas (EPOS, S.A), Lundin Mining, ALMINA, Empresa de Desenvolvimento Mineiro (EDM), ESAN and AVRUPA Minerals is truly appreciated. The authors are grateful to Dr. Maurício Borba for the proficient assistance in samples preparation and lab running at the Centro de Pesquisas Geocronológicas (CPGeo), Instituto de Geociências, Universidade de São Paulo, Brazil. Filipa Luz acknowledges the FCT (Fundação para a Ciência e Tecnologia) grant PD/BD/114485/2016. Additional backing from the project FCT/UID/GEO/50019/2019 (IDL) is acknowledged.

References

Abat, I., Mata, J.P., Nieto, F., Velilla, N., 2001, The phyllosilicates in diagenetic-metamorphic rocks of the South Portuguese Zone, Southwestern Portugal: Canadian Mineralogist, v. 39, p. 1571-1589.

Almodóvar, G.R., Saéz, R., Pons, J.M., Maestre, A., Toscano, M., Pascual, E., 1998, Geology and genesis of the Aznalcóllar massive sulfide deposits, Iberian Pyrite Belt, Spain: Mineralium Deposita, v. 33, p. 111-136.

Almodóvar, G.R., Yesares, L., Sáez, R., Toscano, M., González, F., Pons, J.M., 2019, Massive sulfide ores in the Iberian Pyrite Belt: mineralogical and textural evolution: Minerals, v. 9, p. 653.

Ayuso, R. A., Kelley, K. D., Leach, D. L., Young, L. E., Slack, J. F., Wandless, G., Lyon, A. M., Dillingham, J. D., 2004, Origin of the Red Dog Zn-Pb-Ag deposits, Brooks Range, Alaska: Evidence from regional Pb and Sr isotope sources: Economic Geology, v. 99, p. 1533-1553.

Barrie, C., Amelin, Y., Pascual, E., 2002, U-Pb geochronology of VMS mineralization in the Iberian Pyrite Belt: Mineralium Deposita, v. 37/8, p. 684-703.

Barrie, T., Cousens, B. L., Hannington, M. D., Bleeker, W., Gibson, H., 1999, Lead and neodymium isotope systematics of the giant Kidd Creek mine stratigraphic sequence and ore: Economic Geology Monograph 10, p. 497-510.

Barrett, J.T., Dawson, G.L., MacLean, W.H., 2008, Volcanic stratigraphy, alteration, and seafloor setting of the Paleozoic Feitais massive sulfide deposit, Aljustrel, Portugal: Economic Geology, v. 103, p. 215-239.

Barriga, F.A.J.S., 1983, Hydrothermal Metamorphism and Ore Genesis at Aljustrel, Portugal. PhD thesis, University of Western Ontario, 368 p.

Barriga, F.A.J.S., Carvalho D., Ribeiro A., 1997, Introduction to the Iberian Pyrite Belt. In: Barriga, F.A.J.S., Carvalho, D. (Eds), Geology and VMS Deposits of the Iberian Pyrite Belt. Society of Economic Geologists, Guidebook series 27, p. 1-20.

Barriga, F.J.A.S, Fyfe, W.S., 1998, Multi-phase water-rhyolite interaction and ore fluid generation at Aljustrel, Portugal: Mineralium Deposita, v.33, p. 188-207.

Barriga, F.J.A.S., Kerrich, R., 1984, Extreme ^{18}O-enriched volcanics and ^{18}O-evolved marine water, Aljustrel, Iberian Pyrite Belt: Transition from high to low Rayleigh number convective regimes: Geochimica et Cosmochimica Acta, v. 48, p. 1021-1031.

Boulter, C.A., 1996, Extensional tectonics and magmatism as drivers of convection leading to Iberian massive sulfide deposits?: Journal of Geological Society of London, v. 153, p. 181-184.

Braid, J.A., Murphy, J.B., Quesada, C., Bickerton, L., Mortensen, J.K., 2012. Probing the composition of unexposed basement, South Portuguese Zone, southern Iberia: implications for the connections between the Appalachian and Variscan Orogen. Canadian Journal of Earth Science 49, 591-613.

Carvalho, D., 1976, Considerações sobre o vulcanismo da região de Cercal-Odemira. Suas relações com a Faixa Piritosa: Comunicações dos Serviços Geológicos de Portugal, v. 60, p. 215-238.

Carvalho, D., Barriga, F.J.A.S., Munhá, J., 1999, Bimodal-siliciclastic systems – the case of the Iberian Pyrite Belt: Reviews in Economic Geology, v. 8, p. 375-408.

Carvalho, J. R. S., 2016, Zinc metallogenesis, and indium and selenium distribution at the Neves Corvo Deposit, Iberian Pyrite Belt, Portugal. PhD thesis, University of Lisbon, Portugal, 817 p.

Castroviejo R., Quesada C., Soler M., 2011, Post-depositional tectonic modification of VMS deposits in Iberia and its economic significance: Mineralium Deposita, v.46, p. 615-637.

Chesley, J. T., Ruiz, J., 1998, Crust-mantle interaction in large igneous provinces: implications from Re-Os systematics of the Colombia River flood basalts: Earth and Planetary Science Letters, v. 154, p. 1-11.

Chiaradia, M., Fontboté, L., 2001, Radiogenic lead signatures in Au-Rich volcanic-hosted massive sulfide ores and associated volcanic rocks of the Early Tertiary Macuchi Island Arc (Western Cordillera of Equador): Economic Geology, v. 96, p. 1361-1378.

Clarke, D.B., Halliday, A.N., 1985, Sm/Nd isotopic investigation of the age and origin of the Meguma Zone Metasedimentary rocks: Canadian Journal of Earth Science, v. 22, p. 102-107.

Clarke, D.B., Halliday, A.N., Hamilton, P.J., 1988, Neodymium and Strontium isotopic constraints on the origin of the peraluminous granitoids of the South Mountain batholith, Nova Scotia, Canada: Chemical Geology, v. 73, p. 15-24.

Clarke, D.B., MacDonald, M.A., Tate, M.C., 1997, Late Devonian mafic-felsic magmatism in the Meguma Zone, Nova Scotia. *In* The nature of magmatism in the Appalachian orogen. *Edited by* A.K. Sinha, J.B. Whalen and J.P. Hogan: Geological Society of America, Memoir 191, p. 107-127.

Codeço, M., Mateus, A., Figueiras, J., Gonçalves, L., Rodrigues, P., 2018. Development of the Ervidel-Roxo and Figueirinha-Albernoa volcanic sequences in Iberian Pyrite Belt, Portugal: metallogenic and geodynamic implications. Ore Geology Reviews 98: 80-108.

Conde, C., Tornos, F., 2019, Geochemistry and architecture of the host sequence of the massive sulfides in the northern Iberian Pyrite Belt: Ore Geology Reviews, https://doi.org/10.1016/j.oregeorev.2019.103042

Creaser, R. A., Sannigrahi, P., Chacko, T., Selby, D., 2002, Further evaluation of the Re-Os geochronometer in organic-rich sedimentary rocks: A test of hydrocharbon maturation effects in the Exshan Formation, Western Canada sedimentary basin: Geochimica et Cosmochimica Acta, v. 66, p. 3441-3452.

De Paolo, D.J., 1981. Neodymium isotopes in the Colorado Front Range and crust-mantle evolution in the Proterozoic: Nature, v. 291, p. 193-196.

Doe, B.R., and Zartman, R.E., 1979. Chapter 2. Plumbotectonics I, The Phanerozoic., in: H.L. Barnes (Editor), Geochemistry of Hydrothermal Ore Deposits, 2nd Ed. Wiley-Interscience, New York, N.Y, p. 22-70.

Donaire, T., Sáez, R., Pascual., E., 2002, Rhyolitic globular peperites from the Aznalcóllar mining district (Iberian Pyrite Belt, Spain): physical and chemical controls: Journal of Volcanology and Geothermal Research, v. 114, p. 119-128.

Donaire, T., Pascual, E., Sáez, R., Pin, C., Hamilton, M.A., Toscano, M., 2020, Geochemical and Nd isotopic signature of felsic volcanic rocks as a proxy of Volcanic-Hosted Massive

Sulphide deposits in the Iberian Pyrite Belt (SW, Spain): the Paymogo Volcano-Sedimentary Alignment: Ore Geology Reviews, v. 120, 10.1016/j.oregeorev.2020.103408

Dunning, G.R., Díez-Montes, A., Matas, J., Martín Parra, L.M., Almarza, J., Donaire, M., 2002, Geocronologia U/Pb del volcanismo ácido y granitódies de la Faja Pirítica Ibérica (Zona Sud Portuguesa): Geogaceta, v. 32, p. 127-130.

Faria, R., Pereira, Z., Matos, J.X., Rosa, C., Caetano Alves, M.I., Oliveira, J.T., 2015, Palynostratigraphic study of the Malhadinha sector, NE of Alvares, Mértola, Iberian Pyrite Belt: Comunicações Geológicas, v. 102(1), p. 5-11.

Faure, G., Mensing, T.M., 2005, Isotopes – Principles and Applications. Third Edition. John Wiley & Sons, 897 p.

Fernandes, A., 2011, Caracterização petrográfica, mineralógica e geoquímica do padrão de alteração hidrotermal a muro das massas de sulfuretos maciços do Lousal, Faixa Piritosa Ibérica: MSc thesis, University of Lisbon, 194 p.

Franklin, J. M., and Thorpe, R. I., 1982, Comparative metallogeny of the Superior, Slave and Churchill provinces: Geological Association of Canada, Special Paper 25, p. 3-90.

Godwin, C. I., and Sinclair, A. J., 1982, Average lead isotope growth curve for shale-hosted zinc-lead deposits, Canadian Cordillera: Economic Geology, v. 77, p. 675-690.

Goldstein, S.I., Ónions, R.K., Hamilton, P.J., 1984, A Sm-Nd isotopic study of atmospheric dust and particles from major river systems: Earth Planetary Science Letters, v. 70, p. 221-236.

Habicht, K. S., Canfield, D. E., 1997, Sulfur isotope fractionation during bacterial sulfate reduction in organic-rich sediments: Geochimica et Cosmochimica Acta, v. 61, p. 5351-5361.

Habicht, K. S., Canfield, D. E., 2001, Isotope fractionation by sulfate reducing natural populations and the isotopic composition of sulfide in marine sediments: Geology, v. 29, p. 555-558.

Hannington, M. D., 2014, Volcanogenic massive sulphide deposits, in: Holland, H. D., Turekian K. K. (Eds.): Treatise on Geochemistry 2nd edition. Elsevier Ltd., p. 319-350.

Huston, D.L., 1999, Stable isotopes and their significance for understanding the genesis of volcanic-hosted massive sulfide deposits: a review. In: Barrie, C.T., Hannington, M.D. (Eds), Volcanic-associated massive sulfide deposits: processes and examples in modern and ancient settings: Reviews in Economic Geology, v. 8, p. 157-181.

Huston, D.L., Relvas, J.M.R.S., Gemmel, J.B., Drieberg, S., 2011, The role of granites in volcanic-hosted ore forming systems: an assessment of magmatic-hydrothermal contributions: Mineralium Deposita, v. 46, p. 473-507.

Inverno, C., Díez-Montes, A., Rosa, C., García-Crespo, J., Matos, J., García-Lobón, J.L., Carvalho, J., Bellido, F., Castello-Branco, J.M., Ayala, C., Batista, M.J., Rubio, F., Granado, J., Tornos, F., Oliveira, J.T., Rey, C., Araújo, V., Sánchez-Garcá, T., Pereira, Z., Represas, P., Solá, A.R., Sousa, P., 2015. Introduction and geological setting of the Iberian Pyrite Belt. In:

Weihed, P. (Eds.),3D, 4D and Predictive Modelling of Major Mineral Belts in Europe: Mineral Resources Reviews, Switzerland, Springer, p. 191-208.

Inverno, C. M. C., Lopes, C. J. C. D., d'Orey, F. L. C., Carvalho, D., 2000, The Cu(-Au) stockwork deposito f Salgadinho, Cercal, Pyrite Belt, SW Portugal – paragenetic sequence and fluid inclusion investigation. In: Gemmell, J.B., Pongratz, J. (Eds.) Volcanic environments and massive sulphide deposits: International Conference and Field Meeting (Tasmania), p. 99-100.

Inverno, C.M.C., Solomon, M., Barton, M.D., Foden, J., 2008. The Cu stockwork and massive sulfide ore of the Feitais volcanic-hosted massive sulfide deposit, Aljustrel, Iberian Pyrite Belt, Portugal: a mineralogical, fluid Inclusion, and isotopic investigation: Economic Geology, v. 103, p. 241-267.

Jorge, R. C. G. S., 2009, Caracterização petrográfica, geoquímica e isotópica dos reservatórios metalíferos crustais, dos processos de extracção de metais e dos fluidos hidrotermais envolvidos em sistemas mineralizantes híbridos na Faixa Piritosa Ibérica: PhD thesis, University of Lisbon, Portugal, 272 p.

Jorge, R.C.G.S., Pinto, A.M.M., Tassinari, C.C.G, Relvas, J.M.R.S., Munhá, J., 2007, VHMS metal sources in the Iberian Pyrite Belt: new insights from Pb isotope data [ext. abs.]: 9th Biennal SGA Meeting Dublin, Ireland, 2007, Extended Abstract, p. 1097-1100.

Jorge, R.C.G.S., Relvas, J.M.R.S., Matos, J.X., 2006. Geochemistry of metasediments from the Phyllite-Quartzite Group, Iberian Pyrite Belt: implications for provenance and source-area weathering (progress report), VII Congresso Nacional de Geologia, Livro de Resumos I, Estremoz, Universidade de Évora, Portugal: 175-178.

Kerrich, R., 1991, Radiogenic isotope systems applied to mineral deposits. in: Heaman, L., Luden, J. N. (Eds.) Applications of radiogenic isotope systems to problems in geology: Mineralogical Association of Canada Short Course Handbook 19, p. 365-421.

Layton-Matthews, D., Leybourne, M. I., Peter, J. M., Scott, S. D., Cousens, B., Eglington, B. M., 2013, Multiple sources of selenium in ancient seafloor hydrothermal systems: Compositional and Se, S, and Pb isotopic evidence from volcanic-hosted and volcanic-sediment-hosted massive sulfide deposits of the Finlayson Lake district, Yukon, Canada: Geochimica et Cosmochimica Acta, v. 117, p. 313-331.

Leca, X., Ribeiro, A., Oliveira, J.T., Silva, J.B., Albouy, L., Carvalho, P., Merino, H., 1983, Cadre géologique des minéralisations de Neves Corvo (Baixo-Alentejo, Portugal)-Lithostratigraphie, paléogéographie et tectonique: *Mémories BRGM*, 121-1983. Éditions du BRGM, Orléans, France, p. 79.

Leistel, J. M., Marcoux, E., Deschamps, Y., 1998a, Chert in the IPB. Mineralium Deposita, v. 33, p. 59-81.

Leistel, J.M., Marcoux, E., Thiéblemont, D., Quesada, C., Sánchez, A., Ruiz de Amodóvar, G., Pascual, E., Sáez, R., 1998b, The volcanic-hosted massive sulphide deposits of the Iberian Pyrite Belt: Mineralium Deposita, v. 33, p. 2-30.

Lerouge, C., Deschamps, Y., Joubert, M., Béchu, E., Fouillac, A. M., Castro, J. A., 2001, Regional oxygen isotope systematics of felsic volcanics: a potential exploration tool for volcanogenic massive sulphide deposits in the Iberian Pyrite Belt: Journal of Geochemical Exploration, v. 72, p. 193-210.

Li, X., Zhao, K.D., Jiang, S.Y., Palmer, M.R., 2019, *In situ* U-Pb geochronology and sulfur isotopes constrains the metallogenesis of the giant Neves Corvo deposit, Iberian Pyrite Belt: Ore Geology Reviews, v. 105, 223-235.

Li, Y.-H., Schoonmaker, J.E., 2014, Chemical composition and mineralogy of marine sediments. In: Holland, H.D., Turekian, K.K. (Eds.), Sediments, Diagenesis and Sedimentary Rocks: Treatise on Geochemistry 2nd edition, Vol. 9. Elsevier Ltd., p. 1-32.

Lode, S., Piercey, S. J., Layne, G. D., Piercey, G., Cloutier, J. 2017, Multiple sulphur and lead sources recorded in hydrothermal exhalites associated with the Lemarchant volcanogenic massive sulphide deposit, central Newfoundland, Canada: Mineralium Deposita, v. 52, p. 105-128.

Luz, F., Mateus, A., Figueiras, J., Tassinari, C.C.G., Ferreira, E., Gonçalves, L., 2019, Recognizing metasedimentary sequences potentially hosting concealed massive sulphide accumulations in the Iberian Pyrite Belt using geochemical fingerprints: Ore Geology Reviews v. 107, p. 973-998.

Luz, F., Mateus, A., Rosa, C., Figueiras, J., 2020, Geochemistry of Famennian to Visean metapelites from the Iberian Pyrite Belt: Implications for Provenance, Paleo-Redox Conditions and Vectoring to Massive Sulfide Deposits: Natural Resources Research. DOI: 10.1007/s11053-020-09686-4

Maas, R., McCulloch, M. T., Campbell, I. H., Coad P. R., 1986, Sm-Nd and Rb-Sr dating of an Archean massive sulfide deposit: Kidd Creek, Ontario: Geology, v. 14, p. 585-588.

Mathur, R., Ruiz, J., Tornos, F., 1999, Age and sources of the ore at Tharsis and Rio Tinto, Iberian Pyrite Belt, from Re-Os isotopes: Mineralium Deposita, v. 34, p. 790-793.

Marcoux, E., 1998. Lead isotope systematics of the giant massive sulphide deposits in the Iberian Pyrite Belt. Mineralium Deposita 33: 45-58.

Marcoux, E., Leistel, J. M., Sobol, F., Milési, J. P., Lescuyer, J. L., Leca, X., 1992, Signature isotopique du plomb des amas sulfurés de la province de Huelva Espagne: conséquences métallogéniques et géodynamiques [ext. abs] C.R. Acad. Sci. Paris 314 II. Extended Bastracts, p. 1469-1476.

Marcoux, E., Sáez, R., 1994, Geoquímica isotópica de plomo de las mineralizaciones hidrothermales tardihercínicas de la Faja Pirítica Ibéric: Boletín Sociedad España, Mineralogia v. 17, p. 202-203.

Marignac, C., Cathelineau, M., 2005, Comment on the paper by Sánchez-España et al: Source and evolution of ore-forming hydrothermal fluids in the northern Iberian Pyrite Belt massive

sulphide deposits (SW Spain): evidence from fluid inclusions and stable isotopes: Mineralium Deposita, v. 40 (6-7), DOI: 10.1007/s00126-004-0460-x.

Marignac, C., Diagana, B., Cathelineau, M., Boiron, M.C., Banks, D., Fourcade, S., Vallance, J., 2003, Remobilisation of base metals and gold by Variscan metamorphic fluids in the south Iberian Pyrite Belt: evidence from Tharsis VMS deposit: Chemical Geology, v. 194, p. 143-165.

Martin-Izard, A., Arias, D., Arias, M., Gumiel, P., Sanderson, D.J., Castañon, C., Lavandeira, A., Sanchez, J., 2015, A new 3D geological model and interpretation of structural evolution of the world-class Rio Tinto VMS deposit, Iberian Pyrite Belt (Spain): Ore Geology Reviews, v. 71, p. 457-476.

Martín-Izard, A., Arias, D., Arias, M., Gumiel, P., Sanderson, D.J., Castañon, C., Sanchez, J., 2016. Ore deposit types and tectonic evolution of the Iberian Pyrite Belt: From transtensional basins and magmatism to transpression and inversion tectonics: Ore Geology Reviews, v. 79, p. 254-267.

Mathur, R., Ruiz, J., Tornos, F., 1999, Ages and sources of the ore at Tharsis and Rio Tinto, Iberian Pyrite Belt, from Re-Os isotopes: Mineralium Deposita, v. 34, p. 790-793.

Matos, J.X., Pereira, Z., Rosa, C.J.P., Rosa, D.R.N., Oliveira, J.T., Relvas, J.M.R.S., 2011. Late Strunian age: a key time frame for VMS deposit exploration in the Iberian Pyrite Belt. [ext. abs] 11th SGA Biennal Meeting: Let's talk about Ore Deposits, Antofagasta, Chile, 2011. Extended Abstracts, p. 790-792.

Mitjavila, J., Martí, J., Soriano, C., 1997, Magmatic evolution and tectonic setting of the Iberian Pyrite Belt: Journal of Petrology, v. 38, p. 727-755.

Moreno, C., Sierra, S., Saéz, R., 1996, Evidence for catastrophism at the Famennian-Dinantian boundary in the Iberian Pyrite Belt. in Strogen, P., Sommerville, I.D., Jones, J.L. (Ed.), Recent Advances in Lower Carboniferous Geology, London, The Geological Society of London, Special Publication, v. 106, p. 153-162.

Mortensen, J. K., Dusel-Bacon, C., Hunt, J. A., Gabites, J., 2006, Lead isotopic constraints on the metallogeny of middle and late Paleozoic syngenetic base metal occurrences in the Yukon-Tanana and Slide Mountain/Seventymile terranes and adjacent portions of the North American miogeocline: Geological Association of Canada, Special Paper 45, p. 261-279.

Mortensen, J. K., Hall, B. V., Bissig, T., Friedman, R. M., Danielson, T., Oliver, J., Rhys, D. A., Ross, K. V., Gabites, J. E., 2008, Age and paleotectonic setting of volcanogenic massive sulfide deposits in the Guerrero terrane of central Mexico: Constraints from U-Pb age and Pb isotope studies: Economic Geology, v. 103, p. 117-140.

Moura, A., 2008, Metallogenesis at the Neves Corvo VHMS deposit (Portugal): A contribution from the study of fluid inclusions: Ore Geology Reviews, v. 34(3), p. 354-368.

Moura, A., Noronha, F., Cathelineau, M., Boiron, M.-C., 1999, Metamorphic fluids in cassiterites from the Neves Corvo VMS deposit, Southern Portugal, in: Stanley, C.J. et al. (Eds.) Mineral Deposits Processes to Processing, Balkema, Rotterdam, p. 959-961.

Munhá, J., 1979, Blue amphiboles, metamorphic regime and plate tectonic modelling in the Iberian Pyrite Belt: Contributions to Mineralogy and Petrology, v. 69, p. 279-289

Munhá, J., 1981, Igneous and metamorphic petrology of the Iberian Pyrite Belt volcanic rocks: Doctoral Thesis, University of Western Ontario, Canada.

Munhá, J., 1983, Low-grade regional metamorphism in the Iberian Pyrite Belt: Comunicações dos Serviços Geológicos de Portugal, v. 69, p. 3-36.

Munhá, J., 1990, Metamorphic evolution of the South Portuguese/ Pulo do Lobo Zone, in: Dallmeyer, R.D., Martínez García, E. (Eds), Pre-Mesozoic Geology of Iberia, Berlin, Springer Berlin Heidelberg, p. 363-369.

Munhá, J., Barriga, F.J.A.S., Kerrich, R., 1986, High ^{18}O ore-forming fluids in volcanic-hosted base metal massive sulfide deposits; geologic, $^{18}O/^{16}O$, and D/H evidence from the Iberian Pyrite Belt; Crandon, Wisconsin; and Blue Hill, Maine: Economic Geology, v. 81(3), p. 530-552.

Munhá, J., Fyfe, W.S., Kerrich, R., 1980, Adularia, the characteristic mineral of felsic spilites: Contributions to Mineralogy and Petrology, v. 75, p. 15-19.

Munhá, J., Kerrich, R., 1980. Seawater basalt interaction in spilites from the Iberian Pyrite Belt: Contributions to Mineralogy and Petrology, v. 73, p. 191-200.

Munhá, J., Relvas, J. M. R. S., Barriga, F. J. A. S., Conceição, P., Jorge, R. C. G. S., Mathur, R., Ruiz, J., Tassinari, C. C. G., 2005, Os isotopes systematics in the Iberian Pyrite Belt, in: Mao J, Bierlein FP (eds) Mineral Deposit Research: meeting the global challenge. Springer, Berlin, p. 663-666.

Murphy, J.B., Keppie, J.D., Dostal, J., Waldron, J.W.F., Cude, M., 1996, Geochemical and isotopic characteristics of Early Silurian clastic sequences in Antigonish Highlands, Nova Scotia, Canada: constraints on the accretion of Avalonia in the Appalachian – Caledonide Orogen: Canadian Journal of Earth Sciences, v. 33(3), p. 379-388.

Murphy, J.B., Strachan, R.A., Nance, R.D., Parker, K.D., Fowler, M.B., 2000, Proto-Avalonia: a 1.2-1.0 Ga tectonothermal event and constraints for the evolution of Rodinia: Geology, v. 28(12), p. 1071-1074.

Nesbitt, R.W., Pascual, E., Fenning, C.M., Toscano, M., Sáez, R., Almodóvar, R.G., 1999, U-Pb dating of stockwork zircons from the eastern Iberian Pyrite Belt: Journal of Geological Society of London, v. 156, p. 7-10.

Ohmoto, H., 1986, Stable isotope geochemistry of ore deposits, in: Valley, J. W., Taylor H. P., O'Neil, J. R. (Eds.) Stable isotopes: Reviews in Mineralogy, v. 16, p. 491-559.

Oliveira, D.P.S., Matos, J.X., Rosa, C.J.P., Rosa, D.R.N., Figueiredo, M.O., Silva, T.P., Guimarães, F., Carvalho, J.R.S., Pinto, Á.M.M., Relvas, J.M.R.S., Reiser, F.K.M., 2011, The Lagoa Salgada orebody, Iberian Pyrite Belt, Portugal: Economic Geology, v. 106, p. 1111-1128.

Oliveira, J.T., 1990, Stratigraphy and syn-sedimentary tectonism in the South Portuguese Zone. in: Dallmeyer, R.F. & Martinez-Garcia (Eds). Pre-Mesozoic Geology of Iberia, Springer-Verlag, p. 334-347.

Oliveira, J.T., Quesada, C., Pereira, Z., Matos, J.X., Solá, A.R., Rosa, D., Albardeiro L., Díez-Montes, A., Morais, I., Inverno, C., Rosa, C., Relvas, J., 2019, South Portuguese Terrane: A continental affinity exotic unit, in: C. Quesada and J. T. Oliveira (eds.), The Geology of Iberia: A Geodynamic Approach, Regional Geology Reviews, vol. 2, Springer-Verlag, p. 173-206.

Oliveira, J.T., Relvas, J.M.R.S., Pereira, Z., Matos, J.X., Rosa, C.J., Rosa, D., Munhá, J.M., Fernandes, P., Jorge, R.C.G.S., Pinto, A.M.M., 2013a, Geologia da Zona Sul Portuguesa, com ênfase na estratigrafia, vulcanologia física, geoquímica e mineralizações da Faixa Piritosa, in: Dias, R., Araújo, A., Terrinha, P.E., Kullberg, J.C. (Eds). Geologia de Portugal. Vol. I – Geologia Pré-Mesozóica de Portugal, Escolar Editora, p. 673-766.

Oliveira, J.T., Rosa, C.J.P., Rosa, D.R.N., Pereira, Z., Matos, J.X., Inverno, C.M.C., Andersen, T., 2013b, Geology of the Neves-Corvo antiform, Iberian Pyrite Belt, Portugal: new insights from physical volcanology, palynostratigraphy and isotope geochronology studies: Mineralium Deposita, v. 48, p. 748-766.

Pereira M.P., Brandão Silva J., Gama C. (2019). Comment on Baltic provenance of top-Famennian siliciclastic material of the northern Rhenish Massif, Rhenohercynian zone of the Variscan orogen, by Koltonik et al., International Journal of Earth Sciences (2018) 107:2645–2669. International Journal of Earth Sciences, 108:1067–1073

Pereira, Z., Matos, J.X., Fernandes, P., Jorge, R.G.S., Oliveira, J.T., 2010, Qual a idade mais antiga da Faixa Piritosa. Nova idade Givetiano inferior para o Grupo Filito-Quartzítico (Anticlinal São Francisco da Serra), Faixa Piritosa: Revista Electrónica de Ciências da Terra, v. 17(13), p. 4.

Pereira, Z., Matos, J., Fernandes, P., Oliveira, J.T., 2007, Devonian and Carboniferous palynostratigraphy of the South Portuguese Zone, Portugal – an overview: Comunicações Geológicas, v. 94, p. 53-79.

Pereira, Z., Matos, J.X., Rosa, C., Oliveira, J.T., 2012, Palynostratigraphic importance of the Strunian in the Iberian Pyrite Belt. [ext. abs]: 45th Annual Meeting AASP Abs, Lexington, KY, USA, Extended Abstract, p. 42-43.

Peucat, J.J., Vidal, O., Bernard-Griffiths, J., Condie, K.C., 1989, Sr, Nd, and Pb isotopic systematics in the Archean low- to high-grade transition zone of southern India: syn-accretion vs post-accretion granulites: Journal of Geology, v. 97, p. 537-549.

Piercey S. J., Kamber, B. S., 2019, Lead isotope geochemistry of shales from the Wolverine volcanogenic massive sulfide deposit, Yukon: implications for Pb isotope vectoring in exhalative ore systems: Economic Geology, v. 114, p. 47-66.

Pomiès, C., Cocherie, A., Guerrot, C., Marcoux, E., Lancelot, J., 1998, Assessment of the precision and accuracy of lead-isotope ratios measured by TIMS for geochemical applications: example of massive sulphide deposits (Rio Tinto, Spain): Chemical Geology, v. 144, p. 137-149.

Priem, H.N.A., Boelrijk, N.A.I.M., Hebeda, E.H., Schermerhorn, L.J.G., Verdurmen, E.A.Th., Verschure, R.H., 1978, Sr isotopic homogenization through whole-rock systems under low greenschist facies metamorphism in Carboniferous pyroclastics at Aljustrel (Southern Portugal): Chemical Geology, v. 21, p. 307-314.

Prior, G. J., Gibson, H. L., Watkinson, D. H., Cousens, B. L., Cook, E. E., Batie, T., 1999, Sm-Nd isotope study of rhyolites from the Kidd Creek Mine area, Abitibi Subprovince, Canada. In Hannington, M. D. and Barrie, T. (Eds): Economic Geology Monograph 10: The Giant Kidd Creek Volcanogenic Massive Sulfide Deposit, Western Abitibi Subprovince, Canada, p. 485-496.

Quesada, C., 1991, Geological constraints on the Paleozoic tectonic evolution of the tectonostratigraphic terranes in the Iberian Massif: Tectonophysics, v. 185, p. 225-245.

Quesada, C., 1998, A reappraisal of the structure of the Spanish segment of the Iberian Pyrite Belt: Mineralium Deposita, v. 33, p. 31-44.

Quesada, C., Fonseca, P., Munhá, J., Oliveira, J., Ribeiro, A., 1984, The Beja-Acebuches Ophiolite (Southern Iberia Variscan fold belt): geological characterization and geodynamic significance: Boletin Geológico y Minero, v. 105(1), p. 3-49.

Relvas, J.M.R.S., 2000, Geology and metallogenesis at the Neves Corvo, Portugal: PhD Thesis. University of Lisbon, Portugal, 250 p.

Relvas, J.M.R.S., Barriga, F.J.A.S., Bernardino, F.B.C.P., Oliveira, V.M.S., Matos, J.X., 1994, Ore zone hydrothermal alteration in drill hole IGM-LS1 Lagoa Salgada, Grândola, Portugal: A first report on pyrophyllite in a central stockwork: Boletín Sociedad Española Mineralogia, v. 17, p. 157-158.

Relvas, J.M.R.S., Barriga, F.J.A.S., Pinto, A., Ferreira, A., Pacheco, N., Noiva, P., Barriga, G., Baptista, R., Carvalho, D., Oliveira, V., Munhá, J., Hutchinson, R.W., 2002, The Neves-Corvo deposit, Iberian Pyrite Belt, Portugal: Impacts and future, 25 years after the discovery, in: Goldfarb R, Nielsen J (Ed) Integrated Methods for discovery. SEG Special Publication 9, p. 155-176.

Relvas, J. M. R. S., Tassinari, C. C. G., Munhá, J., Barriga, F. J. A. S., 2001, Multiple sources for ore-forming fluids in the Neves-Corvo VHMS deposit of the Iberian Pyrite Belt (Portugal): strontium, neodymium and lead isotope evidence: Mineralium Deposita, v. 36, p. 416-427.

Relvas, J.M.R.S., Barriga, F.J.A.S., Ferreira, A., Noiva, P.C., Pacheco, N., Barriga, G., 2006a, Hydrothermal alteration and mineralization in the Neves-Corvo volcanic hosted massive sulfide deposit, Portugal: I. Geology, mineralogy and geochemistry: Economic Geology, v. 101, p. 791-804.

Relvas, J.M.R.S., Barriga, F.J.A.S., Longstaffe, F.J., 2006b, Hydrothermal alteration and mineralization in the Neves-Corvo volcanic-hosted massive sulfide deposit, Portugal: II. Oxygen, hydrogen, and carbon isotopes: Economic Geology, v. 101, p. 753-790.

Ribeiro, A., Quesada, C., Dallmeyer, R.D., 1990, Geodynamic evolution of the Iberian Massif, in: Dallmeyer, R.D., Martínez Garcia, E. (Ed), Pre-Mesozoic Geology of Iberia, Berlin, Springer Berlin Heidelberg, p. 334-347.

Ribeiro, A., Munhá, J., Dias, D., Mateus, A., Pereira, E., Ribeiro, L., Fonseca, P., Araújo, A., Oliveira, J.T., Romão, J., Chaminé, H., Coke, C., Pedro, J., 2007, Geodynamic evolution of the SW Europe Variscides: Tectonics, v. 26, TC6009.

Ribeiro, A., Munhá, J., Fonseca, P.E., Araújo, A., Pedro, J.C., Mateus, A., Tassinari, C., Machado, G., Jesus, A.P., 2010, Variscan ophiolite belts in the Ossa-Morena Zone (Southwest Iberia): geological characterization and geodynamic significance: Gondwana Research, v. 17, p. 408-421.

Rodrigues, B., Chew, D.M., Jorge, R.C.G.S., Fernandes, P., Veiga-Pires, C., Oliveira, J.T., 2015, Detrital zircon geochronology of the Carboniferous Baixo Alentejo Flysch Group (South Portugal); constraints on the provenance and geodynamic evolution of the South Portuguese Zone: Journal of the Geological Society, v. 172, p. 294-308.

Rosa, C.J.P., McPhie, J., Relvas, J., 2010, Type of volcanoes hosting the massive sulfide deposits of the Iberian Pyrite Belt: Journal of Volcanology and Geothermal Resources, v. 194, p. 107-126.

Rosa, C.J.P., McPhie, J., Relvas, J., 2011, Sediment-matrix igneous breccias at the top contacts of felsic units in the IPB: implications for VHMS exploration, [ext. abs.]11th SGA Biennal Meeting Abstracts, Antofagasta, Chile, Extended abstract, p. 754-756.

Rosa, C.J.P., McPhie, J., Relvas, J., Pereira, Z., Oliveira, T., Pacheco, N., 2008. Volcanic setting of the giant Neves Corvo massive sulfide deposit, Iberian Pyrite Belt, Portugal. Mineralium Deposita 43: 449-466.

Rosa, D., Inverno, C., Oliveira, V., Rosa, C., 2004, Geochemistry of volcanic rocks, Albernoa area, Iberian Pyrite Belt, Portugal: International Geology Reviews, v. 46, p. 366-383.

Rosa, D., Inverno, C., Oliveira, V., Rosa, C., 2006. Geochemistry and geothermometry of volcanic rocks from Serra Branca, Iberian Pyrite Belt, Portugal. Gondwana Research 10: 328-339.

Rosa, D.R.N., Finch, A.A., Andersen, T., Inverno, C.M.C., 2009, U-Pb geochronology and Hf isotope ratios of magmatic zircons from the Iberian Pyrite Belt: Mineralogy and Petrology, v. 95, p. 47-69.

Rudnicki, M. D., Elderfield, H., Spiro, B., 2001, Fractionation of sulfur isotopes during bacterial sulfate reduction in deep ocean sediments at elevated temperatures, Geochimica et Cosmochimica Acta, v. 65, p. 777-789.

Saéz, R., Almodóvar, G.R., Pascual, E., 1996, Geological constraints on massive sulphide genesis in the Iberian Pyrite Belt: Ore Geology Reviews, v. 11, p. 429-451.

Saéz, R., Pascual, E., Toscano, M., Almodóvar, G.R., 1999, The Iberian type of volcano-sedimentary massive sulphide deposits: Mineralium Deposita, v. 34, p. 549-570.

Saéz, R., Moreno, C., González, F., Almodóvar, G.R., 2011, Black shales and massive sulfide deposits: causal or casual relationships? Insights from Rammelsberg, Tharsis, and Draa Sfar: Mineralium Deposita, v. 46, p. 585-614.

Sánchez-España, J., Velasco, F., Boyce, A. J., Fallick, A. E., 2003, Source and evolution of ore-forming hydrothermal fluids in the northern Iberian Pyrite Belt massive sulphide deposits (SW Spain): evidence from fluid inclusions and stable isotopes: Mineralium Deposita, v. 38, p. 519-537.

Sánchez-España, J., Velasco, F., Yusta, I., 2000, Hydrothermal alteration of felsic volcanic rocks associated with massive sulfide deposition in the northern Iberian Pyrite Belt (SW Spain): Applied Geochemistry, v. 15, p. 1265-1290.

Samson, S.D., Barr, S.M., White, C.E., 2000, Nd isotopic characteristics of terranes within the Avalon zone, southern New Brunswick: Canadian Journal of Earth Sciences, v. 37(7), p. 1039-1052.

Schermerhorn, L.J.G., 1971, An outline stratigraphy of the Iberian Pyrite Belt: Boletin Geológico y Minero, v. 82 (3/4), p. 239-268.

Schermerhorn, L.J.G., Stanton, W.I., 1969, Folded overthrusts at Aljustrel (South Portugal). Geological Magazine, v. 160(2), p. 130-141.

Seal, R. R. II, 2006, Sulphur isotope geochemistry of sulphide minerals: Reviews in Mineralogy and Geochemistry, v. 61, p. 633-677.

Shanks, W. C., 2014, Stable isotope geochemistry of mineral deposits, in: Turekian, H. D. H. K. (Ed.): Treatise on geochemistry, 2nd ed. Elsevier, Oxford, p. 59-85.

Shirey, S. B., Walker, R. J., 1998, The Re-Os isotope system in cosmochemistry and high temperature geochemistry: Annual Review of Earth Planetary Sciences, v. 26, p. 423-500.

Silva, J.B., Oliveira, J.T., Ribeiro, A., 1990, Structural outline of the South Portuguese Zone. in: Dallmeyer, R.D., Martínez García, E. (Eds.), Pre-Mesozoic Geology of Iberia, Berlin, Springer Berlin Heidelberg, p. 348-362.

Silva, J.B., Pereira, M.F., Chichorro, M., 2013, Estruturas das áreas internas da Zona Sul Portuguesa, no contexto do órogeno Varisco, in: Dias, R., Araújo, A., Terrinha, P.E., Kullberg, J.C. (Eds). Geologia de Portugal. Vol. I – Geologia Pré-Mesozóica de Portugal, Escolar Editora, p. 767-780.

Solá, A.R., Salgueiro, R., Pereira, Z., Matos, J.X., Rosa, C., Araújo, V., Neto, R., Lains, J.A., 2015. Time span of the volcanic setting of the Neves-Corvo VHMS deposit. [ext. abs]: X Congresso Ibérico de Geoquímica/XVII Semana da Geoquímica, Extended Abstract, p. 120-123.

Soriano, C., Martí, J., 1999, Facies analysis of volcano-sedimentary successions hosting massive sulfide deposits in the Iberian Pyrite Belt, Spain: Economic Geology, v. 94, p. 867-882.

Solomon M., Gemmell J. B., Zaw, K., 2004, Nature and origin of the fluids responsible for forming the Hellyer Zn-Pb-Cu, volcanic-hosted massive sulfide deposit, Tasmania, using fluid inclusions, and stable and radiogenic isotopes: Ore Geology Reviews, v. 25, p. 89-124.

Solomon, M., Quesada, C., 2003, Zn-Pb-Cu massive sulphide deposits: brine-pool types occur in collisional orogens, black smoker types occur in back arc and/or arc basins: Geology, v. 31, p. 1029-1032.

Solomon, M., Tornos, F., Gaspar, O.C., 2002, A possible explanation for many of the unusual features of the massive sulfide deposits of the Iberian Pyrite Belt: Geology, v. 30, p. 87-90.

Stacey, J. S., Kramers, J. D., 1975, Approximation of terrestrial lead isotopic evolution by a two-stage model: Earth and Planetary Science Letters, v. 26, p. 207-221.

Strauss, G., 1970, Sobre la geologia de la provincia piritífera del SW de la Península Ibérica y de sus yacimientos, en especial sobre la mina de pirita de Lousal (Portugal): Memoria Instituto Tecnológico Geominero de España, v. 77, 266 p.

Strauss, G.K., Madel, J., Fernández Alonso, F. 1977, Exploration practice for stratabound volcanogenic sulphide deposits in the Spanish-Portuguese Pyrite Belt: Geology, geophysics, and geochemistry, in: Klemm, D.D., Schneider, H.J. (eds.). Time and stratabound ore deposits. Berlin, Springer-Verlag, p. 55-93.

Swinden, H. S., Thorpe, R. I., 1984, Variations in style of volcanism and massive sulfide deposition in Early to Middle Ordovician island-arc sequences of the Newfoundland Central mobile belt: Economic Geology, v. 79 p. 1596-1619.

Tessalina S. G., Herrington, R. J., Taylor, R. N., Sundblad, K., Maslennikov, V.V., Orgeval, J.-J., 2016, Lead isotopic systematics of massive sulphide deposits in the Urals: applications for geodynamic setting and metal sources: Ore Geology Reviews, v. 72, p. 22-36.

Thiéblemont, D., Pascual, E., Stein, G., 1998, Magmatism in the Iberian Pyrite Belt: petrological constraints on a metallogenetic model: Mineralium Deposita, v. 33, p. 98-110.

Thorpe, R. I., 1999, The Pb isotope linear array for volcanogenic massive sulfide deposits of the Abitibi and Waawa subprovinces, Canadian Shield: Economic Geology Monograph 10, p. 555-575.

Tornos, F., 2006, Environment of formation and styles of volcanogenic massive sulfides: the Iberian Pyrite Belt: Ore Geology Reviews, v. 28, p. 259-307.

Tornos, F., Barriga, F., Marcoux, E., Pascual, E., Pons, J.M., Relvas, J., Velasco, F., 2000, The Iberian Pyrite Belt, in: Large, R., Blundell, D. (Eds), Database on global VMS districts: CODES-GEODE, p. 19-52.

Tornos, F., Conde, C., 2002, La influencia biogénica en la formación de los yacimientos de sulfuros masivos de la Faja Pirítica Ibérica: Geogaceta, v. 32, p. 235-238.

Tornos, F., González Clavijo E., Spiro, B., 1998, The Filon Norte orebody (Tharsis, Iberian Pyrite Belt): a proximal low-temperature shale hosted massive sulfide in a thin-skinned tectonic belt: Mineralium Deposita, v. 33, p. 150-169.

Tornos, F., Heinrich, C.A., 2008. Shale basins, sulfur-deficient ore brines and the formation of exhalative base metals deposits: Chemical Geology, v. 247, p. 195-207.

Tornos, F., Peter, J.M., Allen, R.L., Conde, C., Peter, F., Conde, R., 2015, Controls on the siting and style of volcanogenic massive sulphide deposits: Ore Geology Reviews, v. 68, p. 142-163.

Tornos, F., Solomon, M., Conde, C., Spiro, B., 2008, Formation of the Tharsis massive sulfide deposit, Iberian Pyrite Belt: geological, lithogeochemical, and stable Isotope evidence for a deposition in a brine Pool: Economic Geology, v. 103, p. 185-214.

Tornos, F., Spiro, B., 1999, The genesis of shale-hosted massive sulfides in the IPB, in: Stanley et al (Eds) Mineral Deposits: Processes to Processing, Rotterdam Balkema, p. 605-608.

Tosdal, R. M., Wooden, J. L., Bouse, R. M., 1999, Pb isotopes, ore deposits, and metallogenic terranes, in Lambert, D. Ruiz, J. (Eds), Reviews in Economic Geology, Vol. 12: Application of Radiogenic Isotopes to Ore Deposit Research and Exploration, p. 1-28.

Turner, E. C., Kamber, B. S., 2012, Arctic Bay Formation, Borden Basin, Nunavut (Canada): basin evolution, black shale, and dissolved metal systematics in the Mesoproterozoic Ocean: Precambrian Research, v. 208-211, p. 1-18.

Valenzuela, A., Donaire, T., Pascual, E., 2002, Secuencia de fácies volcânicas en el area del rio Odiel (Faja Piritica Iberica, España): Geogaceta, v. 32, p. 131-134.

Valenzuela, A., Donaire, T., Pin, C., Toscano, M., Hamilton, M., Pascual, E., 2011, Geochemistry and U-Pb Dating of felsic volcanic rocks in the Rio Tinto-Nerva unit, Iberian

Pyrite Belt, Spain: crustal thinning, progressive crustal melting and massive sulphide genesis: Journal of the Geological Society, v. 168, p. 717-731.

Van den Boogard, M., 1963, Conodonts of Upper Devonian and Lower Carboniferous age from southern Portugal: Geologie en Mijnbouw, v. 42, p. 248-259.

Veizer, J., Ala, D., Azmy, K., Bruckschen, P., Buhl, D., Bruhn, F., Carden, G. A. F., Diener, A., Ebneth, S., Godderis, Y., Jasper, T., Korte, C., Pawellek, F., Podlaha, O.G., Strauss, H., 1999, $^{87}Sr/^{86}Sr$, $\delta^{13}C$ and $\delta^{18}O$ evolution of Phanerozoic seawater: Chemical Geology, v. 161, p. 59-88.

Velasco, F., Sánchez-España, J., Boyce, A. J., Fallick, A. E., Sáez, R., Almodóvar, G. R., 1998, A new sulphur isotopic study of some Iberian Pyrite Belts deposits: evidence of a textural control on sulphur isotope composition: Mineralium Deposita, v. 34, p. 4-18.

Velasco-Acebes, J., Tornos, F., Kidane, A., Wiedenbeck, Mi, Velasco, F., 2018, Isotope geochemistry tracks the maturation of submarine massive sulfide mounds (Iberian Pyrite Belt): Mineralium Deposita, v. 54(6), p. 913-934.

Woodard, S., Thomas, D.J., Grossman, E.L., Olszewski, T.D., 2013, Radiogenic isotopic composition of Carboniferous seawater from North American epicontinental seas: Palaeogeography Palaeoclimatology Palaeoecology, v. 370, p. 51-63.

Yamamoto, M., Kase, K., Carvalho, D., Nakamura, T., Mitsuno, C., 1993, Ore mineralogy and sulphur isotopes of the volcanogenic massive sulphide deposits in the Iberian Pyrite Belt: Resource Geology Special Issue, v. 15, p. 67-80.

Zartman, R. E.; Doe, B. R., 1981, Plumbotectonics: the model: Tectonophysics, v. 75, p. 135-162.

Figure and Table Captions

Fig. 1: Geological setting and simplified geological map of the South Portuguese Zone in SW Iberia, illustrating the Iberian Pyrite Belt extension and the main massive sulfide ore deposits location. The four sectors considered in this study are traced by grey-polygons and referred in text as: Lousal (including the Sesmarias prospect), Aljustrel (active mine and including the Gavião and Monte das Mesas prospects), Albernoa and Neves Corvo (including the Montinho prospect). Modified after Oliveira (1992), Barriga et al. (1997), Marcoux (1998), Leistel et al. (1998), Carvalho et al. (1999), Matos et al. (2000, 2006) and Tornos (2006).

Fig. 2: **(A)** $(^{87}Sr/^{86}Sr)_i$ values from published data, excluding unreasonably geological values (< 0.7000; *n= 6*); **(B)** Sr (ppm) vs. $(^{87}Sr/^{86}Sr)_i$ values for regional volcanic rocks included in VSC (*n=10*) and fine-grained siliciclastic (*n=17*), considering data reported in Mitjavilla et al., (1997) and Jorge (2009), respectively. The available data for some of the ore types forming the Neves Corvo deposit (*n=10*; Relvas et al., 2001; Carvalho, 2016) are also shown. The star indicates a possible starting position for seawater at Devonian-Carboniferous boundary (Veizer et al., 1999), thus representing an end-member of simple binary mixtures that could have developed by means of variable interaction with siliciclastic and/or volcanic rocks. The $(^{87}Sr/^{86}Sr)_i$ are 360 Ma for PQG and *lower* VSC samples, and 350 Ma for *middle/upper* VSC (Luz et al., 2020). Reference data from literature are listed in the electronic supplementary material 3.

Fig. 3: Nd (ppm) vs. εNd*i* for regional volcanic rocks included in VSC (*n=22*) and fine-grained siliciclastic sediments of PQG (*n=7*), considering the data reported in Mitjavila et al. (1997), Donaire et al., (2020) and Jorge (2009), respectively. The available data for some of the ore types forming the Neves Corvo deposit (*n= 27*; Relvas et al., 2001; Jorge et al., 2007; Carvalho, 2016) are also shown, documenting different Nd - εNd trends related to the incorporation of REE derived from distinct sources. The star indicates an exploratory starting position for ambient seawater at Devonian-Carboniferous boundary that could have acted as an end-member of simple binary mixtures involving siliciclastic and/or volcanic rocks. The εNd*i* are 360 Ma for PQG and *lower* VSC samples, and 350 Ma for *middle/upper* VSC (Luz et al., 2020). Reference data from literature are listed in the electronic supplementary material 3.

Fig. 4: (**A**) $^{206}Pb/^{204}Pb_i$ vs. $^{207}Pb/^{204}Pb_i$ and $^{208}Pb/^{204}Pb_i$ diagrams for the IPB sulfide ores (*n=106*; Marcoux, 1998; Pomiés et al., 1999; Relvas et al., 2001; Jorge et al., 2007; Carvalho, 2016), as well as for common IPB volcanic (*n=16;* Marcoux, 1998) and siliciclastic rocks (*n=5*; Jorge, 2009). (**B**) Relative positioning of the available Pb-Pb isotopic results regarding the orogenic curve of Zartman and Doe (1979). The Pb initial compositions are 360 Ma

for PQG and *lower* VSC samples, and 350 Ma for *middle/upper* VSC (Luz et al., 2020). Reference data from literature are listed in the electronic supplementary material 3.

Fig. 5: (A) $^{206}Pb/^{204}Pb$ vs. $^{207}Pb/^{204}Pb$ (age corrected) diagrams for the IPB sulfide ores (*n=106*; Marcoux, 1998; Pomiés et al., 1999; Relvas et al., 2001; Jorge et al., 2007; Carvalho, 2016). **(B)** Zoom in the $^{206}Pb/^{204}Pb$ vs. $^{207}Pb/^{204}Pb$ (age corrected) diagram for the IPB sulfide ores. Portuguese and Spanish deposits were grouped according to the nature of the hosting rocks: shale-hosted (S) and volcanic-hosted (N). For the Neves Corvo deposit 5 major trends can be identified considering all the available published data (*n=42*; Marcoux, 1998; Relvas et al., 2001; Jorge et al., 2007; Carvalho, 2016). **(C)** Zoom of the previous diagram, identifying each IPB deposit for which there are available Pb-Pb data. Reference data from literature are listed in the electronic supplementary material 3.

Fig. 6: Spatial distribution of the sampled sites and drillings (**A**), and schematic representation of samples distribution across the stratigraphic units and sectors (**B**) making use of the reconstructed lithostratigraphic columns and chronostratigraphic regional correlation for the Portuguese segment of the IPB, as reported in Luz et al. (2020). Details on sample attributes (coordinates of the sampling site, depth in selected drillings, lithostratigraphic unit and stratigraphic relationship to massive sulfide orebodies) are summarized in Table 1. Supplementary information regarding petrographic and whole-rock geochemical features for each sample is reported in Luz et al. (2020) reported in Luz et al. (2020).

Fig. 7: $^{87}Sr/^{86}Sr_i$ variation displayed by metapelites from PQG and VSC sections, considering the data gathered for all the studied sectors. **(B)** $1/Sr\ (ppm)^{-1}$ vs. age-corrected $(^{87}Sr/^{86}Sr)_i$ plot discriminating all the samples. $^{87}Sr/^{86}Sr_i$ are360 Ma for PQG and *lower* VSC samples, and 350 Ma for *middle/upper* VSC (Luz et al., 2020).

Fig. 8: (A) εNd_i variation displayed by metapelites from PQG and VSC sections, considering the data gathered for all the studied sectors. **(B)** $1/Nd\ (ppm)^{-1}$ vs. εNd (age-corrected) plot discriminating all the samples. The asterisk indicates differences in the age-corrections: 360 Ma for PQG and *lower* VSC samples, and 350 Ma for *middle/upper* VSC (Luz et al., 2020).

Fig. 9: Present day compositions of $^{206}Pb/^{204}Pb$ vs. $^{207}Pb/^{204}Pb$ and $^{208}Pb/^{204}Pb$ diagrams for the studied samples (*n = 98*); symbols as in previous cross-plots. The boxplots on the right for each isotopic ratio separate the "No-sulfide", "Py-bearing" and "Mineralized" groups of samples. Orogenic and upper crust curves according to Zartman and Doe (1979).

Fig. 10: U/Th vs. U/Pb and Th/Pb diagrams for studied samples (n = 98). **(A)** Samples divided by stratigraphic position, sector and sulfide abundance; **(B)** Samples classified according to the measured Pb concentration: i) Pb < 5 ppm; ii) 5 ≤ Pb ≤ 10 ppm; and Pb > 10 ppm.

Fig. 11: $^{206}Pb/^{204}Pb_i$ vs. $^{207}Pb/^{204}Pb_i$ and $^{208}Pb/^{204}Pb_i$ diagrams for 75 metapelite samples, excluding 19 with Pb abundances below the detection limit of the analytical method used and 4 additional samples recording overcorrected isotopic ratios due to radiogenic Pb. The boxplots on the right for each isotopic ratio separate the "No-sulfide", "Py-bearing" and "Mineralized" groups of samples. Orogenic curve by Zartman and Doe (1979).

Fig. 12: Sr and Nd isotopic compositions and trace element ratios for PQG and VSC samples included in "No-sulfide" and "Py-bearing" groups (*n* = 75)**: (A)** Nd (ppm) vs. εNd_i; **(B)** Th/Sc **vs.** εNd_i; **(C)** $^{87}Sr/^{86}Sr_i$ vs. Sr (ppm) and **(D)** $^{87}Sr/^{86}Sr_i$ ***vs.*** εNd_i for PQG and *lower* VSC at 360 Ma. **(E)** $^{87}Sr/^{86}Sr_i$ ***vs.*** εNd_i for middle and upper VSC at 350 Ma. Crustal reservoirs data from the literature (Clarke & Halliday, 1985; Clarke et al., 1988, 1997; Mitjavilla et al., 1997; Jorge, 2009; Donaire et al., 2020). The star indicates an exploratory reference for ambient seawater at Devonian-Carboniferous boundary that could have acted as an end-member of simple binary mixtures established with siliciclastic and/or volcanic rocks. The data used are reported in Tables 2 and 3 (sections 5.1 and 5.2), excepting Sc concentrations which are listed in the electronic supplementary material 2. Reference data from literature are listed in the electronic supplementary material 3.

Fig. 13: εNd_i vs. time diagrams: **(A)** Time in Ga, The Nd T_{DM} model ages were calculated assuming a linear depletion model with present-day depleted values of $^{143}N/^{144}Nd = 0.513151$ and $^{147}Sm/^{144}Nd = 0.2137$ (Peucat et al., 1998). Two-stage T_{DM} model ages were computed for samples with $^{147}Sm/^{144}Nd$ ratio outside the typical range of upper continental crust-derived sediments (0.09 - 0.13; e.g. Goldstein et al., 1984); a $^{147}Sm/^{144}Nd$ value of 0.114 was used to estimate the sample evolution path prior to depositional age (Goldstein and Jacobsen, 1988; Li and Schoornmaker, 2014) **.(B)** Time in Ma, comparing Sm-Nd isotope data for PQG, *lower* VSC, *middle* VSC, *upper* VSC and reference samples of Gafo, Ribeira de Limas and Sta. Iria Formations (Chança and Pulo do Lobo Groups) with data for the Meguma Metasedimentary rocks (Clark et al., 1980, 1988, 1997), the Avalonia crust (Murphy et al., 1996, 2000) and the IPB volcanic rocks (Mitjavilla et al., 1997; Donaire et al., 2020). Depleted mantle evolution curve from the model of De Paolo (1981). The data used are reported in Tables 2 and 3 (sections 5.1 and 5.2). Reference data from literature are listed in the electronic supplementary material 3.

Fig. 14: $^{206}Pb/^{204}Pb_i$ vs. $^{207}Pb/^{204}Pb_i$ diagrams for studied samples (*n* = 75) classified according to their Pb abundances. The numbered arrows illustrated the trends discussed in section 3.2.4 on the basis of published data (*n=42*; Marcoux, 1998; Relvas et al., 2001; Jorge et al., 2007; Carvalho, 2016). The fields indicated for PQG and IPB metavolcanic rocks encircle data points compiled from literature: PQG siliciclastic rocks (*n=5*; Jorge, 2009), common IPB volcanic rocks (*n=16;* Marcoux, 1998). The data used are reported in Table 4 (section 5.3). Reference data from literature are listed in the electronic supplementary material 3.

Fig. 15: $^{206}Pb/^{204}Pb_i$ vs. $^{207}Pb/^{204}Pb_i$ diagrams for studied samples (*n* = 75). Numbered arrows and reference fields as in Fig. 14. The common massive sulfide ores in the Portuguese and Spanish segments of IPB were separated into two fields, considering the data (*n* =106) reported in Marcoux (1998), Pomiés et al. (1999), Relvas et al. (2001), Jorge et al. (2007) and Carvalho (2016). The data used are reported in Table 4 (section 5.3). Reference data from literature are listed in the electronic supplementary material 3.

Fig. 16: (Cu+Zn+Pb)/Sc and Fe_2O_3/TiO_2 vs**.** $^{207}Pb/^{204}Pb_i$ diagrams showing the potential use of these cross-plots in vectoring massive sulfide accumulations. (Cu+Zn+Pb)/Sc and Fe_2O_3/TiO_2 thresholds (>10) described in Luz et al. (2019, 2020). $^{207}Pb/^{204}Pb_i$ for Portuguese massive sulfide ores according with literature data (*n* = 106; Marcoux, 1998; Pomiés et al., 1999; Relvas et al., 2001; Jorge et al., 2007; Carvalho, 2016). Element concentrations for the studied metasediments are listed in the electronic supplementary material 2. Reference data from literature are listed in the electronic supplementary material 3.

Table 1 – Main attributes of the studied samples.

Table 2 - Rb-Sr whole-rock and isotopic compositions for all dataset. The $(^{87}Sr/^{86}Sr)_i$ was calculated for 350 Ma or 360 Ma (Luz et al., 2020). The εSr(0) was computed considering the chondritic uniform reservoir (CHUR) with present-day composition of $^{87}Sr/^{86}Sr = 0.7042$ and $^{87}Rb/^{86}Sr = 0.0827$ (Faure and Mensing, 2005).

Table 3- Sm-Nd whole-rock and isotopic compositions for all datset. The $\varepsilon Nd_{(0)}$ was determined considering the chondritic uniform reservoir (CHUR) with present-day composition of $^{143}Nd/^{144}Nd= 0.512638$ and $^{147}Sm/^{144}Nd= 0.1967$ (Jacobsen and Wasserburg, 1980). The εNd_i was calculated for 350 Ma or 360 Ma (Luz et al., 2020). The two-stage (T_{DM}) neodymium model ages were computed according to the depleted mantle model of DePaolo (1981). $f_{Sm/Nd} = (^{147}Sm/^{144}Nd)_{sample}/(^{147}Sm/^{144}Nd)_{CHUR} - 1$.

Table 4 - Whole-rock, Pb-Pb isotopic compositions for all samples (n = 98). The Pb-Pb initial isotopic ratios were estimated by considering the $^{238}U/^{204}Pb$, $^{235}U/^{204}Pb$ and $^{232}Th/^{204}Pb$ ratios determined on the basis of the measured

Pb isotopic compositions (i.e. $^{206}Pb/^{204}Pb$, $^{207}Pb/^{204}Pb$ and $^{208}Pb/^{204}Pb$), and U, Th and Pb concentration values. Calculation of $\mu = {}^{238}U/^{204}Pb$, $\omega = {}^{232}Th/^{204}Pb$ and $k = {}^{232}Th/^{238}U$ values was performed using the age corrected $^{208}Pb/^{204}Pb$, $^{207}Pb/^{204}Pb$, $^{206}Pb/^{204}Pb$ ratios and the 3.7 Ga reference point of the Stacey & Kramers (1975) model. The Pb-Pb initial isotopic ratios were calculated to 360 Ma for PQG and *lower* VSC samples, and 350 Ma for *middle/upper* VSC (Luz et al., 2020).

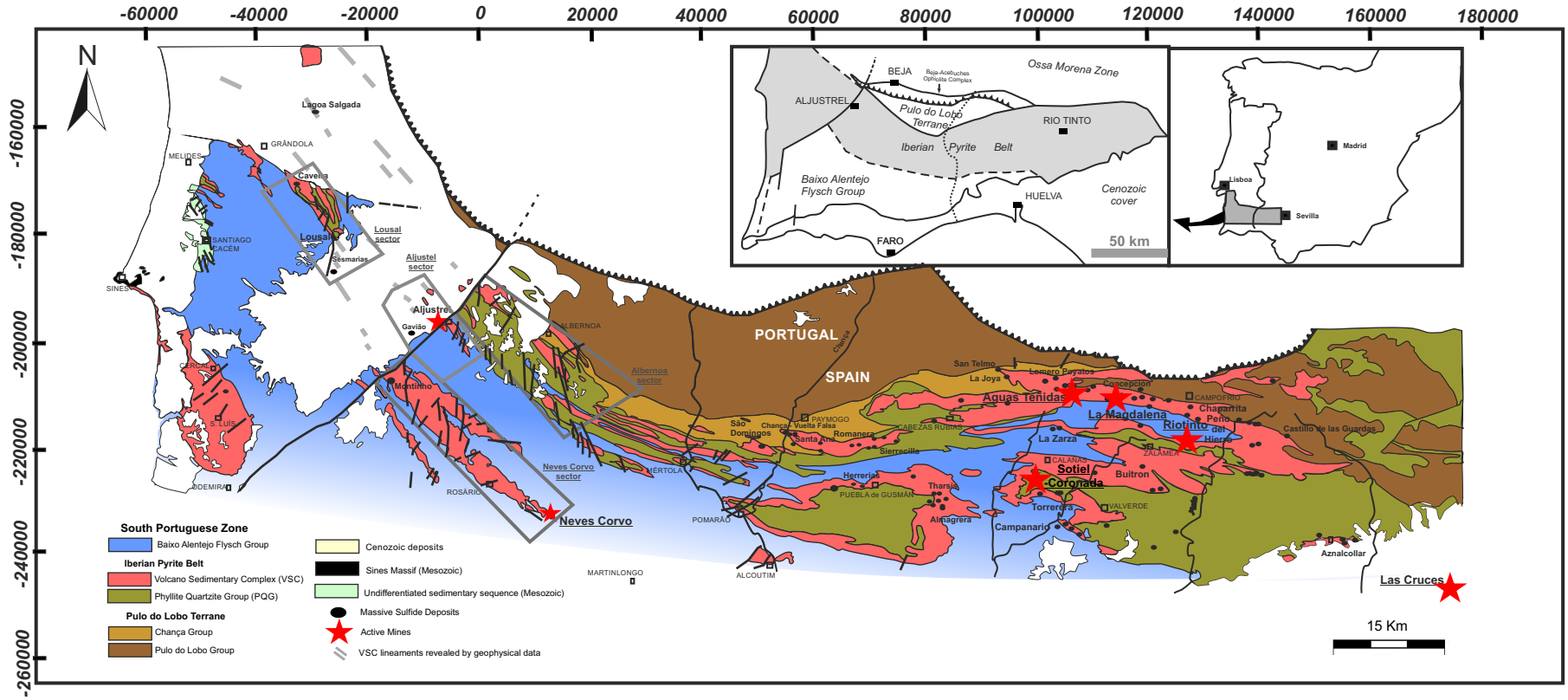
-60000
-40000
-20000
0
20000
40000
60000
80000
100000
120000
140000
160000
180000
-160000
-180000
-200000
-220000
-240000
-260000
N
Lagoa Salgada
GRÂNDOLA
MELIDES
Caveira
SANTIAGO DO CACÉM
Lousal
Lousal sector
Sesmarias
Aljustrel sector
Aljustrel
Gavião
SINES
ALBERNOA
Albernoa sector
PORTUGAL
SPAIN
Chança
Montinho
CASTRO VERDE
S. LUÍS
ODEMIRA
ROSÁRIO
Neves Corvo sector
Neves Corvo
MERTOLA
POMARÃO
MARTINLONGO
ALCOUTIM
São Domingos
Chança
Vuelta Falsa
PAYMOGO
Santa Ana
Romanera
CABEZAS RUBIAS
Sierrecilla
Herrerías
PUEBLA de GUZMÁN
Tharsis
Almagrera
San Telmo
La Joya
Lomero Poyatos
Concepción
Aguas Tenidas
CAMPOFRÍO
La Magdalena
Chapparrita
Peña del Hierro
Riotinto
Castillo de las Guardas
La Zarza
ZALAMEA
CALAÑAS
Sotiel Coronada
Buitron
Torrerera
VALVERDE
Campanario
Aznalcollar
Las Cruces
15 Km
BEJA
Beja-Acebuches Ophiolite Complex
Ossa Morena Zone
ALJUSTREL
Pulo do Lobo Terrane
RIO TINTO
Iberian Pyrite Belt
Baixo Alentejo Flysch Group
HUELVA
Cenozoic cover
FARO
50 km
Madrid
Lisboa
Sevilla
South Portuguese Zone
Baixo Alentejo Flysch Group
Iberian Pyrite Belt
Volcano Sedimentary Complex (VSC)
Phyllite Quartzite Group (PQG)
Pulo do Lobo Terrane
Chança Group
Pulo do Lobo Group
Cenozoic deposits
Sines Massif (Mesozoic)
Undifferentiated sedimentary sequence (Mesozoic)
Massive Sulfide Deposits
Active Mines
VSC lineaments revealed by geophysical data

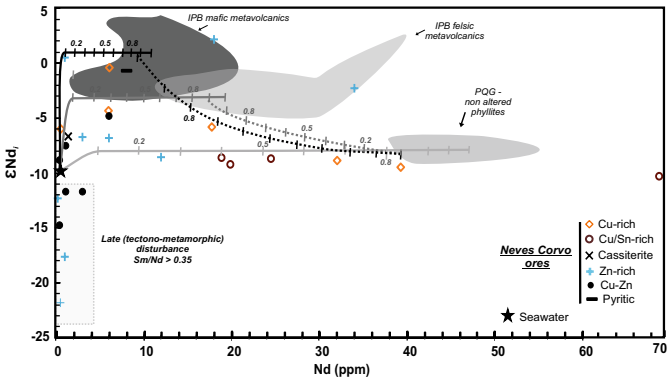
IPB mafic metavolcanics
IPB felsic metavolcanics
PQG - non altered phyllites
Late (tectono-metamorphic) disturbance Sm/Nd > 0.35
Neves Corvo ores
Cu-rich
Cu/Sn-rich
Cassiterite
Zn-rich
Cu-Zn
Pyritic
Seawater
εNdi
Nd (ppm)
5
0
-5
-10
-15
-20
-25
0
10
20
30
40
50
60
70

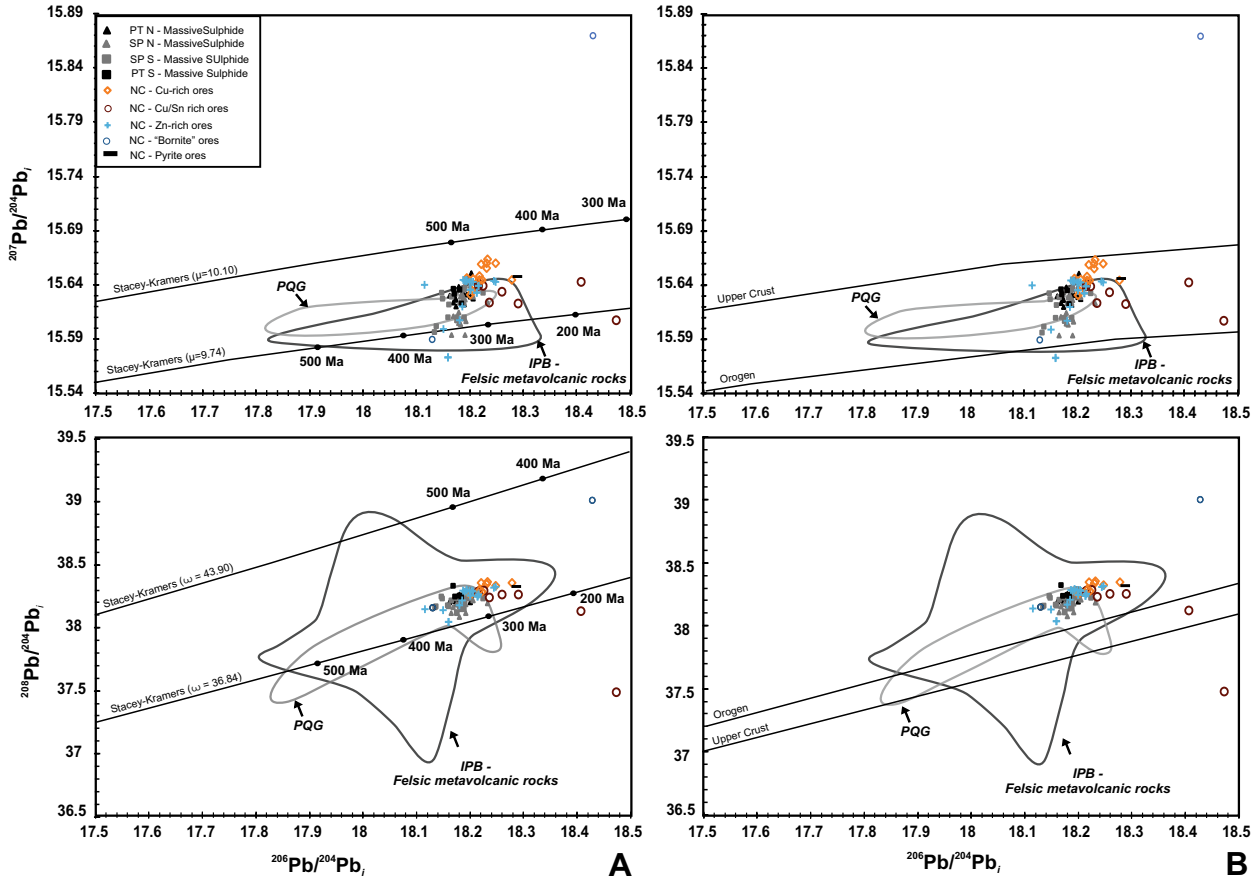
PT N - MassiveSulphide
SP N - MassiveSulphide
SP S - Massive SUlphide
PT S - Massive Sulphide
NC - Cu-rich ores
NC - Cu/Sn rich ores
NC - Zn-rich ores
NC - "Bornite" ores
NC - Pyrite ores
Stacey-Kramers (μ=10.10)
Stacey-Kramers (μ=9.74)
Upper Crust
Orogen
PQG
IPB - Felsic metavolcanic rocks
500 Ma
400 Ma
300 Ma
200 Ma
Stacey-Kramers (ω = 43.90)
Stacey-Kramers (ω = 36.84)
207Pb/204Pbi
208Pb/204Pbi
206Pb/204Pbi
A
B

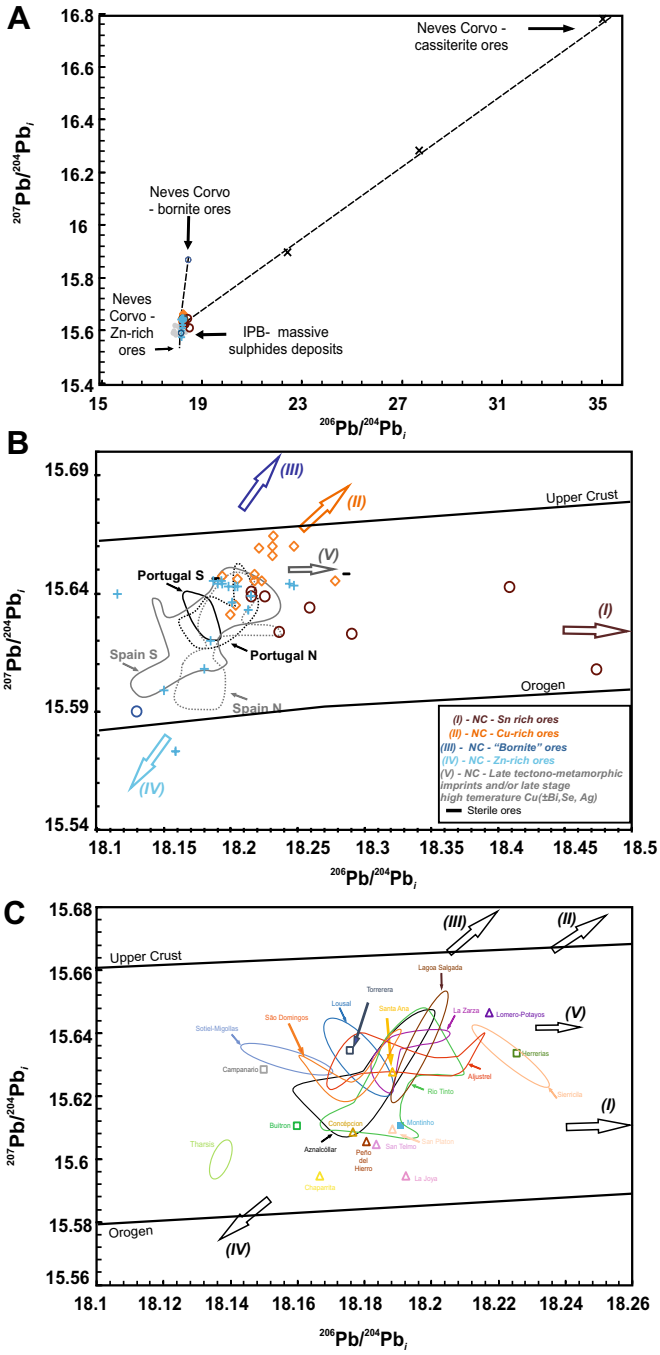
A
Neves Corvo - cassiterite ores
Neves Corvo - bornite ores
Neves Corvo - Zn-rich ores
IPB- massive sulphides deposits
$^{207}Pb/^{204}Pb_i$
$^{206}Pb/^{204}Pb_i$
B
(III)
(II)
(V)
(I)
(IV)
Upper Crust
Orogen
Portugal S
Portugal N
Spain S
Spain N
(I) - NC - Sn rich ores
(II) - NC - Cu-rich ores
(III) - NC - "Bornite" ores
(IV) - NC - Zn-rich ores
(V) - NC - Late tectono-metamorphic imprints and/or late stage high temerature Cu(±Bi,Se, Ag)
Sterile ores
$^{207}Pb/^{204}Pb_i$
$^{206}Pb/^{204}Pb_i$
C
(III)
(II)
(V)
(I)
(IV)
Upper Crust
Orogen
Lagoa Salgada
Torreiera
Lousal
São Domingos
Santa Ana
La Zarza
Lomero-Poyatos
Sotiel-Migollas
Herrerias
Campanario
Aljustrel
Rio Tinto
Sierrecilla
Montinho
Buitron
Concepcion
San Platon
San Telmo
Azmalcóllar
Peño del Hierro
La Joya
Chapparita
Thansis
$^{207}Pb/^{204}Pb_i$
$^{206}Pb/^{204}Pb_i$

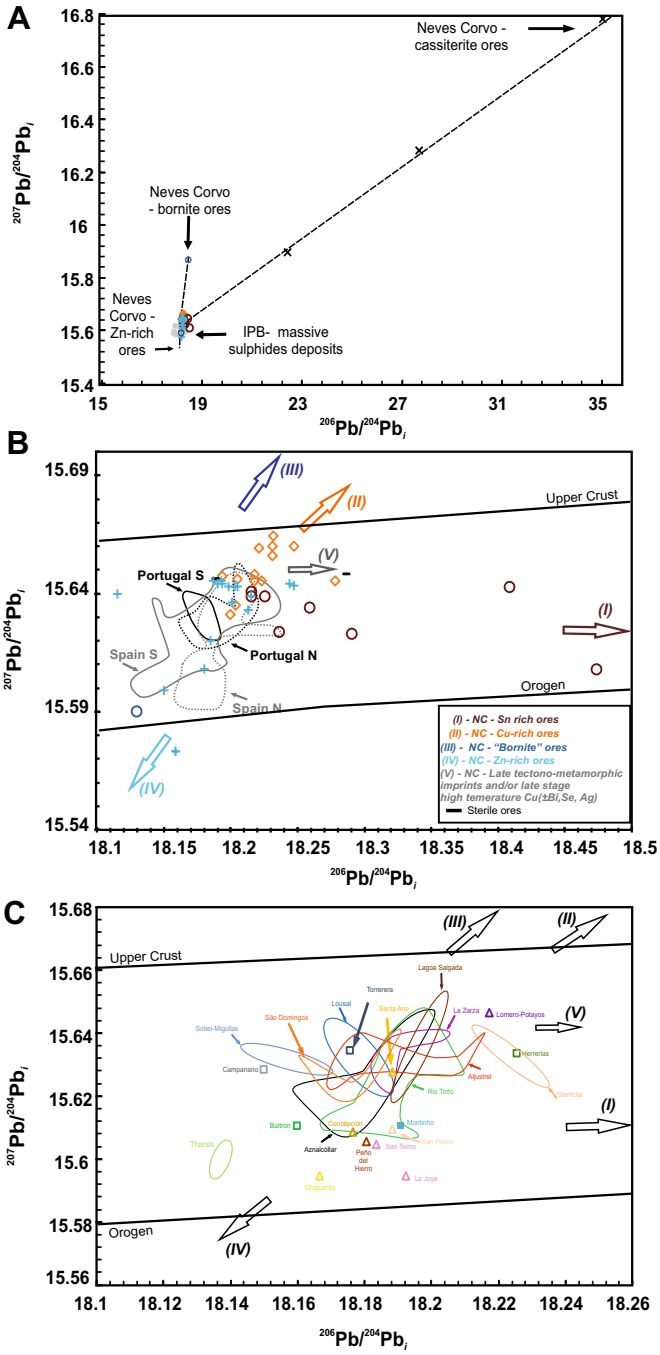
A
Neves Corvo - cassiterite ores
Neves Corvo - bornite ores
Neves Corvo - Zn-rich ores
IPB- massive sulphides deposits
$^{207}Pb/^{204}Pb_i$
$^{206}Pb/^{204}Pb_i$
B
(III)
(II)
(V)
(I)
(IV)
Upper Crust
Orogen
Portugal S
Portugal N
Spain S
Spain N
(I) - NC - Sn rich ores
(II) - NC - Cu-rich ores
(III) - NC - "Bornite" ores
(IV) - NC - Zn-rich ores
(V) - NC - Late tectono-metamorphic imprints and/or late stage high temerature Cu(±Bi,Se, Ag)
Sterile ores
$^{207}Pb/^{204}Pb_i$
$^{206}Pb/^{204}Pb_i$
C
(III)
(II)
(V)
(I)
(IV)
Upper Crust
Orogen
Lagoa Salgada
Torreiera
Lousal
São Domingos
Santa Ana
La Zarza
Lomero-Poyatos
Sotiel-Migollas
Herrerias
Campanario
Aljustrel
Rio Tinto
Sierrecilla
Montinho
Buitron
Concepcion
San Platon
San Telmo
Azmalcóllar
Peño del Hierro
La Joya
Chapparita
Thansis
$^{207}Pb/^{204}Pb_i$
$^{206}Pb/^{204}Pb_i$

Figure

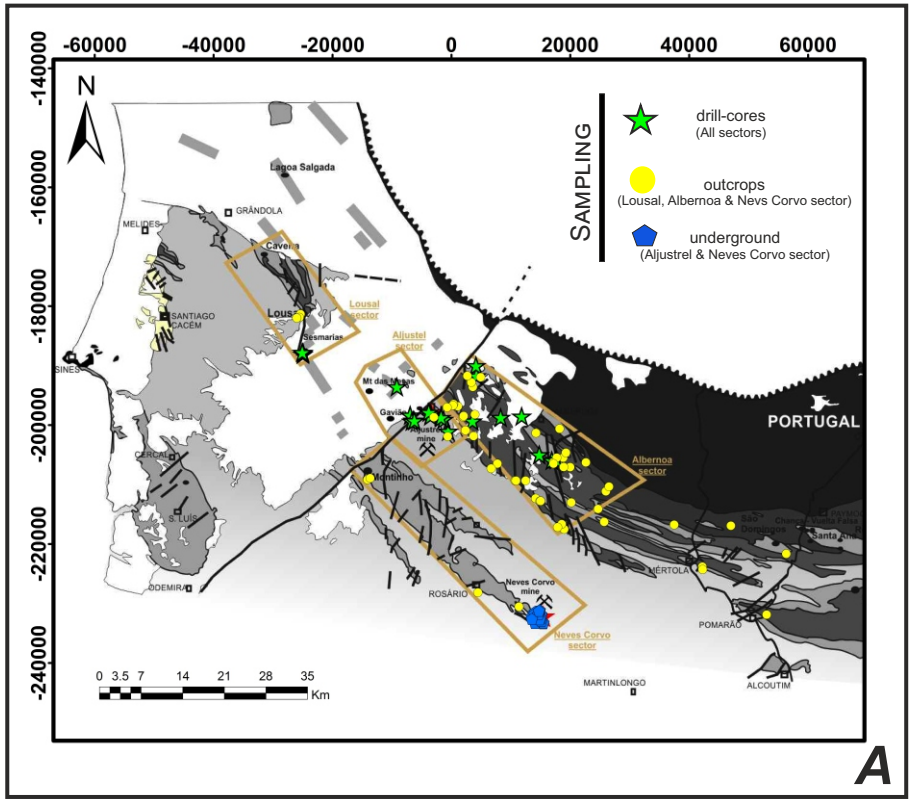
-60000
-40000
-20000
0
20000
40000
60000
-140000
-160000
-180000
-200000
-220000
-240000
N
SAMPLING
drill-cores
(All sectors)
outcrops
(Lousal, Albernoa & Nevs Corvo sector)
underground
(Aljustrel & Neves Corvo sector)
Lagoa Salgada
GRÂNDOLA
MELIDES
SANTIAGO CACÉM
SINES
Lousal
Sesmarias
Lousal sector
Aljustel sector
Mt das Minas
Gavião
Albernoa sector
PORTUGAL
Montinho
CERCAL
ODEMIRA
ROSÁRIO
Neves Corvo mine
Neves Corvo sector
MÉRTOLA
POMARÃO
MARTINLONGO
ALCOUTIM
0 3.5 7 14 21 28 35
Km
A

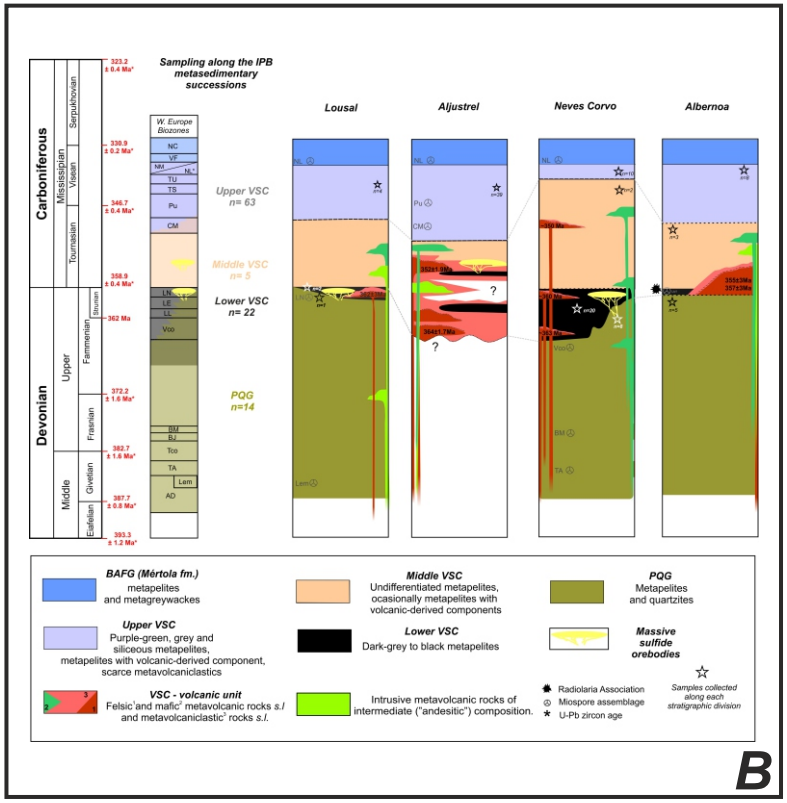
Sampling along the IPB metasedimentary successions
Lousal
Aljustrel
Neves Corvo
Albernoa
Carboniferous
Devonian
Upper VSC n= 63
Middle VSC n= 5
Lower VSC n= 22
PQG n=14
BAFG (Mértola fm.)
metapelites and metagreywackes
Upper VSC
Purple-green, grey and siliceous metapelites, metapelites with volcanic-derived component, scarce metavolcaniclastics
VSC - volcanic unit
Felsic and mafic metavolcanic rocks s.l and metavolcaniclastic rocks s.l.
Middle VSC
Undifferentiated metapelites, ocasionally metapelites with volcanic-derived components
Lower VSC
Dark-grey to black metapelites
Intrusive metavolcanic rocks of intermediate ("andesitic") composition.
PQG
Metapelites and quartzites
Massive sulfide orebodies
Radiolaria Association
Miospore assemblage
U-Pb zircon age
Samples collected along each stratigraphic division
B

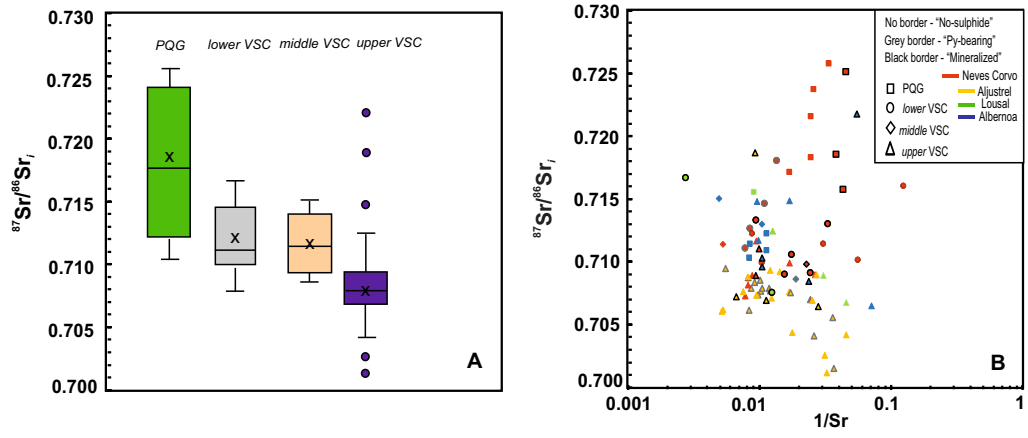
PQG
lower VSC
middle VSC
upper VSC
0.730
0.725
0.720
0.715
0.710
0.705
0.700
$^{87}Sr/^{86}Sr_i$
A
No border - "No-sulphide"
Grey border - "Py-bearing"
Black border - "Mineralized"
PQG
lower VSC
middle VSC
upper VSC
Neves Corvo
Aljustrel
Lousal
Albernoa
0.001
0.01
0.1
1
1/Sr
B

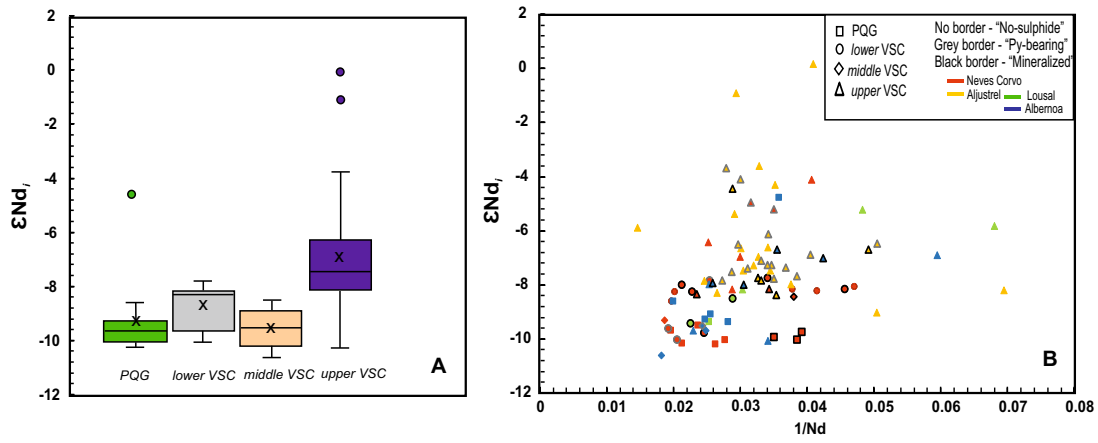
εNdi
2
0
-2
-4
-6
-8
-10
-12
PQG
lower VSC
middle VSC
upper VSC
A
PQG
lower VSC
middle VSC
upper VSC
No border - "No-sulphide"
Grey border - "Py-bearing"
Black border - "Mineralized"
Neves Corvo
Aljustrel
Lousal
Albernoa
B
0
0.01
0.02
0.03
0.04
0.05
0.06
0.07
0.08
1/Nd

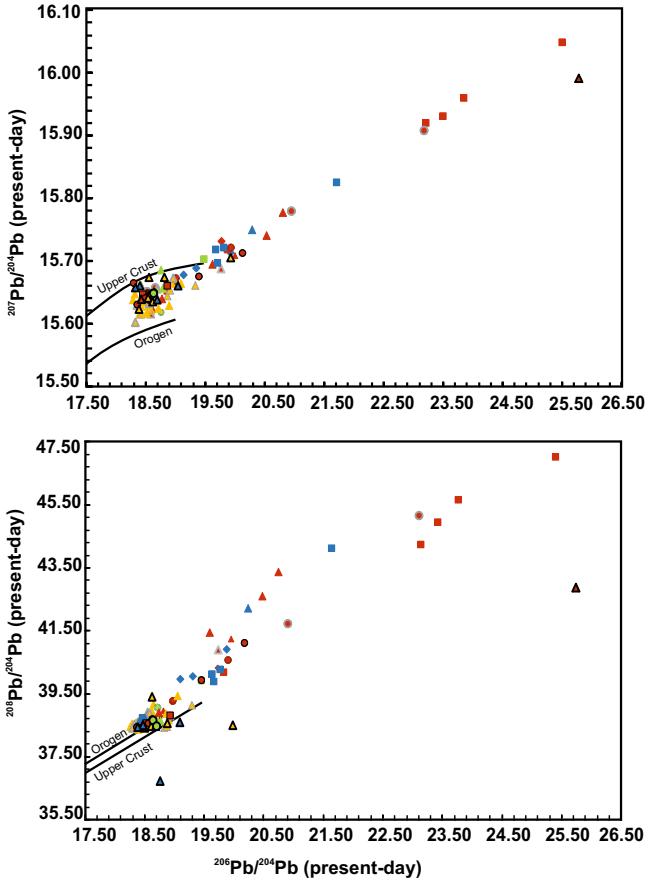
16.10
16.00
15.90
15.80
15.70
15.60
15.50
$^{207}Pb/^{204}Pb$ (present-day)
Upper Crust
Orogen
17.50 18.50 19.50 20.50 21.50 22.50 23.50 24.50 25.50 26.50
47.50
45.50
43.50
41.50
39.50
37.50
35.50
$^{208}Pb/^{204}Pb$ (present-day)
Orogen
Upper Crust
17.50 18.50 19.50 20.50 21.50 22.50 23.50 24.50 25.50 26.50
$^{206}Pb/^{204}Pb$ (present-day)

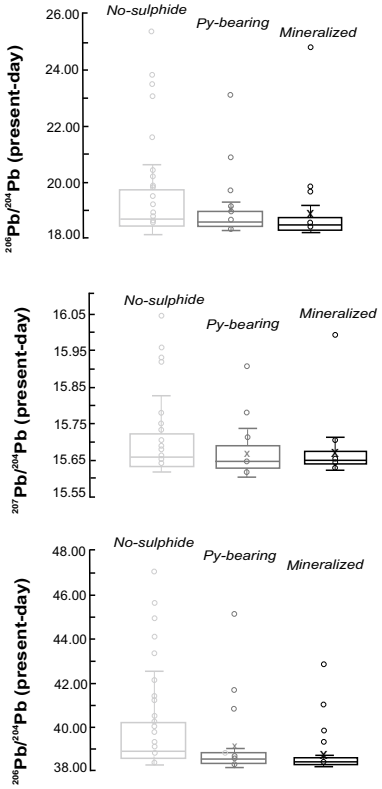
No-sulphide
Py-bearing
Mineralized
26.00
24.00
22.00
20.00
18.00
$^{206}Pb/^{204}Pb$ (present-day)
No-sulphide
Py-bearing
Mineralized
16.05
15.95
15.85
15.75
15.65
15.55
$^{207}Pb/^{204}Pb$ (present-day)
No-sulphide
Py-bearing
Mineralized
48.00
46.00
44.00
42.00
40.00
38.00
$^{208}Pb/^{204}Pb$ (present-day)

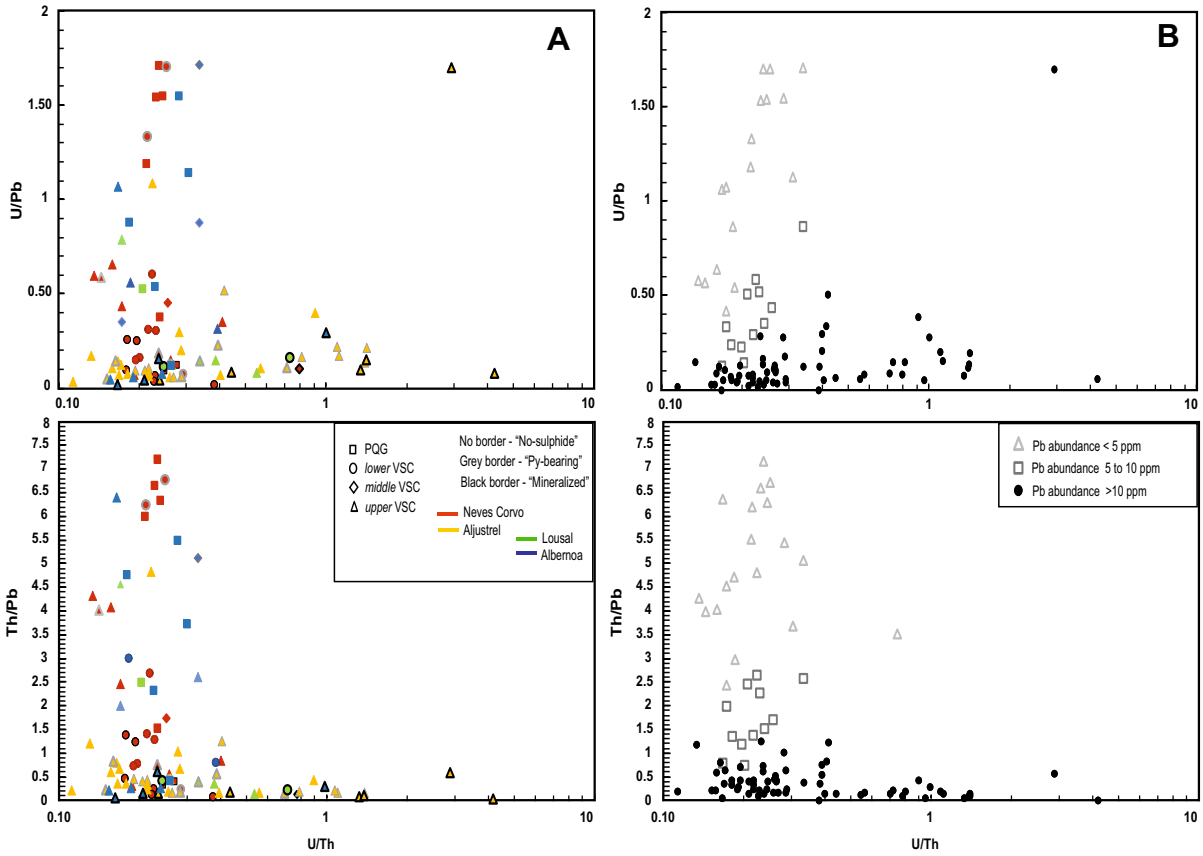
A
B
U/Pb
Th/Pb
U/Th
0.10
1
10
PQG
lower VSC
middle VSC
upper VSC
No border - "No-sulphide"
Grey border - "Py-bearing"
Black border - "Mineralized"
Neves Corvo
Aljustrel
Lousal
Albernoa
Pb abundance < 5 ppm
Pb abundance 5 to 10 ppm
Pb abundance >10 ppm

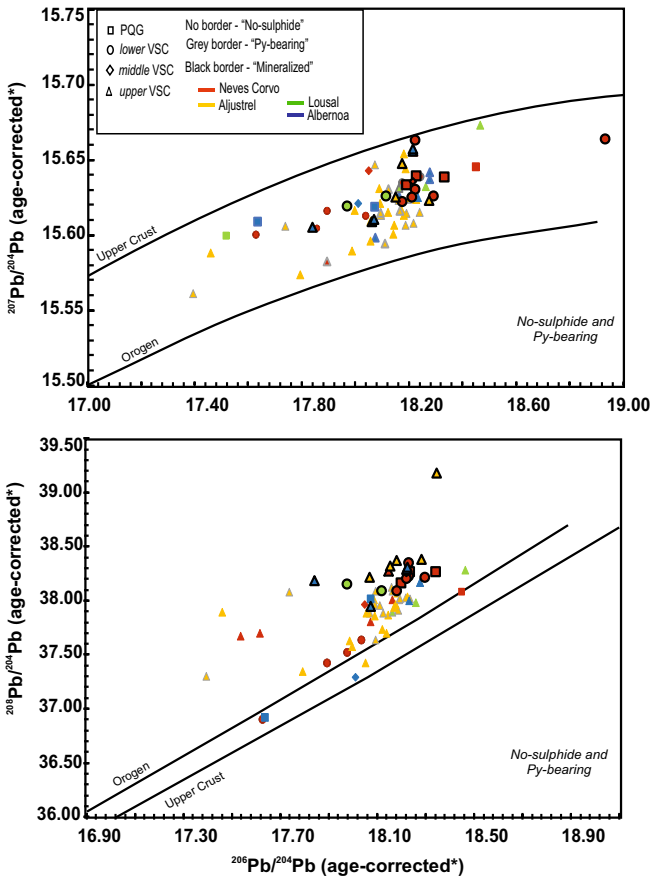
PQG
lower VSC
middle VSC
upper VSC
No border - "No-sulphide"
Grey border - "Py-bearing"
Black border - "Mineralized"
Neves Corvo
Aljustrel
Lousal
Albernoa
Upper Crust
Orogen
No-sulphide and Py-bearing
207Pb/204Pb (age-corrected*)
208Pb/204Pb (age-corrected*)
206Pb/204Pb (age-corrected*)

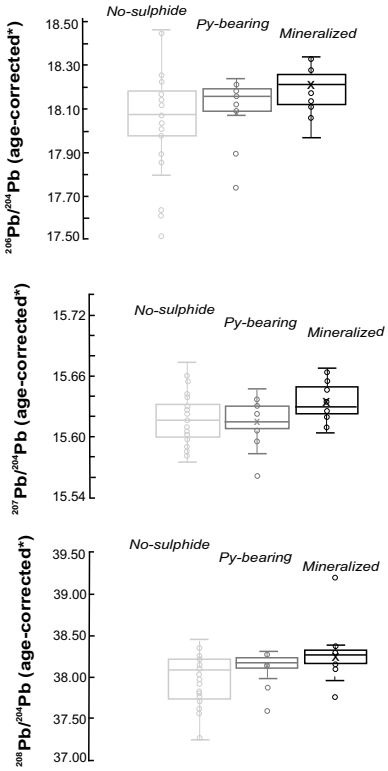
No-sulphide
Py-bearing
Mineralized
206Pb/204Pb (age-corrected*)
207Pb/204Pb (age-corrected*)
208Pb/204Pb (age-corrected*)

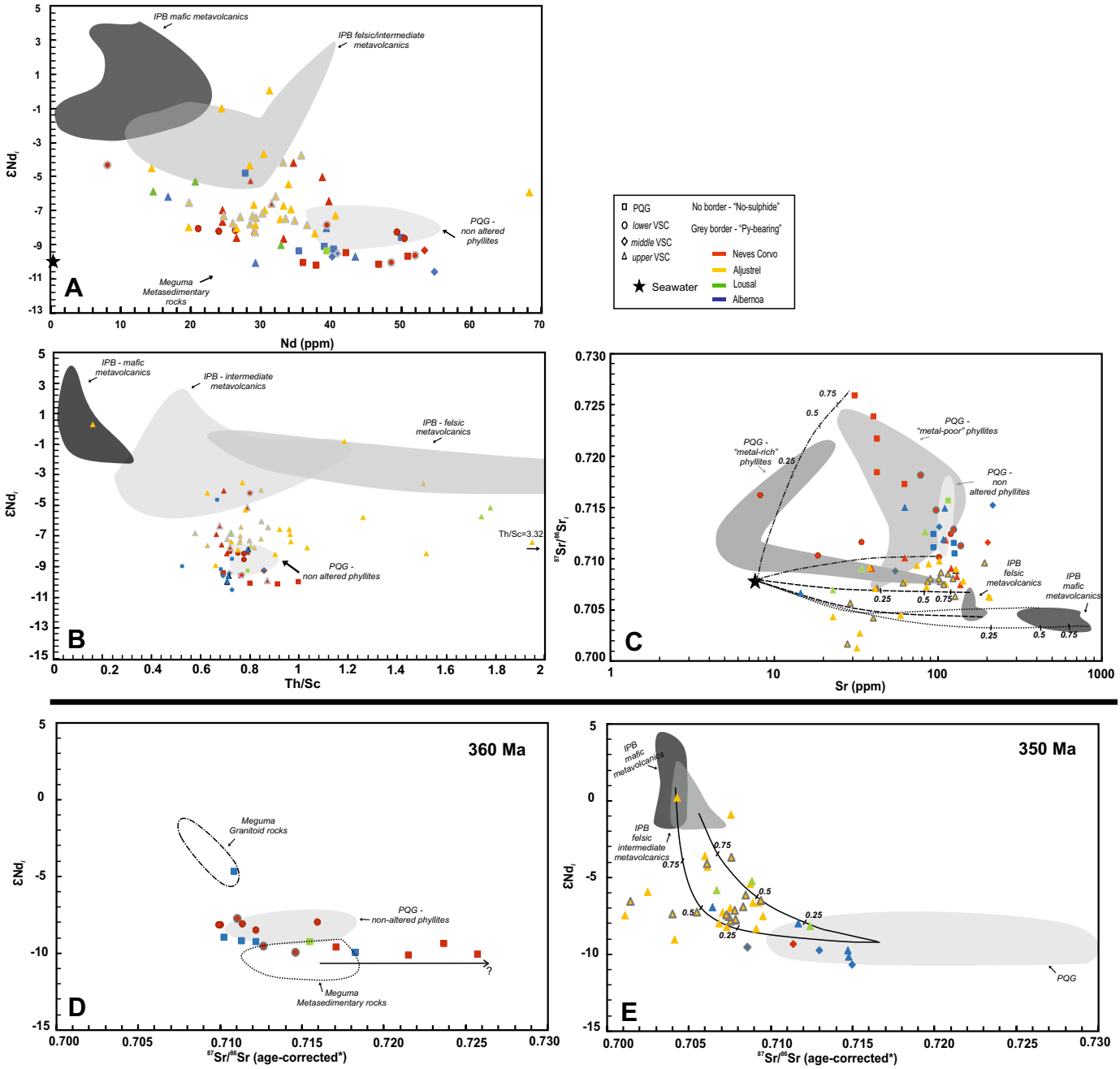
A
IPB mafic metavolcanics
IPB felsic/intermediate metavolcanics
PQG - non altered phyllites
Meguma Metasedimentary rocks
εNdi
Nd (ppm)
PQG
lower VSC
middle VSC
upper VSC
Seawater
No border - "No-sulphide"
Grey border - "Py-bearing"
Neves Corvo
Aljustrel
Lousal
Albernoa
B
IPB - mafic metavolcanics
IPB - intermediate metavolcanics
IPB - felsic metavolcanics
PQG - non altered phyllites
Th/Sc=3.32
Th/Sc
C
PQG - "metal-rich" phyllites
PQG - "metal-poor" phyllites
PQG - non altered phyllites
IPB felsic metavolcanics
IPB mafic metavolcanics
87Sr/86Sri
Sr (ppm)
D
360 Ma
Meguma Granitoid rocks
PQG - non-altered phyllites
Meguma Metasedimentary rocks
87Sr/86Sr (age-corrected*)
E
350 Ma
IPB mafic metavolcanics
IPB felsic intermediate metavolcanics
PQG
87Sr/86Sr (age-corrected*)

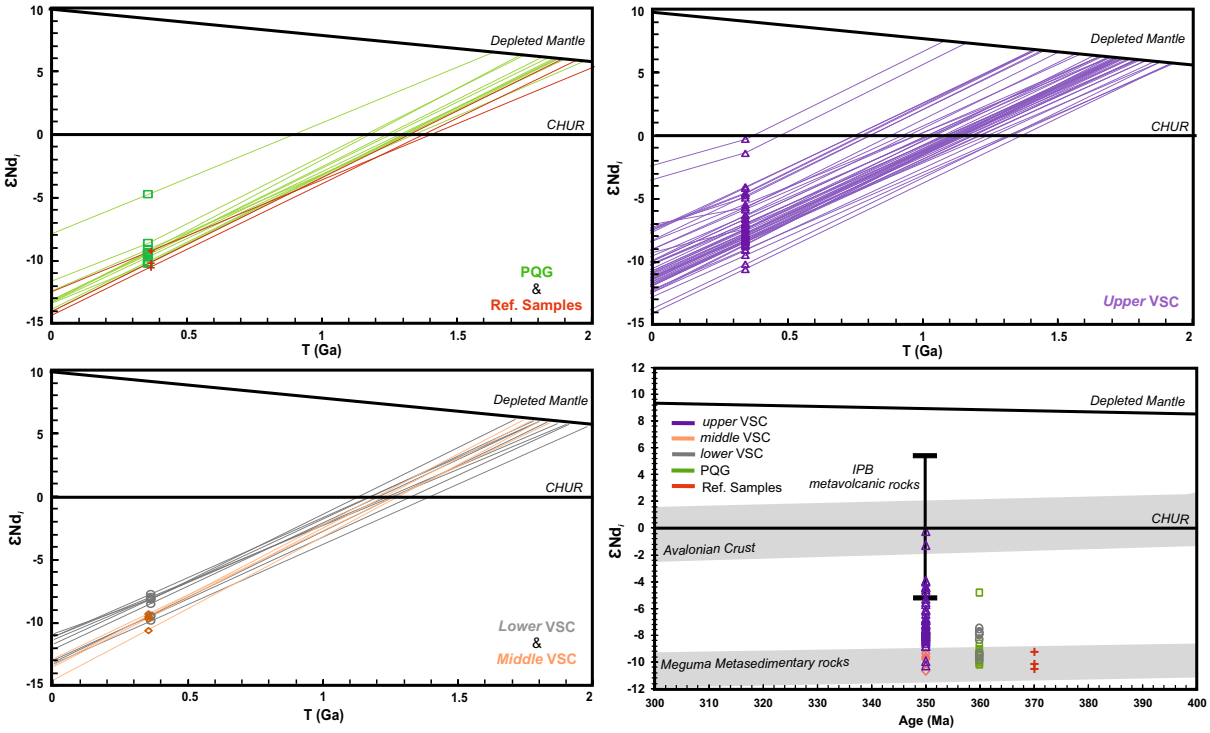
Depleted Mantle
CHUR
PQG
&
Ref. Samples
Upper VSC
Lower VSC
&
Middle VSC
upper VSC
middle VSC
lower VSC
PQG
Ref. Samples
IPB
metavolcanic rocks
Avalonian Crust
Meguma Metasedimentary rocks
εNdi
T (Ga)
Age (Ma)

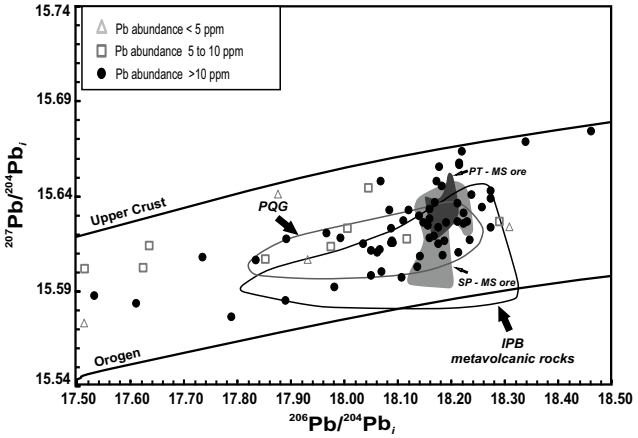
Pb abundance < 5 ppm
Pb abundance 5 to 10 ppm
Pb abundance >10 ppm
Upper Crust
Orogen
PQG
PT - MS ore
SP - MS ore
IPB
metavolcanic rocks
15.74
15.69
15.64
15.59
15.54
17.50
17.60
17.70
17.80
17.90
18.00
18.10
18.20
18.30
18.40
18.50
$^{207}Pb/^{204}Pb_i$
$^{206}Pb/^{204}Pb_i$

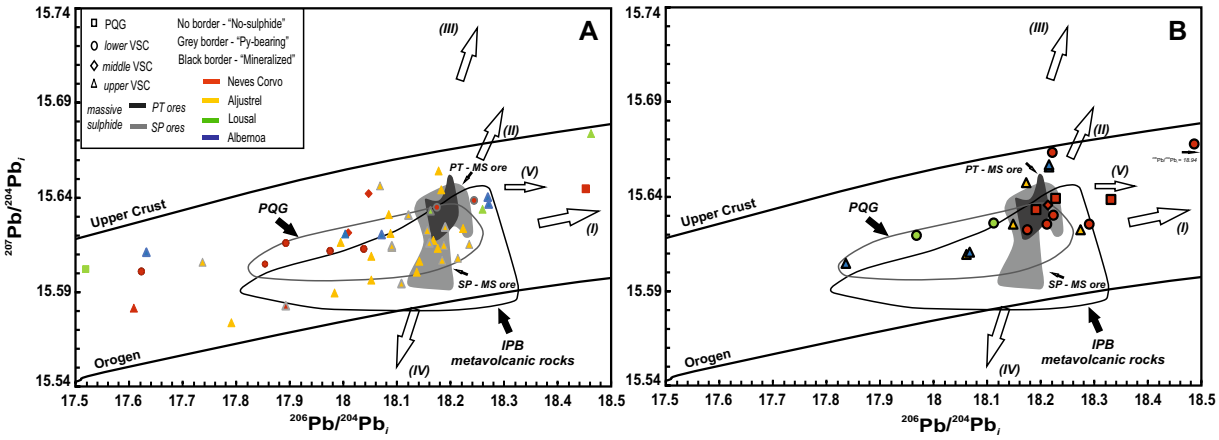
A
B
PQG
lower VSC
middle VSC
upper VSC
massive sulphide
PT ores
SP ores
No border - "No-sulphide"
Grey border - "Py-bearing"
Black border - "Mineralized"
Neves Corvo
Aljustrel
Lousal
Albernoa
Upper Crust
Orogen
PQG
PT - MS ore
SP - MS ore
IPB
metavolcanic rocks
(I)
(II)
(III)
(IV)
(V)
15.74
15.69
15.64
15.59
15.54
17.5
17.6
17.7
17.8
17.9
18
18.1
18.2
18.3
18.4
18.5
$^{207}Pb/^{204}Pb_i$
$^{206}Pb/^{204}Pb_i$

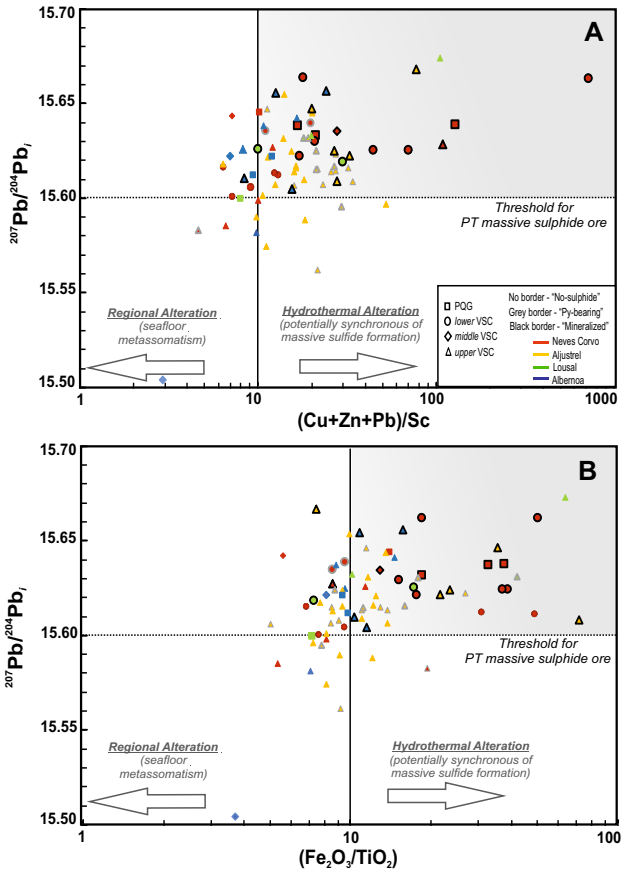
A
15.70
15.65
15.60
15.55
15.50
$^{207}Pb/^{204}Pb_i$
1
10
100
1000
(Cu+Zn+Pb)/Sc
Threshold for
PT massive sulphide ore
Regional Alteration
(seafloor metassomatism)
Hydrothermal Alteration
(potentially synchronous of massive sulfide formation)
POG
lower VSC
middle VSC
upper VSC
No border - "No-sulphide"
Grey border - "Py-bearing"
Black border - "Mineralized"
Neves Corvo
Aljustrel
Lousal
Albernoa
B
15.70
15.65
15.60
15.55
15.50
$^{207}Pb/^{204}Pb_i$
1
10
100
(Fe_2O_3/TiO_2)
Threshold for
PT massive sulphide ore
Regional Alteration
(seafloor metassomatism)
Hydrothermal Alteration
(potentially synchronous of massive sulfide formation)

Table

Click here to access/download;Table;Table1_2_3_4_PbNdSrIsotopes.xlsx

	Ref	Coordinates (ETRS89)			Sector	Stratigraphic division	Relative position to Massive sulfide
		x	*y*	*depth (m)*			
Metapelites	**NCL#9**	*13812*	*-231566*	*n.a.*	*Neves Corvo*	*PQG*	*Footwall*
	NCL#10	*14419*	*-231437*	*n.a.*	*Neves Corvo*	*PQG*	*Footwall*
	NCL#11	*14509*	*-231432*	*n.a.*	*Neves Corvo*	*PQG*	*Footwall*
	NCL#12	*14254*	*-231370*	*n.a.*	*Neves Corvo*	*PQG*	*Footwall*
	NCL#13	*14110*	*-231465*	*n.a.*	*Neves Corvo*	*PQG*	*Footwall*
	NCL#14	*14120*	*-231418*	*n.a.*	*Neves Corvo*	*PQG*	*Footwall*
	NCL#15	*14078*	*-231379*	*n.a.*	*Neves Corvo*	*PQG*	*Footwall*
	NCL#35	*n.a.*	*n.a.*	*n.a.*	*Neves Corvo*	*PQG*	*Footwall*
	NCC#25	*14745*	*-231837*	*n.a.*	*Neves Corvo*	*PQG*	*Footwall*
	NCC#27	*14648*	*-231786*	*n.a.*	*Neves Corvo*	*PQG*	*Footwall*
	PC24	*3557*	*-199306*	*-604.20*	*Albernoa*	*PQG*	*n.a.*
	PC32	*3557*	*-199306*	*-768.90*	*Albernoa*	*PQG*	*n.a.*
	PC19	*3557*	*-199306*	*-475.30*	*Albernoa*	*PQG*	*n.a.*
	11-1-MM	*17603*	*-205799*	*-399.80*	*Albernoa*	*PQG*	*n.a.*
	ABNSTR1	*53032*	*-231885*	*n.a.*	*Albernoa*	*PQG*	*n.a.*
	L MS#1	*n.a.*	*n.a.*	*n.a.*	*Lousal*	*PQG*	*Footwall*
	NCZ#1	*15175*	*-233119*	*n.a.*	*Neves Corvo*	*Lower VSC*	*Footwall*
	NCZ#21	*15143*	*-232927*	*n.a.*	*Neves Corvo*	*Lower VSC*	*Footwall*
	NCZ#40	*n.a.*	*n.a.*	*n.a.*	*Neves Corvo*	*Lower VSC*	*Footwall*
	NCL#7	*14305*	*-231809*	*n.a.*	*Neves Corvo*	*Lower VSC*	*Footwall*
	NCL#8	*14023*	*-232150*	*n.a.*	*Neves Corvo*	*Lower VSC*	*Footwall*
	NCL#36	*n.a.*	*n.a.*	*n.a.*	*Neves Corvo*	*Lower VSC*	*Footwall*
	NCL#37	*n.a.*	*n.a.*	*n.a.*	*Neves Corvo*	*Lower VSC*	*Footwall*
	NCN#16	*13545*	*-232243*	*n.a.*	*Neves Corvo*	*Lower VSC*	*Footwall*
	NCN#17	*13984*	*-232270*	*n.a.*	*Neves Corvo*	*Lower VSC*	*Footwall*
	NCN#18	*13990*	*-232270*	*n.a.*	*Neves Corvo*	*Lower VSC*	*Footwall*
	NCN#19	*14041*	*-232220*	*n.a.*	*Neves Corvo*	*Lower VSC*	*Footwall*
	NCN#22	*13544*	*-232592*	*n.a.*	*Neves Corvo*	*Lower VSC*	*Footwall*
	NCN#30	*13544*	*-232592*	*n.a.*	*Neves Corvo*	*Lower VSC*	*Footwall*
	NCC#23	*15127*	*-231817*	*n.a.*	*Neves Corvo*	*Lower VSC*	*Footwall*
	NCC#24	*15134*	*-231811*	*n.a.*	*Neves Corvo*	*Lower VSC*	*Footwall*
	NCN#20	*14018*	*-231726*	*n.a.*	*Neves Corvo*	*Lower VSC*	*Footwall*
	NCC#28	*14869*	*-232654*	*n.a.*	*Neves Corvo*	*Lower VSC*	*Footwall*
	L MS#2	*-25573*	*-181885*	*n.a.*	*Lousal*	*Lower VSC*	*Footwall*

SES20#10	-25066	-187756	-288.50	Lousal	Lower VSC	Footwall
NCG#4	14054	-233292	n.a.	Neves Corvo	Middle VSC	Footwall
NCL#34	14755	-231210	n.a.	Neves Corvo	Middle VSC	Footwall
37-1-B	8303	-198699	-91.57	Albernoa	Middle VSC	n.a.
X93	19263	-204661	n.a.	Albernoa	Middle VSC	n.a.
X64	26497	-210362	n.a.	Albernoa	Middle VSC	n.a.
NCZ#41	n.a.	n.a.	n.a.	Neves Corvo	Upper VSC	Hangingwall
NCZ#42	n.a.	n.a.	n.a.	Neves Corvo	Upper VSC	Hangingwall
NCL#6	14385	-231332	n.a.	Neves Corvo	Upper VSC	Hangingwall
NCL#31	14861	-231090	n.a.	Neves Corvo	Upper VSC	Hangingwall
NCL#33	14848	-231110	n.a.	Neves Corvo	Upper VSC	Hangingwall
NCC#38	n.a.	n.a.	n.a.	Neves Corvo	Upper VSC	Hangingwall
NCC#39	n.a.	n.a.	n.a.	Neves Corvo	Upper VSC	Hangingwall
ALJ_FM#4	-1303	-1999029	-107.23	Aljustrel	Upper VSC	Hangingwall
ALJ_FM#5	-1303	-1999029	-113.50	Aljustrel	Upper VSC	Hangingwall
ALJ_RS#7	-1729	-198714	-486.15	Aljustrel	Upper VSC	Hangingwall
FFM#1	n.a.	n.a.	n.a.	Aljustrel	Upper VSC	Hangingwall
FFM#2	n.a.	n.a.	n.a.	Aljustrel	Upper VSC	Hangingwall
ALJ_FM#1	-1303	-1999029	-94.45	Aljustrel	Upper VSC	Hangingwall
ALJ_FM#2	-1303	-1999029	-98.59	Aljustrel	Upper VSC	Hangingwall
ALJ_RS#1	-1729	-198714	-408.55	Aljustrel	Upper VSC	Hangingwall
ALJ_RS#3	-1729	-198714	-428.45	Aljustrel	Upper VSC	Hangingwall
ALJ_RS#6	-1729	-198714	-461.75	Aljustrel	Upper VSC	Hangingwall
ALJ_MM10-03#3	-3531	-198454	-63.50	Aljustrel	Upper VSC	Hangingwall
MFM#1	n.a.	n.a.	n.a.	Aljustrel	Upper VSC	Hangingwall
ALJ_MM16-15#1	-3469	-198137	-237.00	Aljustrel	Upper VSC	Hangingwall
GV7#3	-6403	-199158	-782.30	Aljustrel	Upper VSC	Hangingwall
GV7#4	-6403	-199158	-797.00	Aljustrel	Upper VSC	Hangingwall
GV8#1	-6663	-199331	-243.70	Aljustrel	Upper VSC	Hangingwall
GV9#7	-6219	-199247	-244.20	Aljustrel	Upper VSC	Hangingwall
X23	-624	-201919	n.a.	Aljustrel	Upper VSC	n.a.
EDS1-B	-257	-201023	-304.56	Aljustrel	Upper VSC	n.a.
L MS#3	-26006	-181998	n.a.	Lousal	Upper VSC	Hangingwall
L MS#4	-26006	-181998	n.a.	Lousal	Upper VSC	Hangingwall
SES20#6	-25066	-187756	273.78	Lousal	Upper VSC	Hangingwall
18-1-E	11823	-198489	-80.70	Albernoa	Upper VSC	n.a.
18-1-FF	11823	-198489	-159.60	Albernoa	Upper VSC	n.a.
ALB02# 2	14787	-204973	-93.80	Albernoa	Upper VSC	n.a.

	ALB02# 9	*14787*	*-204973*	*-244.16*	*Albernoa*	*Upper VSC*	*n.a.*
	ALB02# 48	14787	-204973	-473.00	*Albernoa*	*Upper VSC*	*n.a.*
	MM02#2	*-6931*	*-198313*	*-238.45*	*Aljustrel*	*Upper VSC*	*n.a.*
	MM02#3	*-6931*	*-198313*	*-255.30*	*Aljustrel*	*Upper VSC*	*n.a.*
	MDM02#1	*-9155*	*-193552*	*-86.50*	*Aljustrel*	*Upper VSC*	*n.a.*
	MDM02#7	*-9155*	*-193552*	*-151.00*	*Aljustrel*	*Upper VSC*	*n.a.*
	R MS#4	*4457*	*-228160*	*n.a.*	*Neves Corvo*	*Upper VSC*	*Hangingwall*
	R MS#5	*11359*	*-230546*	*n.a.*	*Neves Corvo*	*Upper VSC*	*Hangingwall*
Metapelites with a volcanic derived component	**NCS#2**	*15436*	*-233332*	*n.a.*	*Neves Corvo*	*Lower VSC*	*Footwall*
	NCS#3	*15480*	*-233202*	*n.a.*	*Neves Corvo*	*Lower VSC*	*Footwall*
	NCC#26	*15048*	*-232493*	*n.a.*	*Neves Corvo*	*Lower VSC*	*Footwall*
	NCL#5	*14444*	*-231728*	*n.a.*	*Neves Corvo*	*Upper VSC*	*Hangingwall*
	NCC#29	*14662*	*-231774*	*n.a.*	*Neves Corvo*	*Upper VSC*	*Hangingwall*
	NCL#32	*14853*	*-231102*	*n.a.*	*Neves Corvo*	*Upper VSC*	*Hangingwall*
	ALJ_FM#6	*-1303*	*-199029*	*-115.45*	*Aljustrel*	*Upper VSC*	*Hangingwall*
	ALJ_RS#12	*-1729*	*-198714*	*-550.93*	*Aljustrel*	*Upper VSC*	*Hangingwall*
	ALJ_RS#13	*-1729*	*-198714*	*-560.85*	*Aljustrel*	*Upper VSC*	*Hangingwall*
	ALJ_RS#15	*-1729*	*-198714*	*-585.55*	*Aljustrel*	*Upper VSC*	*Hangingwall*
	ALJ_MM10-03#1	*-3531*	*-198454*	*-41.50*	*Aljustrel*	*Upper VSC*	*Hangingwall*
	ALJ_MM10-03#4	-3531	-198454	-77.35	*Aljustrel*	*Upper VSC*	*Hangingwall*
	ALJ_MM16-15#9	*-3469*	*-198137*	*-340.47*	*Aljustrel*	*Upper VSC*	*Hangingwall*
	ALJ_MM16-15#10	*-3469*	*-198137*	*-356.55*	*Aljustrel*	*Upper VSC*	*Hangingwall*
	ALJ_MM16-15#11	*-3469*	*-198137*	*-383.80*	*Aljustrel*	*Upper VSC*	*Hangingwall*
	ALJ_MS#5	*-3795*	*-197814*	*-113.00*	*Aljustrel*	*Upper VSC*	*Hangingwall*
	GV8#5	*-6663*	*-199331*	*-391.20*	*Aljustrel*	*Upper VSC*	*Hangingwall*
	GV9#3	*-6219*	*-199247*	*-160.45*	*Aljustrel*	*Upper VSC*	*Hangingwall*
	GV9#6	*-6219*	*-199247*	*-223.60*	*Aljustrel*	*Upper VSC*	*Hangingwall*
	EDS1-T	*-527*	*-201023*	*-497*	*Aljustrel*	*Upper VSC*	*n.a.*
	SES18#1	*-24931*	*-187850*	*-262.35*	*Lousal*	*Upper VSC*	*n.a.*
	MDM02#9	*-9155*	*-193552*	*-371.55*	*Aljustrel*	*Upper VSC*	*n.a.*
	CW2-CC	*4228*	*-191707*	*-214.75*	*Albernoa*	*Upper VSC*	*n.a.*
	CW2-LL	*4228*	*-191707*	*-333.70*	*Albernoa*	*Upper VSC*	*n.a.*
	RT49	*4905*	*-191952*	*n.a.*	*Albernoa*	*Upper VSC*	*n.a.*

	Ref	Stratigraphic Division	Sector - Position	Sulphide abundance
Metapelites	**NCL#9**	*PQG*	*Neves Corvo (FW)*	*Mineralized*
	NCL#10	*PQG*	*Neves Corvo (FW)*	*Mineralized*
	NCL#11	*PQG*	*Neves Corvo (FW)*	*Mineralized*
	NCL#12	*PQG*	*Neves Corvo (FW)*	*No-sulphide*
	NCL#13	*PQG*	*Neves Corvo (FW)*	*No-sulphide*
	NCL#14	*PQG*	*Neves Corvo (FW)*	*Py-bearing*
	NCL#15	*PQG*	*Neves Corvo (FW)*	*No-sulphide*
	NCL#35	*PQG*	*Neves Corvo (FW)*	*No-sulphide*
	NCC#25	*PQG*	*Neves Corvo (FW)*	*No-sulphide*
	NCC#27	*PQG*	*Neves Corvo (FW)*	*No-sulphide*
	PC24	*PQG*	*Albernoa*	*No-sulphide*
	PC32	*PQG*	*Albernoa*	*No-sulphide*
	PC19	*PQG*	*Albernoa*	*No-sulphide*
	11-1-MM	*PQG*	*Albernoa*	*No-sulphide*
	ABNSTR1	*PQG*	*Albernoa*	*No-sulphide*
	L MS#1	*PQG*	*Lousal (FW)*	*No-sulphide*
	NCZ#1	*Lower VSC*	*Neves Corvo (FW)*	*Mineralized*
	NCZ#21	*Lower VSC*	*Neves Corvo (FW)*	*Mineralized*
	NCZ#40	*Lower VSC*	*Neves Corvo (FW)*	*Mineralized*
	NCL#7	*Lower VSC*	*Neves Corvo (FW)*	*Mineralized*
	NCL#8	*Lower VSC*	*Neves Corvo (FW)*	*Py-bearing*
	NCL#36	*Lower VSC*	*Neves Corvo (FW)*	*No-sulphide*
	NCL#37	*Lower VSC*	*Neves Corvo (FW)*	*No-sulphide*
	NCN#16	*Lower VSC*	*Neves Corvo (FW)*	*Mineralized*
	NCN#17	*Lower VSC*	*Neves Corvo (FW)*	*Py-bearing*
	NCN#18	*Lower VSC*	*Neves Corvo (FW)*	*Py-bearing*
	NCN#19	*Lower VSC*	*Neves Corvo (FW)*	*Mineralized*
	NCN#22	*Lower VSC*	*Neves Corvo (FW)*	*No-sulphide*
	NCN#30	*Lower VSC*	*Neves Corvo (FW)*	*No-sulphide*
	NCC#23	*Lower VSC*	*Neves Corvo (FW)*	*Mineralized*
	NCC#24	*Lower VSC*	*Neves Corvo (FW)*	*Py-bearing*
	NCN#20	*Lower VSC*	*Neves Corvo (FW)*	*Mineralized*
	NCC#28	*Lower VSC*	*Neves Corvo (FW)*	*No-sulphide*
	L MS#2	*Lower VSC*	*Lousal (FW)*	*Mineralized*
	SES20#10	*Lower VSC*	*Lousal (FW)*	*Mineralized*
	NCG#4	*Middle VSC*	*Neves Corvo (FW)*	*No-sulphide*
	NCL#34	*Middle VSC*	*Neves Corvo (FW)*	*Mineralized*
	37-1-B	*Middle VSC*	*Albernoa*	*No-sulphide*
	X93	*Middle VSC*	*Albernoa*	*No-sulphide*
	X64	*Middle VSC*	*Albernoa*	*Py-bearing*
	NCZ#41	*Upper VSC*	*Neves Corvo (HW)*	*No-sulphide*
	NCZ#42	*Upper VSC*	*Neves Corvo (HW)*	*No-sulphide*
	NCL#6	*Upper VSC*	*Neves Corvo (HW)*	*Mineralized*
	NCL#31	*Upper VSC*	*Neves Corvo (HW)*	*Py-bearing*
	NCL#33	*Upper VSC*	*Neves Corvo (HW)*	*No-sulphide*
	NCC#38	*Upper VSC*	*Neves Corvo (HW)*	*Mineralized*
	NCC#39	*Upper VSC*	*Neves Corvo (HW)*	*No-sulphide*

	ALJ_FM#4	*Upper VSC*	*Aljustrel (HW)*	*No-sulphide*
	ALJ_FM#5	*Upper VSC*	*Aljustrel (HW)*	*Py-bearing*
	ALJ_RS#7	*Upper VSC*	*Aljustrel (HW)*	*No-sulphide*
	FFM#1	*Upper VSC*	*Aljustrel (HW)*	*No-sulphide*
	FFM#2	*Upper VSC*	*Aljustrel (HW)*	*No-sulphide*
	ALJ_FM#1	*Upper VSC*	*Aljustrel (HW)*	*Py-bearing*
	ALJ_FM#2	*Upper VSC*	*Aljustrel (HW)*	*Py-bearing*
	ALJ_RS#1	*Upper VSC*	*Aljustrel (HW)*	*Py-bearing*
	ALJ_RS#3	*Upper VSC*	*Aljustrel (HW)*	*Py-bearing*
	ALJ_RS#6	*Upper VSC*	*Aljustrel (HW)*	*No-sulphide*
	ALJ_MM10-03#3	*Upper VSC*	*Aljustrel (HW)*	*Py-bearing*
	MFM#1	*Upper VSC*	*Aljustrel (HW)*	*Mineralized*
	ALJ_MM16-15#1	*Upper VSC*	*Aljustrel (HW)*	*Py-bearing*
	GV7#3	*Upper VSC*	*Aljustrel (HW)*	*Mineralized*
	GV7#4	*Upper VSC*	*Aljustrel (HW)*	*Py-bearing*
	GV8#1	*Upper VSC*	*Aljustrel (HW)*	*Py-bearing*
	GV9#7	*Upper VSC*	*Aljustrel (HW)*	*Py-bearing*
	X23	*Upper VSC*	*Aljustrel*	*Mineralized*
	EDS1-B	*Upper VSC*	*Aljustrel*	*Mineralized*
	L MS#3	*Upper VSC*	*Lousal (HW)*	*No-sulphide*
	L MS#4	*Upper VSC*	*Lousal (HW)*	*No-sulphide*
	SES20#6	*Upper VSC*	*Lousal (HW)*	*Py-bearing*
	18-1-E	*Upper VSC*	*Albernoa*	*Mineralized*
	18-1-FF	*Upper VSC*	*Albernoa*	*Mineralized*
	ALB02# 2	*Upper VSC*	*Albernoa*	*No-sulphide*
	ALB02# 9	*Upper VSC*	*Albernoa*	*No-sulphide*
	ALB02# 48	*Upper VSC*	*Albernoa*	*No-sulphide*
	MM02#2	*Upper VSC*	*Aljustrel*	*No-sulphide*
	MM02#3	*Upper VSC*	*Aljustrel*	*Py-bearing*
	MDM02#1	*Upper VSC*	*Aljustrel*	*No-sulphide*
	MDM02#7	*Upper VSC*	*Aljustrel*	*No-sulphide*
	R MS#4	*Upper VSC*	*Neves Corvo (HW)*	*No-sulphide*
	R MS#5	*Upper VSC*	*Neves Corvo (HW)*	*No-sulphide*
Metapelites with a volcanic derived component	**NCS#2**	*Lower VSC*	*Neves Corvo (FW)*	*No-sulphide*
	NCS#3	*Lower VSC*	*Neves Corvo (FW)*	*No-sulphide*
	NCC#26	*Lower VSC*	*Neves Corvo (FW)*	*Py-bearing*
	NCL#5	*Upper VSC*	*Neves Corvo (HW)*	*No-sulphide*
	NCC#29	*Upper VSC*	*Neves Corvo (HW)*	*Py-bearing*
	NCL#32	*Upper VSC*	*Neves Corvo (HW)*	*Py-bearing*
	ALJ_FM#6	*Upper VSC*	*Aljustrel (HW)*	*Py-bearing*
	ALJ_RS#12	*Upper VSC*	*Aljustrel (HW)*	*No-sulphide*
	ALJ_RS#13	*Upper VSC*	*Aljustrel (HW)*	*No-sulphide*
	ALJ_RS#15	*Upper VSC*	*Aljustrel (HW)*	*No-sulphide*
	ALJ_MM10-03#1	*Upper VSC*	*Aljustrel (HW)*	*No-sulphide*
	ALJ_MM10-03#4	*Upper VSC*	*Aljustrel (HW)*	*No-sulphide*
	ALJ_MM16-15#9	*Upper VSC*	*Aljustrel (HW)*	*No-sulphide*
	ALJ_MM16-15#10	*Upper VSC*	*Aljustrel (HW)*	*No-sulphide*
	ALJ_MM16-15#11	*Upper VSC*	*Aljustrel (HW)*	*Py-bearing*
	ALJ_MS#5	*Upper VSC*	*Aljustrel (HW)*	*Py-bearing*

GV8#5	*Upper VSC*	*Aljustrel (HW)*	*Py-bearing*
GV9#3	*Upper VSC*	*Aljustrel (HW)*	*Py-bearing*
GV9#6	*Upper VSC*	*Aljustrel (HW)*	*No-sulphide*
EDS1-T	*Upper VSC*	*Aljustrel*	*Mineralized*
SES18#1	*Upper VSC*	*Lousal*	*No-sulphide*
MDM02#9	*Upper VSC*	*Aljustrel*	*No-sulphide*
CW2-CC	*Upper VSC*	*Albernoa*	*Mineralized*
CW2-LL	*Upper VSC*	*Albernoa*	*Mineralized*
RT49	*Upper VSC*	*Albernoa*	*No-sulphide*

Rb ppm	Sr ppm	$^{87}Rb/^{86}Sr$	$^{87}Sr/^{86}Sr$	Error (± 2σ)	$^{87}Sr/^{86}Sr$ (i)	Ɛ Sr(0)	Ɛ Sr(i)
13	22	1.714	0.7341771	0.00002	0.7254472	421	297
45	23	5.675	0.7448991	0.000077	0.7159941	573	163
84	26	9.370	0.7665809	0.000018	0.7188506	881	204
211	39	15.692	0.8046551	0.000022	0.7236812	1422	287
239	60	11.553	0.7765761	0.000069	0.7171208	1023	188
184	67	-	-	-	-	-	-
179	30	17.306	0.8151098	0.000074	0.7257178	1570	319
91	41	6.437	0.7546034	0.000052	0.7215456	711	246
152	58	-	-	-	-	-	-
108	41	7.640	0.7575069	0.000062	0.7182625	752	200
160	120	3.867	0.7311692	0.000021	0.7113557	379	99
93	121	2.229	0.7216981	0.000041	0.7102872	244	83
146	90	4.705	0.7349845	0.00002	0.7108691	433	93
138	90	4.447	0.734998	0.000029	0.7122039	433	111
151	82	5.341	0.8475608	0.000024	0.8198855	2031	1645
161	111	4.207	0.7370744	0.000055	0.7155081	462	158
50	30	4.834	0.7380438	0.00002	0.7132603	476	127
154	41	10.894	0.7653513	0.000021	0.7093489	864	76
172	57	8.752	0.7557946	0.000025	0.7108456	728	95
6	11	-	-	-	-	-	-
226	75	8.740	0.7629389	0.000059	0.7180214	830	198
9	8	3.263	0.7326948	0.000027	0.7159747	400	164
99	33	8.701	0.7560726	0.000015	0.7113838	732	103
248	64	11.239	0.7670315	0.000018	0.7092468	888	75
163	148	-	-	-	-	-	-
198	120	4.786	0.7371846	0.000017	0.7126509	464	118
162	79	-	-	-	-	-	-
178	104	-	-	-	-	-	-
196	115	4.943	0.7375553	0.000018	0.7122126	469	112
191	131	-	-	-	-	-	-
150	146	-	-	-	-	-	-
180	106	4.925	0.7388164	0.000019	0.7135634	487	131
73	18	11.763	0.7705726	0.000038	0.7100747	938	87
185	80	6.707	0.7421624	0.000021	0.7077614	535	50
60	363	0.479	0.8075321	0.000019	0.7169581	1462	1428
187	193	2.810	0.7253912	0.000018	0.7114019	297	99
204	43	13.760	0.7788631	0.000017	0.710008	1056	88
278	207	3.895	0.7344201	0.000024	0.7150126	425	151
216	98	6.393	0.7448518	0.000021	0.7129683	573	123
195	53	10.671	0.761882	0.000058	0.708571	815	64
205	116	5.126	0.7344024	0.000022	0.7088641	424	64
145	131	3.210	0.7232245	0.00004	0.7072466	266	40
282	99	8.262	0.7525204	0.000068	0.7112845	682	101
102	41	7.216	0.7429352	0.000054	0.7069542	546	38
78	38	5.953	0.7385691	0.000049	0.7088946	484	65
146	105	4.033	0.7292084	0.000035	0.709125	351	67
144	125	3.341	0.7247099	0.00002	0.7080782	287	52

120	60	5.801	0.7364707	0.000027	0.707563	454	46
170	28	17.609	0.7937399	0.000023	0.7054943	1267	29
137	40	9.934	0.756495	0.000031	0.706894	738	40
104	194	1.555	0.713862	0.000037	0.7061307	133	24
133	198	1.948	0.7157063	0.000044	0.706017	159	22
140	86	4.722	0.7313773	0.000015	0.7078595	382	50
157	99	4.600	0.7305006	0.000019	0.7075922	369	46
124	118	3.048	0.7230359	0.00002	0.707867	263	49
112	97	3.349	0.7245129	0.000021	0.7078434	284	49
92	98	2.723	0.7231214	0.00002	0.7095702	264	73
32	184	0.504	0.7119014	0.000039	0.7093937	105	70
91	35	7.541	0.744261	0.000091	0.7066525	564	34
197	39	14.651	0.7773317	0.000021	0.7040304	1034	4
126	149	2.453	0.7196587	0.000028	0.7074561	215	43
157	122	3.732	0.7246812	0.000068	0.7061022	286	24
215	59	10.569	0.7602573	0.000063	0.7074643	791	48
136	88	4.482	0.7294843	0.000022	0.7071618	355	40
4	121	0.096	0.7344201	0.000037	0.7339424	425	418
119	107	3.226	0.734998	0.000018	0.7189255	433	206
25	33	2.197	0.7198086	0.000057	0.7088766	217	63
137	22	18.061	0.7972615	0.00003	0.7067199	1317	47
308	38	23.508	0.816108	0.000021	0.6980459	1584	-68
114	94	3.517	0.7280498	0.000037	0.7105351	334	87
101	18	16.274	0.803682	0.000138	0.7220482	1408	264
115	60	5.559	0.7425167	0.000014	0.7147972	540	149
230	106	6.293	0.7461319	0.000016	0.7147403	591	149
155	104	4.323	0.7332297	0.000012	0.7116948	408	104
168	84	5.801	0.7381759	0.000064	0.7092635	478	70
117	83	4.088	0.7279762	0.000054	0.7076184	333	46
198	71	8.088	0.7494983	0.000026	0.7091393	639	70
262	32	23.747	0.8218344	0.000048	0.7025083	1665	-4
152	22	20.039	0.8073836	0.000021	0.7081462	1460	52
103	22	13.579	0.7782268	0.000052	0.7109804	1047	92
170	98	5.031	0.7357206	0.000017	0.7099314	443	79
131	132	2.878	0.7257985	0.000018	0.7110587	302	94
170	93	5.302	0.7417916	0.00002	0.7145997	529	146
184	107	4.988	0.7364801	0.00002	0.7116249	454	103
197	60	9.523	0.7574277	0.000053	0.7098739	751	82
134	123	3.160	0.7244186	0.000018	0.7086907	283	61
221	27	23.740	0.8207155	0.000025	0.701436	1650	-19
164	31	15.344	0.7778714	0.000061	0.7010972	1041	-37
208	37	16.305	0.7906267	0.000047	0.7089435	1223	76
217	24	26.224	0.831647	0.000079	0.699747	1805	-39
166	82	5.871	0.7363216	0.000019	0.7070619	452	39
135	57	6.869	0.7385452	0.000022	0.7043055	483	0
164	136	3.498	0.7249978	0.000018	0.7075877	291	45
148	124	3.462	0.7260054	0.000019	0.7087717	305	62
101	111	2.639	0.7214452	0.000018	0.7083128	241	55
141	13	-	-	-	-	-	-

100	104	2.789	0.7212018	0.000053	0.7073246	237	41
127	100	3.683	0.7268182	0.000038	0.7084792	317	58
117	107	3.171	0.7230944	0.000065	0.7073104	264	41
197	41	13.936	0.7426405	0.000067	0.6731498	541	-438
177	80	6.417	0.7444259	0.000028	0.712422	567	116
127	22	16.743	0.7880023	0.000023	0.7041449	1185	8
107	95	3.267	0.7261188	0.000039	0.7098557	307	77
64	42	4.420	0.7306597	0.000041	0.7086473	371	61
38	14	7.872	0.745731	0.000042	0.7064637	585	32

	Ref	Stratigraphic Division	Sector - Position	Sulphide abundance
Metapelites	**NCL#9**	*PQG*	*Neves Corvo (FW)*	*Mineralized*
	NCL#10	*PQG*	*Neves Corvo (FW)*	*Mineralized*
	NCL#11	*PQG*	*Neves Corvo (FW)*	*Mineralized*
	NCL#12	*PQG*	*Neves Corvo (FW)*	*No-sulphide*
	NCL#13	*PQG*	*Neves Corvo (FW)*	*No-sulphide*
	NCL#14	*PQG*	*Neves Corvo (FW)*	*Py-bearing*
	NCL#15	*PQG*	*Neves Corvo (FW)*	*No-sulphide*
	NCL#35	*PQG*	*Neves Corvo (FW)*	*No-sulphide*
	NCC#25	*PQG*	*Neves Corvo (FW)*	*No-sulphide*
	NCC#27	*PQG*	*Neves Corvo (FW)*	*No-sulphide*
	PC24	*PQG*	*Albernoa*	*No-sulphide*
	PC32	*PQG*	*Albernoa*	*No-sulphide*
	PC19	*PQG*	*Albernoa*	*No-sulphide*
	11-1-MM	*PQG*	*Albernoa*	*No-sulphide*
	ABNSTR1	*PQG*	*Albernoa*	*No-sulphide*
	L MS#1	*PQG*	*Lousal (FW)*	*No-sulphide*
	NCZ#1	*Lower VSC*	*Neves Corvo (FW)*	*Mineralized*
	NCZ#21	*Lower VSC*	*Neves Corvo (FW)*	*Mineralized*
	NCZ#40	*Lower VSC*	*Neves Corvo (FW)*	*Mineralized*
	NCL#7	*Lower VSC*	*Neves Corvo (FW)*	*Mineralized*
	NCL#8	*Lower VSC*	*Neves Corvo (FW)*	*Py-bearing*
	NCL#36	*Lower VSC*	*Neves Corvo (FW)*	*No-sulphide*
	NCL#37	*Lower VSC*	*Neves Corvo (FW)*	*No-sulphide*
	NCN#16	*Lower VSC*	*Neves Corvo (FW)*	*Mineralized*
	NCN#17	*Lower VSC*	*Neves Corvo (FW)*	*Py-bearing*
	NCN#18	*Lower VSC*	*Neves Corvo (FW)*	*Py-bearing*
	NCN#19	*Lower VSC*	*Neves Corvo (FW)*	*Mineralized*
	NCN#22	*Lower VSC*	*Neves Corvo (FW)*	*No-sulphide*
	NCN#30	*Lower VSC*	*Neves Corvo (FW)*	*No-sulphide*
	NCC#23	*Lower VSC*	*Neves Corvo (FW)*	*Mineralized*
	NCC#24	*Lower VSC*	*Neves Corvo (FW)*	*Py-bearing*
	NCN#20	*Lower VSC*	*Neves Corvo (FW)*	*Mineralized*
	NCC#28	*Lower VSC*	*Neves Corvo (FW)*	*No-sulphide*
	L MS#2	*Lower VSC*	*Lousal (FW)*	*Mineralized*
	SES20#10	*Lower VSC*	*Lousal (FW)*	*Mineralized*
	NCG#4	*Middle VSC*	*Neves Corvo (FW)*	*No-sulphide*
	NCL#34	*Middle VSC*	*Neves Corvo (FW)*	*Mineralized*
	37-1-B	*Middle VSC*	*Albernoa*	*No-sulphide*
	X93	*Middle VSC*	*Albernoa*	*No-sulphide*
	X64	*Middle VSC*	*Albernoa*	*Py-bearing*
	NCZ#41	*Upper VSC*	*Neves Corvo (HW)*	*No-sulphide*
	NCZ#42	*Upper VSC*	*Neves Corvo (HW)*	*No-sulphide*
	NCL#6	*Upper VSC*	*Neves Corvo (HW)*	*Mineralized*
	NCL#31	*Upper VSC*	*Neves Corvo (HW)*	*Py-bearing*
	NCL#33	*Upper VSC*	*Neves Corvo (HW)*	*No-sulphide*
	NCC#38	*Upper VSC*	*Neves Corvo (HW)*	*Mineralized*
	NCC#39	*Upper VSC*	*Neves Corvo (HW)*	*No-sulphide*

	ALJ_FM#4	*Upper VSC*	*Aljustrel (HW)*	*No-sulphide*
	ALJ_FM#5	*Upper VSC*	*Aljustrel (HW)*	*Py-bearing*
	ALJ_RS#7	*Upper VSC*	*Aljustrel (HW)*	*No-sulphide*
	FFM#1	*Upper VSC*	*Aljustrel (HW)*	*No-sulphide*
	FFM#2	*Upper VSC*	*Aljustrel (HW)*	*No-sulphide*
	ALJ_FM#1	*Upper VSC*	*Aljustrel (HW)*	*Py-bearing*
	ALJ_FM#2	*Upper VSC*	*Aljustrel (HW)*	*Py-bearing*
	ALJ_RS#1	*Upper VSC*	*Aljustrel (HW)*	*Py-bearing*
	ALJ_RS#3	*Upper VSC*	*Aljustrel (HW)*	*Py-bearing*
	ALJ_RS#6	*Upper VSC*	*Aljustrel (HW)*	*No-sulphide*
	ALJ_MM10-03#3	*Upper VSC*	*Aljustrel (HW)*	*Py-bearing*
	MFM#1	*Upper VSC*	*Aljustrel (HW)*	*Mineralized*
	ALJ_MM16-15#1	*Upper VSC*	*Aljustrel (HW)*	*Py-bearing*
	GV7#3	*Upper VSC*	*Aljustrel (HW)*	*Mineralized*
	GV7#4	*Upper VSC*	*Aljustrel (HW)*	*Py-bearing*
	GV8#1	*Upper VSC*	*Aljustrel (HW)*	*Py-bearing*
	GV9#7	*Upper VSC*	*Aljustrel (HW)*	*Py-bearing*
	X23	*Upper VSC*	*Aljustrel*	*Mineralized*
	EDS1-B	*Upper VSC*	*Aljustrel*	*Mineralized*
	L MS#3	*Upper VSC*	*Lousal (HW)*	*No-sulphide*
	L MS#4	*Upper VSC*	*Lousal (HW)*	*No-sulphide*
	SES20#6	*Upper VSC*	*Lousal (HW)*	*Py-bearing*
	18-1-E	*Upper VSC*	*Albernoa*	*Mineralized*
	18-1-FF	*Upper VSC*	*Albernoa*	*Mineralized*
	ALB02# 2	*Upper VSC*	*Albernoa*	*No-sulphide*
	ALB02# 9	*Upper VSC*	*Albernoa*	*No-sulphide*
	ALB02# 48	*Upper VSC*	*Albernoa*	*No-sulphide*
	MM02#2	*Upper VSC*	*Aljustrel*	*No-sulphide*
	MM02#3	*Upper VSC*	*Aljustrel*	*Py-bearing*
	MDM02#1	*Upper VSC*	*Aljustrel*	*No-sulphide*
	MDM02#7	*Upper VSC*	*Aljustrel*	*No-sulphide*
	R MS#4	*Upper VSC*	*Neves Corvo (HW)*	*No-sulphide*
	R MS#5	*Upper VSC*	*Neves Corvo (HW)*	*No-sulphide*
Metapelites with a volcanic derived component	**NCS#2**	*Lower VSC*	*Neves Corvo (FW)*	*No-sulphide*
	NCS#3	*Lower VSC*	*Neves Corvo (FW)*	*No-sulphide*
	NCC#26	*Lower VSC*	*Neves Corvo (FW)*	*Py-bearing*
	NCL#5	*Upper VSC*	*Neves Corvo (HW)*	*No-sulphide*
	NCC#29	*Upper VSC*	*Neves Corvo (HW)*	*Py-bearing*
	NCL#32	*Upper VSC*	*Neves Corvo (HW)*	*Py-bearing*
	ALJ_FM#6	*Upper VSC*	*Aljustrel (HW)*	*Py-bearing*
	ALJ_RS#12	*Upper VSC*	*Aljustrel (HW)*	*No-sulphide*
	ALJ_RS#13	*Upper VSC*	*Aljustrel (HW)*	*No-sulphide*
	ALJ_RS#15	*Upper VSC*	*Aljustrel (HW)*	*No-sulphide*
	ALJ_MM10-03#1	*Upper VSC*	*Aljustrel (HW)*	*No-sulphide*
	ALJ_MM10-03#4	*Upper VSC*	*Aljustrel (HW)*	*No-sulphide*
	ALJ_MM16-15#9	*Upper VSC*	*Aljustrel (HW)*	*No-sulphide*
	ALJ_MM16-15#10	*Upper VSC*	*Aljustrel (HW)*	*No-sulphide*
	ALJ_MM16-15#11	*Upper VSC*	*Aljustrel (HW)*	*Py-bearing*
	ALJ_MS#5	*Upper VSC*	*Aljustrel (HW)*	*Py-bearing*

GV8#5	*Upper VSC*	*Aljustrel (HW)*	*Py-bearing*
GV9#3	*Upper VSC*	*Aljustrel (HW)*	*Py-bearing*
GV9#6	*Upper VSC*	*Aljustrel (HW)*	*No-sulphide*
EDS1-T	*Upper VSC*	*Aljustrel*	*Mineralized*
SES18#1	*Upper VSC*	*Lousal*	*No-sulphide*
MDM02#9	*Upper VSC*	*Aljustrel*	*No-sulphide*
CW2-CC	*Upper VSC*	*Albernoa*	*Mineralized*
CW2-LL	*Upper VSC*	*Albernoa*	*Mineralized*
RT49	*Upper VSC*	*Albernoa*	*No-sulphide*

Sm ppm	Nd ppm	$^{147}Sm/^{144}Nd$	$^{143}Nd/^{144}Nd$	Error (± 2σ)	Ɛ Nd(0)	Ɛ Nd(i)	T_{DM^*} (Ga)	$f_{Sm/Nd}$
4.98	25.5	0.117582297	0.511953	0.000004	-13.4	-9.7	1.90	-0.40
6.26	28.5	0.13224591	0.5119794	0.000004	-12.8	-9.9	1.85	-0.32
5.3	26	0.12273129	0.511951	0.000004	-13.4	-10.0	2.02	-0.37
8.22	42.2	0.11727681	0.5119654	0.000004	-13.1	-9.5	1.88	-0.40
9.96	51	0.117582297	0.511956	0.000005	-13.3	-9.7	1.90	-0.40
9.5	46	-	-	-	-	-	-	-
8.77	46.9	0.112584739	0.5119194	0.000005	-14.0	-10.2	1.86	-0.43
8.09	38	0.128179243	0.5119548	0.000005	-13.3	-10.2	1.88	-0.35
8	40.5	-	-	-	-	-	-	-
6.83	36.1	0.113911161	0.5119289	0.000004	-13.8	-10.0	1.87	-0.42
7.3	40.4	0.108791326	0.5119559	0.000005	-13.3	-9.3	1.74	-0.44
8.09	39.1	0.124573177	0.512004	0.000006	-12.4	-9.1	1.97	-0.36
5.93	27.9	0.127968555	0.5122318	0.000005	-7.9	-4.8	1.64	-0.35
6.8	35.5	0.115327622	0.5119668	0.000003	-13.1	-9.4	1.84	-0.41
10.9	50	0.13125301	0.5120442	0.000004	-11.6	-8.6	1.75	-0.33
7.49	39.5	0.114166188	0.5119642	0.000005	-13.1	-9.4	1.82	-0.42
5.85	29.3	0.120210118	0.5120615	0.000005	-11.2	-7.7	1.78	-0.39
7.9	40.6	0.117153113	0.5119516	0.000005	-13.4	-9.7	1.90	-0.40
8.88	43.9	0.121787081	0.5120407	0.000005	-11.7	-8.2	1.85	-0.38
5.36	26.6	0.121320986	0.5120444	0.000005	-11.6	-8.1	1.83	-0.38
42.8	8.13	3.169611252	0.5119554	0.000004	-13.3	-150.0	1.84	-
4.45	21.2	0.126379585	0.5120601	0.000006	-11.3	-8.0	1.91	-0.35
5.45	26.4	0.124292623	0.5120497	0.000005	-11.5	-8.1	1.88	-0.37
5.03	21.9	0.138285501	0.5120914	0.000006	-10.7	-8.0	1.71	-0.29
13.4	65	-	-	-	-	-	-	-
10.3	52	0.119257763	0.5119646	0.000005	-13.1	-9.6	1.92	-0.39
8.64	40.5	-	-	-	-	-	-	-
9.12	46.6	-	-	-	-	-	-	-
9.83	50.5	0.117196574	0.5120108	0.000004	-12.2	-8.6	1.81	-0.40
7.62	41	-	-	-	-	-	-	-
5.87	29.1	-	-	-	-	-	-	-
9.43	46.9	0.121057479	0.51196	0.000005	-13.2	-9.8	1.96	-0.38
5.42	24.1	0.135405099	0.5120735	0.000005	-11.0	-8.2	1.72	-0.31
8.81	44.3	0.119736059	0.5119757	0.000006	-12.9	-9.4	1.91	-0.39
6.41	34.6	0.111541045	0.5120031	0.000006	-12.4	-8.5	1.72	-0.43
10.3	53.4	0.116131155	0.5119718	0.000004	-13.0	-9.3	1.85	-0.41
5.21	26.3	0.11927097	0.5120235	0.000005	-12.0	-8.4	1.82	-0.39
9.73	54.7	0.107097243	0.5118843	0.000003	-14.7	-10.6	1.81	-0.45
7.33	40.2	0.109781889	0.5119378	0.000005	-13.7	-9.7	1.78	-0.44
7.4	41	0.108667741	0.511944	0.000004	-13.5	-9.5	1.75	-0.45
5.43	29.1	0.112346518	0.512015	0.000005	-12.2	-8.3	1.71	-0.43
7.52	34.7	0.130479157	0.5122631	0.000005	-7.3	-4.3	1.42	-0.33
8.46	42.6	0.119567608	0.5120217	0.000004	-12.0	-8.5	1.83	-0.39
5.67	28.5	0.119781839	0.5121831	0.000006	-8.9	-5.3	1.58	-0.39
4.78	24.6	0.116989145	0.5120871	0.000006	-10.7	-7.1	1.68	-0.40
5.33	29.1	0.110277521	0.5120107	0.000005	-12.2	-8.3	1.68	-0.44
6.95	33.3	0.125658927	0.5120719	0.000005	-11.0	-7.8	1.87	-0.36

6.13	30.6	0.120612363	0.5120953	0.000005	-10.6	-7.1	1.73	-0.38
5.59	28.8	0.116861672	0.5120714	0.000005	-11.1	-7.4	1.70	-0.40
5.21	26.6	0.117925809	0.5120374	0.000004	-11.7	-8.1	1.78	-0.40
5.45	28.4	0.115539621	0.5122203	0.000005	-8.1	-4.4	1.45	-0.41
5.95	30.4	0.117840929	0.5122612	0.000005	-7.4	-3.7	1.42	-0.40
5.53	28.5	0.116824262	0.5120452	0.00005	-11.6	-7.9	1.74	-0.40
7.01	36.6	0.115316037	0.5120383	0.000005	-11.7	-8.0	1.73	-0.41
5.12	26	0.118563057	0.5120535	0.000004	-11.4	-7.8	1.76	-0.39
6.09	30.2	0.121412423	0.51209	0.000005	-10.7	-7.2	1.76	-0.38
6.65	32.8	0.122067648	0.5120722	0.000004	-11.0	-7.6	1.80	-0.38
4.04	19.8	0.122848244	0.5121251	0.000004	-11.1	-7.7	1.73	-0.37
1.43	5.85	0.147174628	0.512255	0.000008	-7.5	-5.2	1.49	-0.25
5.27	27.1	0.11708307	0.5120668	0.000004	-11.1	-7.5	1.72	-0.40
5.95	30.6	0.117070727	0.5120468	0.000005	-11.5	-7.9	1.75	-0.40
7.28	33.2	0.132021928	0.5122687	0.000005	-7.2	-4.2	1.41	-0.33
6.79	34.8	0.117474419	0.5120587	0.000005	-11.3	-7.7	1.73	-0.40
5.74	30.2	0.114434698	0.5120362	0.000005	-11.7	-8.0	1.72	-0.42
3.58	20.3	0.106179277	0.5120754	0.000004	-11.0	-6.8	1.53	-0.46
5.63	28.2	0.120202102	0.5120226	0.000005	-12.0	-8.5	1.84	-0.39
5.69	20.7	0.165498742	0.5122868	0.000005	-6.9	-5.4	1.50	-0.16
2.8	14.7	0.114681529	0.5121399	0.000005	-9.7	-5.9	1.56	-0.41
4.73	18.7	0.152290324	0.5121713	0.000012	-9.1	-7.1	1.63	-0.22
4.6	23.6	0.117354191	0.5120855	0.000003	-10.8	-7.1	1.69	-0.40
5.14	28.1	0.110130998	0.5120849	0.000004	-10.8	-6.8	1.57	-0.44
5.63	29.3	0.115689395	0.511924	0.000005	-13.9	-10.2	1.91	-0.41
8.3	43.5	0.114879255	0.5119414	0.000005	-13.6	-9.8	1.87	-0.41
7.72	39.4	0.117970618	0.5120369	0.000005	-11.7	-8.1	1.78	-0.40
6.93	33.2	0.12567472	0.5121229	0.000005	-10.0	-6.8	1.79	-0.36
6.93	35.8	0.116547506	0.512254	0.000006	-7.5	-3.8	1.41	-0.40
7.26	37.7	0.115943938	0.5120158	0.000005	-12.1	-8.4	1.77	-0.41
14	68.3	0.123412772	0.5121562	0.000005	-9.4	-6.0	1.69	-0.37
5.28	26.6	0.119510225	0.5120084	0.000005	-12.3	-8.7	1.85	-0.39
4.8	23.4	0.123503185	0.5120197	0.000005	-12.1	-8.7	1.92	-0.37
9.69	49.5	0.117861335	0.5120306	0.000004	-11.8	-8.2	1.79	-0.40
7.95	39.4	0.121485287	0.5120605	0.000005	-11.3	-7.8	1.81	-0.38
9.8	48.6	0.12140668	0.5119488	0.000005	-13.4	-10.0	1.99	-0.38
8.26	39.7	0.125268627	0.5121331	0.000005	-9.8	-6.6	1.76	-0.36
8.32	38.8	0.129105391	0.5122172	0.000006	-8.2	-5.1	1.69	-0.34
6.46	31.6	0.123083039	0.5121236	0.000006	-10.0	-6.6	1.73	-0.37
6.52	33.6	0.116831807	0.5120609	0.000005	-11.3	-7.6	1.72	-0.40
5.66	29	0.117509021	0.5121049	0.000004	-10.4	-6.8	1.66	-0.40
5.89	29.3	0.121032067	0.5120501	0.000005	-11.5	-8.0	1.82	-0.38
8.28	40.6	0.122788326	0.512084	0.000004	-10.8	-7.4	1.79	-0.37
7.66	31.2	0.147817874	0.512523	0.000004	-2.2	0.0	1.08	-0.25
6	24.4	0.148051973	0.5124681	0.000005	-3.3	-1.1	1.16	-0.24
6.99	34	0.123780159	0.5121831	0.000004	-8.9	-5.5	1.65	-0.37
6.79	34.3	0.119186874	0.5120954	0.000004	-10.6	-7.0	1.71	-0.39
4.93	24.7	0.120171849	0.5120784	0.000005	-10.9	-7.4	1.75	-0.39
5.66	29.3	0.116305857	0.5120633	0.000005	-11.2	-7.5	1.71	-0.41

6.38	32.1	0.119665352	0.5121357	0.000005	-9.8	-6.3	1.65	-0.39
5.36	29.2	0.110518432	0.512008	0.000005	-12.3	-8.3	1.69	-0.44
3.4	14.4	0.142157312	0.512274	0.000006	-7.1	-4.6	1.44	-0.27
6.5	34.7	0.112781186	0.5120161	0.000006	-12.1	-8.3	1.72	-0.42
6.62	32.9	0.121147615	0.5119912	0.000004	-12.6	-9.1	1.91	-0.38
3.97	19.8	0.120719685	0.5120453	0.000005	-11.6	-8.1	1.82	-0.38
6.95	38.6	0.10840524	0.5120143	0.000004	-12.2	-8.1	1.65	-0.45
7.01	32.7	0.129069326	0.5121172	0.000003	-10.2	-7.0	1.87	-0.34
3.34	16.8	0.119698846	0.5121343	0.000004	-9.8	-6.3	1.65	-0.39

	Ref	Stratigraphic Division	Sector - Position
Metapelites	**NCL#9**	*PQG*	*Neves Corvo (FW)*
	NCL#10	*PQG*	*Neves Corvo (FW)*
	NCL#11	*PQG*	*Neves Corvo (FW)*
	NCL#12	*PQG*	*Neves Corvo (FW)*
	NCL#13	*PQG*	*Neves Corvo (FW)*
	NCL#14	*PQG*	*Neves Corvo (FW)*
	NCL#15	*PQG*	*Neves Corvo (FW)*
	NCL#35	*PQG*	*Neves Corvo (FW)*
	NCC#25	*PQG*	*Neves Corvo (FW)*
	NCC#27	*PQG*	*Neves Corvo (FW)*
	PC24	*PQG*	*Albernoa*
	PC32	*PQG*	*Albernoa*
	PC19	*PQG*	*Albernoa*
	11-1-MM	*PQG*	*Albernoa*
	ABNSTR1	*PQG*	*Albernoa*
	L MS#1	*PQG*	*Lousal (FW)*
	NCZ#1	*Lower VSC*	*Neves Corvo (FW)*
	NCZ#21	*Lower VSC*	*Neves Corvo (FW)*
	NCZ#40	*Lower VSC*	*Neves Corvo (FW)*
	NCL#7	*Lower VSC*	*Neves Corvo (FW)*
	NCL#8	*Lower VSC*	*Neves Corvo (FW)*
	NCL#36	*Lower VSC*	*Neves Corvo (FW)*
	NCL#37	*Lower VSC*	*Neves Corvo (FW)*
	NCN#16	*Lower VSC*	*Neves Corvo (FW)*
	NCN#17	*Lower VSC*	*Neves Corvo (FW)*
	NCN#18	*Lower VSC*	*Neves Corvo (FW)*
	NCN#19	*Lower VSC*	*Neves Corvo (FW)*
	NCN#22	*Lower VSC*	*Neves Corvo (FW)*
	NCN#30	*Lower VSC*	*Neves Corvo (FW)*
	NCC#23	*Lower VSC*	*Neves Corvo (FW)*
	NCC#24	*Lower VSC*	*Neves Corvo (FW)*
	NCN#20	*Lower VSC*	*Neves Corvo (FW)*
	NCC#28	*Lower VSC*	*Neves Corvo (FW)*
	L MS#2	*Lower VSC*	*Lousal (FW)*
	SES20#10	*Lower VSC*	*Lousal (FW)*
	NCG#4	*Middle VSC*	*Neves Corvo (FW)*
	NCL#34	*Middle VSC*	*Neves Corvo (FW)*
	37-1-B	*Middle VSC*	*Albernoa*
	X93	*Middle VSC*	*Albernoa*
	X64	*Middle VSC*	*Albernoa*
	NCZ#41	*Upper VSC*	*Neves Corvo (HW)*
	NCZ#42	*Upper VSC*	*Neves Corvo (HW)*
	NCL#6	*Upper VSC*	*Neves Corvo (HW)*
	NCL#31	*Upper VSC*	*Neves Corvo (HW)*
	NCL#33	*Upper VSC*	*Neves Corvo (HW)*
	NCC#38	*Upper VSC*	*Neves Corvo (HW)*
	NCC#39	*Upper VSC*	*Neves Corvo (HW)*
	ALJ_FM#4	*Upper VSC*	*Aljustrel (HW)*
	ALJ_FM#5	*Upper VSC*	*Aljustrel (HW)*
	ALJ_RS#7	*Upper VSC*	*Aljustrel (HW)*
	FFM#1	*Upper VSC*	*Aljustrel (HW)*
	FFM#2	*Upper VSC*	*Aljustrel (HW)*
	ALJ_FM#1	*Upper VSC*	*Aljustrel (HW)*
	ALJ_FM#2	*Upper VSC*	*Aljustrel (HW)*
	ALJ_RS#1	*Upper VSC*	*Aljustrel (HW)*
	ALJ_RS#3	*Upper VSC*	*Aljustrel (HW)*
	ALJ_RS#6	*Upper VSC*	*Aljustrel (HW)*
	ALJ_MM10-03#3	*Upper VSC*	*Aljustrel (HW)*
	MFM#1	*Upper VSC*	*Aljustrel (HW)*
	ALJ_MM16-15#1	*Upper VSC*	*Aljustrel (HW)*

	GV7#3	*Upper VSC*	*Aljustrel (HW)*
	GV7#4	*Upper VSC*	*Aljustrel (HW)*
	GV8#1	*Upper VSC*	*Aljustrel (HW)*
	GV9#7	*Upper VSC*	*Aljustrel (HW)*
	X23	*Upper VSC*	*Aljustrel*
	EDS1-B	*Upper VSC*	*Aljustrel*
	L MS#3	*Upper VSC*	*Lousal (HW)*
	L MS#4	*Upper VSC*	*Lousal (HW)*
	SES20#6	*Upper VSC*	*Lousal (HW)*
	18-1-E	*Upper VSC*	*Albernoa*
	18-1-FF	*Upper VSC*	*Albernoa*
	ALB02# 2	*Upper VSC*	*Albernoa*
	ALB02# 9	*Upper VSC*	*Albernoa*
	ALB02# 48	*Upper VSC*	*Albernoa*
	MM02#2	*Upper VSC*	*Aljustrel*
	MM02#3	*Upper VSC*	*Aljustrel*
	MDM02#1	*Upper VSC*	*Aljustrel*
	MDM02#7	*Upper VSC*	*Aljustrel*
	R MS#4	*Upper VSC*	*Neves Corvo (HW)*
	R MS#5	*Upper VSC*	*Neves Corvo (HW)*
Metapelites with a volcanic derived component	**NCS#2**	*Lower VSC*	*Neves Corvo (FW)*
	NCS#3	*Lower VSC*	*Neves Corvo (FW)*
	NCC#26	*Lower VSC*	*Neves Corvo (FW)*
	NCL#5	*Upper VSC*	*Neves Corvo (HW)*
	NCC#29	*Upper VSC*	*Neves Corvo (HW)*
	NCL#32	*Upper VSC*	*Neves Corvo (HW)*
	ALJ_FM#6	*Upper VSC*	*Aljustrel (HW)*
	ALJ_RS#12	*Upper VSC*	*Aljustrel (HW)*
	ALJ_RS#13	*Upper VSC*	*Aljustrel (HW)*
	ALJ_RS#15	*Upper VSC*	*Aljustrel (HW)*
	ALJ_MM10-03#1	*Upper VSC*	*Aljustrel (HW)*
	ALJ_MM10-03#4	*Upper VSC*	*Aljustrel (HW)*
	ALJ_MM16-15#9	*Upper VSC*	*Aljustrel (HW)*
	ALJ_MM16-15#10	*Upper VSC*	*Aljustrel (HW)*
	ALJ_MM16-15#11	*Upper VSC*	*Aljustrel (HW)*
	ALJ_MS#5	*Upper VSC*	*Aljustrel (HW)*
	GV8#5	*Upper VSC*	*Aljustrel (HW)*
	GV9#3	*Upper VSC*	*Aljustrel (HW)*
	GV9#6	*Upper VSC*	*Aljustrel (HW)*
	EDS1-T	*Upper VSC*	*Aljustrel*
	SES18#1	*Upper VSC*	*Lousal*
	MDM02#9	*Upper VSC*	*Aljustrel*
	CW2-CC	*Upper VSC*	*Albernoa*
	CW2-LL	*Upper VSC*	*Albernoa*
	RT49	*Upper VSC*	*Albernoa*

Sulphide abundance	U ppm	Th ppm	Pb ppm	$^{206}Pb/^{204}Pb$	Error (± 2σ)	$^{207}Pb/^{204}Pb$	Error (± 2σ)
Mineralized	2.42	8.79	22	18.739	0.006	15.660	0.006
Mineralized	2.43	10.7	62	18.372	0.004	15.646	0.003
Mineralized	2.93	11.8	37	18.483	0.004	15.648	0.003
No-sulphide	3.85	15.7	(*)	23.454	0.01	15.931	0.008
No-sulphide	4.26	17.9	(*)	25.447	0.014	16.047	0.009
Py-bearing	3.87	16.6	(*)	-	-	-	-
No-sulphide	3.84	16.5	(*)	23.166	0.006	15.920	0.005
No-sulphide	2.96	13.8	(*)	23.797	0.008	15.960	0.007
No-sulphide	3.93	14.9	(*)	-	-	-	-
No-sulphide	3.26	13.6	9	19.829	0.004	15.719	0.004
No-sulphide	3.86	13.6	(*)	21.662	0.007	15.826	0.006
No-sulphide	2.83	9.21	(*)	19.775	0.008	15.722	0.009
No-sulphide	2.17	11.8	(*)	19.668	0.008	15.699	0.006
No-sulphide	3.16	13.7	6	19.636	0.006	15.720	0.005
No-sulphide	2.4	9.06	23	18.459	0.005	15.642	0.005
No-sulphide	3.07	14.8	6	19.447	0.007	15.704	0.007
Mineralized	1.47	8.1	6	19.213	0.005	15.675	0.004
Mineralized	3.2	13.9	62	18.414	0.004	15.640	0.004
Mineralized	1.97	10.9	25	18.466	0.004	15.638	0.004
Mineralized	1.66	8.41	7	19.854	0.007	15.712	0.006
Py-bearing	3.33	15.5	(*)	23.130	0.011	15.908	0.008
No-sulphide	1.2	5.96	8	18.527	0.004	15.641	0.003
No-sulphide	1.92	9.85	14	18.541	0.005	15.640	0.005
Mineralized	3.93	10.2	903	18.239	0.007	15.664	0.008
Py-bearing	6.04	22	(*)	-	-	-	-
Py-bearing	4.25	16.8	(*)	20.910	0.005	15.781	0.004
Mineralized	3.46	13.7	255	-	-	-	-
No-sulphide	3.69	15.7	(*)	-	-	-	-
No-sulphide	3.56	15.9	6	19.899	0.004	15.723	0.003
Mineralized	3.17	15.8	6	-	-	-	-
Py-bearing	8.63	9.53	71	-	-	-	-
Mineralized	2.07	9.09	94	18.294	0.004	15.629	0.004
No-sulphide	3.79	16.3	13	18.977	0.004	15.674	0.003
Mineralized	3.73	15.1	37	18.482	0.007	15.646	0.008
Mineralized	9.19	12.6	60	18.529	0.003	15.649	0.003
No-sulphide	4.4	17.1	10	19.723	0.007	15.733	0.007
Mineralized	7.24	9.13	82	18.537	0.004	15.652	0.003
No-sulphide	6.94	20.6	8	19.087	0.005	15.680	0.004
No-sulphide	2.4	13.9	7	19.302	0.006	15.691	0.005
Py-bearing	4.27	12.7	(*)	19.880	0.004	15.715	0.005
No-sulphide	5.14	12.5	15	18.801	0.006	15.653	0.006
No-sulphide	3.6	13.7	26	18.580	0.004	15.626	0.004
Mineralized	14.1	14.7	244	18.352	0.006	15.639	0.006
Py-bearing	1.44	9.97	(*)	19.726	0.005	15.690	0.004
No-sulphide	1.06	6.12	(*)	19.950	0.012	15.710	0.008
Mineralized	6.62	8.79	(*)	24.841	0.017	15.993	0.011
No-sulphide	2.07	10.8	37	18.367	0.012	15.638	0.015
No-sulphide	1.33	8.36	14	18.343	0.006	15.635	0.006
Py-bearing	1.42	7.32	17	18.496	0.006	15.632	0.005
No-sulphide	1.34	7.82	12	18.549	0.005	15.623	0.005
No-sulphide	2.99	10.4	16	18.670	0.010	15.627	0.012
No-sulphide	3.14	11.1	11	18.844	0.008	15.631	0.009
Py-bearing	8.05	9.96	53	18.649	0.005	15.644	0.005
Py-bearing	2.57	11.8	28	18.522	0.005	15.625	0.005
Py-bearing	11.9	8.49	94	18.621	0.005	15.648	0.004
Py-bearing	2.38	8.83	54	18.377	0.004	15.617	0.004
No-sulphide	1.47	8.7	25	18.358	0.006	15.618	0.005
Py-bearing	6.66	5.95	42	18.818	0.006	15.647	0.006
Mineralized	37.3	12.7	22	19.677	0.008	15.706	0.008
Py-bearing	8.85	8.07	42	18.864	0.004	15.655	0.004

Mineralized	12.5	9.28	152	18.451	0.006	15.641	0.006
Py-bearing	2.75	13.1	33	18.374	0.006	15.663	0.005
Py-bearing	15	10.6	74	18.477	0.005	15.646	0.006
Py-bearing	5.53	1.3	84	18.517	0.005	15.635	0.006
Mineralized	2.11	4.75	30	18.319	0.005	15.623	0.004
Mineralized	11.9	8.43	84	18.694	0.006	15.675	0.005
No-sulphide	4.9	8.92	73	18.710	0.007	15.687	0.008
No-sulphide	4.02	10.4	30	18.752	0.009	15.659	0.011
Py-bearing	3.65	10.8	28	18.640	0.006	15.657	0.005
Mineralized	1.73	7.27	12	18.584	0.004	15.638	0.004
Mineralized	7.42	7.4	26	18.887	0.004	15.661	0.004
No-sulphide	1.6	10.2	48	18.398	0.004	15.648	0.004
No-sulphide	2.66	15.9	(*)	20.237	0.006	15.752	0.006
No-sulphide	3.37	13.8	55	18.501	0.007	15.650	0.007
No-sulphide	2.63	10.1	58	18.251	0.005	15.640	0.005
Py-bearing	5.61	13.5	11	19.290	0.010	15.664	0.012
No-sulphide	2.72	12.5	54	18.364	0.023	15.664	0.028
No-sulphide	2.3	20.2	99	18.269	0.030	15.649	0.021
No-sulphide	3.34	8.46	11	18.731	0.004	15.642	0.004
No-sulphide	1.38	7.42	(*)	20.752	0.013	15.779	0.01
No-sulphide	3.01	13.8	10	18.974	0.007	15.665	0.006
No-sulphide	3.54	12.2	53	18.485	0.005	15.653	0.005
Py-bearing	4.3	16.4	36	18.610	0.004	15.659	0.003
No-sulphide	1.6	10.1	(*)	20.484	0.005	15.742	0.005
Py-bearing	1.5	10.7	(*)	19.583	0.008	15.697	0.008
Py-bearing	2.3	9.6	13.0	18.538	0.003	15.618	0.003
Py-bearing	1.4	9.2	41.0	18.317	0.006	15.631	0.005
No-sulphide	1.3	7.9	10.0	18.605	0.009	15.642	0.009
No-sulphide	1.6	9.0	26.0	18.455	0.004	15.637	0.004
No-sulphide	2.7	12.0	(*)	19.043	0.003	15.666	0.003
No-sulphide	2.1	15.4	13.0	18.635	0.005	15.641	0.007
No-sulphide	1.8	4.4	30.0	18.386	0.006	15.629	0.006
No-sulphide	3.6	13.4	31.0	18.472	0.005	15.619	0.006
No-sulphide	2.2	9.9	30.0	18.351	0.008	15.636	0.009
Py-bearing	5.6	7.9	58.0	18.515	0.006	15.635	0.007
Py-bearing	3.3	8.2	15.0	18.922	0.007	15.674	0.006
Py-bearing	1.5	8.9	11.0	18.577	0.008	15.641	0.008
Py-bearing	2.8	9.6	58.0	18.284	0.004	15.605	0.004
No-sulphide	6.2	6.9	16.0	18.891	0.004	15.666	0.003
Mineralized	1.9	8.1	58.0	18.464	0.008	15.674	0.008
No-sulphide	2.0	11.3	(*)	18.712	0.004	15.620	0.004
No-sulphide	3.9	6.9	43.0	18.510	0.005	15.631	0.004
Mineralized	2.9	13.9	99.0	18.325	0.005	15.661	0.004
Mineralized	1.3	7.5	133.0	18.252	0.007	15.658	0.008
No-sulphide	0.6	3.0	12.0	18.405	0.005	15.635	0.004

$^{208}Pb/^{204}Pb$	Error (± 2σ)	μ	ω	κ	$^{206}Pb/^{204}Pb$ (i)	$^{207}Pb/^{204}Pb$ (i)	$^{208}Pb/^{204}Pb$ (i)
38.752	0.018	9.86	37.87	3.84	18.334	15.638	38.277
38.481	0.009	9.90	38.70	3.91	18.229	15.639	38.277
38.548	0.009	9.88	38.28	3.87	18.193	15.633	38.171
44.938	0.022	10.20	36.85	3.61	16.933	15.581	36.340
47.007	0.024	10.02	32.53	3.25	17.878	15.640	36.724
-	-	-	-	-	-	-	-
44.200	0.016	10.31	30.68	2.98	16.741	15.574	35.273
45.640	0.022	9.99	34.59	3.46	18.720	15.687	37.988
-	-	-	-	-	-	-	-
40.137	0.01	9.87	37.16	3.77	18.450	15.645	38.278
44.108	0.015	11.91	69.57	5.84	15.333	15.486	36.898
40.228	0.027	11.59	51.40	4.44	15.465	15.490	35.692
39.833	0.017	10.32	23.18	2.25	16.385	15.522	34.062
40.074	0.011	9.98	37.18	3.73	17.638	15.612	37.273
38.680	0.013	9.86	39.22	3.98	18.076	15.622	38.214
39.861	0.018	9.97	35.33	3.54	17.517	15.600	36.852
39.868	0.010	9.82	37.66	3.84	18.292	15.625	38.227
38.502	0.01	9.86	38.33	3.89	18.226	15.630	38.238
38.618	0.009	9.84	37.79	3.84	18.177	15.622	38.102
41.057	0.014	9.84	40.43	4.11	18.940	15.663	39.560
45.145	0.022	10.01	34.44	3.44	17.499	15.605	36.670
38.668	0.009	9.85	37.39	3.80	17.977	15.612	37.786
38.723	0.013	9.84	37.52	3.81	18.038	15.613	37.888
38.377	0.025	10.01	39.75	3.97	18.223	15.663	38.364
-	-	-	-	-	-	-	-
41.687	0.013	20.22	56.37	2.79	14.213	15.422	33.128
-	-	-	-	-	-	-	-
-	-	-	-	-	-	-	-
40.536	0.008	9.93	36.92	3.72	17.627	15.601	37.255
-	-	-	-	-	-	-	-
-	-	-	-	-	-	-	-
38.328	0.009	9.84	38.19	3.88	18.214	15.625	38.215
39.210	0.007	9.90	37.69	3.81	17.894	15.616	37.704
38.590	0.026	9.87	38.42	3.89	18.113	15.626	38.108
38.409	0.008	9.89	39.76	4.02	17.970	15.619	38.161
40.279	0.021	9.97	39.70	3.98	18.047	15.643	38.173
38.403	0.008	9.88	38.70	3.92	18.215	15.635	38.271
39.939	0.01	10.94	55.27	5.05	15.827	15.504	36.810
40.018	0.012	9.89	36.26	3.67	18.009	15.622	37.596
40.884	0.013	10271	73554	7	13.312	15.362	34.568
38.920	0.015	9.89	41.54	4.20	17.536	15.585	37.925
38.662	0.009	9.76	37.77	3.87	18.073	15.599	38.038
38.360	0.017	9.87	39.25	3.97	18.142	15.628	38.289
40.881	0.012	9.83	29.08	2.96	17.516	15.571	35.935
41.219	0.024	9.80	37.10	3.79	18.311	15.622	38.160
42.832	0.033	3.31	33.98	10.27	13.717	15.395	38.057
38.556	0.050	9.86	38.61	3.92	18.162	15.627	38.212
38.545	0.015	9.87	37.65	3.82	17.996	15.617	37.840
38.727	0.015	9.80	38.18	3.90	18.190	15.615	38.217
38.719	0.012	9.75	36.81	3.77	18.139	15.601	37.946
38.657	0.039	9.75	37.45	3.84	17.984	15.590	37.886
38.844	0.027	9.74	37.28	3.83	17.792	15.575	37.640
38.505	0.016	9.82	39.30	4.00	18.093	15.614	38.282
38.630	0.013	9.77	37.58	3.85	18.186	15.607	38.131
38.417	0.01	9.85	39.12	3.97	18.159	15.623	38.310
38.425	0.009	9.76	37.93	3.88	18.216	15.609	38.232
38.505	0.015	9.78	37.70	3.86	18.144	15.607	38.095
38.392	0.011	9.79	37.87	3.87	18.237	15.616	38.224
38.460	0.024	2.87	32.54	11.32	13.380	15.368	37.767
38.405	0.013	9.82	38.73	3.94	18.090	15.614	38.177

38.402	0.019	9.86	39.33	3.99	18.151	15.625	38.330
38.579	0.014	9.98	39.23	3.93	18.070	15.647	38.110
38.443	0.02	9.91	42.22	4.26	17.737	15.606	38.274
38.410	0.011	9.81	38.61	3.94	18.276	15.622	38.392
38.419	0.010	9.81	39.15	3.99	18.063	15.609	38.232
38.506	0.013	9.95	39.93	4.01	18.175	15.647	38.387
38.598	0.023	9.99	38.57	3.86	18.463	15.674	38.453
38.604	0.035	9.86	37.87	3.84	18.260	15.633	38.192
38.571	0.013	9.88	38.18	3.86	18.162	15.632	38.114
36.680	0.010	9.81	37.72	3.84	18.055	15.610	37.962
38.531	0.011	9.86	40.77	4.13	17.838	15.605	38.193
38.599	0.01	9.90	38.79	3.92	18.276	15.642	38.348
42.181	0.019	10.75	26.45	2.46	16.056	15.527	34.100
38.645	0.021	9.88	38.69	3.92	18.277	15.638	38.348
38.422	0.015	9.91	39.37	3.97	18.086	15.631	38.217
39.085	0.037	9.84	40.40	4.11	17.391	15.562	37.608
38.564	0.091	9.98	39.51	3.96	18.180	15.655	38.291
38.508	0.064	9.93	39.13	3.94	18.185	15.644	38.267
38.864	0.01	9.84	40.84	4.15	17.613	15.581	37.948
43.364	0.026	9.91	43.28	4.37	18.536	15.660	39.511
39.239	0.017	9.86	37.06	3.76	17.855	15.605	37.581
38.516	0.012	9.90	38.45	3.89	18.241	15.640	38.244
38.721	0.008	9.90	38.56	3.90	18.172	15.636	38.180
42.573	0.013	9.83	35.38	3.60	17.934	15.605	37.399
41.427	0.024	9.94	31.51	3.17	17.330	15.576	36.090
38.863	0.008	9.74	38.60	3.96	17.893	15.583	37.984
38.486	0.013	9.84	38.39	3.90	18.192	15.625	38.222
38.914	0.029	9.82	37.43	3.81	18.119	15.616	37.976
38.645	0.01	9.83	38.20	3.88	18.226	15.624	38.236
39.385	0.009	12.66	33.80	2.67	15.017	15.450	33.600
39.127	0.024	9.82	36.34	3.70	18.053	15.610	37.712
38.330	0.016	9.82	38.06	3.88	18.170	15.618	38.156
38.618	0.018	9.76	38.27	3.92	18.053	15.597	38.106
38.473	0.029	9.86	38.39	3.89	18.090	15.622	38.086
38.440	0.024	9.81	38.77	3.95	18.163	15.616	38.280
38.763	0.015	9.89	38.46	3.89	18.123	15.631	38.109
38.855	0.024	9.83	37.17	3.78	18.092	15.615	37.895
38.361	0.010	9.73	38.12	3.92	18.109	15.595	38.166
38.628	0.008	9.94	43.62	4.39	17.457	15.589	38.118
39.359	0.024	9.99	43.43	4.35	18.341	15.668	39.193
39.018	0.010	10.64	22.97	2.16	15.834	15.466	33.625
38.366	0.011	9.80	38.02	3.88	18.178	15.614	38.177
38.461	0.011	9.97	39.25	3.94	18.218	15.655	38.296
38.384	0.027	9.98	39.39	3.95	18.218	15.657	38.317
38.503	0.009	9.84	38.02	3.87	18.232	15.625	38.208

Appendix Figure 1

Appendix Table 1

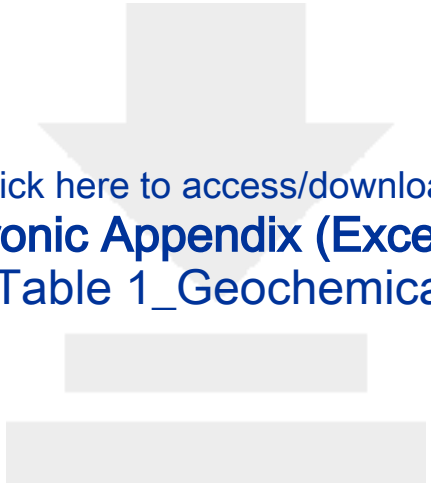

Click here to access/download

Electronic Appendix (Excel etc.)

Appendix Table 1_GeochemicalData.xlsx

Appendix Table 2

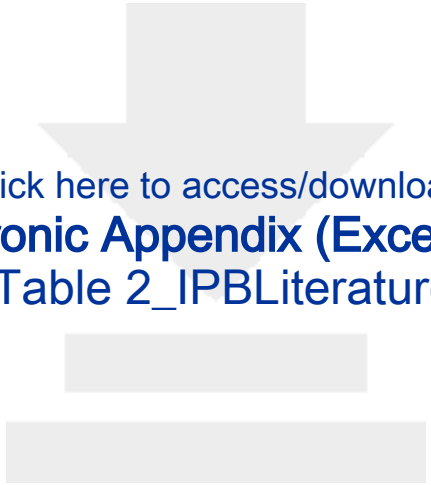

Click here to access/download

Electronic Appendix (Excel etc.)

Appendix Table 2_IPBLiteratureData.xlsx

Appendix 2

Multi-elemental and isotope geochemistry of metapelites from the Volcano-Sedimenatry Complex (Iberian Pyrtite Belt): unravelling fingerprints of differente sources, sedimenatry environments and exhalative-hydrothermal activity

Filipa Luz - PhD Thesis - Dataset information

Supplementary information on sampling, including the coordinates of each sampling site and which study each sample was subjected

Appendix 2

Sample Ref		NCL#9	NCL#10	NCL#11	NCL#12	NCL#13	NCL#14	NCL#15	NCL#35	NCC#25	NCC#27	NCZ#1	NCZ#21
Sector		Neves Corvo	Neves Corvo	Neves Corvo	Neves Corvo	Neves Corvo	Neves Corvo	Neves Corvo	Neves Corvo	Neves Corvo	Neves Corvo	Neves Corvo	Neves Corvo
Stratigraphic division		*PQG*	*PQG*	*PQG*	*PQG*	*PQG*	*PQG*	*PQG*	*PQG*	*PQG*	*PQG*	*lower* VSC	*lower* VSC
Mineralization type/occurrence		*Mineralized*	*Mineralized*	*Mineralized*	*No sulphide*	*No sulphide*	*Py-bearing*	*No sulphide*	*No sulphide*	*No sulphide*	*No sulphide*	*Mineralized*	*Mineralized*
Footwall/Hangingwall		*Footwall*	*Footwall*	*Footwall*	*Footwall*	*Footwall*	*Footwall*	*Footwall*	*Footwall*	*Footwall*	*Footwall*	*Footwall*	*Footwall*
Location - ETRS89	x	13812	14419	14509	14254	14110	14120	14078	*n.a.*	14745	14648	15175	15143
	y	-231566	-231437	-231432	-231370	-231465	-231418	-231379	*n.a.*	-231837	-231786	-233119	-232927
Depth (m)		*n.a.*	*n.a.*	*n.a.*	*n.a.*	*n.a.*	*n.a.*	*n.a.*	*n.a.*	*n.a.*	*n.a.*	*n.a.*	*n.a.*
Petrograpphy		√	√	√		√	√	√			√	√	√
Whole-rock chemistry		√	√	√	√	√	√	√	√	√	√	√	√
Isotopic geochemistry		√	√	√	√	√	√	√	√	√	√	√	√
Mineral Chemistry			√					√					√

Sample Ref		NCL#36	NCL#37	NCN#16	NCN#17	NCN#18	NCN#19	NCN#22	NCN#30	NCC#23	NCC#24	NCC#26	NCC#28
Sector		Neves Corvo	Neves Corvo	Neves Corvo	Neves Corvo	Neves Corvo	Neves Corvo	Neves Corvo	Neves Corvo	Neves Corvo	Neves Corvo	Neves Corvo	Neves Corvo
Stratigraphic division		*lower* VSC	*lower* VSC	*lower* VSC	*lower* VSC	*lower* VSC	*lower* VSC	*lower* VSC	*lower* VSC	*lower* VSC	*lower* VSC	*lower* VSC	*lower* VSC
Mineralization type/occurrence		*No sulphide*	*No sulphide*	*Mineralized*	*Py-bearing*	*Py-bearing*	*Mineralized*	*No sulphide*	*No sulphide*	*Mineralized*	*Py-bearing*	*Py-bearing*	*No sulphide*
Footwall/Hangingwall		*Footwall*	*Footwall*	*Footwall*	*Footwall*	*Footwall*	*Footwall*	*Footwall*	*Footwall*	*Footwall*	*Footwall*	*Footwall*	*Footwall*
Location - ETRS89	x	*n.a.*	*n.a.*	13545	13984	13990	14041	13544	13544	15127	15134	15048	14869
	y	*n.a.*	*n.a.*	-232243	-232270	-232270	-232220	-232592	-232592	-231817	-231811	-232493	-232654
Depth (m)		*n.a.*	*n.a.*	*n.a.*	*n.a.*	*n.a.*	*n.a.*	*n.a.*	*n.a.*	*n.a.*	*n.a.*	*n.a.*	*n.a.*
Petrograpphy		√		√	√		√				√		
Whole-rock chemistry		√	√	√	√	√	√	√	√	√	√	√	√
Isotopic geochemistry		√	√	√	√	√	√	√	√	√	√	√	√
Mineral Chemistry		√		√	√						√		

Sample Ref		NCL#6	NCL#31	NCL#33	NCN#20	NCC#38	NCC#39	NCL#5	NCC#29	X23	EDS1-B	EDS1-E	EDS1-L
Sector		Neves Corvo	Neves Corvo	Neves Corvo	Neves Corvo	Neves Corvo	Neves Corvo	Neves Corvo	Neves Corvo	Aljustrel	Aljustrel	Aljustrel	Aljustrel
Stratigraphic division		*upper* VSC	*upper* VSC	*upper* VSC	*upper* VSC	*upper* VSC	*upper* VSC	*upper* VSC	*upper* VSC	*upper* VSC	*upper* VSC	*upper* VSC	*upper* VSC
Mineralization type/occurrence		*Mineralized*	*Py-bearing*	*No sulphide*	*Mineralized*	*Mineralized*	*No sulphide*	*No sulphide*	*No sulphide*	*Mineralized*	*Mineralized*	*No sulphide*	*No sulphide*
Footwall/Hangingwall		*Hangingwall*	*Hangingwall*	*Hangingwall*	*Hangingwall*	*Hangingwall*	*Hangingwall*	*Hangingwall*	*Hangingwall*	*n.a.*	*n.a.*	*n.a.*	*n.a.*
Location - ETRS89	x	14385	14861	14848	14018	*n.a.*	*n.a.*	14444	14662	-624	-257	-257	-257
	y	-231332	-231090	-231110	-231726	*n.a.*	*n.a.*	-231728	-231774	-201919	-201023	-201023	-201023
Depth (m)		*n.a.*	*n.a.*	*n.a.*	*n.a.*	*n.a.*	*n.a.*	*n.a.*	*n.a.*	*n.a.*	-304.56	-350.57	-434.28
Petrograpphy		√	√		√					√	√	√	√
Whole-rock chemistry		√	√	√	√	√	√	√	√	√	√	√	√
Isotopic geochemistry		√	√	√	√	√	√	√	√	√	√		
Mineral Chemistry		√									√		

Appendix 2

Sample Ref	NCZ#40	NCS#2	NCS#3	NCL#7	NCG#4	NCL#34	NCZ#41	NCZ#42	EDS1-R	GV7#1	GV7#2	GV7#3
Sector	Neves Corvo	Neves Corvo	Neves Corvo	Neves Corvo	Neves Corvo	Neves Corvo	Neves Corvo	Neves Corvo	Aljustrel	Aljustrel	Aljustrel	Aljustrel
Stratigraphic division	*lower* VSC	*lower* VSC	*lower* VSC	*lower* VSC	*middle* VSC	*middle* VSC	*upper* VSC	*upper* VSC	*upper* VSC	*upper* VSC	*upper* VSC	*upper* VSC
Mineralization type/occurrence	*Mineralized*	*No sulphide*	*Py-bearing*	*Mineralized*	*No sulphide*	*Mineralized*	*No sulphide*	*No sulphide*	*No sulphide*	*Py-bearing*	*No sulphide*	*Mineralized*
Footwall/Hangingwall	*Footwall*	*Footwall*	*Footwall*	*Footwall*	*Footwall*	*Footwall*	*Hangingwall*	*Hangingwall*	*n.a.*	*Hangingwall*	*Hangingwall*	*Hangingwall*
Location - ETRS89 x	*n.a.*	15436	15480	14305	14054	14755	*n.a.*	*n.a.*	-257	-6403	-6403	-6403
Location - ETRS89 y	*n.a.*	-233332	-233202	-231809	-233292	-231210	*n.a.*	*n.a.*	-201023	-199158	-199158	-199158
Depth (m)	*n.a.*	*n.a.*	*n.a.*	*n.a.*	*n.a.*	*n.a.*	*n.a.*	*n.a.*	-478.23	-162.70	-778.60	-782.30
Petrography	√			√	√		√		√	√		√
Whole-rock chemistry	√	√	√	√	√	√	√	√	√	√	√	√
Isotopic geochemistry	√	√	√	√	√	√	√	√				√
Mineral Chemistry				√								

Sample Ref	GV7#4	GV8#1	GV8#2	GV8#3	GV8#4	GV9#2	GV9#4	GV9#5	GV9#7	GV9#8	GV9#9	GV9#10
Sector	Aljustrel	Aljustrel	Aljustrel	Aljustrel	Aljustrel	Aljustrel	Aljustrel	Aljustrel	Aljustrel	Aljustrel	Aljustrel	Aljustrel
Stratigraphic division	*upper* VSC	*upper* VSC	*upper* VSC	*upper* VSC	*upper* VSC	*upper* VSC	*upper* VSC	*upper* VSC	*upper* VSC	*upper* VSC	*upper* VSC	*upper* VSC
Mineralization type/occurrence	*Py-bearing*	*Py-bearing*	*No sulphide*	*No sulphide*	*No sulphide*	*Mineralized*	*No sulphide*	*No sulphide*	*Mineralized*	*No sulphide*	*No sulphide*	*Py-bearing*
Footwall/Hangingwall	*Hangingwall*	*Hangingwall*	*Hangingwall*	*Hangingwall*	*Hangingwall*	*Hangingwall*	*Hangingwall*	*Hangingwall*	*Hangingwall*	*Hangingwall*	*Hangingwall*	*Hangingwall*
Location - ETRS89 x	-6403	-6663	-6663	-6663	-6663	-6219	-6219	-6219	-6219	-6219	-6219	-6219
Location - ETRS89 y	-199158	-199331	-199331	-199331	-199331	-199247	-199247	-199247	-199247	-199247	-199247	-199247
Depth (m)	-797.00	-243.70	-337.55	-345.60	-365.85	-148.65	-175.90	-201.90	-244.20	-246.75	-271.45	-294.05
Petrography	√	√				√			√			√
Whole-rock chemistry	√	√	√	√	√	√	√	√	√	√	√	√
Isotopic geochemistry	√	√				√			√			√
Mineral Chemistry												

Sample Ref	GV8#5	GV9#3	GV9#6	ALJ_FM#4	ALJ_FM#5	ALJ_RS#7	ALJ_RS#8	ALJ_RS#9	ALJ_RS#10	FFM#1	FFM#2	ALJ_MM10-03#3
Sector	Aljustrel	Aljustrel	Aljustrel	Aljustrel	Aljustrel	Aljustrel	Aljustrel	Aljustrel	Aljustrel	Aljustrel	Aljustrel	Aljustrel
Stratigraphic division	*upper* VSC	*upper* VSC	*upper* VSC	*upper* VSC	*upper* VSC	*upper* VSC	*upper* VSC	*upper* VSC	*upper* VSC	*upper* VSC	*upper* VSC	*upper* VSC
Mineralization type/occurrence	*No sulphide*	*No sulphide*	*No sulphide*	*No sulphide*	*Py-bearing*	*No sulphide*	*No sulphide*	*Py-bearing*	*Py-bearing*	*No sulphide*	*No sulphide*	*Py-bearing*
Footwall/Hangingwall	*Hangingwall*	*Hangingwall*	*Hangingwall*	*Hangingwall*	*Hangingwall*	*Hangingwall*	*Hangingwall*	*Hangingwall*	*Hangingwall*	*Hangingwall*	*Hangingwall*	*Hangingwall*
Location - ETRS89 x	-6663	-6219	-6219	-1303	-1303	-1729	-1729	-1729	-1729	*n.a.*	*n.a.*	-3531
Location - ETRS89 y	-199331	-199247	-199247	-1999029	-1999029	-198714	-198714	-198714	-198714	*n.a.*	*n.a.*	-198454
Depth (m)	-391.20	-160.45	-223.60	-107.23	-113.50	-486.15	-501.45	-519.85	-529.90	*n.a.*	*n.a.*	-63.50
Petrography	√	√	√	√	√	√	√	√	√	√	√	√
Whole-rock chemistry	√	√	√	√	√	√	√	√	√	√	√	√
Isotopic geochemistry	√	√	√	√						√	√	√
Mineral Chemistry				√	√						√	

Appendix 2

Sample Ref		MFM#1	ALJ_FM#6	ALJ_RS#11	ALJ_RS#12	ALJ_RS#13	ALJ_RS#14	ALJ_RS#15	ALJ_MM10-03#1	ALJ_MM10-03#2	ALJ_MM10-03#4	ALJ_MM10-03#5	ALJ_MM16-15#9	ALJ_MM16-15#10
Sector		**Aljustrel**	**Aljustrel**	**Aljustrel**	**Aljustrel**	**Aljustrel**	**Aljustrel**	**Aljustrel**	**Aljustrel**	**Aljustrel**	**Aljustrel**	**Aljustrel**	**Aljustrel**	**Aljustrel**
Stratigraphic division		***upper* VSC**	***upper* VSC**	***upper* VSC**	***upper* VSC**	***upper* VSC**	***upper* VSC**	***upper* VSC**	***upper* VSC**	***upper* VSC**	***upper* VSC**	***upper* VSC**	***upper* VSC**	***upper* VSC**
Mineralization type/occurrence		***Mineralized***	***No sulphide***	***No sulphide***	***No sulphide***	***No sulphide***	***No sulphide***	***No sulphide***	***No sulphide***	***No sulphide***	***No sulphide***	***No sulphide***	***No sulphide***	***No sulphide***
Footwall/Hangingwall		***Hangingwall***	***Hangingwall***	***Hangingwall***	***Hangingwall***	***Hangingwall***	***Hangingwall***	***Hangingwall***	***Hangingwall***	***Hangingwall***	***Hangingwall***	***Hangingwall***	***Hangingwall***	***Hangingwall***
Location - ETRS89	**x**	*n.a.*	-1303	-1729	-1729	-1729	-1729	-1729	-3531	-3531	-3531	-3531	-3469	-3469
	y	*n.a.*	-1999029	-198714	-198714	-198714	-198714	-198714	-198454	-198454	-198454	-198454	-198137	-198137
Depth (m)		*n.a.*	-115.45	-542.42	-550.93	-560.85	-576.93	-585.55	-41.50	-50.95	-77.35	-109.20	-340.47	-356.55
Petrography		√	√	√	√	√	√	√	√	√	√	√	√	√
Whole-rock chemistry		√	√	√	√	√	√	√	√	√	√	√	√	√
Isotopic geochemistry		√	√		√	√		√	√		√			√
Mineral Chemistry		√											√	

Sample Ref		ALJ_MM16-15#11	ALJ_MS#5	ALJ_FM#1	ALJ_FM#2	ALJ_RS#1	ALJ_RS#2	ALJ_RS#5	ALJ_RS#6	ALJ_MM16-15#1	ABNSTR1	11-1-KK	11-1-LL	11-1-MM
Sector		**Aljustrel**	**Aljustrel**	**Aljustrel**	**Aljustrel**	**Aljustrel**	**Aljustrel**	**Aljustrel**	**Aljustrel**	**Aljustrel**	**Albernoa**	**Albernoa**	**Albernoa**	**Albernoa**
Stratigraphic division		***upper* VSC**	***upper* VSC**	***upper* VSC**	***upper* VSC**	***upper* VSC**	***upper* VSC**	***upper* VSC**	***upper* VSC**	***upper* VSC**	**PQG**	**PQG**	**PQG**	**PQG**
Mineralization type/occurrence		***No sulphide***	***No sulphide***	***Py-bearing***	***Py-bearing***	***Py-bearing***	***Py-bearing***	***No sulphide***	***No sulphide***	***Py-bearing***	***No sulphide***	***No sulphide***	***No sulphide***	***No sulphide***
Footwall/Hangingwall		***Hangingwall***	***Hanginwall***	***Hanginwall***	***Hanginwall***	***Hanginwall***	***Hanginwall***	***Hanginwall***	***Hanginwall***	***Hanginwall***	***n.a.***	***n.a.***	***n.a.***	***n.a.***
Location - ETRS89	**x**	-3469	-3795	-1303	-1303	-1729	-1729	-1729	-1729	-3469	53032	17603	17603	17603
	y	-198137	-197814	-1999029	-1999029	-198714	-198714	-198714	-198714	-198137	-231885	-205799	-205799	-205799
Depth (m)		-383.80	-113.00	-94.45	-98.59	-408.55	-416.70	-454.50	-461.75	-237.00	*n.a.*	-363.60	-365.65	-399.80
Petrography		√	√	√	√	√	√	√	√	√	√		√	√
Whole-rock chemistry		√	√	√	√	√	√	√	√	√	√	√	√	√
Isotopic geochemistry		√	√			√	√		√		√			√
Mineral Chemistry														

Sample Ref		11-1-NN	ALB03#30	ALB03#31	ALB03#32	ALB03#34	PC34	PC32	PC38	PC6	PC19	PC27	X32	X42
Sector		**Albernoa**	**Albernoa**	**Albernoa**	**Albernoa**	**Albernoa**	**Albernoa**	**Albernoa**	**Albernoa**	**Albernoa**	**Albernoa**	**Albernoa**	**Albernoa**	**Albernoa**
Stratigraphic division		**PQG**	**PQG**	**PQG**	**PQG**	**PQG**	**PQG**	**PQG**	**PQG**	**PQG**	**PQG**	**PQG**	**PQG**	**PQG**
Mineralization type/occurrence		***No sulphide***	***No sulphide***	***No sulphide***	***No sulphide***	***No sulphide***	***No sulphide***	***No sulphide***	***No sulphide***	***No sulphide***	***No sulphide***	***No sulphide***	***No sulphide***	***No sulphide***
Footwall/Hangingwall		***n.a.***	***n.a.***	***n.a.***	***n.a.***	***n.a.***	***n.a.***	***n.a.***	***n.a.***	***n.a.***	***n.a.***	***n.a.***	***n.a.***	***n.a.***
Location - ETRS89	**x**	17603	14790	14790	14790	14790	3557	3557	3557	3557	3557	3557	5307	10725
	y	-205799	-204961	-204961	-204961	-204961	-199306	-199306	-199306	-199306	-199306	-199306	-204250	-209321
Depth (m)		-400.80	-513.60	-542.80	-577.95	-593.20	*n.a.*	*n.a.*	*n.a.*	*n.a.*	*n.a.*	*n.a.*	*n.a.*	*n.a.*
Petrography					√		√	√	√	√	√	√	√	√
Whole-rock chemistry		√	√	√	√	√	√	√	√	√	√	√	√	√
Isotopic geochemistry								√			√			
Mineral Chemistry								√			√	√		√

Appendix 2

Sample Ref		X43	X44	X46	X47	X48	X50	X51	X60	X61	X29	X30	X31	X7
Sector		Albernoa	Albernoa	Albernoa	Albernoa	Albernoa	Albernoa	Albernoa	Albernoa	Albernoa	Aljustrel	Aljustrel	Aljustrel	Albernoa
Stratigraphic division		PQG	PQG	PQG	PQG	PQG	PQG	PQG	PQG	PQG	PQG	PQG	PQG	PQG
Mineralization type/occurrence		*No sulphide*	*No sulphide*	*No sulphide*	*No sulphide*	*No sulphide*	*No sulphide*	*No sulphide*	*No sulphide*	*No sulphide*	*No sulphide*	*No sulphide*	*No sulphide*	*No sulphide*
Footwall/Hangingwall		*n.a.*	*n.a.*	*n.a.*	*n.a.*	*n.a.*	*n.a.*	*n.a.*	*n.a.*	*n.a.*	*n.a.*	*n.a.*	*n.a.*	*n.a.*
Location - ETRS89	x	10868	14163	14903	14989	14989	18960	25690	18540	18540	2366	3728	3728	3957
	y	-209353	-212329	-212789	-212768	-212768	-217525	-216294	-216670	-216670	-200888	-201856	-201856	-198222
Depth (m)		*n.a.*	*n.a.*	*n.a.*	*n.a.*	*n.a.*	*n.a.*	*n.a.*	*n.a.*	*n.a.*	*n.a.*	*n.a.*	*n.a.*	*n.a.*
Petrography		√	√	√	√	√	√	√	√	√	√	√	√	√
Whole-rock chemistry		√	√	√	√	√	√	√	√	√	√	√	√	√
Isotopic geochemistry														
Mineral Chemistry														

Sample Ref		X11	X12	X13	X14	X16	X17	X19	ALB02#51	PC1	PC5	PC24	PC17	ABNSTR7
Sector		Albernoa	Albernoa	Albernoa	Albernoa	Albernoa	Albernoa	Albernoa	Albernoa	Albernoa	Albernoa	Albernoa	Albernoa	Albernoa
Stratigraphic division		PQG	PQG	PQG	PQG	PQG	PQG	PQG	PQG	PQG	PQG	PQG	PQG	PQG
Mineralization type/occurrence		*No sulphide*	*No sulphide*	*No sulphide*	*No sulphide*	*No sulphide*	*No sulphide*	*No sulphide*	*No sulphide*	*No sulphide*	*No sulphide*	*No sulphide*	*Py-bearing*	*No sulphide*
Footwall/Hangingwall		*n.a.*	*n.a.*	*n.a.*	*n.a.*	*n.a.*	*n.a.*	*n.a.*	*n.a.*	*n.a.*	*n.a.*	*n.a.*	*n.a.*	*n.a.*
Location - ETRS89	x	2050	1070	370	370	252	-730	-730	144787	3557	3557	3557	3557	42206
	y	-198465	-196842	-196470	-196470	-196686	-197030	-197030	-204973	-199306	-199306	-199306	-199306	-223825
Depth (m)		*n.a.*	*n.a.*	*n.a.*	*n.a.*	*n.a.*	*n.a.*	*n.a.*	*n.a.*	*n.a.*	*n.a.*	*n.a.*	*n.a.*	*n.a.*
Petrography		√	√	√	√	√	√	√	√	√	√	√	√	√
Whole-rock chemistry		√	√	√	√	√	√	√	√	√	√	√	√	√
Isotopic geochemistry												√		
Mineral Chemistry												√	√	

Sample Ref		T8	T18	T59	L MS#2	SES20#10	37-1-A	37-1-B	37-1-C	37-1-D	37-1-F	X68	X71	X93
Sector		Albernoa	Albernoa	Albernoa	Lousal	Lousal	Albernoa	Albernoa	Albernoa	Albernoa	Albernoa	Albernoa	Albernoa	Albernoa
Stratigraphic division		PQG	PQG	PQG	lower VSC	lower VSC	middle VSC	middle VSC	middle VSC	middle VSC	*middle* VSC	*middle* VSC	*middle* VSC	*middle* VSC
Mineralization type/occurrence		*No sulphide*	*No sulphide*	*No sulphide*	*Mineralized*	*Mineralized*	*Py-bearing*	*No sulphide*	*No sulphide*	*No sulphide*	*No sulphide*	*No sulphide*	*No sulphide*	*No sulphide*
Footwall/Hangingwall		*n.a.*	*n.a.*	*n.a.*	*Footwall*	*Footwall*	*n.a.*	*n.a.*	*n.a.*	*n.a.*	*n.a.*	*n.a.*	*n.a.*	*n.a.*
Location - ETRS89	x	3957	-730	18540	-25573	-25066	8303	8303	8303	8303	8303	22622	19970	19263
	y	-198221	-197030	-216670	-181885	-187756	-198699	-198699	-198699	-198699	-198699	-206283	-207079	-204661
Depth (m)		*n.a.*	*n.a.*	*n.a.*	*n.a.*	-288.50	-82.85	-91.57	-124.40	-134.50	-250.00	*n.a.*	*n.a.*	*n.a.*
Petrography		√	√	√		√	√	√	√	√	√	√	√	√
Whole-rock chemistry		√	√	√	√	√	√	√	√	√	√	√	√	√
Isotopic geochemistry						√		√				√		√
Mineral Chemistry						√		√						

Appendix 2

Sample Ref		X10	ABNSTR2	X64	X54	T67	T83	RT56	S3-B	S3-F	S3-I	S3-J	CW2-CC
Sector		Albernoa	Albernoa	Albernoa	Albernoa	Albernoa	Albernoa	Albernoa	Albernoa	Albernoa	Albernoa	Albernoa	Albernoa
Stratigraphic division		PQG	PQG	*middle* VSC	*middle* VSC	*middle* VSC	*middle* VSC	*middle* VSC	*upper* VSC	*upper* VSC	*upper* VSC	*upper* VSC	*upper* VSC
Mineralization type/occurrence		*No sulphide*	*No sulphide*	*Py-bearing*	*No sulphide*	*No sulphide*	*No sulphide*	*No sulphide*	*No sulphide*	*No sulphide*	*No sulphide*	*No sulphide*	*Mineralized*
Footwall/Hangingwall		*n.a.*	*n.a.*	*n.a.*	*n.a.*	*n.a.*	*n.a.*	*n.a.*	*n.a.*	*n.a.*	*n.a.*	*n.a.*	*n.a.*
Location - ETRS89	x	1986	56327	26497	24677	22622	18808	3587	-597	-597	-597	-597	4228
	y	-198632	-221658	-210362	-214114	-206283	-205487	-193577	-201299	-201299	-201299	-201299	-191707
Depth (m)		*n.a.*	*n.a.*	*n.a.*	*n.a.*	*n.a.*	*n.a.*	*n.a.*	-262.20	-313.60	-350.63	-359.38	-214.75
Petrography		√	√	√	√	√	√	√	√	√	√	√	√
Whole-rock chemistry		√	√	√	√	√	√	√	√	√	√	√	√
Isotopic geochemistry				√									√
Mineral Chemistry													

Sample Ref		CW2-LL	CW2-QQ	CW2-ZZ	X72	X84	X92	18-1-E	18-1-H	18-1-FF	18-1-T	18-1-U	18-1-OO
Sector		Albernoa	Albernoa	Albernoa	Albernoa	Albernoa	Albernoa	Albernoa	Albernoa	Albernoa	Albernoa	Albernoa	Albernoa
Stratigraphic division		*upper* VSC	*upper* VSC	*upper* VSC	*upper* VSC	*upper* VSC	*upper* VSC	*upper* VSC	*upper* VSC	*upper* VSC	*upper* VSC	*upper* VSC	*upper* VSC
Mineralization type/occurrence		*Mineralized*	*No sulphide*	*No sulphide*	*No sulphide*	*No sulphide*	*No sulphide*	*Mineralized*	*No sulphide*	*Mineralized*	*No sulphide*	*No sulphide*	*No sulphide*
Footwall/Hangingwall		*n.a.*	*n.a.*	*n.a.*	*n.a.*	*n.a.*	*n.a.*	*n.a.*	*n.a.*	*n.a.*	*n.a.*	*n.a.*	*n.a.*
Location - ETRS89	x	4228	4228	4228	14234	17717	17164	11823	11823	11823	11823	11823	11823
	y	-191707	-191707	-191707	-201324	-205484	-206482	-198489	-198489	-198489	-198489	-198489	-198489
Depth (m)		-333.70	-412.00	-517.84	*n.a.*	*n.a.*	*n.a.*	-80.70	-90.38	-159.60	-130.22	-133.20	-204.50
Petrography		√	√	√	√	√	√	√	√	√	√	√	√
Whole-rock chemistry		√	√	√	√	√	√	√	√	√	√	√	√
Isotopic geochemistry		√											
Mineral Chemistry		√								√			

Sample Ref		ALB02# 2	ALB02# 15	ALB02# 4	ALB02# 6	ALB02# 9	ALB02# 24	ALB02# 28	ALB02# 45	ALB02# 48	ALB03#3	ALB03#7	ALB03#12b
Sector		Albernoa	Albernoa	Albernoa	Albernoa	Albernoa	Albernoa	Albernoa	Albernoa	Albernoa	Albernoa	Albernoa	Albernoa
Stratigraphic division		*upper* VSC	*upper* VSC	*upper* VSC	*upper* VSC	*upper* VSC	*upper* VSC	*upper* VSC	*upper* VSC	*upper* VSC	*upper* VSC	*upper* VSC	*upper* VSC
Mineralization type/occurrence		*No sulphide*	*No sulphide*	*No sulphide*	*No sulphide*	*No sulphide*	*No sulphide*	*No sulphide*	*No sulphide*	*No sulphide*	*No sulphide*	*No sulphide*	*No sulphide*
Footwall/Hangingwall		*n.a.*	*n.a.*	*n.a.*	*n.a.*	*n.a.*	*n.a.*	*n.a.*	*n.a.*	*n.a.*	*n.a.*	*n.a.*	*n.a.*
Location - ETRS89	x	14787	14787	14787	14787	14787	14787	14787	14787	14787	14790	14790	14790
	y	-204973	-204973	-204973	-204973	-204973	-204973	-204973	-204973	-204973	-204961	-204961	-204961
Depth (m)		-93.80	-75.25	-124.50	-197.75	-244.16	-260.00	-378.25	-411.30	-473.00	-88.70	-233.25	-299.40
Petrography		√	√	√	√	√	√	√	√	√	√	√	√
Whole-rock chemistry		√	√	√	√	√	√	√	√	√	√	√	√
Isotopic geochemistry		√				√				√			
Mineral Chemistry		√											

Appendix 2

Sample Ref		ALB03#13c	ALB03#14	ALB03#29	S3-H	CW2-O	CW2-P	CW2-BB	CW2-II	CW2-VV	RT49	RT59-1	RT59-2
Sector		Albernoa	Albernoa	Albernoa	Aljustrel	Albernoa	Albernoa	Albernoa	Albernoa	Albernoa	Albernoa	Albernoa	Albernoa
Stratigraphic division		*upper* VSC	*upper* VSC	*upper* VSC	*upper* VSC	*upper* VSC	*upper* VSC	*upper* VSC	*upper* VSC	*upper* VSC	*upper* VSC	*upper* VSC	*upper* VSC
Mineralization type/occurrence		*No sulphide*	*No sulphide*	*No sulphide*	*No sulphide*	*No sulphide*	*No sulphide*	*No sulphide*	*No sulphide*	*No sulphide*	*No sulphide*	*No sulphide*	*No sulphide*
Footwall/Hangingwall		*n.a.*	*n.a.*	*n.a.*	*n.a.*	*n.a.*	*n.a.*	*n.a.*	*n.a.*	*n.a.*	*n.a.*	*n.a.*	*n.a.*
Location - ETRS89	x	14790	14790	14790	-597	4228	4228	4228	4228	4228	4905	3354	3354
	y	-204961	-204961	-204961	-201299	-191707	-191707	-191707	-191707	-191707	-191952	-192818	-192818
Depth (m)		-311.50	-322	-478	-321	-82	-93	-212	-303	-478	*n.a.*	*n.a.*	*n.a.*
Petrography		√	√	√	√	√	√	√	√	√	√	√	√
Whole-rock chemistry		√	√	√	√	√	√	√	√	√	√	√	√
Isotopic geochemistry											√		
Mineral Chemistry					√		√				√		

Sample Ref		T24	T73	T88	18-1-F	18-1-EE	18-1-II	EDS1-G	EDS1-H	EDS1-I	EDS1-P	EDS1-T	ALB02# 18
Sector		Albernoa	Albernoa	Albernoa	Albernoa	Albernoa	Albernoa	Aljustrel	Aljustrel	Aljustrel	Aljustrel	Aljustrel	Albernoa
Stratigraphic division		*upper* VSC	*upper* VSC	*upper* VSC	*upper* VSC	*upper* VSC	*upper* VSC	*upper* VSC	*upper* VSC	*upper* VSC	*upper* VSC	*upper* VSC	*upper* VSC
Mineralization type/occurrence		*No sulphide*	*No sulphide*	*No sulphide*	*No sulphide*	*No sulphide*	*No sulphide*	*No sulphide*	*No sulphide*	*No sulphide*	*No sulphide*	*No sulphide*	*No sulphide*
Footwall/Hangingwall		*n.a.*	*n.a.*	*n.a.*	*n.a.*	*n.a.*	*n.a.*	*n.a.*	*n.a.*	*n.a.*	*n.a.*	*n.a.*	*n.a.*
Location - ETRS89	x	2684	14234	17133	11823	11823	11823	-527	-527	-527	-527	-527	14787
	y	-191737	-201324	-206276	-198489	-198489	-198489	-201023	-201023	-201023	-201023	-201023	-204973
Depth (m)		*n.a.*	*n.a.*	*n.a.*	-88	-157	-173	-372	-385	-387	-474	-497	-302
Petrography		√	√	√	√	√	√	√	√	√	√	√	√
Whole-rock chemistry		√	√	√	√	√	√	√	√	√	√	√	√
Isotopic geochemistry									√			√	√
Mineral Chemistry		√	√		√	√			√				√

Sample Ref		ALB03#13b	ALB03#13e	L MS#3	L MS#4	SES20#2	SES20#4	SES20#5	SES18#3	SES20#1	SES20#3	SES18#1	SES18#2
Sector		Albernoa	Albernoa	Lousal	Lousal	Lousal	Lousal	Lousal	Lousal	Lousal	Lousal	Lousal	Lousal
Stratigraphic division		*upper* VSC	*upper* VSC	*upper* VSC	*upper* VSC	*upper* VSC	*upper* VSC	*upper* VSC	*upper* VSC	*upper* VSC	*upper* VSC	*upper* VSC	*upper* VSC
Mineralization type/occurrence		*No sulphide*	*No sulphide*	*No sulphide*	*No sulphide*	*No sulphide*	*No sulphide*	*No sulphide*	*No sulphide*	*No sulphide*	*No sulphide*	*No sulphide*	*No sulphide*
Footwall/Hangingwall		*n.a.*	*n.a.*	*Hangingwall*	*Hangingwall*	*Hangingwall*	*Hangingwall*	*Hangingwall*	*Hangingwall*	*Hangingwall*	*Hangingwall*	*Hangingwall*	*Hangingwall*
Location - ETRS89	x	14790	14790	-26006	-26006	-25066	-25066	-25066	-24931	-25066	-25066	-24931	-24931
	y	-204961	-204961	-181998	-181998	-187756	-187756	-187756	-187850	-187756	-187756	-187850	-187850
Depth (m)		-309	-316	*n.a.*	*n.a.*	-236.46	-252.20	-255.60	-277.10	-166.30	-240.20	-262.35	-214.55
Petrography		√	√			√	√			√	√	√	√
Whole-rock chemistry		√	√	√	√	√	√	√	√	√	√	√	√
Isotopic geochemistry				√	√							√	
Mineral Chemistry			√										

Appendix 2

Sample Ref		SES18#4	SES18#5	MM02#2	MM02#3	MDM02#1	MDM02#2	MDM02#3	MDM02#4	MDM02#5	MDM02#6	MM02#1	MDM02#8
Sector		Lousal	Lousal	Aljustrel	Aljustrel	Aljustrel	Aljustrel	Aljustrel	Aljustrel	Aljustrel	Aljustrel	Aljustrel	Aljustrel
Stratigraphic division		upper VSC	upper VSC	upper VSC	upper VSC	upper VSC	upper VSC	upper VSC	upper VSC	upper VSC	upper VSC	upper VSC	upper VSC
Mineralization type/occurrence		*No sulphide*	*No sulphide*	*No sulphide*	*Py-bearing*	*No sulphide*	*No sulphide*	*No sulphide*	*Mineralized*	*No sulphide*	*Mineralized*	*No sulphide*	*No sulphide*
Footwall/Hangingwall		*Hangingwall*	*Hangingwall*	*Hangingwall*	*Hangingwall*	*Hangingwall*	*Hangingwall*	*Hangingwall*	*Hangingwall*	*Hangingwall*	*Hangingwall*	*Hangingwall*	*Hangingwall*
Location - ETRS89	x	-24931	-24931	-6931	-6931	-9155	-9155	-9155	-9155	-9155	-9155	-6931	-9155
	y	-187850	-187850	-198313	-198313	-193552	-193552	-193552	-193552	-193552	-193552	-198313	-193552
Depth (m)		-340.30	-361.40	-238.45	-255.30	-86.50	-110.25	-114.00	-117.00	-136.20	-145.80	-230.80	-361.70
Petrograpphy				√	√	√	√		√		√	√	√
Whole-rock chemistry		√	√	√	√	√	√	√	√	√	√	√	√
Isotopic geochemistry				√	√	√			√		√		√
Mineral Chemistry									√				

Sample Ref		MDM02#9	MDM02#10	R MS#1	R MS#2	R MS#4	R MS#5	L MS#1	X99	X100	ABNSTR7	ABNSTR2	SES20#7
Sector		Aljustrel	Aljustrel	Neves Corvo	Neves Corvo	Neves Corvo	Neves Corvo	Lousal	Albernoa	Albernoa	Albernoa	Albernoa	Lousal
Stratigraphic division		upper VSC	upper VSC	upper VSC	upper VSC	upper VSC	*upper* VSC	PQG	PQG	PQG	PQG	PQG	BAFG (Flysch)
Mineralization type/occurrence		*No sulphide*	*No sulphide*	*No sulphide*	*No sulphide*	*No sulphide*	*No sulphide*	*No sulphide*	*No sulphide*	*No sulphide*	*No sulphide*	*No sulphide*	*No sulphide*
Footwall/Hangingwall		*Hangingwall*	*Hangingwall*	*Hangingwall*	*Hangingwall*	*Hangingwall*	*Hangingwall*	*Footwall*	*n.a.*	*n.a.*	*n.a.*	*n.a.*	*n.a.*
Location - ETRS89	x	-9155	-9155	-14111	-13674	4457	11359	*n.a.*	*n.a.*	*n.a.*	*n.a.*	*n.a.*	-25066
	y	-193552	-193552	-209159	-208943	-228160	-230546	*n.a.*	*n.a.*	*n.a.*	*n.a.*	*n.a.*	-187756
Depth (m)		-371.55	-377.30	*n.a.*	*n.a.*	*n.a.*	*n.a.*	*n.a.*	*n.a.*	*n.a.*	*n.a.*	*n.a.*	*n.a.*
Petrograpphy		√	√								√	√	√
Whole-rock chemistry		√	√	√	√	√	√	√	√	√	√	√	√
Isotopic geochemistry		√				√	√	√					
Mineral Chemistry		√											

Sample Ref		SES18#6	ALJ_MM16-15#2	ALJ_MS#1	ALJ_MS#3	ALJ_MS#4	X38	X57	X62	T58	SES20#6	SES20#9
Sector		Lousal	Aljustrel	Aljustrel	Aljustrel	Aljustrel	Albernoa	Albernoa	Albernoa	Albernoa	Sesamrias	Sesamrias
Stratigraphic division		BAFG (Flysch)	BAFG (Flysch)	BAFG (Flysch)	BAFG (Flysch)	BAFG (Flysch)	BAFG (Flysch)	BAFG (Flysch)	BAFG (Flysch)	BAFG (Flysch)	upper VSC?	footwall - stockwork
Mineralization type/occurrence		*No sulphide*	*No sulphide*	*No sulphide*	*No sulphide*	*No sulphide*	*No sulphide*	*No sulphide*	*No sulphide*	*No sulphide*	*Py Beraring*	*Mineralized*
Footwall/Hangingwall		*n.a.*	*n.a.*	*n.a.*	*n.a.*	*n.a.*	*n.a.*	*n.a.*	*n.a.*	*n.a.*	*hamging wall*	*hamging wall*
Location - ETRS89	x	-24931	-3469	-3795	-3795	-3795	6684	20152	17865	20152	-25066	-25066
	y	-187850	-198137	-197814	-197814	-197814	-207298	-213030	-217172	-213030	-187756	-187756
Depth (m)		*n.a.*	-238.60	-61.50	-72.35	-77.00	*n.a.*	*n.a.*	*n.a.*	*n.a.*		
Petrograpphy		√	√	√	√	√	√	√	√	√	√	√
Whole-rock chemistry		√	√	√	√	√	√	√	√	√	√	√
Isotopic geochemistry												
Mineral Chemistry											√	√

Appendix 3

Mineral Chemistry Data

Appendix 3 - Mineral Chemistry Data

Summary of the main group of analyses per sector

Total	Albernoa				Aljustrel			
	No sulphide	*Py Bearing*	*Mineralized*	*#*	*No sulphide*	*Py Bearing*	*Mineralized*	*#*
Chlorite *(#267)*	*67*	*21*	*3*	***91***	*27*	*10*	*41*	***78***
White Mica *(#217)*	*33*	*3*	*3*	***43***	*14*	*8*	*68*	***107***
Pyrite *(#170)*	*34*	*2*	*6*	***42***	*12*	*14*	*16*	***42***
Chalcopyrite *(#61)*	*26*	*11*	*9*	***46***	*7*	*8*	*0*	***15***
Carbonates *(#105)*	*55*	*1*	*1*	***57***	*1*	*0*	*3*	***4***
Feldspars *(#41)*	*19*	*0*	*0*	***19***	*4*	*10*	*8*	***22***
Zircon *(#39)*	*35*	*0*	*0*	***35***	*0*	*1*	*2*	***3***
Rutile *(#27)*	*6*	*0*	*0*	***6***	*1*	*0*	*6*	***7***
Sphalerite *(#41)*	*11*	*0*	*0*	***11***	*5*	*6*	*12*	***23***
Galena *(#14)*	*4*	*0*	*0*	***4***	*0*	*0*	*7*	***7***

Appendix 3 - Mineral Chemistry Data

Summary of the main group of analyses per sector

Total	Neves Corvo					Lousal				
	No sulphide	*Py Bearing*	*Mineralized*	*Position*	*#*	*No sulphide*	*Py Bearing*	*Mineralized*	*Position*	*#*
Chlorite *(#267)*	*18*	*2*	*64*	***FW to FW below OH***	***84***	*0*	*5 (1)*	*9 (2)*	***[1] HG [2] FW below OH***	***14***
White Mica *(#217)*	*3*	*28*	*33 (1)*	***[1] 9 HG - 24 FW***	***64***	*0*	*11 (1)*	*9 (2)*	***[1] HG [2] FW below OH***	***20***
Pyrite *(#170)*	*6*	*22*	*30 (1)*	***[1] 3 HG - 27 FW***	***58***	*0*	*10 (1)*	*18 (2)*	***[2] HG [2] FW below OH***	***28***
Chalcopyrite *(#61)*	*0*	*0*	*0*		***0***	*0*	*0*	*0*		***0***
Carbonates *(#105)*	*0*	*0*	*17 (1)*	***[1] 3 HG - 14 FW***	***17***	*0*	*10 (1)*	*17 (2)*	***[2] HG [2] FW below OH***	***27***
Feldspars *(#41)*	*0*	*0*	*0*		***0***	*0*	*0*	*0*		***0***
Zircon *(#39)*	*0*	*0*	*0*		***0***	*0*	*1*	*0*		***1***
Rutile *(#27)*	*4*	*1*	*9*	***only HW***	***14***	*0*	*0*	*0*		***0***
Sphalerite *(#41)*	*0*	*0*	*7 (1)*	***[1] 6 HG - 1 FW***	***7***	*0*	*0*	*0*		***0***
Galena *(#14)*	*0*	*0*	*0*		***0***	*0*	*0*	*3*		***3***

Chlorite

n = 267

Chlorite

Sector	*Albernoa*	*Albernoa*	*Albernoa*	*Albernoa*	*Albernoa*	*Albernoa*	*Albernoa*	*Albernoa*	*Albernoa*	*Albernoa*	*Albernoa*	*Albernoa*
Sub-sector												
Stratigraphic division	*middleVSC*	*middleVSC*	*middleVSC*	*middleVSC*	*upperVSC*	*upperVSC*	*upperVSC*	*middleVSC*	*middleVSC*	*middleVSC*	*middleVSC*	*middleVSC*
Mineralization type	*Py-bearing*	*Py-bearing*	*Py-bearing*	*Py-bearing*	*Mineralized*	*Mineralized*	*Mineralized*	*Py-bearing*	*Py-bearing*	*Py-bearing*	*Py-bearing*	*Py-bearing*
Occurrence	*Late-formed*	*Late-formed*	*Late-formed*	*Late-formed*	*Late-formed*	*Late-formed*	*Late-formed*	*Early-formed*	*Early-formed*	*Early-formed*	*Early-formed*	*Early-formed*
Sample ref.	*37-1-E*	*37-1-E*	*37-1-E*	*37-1-E*	*18-1-FF*	*18-1-FF*	*18-1-FF*	*37-1-A*	*37-1-A*	*37-1-A*	*37-1-A*	*37-1-A*
# analysis	*#1*	*#2*	*#3*	*#4*	*#5*	*#6*	*#7*	*#8*	*#9*	*#10*	*#11*	*#12*
SiO2	23.84	24.25	23.74	24.91	25.80	25.69	25.41	24.77	23.37	23.95	24.57	24.43
Al2O3	24.08	24.17	24.03	24.52	22.87	22.89	23.21	22.51	25.11	39.67	38.83	39.72
FeO	29.54	29.14	29.73	28.82	25.95	25.83	25.97	31.01	31.49	24.07	23.70	24.51
Fe2O3	0.00	0.00	0.00	0.00	0.00	0.00	0.00	0.00	0.00	0.00	0.00	0.00
MnO	0.47	0.38	0.44	0.36	0.04	0.04	0.05	0.13	0.20	0.44	0.40	0.34
MgO	9.61	9.65	9.79	9.60	13.37	13.22	12.82	9.74	8.17	1.17	1.38	1.11
CaO	0.05	0.05	0.01	0.02	0.06	0.10	0.06	0.04	0.02	0.03	0.19	0.01
Na2O	0.01	0.06	0.01	0.05	0.00	0.02	0.00	0.00	0.00	0.00	0.00	0.00
K2O	0.03	0.21	0.01	0.38	0.01	0.05	0.00	0.02	0.04	0.05	0.07	0.03
F	0.00	0.00	0.00	0.00	0.04	0.00	0.00	0.12	0.00	0.00	0.13	0.11
Cl	0.00	0.00	0.00	0.00	0.00	0.00	0.00	0.00	0.00	0.01	0.03	0.00
TiO2	0.01	0.05	0.04	0.05	0.00	0.01	0.03	0.03	0.01	0.74	0.14	0.40
Cr2O3	0.11	0.07	0.10	0.10	0.10	0.12	0.07	0.10	0.10	0.06	0.11	0.14
ZnO	0.18	0.00	0.08	0.13	0.11	0.08	0.10	0.05	0.07	0.00	0.00	0.00
V2O3	0.00	0.00	0.00	0.00	0.00	0.00	0.00	0.00	0.00	0.00	0.00	0.00
NiO	0.00	0.00	0.00	0.00	0.00	0.00	0.00	0.00	0.00	0.00	0.00	0.00
Cs2O	0.00	0.00	0.00	0.00	0.00	0.00	0.00	0.00	0.02	0.00	0.00	0.00
BaO	0.05	0.02	0.05	0.00	0.05	0.07	0.00	0.02	0.05	0.00	0.02	0.05
H2O	11.14	11.20	11.14	11.35	11.46	11.45	11.39	11.10	11.14	12.12	11.98	12.14
Total#	99.13	99.26	99.18	100.29	99.85	99.57	99.10	99.63	99.78	102.31	101.54	102.98
O=F	0.00	0.00	0.00	0.00	-0.02	0.00	0.00	-0.05	0.00	0.00	-0.05	-0.05
O=Cl	0.00	0.00	0.00	0.00	0.00	0.00	0.00	0.00	0.00	0.00	-0.01	0.00
Total	99.13	99.26	99.18	100.29	99.84	99.57	99.10	99.59	99.78	102.31	101.47	102.94

Chlorite

# analysis	#1	#2	#3	#4	#5	#6	#7	#8	#9	#10	#11	#12
Ion Distribution												
Si	2.57	2.60	2.56	2.63	2.70	2.69	2.68	2.66	2.52	2.37	2.45	2.40
Al	1.43	1.40	1.45	1.37	1.31	1.31	1.33	1.34	1.49	1.63	1.55	1.60
Total	4.00	4.00	4.00	4.00	4.00	4.00	4.00	4.00	4.00	4.00	4.00	4.00
Al	1.62	1.65	1.60	1.69	1.51	1.52	1.56	1.52	1.70	3.00	3.00	3.01
Mn	0.04	0.03	0.04	0.03	0.00	0.00	0.01	0.01	0.02	0.04	0.03	0.03
Zn	0.01	0.00	0.01	0.01	0.01	0.01	0.01	0.00	0.01	0.00	0.00	0.00
Fe2+	2.66	2.61	2.68	2.55	2.27	2.26	2.29	2.79	2.84	1.99	1.97	2.02
Ti	0.00	0.00	0.00	0.00	0.00	0.00	0.00	0.00	0.00	0.06	0.01	0.03
Ca	0.01	0.01	0.00	0.00	0.01	0.01	0.01	0.01	0.00	0.00	0.02	0.00
V	0.00	0.00	0.00	0.00	0.00	0.00	0.00	0.00	0.00	0.00	0.00	0.00
Ba	0.00	0.00	0.00	0.00	0.00	0.00	0.00	0.00	0.00	0.00	0.00	0.00
Fe3+	0.00	0.00	0.00	0.00	0.00	0.00	0.00	0.00	0.00	0.00	0.00	0.00
Mg	1.54	1.54	1.57	1.51	2.08	2.06	2.01	1.56	1.31	0.17	0.21	0.16
Na	0.00	0.01	0.00	0.01	0.00	0.00	0.00	0.00	0.00	0.00	0.00	0.00
Cr	0.01	0.01	0.01	0.01	0.01	0.01	0.01	0.01	0.01	0.00	0.01	0.01
K	0.00	0.03	0.00	0.05	0.00	0.01	0.00	0.00	0.01	0.01	0.01	0.00
Cs	0.00	0.00	0.00	0.00	0.00	0.00	0.00	0.00	0.00	0.00	0.00	0.00
Ni	0.00	0.00	0.00	0.00	0.00	0.00	0.00	0.00	0.00	0.00	0.00	0.00
Total	5.90	5.89	5.92	5.86	5.89	5.89	5.88	5.90	5.89	5.26	5.26	5.26
OH	8.00	8.00	8.00	8.00	7.99	8.00	8.00	7.96	8.00	8.00	7.96	7.97
F	0.00	0.00	0.00	0.00	0.01	0.00	0.00	0.04	0.00	0.00	0.04	0.03
Cl	0.00	0.00	0.00	0.00	0.00	0.00	0.00	0.00	0.00	0.00	0.01	0.00
Total	8.00	8.00	8.00	8.00	8.00	8.00	8.00	8.00	8.00	8.00	8.00	8.00

Chlorite

Sector	*Albernoa*	*Albernoa*	*Albernoa*	*Albernoa*	*Albernoa*	*Albernoa*	*Albernoa*	*Albernoa*	*Albernoa*	*Albernoa*	*Albernoa*	*Albernoa*
Sub-sector												
Stratigraphic division	*middleVSC*	*middleVSC*	*middleVSC*	*middleVSC*	*middleVSC*	*middleVSC*	*middleVSC*	*middleVSC*	*middleVSC*	*middleVSC*	*middleVSC*	*middleVSC*
Mineralization type	*Py-bearing*	*Py-bearing*	*Py-bearing*	*Py-bearing*	*Py-bearing*	*Py-bearing*	*Py-bearing*	*Py-bearing*	*Py-Bearing*	*Py-Bearing*	*Py-Bearing*	*Py-Bearing*
Occurrence	*Early-formed*	*Early-formed*	*Early-formed*	*Early-formed*	*Early-formed*	*Early-formed*	*Early-formed*	*Early-formed*	*Early-formed*	*Early-formed*	*Early-formed*	*Early-formed*
Sample ref.	*37-1-A*	*37-1-A*	*37-1-A*	*37-1-A*	*37-1-A*	*37-1-A*	*37-1-A*	*37-1-A*	*37-1-E*	*37-1-A*	*37-1-A*	*37-1-A*
# analysis	*#13*	*#14*	*#15*	*#16*	*#17*	*#18*	*#19*	*#20*	*#21*	*#22*	*#23*	*#24*
SiO2	24.50	23.11	22.81	23.36	36.35	24.30	24.91	21.09	24.57	23.03	23.22	23.26
Al2O3	39.98	25.62	25.77	25.38	29.17	39.90	39.92	33.05	24.50	24.71	25.08	24.69
FeO	24.86	31.96	32.17	31.82	18.78	25.00	24.50	30.58	29.72	31.39	31.24	31.19
Fe2O3	0.00	0.00	0.00	0.00	0.00	0.00	0.00	0.00	0.00	0.00	0.00	0.00
MnO	0.39	0.14	0.13	0.10	0.37	0.37	0.45	0.60	0.50	0.18	0.21	0.12
MgO	1.18	7.79	7.65	7.76	0.76	1.05	1.10	1.91	9.72	8.16	8.16	8.22
CaO	0.03	0.02	0.02	0.01	0.00	0.04	0.01	0.21	0.05	0.04	0.04	0.07
Na2O	0.00	0.01	0.01	0.00	0.00	0.01	0.01	0.04	0.04	0.01	0.01	0.04
K2O	0.03	0.00	0.00	0.00	0.04	0.04	0.06	0.02	0.11	0.02	0.02	0.03
F	0.03	0.00	0.00	0.02	0.00	0.00	0.00	0.00	0.00	0.00	0.00	0.02
Cl	0.01	0.00	0.00	0.00	0.00	0.00	0.01	0.00	0.00	0.00	0.00	0.00
TiO2	0.16	0.00	0.00	0.00	0.19	0.23	0.04	0.05	0.00	0.03	0.05	0.04
Cr2O3	0.14	0.02	0.09	0.06	0.09	0.10	0.11	0.11	0.12	0.07	0.09	0.11
ZnO	0.00	0.09	0.11	0.04	0.00	0.00	0.00	0.00	0.14	0.09	0.07	0.09
V2O3	0.00	0.00	0.00	0.00	0.00	0.00	0.00	0.00	0.00	0.00	0.00	0.00
NiO	0.00	0.00	0.00	0.00	0.00	0.00	0.00	0.00	0.00	0.00	0.00	0.00
Cs2O	0.00	0.00	0.00	0.00	0.00	0.00	0.00	0.00	0.00	0.00	0.01	0.00
BaO	0.03	0.04	0.00	0.05	0.06	0.00	0.05	0.00	0.06	0.04	0.02	0.05
H2O	12.24	11.15	11.12	11.13	12.15	12.21	12.26	11.14	11.36	11.02	11.10	11.04
Total#	103.56	99.94	99.87	99.73	97.97	103.25	103.44	98.79	100.90	98.78	99.31	98.96
O=F	-0.01	0.00	0.00	-0.01	0.00	0.00	0.00	0.00	0.00	0.00	0.00	-0.01
O=Cl	0.00	0.00	0.00	0.00	0.00	0.00	0.00	0.00	0.00	0.00	0.00	0.00
Total	103.54	99.94	99.87	99.72	97.97	103.25	103.43	98.79	100.90	98.78	99.31	98.95

Chlorite

# analysis		#13	#14	#15	#16	#17	#18	#19	#20	#21	#22	#23	#24
Ion Distribution													
Si		2.40	2.49	2.46	2.52	3.59	2.39	2.44	2.27	2.59	2.51	2.51	2.53
Al		1.60	1.51	1.54	1.48	0.41	1.61	1.56	1.73	1.41	1.49	1.49	1.48
	Total	4.00	4.00	4.00	4.00	4.00	4.00	4.00	4.00	4.00	4.00	4.00	4.00
Al		3.01	1.74	1.74	1.74	2.98	3.01	3.04	2.47	1.64	1.68	1.70	1.68
Mn		0.03	0.01	0.01	0.01	0.03	0.03	0.04	0.06	0.05	0.02	0.02	0.01
Zn		0.00	0.01	0.01	0.00	0.00	0.00	0.00	0.00	0.01	0.01	0.01	0.01
Fe2+		2.04	2.88	2.90	2.87	1.55	2.06	2.00	2.75	2.62	2.86	2.82	2.83
Ti		0.01	0.00	0.00	0.00	0.01	0.02	0.00	0.00	0.00	0.00	0.00	0.00
Ca		0.00	0.00	0.00	0.00	0.00	0.01	0.00	0.02	0.01	0.00	0.01	0.01
V		0.00	0.00	0.00	0.00	0.00	0.00	0.00	0.00	0.00	0.00	0.00	0.00
Ba		0.00	0.00	0.00	0.00	0.00	0.00	0.00	0.00	0.00	0.00	0.00	0.00
Fe3+		0.00	0.00	0.00	0.00	0.00	0.00	0.00	0.00	0.00	0.00	0.00	0.00
Mg		0.17	1.25	1.23	1.25	0.11	0.15	0.16	0.31	1.53	1.33	1.32	1.33
Na		0.00	0.00	0.00	0.00	0.00	0.00	0.00	0.01	0.01	0.00	0.00	0.01
Cr		0.01	0.00	0.01	0.01	0.01	0.01	0.01	0.01	0.01	0.01	0.01	0.01
K		0.00	0.00	0.00	0.00	0.01	0.01	0.01	0.00	0.02	0.00	0.00	0.01
Cs		0.00	0.00	0.00	0.00	0.00	0.00	0.00	0.00	0.00	0.00	0.00	0.00
Ni		0.00	0.00	0.00	0.00	0.00	0.00	0.00	0.00	0.00	0.00	0.00	0.00
	Total	5.28	5.89	5.90	5.87	4.70	5.28	5.26	5.63	5.89	5.91	5.89	5.90
OH		7.99	8.00	8.00	7.99	8.00	8.00	8.00	8.00	8.00	8.00	8.00	7.99
F		0.01	0.00	0.00	0.01	0.00	0.00	0.00	0.00	0.00	0.00	0.00	0.01
Cl		0.00	0.00	0.00	0.00	0.00	0.00	0.00	0.00	0.00	0.00	0.00	0.00
	Total	8.00	8.00	8.00	8.00	8.00	8.00	8.00	8.00	8.00	8.00	8.00	8.00

Chlorite

Sector	*Albernoa*	*Albernoa*	*Albernoa*	*Albernoa*	*Albernoa*	*Albernoa*	*Albernoa*	*Albernoa*	*Albernoa*	*Albernoa*	*Albernoa*	*Albernoa*
Sub-sector												
Stratigraphic division												*middle VSC*
Mineralization type	*No Sulph*	*No Sulph*	*No Sulph*	*No Sulph*	*No Sulph*	*No Sulph*	*No Sulph*	*No Sulph*	*No Sulph*	*No Sulph*	*No Sulph*	*No Sulph*
Occurrence	*Early-formed*	*Early-formed*	*Early-formed*	*Early-formed*	*Early-formed*	*Early-formed*	*Early-formed*	*Early-formed*	*Early-formed*	*Early-formed*	*Early-formed*	*Early-formed*
Sample ref.	*ABNSTR3*	*ABNSTR3*	*ABNSTR3*	*ABNSTR3*	*ABNSTR3*	*ABNSTR3*	*ABNSTR3*	*ABNSTR3*	*ABNSTR3*	*ABNSTR3*	*ABNSTR3*	*X68*
# analysis	*#25*	*#26*	*#27*	*#28*	*#29*	*#30*	*#31*	*#32*	*#33*	*#34*	*#35*	*#36*
SiO2	23.80	23.93	24.15	23.82	23.82	23.53	23.67	23.73	23.54	23.57	23.76	23.39
Al2O3	22.75	22.77	22.84	22.26	23.25	22.98	22.68	22.87	22.63	22.53	22.64	24.14
FeO	33.07	33.11	31.99	33.21	31.97	32.65	32.58	31.88	32.57	33.21	33.08	30.86
Fe2O3	0.00	0.00	0.00	0.00	0.00	0.00	0.00	0.00	0.00	0.00	0.00	0.00
MnO	0.56	0.42	0.54	0.56	0.54	0.56	0.61	0.64	0.52	0.53	0.60	0.18
MgO	8.57	8.42	8.58	8.62	8.89	8.76	8.96	9.03	8.69	8.47	8.64	7.14
CaO	0.02	0.04	0.05	0.04	0.09	0.03	0.05	0.06	0.07	0.04	0.06	0.03
Na2O	0.02	0.01	0.01	0.00	0.03	0.01	0.01	0.03	0.02	0.00	0.00	0.01
K2O	0.01	0.00	0.14	0.01	0.06	0.01	0.00	0.02	0.06	0.02	0.01	0.01
F	0.02	0.00	0.00	0.17	0.00	0.01	0.07	0.00	0.00	0.08	0.00	0.00
Cl	0.00	0.00	0.00	0.00	0.00	0.00	0.00	0.00	0.00	0.00	0.00	0.00
TiO2	0.02	0.02	0.05	0.04	0.02	0.00	0.05	0.00	0.01	0.02	0.03	0.04
Cr2O3	0.07	0.05	0.08	0.08	0.10	0.05	0.07	0.05	0.10	0.07	0.05	0.07
ZnO	0.01	0.11	0.18	0.00	0.13	0.10	0.14	0.12	0.19	0.05	0.02	0.03
V2O3	0.00	0.00	0.00	0.00	0.00	0.00	0.00	0.00	0.00	0.00	0.00	0.00
NiO	0.00	0.00	0.00	0.00	0.00	0.00	0.00	0.00	0.00	0.00	0.00	0.00
Cs2O	0.00	0.00	0.00	0.00	0.00	0.00	0.00	0.00	0.00	0.00	0.00	0.06
BaO	0.00	0.01	0.00	0.00	0.05	0.05	0.00	0.00	0.10	0.00	0.02	0.02
H2O	11.03	11.04	11.06	10.91	11.10	11.02	11.01	11.03	10.98	10.93	11.03	10.82
Total#	99.94	99.92	99.65	99.73	100.04	99.75	99.90	99.46	99.47	99.50	99.93	96.80
O=F	-0.01	0.00	0.00	-0.07	0.00	0.00	-0.03	0.00	0.00	-0.03	0.00	0.00
O=Cl	0.00	0.00	0.00	0.00	0.00	0.00	0.00	0.00	0.00	0.00	0.00	0.00
Total	99.93	99.92	99.65	99.65	100.04	99.75	99.87	99.46	99.47	99.46	99.93	96.80

Chlorite

# analysis	#25	#26	#27	#28	#29	#30	#31	#32	#33	#34	#35	#36
Ion Distribution												
Si	2.59	2.60	2.62	2.60	2.57	2.56	2.57	2.58	2.57	2.58	2.58	2.59
Al	1.42	1.40	1.38	1.40	1.43	1.44	1.43	1.42	1.43	1.42	1.42	1.41
Total	4.00	4.00	4.00	4.00	4.00	4.00	4.00	4.00	4.00	4.00	4.00	4.00
Al	1.50	1.51	1.54	1.46	1.53	1.51	1.47	1.51	1.49	1.48	1.48	1.75
Mn	0.05	0.04	0.05	0.05	0.05	0.05	0.06	0.06	0.05	0.05	0.06	0.02
Zn	0.00	0.01	0.01	0.00	0.01	0.01	0.01	0.01	0.02	0.00	0.00	0.00
Fe2+	3.01	3.01	2.90	3.03	2.89	2.97	2.96	2.90	2.98	3.04	3.01	2.86
Ti	0.00	0.00	0.00	0.00	0.00	0.00	0.00	0.00	0.00	0.00	0.00	0.00
Ca	0.00	0.01	0.01	0.01	0.01	0.00	0.01	0.01	0.01	0.01	0.01	0.00
V	0.00	0.00	0.00	0.00	0.00	0.00	0.00	0.00	0.00	0.00	0.00	0.00
Ba	0.00	0.00	0.00	0.00	0.00	0.00	0.00	0.00	0.00	0.00	0.00	0.00
Fe3+	0.00	0.00	0.00	0.00	0.00	0.00	0.00	0.00	0.00	0.00	0.00	0.00
Mg	1.39	1.36	1.39	1.40	1.43	1.42	1.45	1.46	1.42	1.38	1.40	1.18
Na	0.00	0.00	0.00	0.00	0.01	0.00	0.00	0.01	0.00	0.00	0.00	0.00
Cr	0.01	0.00	0.01	0.01	0.01	0.00	0.01	0.00	0.01	0.01	0.00	0.01
K	0.00	0.00	0.02	0.00	0.01	0.00	0.00	0.00	0.01	0.00	0.00	0.00
Cs	0.00	0.00	0.00	0.00	0.00	0.00	0.00	0.00	0.00	0.00	0.00	0.00
Ni	0.00	0.00	0.00	0.00	0.00	0.00	0.00	0.00	0.00	0.00	0.00	0.00
Total	5.96	5.94	5.93	5.96	5.95	5.97	5.97	5.96	5.97	5.97	5.96	5.83
OH	8.00	8.00	8.00	7.94	8.00	8.00	7.98	8.00	8.00	7.97	8.00	8.00
F	0.01	0.00	0.00	0.06	0.00	0.00	0.02	0.00	0.00	0.03	0.00	0.00
Cl	0.00	0.00	0.00	0.00	0.00	0.00	0.00	0.00	0.00	0.00	0.00	0.00
Total	8.00	8.00	8.00	8.00	8.00	8.00	8.00	8.00	8.00	8.00	8.00	8.00

Chlorite

Sector	*Albernoa*	*Albernoa*	*Albernoa*	*Albernoa*	*Albernoa*	*Albernoa*	*Albernoa*	*Albernoa*	*Albernoa*	*Albernoa*	*Albernoa*	*Albernoa*
Sub-sector												
Stratigraphic division	*middle VSC*	*middle VSC*	*upperVSC*	*upperVSC*	*upperVSC*	*upperVSC*	*upperVSC*	*upperVSC*	*upperVSC*	*upperVSC*	*upperVSC*	*upperVSC*
Mineralization type	*No Sulph*	*No Sulph*	*No Sulph*	*No Sulph*	*No Sulph*	*No Sulph*	*No Sulph*	*No Sulph*	*No Sulph*	*No Sulph*	*No Sulph*	*No Sulph*
Occurrence	*Early-formed*	*Early-formed*	*Late-formed*	*Late-formed*	*Late-formed*	*Late-formed*	*Late-formed*	*Late-formed*	*Late-formed*	*Late-formed*	*Late-formed*	*Early-formed*
Sample ref.	***x68***	***x68***	***18-1-G***	***18-1-G***	***18-1-EE***	***18-1-EE***	***18-1-EE***	***18-1-EE***	***18-1-EE***	***18-1-EE***	***18-1-EE***	***18-1-G***
# analysis	*#37*	*#38*	*#39*	*#40*	*#41*	*#42*	*#43*	*#44*	*#45*	*#46*	*#47*	*#48*
SiO2	23.87	23.51	26.00	25.11	26.39	27.11	26.13	26.52	26.49	25.95	26.21	24.55
Al2O3	23.60	23.68	21.70	21.78	21.47	21.48	21.44	20.77	21.46	21.54	21.05	23.33
FeO	28.56	30.68	24.74	29.10	26.27	24.61	26.25	25.57	26.01	26.34	25.69	29.52
Fe2O3	0.00	0.00	0.00	0.00	0.00	0.00	0.00	0.00	0.00	0.00	0.00	0.00
MnO	0.19	0.10	0.52	0.40	0.22	0.22	0.18	0.21	0.22	0.19	0.21	0.30
MgO	8.86	7.69	15.31	12.05	14.22	14.48	14.28	14.79	14.57	13.78	14.80	10.91
CaO	0.04	0.06	0.11	0.14	0.05	0.16	0.04	0.30	0.07	0.39	0.06	0.02
Na2O	0.03	0.01	0.01	0.05	0.00	0.04	0.01	0.00	0.01	0.01	0.00	0.02
K2O	0.01	0.01	0.00	0.00	0.06	0.23	0.01	0.02	0.01	0.00	0.01	0.00
F	0.00	0.00	0.04	0.03	0.00	0.00	0.00	0.00	0.00	0.00	0.00	0.07
Cl	0.00	0.00	0.00	0.00	0.00	0.00	0.00	0.00	0.00	0.00	0.00	0.00
TiO2	0.02	0.01	0.04	0.00	0.00	0.01	0.03	0.00	0.00	0.01	0.00	0.01
Cr2O3	0.09	0.06	0.06	0.05	0.11	0.11	0.10	0.10	0.03	0.10	0.10	0.05
ZnO	0.10	0.08	0.21	0.00	0.13	0.11	0.05	0.07	0.01	0.24	0.05	0.00
V2O3	0.00	0.00	0.00	0.00	0.00	0.00	0.00	0.00	0.00	0.00	0.00	0.00
NiO	0.00	0.00	0.00	0.00	0.00	0.00	0.00	0.00	0.00	0.00	0.00	0.00
Cs2O	0.00	0.01	0.00	0.00	0.02	0.00	0.00	0.00	0.00	0.00	0.00	0.00
BaO	0.03	0.03	0.00	0.03	0.05	0.00	0.03	0.00	0.00	0.03	0.04	0.02
H2O	10.88	10.82	11.52	11.27	11.52	11.58	11.46	11.47	11.54	11.43	11.44	11.25
Total#	96.28	96.74	100.24	100.01	100.51	100.13	100.00	99.81	100.44	100.01	99.65	100.06
O=F	0.00	0.00	0.00	0.00	0.00	0.00	0.00	0.00	0.00	0.00	0.00	0.00
O=Cl	0.00	0.00	0.00	0.00	0.00	0.00	0.00	0.00	0.00	0.00	0.00	0.00
Total	96.28	96.74	100.24	100.01	100.51	100.13	100.00	99.81	100.44	100.01	99.65	100.06

Chlorite

# analysis	#37	#38	#39	#40	#41	#42	#43	#44	#45	#46	#47	#48
Ion Distribution												
Si	2.63	2.61	2.70	2.67	2.75	2.81	2.73	2.77	2.75	2.72	2.75	2.61
Al	1.37	1.40	1.30	1.33	1.25	1.19	1.27	1.23	1.25	1.28	1.25	1.39
Total	4.00	4.00	4.00	4.00	4.00	4.00	4.00	4.00	4.00	4.00	4.00	4.00
Al	1.70	1.70	1.36	1.40	1.38	1.43	1.38	1.33	1.38	1.39	1.35	1.53
Mn	0.02	0.01	0.05	0.04	0.02	0.02	0.02	0.02	0.02	0.02	0.02	0.03
Zn	0.01	0.01	0.02	0.00	0.01	0.01	0.00	0.01	0.00	0.02	0.00	0.00
Fe2+	2.63	2.84	2.15	2.59	2.29	2.13	2.30	2.24	2.26	2.31	2.25	2.63
Ti	0.00	0.00	0.00	0.00	0.00	0.00	0.00	0.00	0.00	0.00	0.00	0.00
Ca	0.00	0.01	0.01	0.02	0.01	0.02	0.01	0.03	0.01	0.04	0.01	0.00
V	0.00	0.00	0.00	0.00	0.00	0.00	0.00	0.00	0.00	0.00	0.00	0.00
Ba	0.00	0.00	0.00	0.00	0.00	0.00	0.00	0.00	0.00	0.00	0.00	0.00
Fe3+	0.00	0.00	0.00	0.00	0.00	0.00	0.00	0.00	0.00	0.00	0.00	0.00
Mg	1.46	1.27	2.37	1.91	2.21	2.24	2.23	2.31	2.26	2.16	2.31	1.73
Na	0.01	0.00	0.00	0.01	0.00	0.01	0.00	0.00	0.00	0.00	0.00	0.01
Cr	0.01	0.01	0.01	0.00	0.01	0.01	0.01	0.01	0.00	0.01	0.01	0.00
K	0.00	0.00	0.00	0.00	0.01	0.03	0.00	0.00	0.00	0.00	0.00	0.00
Cs	0.00	0.00	0.00	0.00	0.00	0.00	0.00	0.00	0.00	0.00	0.00	0.00
Ni	0.00	0.00	0.00	0.00	0.00	0.00	0.00	0.00	0.00	0.00	0.00	0.00
Total	5.83	5.85	5.96	5.97	5.93	5.89	5.94	5.94	5.93	5.94	5.95	5.93
OH	8.00	8.00	7.99	7.99	8.00	8.00	8.00	8.00	8.00	8.00	8.00	7.98
F	0.00	0.00	0.01	0.01	0.00	0.00	0.00	0.00	0.00	0.00	0.00	0.03
Cl	0.00	0.00	0.00	0.00	0.00	0.00	0.00	0.00	0.00	0.00	0.00	0.00
Total	8.00	8.00	8.00	8.00	8.00	8.00	8.00	8.00	8.00	8.00	8.00	8.00

Chlorite

Sector	Albernoa	Albernoa	Albernoa	Albernoa	Albernoa	Albernoa	Albernoa	Albernoa	Albernoa	Albernoa	Albernoa	Albernoa
Sub-sector												
Stratigraphic division	upperVSC	upperVSC	upperVSC	upperVSC	upperVSC	upperVSC	upperVSC	upperVSC	upperVSC	upperVSC	upperVSC	upperVSC
Mineralization type	No Sulph	No Sulph	No Sulph	No Sulph	No Sulph	No Sulph	No Sulph	No Sulph	No Sulph	No Sulph	No Sulph	No Sulph
Occurrence	Early-formed	Early-formed	Early-formed	Early-formed	Early-formed	Early-formed	Early-formed	Early-formed	Early-formed	Early-formed	Early-formed	Early-formed
Sample ref.	18-1-G	CW2-AA	18-1-G	CW2-P	CW2-P	CW2-P	CW2-P	CW2-P	CW2-P	CW2-P	CW2-VV	CW2-VV
# analysis	#49	#50	#51	#52	#53	#54	#55	#56	#57	#58	#59	#60
SiO2	25.89	24.89	25.04	26.63	26.31	26.11	26.93	26.76	27.44	27.07	25.47	26.55
Al2O3	24.46	22.88	23.30	21.42	21.71	21.45	20.67	20.80	21.07	20.72	21.87	21.77
FeO	29.03	26.58	29.35	23.11	23.31	22.38	21.54	23.12	17.23	21.31	28.33	26.40
Fe2O3	0.00	0.00	0.00	0.00	0.00	0.00	0.00	0.00	0.00	0.00	0.00	0.00
MnO	0.24	0.96	0.29	1.00	1.05	1.00	1.00	1.08	1.16	1.01	0.41	0.44
MgO	10.16	12.60	10.59	16.48	15.65	16.83	17.51	16.71	20.73	17.90	11.48	13.42
CaO	0.01	0.02	0.04	0.04	0.01	0.03	0.04	0.03	0.01	0.04	0.04	0.04
Na2O	0.02	0.01	0.01	0.00	0.01	0.00	0.00	0.11	0.04	0.02	0.01	0.02
K2O	0.00	0.00	0.00	0.00	0.02	0.01	0.03	0.01	0.01	0.00	0.01	0.01
F	0.04	0.00	0.05	0.07	0.00	0.06	0.07	0.09	0.15	0.04	0.00	0.00
Cl	0.00	0.00	0.00	0.00	0.00	0.00	0.00	0.00	0.00	0.00	0.00	0.00
TiO2	0.00	0.04	0.01	0.00	0.00	0.00	0.00	0.00	0.01	0.00	0.00	0.01
Cr2O3	0.04	0.08	0.08	0.03	0.06	0.08	0.07	0.08	0.02	0.05	0.11	0.10
ZnO	0.07	0.08	0.00	0.10	0.11	0.00	0.07	0.05	0.08	0.05	0.10	0.03
V2O3	0.00	0.00	0.00	0.00	0.00	0.00	0.00	0.00	0.00	0.00	0.00	0.00
NiO	0.00	0.00	0.00	0.00	0.00	0.00	0.00	0.00	0.00	0.00	0.00	0.00
Cs2O	0.00	0.00	0.00	0.00	0.00	0.04	0.00	0.00	0.02	0.00	0.01	0.00
BaO	0.00	0.02	0.00	0.00	0.03	0.02	0.00	0.08	0.00	0.01	0.00	0.01
H2O	11.53	11.34	11.28	11.62	11.56	11.53	11.58	11.59	11.80	11.66	11.22	11.50
Total#	101.51	99.50	100.03	100.49	99.81	99.52	99.49	100.51	99.78	99.88	99.04	100.30
O=F	0.00	0.00	0.00	0.00	0.00	0.00	0.00	0.00	0.00	0.00	0.00	0.00
O=Cl	0.00	0.00	0.00	0.00	0.00	0.00	0.00	0.00	0.00	0.00	0.00	0.00
Total	101.51	99.50	100.03	100.49	99.81	99.52	99.49	100.51	99.78	99.88	99.04	100.30

Chlorite

# analysis	#49	#50	#51	#52	#53	#54	#55	#56	#57	#58	#59	#60
Ion Distribution												
Si	2.69	2.63	2.66	2.74	2.73	2.71	2.78	2.76	2.77	2.78	2.72	2.77
Al	1.31	1.37	1.34	1.26	1.27	1.29	1.22	1.24	1.23	1.22	1.28	1.23
Total	4.00	4.00	4.00	4.00	4.00	4.00	4.00	4.00	4.00	4.00	4.00	4.00
Al	1.68	1.49	1.57	1.34	1.39	1.33	1.30	1.29	1.28	1.29	1.48	1.44
Mn	0.02	0.09	0.03	0.09	0.09	0.09	0.09	0.09	0.10	0.09	0.04	0.04
Zn	0.01	0.01	0.00	0.01	0.01	0.00	0.01	0.00	0.01	0.00	0.01	0.00
Fe2+	2.52	2.35	2.60	1.99	2.02	1.94	1.86	1.99	1.46	1.83	2.53	2.30
Ti	0.00	0.00	0.00	0.00	0.00	0.00	0.00	0.00	0.00	0.00	0.00	0.00
Ca	0.00	0.00	0.00	0.00	0.00	0.00	0.00	0.00	0.00	0.01	0.01	0.01
V	0.00	0.00	0.00	0.00	0.00	0.00	0.00	0.00	0.00	0.00	0.00	0.00
Ba	0.00	0.00	0.00	0.00	0.00	0.00	0.00	0.00	0.00	0.00	0.00	0.00
Fe3+	0.00	0.00	0.00	0.00	0.00	0.00	0.00	0.00	0.00	0.00	0.00	0.00
Mg	1.57	1.99	1.68	2.53	2.42	2.60	2.70	2.57	3.12	2.74	1.83	2.09
Na	0.01	0.00	0.00	0.00	0.00	0.00	0.00	0.02	0.01	0.00	0.00	0.00
Cr	0.00	0.01	0.01	0.00	0.01	0.01	0.01	0.01	0.00	0.00	0.01	0.01
K	0.00	0.00	0.00	0.00	0.00	0.00	0.00	0.00	0.00	0.00	0.00	0.00
Cs	0.00	0.00	0.00	0.00	0.00	0.00	0.00	0.00	0.00	0.00	0.00	0.00
Ni	0.00	0.00	0.00	0.00	0.00	0.00	0.00	0.00	0.00	0.00	0.00	0.00
Total	5.81	5.93	5.89	5.96	5.94	5.98	5.96	5.99	5.98	5.97	5.90	5.89
OH	7.99	8.00	7.98	7.98	8.00	7.98	7.98	7.97	7.95	7.99	8.00	8.00
F	0.01	0.00	0.02	0.02	0.00	0.02	0.02	0.03	0.05	0.01	0.00	0.00
Cl	0.00	0.00	0.00	0.00	0.00	0.00	0.00	0.00	0.00	0.00	0.00	0.00
Total	8.00	8.00	8.00	8.00	8.00	8.00	8.00	8.00	8.00	8.00	8.00	8.00

Chlorite

Sector	*Albernoa*	*Albernoa*	*Albernoa*	*Albernoa*	*Albernoa*	*Albernoa*	*Albernoa*	*Albernoa*	*Albernoa*	*Albernoa*	*Albernoa*	*Albernoa*
Sub-sector												
Stratigraphic division	*upperVSC*	*upperVSC*	*upperVSC*	*upperVSC*	*upperVSC*	*upperVSC*	*upperVSC*	*upperVSC*	*upperVSC*	*upperVSC*	*upperVSC*	*upperVSC*
Mineralization type	*No Sulph*	*No Sulph*	*No Sulph*	*No Sulph*	*No Sulph*	*No Sulph*	*No Sulph*	*No Sulph*	*No Sulph*	*No Sulph*	*No Sulph*	*No Sulph*
Occurrence	*Early-formed*	*Early-formed*	*Early-formed*	*Early-formed*	*Early-formed*	*Early-formed*	*Early-formed*	*Early-formed*	*Early-formed*	*Early-formed*	*Early-formed*	*Early-formed*
Sample ref.	***CW2-VV***	***CW2-VV***	***CW2-VV***	***18-1-II***	***18-1-II***	***18-1-II***	***18-1-II***	***CW2-AA***	***CW2-AA***	***CW2-AA***	***CW2-AA***	***CW2-AA***
# analysis	*#61*	*#62*	*#63*	*#64*	*#65*	*#66*	*#67*	*#68*	*#69*	*#70*	*#71*	*#74*
SiO2	24.88	25.79	25.84	27.57	27.89	27.70	27.97	24.70	24.81	25.61	24.75	24.88
Al2O3	22.75	22.18	21.81	20.77	20.17	20.59	20.80	22.43	22.57	23.59	22.88	21.42
FeO	30.69	26.04	26.39	21.99	21.25	21.60	21.59	26.52	26.34	26.37	27.77	31.52
Fe2O3	0.00	0.00	0.00	0.00	0.00	0.00	0.00	0.00	0.00	0.00	0.00	0.00
MnO	0.32	0.42	0.41	0.14	0.15	0.15	0.12	1.15	1.05	0.87	0.92	1.35
MgO	9.62	13.83	13.26	17.88	18.35	17.34	17.61	12.68	12.74	11.36	11.90	10.29
CaO	0.03	0.03	0.03	0.07	0.05	0.10	0.09	0.16	0.14	0.05	0.11	0.02
Na2O	0.01	0.02	0.02	0.00	0.00	0.02	0.02	0.01	0.02	0.02	0.00	0.03
K2O	0.02	0.00	0.02	0.01	0.02	0.00	0.01	0.00	0.00	0.23	0.01	0.00
F	0.00	0.02	0.01	0.05	0.21	0.12	0.04	0.04	0.00	0.00	0.04	0.01
Cl	0.00	0.00	0.00	0.00	0.00	0.00	0.00	0.00	0.00	0.00	0.00	0.00
TiO2	0.00	0.00	0.01	0.00	0.00	0.01	0.01	0.03	0.03	0.05	0.02	0.02
Cr2O3	0.08	0.08	0.13	0.09	0.07	0.05	0.04	0.09	0.09	0.09	0.08	0.07
ZnO	0.03	0.17	0.11	0.06	0.12	0.12	0.04	0.04	0.06	0.03	0.00	0.22
V2O3	0.00	0.00	0.00	0.00	0.00	0.00	0.00	0.00	0.00	0.00	0.00	0.00
NiO	0.00	0.00	0.00	0.00	0.00	0.00	0.00	0.00	0.00	0.00	0.00	0.00
Cs2O	0.02	0.02	0.01	0.00	0.00	0.00	0.01	0.00	0.00	0.00	0.00	0.00
BaO	0.02	0.07	0.01	0.06	0.00	0.00	0.00	0.00	0.03	0.00	0.01	0.00
H2O	11.17	11.45	11.37	11.73	11.63	11.60	11.75	11.24	11.29	11.40	11.28	11.20
Total#	99.63	100.11	99.43	100.41	99.90	99.40	100.10	99.09	99.17	99.65	99.75	101.02
O=F	0.00	0.00	0.00	0.00	0.00	0.00	0.00	0.00	0.00	0.00	0.00	0.00
O=Cl	0.00	0.00	0.00	0.00	0.00	0.00	0.00	0.00	0.00	0.00	0.00	0.00
Total	99.63	100.11	99.43	100.41	99.90	99.40	100.10	99.09	99.17	99.65	99.75	101.02

Chlorite

# analysis	#61	#62	#63	#64	#65	#66	#67	#68	#69	#70	#71	#74
Ion Distribution												
Si	2.67	2.70	2.73	2.81	2.85	2.85	2.85	2.63	2.64	2.70	2.63	2.66
Al	1.33	1.30	1.28	1.19	1.15	1.15	1.15	1.37	1.37	1.31	1.37	1.34
Total	4.00	4.00	4.00	4.00	4.00	4.00	4.00	4.00	4.00	4.00	4.00	4.00
Al	1.55	1.43	1.44	1.31	1.28	1.35	1.35	1.45	1.46	1.62	1.49	1.37
Mn	0.03	0.04	0.04	0.01	0.01	0.01	0.01	0.10	0.09	0.08	0.08	0.12
Zn	0.00	0.01	0.01	0.00	0.01	0.01	0.00	0.00	0.01	0.00	0.00	0.02
Fe2+	2.76	2.28	2.33	1.88	1.82	1.86	1.84	2.36	2.34	2.32	2.47	2.82
Ti	0.00	0.00	0.00	0.00	0.00	0.00	0.00	0.00	0.00	0.00	0.00	0.00
Ca	0.00	0.00	0.00	0.01	0.01	0.01	0.01	0.02	0.02	0.01	0.01	0.00
V	0.00	0.00	0.00	0.00	0.00	0.00	0.00	0.00	0.00	0.00	0.00	0.00
Ba	0.00	0.00	0.00	0.00	0.00	0.00	0.00	0.00	0.00	0.00	0.00	0.00
Fe3+	0.00	0.00	0.00	0.00	0.00	0.00	0.00	0.00	0.00	0.00	0.00	0.00
Mg	1.54	2.16	2.09	2.72	2.80	2.66	2.68	2.01	2.02	1.78	1.88	1.64
Na	0.00	0.00	0.00	0.00	0.00	0.00	0.01	0.00	0.00	0.00	0.00	0.01
Cr	0.01	0.01	0.01	0.01	0.01	0.00	0.00	0.01	0.01	0.01	0.01	0.01
K	0.00	0.00	0.00	0.00	0.00	0.00	0.00	0.00	0.00	0.03	0.00	0.00
Cs	0.00	0.00	0.00	0.00	0.00	0.00	0.00	0.00	0.00	0.00	0.00	0.00
Ni	0.00	0.00	0.00	0.00	0.00	0.00	0.00	0.00	0.00	0.00	0.00	0.00
Total	5.89	5.93	5.92	5.94	5.93	5.90	5.90	5.96	5.95	5.85	5.94	5.98
OH	8.00	7.99	8.00	7.98	7.93	7.96	7.99	7.99	8.00	8.00	7.99	8.00
F	0.00	0.01	0.00	0.02	0.07	0.04	0.01	0.01	0.00	0.00	0.01	0.00
Cl	0.00	0.00	0.00	0.00	0.00	0.00	0.00	0.00	0.00	0.00	0.00	0.00
Total	8.00	8.00	8.00	8.00	8.00	8.00	8.00	8.00	8.00	8.00	8.00	8.00

Chlorite

Sector	*Albernoa*	*Albernoa*	*Albernoa*	*Albernoa*	*Albernoa*	*Albernoa*	*Albernoa*	*Albernoa*	*Albernoa*	*Albernoa*	*Albernoa*	*Albernoa*
Sub-sector												
Stratigraphic division	*upperVSC*	*upperVSC*	*upperVSC*	*upperVSC*	*upperVSC*	*upperVSC*	*upper VSC*	*upper VSC*	*upper VSC*	*upper VSC*	*upper VSC*	*upper VSC*
Mineralization type	*No Sulph*	*No Sulph*	*No Sulph*	*No Sulph*	*No Sulph*	*No Sulph*	*No Sulph*	*No Sulph*	*No Sulph*	*No Sulph*	*No Sulph*	*No Sulph*
Occurrence	*Early-formed*	*Early-formed*	*Early-formed*	*Early-formed*	*Early-formed*	*Early-formed*						
Sample ref.	*CW2-AA*	*CW2-AA*	*CW2-M*	*CW2-M*	*CW2-M*	*CW2-M*	*ALB#13a*	*ALB#13a*	*ALB#13a*	*ALB#13a*	*ALB#13a*	*ALB#13a*
# analysis	*#75*	*#76*	*#77*	*#78*	*#79*	*#80*	*#81*	*#82*	*#83*	*#84*	*#85*	*#86*
SiO2	25.46	25.26	26.76	27.18	27.11	28.52	25.15	25.46	25.53	25.40	25.80	24.37
Al2O3	22.91	21.17	21.82	22.04	22.09	22.27	21.37	21.01	21.63	21.33	21.30	20.14
FeO	26.25	26.52	14.92	14.42	14.97	13.68	29.66	29.92	29.70	29.67	30.01	30.35
Fe2O3	0.00	0.00	0.00	0.00	0.00	0.00	0.00	0.00	0.00	0.00	0.00	0.00
MnO	1.08	0.25	0.18	0.06	0.13	0.11	0.70	0.51	0.59	0.55	0.52	0.71
MgO	13.06	13.52	21.82	22.50	21.73	24.92	11.34	11.22	11.43	11.29	10.84	11.56
CaO	0.03	0.28	0.06	0.01	0.15	0.04	0.09	0.10	0.06	0.02	0.08	0.10
Na2O	0.00	0.00	0.01	0.00	0.02	0.02	0.00	0.03	0.05	0.05	0.02	0.00
K2O	0.00	0.08	0.00	0.00	0.00	0.01	0.04	0.01	0.02	0.01	0.05	0.01
F	0.00	0.01	0.03	0.01	0.02	0.01	0.00	0.00	0.02	0.00	0.00	0.00
Cl	0.00	0.00	0.00	0.00	0.00	0.01	0.00	0.00	0.00	0.00	0.00	0.00
TiO2	0.12	0.19	0.01	0.04	0.01	0.00	0.58	0.24	0.04	0.04	0.28	0.09
Cr2O3	0.08	0.05	0.08	0.06	0.05	0.07	0.09	0.11	0.07	0.04	0.10	0.06
ZnO	0.05	0.00	0.00	0.06	0.00	0.00	0.22	0.15	0.12	0.14	0.09	0.05
V2O3	0.00	0.07	0.00	0.00	0.00	0.00	0.00	0.00	0.00	0.00	0.00	0.00
NiO	0.00	0.00	0.00	0.00	0.00	0.00	0.13	0.11	0.15	0.11	0.10	0.18
Cs2O	0.00	0.00	0.02	0.00	0.00	0.00	0.00	0.00	0.00	0.03	0.00	0.00
BaO	0.03	0.03	0.00	0.01	0.00	0.08	0.03	0.00	0.01	0.00	0.00	0.05
H2O	11.49	11.24	11.76	11.92	11.86	12.44	11.29	11.23	11.31	11.22	11.29	10.97
Total#	100.56	98.66	97.46	98.30	98.14	102.15	100.68	100.11	100.72	99.90	100.48	98.62
O=F	0.00	0.00	0.00	0.00	0.00	0.00	0.00	0.00	-0.01	0.00	0.00	0.00
O=Cl	0.00	0.00	0.00	0.00	0.00	0.00	0.00	0.00	0.00	0.00	0.00	0.00
Total	100.56	98.66	97.46	98.30	98.14	102.15	100.68	100.11	100.71	99.90	100.48	98.62

Chlorite

# analysis		#75	#76	#77	#78	#79	#80	#81	#82	#83	#84	#85	#86
Ion Distribution													
Si		2.66	2.69	2.73	2.74	2.74	2.75	2.67	2.72	2.70	2.71	2.74	2.66
Al		1.34	1.31	1.27	1.27	1.26	1.25	1.33	1.28	1.30	1.29	1.26	1.34
	Total	4.00	4.00	4.00	4.00	4.00	4.00	4.00	4.00	4.00	4.00	4.00	4.00
Al		1.48	1.36	1.35	1.35	1.37	1.28	1.35	1.36	1.41	1.40	1.41	1.26
Mn		0.10	0.02	0.02	0.01	0.01	0.01	0.06	0.05	0.05	0.05	0.05	0.07
Zn		0.00	0.00	0.00	0.00	0.00	0.00	0.02	0.01	0.01	0.01	0.01	0.00
Fe2+		2.29	2.37	1.27	1.21	1.27	1.10	2.64	2.67	2.63	2.65	2.67	2.77
Ti		0.01	0.02	0.00	0.00	0.00	0.00	0.05	0.02	0.00	0.00	0.02	0.01
Ca		0.00	0.03	0.01	0.00	0.02	0.00	0.01	0.01	0.01	0.00	0.01	0.01
V		0.00	0.01	0.00	0.00	0.00	0.00	0.00	0.00	0.00	0.00	0.00	0.00
Ba		0.00	0.00	0.00	0.00	0.00	0.00	0.00	0.00	0.00	0.00	0.00	0.00
Fe3+		0.00	0.00	0.00	0.00	0.00	0.00	0.00	0.00	0.00	0.00	0.00	0.00
Mg		2.03	2.15	3.31	3.37	3.27	3.58	1.80	1.79	1.81	1.80	1.72	1.88
Na		0.00	0.00	0.00	0.00	0.00	0.00	0.00	0.01	0.01	0.01	0.00	0.00
Cr		0.01	0.00	0.01	0.01	0.00	0.01	0.01	0.01	0.01	0.00	0.01	0.01
K		0.00	0.01	0.00	0.00	0.00	0.00	0.01	0.00	0.00	0.00	0.01	0.00
Cs		0.00	0.00	0.00	0.00	0.00	0.00	0.00	0.00	0.00	0.00	0.00	0.00
Ni		0.00	0.00	0.00	0.00	0.00	0.00	0.01	0.01	0.01	0.01	0.01	0.02
	Total	5.92	5.96	5.96	5.95	5.95	5.99	5.94	5.94	5.95	5.94	5.90	6.03
OH		8.00	8.00	7.99	8.00	8.00	8.00	8.00	8.00	7.99	8.00	8.00	8.00
F		0.00	0.00	0.01	0.00	0.01	0.00	0.00	0.00	0.01	0.00	0.00	0.00
Cl		0.00	0.00	0.00	0.00	0.00	0.00	0.00	0.00	0.00	0.00	0.00	0.00
	Total	8.00	8.00	8.00	8.00	8.00	8.00	8.00	8.00	8.00	8.00	8.00	8.00

Chlorite

Sector	*Albernoa*	*Albernoa*	*Albernoa*	*Albernoa*	*Albernoa*	*Albernoa*	*Albernoa*	*Aljustrel*	*Aljustrel*	*Aljustrel*	*Aljustrel*	*Aljustrel*
Sub-sector												
Stratigraphic division	*upper VSC*	*upper VSC*	*upper VSC*	*upper VSC*	*upper VSC*	*upper VSC*	*upper VSC*	*upperVSC*	*upperVSC*	*upperVSC*	*upperVSC*	*upperVSC*
Mineralization type	*No Sulph*	*No Sulph*	*No Sulph*	*No Sulph*	*No Sulph*	*No Sulph*	*No Sulph*	*No Sulph*	*No Sulph*	*No Sulph*	*No Sulph*	*No Sulph*
Occurrence								*Early-formed*	*Early-formed*	*Late-formed*	*Late-formed*	*Late-formed*
Sample ref.	*ALB#13a*	*ALB#13a*	*ALB#13a*	*ALB#18*	*ALB#18*	*ALB#18*	*ALB#18*	*EDS1-S*	*EDS1-S*	*EDS1-K*	*EDS1-K*	*EDS1-K*
# analysis	*#87*	*#88*	*#89*	*#90*	*#91*	*#92*	*#93*	*#72*	*#73*	*#94*	*#95*	*#96*
SiO2	24.29	24.33	26.81	25.89	26.59	24.89	26.53	25.21	25.33	26.23	27.44	25.64
Al2O3	21.03	20.39	20.31	20.89	21.17	20.78	20.40	22.59	22.77	23.02	22.53	23.05
FeO	30.94	30.10	31.69	32.29	32.81	32.58	32.41	27.21	27.24	20.24	20.13	21.14
Fe2O3	0.00	0.00	0.00	0.00	0.00	0.00	0.00	0.00	0.00	0.00	0.00	0.00
MnO	0.58	0.72	0.53	0.54	0.59	0.63	0.66	1.74	1.86	3.54	3.67	3.67
MgO	10.59	11.33	7.95	9.14	8.29	8.12	9.32	11.22	11.50	15.31	13.90	14.52
CaO	0.04	0.16	0.05	0.03	0.02	0.06	0.03	0.07	0.01	0.03	0.04	0.09
Na2O	0.02	0.01	0.02	0.00	0.00	0.01	0.00	0.01	0.00	0.00	0.01	0.00
K2O	0.02	0.00	0.05	0.10	0.04	0.01	0.11	0.01	0.02	0.00	0.00	0.00
F	0.00	0.00	0.00	0.00	0.00	0.00	0.20	0.01	0.03	0.07	0.05	0.03
Cl	0.00	0.00	0.00	0.00	0.00	0.00	0.00	0.00	0.00	0.00	0.00	0.00
TiO2	0.04	0.03	0.15	0.26	0.69	0.32	0.27	0.03	0.00	0.04	0.01	0.00
Cr2O3	0.07	0.06	0.06	0.07	0.06	0.07	0.07	0.04	0.06	0.10	0.05	0.06
ZnO	0.09	0.25	0.05	0.06	0.11	0.01	0.00	0.22	0.06	0.10	0.13	0.02
V2O3	0.00	0.00	0.00	0.00	0.00	0.00	0.00	0.00	0.00	0.00	0.00	0.00
NiO	0.09	0.14	0.03	0.12	0.05	0.00	0.06	0.00	0.00	0.00	0.00	0.00
Cs2O	0.02	0.00	0.00	0.00	0.00	0.00	0.00	0.00	0.00	0.00	0.01	0.00
BaO	0.00	0.03	0.04	0.00	0.03	0.04	0.00	0.01	0.02	0.00	0.01	0.01
H2O	10.99	10.96	11.03	11.18	11.32	10.88	11.16	11.27	11.34	11.63	11.59	11.52
Total#	98.81	98.51	98.77	100.58	101.78	98.40	101.22	99.63	100.24	100.30	99.57	99.74
O=F	0.00	0.00	0.00	0.00	0.00	0.00	-0.08	0.00	0.00	-0.03	-0.02	-0.01
O=Cl	0.00	0.00	0.00	0.00	0.00	0.00	0.00	0.00	0.00	0.00	0.00	0.00
Total	98.81	98.51	98.77	100.58	101.78	98.40	101.13	99.63	100.24	100.27	99.54	99.73

Chlorite

# analysis	*#87*	*#88*	*#89*	*#90*	*#91*	*#92*	*#93*	*#72*	*#73*	*#94*	*#95*	*#96*
Ion Distribution												
Si	2.65	2.66	2.91	2.78	2.82	2.74	2.83	2.68	2.68	2.70	2.83	2.67
Al	1.35	1.34	1.09	1.22	1.18	1.26	1.17	1.32	1.33	1.30	1.17	1.33
Total	4.00	4.00	4.00	4.00	4.00	4.00	4.00	4.00	4.00	4.00	4.00	4.00
Al	1.36	1.29	1.52	1.42	1.46	1.44	1.39	1.51	1.51	1.49	1.58	1.49
Mn	0.05	0.07	0.05	0.05	0.05	0.06	0.06	0.16	0.17	0.31	0.32	0.32
Zn	0.01	0.02	0.00	0.00	0.01	0.00	0.00	0.02	0.01	0.01	0.01	0.00
Fe2+	2.82	2.75	2.88	2.90	2.91	3.00	2.89	2.42	2.41	1.74	1.74	1.84
Ti	0.00	0.00	0.01	0.02	0.05	0.03	0.02	0.00	0.00	0.00	0.00	0.00
Ca	0.00	0.02	0.01	0.00	0.00	0.01	0.00	0.01	0.00	0.00	0.00	0.01
V	0.00	0.00	0.00	0.00	0.00	0.00	0.00	0.00	0.00	0.00	0.00	0.00
Ba	0.00	0.00	0.00	0.00	0.00	0.00	0.00	0.00	0.00	0.00	0.00	0.00
Fe3+	0.00	0.00	0.00	0.00	0.00	0.00	0.00	0.00	0.00	0.00	0.00	0.00
Mg	1.72	1.85	1.29	1.46	1.31	1.33	1.48	1.78	1.81	2.35	2.14	2.25
Na	0.00	0.00	0.00	0.00	0.00	0.00	0.00	0.00	0.00	0.00	0.00	0.00
Cr	0.01	0.01	0.01	0.01	0.00	0.01	0.01	0.00	0.01	0.01	0.00	0.01
K	0.00	0.00	0.01	0.01	0.01	0.00	0.02	0.00	0.00	0.00	0.00	0.00
Cs	0.00	0.00	0.00	0.00	0.00	0.00	0.00	0.00	0.00	0.00	0.00	0.00
Ni	0.01	0.01	0.00	0.01	0.00	0.00	0.01	0.00	0.00	0.00	0.00	0.00
Total	5.99	6.02	5.77	5.88	5.81	5.88	5.87	5.90	5.91	5.90	5.79	5.92
OH	8.00	8.00	8.00	8.00	8.00	8.00	7.93	8.00	7.99	7.98	7.98	7.99
F	0.00	0.00	0.00	0.00	0.00	0.00	0.07	0.00	0.01	0.02	0.02	0.01
Cl	0.00	0.00	0.00	0.00	0.00	0.00	0.00	0.00	0.00	0.00	0.00	0.00
Total	8.00	8.00	8.00	8.00	8.00	8.00	8.00	8.00	8.00	8.00	8.00	8.00

Chlorite

Sector	*Aljustrel*	*Aljustrel*	*Aljustrel*	*Aljustrel*	*Aljustrel*	*Aljustrel*	*Aljustrel*	*Aljustrel*	*Aljustrel*	*Aljustrel*	*Aljustrel*	*Aljustrel*
Sub-sector												
Stratigraphic division	*upperVSC*	*upperVSC*	*upperVSC*	*upperVSC*	*upperVSC*	*upperVSC*	*upperVSC*	*upperVSC*	*upperVSC*	*upperVSC*	*upperVSC*	*upperVSC*
Mineralization type	*No Sulph*	*No Sulph*	*No Sulph*	*No Sulph*	*No Sulph*	*No Sulph*	*No Sulph*	*No Sulph*	*No Sulph*	*No Sulph*	*No Sulph*	*No Sulph*
Occurrence	*Late-formed*	*Late-formed*	*Late-formed*	*Late-formed*	*Late-formed*	*Late-formed*	*Late-formed*	*Late-formed*	*Late-formed*	*Late-formed*	*Late-formed*	*Late-formed*
Sample ref.	***EDS1-K***	***EDS1-K***	***EDS1-K***	***EDS1-S***	***EDS1-S***	***EDS1-F***	***EDS1-F***	***EDS1-F***	***EDS1-F***	***EDS1-F***	***EDS1-F***	***EDS1-F***
# analysis	*#97*	*#98*	*#99*	*#100*	*#101*	*#102*	*#103*	*#104*	*#105*	*#106*	*#107*	*#108*
SiO2	31.75	26.97	24.66	24.68	24.66	27.28	25.57	25.58	24.82	24.47	25.35	25.25
Al2O3	20.76	22.48	24.62	23.05	23.05	20.62	21.30	21.14	21.85	20.92	22.13	22.34
FeO	20.92	21.37	29.20	26.75	26.58	28.66	29.43	28.37	29.65	28.36	28.63	28.11
Fe2O3	0.00	0.00	0.00	0.00	0.00	0.00	0.00	0.00	0.00	0.00	0.00	0.00
MnO	3.61	3.55	0.43	1.88	1.82	2.46	2.56	2.59	2.60	2.89	2.63	2.57
MgO	12.40	14.03	9.56	11.93	12.32	9.68	9.68	10.84	9.88	10.62	9.83	9.13
CaO	0.34	0.01	0.03	0.06	0.02	0.05	0.04	0.05	0.05	0.07	0.02	0.06
Na2O	0.00	0.00	0.03	0.00	0.01	0.05	0.00	0.00	0.00	0.03	0.01	0.03
K2O	0.01	0.00	0.21	0.07	0.02	0.18	0.00	0.01	0.00	0.01	0.10	0.25
F	0.00	0.05	0.00	0.00	0.01	0.00	0.00	0.02	0.01	0.00	0.01	0.00
Cl	0.00	0.00	0.00	0.00	0.01	0.00	0.00	0.00	0.00	0.00	0.00	0.00
TiO2	0.03	0.00	0.04	0.09	0.06	0.08	0.02	0.00	0.02	0.05	0.00	0.00
Cr2O3	0.09	0.07	0.11	0.08	0.05	0.07	0.02	0.06	0.05	0.03	0.07	0.07
ZnO	0.16	0.21	0.06	0.00	0.00	0.13	0.00	0.00	0.05	0.12	0.04	0.15
V2O3	0.00	0.00	0.00	0.00	0.00	0.00	0.00	0.00	0.00	0.00	0.00	0.00
NiO	0.00	0.00	0.00	0.00	0.00	0.00	0.00	0.00	0.00	0.00	0.00	0.00
Cs2O	0.00	0.00	0.00	0.00	0.02	0.00	0.00	0.00	0.00	0.00	0.02	0.00
BaO	0.00	0.03	0.00	0.00	0.02	0.00	0.00	0.01	0.01	0.01	0.00	0.01
H2O	11.98	11.61	11.34	11.32	11.33	11.31	11.15	11.19	11.15	10.98	11.21	11.11
Total#	102.04	100.38	100.29	99.92	99.98	100.58	99.77	99.84	100.13	98.56	100.03	99.08
O=F	0.00	-0.02	0.00	0.00	0.00	0.00	0.00	0.00	0.00	0.00	0.00	0.00
O=Cl	0.00	0.00	0.00	0.00	0.00	0.00	0.00	0.00	0.00	0.00	0.00	0.00
Total	102.04	100.36	100.29	99.92	99.98	100.58	99.77	99.84	100.13	98.56	100.03	99.08

Chlorite

# analysis	#97	#98	#99	#100	#101	#102	#103	#104	#105	#106	#107	#108
Ion Distribution												
Si	3.18	2.78	2.61	2.61	2.61	2.89	2.75	2.74	2.67	2.67	2.71	2.73
Al	0.82	1.22	1.39	1.39	1.39	1.11	1.25	1.26	1.33	1.33	1.29	1.28
Total	4.00	4.00	4.00	4.00	4.00	4.00	4.00	4.00	4.00	4.00	4.00	4.00
Al	1.63	1.51	1.68	1.49	1.48	1.47	1.45	1.41	1.44	1.36	1.50	
Mn	0.31	0.31	0.04	0.17	0.16	0.22	0.23	0.24	0.24	0.27	0.24	0.24
Zn	0.01	0.02	0.01	0.00	0.00	0.01	0.00	0.00	0.00	0.01	0.00	0.01
Fe2+	1.75	1.84	2.58	2.37	2.35	2.54	2.65	2.54	2.67	2.59	2.56	2.54
Ti	0.00	0.00	0.00	0.01	0.01	0.01	0.00	0.00	0.00	0.00	0.00	0.00
Ca	0.04	0.00	0.00	0.01	0.00	0.01	0.01	0.01	0.01	0.01	0.00	0.01
V	0.00	0.00	0.00	0.00	0.00	0.00	0.00	0.00	0.00	0.00	0.00	0.00
Ba	0.00	0.00	0.00	0.00	0.00	0.00	0.00	0.00	0.00	0.00	0.00	0.00
Fe3+	0.00	0.00	0.00	0.00	0.00	0.00	0.00	0.00	0.00	0.00	0.00	0.00
Mg	1.85	2.16	1.51	1.88	1.94	1.53	1.55	1.73	1.59	1.73	1.57	1.47
Na	0.00	0.00	0.01	0.00	0.00	0.01	0.00	0.00	0.00	0.01	0.00	0.01
Cr	0.01	0.01	0.01	0.01	0.00	0.01	0.00	0.01	0.00	0.00	0.01	0.01
K	0.00	0.00	0.03	0.01	0.00	0.02	0.00	0.00	0.00	0.00	0.01	0.03
Cs	0.00	0.00	0.00	0.00	0.00	0.00	0.00	0.00	0.00	0.00	0.00	0.00
Ni	0.00	0.00	0.00	0.00	0.00	0.00	0.00	0.00	0.00	0.00	0.00	0.00
Total	5.59	5.85	5.87	5.94	5.95	5.83	5.90	5.93	5.94	5.98	5.90	5.87
OH	8.00	7.98	8.00	8.00	7.99	8.00	8.00	7.99	8.00	8.00	8.00	8.00
F	0.00	0.02	0.00	0.00	0.00	0.00	0.00	0.01	0.00	0.00	0.00	0.00
Cl	0.00	0.00	0.00	0.00	0.00	0.00	0.00	0.00	0.00	0.00	0.00	0.00
Total	8.00	8.00	8.00	8.00	8.00	8.00	8.00	8.00	8.00	8.00	8.00	8.00

Chlorite

Sector	*Aljustrel*	*Aljustrel*	*Aljustrel*	*Aljustrel*	*Aljustrel*	*Aljustrel*	*Aljustrel*	*Aljustrel*	*Aljustrel*	*Aljustrel*	*Aljustrel*	*Aljustrel*
Sub-sector								Feitais mine	Feitais mine	Feitais mine	Feitais mine	Feitais mine
Stratigraphic division	*upperVSC*	*upperVSC*	*upperVSC*	*upperVSC*	*upperVSC*	*upperVSC*	*upperVSC*	*upperVSC*	*upperVSC*	*upperVSC*	*upperVSC*	*upperVSC*
Mineralization type	*No Sulph*	*Mineralized*	*Mineralized*	*Mineralized*	*No Sulph*	*No Sulph*	*No Sulph*	*No Sulph*	*No Sulph*	*No Sulph*	*No Sulph*	*No Sulph*
Occurrence	*Late-formed*	*Early-formed*	*Early-formed*	*Early-formed*	*Early-formed*	*Early-formed*	*Early-formed*					
Sample ref.	***EDS1-F***	***EDS1-H***	***EDS1-H***	***EDS1-H***	***EDS1-S***	***EDS1-S***	***EDS1-S***	***FFM#2***	***FFM#2***	***FFM#2***	***FFM#2***	***FFM#2***
# analysis	*#109*	*#110*	*#111*	*#112*	*#113*	*#114*	*#115*	*#116*	*#117*	*#118*	*#119*	*#120*
SiO2	24.62	25.94	26.55	25.31	24.34	24.76	24.98	25.70	25.04	25.56	24.37	24.80
Al2O3	22.37	23.45	23.23	22.03	22.81	22.49	22.35	22.87	22.00	20.80	21.73	21.59
FeO	28.86	28.31	26.47	28.54	27.87	28.03	27.81	29.28	29.48	29.61	30.61	30.21
Fe2O3	0.00	0.00	0.00	0.00	0.00	0.00	0.00	0.00	0.00	0.00	0.00	0.00
MnO	2.63	0.76	0.74	0.81	2.63	2.75	2.78	0.35	0.29	0.32	0.45	0.42
MgO	10.15	10.54	10.64	11.63	10.98	11.25	11.27	10.40	10.42	11.30	10.38	10.55
CaO	0.02	0.03	0.06	0.22	0.03	0.01	0.04	0.02	0.02	0.02	0.01	0.04
Na2O	0.00	0.00	0.08	0.01	0.01	0.00	0.02	0.03	0.00	0.02	0.02	0.00
K2O	0.00	0.11	0.07	0.00	0.00	0.00	0.01	0.39	0.09	0.02	0.01	0.03
F	0.00	0.00	0.00	0.00	0.00	0.03	0.02	0.00	0.00	0.03	0.01	0.01
Cl	0.00	0.01	0.02	0.00	0.00	0.00	0.00	0.00	0.00	0.00	0.00	0.00
TiO2	0.06	0.00	0.04	0.00	0.02	0.03	0.03	0.02	0.04	0.01	0.03	0.00
Cr2O3	0.09	0.06	0.05	0.11	0.06	0.09	0.08	0.08	0.08	0.06	0.11	0.09
ZnO	0.08	0.00	0.00	0.00	0.05	0.09	0.00	0.14	0.01	0.00	0.03	0.06
V2O3	0.00	0.00	0.00	0.00	0.00	0.00	0.00	0.00	0.00	0.00	0.00	0.00
NiO	0.00	0.00	0.00	0.00	0.00	0.00	0.00	0.06	0.09	0.00	0.00	0.00
Cs2O	0.00	0.01	0.00	0.00	0.00	0.00	0.00	0.03	0.00	0.02	0.00	0.01
BaO	0.02	0.09	0.00	0.01	0.00	0.04	0.02	0.00	0.00	0.05	0.03	0.04
H2O	11.18	11.44	11.40	11.29	11.23	11.30	11.31	11.37	11.11	11.12	11.03	11.07
Total#	100.08	100.74	99.34	99.95	100.02	100.86	100.71	100.75	98.68	98.94	98.82	98.93
O=F	0.00	0.00	0.00	0.00	0.00	0.00	0.00	0.00	0.00	-0.01	0.00	-0.01
O=Cl	0.00	0.00	0.00	0.00	0.00	0.00	0.00	0.00	0.00	0.00	0.00	0.00
Total	100.08	100.74	99.34	99.95	100.02	100.86	100.71	100.75	98.68	98.93	98.82	98.92

Chlorite

# analysis		#109	#110	#111	#112	#113	#114	#115	#116	#117	#118	#119	#120
Ion Distribution													
Si		2.64	2.72	2.79	2.69	2.60	2.63	2.65	2.71	2.70	2.75	2.65	2.68
Al		1.36	1.28	1.21	1.31	1.40	1.38	1.35	1.29	1.30	1.25	1.35	1.32
	Total	4.00	4.00	4.00	4.00	4.00	4.00	4.00	4.00	4.00	4.00	4.00	4.00
Al		1.47	1.62	1.67	1.45	1.47	1.44	1.44	1.56	1.50	1.39	1.43	1.44
Mn		0.24	0.07	0.07	0.07	0.24	0.25	0.25	0.03	0.03	0.03	0.04	0.04
Zn		0.01	0.00	0.00	0.00	0.00	0.01	0.00	0.01	0.00	0.00	0.00	0.01
Fe2+		2.59	2.48	2.33	2.53	2.49	2.49	2.47	2.58	2.66	2.67	2.78	2.73
Ti		0.01	0.00	0.00	0.00	0.00	0.00	0.00	0.00	0.00	0.00	0.00	0.00
Ca		0.00	0.00	0.01	0.03	0.00	0.00	0.00	0.00	0.00	0.00	0.00	0.01
V		0.00	0.00	0.00	0.00	0.00	0.00	0.00	0.00	0.00	0.00	0.00	0.00
Ba		0.00	0.00	0.00	0.00	0.00	0.00	0.00	0.00	0.00	0.00	0.00	0.00
Fe3+		0.00	0.00	0.00	0.00	0.00	0.00	0.00	0.00	0.00	0.00	0.00	0.00
Mg		1.62	1.65	1.67	1.84	1.75	1.78	1.78	1.64	1.68	1.82	1.68	1.70
Na		0.00	0.00	0.02	0.00	0.00	0.00	0.00	0.01	0.00	0.00	0.00	0.00
Cr		0.01	0.01	0.00	0.01	0.01	0.01	0.01	0.01	0.01	0.00	0.01	0.01
K		0.00	0.02	0.01	0.00	0.00	0.00	0.00	0.05	0.01	0.00	0.00	0.00
Cs		0.00	0.00	0.00	0.00	0.00	0.00	0.00	0.00	0.00	0.00	0.00	0.00
Ni		0.00	0.00	0.00	0.00	0.00	0.00	0.00	0.01	0.01	0.00	0.00	0.00
	Total	5.94	5.84	5.78	5.93	5.96	5.96	5.95	5.89	5.90	5.93	5.96	5.94
OH		8.00	8.00	8.00	8.00	8.00	7.99	7.99	8.00	8.00	7.99	8.00	8.00
F		0.00	0.00	0.00	0.00	0.00	0.01	0.01	0.00	0.00	0.01	0.00	0.00
Cl		0.00	0.00	0.00	0.00	0.00	0.00	0.00	0.00	0.00	0.00	0.00	0.00
	Total	8.00	8.00	8.00	8.00	8.00	8.00	8.00	8.00	8.00	8.00	8.00	8.00

Chlorite

Sector	*Aljustrel*	*Aljustrel*	*Aljustrel*	*Aljustrel*	*Aljustrel*	*Aljustrel*	*Aljustrel*	*Aljustrel*	*Aljustrel*	*Aljustrel*	*Aljustrel*	*Aljustrel*
Sub-sector	Feitais mine	Gavião	Gavião	Gavião	Gavião	Gavião	Gavião	Gavião	Gavião	Gavião	Gavião	Gavião
Stratigraphic division	*upperVSC*	*upperVSC*	*upperVSC*	*upperVSC*	*upperVSC*	*upperVSC*	*upperVSC*	*upperVSC*	*upperVSC*	*upperVSC*	*upperVSC*	*upperVSC*
Mineralization type	*No Sulph*	*Py-bearing*	*Py-bearing*	*Py-bearing*	*Py-bearing*	*Py-bearing*	*Py-bearing*	*Py-bearing*	*Py-bearing*	*Py-bearing*	*Py-bearing*	*Mineralized*
Occurrence												
Sample ref.	*FFM#2*	*GV7#4*	*GV7#4*	*GV7#4*	*GV9#10*	*GV9#10*	*GV9#10*	*GV9#10*	*GV9#10*	*GV9#10*	*GV9#10*	*GV9#2*
# analysis	*#121*	*#122*	*#123*	*#124*	*#125*	*#126*	*#127*	*#128*	*#129*	*#130*	*#131*	*#132*
SiO2	24.39	27.52	27.21	27.45	25.36	25.74	25.90	25.94	26.18	26.10	26.17	24.96
Al2O3	22.85	21.42	21.50	21.69	21.71	21.41	21.31	21.76	20.80	21.32	21.20	21.15
FeO	32.84	14.92	15.35	15.21	28.67	28.65	28.58	28.02	28.70	28.37	28.49	31.22
Fe2O3	0.00	0.00	0.00	0.00	0.00	0.00	0.00	0.00	0.00	0.00	0.00	0.00
MnO	0.18	4.00	3.89	4.05	0.44	0.44	0.45	0.43	0.45	0.46	0.46	3.20
MgO	7.86	20.04	19.63	19.90	11.32	11.02	10.77	11.45	11.93	11.95	12.12	8.92
CaO	0.02	0.05	0.00	0.03	0.03	0.02	0.04	0.04	0.01	0.03	0.04	0.00
Na2O	0.00	0.02	0.02	0.05	0.00	0.00	0.13	0.03	0.01	0.02	0.05	0.00
K2O	0.05	0.00	0.03	0.01	0.02	0.01	0.05	0.21	0.00	0.03	0.02	0.02
F	0.00	0.33	0.26	0.46	0.00	0.06	0.00	0.00	0.02	0.00	0.08	0.00
Cl	0.00	0.00	0.00	0.00	0.00	0.00	0.00	0.00	0.00	0.00	0.00	0.00
TiO2	0.04	0.00	0.03	0.00	0.04	0.04	0.04	0.07	0.03	0.03	0.02	0.02
Cr2O3	0.12	0.09	0.06	0.07	0.11	0.06	0.09	0.04	0.07	0.06	0.10	0.10
ZnO	0.04	0.18	0.11	0.13	0.01	0.07	0.15	0.03	0.07	0.15	0.00	0.15
V2O3	0.00	0.00	0.00	0.00	0.00	0.00	0.00	0.00	0.00	0.00	0.00	0.00
NiO	0.06	0.02	0.06	0.00	0.00	0.00	0.00	0.00	0.00	0.00	0.08	0.07
Cs2O	0.02	0.02	0.00	0.00	0.03	0.01	0.00	0.00	0.00	0.00	0.04	0.00
BaO	0.05	0.00	0.00	0.00	0.03	0.01	0.00	0.07	0.06	0.04	0.00	0.00
H2O	11.04	11.75	11.71	11.72	11.18	11.13	11.16	11.28	11.26	11.32	11.31	11.12
Total#	99.56	100.35	99.87	100.76	98.93	98.66	98.65	99.36	99.58	99.88	100.16	100.93
O=F	0.00	-0.14	-0.11	-0.19	0.00	-0.02	0.00	0.00	-0.01	0.00	-0.03	0.00
O=Cl	0.00	0.00	0.00	0.00	0.00	0.00	0.00	0.00	0.00	0.00	0.00	0.00
Total	99.56	100.21	99.76	100.56	98.93	98.63	98.65	99.36	99.57	99.88	100.13	100.93

Chlorite

# analysis		#121	#122	#123	#124	#125	#126	#127	#128	#129	#130	#131	#132
Ion Distribution													
Si		2.65	2.77	2.76	2.76	2.72	2.77	2.78	2.76	2.79	2.77	2.77	2.69
Al		1.35	1.23	1.24	1.24	1.28	1.23	1.22	1.24	1.21	1.23	1.23	1.31
	Total	4.00	4.00	4.00	4.00	4.00	4.00	4.00	4.00	4.00	4.00	4.00	4.00
Al		1.58	1.32	1.33	1.33	1.46	1.48	1.48	1.49	1.40	1.43	1.41	1.38
Mn		0.02	0.34	0.33	0.34	0.04	0.04	0.04	0.04	0.04	0.04	0.04	0.29
Zn		0.00	0.01	0.01	0.01	0.00	0.01	0.01	0.00	0.01	0.01	0.00	0.01
Fe2+		2.98	1.26	1.30	1.28	2.57	2.57	2.57	2.49	2.55	2.51	2.52	2.82
Ti		0.00	0.00	0.00	0.00	0.00	0.00	0.00	0.01	0.00	0.00	0.00	0.00
Ca		0.00	0.01	0.00	0.00	0.00	0.00	0.01	0.00	0.00	0.00	0.00	0.00
V		0.00	0.00	0.00	0.00	0.00	0.00	0.00	0.00	0.00	0.00	0.00	0.00
Ba		0.00	0.00	0.00	0.00	0.00	0.00	0.00	0.00	0.00	0.00	0.00	0.00
Fe3+		0.00	0.00	0.00	0.00	0.00	0.00	0.00	0.00	0.00	0.00	0.00	0.00
Mg		1.27	3.01	2.97	2.98	1.81	1.77	1.72	1.82	1.89	1.89	1.91	1.43
Na		0.00	0.00	0.00	0.01	0.00	0.00	0.03	0.01	0.00	0.00	0.01	0.00
Cr		0.01	0.01	0.00	0.01	0.01	0.01	0.01	0.00	0.01	0.01	0.01	0.01
K		0.01	0.00	0.00	0.00	0.00	0.00	0.01	0.03	0.00	0.00	0.00	0.00
Cs		0.00	0.00	0.00	0.00	0.00	0.00	0.00	0.00	0.00	0.00	0.00	0.00
Ni		0.00	0.00	0.00	0.00	0.00	0.00	0.00	0.00	0.00	0.00	0.01	0.01
	Total	5.88	5.95	5.96	5.96	5.90	5.87	5.88	5.89	5.90	5.90	5.91	5.96
OH		8.00	7.89	7.92	7.85	8.00	7.98	8.00	8.00	8.00	8.00	7.97	8.00
F		0.00	0.11	0.08	0.15	0.00	0.02	0.00	0.00	0.01	0.00	0.03	0.00
Cl		0.00	0.00	0.00	0.00	0.00	0.00	0.00	0.00	0.00	0.00	0.00	0.00
	Total	8.00	8.00	8.00	8.00	8.00	8.00	8.00	8.00	8.00	8.00	8.00	8.00

Chlorite

Sector	*Aljustrel*	*Aljustrel*	*Aljustrel*	*Aljustrel*	*Aljustrel*	*Aljustrel*	*Aljustrel*	*Aljustrel*	*Aljustrel*	*Aljustrel*	*Aljustrel*	*Aljustrel*
Sub-sector	Gavião	Gavião	Gavião	Gavião	Gavião	Gavião	Gavião	Mte Mesas	Mte Mesas	Mte Mesas	Mte Mesas	Mte Mesas
Stratigraphic division	*upperVSC*	*upperVSC*	*upperVSC*	*upperVSC*	*upperVSC*	*upperVSC*	*upperVSC*	*upperVSC*	*upperVSC*	*upperVSC*	*upperVSC*	*upperVSC*
Mineralization type	*Mineralized*	*Mineralized*	*Mineralized*	*Mineralized*	*Mineralized*	*Mineralized*	*Mineralized*	*Mineralized*	*Mineralized*	*Mineralized*	*Mineralized*	*Mineralized*
Occurrence							*mtx*	*mtx*	*mtx*	*mtx*	*mtx*	*mtx*
Sample ref.	***GV9#2***	***GV9#2***	***GV9#2***	***GV9#2***	***GV9#2***	***GV9#2***	***MDM02#4***	***MDM02#4***	***MDM02#4***	***MDM02#4***	***MDM02#4***	***MDM02#4***
# analysis	***#133***	***#134***	***#135***	***#136***	***#137***	***#138***	***#139***	***#140***	***#141***	***#142***	***#143***	***#144***
SiO2	24.95	24.53	24.65	24.13	25.07	25.18	28.60	24.45	25.31	25.37	25.32	25.48
Al2O3	20.79	21.39	21.22	20.77	19.80	20.12	20.31	21.79	21.19	21.19	21.42	20.97
FeO	30.57	31.10	31.13	31.09	30.59	30.45	25.92	32.84	32.71	32.76	31.44	31.84
Fe2O3	0.00	0.00	0.00	0.00	0.00	0.00	3.70	0.00	0.00	0.00	0.00	0.00
MnO	3.07	3.13	3.17	3.13	3.13	3.08	2.95	1.02	1.04	1.03	0.96	0.97
MgO	9.16	8.81	8.87	8.50	9.61	9.80	8.13	8.92	9.37	9.30	8.36	8.69
CaO	0.32	0.13	0.03	0.03	0.03	0.05	0.05	0.04	0.09	0.08	0.04	0.05
Na2O	0.00	0.02	0.00	0.00	0.02	0.00	0.00	0.00	0.01	0.00	0.00	0.02
K2O	0.01	0.02	0.02	0.04	0.01	0.01	0.02	0.03	0.02	0.02	0.00	0.02
F	0.00	0.00	0.07	0.00	0.03	0.11	0.00	0.19	0.06	0.00	0.07	0.00
Cl	0.00	0.00	0.00	0.00	0.00	0.00	0.00	0.00	0.00	0.00	0.00	0.00
TiO2	0.09	0.02	0.04	0.01	0.03	0.26	0.16	0.03	0.01	0.00	0.05	0.05
Cr2O3	0.03	0.05	0.12	0.08	0.06	0.07	0.06	0.14	0.12	0.11	0.12	0.10
ZnO	0.08	0.06	0.15	0.13	0.19	0.08	0.12	0.05	0.22	0.03	0.03	0.00
V2O3	0.00	0.00	0.00	0.00	0.00	0.00	0.00	0.00	0.00	0.00	0.00	0.00
NiO	0.05	0.06	0.11	0.07	0.08	0.00	0.00	0.00	0.02	0.04	0.00	0.05
Cs2O	0.00	0.00	0.00	0.00	0.00	0.00	0.00	0.00	0.00	0.00	0.00	0.01
BaO	0.04	0.03	0.04	0.09	0.02	0.05	0.00	0.02	0.04	0.00	0.00	0.04
H2O	11.06	11.05	11.03	10.85	10.96	11.02	11.48	10.99	11.17	11.19	10.96	11.03
Total#	100.25	100.37	100.65	98.90	99.61	100.26	101.48	100.51	101.37	101.11	98.77	99.32
O=F	0.00	0.00	-0.03	0.00	-0.01	-0.05	0.00	-0.08	-0.02	0.00	-0.03	0.00
O=Cl	0.00	0.00	0.00	0.00	0.00	0.00	0.00	0.00	0.00	0.00	0.00	0.00
Total	100.24	100.37	100.62	98.90	99.60	100.22	101.48	100.43	101.35	101.11	98.74	99.32

Chlorite

# analysis		#133	#134	#135	#136	#137	#138	#139	#140	#141	#142	#143	#144
Ion Distribution													
Si		2.71	2.66	2.67	2.67	2.74	2.73	2.99	2.65	2.71	2.72	2.76	2.77
Al		1.29	1.34	1.33	1.33	1.26	1.27	1.01	1.35	1.29	1.28	1.24	1.23
	Total	4.00	4.00	4.00	4.00	4.00	4.00	4.00	4.00	4.00	4.00	4.00	4.00
Al		1.36	1.40	1.38	1.37	1.29	1.30	1.49	1.43	1.38	1.40	1.52	1.46
Mn		0.28	0.29	0.29	0.29	0.29	0.28	0.26	0.09	0.09	0.09	0.09	0.09
Zn		0.01	0.00	0.01	0.01	0.01	0.01	0.01	0.00	0.02	0.00	0.00	0.00
Fe2+		2.77	2.82	2.82	2.87	2.80	2.76	2.26	2.97	2.93	2.94	2.87	2.90
Ti		0.01	0.00	0.00	0.00	0.00	0.02	0.01	0.00	0.00	0.00	0.00	0.00
Ca		0.04	0.02	0.00	0.00	0.00	0.01	0.01	0.00	0.01	0.01	0.00	0.01
V		0.00	0.00	0.00	0.00	0.00	0.00	0.00	0.00	0.00	0.00	0.00	0.00
Ba		0.00	0.00	0.00	0.00	0.00	0.00	0.00	0.00	0.00	0.00	0.00	0.00
Fe3+		0.00	0.00	0.00	0.00	0.00	0.00	0.29	0.00	0.00	0.00	0.00	0.00
Mg		1.48	1.42	1.43	1.40	1.57	1.58	1.27	1.44	1.50	1.49	1.36	1.41
Na		0.00	0.00	0.00	0.00	0.00	0.00	0.00	0.00	0.00	0.00	0.00	0.00
Cr		0.00	0.00	0.01	0.01	0.01	0.01	0.00	0.01	0.01	0.01	0.01	0.01
K		0.00	0.00	0.00	0.01	0.00	0.00	0.00	0.00	0.00	0.00	0.00	0.00
Cs		0.00	0.00	0.00	0.00	0.00	0.00	0.00	0.00	0.00	0.00	0.00	0.00
Ni		0.00	0.01	0.01	0.01	0.01	0.00	0.00	0.00	0.00	0.00	0.00	0.00
	Total	5.96	5.97	5.97	5.98	5.98	5.96	5.60	5.96	5.95	5.94	5.85	5.88
OH		8.00	8.00	7.97	8.00	7.99	7.96	8.00	7.94	7.98	8.00	7.98	8.00
F		0.00	0.00	0.03	0.00	0.01	0.04	0.00	0.06	0.02	0.00	0.02	0.00
Cl		0.00	0.00	0.00	0.00	0.00	0.00	0.00	0.00	0.00	0.00	0.00	0.00
	Total	8.00	8.00	8.00	8.00	8.00	8.00	8.00	8.00	8.00	8.00	8.00	8.00

Chlorite

Sector	*Aljustrel*	*Aljustrel*	*Aljustrel*	*Aljustrel*	*Aljustrel*	*Aljustrel*	*Aljustrel*	*Aljustrel*	*Aljustrel*	*Aljustrel*	*Aljustrel*	*Aljustrel*
Sub-sector	Mte Mesas	Mte Mesas	Mte Mesas	Mte Mesas	Mte Mesas	Mte Mesas	Mte Mesas	Mte Mesas	Mte Mesas	Mte Mesas	Mte Mesas	Mte Mesas
Stratigraphic division	*upperVSC*	*upperVSC*	*upperVSC*	*upperVSC*	*upperVSC*	*upperVSC*	*upperVSC*	*upperVSC*	*upperVSC*	*upperVSC*	*upperVSC*	*upperVSC*
Mineralization type	*Mineralized*	*Mineralized*	*Mineralized*	*Mineralized*	*Mineralized*	*Mineralized*	*Mineralized*	*Mineralized*	*Mineralized*	*Mineralized*	*Mineralized*	*Mineralized*
Occurrence	*mtx*	*mtx*	*mtx*	*mtx*	*miner - rel*	*miner - rel*	*miner - rel*	*miner - rel*	*miner - rel*	*miner - rel*	*miner - rel*	*miner - rel*
Sample ref.	*MDM02#4*	*MDM02#4*	*MDM02#4*	*MDM02#4*	*MDM02#4*	*MDM02#4*	*MDM02#4*	*MDM02#4*	*MDM02#4*	*MDM02#4*	*MDM02#4*	*MDM02#4*
# analysis	*#145*	*#146*	*#147*	*#148*	*#149*	*#150*	*#151*	*#152*	*#153*	*#154*	*#155*	*#156*
SiO2	25.38	25.05	24.93	26.52	24.73	24.55	24.86	24.21	24.71	24.54	23.66	24.02
Al2O3	21.58	21.55	21.05	20.77	21.40	21.92	21.64	20.93	21.34	21.30	21.59	21.34
FeO	31.15	31.88	32.43	32.68	32.58	31.73	32.73	31.82	32.80	32.91	32.71	32.57
Fe2O3	0.00	0.00	0.00	0.00	0.00	0.00	0.00	0.00	0.00	0.00	0.00	0.00
MnO	0.95	1.04	1.00	1.00	1.01	1.01	1.04	1.03	1.06	1.10	1.01	0.99
MgO	8.37	9.20	8.76	8.57	9.10	8.91	8.84	8.50	9.10	8.95	8.92	8.89
CaO	0.03	0.01	0.04	0.06	0.04	0.06	0.04	0.05	0.01	0.03	0.36	0.34
Na2O	0.02	0.03	0.00	0.02	0.00	0.05	0.00	0.01	0.02	0.02	0.00	0.01
K2O	0.36	0.22	0.00	0.01	0.00	0.10	0.00	0.00	0.00	0.00	0.02	0.00
F	0.00	0.05	0.06	0.00	0.13	0.04	0.00	0.05	0.00	0.06	0.05	0.04
Cl	0.00	0.00	0.00	0.00	0.00	0.00	0.00	0.00	0.00	0.00	0.00	0.00
TiO2	0.08	0.05	0.06	0.04	0.20	0.03	0.04	1.67	0.09	0.10	0.09	0.07
Cr2O3	0.11	0.10	0.11	0.09	0.08	0.08	0.09	0.06	0.07	0.08	0.13	0.06
ZnO	0.17	0.15	0.07	0.09	0.05	0.16	0.05	0.12	0.06	0.00	0.00	0.12
V2O3	0.00	0.00	0.00	0.00	0.00	0.00	0.00	0.00	0.00	0.00	0.00	0.00
NiO	0.00	0.01	0.00	0.05	0.00	0.11	0.00	0.00	0.00	0.01	0.02	0.02
Cs2O	0.00	0.00	0.00	0.01	0.00	0.03	0.00	0.00	0.00	0.00	0.00	0.00
BaO	0.00	0.03	0.01	0.03	0.00	0.00	0.07	0.00	0.05	0.01	0.07	0.06
H2O	11.04	11.11	10.97	11.23	11.02	11.04	11.11	10.97	11.08	11.01	10.92	10.93
Total#	99.24	100.47	99.48	101.17	100.34	99.78	100.50	99.43	100.37	100.13	99.55	99.46
O=F	0.00	-0.02	-0.02	0.00	-0.06	-0.02	0.00	-0.02	0.00	-0.02	-0.02	-0.02
O=Cl	0.00	0.00	0.00	0.00	0.00	0.00	0.00	0.00	0.00	0.00	0.00	0.00
Total	99.24	100.45	99.46	101.17	100.28	99.77	100.50	99.41	100.37	100.10	99.52	99.45

Chlorite

# analysis	#145	#146	#147	#148	#149	#150	#151	#152	#153	#154	#155	#156
Ion Distribution												
Si	2.76	2.70	2.72	2.83	2.68	2.66	2.68	2.64	2.67	2.67	2.59	2.63
Al	1.24	1.30	1.28	1.17	1.32	1.34	1.32	1.36	1.33	1.33	1.41	1.37
Total	4.00	4.00	4.00	4.00	4.00	4.00	4.00	4.00	4.00	4.00	4.00	4.00
Al	1.52	1.44	1.42	1.45	1.40	1.47	1.44	1.33	1.40	1.39	1.38	1.39
Mn	0.09	0.10	0.09	0.09	0.09	0.09	0.10	0.10	0.10	0.10	0.09	0.09
Zn	0.01	0.01	0.01	0.01	0.00	0.01	0.00	0.01	0.00	0.00	0.00	0.01
Fe2+	2.83	2.87	2.96	2.92	2.95	2.88	2.96	2.90	2.97	2.99	3.00	2.98
Ti	0.01	0.00	0.00	0.00	0.02	0.00	0.00	0.14	0.01	0.01	0.01	0.01
Ca	0.00	0.00	0.00	0.01	0.00	0.01	0.00	0.01	0.00	0.00	0.04	0.04
V	0.00	0.00	0.00	0.00	0.00	0.00	0.00	0.00	0.00	0.00	0.00	0.00
Ba	0.00	0.00	0.00	0.00	0.00	0.00	0.00	0.00	0.00	0.00	0.00	0.00
Fe3+	0.00	0.00	0.00	0.00	0.00	0.00	0.00	0.00	0.00	0.00	0.00	0.00
Mg	1.36	1.48	1.42	1.37	1.47	1.44	1.42	1.38	1.47	1.45	1.46	1.45
Na	0.00	0.01	0.00	0.00	0.00	0.01	0.00	0.00	0.00	0.00	0.00	0.00
Cr	0.01	0.01	0.01	0.01	0.01	0.01	0.01	0.01	0.01	0.01	0.01	0.01
K	0.05	0.03	0.00	0.00	0.00	0.01	0.00	0.00	0.00	0.00	0.00	0.00
Cs	0.00	0.00	0.00	0.00	0.00	0.00	0.00	0.00	0.00	0.00	0.00	0.00
Ni	0.00	0.00	0.00	0.00	0.00	0.01	0.00	0.00	0.00	0.00	0.00	0.00
Total	5.88	5.94	5.92	5.86	5.94	5.94	5.93	5.87	5.96	5.96	6.00	5.98
OH	8.00	7.98	7.98	8.00	7.95	7.99	8.00	7.98	8.00	7.98	7.98	7.99
F	0.00	0.02	0.02	0.00	0.05	0.01	0.00	0.02	0.00	0.02	0.02	0.01
Cl	0.00	0.00	0.00	0.00	0.00	0.00	0.00	0.00	0.00	0.00	0.00	0.00
Total	8.00	8.00	8.00	8.00	8.00	8.00	8.00	8.00	8.00	8.00	8.00	8.00

Chlorite

Sector	*Aljustrel*	*Aljustrel*	*Aljustrel*	*Aljustrel*	*Aljustrel*	*Aljustrel*	*Aljustrel*	*Aljustrel*	*Aljustrel*	*Aljustrel*	*Aljustrel*	*Aljustrel*
Sub-sector	Mte Mesas	Mte Mesas	Mte Mesas	Mte Mesas	Mte Mesas	Mte Mesas	Mte Mesas	Mte Mesas	Moinho mine	Moinho mine	Moinho mine	Moinho mine
Stratigraphic division	*upperVSC*	*upperVSC*	*upperVSC*	*upperVSC*	*upperVSC*	*upperVSC*	*upperVSC*	*upperVSC*	*upperVSC*	*upperVSC*	*upperVSC*	*upperVSC*
Mineralization type	*Mineralized*	*Mineralized*	*Mineralized*	*Mineralized*	*Mineralized*	*Mineralized*	*Mineralized*	*Mineralized*	*Mineralized*	*Mineralized*	*Mineralized*	*Mineralized*
Occurrence	*miner - rel*	*miner - rel*	*miner - rel*	*miner - rel*	*miner - rel*	*mtx*	*mtx*	*mtx*				
Sample ref.	***MDM2#6***	***MDM2#6***	***MDM2#6***	***MDM2#6***	***MDM2#6***	***MDM2#6***	***MDM2#6***	***MDM2#6***	***MM16#9***	***MM16#9***	***MM16#9***	***MM16#9***
# analysis	***#157***	***#158***	***#159***	***#160***	***#161***	***#162***	***#163***	***#164***	***#165***	***#166***	***#167***	***#168***
SiO2	25.86	25.37	25.89	25.73	26.37	26.27	26.17	25.87	25.01	24.74	27.22	24.58
Al2O3	21.80	20.99	20.22	20.32	19.23	20.33	20.44	20.52	21.25	20.82	21.24	21.67
FeO	29.44	29.33	29.33	29.44	28.67	29.31	28.90	29.57	28.13	27.92	27.62	26.65
Fe2O3	0.00	0.00	0.00	0.00	0.00	0.00	0.00	0.00	0.00	0.00	0.00	0.00
MnO	0.70	0.48	0.46	0.48	0.40	0.46	0.50	0.49	2.57	2.66	2.52	2.64
MgO	9.53	11.55	12.19	11.89	12.30	12.10	11.91	11.63	10.94	10.81	10.73	11.46
CaO	0.02	0.04	0.05	0.03	0.03	0.06	0.07	0.00	0.03	0.03	0.02	0.04
Na2O	0.00	0.01	0.01	0.00	0.00	0.00	0.02	0.00	0.01	0.00	0.01	0.00
K2O	0.35	0.02	0.04	0.02	0.07	0.04	0.12	0.18	0.07	0.05	0.12	0.03
F	0.03	0.00	0.14	0.07	0.05	0.00	0.00	0.00	0.10	0.00	0.10	0.01
Cl	0.00	0.00	0.00	0.00	0.00	0.00	0.00	0.00	0.00	0.00	0.00	0.00
TiO2	0.04	0.01	0.03	0.01	0.04	0.07	0.20	0.07	0.08	0.03	0.03	0.03
Cr2O3	0.10	0.06	0.11	0.08	0.19	0.07	0.07	0.10	0.05	0.06	0.03	0.07
ZnO	0.00	0.08	0.02	0.10	0.10	0.11	0.19	0.15	0.13	0.04	0.12	0.17
V2O3	0.00	0.00	0.00	0.00	0.00	0.00	0.00	0.00	0.00	0.00	0.00	0.00
NiO	0.01	0.02	0.07	0.00	0.00	0.03	0.01	0.03	0.11	0.07	0.11	0.01
Cs2O	0.00	0.00	0.00	0.00	0.00	0.00	0.00	0.00	0.00	0.00	0.00	0.00
BaO	0.00	0.03	0.06	0.00	0.00	0.01	0.06	0.02	0.00	0.00	0.04	0.06
H2O	11.13	11.16	11.15	11.13	11.10	11.29	11.27	11.22	11.09	10.99	11.40	11.08
Total#	99.00	99.16	99.77	99.30	98.54	100.15	99.94	99.85	99.55	98.19	101.29	98.51
O=F	-0.01	0.00	-0.06	-0.03	-0.02	0.00	0.00	0.00	-0.04	0.00	-0.04	0.00
O=Cl	0.00	0.00	0.00	0.00	0.00	0.00	0.00	0.00	0.00	0.00	0.00	0.00
Total	98.99	99.16	99.71	99.27	98.52	100.15	99.94	99.85	99.51	98.19	101.25	98.50

Chlorite

# analysis		#157	#158	#159	#160	#161	#162	#163	#164	#165	#166	#167	#168
Ion Distribution													
Si		2.78	2.73	2.77	2.76	2.84	2.79	2.79	2.76	2.69	2.70	2.85	2.66
Al		1.22	1.27	1.23	1.24	1.16	1.21	1.21	1.24	1.31	1.30	1.15	1.34
	Total	4.00	4.00	4.00	4.00	4.00	4.00	4.00	4.00	4.00	4.00	4.00	4.00
Al		1.55	1.39	1.32	1.34	1.29	1.34	1.35	1.35	1.39	1.38	1.48	1.42
Mn		0.06	0.04	0.04	0.04	0.04	0.04	0.05	0.04	0.23	0.25	0.22	0.24
Zn		0.00	0.01	0.00	0.01	0.01	0.01	0.02	0.01	0.01	0.00	0.01	0.01
Fe2+		2.65	2.64	2.62	2.64	2.59	2.60	2.57	2.64	2.53	2.55	2.42	2.41
Ti		0.00	0.00	0.00	0.00	0.00	0.01	0.02	0.01	0.01	0.00	0.00	0.00
Ca		0.00	0.00	0.01	0.00	0.00	0.01	0.01	0.00	0.00	0.00	0.00	0.01
V		0.00	0.00	0.00	0.00	0.00	0.00	0.00	0.00	0.00	0.00	0.00	0.00
Ba		0.00	0.00	0.00	0.00	0.00	0.00	0.00	0.00	0.00	0.00	0.00	0.00
Fe3+		0.00	0.00	0.00	0.00	0.00	0.00	0.00	0.00	0.00	0.00	0.00	0.00
Mg		1.53	1.85	1.94	1.90	1.98	1.92	1.89	1.85	1.76	1.76	1.68	1.85
Na		0.00	0.00	0.00	0.00	0.00	0.00	0.00	0.00	0.00	0.00	0.00	0.00
Cr		0.01	0.01	0.01	0.01	0.02	0.01	0.01	0.01	0.00	0.00	0.00	0.01
K		0.05	0.00	0.01	0.00	0.01	0.01	0.02	0.02	0.01	0.01	0.02	0.00
Cs		0.00	0.00	0.00	0.00	0.00	0.00	0.00	0.00	0.00	0.00	0.00	0.00
Ni		0.00	0.00	0.01	0.00	0.00	0.00	0.00	0.00	0.01	0.01	0.01	0.00
	Total	5.85	5.94	5.96	5.95	5.93	5.93	5.92	5.94	5.96	5.96	5.84	5.96
OH		7.99	8.00	7.95	7.98	7.98	8.00	8.00	8.00	7.97	8.00	7.97	8.00
F		0.01	0.00	0.05	0.02	0.02	0.00	0.00	0.00	0.03	0.00	0.03	0.00
Cl		0.00	0.00	0.00	0.00	0.00	0.00	0.00	0.00	0.00	0.00	0.00	0.00
	Total	8.00	8.00	8.00	8.00	8.00	8.00	8.00	8.00	8.00	8.00	8.00	8.00

Chlorite

Sector	***Aljustrel***	***Neves Corvo***	***Neves Corvo***	***Neves Corvo***	***Neves Corvo***	***Neves Corvo***	***Neves Corvo***	***Neves Corvo***	***Neves Corvo***	***Neves Corvo***	***Neves Corvo***
Sub-sector	Moinho mine	Corvo	Corvo	Lombador	Lombador	Lombador	Lombador	Lombador	Lombador	Lombador	Lombador
Stratigraphic division	*upperVSC*	*lower VSC*	*lower VSC*	*PQG*	*PQG*	*PQG*	*PQG*	*PQG*	*PQG*	*PQG*	*PQG*
Mineralization type	*Mineralized*	*Py-bearing*	*Py-bearing*	*Mineralized*	*Mineralized*	*Mineralized*	*Mineralized*	*Mineralized*	*Mineralized*	*Mineralized*	*Mineralized*
Occurrence											
Sample ref.	***MM16#9***	***NCC#24***	***NCC#24***	***NCL#10***	***NCL#10***	***NCL#10***	***NCL#10***	***NCL#10***	***NCL#10***	***NCL#10***	***NCL#10***
# analysis	***#169***	***#170***	***#171***	***#172***	***#173***	***#174***	***#175***	***#176***	***#177***	***#178***	***#179***
SiO2	25.15	30.27	27.29	23.78	23.97	24.16	24.20	24.23	24.10	24.22	24.40
Al2O3	21.46	22.13	22.80	21.47	21.35	21.91	21.81	21.67	21.87	21.42	21.65
FeO	26.97	18.77	19.14	37.37	38.37	38.07	37.80	38.30	36.97	37.67	36.61
Fe2O3	0.00	0.00	0.00	0.00	0.00	0.00	0.00	0.00	0.00	0.00	0.00
MnO	2.64	0.08	0.10	0.14	0.18	0.26	0.23	0.23	0.23	0.30	0.21
MgO	11.27	18.07	18.35	5.34	5.47	5.34	5.18	5.26	5.52	5.56	5.85
CaO	0.03	0.02	0.02	0.02	0.01	0.02	0.01	0.02	0.00	0.01	0.01
Na2O	0.04	0.03	0.01	0.00	0.03	0.02	0.00	0.00	0.00	0.00	0.00
K2O	0.10	0.05	0.03	0.00	0.00	0.00	0.00	0.00	0.01	0.00	0.00
F	0.00	0.25	0.38	0.07	0.03	0.00	0.00	0.00	0.00	0.00	0.00
Cl	0.00	0.00	0.00	0.00	0.00	0.00	0.00	0.00	0.00	0.00	0.00
TiO2	0.04	0.00	0.00	0.01	0.01	0.00	0.03	0.00	0.02	0.04	0.02
Cr2O3	0.04	0.14	0.10	0.06	0.06	0.09	0.06	0.09	0.02	0.08	0.06
ZnO	0.18	0.15	0.15	0.14	0.13	0.01	0.13	0.06	0.19	0.07	0.07
V2O3	0.00	0.00	0.00	0.00	0.00	0.00	0.00	0.00	0.00	0.00	0.00
NiO	0.07	0.02	0.00	0.05	0.00	0.07	0.00	0.00	0.00	0.04	0.00
Cs2O	0.00	0.00	0.00	0.00	0.00	0.03	0.00	0.00	0.01	0.01	0.00
BaO	0.00	0.02	0.01	0.09	0.08	0.06	0.00	0.01	0.00	0.00	0.01
H2O	11.16	12.11	11.69	10.69	10.81	10.90	10.85	10.88	10.83	10.85	10.86
Total#	99.14	102.10	100.07	99.21	100.47	100.92	100.27	100.74	99.75	100.26	99.74
O=F	0.00	-0.11	-0.16	-0.03	-0.01	0.00	0.00	0.00	0.00	0.00	0.00
O=Cl	0.00	0.00	0.00	0.00	0.00	0.00	0.00	0.00	0.00	0.00	0.00
Total	99.14	102.00	99.91	99.18	100.46	100.92	100.27	100.74	99.75	100.26	99.74

Chlorite

# analysis		#169	#170	#171	#172	#173	#174	#175	#176	#177	#178	#179
Ion Distribution												
Si		2.70	2.97	2.76	2.66	2.66	2.66	2.67	2.67	2.67	2.68	2.70
Al		1.30	1.03	1.24	1.34	1.34	1.34	1.33	1.33	1.33	1.32	1.30
	Total	4.00	4.00	4.00	4.00	4.00	4.00	4.00	4.00	4.00	4.00	4.00
Al		1.42	1.53	1.47	1.49	1.45	1.50	1.51	1.49	1.52	1.47	1.51
Mn		0.24	0.01	0.01	0.01	0.02	0.02	0.02	0.02	0.02	0.03	0.02
Zn		0.01	0.01	0.01	0.01	0.01	0.00	0.01	0.00	0.02	0.01	0.01
Fe2+		2.42	1.54	1.62	3.50	3.56	3.50	3.49	3.53	3.42	3.48	3.38
Ti		0.00	0.00	0.00	0.00	0.00	0.00	0.00	0.00	0.00	0.00	0.00
Ca		0.00	0.00	0.00	0.00	0.00	0.00	0.00	0.00	0.00	0.00	0.00
V		0.00	0.00	0.00	0.00	0.00	0.00	0.00	0.00	0.00	0.00	0.00
Ba		0.00	0.00	0.00	0.00	0.00	0.00	0.00	0.00	0.00	0.00	0.00
Fe3+		0.00	0.00	0.00	0.00	0.00	0.00	0.00	0.00	0.00	0.00	0.00
Mg		1.81	2.64	2.76	0.89	0.90	0.87	0.85	0.86	0.91	0.92	0.96
Na		0.01	0.01	0.00	0.00	0.01	0.00	0.00	0.00	0.00	0.00	0.00
Cr		0.00	0.01	0.01	0.01	0.00	0.01	0.00	0.01	0.00	0.01	0.00
K		0.01	0.01	0.00	0.00	0.00	0.00	0.00	0.00	0.00	0.00	0.00
Cs		0.00	0.00	0.00	0.00	0.00	0.00	0.00	0.00	0.00	0.00	0.00
Ni		0.01	0.00	0.00	0.00	0.00	0.01	0.00	0.00	0.00	0.00	0.00
	Total	5.94	5.75	5.89	5.92	5.95	5.92	5.90	5.92	5.90	5.92	5.89
OH		8.00	7.92	7.88	7.98	7.99	8.00	8.00	8.00	8.00	8.00	8.00
F		0.00	0.08	0.12	0.02	0.01	0.00	0.00	0.00	0.00	0.00	0.00
Cl		0.00	0.00	0.00	0.00	0.00	0.00	0.00	0.00	0.00	0.00	0.00
	Total	8.00	8.00	8.00	8.00	8.00	8.00	8.00	8.00	8.00	8.00	8.00

Chlorite

Sector	*Neves Corvo*	*Neves Corvo*	*Neves Corvo*	*Neves Corvo*	*Neves Corvo*	*Neves Corvo*	*Neves Corvo*	*Neves Corvo*	*Neves Corvo*	*Neves Corvo*	*Neves Corvo*	*Neves Corvo*
Sub-sector	Lombador	Lombador	Lombador	Lombador	Lombador	Lombador	Lombador	Lombador	Lombador	Lombador	Lombador	Lombador
Stratigraphic division	*PQG*	*PQG*	*PQG*	*PQG*	*PQG*	*PQG*	*PQG*	*PQG*	*PQG*	*PQG*	*PQG*	*PQG*
Mineralization type	*Mineralized*	*Mineralized*	*Mineralized*	*Mineralized*	*Mineralized*	*Mineralized*	*Mineralized*	*Mineralized*	*Mineralized*	*Mineralized*	*Mineralized*	*Mineralized*
Occurrence												
Sample ref.	*NCL#10*	*NCL#10*	*NCL#10*	*NCL#10*	*NCL#10*	*NCL#10*	*NCL#10*	*NCL#10*	*NCL#10*	*NCL#10*	*NCL#10*	*NCL#10*
# analysis	*#180*	*#181*	*#182*	*#183*	*#184*	*#185*	*#186*	*#187*	*#188*	*#189*	*#190*	*#191*
SiO2	24.40	24.46	24.66	24.61	24.53	24.17	24.48	26.27	24.54	24.61	23.99	26.03
Al2O3	20.54	20.03	21.24	20.75	21.45	20.89	20.84	22.64	20.23	20.68	21.61	22.87
FeO	38.03	37.76	37.19	37.81	37.04	37.07	36.97	34.55	38.03	36.95	37.18	34.76
Fe2O3	0.00	0.00	0.00	0.00	0.00	0.00	0.00	0.00	0.00	0.00	0.00	0.00
MnO	0.18	0.16	0.10	0.17	0.16	0.17	0.18	0.15	0.15	0.16	0.18	0.09
MgO	5.67	5.72	5.92	5.81	5.75	6.05	6.30	5.26	5.76	6.23	5.94	5.50
CaO	0.03	0.03	0.04	0.03	0.03	0.00	0.01	0.02	0.02	0.03	0.03	0.03
Na2O	0.01	0.04	0.04	0.01	0.01	0.02	0.00	0.00	0.02	0.03	0.00	0.00
K2O	0.00	0.00	0.00	0.01	0.00	0.00	0.00	0.01	0.00	0.01	0.00	0.01
F	0.00	0.02	0.04	0.00	0.03	0.00	0.03	0.00	0.02	0.00	0.00	0.00
Cl	0.00	0.00	0.00	0.00	0.00	0.00	0.00	0.00	0.00	0.00	0.00	0.00
TiO2	0.04	0.03	0.06	0.02	0.04	0.05	0.02	0.02	0.03	0.00	0.05	0.01
Cr2O3	0.03	0.08	0.10	0.06	0.06	0.03	0.10	0.07	0.04	0.07	0.03	0.08
ZnO	0.01	0.00	0.15	0.10	0.09	0.12	0.01	0.02	0.06	0.00	0.08	0.01
V2O3	0.00	0.00	0.00	0.00	0.00	0.00	0.00	0.00	0.00	0.00	0.00	0.00
NiO	0.05	0.00	0.00	0.00	0.00	0.00	0.06	0.00	0.00	0.00	0.00	0.03
Cs2O	0.00	0.00	0.00	0.00	0.00	0.00	0.00	0.00	0.02	0.00	0.00	0.02
BaO	0.03	0.00	0.02	0.00	0.02	0.03	0.00	0.06	0.04	0.00	0.06	0.02
H2O	10.77	10.68	10.88	10.84	10.86	10.77	10.82	11.10	10.75	10.82	10.84	11.14
Total#	99.79	99.00	100.42	100.20	100.07	99.37	99.83	100.18	99.70	99.59	99.98	100.61
O=F	0.00	-0.01	-0.02	0.00	-0.01	0.00	-0.01	0.00	-0.01	0.00	0.00	0.00
O=Cl	0.00	0.00	0.00	0.00	0.00	0.00	0.00	0.00	0.00	0.00	0.00	0.00
Total	99.79	98.99	100.40	100.20	100.06	99.37	99.82	100.18	99.70	99.59	99.98	100.61

Chlorite

# analysis		#180	#181	#182	#183	#184	#185	#186	#187	#188	#189	#190	#191
Ion Distribution													
Si		2.72	2.74	2.71	2.72	2.71	2.69	2.71	2.84	2.74	2.73	2.66	2.80
Al		1.28	1.26	1.29	1.28	1.29	1.31	1.29	1.16	1.26	1.27	1.34	1.20
	Total	4.00	4.00	4.00	4.00	4.00	4.00	4.00	4.00	4.00	4.00	4.00	4.00
Al		1.41	1.39	1.47	1.43	1.49	1.44	1.43	1.72	1.39	1.43	1.47	1.70
Mn		0.02	0.02	0.01	0.02	0.01	0.02	0.02	0.01	0.01	0.02	0.02	0.01
Zn		0.00	0.00	0.01	0.01	0.01	0.01	0.00	0.00	0.00	0.00	0.01	0.00
Fe2+		3.54	3.54	3.42	3.50	3.42	3.45	3.42	3.12	3.55	3.43	3.44	3.13
Ti		0.00	0.00	0.00	0.00	0.00	0.00	0.00	0.00	0.00	0.00	0.00	0.00
Ca		0.00	0.00	0.00	0.00	0.00	0.00	0.00	0.00	0.00	0.00	0.00	0.00
V		0.00	0.00	0.00	0.00	0.00	0.00	0.00	0.00	0.00	0.00	0.00	0.00
Ba		0.00	0.00	0.00	0.00	0.00	0.00	0.00	0.00	0.00	0.00	0.00	0.00
Fe3+		0.00	0.00	0.00	0.00	0.00	0.00	0.00	0.00	0.00	0.00	0.00	0.00
Mg		0.94	0.96	0.97	0.96	0.95	1.00	1.04	0.85	0.96	1.03	0.98	0.88
Na		0.00	0.01	0.01	0.00	0.00	0.00	0.00	0.00	0.00	0.01	0.00	0.00
Cr		0.00	0.01	0.01	0.00	0.01	0.00	0.01	0.01	0.00	0.01	0.00	0.01
K		0.00	0.00	0.00	0.00	0.00	0.00	0.00	0.00	0.00	0.00	0.00	0.00
Cs		0.00	0.00	0.00	0.00	0.00	0.00	0.00	0.00	0.00	0.00	0.00	0.00
Ni		0.00	0.00	0.00	0.00	0.00	0.00	0.01	0.00	0.00	0.00	0.00	0.00
	Total	5.93	5.93	5.91	5.92	5.89	5.93	5.93	5.72	5.93	5.92	5.93	5.74
OH		8.00	7.99	7.99	8.00	7.99	8.00	7.99	8.00	7.99	8.00	8.00	8.00
F		0.00	0.01	0.01	0.00	0.01	0.00	0.01	0.00	0.01	0.00	0.00	0.00
Cl		0.00	0.00	0.00	0.00	0.00	0.00	0.00	0.00	0.00	0.00	0.00	0.00
	Total	8.00	8.00	8.00	8.00	8.00	8.00	8.00	8.00	8.00	8.00	8.00	8.00

Chlorite

Sector	*Neves Corvo*	*Neves Corvo*	*Neves Corvo*	*Neves Corvo*	*Neves Corvo*	*Neves Corvo*	*Neves Corvo*	*Neves Corvo*	*Neves Corvo*	*Neves Corvo*	*Neves Corvo*	*Neves Corvo*
Sub-sector	Lombador	Lombador	Lombador	Lombador	Lombador	Lombador	Lombador	Lombador	Lombador	Lombador	Lombador	Lombador
Stratigraphic division	*PQG*	*PQG*	*PQG*	*PQG*	*PQG*	*PQG*	*PQG*	*PQG*	*PQG*	*PQG*	*PQG*	*PQG*
Mineralization type	*Mineralized*	*Mineralized*	*Mineralized*	*Mineralized*	*Mineralized*	*Mineralized*	*No sulphide*	*No sulphide*	*No sulphide*	*No sulphide*	*No sulphide*	*No sulphide*
Occurrence												
Sample ref.	*NCL#10*	*NCL#10*	*NCL#10*	*NCL#10*	*NCL#10*	*NCL#10*	*NCL#15*	*NCL#15*	*NCL#15*	*NCL#15*	*NCL#15*	*NCL#15*
# analysis	*#192*	*#193*	*#194*	*#195*	*#196*	*#197*	*#198*	*#199*	*#200*	*#201*	*#202*	*#203*
SiO2	23.99	25.50	24.83	24.04	25.57	23.81	23.92	23.99	24.96	24.23	24.14	23.70
Al2O3	21.10	22.02	22.55	21.34	20.51	20.37	22.28	22.22	22.29	22.42	22.20	22.39
FeO	36.41	35.01	35.07	36.55	35.77	37.07	36.39	35.85	35.45	36.14	36.32	36.79
Fe2O3	0.00	0.00	0.00	0.00	0.00	0.00	0.00	0.00	0.00	0.00	0.00	0.00
MnO	0.11	0.16	0.36	0.23	0.16	0.16	0.29	0.31	0.30	0.34	0.30	0.31
MgO	6.31	5.94	5.65	5.80	5.97	5.93	6.34	6.52	6.45	6.51	6.47	6.38
CaO	0.04	0.07	0.24	0.14	0.04	0.04	0.03	0.02	0.00	0.00	0.03	0.00
Na2O	0.00	0.00	0.01	0.02	0.03	0.01	0.00	0.00	0.02	0.02	0.01	0.02
K2O	0.00	0.08	0.03	0.02	0.10	0.08	0.07	0.13	0.34	0.08	0.01	0.02
F	0.00	0.06	0.00	0.00	0.00	0.05	0.00	0.00	0.00	0.00	0.00	0.00
Cl	0.00	0.00	0.00	0.00	0.00	0.00	0.00	0.00	0.00	0.00	0.00	0.00
TiO2	0.00	0.01	0.06	0.05	0.05	0.03	0.06	0.10	0.06	0.04	0.01	0.03
Cr2O3	0.03	0.06	0.03	0.09	0.08	0.08	0.10	0.10	0.09	0.10	0.09	0.09
ZnO	0.07	0.06	0.17	0.17	0.00	0.01	0.00	0.04	0.00	0.00	0.00	0.10
V2O3	0.00	0.00	0.00	0.00	0.00	0.00	0.00	0.00	0.00	0.00	0.00	0.00
NiO	0.00	0.01	0.06	0.00	0.03	0.00	0.06	0.00	0.00	0.03	0.00	0.04
Cs2O	0.00	0.02	0.02	0.00	0.02	0.00	0.00	0.00	0.00	0.00	0.00	0.05
BaO	0.00	0.06	0.03	0.03	0.00	0.00	0.00	0.00	0.07	0.01	0.05	0.03
H2O	10.74	10.98	10.98	10.77	10.85	10.58	10.94	10.93	11.08	11.01	10.96	10.95
Total#	98.80	100.04	100.10	99.25	99.18	98.22	100.48	100.21	101.11	100.92	100.60	100.89
O=F	0.00	-0.02	0.00	0.00	0.00	-0.02	0.00	0.00	0.00	0.00	0.00	0.00
O=Cl	0.00	0.00	0.00	0.00	0.00	0.00	0.00	0.00	0.00	0.00	0.00	0.00
Total	98.80	100.01	100.10	99.25	99.18	98.20	100.48	100.21	101.11	100.92	100.60	100.89

Chlorite

# analysis		#192	#193	#194	#195	#196	#197	#198	#199	#200	#201	#202	#203
Ion Distribution													
Si		2.68	2.78	2.71	2.68	2.83	2.69	2.62	2.63	2.70	2.64	2.64	2.60
Al		1.32	1.22	1.29	1.32	1.17	1.31	1.38	1.37	1.30	1.36	1.36	1.40
	Total	4.00	4.00	4.00	4.00	4.00	4.00	4.00	4.00	4.00	4.00	4.00	4.00
Al		1.46	1.61	1.61	1.48	1.50	1.40	1.50	1.50	1.55	1.51	1.50	1.49
Mn		0.01	0.02	0.03	0.02	0.01	0.02	0.03	0.03	0.03	0.03	0.03	0.03
Zn		0.01	0.00	0.01	0.01	0.00	0.00	0.00	0.00	0.00	0.00	0.00	0.01
Fe2+		3.40	3.19	3.20	3.40	3.31	3.50	3.34	3.29	3.21	3.29	3.32	3.37
Ti		0.00	0.00	0.00	0.00	0.00	0.00	0.01	0.01	0.01	0.00	0.00	0.00
Ca		0.00	0.01	0.03	0.02	0.00	0.01	0.00	0.00	0.00	0.00	0.00	0.00
V		0.00	0.00	0.00	0.00	0.00	0.00	0.00	0.00	0.00	0.00	0.00	0.00
Ba		0.00	0.00	0.00	0.00	0.00	0.00	0.00	0.00	0.00	0.00	0.00	0.00
Fe3+		0.00	0.00	0.00	0.00	0.00	0.00	0.00	0.00	0.00	0.00	0.00	0.00
Mg		1.05	0.96	0.92	0.96	0.98	1.00	1.04	1.07	1.04	1.06	1.05	1.04
Na		0.00	0.00	0.00	0.00	0.01	0.00	0.00	0.00	0.00	0.00	0.00	0.00
Cr		0.00	0.01	0.00	0.01	0.01	0.01	0.01	0.01	0.01	0.01	0.01	0.01
K		0.00	0.01	0.00	0.00	0.01	0.01	0.01	0.02	0.05	0.01	0.00	0.00
Cs		0.00	0.00	0.00	0.00	0.00	0.00	0.00	0.00	0.00	0.00	0.00	0.00
Ni		0.00	0.00	0.01	0.00	0.00	0.00	0.01	0.00	0.00	0.00	0.00	0.00
	Total	5.93	5.81	5.83	5.92	5.84	5.95	5.93	5.93	5.89	5.92	5.93	5.96
OH		8.00	7.98	8.00	8.00	8.00	7.98	8.00	8.00	8.00	8.00	8.00	8.00
F		0.00	0.02	0.00	0.00	0.00	0.02	0.00	0.00	0.00	0.00	0.00	0.00
Cl		0.00	0.00	0.00	0.00	0.00	0.00	0.00	0.00	0.00	0.00	0.00	0.00
	Total	8.00	8.00	8.00	8.00	8.00	8.00	8.00	8.00	8.00	8.00	8.00	8.00

Chlorite

Sector	*Neves Corvo*	*Neves Corvo*	*Neves Corvo*	*Neves Corvo*	*Neves Corvo*	*Neves Corvo*	*Neves Corvo*	*Neves Corvo*	*Neves Corvo*	*Neves Corvo*	*Neves Corvo*	*Neves Corvo*
Sub-sector	Lombador	Lombador	Lombador	Lombador	Lombador	Lombador	Lombador	Lombador	Lombador	Lombador	Lombador	Lombador
Stratigraphic division	*PQG*	*PQG*	*PQG*	*PQG*	*PQG*	*PQG*	*PQG*	*PQG*	*PQG*	*PQG*	*PQG*	*PQG*
Mineralization type	*No sulphide*	*No sulphide*	*No sulphide*	*No sulphide*	*No sulphide*	*No sulphide*	*No sulphide*	*No sulphide*	*No sulphide*	*No sulphide*	*No sulphide*	*No sulphide*
Occurrence												
Sample ref.	*NCL#15*	*NCL#15*	*NCL#15*	*NCL#15*	*NCL#15*	*NCL#15*	*NCL#15*	*NCL#15*	*NCL#15*	*NCL#15*	*NCL#15*	*NCL#15*
# analysis	*#204*	*#205*	*#206*	*#207*	*#208*	*#209*	*#210*	*#211*	*#212*	*#213*	*#214*	*#215*
SiO2	24.36	24.28	24.05	23.90	24.07	24.23	23.87	24.24	24.48	24.37	24.55	23.75
Al2O3	22.26	22.20	22.36	22.18	21.67	21.76	21.97	21.80	21.92	21.67	21.52	21.77
FeO	36.05	36.04	36.20	36.18	36.54	36.65	36.20	36.44	35.87	36.47	35.43	36.34
Fe2O3	0.00	0.00	0.00	0.00	0.00	0.00	0.00	0.00	0.00	0.00	0.00	0.00
MnO	0.29	0.31	0.23	0.30	0.32	0.42	0.31	0.31	0.24	0.27	0.24	0.33
MgO	6.61	6.50	6.43	6.62	6.63	6.49	6.77	6.66	6.42	6.42	6.52	6.47
CaO	0.01	0.00	0.02	0.00	0.01	0.03	0.02	0.01	0.04	0.01	0.01	0.02
Na2O	0.01	0.00	0.02	0.01	0.01	0.00	0.01	0.00	0.02	0.00	0.01	0.00
K2O	0.16	0.06	0.20	0.03	0.01	0.02	0.00	0.01	0.18	0.00	0.01	0.04
F	0.03	0.00	0.00	0.06	0.00	0.00	0.00	0.00	0.00	0.00	0.12	0.00
Cl	0.00	0.00	0.00	0.00	0.00	0.00	0.00	0.00	0.00	0.00	0.00	0.00
TiO2	0.03	0.02	0.04	0.04	0.00	0.02	0.03	0.04	0.04	0.01	0.04	0.04
Cr2O3	0.12	0.12	0.09	0.07	0.07	0.06	0.09	0.07	0.05	0.08	0.07	0.04
ZnO	0.03	0.07	0.07	0.00	0.03	0.01	0.03	0.05	0.00	0.05	0.03	0.00
V2O3	0.00	0.00	0.00	0.00	0.00	0.00	0.00	0.00	0.00	0.00	0.00	0.00
NiO	0.00	0.05	0.00	0.00	0.01	0.05	0.06	0.04	0.07	0.00	0.00	0.04
Cs2O	0.00	0.00	0.03	0.00	0.00	0.00	0.03	0.00	0.02	0.00	0.00	0.00
BaO	0.00	0.00	0.05	0.00	0.05	0.04	0.00	0.03	0.00	0.01	0.00	0.00
H2O	11.01	10.98	10.97	10.90	10.91	10.95	10.92	10.96	10.95	10.92	10.81	10.84
Total#	100.96	100.62	100.77	100.30	100.31	100.74	100.31	100.66	100.31	100.29	99.35	99.67
O=F	-0.01	0.00	0.00	-0.03	0.00	0.00	0.00	0.00	0.00	0.00	-0.05	0.00
O=Cl	0.00	0.00	0.00	0.00	0.00	0.00	0.00	0.00	0.00	0.00	0.00	0.00
Total	100.94	100.62	100.77	100.27	100.31	100.74	100.31	100.66	100.31	100.29	99.30	99.67

Chlorite

# analysis		#204	#205	#206	#207	#208	#209	#210	#211	#212	#213	#214	#215
Ion Distribution													
Si		2.65	2.65	2.63	2.62	2.65	2.65	2.62	2.65	2.68	2.68	2.71	2.63
Al		1.35	1.35	1.37	1.38	1.35	1.35	1.38	1.35	1.32	1.32	1.29	1.37
	Total	4.00	4.00	4.00	4.00	4.00	4.00	4.00	4.00	4.00	4.00	4.00	4.00
Al		1.51	1.51	1.51	1.49	1.46	1.46	1.47	1.46	1.51	1.48	1.51	1.47
Mn		0.03	0.03	0.02	0.03	0.03	0.04	0.03	0.03	0.02	0.03	0.02	0.03
Zn		0.00	0.01	0.01	0.00	0.00	0.00	0.00	0.00	0.00	0.00	0.00	0.00
Fe2+		3.28	3.29	3.31	3.32	3.36	3.36	3.33	3.34	3.28	3.35	3.27	3.36
Ti		0.00	0.00	0.00	0.00	0.00	0.00	0.00	0.00	0.00	0.00	0.00	0.00
Ca		0.00	0.00	0.00	0.00	0.00	0.00	0.00	0.00	0.01	0.00	0.00	0.00
V		0.00	0.00	0.00	0.00	0.00	0.00	0.00	0.00	0.00	0.00	0.00	0.00
Ba		0.00	0.00	0.00	0.00	0.00	0.00	0.00	0.00	0.00	0.00	0.00	0.00
Fe3+		0.00	0.00	0.00	0.00	0.00	0.00	0.00	0.00	0.00	0.00	0.00	0.00
Mg		1.07	1.06	1.05	1.08	1.09	1.06	1.11	1.09	1.05	1.05	1.07	1.07
Na		0.00	0.00	0.01	0.00	0.00	0.00	0.00	0.00	0.00	0.00	0.00	0.00
Cr		0.01	0.01	0.01	0.01	0.01	0.01	0.01	0.01	0.00	0.01	0.01	0.00
K		0.02	0.01	0.03	0.00	0.00	0.00	0.00	0.00	0.02	0.00	0.00	0.00
Cs		0.00	0.00	0.00	0.00	0.00	0.00	0.00	0.00	0.00	0.00	0.00	0.00
Ni		0.00	0.00	0.00	0.00	0.00	0.00	0.00	0.00	0.01	0.00	0.00	0.00
	Total	5.93	5.92	5.94	5.94	5.95	5.94	5.95	5.94	5.91	5.92	5.89	5.95
OH		7.99	8.00	8.00	7.98	8.00	8.00	8.00	8.00	8.00	8.00	7.96	8.00
F		0.01	0.00	0.00	0.02	0.00	0.00	0.00	0.00	0.00	0.00	0.04	0.00
Cl		0.00	0.00	0.00	0.00	0.00	0.00	0.00	0.00	0.00	0.00	0.00	0.00
	Total	8.00	8.00	8.00	8.00	8.00	8.00	8.00	8.00	8.00	8.00	8.00	8.00

Chlorite

Sector	*Neves Corvo*	*Neves Corvo*	*Neves Corvo*	*Neves Corvo*	*Neves Corvo*	*Neves Corvo*	*Neves Corvo*	*Neves Corvo*	*Neves Corvo*	*Neves Corvo*	*Neves Corvo*	*Neves Corvo*
Sub-sector	Neves	Neves	Neves	Neves	Neves	Neves	Neves	Neves	Neves	Neves	Neves	Neves
Stratigraphic division	*lower VSC*	*lower VSC*	*lower VSC*	*lower VSC*	*lower VSC*	*lower VSC*	*lower VSC*	*lower VSC*	*lower VSC*	*lower VSC*	*lower VSC*	*lower VSC*
Mineralization type	*Mineralized*	*Mineralized*	*Mineralized*	*Mineralized*	*Mineralized*	*Mineralized*	*Mineralized*	*Mineralized*	*Mineralized*	*Mineralized*	*Mineralized*	*Mineralized*
Occurrence												
Sample ref.	*NCN#17*	*NCN#17*	*NCN#17*	*NCN#17*	*NCN#17*	*NCN#17*	*NCN#17*	*NCN#17*	*NCN#17*	*NCN#17*	*NCN#17*	*NCN#17*
# analysis	*#216*	*#217*	*#218*	*#219*	*#220*	*#221*	*#222*	*#223*	*#224*	*#225*	*#226*	*#227*
SiO2	27.50	27.74	26.25	26.51	26.31	26.32	26.85	27.02	26.38	26.27	26.85	26.75
Al2O3	23.48	23.63	21.52	22.97	22.69	22.84	22.83	22.73	21.46	21.31	20.62	20.73
FeO	28.59	28.68	27.80	29.02	29.04	28.92	28.38	28.44	26.30	26.03	26.42	26.49
Fe2O3	0.00	0.00	0.00	0.00	0.00	0.00	0.00	0.00	0.00	0.00	0.00	0.00
MnO	0.11	0.09	0.17	0.11	0.14	0.08	0.16	0.11	0.21	0.22	0.20	0.22
MgO	8.94	8.96	12.11	9.14	9.17	9.13	10.36	10.17	13.14	13.33	13.46	13.58
CaO	0.08	0.07	0.04	0.09	0.07	0.07	0.06	0.07	0.02	0.00	0.05	0.03
Na2O	0.01	0.00	0.03	0.06	0.02	0.04	0.01	0.02	0.00	0.02	0.00	0.01
K2O	0.04	0.04	0.00	0.02	0.03	0.02	0.02	0.01	0.01	0.00	0.01	0.00
F	0.00	0.00	0.11	0.09	0.02	0.00	0.02	0.06	0.02	0.07	0.05	0.05
Cl	0.00	0.00	0.00	0.00	0.00	0.00	0.00	0.00	0.00	0.00	0.00	0.00
TiO2	0.04	0.01	0.00	0.03	1.20	1.18	0.16	0.18	0.01	0.00	0.01	0.00
Cr2O3	0.07	0.06	0.09	0.05	0.10	0.12	0.08	0.05	0.06	0.08	0.05	0.05
ZnO	0.06	0.00	0.01	0.08	0.05	0.00	0.08	0.02	0.03	0.00	0.07	0.00
V2O3	0.00	0.00	0.00	0.00	0.00	0.00	0.00	0.00	0.00	0.00	0.00	0.00
NiO	0.00	0.05	0.00	0.01	0.01	0.00	0.05	0.01	0.00	0.01	0.00	0.06
Cs2O	0.00	0.00	0.00	0.01	0.00	0.00	0.00	0.00	0.01	0.01	0.00	0.03
BaO	0.00	0.04	0.04	0.05	0.06	0.04	0.03	0.04	0.00	0.04	0.00	0.01
H2O	11.49	11.56	11.27	11.26	11.38	11.39	11.46	11.43	11.35	11.29	11.34	11.36
Total#	100.41	100.92	99.44	99.51	100.30	100.14	100.53	100.33	99.01	98.69	99.13	99.36
O=F	0.00	0.00	-0.05	-0.04	-0.01	0.00	-0.01	-0.02	-0.01	-0.03	-0.02	-0.02
O=Cl	0.00	0.00	0.00	0.00	0.00	0.00	0.00	0.00	0.00	0.00	0.00	0.00
Total	100.41	100.92	99.39	99.47	100.29	100.14	100.52	100.30	99.00	98.66	99.10	99.34

Chlorite

# analysis		#216	#217	#218	#219	#220	#221	#222	#223	#224	#225	#226	#227
Ion Distribution													
Si		2.87	2.88	2.78	2.81	2.77	2.77	2.81	2.83	2.79	2.78	2.83	2.82
Al		1.13	1.12	1.22	1.19	1.23	1.23	1.19	1.17	1.21	1.22	1.17	1.18
	Total	4.00	4.00	4.00	4.00	4.00	4.00	4.00	4.00	4.00	4.00	4.00	4.00
Al		1.76	1.77	1.47	1.68	1.59	1.61	1.62	1.63	1.46	1.44	1.40	1.39
Mn		0.01	0.01	0.02	0.01	0.01	0.01	0.01	0.01	0.02	0.02	0.02	0.02
Zn		0.00	0.00	0.00	0.01	0.00	0.00	0.01	0.00	0.00	0.00	0.01	0.00
Fe2+		2.50	2.49	2.46	2.57	2.56	2.55	2.48	2.49	2.32	2.31	2.33	2.33
Ti		0.00	0.00	0.00	0.00	0.10	0.09	0.01	0.01	0.00	0.00	0.00	0.00
Ca		0.01	0.01	0.00	0.01	0.01	0.01	0.01	0.01	0.00	0.00	0.01	0.00
V		0.00	0.00	0.00	0.00	0.00	0.00	0.00	0.00	0.00	0.00	0.00	0.00
Ba		0.00	0.00	0.00	0.00	0.00	0.00	0.00	0.00	0.00	0.00	0.00	0.00
Fe3+		0.00	0.00	0.00	0.00	0.00	0.00	0.00	0.00	0.00	0.00	0.00	0.00
Mg		1.39	1.39	1.91	1.45	1.44	1.43	1.62	1.59	2.07	2.10	2.12	2.13
Na		0.00	0.00	0.01	0.01	0.00	0.01	0.00	0.00	0.00	0.00	0.00	0.00
Cr		0.01	0.01	0.01	0.00	0.01	0.01	0.01	0.00	0.01	0.01	0.00	0.00
K		0.00	0.01	0.00	0.00	0.00	0.00	0.00	0.00	0.00	0.00	0.00	0.00
Cs		0.00	0.00	0.00	0.00	0.00	0.00	0.00	0.00	0.00	0.00	0.00	0.00
Ni		0.00	0.00	0.00	0.00	0.00	0.00	0.00	0.00	0.00	0.00	0.00	0.00
	Total	5.68	5.68	5.88	5.76	5.72	5.72	5.77	5.75	5.88	5.89	5.88	5.89
OH		8.00	8.00	7.96	7.97	7.99	8.00	7.99	7.98	8.00	7.98	7.98	7.98
F		0.00	0.00	0.04	0.03	0.01	0.00	0.01	0.02	0.01	0.02	0.02	0.02
Cl		0.00	0.00	0.00	0.00	0.00	0.00	0.00	0.00	0.00	0.00	0.00	0.00
	Total	8.00	8.00	8.00	8.00	8.00	8.00	8.00	8.00	8.00	8.00	8.00	8.00

Chlorite

Sector	*Neves Corvo*	*Neves Corvo*	*Neves Corvo*	*Neves Corvo*	*Neves Corvo*	*Neves Corvo*	*Neves Corvo*	*Neves Corvo*	*Neves Corvo*	*Neves Corvo*	*Neves Corvo*	*Neves Corvo*
Sub-sector	Neves	Neves	Neves	Neves	Neves	Neves	Neves	Neves	Neves	Neves	Neves	Zambujal
Stratigraphic division	*lower VSC*	*lower VSC*	*lower VSC*	*lower VSC*	*lower VSC*	*lower VSC*	*lower VSC*	*lower VSC*	*lower VSC*	*lower VSC*	*lower VSC*	*lower VSC*
Mineralization type	*Mineralized*	*Mineralized*	*Mineralized*	*Mineralized*	*Mineralized*	*Mineralized*	*Mineralized*	*Mineralized*	*Mineralized*	*Mineralized*	*Mineralized*	*Mineralized*
Occurrence												
Sample ref.	***NCN#17***	***NCN#17***	***NCN#20***	***NCN#20***	***NCN#20***	***NCN#20***	***NCN#20***	***NCN#20***	***NCN#20***	***NCN#20***	***NCN#20***	***NCZ#21***
# analysis	***#228***	***#229***	***#230***	***#231***	***#232***	***#233***	***#234***	***#235***	***#236***	***#237***	***#238***	***#239***
SiO2	26.66	26.97	29.63	23.95	26.15	24.47	27.12	24.65	24.46	24.72	24.22	24.04
Al2O3	21.10	20.90	21.11	21.71	22.16	21.77	20.64	22.40	21.55	21.44	21.27	22.12
FeO	25.89	26.55	12.37	35.84	33.95	35.21	34.02	34.50	35.81	34.68	35.35	36.29
Fe2O3	0.00	0.00	20.19	0.00	0.00	0.00	0.00	0.00	0.00	0.00	0.00	0.00
MnO	0.24	0.24	0.25	0.25	0.26	0.30	0.30	0.27	0.30	0.30	0.23	0.09
MgO	13.58	14.29	5.53	5.96	6.39	6.83	6.62	6.95	6.09	6.54	7.12	6.25
CaO	0.00	0.00	0.03	0.02	0.00	0.10	0.07	0.02	0.00	0.00	0.07	0.00
Na2O	0.01	0.00	0.00	0.02	0.00	0.05	0.07	0.02	0.00	0.03	0.00	0.00
K2O	0.00	0.00	0.32	0.12	0.43	0.02	0.04	0.25	0.01	0.04	0.11	0.01
F	0.16	0.10	0.00	0.02	0.00	0.00	0.00	0.00	0.03	0.07	0.00	0.00
Cl	0.00	0.00	0.00	0.00	0.00	0.00	0.00	0.00	0.00	0.00	0.00	0.00
TiO2	0.00	0.00	0.12	0.06	0.26	0.04	0.01	0.08	0.00	0.02	0.01	0.09
Cr2O3	0.09	0.03	0.07	0.10	0.08	0.06	0.08	0.09	0.03	0.07	0.10	0.11
ZnO	0.10	0.18	0.00	0.06	0.11	0.05	0.08	0.03	0.18	0.03	0.00	0.10
V2O3	0.00	0.00	0.00	0.00	0.00	0.00	0.00	0.00	0.00	0.00	0.00	0.00
NiO	0.03	0.02	0.06	0.05	0.06	0.00	0.01	0.01	0.08	0.02	0.07	0.01
Cs2O	0.00	0.00	0.00	0.00	0.00	0.00	0.00	0.00	0.00	0.00	0.00	0.00
BaO	0.02	0.00	0.00	0.05	0.07	0.05	0.02	0.04	0.06	0.00	0.00	0.00
H2O	11.31	11.50	11.88	10.76	11.18	10.94	11.11	11.03	10.83	10.81	10.86	10.90
Total#	99.19	100.79	101.54	98.96	101.10	99.88	100.17	100.34	99.43	98.77	99.41	100.02
O=F	-0.07	-0.04	0.00	-0.01	0.00	0.00	0.00	0.00	-0.01	-0.03	0.00	0.00
O=Cl	0.00	0.00	0.00	0.00	0.00	0.00	0.00	0.00	0.00	0.00	0.00	0.00
Total	99.12	100.75	101.54	98.95	101.10	99.88	100.17	100.34	99.42	98.74	99.41	100.02

Chlorite

# analysis	#228	#229	#230	#231	#232	#233	#234	#235	#236	#237	#238	#239
Ion Distribution												
Si	2.81	2.80	2.99	2.67	2.80	2.68	2.93	2.68	2.71	2.73	2.68	2.64
Al	1.19	1.20	1.01	1.33	1.20	1.32	1.07	1.32	1.29	1.27	1.32	1.36
Total	4.00	4.00	4.00	4.00	4.00	4.00	4.00	4.00	4.00	4.00	4.00	4.00
Al	1.43	1.36	1.50	1.51	1.61	1.50	1.56	1.55	1.52	1.53	1.44	1.51
Mn	0.02	0.02	0.02	0.02	0.02	0.03	0.03	0.02	0.03	0.03	0.02	0.01
Zn	0.01	0.01	0.00	0.00	0.01	0.00	0.01	0.00	0.01	0.00	0.00	0.01
Fe2+	2.28	2.31	1.04	3.34	3.04	3.23	3.07	3.14	3.31	3.21	3.27	3.34
Ti	0.00	0.00	0.01	0.00	0.02	0.00	0.00	0.01	0.00	0.00	0.00	0.01
Ca	0.00	0.00	0.00	0.00	0.00	0.01	0.01	0.00	0.00	0.00	0.01	0.00
V	0.00	0.00	0.00	0.00	0.00	0.00	0.00	0.00	0.00	0.00	0.00	0.00
Ba	0.00	0.00	0.00	0.00	0.00	0.00	0.00	0.00	0.00	0.00	0.00	0.00
Fe3+	0.00	0.00	1.53	0.00	0.00	0.00	0.00	0.00	0.00	0.00	0.00	0.00
Mg	2.13	2.21	0.83	0.99	1.02	1.12	1.07	1.13	1.00	1.08	1.17	1.02
Na	0.00	0.00	0.00	0.00	0.00	0.01	0.01	0.00	0.00	0.01	0.00	0.00
Cr	0.01	0.00	0.01	0.01	0.01	0.01	0.01	0.01	0.00	0.01	0.01	0.01
K	0.00	0.00	0.04	0.02	0.06	0.00	0.01	0.03	0.00	0.01	0.02	0.00
Cs	0.00	0.00	0.00	0.00	0.00	0.00	0.00	0.00	0.00	0.00	0.00	0.00
Ni	0.00	0.00	0.00	0.00	0.01	0.00	0.00	0.00	0.01	0.00	0.01	0.00
Total	5.88	5.92	5.00	5.91	5.80	5.91	5.76	5.90	5.89	5.87	5.94	5.91
OH	7.95	7.97	8.00	7.99	8.00	8.00	8.00	8.00	7.99	7.98	8.00	8.00
F	0.05	0.03	0.00	0.01	0.00	0.00	0.00	0.00	0.01	0.02	0.00	0.00
Cl	0.00	0.00	0.00	0.00	0.00	0.00	0.00	0.00	0.00	0.00	0.00	0.00
Total	8.00	8.00	8.00	8.00	8.00	8.00	8.00	8.00	8.00	8.00	8.00	8.00

Chlorite

Sector	*Neves Corvo*	*Neves Corvo*	*Neves Corvo*	*Neves Corvo*	*Neves Corvo*	*Neves Corvo*	*Neves Corvo*	*Neves Corvo*	*Neves Corvo*	*Neves Corvo*	*Neves Corvo*	*Neves Corvo*
Sub-sector	Zambujal	Zambujal	Zambujal	Zambujal	Zambujal	Zambujal	Zambujal	Zambujal	Zambujal	Zambujal	Zambujal	Zambujal
Stratigraphic division	*lower VSC*	*lower VSC*	*lower VSC*	*lower VSC*	*lower VSC*	*lower VSC*	*lower VSC*	*lower VSC*	*lower VSC*	*lower VSC*	*lower VSC*	*lower VSC*
Mineralization type	*Mineralized*	*Mineralized*	*Mineralized*	*Mineralized*	*Mineralized*	*Mineralized*	*Mineralized*	*Mineralized*	*Mineralized*	*Mineralized*	*Mineralized*	*Mineralized*
Occurrence												
Sample ref.	***NCZ#21***	***NCZ#21***	***NCZ#21***	***NCZ#21***	***NCZ#21***	***NCZ#21***	***NCZ#21***	***NCZ#21***	***NCZ#21***	***NCZ#21***	***NCZ#21***	***NCZ#21***
# analysis	***#240***	***#241***	***#242***	***#243***	***#244***	***#245***	***#246***	***#247***	***#248***	***#249***	***#250***	***#251***
SiO2	23.90	24.01	23.94	24.04	24.00	23.75	24.26	24.30	24.15	23.93	24.66	23.96
Al2O3	21.78	22.87	22.64	22.74	22.85	22.60	22.66	21.72	22.24	21.99	22.32	21.51
FeO	36.27	35.09	34.25	35.62	34.61	35.32	35.11	33.65	34.32	35.66	34.55	35.58
Fe2O3	0.00	0.00	0.00	0.00	0.00	0.00	0.00	0.00	0.00	0.00	0.00	0.00
MnO	0.14	0.06	0.06	0.16	0.10	0.08	0.10	0.12	0.10	0.16	0.12	0.08
MgO	6.10	6.75	7.14	6.82	7.21	6.61	6.67	7.63	7.51	6.69	6.85	6.34
CaO	0.00	0.02	0.03	0.00	0.04	0.03	0.01	0.07	0.03	0.00	0.01	0.02
Na2O	0.03	0.00	0.03	0.03	0.00	0.04	0.01	0.06	0.01	0.01	0.01	0.06
K2O	0.01	0.02	0.00	0.01	0.06	0.01	0.01	0.03	0.01	0.01	0.01	0.02
F	0.00	0.03	0.00	0.00	0.00	0.00	0.02	0.05	0.17	0.19	0.00	0.00
Cl	0.00	0.00	0.00	0.00	0.00	0.00	0.00	0.00	0.00	0.00	0.00	0.00
TiO2	0.03	0.05	0.00	0.02	0.04	0.01	0.01	0.01	0.03	0.01	0.00	0.01
Cr2O3	0.06	0.07	0.09	0.06	0.05	0.04	0.10	0.11	0.07	0.07	0.05	0.08
ZnO	0.17	0.05	0.02	0.08	0.17	0.08	0.04	0.15	0.15	0.07	0.09	0.15
V2O3	0.00	0.00	0.00	0.00	0.00	0.00	0.00	0.00	0.00	0.00	0.00	0.00
NiO	0.05	0.01	0.01	0.02	0.03	0.01	0.00	0.00	0.05	0.02	0.04	0.08
Cs2O	0.00	0.00	0.00	0.00	0.00	0.04	0.00	0.00	0.00	0.02	0.00	0.02
BaO	0.04	0.00	0.00	0.00	0.04	0.02	0.01	0.07	0.00	0.00	0.02	0.05
H2O	10.81	10.96	10.92	11.01	11.01	10.89	10.97	10.86	10.88	10.78	10.98	10.76
Total#	99.40	99.98	99.15	100.61	100.20	99.53	99.95	98.82	99.73	99.59	99.71	98.74
O=F	0.00	-0.01	0.00	0.00	0.00	0.00	-0.01	-0.02	-0.07	-0.08	0.00	0.00
O=Cl	0.00	0.00	0.00	0.00	0.00	0.00	0.00	0.00	0.00	0.00	0.00	0.00
Total	99.40	99.97	99.15	100.61	100.20	99.53	99.94	98.79	99.65	99.51	99.71	98.74

Chlorite

# analysis	#240	#241	#242	#243	#244	#245	#246	#247	#248	#249	#250	#251
Ion Distribution												
Si	2.65	2.62	2.63	2.62	2.61	2.62	2.65	2.68	2.64	2.64	2.69	2.67
Al	1.35	1.38	1.37	1.38	1.39	1.38	1.35	1.32	1.36	1.36	1.31	1.33
Total	4.00	4.00	4.00	4.00	4.00	4.00	4.00	4.00	4.00	4.00	4.00	4.00
Al	1.50	1.57	1.56	1.54	1.55	1.55	1.57	1.50	1.51	1.50	1.57	1.49
Mn	0.01	0.01	0.01	0.01	0.01	0.01	0.01	0.01	0.01	0.01	0.01	0.01
Zn	0.01	0.00	0.00	0.01	0.01	0.01	0.00	0.01	0.01	0.01	0.01	0.01
Fe2+	3.37	3.21	3.15	3.24	3.15	3.25	3.21	3.10	3.14	3.29	3.16	3.32
Ti	0.00	0.00	0.00	0.00	0.00	0.00	0.00	0.00	0.00	0.00	0.00	0.00
Ca	0.00	0.00	0.00	0.00	0.00	0.00	0.00	0.01	0.00	0.00	0.00	0.00
V	0.00	0.00	0.00	0.00	0.00	0.00	0.00	0.00	0.00	0.00	0.00	0.00
Ba	0.00	0.00	0.00	0.00	0.00	0.00	0.00	0.00	0.00	0.00	0.00	0.00
Fe3+	0.00	0.00	0.00	0.00	0.00	0.00	0.00	0.00	0.00	0.00	0.00	0.00
Mg	1.01	1.10	1.17	1.11	1.17	1.08	1.09	1.25	1.22	1.10	1.11	1.05
Na	0.01	0.00	0.01	0.01	0.00	0.01	0.00	0.01	0.00	0.00	0.00	0.01
Cr	0.01	0.01	0.01	0.01	0.00	0.00	0.01	0.01	0.01	0.01	0.00	0.01
K	0.00	0.00	0.00	0.00	0.01	0.00	0.00	0.00	0.00	0.00	0.00	0.00
Cs	0.00	0.00	0.00	0.00	0.00	0.00	0.00	0.00	0.00	0.00	0.00	0.00
Ni	0.00	0.00	0.00	0.00	0.00	0.00	0.00	0.00	0.00	0.00	0.00	0.01
Total	5.92	5.90	5.90	5.92	5.92	5.92	5.89	5.91	5.92	5.93	5.87	5.92
OH	8.00	7.99	8.00	8.00	8.00	8.00	7.99	7.98	7.94	7.93	8.00	8.00
F	0.00	0.01	0.00	0.00	0.00	0.00	0.01	0.02	0.06	0.07	0.00	0.00
Cl	0.00	0.00	0.00	0.00	0.00	0.00	0.00	0.00	0.00	0.00	0.00	0.00
Total	8.00	8.00	8.00	8.00	8.00	8.00	8.00	8.00	8.00	8.00	8.00	8.00

Chlorite

Sector	*Neves Corvo*	*Neves Corvo*	*Lousal*	*Lousal*	*Lousal*	*Lousal*	*Lousal*	*Lousal*	*Lousal*	*Lousal*	*Lousal*	*Lousal*
Sub-sector	Zambujal	Zambujal	Sesmarias	Sesmarias	Sesmarias	Sesmarias	Sesmarias	Sesmarias	Sesmarias	Sesmarias	Sesmarias	Sesmarias
Stratigraphic division	*lower VSC*	*lower VSC*	*lower VSC*	*upper VSC*	*upper VSC*	*upper VSC*	*upper VSC*	*upper VSC*	*lower VSC*	*lower VSC*	*lower VSC*	*lower VSC*
Mineralization type	*Mineralized*	*Mineralized*	*Mineralized*	*Py-bearing*	*Py-bearing*	*Py-bearing*	*Py-bearing*	*Py-bearing*	*Mineralized*	*Mineralized*	*Mineralized*	*Mineralized*
Occurrence												
Sample ref.	***NCZ#21***	***NCZ#21***	***SES20#10***	***SES20#6***	***SES20#6***	***SES20#6***	***SES20#6***	***SES20#6***	***SES20#9***	***SES20#9***	***SES20#9***	***SES20#9***
# analysis	***#252***	***#253***	***#254***	***#255***	***#256***	***#257***	***#258***	***#259***	***#260***	***#261***	***#262***	***#263***
SiO2	24.83	25.29	26.76	25.62	25.51	25.37	25.12	24.14	24.17	24.62	24.08	24.84
Al2O3	22.17	22.52	22.39	21.94	21.73	21.94	21.84	22.42	19.77	20.08	20.01	20.13
FeO	33.44	33.14	28.13	28.78	29.55	29.06	29.10	39.76	37.15	36.87	37.33	34.90
Fe2O3	0.00	0.00	0.00	0.00	0.00	0.00	0.00	0.00	0.00	0.00	0.00	0.00
MnO	0.06	0.04	0.61	0.59	0.63	0.60	0.66	0.05	1.43	1.71	1.60	1.81
MgO	7.43	6.30	10.66	11.69	11.25	11.79	11.62	1.70	5.71	5.39	5.20	7.00
CaO	0.05	0.05	0.01	0.02	0.02	0.00	0.01	0.09	0.08	0.02	0.01	0.00
Na2O	0.03	0.06	0.01	0.00	0.01	0.03	0.02	0.00	0.02	0.01	0.00	0.01
K2O	0.00	0.26	0.17	0.04	0.04	0.04	0.03	0.14	0.00	0.00	0.00	0.00
F	0.00	0.06	0.00	0.12	0.03	0.06	0.00	0.00	0.00	0.00	0.00	0.08
Cl	0.00	0.00	0.00	0.00	0.00	0.00	0.00	0.00	0.00	0.00	0.00	0.00
TiO2	0.02	0.03	0.05	0.02	0.04	0.04	0.03	0.03	0.00	0.00	0.03	0.03
Cr2O3	0.10	0.06	0.14	0.02	0.05	0.03	0.06	0.09	0.21	0.11	0.17	0.24
ZnO	0.06	0.07	0.06	0.06	0.02	0.10	0.11	0.11	0.05	0.13	0.06	0.01
V2O3	0.00	0.00	0.00	0.00	0.00	0.00	0.00	0.00	0.00	0.00	0.00	0.00
NiO	0.01	0.00	0.05	0.00	0.06	0.00	0.00	0.05	0.02	0.00	0.00	0.01
Cs2O	0.00	0.00	0.00	0.00	0.00	0.00	0.00	0.01	0.00	0.00	0.00	0.00
BaO	0.05	0.09	0.04	0.01	0.04	0.03	0.07	0.00	0.03	0.04	0.02	0.01
H2O	10.99	10.94	11.44	11.27	11.27	11.29	11.25	10.64	10.67	10.74	10.64	10.82
Total#	99.22	98.91	100.51	100.18	100.24	100.38	99.93	99.22	99.31	99.72	99.15	99.90
O=F	0.00	-0.02	0.00	-0.05	-0.01	-0.03	0.00	0.00	0.00	0.00	0.00	-0.03
O=Cl	0.00	0.00	0.00	0.00	0.00	0.00	0.00	0.00	0.00	0.00	0.00	0.00
Total	99.22	98.89	100.51	100.13	100.22	100.35	99.93	99.22	99.31	99.72	99.15	99.87

Chlorite

# analysis		#252	#253	#254	#255	#256	#257	#258	#259	#260	#261	#262	#263
Ion Distribution													
Si		2.71	2.77	2.81	2.71	2.71	2.69	2.68	2.72	2.72	2.75	2.71	2.74
Al		1.29	1.23	1.19	1.29	1.29	1.31	1.32	1.28	1.28	1.25	1.29	1.26
	Total	4.00	4.00	4.00	4.00	4.00	4.00	4.00	4.00	4.00	4.00	4.00	4.00
Al		1.56	1.67	1.57	1.45	1.43	1.43	1.42	1.70	1.34	1.39	1.37	1.36
Mn		0.01	0.00	0.05	0.05	0.06	0.05	0.06	0.01	0.14	0.16	0.15	0.17
Zn		0.00	0.01	0.00	0.00	0.00	0.01	0.01	0.01	0.00	0.01	0.01	0.00
Fe2+		3.05	3.03	2.47	2.55	2.63	2.57	2.59	3.75	3.49	3.44	3.52	3.22
Ti		0.00	0.00	0.00	0.00	0.00	0.00	0.00	0.00	0.00	0.00	0.00	0.00
Ca		0.01	0.01	0.00	0.00	0.00	0.00	0.00	0.01	0.01	0.00	0.00	0.00
V		0.00	0.00	0.00	0.00	0.00	0.00	0.00	0.00	0.00	0.00	0.00	0.00
Ba		0.00	0.00	0.00	0.00	0.00	0.00	0.00	0.00	0.00	0.00	0.00	0.00
Fe3+		0.00	0.00	0.00	0.00	0.00	0.00	0.00	0.00	0.00	0.00	0.00	0.00
Mg		1.21	1.03	1.67	1.85	1.78	1.86	1.85	0.29	0.96	0.90	0.87	1.15
Na		0.01	0.01	0.00	0.00	0.00	0.01	0.00	0.00	0.00	0.00	0.00	0.00
Cr		0.01	0.01	0.01	0.00	0.00	0.00	0.01	0.01	0.02	0.01	0.02	0.02
K		0.00	0.04	0.02	0.00	0.01	0.00	0.00	0.02	0.00	0.00	0.00	0.00
Cs		0.00	0.00	0.00	0.00	0.00	0.00	0.00	0.00	0.00	0.00	0.00	0.00
Ni		0.00	0.00	0.00	0.00	0.01	0.00	0.00	0.00	0.00	0.00	0.00	0.00
	Total	5.86	5.80	5.81	5.92	5.93	5.94	5.95	5.79	5.97	5.92	5.95	5.94
OH		8.00	7.98	8.00	7.96	7.99	7.98	8.00	8.00	8.00	8.00	8.00	7.97
F		0.00	0.02	0.00	0.04	0.01	0.02	0.00	0.00	0.00	0.00	0.00	0.03
Cl		0.00	0.00	0.00	0.00	0.00	0.00	0.00	0.00	0.00	0.00	0.00	0.00
	Total	8.00	8.00	8.00	8.00	8.00	8.00	8.00	8.00	8.00	8.00	8.00	8.00

Chlorite

Sector	***Lousal***	***Lousal***	***Lousal***	***Lousal***
Sub-sector	Sesmarias	Sesmarias	Sesmarias	Sesmarias
Stratigraphic division	*lower VSC*	*lower VSC*	*lower VSC*	*lower VSC*
Mineralization type	*Mineralized*	*Mineralized*	*Mineralized*	*Mineralized*
Occurrence				
Sample ref.	***SES20#9***	***SES20#9***	***SES20#9***	***SES20#9***
# analysis	***#264***	***#265***	***#266***	***#267***
SiO2	25.28	25.29	24.84	25.14
Al2O3	20.18	20.14	19.83	20.09
FeO	29.15	30.03	32.09	31.04
Fe2O3	0.00	0.00	0.00	0.00
MnO	1.67	1.52	1.54	1.71
MgO	11.04	10.88	9.09	9.89
CaO	0.04	0.03	0.04	0.02
Na2O	0.02	0.01	0.02	0.00
K2O	0.01	0.00	0.01	0.01
F	0.02	0.07	0.04	0.00
Cl	0.00	0.00	0.00	0.00
TiO2	0.02	0.01	0.04	0.08
Cr2O3	0.31	0.30	0.21	0.29
ZnO	0.09	0.02	0.09	0.04
V2O3	0.00	0.00	0.00	0.00
NiO	0.00	0.00	0.04	0.00
Cs2O	0.00	0.00	0.00	0.00
BaO	0.05	0.01	0.02	0.05
H2O	11.05	11.04	10.85	11.01
Total#	98.93	99.35	98.77	99.37
O=F	-0.01	-0.03	-0.02	0.00
O=Cl	0.00	0.00	0.00	0.00
Total	98.92	99.32	98.75	99.37

Chlorite

# analysis		#264	#265	#266	#267
Ion Distribution					
Si		2.74	2.74	2.74	2.74
Al		1.26	1.26	1.26	1.26
	Total	4.00	4.00	4.00	4.00
Al		1.32	1.31	1.32	1.32
Mn		0.15	0.14	0.14	0.16
Zn		0.01	0.00	0.01	0.00
Fe2+		2.65	2.72	2.96	2.83
Ti		0.00	0.00	0.00	0.01
Ca		0.00	0.00	0.01	0.00
V		0.00	0.00	0.00	0.00
Ba		0.00	0.00	0.00	0.00
Fe3+		0.00	0.00	0.00	0.00
Mg		1.79	1.76	1.49	1.61
Na		0.00	0.00	0.00	0.00
Cr		0.03	0.03	0.02	0.03
K		0.00	0.00	0.00	0.00
Cs		0.00	0.00	0.00	0.00
Ni		0.00	0.00	0.00	0.00
	Total	5.96	5.96	5.96	5.95
OH		7.99	7.98	7.99	8.00
F		0.01	0.03	0.02	0.00
Cl		0.00	0.00	0.00	0.00
	Total	8.00	8.00	8.00	8.00

White Mica

n = 217

White mica

Sector	*Albernoa*	*Albernoa*	*Albernoa*	*Albernoa*	*Albernoa*	*Albernoa*	*Albernoa*	*Albernoa*	*Albernoa*	*Albernoa*	*Albernoa*
Sub-sector											
Stratigraphic division	*upper VSC*	*upper VSC*	*middle VSC*	*upper VSC*	*upper VSC*	*upper VSC*	*upper VSC*	*upper VSC*	*upper VSC*	*upper VSC*	*upper VSC*
Mineralization type	*No Sulph*	*No Sulph*	*Py-bearing*	*No Sulph*	*No Sulph*	*No Sulph*	*No Sulph*	*No Sulph*	*Mineralized*	*Mineralized*	*Mineralized*
Occurrence	*Early-formed*	*Early-formed*	*Early-formed*	*Early-formed*	*Early-formed*	*Early-formed*	*Early-formed*	*Early-formed*	*Early-formed*	*Early-formed*	*Early-formed*
Sample ref.	***18-1-G***	***18-1-G***	***37-1-A***	***CW2-AA***	***CW2-M***	***T24a***	***T24a***	***EDS1-F***	***EDS1-H***	***EDS1-H***	***EDS1-H***
Observations						***fsp alteration***	***fsp alteration***				
# analysis	***#1***	***#2***	***#3***	***#4***	***#5***	***#6***	***#7***	***#8***	***#9***	***#10***	***#11***
SiO2	49.042	48.539	57.704	47.670	48.738	49.659	49.454	49.247	48.392	47.911	48.462
Al2O3	28.663	31.391	26.590	33.626	31.755	30.824	31.354	30.248	33.859	34.457	33.870
FeO	3.500	3.003	1.796	1.024	0.745	0.635	0.644	2.770	1.118	1.155	1.079
Fe2O3	0.000	0.000	0.000	0.000	0.000	0.000	0.000	0.000	0.000	0.000	0.000
MnO	0.013	0.046	0.004	0.000	0.008	0.000	0.037	0.063	0.000	0.026	0.024
MgO	2.355	1.533	0.596	1.396	2.636	2.511	2.526	0.500	1.095	1.144	1.106
CaO	0.089	0.073	0.110	0.107	0.040	0.032	0.037	0.030	0.044	0.061	0.068
Na2O	0.278	0.343	1.121	0.290	0.187	0.208	0.237	0.416	0.260	0.356	0.287
K2O	9.967	8.742	5.906	9.668	10.170	10.018	10.329	8.809	9.345	9.968	9.797
F	0.345	0.117	0.089	0.016	0.045	0.014	0.093	0.079	0.045	0.019	0.038
Cl	0.002	0.017	0.021	0.000	0.000	0.000	0.000	0.000	0.001	0.003	0.000
TiO2	0.020	0.119	0.356	0.177	0.032	0.032	0.041	0.130	0.240	0.216	0.237
Cr2O3	0.045	0.069	0.111	0.056	0.061	0.034	0.088	0.084	0.064	0.030	0.056
ZnO	0.000	0.000	0.000	0.000	0.000	0.000	0.000	0.000	0.000	0.000	0.000
Cs2O	0.000	0.000	0.000	0.000	0.000	0.000	0.007	0.000	0.000	0.000	0.000
BaO	0.104	0.293	0.075	0.045	0.090	0.057	0.035	0.142	0.108	0.089	0.161
SnO	0.000	0.000	0.000	0.000	0.000	0.000	0.000	0.000	0.000	0.000	0.000
Mn2O3	0.000	0.000	0.000	0.000	0.000	0.000	0.000	0.000	0.000	0.000	0.000
LiO2	0.000	0.000	0.000	0.000	0.000	0.000	0.000	0.000	0.000	0.000	0.000
H2O	4.253	4.404	4.599	4.480	4.477	4.486	4.473	4.364	4.502	4.531	4.519
Total#	98.676	98.689	99.078	98.555	98.984	98.510	99.355	96.882	99.073	99.966	99.704
O=F	-0.145	-0.049	-0.037	-0.007	-0.019	-0.006	-0.039	-0.033	-0.019	-0.008	-0.016
O=Cl	0.000	-0.004	-0.005	0.000	0.000	0.000	0.000	0.000	0.000	-0.001	0.000
Total	98.530	98.636	99.036	98.548	98.965	98.504	99.316	96.849	99.054	99.958	99.688

White mica

# analysis		*#1*	*#2*	*#3*	*#4*	*#5*	*#6*	*#7*	*#8*	*#9*	*#10*	*#11*
Ion Distribution												
Group iv												
Si		3.329	3.260	3.723	3.185	3.248	3.314	3.283	3.355	3.208	3.163	3.202
Al		0.671	0.740	0.277	0.815	0.752	0.686	0.717	0.645	0.792	0.837	0.798
	Total	4.000	4.000	4.000	4.000	4.000	4.000	4.000	4.000	4.000	4.000	4.000
Group vi												
Cr		0.002	0.004	0.006	0.003	0.003	0.002	0.005	0.005	0.003	0.002	0.003
Al		1.622	1.745	1.745	1.833	1.743	1.739	1.736	1.783	1.853	1.845	1.840
Zn		0.000	0.000	0.000	0.000	0.000	0.000	0.000	0.000	0.000	0.000	0.000
Mn		0.001	0.003	0.000	0.000	0.000	0.000	0.002	0.004	0.000	0.001	0.001
Mg		0.238	0.153	0.057	0.139	0.262	0.250	0.250	0.051	0.108	0.113	0.109
Fe3+		0.000	0.000	0.000	0.000	0.000	0.000	0.000	0.000	0.000	0.000	0.000
Fe2+		0.199	0.169	0.097	0.057	0.042	0.035	0.036	0.158	0.062	0.064	0.060
Ti4		0.001	0.006	0.017	0.009	0.002	0.002	0.002	0.007	0.012	0.011	0.012
Sn		0.000	0.000	0.000	0.000	0.000	0.000	0.000	0.000	0.000	0.000	0.000
Mn		0.000	0.000	0.000	0.000	0.000	0.000	0.000	0.000	0.000	0.000	0.000
	Total	2.063	2.080	1.923	2.041	2.052	2.027	2.030	2.006	2.038	2.035	2.025
Group xii												
Ca		0.006	0.005	0.008	0.008	0.003	0.002	0.003	0.002	0.003	0.004	0.005
Ba		0.003	0.008	0.002	0.001	0.002	0.001	0.001	0.004	0.003	0.002	0.004
Na		0.037	0.045	0.140	0.038	0.024	0.027	0.031	0.055	0.033	0.046	0.037
K		0.863	0.749	0.486	0.824	0.865	0.853	0.875	0.765	0.790	0.840	0.826
Cs		0.000	0.000	0.000	0.000	0.000	0.000	0.000	0.000	0.000	0.000	0.000
	Total	0.909	0.807	0.636	0.870	0.894	0.884	0.909	0.826	0.830	0.892	0.872
OH		1.926	1.973	1.980	1.997	1.991	1.997	1.980	1.983	1.990	1.996	1.992
F		0.074	0.025	0.018	0.003	0.009	0.003	0.020	0.017	0.009	0.004	0.008
Cl		0.000	0.002	0.002	0.000	0.000	0.000	0.000	0.000	0.000	0.000	0.000
O		0.000	0.000	0.000	0.000	0.000	0.000	0.000	0.000	0.000	0.000	0.000
	Total	2.000	2.000	2.000	2.000	2.000	2.000	2.000	2.000	2.000	2.000	2.000

White mica

Sector	*Albernoa*	*Albernoa*	*Albernoa*	*Albernoa*	*Albernoa*	*Albernoa*	*Albernoa*	*Albernoa*	*Albernoa*	*Albernoa*	*Albernoa*
Sub-sector											
Stratigraphic division	*upper VSC*	*upper VSC*	*upper VSC*	*upper VSC*	*middle VSC*	*middle VSC*	*middle VSC*	*middle VSC*	*middle VSC*	*middle VSC*	*upper VSC*
Mineralization type	*No Sulph*	*No Sulph*	*No Sulph*	*No Sulph*	*Py-bearing*	*Py-bearing*	*No Sulph*	*No Sulph*	*No Sulph*	*No Sulph*	*No Sulph*
Occurrence	*Early-formed*	*Early-formed*	*Early-formed*	*Early-formed*	*Early-formed*	*Early-formed*	*Early-formed*	*Early-formed*	*Early-formed*	*Early-formed*	*Early-formed*
Sample ref.	***EDS1-S***	***EDS1-S***	***EDS1-S***	***EDS1-H***	***37-1-A***	***37-1-A***	***X68***	***X68***	***X68***	***X68***	***EDS1-K***
Observations	***fsp alteration***		***fsp alteration***	***fsp alteration***							
# analysis	***#12***	***#13***	***#14***	***#15***	***#16***	***#17***	***#18***	***#19***	***#20***	***#21***	***#22***
SiO2	46.646	47.180	47.862	48.310	52.136	44.842	47.791	50.251	48.191	45.781	51.765
Al2O3	32.321	32.955	33.735	34.525	28.986	34.834	36.259	32.521	33.143	35.030	29.739
FeO	2.955	3.089	1.113	1.194	3.785	1.991	0.491	1.530	1.410	1.218	2.498
Fe2O3	0.000	0.000	0.000	0.000	0.000	0.000	0.000	0.000	0.000	0.000	0.000
MnO	0.044	0.028	0.000	0.000	0.000	0.041	0.000	0.045	0.026	0.000	0.008
MgO	1.103	0.778	1.118	0.923	1.215	0.867	0.232	0.805	0.778	0.944	0.775
CaO	0.115	0.029	0.046	0.040	0.138	0.157	0.025	0.017	0.031	0.054	0.025
Na2O	0.569	0.504	0.286	0.384	1.238	1.410	1.856	0.370	0.434	0.364	0.670
K2O	9.503	9.121	9.798	10.124	6.161	8.203	7.501	8.960	9.383	9.844	8.662
F	0.034	0.073	0.000	0.000	0.143	0.000	0.086	0.014	0.086	0.056	0.077
Cl	0.007	0.003	0.000	0.000	0.009	0.005	0.007	0.009	0.004	0.028	0.003
TiO2	0.128	0.098	0.106	0.093	0.573	0.630	0.072	0.166	0.177	0.204	0.115
Cr2O3	0.054	0.045	0.000	0.000	0.061	0.021	0.116	0.078	0.081	0.103	0.076
ZnO	0.000	0.000	0.000	0.000	0.000	0.000	0.000	0.000	0.000	0.000	0.000
Cs2O	0.000	0.000	0.000	0.000	0.000	0.000	0.000	0.000	0.000	0.000	0.000
BaO	0.152	0.152	0.190	0.145	0.097	0.149	0.067	0.177	0.193	0.171	0.165
SnO	0.000	0.000	0.000	0.000	0.000	0.000	0.000	0.000	0.000	0.000	0.000
Mn2O3	0.000	0.000	0.000	0.000	0.000	0.000	0.000	0.000	0.000	0.000	0.000
LiO2	0.000	0.000	0.000	0.000	0.000	0.000	0.000	0.000	0.000	0.000	0.000
H2O	4.388	4.407	4.491	4.555	4.475	4.416	4.518	4.544	4.434	4.412	4.484
Total#	98.019	98.462	98.745	100.293	99.017	97.566	99.021	99.487	98.371	98.209	99.062
O=F	-0.014	-0.031	0.000	0.000	-0.060	0.000	-0.036	-0.006	-0.036	-0.024	-0.032
O=Cl	-0.002	-0.001	0.000	0.000	-0.002	-0.001	-0.002	-0.002	-0.001	-0.006	-0.001
Total	98.003	98.431	98.745	100.293	98.955	97.565	98.983	99.479	98.334	98.179	99.029

White mica

# analysis		*#12*	*#13*	*#14*	*#15*	*#16*	*#17*	*#18*	*#19*	*#20*	*#21*	*#22*
Ion Distribution												
Group iv												
Si		3.174	3.184	3.195	3.180	3.439	3.044	3.142	3.310	3.228	3.088	3.433
Al		0.826	0.816	0.805	0.820	0.561	0.956	0.858	0.690	0.772	0.912	0.567
	Total	4.000	4.000	4.000	4.000	4.000	4.000	4.000	4.000	4.000	4.000	4.000
Group vi												
Cr		0.003	0.002	0.000	0.000	0.003	0.001	0.006	0.004	0.004	0.005	0.004
Al		1.767	1.806	1.850	1.859	1.693	1.830	1.951	1.834	1.845	1.872	1.757
Zn		0.000	0.000	0.000	0.000	0.000	0.000	0.000	0.000	0.000	0.000	0.000
Mn		0.003	0.002	0.000	0.000	0.000	0.002	0.000	0.003	0.001	0.000	0.000
Mg		0.112	0.078	0.111	0.091	0.119	0.088	0.023	0.079	0.078	0.095	0.077
Fe3+		0.000	0.000	0.000	0.000	0.000	0.000	0.000	0.000	0.000	0.000	0.000
Fe2+		0.168	0.174	0.062	0.066	0.209	0.113	0.027	0.084	0.079	0.069	0.139
Ti4		0.007	0.005	0.005	0.005	0.028	0.032	0.004	0.008	0.009	0.010	0.006
Sn		0.000	0.000	0.000	0.000	0.000	0.000	0.000	0.000	0.000	0.000	0.000
Mn		0.000	0.000	0.000	0.000	0.000	0.000	0.000	0.000	0.000	0.000	0.000
	Total	2.059	2.067	2.028	2.020	2.053	2.067	2.011	2.012	2.016	2.051	1.982
Group xii												
Ca		0.008	0.002	0.003	0.003	0.010	0.011	0.002	0.001	0.002	0.004	0.002
Ba		0.004	0.004	0.005	0.004	0.003	0.004	0.002	0.005	0.005	0.005	0.004
Na		0.075	0.066	0.037	0.049	0.158	0.186	0.237	0.047	0.056	0.048	0.086
K		0.825	0.785	0.834	0.850	0.519	0.710	0.629	0.753	0.802	0.847	0.733
Cs		0.000	0.000	0.000	0.000	0.000	0.000	0.000	0.000	0.000	0.000	0.000
	Total	0.913	0.857	0.880	0.906	0.689	0.911	0.869	0.806	0.865	0.903	0.825
OH		1.992	1.984	2.000	2.000	1.969	1.999	1.981	1.996	1.981	1.985	1.984
F		0.007	0.016	0.000	0.000	0.030	0.000	0.018	0.003	0.018	0.012	0.016
Cl		0.001	0.000	0.000	0.000	0.001	0.001	0.001	0.001	0.000	0.003	0.000
O		0.000	0.000	0.000	0.000	0.000	0.000	0.000	0.000	0.000	0.000	0.000
	Total	2.000	2.000	2.000	2.000	2.000	2.000	2.000	2.000	2.000	2.000	2.000

White mica

Sector	*Albernoa*	*Albernoa*	*Albernoa*	*Albernoa*	*Albernoa*	*Albernoa*	*Albernoa*	*Albernoa*	*Albernoa*	*Albernoa*	*Albernoa*	*Albernoa*
Sub-sector												
Stratigraphic division	*PQG*	*PQG*	*PQG*	*PQG*	*PQG*	*PQG*	*PQG*	*PQG*	*upper VSC*			
Mineralization type	*No Sulph*	*No Sulph*	*No Sulph*	*No Sulph*	*No Sulph*	*No Sulph*	*No Sulph*	*No Sulph*	*No Sulph*			
Occurrence	*Early-formed*	*Early-formed*	*Early-formed*	*Early-formed*	*Early-formed*	*Early-formed*	*Early-formed*	*Early-formed*	*Early-formed*	*Early-formed*	*Early-formed*	*Early-formed*
Sample ref.	***X32***	***X32***	***X32***	***X32***	***X32***	***X32***	***X32***	***X32***	***EDS1-K***	***ABNSTR3***	***ABNSTR3***	***ABNSTR3***
Observations												
# analysis	***#23***	***#24***	***#25***	***#26***	***#27***	***#28***	***#29***	***#30***	***#31***	***#32***	***#33***	***#34***
SiO2	46.798	47.281	44.551	47.378	48.232	47.706	45.627	46.995	55.875	50.858	46.969	48.204
Al2O3	37.405	37.124	35.145	37.786	34.805	31.953	36.486	36.989	25.153	30.946	32.877	33.402
FeO	1.097	1.066	1.875	0.417	1.548	2.741	1.133	1.003	4.659	1.542	1.515	1.499
Fe2O3	0.000	0.000	0.000	0.000	0.000	0.000	0.000	0.000	0.000	0.000	0.000	0.000
MnO	0.019	0.000	0.000	0.015	0.016	0.000	0.023	0.000	0.516	0.024	0.000	0.020
MgO	0.489	0.570	0.819	0.314	0.868	1.141	0.731	0.485	2.042	0.700	0.810	0.795
CaO	0.073	0.118	0.159	0.078	0.096	0.064	0.147	0.132	0.054	0.102	0.111	0.260
Na2O	2.421	3.196	2.066	3.042	1.117	0.943	1.553	2.660	0.449	0.671	0.679	0.634
K2O	5.813	5.594	6.500	5.822	8.284	9.003	7.338	5.834	6.509	8.613	8.960	8.998
F	0.116	0.050	0.155	0.075	0.122	0.233	0.214	0.108	0.000	0.109	0.058	0.213
Cl	0.006	0.001	0.024	0.000	0.004	0.010	0.000	0.009	0.000	0.002	0.000	0.000
TiO2	0.241	0.098	3.074	0.154	0.548	0.532	0.114	0.343	0.099	1.210	0.238	1.481
Cr2O3	0.073	0.089	0.069	0.083	0.060	0.077	0.091	0.073	0.052	0.085	0.046	0.105
ZnO	0.000	0.000	0.000	0.000	0.000	0.000	0.000	0.000	0.000	0.000	0.000	0.000
Cs2O	0.000	0.000	0.000	0.000	0.000	0.000	0.000	0.000	0.000	0.000	0.000	0.000
BaO	0.109	0.157	0.106	0.121	0.197	0.168	0.114	0.079	0.096	0.159	0.187	0.193
SnO	0.000	0.000	0.000	0.000	0.000	0.000	0.000	0.000	0.000	0.000	0.000	0.000
Mn2O3	0.000	0.000	0.000	0.000	0.000	0.000	0.000	0.000	0.000	0.000	0.000	0.000
LiO2	0.000	0.000	0.000	0.000	0.000	0.000	0.000	0.000	0.000	0.000	0.000	0.000
H2O	4.523	4.584	4.420	4.585	4.521	4.346	4.382	4.526	4.593	4.500	4.375	4.450
Total#	99.183	99.928	98.963	99.870	100.418	98.917	97.953	99.236	100.097	99.521	96.825	100.254
O=F	-0.049	-0.021	-0.065	-0.032	-0.051	-0.098	-0.090	-0.045	0.000	-0.046	-0.024	-0.090
O=Cl	-0.001	0.000	-0.005	0.000	-0.001	-0.002	0.000	-0.002	0.000	0.000	0.000	0.000
Total	99.133	99.906	98.893	99.838	100.366	98.816	97.863	99.189	100.097	99.475	96.801	100.165

White mica

# analysis		*#23*	*#24*	*#25*	*#26*	*#27*	*#28*	*#29*	*#30*	*#31*	*#32*	*#33*	*#34*
Ion Distribution													
Group iv													
Si		3.064	3.077	2.968	3.075	3.157	3.208	3.051	3.077	3.648	3.350	3.199	3.176
Al		0.936	0.923	1.032	0.925	0.843	0.792	0.949	0.923	0.352	0.650	0.801	0.824
	Total	4.000	4.000	4.000	4.000	4.000	4.000	4.000	4.000	4.000	4.000	4.000	4.000
Group vi													
Cr		0.004	0.005	0.004	0.004	0.003	0.004	0.005	0.004	0.003	0.004	0.002	0.005
Al		1.950	1.924	1.728	1.964	1.843	1.741	1.927	1.931	1.583	1.752	1.838	1.769
Zn		0.000	0.000	0.000	0.000	0.000	0.000	0.000	0.000	0.000	0.000	0.000	0.000
Mn		0.001	0.000	0.000	0.001	0.001	0.000	0.001	0.000	0.029	0.001	0.000	0.001
Mg		0.048	0.055	0.081	0.030	0.085	0.114	0.073	0.047	0.199	0.069	0.082	0.078
Fe3+		0.000	0.000	0.000	0.000	0.000	0.000	0.000	0.000	0.000	0.000	0.000	0.000
Fe2+		0.060	0.058	0.104	0.023	0.085	0.154	0.063	0.055	0.254	0.085	0.086	0.083
Ti4		0.012	0.005	0.154	0.008	0.027	0.027	0.006	0.017	0.005	0.060	0.012	0.073
Sn		0.000	0.000	0.000	0.000	0.000	0.000	0.000	0.000	0.000	0.000	0.000	0.000
Mn		0.000	0.000	0.000	0.000	0.000	0.000	0.000	0.000	0.000	0.000	0.000	0.000
	Total	2.075	2.047	2.072	2.030	2.043	2.040	2.075	2.054	2.072	1.971	2.021	2.010
Group xii													
Ca		0.005	0.008	0.011	0.005	0.007	0.005	0.011	0.009	0.004	0.007	0.008	0.018
Ba		0.003	0.004	0.003	0.003	0.005	0.004	0.003	0.002	0.002	0.004	0.005	0.005
Na		0.307	0.403	0.267	0.383	0.142	0.123	0.201	0.338	0.057	0.086	0.090	0.081
K		0.486	0.464	0.553	0.482	0.692	0.772	0.626	0.487	0.542	0.724	0.778	0.756
Cs		0.000	0.000	0.000	0.000	0.000	0.000	0.000	0.000	0.000	0.000	0.000	0.000
	Total	0.801	0.880	0.834	0.873	0.845	0.904	0.841	0.836	0.605	0.821	0.881	0.861
OH		1.975	1.990	1.965	1.985	1.974	1.949	1.955	1.977	2.000	1.977	1.988	1.956
F		0.024	0.010	0.033	0.015	0.025	0.050	0.045	0.022	0.000	0.023	0.012	0.044
Cl		0.001	0.000	0.003	0.000	0.000	0.001	0.000	0.001	0.000	0.000	0.000	0.000
O		0.000	0.000	0.000	0.000	0.000	0.000	0.000	0.000	0.000	0.000	0.000	0.000
	Total	2.000	2.000	2.000	2.000	2.000	2.000	2.000	2.000	2.000	2.000	2.000	2.000

White mica

Sector	*Albernoa*	*Albernoa*	*Albernoa*	*Albernoa*	*Albernoa*	*Albernoa*	*Albernoa*	*Albernoa*	*Albernoa*	*Aljustrel*	*Aljustrel*	*Aljustrel*
Sub-sector										*Mina F*	*Mina F*	*Mina F*
Stratigraphic division		*upper VSC*	*upper VSC*	*upper VSC*	*upper VSC*	*upper VSC*	*upper VSC*	*upper VSC*	*upper VSC*	*upper VSC*	*upper VSC*	*upper VSC*
Mineralization type		*No Sulph*	*No Sulph*	*No Sulph*	*No Sulph*	*No Sulph*	*No Sulph*	*No Sulph*	*No Sulph*	*No Sulph*	*No Sulph*	*No Sulph*
Occurrence	*Early-formed*											
Sample ref.	*ABNSTR3*	*ALB03#22a*	*ALB03#22a*	*ALB03#13a*	*ALB03#13a*	*ALB03#22a*	*ALB03#22a*	*ALB03#22a*	*ALB03#22a*	*FFM#2*	*FFM#2*	*FFM#2*
Observations												
# analysis	*#35*	*#36*	*#37*	*#38*	*#39*	*#40*	*#41*	*#42*	*#43*	*#44*	*#45*	*#46*
SiO2	48.236	50.486	52.395	52.093	49.960	50.486	50.653	49.611	52.395	48.213	48.017	48.136
Al2O3	32.552	34.167	30.412	28.538	28.614	34.167	31.943	32.074	30.412	34.805	35.058	34.880
FeO	1.524	0.493	0.724	0.386	3.920	0.000	0.659	0.554	0.000	0.226	0.330	1.133
Fe2O3	0.000			3.906	0.000	0.548	0.000	0.120	0.805	1.074	1.979	0.000
MnO	0.000	0.015	0.000	0.113	0.083	0.000	0.035	0.030	0.000	0.055	0.000	0.000
MgO	0.753	0.821	1.933	2.014	1.828	0.821	1.582	1.567	1.933	0.938	0.980	0.947
CaO	0.114	0.310	0.006	0.062	0.032	0.310	0.042	0.032	0.006	0.050	0.085	0.047
Na2O	0.615	0.215	0.252	0.440	0.230	0.215	0.288	0.281	0.252	0.270	0.298	0.367
K2O	8.924	9.659	9.980	9.185	10.757	9.659	10.415	10.315	9.980	9.653	9.075	10.427
F	0.147	0.203	0.066	0.121	0.084	0.203	0.443	0.244	0.066	0.029	0.164	0.138
Cl	0.016	0.017	0.000	0.000	0.000	0.017	0.007	0.000	0.000	0.000	0.000	0.008
TiO2	1.381	0.002	0.049	0.013	0.022	0.002	0.034	0.109	0.049	0.059	0.045	0.010
Cr2O3	0.095	0.070	0.046	0.063	0.050	0.070	0.062	0.088	0.046	0.128	0.071	0.062
ZnO	0.000	0.000	0.000	0.000	0.000	0.000	0.000	0.000	0.000	0.000	0.000	0.000
Cs2O	0.000	0.000	0.000	0.017	0.000	0.000	0.000	0.000	0.000	0.000	0.000	0.000
BaO	0.100	0.140	0.046	0.115	0.101	0.140	0.104	0.117	0.046	0.214	0.249	0.235
SnO	0.000	0.000	0.000	0.000	0.000	0.000	0.000	0.000	0.000	0.000	0.000	0.000
Mn2O3	0.000	0.000	0.000	0.000	0.000	0.017	0.000	0.000	0.000	0.000	0.000	0.000
LiO2	0.000	0.000	0.000	0.181	0.000	0.156	0.000	0.443	0.145	0.239	0.102	0.000
H2O	4.425	4.530	4.570	4.556	4.423	4.544	4.359	4.422	4.580	4.561	4.512	4.498
Total#	98.882	101.128	100.479	101.803	100.104	101.354	100.626	100.007	100.715	100.514	100.964	100.888
O=F	-0.062	-0.086	-0.028	-0.051	-0.035	-0.086	-0.187	-0.103	-0.028	-0.012	-0.069	-0.058
O=Cl	-0.004	-0.004	0.000	0.000	0.000	-0.004	-0.002	0.000	0.000	0.000	0.000	-0.002
Total	98.817	101.038	100.451	101.752	100.069	101.265	100.438	99.905	100.687	100.502	100.895	100.828

White mica

# analysis		*#35*	*#36*	*#37*	*#38*	*#39*	*#40*	*#41*	*#42*	*#43*	*#44*	*#45*	*#46*
Ion Distribution													
Group iv													
Si		3.215	3.269	3.414	3.384	3.355	3.259	3.320	3.269	3.403	3.156	3.133	3.161
Al		0.785	0.731	0.586	0.616	0.645	0.741	0.680	0.731	0.597	0.844	0.867	0.839
	Total	4.000	4.000	4.000	4.000	4.000	4.000	4.000	4.000	4.000	4.000	4.000	4.000
Group vi													
Cr		0.005	0.004	0.002	0.003	0.003	0.004	0.003	0.005	0.002	0.007	0.004	0.003
Al		1.771	1.877	1.750	1.569	1.619	1.859	1.787	1.760	1.730	1.841	1.829	1.860
Zn		0.000	0.000	0.000	0.000	0.000	0.000	0.000	0.000	0.000	0.000	0.000	0.000
Mn		0.000	0.001	0.000	0.006	0.005	0.000	0.002	0.002	0.000	0.003	0.000	0.000
Mg		0.075	0.079	0.188	0.195	0.183	0.079	0.155	0.154	0.187	0.092	0.095	0.093
Fe3+		0.000	0.000	0.000	0.191	0.000	0.027	0.000	0.006	0.039	0.053	0.097	0.000
Fe2+		0.085	0.027	0.040	0.021	0.220	0.000	0.036	0.031	0.000	0.012	0.018	0.062
Ti4		0.069	0.000	0.002	0.001	0.001	0.000	0.002	0.005	0.002	0.003	0.002	0.001
Sn		0.000	0.000	0.000	0.000	0.000	0.000	0.000	0.000	0.000	0.000	0.000	0.000
Mn		0.000	0.000	0.000	0.000	0.000	0.001	0.000	0.000	0.000	0.000	0.000	0.000
	Total	2.005	1.987	1.982	2.034	2.031	2.009	1.985	2.080	2.000	2.073	2.072	2.019
Group xii													
Ca		0.008	0.022	0.000	0.004	0.002	0.021	0.003	0.002	0.000	0.004	0.006	0.003
Ba		0.003	0.004	0.001	0.003	0.003	0.004	0.003	0.003	0.001	0.006	0.006	0.006
Na		0.079	0.027	0.032	0.055	0.030	0.027	0.037	0.036	0.032	0.034	0.038	0.047
K		0.759	0.798	0.830	0.761	0.921	0.796	0.871	0.867	0.827	0.806	0.755	0.873
Cs		0.000	0.000	0.000	0.001	0.000	0.000	0.000	0.000	0.000	0.000	0.000	0.000
	Total	0.849	0.850	0.863	0.824	0.956	0.847	0.913	0.908	0.860	0.849	0.805	0.930
OH		1.967	1.957	1.986	1.975	1.981	1.957	1.906	1.944	1.984	1.991	1.964	1.970
F		0.031	0.002	0.000	0.000	0.000	0.002	0.001	0.000	0.000	0.000	0.000	0.001
Cl		0.002	0.042	0.014	0.025	0.018	0.041	0.092	0.051	0.014	0.006	0.034	0.029
O		0.000	0.000	0.000	0.001	0.001	0.000	0.002	0.005	0.002	0.003	0.002	0.001
	Total	2.000	2.000	2.000	2.000	2.000	2.000	2.000	2.000	2.000	2.000	2.000	2.000

White mica

Sector	*Aljustrel*	*Aljustrel*	*Aljustrel*	*Aljustrel*	*Aljustrel*	*Aljustrel*	*Aljustrel*	*Aljustrel*	*Aljustrel*	*Aljustrel*	*Aljustrel*	*Aljustrel*
Sub-sector	*Mina F*	*Mina F*	*Mina F*	*Mina F*	*Mina F*	*Mina F*	*Mina F*	*Mina F*	*Mina F*	*Mina F*	*Mina F*	*Mina F*
Stratigraphic division	*upper VSC*	*upper VSC*	*upper VSC*	*upper VSC*	*upper VSC*	*upper VSC*	*upper VSC*	*upper VSC*	*upper VSC*	*upper VSC*	*upper VSC*	*upper VSC*
Mineralization type	*No Sulph*	*No Sulph*	*No Sulph*	*No Sulph*	*No Sulph*	*No Sulph*	*No Sulph*	*No Sulph*	*No Sulph*	*No Sulph*	*No Sulph*	*Py-bearing*
Occurrence												
Sample ref.	*FFM#2*	*FFM#2*	*FFM#2*	*FFM#2*	*FFM#2*	*FFM#2*	*FFM#2*	*FFM#2*	*FFM#2*	*FFM#2*	*FFM#2*	*FM#5*
Observations												
# analysis	*#47*	*#48*	*#49*	*#50*	*#51*	*#52*	*#53*	*#54*	*#55*	*#56*	*#57*	*#58*
SiO2	48.426	48.466	47.527	48.416	48.229	47.830	48.361	48.083	48.228	47.241	48.471	49.272
Al2O3	35.297	35.225	34.966	34.913	34.347	34.432	35.232	35.040	33.050	35.280	32.323	32.151
FeO	0.090	1.038	1.070	1.090	1.176	1.645	0.797	1.114	0.784	1.030	1.492	0.000
Fe2O3	0.943	0.000	0.000	0.000	0.000	0.000	0.000	0.000	0.233	0.000	0.000	1.767
MnO	0.001	0.012	0.000	0.000	0.021	0.028	0.026	0.005	0.000	0.000	0.000	0.000
MgO	0.790	0.923	0.864	0.886	1.013	0.998	0.843	0.876	0.879	0.847	1.691	1.782
CaO	0.054	0.016	0.096	0.048	0.088	0.148	0.123	0.010	0.007	0.023	0.037	0.028
Na2O	0.320	0.284	0.789	0.348	0.316	0.399	0.352	0.321	0.403	0.303	0.416	0.147
K2O	9.918	10.252	9.925	10.316	10.358	10.032	10.030	10.550	10.619	10.650	10.881	9.550
F	0.099	0.026	0.130	0.000	0.158	0.000	0.000	0.028	0.065	0.130	0.000	0.525
Cl	0.007	0.008	0.000	0.007	0.009	0.000	0.000	0.000	0.004	0.000	0.001	0.000
TiO2	0.012	0.051	0.189	0.021	0.065	0.059	0.069	0.072	0.024	0.053	0.369	0.138
Cr2O3	0.081	0.087	0.126	0.055	0.069	0.110	0.063	0.102	0.028	0.109	0.069	0.073
ZnO	0.000	0.000	0.000	0.000	0.000	0.000	0.000	0.000	0.000	0.000	0.000	0.000
Cs2O	0.000	0.000	0.000	0.000	0.011	0.000	0.000	0.000	0.009	0.000	0.000	0.000
BaO	0.228	0.216	0.182	0.161	0.280	0.241	0.244	0.156	0.186	0.244	0.403	0.304
SnO	0.000	0.000	0.000	0.000	0.000	0.000	0.000	0.000	0.000	0.000	0.000	0.000
Mn2O3	0.000	0.000	0.000	0.000	0.000	0.000	0.000	0.000	0.000	0.000	0.000	0.008
LiO2	0.222	0.000	0.000	0.000	0.000	0.000	0.000	0.000	0.968	0.000	0.000	0.059
H2O	4.554	4.574	4.461	4.573	4.467	4.536	4.573	4.549	4.500	4.467	4.480	4.282
Total#	101.042	101.178	100.325	100.834	100.607	100.458	100.713	100.906	99.988	100.377	100.633	100.085
O=F	-0.042	-0.011	-0.055	0.000	-0.067	0.000	0.000	-0.012	-0.027	-0.055	0.000	-0.221
O=Cl	-0.002	-0.002	0.000	-0.002	-0.002	0.000	0.000	0.000	-0.001	0.000	0.000	0.000
Total	100.999	101.165	100.270	100.832	100.538	100.458	100.713	100.894	99.960	100.323	100.633	99.864

White mica

# analysis		*#47*	*#48*	*#49*	*#50*	*#51*	*#52*	*#53*	*#54*	*#55*	*#56*	*#57*	*#58*
Ion Distribution													
Group iv													
	Si	3.154	3.163	3.136	3.172	3.177	3.157	3.165	3.155	3.189	3.123	3.214	3.250
	Al	0.846	0.837	0.864	0.828	0.823	0.843	0.835	0.846	0.811	0.877	0.786	0.750
	Total	4.000	4.000	4.000	4.000	4.000	4.000	4.000	4.000	4.000	4.000	4.000	4.000
Group vi													
	Cr	0.004	0.005	0.007	0.003	0.004	0.006	0.003	0.005	0.002	0.006	0.004	0.004
	Al	1.863	1.873	1.856	1.868	1.844	1.836	1.883	1.864	1.764	1.873	1.740	1.749
	Zn	0.000	0.000	0.000	0.000	0.000	0.000	0.000	0.000	0.000	0.000	0.000	0.000
	Mn	0.000	0.001	0.000	0.000	0.001	0.002	0.001	0.000	0.000	0.000	0.000	0.000
	Mg	0.077	0.090	0.085	0.087	0.100	0.098	0.082	0.086	0.087	0.084	0.167	0.175
	Fe3+	0.046	0.000	0.000	0.000	0.000	0.000	0.000	0.000	0.012	0.000	0.000	0.088
	Fe2+	0.005	0.057	0.059	0.060	0.065	0.091	0.044	0.061	0.043	0.057	0.083	0.000
	Ti4	0.001	0.003	0.009	0.001	0.003	0.003	0.003	0.004	0.001	0.003	0.018	0.007
	Sn	0.000	0.000	0.000	0.000	0.000	0.000	0.000	0.000	0.000	0.000	0.000	0.000
	Mn	0.000	0.000	0.000	0.000	0.000	0.000	0.000	0.000	0.000	0.000	0.000	0.000
	Total	2.054	2.027	2.016	2.018	2.017	2.035	2.017	2.020	2.166	2.021	2.012	2.038
Group xii													
	Ca	0.004	0.001	0.007	0.003	0.006	0.011	0.009	0.001	0.001	0.002	0.003	0.002
	Ba	0.006	0.006	0.005	0.004	0.007	0.006	0.006	0.004	0.005	0.006	0.011	0.008
	Na	0.040	0.036	0.101	0.044	0.040	0.051	0.045	0.041	0.052	0.039	0.054	0.019
	K	0.824	0.854	0.836	0.862	0.871	0.845	0.837	0.883	0.896	0.898	0.920	0.804
	Cs	0.000	0.000	0.000	0.000	0.000	0.000	0.000	0.000	0.000	0.000	0.000	0.000
	Total	0.874	0.896	0.948	0.914	0.925	0.913	0.897	0.929	0.953	0.945	0.987	0.832
	OH	1.978	1.991	1.964	1.998	1.963	1.997	1.997	1.991	1.985	1.970	1.982	1.884
	F	0.001	0.001	0.000	0.001	0.001	0.000	0.000	0.000	0.000	0.000	0.000	0.000
	Cl	0.020	0.005	0.027	0.000	0.033	0.000	0.000	0.006	0.014	0.027	0.000	0.110
	O	0.001	0.003	0.009	0.001	0.003	0.003	0.003	0.004	0.001	0.003	0.018	0.007
		2.000	2.000	2.000	2.000	2.000	2.000	2.000	2.000	2.000	2.000	2.000	2.000

White mica

Sector	*Aljustrel*	*Aljustrel*	*Aljustrel*	*Aljustrel*	*Aljustrel*	*Aljustrel*	*Aljustrel*	*Aljustrel*	*Aljustrel*	*Aljustrel*	*Aljustrel*	*Aljustrel*
Sub-sector	*Mina F*	*Gavião*	*Gavião*	*Gavião*	*Gavião*	*Gavião*	*Gavião*	*Gavião*	*Gavião*	*Gavião*	*Mte Mesas*	*Mte Mesas*
Stratigraphic division	*upper VSC*	*upper VSC*	*upper VSC*	*upper VSC*	*upper VSC*	*upper VSC*	*upper VSC*	*upper VSC*	*upper VSC*	*upper VSC*	*upper VSC*	*upper VSC*
Mineralization type	*Py-bearing*	*Py-bearing*	*Py-bearing*	*Py-bearing*	*Py-bearing*	*Py-bearing*	*Py-bearing*	*Mineralized*	*Mineralized*	*Mineralized*	*Mineralized*	*Mineralized*
Occurrence												
Sample ref.	*FM#5*	*GV7#4*	*GV7#4*	*GV7#4*	*GV7#4*	*GV7#4*	*GV7#4*	*GV9#2*	*GV9#2*	*GV9#2*	*MDM02#4*	*MDM02#4*
Observations												
# analysis	*#59*	*#60*	*#61*	*#62*	*#63*	*#64*	*#65*	*#66*	*#67*	*#68*	*#69*	*#70*
SiO2	49.701	42.323	49.408	47.256	47.719	49.435	47.581	47.458	47.135	47.178	53.107	46.514
Al2O3	32.170	26.374	31.101	32.904	32.977	31.990	32.893	33.742	34.109	33.649	26.707	31.448
FeO	0.526	0.566	0.000	3.575	3.395	2.906	3.327	0.000	2.980	3.839	0.000	5.078
Fe2O3	1.216	6.912	3.541	0.000	0.000	0.000	0.000	3.722	0.000	0.000	4.441	0.000
MnO	0.001	1.387	0.000	0.057	0.034	0.108	0.043	0.000	0.047	0.118	0.004	0.015
MgO	1.800	6.801	1.487	0.986	1.083	1.460	1.113	0.711	0.701	0.796	1.194	1.399
CaO	0.024	0.081	0.032	0.042	0.051	0.085	0.066	0.037	0.005	0.014	0.552	0.026
Na2O	0.147	1.934	0.354	0.426	0.483	0.575	0.454	0.342	0.465	0.429	0.367	0.200
K2O	9.222	4.599	9.243	9.847	9.900	9.811	9.828	9.499	10.181	10.097	9.313	10.879
F	0.122	0.231	0.067	0.132	0.134	0.180	0.103	0.090	0.000	0.127	0.162	0.222
Cl	0.000	0.000	0.000	0.007	0.000	0.000	0.000	0.003	0.004	0.008	0.008	0.016
TiO2	0.163	0.072	0.021	0.229	0.184	0.066	0.181	0.252	0.074	0.149	0.165	0.377
Cr2O3	0.060	0.049	0.072	0.038	0.008	0.056	0.000	0.088	0.075	0.034	0.077	0.050
ZnO	0.000	0.068	0.000	0.000	0.000	0.000	0.000	0.000	0.000	0.000	0.000	0.000
Cs2O	0.000	0.000	0.000	0.000	0.000	0.000	0.000	0.000	0.000	0.000	0.007	0.000
BaO	0.333	0.174	0.150	0.289	0.194	0.158	0.280	0.140	0.196	0.187	0.242	0.399
SnO	0.000	0.000	0.000	0.000	0.000	0.000	0.000	0.000	0.000	0.000	0.000	0.000
Mn2O3	0.000	0.000	0.087	0.000	0.000	0.000	0.000	0.075	0.000	0.000	0.073	0.000
LiO2	0.208	2.596	0.241	0.000	0.000	0.000	0.000	0.000	0.000	0.000	0.659	0.000
H2O	4.493	4.277	4.519	4.390	4.423	4.466	4.425	4.474	4.498	4.432	4.506	4.285
Total#	100.185	98.445	100.322	100.178	100.585	101.296	100.294	100.633	100.470	101.057	101.584	100.908
O=F	-0.051	-0.097	-0.028	-0.056	-0.056	-0.076	-0.043	-0.038	0.000	-0.054	-0.068	-0.094
O=Cl	0.000	0.000	0.000	-0.002	0.000	0.000	0.000	-0.001	-0.001	-0.002	-0.002	-0.004
Total	100.134	98.347	100.294	100.120	100.528	101.220	100.251	100.594	100.469	101.002	101.514	100.811

White mica

# analysis		*#59*	*#60*	*#61*	*#62*	*#63*	*#64*	*#65*	*#66*	*#67*	*#68*	*#69*	*#70*
Ion Distribution													
Group iv													
Si		3.262	2.887	3.254	3.163	3.175	3.252	3.174	3.130	3.136	3.136	3.459	3.143
Al		0.739	1.113	0.746	0.837	0.826	0.748	0.826	0.870	0.864	0.864	0.541	0.857
	Total	4.000	4.000	4.000	4.000	4.000	4.000	4.000	4.000	4.000	4.000	4.000	4.000
Group vi													
Cr		0.003	0.003	0.004	0.002	0.000	0.003	0.000	0.005	0.004	0.002	0.004	0.003
Al		1.750	1.008	1.668	1.759	1.760	1.732	1.761	1.753	1.810	1.772	1.509	1.648
Zn		0.000	0.003	0.000	0.000	0.000	0.000	0.000	0.000	0.000	0.000	0.000	0.000
Mn		0.000	0.080	0.000	0.003	0.002	0.006	0.002	0.000	0.003	0.007	0.000	0.001
Mg		0.176	0.692	0.146	0.098	0.107	0.143	0.111	0.070	0.070	0.079	0.116	0.141
Fe3+		0.060	0.355	0.176	0.000	0.000	0.000	0.000	0.185	0.000	0.000	0.218	0.000
Fe2+		0.029	0.032	0.000	0.200	0.189	0.160	0.186	0.000	0.166	0.213	0.000	0.287
Ti4		0.008	0.004	0.001	0.012	0.009	0.003	0.009	0.013	0.004	0.008	0.008	0.019
Sn		0.000	0.000	0.000	0.000	0.000	0.000	0.000	0.000	0.000	0.000	0.000	0.000
Mn		0.000	0.000	0.004	0.000	0.000	0.000	0.000	0.004	0.000	0.000	0.004	0.000
	Total	2.081	2.889	2.062	2.074	2.068	2.047	2.068	2.028	2.056	2.080	2.031	2.099
Group xii													
Ca		0.002	0.006	0.002	0.003	0.004	0.006	0.005	0.003	0.000	0.001	0.039	0.002
Ba		0.009	0.005	0.004	0.008	0.005	0.004	0.007	0.004	0.005	0.005	0.006	0.011
Na		0.019	0.256	0.045	0.055	0.062	0.073	0.059	0.044	0.060	0.055	0.046	0.026
K		0.772	0.400	0.777	0.841	0.840	0.823	0.836	0.799	0.864	0.856	0.774	0.938
Cs		0.000	0.000	0.000	0.000	0.000	0.000	0.000	0.000	0.000	0.000	0.000	0.000
	Total	0.801	0.667	0.828	0.907	0.911	0.907	0.907	0.849	0.930	0.917	0.865	0.977
OH		1.967	1.947	1.985	1.960	1.963	1.959	1.969	1.968	1.996	1.965	1.958	1.932
F		0.000	0.000	0.000	0.001	0.000	0.000	0.000	0.000	0.001	0.001	0.001	0.002
Cl		0.025	0.050	0.014	0.028	0.028	0.037	0.022	0.019	0.000	0.027	0.033	0.047
O		0.008	0.004	0.001	0.012	0.009	0.003	0.009	0.013	0.004	0.008	0.008	0.019
		2.000	2.000	2.000	2.000	2.000	2.000	2.000	2.000	2.000	2.000	2.000	2.000

White mica

Sector	*Aljustrel*	*Aljustrel*	*Aljustrel*	*Aljustrel*	*Aljustrel*	*Aljustrel*	*Aljustrel*	*Aljustrel*	*Aljustrel*	*Aljustrel*	*Aljustrel*	*Aljustrel*
Sub-sector	*Mte Mesas*	*Mte Mesas*	*Mte Mesas*	*Mte Mesas*	*Mte Mesas*	*Mte Mesas*	*Mte Mesas*	*Mte Mesas*	*Mte Mesas*	*Mte Mesas*	*Mte Mesas*	*Mte Mesas*
Stratigraphic division	*upper VSC*	*upper VSC*	*upper VSC*	*upper VSC*	*upper VSC*	*upper VSC*	*upper VSC*	*upper VSC*	*upper VSC*	*upper VSC*	*upper VSC*	*upper VSC*
Mineralization type	*Mineralized*	*Mineralized*	*Mineralized*	*Mineralized*	*Mineralized*	*Mineralized*	*Mineralized*	*Mineralized*	*Mineralized*	*Mineralized*	*Mineralized*	*Mineralized*
Occurrence												
Sample ref.	*MDM02#4*	*MDM02#4*	*MDM02#4*	*MDM02#4*	*MDM02#4*	*MDM02#4*	*MDM02#4*	*MDM02#4*	*MDM02#4*	*MDM02#4*	*MDM02#4*	*MDM02#4*
Observations												
# analysis	*#71*	*#72*	*#73*	*#74*	*#75*	*#76*	*#77*	*#78*	*#79*	*#80*	*#81*	*#82*
SiO2	46.778	48.819	50.783	51.007	53.556	49.818	47.401	50.231	50.773	50.301	50.770	39.785
Al2O3	31.350	31.099	29.968	31.303	28.341	32.038	28.712	31.212	31.118	31.227	30.928	30.627
FeO	4.994	2.771	2.510	0.551	0.000	0.534	0.000	0.546	0.699	0.593	0.619	3.001
Fe2O3	0.000	0.000	0.000	0.000	0.503	0.000	4.873	0.000	0.000	0.000	0.000	0.000
MnO	0.081	0.056	0.010	0.000	0.000	0.044	0.000	0.032	0.000	0.019	0.014	0.000
MgO	1.426	1.776	1.492	2.729	2.354	2.418	6.756	2.763	2.759	2.599	2.668	9.844
CaO	0.011	0.025	0.012	0.023	0.046	0.006	0.022	0.019	0.034	0.023	0.012	0.004
Na2O	0.213	0.124	0.169	0.207	0.687	0.242	0.189	0.235	0.211	0.233	0.223	0.201
K2O	10.798	11.335	10.532	10.996	10.599	11.020	8.450	11.106	10.952	10.988	10.978	8.540
F	0.146	0.244	0.245	0.113	0.182	0.135	0.013	0.356	0.097	0.285	0.180	0.181
Cl	0.009	0.003	0.018	0.000	0.000	0.000	0.000	0.007	0.003	0.000	0.000	0.000
TiO2	0.373	0.281	0.640	0.010	0.010	0.000	0.022	0.013	0.034	0.000	0.027	0.023
Cr2O3	0.069	0.082	0.072	0.079	0.067	0.071	0.025	0.052	0.077	0.075	0.058	0.039
ZnO	0.000	0.000	0.000	0.000	0.000	0.000	0.000	0.000	0.000	0.000	0.000	0.000
Cs2O	0.000	0.000	0.000	0.004	0.000	0.000	0.050	0.003	0.000	0.006	0.028	0.000
BaO	0.418	0.158	0.156	0.210	0.184	0.252	0.134	0.222	0.166	0.234	0.120	0.135
SnO	0.000	0.000	0.000	0.000	0.000	0.000	0.000	0.000	0.000	0.000	0.000	0.000
Mn2O3	0.000	0.000	0.000	0.000	0.000	0.000	0.050	0.000	0.000	0.000	0.000	0.000
LiO2	0.000	0.000	0.000	0.000	0.453	0.000	0.440	0.000	0.000	0.000	0.000	2.411
H2O	4.333	4.363	4.349	4.560	4.542	4.510	4.565	4.400	4.547	4.434	4.494	4.314
Total#	100.999	101.136	100.956	101.792	101.524	101.088	101.702	101.197	101.470	101.017	101.119	99.106
O=F	-0.062	-0.103	-0.103	-0.048	-0.077	-0.057	-0.006	-0.150	-0.041	-0.120	-0.076	-0.076
O=Cl	-0.002	-0.001	-0.004	0.000	0.000	0.000	0.000	-0.002	-0.001	0.000	0.000	0.000
Total	100.935	101.032	100.849	101.745	101.448	101.031	101.697	101.046	101.429	100.897	101.043	99.029

White mica

# analysis		*#71*	*#72*	*#73*	*#74*	*#75*	*#76*	*#77*	*#78*	*#79*	*#80*	*#81*	*#82*
Ion Distribution													
Group iv													
Si		3.154	3.245	3.352	3.314	3.469	3.266	3.108	3.294	3.311	3.301	3.322	2.710
Al		0.846	0.755	0.648	0.686	0.531	0.735	0.893	0.706	0.689	0.699	0.678	1.291
	Total	4.000	4.000	4.000	4.000	4.000	4.000	4.000	4.000	4.000	4.000	4.000	4.000
Group vi													
Cr		0.004	0.004	0.004	0.004	0.003	0.004	0.001	0.003	0.004	0.004	0.003	0.002
Al		1.646	1.682	1.684	1.711	1.632	1.741	1.326	1.706	1.703	1.716	1.707	1.168
Zn		0.000	0.000	0.000	0.000	0.000	0.000	0.000	0.000	0.000	0.000	0.000	0.000
Mn		0.005	0.003	0.001	0.000	0.000	0.002	0.000	0.002	0.000	0.001	0.001	0.000
Mg		0.143	0.176	0.147	0.264	0.227	0.236	0.660	0.270	0.268	0.254	0.260	0.999
Fe3+		0.000	0.000	0.000	0.000	0.025	0.000	0.240	0.000	0.000	0.000	0.000	0.000
Fe2+		0.282	0.154	0.139	0.030	0.000	0.029	0.000	0.030	0.038	0.033	0.034	0.171
Ti4		0.019	0.014	0.032	0.001	0.001	0.000	0.001	0.001	0.002	0.000	0.001	0.001
Sn		0.000	0.000	0.000	0.000	0.000	0.000	0.000	0.000	0.000	0.000	0.000	0.000
Mn		0.000	0.000	0.000	0.000	0.000	0.000	0.003	0.000	0.000	0.000	0.000	0.000
	Total	2.098	2.033	2.005	2.010	2.006	2.012	2.348	2.012	2.015	2.007	2.007	3.002
Group xii													
Ca		0.001	0.002	0.001	0.002	0.003	0.000	0.002	0.001	0.002	0.002	0.001	0.000
Ba		0.011	0.004	0.004	0.005	0.005	0.007	0.003	0.006	0.004	0.006	0.003	0.004
Na		0.028	0.016	0.022	0.026	0.086	0.031	0.024	0.030	0.027	0.030	0.028	0.027
K		0.929	0.961	0.887	0.911	0.876	0.922	0.707	0.929	0.911	0.920	0.916	0.742
Cs		0.000	0.000	0.000	0.000	0.000	0.000	0.001	0.000	0.000	0.000	0.001	0.000
	Total	0.969	0.983	0.913	0.945	0.970	0.959	0.737	0.966	0.944	0.957	0.949	0.772
OH		1.949	1.934	1.915	1.976	1.962	1.972	1.996	1.925	1.978	1.941	1.961	1.960
F		0.001	0.000	0.002	0.000	0.000	0.000	0.000	0.001	0.000	0.000	0.000	0.000
Cl		0.031	0.051	0.051	0.023	0.037	0.028	0.003	0.074	0.020	0.059	0.037	0.039
O		0.019	0.014	0.032	0.001	0.001	0.000	0.001	0.001	0.002	0.000	0.001	0.001
		2.000	2.000	2.000	2.000	2.000	2.000	2.000	2.000	2.000	2.000	2.000	2.000

White mica

Sector	*Aljustrel*	*Aljustrel*	*Aljustrel*	*Aljustrel*	*Aljustrel*	*Aljustrel*	*Aljustrel*	*Aljustrel*	*Aljustrel*	*Aljustrel*	*Aljustrel*	*Aljustrel*
Sub-sector	*Mte Mesas*	*Mte Mesas*	*Mte Mesas*	*Mina M*	*Mina M*	*Mina M*	*Mina M*	*Mina M*	*Mina M*	*Mina M*	*Mina M*	*Mina M*
Stratigraphic division	*upper VSC*	*upper VSC*	*upper VSC*	*upper VSC*	*upper VSC*	*upper VSC*	*upper VSC*	*upper VSC*	*upper VSC*	*upper VSC*	*upper VSC*	*upper VSC*
Mineralization type	*Mineralized*	*Mineralized*	*Mineralized*	*Mineralized*	*Mineralized*	*Mineralized*	*Mineralized*	*Mineralized*	*Mineralized*	*Mineralized*	*Mineralized*	*Mineralized*
Occurrence												
Sample ref.	*MDM02#4*	*MDM02#4*	*MDM02#4*	*MFM#3*	*MFM#3*	*MFM#3*	*MFM#3*	*MFM#3*	*MFM#3*	*MFM#3*	*MFM#3*	*MFM#3*
Observations												
# analysis	*#83*	*#84*	*#85*	*#86*	*#87*	*#88*	*#89*	*#90*	*#91*	*#92*	*#93*	*#94*
SiO2	50.166	50.480	50.864	47.297	46.254	47.647	46.695	47.089	47.585	46.019	48.293	49.778
Al2O3	31.538	30.537	30.783	35.723	35.595	34.540	34.710	34.583	35.043	35.845	36.020	33.799
FeO	0.541	0.619	0.578	0.000	0.423	0.603	0.453	0.561	0.404	0.350	0.000	0.000
Fe2O3	0.000	0.000	0.000	0.665	0.000	0.000	0.000	0.011	0.000	0.000	0.497	0.629
MnO	0.000	0.000	0.000	0.000	0.000	0.015	0.000	0.002	0.000	0.021	0.000	0.000
MgO	2.406	2.619	2.601	1.079	0.968	1.003	1.021	1.181	0.999	0.995	1.103	1.004
CaO	0.026	0.020	0.027	0.048	0.025	0.040	0.049	0.018	0.083	0.113	0.029	0.083
Na2O	0.287	0.514	0.216	0.508	0.767	0.739	0.628	0.701	0.691	0.550	0.421	0.565
K2O	11.052	10.846	11.106	8.926	9.302	9.163	9.484	9.602	9.010	9.078	8.779	8.887
F	0.117	0.307	0.104	0.203	0.195	0.305	0.045	0.316	0.287	0.294	0.227	0.211
Cl	0.000	0.006	0.016	0.017	0.000	0.008	0.000	0.000	0.011	0.001	0.011	0.000
TiO2	0.000	0.010	0.000	0.114	0.100	0.285	0.086	0.122	0.105	0.451	0.216	0.274
Cr2O3	0.082	0.071	0.055	0.061	0.041	0.057	0.079	0.041	0.027	0.066	0.035	0.033
ZnO	0.000	0.000	0.000	0.000	0.000	0.000	0.000	0.000	0.000	0.000	0.000	0.000
Cs2O	0.000	0.000	0.044	0.021	0.000	0.000	0.002	0.000	0.000	0.000	0.000	0.000
BaO	0.214	0.184	0.168	0.975	1.030	0.994	0.903	0.799	1.015	1.142	1.053	0.857
SnO	0.000	0.000	0.000	0.000	0.000	0.000	0.000	0.000	0.000	0.000	0.000	0.000
Mn2O3	0.000	0.000	0.000	0.000	0.000	0.000	0.000	0.000	0.000	0.000	0.033	0.023
LiO2	0.000	0.000	0.000	0.286	0.839	0.000	1.269	0.622	0.329	0.737	0.174	0.168
H2O	4.515	4.403	4.525	4.452	4.426	4.339	4.506	4.365	4.392	4.339	4.488	4.472
Total#	100.944	100.616	101.087	100.375	99.966	99.738	99.930	100.012	99.981	100.001	101.379	100.783
O=F	-0.049	-0.129	-0.044	-0.086	-0.082	-0.128	-0.019	-0.133	-0.121	-0.124	-0.096	-0.089
O=Cl	0.000	-0.001	-0.004	-0.004	0.000	-0.002	0.000	0.000	-0.003	0.000	-0.003	0.000
Total	100.894	100.485	101.040	100.285	99.883	99.608	99.911	99.879	99.858	99.877	101.281	100.695

White mica

# analysis		*#83*	*#84*	*#85*	*#86*	*#87*	*#88*	*#89*	*#90*	*#91*	*#92*	*#93*	*#94*
Ion Distribution													
Group iv													
	Si	3.291	3.326	3.331	3.106	3.062	3.162	3.086	3.118	3.141	3.047	3.132	3.243
	Al	0.709	0.674	0.669	0.894	0.938	0.838	0.914	0.882	0.859	0.954	0.868	0.758
	Total	4.000	4.000	4.000	4.000	4.000	4.000	4.000	4.000	4.000	4.000	4.000	4.000
Group vi													
	Cr	0.004	0.004	0.003	0.003	0.002	0.003	0.004	0.002	0.001	0.004	0.002	0.002
	Al	1.730	1.697	1.707	1.871	1.838	1.864	1.789	1.817	1.867	1.843	1.886	1.837
	Zn	0.000	0.000	0.000	0.000	0.000	0.000	0.000	0.000	0.000	0.000	0.000	0.000
	Mn	0.000	0.000	0.000	0.000	0.000	0.001	0.000	0.000	0.000	0.001	0.000	0.000
	Mg	0.235	0.257	0.254	0.106	0.096	0.099	0.101	0.117	0.098	0.098	0.107	0.098
	Fe3+	0.000	0.000	0.000	0.033	0.000	0.000	0.000	0.001	0.000	0.000	0.024	0.031
	Fe2+	0.030	0.034	0.032	0.000	0.023	0.034	0.025	0.031	0.022	0.019	0.000	0.000
	Ti4	0.000	0.001	0.000	0.006	0.005	0.014	0.004	0.006	0.005	0.023	0.011	0.013
	Sn	0.000	0.000	0.000	0.000	0.000	0.000	0.000	0.000	0.000	0.000	0.000	0.000
	Mn	0.000	0.000	0.000	0.000	0.000	0.000	0.000	0.000	0.000	0.000	0.002	0.001
	Total	1.999	1.992	1.995	2.094	2.188	2.014	2.260	2.139	2.081	2.184	2.076	2.026
Group xii													
	Ca	0.002	0.001	0.002	0.003	0.002	0.003	0.004	0.001	0.006	0.008	0.002	0.006
	Ba	0.006	0.005	0.004	0.025	0.027	0.026	0.023	0.021	0.026	0.030	0.027	0.022
	Na	0.037	0.066	0.027	0.065	0.098	0.095	0.081	0.090	0.088	0.071	0.053	0.071
	K	0.925	0.912	0.928	0.748	0.786	0.776	0.800	0.811	0.759	0.767	0.726	0.739
	Cs	0.000	0.000	0.001	0.001	0.000	0.000	0.000	0.000	0.000	0.000	0.000	0.000
	Total	0.969	0.983	0.963	0.842	0.912	0.900	0.907	0.923	0.879	0.875	0.808	0.838
	OH	1.976	1.935	1.977	1.950	1.954	1.921	1.986	1.928	1.934	1.916	1.942	1.943
	F	0.000	0.001	0.002	0.002	0.000	0.001	0.000	0.000	0.001	0.000	0.001	0.000
	Cl	0.024	0.064	0.022	0.042	0.041	0.064	0.009	0.066	0.060	0.062	0.047	0.044
	O	0.000	0.001	0.000	0.006	0.005	0.014	0.004	0.006	0.005	0.023	0.011	0.013
		2.000	2.000	2.000	2.000	2.000	2.000	2.000	2.000	2.000	2.000	2.000	2.000

White mica

Sector	*Aljustrel*	*Aljustrel*	*Aljustrel*	*Aljustrel*	*Aljustrel*	*Aljustrel*	*Aljustrel*	*Aljustrel*	*Aljustrel*	*Aljustrel*	*Aljustrel*	*Aljustrel*
Sub-sector	*Mina M*	*Mina M*	*Mina M*	*Mina M*	*Mina M*	*Mina M*	*Mina M*	*Mina M*	*Mina M*	*Mina M*	*Mina M*	*Mina M*
Stratigraphic division	*upper VSC*	*upper VSC*	*upper VSC*	*upper VSC*	*upper VSC*	*upper VSC*	*upper VSC*	*upper VSC*	*upper VSC*	*upper VSC*	*upper VSC*	*upper VSC*
Mineralization type	*Mineralized*	*Mineralized*	*Mineralized*	*Mineralized*	*Mineralized*	*Mineralized*	*Mineralized*	*Mineralized*	*Mineralized*	*Mineralized*	*Mineralized*	*Mineralized*
Occurrence												
Sample ref.	*MFM#3*	*MFM#3*	*MFM#3*	*MFM#3*	*MFM#3*	*MFM#3*	*MFM#3*	*MFM#3*	*MFM#3*	*MFM#3*	*MFM#3*	*MFM#3*
Observations												
# analysis	*#95*	*#96*	*#97*	*#98*	*#99*	*#100*	*#101*	*#102*	*#103*	*#104*	*#105*	*#106*
SiO2	48.087	47.162	47.257	47.352	47.276	47.084	46.281	46.444	46.379	47.746	48.351	48.177
Al2O3	35.400	35.534	35.199	35.469	34.651	34.474	34.162	34.326	33.720	34.365	32.428	34.210
FeO	0.000	0.435	0.364	0.416	0.565	0.501	0.577	0.491	2.258	0.468	0.350	0.000
Fe2O3	0.496	0.000	0.000	0.000	0.000	0.000	0.058	0.000	0.489	0.000	0.134	0.515
MnO	0.000	0.000	0.040	0.003	0.001	0.000	0.004	0.000	0.000	0.024	0.000	0.000
MgO	1.001	0.986	0.933	1.027	0.985	1.008	0.919	0.963	1.028	0.946	0.946	1.025
CaO	0.090	0.050	0.044	0.074	0.094	0.123	0.094	0.089	0.101	0.156	0.165	0.112
Na2O	0.624	0.659	0.722	0.617	0.653	0.639	0.821	0.604	0.672	0.646	0.767	0.678
K2O	9.155	9.313	9.550	9.265	9.333	9.242	8.875	9.062	8.953	8.810	8.411	8.941
F	0.247	0.140	0.351	0.451	0.305	0.278	0.196	0.317	0.302	0.221	0.264	0.381
Cl	0.008	0.000	0.007	0.002	0.000	0.000	0.014	0.000	0.017	0.007	0.005	0.000
TiO2	0.120	0.102	0.318	0.383	0.391	0.488	2.026	1.947	0.098	0.923	3.051	1.294
Cr2O3	0.034	0.085	0.064	0.040	0.061	0.044	0.070	0.031	0.050	0.032	0.054	0.011
ZnO	0.000	0.000	0.000	0.000	0.000	0.000	0.000	0.000	0.000	0.000	0.000	0.000
Cs2O	0.000	0.008	0.000	0.000	0.000	0.000	0.000	0.000	0.000	0.000	0.000	0.000
BaO	0.963	0.960	0.994	1.113	1.023	0.937	0.900	1.047	0.866	1.075	0.893	0.835
SnO	0.000	0.000	0.000	0.000	0.000	0.000	0.000	0.000	0.000	0.000	0.000	0.000
Mn2O3	0.029	0.000	0.000	0.000	0.000	0.000	0.000	0.000	0.000	0.000	0.000	0.021
LiO2	0.171	0.000	0.000	0.000	0.000	0.840	0.800	0.541	0.885	0.205	0.124	0.170
H2O	4.454	4.452	4.324	4.289	4.318	4.347	4.193	4.144	4.342	4.325	4.062	4.242
Total#	100.879	99.886	100.167	100.501	99.656	100.006	99.990	100.006	100.159	99.949	100.004	100.611
O=F	-0.104	-0.059	-0.148	-0.190	-0.128	-0.117	-0.083	-0.134	-0.127	-0.093	-0.111	-0.160
O=Cl	-0.002	0.000	-0.002	-0.001	0.000	0.000	-0.003	0.000	-0.004	-0.002	-0.001	0.000
Total	100.773	99.828	100.018	100.311	99.528	99.889	99.904	99.873	100.028	99.854	99.892	100.451

White mica

# analysis		*#95*	*#96*	*#97*	*#98*	*#99*	*#100*	*#101*	*#102*	*#103*	*#104*	*#105*	*#106*
Ion Distribution													
Group iv													
Si		3.143	3.121	3.129	3.123	3.145	3.114	3.071	3.085	3.090	3.156	3.199	3.162
Al		0.857	0.879	0.871	0.877	0.855	0.886	0.929	0.915	0.910	0.844	0.801	0.838
	Total	4.000	4.000	4.000	4.000	4.000	4.000	4.000	4.000	4.000	4.000	4.000	4.000
Group vi													
Cr		0.002	0.004	0.003	0.002	0.003	0.002	0.004	0.002	0.003	0.002	0.003	0.001
Al		1.871	1.893	1.876	1.880	1.862	1.801	1.743	1.772	1.738	1.834	1.727	1.809
Zn		0.000	0.000	0.000	0.000	0.000	0.000	0.000	0.000	0.000	0.000	0.000	0.000
Mn		0.000	0.000	0.002	0.000	0.000	0.000	0.000	0.000	0.000	0.001	0.000	0.000
Mg		0.098	0.097	0.092	0.101	0.098	0.099	0.091	0.095	0.102	0.093	0.093	0.100
Fe3+		0.024	0.000	0.000	0.000	0.000	0.000	0.003	0.000	0.025	0.000	0.007	0.025
Fe2+		0.000	0.024	0.020	0.023	0.031	0.028	0.032	0.027	0.126	0.026	0.019	0.000
Ti4		0.006	0.005	0.016	0.019	0.020	0.024	0.101	0.097	0.005	0.046	0.152	0.064
Sn		0.000	0.000	0.000	0.000	0.000	0.000	0.000	0.000	0.000	0.000	0.000	0.000
Mn		0.001	0.000	0.000	0.000	0.000	0.000	0.000	0.000	0.000	0.000	0.000	0.001
	Total	2.047	2.024	2.009	2.025	2.014	2.178	2.187	2.138	2.235	2.057	2.034	2.045
Group xii													
Ca		0.006	0.004	0.003	0.005	0.007	0.009	0.007	0.006	0.007	0.011	0.012	0.008
Ba		0.025	0.025	0.026	0.029	0.027	0.024	0.023	0.027	0.023	0.028	0.023	0.022
Na		0.079	0.085	0.093	0.079	0.084	0.082	0.106	0.078	0.087	0.083	0.098	0.086
K		0.763	0.786	0.807	0.780	0.792	0.780	0.751	0.768	0.761	0.743	0.710	0.749
Cs		0.000	0.000	0.000	0.000	0.000	0.000	0.000	0.000	0.000	0.000	0.000	0.000
	Total	0.874	0.900	0.928	0.892	0.910	0.895	0.887	0.879	0.878	0.865	0.843	0.864
OH		1.942	1.966	1.910	1.887	1.916	1.918	1.856	1.836	1.930	1.907	1.792	1.857
F		0.001	0.000	0.001	0.000	0.000	0.000	0.002	0.000	0.002	0.001	0.001	0.000
Cl		0.051	0.029	0.074	0.094	0.064	0.058	0.041	0.067	0.064	0.046	0.055	0.079
O		0.006	0.005	0.016	0.019	0.020	0.024	0.101	0.097	0.005	0.046	0.152	0.064
		2.000	2.000	2.000	2.000	2.000	2.000	2.000	2.000	2.000	2.000	2.000	2.000

White mica

Sector	*Aljustrel*	*Aljustrel*	*Aljustrel*	*Aljustrel*	*Aljustrel*	*Aljustrel*	*Aljustrel*	*Aljustrel*	*Aljustrel*	*Aljustrel*	*Aljustrel*	*Aljustrel*
Sub-sector	*Mina M*	*Mina M*	*Mina M*	*Mina M*	*Mina M*	*Mina M*	*Mina M*	*Mina M*	*Mina M*	*Mina M*	*Mina M*	*Mina M*
Stratigraphic division	*upper VSC*	*upper VSC*	*upper VSC*	*upper VSC*	*upper VSC*	*upper VSC*	*upper VSC*	*upper VSC*	*upper VSC*	*upper VSC*	*upper VSC*	*upper VSC*
Mineralization type	*Mineralized*	*Mineralized*	*Mineralized*	*Mineralized*	*Mineralized*	*Mineralized*	*Mineralized*	*Mineralized*	*Mineralized*	*Mineralized*	*Mineralized*	*Mineralized*
Occurrence												
Sample ref.	*MFM#3*	*MFM#3*	*MFM#3*	*MFM#3*	*MFM#3*	*MM16#9*	*MM16#9*	*MM16#9*	*MM16#9*	*MM16#9*	*MM16#9*	*MM16#9*
Observations												
# analysis	*#107*	*#108*	*#109*	*#110*	*#111*	*#112*	*#113*	*#114*	*#115*	*#116*	*#117*	*#118*
SiO2	56.429	59.210	49.016	47.876	46.155	48.259	48.617	48.746	48.393	49.168	48.389	48.651
Al2O3	28.745	26.232	32.492	34.817	33.250	33.714	33.724	32.935	32.560	31.959	33.550	33.296
FeO	0.420	0.535	0.508	0.460	1.741	1.402	1.174	1.293	1.744	1.516	1.302	1.034
Fe2O3	0.000	0.000	0.000	0.000	0.341	0.000	0.000	0.000	0.000	0.000	0.000	0.000
MnO	0.000	0.033	0.019	0.015	0.020	0.116	0.110	0.099	0.177	0.091	0.096	0.077
MgO	0.865	0.937	1.099	1.023	1.010	1.217	1.281	1.326	1.585	1.626	1.271	1.215
CaO	0.119	0.066	0.095	0.122	0.088	0.036	0.035	0.045	0.031	0.111	0.014	0.043
Na2O	0.502	0.396	0.559	0.593	0.603	0.269	0.289	0.213	0.163	0.351	0.340	0.295
K2O	7.849	7.134	8.646	9.228	9.140	10.215	10.365	11.064	11.125	10.448	10.614	10.427
F	0.278	0.215	0.224	0.342	0.222	0.092	0.101	0.119	0.156	0.176	0.120	0.043
Cl	0.019	0.016	0.000	0.007	0.004	0.000	0.005	0.000	0.000	0.011	0.000	0.001
TiO2	0.040	0.082	0.491	0.095	1.371	0.197	0.174	0.289	0.250	0.177	0.032	0.249
Cr2O3	0.043	0.052	0.072	0.049	0.051	0.059	0.039	0.041	0.067	0.045	0.081	0.082
ZnO	0.000	0.000	0.000	0.000	0.000	0.000	0.000	0.000	0.000	0.000	0.000	0.000
Cs2O	0.000	0.002	0.000	0.000	0.000	0.000	0.000	0.000	0.000	0.000	0.000	0.000
BaO	0.749	0.769	0.966	0.859	0.863	0.251	0.242	0.208	0.180	0.228	0.262	0.234
SnO	0.000	0.000	0.000	0.000	0.000	0.000	0.000	0.000	0.000	0.000	0.000	0.000
Mn2O3	0.000	0.000	0.000	0.000	0.000	0.000	0.000	0.000	0.000	0.000	0.000	0.000
LiO2	0.772	0.897	1.430	0.000	1.001	0.000	0.000	0.000	0.000	0.000	0.000	0.000
H2O	4.571	4.626	4.407	4.359	4.235	4.470	4.486	4.453	4.424	4.421	4.478	4.486
Total#	101.402	101.202	100.024	99.845	100.094	100.297	100.642	100.831	100.855	100.328	100.549	100.133
O=F	-0.117	-0.091	-0.094	-0.144	-0.094	-0.039	-0.043	-0.050	-0.066	-0.074	-0.051	-0.018
O=Cl	-0.004	-0.004	0.000	-0.002	-0.001	0.000	-0.001	0.000	0.000	-0.003	0.000	0.000
Total	101.280	101.108	99.930	99.699	100.000	100.258	100.598	100.781	100.789	100.251	100.499	100.115

White mica

# analysis		*#107*	*#108*	*#109*	*#110*	*#111*	*#112*	*#113*	*#114*	*#115*	*#116*	*#117*	*#118*
Ion Distribution													
Group iv													
Si		3.591	3.745	3.217	3.166	3.079	3.190	3.200	3.218	3.206	3.257	3.197	3.217
Al		0.410	0.255	0.783	0.834	0.922	0.810	0.800	0.782	0.794	0.743	0.803	0.783
	Total	4.000	4.000	4.000	4.000	4.000	4.000	4.000	4.000	4.000	4.000	4.000	4.000
Group vi													
Cr		0.002	0.003	0.004	0.003	0.003	0.003	0.002	0.002	0.004	0.002	0.004	0.004
Al		1.746	1.700	1.730	1.880	1.692	1.817	1.817	1.781	1.748	1.752	1.809	1.812
Zn		0.000	0.000	0.000	0.000	0.000	0.000	0.000	0.000	0.000	0.000	0.000	0.000
Mn		0.000	0.002	0.001	0.001	0.001	0.007	0.006	0.006	0.010	0.005	0.005	0.004
Mg		0.082	0.088	0.108	0.101	0.100	0.120	0.126	0.131	0.157	0.161	0.125	0.120
Fe3+		0.000	0.000	0.000	0.000	0.017	0.000	0.000	0.000	0.000	0.000	0.000	0.000
Fe2+		0.022	0.028	0.028	0.025	0.097	0.078	0.065	0.071	0.097	0.084	0.072	0.057
Ti4		0.002	0.004	0.024	0.005	0.069	0.010	0.009	0.014	0.013	0.009	0.002	0.012
Sn		0.000	0.000	0.000	0.000	0.000	0.000	0.000	0.000	0.000	0.000	0.000	0.000
Mn		0.000	0.000	0.000	0.000	0.000	0.000	0.000	0.000	0.000	0.000	0.000	0.000
	Total	2.052	2.053	2.272	2.015	2.248	2.033	2.024	2.004	2.027	2.013	2.017	2.010
Group xii													
Ca		0.008	0.005	0.007	0.009	0.006	0.003	0.003	0.003	0.002	0.008	0.001	0.003
Ba		0.019	0.019	0.025	0.022	0.023	0.007	0.006	0.005	0.005	0.006	0.007	0.006
Na		0.062	0.049	0.071	0.076	0.078	0.035	0.037	0.027	0.021	0.045	0.044	0.038
K		0.637	0.576	0.724	0.779	0.778	0.861	0.870	0.932	0.940	0.883	0.895	0.880
Cs		0.000	0.000	0.000	0.000	0.000	0.000	0.000	0.000	0.000	0.000	0.000	0.000
	Total	0.726	0.648	0.827	0.886	0.885	0.905	0.916	0.968	0.968	0.942	0.946	0.927
OH		1.940	1.951	1.929	1.923	1.884	1.971	1.970	1.961	1.955	1.953	1.973	1.979
F		0.002	0.002	0.000	0.001	0.001	0.000	0.001	0.000	0.000	0.001	0.000	0.000
Cl		0.056	0.043	0.047	0.072	0.047	0.019	0.021	0.025	0.033	0.037	0.025	0.009
O		0.002	0.004	0.024	0.005	0.069	0.010	0.009	0.014	0.013	0.009	0.002	0.012
		2.000	2.000	2.000	2.000	2.000	2.000	2.000	2.000	2.000	2.000	2.000	2.000

White mica

Sector	*Aljustrel*	*Aljustrel*	*Aljustrel*	*Aljustrel*	*Aljustrel*	*Aljustrel*	*Aljustrel*	*Aljustrel*	*Aljustrel*	*Aljustrel*	*Aljustrel*	*Aljustrel*
Sub-sector	*Mina M*	*Mina M*	*Mina M*	*Mina M*	*Mina M*	*Mina M*	*Mina M*	*Mina M*	*Mina M*	*Gavião*	*Gavião*	*Gavião*
Stratigraphic division	*upper VSC*	*upper VSC*	*upper VSC*	*upper VSC*	*upper VSC*	*upper VSC*	*upper VSC*	*upper VSC*	*upper VSC*	*upper VSC*	*upper VSC*	*upper VSC*
Mineralization type	*Mineralized*	*Mineralized*	*Mineralized*	*Mineralized*	*Mineralized*	*Mineralized*	*Mineralized*	*Mineralized*	*Mineralized*	*Mineralized*	*Mineralized*	*Mineralized*
Occurrence												
Sample ref.	*MM16#9*	*MM16#9*	*MM16#9*	*MM16#9*	*MM16#9*	*MM16#9*	*MM16#9*	*MM16#9*	*MM16#9*	*GV7#3*	*GV7#3*	*GV7#3*
Observations												
# analysis	*#119*	*#120*	*#121*	*#122*	*#123*	*#124*	*#125*	*#126*	*#127*	*#128*	*#129*	*#130*
SiO2	47.327	46.506	48.086	49.160	49.106	48.317	48.692	48.519	47.715	48.519	46.864	58.484
Al2O3	34.033	32.532	33.114	31.366	34.212	34.343	32.844	32.651	34.186	34.573	32.684	26.569
FeO	0.473	3.375	1.328	2.271	0.184	0.853	1.299	1.242	0.986	0.609	0.000	0.652
Fe2O3	0.586	0.000	0.000	0.000	1.142	0.000	0.000	0.000	0.000	0.528	1.087	0.000
MnO	0.092	0.227	0.044	0.141	0.108	0.103	0.074	0.048	0.058	0.004	0.000	0.025
MgO	1.188	1.866	1.463	1.675	1.487	1.026	1.413	1.425	1.160	0.631	0.647	0.525
CaO	0.000	0.085	0.031	0.094	0.037	0.030	0.065	0.000	0.028	0.073	0.003	0.003
Na2O	0.334	0.272	0.189	0.232	0.223	0.406	0.277	0.178	0.391	0.800	0.603	0.327
K2O	10.447	10.577	10.735	10.139	9.739	10.533	10.885	11.242	10.622	8.936	9.324	8.052
F	0.197	0.139	0.140	0.055	0.239	0.064	0.221	0.379	0.251	0.175	0.244	0.186
Cl	0.007	0.000	0.006	0.006	0.008	0.000	0.007	0.000	0.000	0.003	0.000	0.000
TiO2	0.178	0.273	0.218	0.142	0.126	0.056	0.221	0.257	0.130	0.241	1.182	0.147
Cr2O3	0.045	0.065	0.096	0.103	0.052	0.074	0.044	0.099	0.067	0.061	0.093	0.063
ZnO	0.000	0.000	0.000	0.000	0.000	0.000	0.000	0.000	0.000	0.000	0.000	0.000
Cs2O	0.000	0.000	0.000	0.000	0.000	0.037	0.000	0.000	0.000	0.000	0.000	0.000
BaO	0.217	0.211	0.329	0.215	0.202	0.187	0.245	0.254	0.246	0.164	0.247	0.177
SnO	0.000	0.000	0.000	0.000	0.000	0.000	0.000	0.000	0.000	0.000	0.000	0.000
Mn2O3	0.000	0.000	0.000	0.000	0.000	0.000	0.000	0.000	0.000	0.000	0.002	0.000
LiO2	0.572	0.000	0.000	0.000	0.244	0.000	0.000	0.000	0.000	0.278	2.735	1.026
H2O	4.415	4.371	4.421	4.466	4.496	4.517	4.404	4.311	4.390	4.461	4.311	4.614
Total#	100.111	100.499	100.200	100.065	101.605	100.546	100.691	100.605	100.230	100.056	100.025	100.850
O=F	-0.083	-0.059	-0.059	-0.023	-0.101	-0.027	-0.093	-0.160	-0.106	-0.074	-0.103	-0.078
O=Cl	-0.002	0.000	-0.001	-0.001	-0.002	0.000	-0.002	0.000	0.000	-0.001	0.000	0.000
Total	100.026	100.440	100.140	100.041	101.502	100.519	100.596	100.445	100.125	99.982	99.922	100.771

White mica

# analysis		*#119*	*#120*	*#121*	*#122*	*#123*	*#124*	*#125*	*#126*	*#127*	*#128*	*#129*	*#130*
Ion Distribution													
Group iv													
Si		3.132	3.121	3.194	3.269	3.183	3.182	3.219	3.219	3.162	3.182	3.082	3.716
Al		0.868	0.879	0.806	0.732	0.817	0.819	0.781	0.781	0.838	0.818	0.918	0.284
	Total	4.000	4.000	4.000	4.000	4.000	4.000	4.000	4.000	4.000	4.000	4.000	4.000
Group vi													
Cr		0.002	0.003	0.005	0.005	0.003	0.004	0.002	0.005	0.004	0.003	0.005	0.003
Al		1.787	1.695	1.787	1.726	1.797	1.847	1.778	1.772	1.833	1.854	1.615	1.706
Zn		0.000	0.000	0.000	0.000	0.000	0.000	0.000	0.000	0.000	0.000	0.000	0.000
Mn		0.005	0.013	0.003	0.008	0.006	0.006	0.004	0.003	0.003	0.000	0.000	0.001
Mg		0.117	0.187	0.145	0.166	0.144	0.101	0.139	0.141	0.115	0.062	0.063	0.050
Fe3+		0.029	0.000	0.000	0.000	0.056	0.000	0.000	0.000	0.000	0.026	0.054	0.000
Fe2+		0.026	0.189	0.074	0.126	0.010	0.047	0.072	0.069	0.055	0.033	0.000	0.035
Ti4		0.009	0.014	0.011	0.007	0.006	0.003	0.011	0.013	0.007	0.012	0.059	0.007
Sn		0.000	0.000	0.000	0.000	0.000	0.000	0.000	0.000	0.000	0.000	0.000	0.000
Mn		0.000	0.000	0.000	0.000	0.000	0.000	0.000	0.000	0.000	0.000	0.000	0.000
	Total	2.128	2.101	2.024	2.039	2.085	2.007	2.007	2.002	2.015	2.064	2.519	2.064
Group xii													
Ca		0.000	0.006	0.002	0.007	0.003	0.002	0.005	0.000	0.002	0.005	0.000	0.000
Ba		0.006	0.006	0.009	0.006	0.005	0.005	0.006	0.007	0.006	0.004	0.006	0.004
Na		0.043	0.035	0.024	0.030	0.028	0.052	0.036	0.023	0.050	0.102	0.077	0.040
K		0.882	0.906	0.910	0.860	0.805	0.885	0.918	0.951	0.898	0.748	0.782	0.653
Cs		0.000	0.000	0.000	0.000	0.000	0.001	0.000	0.000	0.000	0.000	0.000	0.000
	Total	0.931	0.953	0.945	0.902	0.841	0.945	0.965	0.981	0.957	0.859	0.866	0.698
OH		1.949	1.957	1.959	1.981	1.944	1.984	1.942	1.908	1.941	1.952	1.891	1.956
F		0.001	0.000	0.001	0.001	0.001	0.000	0.001	0.000	0.000	0.036	0.051	0.037
Cl		0.041	0.030	0.029	0.012	0.049	0.013	0.046	0.080	0.053	0.000	0.000	0.000
O		0.009	0.014	0.011	0.007	0.006	0.003	0.011	0.013	0.007	0.000	0.000	0.000
		2.000	2.000	2.000	2.000	2.000	2.000	2.000	2.000	2.000	2.000	2.000	2.000

White mica

Sector	*Aljustrel*	*Aljustrel*	*Aljustrel*	*Neves Corvo*	*Neves Corvo*	*Neves Corvo*	*Neves Corvo*	*Neves Corvo*	*Neves Corvo*	*Neves Corvo*
Sub-sector	*Gavião*	*Gavião*	*Gavião*	*Lombador*	*Neves*	*Neves*	*Neves*	*Neves*	*Neves*	*Lombador*
Stratigraphic division	*upper VSC*	*upper VSC*	*upper VSC*	*PQG*	*lower VSC*	*lower VSC*	*lower VSC*	*lower VSC*	*lower VSC*	*PQG*
Mineralization type	*Mineralized*	*Mineralized*	*Mineralized*	*No Sulph*	*Mineralized*	*Mineralized*	*Mineralized*	*Mineralized*	*Mineralized*	*No sulph*
Occurrence										
Sample ref.	*GV7#3*	*GV7#3*	*GV7#3*	*NCL#15*	*NCN#16*	*NCN#16*	*NCN#16*	*NCN#16*	*NCN#16*	*NCLl#15*
Observations										
# analysis	*#131*	*#132*	*#133*	*#134*	*#135*	*#136*	*#137*	*#138*	*#139*	*#140*
SiO2	47.696	51.609	57.718	54.249	48.989	47.887	47.876	48.809	48.206	49.047
Al2O3	31.733	28.678	28.026	29.075	35.705	36.548	34.339	35.830	35.783	32.777
FeO	0.493	0.145	1.071	2.563	0.892	0.808	1.214	0.850	0.956	0.383
Fe2O3	1.442	1.570	0.178							2.242
MnO	0.000	0.012	0.045	0.000	0.010	0.000	0.021	0.015	0.019	0.009
MgO	0.934	0.568	0.375	0.836	0.559	0.502	0.799	0.486	0.506	1.486
CaO	0.024	0.008	0.034	0.036	0.091	0.123	0.110	0.023	0.053	0.023
Na2O	0.416	0.440	0.264	0.223	0.447	0.511	0.405	0.385	0.398	0.324
K2O	9.656	8.970	6.017	8.809	8.699	9.428	9.622	8.921	9.638	9.826
F	0.196	0.000	0.019	0.200	0.266	0.069	0.114	0.168	0.168	0.357
Cl	0.012	0.014	0.000	0.000	0.000	0.000	0.004	0.076	0.000	0.010
TiO2	0.761	0.892	0.407	0.728	0.251	0.111	0.856	0.195	0.201	0.751
Cr2O3	0.073	0.093	0.100	0.053	0.060	0.085	0.065	0.040	0.063	0.051
ZnO	0.000	0.000	0.000	0.000	0.000	0.000	0.000	0.000	0.000	0.000
Cs2O	0.000	0.000	0.000	0.000	0.000	0.000	0.000	0.000	0.000	0.000
BaO	0.182	0.131	0.125	0.110	0.165	0.199	0.182	0.113	0.177	0.191
SnO	0.000	0.000	0.000	0.047	0.000	0.000	0.000	0.000	0.000	0.000
Mn2O3	0.000	0.000	0.000	0.000	0.000	0.000	0.000	0.000	0.000	0.000
LiO2	2.081	2.362	1.035	0.000	0.000	0.000	0.000	0.000	0.000	0.141
H2O	4.362	4.495	4.675	4.550	4.488	4.568	4.491	4.504	4.507	4.350
Total#	100.061	99.987	100.089	101.479	100.622	100.839	100.098	100.415	100.675	101.968
O=F	-0.083	0.000	-0.008	-0.084	-0.112	-0.029	-0.048	-0.071	-0.071	-0.150
O=Cl	-0.003	-0.003	0.000	0.000	0.000	0.000	-0.001	-0.017	0.000	-0.002
Total	99.976	99.984	100.081	101.395	100.510	100.810	100.049	100.328	100.605	101.815

White mica

# analysis		*#131*	*#132*	*#133*	*#134*	*#135*	*#136*	*#137*	*#138*	*#139*	*#140*
Ion Distribution											
Group iv											
Si		3.147	3.364	3.659	3.502	3.183	3.121	3.158	3.179	3.151	3.193
Al		0.853	0.636	0.341	0.498	0.817	0.879	0.842	0.821	0.849	0.807
	Total	4.000	4.000	4.000	4.000	4.000	4.000	4.000	4.000	4.000	4.000
Group vi											
Cr		0.004	0.005	0.005	0.003	0.003	0.004	0.003	0.002	0.003	0.003
Al		1.615	1.568	1.753	1.714	1.918	1.928	1.827	1.930	1.908	1.707
Zn		0.000	0.000	0.000	0.000	0.000	0.000	0.000	0.000	0.000	0.000
Mn		0.000	0.001	0.002	0.000	0.001	0.000	0.001	0.001	0.001	0.001
Mg		0.092	0.055	0.035	0.081	0.054	0.049	0.079	0.047	0.049	0.144
Fe3+		0.072	0.077	0.009	0.000	0.000	0.000	0.000	0.000	0.000	0.110
Fe2+		0.027	0.008	0.057	0.138	0.049	0.044	0.067	0.046	0.052	0.021
Ti4		0.038	0.044	0.019	0.035	0.012	0.005	0.043	0.010	0.010	0.037
Sn		0.000	0.000	0.000	0.001	0.000	0.000	0.000	0.000	0.000	0.000
Mn		0.000	0.000	0.000	0.000	0.000	0.000	0.000	0.000	0.000	0.000
	Total	2.399	2.376	2.145	1.972	2.036	2.030	2.020	2.036	2.024	2.059
Group xii											
Ca		0.002	0.001	0.002	0.003	0.006	0.009	0.008	0.002	0.004	0.002
Ba		0.005	0.003	0.003	0.003	0.004	0.005	0.005	0.003	0.005	0.005
Na		0.053	0.056	0.032	0.028	0.056	0.065	0.052	0.049	0.050	0.041
K		0.813	0.746	0.487	0.725	0.721	0.784	0.810	0.741	0.804	0.816
Cs		0.000	0.000	0.000	0.000	0.000	0.000	0.000	0.000	0.000	0.000
	Total	0.872	0.806	0.525	0.759	0.788	0.862	0.874	0.794	0.862	0.863
OH		1.920	1.955	1.977	1.959	1.945	1.986	1.976	1.957	1.965	1.889
F		0.041	0.000	0.004	0.000	0.000	0.000	0.000	0.008	0.000	0.001
Cl		0.001	0.002	0.000	0.041	0.055	0.014	0.024	0.035	0.035	0.074
O		0.000	0.000	0.000	0.000	0.000	0.000	0.000	0.000	0.000	0.037
		2.000	2.000	2.000	2.000	2.000	2.000	2.000	2.000	2.000	2.000

White mica

Sector	*Neves Corvo*	*Neves Corvo*	*Neves Corvo*	*Neves Corvo*	*Neves Corvo*	*Neves Corvo*	*Neves Corvo*	*Neves Corvo*	*Neves Corvo*	*Neves Corvo*	*Neves Corvo*	*Neves Corvo*
Sub-sector	*Lombador*	*Neves*	*Neves*	*Neves*	*Neves*	*Neves*	*Neves*	*Neves*	*Neves*	*Neves*	*Neves*	*Neves*
Stratigraphic division	*PQG*	*lower VSC*	*lower VSC*	*lower VSC*	*lower VSC*	*lower VSC*	*lower VSC*	*lower VSC*	*lower VSC*	*lower VSC*	*lower VSC*	*lower VSC*
Mineralization type	*No sulph*	*Mineralized*	*Mineralized*	*Mineralized*	*Mineralized*	*Mineralized*	*Mineralized*	*Mineralized*	*Mineralized*	*Mineralized*	*Mineralized*	*Mineralized*
Occurrence												
Sample ref.	*NCLl#15*	*NCNl#16*	*NCNl#16*	*NCNl#16*	*NCNl#16*	*NCNl#16*	*NCNl#16*	*NCNl#16*	*NCNl#16*	*NCNl#16*	*NCNl#16*	*NCNl#16*
Observations												
# analysis	*#141*	*#142*	*#143*	*#144*	*#145*	*#146*	*#147*	*#148*	*#149*	*#150*	*#151*	*#152*
SiO2	49.118	60.143	48.989	47.887	47.876	48.809	48.206	49.173	48.059	48.259	47.997	47.756
Al2O3	30.784	24.989	35.705	36.548	34.339	35.830	35.783	30.117	30.998	31.494	31.204	30.105
FeO	3.101	0.516	0.038	0.010	0.208	0.009	0.091	1.157	0.361	0.951	0.975	0.000
Fe2O3	0.000	0.000	0.950	0.887	1.119	0.935	0.962	0.000	0.501	0.000	0.000	1.087
MnO	0.022	0.003	0.010	0.000	0.021	0.015	0.019	0.004	0.027	0.000	0.002	0.000
MgO	2.018	0.342	0.559	0.502	0.799	0.486	0.506	0.704	0.564	0.574	0.649	0.590
CaO	0.006	0.029	0.091	0.123	0.110	0.023	0.053	0.028	0.002	0.038	0.021	0.035
Na2O	0.073	0.336	0.447	0.511	0.405	0.385	0.398	0.503	0.586	0.485	0.429	0.485
K2O	11.338	6.536	8.699	9.428	9.622	8.921	9.638	7.707	7.838	7.864	8.215	7.806
F	0.294	0.045	0.266	0.069	0.114	0.168	0.168	0.184	0.000	0.073	0.266	0.180
Cl	0.000	0.006	0.000	0.000	0.004	0.076	0.000	0.001	0.012	0.004	0.000	0.000
TiO2	0.366	0.044	0.251	0.111	0.856	0.195	0.201	0.138	0.117	0.221	0.380	2.619
Cr2O3	0.050	0.078	0.060	0.085	0.065	0.040	0.063	0.072	0.048	0.055	0.070	0.097
ZnO	0.000	0.000	0.000	0.000	0.000	0.000	0.000	0.000	0.000	0.000	0.000	0.000
Cs2O	0.000	0.007	0.000	0.000	0.000	0.000	0.000	0.000	0.000	0.000	0.000	0.000
BaO	0.156	0.128	0.165	0.199	0.182	0.113	0.177	0.054	0.102	0.150	0.149	0.082
SnO	0.000	0.000	0.000	0.000	0.000	0.000	0.000	0.000	0.000	0.018	0.000	0.000
Mn2O3	0.000	0.000	0.000	0.000	0.000	0.000	0.000	0.000	0.000	0.000	0.000	0.022
LiO2	0.000	2.121	0.217	0.226	0.048	0.216	0.228	4.912	5.144	5.029	5.068	5.101
H2O	4.347	4.726	4.479	4.576	4.399	4.502	4.505	4.508	4.585	4.570	4.448	4.245
Total#	101.673	100.049	100.925	101.162	100.167	100.722	100.997	99.263	98.944	99.785	99.873	100.210
O=F	-0.124	-0.019	-0.112	-0.029	-0.048	-0.071	-0.071	-0.078	0.000	-0.031	-0.112	-0.076
O=Cl	0.000	-0.001	0.000	0.000	-0.001	-0.017	0.000	0.000	-0.003	-0.001	0.000	0.000
Total	101.550	100.028	100.813	101.133	100.118	100.634	100.927	99.185	98.941	99.754	99.761	100.134

White mica

# analysis		*#141*	*#142*	*#143*	*#144*	*#145*	*#146*	*#147*	*#148*	*#149*	*#150*	*#151*	*#152*
Ion Distribution													
Group iv													
Si		3.252	3.794	3.170	3.107	3.154	3.166	3.137	3.197	3.132	3.125	3.117	3.095
Al		0.748	0.206	0.830	0.893	0.846	0.834	0.863	0.803	0.868	0.875	0.883	0.905
	Total	4.000	4.000	4.000	4.000	4.000	4.000	4.000	4.000	4.000	4.000	4.000	4.000
Group vi													
Cr		0.003	0.004	0.003	0.004	0.003	0.002	0.003	0.004	0.003	0.003	0.004	0.005
Al		1.655	1.651	1.894	1.902	1.821	1.905	1.882	1.505	1.513	1.529	1.505	1.395
Zn		0.000	0.000	0.000	0.000	0.000	0.000	0.000	0.000	0.000	0.000	0.000	0.000
Mn		0.001	0.000	0.001	0.000	0.001	0.001	0.001	0.000	0.002	0.000	0.000	0.000
Mg		0.199	0.032	0.054	0.049	0.079	0.047	0.049	0.068	0.055	0.055	0.063	0.057
Fe3+		0.000	0.000	0.046	0.043	0.056	0.046	0.047	0.000	0.025	0.000	0.000	0.053
Fe2+		0.172	0.027	0.002	0.001	0.011	0.001	0.005	0.063	0.020	0.052	0.053	0.000
Ti4		0.018	0.002	0.012	0.005	0.042	0.010	0.010	0.007	0.006	0.011	0.019	0.128
Sn		0.000	0.000	0.000	0.000	0.000	0.000	0.000	0.000	0.000	0.001	0.000	0.000
Mn		0.000	0.000	0.000	0.000	0.000	0.000	0.000	0.000	0.000	0.000	0.000	0.001
	Total	2.048	2.255	2.068	2.063	2.026	2.067	2.057	2.931	2.970	2.959	2.967	2.968
Group xii													
Ca		0.000	0.002	0.006	0.009	0.008	0.002	0.004	0.002	0.000	0.003	0.002	0.002
Ba		0.004	0.003	0.004	0.005	0.005	0.003	0.005	0.001	0.003	0.004	0.004	0.002
Na		0.009	0.041	0.056	0.064	0.052	0.048	0.050	0.063	0.074	0.061	0.054	0.061
K		0.958	0.526	0.718	0.780	0.809	0.738	0.800	0.639	0.652	0.650	0.681	0.646
Cs		0.000	0.000	0.000	0.000	0.000	0.000	0.000	0.000	0.000	0.000	0.000	0.000
	Total	0.972	0.572	0.785	0.858	0.873	0.791	0.859	0.706	0.728	0.717	0.740	0.711
OH		1.920	1.988	1.933	1.980	1.933	1.948	1.956	1.955	1.993	1.974	1.927	1.835
F		0.000	0.001	0.000	0.000	0.000	0.008	0.000	0.000	0.001	0.000	0.000	0.000
Cl		0.062	0.009	0.054	0.014	0.024	0.035	0.035	0.038	0.000	0.015	0.055	0.037
O		0.018	0.002	0.012	0.005	0.042	0.010	0.010	0.007	0.006	0.011	0.019	0.128
		2.000	2.000	2.000	2.000	2.000	2.000	2.000	2.000	2.000	2.000	2.000	2.000

White mica

Sector	*Neves Corvo*	*Neves Corvo*	*Neves Corvo*	*Neves Corvo*	*Neves Corvo*	*Neves Corvo*	*Neves Corvo*	*Neves Corvo*	*Neves Corvo*	*Neves Corvo*	*Neves Corvo*
Sub-sector	*Neves*	*Corvo*	*Corvo*	*Lombador*	*Lombador*	*Lombador*	*Lombador*	*Lombador*	*Lombador*	*Lombador*	*Lombador*
Stratigraphic division	*lower VSC*	*lower VSC*	*lower VSC*	*upper VSC*	*upper VSC*	*upper VSC*	*upper VSC*	*upper VSC*	*upper VSC*	*upper VSC*	*upper VSC*
Mineralization type	*Mineralized*	*Py-bearing*	*Py-bearing*	*Mineralized*	*Mineralized*	*Mineralized*	*Mineralized*	*Mineralized*	*Mineralized*	*Mineralized*	*Mineralized*
Occurrence											
Sample ref.	*NCNl#16*	*NCC#24*	*NCC#24*	*NCL#6*	*NCL#6*	*NCL#6*	*NCL#6*	*NCL#6*	*NCL#6*	*NCL#6*	*NCL#6*
Observations											
# analysis	*#153*	*#154*	*#155*	*#156*	*#157*	*#158*	*#159*	*#160*	*#161*	*#162*	*#163*
SiO2	47.676	50.367	57.291	48.206	49.144	50.864	48.733	48.730	48.026	48.704	47.954
Al2O3	29.547	30.067	27.570	35.371	34.690	33.650	35.193	35.856	32.855	33.931	33.441
FeO	0.991	0.987	1.657	0.794	1.226	0.874	1.096	0.910	2.054	1.319	1.404
Fe2O3	0.000	0.000	0.000	0.000	0.000	0.000	0.000	0.000	0.000	0.000	0.000
MnO	0.000	0.000	0.000	0.000	0.000	0.000	0.000	0.000	0.000	0.000	0.000
MgO	0.679	1.050	1.429	0.629	0.864	0.634	0.666	0.634	1.006	0.770	0.679
CaO	0.059	0.109	0.110	0.007	0.000	0.000	0.052	0.020	0.061	0.016	0.028
Na2O	0.548	1.039	0.949	0.483	0.350	0.356	0.398	0.637	0.427	0.525	0.499
K2O	7.441	7.448	6.263	9.295	9.481	9.010	9.642	9.442	9.538	9.526	9.478
F	0.197	0.213	0.058	0.178	0.157	0.140	0.268	0.288	0.197	0.223	0.149
Cl	0.000	0.013	0.004	0.007	0.001	0.005	0.005	0.010	0.005	0.012	0.000
TiO2	1.673	2.333	0.217	0.854	0.065	0.174	0.097	0.080	0.528	0.382	0.550
Cr2O3	0.060	0.051	0.111	0.105	0.040	0.083	0.067	0.104	0.046	0.079	0.072
ZnO	0.000	0.000	0.000	0.000	0.000	0.000	0.000	0.000	0.000	0.000	0.000
Cs2O	0.000	0.000	0.000	0.000	0.014	0.000	0.000	0.000	0.000	0.000	0.000
BaO	0.179	0.108	0.153	0.195	0.150	0.177	0.175	0.226	0.142	0.178	0.231
SnO	0.000	0.000	0.000	0.000	0.000	0.000	0.000	0.000	0.000	0.000	0.000
Mn2O3	0.000	0.000	0.000	0.031	0.000	0.006	0.001	0.000	0.018	0.034	0.000
LiO2	5.048	0.000	0.000	0.000	0.000	0.000	0.000	0.000	0.000	0.000	0.000
H2O	4.269	4.414	4.670	4.506	4.519	4.550	4.464	4.482	4.398	4.444	4.421
Total#	98.367	98.199	100.482	100.661	100.701	100.523	100.857	101.419	99.301	100.143	98.906
O=F	-0.083	-0.090	-0.024	-0.075	-0.066	-0.059	-0.113	-0.121	-0.083	-0.094	-0.063
O=Cl	0.000	-0.003	-0.001	-0.002	0.000	-0.001	-0.001	-0.002	-0.001	-0.003	0.000
Total	98.284	98.107	100.457	100.584	100.635	100.463	100.743	101.296	99.217	100.046	98.843

White mica

# analysis		*#153*	*#154*	*#155*	*#156*	*#157*	*#158*	*#159*	*#160*	*#161*	*#162*	*#163*
Ion Distribution												
Group iv												
Si		3.141	3.342	3.656	3.148	3.208	3.303	3.182	3.162	3.205	3.208	3.201
Al		0.859	0.658	0.344	0.852	0.792	0.698	0.818	0.839	0.795	0.792	0.799
	Total	4.000	4.000	4.000	4.000	4.000	4.000	4.000	4.000	4.000	4.000	4.000
Group vi												
Cr		0.003	0.003	0.006	0.005	0.002	0.004	0.004	0.005	0.002	0.004	0.004
Al		1.436	1.694	1.729	1.870	1.877	1.877	1.890	1.903	1.789	1.842	1.832
Zn		0.000	0.000	0.000	0.000	0.000	0.000	0.000	0.000	0.000	0.000	0.000
Mn		0.000	0.000	0.000	0.002	0.000	0.000	0.000	0.000	0.001	0.002	0.000
Mg		0.067	0.104	0.136	0.061	0.084	0.061	0.065	0.061	0.100	0.076	0.068
Fe3+		0.000	0.000	0.000	0.000	0.000	0.000	0.000	0.000	0.000	0.000	0.000
Fe2+		0.055	0.055	0.088	0.043	0.067	0.048	0.060	0.049	0.115	0.073	0.078
Ti4		0.083	0.117	0.010	0.042	0.003	0.009	0.005	0.004	0.027	0.019	0.028
Sn		0.000	0.000	0.000	0.000	0.000	0.000	0.000	0.000	0.000	0.000	0.000
Mn		0.000	0.000	0.000	0.000	0.000	0.000	0.000	0.000	0.000	0.000	0.000
	Total	2.981	1.972	1.969	2.023	2.033	1.999	2.023	2.023	2.034	2.015	2.010
Group xii												
Ca		0.004	0.008	0.008	0.001	0.000	0.000	0.004	0.001	0.004	0.001	0.002
Ba		0.005	0.003	0.004	0.005	0.004	0.005	0.005	0.006	0.004	0.005	0.006
Na		0.070	0.134	0.117	0.061	0.044	0.045	0.050	0.080	0.055	0.067	0.065
K		0.626	0.631	0.510	0.774	0.790	0.746	0.803	0.782	0.812	0.800	0.807
Cs		0.000	0.000	0.000	0.000	0.000	0.000	0.000	0.000	0.000	0.000	0.000
	Total	0.704	0.775	0.639	0.841	0.838	0.796	0.862	0.869	0.875	0.873	0.880
OH		1.876	1.954	1.988	1.963	1.968	1.971	1.944	1.940	1.958	1.952	1.969
F		0.000	0.045	0.012	0.037	0.032	0.029	0.055	0.059	0.042	0.047	0.032
Cl		0.041	0.002	0.000	0.001	0.000	0.001	0.001	0.001	0.001	0.001	0.000
O		0.083	0.000	0.000	0.000	0.000	0.000	0.000	0.000	0.000	0.000	0.000
		2.000	2.000	2.000	2.000	2.000	2.000	2.000	2.000	2.000	2.000	2.000

White mica

Sector	*Neves Corvo*	*Neves Corvo*	*Neves Corvo*	*Neves Corvo*	*Neves Corvo*	*Neves Corvo*	*Neves Corvo*	*Neves Corvo*	*Neves Corvo*	*Neves Corvo*	*Neves Corvo*	*Neves Corvo*
Sub-sector	*Lombador*	*neves*	*neves*	*neves*	*neves*	*neves*	*neves*	*Corvo*	*Corvo*	*Corvo*	*Corvo*	*Corvo*
Stratigraphic division	*upper VSC*	*lower VSC*	*lower VSC*	*lower VSC*	*lower VSC*	*lower VSC*	*lower VSC*	*lower VSC*	*lower VSC*	*lower VSC*	*lower VSC*	*lower VSC*
Mineralization type	*Mineralized*	*Py-bearing*	*Py-bearing*	*Py-bearing*	*Py-bearing*	*Py-bearing*	*Py-bearing*	*Py-bearing*	*Py-bearing*	*Py-bearing*	*Py-bearing*	*Py-bearing*
Occurrence												
Sample ref.	*NCL#6*	*NCN#17*	*NCN#17*	*NCN#17*	*NCN#17*	*NCN#17*	*NCN#17*	*NCC#24*	*NCC#24*	*NCC#24*	*NCC#24*	*NCC#24*
Observations												
# analysis	*#164*	*#165*	*#166*	*#167*	*#168*	*#169*	*#170*	*#171*	*#172*	*#173*	*#174*	*#175*
SiO2	47.751	48.402	47.520	47.495	47.658	48.208	47.953	52.654	52.951	50.367	57.291	51.860
Al2O3	33.521	36.342	35.539	36.915	35.811	35.838	35.947	29.607	29.498	30.067	27.570	28.952
FeO	1.477	0.678	1.000	0.477	0.896	0.837	0.570	0.000	0.000	0.756	0.000	2.351
Fe2O3	0.000	0.000	0.000	0.000	0.000	0.000	0.000	1.548	1.499	0.257	1.842	0.371
MnO	0.000	0.000	0.000	0.000	0.000	0.000	0.000	0.000	0.000	0.000	0.000	0.067
MgO	0.645	0.375	0.419	0.296	0.473	0.477	0.490	0.943	0.943	1.050	1.429	2.310
CaO	0.018	0.007	0.003	0.009	0.023	0.052	0.044	0.105	0.079	0.109	0.110	0.083
Na2O	0.492	0.775	0.786	0.734	0.820	0.905	0.730	0.902	0.943	1.039	0.949	1.340
K2O	9.423	8.975	8.863	9.108	8.695	8.900	8.836	6.419	6.393	7.448	6.263	6.185
F	0.000	0.135	0.123	0.011	0.183	0.000	0.000	0.046	0.184	0.213	0.058	0.182
Cl	0.003	0.000	0.002	0.000	0.000	0.000	0.001	0.025	0.038	0.013	0.004	0.000
TiO2	0.553	0.108	1.269	0.482	0.467	0.058	0.032	0.395	0.392	2.333	0.217	0.736
Cr2O3	0.080	0.078	0.092	0.078	0.039	0.099	0.058	0.075	0.102	0.051	0.111	0.052
ZnO	0.000	0.000	0.000	0.000	0.000	0.000	0.000	0.000	0.000	0.000	0.000	0.000
Cs2O	0.000	0.000	0.000	0.000	0.000	0.009	0.002	0.000	0.000	0.000	0.000	0.000
BaO	0.166	0.115	0.085	0.125	0.062	0.149	0.165	0.187	0.169	0.108	0.153	0.125
SnO	0.000	0.000	0.000	0.000	0.000	0.000	0.000	0.000	0.000	0.000	0.000	0.000
Mn2O3	0.000	0.001	0.013	0.000	0.016	0.017	0.000	0.000	0.035	0.000	0.000	0.000
LiO2	0.000	0.000	0.000	0.000	0.000	0.000	0.000	2.472	2.258	2.078	0.396	1.024
H2O	4.482	4.542	4.515	4.587	4.472	4.581	4.558	4.601	4.532	4.244	4.684	4.441
Total#	98.611	100.533	100.229	100.317	99.615	100.130	99.386	99.979	100.016	100.132	101.076	100.079
O=F	0.000	-0.057	-0.052	-0.005	-0.077	0.000	0.000	-0.019	-0.078	-0.090	-0.024	-0.077
O=Cl	-0.001	0.000	-0.001	0.000	0.000	0.000	0.000	-0.006	-0.009	-0.003	-0.001	0.000
Total	98.610	100.476	100.177	100.313	99.538	100.130	99.386	99.954	99.930	100.040	101.051	100.003

White mica

# analysis		*#164*	*#165*	*#166*	*#167*	*#168*	*#169*	*#170*	*#171*	*#172*	*#173*	*#174*	*#175*
Ion Distribution													
Group iv													
Si		3.194	3.151	3.115	3.101	3.135	3.155	3.154	3.378	3.398	3.275	3.626	3.373
Al		0.806	0.849	0.885	0.899	0.865	0.845	0.846	0.622	0.602	0.725	0.374	0.627
	Total	4.000	4.000	4.000	4.000	4.000	4.000	4.000	4.000	4.000	4.000	4.000	4.000
Group vi													
Cr		0.004	0.004	0.005	0.004	0.002	0.005	0.003	0.004	0.005	0.003	0.006	0.003
Al		1.836	1.940	1.861	1.941	1.911	1.920	1.941	1.617	1.628	1.579	1.683	1.592
Zn		0.000	0.000	0.000	0.000	0.000	0.000	0.000	0.000	0.000	0.000	0.000	0.000
Mn		0.000	0.000	0.001	0.000	0.001	0.001	0.000	0.000	0.000	0.000	0.000	0.004
Mg		0.064	0.036	0.041	0.029	0.046	0.047	0.048	0.090	0.090	0.102	0.135	0.224
Fe3+		0.000	0.000	0.000	0.000	0.000	0.000	0.000	0.075	0.072	0.013	0.088	0.018
Fe2+		0.083	0.037	0.055	0.026	0.049	0.046	0.031	0.000	0.000	0.041	0.000	0.128
Ti4		0.028	0.005	0.063	0.024	0.023	0.003	0.002	0.019	0.019	0.114	0.010	0.036
Sn		0.000	0.000	0.000	0.000	0.000	0.000	0.000	0.000	0.000	0.000	0.000	0.000
Mn		0.000	0.000	0.000	0.000	0.000	0.000	0.000	0.000	0.002	0.000	0.000	0.000
	Total	2.015	2.022	2.024	2.024	2.033	2.021	2.025	2.442	2.399	2.395	2.022	2.273
Group xii													
Ca		0.001	0.001	0.000	0.001	0.002	0.004	0.003	0.007	0.005	0.008	0.008	0.006
Ba		0.004	0.003	0.002	0.003	0.002	0.004	0.004	0.005	0.004	0.003	0.004	0.003
Na		0.064	0.098	0.100	0.093	0.105	0.115	0.093	0.112	0.117	0.131	0.117	0.169
K		0.804	0.745	0.741	0.759	0.730	0.743	0.741	0.525	0.523	0.618	0.506	0.513
Cs		0.000	0.000	0.000	0.000	0.000	0.000	0.000	0.000	0.000	0.000	0.000	0.000
	Total	0.874	0.847	0.844	0.855	0.837	0.866	0.842	0.650	0.650	0.759	0.633	0.691
OH		2.000	1.972	1.974	1.998	1.962	2.000	2.000	1.969	1.940	1.841	1.978	1.927
F		0.000	0.028	0.026	0.002	0.038	0.000	0.000	0.009	0.037	0.044	0.012	0.037
Cl		0.000	0.000	0.000	0.000	0.000	0.000	0.000	0.003	0.004	0.001	0.000	0.000
O		0.000	0.000	0.000	0.000	0.000	0.000	0.000	0.000	0.000	0.000	0.000	0.000
		2.000	2.000	2.000	2.000	2.000	2.000	2.000	2.000	2.000	2.000	2.000	2.000

White mica

Sector	*Neves Corvo*	*Neves Corvo*	*Neves Corvo*	*Neves Corvo*	*Neves Corvo*	*Neves Corvo*	*Neves Corvo*	*Neves Corvo*	*Neves Corvo*	*Neves Corvo*	*Neves Corvo*	*Neves Corvo*
Sub-sector	*neves*	*neves*	*neves*	*neves*	*neves*	*neves*	*neves*	*neves*	*neves*	*neves*	*neves*	*neves*
Stratigraphic division	*lower VSC*	*lower VSC*	*lower VSC*	*lower VSC*	*lower VSC*	*lower VSC*	*lower VSC*	*lower VSC*	*lower VSC*	*lower VSC*	*lower VSC*	*lower VSC*
Mineralization type	*Py-bearing*	*Py-bearing*	*Py-bearing*	*Py-bearing*	*Py-bearing*	*Py-bearing*	*Py-bearing*	*Py-bearing*	*Py-bearing*	*Py-bearing*	*Py-bearing*	*Py-bearing*
Occurrence												
Sample ref.	*NCN#17*	*NCN#17*	*NCN#17*	*NCN#17*	*NCN#17*	*NCN#17*	*NCN#17*	*NCN#17*	*NCN#17*	*NCN#17*	*NCN#17*	*NCN#17*
Observations												
# analysis	*#176*	*#177*	*#178*	*#179*	*#180*	*#181*	*#182*	*#183*	*#184*	*#185*	*#186*	*#187*
SiO2	47.320	47.363	48.402	43.960	47.561	47.667	47.520	47.090	47.495	47.658	48.208	47.953
Al2O3	37.964	38.053	36.342	35.666	36.215	36.356	35.539	36.285	36.915	35.811	35.838	35.947
FeO	0.000	0.000	0.000	2.605	0.727	0.741	0.144	0.465	0.000	0.590	0.015	0.570
Fe2O3	0.671	0.699	0.754	1.648	0.168	0.142	0.951	0.849	0.530	0.341	0.913	0.000
MnO	0.000	0.000	0.000	0.009	0.037	0.004	0.013	0.018	0.000	0.016	0.017	0.000
MgO	0.346	0.329	0.375	2.291	0.439	0.444	0.419	0.565	0.296	0.473	0.477	0.490
CaO	0.028	0.020	0.007	0.096	0.034	0.043	0.003	0.019	0.009	0.023	0.052	0.044
Na2O	0.653	0.658	0.775	0.804	0.727	0.653	0.786	0.792	0.734	0.820	0.905	0.730
K2O	8.542	8.408	8.975	5.956	8.275	8.094	8.863	8.926	9.108	8.695	8.900	8.836
F	0.027	0.189	0.135	0.000	0.049	0.124	0.123	0.114	0.011	0.183	0.000	0.000
Cl	0.002	0.011	0.000	0.000	0.015	0.014	0.002	0.008	0.000	0.000	0.000	0.001
TiO2	0.870	0.904	0.108	0.187	0.211	0.184	1.269	0.074	0.482	0.467	0.058	0.032
Cr2O3	0.078	0.072	0.078	0.097	0.081	0.099	0.092	0.079	0.078	0.039	0.099	0.058
ZnO	0.000	0.000	0.000	0.000	0.000	0.000	0.000	0.000	0.000	0.000	0.000	0.000
Cs2O	0.000	0.000	0.000	0.000	0.000	0.000	0.000	0.000	0.000	0.000	0.009	0.002
BaO	0.133	0.180	0.115	0.097	0.133	0.165	0.085	0.128	0.125	0.062	0.149	0.165
SnO	0.000	0.000	0.000	0.000	0.000	0.000	0.000	0.000	0.000	0.000	0.000	0.000
Mn2O3	0.000	0.005	0.001	0.000	0.000	0.000	0.000	0.000	0.000	0.000	0.000	0.000
LiO2	0.208	0.213	0.200	2.099	0.727	0.718	0.237	0.192	0.179	0.404	0.220	0.454
H2O	4.541	4.464	4.547	4.550	4.542	4.516	4.382	4.505	4.543	4.440	4.596	4.579
Total#	101.383	101.568	100.814	100.065	99.941	99.964	100.428	100.109	100.505	100.020	100.456	99.861
O=F	-0.011	-0.080	-0.057	0.000	-0.021	-0.052	-0.052	-0.048	-0.005	-0.077	0.000	0.000
O=Cl	-0.001	-0.003	0.000	0.000	-0.003	-0.003	-0.001	-0.002	0.000	0.000	0.000	0.000
Total	101.371	101.486	100.757	100.065	99.917	99.909	100.376	100.059	100.501	99.943	100.456	99.861

White mica

# analysis		*#176*	*#177*	*#178*	*#179*	*#180*	*#181*	*#182*	*#183*	*#184*	*#185*	*#186*	*#187*
Ion Distribution													
Group iv													
	Si	3.050	3.048	3.139	2.884	3.105	3.108	3.108	3.090	3.094	3.121	3.141	3.137
	Al	0.950	0.952	0.861	1.117	0.895	0.892	0.892	0.910	0.906	0.880	0.859	0.863
	Total	4.000	4.000	4.000	4.000	4.000	4.000	4.000	4.000	4.000	4.000	4.000	4.000
Group vi													
	Cr	0.004	0.004	0.004	0.005	0.004	0.005	0.005	0.004	0.004	0.002	0.005	0.003
	Al	1.933	1.935	1.917	1.641	1.891	1.901	1.848	1.897	1.928	1.884	1.893	1.909
	Zn	0.000	0.000	0.000	0.000	0.000	0.000	0.000	0.000	0.000	0.000	0.000	0.000
	Mn	0.000	0.000	0.000	0.001	0.002	0.000	0.001	0.001	0.000	0.001	0.001	0.000
	Mg	0.033	0.032	0.036	0.224	0.043	0.043	0.041	0.055	0.029	0.046	0.046	0.048
	Fe3+	0.033	0.034	0.037	0.081	0.008	0.007	0.047	0.042	0.026	0.017	0.045	0.000
	Fe2+	0.000	0.000	0.000	0.143	0.040	0.040	0.008	0.026	0.000	0.032	0.001	0.031
	Ti4	0.042	0.044	0.005	0.009	0.010	0.009	0.062	0.004	0.024	0.023	0.003	0.002
	Sn	0.000	0.000	0.000	0.000	0.000	0.000	0.000	0.000	0.000	0.000	0.000	0.000
	Mn	0.000	0.000	0.000	0.000	0.000	0.000	0.000	0.000	0.000	0.000	0.000	0.000
	Total	2.099	2.103	2.052	2.657	2.190	2.194	2.074	2.079	2.057	2.112	2.051	2.112
Group xii													
	Ca	0.002	0.001	0.001	0.007	0.002	0.003	0.000	0.001	0.001	0.002	0.004	0.003
	Ba	0.003	0.005	0.003	0.003	0.003	0.004	0.002	0.003	0.003	0.002	0.004	0.004
	Na	0.082	0.082	0.098	0.102	0.092	0.083	0.100	0.101	0.093	0.104	0.114	0.093
	K	0.702	0.690	0.743	0.498	0.689	0.673	0.740	0.747	0.757	0.726	0.740	0.738
	Cs	0.000	0.000	0.000	0.000	0.000	0.000	0.000	0.000	0.000	0.000	0.000	0.000
	Total	0.789	0.778	0.843	0.610	0.787	0.763	0.842	0.853	0.853	0.834	0.862	0.837
	OH	1.952	1.917	1.967	1.991	1.978	1.964	1.912	1.972	1.974	1.939	1.997	1.998
	F	0.006	0.039	0.028	0.000	0.010	0.026	0.025	0.024	0.002	0.038	0.000	0.000
	Cl	0.000	0.001	0.000	0.000	0.002	0.002	0.000	0.001	0.000	0.000	0.000	0.000
	O	0.000	0.000	0.000	0.000	0.000	0.000	0.000	0.000	0.000	0.000	0.000	0.000
		2.000	2.000	2.000	2.000	2.000	2.000	2.000	2.000	2.000	2.000	2.000	2.000

White mica

Sector	*Neves Corvo*	*Neves Corvo*	*Neves Corvo*	*Neves Corvo*	*Neves Corvo*	*Neves Corvo*	*Neves Corvo*	*Neves Corvo*	*Neves Corvo*	*Neves Corvo*	*Lousal*	*Lousal*
Sub-sector	*neves*	*neves*	*neves*	*neves*	*neves*	*neves*	*zambujal*	*zambujal*	*zambujal*	*zambujal*	*Sesmarias*	*Sesmarias*
Stratigraphic division	*lower VSC*	*lower VSC*	*lower VSC*	*lower VSC*	*lower VSC*	*lower VSC*	*lower VSC*	*lower VSC*	*lower VSC*	*lower VSC*	*lower VSC*	*lower VSC*
Mineralization type	*Py-bearing*	*Py-bearing*	*Py-bearing*	*Mineralized*	*Mineralized*	*Mineralized*	*Mineralized*	*Mineralized*	*Mineralized*	*Mineralized*	*Mineralized*	*Mineralized*
Occurrence												
Sample ref.	*NCN#17*	*NCN#17*	*NCN#17*	*NCN#20*	*NCN#20*	*NCN#20*	*NCZ#21*	*NCZ#21*	*NCZ#21*	*NCZ#21*	*SES20#10*	*SES20#10*
Observations												
# analysis	*#188*	*#189*	*#190*	*#191*	*#192*	*#193*	*#194*	*#195*	*#196*	*#197*	*#198*	*#199*
SiO2	48.992	49.766	46.902	47.048	48.019	38.453	47.008	38.047	54.568	52.163	51.065	49.115
Al2O3	37.247	37.195	35.892	31.104	33.412	31.034	33.200	28.382	28.416	30.379	30.951	34.616
FeO	0.105	0.088	0.415	0.000	2.127	2.792	0.000	4.789	0.959	0.664	1.418	1.266
Fe2O3	1.019	1.032	2.225	6.295	0.000	8.542	6.681	15.108	0.260	0.919		
MnO	0.000	0.000	0.016	0.000	0.040	0.074	0.000	0.000	0.000	0.004	0.000	0.000
MgO	0.626	0.603	0.899	1.337	0.757	2.894	1.170	2.930	0.576	0.457	1.237	1.038
CaO	0.036	0.035	0.040	0.007	0.016	0.028	0.091	0.035	0.031	0.063	0.016	0.006
Na2O	0.473	0.443	0.695	0.258	0.687	0.312	0.352	0.289	0.394	0.756	0.159	0.306
K2O	7.514	7.320	8.299	9.494	9.922	9.529	7.074	5.687	8.131	9.188	9.716	10.133
F	0.036	0.092	0.065	0.391	0.287	0.219	0.154	0.239	0.100	0.154	0.291	0.142
Cl	0.006	0.009	0.002	0.003	0.000	0.003	0.000	0.008	0.002	0.000	0.000	0.005
TiO2	0.014	0.049	0.323	0.180	0.173	0.242	0.980	0.051	0.689	0.101	0.388	0.089
Cr2O3	0.091	0.075	0.026	0.015	0.069	0.102	0.112	0.094	0.076	0.090	0.118	0.056
ZnO	0.000	0.000	0.000	0.000	0.000	0.000	0.000	0.000	0.000	0.000	0.000	0.000
Cs2O	0.000	0.000	0.000	0.000	0.000	0.000	0.000	0.000	0.000	0.000	0.000	0.000
BaO	0.123	0.120	0.113	0.154	0.159	0.187	0.209	0.071	0.186	0.180	0.135	0.138
SnO	0.000	0.000	0.000	0.000	0.000	0.000	0.000	0.000	0.000	0.000	0.000	0.000
Mn2O3	0.000	0.000	0.000	0.022	0.000	0.000	0.000	0.000	0.000	0.000	0.000	0.000
LiO2	0.233	0.228	0.163	0.671	0.000	1.524	0.460	0.261	1.113	0.497	0.000	0.000
H2O	4.666	4.670	4.518	4.322	4.353	4.177	4.428	4.141	4.511	4.502	4.415	4.539
Total#	101.182	101.725	100.593	101.301	100.021	100.112	101.920	100.131	100.012	100.117	99.909	101.449
O=F	-0.015	-0.039	-0.027	-0.165	-0.121	-0.092	-0.065	-0.101	-0.042	-0.065	-0.123	-0.060
O=Cl	-0.001	-0.002	-0.001	-0.001	0.000	-0.001	0.000	-0.002	-0.001	0.000	0.000	-0.001
Total	101.165	101.684	100.566	101.136	99.900	100.019	101.855	100.029	99.969	100.052	99.786	101.389

White mica

# analysis		*#188*	*#189*	*#190*	*#191*	*#192*	*#193*	*#194*	*#195*	*#196*	*#197*	*#198*	*#199*
Ion Distribution													
Group iv													
Si		3.134	3.161	3.067	3.115	3.194	2.676	3.056	2.677	3.529	3.410	3.363	3.196
Al		0.866	0.840	0.934	0.885	0.806	1.324	0.944	1.323	0.471	0.590	0.637	0.804
	Total	4.000	4.000	4.000	4.000	4.000	4.000	4.000	4.000	4.000	4.000	4.000	4.000
Group vi													
Cr		0.005	0.004	0.001	0.001	0.004	0.006	0.006	0.005	0.004	0.005	0.006	0.003
Al		1.943	1.944	1.832	1.542	1.813	1.221	1.600	1.030	1.694	1.751	1.766	1.850
Zn		0.000	0.000	0.000	0.000	0.000	0.000	0.000	0.000	0.000	0.000	0.000	0.000
Mn		0.000	0.000	0.001	0.000	0.002	0.004	0.000	0.000	0.000	0.000	0.000	0.000
Mg		0.060	0.057	0.088	0.132	0.075	0.300	0.113	0.307	0.056	0.045	0.121	0.101
Fe3+		0.049	0.049	0.110	0.314	0.000	0.447	0.327	0.800	0.013	0.045	0.000	0.000
Fe2+		0.006	0.005	0.023	0.000	0.118	0.163	0.000	0.282	0.052	0.036	0.078	0.069
Ti4		0.001	0.002	0.016	0.009	0.009	0.013	0.048	0.003	0.034	0.005	0.019	0.004
Sn		0.000	0.000	0.000	0.000	0.000	0.000	0.000	0.000	0.000	0.000	0.000	0.000
Mn		0.000	0.000	0.000	0.001	0.000	0.000	0.000	0.000	0.000	0.000	0.000	0.000
	Total	2.123	2.120	2.113	2.177	2.020	2.581	2.214	2.500	2.141	2.017	1.991	2.027
Group xii													
Ca		0.003	0.002	0.003	0.001	0.001	0.002	0.006	0.003	0.002	0.004	0.001	0.000
Ba		0.003	0.003	0.003	0.004	0.004	0.005	0.005	0.002	0.005	0.005	0.004	0.004
Na		0.059	0.055	0.088	0.033	0.089	0.042	0.044	0.039	0.049	0.096	0.020	0.039
K		0.613	0.593	0.692	0.802	0.842	0.846	0.587	0.510	0.671	0.766	0.816	0.841
Cs		0.000	0.000	0.000	0.000	0.000	0.000	0.000	0.000	0.000	0.000	0.000	0.000
	Total	0.678	0.653	0.786	0.840	0.936	0.895	0.643	0.554	0.727	0.871	0.841	0.884
OH		1.991	1.978	1.971	1.909	1.931	1.939	1.920	1.943	1.946	1.963	1.939	1.970
F		0.007	0.019	0.013	0.082	0.060	0.048	0.032	0.053	0.021	0.032	0.000	0.001
Cl		0.001	0.001	0.000	0.000	0.000	0.000	0.000	0.001	0.000	0.000	0.061	0.029
O		0.000	0.000	0.000	0.000	0.000	0.000	0.000	0.000	0.000	0.000	0.000	0.000
		2.000	2.000	2.000	2.000	2.000	2.000	2.000	2.000	2.000	2.000	2.000	2.000

White mica

Sector	*Lousal*	*Lousal*	*Lousal*	*Lousal*	*Lousal*	*Lousal*	*Lousal*	*Lousal*	*Lousal*	*Lousal*	*Lousal*	*Lousal*
Sub-sector	*Sesmarias*	*Sesmarias*	*Sesmarias*	*Sesmarias*	*Sesmarias*	*Sesmarias*	*Sesmarias*	*Sesmarias*	*Sesmarias*	*Sesmarias*	*Sesmarias*	*Sesmarias*
Stratigraphic division	*upper VSC*	*lower VSC*	*lower VSC*	*lower VSC*	*lower VSC*	*lower VSC*	*lower VSC*	*lower VSC*	*upper VSC*	*upper VSC*	*upper VSC*	*upper VSC*
Mineralization type	*Py-bearing*	*Mineralized*	*Mineralized*	*Mineralized*	*Mineralized*	*Mineralized*	*Mineralized*	*Mineralized*	*Py-bearing*	*Py-bearing*	*Py-bearing*	*Py-bearing*
Occurrence												
Sample ref.	*SES20#6*	*SES20#10*	*SES20#10*	*SES20#10*	*SES20#10*	*SES20#10*	*SES20#10*	*SES20#10*	*SES20#6*	*SES20#6*	*SES20#6*	*SES20#6*
Observations												
# analysis	*#200*	*#201*	*#202*	*#203*	*#204*	*#205*	*#206*	*#207*	*#208*	*#209*	*#210*	*#211*
SiO2	49.069	42.541	51.065	49.181	55.451	59.452	49.283	49.115	56.701	48.482	48.889	53.047
Al2O3	33.718	31.411	30.951	32.162	27.887	24.687	32.405	34.616	27.519	33.641	32.359	29.966
FeO	1.170	7.094	0.543	1.565	0.000	1.164	1.454	0.281	0.000	1.365	1.632	0.000
Fe2O3		1.230	0.973	0.000	1.584	0.134	0.000	1.095	1.420	0.000	0.000	1.240
MnO	0.020	0.153	0.000	0.057	0.000	0.011	0.000	0.000	0.000	0.018	0.023	0.000
MgO	1.090	2.539	1.237	1.324	1.086	1.124	1.581	1.038	1.193	1.288	1.352	1.161
CaO	0.052	0.018	0.016	0.000	0.045	0.031	0.039	0.006	0.013	0.047	0.074	0.066
Na2O	0.208	0.685	0.159	0.204	0.180	0.133	0.160	0.306	0.145	0.227	0.186	0.215
K2O	9.935	6.502	9.716	10.573	8.691	8.353	10.450	10.133	8.335	10.314	10.369	9.391
F	0.191	0.000	0.291	0.318	0.272	0.204	0.267	0.142	0.269	0.268	0.124	0.095
Cl	0.004	0.000	0.000	0.003	0.008	0.000	0.000	0.005	0.000	0.003	0.000	0.004
TiO2	0.125	0.274	0.388	0.152	1.692	1.038	0.103	0.089	0.141	0.148	0.164	0.159
Cr2O3	0.045	0.105	0.118	0.036	0.074	0.071	0.038	0.056	0.049	0.052	0.038	0.044
ZnO	0.000	0.010	0.000	0.000	0.000	0.000	0.000	0.000	0.000	0.000	0.000	0.000
Cs2O	0.000	0.000	0.000	0.000	0.000	0.000	0.000	0.000	0.000	0.000	0.000	0.009
BaO	0.300	0.156	0.135	0.183	0.112	0.123	0.134	0.138	0.274	0.284	0.256	0.269
SnO	0.000	0.000	0.000	0.000	0.000	0.000	0.000	0.000	0.000	0.000	0.000	0.000
Mn2O3	0.000	0.000	0.000	0.000	0.022	0.000	0.000	0.000	0.000	0.000	0.000	0.000
LiO2	0.000	2.348	0.205	0.000	0.465	0.910	0.000	0.237	0.399	0.000	0.000	0.520
H2O	4.469	4.382	4.388	4.350	4.377	4.529	4.400	4.553	4.546	4.399	4.436	4.566
Total#	100.396	99.448	100.184	100.108	101.945	101.963	100.314	101.809	101.004	100.536	99.902	100.752
O=F	-0.080	0.000	-0.123	-0.134	-0.115	-0.086	-0.112	-0.060	-0.113	-0.113	-0.052	-0.040
O=Cl	-0.001	0.000	0.000	-0.001	-0.002	0.000	0.000	-0.001	0.000	-0.001	0.000	-0.001
Total	100.315	99.448	100.062	99.974	101.829	101.877	100.202	101.748	100.890	100.423	99.850	100.712

White mica

# analysis		*#200*	*#201*	*#202*	*#203*	*#204*	*#205*	*#206*	*#207*	*#208*	*#209*	*#210*	*#211*
Ion Distribution													
Group iv													
	Si	3.226	2.890	3.350	3.263	3.539	3.759	3.256	3.180	3.626	3.199	3.248	3.435
	Al	0.774	1.110	0.650	0.737	0.462	0.241	0.744	0.820	0.374	0.801	0.752	0.565
	Total	4.000	4.000	4.000	4.000	4.000	4.000	4.000	4.000	4.000	4.000	4.000	4.000
Group vi													
	Cr	0.002	0.006	0.006	0.002	0.004	0.004	0.002	0.003	0.003	0.003	0.002	0.002
	Al	1.838	1.406	1.744	1.779	1.636	1.599	1.779	1.821	1.699	1.815	1.781	1.723
	Zn	0.000	0.001	0.000	0.000	0.000	0.000	0.000	0.000	0.000	0.000	0.000	0.000
	Mn	0.001	0.009	0.000	0.003	0.000	0.001	0.000	0.000	0.000	0.001	0.001	0.000
	Mg	0.107	0.257	0.121	0.131	0.103	0.106	0.156	0.100	0.114	0.127	0.134	0.112
	Fe3+	0.000	0.063	0.048	0.000	0.076	0.006	0.000	0.053	0.068	0.000	0.000	0.060
	Fe2+	0.064	0.403	0.030	0.087	0.000	0.062	0.080	0.015	0.000	0.075	0.091	0.000
	Ti4	0.006	0.014	0.019	0.008	0.081	0.049	0.005	0.004	0.007	0.007	0.008	0.008
	Sn	0.000	0.000	0.000	0.000	0.000	0.000	0.000	0.000	0.000	0.000	0.000	0.000
	Mn	0.000	0.000	0.000	0.000	0.001	0.000	0.000	0.000	0.000	0.000	0.000	0.000
	Total	2.019	2.799	2.022	2.009	2.021	2.057	2.022	2.059	1.993	2.028	2.017	2.041
Group xii													
	Ca	0.004	0.001	0.001	0.000	0.003	0.002	0.003	0.000	0.001	0.003	0.005	0.005
	Ba	0.008	0.004	0.004	0.005	0.003	0.003	0.004	0.004	0.007	0.007	0.007	0.007
	Na	0.027	0.090	0.020	0.026	0.022	0.016	0.021	0.038	0.018	0.029	0.024	0.027
	K	0.833	0.564	0.813	0.895	0.708	0.674	0.881	0.837	0.680	0.868	0.879	0.776
	Cs	0.000	0.000	0.000	0.000	0.000	0.000	0.000	0.000	0.000	0.000	0.000	0.000
	Total	0.871	0.659	0.838	0.926	0.736	0.695	0.908	0.879	0.706	0.908	0.915	0.815
	OH	1.960	1.986	1.921	1.925	1.863	1.910	1.939	1.966	1.939	1.936	1.966	1.972
	F	0.000	0.000	0.000	0.000	0.001	0.000	0.000	0.001	0.000	0.000	0.000	0.000
	Cl	0.040	0.000	0.060	0.067	0.055	0.041	0.056	0.029	0.054	0.056	0.026	0.020
	O	0.000	0.014	0.019	0.008	0.081	0.049	0.005	0.004	0.007	0.007	0.008	0.008
		2.000	2.000	2.000	2.000	2.000	2.000	2.000	2.000	2.000	2.000	2.000	2.000

White mica

Sector	*Lousal*	*Lousal*	*Lousal*	*Lousal*	*Lousal*	*Lousal*
Sub-sector	*Sesmarias*	*Sesmarias*	*Sesmarias*	*Sesmarias*	*Sesmarias*	*Sesmarias*
Stratigraphic division	*upper VSC*	*upper VSC*	*upper VSC*	*upper VSC*	*upper VSC*	*upper VSC*
Mineralization type	*Py-bearing*	*Py-bearing*	*Py-bearing*	*Py-bearing*	*Py-bearing*	*Py-bearing*
Occurrence						
Sample ref.	*SES20#6*	*SES20#6*	*SES20#6*	*SES20#6*	*SES20#6*	*SES20#6*
Observations						
# analysis	*#212*	*#213*	*#214*	*#215*	*#216*	*#217*
SiO2	49.017	47.518	47.835	49.069	48.815	48.734
Al2O3	33.016	33.769	32.500	33.718	33.693	33.978
FeO	1.615	0.407	0.885	0.223	1.385	1.190
Fe2O3	0.000	2.219	0.351	1.053	0.000	0.000
MnO	0.006	0.007	0.023	0.020	0.000	0.000
MgO	1.415	1.405	1.308	1.090	1.234	1.152
CaO	0.072	0.050	0.081	0.052	0.012	0.058
Na2O	0.213	0.276	0.174	0.208	0.159	0.216
K2O	10.360	9.851	10.181	9.935	10.431	10.315
F	0.076	0.162	0.254	0.191	0.152	0.160
Cl	0.000	0.003	0.000	0.004	0.000	0.002
TiO2	0.111	0.117	0.156	0.125	0.124	0.191
Cr2O3	0.043	0.017	0.035	0.045	0.034	0.103
ZnO	0.000	0.000	0.000	0.000	0.000	0.000
Cs2O	0.000	0.000	0.000	0.000	0.000	0.003
BaO	0.217	0.283	0.198	0.300	0.292	0.337
SnO	0.000	0.000	0.000	0.000	0.000	0.000
Mn2O3	0.000	0.000	0.000	0.000	0.000	0.000
LiO2	0.000	0.155	1.758	0.222	0.000	0.000
H2O	4.504	4.457	4.409	4.477	4.474	4.470
Total#	100.665	100.697	100.148	100.731	100.805	100.909
O=F	-0.032	-0.068	-0.107	-0.080	-0.064	-0.067
O=Cl	0.000	-0.001	0.000	-0.001	0.000	-0.001
Total	100.633	100.628	100.041	100.650	100.741	100.841

White mica

# analysis		*#212*	*#213*	*#214*	*#215*	*#216*	*#217*
Ion Distribution							
Group iv							
Si		3.228	3.133	3.154	3.211	3.209	3.199
Al		0.772	0.868	0.846	0.789	0.791	0.801
	Total	4.000	4.000	4.000	4.000	4.000	4.000
Group vi							
Cr		0.002	0.001	0.002	0.002	0.002	0.005
Al		1.791	1.756	1.680	1.811	1.820	1.828
Zn		0.000	0.000	0.000	0.000	0.000	0.000
Mn		0.000	0.000	0.001	0.001	0.000	0.000
Mg		0.139	0.138	0.129	0.106	0.121	0.113
Fe3+		0.000	0.110	0.017	0.052	0.000	0.000
Fe2+		0.089	0.023	0.049	0.012	0.076	0.065
Ti4		0.006	0.006	0.008	0.006	0.006	0.009
Sn		0.000	0.000	0.000	0.000	0.000	0.000
Mn		0.000	0.000	0.000	0.000	0.000	0.000
	Total	2.027	2.075	2.352	2.049	2.025	2.021
Group xii							
Ca		0.005	0.004	0.006	0.004	0.001	0.004
Ba		0.006	0.007	0.005	0.008	0.008	0.009
Na		0.027	0.035	0.022	0.026	0.020	0.028
K		0.870	0.829	0.857	0.829	0.875	0.864
Cs		0.000	0.000	0.000	0.000	0.000	0.000
	Total	0.908	0.875	0.890	0.867	0.904	0.904
OH		1.979	1.960	1.939	1.954	1.962	1.957
F		0.000	0.000	0.000	0.000	0.000	0.000
Cl		0.016	0.034	0.053	0.040	0.032	0.033
O		0.006	0.006	0.008	0.006	0.006	0.009
		2.000	2.000	2.000	2.000	2.000	2.000

Carbonates

n = 105

Carbonates

Sector	Neves Corvo	Neves Corvo	Neves Corvo	Neves Corvo	Neves Corvo	Neves Corvo	Neves Corvo	Neves Corvo	Neves Corvo	Neves Corvo
Sub-sector	*Lombador*	*Lombador*	*Lombador*	*Lombador*	*Lombador*	*Lombador*	*Lombador*	*Lombador*	*Lombador*	*Neves*
Stratigraphic division	*PQG*	*PQG*	*PQG*	*PQG*	*PQG*	*PQG*	*PQG*	*PQG*	*PQG*	*lower VSC*
Mineralization type	*Mineralized*	*Mineralized*	*Mineralized*	*Mineralized*	*Mineralized*	*Mineralized*	*Mineralized*	*Mineralized*	*Mineralized*	*Mineralized*
Occurrence										
Sample ref.	*NCL#10*	*NCL#10*	*NCL#10*	*NCL#10*	*NCL#10*	*NCL#10*	*NCL#10*	*NCL#10*	*NCL#10*	*NCN#16*
# analysis	*#1*	*#2*	*#3*	*#4*	*#5*	*#6*	*#7*	*#8*	*#9*	*#10*
TiO2	0.000	0.000	0.014	0.000	0.014	0.030	0.000	0.007	0.000	0.008
CO2	39.663	39.417	39.644	39.807	40.005	39.859	40.921	40.350	40.086	40.264
Ce2O3	0.037	0.000	0.012	0.000	0.047	0.033	0.037	0.040	0.033	0.000
La2O3	0.000	0.000	0.029	0.041	0.024	0.032	0.000	0.000	0.030	0.002
BaO	0.000	0.000	0.000	0.012	0.058	0.000	0.000	0.014	0.000	0.037
SrO	0.000	0.000	0.004	0.000	0.000	0.006	0.000	0.004	0.022	0.000
ZnO	0.000	0.076	0.000	0.017	0.055	0.000	0.004	0.021	0.000	0.051
FeO	51.251	52.408	50.914	52.193	49.852	51.173	45.675	52.003	50.984	47.843
MnO	0.414	0.906	3.191	0.980	1.925	0.847	3.130	2.413	3.812	0.321
CaO	0.518	0.488	0.292	0.475	0.603	0.720	0.401	0.246	0.577	0.849
MgO	6.965	5.795	5.719	6.266	7.101	6.794	9.784	6.216	5.520	9.207
Na2O	0.024	0.021	0.000	0.000	0.003	0.035	0.007	0.000	0.016	0.089
Total#	98.872	99.111	99.819	99.791	99.687	99.529	99.959	101.314	101.080	98.671
Total	98.872	99.111	99.819	99.791	99.687	99.529	99.959	101.314	101.080	98.671

Ion Distribution											
Group C											
C		1.000	1.000	1.000	1.000	1.000	1.000	1.000	1.000	1.000	1.000
	Total	1.000	1.000	1.000	1.000	1.000	1.000	1.000	1.000	1.000	1.000
Group Z											
Ba		0.000	0.000	0.000	0.000	0.000	0.000	0.000	0.000	0.000	0.000
Sr		0.000	0.000	0.000	0.000	0.000	0.000	0.000	0.000	0.000	0.000
Zn		0.000	0.001	0.000	0.000	0.001	0.000	0.000	0.000	0.000	0.001
Fe2+		0.792	0.814	0.787	0.803	0.763	0.787	0.684	0.790	0.779	0.728
Mn		0.007	0.014	0.050	0.015	0.030	0.013	0.048	0.037	0.059	0.005
Ca		0.010	0.010	0.006	0.009	0.012	0.014	0.008	0.005	0.011	0.017
Mg		0.192	0.161	0.158	0.172	0.194	0.186	0.261	0.168	0.150	0.250
	Total	1.000	1.000	1.000	1.000	1.000	1.000	1.000	1.000	1.000	1.000
Group I											
Ti		0.000	0.000	0.000	0.000	0.000	0.000	0.000	0.000	0.000	0.000
Ce		0.000	0.000	0.000	0.000	0.000	0.000	0.000	0.000	0.000	0.000
La		0.000	0.000	0.000	0.000	0.000	0.000	0.000	0.000	0.000	0.000
Na		0.001	0.001	0.000	0.000	0.000	0.001	0.000	0.000	0.001	0.003
	Total	0.001	0.001	0.001	0.000	0.001	0.002	0.001	0.000	0.001	0.003

Carbonates

Sector	*Neves Corvo*	*Neves Corvo*	*Neves Corvo*	*Neves Corvo*	*Neves Corvo*	*Neves Corvo*	*Neves Corvo*	**Lousal**	**Lousal**	**Lousal**	**Lousal**	**Lousal**
Sub-sector	*Lombador*	*Lombador*	*Lombador*	*Lombador*	*Zambujal*	*Zambujal*	*Zambujal*	*Sesmarias*	*Sesmarias*	*Sesmarias*	*Sesmarias*	*Sesmarias*
Stratigraphic division	*upper VSC*	*upper VSC*	*upper VSC*	*upper VSC*	*lower VSC*	*lower VSC*	*lower VSC*	*lower VSC*	*lower VSC*	*lower VSC*	*lower VSC*	*lower VSC*
Mineralization type	*Mineralized*	*Mineralized*	*Mineralized*	*Mineralized*	*Mineralized*	*Mineralized*	*Mineralized*	*Mineralized*	*Mineralized*	*Mineralized*	*Mineralized*	*Mineralized*
Occurrence												
Sample ref.	*NCL#6*	*NCL#6*	*NCL#6*	*NCL#6*	*NCZ#21*	*NCZ#21*	*NCZ#21*	*SES20#10*	*SES20#10*	*SES20#10*	*SES20#10*	*SES20#10*
# analysis	*#11*	*#12*	*#13*	*#14*	*#15*	*#16*	*#17*	*#18*	*#19*	*#20*	*#21*	*#22*
TiO2	0.000	0.000	0.011	0.059	0.022	0.012	0.000	0.049	0.308	0.814	0.110	0.000
CO2	39.750	39.798	41.325	41.409	39.912	40.469	41.342	38.866	38.457	38.643	38.328	38.582
Ce2O3	0.081	0.012	0.000	0.026	0.000	0.000	0.000	0.000	0.035	0.000	0.000	0.000
La2O3	0.000	0.059	0.000	0.000	0.000	0.056	0.019	0.004	0.013	0.000	0.000	0.000
BaO	0.000	0.000	0.000	0.000	0.000	0.002	0.000	0.000	0.000	0.019	0.000	0.000
SrO	0.029	0.000	0.019	0.011	0.033	0.007	0.000	0.002	0.013	0.002	0.007	0.000
ZnO	6.327	6.274	0.069	0.032	0.042	0.067	0.030	0.019	0.000	0.012	0.000	0.014
FeO	41.829	41.758	46.065	48.107	48.698	47.947	50.575	55.347	53.209	52.329	57.946	58.273
MnO	0.396	0.425	0.283	0.254	0.555	1.310	1.096	0.773	1.344	2.239	0.254	0.262
CaO	0.116	0.079	0.465	0.225	0.309	0.234	0.171	0.230	0.544	0.519	0.356	0.377
MgO	9.484	9.616	11.467	10.609	8.661	9.215	8.729	3.930	4.210	4.376	2.191	2.216
Na2O	0.611	0.665	0.226	0.043	0.023	0.028	0.031	0.000	0.004	0.000	0.000	0.000
Total#	98.623	98.686	99.930	100.775	98.255	99.347	101.993	99.220	98.137	98.953	99.192	99.724
Total	98.623	98.686	99.930	100.775	98.255	99.347	101.993	99.220	98.137	98.953	99.192	99.724
Ion Distribution												
Group C												
C	1.000	1.000	1.000	1.000	1.000	1.000	1.000	1.000	1.000	1.000	1.000	1.000
Total	1.000	1.000	1.000	1.000	1.000	1.000	1.000	1.000	1.000	1.000	1.000	1.000
Group Z												
Ba	0.000	0.000	0.000	0.000	0.000	0.000	0.000	0.000	0.000	0.000	0.000	0.000
Sr	0.000	0.000	0.000	0.000	0.000	0.000	0.000	0.000	0.000	0.000	0.000	0.000
Zn	0.086	0.085	0.001	0.000	0.001	0.001	0.000	0.000	0.000	0.000	0.000	0.000
Fe2+	0.645	0.643	0.683	0.712	0.747	0.726	0.749	0.872	0.848	0.830	0.926	0.925
Mn	0.006	0.007	0.004	0.004	0.009	0.020	0.016	0.012	0.022	0.036	0.004	0.004
Ca	0.002	0.002	0.009	0.004	0.006	0.005	0.003	0.005	0.011	0.011	0.007	0.008
Mg	0.261	0.264	0.303	0.280	0.237	0.249	0.231	0.110	0.120	0.124	0.062	0.063
Total	1.000	1.000	1.000	1.000	1.000	1.000	1.000	1.000	1.000	1.000	1.000	1.000
Group I												
Ti	0.000	0.000	0.000	0.001	0.000	0.000	0.000	0.001	0.004	0.012	0.002	0.000
Ce	0.001	0.000	0.000	0.000	0.000	0.000	0.000	0.000	0.000	0.000	0.000	0.000
La	0.000	0.000	0.000	0.000	0.000	0.000	0.000	0.000	0.000	0.000	0.000	0.000
Na	0.022	0.024	0.008	0.002	0.001	0.001	0.001	0.000	0.000	0.000	0.000	0.000
Total	0.022	0.024	0.008	0.002	0.001	0.002	0.001	0.001	0.005	0.012	0.002	0.000

Carbonates

Sector	Lousal	Lousal	Lousal	Lousal	Lousal	Lousal	Lousal	Lousal	Lousal	Lousal	Lousal	Lousal
Sub-sector	*Sesmarias*	*Sesmarias*	*Sesmarias*	*Sesmarias*	*Sesmarias*	*Sesmarias*	*Sesmarias*	*Sesmarias*	*Sesmarias*	*Sesmarias*	*Sesmarias*	*Sesmarias*
Stratigraphic division	*lower VSC*	*lower VSC*	*upper VSC*	*upper VSC*	*upper VSC*	*upper VSC*	*upper VSC*	*upper VSC*	*upper VSC*	*upper VSC*	*upper VSC*	*upper VSC*
Mineralization type	*Mineralized*	*Mineralized*	*Py-bearing*	*Py-bearing*	*Py-bearing*	*Py-bearing*	*Py-bearing*	*Py-bearing*	*Py-bearing*	*Py-bearing*	*Py-bearing*	*Py-bearing*
Occurrence												
Sample ref.	*SES20#10*	*SES20#10*	*SES20#6*	*SES20#6*	*SES20#6*	*SES20#6*	*SES20#6*	*SES20#6*	*SES20#6*	*SES20#6*	*SES20#6*	*SES20#6*
# analysis	*#23*	*#24*	*#25*	*#26*	*#27*	*#28*	*#29*	*#30*	*#31*	*#32*	*#33*	*#34*
TiO2	0.032	0.120	0.000	0.000	0.000	0.013	0.000	0.018	0.000	0.005	0.000	0.000
CO2	38.710	37.464	38.422	37.958	39.114	37.973	38.313	38.415	39.010	38.943	38.539	38.363
Ce2O3	0.000	0.000	0.025	0.000	0.026	0.000	0.002	0.000	0.048	0.042	0.000	0.000
La2O3	0.000	0.020	0.000	0.026	0.027	0.000	0.041	0.000	0.000	0.031	0.000	0.000
BaO	0.000	0.000	0.023	0.000	0.000	0.000	0.000	0.004	0.000	0.000	0.000	0.032
SrO	0.019	0.019	0.000	0.000	0.000	0.000	0.000	0.004	0.000	0.027	0.009	0.000
ZnO	0.336	0.000	0.017	0.000	0.000	0.000	0.029	0.022	0.007	0.051	0.000	0.000
FeO	58.099	59.107	55.263	58.123	52.324	57.995	58.394	58.137	59.371	60.137	58.665	58.471
MnO	0.381	0.596	0.463	0.296	1.487	0.136	0.113	1.090	0.167	0.511	0.092	0.406
CaO	0.326	0.009	0.333	0.301	0.844	0.465	0.482	0.359	0.629	0.251	0.718	0.519
MgO	2.233	0.799	3.668	1.771	5.016	1.830	1.904	1.675	1.868	1.421	1.812	1.719
Na2O	0.038	0.000	0.000	0.010	0.003	0.022	0.015	0.000	0.009	0.014	0.025	0.000
Total#	100.174	98.134	98.214	98.485	98.841	98.434	99.293	99.724	101.109	101.433	99.860	99.510
Total	100.174	98.134	98.214	98.485	98.841	98.434	99.293	99.724	101.109	101.433	99.860	99.510
Ion Distribution												
Group C												
C	1.000	1.000	1.000	1.000	1.000	1.000	1.000	1.000	1.000	1.000	1.000	1.000
Total	1.000	1.000	1.000	1.000	1.000	1.000	1.000	1.000	1.000	1.000	1.000	1.000
Group Z												
Ba	0.000	0.000	0.000	0.000	0.000	0.000	0.000	0.000	0.000	0.000	0.000	0.000
Sr	0.000	0.000	0.000	0.000	0.000	0.000	0.000	0.000	0.000	0.000	0.000	0.000
Zn	0.005	0.000	0.000	0.000	0.000	0.000	0.000	0.000	0.000	0.001	0.000	0.000
Fe2+	0.919	0.966	0.881	0.938	0.820	0.936	0.934	0.927	0.932	0.946	0.933	0.934
Mn	0.006	0.010	0.008	0.005	0.024	0.002	0.002	0.018	0.003	0.008	0.002	0.007
Ca	0.007	0.000	0.007	0.006	0.017	0.010	0.010	0.007	0.013	0.005	0.015	0.011
Mg	0.063	0.023	0.104	0.051	0.140	0.053	0.054	0.048	0.052	0.040	0.051	0.049
Total	1.000	1.000	1.000	1.000	1.000	1.000	1.000	1.000	1.000	1.000	1.000	1.000
Group I												
Ti	0.001	0.002	0.000	0.000	0.000	0.000	0.000	0.000	0.000	0.000	0.000	0.000
Ce	0.000	0.000	0.000	0.000	0.000	0.000	0.000	0.000	0.000	0.000	0.000	0.000
La	0.000	0.000	0.000	0.000	0.000	0.000	0.000	0.000	0.000	0.000	0.000	0.000
Na	0.001	0.000	0.000	0.000	0.000	0.001	0.001	0.000	0.000	0.001	0.001	0.000
Total	0.002	0.002	0.000	0.001	0.001	0.001	0.001	0.000	0.001	0.001	0.001	0.000

Carbonates

Sector	Lousal	Lousal	Lousal	Lousal	Lousal	Lousal	Lousal	Lousal	Lousal	Lousal	*Aljustrel*	*Aljustrel*
Sub-sector	*Sesmarias*	*Sesmarias*	*Sesmarias*	*Sesmarias*	*Sesmarias*	*Sesmarias*	*Sesmarias*	*Sesmarias*	*Sesmarias*	*Sesmarias*	*Mina F.*	*Gavião*
Stratigraphic division	*lower VSC*	*lower VSC*	*lower VSC*	*lower VSC*	*lower VSC*	*lower VSC*	*lower VSC*	*lower VSC*	*lower VSC*	*lower VSC*	*upper VSC*	*upper VSC*
Mineralization type	*stockwork*	*stockwork*	*stockwork*	*stockwork*	*stockwork*	*stockwork*	*stockwork*	*stockwork*	*stockwork*	*stockwork*	*No-sulphide*	*Mineralized*
Occurrence												
Sample ref.	*SES20#9_2*	*SES20#9_2*	*SES20#9_2*	*SES20#9_2*	*SES20#9_2*	*SES20#9_2*	*SES20#9_2*	*SES20#9_2*	*SES20#9_2*	*SES20#9_2*	*FM#4*	*GV7#3*
# analysis	*#35*	*#36*	*#37*	*#38*	*#39*	*#40*	*#41*	*#42*	*#43*	*#44*	*#45*	*#46*
TiO2	0.000	0.000	0.000	0.000	0.000	0.000	0.010	0.000	0.000	0.000	0.000	0.000
CO2	38.502	38.432	38.303	38.320	38.139	38.392	38.227	38.341	38.011	38.274	43.413	39.579
Ce2O3	0.054	0.000	0.034	0.044	0.025	0.016	0.045	0.006	0.011	0.000	0.066	0.000
La2O3	0.000	0.066	0.000	0.011	0.000	0.000	0.000	0.000	0.051	0.044	0.005	0.003
BaO	0.023	0.015	0.000	0.041	0.019	0.029	0.020	0.007	0.042	0.000	0.000	0.000
SrO	0.000	0.000	0.000	0.025	0.021	0.000	0.000	0.000	0.021	0.000	0.000	0.032
ZnO	0.000	0.000	0.045	0.031	0.000	0.004	0.000	0.015	0.040	0.006	0.019	0.095
FeO	60.871	60.651	59.308	61.578	61.245	61.761	61.451	61.006	60.463	60.055	1.368	51.131
MnO	0.663	0.260	0.985	0.208	0.199	0.208	0.193	0.555	0.263	0.293	0.000	0.271
CaO	0.023	0.414	0.082	0.126	0.058	0.027	0.064	0.119	0.121	0.354	53.175	0.164
MgO	0.713	0.722	1.166	0.304	0.402	0.365	0.374	0.479	0.616	0.937	0.519	7.231
Na2O	0.000	0.022	0.001	0.025	0.014	0.000	0.000	0.000	0.011	0.028	0.018	0.029
Total#	100.849	100.582	99.924	100.713	100.122	100.802	100.384	100.528	99.650	99.991	98.583	98.535
Total	100.849	100.582	99.924	100.713	100.122	100.802	100.384	100.528	99.650	99.991	98.583	98.535

Ion Distribution													
Group C													
C		1.000	1.000	1.000	1.000	1.000	1.000	1.000	1.000	1.000	1.000	1.000	1.000
	Total	1.000	1.000	1.000	1.000	1.000	1.000	1.000	1.000	1.000	1.000	1.000	1.000
Group Z													
Ba		0.000	0.000	0.000	0.000	0.000	0.000	0.000	0.000	0.000	0.000	0.000	0.000
Sr		0.000	0.000	0.000	0.000	0.000	0.000	0.000	0.000	0.000	0.000	0.000	0.000
Zn		0.000	0.000	0.001	0.000	0.000	0.000	0.000	0.000	0.001	0.000	0.000	0.001
Fe2+		0.969	0.967	0.949	0.984	0.984	0.985	0.985	0.975	0.974	0.961	0.019	0.791
Mn		0.011	0.004	0.016	0.003	0.003	0.003	0.003	0.009	0.004	0.005	0.007	0.004
Ca		0.001	0.009	0.002	0.003	0.001	0.001	0.001	0.002	0.003	0.007	0.961	0.003
Mg		0.020	0.021	0.033	0.009	0.012	0.010	0.011	0.014	0.018	0.027	0.012	0.200
	Total	1.000	1.000	1.000	1.000	1.000	1.000	1.000	1.000	1.000	1.000	1.000	1.000
Group I													
Ti		0.000	0.000	0.000	0.000	0.000	0.000	0.000	0.000	0.000	0.000	0.000	0.000
Ce		0.000	0.000	0.000	0.000	0.000	0.000	0.000	0.000	0.000	0.000	0.000	0.000
La		0.000	0.001	0.000	0.000	0.000	0.000	0.000	0.000	0.000	0.000	0.000	0.000
Na		0.000	0.001	0.000	0.001	0.001	0.000	0.000	0.000	0.000	0.001	0.001	0.001
	Total	0.000	0.001	0.000	0.001	0.001	0.000	0.001	0.000	0.001	0.001	0.001	0.001

Carbonates

Sector	*Aljustrel*	*Aljustrel*	*Albernoa*	*Albernoa*	*Albernoa*	*Albernoa*	*Albernoa*	*Albernoa*	*Albernoa*	*Albernoa*	*Albernoa*	*Albernoa*
Sub-sector	*Gavião*	*Gavião*										
Stratigraphic division	*upper VSC*	*upper VSC*	*upper VSC*	*upper VSC*	*upper VSC*	*upper VSC*	*upper VSC*	*upper VSC*	*upper VSC*	*upper VSC*	*upper VSC*	*upper VSC*
Mineralization type	*Mineralized*	*Mineralized*	*No-sulphide*	*No-sulphide*	*No-sulphide*	*No-sulphide*	*No-sulphide*	*No-sulphide*	*Mineralized*	*No-sulphide*	*No-sulphide*	*No-sulphide*
Occurrence									Late veins	Late veins	Late veins	Late veins
Sample ref.	*GV7#3*	*GV7#3*	*Alb03#13a*	*Alb03#22a*	*Alb03#22a*	*Alb03#18*	*Alb03#18*	*Alb03#18*	*18-1-FF*	*18-1-G*	*18-1-G*	*18-1-G*
# analysis	*#47*	*#48*	*#49*	*#50*	*#51*	*#52*	*#53*	*#54*	*#55*	*#56*	*#57*	*#58*
TiO2	0.000	0.000	0.347	0.011	0.065	0.000	0.000	0.020	0.005	0.000	0.000	0.000
CO2	41.565	39.354	43.943	44.837	44.893	43.397	43.876	42.936	45.676	44.197	44.311	42.919
Ce2O3	0.042	0.000	0.040	0.000	0.100	0.015	0.000	0.048	0.048	0.020	0.000	0.048
La2O3	0.015	0.028	0.000	0.012	0.025	0.013	0.028	0.011	0.000	0.058	0.000	0.000
BaO	0.000	0.000	0.000	0.000	0.012	0.000	0.000	0.000	0.000	0.000	0.008	0.000
SrO	0.000	0.004	0.000	0.054	0.016	0.000	0.000	0.000	0.015	0.000	0.021	0.006
ZnO	0.027	0.000	0.041	0.021	0.042	0.004	0.008	0.046	0.000	0.055	0.021	0.065
FeO	46.245	51.810	12.689	10.363	10.196	12.916	10.323	13.023	10.854	15.316	15.329	15.432
MnO	0.805	0.178	6.038	6.313	6.162	7.720	7.909	8.056	0.510	1.545	1.393	1.055
CaO	0.494	0.117	28.366	29.020	28.927	27.622	27.905	27.615	30.048	29.525	29.808	26.563
MgO	11.297	6.789	9.287	10.773	11.072	8.257	9.837	7.568	13.792	9.748	9.716	10.842
Na2O	0.018	0.010	0.029	0.000	0.022	0.006	0.000	0.000	0.023	0.004	0.011	0.031
Total#	100.508	98.290	100.780	101.404	101.532	99.950	99.886	99.323	100.971	100.468	100.618	96.961
Total	100.508	98.290	100.780	101.404	101.532	99.950	99.886	99.323	100.971	100.468	100.618	96.961

Ion Distribution												
Group C												
C	1.000	1.000	2.000	2.000	2.000	2.000	2.000	2.000	2.000	2.000	2.000	2.001
Total	1.000	1.000	2.000	2.000	2.000	2.000	2.000	2.000	2.000	2.000	2.000	2.001
Group Z												
Ba	0.000	0.000	0.000	0.000	0.000	0.000	0.000	0.000	0.000	0.000	0.000	0.000
Sr	0.000	0.000	0.000	0.001	0.000	0.000	0.000	0.000	0.000	0.000	0.000	0.000
Zn	0.000	0.000	0.001	0.001	0.001	0.000	0.000	0.001	0.000	0.001	0.001	0.002
Fe2+	0.682	0.806	0.354	0.283	0.278	0.365	0.288	0.372	0.291	0.424	0.424	0.441
Mn	0.012	0.003	0.171	0.175	0.170	0.221	0.224	0.233	0.014	0.043	0.039	0.031
Ca	0.009	0.002	1.013	1.016	1.011	0.999	0.998	1.010	1.033	1.048	1.056	0.972
Mg	0.297	0.188	0.462	0.525	0.539	0.416	0.490	0.385	0.660	0.482	0.479	0.552
Total	1.000	1.000	2.000	2.000	2.000	2.000	2.000	2.000	1.998	1.998	1.999	1.998
Group I												
Ti	0.000	0.000	0.009	0.000	0.002	0.000	0.000	0.001	0.000	0.000	0.000	0.000
Ce	0.000	0.000	0.001	0.000	0.001	0.000	0.000	0.001	0.001	0.000	0.000	0.001
La	0.000	0.000	0.000	0.000	0.000	0.000	0.000	0.000	0.000	0.001	0.000	0.000
Na	0.001	0.000	0.002	0.000	0.001	0.000	0.000	0.000	0.001	0.000	0.001	0.002
Total	0.001	0.001	0.011	0.000	0.005	0.001	0.000	0.001	0.002	0.001	0.001	0.003

Carbonates

Sector	*Albernoa*	*Albernoa*	*Albernoa*	*Albernoa*	*Albernoa*	*Albernoa*	*Albernoa*	*Albernoa*	*Albernoa*	*Albernoa*	*Albernoa*	*Albernoa*
Sub-sector												
Stratigraphic division	*upper VSC*	*upper VSC*	*upper VSC*	*upper VSC*	*upper VSC*	*upper VSC*	*upper VSC*	*upper VSC*	*upper VSC*	*upper VSC*	*upper VSC*	*upper VSC*
Mineralization type	*No-sulphide*	*No-sulphide*	*No-sulphide*	*No-sulphide*	*No-sulphide*	*No-sulphide*	*No-sulphide*	*No-sulphide*	*No-sulphide*	*No-sulphide*	*No-sulphide*	*No-sulphide*
Occurrence	Late veins	Late veins	Late veins	Late veins	Late veins	Late veins	Late veins	Late veins	Late veins	Late veins	Late veins	Late veins
Sample ref.	*18-1-G*	*18-1-G*	*18-1-G*	*18-1-G*	*18-1-G*	*18-1-G*	*18-1-G*	*18-1-G*	*18-1-G*	*18-1-G*	*18-1-G*	*18-1-G*
# analysis	*#59*	*#60*	*#61*	*#62*	*#63*	*#64*	*#65*	*#66*	*#67*	*#68*	*#69*	*#70*
TiO2	0.000	0.000	0.009	0.000	0.000	0.000	0.000	0.005	0.000	0.000	0.000	0.000
CO2	43.482	44.017	44.827	44.830	44.722	44.541	44.331	44.171	44.663	44.029	44.149	44.369
Ce2O3	0.008	0.024	0.062	0.040	0.000	0.064	0.000	0.019	0.000	0.079	0.015	0.000
La2O3	0.016	0.000	0.000	0.033	0.000	0.067	0.030	0.024	0.009	0.000	0.032	0.015
BaO	0.000	0.000	0.000	0.000	0.029	0.000	0.000	0.000	0.011	0.000	0.000	0.000
SrO	0.021	0.032	0.000	0.012	0.026	0.067	0.056	0.050	0.030	0.071	0.002	0.000
ZnO	0.051	0.039	0.057	0.000	0.027	0.033	0.006	0.066	0.035	0.071	0.034	0.071
FeO	16.588	13.498	13.860	13.480	13.846	13.878	17.020	16.392	14.527	16.011	16.175	0.044
MnO	0.501	1.190	1.154	1.203	1.012	0.907	0.788	0.995	1.017	1.093	1.034	0.056
CaO	29.532	29.271	30.010	30.249	30.272	29.936	29.112	28.996	29.597	29.200	29.451	56.371
MgO	8.962	10.993	11.029	11.059	10.800	10.872	9.532	9.786	10.864	9.636	9.536	0.027
Na2O	0.004	0.000	0.000	0.002	0.010	0.023	0.047	0.006	0.003	0.013	0.019	0.000
Total#	99.165	99.064	101.008	100.908	100.744	100.388	100.922	100.510	100.756	100.203	100.447	100.953
Total	99.165	99.064	101.008	100.908	100.744	100.388	100.922	100.510	100.756	100.203	100.447	100.953
Ion Distribution												
Group C												
C	2.000	2.000	1.999	2.000	2.000	2.000	2.001	2.000	2.000	2.000	2.000	2.000
Total	2.000	2.000	1.999	2.000	2.000	2.000	2.001	2.000	2.000	2.000	2.000	2.000
Group Z												
Ba	0.000	0.000	0.000	0.000	0.000	0.000	0.000	0.000	0.000	0.000	0.000	0.000
Sr	0.000	0.001	0.000	0.000	0.000	0.001	0.001	0.001	0.001	0.001	0.000	0.000
Zn	0.001	0.001	0.001	0.000	0.001	0.001	0.000	0.002	0.001	0.002	0.001	0.002
Fe2+	0.467	0.376	0.379	0.368	0.379	0.382	0.471	0.455	0.398	0.445	0.449	0.001
Mn	0.014	0.034	0.032	0.033	0.028	0.025	0.022	0.028	0.028	0.031	0.029	0.002
Ca	1.066	1.044	1.050	1.059	1.063	1.055	1.031	1.030	1.040	1.041	1.047	1.994
Mg	0.450	0.545	0.537	0.539	0.527	0.533	0.470	0.484	0.531	0.478	0.472	0.001
Total	1.998	2.001	1.999	1.999	1.998	1.997	1.995	2.000	1.999	1.998	1.998	2.000
Group I												
Ti	0.000	0.000	0.000	0.000	0.000	0.000	0.000	0.000	0.000	0.000	0.000	0.000
Ce	0.000	0.000	0.001	0.000	0.000	0.001	0.000	0.000	0.000	0.001	0.000	0.000
La	0.000	0.000	0.000	0.000	0.000	0.001	0.000	0.000	0.000	0.000	0.000	0.000
Na	0.000	0.000	0.000	0.000	0.001	0.001	0.003	0.000	0.000	0.001	0.001	0.000
Total	0.000	0.000	0.001	0.000	0.001	0.003	0.003	0.000	0.000	0.002	0.001	0.000

Carbonates

Sector	*Albernoa*	*Albernoa*	*Albernoa*	*Albernoa*	*Albernoa*	*Albernoa*	*Albernoa*	*Albernoa*	*Albernoa*	*Albernoa*	*Albernoa*	*Albernoa*
Sub-sector												
Stratigraphic division	*upper VSC*	*middle VSC*	*upper VSC*	*upper VSC*	*upper VSC*	*upper VSC*	*upper VSC*	*upper VSC*	*upper VSC*	*upper VSC*	*upper VSC*	*upper VSC*
Mineralization type	*No-sulphide*	*Py-bearing*	*No-sulphide*	*No-sulphide*	*No-sulphide*	*No-sulphide*	*No-sulphide*	*No-sulphide*	*No-sulphide*	*No-sulphide*	*No-sulphide*	*No-sulphide*
Occurrence	Late veins	Late veins	Late veins	Late veins	Late veins	Late veins	Late veins	Late veins	Late veins	Late veins	Late veins	Late veins
Sample ref.	***18-1-G***	***37-1-E***	***CW2-AA***	***CW2-AA***	***CW2-AA***	***CW2-AA***	***CW2-AA***	***CW2-AA***	***CW2-AA***	***CW2-AA***	***CW2-AA***	***CW2-AA***
# analysis	***#71***	***#72***	***#73***	***#74***	***#75***	***#76***	***#77***	***#78***	***#79***	***#80***	***#81***	***#82***
TiO2	0.000	0.000	0.000	0.000	0.018	0.000	0.011	0.000	0.000	0.008	0.005	0.000
CO2	44.282	44.244	43.443	43.603	43.845	44.826	42.991	42.888	43.552	44.921	45.038	44.682
Ce2O3	0.010	0.070	0.047	0.039	0.065	0.064	0.000	0.000	0.017	0.000	0.000	0.041
La2O3	0.000	0.000	0.000	0.000	0.000	0.000	0.000	0.000	0.000	0.000	0.000	0.000
BaO	0.022	0.015	0.074	0.088	0.065	0.058	0.038	0.090	0.000	0.001	0.000	0.070
SrO	0.001	0.000	0.000	0.000	0.000	0.000	0.000	0.000	0.000	0.000	0.000	0.000
ZnO	0.076	0.000	0.145	0.102	0.030	0.035	0.000	0.013	0.033	0.036	0.073	0.012
FeO	0.055	0.929	0.204	0.267	0.089	0.413	0.363	0.333	0.395	0.064	0.150	0.093
MnO	0.046	1.331	0.475	0.276	0.186	0.409	0.467	0.423	0.552	0.150	0.237	0.187
CaO	56.166	54.154	54.656	54.965	55.620	56.094	53.868	53.791	54.420	57.001	56.891	56.621
MgO	0.030	0.316	0.025	0.042	0.000	0.229	0.182	0.141	0.221	0.036	0.084	0.035
Na2O	0.021	0.000	0.001	0.002	0.000	0.004	0.000	0.007	0.000	0.000	0.008	0.003
Total#	100.709	101.059	99.070	99.384	99.918	102.132	97.920	97.686	99.190	102.217	102.486	101.744
Total	100.709	101.059	99.070	99.384	99.918	102.132	97.920	97.686	99.190	102.217	102.486	101.744
Ion Distribution												
Group C												
C	2.001	2.000	2.000	2.000	1.999	2.000	2.000	2.000	2.000	2.000	2.000	2.000
Total	2.001	2.000	2.000	2.000	1.999	2.000	2.000	2.000	2.000	2.000	2.000	2.000
Group Z												
Ba	0.000	0.000	0.001	0.001	0.001	0.001	0.001	0.001	0.000	0.000	0.000	0.001
Sr	0.000	0.000	0.000	0.000	0.000	0.000	0.000	0.000	0.000	0.000	0.000	0.000
Zn	0.002	0.000	0.004	0.003	0.001	0.001	0.000	0.000	0.001	0.001	0.002	0.000
Fe2+	0.002	0.026	0.006	0.008	0.002	0.011	0.010	0.010	0.011	0.002	0.004	0.003
Mn	0.001	0.037	0.014	0.008	0.005	0.011	0.013	0.012	0.016	0.004	0.007	0.005
Ca	1.991	1.921	1.974	1.978	1.990	1.964	1.966	1.969	1.961	1.991	1.983	1.989
Mg	0.001	0.016	0.001	0.002	0.000	0.011	0.009	0.007	0.011	0.002	0.004	0.002
Total	1.997	2.000	2.000	2.000	1.999	1.999	1.999	1.999	2.000	2.000	2.000	2.000
Group I												
Ti	0.000	0.000	0.000	0.000	0.000	0.000	0.000	0.000	0.000	0.000	0.000	0.000
Ce	0.000	0.001	0.001	0.000	0.001	0.001	0.000	0.000	0.000	0.000	0.000	0.000
La	0.000	0.000	0.000	0.000	0.000	0.000	0.000	0.000	0.000	0.000	0.000	0.000
Na	0.001	0.000	0.000	0.000	0.000	0.000	0.000	0.000	0.000	0.000	0.001	0.000
Total	0.001	0.001	0.001	0.000	0.001	0.001	0.000	0.000	0.000	0.000	0.001	0.000

Carbonates

Sector		Albernoa	Albernoa	Albernoa	Albernoa	Albernoa	Albernoa	Albernoa	Albernoa	Albernoa	Albernoa	Albernoa	Albernoa
Sub-sector													
Stratigraphic division		upper VSC	upper VSC	upper VSC	upper VSC	upper VSC	upper VSC	upper VSC	upper VSC	upper VSC	upper VSC	upper VSC	upper VSC
Mineralization type		No-sulphide	No-sulphide	No-sulphide	No-sulphide	No-sulphide	No-sulphide	No-sulphide	No-sulphide	No-sulphide	No-sulphide	No-sulphide	No-sulphide
Occurrence		Late veins	Late veins	Late veins	matrix	matrix	matrix	matrix	matrix	matrix	matrix	matrix	matrix
Sample ref.		CW2-M	CW2-M	CW2-M	18-1-G2	18-1-G2	18-1-G2	18-1-G2	18-1-G2	18-1-G2	18-1-G2	18-1-G2	CW2-AA
# analysis		#83	#84	#85	#86	#87	#88	#89	#90	#91	#92	#93	#94
TiO2		0.000	0.000	0.005	0.000	0.000	0.000	0.027	0.000	0.076	0.000	0.004	0.000
CO2		44.346	43.752	44.385	44.694	44.587	44.715	42.937	44.877	44.140	44.697	43.859	45.174
Ce2O3		0.000	0.053	0.000	0.029	0.000	0.031	0.000	0.073	0.074	0.042	0.031	0.103
La2O3		0.000	0.000	0.000	0.062	0.019	0.000	0.000	0.000	0.000	0.002	0.000	0.000
BaO		0.109	0.072	0.052	0.004	0.000	0.000	0.000	0.009	0.000	0.031	0.000	0.023
SrO		0.000	0.000	0.000	0.000	0.013	0.055	0.043	0.000	0.033	0.060	0.017	0.000
ZnO		0.000	0.080	0.058	0.000	0.026	0.017	0.096	0.068	0.096	0.058	0.019	0.000
FeO		0.074	0.030	0.099	14.287	13.409	13.958	14.435	16.226	16.401	13.330	16.507	0.342
MnO		0.006	0.000	0.023	1.115	1.195	1.029	1.176	0.945	1.064	1.156	0.988	0.298
CaO		56.221	55.555	56.266	28.195	30.253	29.929	28.370	29.369	29.162	30.156	29.115	56.879
MgO		0.131	0.064	0.089	10.579	10.870	10.964	10.071	10.315	9.637	11.065	9.384	0.123
Na2O		0.000	0.000	0.004	0.553	0.000	0.012	0.017	0.000	0.000	0.000	0.008	0.000
Total#		100.887	99.606	100.981	99.518	100.372	100.710	97.172	101.882	100.683	100.597	99.932	102.942
	Total	100.887	99.606	100.981	99.518	100.372	100.710	97.172	101.882	100.683	100.597	99.932	102.942
Ion Distribution													
Group C													
C		2.000	2.000	2.000	2.017	2.000	2.000	2.000	2.000	1.998	2.000	2.000	1.999
	Total	2.000	2.000	2.000	2.017	2.000	2.000	2.000	2.000	1.998	2.000	2.000	1.999
Group Z													
Ba		0.001	0.001	0.001	0.000	0.000	0.000	0.000	0.000	0.000	0.000	0.000	0.000
Sr		0.000	0.000	0.000	0.000	0.000	0.001	0.001	0.000	0.001	0.001	0.000	0.000
Zn		0.000	0.002	0.001	0.000	0.001	0.000	0.002	0.002	0.002	0.001	0.000	0.000
Fe2+		0.002	0.001	0.003	0.395	0.368	0.382	0.412	0.443	0.455	0.365	0.461	0.009
Mn		0.000	0.000	0.001	0.031	0.033	0.029	0.034	0.026	0.030	0.032	0.028	0.008
Ca		1.990	1.993	1.990	0.999	1.065	1.051	1.037	1.027	1.036	1.059	1.042	1.976
Mg		0.006	0.003	0.004	0.521	0.532	0.536	0.512	0.502	0.476	0.541	0.467	0.006
	Total	1.999	2.000	2.000	1.946	1.999	1.999	1.998	2.000	2.000	1.999	1.998	1.999
Group I													
Ti		0.000	0.000	0.000	0.000	0.000	0.000	0.001	0.000	0.002	0.000	0.000	0.000
Ce		0.000	0.001	0.000	0.000	0.000	0.000	0.000	0.001	0.001	0.001	0.000	0.001
La		0.000	0.000	0.000	0.001	0.000	0.000	0.000	0.000	0.000	0.000	0.000	0.000
Na		0.000	0.000	0.000	0.035	0.000	0.001	0.001	0.000	0.000	0.000	0.001	0.000
	Total	0.000	0.001	0.000	0.036	0.000	0.001	0.002	0.001	0.003	0.001	0.001	0.001

Carbonates

Sector	*Albernoa*	*Albernoa*	*Albernoa*	*Albernoa*	*Albernoa*	*Albernoa*	*Albernoa*	*Albernoa*	*Albernoa*	*Albernoa*	*Albernoa*
Sub-sector											
Stratigraphic division	*upper VSC*	*upper VSC*	*upper VSC*	*upper VSC*	*upper VSC*	*upper VSC*	*upper VSC*	*upper VSC*	*upper VSC*	*upper VSC*	*upper VSC*
Mineralization type	*No-sulphide*	*No-sulphide*	*No-sulphide*	*No-sulphide*	*No-sulphide*	*No-sulphide*	*No-sulphide*	*No-sulphide*	*No-sulphide*	*No-sulphide*	*No-sulphide*
Occurrence	matrix	matrix	matrix	matrix	matrix	matrix	grains	grains	grains	grains	grains
Sample ref.	*CW2-AA*	*CW2-AA*	*CW2-AA*	*CW2-AA*	*CW2-AA*	*CW2-AA*	*CW2-P*	*CW2-P*	*CW2-P*	*18-1-II*	*18-1-II*
# analysis	*#95*	*#96*	*#97*	*#98*	*#99*	*#100*	*#101*	*#102*	*#103*	*#104*	*#105*
TiO2	0.000	0.000	0.000	0.008	0.024	0.000	0.000	0.000	0.000	0.079	0.000
CO2	44.527	44.562	43.154	44.180	44.282	43.407	45.244	43.982	44.351	43.564	42.493
Ce2O3	0.000	0.037	0.037	0.025	0.061	0.040	0.032	0.000	0.000	0.000	0.000
La2O3	0.000	0.000	0.000	0.000	0.000	0.000	0.000	0.063	0.000	0.060	0.026
BaO	0.059	0.170	0.003	0.120	0.096	0.093	0.000	0.042	0.035	0.000	0.000
SrO	0.000	0.000	0.000	0.000	0.000	0.000	0.100	0.083	0.076	0.022	0.037
ZnO	0.000	0.000	0.052	0.000	0.039	0.043	0.089	0.010	0.039	0.046	0.052
FeO	0.202	0.108	0.116	0.486	0.321	0.189	0.215	0.273	0.258	0.175	0.196
MnO	0.264	0.419	0.401	0.479	0.552	0.498	1.329	1.243	1.215	0.273	0.256
CaO	56.179	56.267	54.462	55.262	55.490	54.600	56.105	54.505	54.993	54.933	53.293
MgO	0.104	0.026	0.035	0.165	0.125	0.036	0.134	0.145	0.155	0.146	0.176
Na2O	0.007	0.000	0.009	0.002	0.008	0.015	0.007	0.020	0.017	0.009	0.054
Total#	101.342	101.589	98.269	100.727	100.998	98.921	103.255	100.366	101.139	99.307	96.583
Total	101.342	101.589	98.269	100.727	100.998	98.921	103.255	100.366	101.139	99.307	96.583
Ion Distribution											
Group C											
C	2.000	2.000	2.000	2.000	1.999	2.000	2.000	2.000	2.001	1.998	2.002
Total	2.000	2.000	2.000	2.000	1.999	2.000	2.000	2.000	2.001	1.998	2.002
Group Z											
Ba	0.001	0.002	0.000	0.002	0.001	0.001	0.000	0.001	0.000	0.000	0.000
Sr	0.000	0.000	0.000	0.000	0.000	0.000	0.002	0.002	0.001	0.000	0.001
Zn	0.000	0.000	0.001	0.000	0.001	0.001	0.002	0.000	0.001	0.001	0.001
Fe2+	0.006	0.003	0.003	0.013	0.009	0.005	0.006	0.008	0.007	0.005	0.006
Mn	0.007	0.012	0.012	0.013	0.015	0.014	0.036	0.035	0.034	0.008	0.007
Ca	1.981	1.982	1.981	1.963	1.966	1.975	1.946	1.945	1.947	1.977	1.970
Mg	0.005	0.001	0.002	0.008	0.006	0.002	0.006	0.007	0.008	0.007	0.009
Total	2.000	2.000	1.999	1.999	1.998	1.998	1.998	1.998	1.998	1.998	1.994
Group I											
Ti	0.000	0.000	0.000	0.000	0.001	0.000	0.000	0.000	0.000	0.002	0.000
Ce	0.000	0.000	0.000	0.000	0.001	0.000	0.000	0.000	0.000	0.000	0.000
La	0.000	0.000	0.000	0.000	0.000	0.000	0.000	0.001	0.000	0.001	0.000
Na	0.000	0.000	0.001	0.000	0.001	0.001	0.000	0.001	0.001	0.001	0.004
Total	0.000	0.000	0.001	0.000	0.003	0.001	0.000	0.002	0.001	0.004	0.004

Feldspar

n = 36

Feldspars *s.l.*

Sector	*Aljustrel*	*Aljustrel*	*Aljustrel*	*Aljustrel*	*Aljustrel*	*Aljustrel*	*Aljustrel*	*Aljustrel*	*Aljustrel*	*Aljustrel*	*Aljustrel*	*Aljustrel*
Sub-sector	*Feitais mine*	*Gavião*	*Gavião*	*Gavião*	*Gavião*	*Gavião*	*Gavião*	*Gavião*	*Gavião*	*Gavião*	*Gavião*	*Mte Mesas*
Stratigraphic division	*upper VSC*	*upper VSC*	*upper VSC*	*upper VSC*	*upper VSC*	*upper VSC*	*upper VSC*	*upper VSC*	*upper VSC*	*upper VSC*	*upper VSC*	*upper VSC*
Mineralization type	*No Sulph*	*Py-bearing*	*Py-bearing*	*Py-bearing*	*Py-bearing*	*Py-bearing*	*Py-bearing*	*Py-bearing*	*Py-bearing*	*Py-bearing*	*Py-bearing*	*Mineralized*
Occurrence												
Sample ref.	*FFM#2*	*GV7#4*	*GV7#4*	*GV7#4*	*GV7#4*	*GV9#10*	*GV9#10*	*GV9#10*	*GV9#10*	*GV9#10*	*GV9#10*	*MDM02#6*
# analysis	*#1*	*#2*	*#3*	*#4*	*#5*	*#6*	*#7*	*#8*	*#9*	*#10*	*#11*	*#12*
TiO2	0.036	0.007	0.010	0.000	0.016	0.000	0.019	0.000	0.000	0.000	0.017	0.009
SiO2	67.752	68.080	67.032	68.735	68.719	69.877	68.600	70.235	68.909	67.447	67.713	68.607
Fe2O3	0.000	0.000	0.000	0.000	1.046	0.187	0.190	0.213	0.000	0.000	0.000	0.000
Al2O3	18.905	19.384	19.327	19.247	18.762	19.082	19.604	19.084	19.123	19.781	19.823	19.055
BaO	0.000	0.045	0.000	0.024	0.000	0.000	0.000	0.031	0.000	0.028	0.000	0.000
SrO	0.136	0.000	0.233	0.014	0.066	0.009	0.157	0.114	0.000	0.000	0.000	0.048
FeO	0.131	0.148	0.405	0.777	0.351	0.000	0.000	0.000	0.344	0.318	0.309	0.239
CaO	0.118	0.469	0.806	0.516	0.322	0.031	0.626	0.177	0.147	0.671	0.673	0.046
MgO	0.000	0.069	0.006	0.000	0.017	0.003	0.000	0.002	0.000	0.044	0.020	0.005
K2O	0.105	0.072	0.028	0.024	0.022	0.063	0.009	0.029	0.023	0.260	0.294	0.057
Na2O	11.196	11.193	10.774	11.212	11.605	12.065	11.644	12.032	11.435	10.970	11.040	11.502
Total	98.379	99.467	98.621	100.549	100.926	101.317	100.849	101.917	99.981	99.519	99.889	99.568
Ion Distribution												
Group Z												
Ti	0.001	0.000	0.000	0.000	0.001	0.000	0.001	0.000	0.000	0.000	0.001	0.000
Si	3.008	2.991	2.978	2.995	2.991	3.014	2.980	3.014	3.010	2.969	2.970	3.009
Fe3+	0.000	0.000	0.000	0.000	0.034	0.006	0.006	0.007	0.000	0.000	0.000	0.000
Al	0.989	1.004	1.012	0.988	0.963	0.970	1.004	0.965	0.984	1.026	1.025	0.985
Fe2+	0.002	0.005	0.009	0.017	0.011	0.000	0.000	0.000	0.006	0.005	0.005	0.005
Total	4.000	4.000	4.000	4.000	4.000	3.990	3.991	3.987	4.000	4.000	4.000	4.000
Group X												
Ba	0.000	0.001	0.000	0.000	0.000	0.000	0.000	0.001	0.000	0.001	0.000	0.000
Sr	0.004	0.000	0.006	0.000	0.002	0.000	0.004	0.003	0.000	0.000	0.000	0.001
Fe2+	0.003	0.001	0.006	0.012	0.002	0.000	0.000	0.000	0.007	0.007	0.007	0.004
Ca	0.006	0.022	0.038	0.024	0.015	0.001	0.029	0.008	0.007	0.032	0.032	0.002
Mg	0.000	0.005	0.000	0.000	0.001	0.000	0.000	0.000	0.000	0.003	0.001	0.000
K	0.006	0.004	0.002	0.001	0.001	0.004	0.001	0.002	0.001	0.015	0.017	0.003
Na	0.964	0.954	0.928	0.947	0.980	1.009	0.981	1.001	0.968	0.936	0.939	0.978
Total	0.981	0.986	0.980	0.985	1.000	1.014	1.014	1.014	0.983	0.993	0.995	0.989

Feldspars *s.l.*

Sector	*Aljustrel*	*Aljustrel*	*Aljustrel*	*Aljustrel*	*Aljustrel*	*Aljustrel*	*Aljustrel*	*Aljustrel*	*Aljustrel*	*Aljustrel*	*Albernoa*	*Albernoa*
Sub-sector	*Mte Mesas*	*Mte Mesas*	*Mte Mesas*	*Mte Mesas*	*Mte Mesas*	*Feitais extensio*	*Feitais extensio*	*Feitais extensio*	*Feitais extensio*	*Feitais extensio*	*Feitais extensio*	*Feitais extensio*
Stratigraphic division	*upper VSC*	*upper VSC*	*upper VSC*	*upper VSC*	*upper VSC*	*upper VSC*	*upper VSC*	*upper VSC*	*upper VSC*	*upper VSC*	*upper VSC*	*upper VSC*
Mineralization type	*Mineralized*	*Mineralized*	*No Sulph*	*No Sulph*	*No Sulph*	*Mineralized*	*Mineralized*	*Mineralized*	*Mineralized*	*Mineralized*	*No Sulph*	*No Sulph*
Occurrence												
Sample ref.	*MDM02#6*	*MDM02#6*	*MDM02#8*	*MDM02#8*	*MDM02#8*	*EDS1-H*	*EDS1-H*	*EDS1-H*	*EDS1-H*	*EDS1-H*	*18-1-EE*	*18-1-EE*
# analysis	*#13*	*#14*	*#15*	*#16*	*#17*	*#37*	*#38*	*#39*	*#40*	*#41*	*#18*	*#19*
TiO2	0.045	0.019	0.000	0.000	0.017	0.000	0.000	0.000	0.014	0.000	0.000	0.002
SiO2	68.528	68.961	67.902	68.678	68.454	69.802	69.848	69.684	70.084	70.452	68.610	68.210
Fe2O3	0.000	0.000	0.000	0.350	0.000	0.000	0.000	0.000	0.000	0.000	0.103	0.103
Al2O3	18.523	17.662	19.837	19.035	19.115	19.596	19.329	19.328	19.234	19.601	19.754	19.566
BaO	0.088	0.000	0.016	0.000	0.000	0.005	0.053	0.028	0.000	0.014	0.000	0.000
SrO	0.000	0.000	0.029	0.000	0.121	0.044	0.073	0.026	0.000	0.056	0.118	0.027
FeO	0.250	0.288	0.377	0.000	0.061	0.232	0.141	0.088	0.114	0.126	0.000	0.000
CaO	0.012	0.048	0.820	0.329	0.399	0.124	0.104	0.149	0.011	0.189	0.244	0.404
MgO	0.032	0.000	0.000	0.000	0.003	0.000	0.004	0.000	0.005	0.000	0.014	0.000
K2O	0.086	0.053	0.035	0.037	0.012	0.012	0.018	0.013	0.002	0.011	0.045	0.062
Na2O	11.419	11.455	11.201	11.703	11.403	11.893	11.602	11.703	11.839	11.560	11.750	11.628
Total	98.983	98.486	100.217	100.132	99.585	101.708	101.172	101.019	101.303	102.009	100.638	100.002
Ion Distribution												
Group Z												
Ti	0.002	0.001	0.000	0.000	0.001	0.000	0.000	0.000	0.000	0.000	0.000	0.000
Si	3.024	3.055	2.969	3.000	3.003	3.000	3.014	3.011	3.018	3.012	2.983	2.984
Fe3+	0.000	0.000	0.000	0.012	0.000	0.000	0.000	0.000	0.000	0.000	0.003	0.003
Al	0.963	0.922	1.022	0.980	0.988	0.993	0.983	0.984	0.976	0.988	1.012	1.009
Fe2+	0.009	0.011	0.009	0.000	0.002	0.007	0.004	0.003	0.004	0.000	0.000	0.000
Total	3.998	3.988	4.000	3.992	3.995	4.000	4.000	3.998	3.999	4.000	3.998	3.996
Group X												
Ba	0.002	0.000	0.000	0.000	0.000	0.000	0.001	0.000	0.000	0.000	0.000	0.000
Sr	0.000	0.000	0.001	0.000	0.003	0.001	0.002	0.001	0.000	0.001	0.003	0.001
Fe2+	0.000	0.000	0.005	0.000	0.000	0.001	0.001	0.000	0.000	0.004	0.000	0.000
Ca	0.001	0.002	0.038	0.015	0.019	0.006	0.005	0.007	0.001	0.009	0.011	0.019
Mg	0.002	0.000	0.000	0.000	0.000	0.000	0.000	0.000	0.000	0.000	0.001	0.000
K	0.005	0.003	0.002	0.002	0.001	0.001	0.001	0.001	0.000	0.001	0.002	0.003
Na	0.977	0.984	0.950	0.991	0.970	0.991	0.971	0.980	0.988	0.958	0.990	0.986
Total	0.986	0.989	0.996	1.009	0.993	1.000	0.981	0.989	0.989	0.973	1.008	1.009

Feldspars *s.l.*

Sector	*Albernoa*	*Albernoa*	*Albernoa*	*Albernoa*	*Albernoa*	*Albernoa*	*Albernoa*	*Albernoa*	*Albernoa*	*Albernoa*	*Albernoa*	*Albernoa*
Sub-sector	*eitais extensio*	*eitais extensio*	*eitais extensio*	*eitais extensio*	*eitais extensio*	*eitais extensio*	*eitais extensio*	*eitais extensio*	*eitais extensio*	*eitais extensio*	*eitais extensio*	*eitais extensio*
Stratigraphic division	*upper VSC*	*upper VSC*	*upper VSC*	*upper VSC*	*upper VSC*	*upper VSC*	*upper VSC*	*upper VSC*	*upper VSC*	*upper VSC*	*upper VSC*	*upper VSC*
Mineralization type	*No Sulph*	*No Sulph*	*No Sulph*	*No Sulph*	*No Sulph*	*No Sulph*	*No Sulph*	*No Sulph*	*No Sulph*	*No Sulph*	*No Sulph*	*No Sulph*
Occurrence												
Sample ref.	*18-1-EE*	*CW2-M*	*CW2-M*	*CW2-M*	*CW2-M*	*CW2-M*	*CW2-P*	*CW2-P*	*CW2-P*	*CW2-P*	*CW2-P*	*CW2-P*
# analysis	*#20*	*#21*	*#22*	*#23*	*#24*	*#25*	*#26*	*#27*	*#28*	*#29*	*#30*	*#31*
TiO2	0.000	0.003	0.000	0.000	0.035	0.018	0.010	0.008	0.000	0.000	0.000	0.000
SiO2	66.825	68.767	66.520	65.672	68.072	69.548	68.214	68.717	68.356	68.078	68.984	68.347
Fe2O3	0.104	0.041	0.076	0.124	0.000	0.058	0.000	0.037	0.022	0.000	0.250	1.336
Al2O3	19.813	20.220	21.643	21.394	20.554	19.822	19.839	19.257	19.232	19.537	19.492	19.469
BaO	0.011	0.000	0.017	0.006	0.000	0.037	0.000	0.000	0.000	0.015	0.000	0.000
SrO	0.009	0.050	0.086	0.099	0.028	0.034	0.103	0.100	0.089	0.089	0.000	0.000
FeO	0.000	0.000	0.000	0.000	0.042	0.000	0.000	0.000	0.000	0.206	0.000	0.000
CaO	0.991	0.492	2.324	2.712	1.074	0.389	0.433	0.410	0.419	0.190	0.136	0.149
MgO	0.000	0.166	0.025	0.000	0.018	0.000	0.000	0.000	0.006	0.002	0.000	0.460
K2O	0.141	0.494	0.263	0.020	0.118	0.024	0.044	0.041	0.060	0.023	0.022	0.034
Na2O	11.142	11.358	10.414	10.566	11.032	11.975	11.632	11.777	11.749	11.484	11.953	11.817
Total	99.036	101.591	101.368	100.593	100.973	101.905	100.275	100.347	99.933	99.624	100.837	101.612
Ion Distribution												
Group Z												
Ti	0.000	0.000	0.000	0.000	0.001	0.001	0.000	0.000	0.000	0.000	0.000	0.000
Si	2.958	2.966	2.888	2.878	2.951	2.986	2.976	2.996	2.994	2.988	2.992	2.956
Fe3+	0.003	0.001	0.002	0.004	0.000	0.002	0.000	0.001	0.001	0.000	0.008	0.043
Al	1.033	1.028	1.108	1.105	1.050	1.003	1.020	0.990	0.993	1.011	0.996	0.993
Fe2+	0.000	0.000	0.000	0.000	0.000	0.000	0.000	0.000	0.000	0.002	0.000	0.000
Total	3.995	3.996	3.999	3.988	4.002	3.992	3.997	3.987	3.987	4.000	3.996	3.992
Group X												
Ba	0.000	0.000	0.000	0.000	0.000	0.001	0.000	0.000	0.000	0.000	0.000	0.000
Sr	0.000	0.001	0.002	0.003	0.001	0.001	0.003	0.003	0.002	0.002	0.000	0.000
Fe2+	0.000	0.000	0.000	0.000	0.002	0.000	0.000	0.000	0.000	0.006	0.000	0.000
Ca	0.047	0.023	0.108	0.127	0.050	0.018	0.020	0.019	0.020	0.009	0.006	0.007
Mg	0.000	0.011	0.002	0.000	0.001	0.000	0.000	0.000	0.000	0.000	0.000	0.030
K	0.008	0.027	0.015	0.001	0.007	0.001	0.002	0.002	0.003	0.001	0.001	0.002
Na	0.956	0.950	0.877	0.898	0.927	0.997	0.984	0.996	0.998	0.977	1.005	0.991
Total	1.011	1.012	1.004	1.029	0.987	1.018	1.009	1.020	1.023	0.996	1.013	1.030

Feldspars *s.l.*

Sector	*Albernoa*	*Albernoa*	*Albernoa*	*Albernoa*	*Albernoa*
Sub-sector	*Feitais extension*	*Feitais extension*	*Feitais extension*	*Feitais extension*	*Feitais extension*
Stratigraphic division	*upper VSC*	*middle VSC*	*middle VSC*	*middle VSC*	*middle VSC*
Mineralization type	*No Sulph*	*No Sulph*	*No Sulph*	*No Sulph*	*No Sulph*
Occurrence					
Sample ref.	*CW2-P*	*Rt56*	*Rt56*	*Rt56*	*T73*
# analysis	*#32*	*#33*	*#34*	*#35*	*#36*
TiO2	0.000	0.030	0.000	0.026	0.009
SiO2	68.690	69.307	68.996	69.066	67.993
Fe2O3	0.200	0.000	0.000	0.000	0.000
Al2O3	19.183	19.379	19.162	19.040	19.237
BaO	0.000	0.000	0.000	0.000	0.000
SrO	0.000	0.000	0.017	0.000	0.199
FeO	0.000	0.149	0.100	0.218	0.002
CaO	0.163	0.032	0.056	0.052	0.087
MgO	0.000	0.016	0.003	0.000	0.001
K2O	0.020	0.030	0.002	0.018	0.044
Na2O	11.825	11.543	11.516	11.786	11.489
Total	100.081	100.486	99.852	100.206	99.061

Ion Distribution					
Group Z					
Ti	0.000	0.001	0.000	0.001	0.000
Si	3.000	3.008	3.013	3.011	2.999
Fe3+	0.007	0.000	0.000	0.000	0.000
Al	0.987	0.991	0.986	0.978	1.000
Fe2+	0.000	0.000	0.001	0.008	0.000
Total	3.994	4.001	4.000	3.998	3.999
Group X					
Ba	0.000	0.000	0.000	0.000	0.000
Sr	0.000	0.000	0.000	0.000	0.005
Fe2+	0.000	0.005	0.003	0.000	0.000
Ca	0.008	0.001	0.003	0.002	0.004
Mg	0.000	0.001	0.000	0.000	0.000
K	0.001	0.002	0.000	0.001	0.002
Na	1.001	0.971	0.975	0.996	0.982
Total	1.010	0.981	0.981	1.000	0.994

Zircon

n = 35

Zircon

Sector	Albernoa	Albernoa	Albernoa	Albernoa	Albernoa	Albernoa	Albernoa	Albernoa	Albernoa	Albernoa	Albernoa	Albernoa
Sub-sector												
Stratigraphic division	lower VSC	PQG	PQG	PQG	upper VSC	upper VSC	upper VSC	upper VSC	upper VSC	upper VSC	upper VSC	lower VSC
Mineralization type	No Sulph	No Sulph	No Sulph	No Sulph	No Sulph	No Sulph	No Sulph	No Sulph	No Sulph	No Sulph	No Sulph	No Sulph
Occurrence	metapel	metapel	metapel	metapel	metapel	metapel	metapel	metapel	Volc Metapel	Volc Metapel	Volc Metapel	Volc Metapel
Sample ref.	18-1-EE	X42	X42	X42	X68	X69	X70	X71	RT56	T73	T74	18-1-G2
Observations	No Alt	No Alt	No Alt	No Alt	No Alt	No Alt	No Alt	No Alt	No Alt	No Alt	No Alt	No Alt
# analysis	#1	#2	#3	#4	#5	#6	#7	#8	#9	#10	#11	#12
MnO	0.045	0.083	0.000	0.000	0.005	0.000	0.006	0.005	0.000	0.006	0.000	0.007
P2O5	2.387	0.199	0.033	0.113	0.119	0.000	0.616	0.000	0.111	0.018	0.033	0.000
HfO2	0.868	1.457	1.005	0.956	1.163	1.040	1.517	1.459	1.149	0.935	0.731	1.305
La2O3	0.006	0.000	0.000	0.000	0.000	0.005	0.000	0.000	0.059	0.020	0.044	0.000
MgO	0.096	0.014	0.015	0.000	0.015	0.000	0.078	0.011	0.137	0.007	0.010	0.000
Ce2O3	0.021	0.000	0.000	0.000	0.115	0.398	0.204	0.000	0.000	0.026	0.069	0.188
Fe2O3	0.400	0.769	0.223	0.336	0.270	0.129	0.392	0.087	0.385	0.116	0.127	0.212
TiO2	0.000	0.023	0.000	0.030	0.000	0.060	0.048	0.000	0.000	0.000	0.000	0.209
Al2O3	0.156	0.343	0.000	0.000	0.086	0.017	0.450	0.015	4.128	0.009	0.000	0.019
ThO2	0.041	0.000	0.067	0.119	0.000	0.079	0.471	0.000	0.063	0.004	0.000	0.048
Nd2O3	0.000	0.000	0.001	0.000	0.000	0.000	0.036	0.003	0.024	0.018	0.030	0.039
CaO	3.711	0.520	0.040	0.000	0.143	0.023	0.586	0.074	0.039	0.032	0.053	0.039
ZrO2	59.826	62.836	64.869	65.870	64.011	64.773	60.956	64.672	58.980	65.621	65.313	65.619
SiO2	32.320	31.985	32.942	32.454	32.183	32.680	30.841	32.883	34.753	32.923	32.807	33.266
Total	99.877	98.229	99.195	99.878	98.110	99.204	96.201	99.209	99.828	99.735	99.217	100.951
Ion Distribution												
Group												
P	0.242	0.021	0.003	0.012	0.013	0.000	0.066	0.000	0.011	0.002	0.003	0.000
Si	3.875	3.978	4.050	3.982	4.010	4.032	3.926	4.050	4.090	4.032	4.035	4.031
Total	4.117	3.999	4.054	3.994	4.023	4.032	3.992	4.050	4.101	4.034	4.038	4.031
Group												
Zr	3.498	3.810	3.889	3.941	3.889	3.897	3.783	3.884	3.384	3.919	3.917	3.877
Th	0.001	0.000	0.002	0.003	0.000	0.002	0.014	0.000	0.002	0.000	0.000	0.001
Nd	0.000	0.000	0.000	0.000	0.000	0.000	0.002	0.000	0.001	0.001	0.001	0.002
Al	0.022	0.050	0.000	0.000	0.013	0.002	0.068	0.002	0.573	0.001	0.000	0.003
Fe3+	0.036	0.072	0.021	0.031	0.025	0.012	0.038	0.008	0.034	0.011	0.012	0.019
Ca	0.477	0.069	0.005	0.000	0.019	0.003	0.080	0.010	0.005	0.004	0.007	0.005
Ti	0.000	0.002	0.000	0.003	0.000	0.006	0.005	0.000	0.000	0.000		0.019
Ce	0.001	0.000	0.000	0.000	0.005	0.018	0.010	0.000	0.000	0.001	0.003	0.008
Mg	0.017	0.003	0.003	0.000	0.003	0.000	0.015	0.002	0.024	0.001	0.002	0.000
La	0.000	0.000	0.000	0.000	0.000	0.000	0.000	0.000	0.003	0.001	0.002	0.000
Hf	0.030	0.052	0.035	0.033	0.041	0.037	0.055	0.051	0.039	0.033	0.026	0.045
Mn2+	0.005	0.009	0.000	0.000	0.001	0.000	0.001	0.001	0.000	0.001	0.000	0.001
Total	4.086	4.067	3.955	4.011	3.996	3.977	4.068	3.958	4.064	3.972	3.970	3.980

Zircon

Sector	Albernoa	Albernoa	Albernoa	Albernoa	Albernoa	Albernoa	Albernoa	Albernoa	Albernoa	Albernoa	Albernoa	Albernoa
Sub-sector												
Stratigraphic division	lower VSC	Upper VSC	Upper VSC	Upper VSC	Upper VSC	Upper VSC	PQG	PQG	Upper VSC	Upper VSC	Upper VSC	Upper VSC
Mineralization type	No Sulph	No Sulph	No Sulph	No Sulph	No Sulph	No Sulph	No Sulph	No Sulph	No Sulph	No Sulph	No Sulph	No Sulph
Occurrence	Volc Metapel	metapel	metapel	metapel	metapel	metapel	metapel	metapel	Volc Metapel	Volc Metapel	Volc Metapel	Volc Metapel
Sample ref.	18-1-II	CW2-M	CW2-M	CW2-M	CW2-M	CW2-M	X32	X32	CW2-P	CW2-P	CW2-P	CW2-P
Observations	Mod Alt	Mod Alt	Mod Alt	Mod Alt	Mod Alt	Mod Alt	Mod Alt	Mod Alt	Alt	Alt	Alt	Alt
# analysis	#13	#14	#15	#16	#17	#18	#19	#20	#21	#22	#23	#24
MnO	0.040	0.000	0.084	0.019	0.000	0.050	0.018	0.021	0.037	0.000	0.050	0.000
P2O5	0.027	0.120	0.015	0.155	0.180	0.000	0.210	0.146	0.041	0.000	0.146	0.065
HfO2	1.124	1.015	1.252	1.354	1.311	1.461	0.935	1.244	1.261	1.284	1.058	0.851
La2O3	0.048	0.068	0.017	0.000	0.000	0.059	0.039	0.057	0.001	0.000	0.027	0.000
MgO	0.144	0.000	0.005	0.008	0.023	0.013	0.014	0.006	0.000	0.002	0.073	0.000
Ce2O3	0.051	0.000	0.013	0.000	0.000	0.000	0.000	0.080	0.019	0.031	0.201	0.000
Fe2O3	0.487	0.097	0.076	0.163	0.718	0.106	0.156	0.136	0.171	0.130	0.438	0.154
TiO2	0.000	0.007	0.011	0.014	0.093	0.000	0.000	0.000	0.000	0.000	0.000	0.000
Al2O3	0.205	0.000	0.000	0.000	0.000	0.000	0.062	0.045	0.000	0.000	0.105	0.000
ThO2	0.061	0.000	0.000	0.137	0.000	0.011	0.097	0.000	0.000	0.121	0.113	0.000
Nd2O3	0.000	0.000	0.000	0.011	0.000	0.000	0.000	0.001	0.000	0.000	0.000	0.000
CaO	0.054	0.021	0.017	0.012	0.044	0.008	0.032	0.024	0.025	0.041	0.094	0.031
ZrO2	65.197	64.431	64.547	63.941	63.396	64.182	65.161	65.772	66.181	65.418	64.542	66.320
SiO2	32.838	34.091	34.199	34.037	34.112	34.316	32.418	32.875	32.309	32.439	32.494	32.947
Total	100.276	99.850	100.236	99.851	99.877	100.206	99.142	100.407	100.045	99.466	99.341	100.368
Ion Distribution												
Group												
P	0.003	0.012	0.002	0.016	0.018	0.000	0.022	0.015	0.004	0.000	0.015	0.007
Si	4.003	4.131	4.136	4.131	4.128	4.151	3.997	4.007	3.970	4.003	4.001	4.012
Total	4.006	4.144	4.137	4.146	4.147	4.151	4.019	4.022	3.974	4.003	4.016	4.018
Group												
Zr	3.875	3.807	3.806	3.784	3.741	3.785	3.917	3.909	3.965	3.936	3.875	3.938
Th	0.002	0.000	0.000	0.004	0.000	0.000	0.003	0.000	0.000	0.003	0.003	0.000
Nd	0.000	0.000	0.000	0.000	0.000	0.000	0.000	0.000	0.000	0.000	0.000	0.000
Al	0.029	0.000	0.000	0.000	0.000	0.000	0.009	0.006	0.000	0.000	0.015	0.000
Fe3+	0.045	0.009	0.007	0.015	0.065	0.010	0.014	0.012	0.016	0.012	0.041	0.014
Ca	0.007	0.003	0.002	0.002	0.006	0.001	0.004	0.003	0.003	0.005	0.012	0.004
Ti	0.000	0.001	0.001	0.001	0.008	0.000	0.000	0.000	0.000	0.000	0.000	0.000
Ce	0.002	0.000	0.001	0.000	0.000	0.000	0.000	0.004	0.001	0.001	0.009	0.000
Mg	0.026	0.000	0.001	0.001	0.004	0.002	0.003	0.001	0.000	0.000	0.013	0.000
La	0.002	0.003	0.001	0.000	0.000	0.003	0.002	0.003	0.000	0.000	0.001	0.000
Hf	0.039	0.035	0.043	0.047	0.045	0.050	0.033	0.043	0.044	0.045	0.037	0.030
Mn2+	0.004	0.000	0.009	0.002	0.000	0.005	0.002	0.002	0.004	0.000	0.005	0.000
Total	4.032	3.858	3.870	3.856	3.870	3.857	3.987	3.984	4.033	4.004	4.012	3.985

Zircon

Sector	Albernoa	Albernoa	Albernoa	Albernoa	Albernoa	Albernoa	Albernoa	Albernoa	Lousal	Albernoa	Albernoa	Albernoa
Sub-sector									Sesmarias			
Stratigraphic division	Upper VSC	Upper VSC	Upper VSC	Upper VSC	Upper VSC	Upper VSC	Upper VSC	Upper VSC	Upper VSC	Upper VSC	Upper VSC	Upper VSC
Mineralization type	No Sulph	No Sulph	No Sulph	No Sulph	No Sulph	No Sulph	No Sulph	No Sulph	Py-bearing	No Sulph	No Sulph	No Sulph
Occurrence	Volc Metapel	Volc Metapel	Volc Metapel	Volc Metapel	Volc Metapel	Volc Metapel	Volc Metapel	Volc Metapel				
Sample ref.	CW2-P	T73	T74	T75	T76	18-1-G2	18-1-G2	18-1-G2	SES20#6	ALB#22a	ALB#22a	ALB#18
Observations	Alt	Alt	Alt	Alt	Alt	Alt	Alt	Alt				
# analysis	#25	#26	#27	#28	#29	#30	#31	#32	#36	#37	#38	#39
MnO	0.051	0.000	0.043	0.231	0.209	0.053	0.000	0.013	0.000	0.000	0.006	0.000
P2O5	0.325	0.000	0.055	0.017	0.042	0.112	0.000	0.026	0.591	0.023	0.000	0.226
HfO2	1.153	0.950	1.056	1.430	1.023	1.209	1.078	0.994	1.345	1.203	1.226	1.520
La2O3	0.000	0.000	0.000	0.090	0.030	0.035	0.004	0.000	0.000	0.021	0.000	0.000
MgO	0.000	0.031	0.000	0.000	0.000	0.002	0.005	0.015	0.001	0.004	0.002	0.015
Ce2O3	0.106	0.062	0.079	0.012	0.106	0.027	0.000	0.000	0.191	0.137	0.147	0.066
Fe2O3	0.288	0.201	0.111	0.198	0.114	0.252	0.198	0.204	0.273	0.073	0.087	0.440
TiO2	0.000	0.000	0.000	0.000	0.000	0.053	0.044	0.037	0.015	0.058	0.004	0.020
Al2O3	0.000	0.714	0.000	0.010	0.020	0.000	0.000	0.085	1.149	0.004	0.000	0.025
ThO2	0.200	0.000	0.000	0.082	0.124	0.085	0.022	0.022	0.067	0.015	0.153	0.000
Nd2O3	0.093	0.016	0.041	0.000	0.014	0.000	0.012	0.061	0.000	0.000	0.009	0.000
CaO	0.350	0.046	0.002	0.038	0.031	0.017	0.027	0.046	0.016	0.050	0.021	0.018
ZrO2	65.224	62.391	65.365	65.050	64.900	65.157	65.454	65.031	62.519	64.963	64.864	65.070
SiO2	32.480	33.324	32.655	32.623	32.617	32.926	32.810	33.060	32.731	32.741	32.781	32.387
Total	100.270	97.735	99.407	99.781	99.230	99.928	99.654	99.594	98.992	99.292	99.300	99.787
Ion Distribution												
Group												
P	0.034	0.000	0.006	0.002	0.004	0.012	0.000	0.003	0.061	0.002	0.000	0.024
Si	3.971	4.112	4.019	4.012	4.023	4.027	4.025	4.046	3.997	4.033	4.041	3.979
Total	4.005	4.112	4.025	4.014	4.028	4.038	4.025	4.049	4.058	4.035	4.041	4.003
Group												
Zr	3.889	3.754	3.923	3.901	3.904	3.886	3.916	3.881	3.723	3.902	3.899	3.898
Th	0.006	0.000	0.000	0.002	0.003	0.002	0.001	0.001	0.002	0.000	0.004	0.000
Nd	0.004	0.001	0.002	0.000	0.001	0.000	0.001	0.003	0.000	0.000	0.000	0.000
Al	0.000	0.104	0.000	0.001	0.003	0.000	0.000	0.012	0.165	0.001	0.000	0.004
Fe3+	0.026	0.019	0.010	0.018	0.011	0.023	0.018	0.019	0.025	0.007	0.008	0.041
Ca	0.046	0.006	0.000	0.005	0.004	0.002	0.004	0.006	0.002	0.007	0.003	0.002
Ti	0.000	0.000	0.000	0.000	0.000	0.005	0.004	0.003	0.001	0.005	0.000	0.002
Ce	0.005	0.003	0.004	0.001	0.005	0.001	0.000	0.000	0.009	0.006	0.007	0.003
Mg	0.000	0.006	0.000	0.000	0.000	0.000	0.001	0.003	0.000	0.001	0.000	0.003
La	0.000	0.000	0.000	0.004	0.001	0.002	0.000	0.000	0.000	0.001	0.000	0.000
Hf	0.040	0.033	0.037	0.050	0.036	0.042	0.038	0.035	0.047	0.042	0.043	0.053
Mn2+	0.005	0.000	0.004	0.024	0.022	0.005	0.000	0.001	0.000	0.000	0.001	0.000
Total	4.021	3.925	3.980	4.007	3.989	3.969	3.982	3.964	3.976	3.972	3.965	4.006

Zircon

Sector	*Aljustrel*	*Aljustrel*	*Aljustrel*
Sub-sector	*Feitais mine*	*Moinho mine*	*Moinho mine*
Stratigraphic division	*Upper VSC*	*Upper VSC*	*Upper VSC*
Mineralization type	*Py-bearing*	*Mineralized*	*Mineralized*
Occurrence			
Sample ref.	*FM#5*	*MFM#3*	*MFM#3*
Observations			
# analysis	*#33*	*#34*	*#35*
MnO	0.073	0.022	0.011
P2O5	0.000	0.047	0.038
HfO2	1.448	1.204	1.152
La2O3	0.000	0.019	0.000
MgO	0.000	0.000	0.000
Ce2O3	0.000	0.150	0.000
Fe2O3	0.180	0.098	0.085
TiO2	0.021	0.000	0.003
Al2O3	0.009	0.001	0.000
ThO2	0.000	0.000	0.032
Nd2O3	0.000	0.004	0.000
CaO	0.057	0.000	0.005
ZrO2	64.680	64.262	64.543
SiO2	32.205	32.554	32.430
Total	98.814	98.406	98.299

Ion Distribution			
Group			
P	0.000	0.005	0.004
Si	4.001	4.043	4.033
Total	4.001	4.048	4.037
Group			
Zr	3.919	3.892	3.914
Th	0.000	0.000	0.001
Nd	0.000	0.000	0.000
Al	0.001	0.000	0.000
Fe3+	0.017	0.009	0.008
Ca	0.008	0.000	0.001
Ti	0.002	0.000	0.000
Ce	0.000	0.007	0.000
Mg	0.000	0.000	0.000
La	0.000	0.001	0.000
Hf	0.051	0.043	0.041
Mn2+	0.008	0.002	0.001
Total	4.009	3.955	3.965

Rutile

n = 27

Rutile s.l.

Sector	*Aljustrel*	*Aljustrel*	*Aljustrel*	*Aljustrel*	*Aljustrel*	*Aljustrel*	*Aljustrel*	*Neves Corvo*	*Neves Corvo*	*Neves Corvo*	*Neves Corvo*
Sub-sector	*Mte Mesas*	*Mte Mesas*	*Mte Mesas*	*Moinho mine*	*Moinho mine*	*Moinho mine*	*Moinho mine*	*Corvo*	*Lombador*	*Lombador*	*Lombador*
Stratigraphic division	*upper VSC*	*upper VSC*	*upper VSC*	*upper VSC*	*upper VSC*	*upper VSC*	*upper VSC*	*lower VSC*	*PQG*	*PQG*	*PQG*
Mineralization type	*Mineralized*	*Mineralized*	*No Sulph*	*Mineralized*	*Mineralized*	*Mineralized*	*Mineralized*	*Py-bearing*	*Mineralized*	*Mineralized*	*No Sulph*
Occurrence	*detrital*	*detrital*	*detrital*	*detrital*	*detrital*	*detrital*	*detrital*	*detrital*	*min-related*	*min-related*	*detrital*
Sample ref.	*MDM02#4*	*MDM02#6*	*MDM02#8*	*MFM#3*	*MFM#3*	*MFM#3*	*MFM#3*	*NCC#24*	*NCL#10*	*NCL#10*	*NCL#15*
# analysis	**#1**	**#2**	**#3**	**#4**	**#5**	**#6**	**#7**	**#8**	**#9**	**#10**	**#11**
WO3	0.000	0.094	0.000	0.000	0.013	0.121	0.000	0.040	0.230	0.210	0.054
Ta2O5	0.085	0.082	0.067	0.000	0.000	0.213	0.000	0.000	0.000	0.058	0.000
Sb2O5	0.000	0.000	0.000	0.000	0.000	0.000	0.000	0.014	0.000	0.000	0.001
Nb2O5	0.271	0.264	0.383	0.236	0.208	0.292	0.488	0.059	0.223	0.314	0.362
As2O5	0.000	0.000	0.000	0.017	0.000	0.001	0.000	0.039	0.008	0.000	0.013
P2O5	0.012	0.028	0.000	0.033	0.000	0.000	0.000	0.032	0.004	0.006	0.034
SnO2	0.000	0.000	0.000	0.027	0.005	0.042	0.071	0.019	0.077	0.035	0.000
ZrO2	0.102	0.033	0.048	0.018	0.001	0.026	0.390	0.027	0.232	0.096	0.053
MnO2	0.000	0.000	0.000	0.015	0.000	0.078	0.000	0.017	0.042	0.016	0.037
TiO2	97.868	99.361	98.966	99.277	98.750	98.049	96.073	98.577	97.856	98.863	97.233
SiO2	0.130	0.142	0.184	0.084	0.182	0.488	0.782	0.239	0.243	0.182	0.383
Ni2O3	0.037	0.004	0.000	0.010	0.000	0.006	0.022	0.000	0.000	0.021	0.022
Co2O3	0.031	0.023	0.000	0.000	0.000	0.000	0.024	0.026	0.000	0.016	0.028
Fe2O3	0.861	0.708	0.411	0.285	0.241	0.428	0.567	0.231	0.744	0.767	1.005
Cr2O3	0.534	0.022	0.007	0.004	0.001	0.000	0.050	0.058	0.026	0.013	0.019
Al2O3	0.062	0.030	0.067	0.029	0.135	0.105	0.334	0.058	0.038	0.045	0.136
PbO	0.034	0.000	0.000	0.060	0.021	0.003	0.030	0.000	0.000	0.000	0.000
BaO	0.057	0.051	0.373	0.095	0.029	0.097	0.034	0.103	0.103	0.044	0.121
ZnO	0.012	0.124	0.000	0.000	0.000	0.000	0.019	0.037	0.004	0.078	0.000
CuO	0.055	0.023	0.000	0.000	0.000	0.000	0.011	0.018	0.000	0.038	0.053
FeO	0.000	0.000	0.000	0.000	0.000	0.000	0.000	0.000	0.000	0.000	0.000
CaO	0.334	0.014	0.237	0.109	0.049	0.046	0.116	0.063	0.054	0.030	0.021
MgO	0.000	0.000	0.003	0.000	0.000	0.013	0.055	0.000	0.014	0.008	0.003
K2O	0.025	0.074	0.001	0.109	0.130	0.104	0.161	0.094	0.023	0.015	0.001
Na2O	0.000	0.000	0.000	0.011	0.010	0.000	0.012	0.009	0.013	0.011	0.000
Total	100.510	101.078	100.747	100.418	99.775	100.112	99.239	99.760	99.933	100.865	99.578

Rutile s.l.

# analysis	#1	#2	#3	#4	#5	#6	#7	#8	#9	#10	#11
Ion Distribution											
Group M											
W	0.000	0.000	0.000	0.000	0.000	0.000	0.000	0.000	0.001	0.001	0.000
Ta	0.000	0.000	0.000	0.000	0.000	0.001	0.000	0.000	0.000	0.000	0.000
Sb	0.000	0.000	0.000	0.000	0.000	0.000	0.000	0.000	0.000	0.000	0.000
Nb	0.002	0.002	0.002	0.001	0.001	0.002	0.003	0.000	0.001	0.002	0.002
As	0.000	0.000	0.000	0.000	0.000	0.000	0.000	0.000	0.000	0.000	0.000
P5+	0.000	0.000	0.000	0.000	0.000	0.000	0.000	0.000	0.000	0.000	0.000
Sn	0.000	0.000	0.000	0.000	0.000	0.000	0.000	0.000	0.000	0.000	0.000
Zr	0.001	0.000	0.000	0.000	0.000	0.000	0.003	0.000	0.002	0.001	0.000
Mn	0.000	0.000	0.000	0.000	0.000	0.001	0.000	0.000	0.000	0.000	0.000
Ti	0.983	0.989	0.990	0.993	0.992	0.984	0.974	0.992	0.985	0.986	0.981
Si	0.002	0.002	0.002	0.001	0.002	0.007	0.011	0.003	0.003	0.002	0.005
Ni	0.000	0.000	0.000	0.000	0.000	0.000	0.000	0.000	0.000	0.000	0.000
Co	0.000	0.000	0.000	0.000	0.000	0.000	0.000	0.000	0.000	0.000	0.000
Fe3+	0.009	0.007	0.004	0.003	0.002	0.004	0.006	0.002	0.008	0.008	0.010
Cr	0.006	0.000	0.000	0.000	0.000	0.000	0.001	0.001	0.000	0.000	0.000
Al	0.001	0.001	0.001	0.001	0.002	0.002	0.005	0.001	0.001	0.001	0.002
Pb	0.000	0.000	0.000	0.000	0.000	0.000	0.000	0.000	0.000	0.000	0.000
Fe2+	0.000	0.000	0.000	0.000	0.000	0.000	0.000	0.000	0.000	0.000	0.000
Total	1.004	1.001	1.001	1.001	1.001	1.001	1.002	1.001	1.001	1.001	1.003
Group I											
Ba	0.000	0.000	0.002	0.001	0.000	0.001	0.000	0.001	0.001	0.000	0.001
Zn	0.000	0.001	0.000	0.000	0.000	0.000	0.000	0.000	0.000	0.001	0.000
Cu	0.001	0.000	0.000	0.000	0.000	0.000	0.000	0.000	0.000	0.000	0.001
Ca	0.005	0.000	0.003	0.002	0.001	0.001	0.002	0.001	0.001	0.000	0.000
Mg	0.000	0.000	0.000	0.000	0.000	0.000	0.001	0.000	0.000	0.000	0.000
K	0.000	0.001	0.000	0.002	0.002	0.002	0.003	0.002	0.000	0.000	0.000
Na	0.000	0.000	0.000	0.000	0.000	0.000	0.000	0.000	0.000	0.000	0.000
Total	0.006	0.003	0.005	0.004	0.003	0.003	0.006	0.004	0.002	0.003	0.002

Rutile s.l.

Sector	*Neves Corvo*	*Neves Corvo*	*Neves Corvo*	*Neves Corvo*	*Neves Corvo*	*Neves Corvo*	*Neves Corvo*	*Neves Corvo*	*Neves Corvo*	*Neves Corvo*	*Albernoa*	*Albernoa*
Sub-sector	*Lombador*	*Lombador*	*Lombador*	*Neves*	*Neves*	*Neves*	*Neves*	*Zambujal*	*Zambujal*	*Zambujal*		
Stratigraphic division	*PQG*	*PQG*	*PQG*	*lower VSC*	*lower VSC*	*lower VSC*	*lower VSC*	*lower VSC*	*lower VSC*	*lower VSC*	*upper VSC*	*upper VSC*
Mineralization type	*No Sulph*	*No Sulph*	*No Sulph*	*Mineralized*	*Mineralized*	*Mineralized*	*Mineralized*	*Mineralized*	*Mineralized*	*Mineralized*		
Occurrence	*detrital*	*detrital*	*detrital*	*min-related*	*min-related*	*min-related*	*min-related*	*min-related*	*min-related*	*min-related*	*detrital*	*detrital*
Sample ref.	*NCL#15*	*NCL#15*	*NCL#15*	*NCN#20*	*NCN#20*	*NCN#20*	*NCN#20*	*NCZ#21*	*NCZ#21*	*NCZ#21*	*ALB#22a*	*ALB#22a*
# analysis	**#12**	**#13**	**#14**	**#15**	**#16**	**#17**	**#18**	**#19**	**#20**	**#21**	**#22**	**#23**
WO3	0.037	0.000	0.025	0.180	0.000	0.000	0.170	0.000	0.000	0.054	0.121	0.000
Ta2O5	0.000	0.000	0.280	0.000	0.024	0.071	0.000	0.173	0.000	0.119	0.126	0.000
Sb2O5	0.011	0.000	0.003	0.000	0.000	0.000	0.000	0.020	0.000	0.000	0.000	0.000
Nb2O5	0.414	0.446	0.272	0.373	0.275	0.262	0.369	0.559	0.275	0.237	0.510	0.512
As2O5	0.036	0.000	0.000	0.010	0.000	0.009	0.018	0.017	0.000	0.013	0.000	0.000
P2O5	0.000	0.000	0.034	0.000	0.000	0.078	0.011	0.024	0.004	0.000	0.011	0.010
SnO2	0.031	0.017	0.020	0.046	0.104	0.002	0.000	0.052	0.010	0.039	0.000	0.004
ZrO2	0.094	0.129	0.040	0.074	0.004	0.043	0.026	0.041	0.094	0.037	0.023	0.028
MnO2	0.004	0.014	0.000	0.015	0.000	0.000	0.033	0.000	0.000	0.000	0.000	0.009
TiO2	97.579	98.284	98.258	97.274	98.076	98.294	97.049	96.963	97.490	96.445	97.965	98.081
SiO2	0.300	0.162	0.064	0.299	0.135	0.127	0.877	0.452	0.555	0.813	0.094	0.113
Ni2O3	0.000	0.026	0.049	0.000	0.000	0.007	0.000	0.000	0.020	0.014	0.000	0.000
Co2O3	0.000	0.026	0.000	0.013	0.027	0.000	0.000	0.000	0.000	0.045	0.000	0.034
Fe2O3	0.862	0.586	0.476	0.979	0.709	0.667	0.986	1.586	0.878	0.585	0.547	0.461
Cr2O3	0.033	0.038	0.000	0.016	0.000	0.021	0.009	0.000	0.000	0.067	0.000	0.001
Al2O3	0.030	0.056	0.026	0.086	0.589	0.060	0.087	0.935	0.170	0.281	0.033	0.073
PbO	0.003	0.000	0.011	0.000	0.048	0.009	0.000	0.000	0.086	0.000	0.000	0.000
BaO	0.044	0.077	0.109	0.124	0.136	0.036	0.019	0.131	0.070	0.029	0.035	0.000
ZnO	0.000	0.000	0.032	0.009	0.000	0.000	0.000	0.000	0.000	0.046	0.013	0.000
CuO	0.012	0.017	0.030	0.000	0.014	0.032	0.009	0.000	0.034	0.012	0.465	0.318
FeO	0.000	0.000	0.000	0.000	0.000	0.000	0.000	0.000	0.000	0.000	0.000	0.000
CaO	0.008	0.087	0.074	0.035	0.007	0.006	0.023	0.032	0.137	0.036	0.023	0.009
MgO	0.000	0.000	0.000	0.006	0.026	0.006	0.000	0.028	0.008	0.010	0.000	0.000
K2O	0.012	0.017	0.012	0.027	0.156	0.047	0.045	0.148	0.013	0.072	0.048	0.039
Na2O	0.000	0.000	0.005	0.030	0.024	0.031	0.012	0.007	0.040	0.031	0.006	0.007
Total	99.510	99.980	99.819	99.596	100.354	99.808	99.743	101.168	99.884	98.985	100.020	99.699

Rutile s.l.

# analysis	#12	#13	#14	#15	#16	#17	#18	#19	#20	#21	#22	#23
Ion Distribution												
Group M												
W	0.000	0.000	0.000	0.001	0.000	0.000	0.001	0.000	0.000	0.000	0.000	0.000
Ta	0.000	0.000	0.001	0.000	0.000	0.000	0.000	0.001	0.000	0.000	0.001	0.000
Sb	0.000	0.000	0.000	0.000	0.000	0.000	0.000	0.000	0.000	0.000	0.000	0.000
Nb	0.003	0.003	0.002	0.002	0.002	0.002	0.002	0.003	0.002	0.001	0.003	0.003
As	0.000	0.000	0.000	0.000	0.000	0.000	0.000	0.000	0.000	0.000	0.000	0.000
P5+	0.000	0.000	0.000	0.000	0.000	0.001	0.000	0.000	0.000	0.000	0.000	0.000
Sn	0.000	0.000	0.000	0.000	0.001	0.000	0.000	0.000	0.000	0.000	0.000	0.000
Zr	0.001	0.001	0.000	0.001	0.000	0.000	0.000	0.000	0.001	0.000	0.000	0.000
Mn	0.000	0.000	0.000	0.000	0.000	0.000	0.000	0.000	0.000	0.000	0.000	0.000
Ti	0.984	0.988	0.991	0.983	0.983	0.989	0.975	0.965	0.981	0.977	0.989	0.990
Si	0.004	0.002	0.001	0.004	0.002	0.002	0.012	0.006	0.007	0.011	0.001	0.002
Ni	0.000	0.000	0.001	0.000	0.000	0.000	0.000	0.000	0.000	0.000	0.000	0.000
Co	0.000	0.000	0.000	0.000	0.000	0.000	0.000	0.000	0.000	0.000	0.000	0.000
Fe3+	0.009	0.006	0.005	0.010	0.007	0.007	0.010	0.016	0.009	0.006	0.006	0.005
Cr	0.000	0.000	0.000	0.000	0.000	0.000	0.000	0.000	0.000	0.001	0.000	0.000
Al	0.001	0.001	0.000	0.001	0.009	0.001	0.001	0.015	0.003	0.005	0.001	0.001
Pb	0.000	0.000	0.000	0.000	0.000	0.000	0.000	0.000	0.000	0.000	0.000	0.000
Fe2+	0.000	0.000	0.000	0.000	0.000	0.000	0.000	0.000	0.000	0.000	0.000	0.000
Total	1.002	1.001	1.001	1.002	1.004	1.001	1.002	1.007	1.003	1.002	1.000	1.001
Group I												
Ba	0.000	0.000	0.001	0.001	0.001	0.000	0.000	0.001	0.000	0.000	0.000	0.000
Zn	0.000	0.000	0.000	0.000	0.000	0.000	0.000	0.000	0.000	0.001	0.000	0.000
Cu	0.000	0.000	0.000	0.000	0.000	0.000	0.000	0.000	0.000	0.000	0.005	0.003
Ca	0.000	0.001	0.001	0.001	0.000	0.000	0.000	0.001	0.002	0.001	0.000	0.000
Mg	0.000	0.000	0.000	0.000	0.001	0.000	0.000	0.001	0.000	0.000	0.000	0.000
K	0.000	0.000	0.000	0.001	0.003	0.001	0.001	0.003	0.000	0.001	0.001	0.001
Na	0.000	0.000	0.000	0.001	0.001	0.001	0.000	0.000	0.001	0.001	0.000	0.000
Total	0.001	0.002	0.003	0.003	0.005	0.002	0.002	0.004	0.004	0.004	0.006	0.004

Rutile s.l.

Sector	*Albernoa*	*Albernoa*	*Albernoa*	*Albernoa*
Sub-sector				
Stratigraphic division	*upper VSC*	*upper VSC*	*upper VSC*	*upper VSC*
Mineralization type				
Occurrence	*detrital*	*min-related*	*detrital*	*detrital*
Sample ref.	*ALB#22a*	*ALB#22a*	*ALB#22a*	*ALB#22a*
# analysis	**#24**	**#25**	**#26**	**#27**
WO3	0.014	0.000	0.000	0.189
Ta2O5	0.036	0.091	0.000	0.000
Sb2O5	0.000	0.000	0.000	0.000
Nb2O5	0.514	0.489	0.587	0.726
As2O5	0.000	0.006	0.000	0.000
P2O5	0.000	0.008	0.000	0.000
SnO2	0.019	0.024	0.000	0.061
ZrO2	0.000	0.012	0.000	0.000
MnO2	0.000	0.000	0.000	0.000
TiO2	98.626	98.482	97.857	98.066
SiO2	0.085	0.095	0.231	0.102
Ni2O3	0.000	0.000	0.000	0.006
Co2O3	0.000	0.000	0.007	0.000
Fe2O3	0.365	0.213	0.546	0.271
Cr2O3	0.002	0.009	0.031	0.052
Al2O3	0.038	0.039	0.045	0.054
PbO	0.000	0.015	0.000	0.015
BaO	0.000	0.023	0.022	0.036
ZnO	0.080	0.000	0.000	0.081
CuO	0.086	0.033	0.359	0.251
FeO	0.000	0.021	0.000	0.063
CaO	0.030	0.017	0.024	0.000
MgO	0.005	0.003	0.000	0.001
K2O	0.101	0.096	0.013	0.067
Na2O	0.021	0.007	0.000	0.000
Total	100.022	99.682	99.721	100.041

Rutile s.l.

# analysis		#24	#25	#26	#27
Ion Distribution					
Group M					
W		0.000	0.000	0.000	0.001
Ta		0.000	0.000	0.000	0.000
Sb		0.000	0.000	0.000	0.000
Nb		0.003	0.003	0.004	0.004
As		0.000	0.000	0.000	0.000
P5+		0.000	0.000	0.000	0.000
Sn		0.000	0.000	0.000	0.000
Zr		0.000	0.000	0.000	0.000
Mn		0.000	0.000	0.000	0.000
Ti		0.991	0.992	0.988	0.988
Si		0.001	0.001	0.003	0.001
Ni		0.000	0.000	0.000	0.000
Co		0.000	0.000	0.000	0.000
Fe3+		0.004	0.002	0.006	0.003
Cr		0.000	0.000	0.000	0.001
Al		0.001	0.001	0.001	0.001
Pb		0.000	0.000	0.000	0.000
Fe2+		0.000	0.000	0.000	0.001
	Total	1.000	1.000	1.001	1.000
Group I					
Ba		0.000	0.000	0.000	0.000
Zn		0.001	0.000	0.000	0.001
Cu		0.001	0.000	0.004	0.003
Ca		0.000	0.000	0.000	0.000
Mg		0.000	0.000	0.000	0.000
K		0.002	0.002	0.000	0.001
Na		0.001	0.000	0.000	0.000
	Total	0.005	0.003	0.004	0.005

Pyrite

n = 170

Pyrites

Sector	*Albernoa*	*Albernoa*	*Albernoa*	*Albernoa*	*Albernoa*	*Albernoa*	*Albernoa*	*Albernoa*	*Albernoa*	*Albernoa*	*Albernoa*	*Albernoa*
Sub-sector												
Stratigraphic division	*upper VSC*	*upper VSC*	*upper VSC*	*upper VSC*	*upper VSC*	*upper VSC*	*upper VSC*	*upper VSC*	*upper VSC*	*upper VSC*	*upper VSC*	*upper VSC*
Mineralization type	*No Sulph*	*No Sulph*	*No Sulph*	*No Sulph*	*No Sulph*	*No Sulph*	*Mineralized*	*Mineralized*	*Mineralized*	*Mineralized*	*Mineralized*	*Mineralized*
Occurrence				Euhedral Pyrites								
Sample ref.	**18-1-EE**	**18-1-EE**	**18-1-EE**	**18-1-EE**	**18-1-EE**	**18-1-EE**	**18-1-FF**	**18-1-FF**	**18-1-FF**	**18-1-FF**	**18-1-FF**	**18-1-FF**
# analysis	*#1*	*#2*	*#3*	*#4*	*#5*	*#6*	*#7*	*#8*	*#9*	*#10*	*#11*	*#12*
Mo	0.000	0.000	0.000	0.000	0.000	0.000	0.000	0.000	0.000	0.000	0.000	0.000
Sn	0.000	0.000	0.047	0.000	0.008	0.004	0.029	0.000	0.010	0.027	0.016	0.003
Ge	0.000	0.000	0.000	0.000	0.000	0.018	0.000	0.001	0.000	0.000	0.000	0.010
In	0.058	0.066	0.003	0.000	0.026	0.018	0.084	0.036	0.000	0.000	0.000	0.000
Pb	0.156	0.042	0.225	0.000	0.061	0.082	0.052	0.009	0.084	0.042	0.000	0.000
Cd	0.000	0.035	0.000	0.029	0.000	0.019	0.000	0.024	0.000	0.008	0.027	0.026
Zn	0.000	0.057	0.000	0.000	0.051	0.047	0.050	0.019	0.055	0.041	0.000	0.000
Cu	0.000	0.020	0.081	0.019	0.051	0.318	0.059	0.012	0.015	0.052	0.026	0.061
Ni	0.019	0.054	0.289	0.015	0.000	0.081	0.068	0.000	0.040	0.403	0.074	0.255
Co	0.069	0.111	0.085	0.067	0.100	0.070	0.123	0.097	0.078	0.094	0.127	0.060
Fe2+	46.270	45.371	45.400	46.641	46.705	46.624	46.335	47.082	46.522	46.172	44.789	46.137
Mn	0.000	0.000	0.009	0.000	0.018	0.015	0.032	0.005	0.000	0.000	0.000	0.009
Au	0.011	0.000	0.000	0.009	0.000	0.007	0.003	0.000	0.028	0.038	0.000	0.058
Ag	0.000	0.000	0.028	0.003	0.003	0.000	0.000	0.019	0.012	0.000	0.016	0.005
Bi	0.000	0.000	0.000	0.000	0.000	0.000	0.000	0.000	0.000	0.000	0.000	0.000
Te	0.000	0.000	0.000	0.000	0.000	0.000	0.000	0.000	0.000	0.000	0.000	0.000
Sb	0.000	0.019	0.000	0.000	0.015	0.004	0.000	0.000	0.000	0.033	0.000	0.000
Se	0.005	0.016	0.009	0.009	0.008	0.037	0.000	0.008	0.000	0.011	0.015	0.012
As	0.066	0.050	0.694	0.090	0.112	0.000	0.042	0.042	0.035	0.000	0.032	0.000
S	53.231	51.936	52.460	53.171	53.198	53.306	53.008	53.589	53.141	53.366	51.327	53.375
Total	99.885	97.777	99.330	100.053	100.356	100.650	99.885	100.943	100.020	100.287	96.449	100.011

Pyrites

# analysis	*#1*	*#2*	*#3*	*#4*	*#5*	*#6*	*#7*	*#8*	*#9*	*#10*	*#11*	*#12*
Ion Distribution												
Group S												
Bi	0.000	0.000	0.000	0.000	0.000	0.000	0.000	0.000	0.000	0.000	0.000	0.000
Te	0.000	0.000	0.000	0.000	0.000	0.000	0.000	0.000	0.000	0.000	0.000	0.000
Sb	0.000	0.000	0.000	0.000	0.000	0.000	0.000	0.000	0.000	0.000	0.000	0.000
Se	0.000	0.000	0.000	0.000	0.000	0.001	0.000	0.000	0.000	0.000	0.000	0.000
As	0.001	0.001	0.011	0.001	0.002	0.000	0.001	0.001	0.001	0.000	0.001	0.000
S	1.998	1.993	1.989	1.992	1.990	1.989	1.992	1.991	1.993	1.995	1.994	1.999
Total	1.999	1.994	2.000	1.993	1.992	1.990	1.993	1.992	1.994	1.995	1.995	1.999
Group M												
Mo	0.000	0.000	0.000	0.000	0.000	0.000	0.000	0.000	0.000	0.000	0.000	0.000
Sn	0.000	0.000	0.000	0.000	0.000	0.000	0.000	0.000	0.000	0.000	0.000	0.000
Ge	0.000	0.000	0.000	0.000	0.000	0.000	0.000	0.000	0.000	0.000	0.000	0.000
In	0.001	0.001	0.001	0.001	0.001	0.001	0.001	0.001	0.001	0.001	0.001	0.001
Pb	0.001	0.001	0.001	0.001	0.001	0.001	0.001	0.001	0.001	0.001	0.001	0.001
Cd	0.000	0.000	0.000	0.000	0.000	0.000	0.000	0.000	0.000	0.000	0.000	0.000
Zn	0.000	0.000	0.000	0.000	0.000	0.000	0.000	0.000	0.000	0.000	0.000	0.000
Cu	0.000	0.000	0.000	0.000	0.000	0.000	0.000	0.000	0.000	0.000	0.000	0.000
Ni	0.000	0.000	0.000	0.000	0.000	0.000	0.000	0.000	0.000	0.000	0.000	0.000
Co	0.001	0.001	0.001	0.001	0.001	0.001	0.001	0.001	0.001	0.001	0.001	0.001
Fe2+	0.997	0.997	0.997	0.997	0.997	0.997	0.997	0.997	0.997	0.997	0.997	0.997
Mn	0.000	0.000	0.000	0.000	0.000	0.000	0.000	0.000	0.000	0.000	0.000	0.000
Au	0.000	0.000	0.000	0.000	0.000	0.000	0.000	0.000	0.000	0.000	0.000	0.000
Ag	0.000	0.000	0.000	0.000	0.000	0.000	0.000	0.000	0.000	0.000	0.000	0.000
Total	1.000	1.000	1.000	1.000	1.000	1.000	1.000	1.000	1.000	1.000	1.000	1.000

Pyrites

Sector	*Albernoa*	*Albernoa*	*Albernoa*	*Albernoa*	*Albernoa*	*Albernoa*	*Albernoa*	*Albernoa*	*Albernoa*	*Albernoa*	*Albernoa*	*Albernoa*
Sub-sector												
Stratigraphic division	*upper VSC*	*upper VSC*	*upper VSC*	*upper VSC*	*upper VSC*	*upper VSC*	*middle VSC*	*middle VSC*	*upper VSC*	*upper VSC*	*upper VSC*	*upper VSC*
Mineralization type	*No Sulph*	*No Sulph*	*No Sulph*	*No Sulph*	*No Sulph*	*No Sulph*	*Py bearing*	*Py bearing*	*No Sulph*	*No Sulph*	*No Sulph*	*No Sulph*
Occurrence							framboidal Py					
Sample ref.	**18-1-G**	**18-1-G**	**18-1-G**	**18-1-G**	**18-1-G**	**18-1-G**	**37-1-E**	**37-1-E**	**ABNSTR3**	**ABNSTR3**	**CW2-AA**	**CW2-AA**
# analysis	***#13***	***#14***	***#15***	***#16***	***#17***	***#18***	***#19***	***#20***	***#21***	***#22***	***#23***	***#24***
Mo	0.000	0.000	0.000	0.000	0.000	0.000	0.000	0.000	0.000	0.000	0.000	0.000
Sn	0.077	0.000	0.022	0.000	0.002	0.010	0.000	0.000	0.049	0.026	0.014	0.024
Ge	0.000	0.000	0.016	0.000	0.000	0.000	0.001	0.000	0.000	0.000	0.000	0.000
In	0.000	0.056	0.006	0.000	0.000	0.000	0.000	0.000	0.034	0.000	0.000	0.004
Pb	0.049	0.030	0.014	0.096	0.051	0.000	0.008	0.028	0.063	0.097	0.488	0.009
Cd	0.000	0.000	0.000	0.000	0.000	0.000	0.000	0.025	0.000	0.031	0.000	0.000
Zn	0.000	0.078	0.000	0.000	0.117	0.000	0.049	0.000	0.000	0.057	0.000	0.000
Cu	0.048	0.035	0.054	0.027	0.018	0.003	0.171	0.164	0.087	0.050	0.030	0.000
Ni	0.007	0.095	0.041	0.000	0.006	0.000	0.000	0.001	0.054	0.053	0.000	0.021
Co	0.094	0.110	0.119	0.105	0.052	0.098	0.120	0.119	0.087	0.037	0.066	0.114
Fe2+	46.258	46.301	46.347	46.118	46.194	46.361	45.854	45.489	46.900	46.912	45.051	46.976
Mn	0.000	0.016	0.052	0.011	0.000	0.017	0.013	0.000	0.000	0.000	0.009	0.000
Au	0.008	0.029	0.055	0.008	0.000	0.027	0.000	0.036	0.000	0.000	0.016	0.000
Ag	0.007	0.000	0.000	0.000	0.006	0.004	0.000	0.000	0.000	0.000	0.000	0.003
Bi	0.000	0.000	0.000	0.000	0.000	0.000	0.000	0.000	0.000	0.000	0.000	0.000
Te	0.000	0.000	0.000	0.000	0.000	0.000	0.000	0.000	0.000	0.000	0.000	0.000
Sb	0.017	0.000	0.000	0.025	0.000	0.001	0.000	0.000	0.000	0.000	0.000	0.000
Se	0.014	0.000	0.018	0.032	0.004	0.000	0.000	0.001	0.020	0.000	0.001	0.000
As	0.000	0.002	0.000	0.000	0.002	0.030	0.060	0.071	0.042	0.099	0.044	0.000
S	53.342	53.427	53.477	53.455	53.029	53.390	52.098	52.034	52.782	52.618	52.711	52.963
Total	99.921	100.179	100.221	99.877	99.481	99.941	98.374	97.968	100.118	99.980	98.430	100.114

Pyrites

# analysis	*#13*	*#14*	*#15*	*#16*	*#17*	*#18*	*#19*	*#20*	*#21*	*#22*	*#23*	*#24*
Ion Distribution												
Group S												
Bi	0.000	0.000	0.000	0.000	0.000	0.000	0.000	0.000	0.000	0.000	0.000	0.000
Te	0.000	0.000	0.000	0.000	0.000	0.000	0.000	0.000	0.000	0.000	0.000	0.000
Sb	0.000	0.000	0.000	0.000	0.000	0.000	0.000	0.000	0.000	0.000	0.000	0.000
Se	0.000	0.000	0.000	0.000	0.000	0.000	0.000	0.000	0.000	0.000	0.000	0.000
As	0.000	0.000	0.000	0.000	0.000	0.000	0.001	0.001	0.001	0.002	0.001	0.000
S	2.000	1.998	1.999	2.003	1.997	2.000	1.988	1.992	1.982	1.980	2.008	1.986
Total	2.000	1.998	1.999	2.003	1.997	2.000	1.989	1.993	1.983	1.982	2.009	1.986
Group M												
Mo	0.000	0.000	0.000	0.000	0.000	0.000	0.000	0.000	0.000	0.000	0.000	0.000
Sn	0.000	0.000	0.000	0.000	0.000	0.000	0.000	0.000	0.000	0.000	0.000	0.000
Ge	0.000	0.000	0.000	0.000	0.000	0.000	0.000	0.000	0.000	0.000	0.000	0.000
In	0.001	0.001	0.001	0.001	0.001	0.001	0.001	0.001	0.001	0.001	0.001	0.001
Pb	0.001	0.001	0.001	0.001	0.001	0.001	0.001	0.001	0.001	0.001	0.001	0.001
Cd	0.000	0.000	0.000	0.000	0.000	0.000	0.000	0.000	0.000	0.000	0.000	0.000
Zn	0.000	0.000	0.000	0.000	0.000	0.000	0.000	0.000	0.000	0.000	0.000	0.000
Cu	0.000	0.000	0.000	0.000	0.000	0.000	0.000	0.000	0.000	0.000	0.000	0.000
Ni	0.000	0.000	0.000	0.000	0.000	0.000	0.000	0.000	0.000	0.000	0.000	0.000
Co	0.001	0.001	0.001	0.001	0.001	0.001	0.001	0.001	0.001	0.001	0.001	0.001
Fe2+	0.997	0.997	0.997	0.997	0.997	0.997	0.997	0.997	0.997	0.997	0.997	0.997
Mn	0.000	0.000	0.000	0.000	0.000	0.000	0.000	0.000	0.000	0.000	0.000	0.000
Au	0.000	0.000	0.000	0.000	0.000	0.000	0.000	0.000	0.000	0.000	0.000	0.000
Ag	0.000	0.000	0.000	0.000	0.000	0.000	0.000	0.000	0.000	0.000	0.000	0.000
Total	1.000	1.000	1.000	1.000	1.000	1.000	1.000	1.000	1.000	1.000	1.000	1.000

Pyrites

Sector	*Albernoa*	*Albernoa*	*Albernoa*	*Albernoa*	*Albernoa*	*Albernoa*	*Albernoa*	*Albernoa*	*Albernoa*	*Albernoa*	*Albernoa*	*Albernoa*
Sub-sector												
Stratigraphic division	*upper VSC*	*upper VSC*	*upper VSC*	*upper VSC*	*upper VSC*	*upper VSC*	*upper VSC*	*upper VSC*	*upper VSC*	*upper VSC*	*upper VSC*	*upper VSC*
Mineralization type	*No Sulph*	*No Sulph*	*No Sulph*	*No Sulph*	*No Sulph*	*No Sulph*	*No Sulph*	*No Sulph*	*No Sulph*	*No Sulph*	*No Sulph*	*No Sulph*
Occurrence												
Sample ref.	**CW2-AA**	**CW2-AA**	**CW2-AA**	**CW2-AA**	**CW2-AA**	**CW2-AA**	**CW2-AA**	**CW2-AA**	**CW2-AA**	**CW2-M**	**CW2-M**	**CW2-M**
# analysis	*#25*	*#26*	*#27*	*#28*	*#29*	*#30*	*#31*	*#32*	*#33*	*#34*	*#35*	*#36*
Mo	0.000	0.000	0.000	0.000	0.000	0.000	0.000	0.000	0.000	0.000	0.000	0.000
Sn	0.000	0.000	0.054	0.004	0.000	0.000	0.000	0.006	0.039	0.000	0.020	0.028
Ge	0.000	0.005	0.000	0.000	0.000	0.000	0.000	0.013	0.000	0.000	0.000	0.000
In	0.038	0.000	0.025	0.025	0.011	0.019	0.017	0.080	0.000	0.000	0.000	0.012
Pb	0.003	0.000	0.008	0.000	0.099	0.809	1.425	0.000	0.007	0.081	0.127	0.070
Cd	0.000	0.000	0.020	0.000	0.000	0.000	0.000	0.000	0.000	0.002	0.007	0.000
Zn	0.000	0.000	0.072	0.226	0.215	0.004	0.000	0.066	0.001	0.010	0.000	0.020
Cu	0.000	0.023	0.000	0.027	0.000	0.094	0.241	0.025	0.000	0.030	0.047	0.040
Ni	0.000	0.015	0.000	0.007	0.000	0.000	0.000	0.032	0.000	0.038	0.023	0.000
Co	0.136	0.118	0.119	0.090	0.074	0.084	0.078	0.073	0.081	0.086	0.101	0.105
Fe2+	47.213	47.004	46.346	47.169	46.784	45.356	44.946	47.338	47.322	46.113	45.927	46.177
Mn	0.000	0.000	0.030	0.000	0.019	0.027	0.000	0.046	0.011	0.091	0.068	0.003
Au	0.020	0.000	0.000	0.037	0.000	0.000	0.000	0.046	0.019	0.010	0.000	0.003
Ag	0.006	0.000	0.000	0.000	0.000	0.009	0.000	0.025	0.000	0.020	0.000	0.000
Bi	0.000	0.000	0.000	0.000	0.000	0.000	0.000	0.000	0.000	0.000	0.000	0.000
Te	0.000	0.000	0.000	0.000	0.000	0.000	0.000	0.000	0.000	0.000	0.000	0.000
Sb	0.000	0.051	0.006	0.050	0.000	0.036	0.035	0.000	0.000	0.016	0.000	0.011
Se	0.000	0.000	0.000	0.000	0.002	0.000	0.012	0.016	0.000	0.001	0.000	0.000
As	0.016	0.000	0.000	0.000	0.000	0.000	0.000	0.000	0.000	0.485	0.524	0.068
S	52.837	52.523	51.859	52.713	52.529	51.865	49.886	53.529	53.407	52.180	52.169	52.401
Total	100.269	99.739	98.539	100.348	99.733	98.303	96.640	101.295	100.887	99.163	99.013	98.938

Pyrites

# analysis	*#25*	*#26*	*#27*	*#28*	*#29*	*#30*	*#31*	*#32*	*#33*	*#34*	*#35*	*#36*
Ion Distribution												
Group S												
Bi	0.000	0.000	0.000	0.000	0.000	0.000	0.000	0.000	0.000	0.000	0.000	0.000
Te	0.000	0.000	0.000	0.000	0.000	0.000	0.000	0.000	0.000	0.000	0.000	0.000
Sb	0.000	0.001	0.000	0.000	0.000	0.000	0.000	0.000	0.000	0.000	0.000	0.000
Se	0.000	0.000	0.000	0.000	0.000	0.000	0.000	0.000	0.000	0.000	0.000	0.000
As	0.000	0.000	0.000	0.000	0.000	0.000	0.000	0.000	0.000	0.008	0.009	0.001
S	1.980	1.979	1.979	1.977	1.981	1.991	1.967	1.985	1.987	1.981	1.983	1.988
Total	1.980	1.980	1.979	1.977	1.981	1.991	1.967	1.985	1.987	1.989	1.992	1.989
Group M												
Mo	0.000	0.000	0.000	0.000	0.000	0.000	0.000	0.000	0.000	0.000	0.000	0.000
Sn	0.000	0.000	0.000	0.000	0.000	0.000	0.000	0.000	0.000	0.000	0.000	0.000
Ge	0.000	0.000	0.000	0.000	0.000	0.000	0.000	0.000	0.000	0.000	0.000	0.000
In	0.001	0.001	0.001	0.001	0.001	0.001	0.001	0.001	0.001	0.001	0.001	0.001
Pb	0.001	0.001	0.001	0.001	0.001	0.001	0.001	0.001	0.001	0.001	0.001	0.001
Cd	0.000	0.000	0.000	0.000	0.000	0.000	0.000	0.000	0.000	0.000	0.000	0.000
Zn	0.000	0.000	0.000	0.000	0.000	0.000	0.000	0.000	0.000	0.000	0.000	0.000
Cu	0.000	0.000	0.000	0.000	0.000	0.000	0.000	0.000	0.000	0.000	0.000	0.000
Ni	0.000	0.000	0.000	0.000	0.000	0.000	0.000	0.000	0.000	0.000	0.000	0.000
Co	0.001	0.001	0.001	0.001	0.001	0.001	0.001	0.001	0.001	0.001	0.001	0.001
Fe2+	0.997	0.997	0.997	0.997	0.997	0.997	0.997	0.997	0.997	0.997	0.997	0.997
Mn	0.000	0.000	0.000	0.000	0.000	0.000	0.000	0.000	0.000	0.000	0.000	0.000
Au	0.000	0.000	0.000	0.000	0.000	0.000	0.000	0.000	0.000	0.000	0.000	0.000
Ag	0.000	0.000	0.000	0.000	0.000	0.000	0.000	0.000	0.000	0.000	0.000	0.000
Total	1.000	1.000	1.000	1.000	1.000	1.000	1.000	1.000	1.000	1.000	1.000	1.000

Pyrites

Sector	*Albernoa*	*Albernoa*	*Albernoa*	*Albernoa*	*Albernoa*	*Albernoa*	*Aljustrel*	*Aljustrel*	*Aljustrel*	*Aljustrel*	*Aljustrel*	*Aljustrel*
Sub-sector												
Stratigraphic division	*upper VSC*	*upper VSC*	*upper VSC*	*upper VSC*	*upper VSC*	*upper VSC*	*upper VSC*	*upper VSC*	*upper VSC*	*upper VSC*	*upper VSC*	*upper VSC*
Mineralization type	*No Sulph*	*No Sulph*	*No Sulph*	*No Sulph*	*No Sulph*	*No Sulph*	*Mineralized*	*Mineralized*	*Mineralized*	*Mineralized*	*Mineralized*	*Mineralized*
Occurrence	Early formed, digested borders								Early formed pyrite			
Sample ref.	**CW2-M**	**CW2-M**	**CW2-M**	**Alb03#18**	**Alb03#18**	**Alb03#13a**	**EDS1-H**	**EDS1-H**	**EDS1-B**	**EDS1-B**	**EDS1-B**	**EDS1-B**
# analysis	*#37*	*#38*	*#39*	*#40*	*#41*	*#42*	*#43*	*#44*	*#45*	*#46*	*#47*	*#48*
Mo	0.000	0.000	0.000	0.000	0.000	0.000	0.000	0.000	0.000	0.000	0.000	0.000
Sn	0.000	0.000	0.000	0.000	0.000	0.014	0.000	0.000	0.000	0.000	0.000	0.022
Ge	0.000	0.000	0.000	0.000	0.000	0.000	0.000	0.000	0.000	0.000	0.003	0.000
In	0.000	0.078	0.004	0.000	0.000	0.000	0.000	0.034	0.000	0.000	0.004	0.000
Pb	1.667	0.112	0.125	0.062	0.025	0.051	0.087	0.196	0.000	0.000	0.051	0.045
Cd	0.000	0.000	0.000	0.040	0.044	0.060	0.000	0.000	0.000	0.000	0.000	0.000
Zn	0.007	0.000	0.000	0.000	0.000	0.000	0.000	0.002	0.007	0.000	0.056	0.000
Cu	0.022	0.028	0.024	0.000	0.000	0.000	0.083	0.060	0.000	0.000	0.000	0.000
Ni	0.121	0.000	0.039	0.056	0.069	0.000	0.011	0.064	0.019	0.009	0.000	0.046
Co	0.357	0.106	0.086	0.114	0.154	0.036	0.062	0.114	0.115	0.080	0.095	0.060
Fe2+	45.552	46.140	45.999	45.906	46.376	45.903	46.496	46.728	46.734	46.581	46.588	46.572
Mn	0.106	0.042	0.078	0.084	0.090	0.000	0.002	0.000	0.001	0.032	0.011	0.000
Au	0.003	0.074	0.005	0.000	0.000	0.017	0.035	0.034	0.013	0.000	0.000	0.000
Ag	0.000	0.001	0.000	0.000	0.060	0.005	0.000	0.025	0.014	0.000	0.000	0.037
Bi	0.000	0.000	0.000	0.018	0.000	0.000	0.000	0.000	0.000	0.000	0.000	0.000
Te	0.000	0.000	0.000	0.000	0.011	0.046	0.000	0.000	0.000	0.000	0.000	0.000
Sb	0.080	0.000	0.052	0.000	0.000	0.030	0.004	0.009	0.000	0.000	0.040	0.000
Se	0.000	0.000	0.010	0.016	0.000	0.000	0.000	0.002	0.003	0.000	0.003	0.006
As	0.435	0.290	0.292	0.419	0.000	0.010	0.093	0.091	0.072	0.024	0.087	0.028
S	51.604	52.409	52.234	52.832	53.445	52.915	53.339	53.539	53.657	53.252	53.387	53.361
Total	99.954	99.280	98.948	99.547	100.274	99.087	100.212	100.898	100.635	99.978	100.325	100.177

Pyrites

# analysis	*#37*	*#38*	*#39*	*#40*	*#41*	*#42*	*#43*	*#44*	*#45*	*#46*	*#47*	*#48*
Ion Distribution												
Group S												
Bi	0.000	0.000	0.000	0.000	0.000	0.000	0.000	0.000	0.000	0.000	0.000	0.000
Te	0.000	0.000	0.000	0.000	0.000	0.000	0.000	0.000	0.000	0.000	0.000	0.000
Sb	0.001	0.000	0.001	0.000	0.000	0.000	0.000	0.000	0.000	0.000	0.000	0.000
Se	0.000	0.000	0.000	0.000	0.000	0.000	0.000	0.000	0.000	0.000	0.000	0.000
As	0.007	0.005	0.005	0.007	0.000	0.000	0.001	0.001	0.001	0.000	0.001	0.000
S	1.971	1.986	1.985	1.993	1.997	2.001	1.996	1.993	1.997	1.995	1.995	1.996
Total	1.979	1.991	1.991	2.000	1.997	2.002	1.997	1.994	1.998	1.995	1.996	1.996
Group M												
Mo	0.000	0.000	0.000	0.000	0.000	0.000	0.000	0.000	0.000	0.000	0.000	0.000
Sn	0.000	0.000	0.000	0.000	0.000	0.000	0.000	0.000	0.000	0.000	0.000	0.000
Ge	0.000	0.000	0.000	0.000	0.000	0.000	0.000	0.000	0.000	0.000	0.000	0.000
In	0.001	0.001	0.001	0.000	0.000	0.000	0.001	0.001	0.001	0.001	0.001	0.001
Pb	0.001	0.001	0.001	0.000	0.000	0.000	0.001	0.001	0.001	0.001	0.001	0.001
Cd	0.000	0.000	0.000	0.000	0.001	0.001	0.000	0.000	0.000	0.000	0.000	0.000
Zn	0.000	0.000	0.000	0.000	0.000	0.000	0.000	0.000	0.000	0.000	0.000	0.000
Cu	0.000	0.000	0.000	0.000	0.000	0.000	0.000	0.000	0.000	0.000	0.000	0.000
Ni	0.000	0.000	0.000	0.001	0.001	0.000	0.000	0.000	0.000	0.000	0.000	0.000
Co	0.001	0.001	0.001	0.002	0.003	0.001	0.001	0.001	0.001	0.001	0.001	0.001
Fe2+	0.997	0.997	0.997	0.994	0.995	0.997	0.997	0.997	0.997	0.997	0.997	0.997
Mn	0.000	0.000	0.000	0.002	0.002	0.000	0.000	0.000	0.000	0.000	0.000	0.000
Au	0.000	0.000	0.000	0.000	0.000	0.000	0.000	0.000	0.000	0.000	0.000	0.000
Ag	0.000	0.000	0.000	0.000	0.001	0.000	0.000	0.000	0.000	0.000	0.000	0.000
Total	1.000	1.000	1.000	1.000	1.003	0.999	1.000	1.000	1.000	1.000	1.000	1.000

Pyrites

Sector	*Aljustrel*	*Aljustrel*	*Aljustrel*	*Aljustrel*	*Aljustrel*	*Aljustrel*	*Aljustrel*	*Aljustrel*	*Aljustrel*	*Aljustrel*	*Aljustrel*	*Aljustrel*
Sub-sector			*Mina F*	*Mina F*	*Mina F*	*Mina F*	*Mina F*	*Mina F*	*Mina F*	*Mina F*	*Mina F*	*Mina F*
Stratigraphic division	*upper VSC*	*upper VSC*	*upper VSC*	*upper VSC*	*upper VSC*	*upper VSC*	*upper VSC*	*upper VSC*	*upper VSC*	*upper VSC*	*upper VSC*	*upper VSC*
Mineralization type	*Mineralized*	*Mineralized*	*No Sulph*	*No Sulph*	*No Sulph*	*No Sulph*	*No Sulph*	*Py-bearing*	*Py-bearing*	*Py-bearing*	*Py-bearing*	*Py-bearing*
Occurrence												
Sample ref.	**EDS1-B**	**EDS1-B**	**FFM#2**	**FFM#2**	**FM#4**	**FM#4**	**FM#4**	**FM#5**	**FM#5**	**FM#5**	**FM#5**	**FM#5**
# analysis	*#49*	*#50*	*#51*	*#52*	*#53*	*#54*	*#55*	*#56*	*#57*	*#58*	*#59*	*#60*
Mo	0.000	0.000	0.047	0.054	0.031	0.053	0.035	0.000	0.000	0.000	0.000	0.000
Sn	0.000	0.023	0.000	0.000	0.000	0.013	0.037	0.055	0.000	0.000	0.000	0.000
Ge	0.000	0.000	0.000	0.006	0.039	0.000	0.000	0.000	0.000	0.000	0.000	0.000
In	0.027	0.000	0.005	0.000	0.023	0.011	0.013	0.018	0.000	0.044	0.002	0.005
Pb	0.028	0.000	0.144	0.035	0.037	0.000	0.000	0.016	0.031	0.078	0.116	0.108
Cd	0.000	0.000	0.020	0.000	0.000	0.050	0.000	0.034	0.039	0.009	0.013	0.000
Zn	0.066	0.071	0.000	0.028	0.057	0.003	0.007	0.014	0.000	0.000	0.000	0.000
Cu	0.001	0.006	0.000	0.000	0.000	0.000	0.000	0.000	0.000	0.000	0.026	0.000
Ni	0.000	0.020	0.019	0.000	0.035	0.000	0.171	0.033	0.019	0.438	0.379	0.286
Co	0.056	0.102	0.193	0.025	0.033	0.000	0.002	0.000	0.030	0.035	0.113	0.082
Fe2+	46.832	46.901	45.813	45.383	46.133	46.329	46.186	46.057	46.038	46.108	45.803	45.875
Mn	0.000	0.000	0.010	0.000	0.000	0.000	0.004	0.000	0.000	0.000	0.006	0.034
Au	0.000	0.078	0.000	0.028	0.009	0.000	0.000	0.011	0.000	0.000	0.003	0.000
Ag	0.012	0.038	0.000	0.027	0.023	0.026	0.000	0.000	0.000	0.000	0.027	0.000
Bi	0.000	0.000	0.000	0.000	0.000	0.000	0.000	0.000	0.000	0.000	0.000	0.000
Te	0.000	0.000	0.014	0.019	0.000	0.000	0.025	0.021	0.000	0.000	0.046	0.033
Sb	0.011	0.000	0.030	0.015	0.000	0.026	0.046	0.038	0.004	0.005	0.000	0.000
Se	0.020	0.003	0.010	0.005	0.034	0.000	0.010	0.005	0.027	0.008	0.021	0.000
As	0.027	0.008	0.076	0.043	0.039	0.007	0.016	0.431	0.444	0.528	0.596	0.571
S	53.445	53.460	53.193	52.608	52.974	52.911	52.988	53.044	52.898	53.015	52.985	52.952
Total	100.525	100.710	99.574	98.276	99.467	99.429	99.540	99.777	99.530	100.268	100.136	99.946

Pyrites

# analysis	*#49*	*#50*	*#51*	*#52*	*#53*	*#54*	*#55*	*#56*	*#57*	*#58*	*#59*	*#60*
Ion Distribution												
Group S												
Bi	0.000	0.000	0.000	0.000	0.000	0.000	0.000	0.000	0.000	0.000	0.000	0.000
Te	0.000	0.000	0.000	0.000	0.000	0.000	0.000	0.000	0.000	0.000	0.000	0.000
Sb	0.000	0.000	0.000	0.000	0.000	0.000	0.001	0.000	0.000	0.000	0.000	0.000
Se	0.000	0.000	0.000	0.000	0.001	0.000	0.000	0.000	0.000	0.000	0.000	0.000
As	0.000	0.000	0.001	0.001	0.001	0.000	0.000	0.007	0.007	0.009	0.010	0.009
S	1.993	1.992	2.002	2.004	1.996	1.995	1.996	1.995	1.994	1.988	1.990	1.991
Total	1.993	1.992	2.004	2.005	1.998	1.995	1.997	2.003	2.002	1.997	2.000	2.001
Group M												
Mo	0.000	0.000	0.001	0.001	0.000	0.001	0.000	0.000	0.000	0.000	0.000	0.000
Sn	0.000	0.000	0.000	0.000	0.000	0.000	0.000	0.001	0.000	0.000	0.000	0.000
Ge	0.000	0.000	0.000	0.000	0.001	0.000	0.000	0.000	0.000	0.000	0.000	0.000
In	0.001	0.001	0.000	0.000	0.000	0.000	0.000	0.000	0.000	0.001	0.000	0.000
Pb	0.001	0.001	0.001	0.000	0.000	0.000	0.000	0.000	0.000	0.001	0.001	0.001
Cd	0.000	0.000	0.000	0.000	0.000	0.001	0.000	0.000	0.000	0.000	0.000	0.000
Zn	0.000	0.000	0.000	0.001	0.001	0.000	0.000	0.000	0.000	0.000	0.000	0.000
Cu	0.000	0.000	0.000	0.000	0.000	0.000	0.000	0.000	0.000	0.000	0.001	0.000
Ni	0.000	0.000	0.000	0.000	0.001	0.000	0.004	0.001	0.000	0.009	0.008	0.006
Co	0.001	0.001	0.004	0.001	0.001	0.000	0.000	0.000	0.001	0.001	0.002	0.002
Fe2+	0.997	0.997	0.990	0.993	0.998	1.003	0.999	0.995	0.997	0.993	0.988	0.990
Mn	0.000	0.000	0.000	0.000	0.000	0.000	0.000	0.000	0.000	0.000	0.000	0.001
Au	0.000	0.000	0.000	0.000	0.000	0.000	0.000	0.000	0.000	0.000	0.000	0.000
Ag	0.000	0.000	0.000	0.000	0.000	0.000	0.000	0.000	0.000	0.000	0.000	0.000
Total	1.000	1.000	0.996	0.995	1.003	1.005	1.003	0.997	0.998	1.003	1.000	0.999

Pyrites

Sector	*Aljustrel*	*Aljustrel*	*Aljustrel*	*Aljustrel*	*Aljustrel*	*Aljustrel*	*Aljustrel*	*Aljustrel*	*Aljustrel*	*Aljustrel*	*Aljustrel*	*Aljustrel*
Sub-sector	*Mte Mesas*	*Mte Mesas*	*Mte Mesas*	*Mte Mesas*	*Mte Mesas*	*Mte Mesas*	*Mte Mesas*	*Mina M*	*Mina M*	*Mina M*	*Mina M*	*Mina M*
Stratigraphic division	*upper VSC*	*upper VSC*	*upper VSC*	*upper VSC*	*upper VSC*	*upper VSC*	*upper VSC*	*upper VSC*	*upper VSC*	*upper VSC*	*upper VSC*	*upper VSC*
Mineralization type	*No-Sulph*	*No-Sulph*	*No-Sulph*	*No-Sulph*	*No-Sulph*	*No-Sulph*	*No-Sulph*	*Mineralized*	*Mineralized*	*Mineralized*	*Mineralized*	*Mineralized*
Occurrence												
Sample ref.	**MDM02#8**	**MDM02#8**	**MDM02#8**	**MDM02#8**	**MDM02#8**	**MDM02#8**	**MDM02#8**	**MFM#3**	**MFM#3**	**MFM#3**	**MFM#3**	**MFM#3**
# analysis	*#61*	*#62*	*#63*	*#64*	*#65*	*#66*	*#67*	*#68*	*#69*	*#70*	*#71*	*#72*
Mo	0.030	0.023	0.041	0.013	0.057	0.067	0.024	0.024	0.002	0.047	0.108	0.100
Sn	0.036	0.000	0.008	0.008	0.000	0.000	0.000	0.000	0.000	0.000	0.024	0.015
Ge	0.000	0.012	0.000	0.000	0.000	0.000	0.000	0.000	0.000	0.000	0.000	0.000
In	0.018	0.045	0.000	0.052	0.012	0.005	0.004	0.034	0.032	0.010	0.091	0.000
Pb	0.121	0.000	0.000	0.000	0.026	0.038	0.000	0.477	1.395	0.033	0.000	0.007
Cd	0.000	0.003	0.000	0.000	0.000	0.016	0.000	0.000	0.027	0.003	0.000	0.045
Zn	0.003	0.003	0.003	0.012	0.000	0.000	0.020	0.105	0.039	0.370	0.046	0.020
Cu	0.000	0.000	0.000	0.000	0.000	0.000	0.000	0.000	0.004	0.000	0.000	0.000
Ni	0.243	0.020	0.081	0.131	0.000	0.030	0.033	0.000	0.003	0.008	0.059	0.003
Co	0.021	0.000	0.000	0.000	0.032	0.000	0.019	0.037	0.050	0.016	0.028	0.000
Fe2+	46.121	46.554	46.646	46.043	46.498	46.430	46.411	45.483	44.797	46.715	46.420	46.796
Mn	0.000	0.022	0.000	0.000	0.012	0.025	0.000	0.114	0.253	0.000	0.009	0.033
Au	0.043	0.040	0.074	0.000	0.000	0.015	0.002	0.003	0.000	0.012	0.019	0.014
Ag	0.047	0.000	0.000	0.002	0.028	0.024	0.011	0.000	0.000	0.000	0.002	0.023
Bi	0.000	0.000	0.000	0.000	0.000	0.000	0.000	0.000	0.000	0.000	0.000	0.000
Te	0.006	0.000	0.000	0.000	0.000	0.010	0.002	0.001	0.000	0.000	0.000	0.000
Sb	0.034	0.019	0.000	0.000	0.026	0.042	0.000	0.000	0.124	0.042	0.000	0.000
Se	0.017	0.011	0.000	0.000	0.023	0.023	0.027	0.011	0.000	0.002	0.000	0.037
As	0.057	0.071	0.086	0.137	0.000	0.013	0.000	0.106	0.078	0.157	0.004	0.020
S	53.338	53.670	53.650	53.022	53.815	53.610	53.736	52.857	52.946	53.396	53.742	53.865
Total	100.135	100.493	100.589	99.420	100.529	100.348	100.289	99.252	99.750	100.811	100.552	100.978

Pyrites

# analysis	*#61*	*#62*	*#63*	*#64*	*#65*	*#66*	*#67*	*#68*	*#69*	*#70*	*#71*	*#72*
Ion Distribution												
Group S												
Bi	0.000	0.000	0.000	0.000	0.000	0.000	0.000	0.000	0.000	0.000	0.000	0.000
Te	0.000	0.000	0.000	0.000	0.000	0.000	0.000	0.000	0.000	0.000	0.000	0.000
Sb	0.000	0.000	0.000	0.000	0.000	0.000	0.000	0.000	0.001	0.000	0.000	0.000
Se	0.000	0.000	0.000	0.000	0.000	0.000	0.000	0.000	0.000	0.000	0.000	0.001
As	0.001	0.001	0.001	0.002	0.000	0.000	0.000	0.002	0.001	0.003	0.000	0.000
S	1.998	2.000	1.998	1.998	2.003	2.001	2.004	2.001	2.006	1.989	2.002	1.999
Total	2.000	2.002	2.000	2.000	2.004	2.002	2.004	2.003	2.009	1.992	2.002	2.000
Group M												
Mo	0.000	0.000	0.001	0.000	0.001	0.001	0.000	0.000	0.000	0.001	0.001	0.001
Sn	0.000	0.000	0.000	0.000	0.000	0.000	0.000	0.000	0.000	0.000	0.000	0.000
Ge	0.000	0.000	0.000	0.000	0.000	0.000	0.000	0.000	0.000	0.000	0.000	0.000
In	0.000	0.001	0.000	0.001	0.000	0.000	0.000	0.000	0.000	0.000	0.001	0.000
Pb	0.001	0.000	0.000	0.000	0.000	0.000	0.000	0.003	0.008	0.000	0.000	0.000
Cd	0.000	0.000	0.000	0.000	0.000	0.000	0.000	0.000	0.000	0.000	0.000	0.001
Zn	0.000	0.000	0.000	0.000	0.000	0.000	0.000	0.002	0.001	0.007	0.001	0.000
Cu	0.000	0.000	0.000	0.000	0.000	0.000	0.000	0.000	0.000	0.000	0.000	0.000
Ni	0.005	0.000	0.002	0.003	0.000	0.001	0.001	0.000	0.000	0.000	0.001	0.000
Co	0.000	0.000	0.000	0.000	0.001	0.000	0.000	0.001	0.001	0.000	0.001	0.000
Fe2+	0.992	0.996	0.998	0.996	0.994	0.995	0.994	0.989	0.975	0.999	0.993	0.997
Mn	0.000	0.001	0.000	0.000	0.000	0.001	0.000	0.003	0.006	0.000	0.000	0.001
Au	0.000	0.000	0.000	0.000	0.000	0.000	0.000	0.000	0.000	0.000	0.000	0.000
Ag	0.001	0.000	0.000	0.000	0.000	0.000	0.000	0.000	0.000	0.000	0.000	0.000
Total	1.000	0.998	1.000	1.000	0.996	0.998	0.996	0.997	0.991	1.008	0.998	1.000

Pyrites

Sector	*Aljustrel*	*Aljustrel*	*Aljustrel*	*Aljustrel*	*Aljustrel*	*Aljustrel*	*Aljustrel*	*Aljustrel*	*Aljustrel*	*Aljustrel*	*Aljustrel*	*Aljustrel*
Sub-sector	*Mina M*	*Mina M*	*Gavião*	*Gavião*	*Gavião*	*Gavião*	*Gavião*	*Gavião*	*Gavião*	*Gavião*	*Gavião*	*Gavião*
Stratigraphic division	*upper VSC*	*upper VSC*	*upper VSC*	*upper VSC*	*upper VSC*	*upper VSC*	*upper VSC*	*upper VSC*	*upper VSC*	*upper VSC*	*upper VSC*	*upper VSC*
Mineralization type	*Mineralized*	*Mineralized*	*Mineralized*	*Py-bearing*	*Py-bearing*	*Py-bearing*	*Py-bearing*	*Py-bearing*	*Py-bearing*	*Py-bearing*	*Py-bearing*	*Py-bearing*
Occurrence												
Sample ref.	**MFM#3**	**MFM#3**	**GV7#3**	**GV9#10**	**GV9#10**	**GV9#10**	**GV9#10**	**GV9#10**	**GV9#10**	**GV9#10**	**GV9#10**	**GV9#10**
# analysis	*#73*	*#74*	*#75*	*#76*	*#77*	*#78*	*#79*	*#80*	*#81*	*#82*	*#83*	*#84*
Mo	0.070	0.048	0.089	0.040	0.070	0.088	0.058	0.073	0.109	0.076	0.093	0.055
Sn	0.050	0.014	0.000	0.000	0.000	0.000	0.000	0.000	0.000	0.000	0.000	0.000
Ge	0.013	0.000	0.000	0.000	0.000	0.000	0.016	0.000	0.000	0.000	0.000	0.000
In	0.008	0.029	0.000	0.000	0.000	0.000	0.000	0.035	0.000	0.000	0.000	0.000
Pb	0.008	0.063	0.002	0.046	0.000	0.000	0.063	0.000	0.000	0.133	0.072	0.094
Cd	0.000	0.012	0.000	0.000	0.000	0.000	0.000	0.000	0.000	0.000	0.000	0.000
Zn	0.144	0.297	0.000	0.120	0.083	0.026	0.000	0.056	0.000	0.023	0.000	0.000
Cu	0.000	0.000	0.000	0.000	0.000	0.000	0.000	0.000	0.000	0.000	0.000	0.000
Ni	0.020	0.000	0.000	0.018	0.000	0.016	0.000	0.040	0.690	0.031	0.016	0.107
Co	0.000	0.056	0.000	0.046	0.043	0.020	0.015	0.012	0.041	0.026	0.088	0.001
Fe2+	46.569	46.563	46.535	46.120	45.982	45.980	46.437	46.028	46.043	46.399	46.720	46.766
Mn	0.003	0.000	0.016	0.148	0.115	0.029	0.000	0.030	0.002	0.000	0.000	0.003
Au	0.005	0.040	0.023	0.000	0.038	0.018	0.000	0.017	0.000	0.004	0.007	0.005
Ag	0.014	0.005	0.000	0.000	0.021	0.011	0.014	0.000	0.041	0.000	0.047	0.006
Bi	0.000	0.000	0.000	0.000	0.000	0.000	0.000	0.000	0.000	0.000	0.000	0.000
Te	0.000	0.000	0.000	0.000	0.000	0.000	0.000	0.052	0.000	0.012	0.034	0.062
Sb	0.000	0.048	0.000	0.001	0.000	0.000	0.000	0.011	0.000	0.000	0.004	0.000
Se	0.000	0.000	0.021	0.000	0.000	0.013	0.021	0.029	0.007	0.002	0.009	0.045
As	0.317	0.009	0.000	0.047	0.013	0.043	0.040	0.100	0.000	0.029	0.066	0.065
S	53.750	53.639	52.110	52.567	52.611	52.097	53.013	51.818	53.236	52.719	52.988	52.967
Total	100.971	100.823	98.796	99.153	98.976	98.341	99.677	98.301	100.169	99.454	100.144	100.176

Pyrites

# analysis	*#73*	*#74*	*#75*	*#76*	*#77*	*#78*	*#79*	*#80*	*#81*	*#82*	*#83*	*#84*
Ion Distribution												
Group S												
Bi	0.000	0.000	0.000	0.000	0.000	0.000	0.000	0.000	0.000	0.000	0.000	0.000
Te	0.000	0.000	0.000	0.000	0.000	0.000	0.000	0.001	0.000	0.000	0.000	0.001
Sb	0.000	0.001	0.000	0.000	0.000	0.000	0.000	0.000	0.000	0.000	0.000	0.000
Se	0.000	0.000	0.000	0.000	0.000	0.000	0.000	0.001	0.000	0.000	0.000	0.001
As	0.005	0.000	0.000	0.001	0.000	0.001	0.001	0.002	0.000	0.001	0.001	0.001
S	1.997	1.996	1.982	1.989	1.993	1.988	1.994	1.982	1.993	1.990	1.988	1.987
Total	2.002	1.997	1.982	1.990	1.993	1.989	1.995	1.985	1.993	1.991	1.989	1.989
Group M												
Mo	0.001	0.001	0.001	0.001	0.001	0.001	0.001	0.001	0.001	0.001	0.001	0.001
Sn	0.001	0.000	0.000	0.000	0.000	0.000	0.000	0.000	0.000	0.000	0.000	0.000
Ge	0.000	0.000	0.000	0.000	0.000	0.000	0.000	0.000	0.000	0.000	0.000	0.000
In	0.000	0.000	0.000	0.000	0.000	0.000	0.000	0.000	0.000	0.000	0.000	0.000
Pb	0.000	0.000	0.000	0.000	0.000	0.000	0.000	0.000	0.000	0.001	0.000	0.001
Cd	0.000	0.000	0.000	0.000	0.000	0.000	0.000	0.000	0.000	0.000	0.000	0.000
Zn	0.003	0.005	0.000	0.002	0.002	0.001	0.000	0.001	0.000	0.000	0.000	0.000
Cu	0.000	0.000	0.000	0.000	0.000	0.000	0.000	0.000	0.000	0.000	0.000	0.000
Ni	0.000	0.000	0.000	0.000	0.000	0.000	0.000	0.001	0.014	0.001	0.000	0.002
Co	0.000	0.001	0.000	0.001	0.001	0.000	0.000	0.000	0.001	0.001	0.002	0.000
Fe2+	0.993	0.995	1.016	1.002	1.000	1.008	1.003	1.011	0.990	1.006	1.006	1.007
Mn	0.000	0.000	0.000	0.003	0.003	0.001	0.000	0.001	0.000	0.000	0.000	0.000
Au	0.000	0.000	0.000	0.000	0.000	0.000	0.000	0.000	0.000	0.000	0.000	0.000
Ag	0.000	0.000	0.000	0.000	0.000	0.000	0.000	0.000	0.001	0.000	0.001	0.000
Total	0.998	1.003	1.018	1.010	1.007	1.011	1.005	1.015	1.007	1.009	1.011	1.011

Pyrites

Sector	*Lousal*	*Lousal*	*Lousal*	*Lousal*	*Lousal*	*Lousal*	*Lousal*	*Lousal*	*Lousal*	*Lousal*	*Lousal*	*Lousal*
Sub-sector	*Sesmarias*	*Sesmarias*	*Sesmarias*	*Sesmarias*	*Sesmarias*	*Sesmarias*	*Sesmarias*	*Sesmarias*	*Sesmarias*	*Sesmarias*	*Sesmarias*	*Sesmarias*
Stratigraphic division	*lower VSC*	*lower VSC*	*lower VSC*	*lower VSC*	*lower VSC*	*lower VSC*	*upper VSC*	*upper VSC*	*upper VSC*	*upper VSC*	*upper VSC*	*upper VSC*
Mineralization type	*Mineralized*	*Mineralized*	*Mineralized*	*Mineralized*	*Mineralized*	*Mineralized*	*Py-bearing*	*Py-bearing*	*Py-bearing*	*Py-bearing*	*Py-bearing*	*Py-bearing*
Occurrence												
Sample ref.	**SES20#10**	**SES20#10**	**SES20#10**	**SES20#10**	**SES20#10**	**SES20#10**	**SES20#6**	**SES20#6**	**SES20#6**	**SES20#6**	**SES20#6**	**SES20#6**
# analysis	*#85*	*#86*	*#87*	*#88*	*#89*	*#90*	*#91*	*#92*	*#93*	*#94*	*#95*	*#96*
Mo	0.038	0.000	0.000	0.000	0.007	0.000	0.000	0.004	0.000	0.012	0.002	0.000
Sn	0.001	0.026	0.002	0.000	0.009	0.000	0.034	0.002	0.019	0.000	0.000	0.022
Ge	0.000	0.000	0.006	0.000	0.000	0.000	0.000	0.000	0.000	0.000	0.000	0.025
In	0.013	0.000	0.000	0.016	0.027	0.040	0.000	0.011	0.043	0.023	0.042	0.059
Pb	0.000	0.010	0.000	0.062	0.168	0.137	0.000	0.085	0.056	0.081	0.000	0.000
Cd	0.000	0.000	0.000	0.000	0.000	0.000	0.000	0.002	0.016	0.000	0.000	0.000
Zn	0.000	0.000	0.047	0.076	0.000	0.014	0.040	0.000	0.047	0.000	0.007	0.029
Cu	0.000	0.000	0.000	0.000	0.000	0.000	0.000	0.000	0.000	0.000	0.000	0.000
Ni	0.109	0.178	0.236	0.037	0.091	0.061	0.000	0.043	0.042	0.038	0.029	0.028
Co	0.051	0.029	0.062	0.031	0.004	0.005	0.033	0.006	0.031	0.019	0.005	0.000
Fe2+	45.528	45.311	44.807	46.022	45.989	45.853	46.275	46.287	46.063	46.203	45.929	46.042
Mn	0.000	0.012	0.000	0.030	0.059	0.038	0.000	0.000	0.000	0.000	0.000	0.000
Au	0.000	0.000	0.000	0.000	0.000	0.003	0.007	0.005	0.018	0.024	0.004	0.000
Ag	0.000	0.006	0.024	0.000	0.013	0.013	0.000	0.000	0.018	0.040	0.014	0.002
Bi	0.000	0.000	0.000	0.000	0.000	0.000	0.000	0.000	0.000	0.000	0.000	0.000
Te	0.000	0.031	0.000	0.018	0.057	0.003	0.016	0.000	0.000	0.000	0.000	0.051
Sb	0.000	0.009	0.000	0.035	0.041	0.074	0.000	0.008	0.050	0.000	0.010	0.002
Se	0.038	0.000	0.012	0.032	0.000	0.000	0.017	0.018	0.029	0.040	0.033	0.008
As	0.018	0.009	0.356	0.001	0.000	0.000	0.000	0.000	0.000	0.000	0.000	0.000
S	52.429	52.661	52.716	52.937	53.016	52.461	52.736	53.166	52.869	52.911	52.846	52.869
Total	98.225	98.282	98.268	99.297	99.481	98.702	99.158	99.637	99.301	99.391	98.921	99.137

Pyrites

# analysis	*#85*	*#86*	*#87*	*#88*	*#89*	*#90*	*#91*	*#92*	*#93*	*#94*	*#95*	*#96*
Ion Distribution												
Group S												
Bi	0.000	0.000	0.000	0.000	0.000	0.000	0.000	0.000	0.000	0.000	0.000	0.000
Te	0.000	0.000	0.000	0.000	0.001	0.000	0.000	0.000	0.000	0.000	0.000	0.001
Sb	0.000	0.000	0.000	0.000	0.000	0.001	0.000	0.000	0.001	0.000	0.000	0.000
Se	0.001	0.000	0.000	0.001	0.000	0.000	0.000	0.000	0.000	0.001	0.001	0.000
As	0.000	0.000	0.006	0.000	0.000	0.000	0.000	0.000	0.000	0.000	0.000	0.000
S	1.999	2.004	2.007	1.998	1.999	1.994	1.993	1.999	1.997	1.996	2.000	1.998
Total	2.000	2.005	2.013	1.999	2.000	1.995	1.994	1.999	1.997	1.997	2.001	1.999
Group M												
Mo	0.001	0.000	0.000	0.000	0.000	0.000	0.000	0.000	0.000	0.000	0.000	0.000
Sn	0.000	0.000	0.000	0.000	0.000	0.000	0.000	0.000	0.000	0.000	0.000	0.000
Ge	0.000	0.000	0.000	0.000	0.000	0.000	0.000	0.000	0.000	0.000	0.000	0.000
In	0.000	0.000	0.000	0.000	0.000	0.000	0.000	0.000	0.001	0.000	0.000	0.001
Pb	0.000	0.000	0.000	0.000	0.001	0.001	0.000	0.001	0.000	0.001	0.000	0.000
Cd	0.000	0.000	0.000	0.000	0.000	0.000	0.000	0.000	0.000	0.000	0.000	0.000
Zn	0.000	0.000	0.001	0.001	0.000	0.000	0.001	0.000	0.001	0.000	0.000	0.001
Cu	0.000	0.000	0.000	0.000	0.000	0.000	0.000	0.000	0.000	0.000	0.000	0.000
Ni	0.002	0.004	0.005	0.001	0.002	0.001	0.000	0.001	0.001	0.001	0.001	0.001
Co	0.001	0.001	0.001	0.001	0.000	0.000	0.001	0.000	0.001	0.000	0.000	0.000
Fe2+	0.997	0.990	0.980	0.997	0.996	1.001	1.004	0.999	0.999	1.001	0.998	0.999
Mn	0.000	0.000	0.000	0.001	0.001	0.001	0.000	0.000	0.000	0.000	0.000	0.000
Au	0.000	0.000	0.000	0.000	0.000	0.000	0.000	0.000	0.000	0.000	0.000	0.000
Ag	0.000	0.000	0.000	0.000	0.000	0.000	0.000	0.000	0.000	0.000	0.000	0.000
Total	1.001	0.995	0.987	1.001	1.000	1.005	1.006	1.001	1.003	1.003	1.000	1.001

Pyrites

Sector	*Lousal*	*Lousal*	*Lousal*	*Lousal*	*Lousal*	*Lousal*	*Lousal*	*Lousal*	*Lousal*	*Lousal*	*Lousal*	*Lousal*
Sub-sector	*Sesmarias*	*Sesmarias*	*Sesmarias*	*Sesmarias*	*Sesmarias*	*Sesmarias*	*Sesmarias*	*Sesmarias*	*Sesmarias*	*Sesmarias*	*Sesmarias*	*Sesmarias*
Stratigraphic division	*upper VSC*	*upper VSC*	*upper VSC*	*upper VSC*	*lower VSC*	*lower VSC*	*lower VSC*	*lower VSC*	*lower VSC*	*lower VSC*	*lower VSC*	*lower VSC*
Mineralization type	*Py-bearing*	*Py-bearing*	*Py-bearing*	*Py-bearing*	*Mineralized*	*Mineralized*	*Mineralized*	*Mineralized*	*Mineralized*	*Mineralized*	*Mineralized*	*Mineralized*
Occurrence												
Sample ref.	**SES20#6**	**SES20#6**	**SES20#6**	**SES20#6**	**SES20#9_2**	**SES20#9_2**	**SES20#9_2**	**SES20#9_2**	**SES20#9_2**	**SES20#9_2**	**SES20#9_2**	**SES20#9_2**
# analysis	*#97*	*#98*	*#99*	*#100*	*#101*	*#102*	*#103*	*#104*	*#105*	*#106*	*#107*	*#108*
Mo	0.015	0.026	0.000	0.000	0.012	0.048	0.079	0.044	0.012	0.085	0.027	0.043
Sn	0.000	0.045	0.032	0.066	0.000	0.000	0.000	0.000	0.038	0.000	0.000	0.000
Ge	0.000	0.000	0.000	0.000	0.000	0.000	0.000	0.000	0.000	0.000	0.000	0.000
In	0.030	0.006	0.031	0.000	0.000	0.015	0.005	0.000	0.000	0.024	0.000	0.000
Pb	0.017	0.000	0.026	0.000	0.017	0.003	0.073	0.144	0.070	0.045	0.016	0.023
Cd	0.000	0.006	0.000	0.000	0.000	0.000	0.039	0.000	0.000	0.019	0.000	0.000
Zn	0.133	0.000	0.006	0.019	0.000	0.000	0.000	0.039	0.034	0.000	0.075	0.022
Cu	0.000	0.000	0.000	0.000	0.002	0.037	0.000	0.000	0.000	0.000	0.000	0.000
Ni	0.000	0.000	0.000	0.215	0.000	0.000	0.000	0.000	0.039	0.026	0.000	0.000
Co	0.027	0.000	0.018	0.016	0.050	0.000	0.002	0.029	0.015	0.006	0.000	0.018
Fe2+	46.119	46.351	46.005	45.649	46.494	46.741	46.321	46.063	46.381	46.325	46.529	46.455
Mn	0.032	0.000	0.000	0.000	0.001	0.000	0.000	0.000	0.000	0.014	0.017	0.000
Au	0.044	0.001	0.021	0.024	0.000	0.000	0.009	0.034	0.000	0.037	0.039	0.043
Ag	0.000	0.000	0.000	0.000	0.000	0.027	0.038	0.000	0.008	0.014	0.022	0.031
Bi	0.000	0.000	0.000	0.000	0.000	0.000	0.000	0.000	0.000	0.000	0.000	0.000
Te	0.000	0.000	0.024	0.015	0.000	0.001	0.034	0.000	0.000	0.000	0.000	0.000
Sb	0.034	0.000	0.036	0.014	0.007	0.007	0.000	0.003	0.022	0.000	0.013	0.000
Se	0.038	0.000	0.000	0.000	0.000	0.000	0.000	0.000	0.000	0.009	0.000	0.007
As	0.000	0.000	0.016	0.000	0.022	0.000	0.000	0.424	0.000	0.000	0.000	0.022
S	52.718	52.946	52.930	52.967	53.496	53.403	53.276	53.063	53.350	53.430	53.570	53.614
Total	99.207	99.381	99.145	98.985	100.101	100.282	99.876	99.843	99.969	100.034	100.308	100.278

Pyrites

# analysis	*#97*	*#98*	*#99*	*#100*	*#101*	*#102*	*#103*	*#104*	*#105*	*#106*	*#107*	*#108*
Ion Distribution												
Group S												
Bi	0.000	0.000	0.000	0.000	0.000	0.000	0.000	0.000	0.000	0.000	0.000	0.000
Te	0.000	0.000	0.000	0.000	0.000	0.000	0.000	0.000	0.000	0.000	0.000	0.000
Sb	0.000	0.000	0.000	0.000	0.000	0.000	0.000	0.000	0.000	0.000	0.000	0.000
Se	0.001	0.000	0.000	0.000	0.000	0.000	0.000	0.000	0.000	0.000	0.000	0.000
As	0.000	0.000	0.000	0.000	0.000	0.000	0.000	0.007	0.000	0.000	0.000	0.000
S	1.993	1.996	2.000	2.003	2.000	1.995	1.999	1.996	1.999	2.001	2.000	2.002
Total	1.994	1.996	2.001	2.003	2.001	1.996	2.000	2.002	1.999	2.001	2.000	2.002
Group M												
Mo	0.000	0.000	0.000	0.000	0.000	0.001	0.001	0.001	0.000	0.001	0.000	0.001
Sn	0.000	0.001	0.000	0.001	0.000	0.000	0.000	0.000	0.000	0.000	0.000	0.000
Ge	0.000	0.000	0.000	0.000	0.000	0.000	0.000	0.000	0.000	0.000	0.000	0.000
In	0.000	0.000	0.000	0.000	0.000	0.000	0.000	0.000	0.000	0.000	0.000	0.000
Pb	0.000	0.000	0.000	0.000	0.000	0.000	0.000	0.001	0.000	0.000	0.000	0.000
Cd	0.000	0.000	0.000	0.000	0.000	0.000	0.000	0.000	0.000	0.000	0.000	0.000
Zn	0.003	0.000	0.000	0.000	0.000	0.000	0.000	0.001	0.001	0.000	0.001	0.000
Cu	0.000	0.000	0.000	0.000	0.000	0.001	0.000	0.000	0.000	0.000	0.000	0.000
Ni	0.000	0.000	0.000	0.004	0.000	0.000	0.000	0.000	0.001	0.001	0.000	0.000
Co	0.001	0.000	0.000	0.000	0.001	0.000	0.000	0.001	0.000	0.000	0.000	0.000
Fe2+	1.001	1.003	0.998	0.991	0.998	1.003	0.998	0.995	0.998	0.996	0.997	0.996
Mn	0.001	0.000	0.000	0.000	0.000	0.000	0.000	0.000	0.000	0.000	0.000	0.000
Au	0.000	0.000	0.000	0.000	0.000	0.000	0.000	0.000	0.000	0.000	0.000	0.000
Ag	0.000	0.000	0.000	0.000	0.000	0.000	0.000	0.000	0.000	0.000	0.000	0.000
Total	1.006	1.004	0.999	0.997	0.999	1.005	1.001	0.998	1.001	0.999	1.000	0.998

Pyrites

Sector	*Lousal*	*Lousal*	*Lousal*	*Lousal*	*Neves Corvo*	*Neves Corvo*	*Neves Corvo*	*Neves Corvo*	*Neves Corvo*	*Neves Corvo*	*Neves Corvo*	*Neves Corvo*
Sub-sector	*Sesmarias*	*Sesmarias*	*Sesmarias*	*Sesmarias*	*Corvo*	*Corvo*	*Corvo*	*Corvo*	*Corvo*	*Corvo*	*Lombador*	*Lombador*
Stratigraphic division	*lower VSC*	*lower VSC*	*lower VSC*	*lower VSC*	*lower VSC*	*lower VSC*	*lower VSC*	*lower VSC*	*lower VSC*	*lower VSC*	*Upper VSC*	*Upper VSC*
Mineralization type	*Mineralized*	*Mineralized*	*Mineralized*	*Mineralized*	*Py-bearing*	*Py-bearing*	*Py-bearing*	*Py-bearing*	*Py-bearing*	*Py-bearing*	*Mineralized*	*Mineralized*
Occurrence												
Sample ref.	**SES20#9_2**	**SES20#9_2**	**SES20#9_2**	**SES20#9_2**	**NCC#24**	**NCC#24**	**NCC#24**	**NCC#24**	**NCC#24**	**NCC#24**	**NCL#6**	**NCL#6**
# analysis	*#109*	*#110*	*#111*	*#112*	*#113*	*#114*	*#115*	*#116*	*#117*	*#118*	*#119*	*#120*
Mo	0.009	0.065	0.072	0.076	0.112	0.118	0.089	0.098	0.065	0.121	0.022	0.049
Sn	0.014	0.000	0.000	0.000	0.000	0.000	0.000	0.000	0.000	0.000	0.000	0.000
Ge	0.005	0.000	0.000	0.000	0.000	0.000	0.000	0.011	0.000	0.000	0.000	0.000
In	0.000	0.016	0.033	0.018	0.000	0.019	0.000	0.061	0.000	0.000	0.000	0.021
Pb	0.000	0.000	0.048	0.000	0.000	0.081	0.072	0.000	0.090	0.000	0.172	0.132
Cd	0.019	0.000	0.013	0.012	0.000	0.000	0.000	0.000	0.000	0.000	0.000	0.000
Zn	0.000	0.000	0.000	0.000	0.000	0.048	0.000	0.040	0.000	0.044	0.000	0.063
Cu	0.365	0.255	0.000	0.000	0.017	0.055	0.158	0.046	0.094	0.000	0.124	0.015
Ni	0.001	0.007	0.368	0.136	0.000	0.058	0.118	0.143	0.204	0.134	0.082	0.000
Co	0.006	0.019	0.474	0.495	0.018	0.007	0.000	0.034	0.028	0.018	0.081	0.014
Fe2+	46.273	46.625	45.686	46.053	46.514	46.010	45.698	45.566	45.774	47.012	46.517	46.282
Mn	0.010	0.000	0.000	0.000	0.000	0.068	0.105	0.108	0.077	0.000	0.000	0.000
Au	0.000	0.000	0.000	0.002	0.006	0.022	0.000	0.000	0.008	0.011	0.000	0.000
Ag	0.000	0.022	0.000	0.027	0.000	0.048	0.000	0.000	0.000	0.000	0.010	0.000
Bi	0.000	0.000	0.000	0.000	0.000	0.000	0.000	0.000	0.000	0.000	0.000	0.000
Te	0.000	0.000	0.007	0.000	0.000	0.052	0.000	0.004	0.000	0.000	0.000	0.000
Sb	0.000	0.015	0.000	0.049	0.000	0.022	0.009	0.009	0.002	0.000	0.000	0.000
Se	0.000	0.001	0.010	0.000	0.010	0.018	0.010	0.021	0.051	0.029	0.027	0.000
As	0.000	0.000	0.009	0.005	0.000	0.015	0.088	0.106	0.119	0.201	0.282	0.586
S	53.566	53.689	53.403	53.487	52.901	52.321	52.022	51.991	52.477	52.679	52.166	51.684
Total	100.268	100.714	100.123	100.360	99.578	98.962	98.369	98.238	98.989	100.249	99.483	98.846

Pyrites

# analysis	*#109*	*#110*	*#111*	*#112*	*#113*	*#114*	*#115*	*#116*	*#117*	*#118*	*#119*	*#120*
Ion Distribution												
Group S												
Bi	0.000	0.000	0.000	0.000	0.000	0.000	0.000	0.000	0.000	0.000	0.000	0.000
Te	0.000	0.000	0.000	0.000	0.000	0.001	0.000	0.000	0.000	0.000	0.000	0.000
Sb	0.000	0.000	0.000	0.001	0.000	0.000	0.000	0.000	0.000	0.000	0.000	0.000
Se	0.000	0.000	0.000	0.000	0.000	0.000	0.000	0.000	0.001	0.000	0.000	0.000
As	0.000	0.000	0.000	0.000	0.000	0.000	0.001	0.002	0.002	0.003	0.005	0.010
S	2.000	1.997	1.999	1.998	1.992	1.988	1.987	1.988	1.991	1.978	1.976	1.973
Total	2.000	1.998	1.999	1.998	1.992	1.989	1.989	1.990	1.993	1.981	1.981	1.982
Group M												
Mo	0.000	0.001	0.001	0.001	0.001	0.002	0.001	0.001	0.001	0.002	0.000	0.001
Sn	0.000	0.000	0.000	0.000	0.000	0.000	0.000	0.000	0.000	0.000	0.000	0.000
Ge	0.000	0.000	0.000	0.000	0.000	0.000	0.000	0.000	0.000	0.000	0.000	0.000
In	0.000	0.000	0.000	0.000	0.000	0.000	0.000	0.001	0.000	0.000	0.000	0.000
Pb	0.000	0.000	0.000	0.000	0.000	0.001	0.000	0.000	0.001	0.000	0.001	0.001
Cd	0.000	0.000	0.000	0.000	0.000	0.000	0.000	0.000	0.000	0.000	0.000	0.000
Zn	0.000	0.000	0.000	0.000	0.000	0.001	0.000	0.001	0.000	0.001	0.000	0.001
Cu	0.007	0.005	0.000	0.000	0.000	0.001	0.003	0.001	0.002	0.000	0.002	0.000
Ni	0.000	0.000	0.008	0.003	0.000	0.001	0.003	0.003	0.004	0.003	0.002	0.000
Co	0.000	0.000	0.010	0.010	0.000	0.000	0.000	0.001	0.001	0.000	0.002	0.000
Fe2+	0.992	0.996	0.982	0.988	1.006	1.004	1.002	1.000	0.997	1.013	1.012	1.014
Mn	0.000	0.000	0.000	0.000	0.000	0.002	0.002	0.002	0.002	0.000	0.000	0.000
Au	0.000	0.000	0.000	0.000	0.000	0.000	0.000	0.000	0.000	0.000	0.000	0.000
Ag	0.000	0.000	0.000	0.000	0.000	0.001	0.000	0.000	0.000	0.000	0.000	0.000
Total	1.000	1.003	1.001	1.002	1.008	1.011	1.012	1.010	1.007	1.019	1.019	1.018

Pyrites

Sector	*Neves Corvo*	*Neves Corvo*	*Neves Corvo*	*Neves Corvo*	*Neves Corvo*	*Neves Corvo*	*Neves Corvo*	*Neves Corvo*	*Neves Corvo*	*Neves Corvo*	*Neves Corvo*	*Neves Corvo*
Sub-sector	*Lombador*	*neves*	*neves*	*neves*	*neves*	*neves*	*neves*	*neves*	*neves*	*neves*	*neves*	*neves*
Stratigraphic division	*Upper VSC*	*lower VSC*	*lower VSC*	*lower VSC*	*lower VSC*	*lower VSC*	*lower VSC*	*lower VSC*	*lower VSC*	*lower VSC*	*lower VSC*	*lower VSC*
Mineralization type	*Mineralized*	*Py-bearing*	*Py-bearing*	*Py-bearing*	*Py-bearing*	*Py-bearing*	*Py-bearing*	*Py-bearing*	*Py-bearing*	*Py-bearing*	*Py-bearing*	*Py-bearing*
Occurrence												
Sample ref.	**NCL#6**	**NCN#17**	**NCN#17**	**NCN#17**	**NCN#17**	**NCN#17**	**NCN#17**	**NCN#17**	**NCN#17**	**NCN#17**	**NCN#17**	**NCN#17**
# analysis	*#121*	*#122*	*#123*	*#124*	*#125*	*#126*	*#127*	*#128*	*#129*	*#130*	*#131*	*#132*
Mo	0.025	0.116	0.128	0.106	0.066	0.080	0.121	0.094	0.133	0.119	0.123	0.134
Sn	0.000	0.000	0.000	0.000	0.000	0.000	0.000	0.000	0.000	0.000	0.000	0.000
Ge	0.000	0.004	0.000	0.000	0.004	0.000	0.000	0.000	0.000	0.000	0.000	0.000
In	0.000	0.000	0.000	0.000	0.000	0.000	0.000	0.000	0.000	0.000	0.000	0.000
Pb	0.000	0.000	0.045	0.000	0.000	0.033	0.016	0.030	0.000	0.087	0.090	0.042
Cd	0.000	0.000	0.000	0.000	0.000	0.000	0.000	0.000	0.000	0.000	0.000	0.000
Zn	0.066	0.037	0.000	0.000	0.000	0.064	0.000	0.000	0.000	0.020	0.000	0.000
Cu	0.017	0.000	0.000	0.000	0.000	0.000	0.000	0.000	0.000	0.000	0.000	0.000
Ni	0.000	0.031	0.000	0.009	0.021	0.009	0.040	0.056	0.000	0.076	0.064	0.018
Co	0.000	0.027	0.015	0.000	0.043	0.011	0.016	0.002	0.010	0.165	0.119	0.092
Fe2+	46.320	45.962	46.264	45.609	46.337	46.276	46.358	46.075	46.232	45.516	45.839	45.816
Mn	0.127	0.004	0.000	0.000	0.028	0.019	0.000	0.000	0.000	0.000	0.014	0.000
Au	0.016	0.018	0.007	0.000	0.033	0.000	0.000	0.000	0.003	0.000	0.000	0.036
Ag	0.000	0.000	0.013	0.023	0.019	0.000	0.021	0.000	0.000	0.019	0.000	0.009
Bi	0.000	0.000	0.000	0.000	0.000	0.000	0.000	0.000	0.000	0.000	0.000	0.000
Te	0.000	0.000	0.000	0.019	0.000	0.000	0.000	0.000	0.000	0.000	0.000	0.000
Sb	0.006	0.000	0.000	0.000	0.000	0.000	0.000	0.000	0.000	0.036	0.059	0.000
Se	0.014	0.014	0.000	0.000	0.000	0.007	0.000	0.000	0.005	0.013	0.027	0.000
As	0.160	0.000	0.000	0.000	0.000	0.000	0.000	0.000	0.000	0.085	0.063	0.000
S	52.499	52.664	52.766	53.074	52.414	52.462	52.152	52.699	52.791	52.459	52.388	52.296
Total	99.250	98.877	99.238	98.840	98.965	98.961	98.724	98.956	99.174	98.595	98.786	98.443

Pyrites

# analysis	*#121*	*#122*	*#123*	*#124*	*#125*	*#126*	*#127*	*#128*	*#129*	*#130*	*#131*	*#132*
Ion Distribution												
Group S												
Bi	0.000	0.000	0.000	0.000	0.000	0.000	0.000	0.000	0.000	0.000	0.000	0.000
Te	0.000	0.000	0.000	0.000	0.000	0.000	0.000	0.000	0.000	0.000	0.000	0.000
Sb	0.000	0.000	0.000	0.000	0.000	0.000	0.000	0.000	0.000	0.000	0.001	0.000
Se	0.000	0.000	0.000	0.000	0.000	0.000	0.000	0.000	0.000	0.000	0.000	0.000
As	0.003	0.000	0.000	0.000	0.000	0.000	0.000	0.000	0.000	0.001	0.001	0.000
S	1.986	1.996	1.994	2.008	1.988	1.989	1.984	1.996	1.995	1.996	1.991	1.993
Total	1.989	1.996	1.994	2.008	1.988	1.989	1.984	1.996	1.995	1.998	1.993	1.993
Group M												
Mo	0.000	0.002	0.002	0.001	0.001	0.001	0.002	0.001	0.002	0.002	0.002	0.002
Sn	0.000	0.000	0.000	0.000	0.000	0.000	0.000	0.000	0.000	0.000	0.000	0.000
Ge	0.000	0.000	0.000	0.000	0.000	0.000	0.000	0.000	0.000	0.000	0.000	0.000
In	0.000	0.000	0.000	0.000	0.000	0.000	0.000	0.000	0.000	0.000	0.000	0.000
Pb	0.000	0.000	0.000	0.000	0.000	0.000	0.000	0.000	0.000	0.001	0.001	0.000
Cd	0.000	0.000	0.000	0.000	0.000	0.000	0.000	0.000	0.000	0.000	0.000	0.000
Zn	0.001	0.001	0.000	0.000	0.000	0.001	0.000	0.000	0.000	0.000	0.000	0.000
Cu	0.000	0.000	0.000	0.000	0.000	0.000	0.000	0.000	0.000	0.000	0.000	0.000
Ni	0.000	0.001	0.000	0.000	0.000	0.000	0.001	0.001	0.000	0.002	0.001	0.000
Co	0.000	0.001	0.000	0.000	0.001	0.000	0.000	0.000	0.000	0.003	0.003	0.002
Fe2+	1.006	1.000	1.004	0.991	1.009	1.008	1.013	1.002	1.003	0.994	1.000	1.003
Mn	0.003	0.000	0.000	0.000	0.001	0.000	0.000	0.000	0.000	0.000	0.000	0.000
Au	0.000	0.000	0.000	0.000	0.000	0.000	0.000	0.000	0.000	0.000	0.000	0.000
Ag	0.000	0.000	0.000	0.000	0.000	0.000	0.000	0.000	0.000	0.000	0.000	0.000
Total	1.011	1.004	1.006	0.992	1.012	1.011	1.016	1.004	1.005	1.002	1.007	1.007

Pyrites

Sector	*Neves Corvo*	*Neves Corvo*	*Neves Corvo*	*Neves Corvo*	*Neves Corvo*	*Neves Corvo*	*Neves Corvo*	*Neves Corvo*	*Neves Corvo*	*Neves Corvo*	*Neves Corvo*	*Neves Corvo*
Sub-sector	*neves*	*neves*	*neves*	*neves*	*neves*	*neves*	*zambujal*	*zambujal*	*zambujal*	*zambujal*	*zambujal*	*zambujal*
Stratigraphic division	*lower VSC*	*lower VSC*	*lower VSC*	*lower VSC*	*lower VSC*	*lower VSC*	*lower VSC*	*lower VSC*	*lower VSC*	*lower VSC*	*lower VSC*	*lower VSC*
Mineralization type	*Py-bearing*	*Py-bearing*	*Py-bearing*	*Py-bearing*	*Py-bearing*	*Mineralized*	*Mineralized*	*Mineralized*	*Mineralized*	*Mineralized*	*Mineralized*	*Mineralized*
Occurrence												
Sample ref.	**NCN#17**	**NCN#17**	**NCN#17**	**NCN#17**	**NCN#17**	**NCN#20**	**NCZ#21**	**NCZ#21**	**NCZ#21**	**NCZ#21**	**NCZ#21**	**NCZ#21**
# analysis	*#133*	*#134*	*#135*	*#136*	*#137*	*#138*	*#139*	*#140*	*#141*	*#142*	*#143*	*#144*
Mo	0.089	0.068	0.097	0.071	0.046	0.100	0.076	0.073	0.069	0.062	0.056	0.092
Sn	0.000	0.000	0.000	0.000	0.000	0.000	0.000	0.000	0.000	0.000	0.000	0.000
Ge	0.000	0.000	0.000	0.000	0.000	0.000	0.000	0.000	0.000	0.000	0.000	0.000
In	0.032	0.000	0.000	0.000	0.033	0.000	0.000	0.000	0.000	0.000	0.027	0.013
Pb	0.042	0.134	0.090	0.030	0.000	0.420	0.000	0.000	0.056	0.189	0.000	0.016
Cd	0.000	0.000	0.000	0.000	0.000	0.000	0.000	0.000	0.000	0.000	0.000	0.000
Zn	0.000	0.000	0.013	0.000	0.009	0.000	0.000	0.065	0.000	0.000	0.065	0.000
Cu	0.000	0.000	0.000	0.000	0.000	0.000	0.226	0.000	0.017	0.081	0.000	0.000
Ni	0.019	0.123	0.002	0.033	0.058	0.375	0.116	0.161	0.005	0.031	0.697	0.077
Co	0.254	0.243	0.095	0.122	0.152	0.483	0.017	0.155	0.022	0.011	0.018	0.031
Fe2+	46.312	46.424	46.500	46.590	46.389	45.308	46.871	46.331	47.136	46.718	46.298	46.525
Mn	0.000	0.005	0.025	0.000	0.000	0.006	0.000	0.000	0.004	0.000	0.000	0.002
Au	0.024	0.000	0.000	0.000	0.000	0.000	0.000	0.000	0.000	0.033	0.002	0.021
Ag	0.000	0.000	0.000	0.000	0.000	0.000	0.000	0.000	0.000	0.000	0.018	0.017
Bi	0.000	0.000	0.000	0.000	0.000	0.000	0.000	0.000	0.000	0.000	0.000	0.000
Te	0.000	0.000	0.000	0.030	0.000	0.000	0.003	0.000	0.000	0.021	0.000	0.000
Sb	0.047	0.046	0.000	0.000	0.008	0.000	0.000	0.004	0.000	0.000	0.000	0.005
Se	0.000	0.010	0.000	0.006	0.017	0.010	0.000	0.000	0.039	0.000	0.000	0.020
As	0.169	0.107	0.051	0.034	0.110	0.516	0.000	0.000	0.068	0.159	0.000	0.015
S	52.215	52.262	52.556	52.471	52.519	51.738	53.129	52.452	53.062	52.757	52.914	52.654
Total	99.203	99.422	99.429	99.387	99.341	98.956	100.438	99.241	100.478	100.062	100.095	99.488

Pyrites

# analysis	*#133*	*#134*	*#135*	*#136*	*#137*	*#138*	*#139*	*#140*	*#141*	*#142*	*#143*	*#144*
Ion Distribution												
Group S												
Bi	0.000	0.000	0.000	0.000	0.000	0.000	0.000	0.000	0.000	0.000	0.000	0.000
Te	0.000	0.000	0.000	0.000	0.000	0.000	0.000	0.000	0.000	0.000	0.000	0.000
Sb	0.001	0.001	0.000	0.000	0.000	0.000	0.000	0.000	0.000	0.000	0.000	0.000
Se	0.000	0.000	0.000	0.000	0.000	0.000	0.000	0.000	0.001	0.000	0.000	0.000
As	0.003	0.002	0.001	0.001	0.002	0.008	0.000	0.000	0.001	0.003	0.000	0.000
S	1.981	1.979	1.986	1.984	1.986	1.976	1.986	1.985	1.984	1.984	1.986	1.987
Total	1.984	1.981	1.987	1.985	1.988	1.985	1.986	1.985	1.986	1.987	1.986	1.988
Group M												
Mo	0.001	0.001	0.001	0.001	0.001	0.001	0.001	0.001	0.001	0.001	0.001	0.001
Sn	0.000	0.000	0.000	0.000	0.000	0.000	0.000	0.000	0.000	0.000	0.000	0.000
Ge	0.000	0.000	0.000	0.000	0.000	0.000	0.000	0.000	0.000	0.000	0.000	0.000
In	0.000	0.000	0.000	0.000	0.000	0.000	0.000	0.000	0.000	0.000	0.000	0.000
Pb	0.000	0.001	0.001	0.000	0.000	0.003	0.000	0.000	0.000	0.001	0.000	0.000
Cd	0.000	0.000	0.000	0.000	0.000	0.000	0.000	0.000	0.000	0.000	0.000	0.000
Zn	0.000	0.000	0.000	0.000	0.000	0.000	0.000	0.001	0.000	0.000	0.001	0.000
Cu	0.000	0.000	0.000	0.000	0.000	0.000	0.004	0.000	0.000	0.002	0.000	0.000
Ni	0.000	0.003	0.000	0.001	0.001	0.008	0.002	0.003	0.000	0.001	0.014	0.002
Co	0.005	0.005	0.002	0.003	0.003	0.010	0.000	0.003	0.000	0.000	0.000	0.001
Fe2+	1.009	1.009	1.009	1.011	1.007	0.994	1.006	1.007	1.012	1.009	0.998	1.008
Mn	0.000	0.000	0.001	0.000	0.000	0.000	0.000	0.000	0.000	0.000	0.000	0.000
Au	0.000	0.000	0.000	0.000	0.000	0.000	0.000	0.000	0.000	0.000	0.000	0.000
Ag	0.000	0.000	0.000	0.000	0.000	0.000	0.000	0.000	0.000	0.000	0.000	0.000
Total	1.016	1.019	1.013	1.016	1.012	1.015	1.014	1.015	1.014	1.013	1.015	1.012

Pyrites

Sector	*Neves Corvo*	*Neves Corvo*	*Neves Corvo*	*Neves Corvo*	*Neves Corvo*	*Neves Corvo*	*Neves Corvo*	*Neves Corvo*	*Neves Corvo*	*Neves Corvo*	*Neves Corvo*	*Neves Corvo*
Sub-sector	*zambujal*	*zambujal*	*zambujal*	*zambujal*	*zambujal*	*zambujal*	*zambujal*	*Lombador*	*Lombador*	*Lombador*	*Lombador*	*Lombador*
Stratigraphic division	*lower VSC*	*lower VSC*	*lower VSC*	*lower VSC*	*lower VSC*	*lower VSC*	*lower VSC*	*lower VSC*	*lower VSC*	*lower VSC*	*lower VSC*	*lower VSC*
Mineralization type	*Mineralized*	*Mineralized*	*Mineralized*	*Mineralized*	*Mineralized*	*Mineralized*	*Mineralized*	*Mineralized*	*Mineralized*	*Mineralized*	*Mineralized*	*Mineralized*
Occurrence												
Sample ref.	**NCZ#21**	**NCZ#21**	**NCZ#21**	**NCZ#21**	**NCZ#21**	**NCZ#21**	**NCZ#21**	**NCL#10**	**NCL#10**	**NCL#10**	**NCL#10**	**NCL#10**
# analysis	*#145*	*#146*	*#147*	*#148*	*#149*	*#150*	*#151*	*#152*	*#153*	*#154*	*#155*	*#156*
Mo	0.068	0.085	0.118	0.080	0.066	0.036	0.063	0.064	0.081	0.080	0.084	0.042
Sn	0.000	0.000	0.000	0.000	0.000	0.000	0.000	0.019	0.000	0.049	0.048	0.000
Ge	0.000	0.000	0.000	0.000	0.000	0.000	0.000	0.000	0.000	0.007	0.000	0.000
In	0.000	0.000	0.000	0.000	0.000	0.000	0.023	0.000	0.049	0.000	0.019	0.033
Pb	0.000	0.000	0.099	0.047	0.355	0.012	0.041	0.024	0.068	0.313	0.000	0.009
Cd	0.000	0.000	0.000	0.000	0.000	0.000	0.000	0.010	0.001	0.041	0.000	0.026
Zn	0.035	0.000	0.000	0.024	0.000	0.000	0.005	0.078	0.000	0.027	0.000	0.000
Cu	0.000	0.000	0.000	0.000	0.000	0.000	0.000	0.000	0.000	0.013	0.000	0.000
Ni	0.041	0.034	0.067	0.057	0.010	0.027	0.042	0.021	0.003	0.060	0.018	0.007
Co	0.012	0.017	0.005	0.026	0.025	0.033	0.000	0.030	0.000	0.087	0.009	0.048
Fe2+	46.819	46.492	47.264	47.180	47.146	47.071	46.692	46.244	46.581	46.101	46.590	46.264
Mn	0.022	0.000	0.001	0.017	0.000	0.000	0.015	0.014	0.000	0.044	0.000	0.000
Au	0.065	0.000	0.032	0.000	0.005	0.032	0.000	0.000	0.020	0.000	0.000	0.027
Ag	0.000	0.000	0.018	0.030	0.044	0.000	0.054	0.001	0.000	0.015	0.021	0.018
Bi	0.000	0.000	0.000	0.000	0.000	0.000	0.000	0.000	0.000	0.000	0.000	0.000
Te	0.000	0.000	0.000	0.000	0.027	0.000	0.000	0.000	0.058	0.001	0.013	0.000
Sb	0.000	0.000	0.019	0.000	0.030	0.000	0.000	0.000	0.000	0.000	0.017	0.048
Se	0.030	0.005	0.000	0.028	0.000	0.000	0.038	0.000	0.000	0.004	0.023	0.015
As	0.032	0.000	0.036	0.000	0.059	0.000	0.000	0.300	0.008	0.124	0.516	1.199
S	52.955	52.503	53.413	53.003	53.189	52.873	53.007	53.218	53.491	53.356	53.330	52.500
Total	100.079	99.136	101.072	100.492	100.956	100.084	99.980	100.023	100.360	100.322	100.688	100.236

Pyrites

# analysis	*#145*	*#146*	*#147*	*#148*	*#149*	*#150*	*#151*	*#152*	*#153*	*#154*	*#155*	*#156*
Ion Distribution												
Group S												
Bi	0.000	0.000	0.000	0.000	0.000	0.000	0.000	0.000	0.000	0.000	0.000	0.000
Te	0.000	0.000	0.000	0.000	0.000	0.000	0.000	0.000	0.001	0.000	0.000	0.000
Sb	0.000	0.000	0.000	0.000	0.000	0.000	0.000	0.000	0.000	0.000	0.000	0.001
Se	0.001	0.000	0.000	0.000	0.000	0.000	0.001	0.000	0.000	0.000	0.000	0.000
As	0.001	0.000	0.001	0.000	0.001	0.000	0.000	0.005	0.000	0.002	0.008	0.019
S	1.987	1.987	1.986	1.982	1.984	1.984	1.990	1.996	1.998	1.998	1.990	1.977
Total	1.988	1.987	1.987	1.983	1.986	1.984	1.990	2.000	1.999	2.000	1.999	1.997
Group M												
Mo	0.001	0.001	0.002	0.001	0.001	0.001	0.001	0.001	0.001	0.001	0.001	0.001
Sn	0.000	0.000	0.000	0.000	0.000	0.000	0.000	0.000	0.000	0.001	0.001	0.000
Ge	0.000	0.000	0.000	0.000	0.000	0.000	0.000	0.000	0.000	0.000	0.000	0.000
In	0.000	0.000	0.000	0.000	0.000	0.000	0.000	0.000	0.001	0.000	0.000	0.000
Pb	0.000	0.000	0.001	0.000	0.002	0.000	0.000	0.000	0.000	0.002	0.000	0.000
Cd	0.000	0.000	0.000	0.000	0.000	0.000	0.000	0.000	0.000	0.000	0.000	0.000
Zn	0.001	0.000	0.000	0.000	0.000	0.000	0.000	0.001	0.000	0.001	0.000	0.000
Cu	0.000	0.000	0.000	0.000	0.000	0.000	0.000	0.000	0.000	0.000	0.000	0.000
Ni	0.001	0.001	0.001	0.001	0.000	0.001	0.001	0.000	0.000	0.001	0.000	0.000
Co	0.000	0.000	0.000	0.001	0.001	0.001	0.000	0.001	0.000	0.002	0.000	0.001
Fe2+	1.009	1.010	1.009	1.013	1.010	1.014	1.006	0.996	0.999	0.991	0.998	1.000
Mn	0.001	0.000	0.000	0.000	0.000	0.000	0.000	0.000	0.000	0.001	0.000	0.000
Au	0.000	0.000	0.000	0.000	0.000	0.000	0.000	0.000	0.000	0.000	0.000	0.000
Ag	0.000	0.000	0.000	0.000	0.001	0.000	0.001	0.000	0.000	0.000	0.000	0.000
Total	1.012	1.013	1.013	1.017	1.014	1.016	1.010	1.000	1.001	1.000	1.001	1.003

Pyrites

Sector	*Neves Corvo*	*Neves Corvo*	*Neves Corvo*	*Neves Corvo*	*Neves Corvo*	*Neves Corvo*	*Neves Corvo*	*Neves Corvo*	*Neves Corvo*	*Neves Corvo*
Sub-sector	***Lombador***	***Lombador***	***Lombador***	***Lombador***	***Lombador***	***Lombador***	***Lombador***	***Lombador***	***Lombador***	***Lombador***
Stratigraphic division	*lower VSC*	*lower VSC*	*lower VSC*	*lower VSC*	*PQG*	*PQG*	*PQG*	*PQG*	*PQG*	*PQG*
Mineralization type	*Mineralized*	*Mineralized*	*Mineralized*	*Mineralized*	*No Sulph*	*No Sulph*	*No Sulph*	*No Sulph*	*No Sulph*	*No Sulph*
Occurrence										
Sample ref.	**NCL#10**	**NCL#10**	**NCL#10**	**NCL#10**	**NCL#15**	**NCL#15**	**NCL#15**	**NCL#15**	**NCL#15**	**NCL#15**
# analysis	***#157***	***#158***	***#159***	***#160***	***#161***	***#162***	***#163***	***#164***	***#165***	***#166***
Mo	0.032	0.076	0.034	0.041	0.039	0.071	0.058	0.084	0.089	0.048
Sn	0.000	0.009	0.032	0.000	0.000	0.000	0.000	0.026	0.000	0.000
Ge	0.000	0.000	0.019	0.000	0.000	0.000	0.000	0.000	0.000	0.000
In	0.000	0.030	0.000	0.000	0.013	0.000	0.004	0.008	0.000	0.000
Pb	0.078	0.013	0.016	0.000	0.000	0.020	0.020	0.075	0.000	0.000
Cd	0.028	0.000	0.000	0.000	0.000	0.000	0.000	0.000	0.000	0.000
Zn	0.025	0.000	0.531	0.034	0.000	0.028	0.075	0.043	0.000	0.017
Cu	0.000	0.000	0.007	0.618	0.000	0.000	0.000	0.000	0.000	0.000
Ni	0.000	0.030	0.000	0.023	0.018	0.081	0.041	0.073	0.068	0.019
Co	0.047	0.001	0.030	0.066	0.084	0.148	0.062	0.228	0.049	0.094
Fe2+	46.658	46.675	46.089	46.071	46.083	45.637	45.749	45.543	46.108	45.916
Mn	0.000	0.028	0.000	0.000	0.015	0.008	0.007	0.000	0.000	0.011
Au	0.016	0.032	0.011	0.000	0.000	0.007	0.041	0.020	0.032	0.020
Ag	0.035	0.000	0.006	0.000	0.016	0.000	0.000	0.036	0.046	0.030
Bi	0.000	0.000	0.000	0.000	0.000	0.000	0.000	0.000	0.000	0.000
Te	0.025	0.000	0.013	0.000	0.000	0.052	0.022	0.000	0.038	0.000
Sb	0.001	0.023	0.000	0.020	0.023	0.024	0.040	0.048	0.063	0.000
Se	0.000	0.000	0.000	0.011	0.000	0.010	0.000	0.015	0.000	0.000
As	0.857	0.290	0.295	0.585	0.032	0.000	0.041	0.060	0.000	0.000
S	53.070	53.560	53.296	52.857	53.371	52.624	53.101	52.706	53.144	52.876
Total	100.872	100.767	100.379	100.326	99.694	98.710	99.261	98.965	99.637	99.031

Pyrites

# analysis	*#157*	*#158*	*#159*	*#160*	*#161*	*#162*	*#163*	*#164*	*#165*	*#166*
Ion Distribution										
Group S										
Bi	0.000	0.000	0.000	0.000	0.000	0.000	0.000	0.000	0.000	0.000
Te	0.000	0.000	0.000	0.000	0.000	0.001	0.000	0.000	0.000	0.000
Sb	0.000	0.000	0.000	0.000	0.000	0.000	0.000	0.001	0.001	0.000
Se	0.000	0.000	0.000	0.000	0.000	0.000	0.000	0.000	0.000	0.000
As	0.014	0.005	0.005	0.009	0.001	0.000	0.001	0.001	0.000	0.000
S	1.982	1.994	1.994	1.983	2.003	1.998	2.003	1.998	1.999	1.999
Total	1.996	1.999	1.998	1.993	2.004	1.999	2.004	1.999	2.000	1.999
Group M										
Mo	0.000	0.001	0.000	0.001	0.001	0.001	0.001	0.001	0.001	0.001
Sn	0.000	0.000	0.000	0.000	0.000	0.000	0.000	0.000	0.000	0.000
Ge	0.000	0.000	0.000	0.000	0.000	0.000	0.000	0.000	0.000	0.000
In	0.000	0.000	0.000	0.000	0.000	0.000	0.000	0.000	0.000	0.000
Pb	0.001	0.000	0.000	0.000	0.000	0.000	0.000	0.000	0.000	0.000
Cd	0.000	0.000	0.000	0.000	0.000	0.000	0.000	0.000	0.000	0.000
Zn	0.001	0.000	0.010	0.001	0.000	0.001	0.001	0.001	0.000	0.000
Cu	0.000	0.000	0.000	0.012	0.000	0.000	0.000	0.000	0.000	0.000
Ni	0.000	0.001	0.000	0.001	0.000	0.002	0.001	0.002	0.001	0.000
Co	0.001	0.000	0.001	0.001	0.002	0.003	0.001	0.005	0.001	0.002
Fe2+	1.001	0.998	0.990	0.993	0.993	0.995	0.991	0.991	0.996	0.997
Mn	0.000	0.001	0.000	0.000	0.000	0.000	0.000	0.000	0.000	0.000
Au	0.000	0.000	0.000	0.000	0.000	0.000	0.000	0.000	0.000	0.000
Ag	0.000	0.000	0.000	0.000	0.000	0.000	0.000	0.000	0.001	0.000
Total	1.004	1.001	1.002	1.007	0.996	1.001	0.996	1.001	1.000	1.001

Pyrites

Sector	*Neves Corvo*	*Neves Corvo*	*Neves Corvo*	*Neves Corvo*
Sub-sector	*Neves*	*Neves*	*Neves*	*Neves*
Stratigraphic division	*lower VSC*	*lower VSC*	*lower VSC*	*lower VSC*
Mineralization type	*Mineralized*	*Mineralized*	*Mineralized*	*Mineralized*
Occurrence				
Sample ref.	**NCN#16**	**NCN#16**	**NCN#16**	**NCN#16**
# analysis	***#167***	***#168***	***#169***	***#170***
Mo	0.045	0.085	0.023	0.048
Sn	0.009	0.000	0.000	0.000
Ge	0.000	0.000	0.007	0.000
In	0.000	0.012	0.019	0.006
Pb	0.120	0.033	0.021	0.012
Cd	0.000	0.000	0.000	0.000
Zn	0.025	0.015	0.017	0.000
Cu	0.114	0.000	0.000	0.000
Ni	0.082	0.000	0.061	0.110
Co	0.011	0.028	0.029	0.016
Fe2+	45.580	45.957	45.871	44.585
Mn	0.000	0.026	0.000	0.000
Au	0.022	0.010	0.054	0.000
Ag	0.000	0.003	0.000	0.021
Bi	0.000	0.000	0.000	0.000
Te	0.010	0.000	0.006	0.000
Sb	0.032	0.004	0.080	0.166
Se	0.000	0.037	0.000	0.010
As	0.000	0.000	0.008	2.451
S	53.246	53.352	53.341	51.129
Total	99.296	99.562	99.537	98.554

Pyrites

# analysis	*#167*	*#168*	*#169*	*#170*
Ion Distribution				
Group S				
Bi	0.000	0.000	0.000	0.000
Te	0.000	0.000	0.000	0.000
Sb	0.000	0.000	0.001	0.002
Se	0.000	0.001	0.000	0.000
As	0.000	0.000	0.000	0.040
S	2.007	2.005	2.006	1.969
Total	2.008	2.006	2.007	2.011
Group M				
Mo	0.001	0.001	0.000	0.001
Sn	0.000	0.000	0.000	0.000
Ge	0.000	0.000	0.000	0.000
In	0.000	0.000	0.000	0.000
Pb	0.001	0.000	0.000	0.000
Cd	0.000	0.000	0.000	0.000
Zn	0.001	0.000	0.000	0.000
Cu	0.002	0.000	0.000	0.000
Ni	0.002	0.000	0.001	0.002
Co	0.000	0.001	0.001	0.000
Fe2+	0.987	0.992	0.990	0.986
Mn	0.000	0.001	0.000	0.000
Au	0.000	0.000	0.000	0.000
Ag	0.000	0.000	0.000	0.000
Total	0.993	0.995	0.994	0.989

Chalcopyrite

n = 61

Chalcopyrite

Sector	*Aljustrel*	*Aljustrel*	*Aljustrel*	*Aljustrel*	*Aljustrel*	*Aljustrel*	*Aljustrel*	*Aljustrel*	*Aljustrel*	*Aljustrel*	*Aljustrel*	*Aljustrel*
Sub-sector	Feitais ext.										*Mina F*	*Mina M*
Stratigraphic division	*upper VSC*	*upper VSC*	*upper VSC*	*upper VSC*	*upper VSC*	*upper VSC*	*upper VSC*	*upper VSC*	*upper VSC*	*upper VSC*	*upper VSC*	*upper VSC*
Mineralization type	*Mineralized*	*Mineralized*	*Mineralized*	*Mineralized*	*No Sulph*	*No Sulph*	*No Sulph*	*No Sulph*	*No Sulph*	*No Sulph*	*No Sulph*	*Mineralized*
Occurrence	Early developed coupled with (As,Co, Ni) phases						Replacements in sigmoide structures					
Sample ref.	*EDS1-H*	*EDS1-H*	*EDS1-H*	*EDS1-H*	*EDS1-S*	*EDS1-S*	*EDS1-F*	*EDS1-F*	*EDS1-F*	*EDS1-F*	*FM#4*	**MM16#9**
# analysis	*#1*	*#2*	*#3*	*#4*	*#5*	*#6*	*#7*	*#8*	*#9*	*#10*	*#11*	*#12*
Mo	0.000	0.000	0.000	0.000	0.000	0.000	0.000	0.000	0.000	0.000	0.102	0.104
Sn	0.005	0.018	0.021	0.035	0.000	0.000	0.000	0.012	0.000	0.015	0.000	0.001
Ge	0.000	0.000	0.000	0.017	0.028	0.019	0.000	0.031	0.000	0.000	0.000	0.025
In	0.023	0.000	0.010	0.000	0.031	0.000	0.000	0.011	0.010	0.015	0.003	0.016
Pb	0.018	0.032	0.017	0.143	0.320	0.233	0.079	0.089	0.002	0.000	0.000	0.000
Cd	0.000	0.000	0.000	0.000	0.000	0.000	0.000	0.000	0.000	0.017	0.000	0.029
Zn	0.060	0.122	0.007	0.047	0.039	0.085	0.000	0.098	0.000	0.015	0.000	0.009
Cu	33.996	33.807	33.223	33.341	32.837	33.022	33.424	33.188	33.900	33.843	29.831	30.314
Ni	0.000	0.000	0.000	0.005	0.000	0.000	0.040	0.033	0.000	0.030	0.000	0.000
Co	0.043	0.030	0.045	0.049	0.055	0.034	0.045	0.077	0.050	0.061	0.000	0.038
Fe2+	30.742	30.618	30.742	30.381	30.452	29.815	30.607	29.992	30.708	30.577	0.182	0.047
Mn	0.006	0.000	0.000	0.000	0.007	0.018	0.034	0.014	0.025	0.000	0.021	0.030
Au	0.000	0.005	0.000	0.000	0.012	0.022	0.000	0.000	0.000	0.040	0.007	0.051
Ag	0.013	0.000	0.001	0.000	0.001	0.000	0.000	0.008	0.000	0.000	0.000	0.000
Bi	0.000	0.000	0.000	0.000	0.082	0.000	0.000	0.000	0.000	0.000	0.042	0.021
Te	0.000	0.000	0.000	0.000	0.000	0.000	0.000	0.000	0.000	0.000	33.522	33.889
Sb-	0.054	0.000	0.000	0.000	0.007	0.000	0.029	0.013	0.021	0.031	0.009	0.000
Se	0.000	0.011	0.000	0.009	0.061	0.030	0.000	0.000	0.012	0.018	0.000	0.051
As	0.000	0.000	0.000	0.000	0.002	0.000	0.000	0.000	0.001	0.000	0.000	0.000
S	34.859	34.803	35.134	35.084	34.945	35.081	35.100	34.699	35.174	34.803	34.389	34.944
Ga	0.000	0.000	0.000	0.000	0.000	0.000	0.000	0.000	0.000	0.000	0.000	0.009
Total	99.819	99.446	99.200	99.111	98.879	98.359	99.358	98.265	99.903	99.465	98.108	99.569

Chalcopyrite

# analysis	*#1*	*#2*	*#3*	*#4*	*#5*	*#6*	*#7*	*#8*	*#9*	*#10*	*#11*	*#12*
Ion Distribution												
Group S												
Bi	0.000	0.000	0.000	0.000	0.001	0.000	0.000	0.000	0.000	0.000	0.000	0.000
Te	0.000	0.000	0.000	0.000	0.000	0.000	0.000	0.000	0.000	0.000	0.000	0.001
Sb	0.001	0.000	0.000	0.000	0.000	0.000	0.000	0.000	0.000	0.000	0.000	0.000
Se-	0.000	0.000	0.000	0.000	0.001	0.001	0.000	0.000	0.000	0.000	0.000	0.000
As	0.000	0.000	0.000	0.000	0.000	0.000	0.000	0.000	0.000	0.000	0.000	0.000
S	1.999	2.002	2.020	2.021	2.021	2.034	2.017	2.017	2.011	2.002	2.006	2.008
Total											2.006	2.009
Group M												
Mo	0.000	0.000	0.000	0.000	0.000	0.000	0.000	0.000	0.000	0.000	0.002	0.002
Sn	0.000	0.000	0.000	0.001	0.000	0.000	0.000	0.000	0.000	0.000	0.000	0.000
Ge	0.000	0.000	0.000	0.000	0.001	0.000	0.000	0.001	0.000	0.000	0.000	0.000
In	0.000	0.000	0.000	0.000	0.001	0.000	0.000	0.000	0.000	0.000	0.000	0.001
Pb	0.000	0.000	0.000	0.001	0.003	0.002	0.001	0.001	0.000	0.000	0.000	0.000
Cd	0.000	0.000	0.000	0.000	0.000	0.000	0.000	0.000	0.000	0.000	0.000	0.001
Zn	0.002	0.003	0.000	0.001	0.001	0.002	0.000	0.003	0.000	0.000	0.005	0.001
Cu	0.984	0.981	0.964	0.969	0.958	0.966	0.969	0.973	0.978	0.982	0.986	0.983
Ni	0.000	0.000	0.000	0.000	0.000	0.000	0.001	0.001	0.000	0.001	0.000	0.000
Co	0.001	0.001	0.001	0.002	0.002	0.001	0.001	0.002	0.002	0.002	0.001	0.001
Fe2+	1.012	1.011	1.015	1.005	1.011	0.993	1.010	1.001	1.008	1.010	0.999	1.000
Mn	0.000	0.000	0.000	0.000	0.000	0.001	0.001	0.000	0.001	0.000	0.000	0.002
Au	0.000	0.000	0.000	0.000	0.000	0.000	0.000	0.000	0.000	0.000	0.000	0.000
Ag	0.000	0.000	0.000	0.000	0.000	0.000	0.000	0.000	0.000	0.000	0.001	0.000
Ga	0.000	0.000	0.000	0.000	0.000	0.000	0.000	0.000	0.000	0.000	0.000	0.000
Total	2.001	1.998	1.980	1.979	1.979	1.966	1.983	1.983	1.989	1.998	1.995	1.991

Chalcopyrite

Sector	*Aljustrel*	*Aljustrel*	*Aljustrel*	*Albernoa*	*Albernoa*	*Albernoa*	*Albernoa*	*Albernoa*	*Albernoa*	*Albernoa*	*Albernoa*	*Albernoa*
Sub-sector	*Mina M*	*Mina M*	*Mina M*									
Stratigraphic division	*upper VSC*	*upper VSC*	*upper VSC*	*upper VSC*	*upper VSC*	*upper VSC*	*upper VSC*	*upper VSC*	*upper VSC*	*upper VSC*	*upper VSC*	*upper VSC*
Mineralization type	*Mineralized*	*Mineralized*	*Mineralized*	*No Sulph*	*No Sulph*	*No Sulph*	*No Sulph*	*No Sulph*	*No Sulph*	*No Sulph*	*No Sulph*	*No Sulph*
Occurrence												
Sample ref.	**MM16#9**	**MM16#9**	**MM16#9**	**ALB02#22a**	**ALB02#22a**	**ALB02#22a**	**ALB02#22a**	**ALB02#22a**	**ALB02#22a**	**ALB02#22a**	**ALB02#22a**	**ALB02#22a**
# analysis	*#13*	*#14*	*#15*	*#16*	*#17*	*#18*	*#19*	*#20*	*#21*	*#22*	*#23*	*#24*
Mo	0.087	0.073	0.054	0.000	0.002	0.006	0.001	0.000	0.000	0.000	0.055	0.009
Sn	0.000	0.011	0.006	0.015	0.000	0.013	0.000	0.001	0.000	0.000	0.057	0.000
Ge	0.000	0.000	0.039	0.000	0.000	0.034	0.004	0.000	0.000	0.000	0.034	0.005
In	0.002	0.000	0.000	0.000	0.000	0.000	0.000	0.006	0.000	0.000	0.000	0.000
Pb	0.023	0.000	0.023	0.000	0.023	0.007	0.000	0.000	0.000	0.008	0.044	0.000
Cd	0.000	0.007	0.026	0.000	0.041	0.054	0.000	0.010	0.000	0.002	0.015	0.023
Zn	0.016	0.000	0.000	0.008	0.017	0.009	0.009	0.000	0.000	0.000	0.008	0.001
Cu	30.240	30.023	29.966	30.384	30.054	30.112	29.972	30.231	30.248	30.521	29.977	30.047
Ni	0.000	0.103	0.062	0.112	0.092	0.038	0.066	0.062	0.000	0.087	0.000	0.054
Co	0.022	0.000	0.000	0.000	0.002	0.000	0.009	0.000	0.017	0.000	0.003	0.000
Fe2+	0.039	0.035	0.064	0.096	0.117	0.095	0.000	0.065	0.022	0.040	0.040	0.138
Mn	0.006	0.388	0.170	0.000	0.002	0.000	0.019	0.000	0.010	0.011	0.029	0.033
Au	0.053	0.010	0.025	0.134	0.209	0.000	0.026	0.000	0.000	0.000	0.000	0.025
Ag	0.000	0.000	0.010	0.001	0.018	0.004	0.000	0.006	0.050	0.038	0.033	0.020
Bi	0.024	0.000	0.071	0.015	0.060	0.028	0.009	0.000	0.048	0.015	0.000	0.002
Te	33.978	33.716	33.637	34.275	33.907	34.245	34.107	34.538	34.455	34.588	34.402	34.545
Sb-	0.000	0.000	0.008	0.000	0.000	0.000	0.059	0.000	0.038	0.000	0.004	0.000
Se	0.000	0.029	0.000	0.042	0.000	0.000	0.007	0.010	0.002	0.000	0.000	0.000
As	0.009	0.002	0.000	0.000	0.034	0.015	0.019	0.013	0.000	0.019	0.000	0.000
S	34.927	34.927	34.670	35.082	35.012	35.094	34.460	34.849	35.022	35.149	34.804	35.025
Ga	0.016	0.000	0.000	0.008	0.017	0.009	0.009	0.000	0.000	0.000	0.008	0.001
Total	99.426	99.324	98.831	100.164	99.590	99.754	98.767	99.791	99.912	100.478	99.505	99.927

Chalcopyrite

# analysis	*#13*	*#14*	*#15*	*#16*	*#17*	*#18*	*#19*	*#20*	*#21*	*#22*	*#23*	*#24*
Ion Distribution												
Group S												
Bi	0.000	0.000	0.000	0.000	0.000	0.000	0.000	0.000	0.000	0.000	0.000	0.000
Te	0.000	0.000	0.000	0.001	0.000	0.000	0.000	0.000	0.000	0.000	0.000	0.000
Sb	0.000	0.000	0.000	0.000	0.000	0.000	0.000	0.000	0.000	0.000	0.000	0.000
Se-	0.000	0.000	0.000	0.000	0.001	0.000	0.000	0.000	0.000	0.000	0.000	0.000
As	0.000	0.000	0.000	0.000	0.000	0.000	0.000	0.000	0.000	0.000	0.000	0.000
S	2.009	2.011	2.008	2.005	2.011	2.012	1.999	2.000	2.006	2.003	2.003	2.006
Total	2.009	2.012	2.008	2.006	2.012	2.012	1.999	2.001	2.006	2.004	2.003	2.006
Group M												
Mo	0.002	0.001	0.001	0.000	0.000	0.000	0.000	0.000	0.000	0.000	0.001	0.000
Sn	0.000	0.000	0.001	0.000	0.000	0.001	0.000	0.000	0.000	0.000	0.001	0.000
Ge	0.000	0.000	0.000	0.000	0.000	0.000	0.000	0.000	0.000	0.000	0.000	0.000
In	0.000	0.000	0.000	0.000	0.001	0.001	0.000	0.000	0.000	0.000	0.000	0.000
Pb	0.000	0.001	0.001	0.001	0.001	0.000	0.001	0.001	0.000	0.001	0.000	0.001
Cd	0.000	0.000	0.000	0.000	0.000	0.000	0.000	0.000	0.000	0.000	0.000	0.000
Zn	0.001	0.001	0.002	0.003	0.003	0.003	0.000	0.002	0.001	0.001	0.001	0.004
Cu	0.986	0.980	0.983	0.988	0.983	0.991	0.998	1.000	0.996	0.995	0.999	0.999
Ni	0.000	0.000	0.000	0.000	0.000	0.000	0.002	0.000	0.001	0.000	0.000	0.000
Co	0.000	0.012	0.005	0.000	0.000	0.000	0.001	0.000	0.000	0.000	0.001	0.001
Fe2+	0.999	0.993	0.996	0.997	0.991	0.991	0.998	0.996	0.995	0.999	0.991	0.988
Mn	0.002	0.000	0.001	0.005	0.007	0.000	0.001	0.000	0.000	0.000	0.000	0.001
Au	0.000	0.000	0.000	0.000	0.000	0.000	0.000	0.000	0.001	0.000	0.000	0.000
Ag	0.000	0.000	0.001	0.000	0.001	0.001	0.000	0.000	0.001	0.000	0.000	0.000
Ga	0.000	0.000	0.000	0.000	0.000	0.000	0.000	0.000	0.000	0.000	0.000	0.000
Total	1.991	1.988	1.992	1.994	1.988	1.987	2.001	2.000	1.994	1.996	1.994	1.994

Chalcopyrite

Sector	*Albernoa*	*Albernoa*	*Albernoa*	*Albernoa*	*Albernoa*	*Albernoa*	*Albernoa*	*Albernoa*	*Albernoa*	*Albernoa*	*Albernoa*	*Albernoa*
Sub-sector												
Stratigraphic division	*upper VSC*	*upper VSC*	*upper VSC*	*upper VSC*	*upper VSC*	*upper VSC*	*upper VSC*	*upper VSC*	*upper VSC*	*upper VSC*	*upper VSC*	*upper VSC*
Mineralization type	*No Sulph*	*No Sulph*	*No Sulph*	*No Sulph*	*No Sulph*	*No Sulph*	*No Sulph*	*No Sulph*	*No Sulph*	*No Sulph*	*No Sulph*	*No Sulph*
Occurrence												*Early developed*
Sample ref.	**ALB02#22a**	**ALB02#22a**	**ALB02#22a**	**ALB02#22a**	**ALB02#22a**	**ALB02#22a**	**ALB02#22a**	**ALB02#22a**	**ALB02#22a**	**ALB02#22a**	**ALB02#22a**	***18-1-EE***
# analysis	***#25***	***#26***	***#27***	***#28***	***#29***	***#30***	***#31***	***#32***	***#33***	***#34***	***#35***	***#36***
Mo	0.039	0.004	0.000	0.000	0.010	0.004	0.000	0.025	0.000	0.000	0.039	0.000
Sn	0.000	0.001	0.000	0.002	0.022	0.000	0.000	0.000	0.010	0.022	0.000	0.016
Ge	0.012	0.000	0.023	0.019	0.051	0.000	0.015	0.000	0.015	0.065	0.000	0.000
In	0.000	0.012	0.000	0.000	0.000	0.000	0.000	0.000	0.000	0.000	0.000	0.004
Pb	0.000	0.000	0.000	0.000	0.000	0.000	0.010	0.009	0.000	0.061	0.023	0.076
Cd	0.000	0.051	0.029	0.000	0.013	0.000	0.013	0.012	0.000	0.054	0.000	0.000
Zn	0.000	0.000	0.000	0.000	0.000	0.001	0.000	0.024	0.000	0.000	0.000	0.010
Cu	29.400	30.479	30.208	30.553	30.623	30.290	30.258	30.311	30.388	30.257	30.128	32.585
Ni	0.017	0.000	0.000	0.000	0.022	0.000	0.021	0.007	0.003	0.052	0.004	0.000
Co	0.000	0.000	0.048	0.004	0.000	0.000	0.030	0.000	0.000	0.027	0.010	0.054
Fe2+	0.000	0.022	0.000	0.065	0.037	0.098	0.000	0.000	0.008	0.017	0.028	29.184
Mn	0.000	0.008	0.020	0.002	0.000	0.018	0.036	0.000	0.083	0.000	0.013	0.000
Au	0.094	0.000	0.000	0.040	0.013	0.013	0.000	0.009	0.000	0.000	0.000	0.000
Ag	0.015	0.000	0.000	0.000	0.000	0.000	0.000	0.038	0.008	0.000	0.021	0.007
Bi	0.006	0.061	0.000	0.000	0.000	0.010	0.000	0.060	0.005	0.000	0.021	0.000
Te	33.748	34.970	34.851	34.498	34.359	34.823	34.414	34.206	34.525	34.460	34.584	0.000
Sb-	0.000	0.000	0.015	0.007	0.044	0.013	0.006	0.003	0.000	0.000	0.000	0.000
Se	0.000	0.064	0.000	0.030	0.020	0.000	0.000	0.015	0.000	0.005	0.038	0.000
As	0.000	0.000	0.000	0.000	0.017	0.000	0.033	0.000	0.022	0.018	0.002	0.042
S	35.197	35.066	35.177	35.507	35.503	35.380	34.866	35.387	35.392	34.881	34.810	34.250
Ga	0.000	0.000	0.000	0.000	0.000	0.001	0.000	0.024	0.000	0.000	0.000	0.000
Total	98.528	100.738	100.371	100.727	100.734	100.650	99.702	100.106	100.459	99.919	99.721	96.228

Chalcopyrite

# analysis	*#25*	*#26*	*#27*	*#28*	*#29*	*#30*	*#31*	*#32*	*#33*	*#34*	*#35*	*#36*
Ion Distribution												
Group S												
Bi	0.000	0.000	0.000	0.000	0.000	0.000	0.000	0.000	0.000	0.000	0.000	0.000
Te	0.000	0.001	0.000	0.000	0.000	0.000	0.000	0.000	0.000	0.000	0.001	0.000
Sb	0.000	0.000	0.000	0.000	0.000	0.000	0.000	0.000	0.000	0.000	0.000	0.000
Se-	0.000	0.000	0.000	0.000	0.000	0.000	0.001	0.000	0.001	0.000	0.000	0.000
As	0.000	0.000	0.000	0.000	0.000	0.000	0.000	0.000	0.000	0.000	0.000	0.000
S	2.035	1.996	2.006	2.014	2.014	2.010	2.002	2.019	2.013	2.001	2.000	2.029
Total	2.035	1.997	2.006	2.014	2.015	2.010	2.003	2.019	2.013	2.001	2.000	
Group M												
Mo	0.001	0.000	0.000	0.000	0.000	0.000	0.000	0.001	0.000	0.000	0.001	0.000
Sn	0.000	0.000	0.000	0.000	0.001	0.000	0.000	0.000	0.000	0.001	0.000	0.000
Ge	0.000	0.000	0.000	0.000	0.000	0.000	0.000	0.000	0.000	0.000	0.000	0.000
In	0.000	0.001	0.001	0.000	0.000	0.000	0.000	0.000	0.000	0.001	0.000	0.000
Pb	0.000	0.000	0.000	0.000	0.000	0.000	0.000	0.000	0.000	0.001	0.000	0.001
Cd	0.000	0.000	0.001	0.000	0.000	0.000	0.001	0.000	0.000	0.000	0.000	0.000
Zn	0.000	0.001	0.000	0.002	0.001	0.003	0.000	0.000	0.000	0.001	0.001	0.000
Cu	0.985	1.004	1.003	0.987	0.983	0.998	0.997	0.985	0.991	0.997	1.003	0.974
Ni	0.000	0.000	0.001	0.000	0.001	0.000	0.000	0.000	0.000	0.000	0.000	0.000
Co	0.000	0.000	0.001	0.000	0.000	0.001	0.001	0.000	0.003	0.000	0.000	0.002
Fe2+	0.976	0.996	0.989	0.995	0.997	0.988	0.998	0.993	0.992	0.997	0.994	0.993
Mn	0.003	0.000	0.000	0.001	0.000	0.000	0.000	0.000	0.000	0.000	0.000	0.000
Au	0.000	0.000	0.000	0.000	0.000	0.000	0.000	0.000	0.000	0.000	0.000	0.000
Ag	0.000	0.001	0.000	0.000	0.000	0.000	0.000	0.001	0.000	0.000	0.000	0.000
Ga	0.000	0.000	0.000	0.000	0.000	0.000	0.000	0.001	0.000	0.000	0.000	0.000
Total	1.965	2.003	1.994	1.986	1.985	1.990	1.997	1.981	1.986	1.997	1.999	1.971

Chalcopyrite

Sector	*Albernoa*	*Albernoa*	*Albernoa*	*Albernoa*	*Albernoa*	*Albernoa*	*Albernoa*	*Albernoa*	*Albernoa*	*Albernoa*	*Albernoa*	*Albernoa*
Sub-sector												
Stratigraphic division	*upper VSC*	*upper VSC*	*upper VSC*	*upper VSC*	*upper VSC*	*upper VSC*	*upper VSC*	*upper VSC*	*upper VSC*	*upper VSC*	*upper VSC*	*upper VSC*
Mineralization type	*No Sulph*	*No Sulph*	*No Sulph*	*No Sulph*	*Mineralized*	*Mineralized*	*Mineralized*	*Mineralized*	*Mineralized*	*Mineralized*	*Mineralized*	*Mineralized*
	Early	*Early*	*Early*	*Early*	*Early*	*Early*	*Early*	*Early*	*Early*	*Early*	*Early*	*Early*
Occurrence	*developed*	*developed*	*developed*	*developed*	*developed*	*developed*	*developed*	*developed*	*developed*	*developed*	*developed*	*developed*
Sample ref.	***18-1-EE***	***18-1-EE***	***18-1-EE***	***18-1-EE***	***18-1-FF***	***18-1-FF***	***18-1-FF***	***18-1-FF***	***18-1-FF***	***18-1-FF***	***18-1-FF***	***18-1-FF***
# analysis	***#37***	***#38***	***#39***	***#40***	***#41***	***#42***	***#43***	***#44***	***#45***	***#46***	***#47***	***#48***
Mo	0.000	0.000	0.000	0.000	0.000	0.000	0.000	0.000	0.000	0.000	0.000	0.000
Sn	0.000	0.000	0.000	0.041	0.000	0.000	0.090	0.000	0.020	0.017	0.000	0.058
Ge	0.005	0.000	0.000	0.009	0.000	0.000	0.000	0.000	0.000	0.000	0.000	0.000
In	0.005	0.000	0.043	0.000	0.000	0.020	0.000	0.027	0.017	0.008	0.000	0.012
Pb	0.012	0.076	0.109	0.148	0.015	0.000	0.000	0.126	0.082	0.000	0.000	0.000
Cd	0.000	0.013	0.000	0.000	0.000	0.003	0.000	0.000	0.003	0.024	0.010	0.000
Zn	0.047	0.018	0.029	0.111	0.003	0.054	0.086	0.041	0.057	0.026	0.091	0.000
Cu	32.987	33.008	33.166	33.343	33.235	33.026	33.192	33.097	33.059	33.398	33.298	33.586
Ni	0.030	0.000	0.032	0.000	0.008	0.007	0.012	0.000	0.008	0.034	0.000	0.000
Co	0.038	0.038	0.033	0.054	0.074	0.049	0.044	0.058	0.067	0.014	0.031	0.042
Fe2+	29.605	29.151	30.240	30.326	29.885	29.616	29.649	30.388	30.183	30.112	30.270	30.486
Mn	0.000	0.009	0.035	0.043	0.095	0.112	0.085	0.049	0.054	0.002	0.000	0.000
Au	0.026	0.014	0.024	0.011	0.003	0.000	0.039	0.006	0.000	0.024	0.000	0.009
Ag	0.000	0.039	0.000	0.020	0.004	0.034	0.000	0.000	0.000	0.016	0.000	0.021
Bi	0.000	0.000	0.000	0.000	0.000	0.000	0.000	0.000	0.000	0.000	0.000	0.000
Te	0.000	0.000	0.000	0.000	0.000	0.000	0.000	0.000	0.000	0.000	0.000	0.000
Sb-	0.000	0.000	0.000	0.000	0.000	0.017	0.000	0.000	0.000	0.000	0.000	0.000
Se	0.000	0.000	0.005	0.011	0.000	0.008	0.014	0.034	0.000	0.000	0.000	0.000
As	0.005	0.006	0.000	0.000	0.000	0.006	0.038	0.015	0.018	0.000	0.000	0.000
S	35.041	34.628	34.945	34.776	35.183	34.703	34.480	35.261	35.001	34.935	34.966	35.159
Ga	0.000	0.000	0.000	0.000	0.000	0.000	0.000	0.000	0.000	0.000	0.000	0.000
Total	97.801	97.000	98.661	98.893	98.505	97.655	97.729	99.102	98.569	98.610	98.666	99.373

Chalcopyrite

# analysis	*#37*	*#38*	*#39*	*#40*	*#41*	*#42*	*#43*	*#44*	*#45*	*#46*	*#47*	*#48*
Ion Distribution												
Group S												
Bi	0.000	0.000	0.000	0.000	0.000	0.000	0.000	0.000	0.000	0.000	0.000	0.000
Te	0.000	0.000	0.000	0.000	0.000	0.000	0.000	0.000	0.000	0.000	0.000	0.000
Sb	0.000	0.000	0.000	0.000	0.000	0.000	0.000	0.000	0.000	0.000	0.000	0.000
Se-	0.000	0.000	0.000	0.000	0.000	0.000	0.000	0.001	0.000	0.000	0.000	0.000
As	0.000	0.000	0.000	0.000	0.000	0.000	0.000	0.000	0.000	0.000	0.000	0.000
S	2.039	2.034	2.021	2.011	2.033	2.026	2.016	2.028	2.025	2.021	2.021	2.019
Total												
Group M												
Mo	0.000	0.000	0.000	0.000	0.000	0.000	0.000	0.000	0.000	0.000	0.000	0.000
Sn	0.000	0.000	0.000	0.001	0.000	0.000	0.001	0.000	0.000	0.000	0.000	0.001
Ge	0.000	0.000	0.000	0.000	0.000	0.000	0.000	0.000	0.000	0.000	0.000	0.000
In	0.000	0.000	0.001	0.000	0.000	0.000	0.000	0.000	0.000	0.000	0.000	0.000
Pb	0.000	0.001	0.001	0.001	0.000	0.000	0.000	0.001	0.001	0.000	0.000	0.000
Cd	0.000	0.000	0.000	0.000	0.000	0.000	0.000	0.000	0.000	0.000	0.000	0.000
Zn	0.001	0.001	0.001	0.003	0.000	0.002	0.002	0.001	0.002	0.001	0.003	0.000
Cu	0.968	0.978	0.968	0.973	0.969	0.973	0.979	0.961	0.965	0.975	0.971	0.973
Ni	0.001	0.000	0.001	0.000	0.000	0.000	0.000	0.000	0.000	0.001	0.000	0.000
Co	0.001	0.001	0.001	0.002	0.002	0.002	0.001	0.002	0.002	0.000	0.001	0.001
Fe2+	0.989	0.983	1.004	1.007	0.992	0.993	0.995	1.004	1.003	1.000	1.004	1.005
Mn	0.000	0.000	0.001	0.001	0.003	0.004	0.003	0.002	0.002	0.000	0.000	0.000
Au	0.000	0.000	0.000	0.000	0.000	0.000	0.000	0.000	0.000	0.000	0.000	0.000
Ag	0.000	0.001	0.000	0.000	0.000	0.001	0.000	0.000	0.000	0.000	0.000	0.000
Ga	0.000	0.000	0.000	0.000	0.000	0.000	0.000	0.000	0.000	0.000	0.000	0.000
Total	1.961	1.966	1.979	1.989	1.967	1.974	1.984	1.972	1.975	1.979	1.979	1.981

Chalcopyrite

Sector	*Albernoa*	*Albernoa*	*Albernoa*	*Albernoa*	*Albernoa*	*Albernoa*	*Albernoa*	*Albernoa*	*Albernoa*	*Albernoa*	*Albernoa*	*Albernoa*
Sub-sector												
Stratigraphic division	*upper VSC*	*Middle VSC*	*Middle VSC*	*Middle VSC*	*Middle VSC*	*Middle VSC*	*Middle VSC*	*Middle VSC*	*Middle VSC*	*Middle VSC*	*Middle VSC*	*Middle VSC*
Mineralization type	*Mineralized*	*Py-bearing*	*Py-bearing*	*Py-bearing*	*Py-bearing*	*Py-bearing*	*Py-bearing*	*Py-bearing*	*Py-bearing*	*Py-bearing*	*Py-bearing*	*Py-bearing*
Occurrence	*Early developed*					*Late-developed*	*Late-developed*	*Late-developed*	*Late-developed*	*Late-developed*	*Late-developed*	*Late-developed*
Sample ref.	***18-1-FF***	**37-1-A**	**37-1-A**	**37-1-A**	**37-1-A**	**37-1-E**	**37-1-E**	**37-1-E**	**37-1-E**	**37-1-E**	**37-1-E**	**37-1-E**
# analysis	***#49***	***#50***	***#51***	***#52***	***#53***	***#54***	***#55***	***#56***	***#57***	***#58***	***#59***	***#60***
Mo	0.000	0.000	0.000	0.000	0.000	0.000	0.000	0.000	0.000	0.000	0.000	0.000
Sn	0.000	0.011	0.000	0.030	0.037	0.000	0.050	0.000	0.000	0.000	0.047	0.004
Ge	0.000	0.000	0.000	0.000	0.000	0.000	0.000	0.001	0.010	0.000	0.000	0.000
In	0.013	0.000	0.010	0.000	0.038	0.013	0.011	0.000	0.034	0.059	0.004	0.029
Pb	0.023	0.062	0.075	0.102	0.000	0.086	0.038	0.014	0.040	0.000	0.085	0.014
Cd	0.030	0.000	0.000	0.000	0.000	0.000	0.000	0.000	0.000	0.000	0.000	0.000
Zn	0.033	0.042	0.004	0.111	0.000	0.043	0.110	0.000	0.022	0.044	0.037	0.028
Cu	33.475	33.118	33.158	33.200	32.766	33.707	33.106	33.323	33.255	33.294	33.059	33.502
Ni	0.000	0.000	0.016	0.000	0.003	0.000	0.000	0.000	0.000	0.041	0.047	0.000
Co	0.025	0.046	0.084	0.071	0.050	0.014	0.071	0.037	0.028	0.030	0.032	0.041
Fe2+	30.617	30.344	29.918	30.537	30.520	30.058	29.660	30.130	29.923	29.746	29.704	30.062
Mn	0.000	0.011	0.000	0.000	0.011	0.015	0.108	0.000	0.045	0.059	0.038	0.079
Au	0.025	0.000	0.000	0.000	0.014	0.021	0.006	0.000	0.000	0.022	0.001	0.022
Ag	0.008	0.026	0.000	0.008	0.001	0.000	0.000	0.004	0.000	0.047	0.000	0.029
Bi	0.000	0.000	0.000	0.035	0.000	0.000	0.000	0.000	0.000	0.000	0.000	0.000
Te	0.000	0.000	0.000	0.000	0.000	0.000	0.000	0.000	0.000	0.000	0.000	0.000
Sb-	0.000	0.020	0.019	0.041	0.006	0.000	0.005	0.000	0.000	0.000	0.031	0.003
Se	0.044	0.000	0.005	0.000	0.000	0.005	0.000	0.026	0.000	0.025	0.021	0.029
As	0.007	0.000	0.000	0.000	0.000	0.001	0.000	0.000	0.019	0.000	0.022	0.000
S	35.373	35.530	34.684	35.090	35.345	34.936	34.784	35.252	35.024	34.531	34.738	34.832
Ga	0.000	0.000	0.000	0.000	0.000	0.000	0.000	0.000	0.000	0.000	0.000	0.000
Total	99.673	99.210	97.973	99.225	98.791	98.899	97.949	98.787	98.400	97.898	97.866	98.674

Chalcopyrite

# analysis	*#49*	*#50*	*#51*	*#52*	*#53*	*#54*	*#55*	*#56*	*#57*	*#58*	*#59*	*#60*
Ion Distribution												
Group S												
Bi	0.000	0.000	0.000	0.000	0.000	0.000	0.000	0.000	0.000	0.000	0.000	0.000
Te	0.000	0.000	0.000	0.000	0.000	0.000	0.000	0.000	0.000	0.000	0.000	0.000
Sb	0.000	0.000	0.000	0.001	0.000	0.000	0.000	0.000	0.000	0.000	0.000	0.000
Se-	0.001	0.000	0.000	0.000	0.000	0.000	0.000	0.001	0.000	0.001	0.000	0.001
As	0.000	0.000	0.000	0.000	0.000	0.000	0.000	0.000	0.000	0.000	0.000	0.000
S	2.024	2.038	2.020	2.019	2.035	2.018	2.025	2.032	2.028	2.015	2.025	2.016
Total												
Group M												
Mo	0.000	0.000	0.000	0.000	0.000	0.000	0.000	0.000	0.000	0.000	0.000	0.000
Sn	0.000	0.000	0.000	0.000	0.001	0.000	0.001	0.000	0.000	0.000	0.001	0.000
Ge	0.000	0.000	0.000	0.000	0.000	0.000	0.000	0.000	0.000	0.000	0.000	0.000
In	0.000	0.000	0.000	0.000	0.001	0.000	0.000	0.000	0.001	0.001	0.000	0.000
Pb	0.000	0.001	0.001	0.001	0.000	0.001	0.000	0.000	0.000	0.000	0.001	0.000
Cd	0.000	0.000	0.000	0.000	0.000	0.000	0.000	0.000	0.000	0.000	0.000	0.000
Zn	0.001	0.001	0.000	0.003	0.000	0.001	0.003	0.000	0.001	0.001	0.001	0.001
Cu	0.966	0.958	0.975	0.964	0.952	0.982	0.973	0.969	0.972	0.980	0.973	0.978
Ni	0.000	0.000	0.001	0.000	0.000	0.000	0.000	0.000	0.000	0.001	0.001	0.000
Co	0.001	0.001	0.003	0.002	0.002	0.000	0.002	0.001	0.001	0.001	0.001	0.001
Fe2+	1.006	0.999	1.001	1.009	1.009	0.997	0.992	0.997	0.995	0.997	0.994	0.999
Mn	0.000	0.000	0.000	0.000	0.000	0.001	0.004	0.000	0.002	0.002	0.001	0.003
Au	0.000	0.000	0.000	0.000	0.000	0.000	0.000	0.000	0.000	0.000	0.000	0.000
Ag	0.000	0.000	0.000	0.000	0.000	0.000	0.000	0.000	0.000	0.001	0.000	0.000
Ga	0.000	0.000	0.000	0.000	0.000	0.000	0.000	0.000	0.000	0.000	0.000	0.000
Total	1.976	1.962	1.980	1.981	1.965	1.982	1.975	1.968	1.972	1.985	1.975	1.984

Chalcopyrite

Sector		***Albernoa***
Sub-sector		
Stratigraphic division		*upper VSC*
Mineralization type		*No Sulph*
Occurrence		
Sample ref.		***CW2-P***
# analysis		***#61***
Mo		0.000
Sn		0.029
Ge		0.000
In		0.000
Pb		0.064
Cd		0.000
Zn		0.084
Cu		33.043
Ni		0.000
Co		0.055
Fe2+		29.805
Mn		0.000
Au		0.181
Ag		0.038
Bi		0.000
Te		0.000
Sb-		0.000
Se		0.022
As		0.000
S		35.242
Ga		0.000
	Total	98.563

Chalcopyrite

# analysis		*#61*
Ion Distribution		
Group S		
Bi		0.000
Te		0.000
Sb		0.000
Se-		0.001
As		0.000
S		2.038
	Total	
Group M		
Mo		0.000
Sn		0.000
Ge		0.000
In		0.000
Pb		0.001
Cd		0.000
Zn		0.002
Cu		0.964
Ni		0.000
Co		0.002
Fe2+		0.990
Mn		0.000
Au		0.002
Ag		0.001
Ga		0.000
	Total	1.962

Sphalerite

n = 41

Sphalerite

Sector	*Albernoa*	*Albernoa*	*Albernoa*	*Albernoa*	*Albernoa*	*Albernoa*	*Albernoa*	*Albernoa*	*Albernoa*	*Albernoa*	*Albernoa*	*Aljustrel*
Sub-sector												
Stratigraphic division	*upper VSC*	*upper VSC*	*upper VSC*	*upper VSC*	*upper VSC*	*upper VSC*	*upper VSC*	*upper VSC*	*upper VSC*	*upper VSC*	*upper VSC*	*upper VSC*
Mineralization type	*No Sulph*	*No Sulph*	*No Sulph*	*No Sulph*	*No Sulph*	*No Sulph*	*No Sulph*	*No Sulph*	*No Sulph*	*No Sulph*	*No Sulph*	*No Sulph*
Occurrence												
Sample ref.	*CW2-AA*	*CW2-AA*	*CW2-AA*	*CW2-AA*	*CW2-AA*	*CW2-AA*	*CW2-AA*	*CW2-P*	*CW2-P*	*CW2-P*	*CW2-P*	*EDS1-F*
# analysis	*#1*	*#2*	*#3*	*#4*	*#5*	*#6*	*#7*	*#8*	*#9*	*#10*	*#11*	*#12*
As	0.029	0.000	0.004	0.000	0.016	0.000	0.004	0.003	0.000	0.000	0.044	0.012
Au	0.000	0.042	0.000	0.020	0.006	0.000	0.000	0.051	0.000	0.000	0.000	0.046
Fe	9.914	10.178	10.040	9.189	9.851	9.690	5.085	0.802	1.530	0.769	1.375	1.054
Pb	0.121	0.083	0.000	0.042	0.109	0.000	0.089	0.000	0.058	0.054	0.113	0.105
Ge	0.000	0.000	0.000	0.025	0.011	0.016	0.000	0.000	0.000	0.001	0.000	0.000
Sn	0.000	0.019	0.028	0.006	0.049	0.001	0.009	0.028	0.000	0.000	0.000	0.061
Ni	0.000	0.000	0.010	0.012	0.000	0.000	0.000	0.002	0.000	0.010	0.000	0.000
Cu	0.086	0.003	0.013	0.025	0.054	0.000	0.000	0.067	0.164	0.000	0.000	0.273
Co	0.049	0.047	0.049	0.036	0.034	0.051	0.001	0.000	0.000	0.000	0.009	0.014
Se	0.018	0.007	0.000	0.034	0.015	0.009	0.011	0.000	0.018	0.031	0.000	0.004
Cd	0.032	0.178	0.081	0.086	0.073	0.032	0.063	0.027	0.022	0.034	0.000	0.035
Sb	0.000	0.000	0.084	0.027	0.000	0.000	0.000	0.000	0.000	0.000	0.000	0.000
Zn	55.386	56.040	55.579	56.380	56.405	56.588	60.905	64.332	63.800	63.079	62.401	63.014
Bi	0.000	0.000	0.000	0.000	0.000	0.000	0.000	0.061	0.000	0.000	0.000	0.000
In	0.000	0.000	0.054	0.000	0.000	0.000	0.000	0.023	0.000	0.000	0.036	0.007
S	33.961	33.877	33.833	33.712	34.010	33.938	33.806	33.888	33.813	33.786	33.789	33.737
Mn	0.007	0.023	0.000	0.000	0.029	0.018	0.022	0.031	0.011	0.061	0.000	0.000
Ag	0.000	0.000	0.000	0.000	0.000	0.000	0.000	0.032	0.014	0.033	0.007	0.005
Mo	0.000	0.000	0.000	0.000	0.000	0.000	0.000	0.000	0.000	0.000	0.000	0.000
Te	0.000	0.000	0.000	0.000	0.000	0.000	0.000	0.000	0.000	0.000	0.000	0.000
Total	99.603	100.497	99.775	99.594	100.662	100.343	99.995	99.347	99.430	97.858	97.774	98.367

Sphalerite

# analysis		#1	#2	#3	#4	#5	#6	#7	#8	#9	#10	#11	#12
Ion Distribution													
Group S													
Te2-		0.000	0.000	0.000	0.000	0.000	0.000	0.000	0.000	0.000	0.000	0.000	0.000
Sb2-		0.000	0.000	0.000	0.000	0.000	0.000	0.000	0.000	0.000	0.000	0.000	0.000
Se2-		0.000	0.000	0.000	0.000	0.000	0.000	0.000	0.000	0.000	0.000	0.000	0.000
S		1.015	1.006	1.010	1.010	1.008	1.008	1.014	1.027	1.023	1.036	1.036	1.031
	Total	1.015	1.006	1.010	1.010	1.008	1.008	1.014	1.027	1.023	1.036	1.036	1.031
Group M													
In		0.000	0.000	0.000	0.000	0.000	0.000	0.000	0.000	0.000	0.000	0.000	0.000
Bi		0.000	0.000	0.000	0.000	0.000	0.000	0.000	0.000	0.000	0.000	0.000	0.000
Zn		0.812	0.816	0.814	0.829	0.820	0.825	0.896	0.956	0.947	0.948	0.938	0.944
Cd		0.000	0.002	0.001	0.001	0.001	0.000	0.001	0.000	0.000	0.000	0.000	0.000
Sb		0.000	0.000	0.001	0.000	0.000	0.000	0.000	0.000	0.000	0.000	0.000	0.000
Se		0.000	0.000	0.000	0.000	0.000	0.000	0.000	0.000	0.000	0.000	0.000	0.000
Ni		0.000	0.000	0.000	0.000	0.000	0.000	0.000	0.000	0.000	0.000	0.000	0.000
Cu		0.001	0.000	0.000	0.000	0.001	0.000	0.000	0.001	0.003	0.000	0.000	0.004
Co		0.001	0.001	0.001	0.001	0.001	0.001	0.000	0.000	0.000	0.000	0.000	0.000
Sn		0.000	0.000	0.000	0.000	0.000	0.000	0.000	0.000	0.000	0.000	0.000	0.001
Ge		0.000	0.000	0.000	0.000	0.000	0.000	0.000	0.000	0.000	0.000	0.000	0.000
Fe		0.170	0.174	0.172	0.158	0.168	0.165	0.088	0.014	0.027	0.014	0.024	0.018
Pb		0.001	0.000	0.000	0.000	0.001	0.000	0.000	0.000	0.000	0.000	0.001	0.000
Mn		0.000	0.000	0.000	0.000	0.001	0.000	0.000	0.001	0.000	0.001	0.000	0.000
Ag		0.000	0.000	0.000	0.000	0.000	0.000	0.000	0.000	0.000	0.000	0.000	0.000
Au		0.000	0.000	0.000	0.000	0.000	0.000	0.000	0.000	0.000	0.000	0.000	0.000
As		0.000	0.000	0.000	0.000	0.000	0.000	0.000	0.000	0.000	0.000	0.001	0.000
Mo		0.000	0.000	0.000	0.000	0.000	0.000	0.000	0.000	0.000	0.000	0.000	0.000
	Total	0.985	0.994	0.990	0.990	0.992	0.992	0.986	0.973	0.977	0.964	0.964	0.969

Sphalerite

Sector	*Aljustrel*	*Aljustrel*	*Aljustrel*	*Aljustrel*	*Aljustrel*	*Aljustrel*	*Aljustrel*	*Aljustrel*	*Aljustrel*	*Aljustrel*	*Aljustrel*	*Aljustrel*
Sub-sector		*feitais mine*	*feitais mine*	*feitais mine*	*feitais mine*	*feitais mine*	*feitais mine*	*Gavião*	*Gavião*	*Gavião*	*Gavião*	*Mte Mesas*
Stratigraphic division	*upper VSC*	*upper VSC*	*upper VSC*	*upper VSC*	*upper VSC*	*upper VSC*	*upper VSC*	*upper VSC*	*upper VSC*	*upper VSC*	*upper VSC*	*upper VSC*
Mineralization type	*No Sulph*	*No Sulph*	*No Sulph*	*No Sulph*	*Py-bearing*	*Py-bearing*	*Py-bearing*	*Mineralized*	*Py-bearing*	*Py-bearing*	*Py-bearing*	*Mineralized*
Occurrence												
Sample ref.	***EDS1-F***	***FM#4***	***FM#4***	***FM#4***	***FM#5***	***FM#5***	***FM#5***	***GV7#3***	***GV9#10***	***GV9#10***	***GV9#10***	***MDM02#4***
# analysis	***#13***	***#14***	***#15***	***#16***	***#17***	***#18***	***#19***	***#20***	***#21***	***#22***	***#23***	***#24***
As	0.000	0.000	0.000	0.000	0.000	0.000	0.025	0.000	0.006	0.000	0.000	0.041
Au	0.000	0.023	0.000	0.000	0.000	0.000	0.010	0.000	0.060	0.000	0.000	0.060
Fe	1.248	1.987	1.769	1.682	4.149	1.384	1.385	3.729	2.826	2.820	2.590	0.976
Pb	6.127	0.000	0.000	0.079	0.000	0.038	0.000	0.054	0.000	0.082	0.015	0.032
Ge	0.000	0.000	0.000	0.000	0.000	0.000	0.000	0.047	0.000	0.004	0.000	0.019
Sn	0.014	0.000	0.033	0.001	0.000	0.000	0.000	0.000	0.006	0.012	0.053	0.043
Ni	0.048	0.000	0.003	0.049	0.000	0.000	0.000	0.006	0.000	0.002	0.015	0.000
Cu	0.097	0.488	0.085	0.052	6.068	0.000	0.025	0.276	0.039	0.060	0.014	0.000
Co	0.037	0.000	0.000	0.006	0.000	0.000	0.000	0.009	0.011	0.020	0.007	0.000
Se	0.000	0.000	0.012	0.015	0.015	0.005	0.014	0.003	0.005	0.017	0.010	0.006
Cd	0.032	0.072	0.099	0.055	0.084	0.181	0.193	0.104	0.193	0.177	0.128	0.068
Sb	0.000	0.018	0.024	0.000	0.000	0.039	0.000	0.000	0.000	0.018	0.000	0.064
Zn	57.071	64.254	64.853	65.012	57.052	65.732	65.219	61.602	62.655	62.591	63.193	65.559
Bi	0.000	0.000	0.000	0.000	0.000	0.000	0.000	0.000	0.000	0.017	0.000	0.000
In	0.012	0.018	0.000	0.000	0.000	0.000	0.001	0.241	0.000	0.000	0.000	0.002
S	31.969	33.949	33.422	33.291	32.948	33.607	33.512	33.489	32.933	33.039	32.985	33.346
Mn	0.016	0.008	0.031	0.000	0.022	0.017	0.011	0.012	0.000	0.000	0.047	0.039
Ag	0.000	0.000	0.042	0.006	0.000	0.005	0.043	0.000	0.000	0.000	0.000	0.027
Mo	0.000	0.135	0.105	0.114	0.081	0.025	0.000	0.124	0.101	0.120	0.096	0.053
Te	0.000	0.006	0.000	0.000	0.014	0.000	0.000	0.000	0.049	0.000	0.000	0.021
Total	96.671	100.958	100.478	100.362	100.433	101.033	100.438	99.696	98.884	98.979	99.153	100.356

Sphalerite

# analysis	*#13*	*#14*	*#15*	*#16*	*#17*	*#18*	*#19*	*#20*	*#21*	*#22*	*#23*	*#24*
Ion Distribution												
Group S												
Te2-	0.000	0.000	0.000	0.000	0.000	0.000	0.000	0.000	0.000	0.000	0.000	0.000
Sb2-	0.000	0.000	0.000	0.000	0.000	0.000	0.000	0.000	0.000	0.000	0.000	0.001
Se2-	0.000	0.000	0.000	0.000	0.000	0.000	0.000	0.000	0.000	0.000	0.000	0.000
S	1.036	1.014	1.007	1.005	0.992	1.007	1.009	1.012	1.007	1.009	1.006	1.007
Total	1.036	1.015	1.007	1.005	0.992	1.008	1.010	1.012	1.007	1.009	1.006	1.008
Group M												
In	0.000	0.000	0.000	0.000	0.000	0.000	0.000	0.002	0.000	0.000	0.000	0.000
Bi	0.000	0.000	0.000	0.000	0.000	0.000	0.000	0.000	0.000	0.000	0.000	0.000
Zn	0.907	0.942	0.958	0.962	0.842	0.966	0.964	0.913	0.939	0.937	0.945	0.971
Cd	0.000	0.001	0.001	0.001	0.001	0.002	0.002	0.001	0.002	0.002	0.001	0.001
Sb	0.000	0.000	0.000	0.000	0.000	0.000	0.000	0.000	0.000	0.000	0.000	0.000
Se	0.000	0.000	0.000	0.000	0.000	0.000	0.000	0.000	0.000	0.000	0.000	0.000
Ni	0.001	0.000	0.000	0.001	0.000	0.000	0.000	0.000	0.000	0.000	0.000	0.000
Cu	0.002	0.007	0.001	0.001	0.092	0.000	0.000	0.004	0.001	0.001	0.000	0.000
Co	0.001	0.000	0.000	0.000	0.000	0.000	0.000	0.000	0.000	0.000	0.000	0.000
Sn	0.000	0.000	0.000	0.000	0.000	0.000	0.000	0.000	0.000	0.000	0.000	0.000
Ge	0.000	0.000	0.000	0.000	0.000	0.000	0.000	0.001	0.000	0.000	0.000	0.000
Fe	0.023	0.034	0.031	0.029	0.072	0.024	0.024	0.065	0.050	0.049	0.045	0.017
Pb	0.031	0.000	0.000	0.000	0.000	0.000	0.000	0.000	0.000	0.000	0.000	0.000
Mn	0.000	0.000	0.001	0.000	0.000	0.000	0.000	0.000	0.000	0.000	0.001	0.001
Ag	0.000	0.000	0.000	0.000	0.000	0.000	0.000	0.000	0.000	0.000	0.000	0.000
Au	0.000	0.000	0.000	0.000	0.000	0.000	0.000	0.000	0.000	0.000	0.000	0.000
As	0.000	0.000	0.000	0.000	0.000	0.000	0.000	0.000	0.000	0.000	0.000	0.001
Mo	0.000	0.001	0.001	0.001	0.001	0.000	0.000	0.001	0.001	0.001	0.001	0.001
Total	0.964	0.985	0.993	0.995	1.008	0.992	0.990	0.988	0.993	0.991	0.994	0.992

Sphalerite

Sector	*Aljustrel*	*Aljustrel*	*Aljustrel*	*Aljustrel*	*Aljustrel*	*Aljustrel*	*Aljustrel*	*Aljustrel*	*Aljustrel*	*Aljustrel*	*Neves Corvo*	*Neves Corvo*
Sub-sector	*Mte Mesas*	*Mte Mesas*	*Mte Mesas*	*Mte Mesas*	*Mte Mesas*	*Mte Mesas*	*Moinho mine*	*Moinho mine*	*Moinho mine*	*Moinho mine*	*Lombador*	*Lombador*
Stratigraphic division	*upper VSC*	*upper VSC*	*upper VSC*	*upper VSC*	*upper VSC*	*upper VSC*	*upper VSC*	*upper VSC*	*upper VSC*	*upper VSC*	*upper VSC*	*upper VSC*
Mineralization type	*Mineralized*	*Mineralized*	*Mineralized*	*Mineralized*	*Mineralized*	*Mineralized*	*Mineralized*	*Mineralized*	*Mineralized*	*Mineralized*	*Mineralized*	*Mineralized*
Occurrence												
Sample ref.	*MDM02#4*	*MDM02#6*	*MDM02#6*	*MDM02#6*	*MDM02#6*	*MDM02#6*	*MFM#3*	*MFM#3*	*MFM#3*	*MFM#3*	*NCL#6*	*NCL#6*
# analysis	*#25*	*#26*	*#27*	*#28*	*#29*	*#30*	*#31*	*#32*	*#33*	*#34*	*#35*	*#36*
As	0.000	0.000	0.002	0.000	0.000	0.000	0.000	0.000	0.000	0.006	0.014	0.000
Au	0.018	0.000	0.000	0.000	0.010	0.002	0.008	0.000	0.005	0.016	0.029	0.007
Fe	0.956	1.578	1.560	1.559	1.609	1.531	2.447	2.248	2.751	2.245	1.769	1.425
Pb	0.001	0.056	0.063	0.000	0.028	0.000	0.000	0.014	0.031	0.000	0.062	0.000
Ge	0.004	0.000	0.000	0.000	0.000	0.000	0.000	0.000	0.006	0.000	0.000	0.000
Sn	0.000	0.000	0.021	0.036	0.000	0.016	0.000	0.000	0.021	0.012	0.034	0.012
Ni	0.004	0.014	0.000	0.000	0.000	0.000	0.000	0.024	0.000	0.000	0.017	0.014
Cu	0.017	0.047	0.000	0.020	0.000	0.000	0.000	0.000	0.000	0.000	0.000	0.021
Co	0.000	0.000	0.014	0.025	0.017	0.032	0.000	0.024	0.000	0.000	0.000	0.000
Se	0.011	0.015	0.000	0.000	0.000	0.008	0.000	0.000	0.000	0.000	0.000	0.000
Cd	0.078	0.091	0.071	0.108	0.103	0.164	0.141	0.097	0.119	0.135	0.148	0.194
Sb	0.014	0.015	0.000	0.000	0.000	0.002	0.000	0.026	0.005	0.000	0.024	0.025
Zn	65.840	64.622	64.996	64.838	64.739	64.894	62.747	63.480	63.748	62.943	62.674	63.703
Bi	0.006	0.000	0.000	0.000	0.000	0.000	0.000	0.000	0.000	0.000	0.000	0.000
In	0.000	0.000	0.000	0.000	0.053	0.045	0.018	0.005	0.052	0.000	0.055	0.130
S	33.476	33.579	33.641	33.748	33.600	33.467	33.226	33.784	33.493	33.309	33.062	33.217
Mn	0.000	0.036	0.024	0.014	0.000	0.000	0.000	0.016	0.006	0.033	0.013	0.005
Ag	0.000	0.018	0.000	0.000	0.000	0.025	0.041	0.019	0.017	0.000	0.075	0.000
Mo	0.081	0.090	0.122	0.116	0.050	0.098	0.078	0.122	0.134	0.110	0.077	0.112
Te	0.000	0.000	0.000	0.000	0.000	0.000	0.000	0.000	0.000	0.000	0.000	0.000
Total	100.506	100.161	100.514	100.464	100.209	100.284	98.706	99.859	100.388	98.809	98.053	98.865

Sphalerite

# analysis		*#25*	*#26*	*#27*	*#28*	*#29*	*#30*	*#31*	*#32*	*#33*	*#34*	*#35*	*#36*
Ion Distribution													
Group S													
Te2-		0.000	0.000	0.000	0.000	0.000	0.000	0.000	0.000	0.000	0.000	0.000	0.000
Sb2-		0.000	0.000	0.000	0.000	0.000	0.000	0.000	0.000	0.000	0.000	0.000	0.000
Se2-		0.000	0.000	0.000	0.000	0.000	0.000	0.000	0.000	0.000	0.000	0.000	0.000
S		1.009	1.013	1.012	1.014	1.013	1.010	1.015	1.019	1.008	1.016	1.018	1.015
	Total	1.009	1.013	1.012	1.014	1.013	1.010	1.015	1.019	1.008	1.016	1.018	1.015
Group M													
In		0.000	0.000	0.000	0.000	0.000	0.000	0.000	0.000	0.000	0.000	0.001	0.001
Bi		0.000	0.000	0.000	0.000	0.000	0.000	0.000	0.000	0.000	0.000	0.000	0.000
Zn		0.973	0.956	0.959	0.956	0.957	0.960	0.940	0.939	0.941	0.942	0.946	0.955
Cd		0.001	0.001	0.001	0.001	0.001	0.001	0.001	0.001	0.001	0.001	0.001	0.002
Sb		0.000	0.000	0.000	0.000	0.000	0.000	0.000	0.000	0.000	0.000	0.000	0.000
Se		0.000	0.000	0.000	0.000	0.000	0.000	0.000	0.000	0.000	0.000	0.000	0.000
Ni		0.000	0.000	0.000	0.000	0.000	0.000	0.000	0.000	0.000	0.000	0.000	0.000
Cu		0.000	0.001	0.000	0.000	0.000	0.000	0.000	0.000	0.000	0.000	0.000	0.000
Co		0.000	0.000	0.000	0.000	0.000	0.001	0.000	0.000	0.000	0.000	0.000	0.000
Sn		0.000	0.000	0.000	0.000	0.000	0.000	0.000	0.000	0.000	0.000	0.000	0.000
Ge		0.000	0.000	0.000	0.000	0.000	0.000	0.000	0.000	0.000	0.000	0.000	0.000
Fe		0.017	0.027	0.027	0.027	0.028	0.027	0.043	0.039	0.048	0.039	0.031	0.025
Pb		0.000	0.000	0.000	0.000	0.000	0.000	0.000	0.000	0.000	0.000	0.000	0.000
Mn		0.000	0.001	0.000	0.000	0.000	0.000	0.000	0.000	0.000	0.001	0.000	0.000
Ag		0.000	0.000	0.000	0.000	0.000	0.000	0.000	0.000	0.000	0.000	0.001	0.000
Au		0.000	0.000	0.000	0.000	0.000	0.000	0.000	0.000	0.000	0.000	0.000	0.000
As		0.000	0.000	0.000	0.000	0.000	0.000	0.000	0.000	0.000	0.000	0.000	0.000
Mo		0.001	0.001	0.001	0.001	0.001	0.001	0.001	0.001	0.001	0.001	0.001	0.001
	Total	0.991	0.987	0.988	0.986	0.987	0.990	0.985	0.981	0.992	0.984	0.982	0.985

Sphalerite

Sector	***Neves Corvo***	***Neves Corvo***	***Neves Corvo***	***Neves Corvo***	***Neves Corvo***
Sub-sector	*Lombador*	*Lombador*	*Lombador*	*Lombador*	*Zambujal*
Stratigraphic division	*upper VSC*	*upper VSC*	*upper VSC*	*upper VSC*	*lower VSC*
Mineralization type	*Mineralized*	*Mineralized*	*Mineralized*	*Mineralized*	*Mineralized*
Occurrence					
Sample ref.	***NCL#6***	***NCL#6***	***NCL#6***	***NCL#6***	***NCZ#21***
# analysis	***#37***	***#38***	***#39***	***#40***	***#41***
As	0.020	0.000	0.000	0.029	0.025
Au	0.024	0.000	0.000	0.000	0.045
Fe	0.931	1.782	0.807	0.337	3.622
Pb	0.000	0.030	0.000	0.025	0.029
Ge	0.000	0.000	0.000	0.000	0.000
Sn	0.002	0.000	0.000	0.000	0.000
Ni	0.000	0.000	0.031	0.000	0.024
Cu	0.134	0.016	0.068	0.034	0.022
Co	0.000	0.005	0.006	0.003	0.016
Se	0.050	0.035	0.000	0.000	0.000
Cd	0.120	0.069	0.163	0.159	0.342
Sb	0.000	0.000	0.000	0.047	0.018
Zn	63.577	62.978	64.648	64.346	61.437
Bi	0.000	0.000	0.000	0.000	0.000
In	0.279	0.003	0.102	0.000	0.000
S	32.941	33.036	33.014	32.986	33.066
Mn	0.000	0.000	0.018	0.000	0.018
Ag	0.019	0.000	0.000	0.000	0.012
Mo	0.113	0.099	0.092	0.071	0.124
Te	0.064	0.000	0.010	0.000	0.000
Total	98.274	98.053	98.959	98.037	98.800

Sphalerite

# analysis		*#37*	*#38*	*#39*	*#40*	*#41*
Ion Distribution						
Group S						
Te2-		0.001	0.000	0.000	0.000	0.000
Sb2-		0.000	0.000	0.000	0.000	0.000
Se2-		0.001	0.000	0.000	0.000	0.000
S		1.015	1.016	1.010	1.017	1.010
	Total	1.016	1.017	1.010	1.018	1.010
Group M						
In		0.002	0.000	0.001	0.000	0.000
Bi		0.000	0.000	0.000	0.000	0.000
Zn		0.961	0.950	0.970	0.973	0.920
Cd		0.001	0.001	0.001	0.001	0.003
Sb		0.000	0.000	0.000	0.000	0.000
Se		0.000	0.000	0.000	0.000	0.000
Ni		0.000	0.000	0.001	0.000	0.000
Cu		0.002	0.000	0.001	0.001	0.000
Co		0.000	0.000	0.000	0.000	0.000
Sn		0.000	0.000	0.000	0.000	0.000
Ge		0.000	0.000	0.000	0.000	0.000
Fe		0.017	0.032	0.014	0.006	0.064
Pb		0.000	0.000	0.000	0.000	0.000
Mn		0.000	0.000	0.000	0.000	0.000
Ag		0.000	0.000	0.000	0.000	0.000
Au		0.000	0.000	0.000	0.000	0.000
As		0.000	0.000	0.000	0.000	0.000
Mo		0.001	0.001	0.001	0.001	0.001
	Total	0.984	0.984	0.990	0.982	0.990

Galena

n = 14

Galena

Sector	*Albernoa*	*Albernoa*	*Albernoa*	*Albernoa*	*Aljustrel*	*Aljustrel*	*Aljustrel*	*Aljustrel*	*Aljustrel*	*Aljustrel*	*Aljustrel*	*Lousal*
Sub-sector					*Mte Mesas*	*Mte Mesas*	*Mte Mesas*	*Mte Mesas*	*Mte Mesas*	*Mte Mesas*	*Mte Mesas*	*Sesmarias*
Stratigraphic division	*upper VSC*	*upper VSC*	*upper VSC*	*upper VSC*	*upper VSC*	*upper VSC*	*upper VSC*	*upper VSC*	*upper VSC*	*upper VSC*	*upper VSC*	*lower VSC*
Mineralization type	*No sulph*	*No sulph*	*No sulph*	*No sulph*	*Mineralized*	*Mineralized*	*Mineralized*	*Mineralized*	*Mineralized*	*Mineralized*	*Mineralized*	*Mineralized*
Occurrence												
Sample ref.	*CW2-AA*	*CW2-AA*	*CW2-AA*	*CW2-AA*	*MDM02#4*	*MDM02#4*	*MDM02#4*	*MDM02#4*	*MDM02#4*	*MDM02#4*	*MDM02#6*	*SES20#9*
# analysis	*#1*	*#2*	*#3*	*#4*	*#5*	*#6*	*#7*	*#8*	*#9*	*#10*	*#11*	*#12*
As	0.009	0.000	0.000	0.000	0.012	0.000	0.021	0.011	0.000	0.000	0.006	0.003
Fe	0.000	0.000	0.036	0.000	0.186	0.204	0.223	0.050	0.166	0.008	0.399	1.008
Pb	87.383	87.722	88.175	88.333	87.356	87.666	86.212	87.866	84.809	87.369	87.490	83.689
Ge	0.009	0.012	0.027	0.006	0.012	0.020	0.000	0.064	0.017	0.034	0.058	0.009
Sn	0.089	0.010	0.064	0.000	0.000	0.004	0.016	0.000	0.000	0.000	0.033	0.000
Ni	0.055	0.017	0.010	0.000	0.000	0.005	0.010	0.000	0.000	0.024	0.048	0.000
Cu	0.000	0.000	0.013	0.000	0.018	0.071	0.965	0.000	0.278	0.000	0.000	0.259
Co	0.000	0.001	0.000	0.000	0.009	0.018	0.000	0.006	0.017	0.000	0.000	0.006
Se	0.000	0.008	0.008	0.006	0.071	0.072	0.115	0.076	0.168	0.112	0.692	0.394
Cd	0.051	0.093	0.020	0.007	0.000	0.000	0.000	0.000	0.000	0.000	0.000	0.000
Sb	0.000	0.000	0.137	0.063	0.000	0.000	0.000	0.000	0.000	0.000	0.000	0.000
Zn	0.000	0.000	0.024	0.000	0.000	0.100	0.000	0.003	0.068	0.068	0.011	0.000
S	13.456	13.361	13.405	13.427	13.288	13.273	13.437	13.602	12.919	13.510	13.043	13.177
Mn	0.032	0.040	0.000	0.000	0.000	0.028	0.000	0.067	0.012	0.000	0.000	0.000
Ga	0.000	0.000	0.000	0.000	0.000	0.007	0.000	0.000	0.000	0.011	0.016	0.020
Ag	0.000	0.000	0.000	0.000	0.000	0.000	0.000	0.019	0.000	0.000	0.068	0.381
Te	0.000	0.000	0.000	0.000	0.070	0.047	0.000	0.047	0.020	0.057	0.016	0.005
Sb	0.000	0.000	0.000	0.000	0.000	0.000	0.000	0.000	0.000	0.020	0.000	0.012
Total	101.084	101.264	101.919	101.842	101.022	101.515	100.999	101.811	98.474	101.213	101.880	98.963

Galena

# analysis	*#1*	*#2*	*#3*	*#4*	*#5*	*#6*	*#7*	*#8*	*#9*	*#10*	*#11*	*#12*
Ion Distribution												
Group												
S	0.994	0.989	0.987	0.990	0.985	0.979	0.979	0.995	0.978	0.995	0.959	0.971
Te	0.000	0.000	0.000	0.000	0.001	0.001	0.000	0.001	0.000	0.001	0.000	0.000
Se	0.000	0.000	0.000	0.000	0.002	0.002	0.003	0.002	0.005	0.003	0.021	0.012
Sb	0.000	0.000	0.000	0.000	0.000	0.000	0.000	0.000	0.000	0.000	0.000	0.000
Total	0.994	0.989	0.987	0.990	0.988	0.982	0.982	0.998	0.984	0.999	0.980	0.983
Group												
Zn	0.000	0.000	0.001	0.000	0.000	0.004	0.000	0.000	0.003	0.003	0.000	0.000
Cd	0.001	0.002	0.000	0.000	0.000	0.000	0.000	0.000	0.000	0.000	0.000	0.000
Sb	0.000	0.000	0.003	0.001	0.000	0.000	0.000	0.000	0.000	0.000	0.000	0.000
Se	0.000	0.000	0.000	0.000	0.000	0.000	0.000	0.000	0.000	0.000	0.000	0.000
Ni	0.002	0.001	0.000	0.000	0.000	0.000	0.000	0.000	0.000	0.001	0.002	0.000
Cu	0.000	0.000	0.000	0.000	0.001	0.003	0.036	0.000	0.011	0.000	0.000	0.010
Co	0.000	0.000	0.000	0.000	0.000	0.001	0.000	0.000	0.001	0.000	0.000	0.000
Sn	0.002	0.000	0.001	0.000	0.000	0.000	0.000	0.000	0.000	0.000	0.001	0.000
Ge	0.000	0.000	0.001	0.000	0.000	0.001	0.000	0.002	0.001	0.001	0.002	0.000
Fe	0.000	0.000	0.002	0.000	0.000	0.000	0.000	0.000	0.000	0.000	0.001	0.001
Pb	0.999	1.005	1.004	1.008	1.002	1.000	0.972	0.994	0.994	0.995	0.996	0.955
Mn	0.001	0.002	0.000	0.000	0.000	0.001	0.000	0.003	0.001	0.000	0.000	0.000
As	0.000	0.000	0.000	0.000	0.000	0.000	0.001	0.000	0.000	0.000	0.000	0.000
Ga	0.000	0.000	0.000	0.000	0.000	0.000	0.000	0.000	0.000	0.000	0.001	0.001
Total	1.006	1.011	1.013	1.010	1.012	1.018	1.018	1.002	1.016	1.001	1.020	1.017

Galena

Sector	***Lousal***	***Lousal***
Sub-sector	*Sesmarias*	*Sesmarias*
Stratigraphic division	*lower VSC*	*lower VSC*
Mineralization type	*Mineralized*	*Mineralized*
Occurrence		
Sample ref.	***SES20#9***	***SES20#9***
# analysis	***#13***	***#14***
As	0.000	0.000
Fe	0.379	0.316
Pb	85.419	85.697
Ge	0.038	0.026
Sn	0.028	0.009
Ni	0.000	0.000
Cu	0.036	0.007
Co	0.000	0.000
Se	0.514	0.113
Cd	0.000	0.000
Sb	0.000	0.000
Zn	0.077	0.000
S	13.012	13.274
Mn	0.008	0.024
Ga	0.044	0.000
Ag	0.425	0.506
Te	0.095	0.078
Sb	0.000	0.000
Total	100.075	100.050

Galena

# analysis	*#13*	*#14*
Ion Distribution		
Group		
S	0.967	0.985
Te	0.002	0.002
Se	0.016	0.003
Sb	0.000	0.000
Total	0.984	0.989
Group		
Zn	0.003	0.000
Cd	0.000	0.000
Sb	0.000	0.000
Se	0.000	0.000
Ni	0.000	0.000
Cu	0.001	0.000
Co	0.000	0.000
Sn	0.001	0.000
Ge	0.001	0.001
Fe	0.002	0.000
Pb	0.982	0.984
Mn	0.000	0.001
As	0.000	0.000
Ga	0.002	0.000
Total	1.016	1.011

Cobaltite

n = 15

Cobaltite

Sector	*Aljustrel*	*Aljustrel*	*Aljustrel*	*Aljustrel*	*Aljustrel*	*Aljustrel*	*Aljustrel*	*Aljustrel*	*Neves Corvo*	*Albernoa*
Sub-sector	***Feitais mine***	***Feitais mine***	***Gavião***	***Gavião***	***Gavião***	***Gavião***	***Gavião***	***Gavião***	***Neves***	
Stratigraphic division	*upper VSC*	*upper VSC*	*upper VSC*	*upper VSC*	*upper VSC*	*upper VSC*	*upper VSC*	*upper VSC*	*lowerVSC*	
Mineralization type	*Mineralized*	*Mineralized*	*Mineralized*	*Mineralized*	*Mineralized*	*Mineralized*	*Mineralized*	*Mineralized*	*Py-bearing*	*No Sulphide?*
Occurrence										
Sample ref.	***FM#5***	***FM#5***	**GV9#10**	**GV9#10**	**GV9#10**	**MM16#9**	**MM16#10**	**MM16#11**	**NCN#17**	**ALB03#22a**
# analysis	***#1***	***#2***	***#3***	***#4***	***#5***	***#6***	***#7***	***#8***	***#9***	***#10***
W	0.062	0.054	0.000	0.000	0.008	0.000	0.096	0.000	0.007	0.000
Mo	0.000	0.024	0.011	0.046	0.013	0.035	0.000	0.016	0.034	0.000
Sn	0.019	0.000	0.011	0.033	0.000	0.011	0.005	0.005	0.000	0.000
In	0.032	0.000	0.000	0.031	0.021	0.007	0.000	0.000	0.000	0.004
Ga	0.000	0.000	0.000	0.000	0.025	0.000	0.000	0.000	0.000	0.000
Pb	0.000	0.000	0.000	0.000	0.000	0.062	0.024	0.004	0.020	0.000
Cd	0.000	0.000	0.000	0.000	0.000	0.022	0.000	0.006	0.008	0.000
Zn	0.027	0.098	0.065	0.000	0.000	0.053	0.060	0.000	0.040	0.000
Cu	0.000	0.000	0.000	0.168	0.179	0.000	0.000	0.000	0.008	0.000
Ni	3.526	3.450	3.226	4.798	4.578	2.665	5.454	2.337	6.699	3.188
Co	29.773	29.872	26.322	22.872	22.902	32.345	28.885	32.494	23.891	30.846
Fe2+	2.640	2.604	6.116	7.919	7.876	1.242	1.306	1.447	4.497	1.528
Mn	0.015	0.000	0.000	0.027	0.006	0.047	0.028	0.038	0.036	0.000
Au	0.007	0.000	0.000	0.000	0.000	0.001	0.078	0.000	0.000	0.069
Ag	0.000	0.048	0.000	0.000	0.000	0.015	0.043	0.000	0.023	0.000
Bi	0.000	0.000	0.000	0.000	0.021	0.000	0.000	0.000	0.000	0.000
Te	0.040	0.055	0.040	0.000	0.000	0.049	0.000	0.009	0.000	0.000
Sb	0.000	0.000	0.000	0.039	0.006	0.000	0.000	0.000	0.614	0.000
Se	0.000	0.000	0.000	0.000	0.000	0.000	0.000	0.000	0.305	0.000
As	39.752	39.702	40.168	39.762	39.539	42.859	41.624	42.269	42.378	41.692
S	20.107	20.165	20.555	20.473	20.900	20.164	19.752	20.111	18.597	20.081
Total	96.000	96.072	96.514	96.168	96.074	99.577	97.355	98.736	97.157	97.408

Cobaltite

# analysis	*#1*	*#2*	*#3*	*#4*	*#5*	*#6*	*#7*	*#8*	*#9*	*#10*
Ion Distribution										
Group M										
W	0.001	0.001	0.000	0.000	0.000	0.000	0.001	0.000	0.000	0.000
Mo	0.000	0.000	0.000	0.001	0.000	0.001	0.000	0.000	0.001	0.000
Sn	0.000	0.000	0.000	0.001	0.000	0.000	0.000	0.000	0.000	0.000
In	0.001	0.000	0.000	0.001	0.000	0.000	0.000	0.000	0.000	0.000
Ga	0.000	0.000	0.000	0.000	0.001	0.000	0.000	0.000	0.000	0.000
Pb	0.000	0.000	0.000	0.000	0.000	0.001	0.000	0.000	0.000	0.000
Cd	0.000	0.000	0.000	0.000	0.000	0.000	0.000	0.000	0.000	0.000
Zn	0.001	0.003	0.002	0.000	0.000	0.001	0.002	0.000	0.001	0.000
Cu	0.000	0.000	0.000	0.004	0.005	0.000	0.000	0.000	0.000	0.000
Ni	0.102	0.099	0.092	0.137	0.131	0.075	0.157	0.066	0.195	0.091
Co	0.855	0.857	0.749	0.652	0.651	0.904	0.826	0.914	0.692	0.878
Fe2+	0.080	0.079	0.184	0.238	0.236	0.037	0.039	0.043	0.138	0.046
Mn	0.001	0.000	0.000	0.001	0.000	0.001	0.001	0.001	0.001	0.000
Au	0.000	0.000	0.000	0.000	0.000	0.000	0.001	0.000	0.000	0.001
Ag	0.000	0.001	0.000	0.000	0.000	0.000	0.001	0.000	0.000	0.000
Total	1.040	1.040	1.026	1.035	1.024	1.021	1.027	1.025	1.028	1.016
Group S										
Bi	0.000	0.000	0.000	0.000	0.000	0.000	0.000	0.000	0.000	0.000
Sb	0.000	0.000	0.000	0.001	0.000	0.000	0.000	0.000	0.009	0.000
As	0.898	0.896	0.899	0.892	0.884	0.943	0.936	0.935	0.966	0.934
S	0.062	0.064	0.075	0.073	0.092	0.037	0.038	0.040	0.000	0.051
Total	0.960	0.960	0.974	0.965	0.976	0.980	0.974	0.975	0.975	0.984
Group X										
Te	0.001	0.001	0.001	0.000	0.000	0.001	0.000	0.000	0.000	0.000
Se	0.000	0.000	0.000	0.000	0.000	0.000	0.000	0.000	0.007	0.000
S	1.000	0.999	1.000	1.000	1.000	0.999	1.000	1.000	0.990	1.000
Total	1.000	1.000	1.000	1.000	1.000	1.000	1.000	1.000	0.997	1.000

Cobaltite

Sector	*Albernoa*	*Albernoa*	*Albernoa*	*Albernoa*	*Albernoa*
Sub-sector					
Stratigraphic division					
Mineralization type	*No Sulphide?*	*No Sulphide?*	*No Sulphide?*	*No Sulphide?*	*No Sulphide?*
Occurrence					
Sample ref.	**ALB03#22a**	**ALB03#22a**	**ALB03#22a**	**ALB03#22a**	**ALB03#22a**
# analysis	*#11*	*#12*	*#13*	*#14*	*#15*
W	0.193	0.081	0.000	0.022	0.055
Mo	0.018	0.000	0.000	0.000	0.000
Sn	0.047	0.000	0.016	0.057	0.009
In	0.000	0.000	0.007	0.000	0.000
Ga	0.000	0.000	0.000	0.000	0.000
Pb	0.000	0.000	0.000	0.094	0.063
Cd	0.011	0.000	0.037	0.000	0.000
Zn	0.000	0.003	0.041	0.000	0.000
Cu	0.067	0.000	0.055	0.000	0.000
Ni	4.554	4.544	4.142	3.115	4.109
Co	29.392	29.055	28.835	30.515	29.245
Fe2+	1.869	2.356	2.487	2.150	2.225
Mn	0.065	0.048	0.045	0.159	0.011
Au	0.005	0.012	0.000	0.061	0.000
Ag	0.048	0.023	0.040	0.000	0.000
Bi	0.000	0.000	0.000	0.000	0.000
Te	0.101	0.025	0.005	0.052	0.045
Sb	0.000	0.000	0.000	0.000	0.000
Se	0.000	0.000	0.000	0.000	0.000
As	41.486	41.597	41.629	41.753	41.540
S	20.099	20.174	20.105	20.183	20.247
Total	97.955	97.918	97.444	98.161	97.549

Cobaltite

# analysis		*#11*	*#12*	*#13*	*#14*	*#15*
Ion Distribution						
Group M						
W		0.002	0.001	0.000	0.000	0.001
Mo		0.000	0.000	0.000	0.000	0.000
Sn		0.001	0.000	0.000	0.001	0.000
In		0.000	0.000	0.000	0.000	0.000
Ga		0.000	0.000	0.000	0.000	0.000
Pb		0.000	0.000	0.000	0.001	0.001
Cd		0.000	0.000	0.001	0.000	0.000
Zn		0.000	0.000	0.001	0.000	0.000
Cu		0.002	0.000	0.002	0.000	0.000
Ni		0.130	0.129	0.118	0.088	0.117
Co		0.833	0.822	0.820	0.863	0.830
Fe2+		0.056	0.070	0.075	0.064	0.067
Mn		0.002	0.002	0.001	0.005	0.000
Au		0.000	0.000	0.000	0.001	0.000
Ag		0.001	0.000	0.001	0.000	0.000
	Total	1.026	1.024	1.018	1.022	1.015
Group S						
Bi		0.000	0.000	0.000	0.000	0.000
Sb		0.000	0.000	0.000	0.000	0.000
As		0.925	0.926	0.931	0.928	0.928
S		0.049	0.050	0.051	0.049	0.057
	Total	0.974	0.976	0.982	0.978	0.985
Group X						
Te		0.001	0.000	0.000	0.001	0.001
Se		0.000	0.000	0.000	0.000	0.000
S		0.999	1.000	1.000	0.999	0.999
	Total	1.000	1.000	1.000	1.000	1.000